28th International QUENCH Workshop

5-7 December 2023
Karlsruhe Institute of Technology
Karlsruhe, Germany

Editor: Martin Steinbrück

DOI: 10.5445/IR/1000165938

AGENDA

28th International QUENCH Workshop*

Karlsruhe Institute of Technology, Campus North, H.-von-Helmholtz-Platz 1, 76344 Egg.-Leopoldshafen, Germany
5-7 December 2023

Meeting Location: Fortbildungszentrum für Technik und Umwelt (FTU), Auditorium (Aula)

Tuesday, 5 Dec 2023

9:00	Welcome	W. Tromm/M. Steinbrück, KIT
9:20	Update of the QUENCH Program	M. Steinbrück, KIT
	LONG-TERM DRY STORAGE – SYSTEM ZR-H (Chair: M. Wolff, ENSI)	
9:40	Update of the SPIZWURZ project investigating the hydrogen behavior in zirconium alloys	M. Grosse, KIT
10:10	Hydrogenation of claddings in the new developed HOKI oven and performance of the long-term bundle test under dry storage conditions in the framework of the SPIZWURZ project	J. Stuckert, KIT
10:40	**Coffee break (Group Photo)**	
11:10	Neutron imaging investigations of hydrogen in cladding tubes	S. Weick, KIT
11:30	Structural integrity of hydrided Zircaloy and its implications for safety of extended dry storage	Y. Lee, SNU
12:00	Hydrogen diffusion and precipitation in fuel cladding under stress, at various temperatures and under the influence of a liner, using neutron imaging	J. Bertsch, PSI
12:30	**Lunch**	
	ATF CLADDING (Chair: M. Grosse, KIT)	
13:30	Accident Tolerant Fuel: Cr Coated Cladding Development at Westinghouse	K. Frederick, WEC
14:00	Exploring safety limits of Cr-coated ATF cladding using separate effect and integral LOCA experiments	Y. Lee, SNU
14:30	Chromium coating (on zirconium based-cladding substrate) cracking monitoring and characterization under thermomechanical loadings	A. Charbal, CEA
14:50	Preliminary BDBA test results of Cr-coated Zr alloy cladding at DEGREE facility	K. Nakamura, CRIEPI
15:10	**Coffee break**	
15:40	The CODEX-ATF experiment	R. Farkas, CER(EK)

**** In Cooperation with the International Atomic Energy Agency (IAEA)***

16:00	Oxidation of various ATF cladding concepts	A. Endrychova, UJP
16:20	Recent and ongoing experiments on the high-temperature oxidation and degradation of Cr-coated Zr alloy	M. Steinbrück, KIT

Wednesday, 6 Dec 2023

	MODELLING AND CODE APPLICATION (Chair: E. Rouge, IRSN)	
9:00	Modelling of hydride morphology in zirconium tubes loaded by internal pressure after slow cooling	M. Kolesnik, KIT (presented by J. Stuckert)
9:20	Development of a model for Cr-coated Claddings for system codes	G. Stahlberg, RUB
9:40	Simulation of QUENCH-15 and QUENCH-03 scenarios with modified AC² for Cr-coated claddings	T. Hollands, GRS
10:10	**Coffee break**	
10:40	NPP accident analyses under LOCA and SBO conditions using system computer codes	M. Valincius, LEI
11:00	KIT Validation Activities of the ASTEC code against the QUENCH Bundle Experiments: Results and Outlook	M. Cazado, KIT
11:20	Estimation of melt oxidation kinetics	J. Stuckert, GRS
12:00	**Lunch**	
	INTERNATIONAL PROGRAMS (Chair: H. Esmaili, USNRC)	
13:30	IAEA ongoing activities to support advanced nuclear fuel technologies development	A. Khaperskaia, IAEA
14:00	Improving chemical thermodynamics knowledge of severe accidents within the OECD-TCOFF2 Project	D. Bottomley, JRC
14:30	Update on NEA activities supporting ATF development	J.F. Martin, OECD-NEA
14:50	Overview on the OECD-NEA Joint Undertaking QUENCH-ATF	M. Steinbrück, KIT
15:20	**Coffee break + Time for discussion**	
16:15	**Bus to former nuclear power station Philippsburg and invited dinner (Löwenbräu Philippsburg)**	

Thursday, 7 Dec 2023

	EXPERIMENTS (Chair: J.- Stuckert, KIT)	
9:00	PNNL Research and Testing Capabilities	G. Wang, PNNL
9:30	A separate effects study of secondary hydriding during a LOCA transient	A.M. Kpemou, IRSN
10:00	High Temperature Creep of Zr Alloys with Internal Overpressure	V. Boucek, UJP

10:20	**Coffee break**	
10:50	The EC SCORPION Project on SiC cladding: Overview and first results	M. Grosse, KIT
11:10	Analysis of Fuel Fragment Dispersal During Post-Burst Vibration Event	P. Doyle, ORNL
11:30	**Closure of the Workshop**	M. Steinbrück, KIT
12:00	**Lunch**	


28th International QUENCH Workshop

W. Tromm

KIT

Outlook Programme NUSAFE at KIT and Helmholtz Association

The Head of the Nuclear Safety program at welcomed the participants and gave a brief overview on the status and future of the nuclear safety research in Karlsruhe within the current political boundary conditions.

Karlsruhe Institute of Technology

Welcome Address:
28th QUENCH workshop at KIT

Outlook Programme NUSAFE at KIT and Helmholtz Association

Th. Walter Tromm, Programme Nuclear Waste Management, Safety and Radiation Research

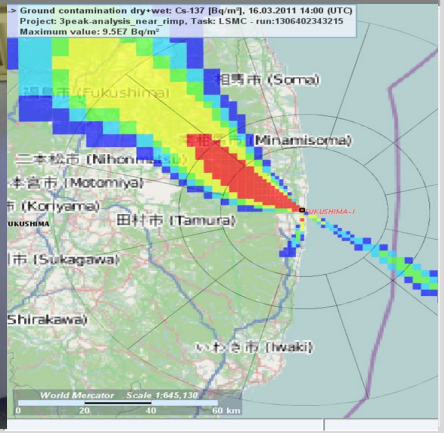

Countries launch joint declaration to triple nuclear energy capacity by 2050 at COP28

President of the French Republic Emmanuel Macron and United States Special Presidential Envoy for Climate John Kerry announced that 20 countries have launched the 'Declaration to Triple Nuclear Energy by 2050' at the 28th United Nations Climate Change Conference or Conference of the Parties of the UNFCCC (COP28).

Leaders from around the world came together on 2 December in Dubai to make the joint declaration which refers to Nuclear Energy Agency analysis which shows that a scenario where nuclear energy capacity is tripled by 2050 provides a feasible path to meet net zero.

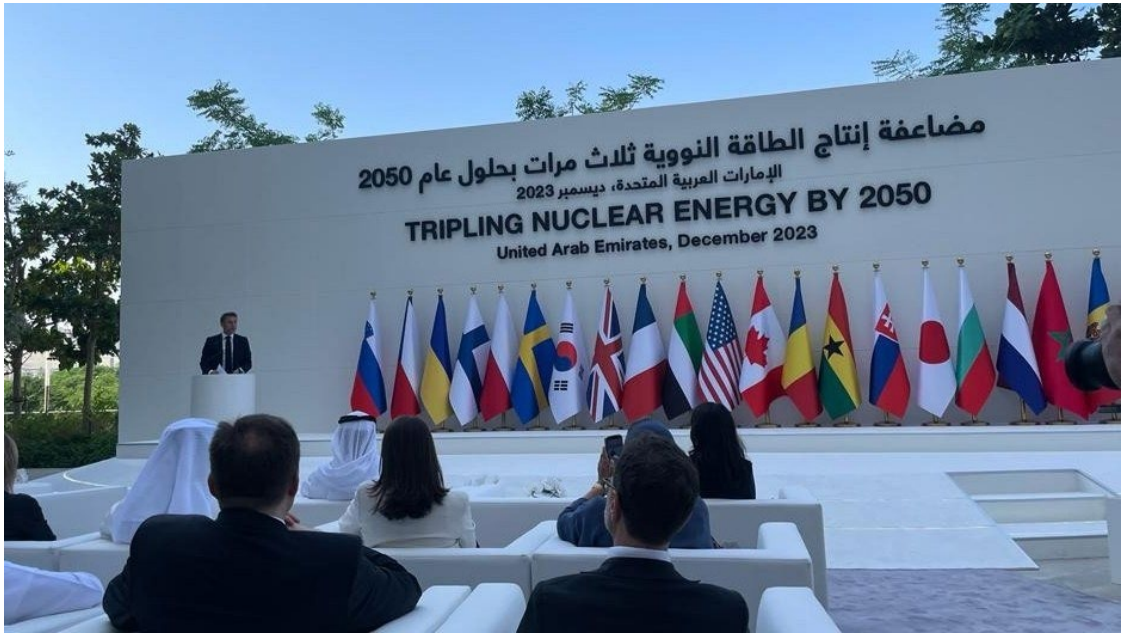

President of the French Republic Emmanuel Macron launching the 'Declaration to Triple Nuclear Energy by 2050' at COP28.

Nuclear Energy Agency Director-General William D. Magwood, commented on the joint declaration:

"I am pleased to see this declaration from the leaders of 20 countries committing to work together to advance a global aspirational goal to triple nuclear energy capacity by 2050. Nuclear Energy Agency analysis shows that tripling nuclear energy capacity by 2050 provides the world with a realistic and practical path to meet net zero carbon emissions goals. We have the research to tell us what needs to be done, and now is the time for action.

The task ahead is not an easy one, but I am optimistic, as this declaration demonstrates a collective recognition of what is required. Those countries that choose this option will need to work in concert to address issues such as affordable financing, enhanced supply chains and the need for a skilled workforce if success is to be in reach. We look forward to working with our members and partners to help them reach this goal."

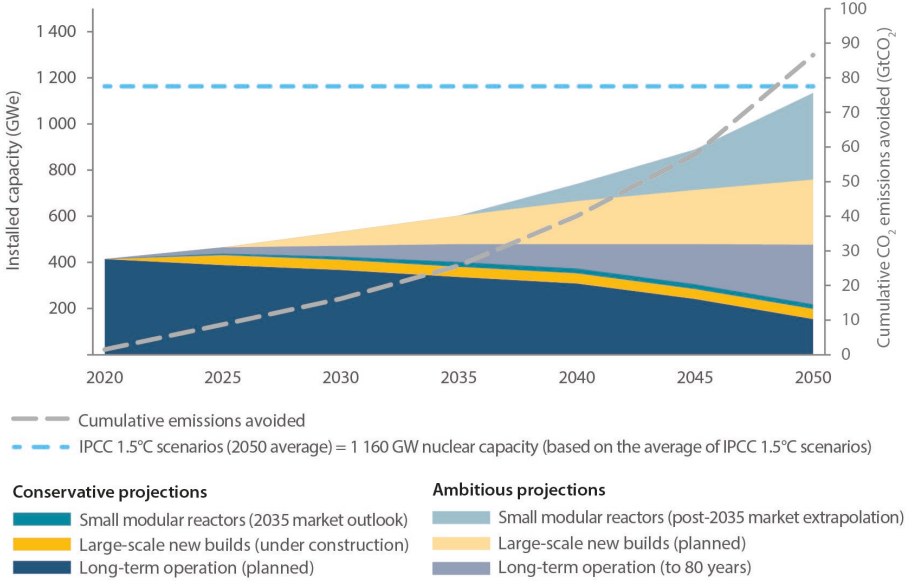

Meeting ambitious goals requires collaboration

Nuclear power has a lot to contribute. **IAEA Director General Rafael Mariano Grossi** said, “To be pro-nuclear is to take our long-term responsibility to this planet and its future generations seriously”.
As the only world forum in the nuclear field, the IAEA contributes to an informed debate on the benefits of nuclear power and nuclear applications by providing the scientific and technical facts at international forums, including COP, where political leaders, industry, scientists and civil society discuss the way forward.

Continuation of the Reactor Safety Topic in PoF V from 2028 until 2035

- Main focus on LWR technology developments, including LWR-SMR.
  - Objective: Contributions within an international collaboration for the safety assessment of existing and new reactor designs
- Investigations as well in **innovative reactor concepts, such as LFR and MSR**
  - Objective: Contributions within an international collaboration for the safety assessment and evaluation of their advantages in comparison with LWR-reactors, e.g. for higher efficiency and possibilities for transmutation.

Motivation: Nuclear Technology Developments in LWRs

Karlsruhe Institute of Technology

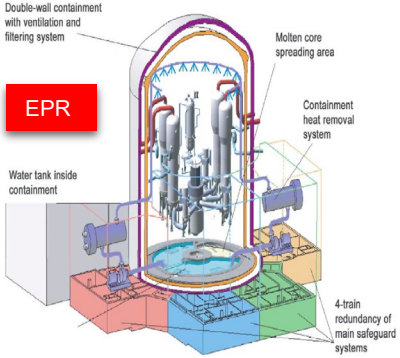

EPR

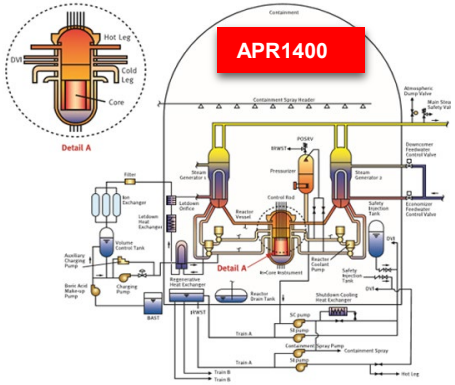

APR1400

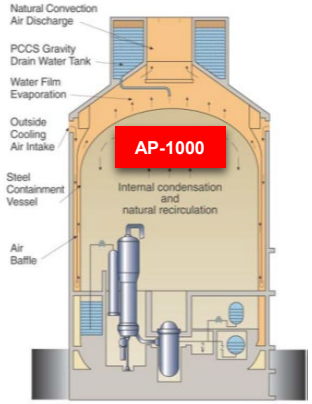

AP-1000

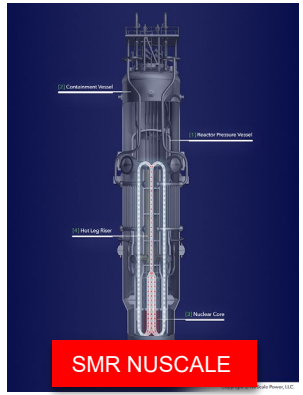

SMR NUSCALE

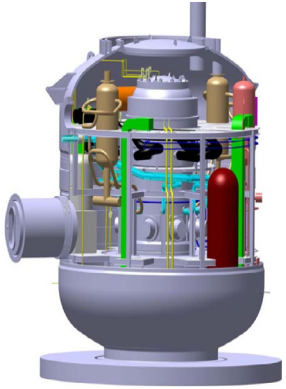

SMR NUWARD

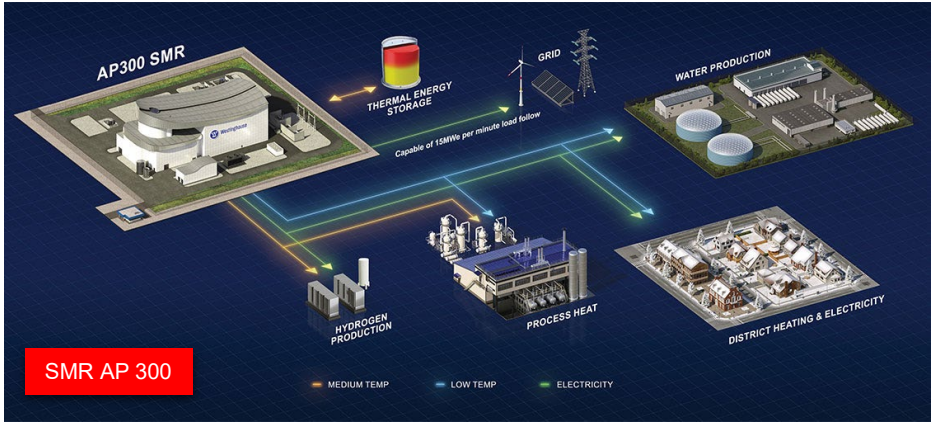

SMR AP 300

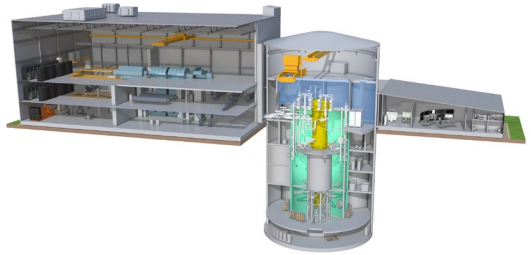

SMR GE Hitachi

KIT approach for safety analysis

- **EU-project McSAFER, coordinated by KIT**: Improving safety analysis methodologies for SMR
- Planned follow-up by EdF: KIT WP coordination
- BMBF initiative „Innovation pool projects“: **Safety assessment of small modular reactors (SMR)**
  - Develop advanced simulation tools for safety analysis of SMR to be build in Europe
  - Combination of in-house with external codes to improve core and plant analysis

Multi-physics and multi-scale developments for core analysis and safety

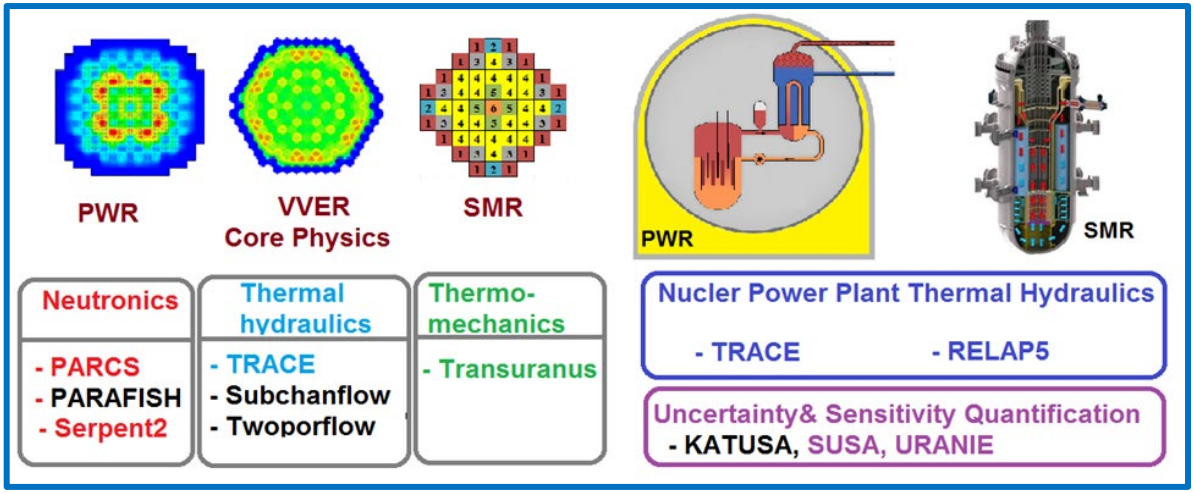

In-house: PARAFISH, SUBCHANFLOW, TWOPORFLOW, KATUSA

Core and Plant Thermal Hydraulics

- SMR with integrated RPV

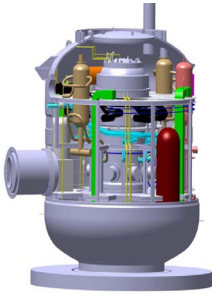

NUWARD Design

Multi-scale/-physics coupling

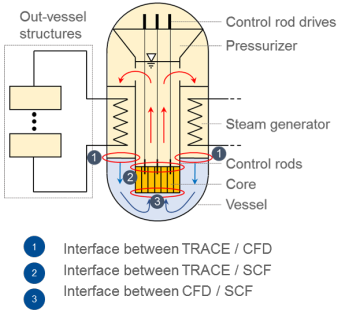

EU McSAFER approach

COSMOS-H

Investigation of, e.g.:

- safety-relevant TH phenomena e.g. boiling, CHF, cross flow
- Natural circulation flow / forced convection transition

In-house code TWOPORFLOW: NuSCALE Core Analysis at FA-Level

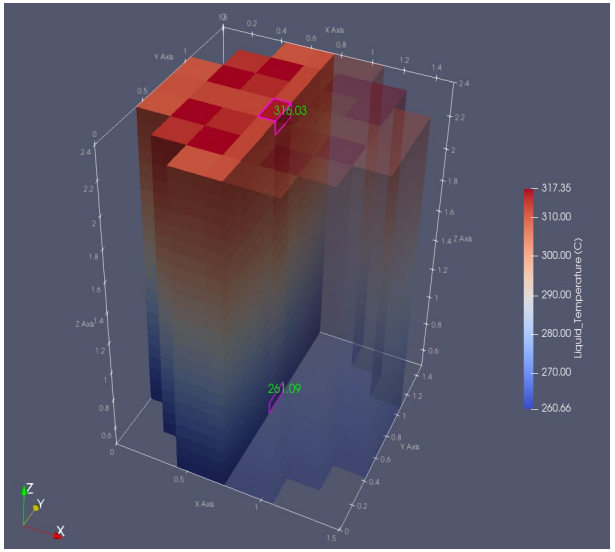

NuScale core: 3D Coolant temperature

QUENCH-ATF Joint Undertaking

Worldwide first large-scale bundle experiments with Accident-Tolerant Fuel (ATF) cladding materials under DBA and severe accident conditions

- Three bundle experiments in the QUENCH facility
- Budget: 1.6 Mio €
- 20 participants from 9 countries

Most promising ATF cladding concepts

- Cr-coated Zr alloys
- FeCrAl alloys
- SiCf-SiC ceramic matrix composites

QUENCH-ATF #1 successfully performed with Cr coated Zr
(provided by Westinghouse)

Assessment of the radiological consequences of severe accidents in nuclear power plants

- Cooperation with IRSN on ASTEC code (including source-code shared with KIT)
- Cooperation under the US-NRC-CSARP agreement with SANDIA-NL MELCOR development
- **Coupling ASTEC with JRODOS:** Innovative computational platform for realistic assessments of fission product release and dispersion into the environment in case of severe accidents in NPPs, i.e. PWR, VVER-1000, BWR and SMRs
  - Quantification of uncertainty and prediction accuracy
  - Emergency management support for beyond-design-basis events
  - Artificial intelligence algorithms to improve ASTEC and JRODOS

European Reference ASTEC code (IRSN)

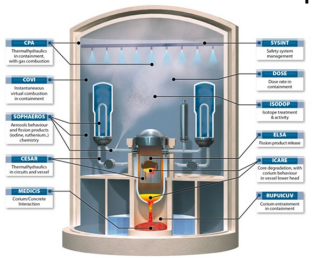

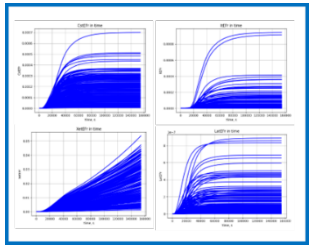

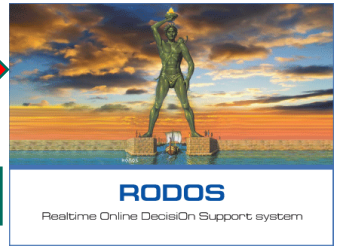

JRODOS

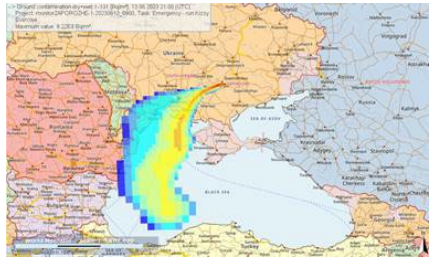

Innovative Reactor concepts: EU Project PATRICIA

PATRICIA

KIT Karlsruhe Institute of Technology

Partitioning And Transmuter Research Initiative in a Collaborative Innovation Action (2020-2024)

- 24 European project partners coordinated by SCK·CEN
- KIT: fuel rod bundle experiments with liquid metal LBE
- Realistic blockage in 19-pin bundle
  - MYRRHA specific geometry
  - Well defined porosity by ZrO2 printed blockage

fuel rod bundle

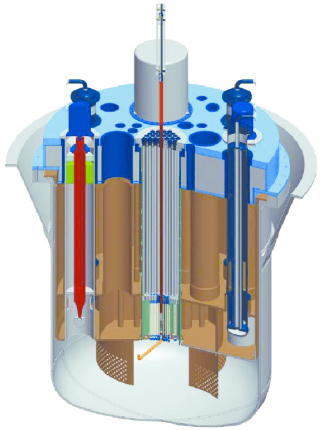

ADS MYRRHA reactor

KALLA Loop

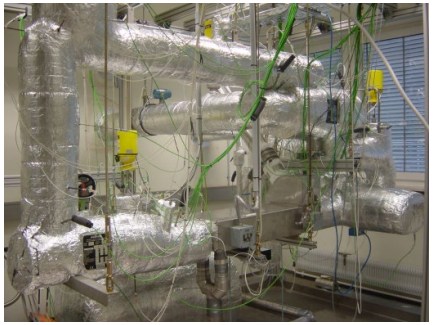

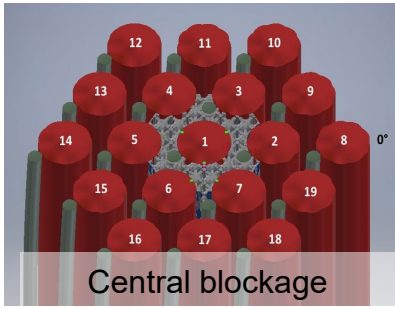

Central blockage

INNUMAT - INNovative strUctural MATerials for fission and fusion

- **Coordinated by KIT**,
  36 Partners (20 research institutions, 9 universities,
  7 private organizations) from 15 countries
- Total budget: 9.24 Mio€ (EU funding: 8 Mio €, 75% fission & 25% fusion)
- Development and qualification of innovative materials, increase of technology readiness level (TRL)
- Cross cutting aspects: one WP dealing with the synergies in terms of innovative materials for fission, fusion and also non-nuclear energies
- KIT involved in all major material research tracks

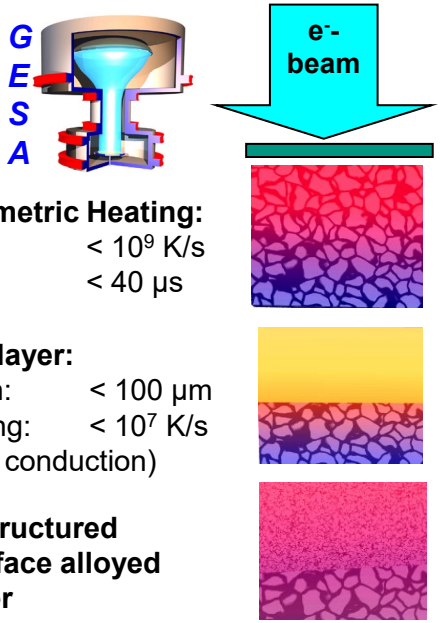

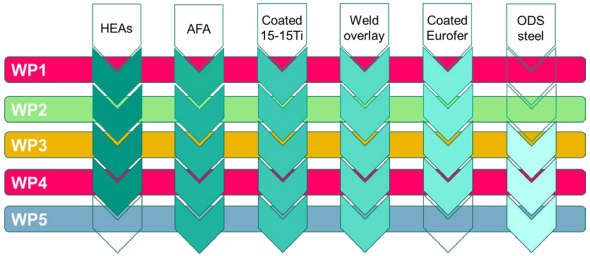

Topic 2 Reactor Safety: Status and Outlook

- Excellent scientific expertise available and unique experimental facilities
- Continue with teaching and education
  - Establishment of min. 3 new professorships at KIT
  - Attract (international, European) students, PhD candidates, etc.
  - Currently, Doctoral Students: 17
    - HGF financed: 2
    - 3rd party financed 9
    - Financed by grant: 6

Acronym	*EC funding for KIT*	*Full title*
new proposals in HORIZON-EURATOM Call 2021 accepted for funding:		
ANSELMUS	68.719,00	Advanced Nuclear Safety Evaluation of Liquid Metal Using Systems
ASSAS	358.313,00	Artificial intelligence for the Simulation of Severe AccidentS
ENEN2plus	105.000,00	Building European Nuclear Competence through continuous Advanced and Structured Education and Training Actions
ESFR-SIMPLE	578.774,00	European Sodium Fast Reactor - Safety by Innovative Monitoring, Power Level flexibility and Experimental research
INNUMAT (coord.: KIT)	1.021.986,00	Innovative Structural Materials for Fission and Fusion
OFFERR	42.500,00	eurOpean platForm For accEssing nucleaR R&d facilities
SASPAM-SA	247.032,00	Safety Analysis of SMR with PAssive Mitigation strategies - Severe Accident
SCORPION	249.930,00	SiC composite claddings: LWR performance optimization for nominal and accident conditions
SEAKNOT	192.047,00	SEvere Accident research and KNOwledge managemenT for LWRs
EC funding for KIT in this call	***2.864.301,00***	

NUSAFE Topic 1 Perspectives

(New strategic laboratory infrastructure: *HOVER* @KIT*)

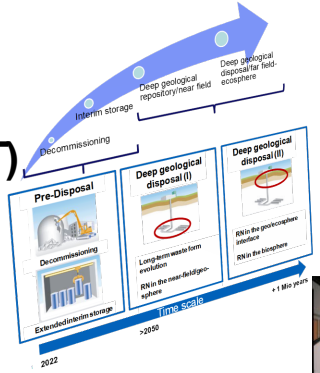

Karlsruhe Institute of Technology

HZDR JÜLICH FORSCHUNGSZENTRUM

Research infrastructure for the **scientific support of the German nuclear waste management programme**

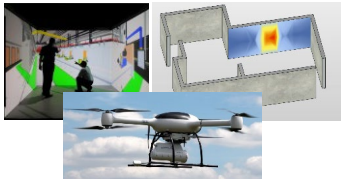

- **Decommissioning Virtual laboratories**
  - BIM D^2 (Deconstruction and Decommissioning) (under construction; ready in 2024; @TMB)
  - Combined Virtual – Experimental Laboratory (ready in 2023; @INR)

  for the development and optimization of decommissioning projects

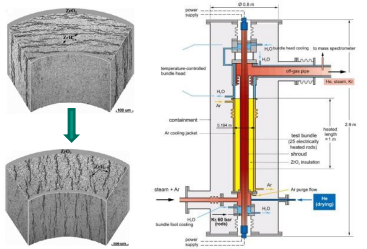

- **Extended interim storage of used nuclear fuel**
  - **LICAS/INCHAMEL:** Test facility to investigate Cladding material under interim storage conditions (operation started; @ IAM)

- **Disposal of radioactive waste**
  - **INE µ-spectrometry-LAB** (µ-XAS extension; µ-CT; FIB-SEM) (focus on impact of heterogeneities of repository subsystems (operation started; @INE)
  - **INE-AMS-LAB** (ultratrace analysis of radionuclides in environmental samples) (planned to be ready 2025/26; @INE)

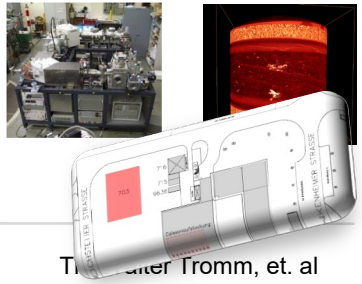

*Helmholtz Research and Technology Platform for the Decommissioning of Nuclear Facilities and for the Management of Radioactive Waste

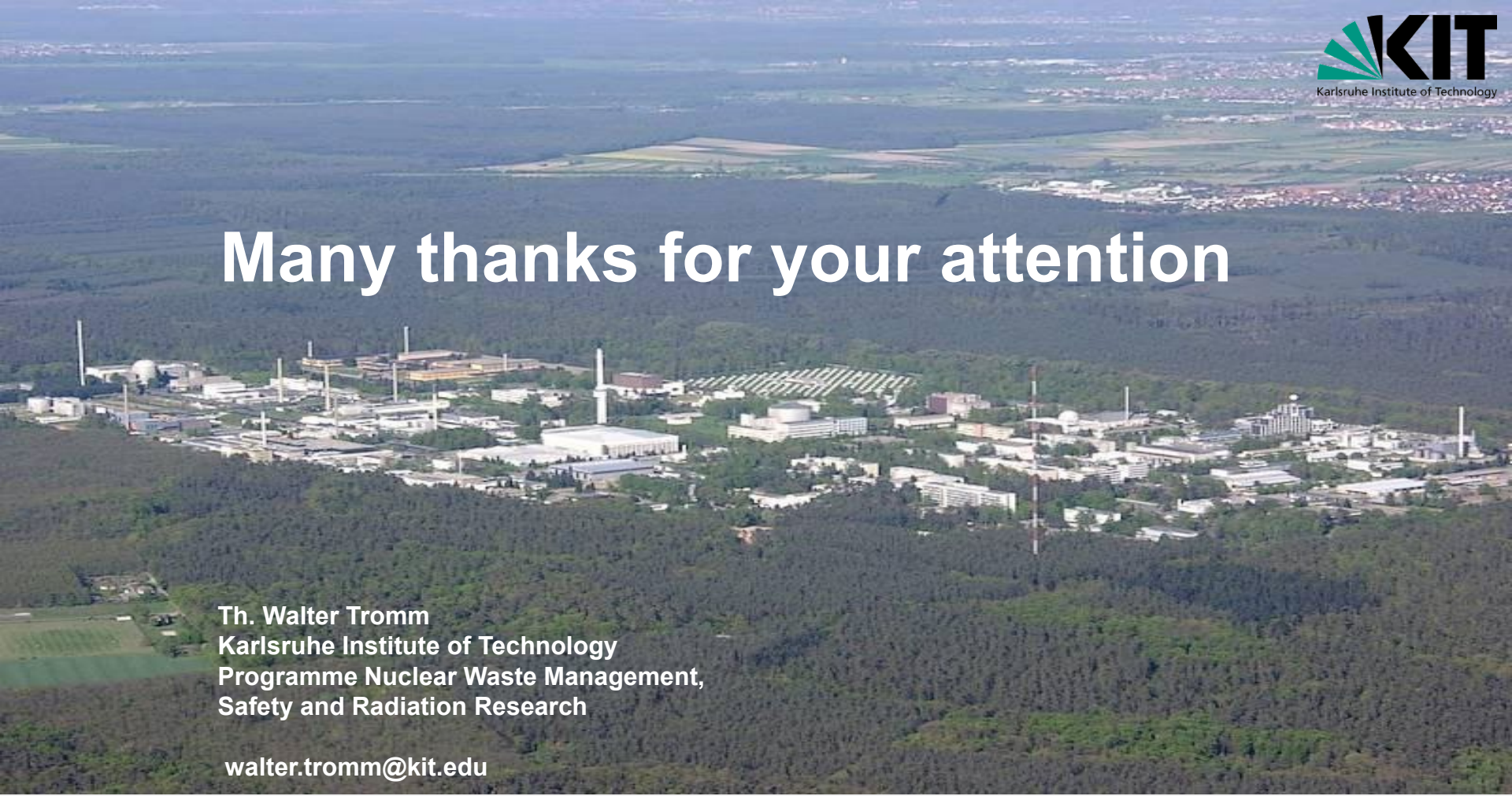

Many thanks for your attention

Th. Walter Tromm
Karlsruhe Institute of Technology
Programme Nuclear Waste Management,
Safety and Radiation Research

walter.tromm@kit.edu

M. Steinbrück

KIT

Update of the QUENCH Program

The main objective of the QUENCH program at KIT is the investigation of the hydrogen source term and materials interactions during LOCA and the early phase of severe accidents including reflood. Bundle experiments as well as separate-effects tests are conducted to provide data for the development of models and the validation of severe fuel damage code systems.

The QUENCH bundle facility is a unique out-of-pile bundle facility with electrically heated fuel rod simulators and extensive instrumentation. So far, 20 experiments with various severe accident (SA) scenarios as well as a series of eight DBA LOCA experiments were conducted. The QUENCH-LOCA series was completed in 2016. One of the main results is the definition of the conditions for secondary hydriding around the burst position and its influence on the mechanical properties of the cladding rods.

The latest QUENCH bundle test under LOCA conditions was conducted in July 2022 with ATF cladding tubes in the framework of the OECD-NEA Joint Undertaking QUENCH-ATF. Currently, an 8-month lasting bundle experiment with pressurized and hydrogen preloaded fuel rod simulators is ongoing in the framework of the German SPIZWURZ project on long-term intermediate dry storage.

Separate-effects tests during 2022/23 were focused on the high-temperature behavior of various ATF cladding candidates as well as on the behavior of hydrogen in Zr alloys under long-term dry storage conditions.

QUENCH bundle tests are part of the validation matrices of most SFD code systems, which was also reflected during the session “Modelling and code validation”.

After the completion of the SPIZWURZ test, two remaining bundle experiments with ATF cladding in the framework of the NEA project are foreseen.

Most activities of the QUENCH group are embedded in international cooperation in the framework of the EC, OECD-NEA and IAEA.

Finally, the status of reporting and publishing as well as the numerous national and international cooperations were briefly described and acknowledged.

Karlsruhe Institute of Technology

Institute for Applied Materials

Update of the QUENCH Program

M. Steinbrück, J. Stuckert, M. Große

28th International QUENCH Workshop, Karlsruhe Institute of Technology, 5-7 Dec 2023

Institute for Applied Materials, Programme NUSAFE

Outlook

- Current topics
- Experimental facilities
- ATF activities
- Long-term dry intermediate storage activities
- Modelling / Code validation
- Reporting
- Cooperation
- Future planning

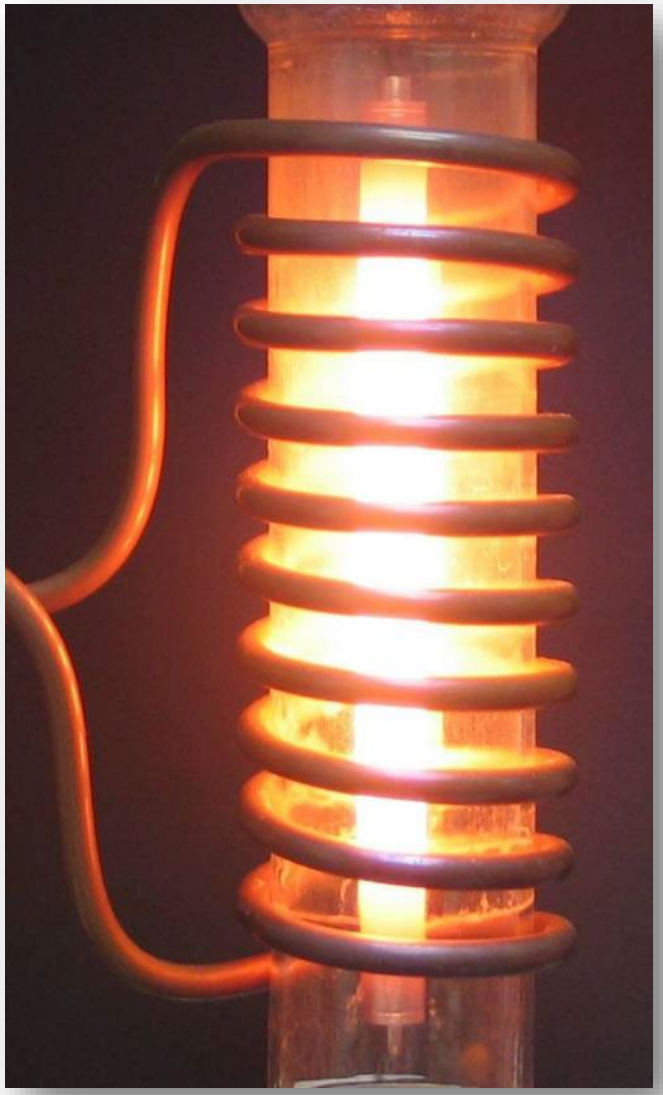

Current topics

- **Accident tolerant fuel (ATF) cladding**
  - ATF research after Fukushima Daiichi accidents
  - Characterization of promising ATF cladding concepts at (very) high temperatures
  - Degradation mechanisms and kinetic data
  - Max. temperature and coping time for AMMs

SiC_f-SiC cladding

- **Long-term dry intermediate storage**
  - No final storage on the horizon in Germany and many other countries
  - Hydrogen/hydride behavior in Zr cladding during 50-100 years storage e.g. in CASTOR casks
  - Hydride reorientation and its effect on mechanical properties

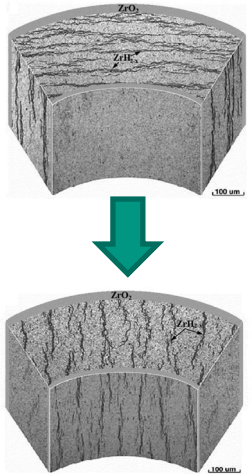

Hydride reorientation

QUENCH/LICAS facility

- Unique out-of-pile bundle facility to investigate reflood of an overheated reactor core
- 21-31 electrically heated fuel rod simulators; T up to >2000°C
- Extensive instrumentation for T, p, flow rates, level, etc. + MS
- So far, 20 experiments on SA performed (1996-today)
  - Influence of pre-oxidation, initial temperature, flooding rate
  - B_4C, Ag-In-Cd control rods
  - Air ingress; debris formation
  - Advanced cladding alloys
- 7+1 DBA LOCA experiments with separately pressurized fuel rods

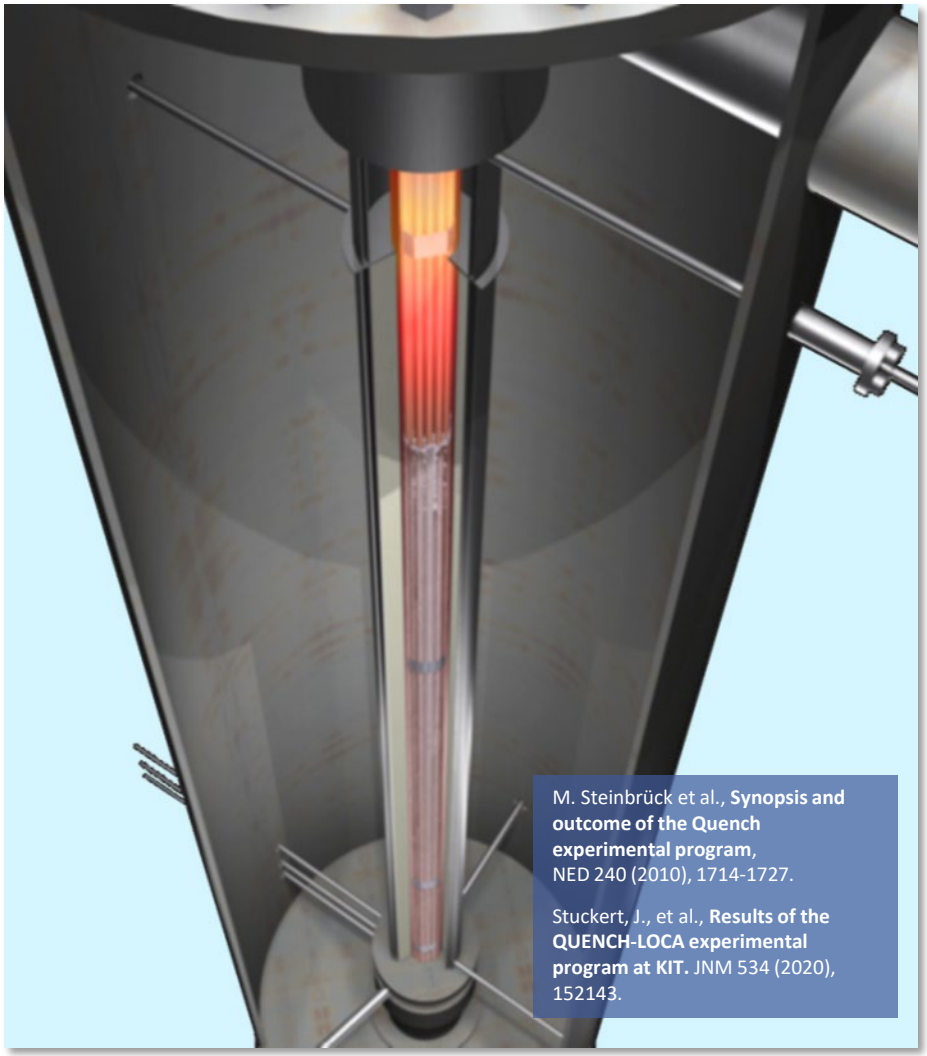

M. Steinbrück et al., **Synopsis and outcome of the Quench experimental program**, NED 240 (2010), 1714-1727.

Stuckert, J., et al., **Results of the QUENCH-LOCA experimental program at KIT.** JNM 534 (2020), 152143.

QUENCH Separate-effects tests: Main HT setups

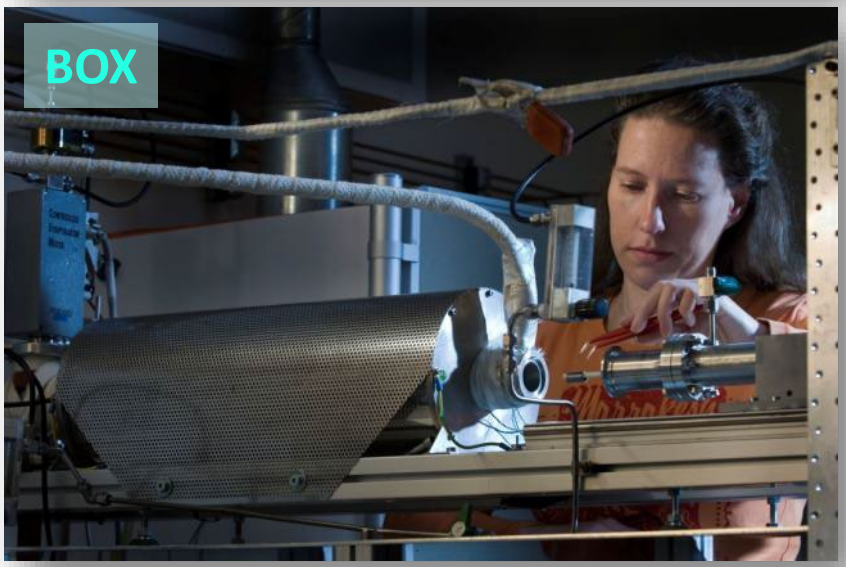

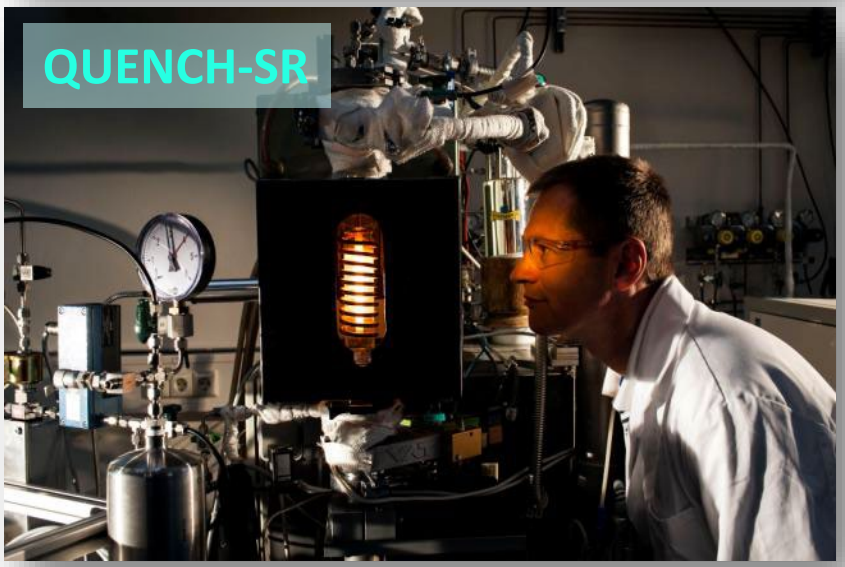

New test facilities devoted to SPIZWURZ activities

Apparatus for in-situ neutron radiography experiments under defined mechanical load and temperature

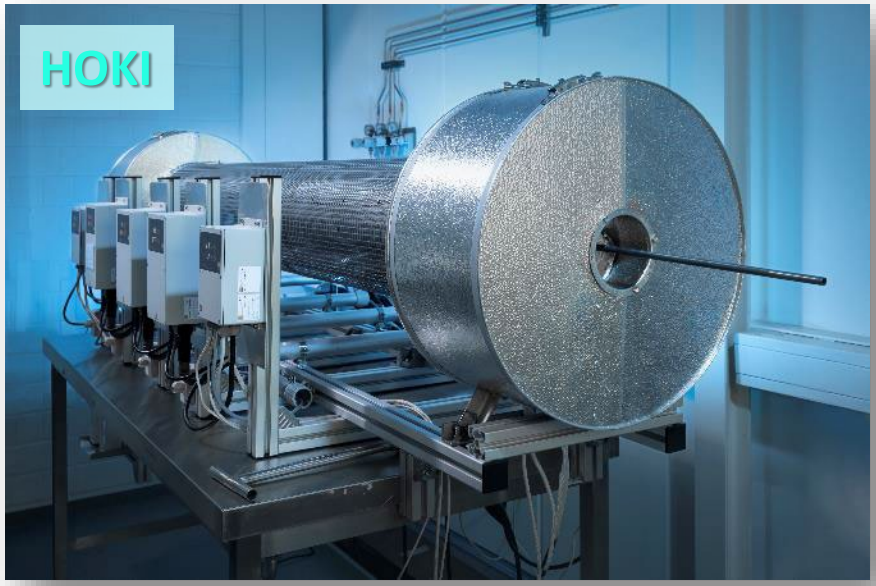

2.5 m long furnace for hydrogen pre-loading of cladding tubes for bundle tests

QUENCH activities on ATF cladding materials

- Bundle tests in the framework of OECD-NEA QUENCH-ATF
- Single-rod oxidation and quench tests of ATF cladding segment samples
- HT furnace tests with small samples in various atmospheres for analysis of oxidation kinetics and degradation mechanisms

- Participation in various international collaborations on ATF
  - EC IL TROVATORE (Coordinator of WP “Coolant-cladding-fuel interaction”)
  - EC SCORPION (Coord. of WP “Coolant/cladding/fuel interaction tests”)
  - IAEA ATF-TS (Coordinator of Benchmark QU-19 and exp. program)
  - OECD NEA QUENCH-ATF (KIT is Operating Agent)
  - OECD NEA TCOFF-2
  - Various bilateral collaborations with CNL, IRSN, CTU Prague, SNU, …

QUENCH-ATF Joint Undertaking

- Three bundle experiments with ATF cladding in the QUENCH facility
  - Focus on Cr-coated Zr alloys
  - Tubes provided by Westinghouse (US) and others
  - Design basis and beyond design basis accident conditions
- Supporting separate-effects tests and PTA
  - at KIT
  - Post-test analyses at IRSN and CEA/ILL (France)
- Code support for test preparation and code benchmark exercises, coordinated by GRS

QUENCH-ATF1 bundle test

- Conducted in July 2022 in the framework of the OECD-NEA Joint Undertaking QUENCH-ATF
- Scenario: Slightly beyond DBA-LOCA with QUENCH-LOCA3HT as reference test
- PTE ongoing
- Benchmark exercises completed

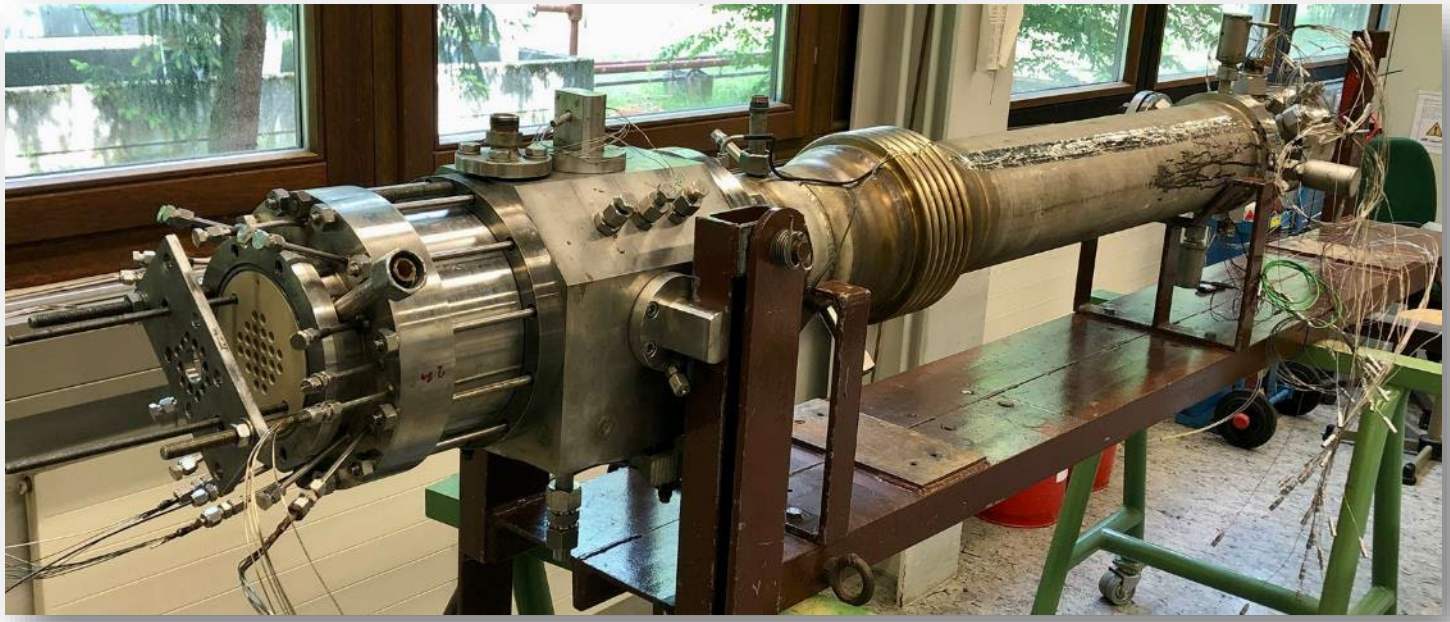

Transient oxidation of Cr-Zry with varying heating rates

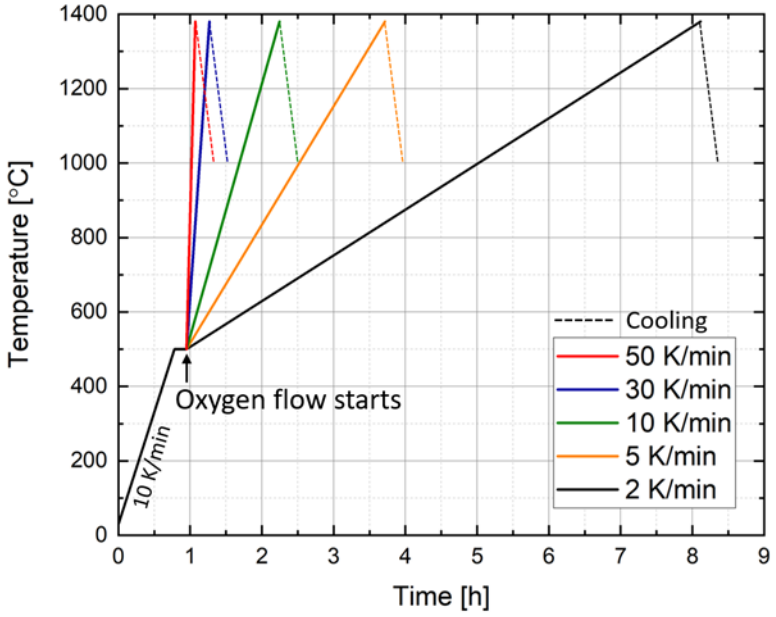

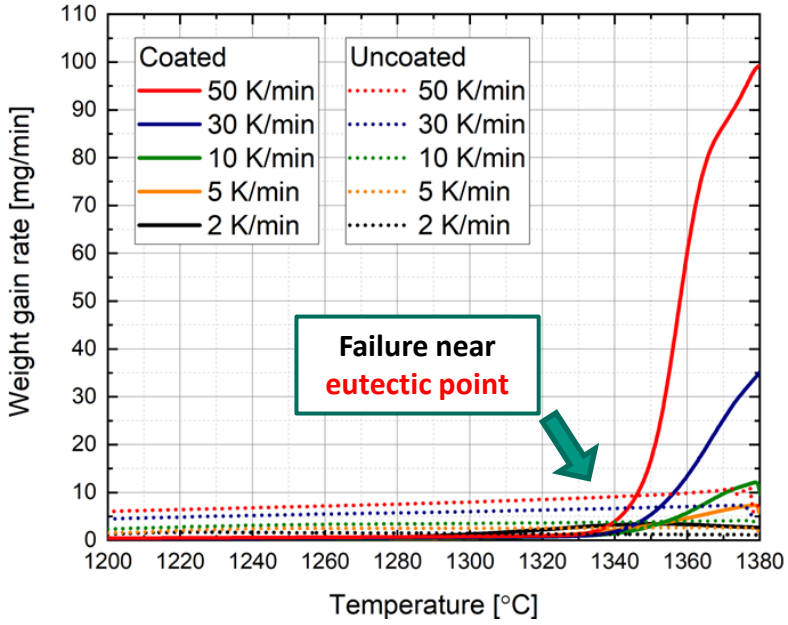

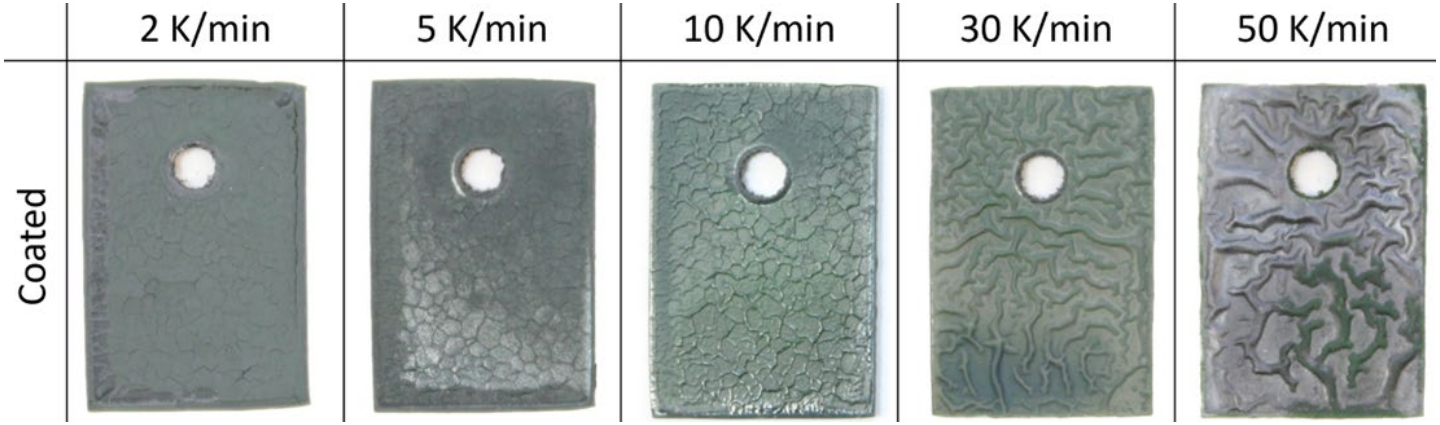

Long-term intermediate storage activities

- Work embedded in the German project SPIZWURZ (GRS, KIT) and the HGF HOVER infrastructure program
  - 8 month lasting bundle test running
  - Various SETs on the system Zr-H
- INCHAMEL test facility
  - Apparatus for in-situ neutron radiography experiments under defined mechanical load and temperature
- Sieverts type chamber for hydrogen loading of small samples (SICHA)
  - Investigation of the hydrogen uptake at temperatures relevant for dry storage of spent fuel
- HOKI test facility
  - 2.5 m long furnace for hydrogen pre-loading of cladding tubes for bundle tests

SPIZWURZ bundle test

- Simulation of dry storage of pre-hydrided fuel cladding
- 8 months (May 23 - Jan 24)
- Starting temperature 400°C
- Cool-down rate 1 K/day
- Cladding types
  - Zircaloy-4
  - DUPLEX
  - ZIRLO
- Hydrogen content 300/100 wppm
- Internal pressure 106/146 bar

SPIZWURZ bundle

SPIZWURZ Separate-effects tests

- Diffusion of Hydrogen in Zry in axial direction (3 h & 400°C)
- Neutron radiographies of hydrogenated claddings
- Results presented at the 6th GRS Workshop on Safety of the Extended Dry Storage of Spent Nuclear Fuel

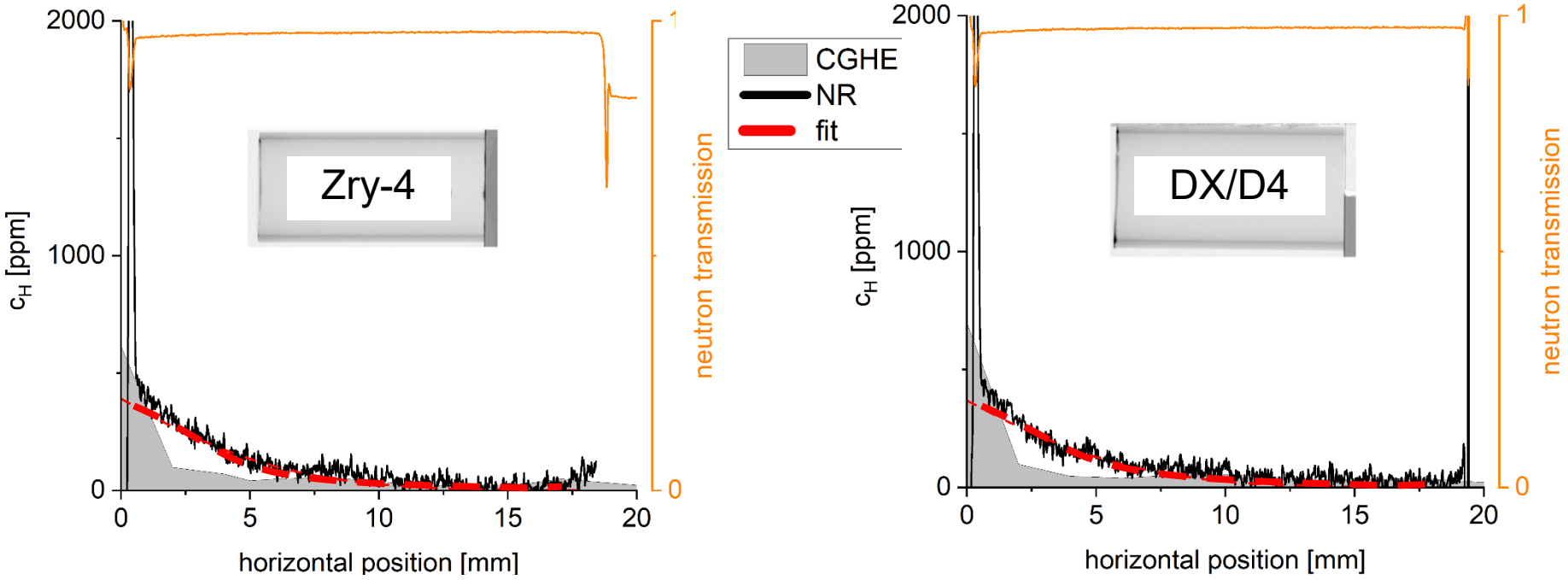

Modelling and code validation

- QUENCH bundle tests are part of validation matrices of most SFD code systems
- Pre-test calculation of CODEX-ATF (4 Cr-coated opt. ZIRLO and 3 uncoated opt. ZIRLO claddings) in the framework of the IAEA ATF-TS project
- Post-test calculations of QUENCH-19 (24 FeCrAl claddings) and DEGREE (9 Cr-coated Zry-4 claddings) in the framework of the IAEA ATF-TS project
- Benchmark exercise (blind & open phase) on QUENCH-ATF1 test coordinated by GRS
- Separate-effects test data are used by various institutions for model development

Reporting

- >20 Scopus referenced papers and conference contributions in 2022/23

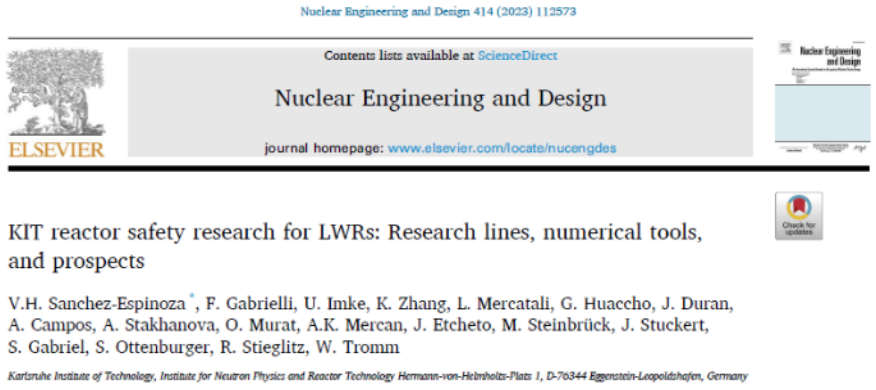

Nuclear Engineering and Design 414 (2023) 112573

Contents lists available at ScienceDirect

Nuclear Engineering and Design

journal homepage: www.elsevier.com/locate/nucengdes

KIT reactor safety research for LWRs: Research lines, numerical tools, and prospects

V.H. Sanchez-Espinoza *, F. Gabrielli, U. Imke, K. Zhang, L. Mercatali, G. Huaccho, J. Duran, A. Campos, A. Stakhanova, O. Murat, A.K. Mercan, J. Etcheto, M. Steinbrück, J. Stuckert, S. Gabriel, S. Ottenburger, R. Stieglitz, W. Tromm

Karlsruhe Institute of Technology, Institute for Neutron Physics and Reactor Technology Hermann-von-Helmholtz-Platz 1, D-76344 Eggenstein-Leopoldshafen, Germany

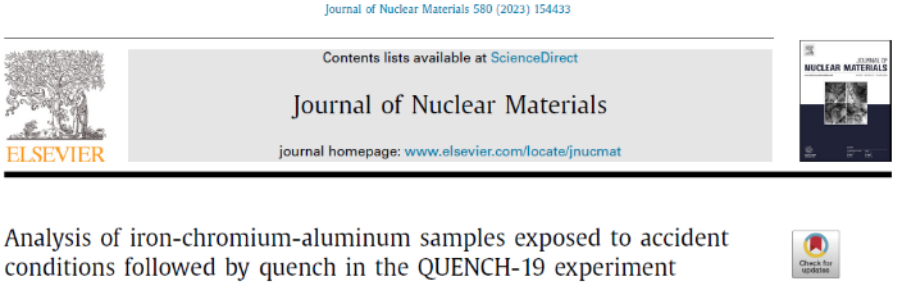

Journal of Nuclear Materials 580 (2023) 154433

Contents lists available at ScienceDirect

Journal of Nuclear Materials

journal homepage: www.elsevier.com/locate/jnucmat

Analysis of iron-chromium-aluminum samples exposed to accident conditions followed by quench in the QUENCH-19 experiment

Peter Doyle [a,*], Juri Stuckert [b], Mirco Grosse [b], Martin Steinbrück [b], Andrew T. Nelson [a], Jason Harp [a], Kurt Terrani [a]

[a] Nuclear Fuel and Energy Cycle Division, Oak Ridge National Laboratory, TN, USA
[b] Institute for Applied Materials, Karlsruhe Institute of Technology, Eggenstein-Leopoldshafen, Germany

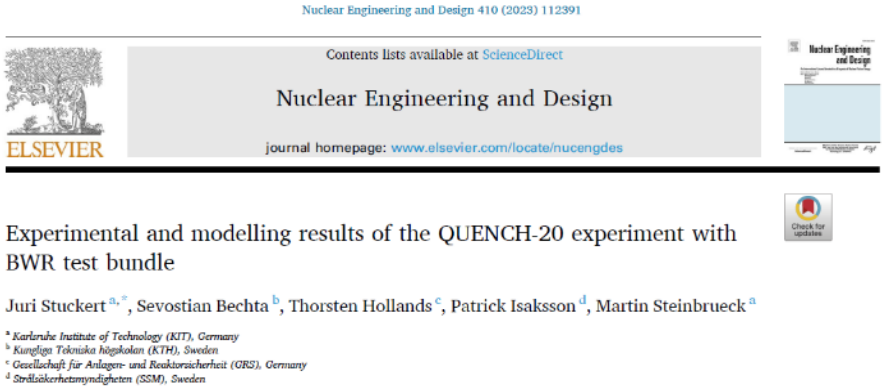

Nuclear Engineering and Design 410 (2023) 112391

Contents lists available at ScienceDirect

Nuclear Engineering and Design

journal homepage: www.elsevier.com/locate/nucengdes

Experimental and modelling results of the QUENCH-20 experiment with BWR test bundle

Juri Stuckert [a,*], Sevostian Bechta [b], Thorsten Hollands [c], Patrick Isaksson [d], Martin Steinbrueck [a]

[a] Karlsruhe Institute of Technology (KIT), Germany
[b] Kungliga Tekniska högskolan (KTH), Sweden
[c] Gesellschaft für Anlagen- und Reaktorsicherheit (GRS), Germany
[d] Strålsäkerhetsmyndigheten (SSM), Sweden

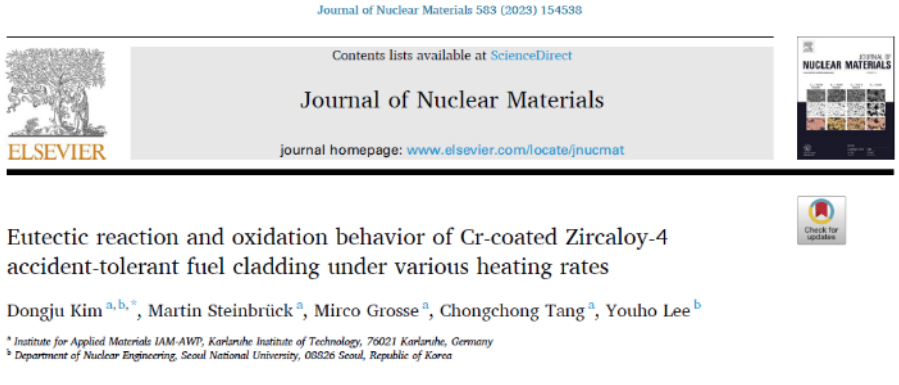

Journal of Nuclear Materials 583 (2023) 154538

Contents lists available at ScienceDirect

Journal of Nuclear Materials

journal homepage: www.elsevier.com/locate/jnucmat

Eutectic reaction and oxidation behavior of Cr-coated Zircaloy-4 accident-tolerant fuel cladding under various heating rates

Dongju Kim [a,b,*], Martin Steinbrück [a], Mirco Grosse [a], Chongchong Tang [a], Youho Lee [b]

[a] Institute for Applied Materials IAM-AWP, Karlsruhe Institute of Technology, 76021 Karlsruhe, Germany
[b] Department of Nuclear Engineering, Seoul National University, 08826 Seoul, Republic of Korea

New papers 2022-2023 (SCOPUS)

Sanchez-Espinoza, V.H., Gabrielli, F., Imke, U., Zhang, K., Mercatali, L., Huaccho, G., Duran, J., Campos, A., Stakhanova, A., Murat, O., Mercan, A.K., Etcheto, J., Steinbrück, M., Stuckert, J., Gabriel, S., Ottenburger, S., Stieglitz, R., Tromm, W.

KIT reactor safety research for LWRs: Research lines, numerical tools, and prospects

(2023) Nuclear Engineering and Design, 414, art. no. 112573, .

DOI: 10.1016/j.nucengdes.2023.112573

Kim, D., Steinbrück, M., Grosse, M., Tang, C., Lee, Y.

Eutectic reaction and oxidation behavior of Cr-coated Zircaloy-4 accident-tolerant fuel cladding under various heating rates

(2023) Journal of Nuclear Materials, 583, art. no. 154538, .

DOI: 10.1016/j.jnucmat.2023.154538

Tang, C., Dürrschnabel, M., Jäntsch, U., Klimenkov, M., Steinbrück, M., Ulrich, S., Hans, M., Schneider, J.M., Stüber, M.

Synthesis of V2AlC thin films by thermal annealing of nanoscale elemental multilayered precursors: Incorporation of layered Ar bubbles and impact on microstructure formation

(2023) Applied Surface Science, 629, art. no. 157340, .

DOI: 10.1016/j.apsusc.2023.157340

Stuckert, J., Bechta, S., Hollands, T., Isaksson, P., Steinbrueck, M.

Experimental and modelling results of the QUENCH-20 experiment with BWR test bundle

(2023) Nuclear Engineering and Design, 410, art. no. 112391, .

DOI: 10.1016/j.nucengdes.2023.112391

Jäckel, B.S., Birchley, J.C., Lind, T., Steinbrück, M., Park, S.

Nitriding model for zirconium based fuel cladding in severe accident codes

(2023) Journal of Nuclear Materials, 582, art. no. 154466, .

DOI: 10.1016/j.jnucmat.2023.154466

Wu, J., Yuan, Y., Chen, T., Tang, A., Wu, L., Li, D., Steinbrück, M., Pan, F.

The oxidation behavior and reaction thermodynamics and kinetics of the Mg-X (X = Ca/Gd/Y) binary alloys

(2023) Corrosion Science, 225, art. no. 111609, .

DOI: 10.1016/j.corsci.2023.111609

Doyle, P., Stuckert, J., Grosse, M., Steinbrück, M., Nelson, A.T., Harp, J., Terrani, K.

Analysis of iron-chromium-aluminum samples exposed to accident conditions followed by quench in the QUENCH-19 experiment

(2023) Journal of Nuclear Materials, 580, art. no. 154433, .

DOI: 10.1016/j.jnucmat.2023.154433

Liu, J., Meng, R., Steinbrück, M., Große, M., Stegmaier, U., Tang, C., Yang, J., Yun, D.

Microstructural evolution of pre-oxidized Cr-coated Zry-4 during annealing in argon

(2023) Journal of Nuclear Materials, 573, art. no. 154144, .

DOI: 10.1016/j.jnucmat.2022.154144

Gómez, A.G., Ponce, J.P., Grosse, M., Soria, S., Condó, A., Flores, A., Schulz, M., Vizcaíno, P., Santisteban, J.R.

Evaluation of the delayed hydrogen cracking behavior and the hydrogen diffusion coefficient for different microstructures of the Zr-2.5%Nb alloy

(2023) Journal of Nuclear Materials, 587, art. no. 154725, .

DOI: 10.1016/j.jnucmat.2023.154725

Grosse, M., Boldt, F., Herm, M., Roessger, C., Stuckert, J., Weick, S., Nahm, D.

The SPIZWURZ project – Experimental investigations and modeling of the behavior of hydrogen in zirconium alloys under long-term dry storage conditions

(2023) Nuclear Engineering and Technology, .

DOI: 10.1016/j.net.2023.09.027

Farkas, R., Hózer, Z., Nagy, I., Vér, N., Horváth, M., Steinbrück, M., Stuckert, J., Grosse, M.

Effect of steam and oxygen starvation on severe accident progression with air ingress

(2022) Nuclear Engineering and Design, 396, art. no. 111884, .

DOI: 10.1016/j.nucengdes.2022.111884

Kashkarov, E.B., Sidelev, D.V., Pushilina, N.S., Yang, J., Tang, C., Steinbrueck, M.

Influence of coating parameters on oxidation behavior of Cr-coated zirconium alloy for accident tolerant fuel claddings

(2022) Corrosion Science, 203, art. no. 110359, .

DOI: 10.1016/j.corsci.2022.110359

New papers 2022-2023 (SCOPUS)

Steinbrueck, M., Grosse, M., Stegmaier, U., Braun, J., Lorrette, C.

Oxidation of Silicon Carbide Composites for Nuclear Applications at Very High Temperatures in Steam

(2022) Coatings, 12 (7), art. no. 875, .

DOI: 10.3390/coatings12070875

Liu, J., Steinbrück, M., Große, M., Stegmaier, U., Tang, C., Yun, D., Yang, J., Cui, Y., Seifert, H.J.

Systematic investigations on the coating degradation mechanism during the steam oxidation of Cr-coated Zry-4 at 1200 °C

(2022) Corrosion Science, 202, art. no. 110310, .

DOI: 10.1016/j.corsci.2022.110310

Kim, C., Tang, C., Grosse, M., Maeng, Y., Jang, C., Steinbrueck, M.

Oxidation mechanism and kinetics of nuclear-grade FeCrAl alloys in the temperature range of 500–1500 °C in steam

(2022) Journal of Nuclear Materials, 564, art. no. 153696, .

DOI: 10.1016/j.jnucmat.2022.153696

Yang, J., Steinbrück, M., Tang, C., Große, M., Liu, J., Zhang, J., Yun, D., Wang, S.

Review on chromium coated zirconium alloy accident tolerant fuel cladding

(2022) Journal of Alloys and Compounds, 895, art. no. 162450, .

DOI: 10.1016/j.jallcom.2021.162450

Tang, C., Steinbrück, M., Grosse, M., Ulrich, S., Stüber, M.

The Effect of Annealing Temperature on the Microstructure and Properties of Cr–C–Al Coatings on Zircaloy-4 for Accident-Tolerant Fuel (ATF) Applications

(2022) Coatings, 12 (2), art. no. 167, .

DOI: 10.3390/coatings12020167

Steinbrück, M., Stegmaier, U., Große, M., Czerniak, L., Lahoda, E., Daum, R., Yueh, K.

High-temperature oxidation and quenching of chromium-coated zirconium alloy ATF cladding tubes with and w/o pre-damage

(2022) Journal of Nuclear Materials, 559, art. no. 153470, .

DOI: 10.1016/j.jnucmat.2021.153470

Wu, J., Yuan, Y., Yang, L., Chen, T., Li, D., Wu, L., Jiang, B., Steinbrück, M., Pan, F.

The oxidation behavior of Mg-Er binary alloys at 500 ℃

(2022) Corrosion Science, 195, art. no. 109961, .

DOI: 10.1016/j.corsci.2021.109961

Santisteban, J.R., Buitrago, N.L., Moya Riffo, A., Soria, S.R., Baruj, A.L., Schulz, M., Grosse, M., Luzin, V., Hache, M., Barrow, L., Daymond, M.R.

Diffusion of H in Zircaloy-2 and Zr-2.5%Nb rolled plates between 250 °C and 350 °C by off-situ neutron imaging experiments

(2022) Journal of Nuclear Materials, 561, art. no. 153547, .

DOI: 10.1016/j.jnucmat.2022.153547

S Weick, M Grosse and M Steinbrueck

The INCHAMEL facility – a new device for in-situ neutron investigations under defined temperatures with applicable mechanical load

(2022) Phys.: Conf. Ser. 2605 012035

DOI 10.1088/1742-6596/2605/1/012035

Co-operations

Programs

- NUGENIA/SARNET
- HORIZON 2020
- IAEA
- OECD-NEA

Bilateral

- PSI
- MTA EK
- IRSN, CEA, EdF
- RUB-LEE
- GRS
- Westinghouse
- USNRC
- KONICOF
- SNU
- NECSA, BAM, HMI
- NRA, JAEA
- ISS
- ORNL
- CNL

Outlook 2024

- SPIZWURZ bundle experiment
  - Running until January 2024
  - Extensive post-test examinations
- QUENCH-ATF2 experiment
  - Severe accident test with Cr-coated Optimized ZIRLO cladding
  - Planned for March/April 2024
  - Post-test analyses
- Post-test examinations of QUENCH-ATF1
  - Should be completed in 2024 by IRSN and KIT
- Preparation and conduct of QUENCH-ATF3
- EC OFFER proposal for the CODEX facility under review
- SETs on various topics, mainly on ATF cladding and Zry/H

Acknowledgement

- Helmholtz Association for funding program NUSAFE at KIT
- Program NUSAFE and IAM institute's management for broad support of our activities
- BMWK for funding of the SPIZWURZ project
- EC for funding the projects SEAKNOT, IL TROVATORE and SCORPION
- OECD-NEA and partners for support of QUENCH-ATF

- And last but not least the QUENCH team:
  J. Laier, J. Moch, U. Peters, C. Roessger, U. Stegmaier, C. Tang, S. Weick

M. Große

KIT

Update of the SPIZWURZ project investigating the hydrogen behavior in zirconium alloys

SPIZWURZ is a joined project of the GRS Garching and the KIT institutes INE and IAM-AWP. It is sponsored by the German Ministry of Environment, Nature Conservation, Nuclear Safety and Consumer Protection. The project started in June 2020 and has a duration of 4.75 years.

The four main topics are:

- A long-term bundle test (duration 240 days) in the QUENCH/LICAS facility,
- Separate effect tests to measure the influence of texture and stress on solubility and diffusivity of hydrogen in zirconium alloys,
- Determination of elastic and residual plastic strain at a spent fuel rod,
- Modelling, pre and posttest computing of the bundle test for validation of the codes (benchmark exercise).

A main result already obtained is that pellet swelling does not induce an additional stress to the cladding, at least after about 50 GWd/t_{HM} and about 30 years of dry storage.

The bundle test runs until middle of January 2024. After the test, an extensive posttest examination of the claddings will be performed to measure hydrogen distributions and hydride morphologies and orientations.

The separate-effect tests are still ongoing. First results are presented.

Pretest calculations were performed predicting the ratio between circumferential and radial oriented hydrides as well as the axial hydrogen redistribution.

Karlsruhe Institute of Technology

Institute for Applied Materials

Update of the SPIZWURZ project investigating the hydrogen behavior in zirconium alloys

M. Grosse, M. Herm, R. Kilger, D. Nahm, C. Roessger, J. Stuckert, S. Weick

KIT / Institute for Applied Materials – Applied Material Physics / Program NUSAFE

Gesellschaft für Anlagen- und Reaktorsicherheit, Garching

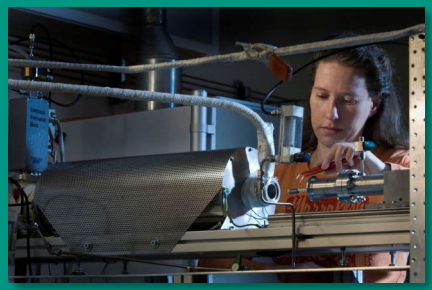
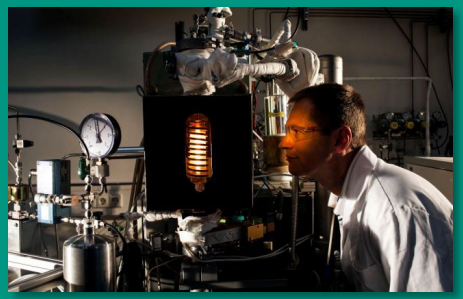
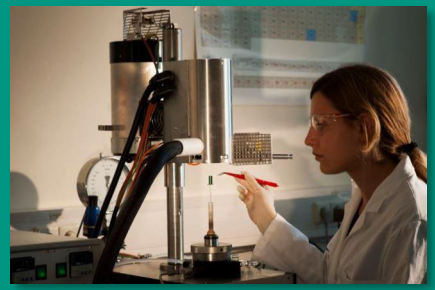
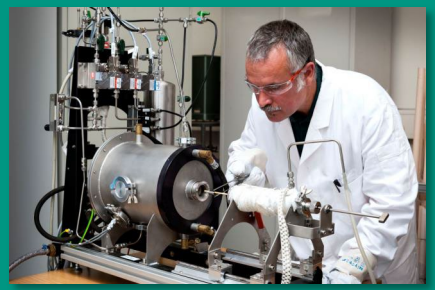

Introduction

The SPIZWURZ project

- SPIZWURZ = acronym for „**Sp**annungs**i**nduz**z**ierte **W**asserstoff**u**mlagerung wäh**r**end Langzeit-**Z**wischenlagerung“ (stress induzed hydrogen re-distribution during long term intermediate storage)
- Joined project between GRS and KIT-INE and KIT-IAM-AWP
- Founded by the German Ministry of Environment, Nature Conservation, Nuclear Safety and Consumer Protection
- Duration 4.75 years until 3/2025
  - Long term bundle test
  - Separate effect tests to measure the influence of texture and stress on solubility and diffusivity of hydrogen in zirconium alloys
  - Determination of elastic and residual plastic strain at a spent fuel rod
  - Modelling, pre and post test computing of the bundle test for validation of the codes (benchmark exercise)

Credit: Audrius Meskauskas

Purpurner Enzian (Spitzwurz)

Purple gentian

Determination of elastic and residual plastic strain at a spent fuel rod

- Fuel rod was used in the NPP Gösgen (Switzerland)
- Burn-up 50.5 GWd/t_{HM}
- Usage until 1984
- 8 mm long segment were cut
- Measurement of the diameter by means of laser micro-meter scanner
- Removing of the fuel using a mixture of $(NH_4)_2CO_3$ / H_2O_2 at room temperature within five days
- Measurement of the diameter by means of laser micro-meter scanner

Determination of elastic and residual plastic strain at a spent fuel rod

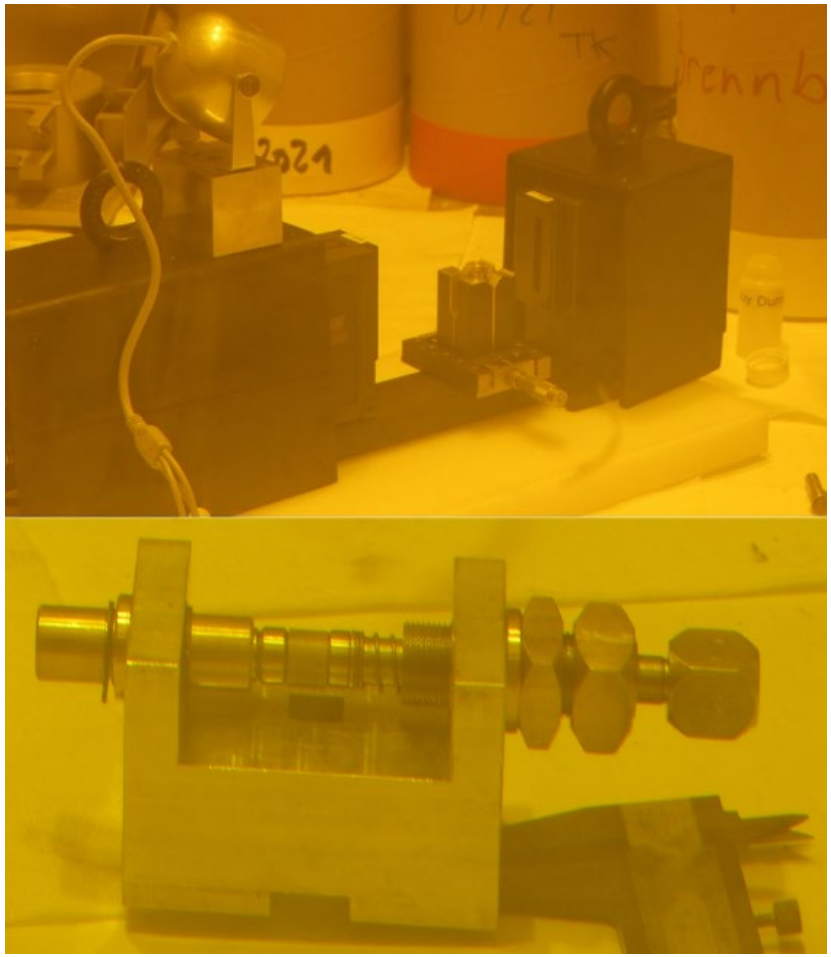

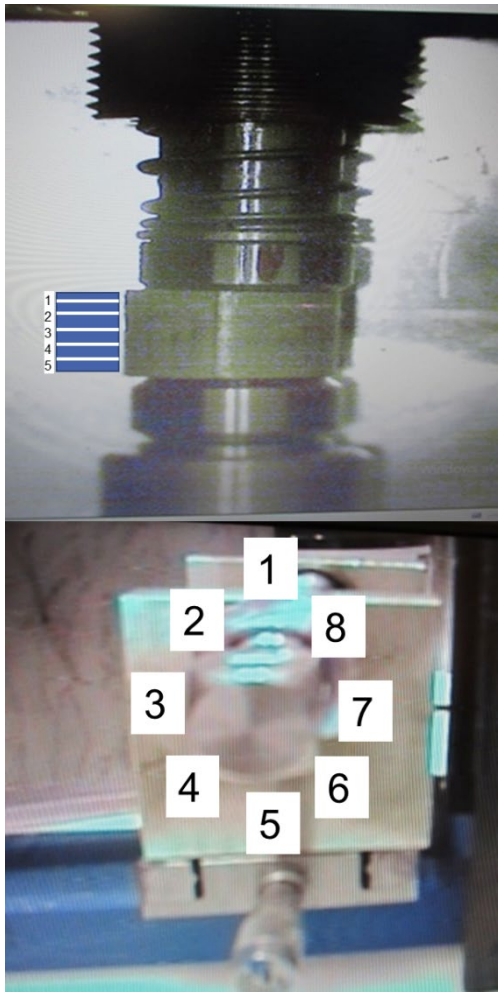

Determination of elastic and residual plastic strain at a spent fuel rod

- Sligthly oval shape of the rod cross section with the fuel, largest diameter is about 30 .. 50 µm larger than the smallest one depending on the axial position.
- The mean value of the outer diameter of the rod still filled with fuel is about 6 µm smaller than the nominal one.
- After fuel removal, the variation of the diameter is 3.3 ± 1.7 µm comperes to the same position measured with fuel; the uncertainty due to the positioning of the pellets is 3.1 ± 2.7 µm.
- Up-initio calculation predicts a decrease of the diameter due to the fuel removal of < 20 µm.

- **Conclusion: Pellet swelling do not induce stress to the cladding tube after 50 GWh/t_{HM} and more than 30 y dry storage.**

Separate effect tests

- Investigation of the influence of texture and elastic strain on hydrogen diffusion and solubility in zirconium alloys.
- Measurements of the hydrogen distribution by means of neutron imaging methods
- This topic is still in progress.
- Ex-situ neutron radiography investigations of the texture dependence of H diffusion as an examples of the results already obtained.

Separate effect tests

Diffusion in axial direction

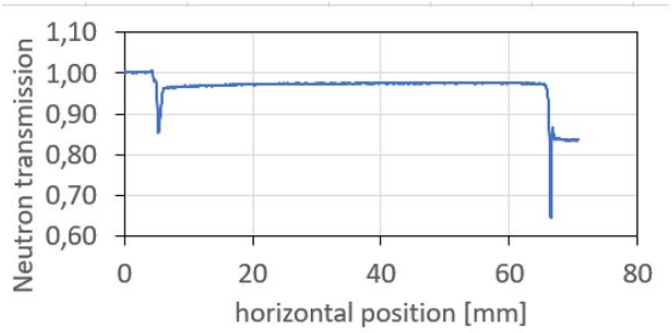

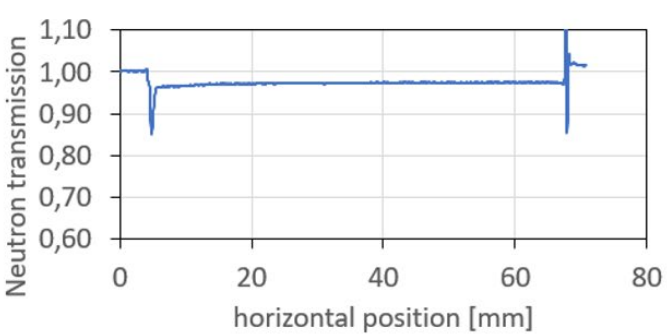

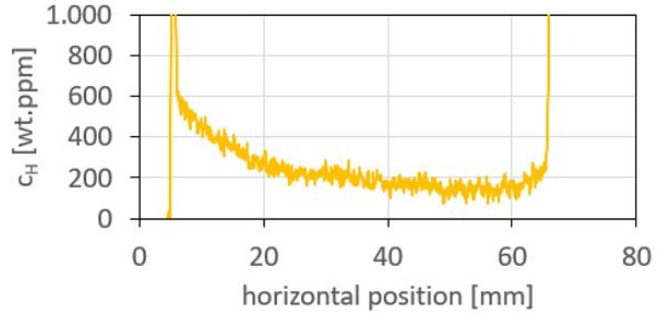

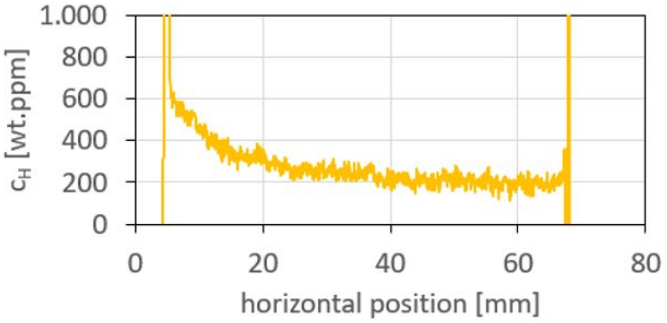

Separate effect tests

Zr single crystals are delivered by MaTeck (Jülich):
20 with a (1 0 -1 0) and 20 with c (0001) orientation perpendicular to the disk plane

Pre-characterization of zirconium single crystals

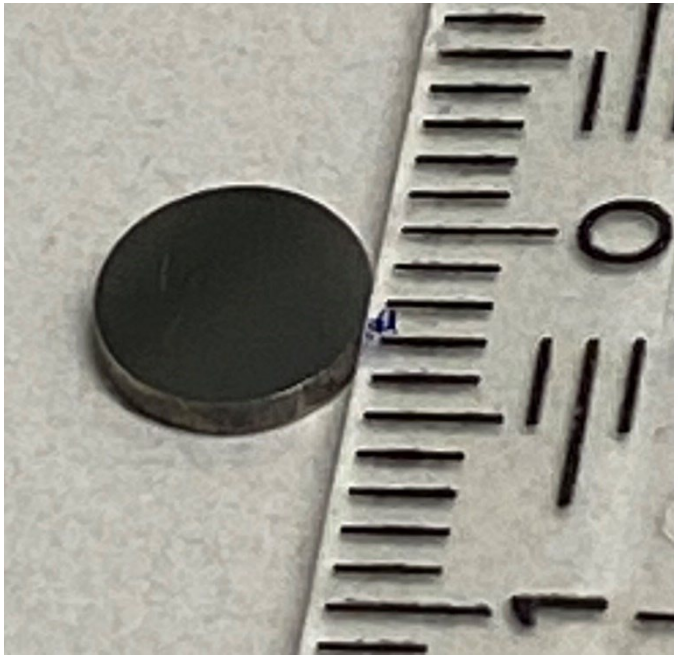

Ø > 6mm, thickness 1 mm

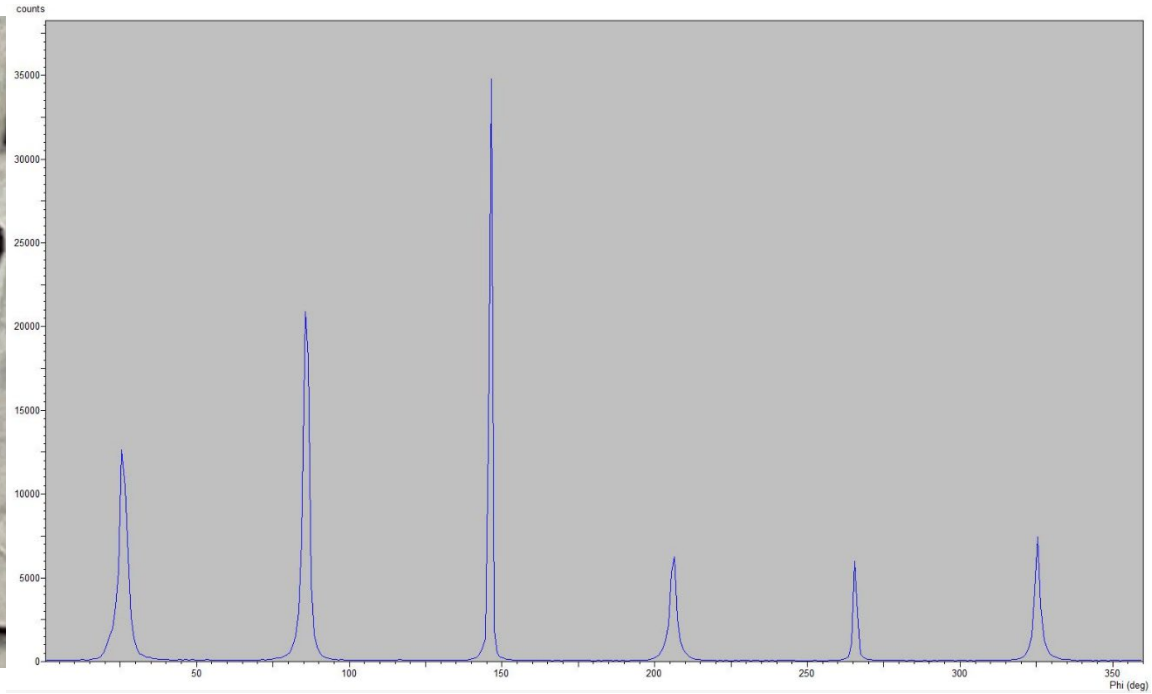

Rotation around (0 0 0 1): (1 0 -1 0) peaks each 60°

Separate effect tests

In-situ neutron radiography

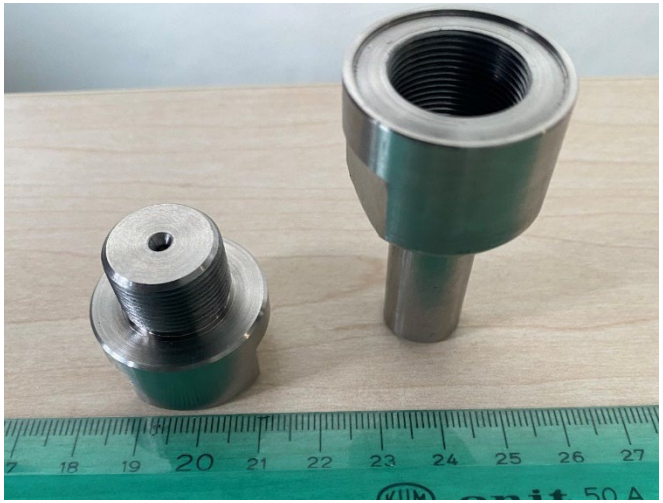

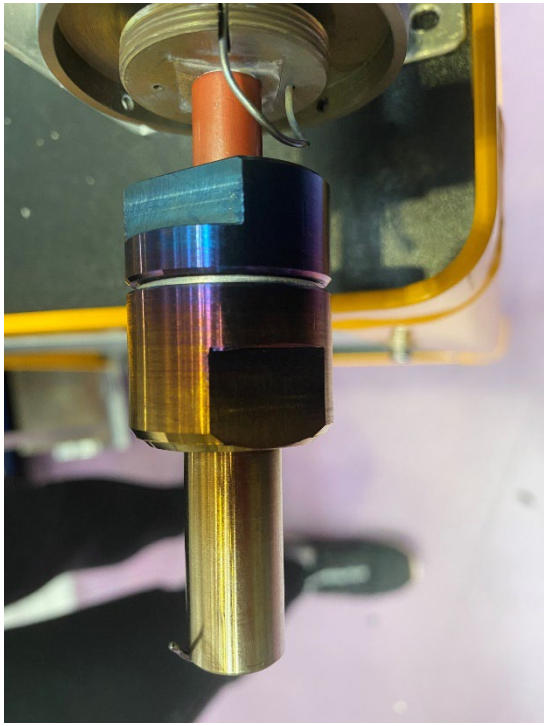

new leak-tight sample holder with aluminium sealing ring

Separate effect tests

In-situ neutron radiography

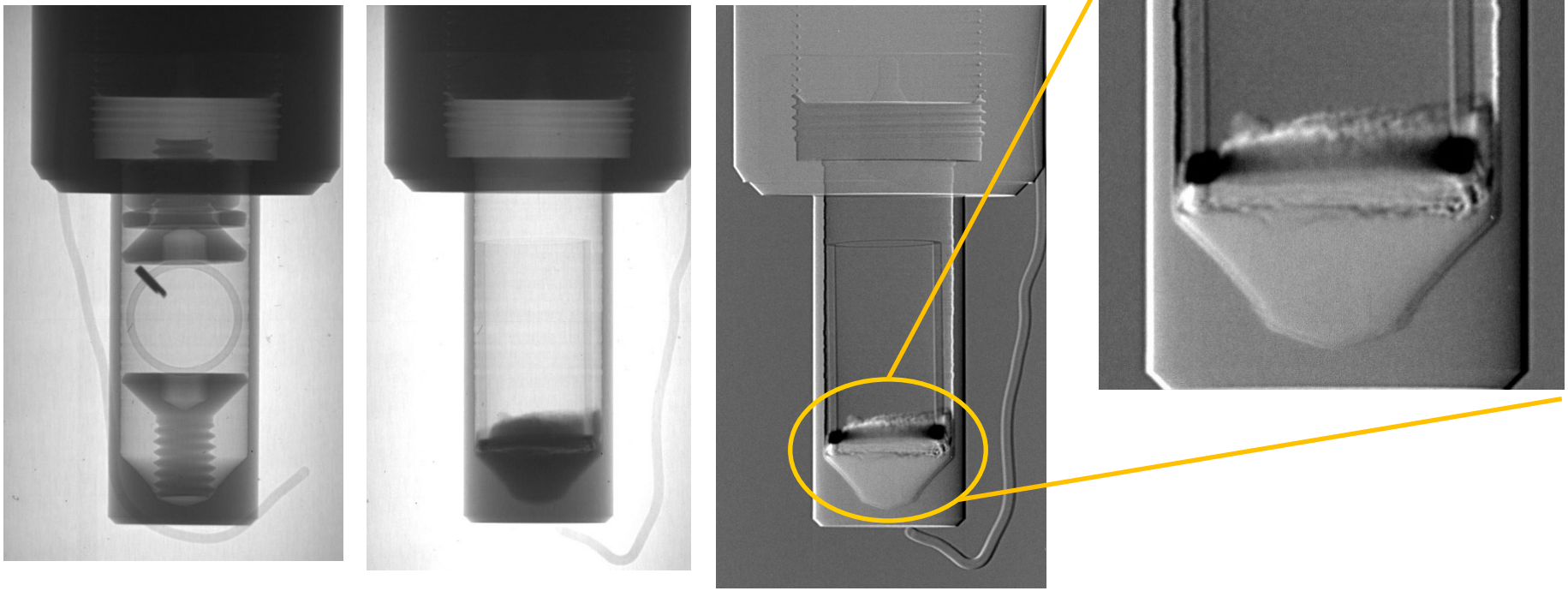

QUENCH bundle test

- Bundle with 21 - 32 fuel rod simulators of ~2.5 m length
- Electrically heated: ~2 m;
- Fuel simulator: ZrO_2 pellets
- Quenching from bottom
- Off-gas analysis by mass spectrometer (H_2, steam …)
- Extensive instrumentation for T, p, flow rates, water level, etc.
- corner rods, can be removed during test

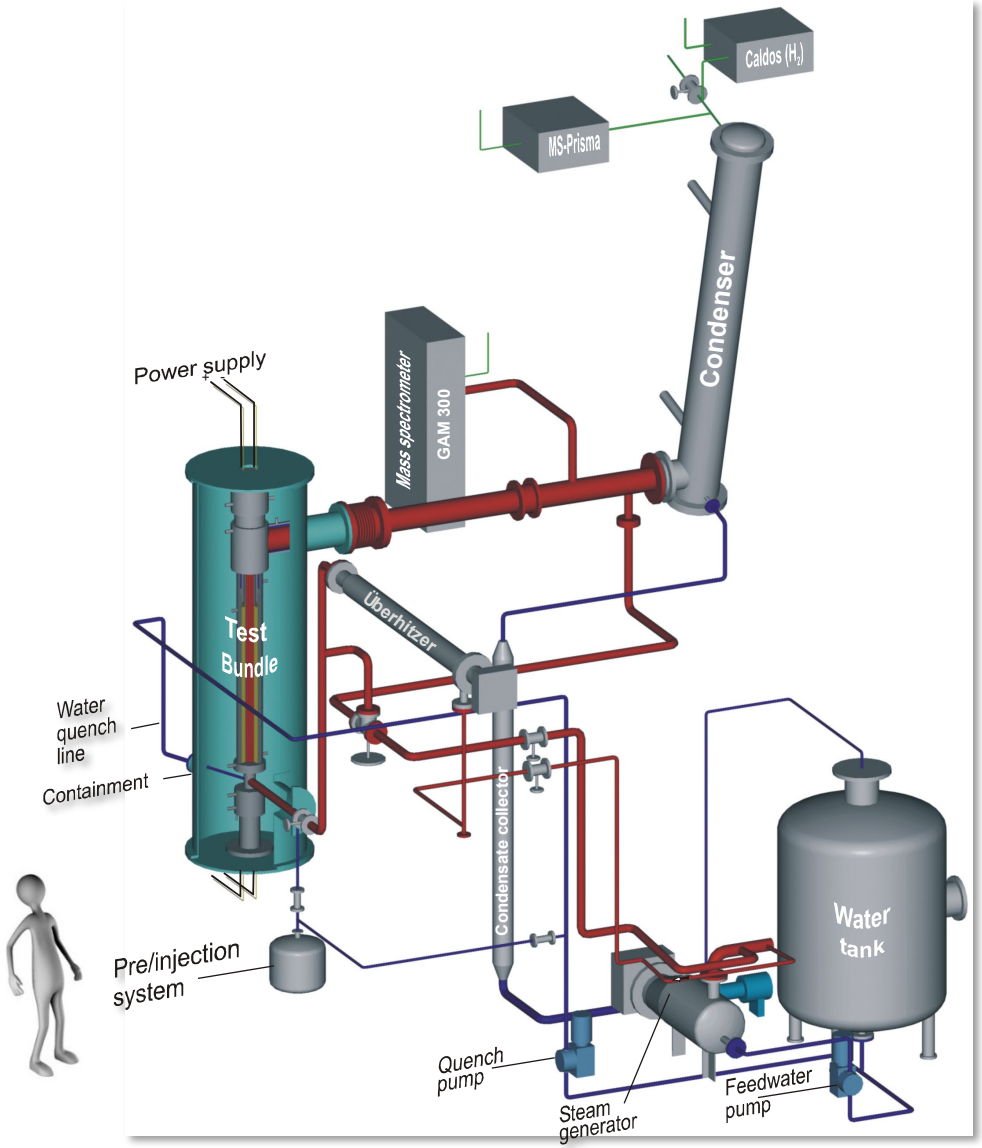

QUENCH bundle test

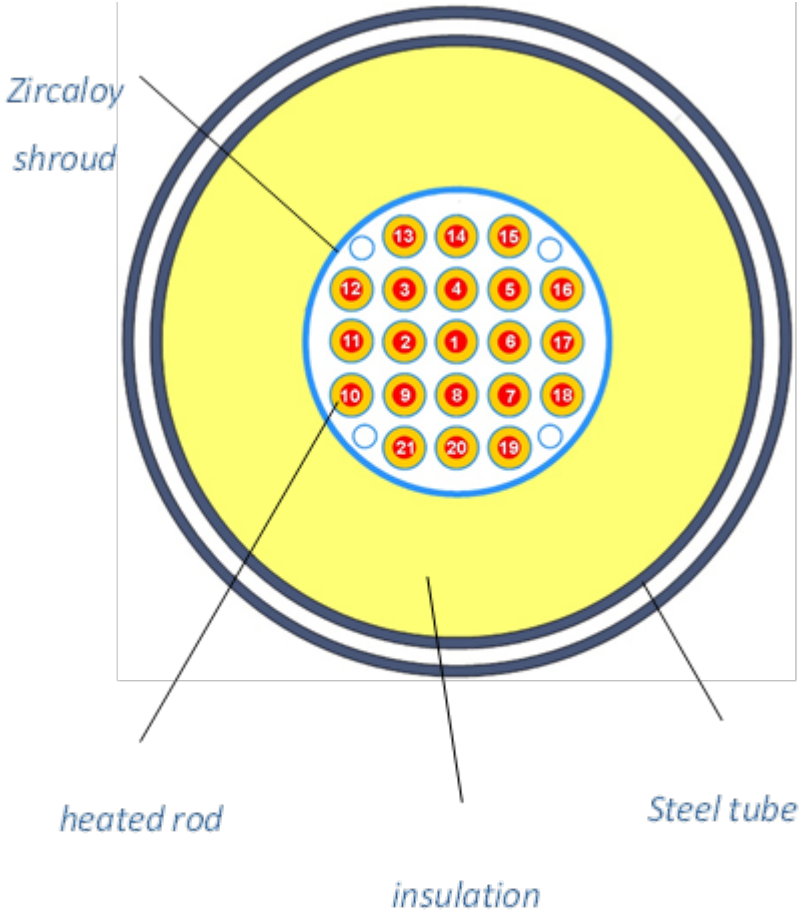

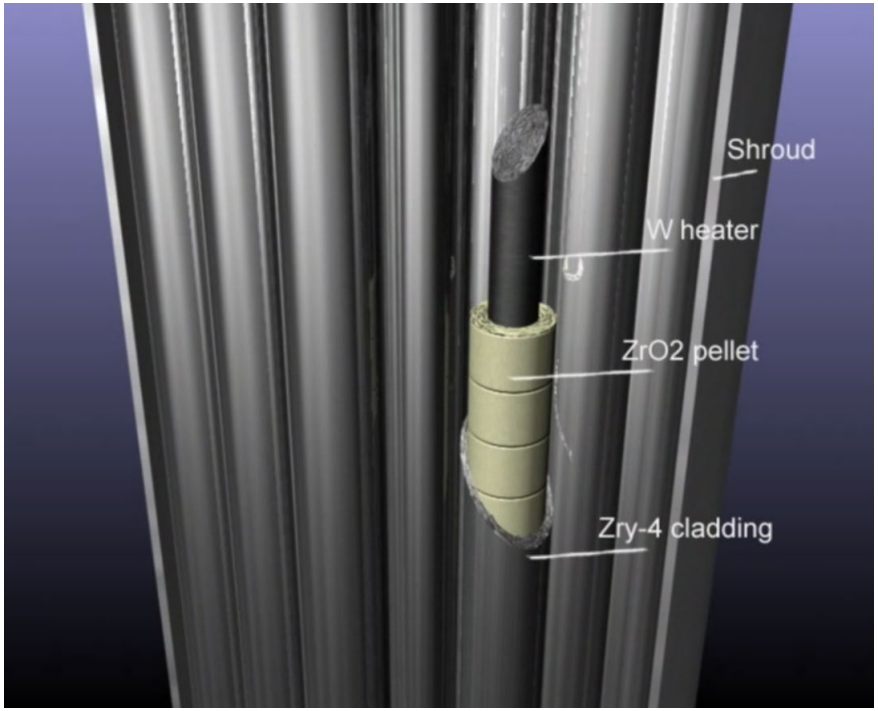

QUENCH bundle test

Hydrogen loading of 2.5 m long cladding tubes

T= 450°C

Loading from the inner side, outer side of the tube is in air atmosphere producing an oxide layer preventing hydrogen release.

After the hydrogen loading, about 20 h annealing to normalize the radial hydrogen distribution

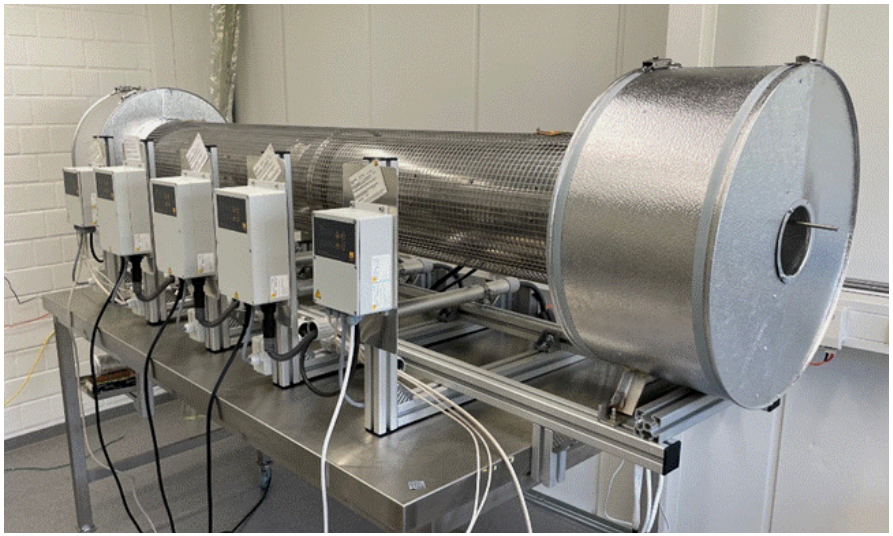

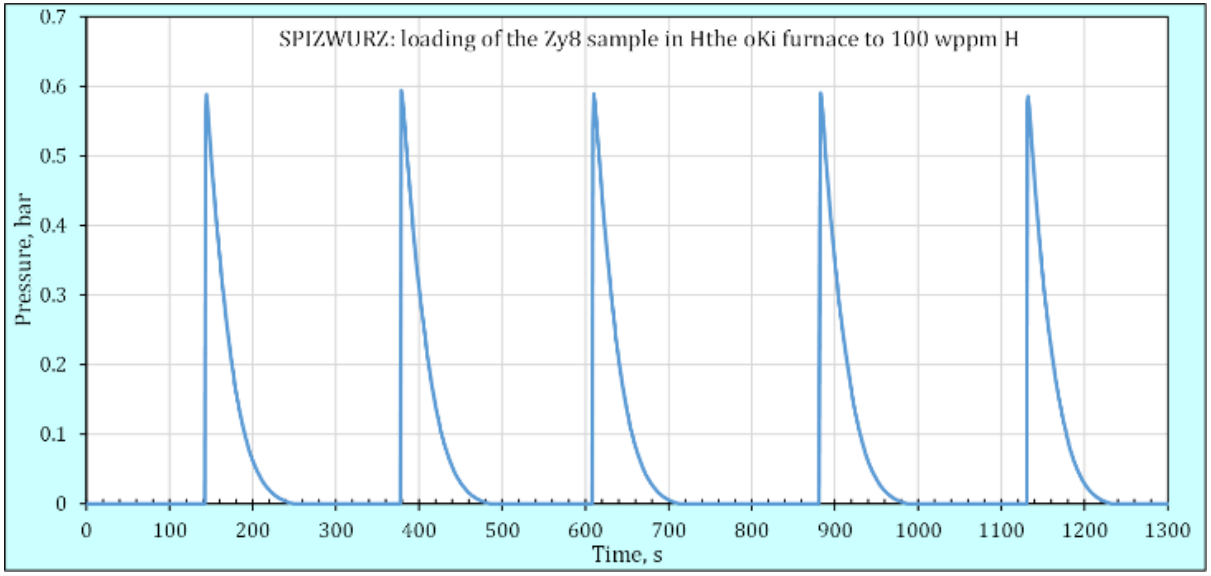

QUENCH bundle test

Material	p_{min}, c_{min}	p_{min}, c_{max}	p_{max}, c_{min}	p_{max}, c_{max}
Zry-4	1, 1	1, 1	1, 1	1, 1
ZIRLO	2	1, 1	1, 1	1, 1
Dx/D4	1	1	1	1, 1

p_{min} = 106 bar (σ = 68 MPa)
p_{max} = 146 bar (σ = 96 MPa)

c_{min} = 100 wt.ppm
c_{max} = 300 wt.ppm

T_{max} = 405°C
ΔT_{max} = 1 K/day

The test has been started at May 16 2023 and will be conducted until January 11 2024 (240 days)

QUENCH bundle test

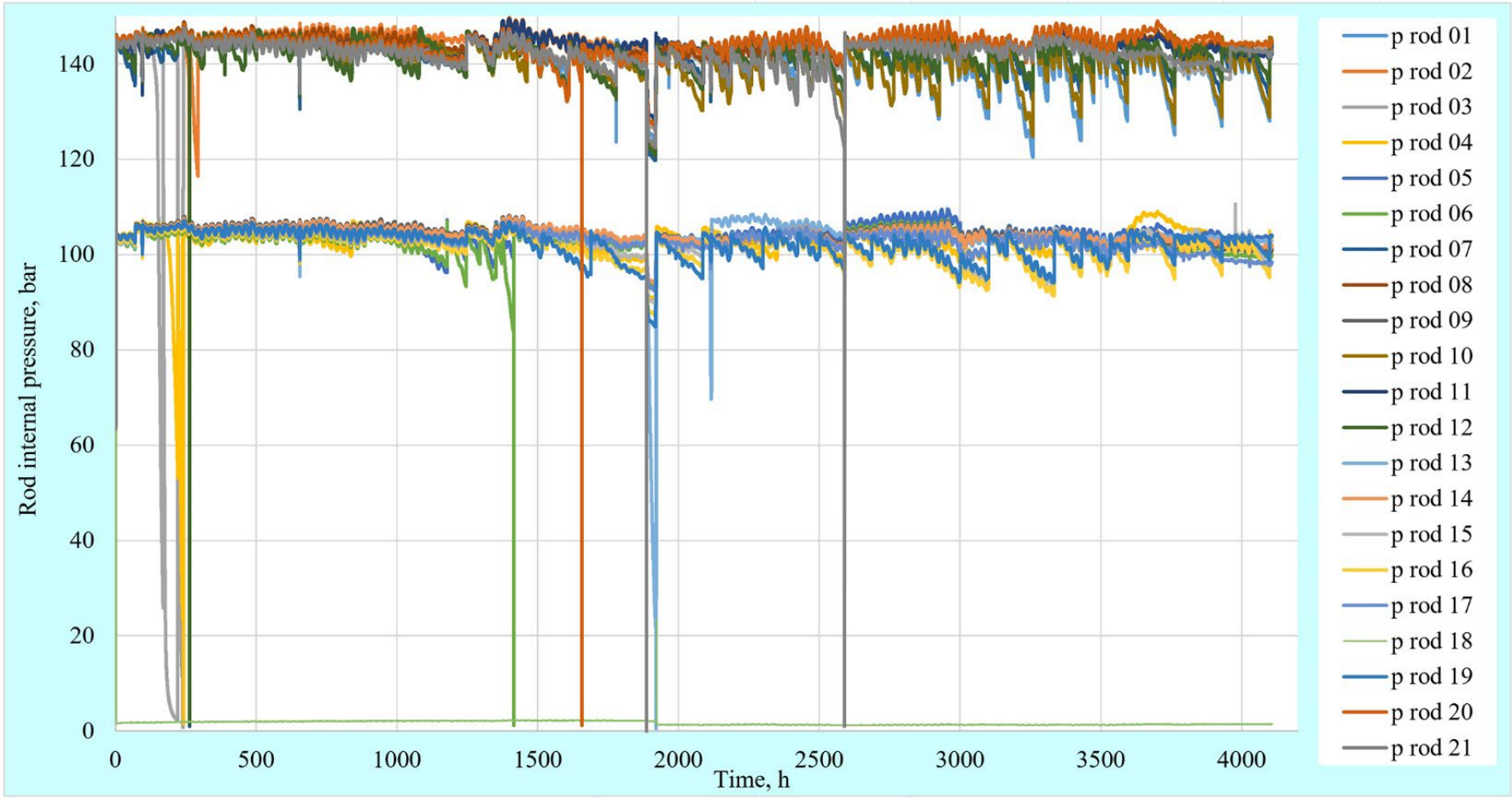

Pressure inside the tubes

QUENCH bundle test

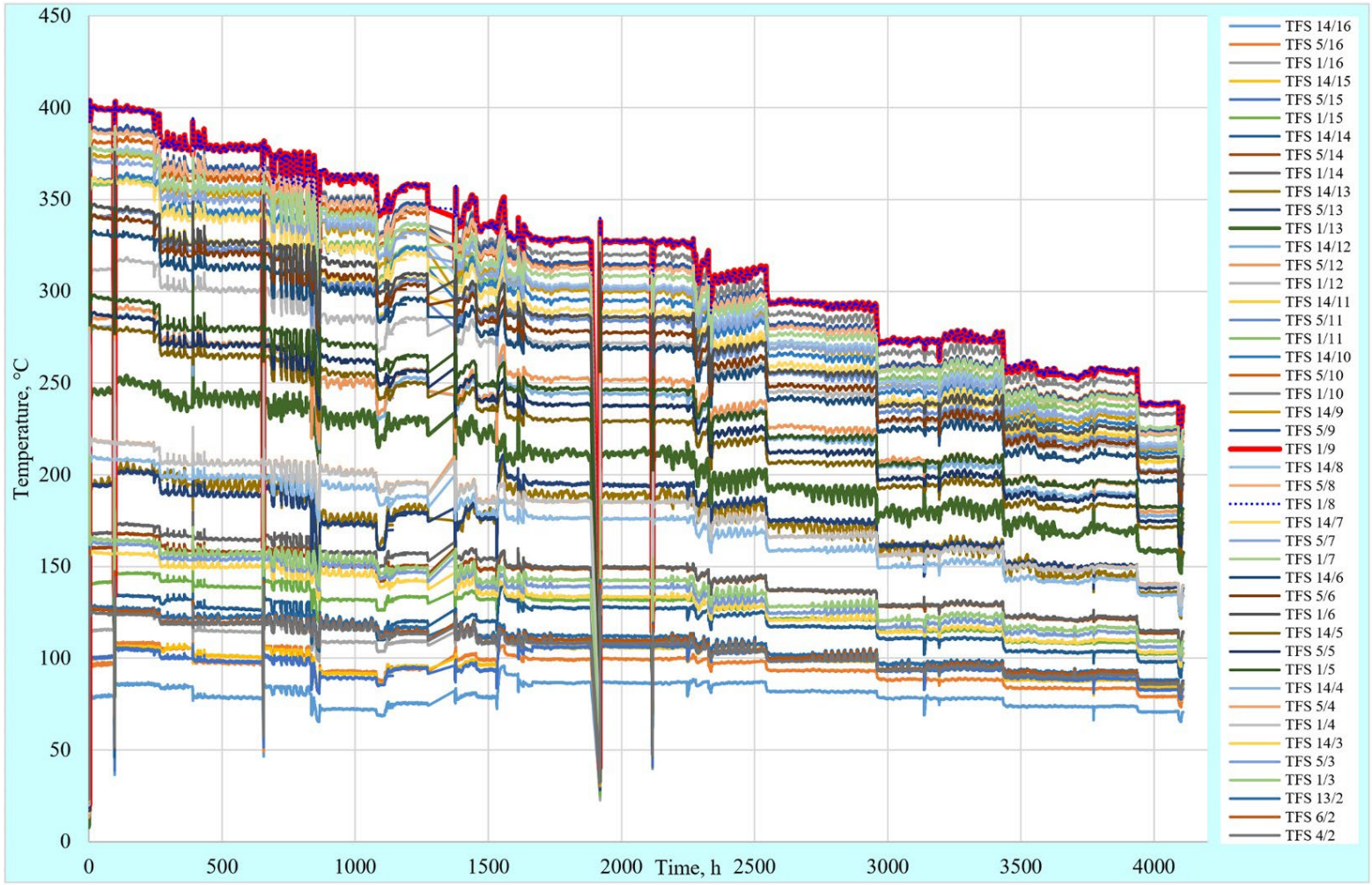

Cool down of the bundle

Planned Post Test Examinations

- Axial hydrogen distribution — neutron imaging
- Amount of hydrides — neutron imaging, metallography
- Morphology of the hydrides — metallography
  - dimensions of the hydrides
- Orientation of the hydrides — metallography

- Derived parameters (refinement of the already known parameters)
  - Threshold temperatures depending on the stress state for general hydride precipitation (TSSP under stress)
  - Threshold stresses for the precipitation of radial oriented hydrides.
  - Axial hydrogen diffusion parameters under the two applied stresses

QUENCH bundle test

Pre-test calculations with the TESPA-ROD code and resulting axial hydrogen redistribution

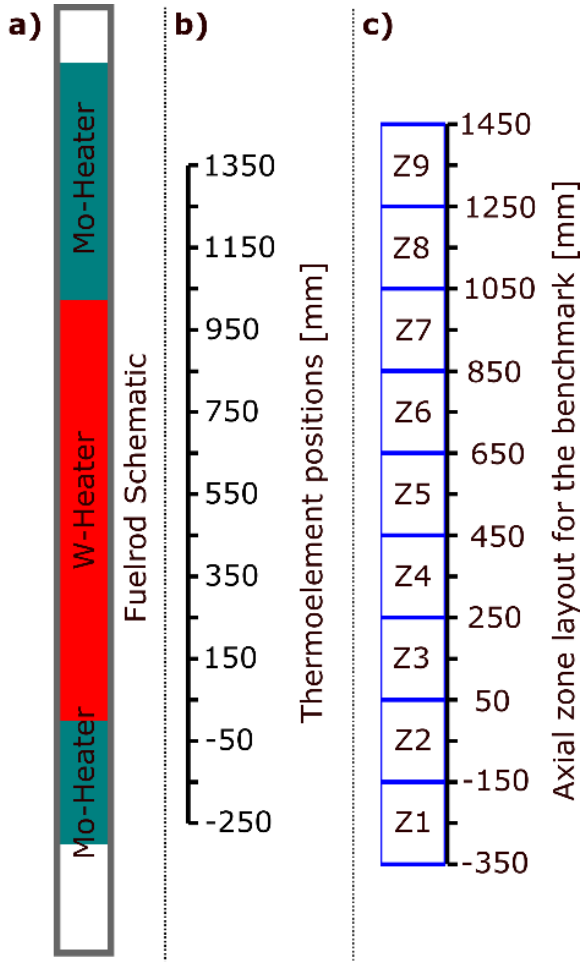

a) Schematic illustration of a fuel rod simulator with heater.
b) Axial positions of the thermo-couples.
c) Axial zone layout for the benchmark.

QUENCH bundle test

Pre-test calculations with the TESPA-ROD code and resulting axial H redistribution

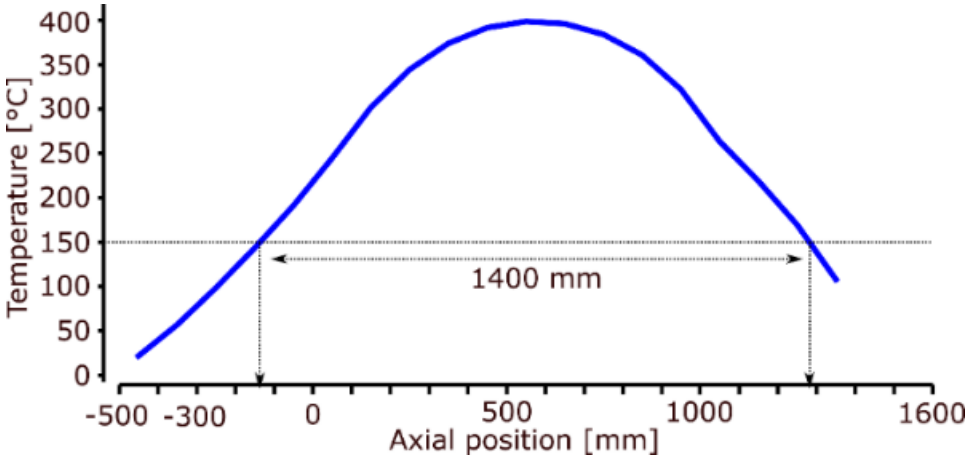

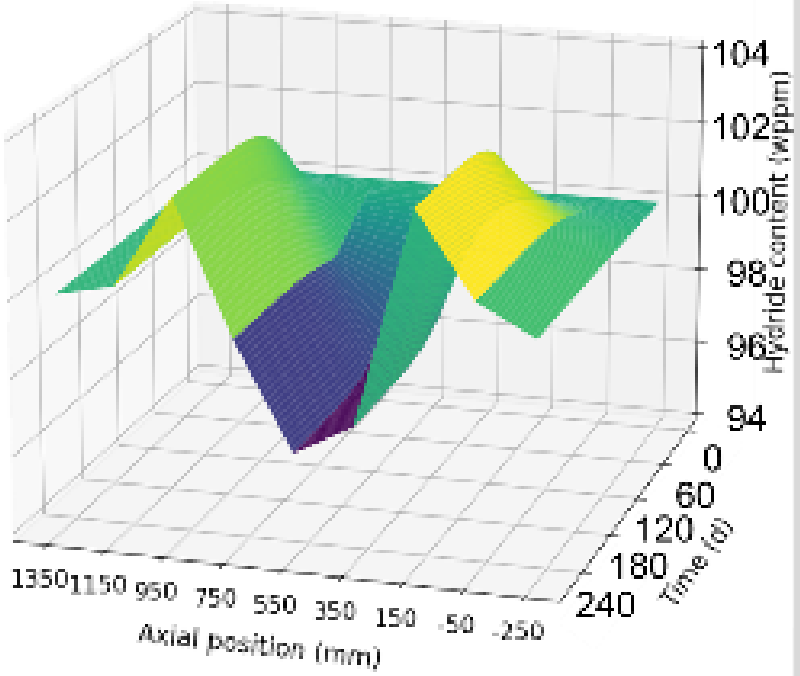

QUENCH bundle test

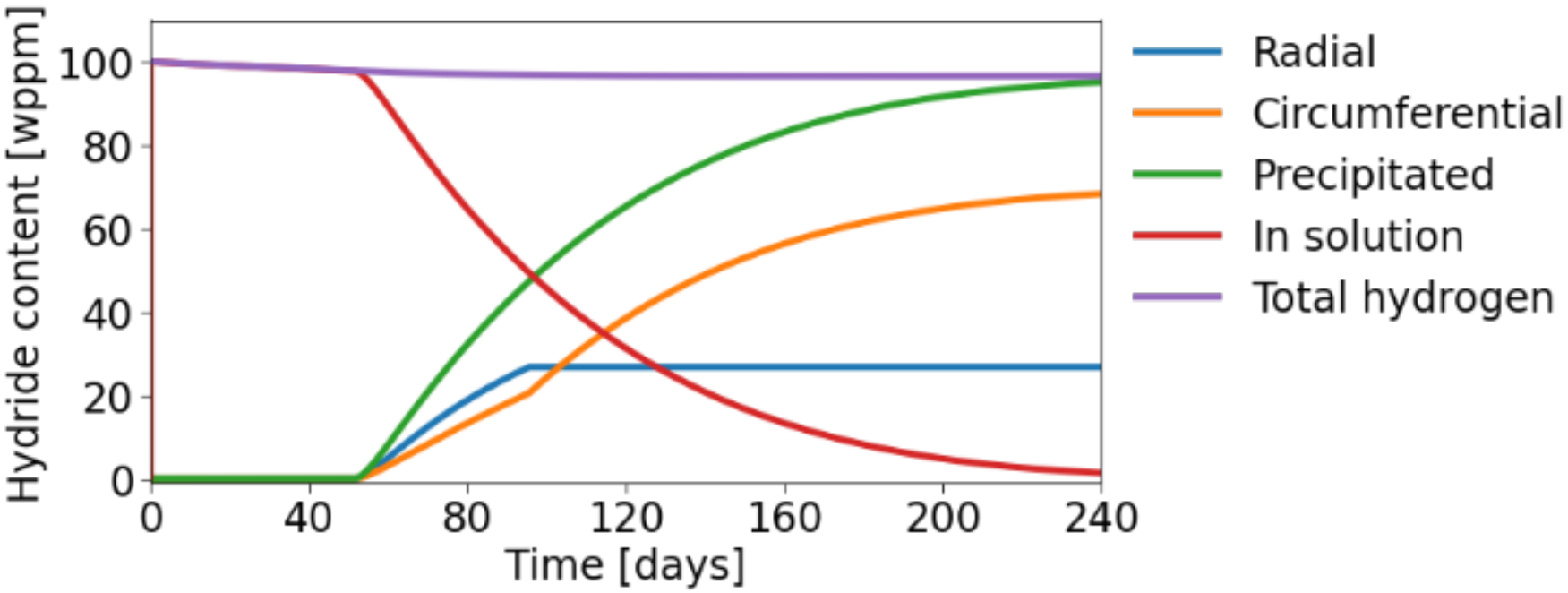

Pre-test calculations with the TESPA-ROD code: Prediction of the hydrogen behaviour at the hottest position of the central rod #01 during the test

Summary

- Investigations at a segment of a real fuel rod after long term dry storage:
  - Elastic and plastic deformations at a spent fuel cladding segment were measured in the range of the resolution limit.
  - No additional stress in the cladding tube due to fuel swelling after 50 GWh/t_{HM} and more than 30 y dry storage.
- The separate effect test will provide quantitative information on hydrogen diffusivity and solubility in zirconium alloys. Still in progress.
- The QUENCH bundle test is started at May 16 2023. It will be provide information about the hydride re-orientation in dependence on
  - Cladding alloy (Zry-4, ZIRLO, Dx/D4 Duplex)
  - Initial hydrogen concentration
  - Gas pressure inside the tubes and hoop stress in the tube wall
  - Initial temperature and cooling rate
  - The test will end at January 11 2024
- Predictions on the behavior were already calculated using the single rod code TESPA-ROD

Acknowledgement

The SPIZWURZ project is supported by

Supported by:

Federal Ministry
for the Environment, Nature Conservation,
Nuclear Safety and Consumer Protection

based on a decision of
the German Bundestag

The authors thank all colleagues contributing to the investigations: Maik Stuke (formerly GRS, now BGZ), Felix Boldt (formerly GRS, now BGZ), Thorsten Holland (GRS), Mara Marchetti (formerly INE), Jürgen Moch, Ursela Peters, Jutta Laier, Ulrike Stegmaier, Martin Steinbrück (IAM)

Thank you for your attention

J. Stuckert

KIT

Hydrogenation of claddings in the new developed HOKI oven and performance of the long-term bundle test under dry storage conditions in the framework of the SPIZWURZ project

During the dry storage of spent nuclear fuel, the initially dissolved hydrogen precipitates as hydrides in the metallic matrix. The orientation of hydrides influences the crack propagation and depends mainly on the hoop stress. In the frame of the SPIZWURZ project, the reorientation of zirconium hydrides in cladding tubes is being investigated under conditions similar to dry storage. For the long-term SPIZWURZ bundle experiment, 21 zirconium alloy tubes were charged with hydrogen to 100 and 300 wppm in the special developed HOKI tube oven as homogeneously as possible along a length of 1.3 m. The developed process allows a stepwise and controlled hydrogen absorption through the specially treated inner surface of claddings placed in the oven heated to 450 °C. The hydrogenation was carried out by successively supplying fixed masses of hydrogen, initially increasing the pressure in the tube sample from the achieved vacuum level to about 0.5 bar. Because of absorption, this pressure dropped to a predetermined vacuum level within a few minutes. During hydrogenation and subsequent heat treatment processes, the outer surface of the tube was exposed to a flow of oxygen to create an outer oxide layer more than 1 µm thick, which served as a barrier to hydrogen accumulating in the tube wall. After the hydrogen loading of the samples, the axial distribution of hydrogen was determined by laser scanning profilometry. This method makes it possible to use the correlation between the swelling of the rod diameter and the hydrogen concentration. This correlation was obtained by hot extraction of hydrogen from pre-hydrogenated reference samples. A long-term bundle test with hydrogenated and pressurized cladding tubes began on 12.05.2023 and will last until mid-January 2024. The peak cladding temperature decreased in steps of about 15 K from 400 to 200 °C currently (the average cooling rate is about 0.9 K/day).

Karlsruhe Institute of Technology

IAM
Institute for Applied Materials

Hydrogenation of claddings in the new developed HOKI oven and performance of the long-term bundle test under dry storage conditions in the framework of the SPIZWURZ project

J. Stuckert, C. Rößger, J. Moch, M. Große, S. Weick

Institute for Applied Materials; Program NUSAFE

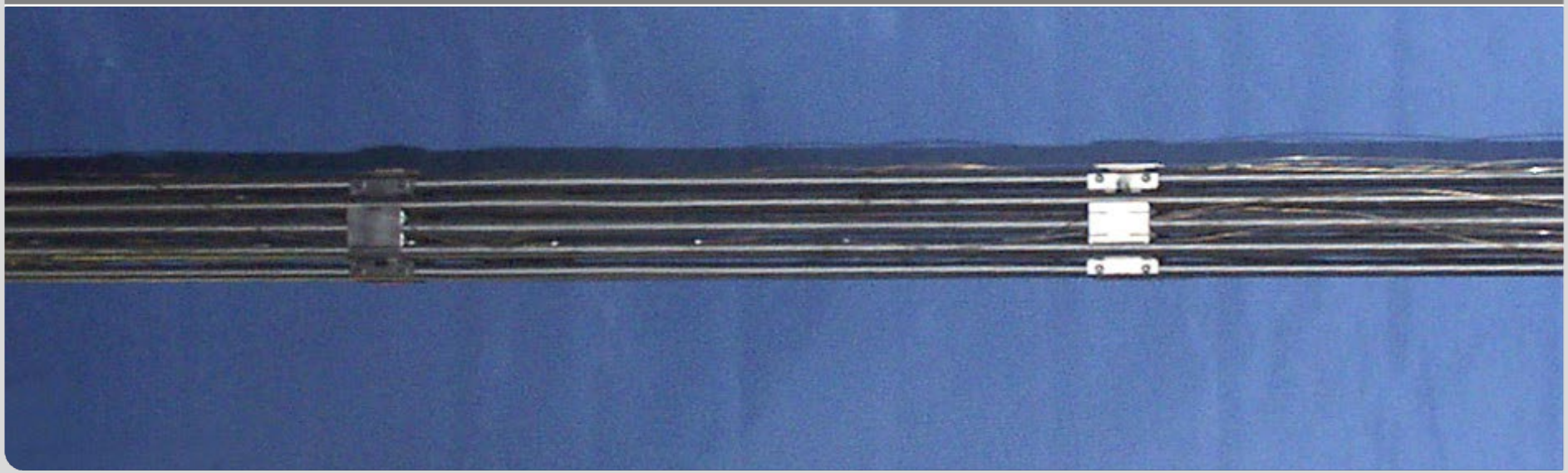

Goal of bundle test:

investigation of behavior of hydrides during the long-time dry storage of spent fuel with

- ***different cladding materials (Zry-4, opt. ZIRLO, DUPLEX)***
- ***different cladding inner pressures (140, 100 bar)***
- ***different hydrogen contents (100, 300 wppm)***
- ***different temperature histories (due to axial T profile in the bundle)***

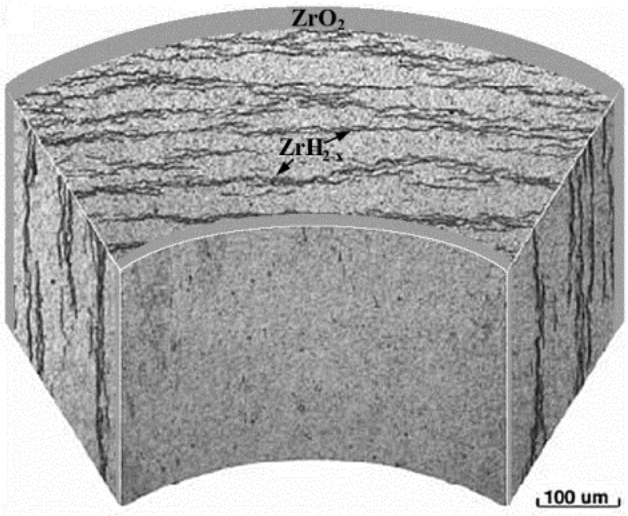

long time cool-down:
reorientation of hydrides

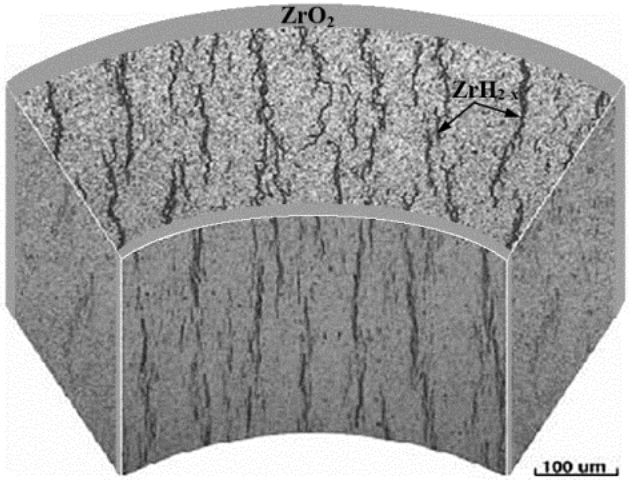

Phase diagram Zr-H

/nach Zuzek et al., Bull Alloy Phase Diagr., 11 (1990), 385/

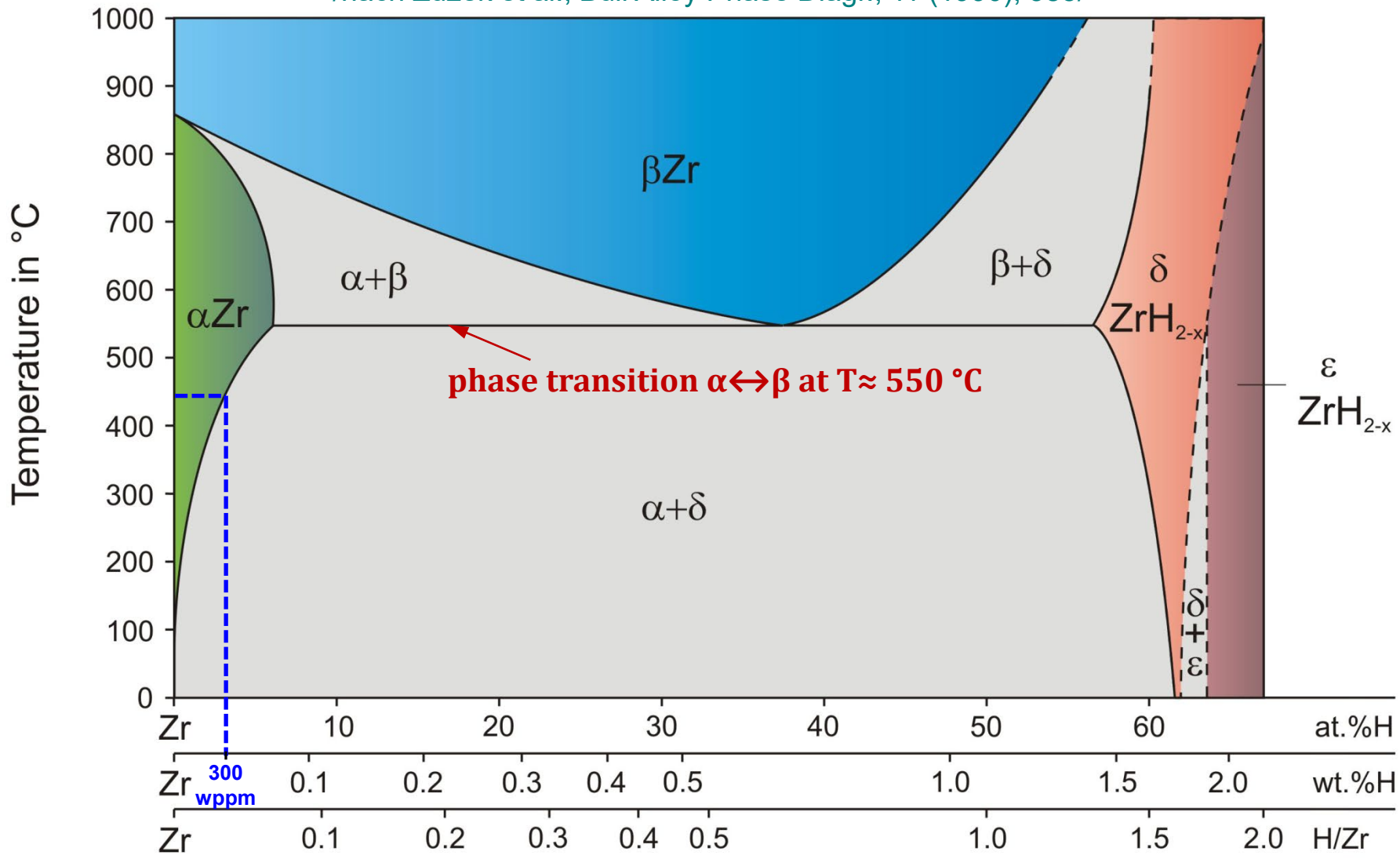

hydriding of claddings should be performed at T<550 °C to avoid the phase transition

Solubility of hydrogen in α-Zirconium

/D. Khatamian, V.C. Ling, JAC vol.253-254, 1997, https://doi.org/10.1016/S0925-8388(96)02947-7/

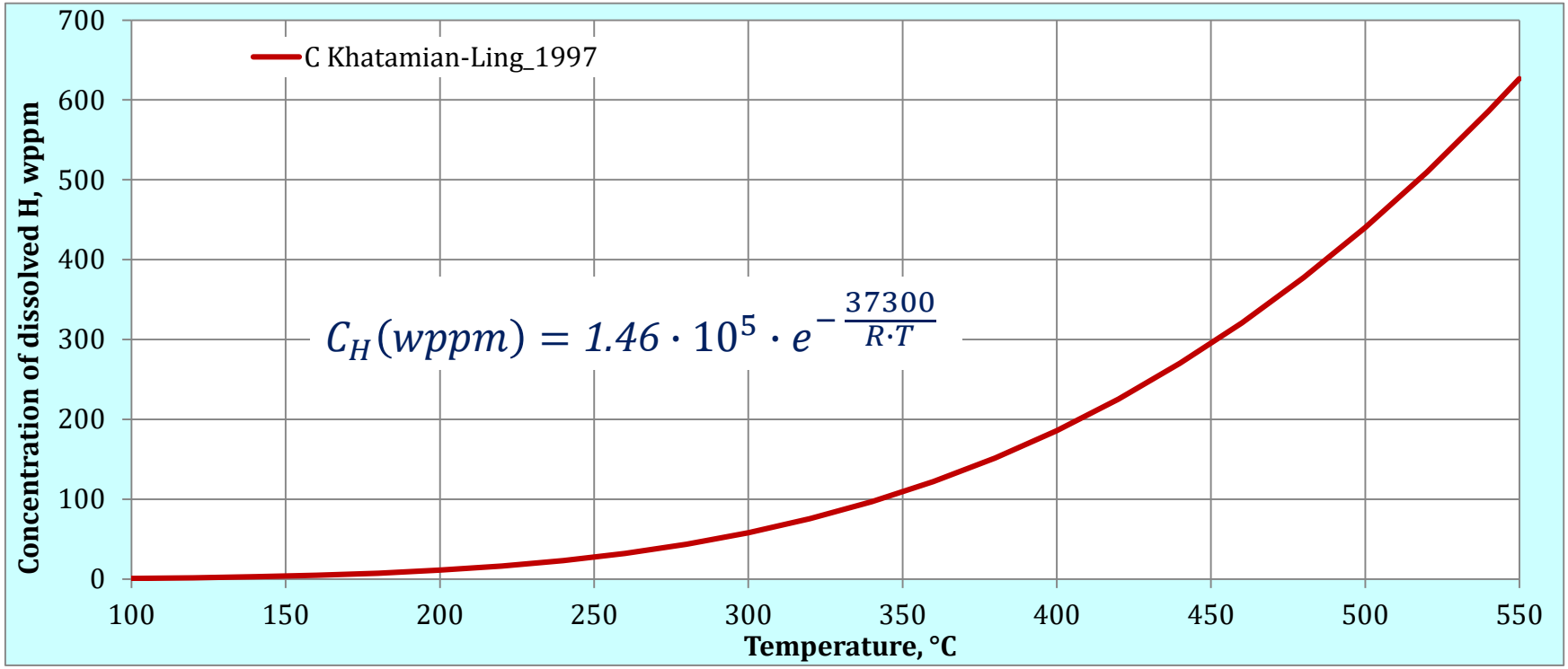

T, °C	175	200	225	250	275	300	325	350	375	400	425	450	475
C_H, wppm	**7**	**11**	18	27	41	58	81	109	144	186	236	**295**	363

dissolved hydrogen at the end of the bundle test

dissolved hydrogen at the beginning of the bundle test

dissolved hydrogen after hydriding in oven

Pre-hydrogenation of claddings in tube oven through the inner cladding surface with simultaneous oxidation of outer cladding surface

For hydriding to 300 wppm:
1) evacuation of cladding tube,
2) filling of cladding tube with H_2 to **8.4 bar** at T=450 °C,
3) p decrease to ≈**0 bar,**
4) annealing (T=450°C) during 3 h to homogenization of H distribution

Duration of hydrogen absorption depends on the diffusion coefficient

$$D_H^{Zr}(\mathrm{cm}^2/\mathrm{s}) = 7 \cdot 10^{-3} \cdot e^{-\frac{44560}{R \cdot T}}$$

/J.J. Kearns, JNM vol. 43, 1972, https://doi.org/10.1016/0022-3115(72)90065-7 /

and is therefore $t \approx \delta_{Zr}^2 / D_H^{Zr} \approx$ **1250 s** for clad thickness δ_{Zr}=725 µm, T=450 °C

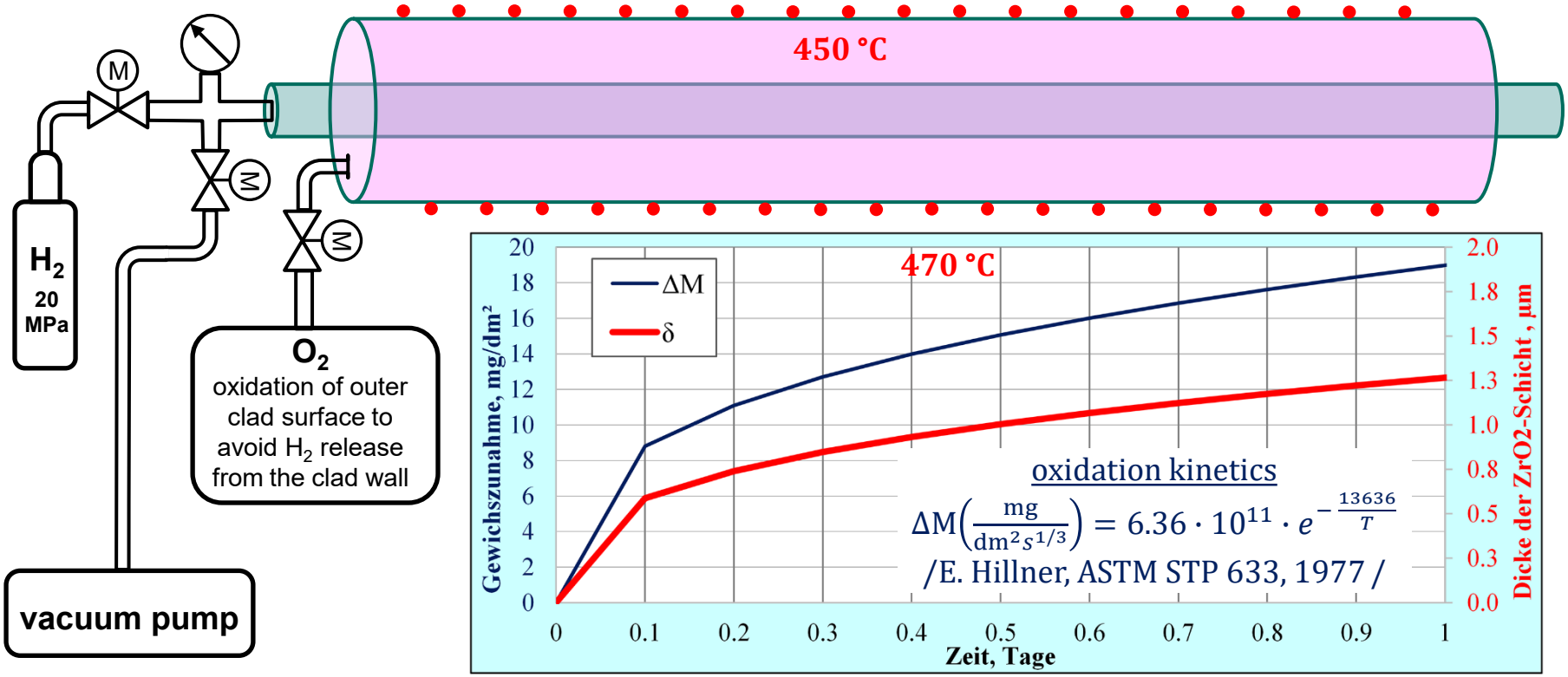

HOKI-facility: hydrogenation of single claddings through the inner cladding surface

and oxidation of the outer cladding surface

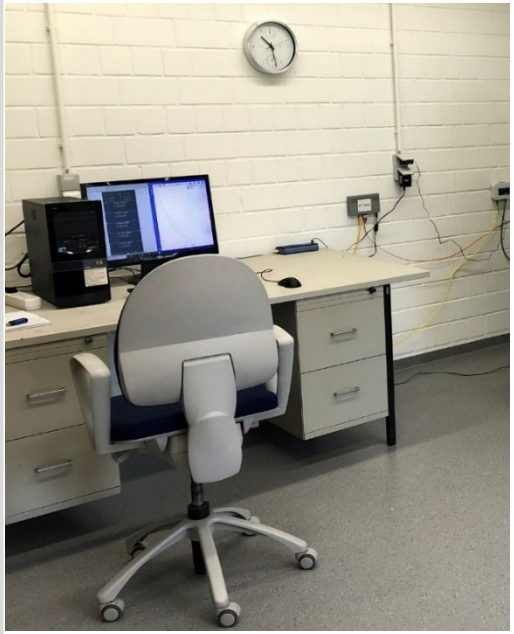

control and recording system

HOKI oven with 5 heated zones and connected gas system

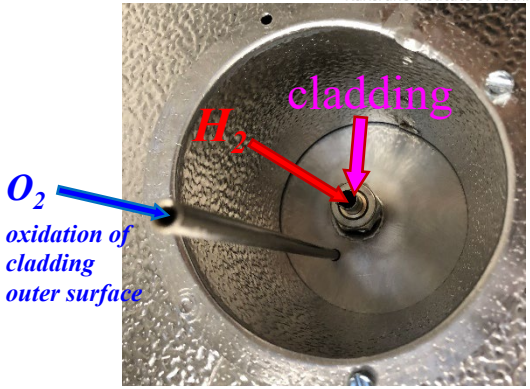

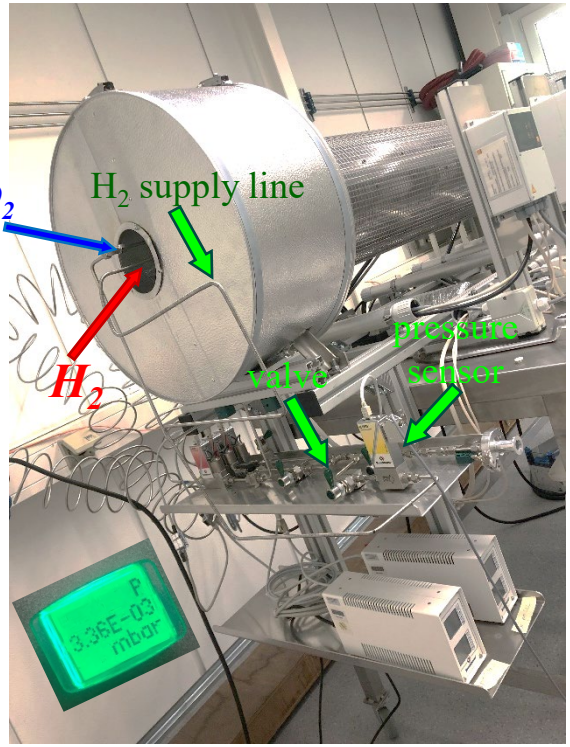

$V_{H2}=V_{hot\ clad} + V_{cold\ supply} = 133\ cm^3 + 20\ cm^3$

Hydrogenation of each cladding in extended pulse mode to prevent rapid formation of hydrides near to the inner cladding surface

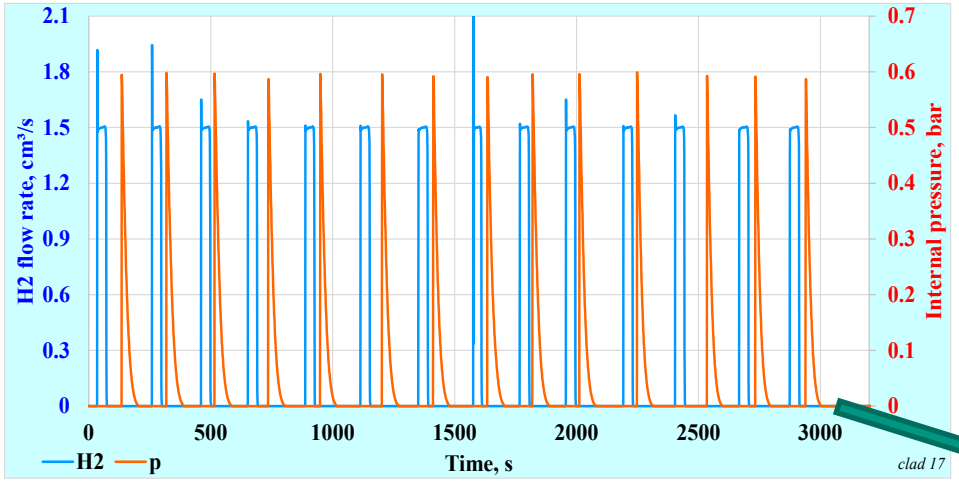

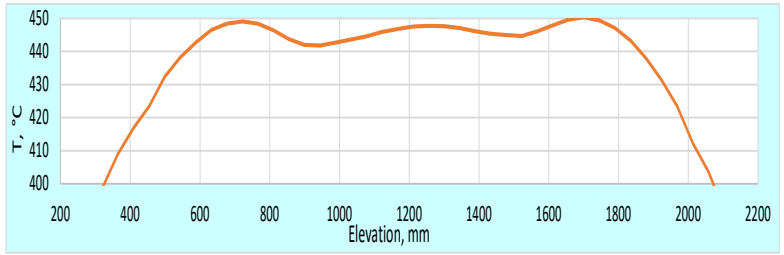

pulse filling of the internal cladding volume after special treatment of the inner cladding surface and evacuation of the cladding tube: repeated depressurization of inner cladding volume due to H_2 absorption

HOKI oven with axial temperature profile: T ≈ 450 °C along the length of ≈ 1250 mm

1) stepwise hydriding of cladding to 300 wppm H
***14 injections** with **p_{max}=0.6 bar** →*

$$\text{total } m_{H2} = 14 \times \left(\frac{\mu p_{max} V_{hot}}{R T_{hot}} + \frac{\mu p_{max} V_{cold}}{R T_{cold}}\right) = 0.05 \text{ g}$$

*$M_{clad\ 125\ cm}$ = 170 g C_H = 0.05/170 ≈ **300 wppm***

2) stepwise hydriding of cladding to 100 wppm H
***5 injections** with **p_{max}=0.6 bar** →*

$$\text{total } m_{H2} = 5 \times \left(\frac{\mu p_{max} V_{hot}}{R T_{hot}} + \frac{\mu p_{max} V_{cold}}{R T_{cold}}\right) = 0.0179 \text{ g}$$

*$M_{clad\ 125\ cm}$ = 170 g C_H = 0.0179/170 ≈ **100 wppm***

Determination of axial distribution of hydrogen concentration by increase of circumferential strain at each elevation

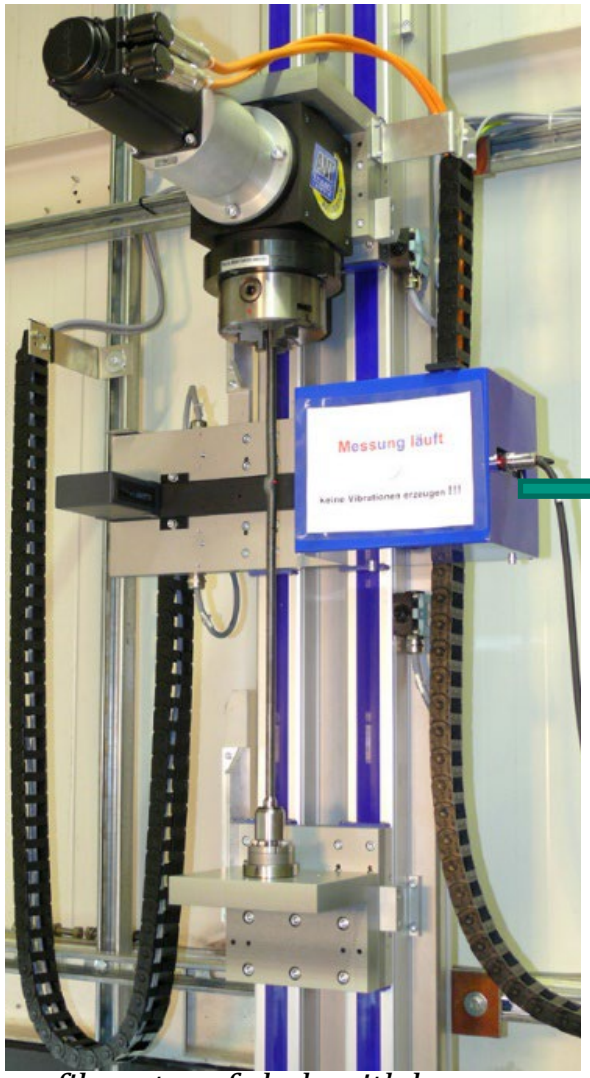

profilometry of clads with laser scanner

(thermal expansion ±0.3 µm for ±5 °C)

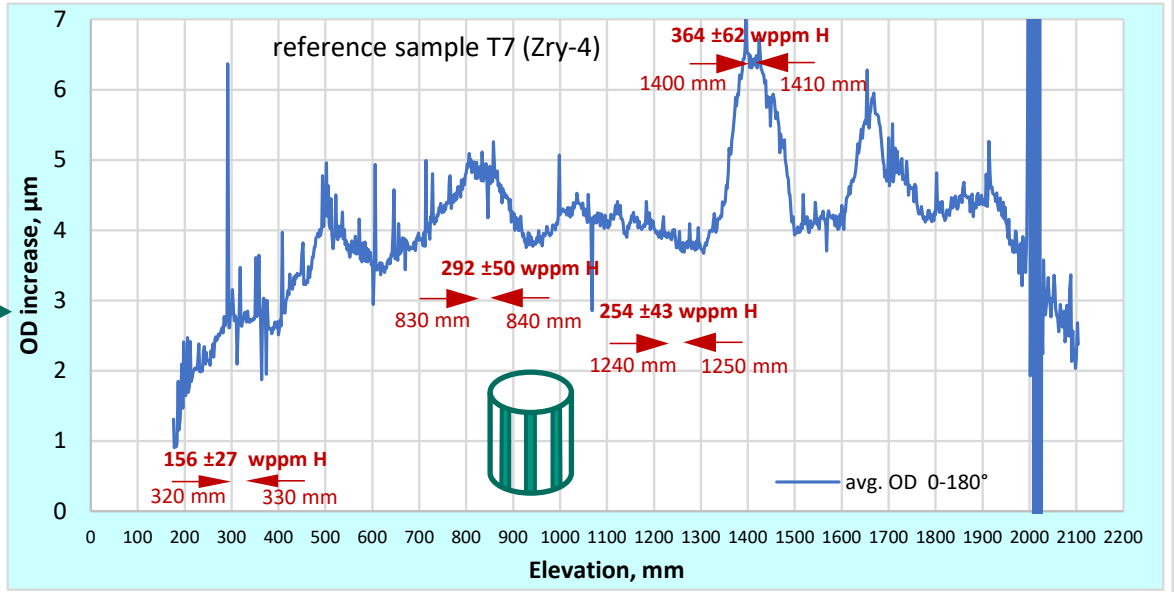

axial profile of cladding diameter increase (laser scanner)

and corresponded hydrogen concentrations
(hot extraction from 3 lamellas 10x1 mm)

Correlation between hydrogen content and cladding diameter increase

sample	T4			T5			T6				T7			
axial position, mm	750	1250	1650	750	1250	1650	405	755	1155	1455	325	835	1245	1405
OD increase, µm (laser scanner)	**7.6**	**4**	**5.5**	**8.2**	**5.5**	**4.5**	**1**	**2.5**	**2.7**	**1.5**	**2.7**	**4.8**	**3.8**	**6.5**
hot extraction, wppm	**318**	**301**	**329**	**421**	**353**	**296**	**66**	**132**	**135**	**115**	**156**	**292**	**254**	**364**
± wppm	48	45	49	105	88	74	17	33	34	29	27	50	43	62
SD				25	3	2	27	2	1	5	4	13	6	3

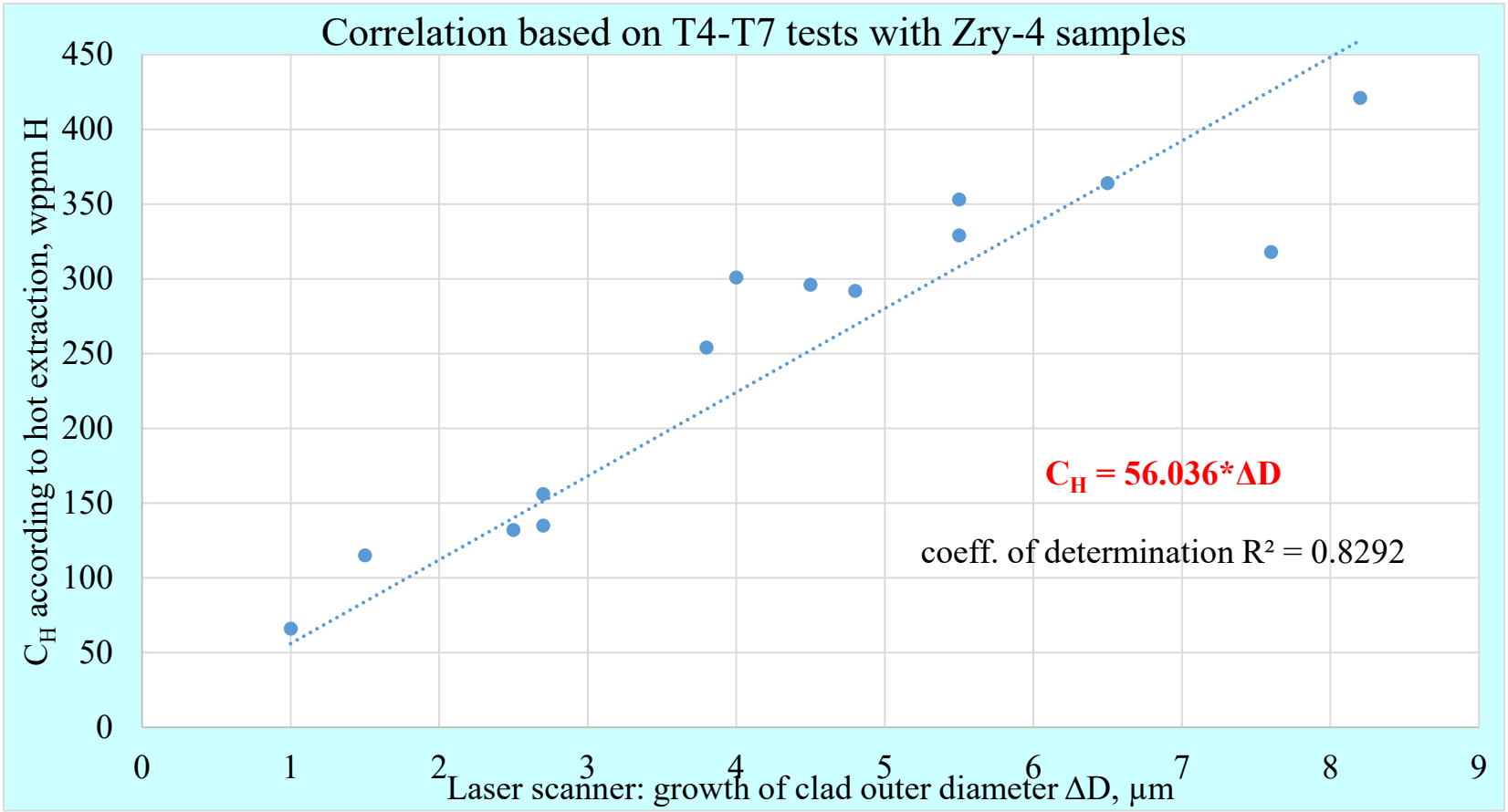

Axial hydrogen distribution for claddings hydrogenated to 100 wppm H

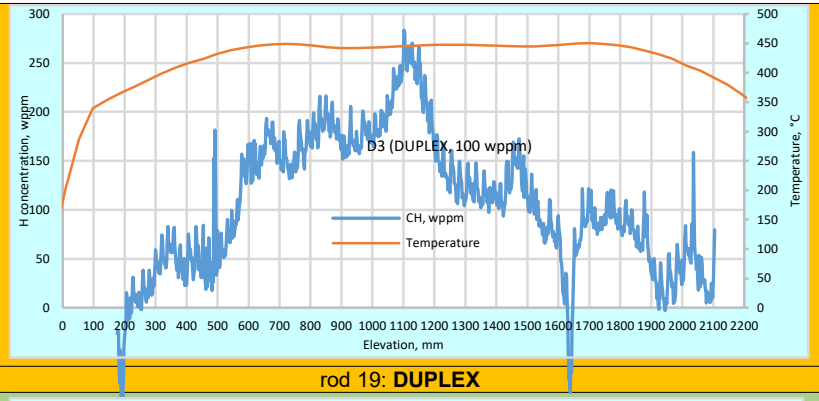

rod 19: **DUPLEX**

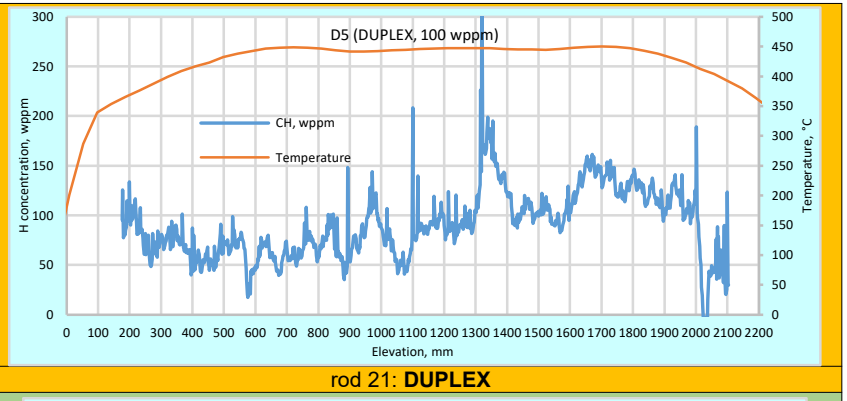

rod 21: **DUPLEX**

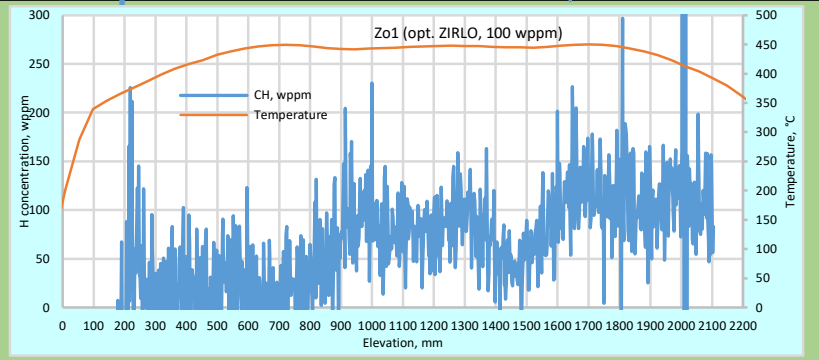

rod 3: **optimized ZIRLO**

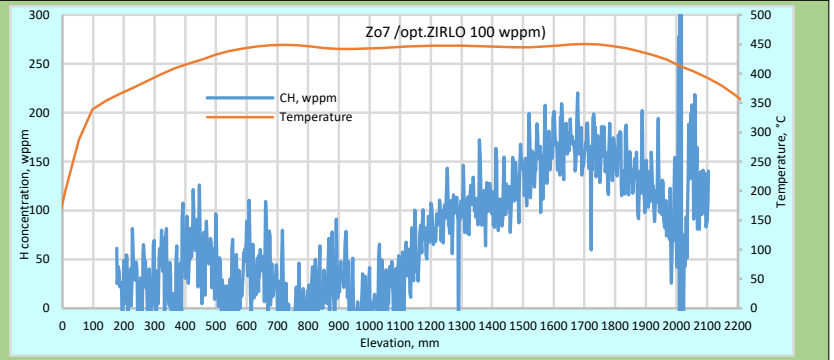

rod 15: **optimized ZIRLO**

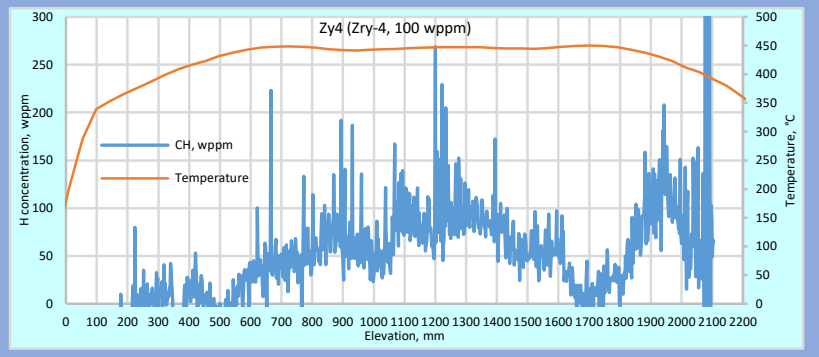

rod 8: **Zircaloy-4**

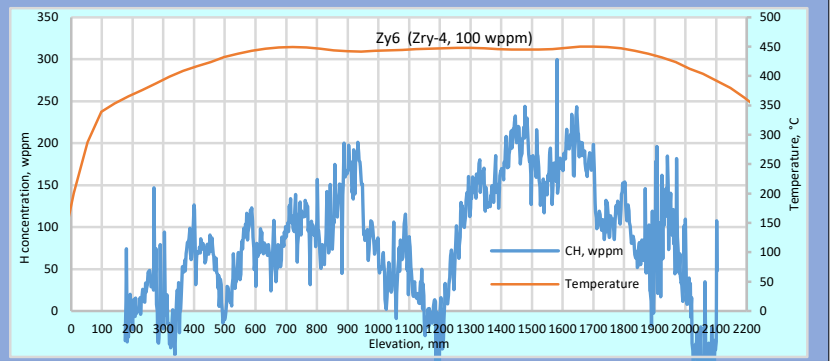

rod 14: **Zircaloy-4**

Axial hydrogen distribution for claddings hydrogenated to 300 wppm H

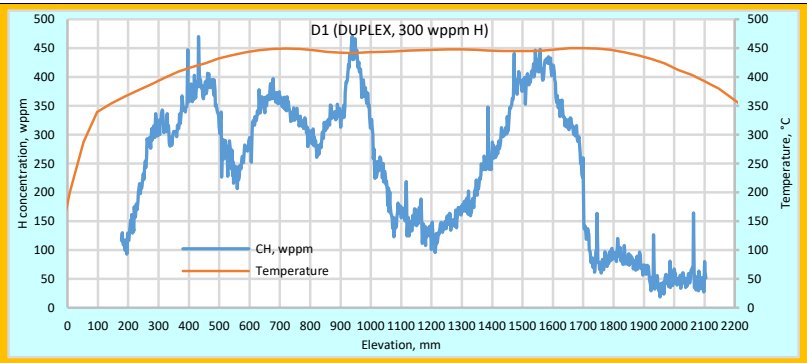

rod 1: **DUPLEX**

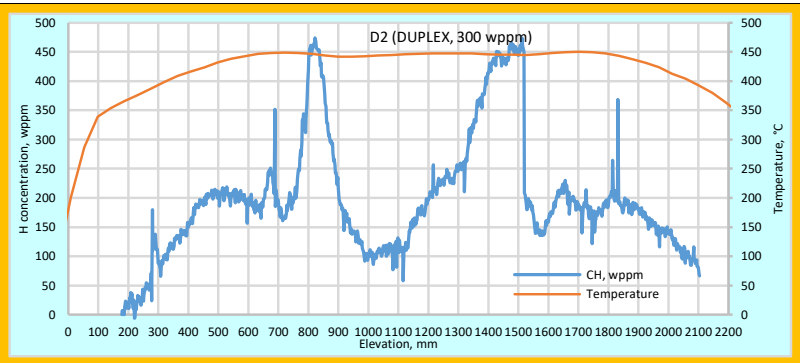

rod 9: **DUPLEX**

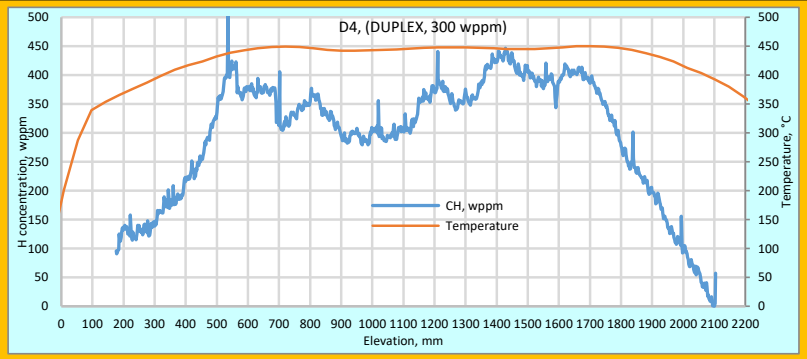

rod 20: **DUPLEX**

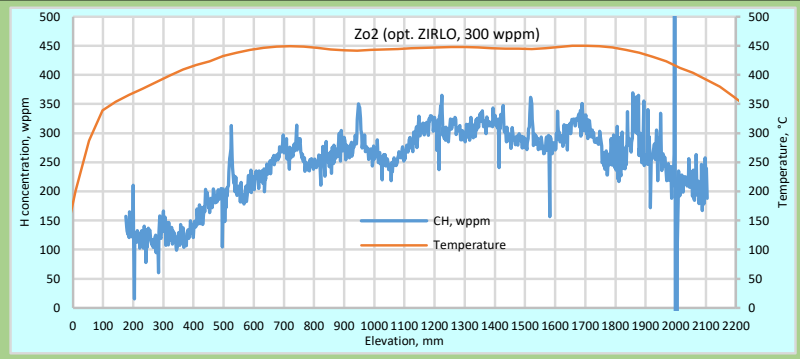

rod 5: **optimized ZIRLO**

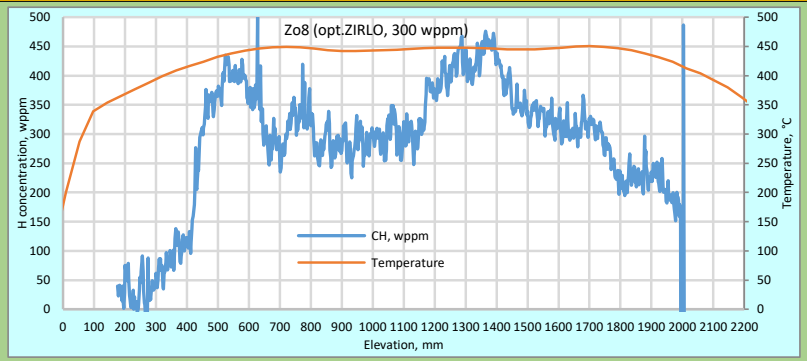

rod 16: **optimized ZIRLO**

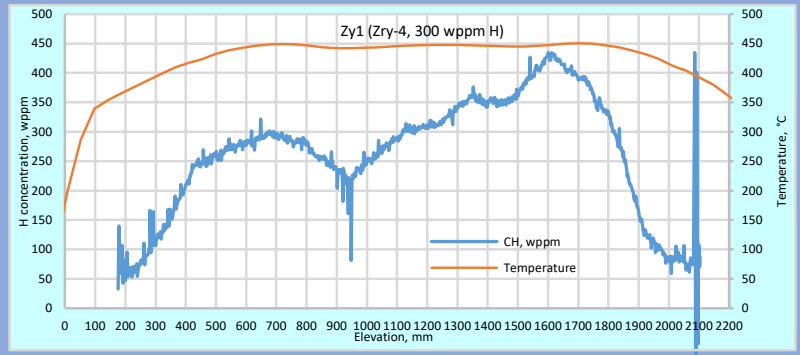

rod 2: **Zry-4**

Metallography of the reference sample D6 (DUPLEX with outer 150 µm liner)

not etched cladding cross-sections

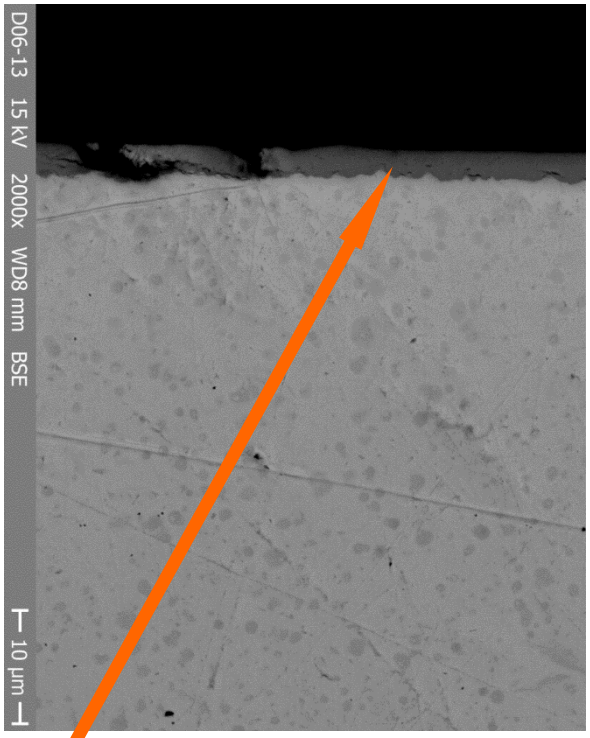

outer ZrO_2 2.4 µm (formed during 4.5 days at 450 °C)
corresponds 0.3% O in whole sample,
what was confirmed also by hot extraction

300 wppm

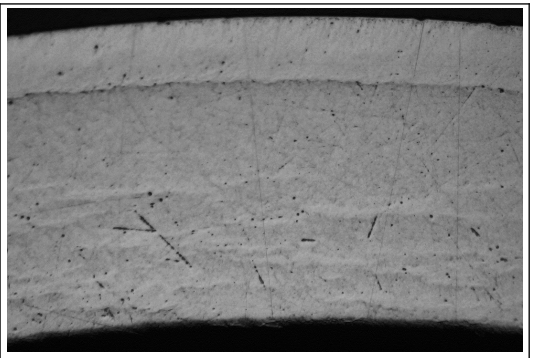

170 wppm

200 wppm

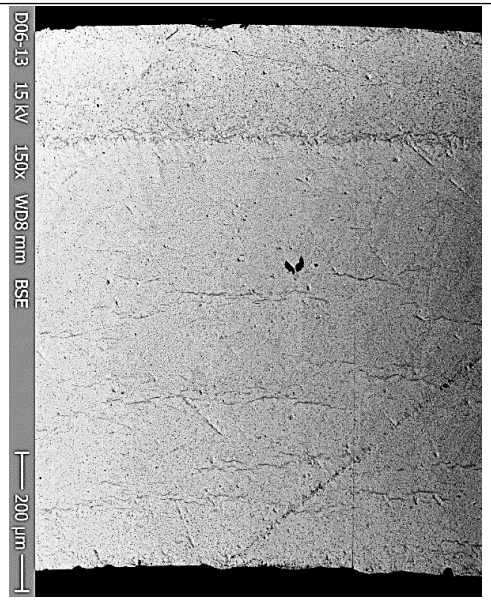

SEM: 170 wppm

hydrides

Relationship between the CASTOR-V/19 container (PWR) and the QUENCH bundle simulator

Trockenlager

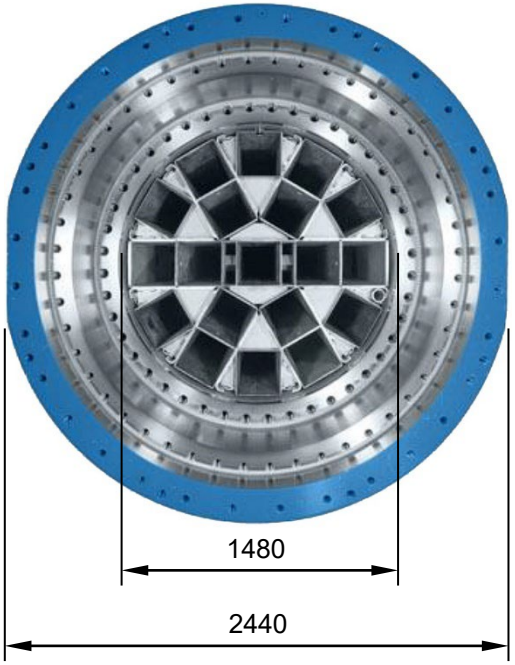

Container for 19 fuel elements
with a maximum height of 4950 mm and a total heat output of 39 kW

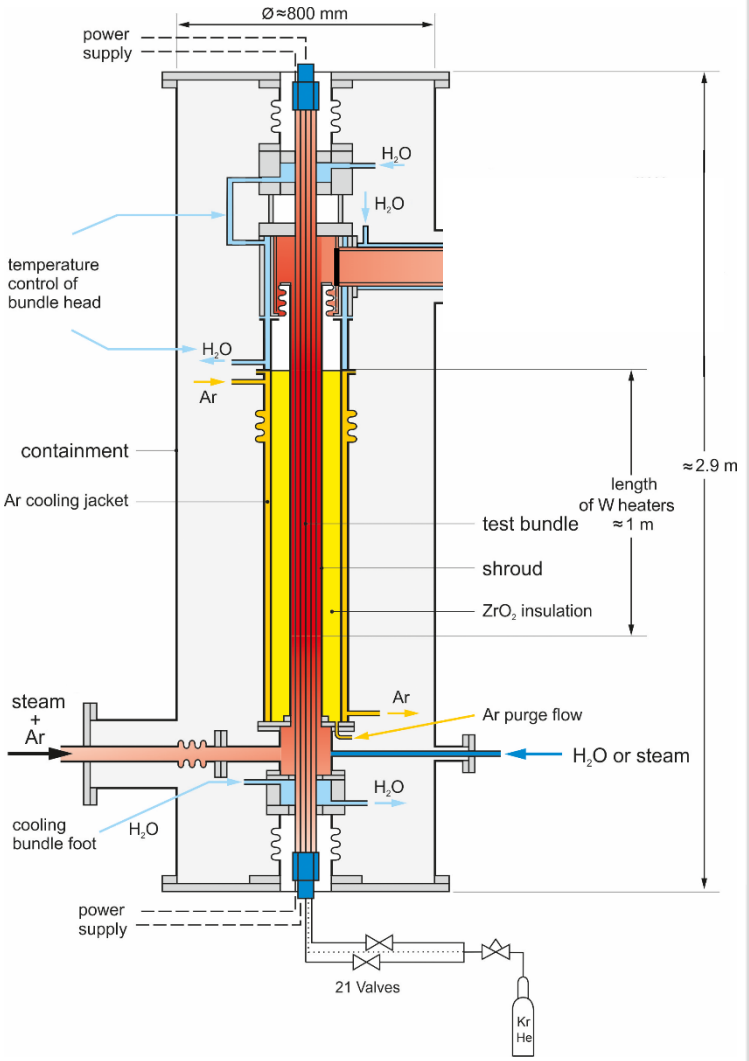

QUENCH test section

SPIZWURZ bundle

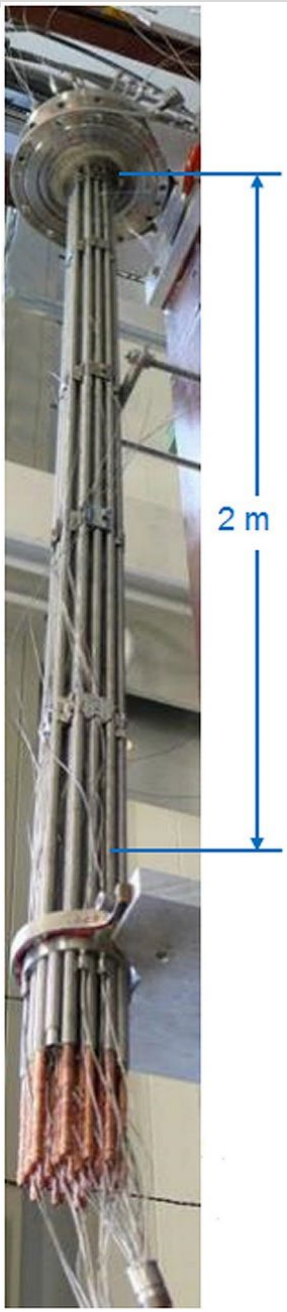

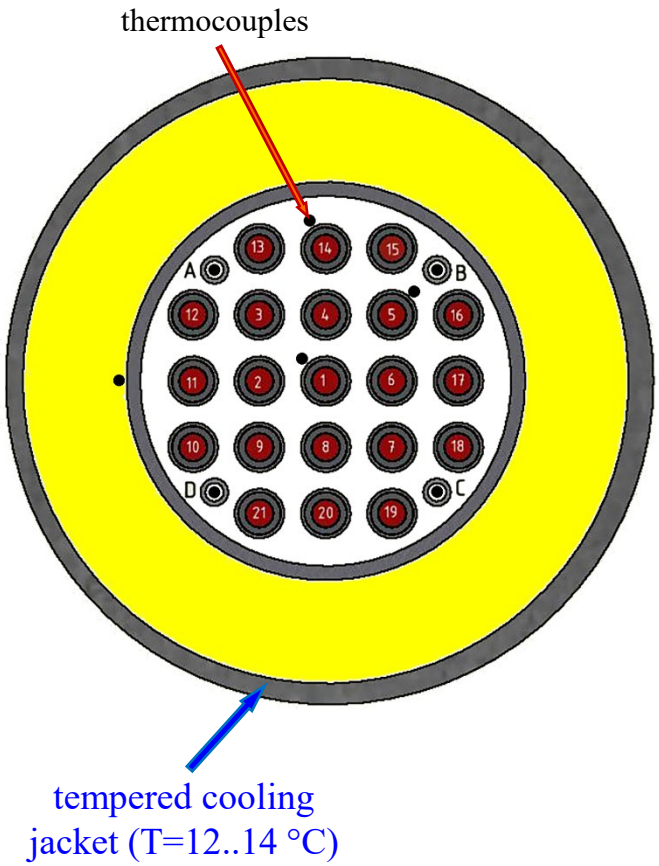

Bundle size		21 heated rods
Pitch		14.3 mm
Corner rod (4)	material	Zircaloy-4
	instrumented (A, B, C, D)	tube ∅ 6x0.5 (bottom: -1140 mm)
Grid spacer	material	Zircaloy-4
	length	42 mm
	sheet thickness	0.5 mm
	elevation of lower edge	Zry: -100, 150, 550, 1050, 1410 mm
Shroud	material	Zirconium 702 (flange: Zry-4)
	wall thickness	3.17 mm
	outside diameter	86.0 mm
	length (extension)	1600 mm (-300 mm to 1300 mm)
Shroud insulation	material	ZrO_2 fiber
	insulation thickness	~ 36 mm
	elevation	-300 to ~1000 mm
Cooling jacket	Material: inner/outer	Inconel 600 (2.4816) / SS (1.4571)
	inner tube	∅ 158.3 / 168.3 mm
	outer tube	∅ 181.7 / 193.7 mm
Thermocouples	at cladding surfaces	rods 1, 5, 9; totally 3x15=45
	inside corner rods	one at each elevation 2-16, totally 15
	at shroud outer surface	one at each elevation 3-15, totally 13

Heat transport in the QUENCH bundle

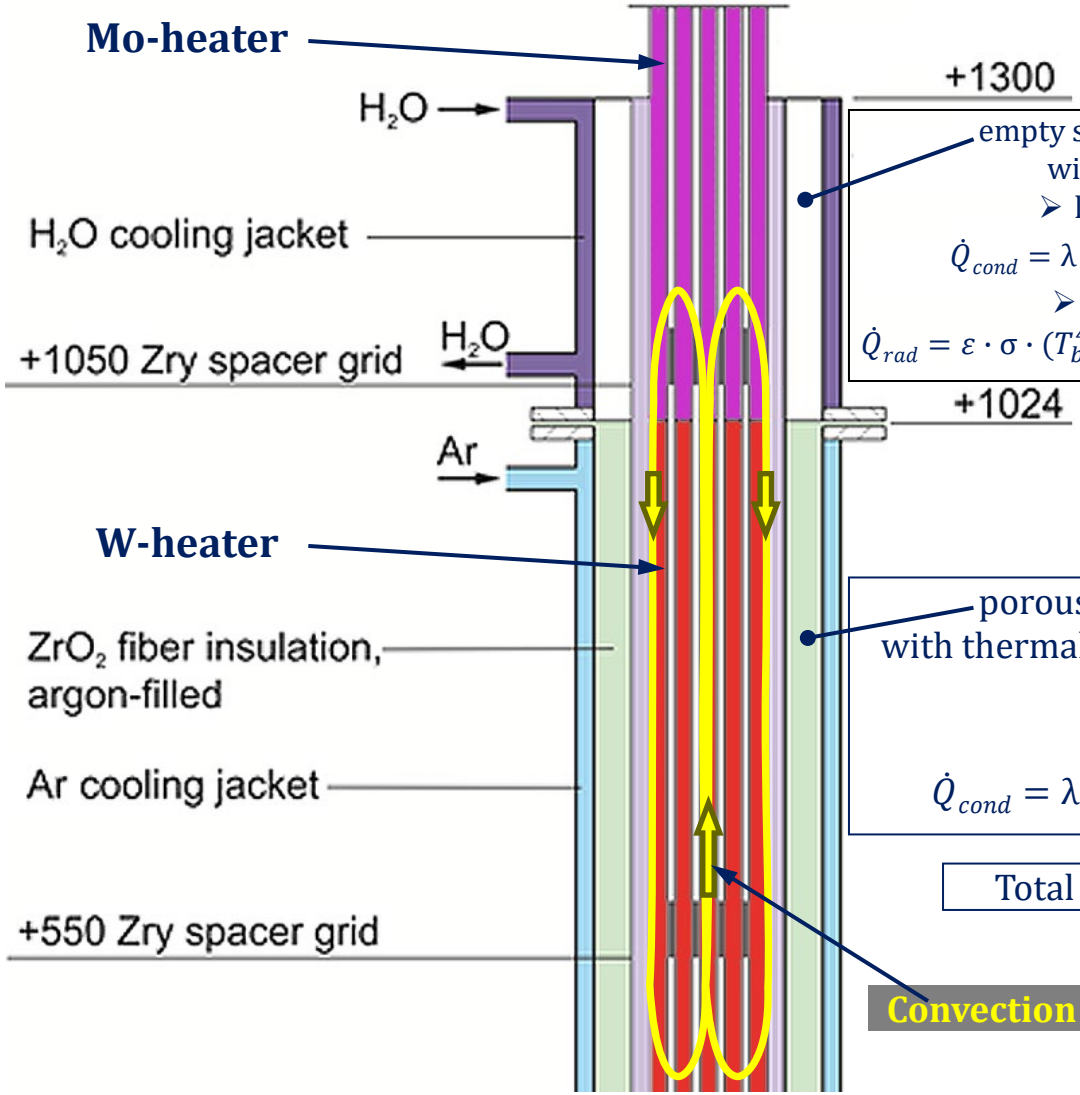

empty space (δ_{gap}=37 mm) at bundle head field with Ar with heat conductivity λ_{Ar}=0.01772 W/(m·K):

- low bundle head cooling due to conductivity

$$\dot{Q}_{cond} = \lambda \cdot \frac{T_{bundle} - T_{jacket}}{\delta} = 0.01772 \cdot \frac{350-15}{0.037} \approx 160\ W/m^2$$

- ***intensive*** *bundle head cooling by radiation*

$$\dot{Q}_{rad} = \varepsilon \cdot \sigma \cdot (T_{bundle}^4 - T_{jacket}^4) = 0.27 \cdot \sigma \cdot (623^4\text{-}288^4) \approx 2200\ W/m^2$$

porous ZrO_2 thermal insulation (porosity 92%) with thermal conductivity $\lambda_{porousZrO2}$=0.08 W/(m·K) (673 K)

heat flow:

$$\dot{Q}_{cond} = \lambda \cdot \frac{T_{bundle} - T_{jacket}}{\delta} = 0.08 \cdot \frac{450-15}{0.037} \approx 940\ W/m^2$$

Total QUENCH bundle heat loss ≈630 W

Heated rod

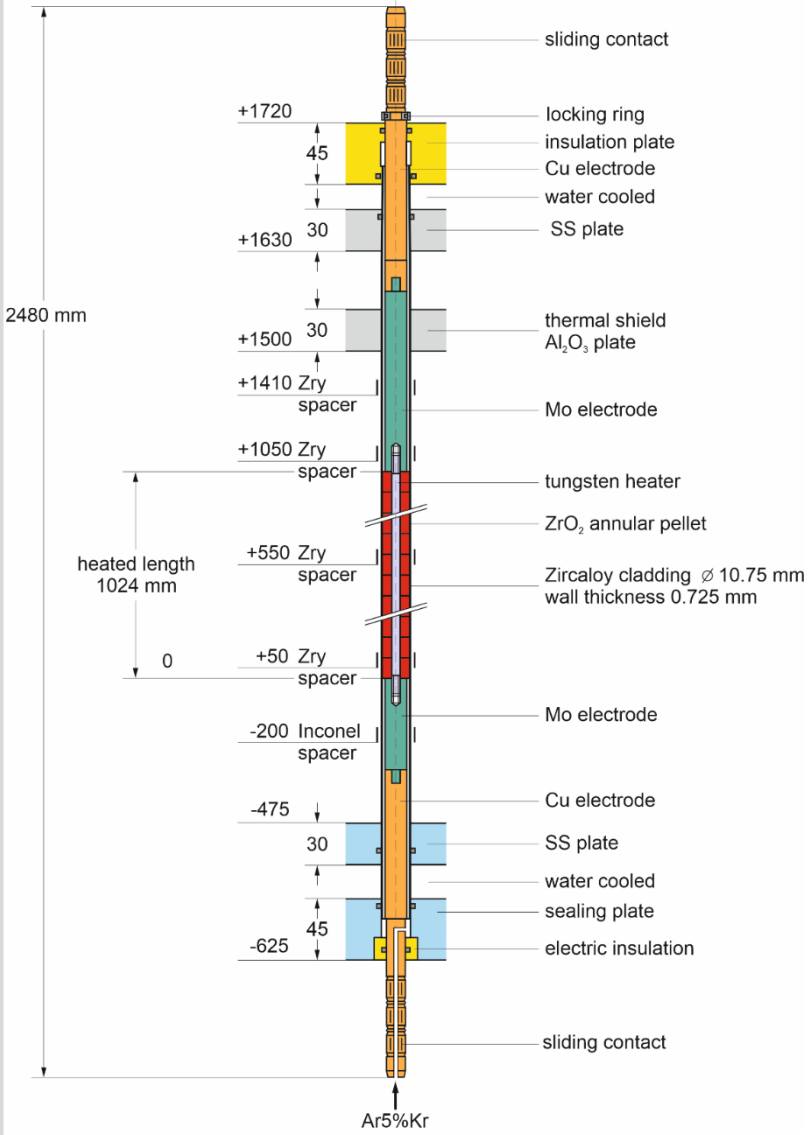

Cladding outside diameter		**10.75 mm**
Cladding thickness		**0.725 mm**
Cladding length	**(position in the bundle)**	**2278 mm (between -593 and 1685 mm)**
Rod length	(elevations)	2480 mm (-690 to 1790 mm)
Internal rod pressure; gas		5.5 MPa abs.; Kr
Material of middle heater		Tungsten (W)
	surface roughness	Ra=1.6 µm
Tungsten heater length		1024 mm (between 0 and 1024 mm)
Tungsten heater diameter		4.6 mm
Annular pellet	material	ZrO_2;Y_2O_3-stabilized
	dimensions	∅ 9.15/4.75 mm; L=11 mm
	surface roughness	Ra=0.3 µm
Pellet stack		0 mm to ~1020 mm
Molybdenum heaters and copper electrodes	length of upper part	766 mm (576 Mo, 190 mm Cu)
	length of lower part	690 mm (300 Mo, 390 mm Cu)
	outer diameter:	
	prior to coating	8.6 mm
	after coating with ZrO_2	9.0 mm
	coat. surface roughness	Ra=6-12 µm
	borehole of Cu-electrodes	diameter 2 mm, length 96 mm
Gas volume inside the rod	**heated**	**15 cm³**
Gas volume outside the rod	**not heated (room T)**	**20 cm³**

Fuel rod simulator, electrically heated with W and Mo heaters

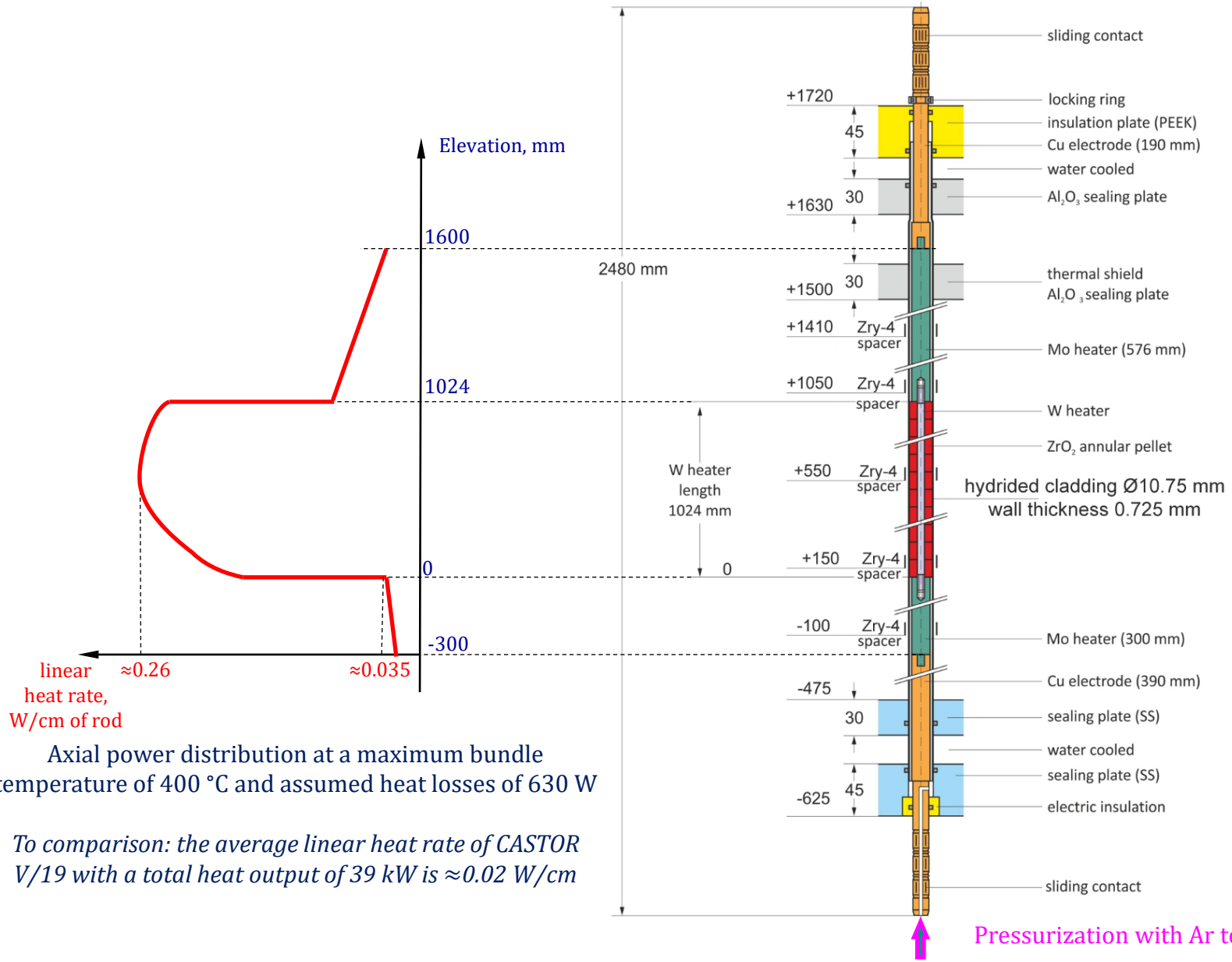

Axial power distribution at a maximum bundle temperature of 400 °C and assumed heat losses of 630 W

To comparison: the average linear heat rate of CASTOR V/19 with a total heat output of 39 kW is ≈0.02 W/cm

Bundle composition

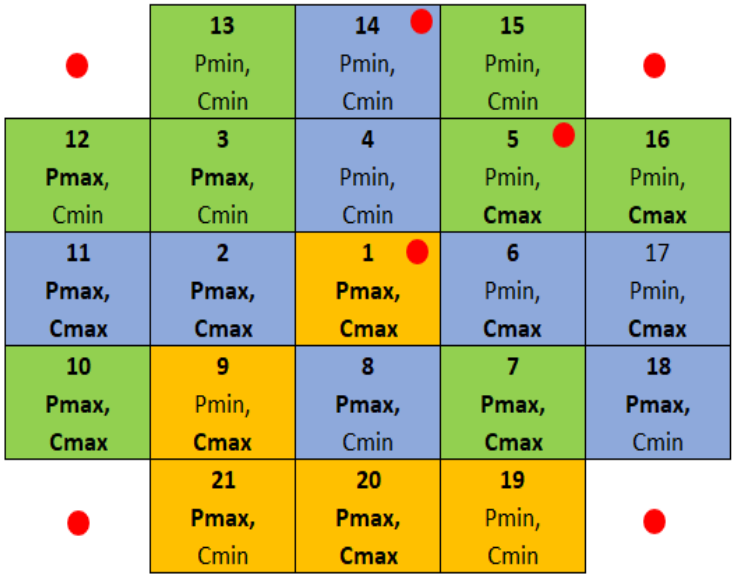

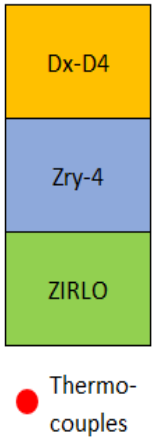

number	rod	alloy	H conc., wppm	mark
D1	1	DUPLEX	300	D1
Zry0212	2	Zry-4	300	Zy1
Zo049	3	ZIRLO	100	Zo1
Zy31	4	Zry-4	100	Zy2
Zo087	5	ZIRLO	300	Zo2
Zy85	6	Zry-4	300	Zy3
Zo156	7	ZIRLO	300	Zo3
Zry197	8	Zry-4	100	Zy4
D2	9	DUPLEX	300	D2
Zo165	10	ZIRLO	300	Zo4
Zry199	11	Zry-4	300	Zy5
Zo220	12	ZIRLO	100	Zo5
Zo221	13	ZIRLO	100	Zo6
Zy914	14	Zry-4	100	Zy6
Zo332	15	ZIRLO	100	Zo7
Zo351	16	ZIRLO	300	Zo8
Zry1021	17	Zry-4	300	Zy7
	18	Zry-4	100	Zy8
D3	19	DUPLEX	100	D3
D4	20	DUPLEX	300	D4
D5	21	DUPLEX	100	D5

Pressures inside the rods between 12.05 and 30.10.2023

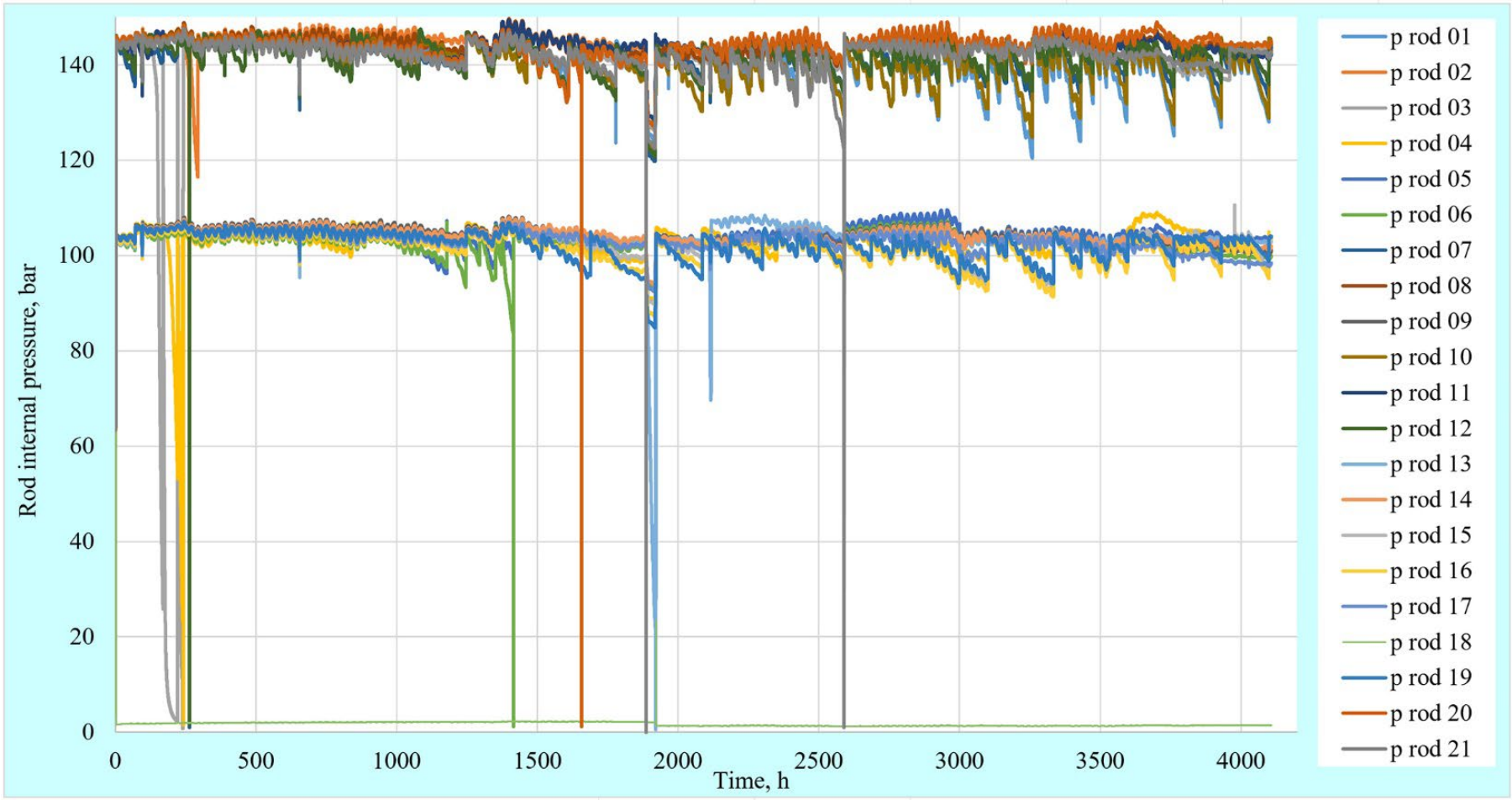

- two pressurization levels of **106 and 146 bar**
- daily refill of 7 rods with Ar+O_2 due to small leakages
- short depressurizations of 6 rods due to change of sealing rings

Reading of cladding surface thermocouples (TFS) between 12.05 and 30.10.2023

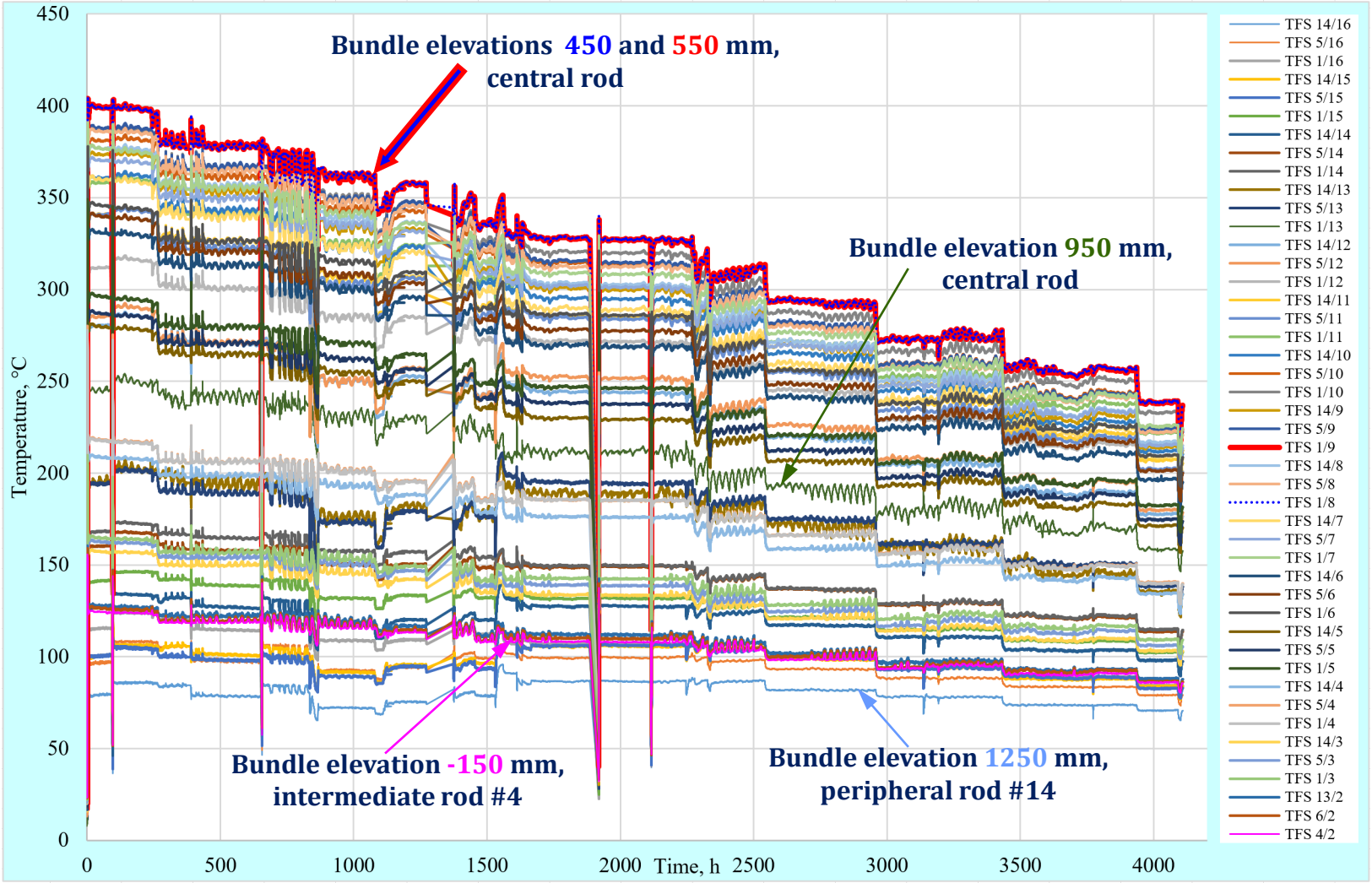

- peak cladding temperature decreased in steps with 15 K decrement and average duration of 400 h, average cooling rate 0.9 K/day
- periodic daily temperature fluctuations ≈±1.5 K for each thermocouple
- 4 el. power breakdowns

Smooth temperature decrease on the time of the power step reduction

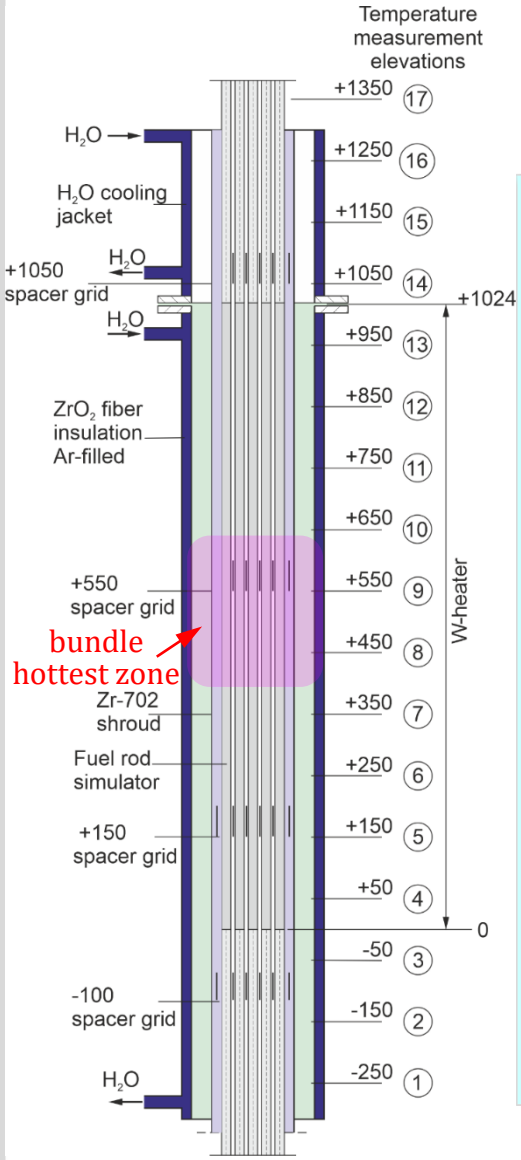

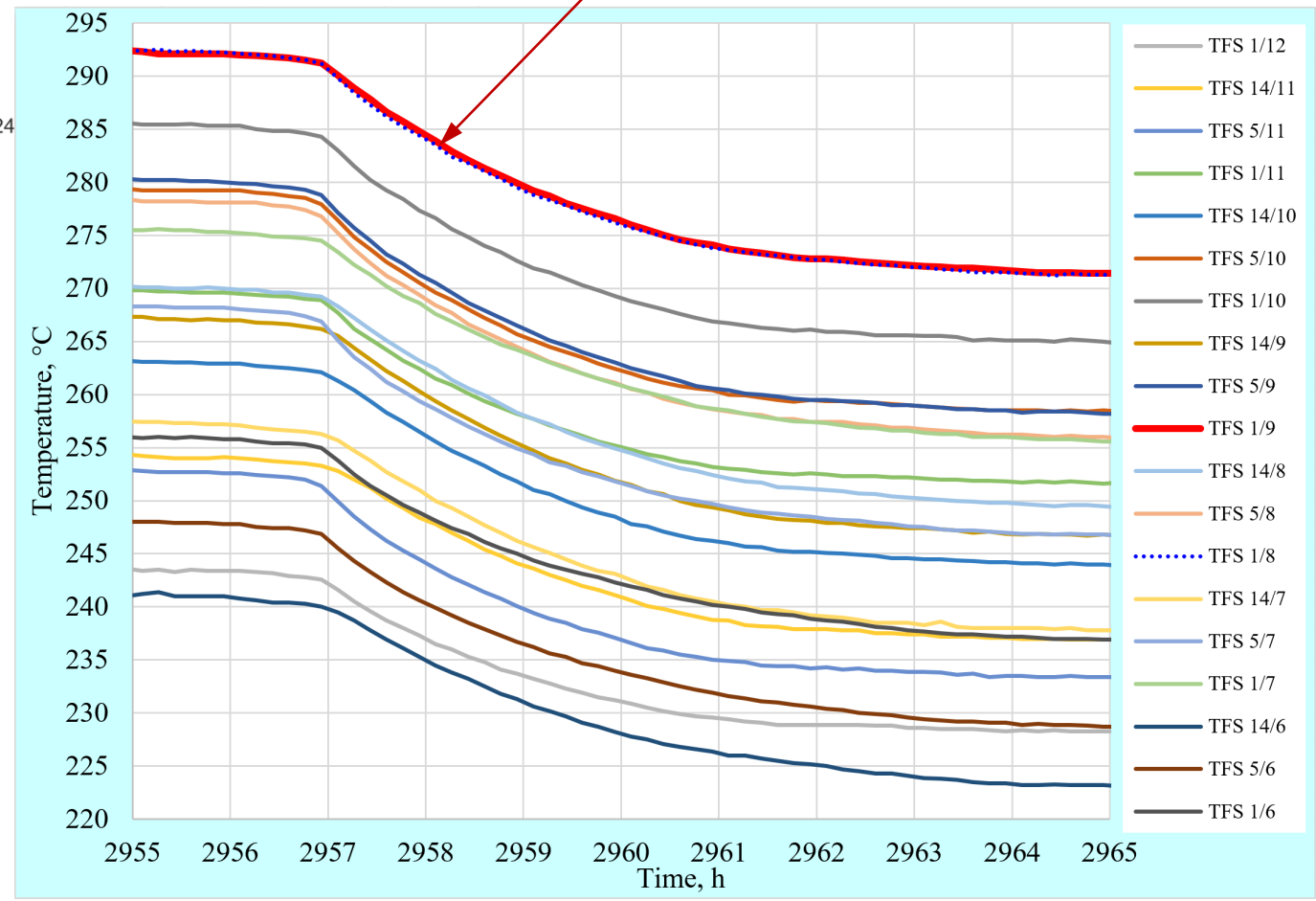

Axial temperature distribution for three rod groups

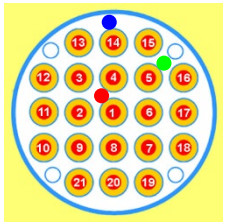

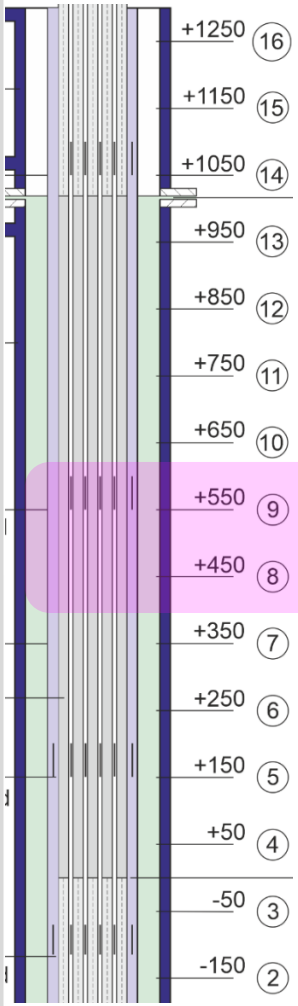

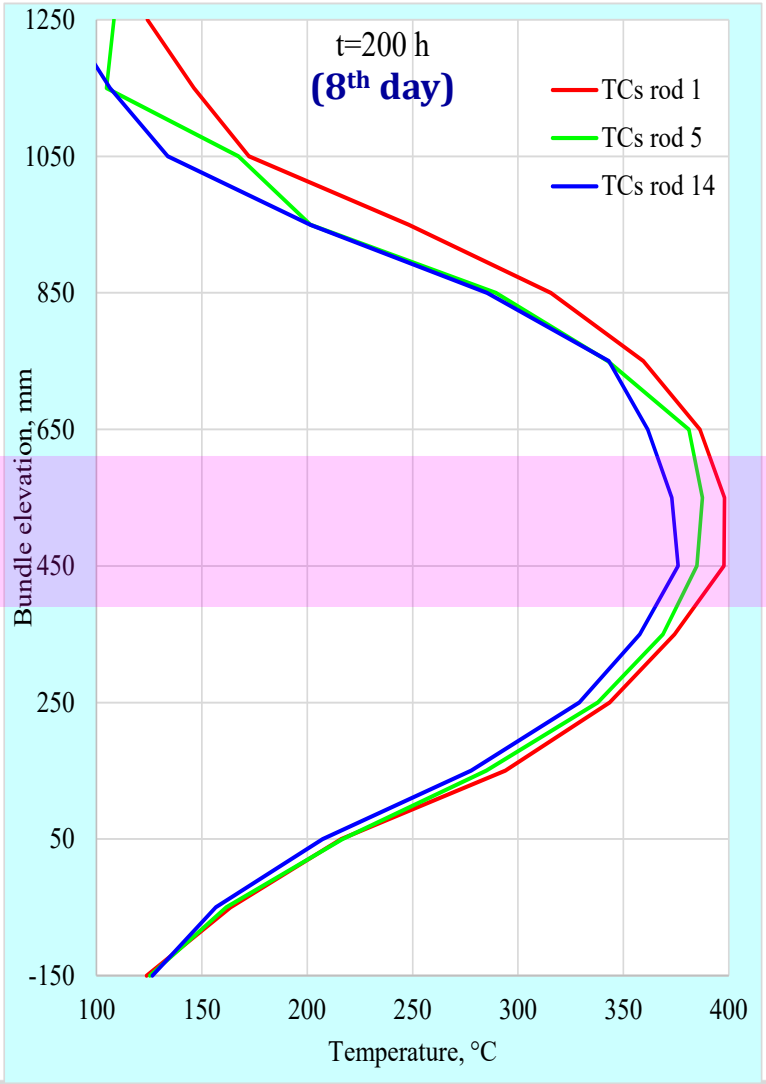

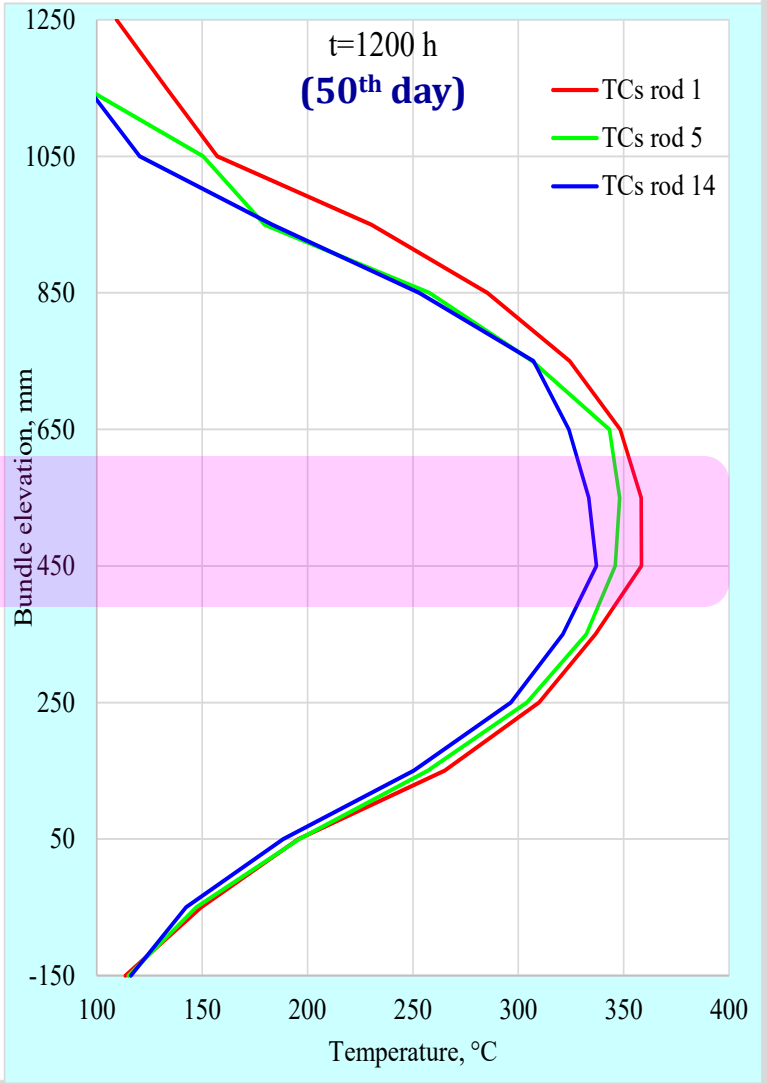

Summary

- For the long-term SPIZWURZ bundle experiment, zirconium alloy tubes were charged with hydrogen to 100 and 300 wppm in the special developed HOKI tube oven as homogeneously as possible along a length of 1.3 m.
- The developed process allows a stepwise and controlled hydrogen absorption through the specially treated **inner** surface of claddings placed in the oven heated to 450 °C.
- The hydrogenation was carried out by successively supplying fixed masses of hydrogen, initially increasing the pressure in the tube sample from the achieved vacuum level to about 0.05 MPa. As a result of absorption, this pressure dropped to a predetermined vacuum level within a few minutes.
- During hydrogenation and subsequent heat treatment processes, the outer surface of the tube was exposed to a flow of oxygen to create an outer oxide layer more than 1 µm thick, which served as a barrier to hydrogen accumulating in the tube wall.
- After the hydrogen loading of the samples, the axial distribution of hydrogen was determined by laser scanning profilometry. This method makes it possible to use the correlation between the swelling of the rod diameter and the hydrogen concentration (verified by hot gas extraction).
- A long-term bundle test with 21 hydrogenated and pressurized cladding tubes began on 12.05.2023 and will last until mid-January 2024. The peak cladding temperature decreased in steps of 15 K from 400 to 200 °C today (average cooling rate ≈0.9 K/day).

Thank you for your attention

http://www.iam.kit.edu/awp/163.php

http://quench.forschung.kit.edu/

S. Weick

KIT

Neutron imaging investigations of hydrogen in cladding tubes

Neutron imaging is a non-destructive method to locally detect precise hydrogen contents within Zirconium – the metal that is used in cladding tubes. Because of the very low neutron cross section of Zirconium, the metal is nearly invisible for neutrons and the contrarily behaving hydrogen that scatters neutrons strongly, appears as dark contrast in neutron images. Thus, the amount of hydrogen within the samples can be visualised and measured mutually.

In this paper, recent measuring campaigns in the context of hydrogen in cladding tubes are presented. These different campaigns were conducted in order to determine diffusion coefficients of hydrogen in axial and circumferential directions of cladding tubes and to determine hydrogen contents in oxide layers of cladding tubes. The cladding tubes for the determination of diffusion coefficients were either pre-hydrogenated at low temperatures below 500°C, or the hydrogen uptake process was investigated in-situ. Other samples were investigated after their heating in oxidizing hydrogen-rich atmospheres.

The paper will help to understand the possibilities of neutron imaging for several applications in the framework of hydrogen in Zirconium and thus the integrity of cladding tubes.

Karlsruher Institut für Technologie

PAUL SCHERRER INSTITUT PSI

Neutron imaging investigations of hydrogen in cladding tubes

S. Weick, M. Grosse, M. Steinbrueck, O. Yetik

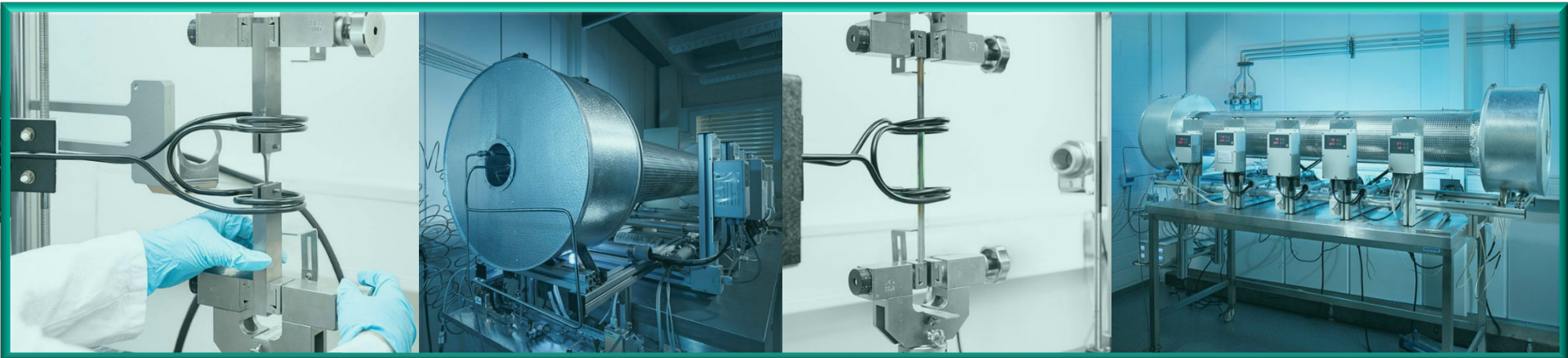

28th QUENCH Workshop
5-7 December 2023, KIT Karlsruhe, Germany

IAM-AWP-HTWC

Introduction – Spent Nuclear Fuel

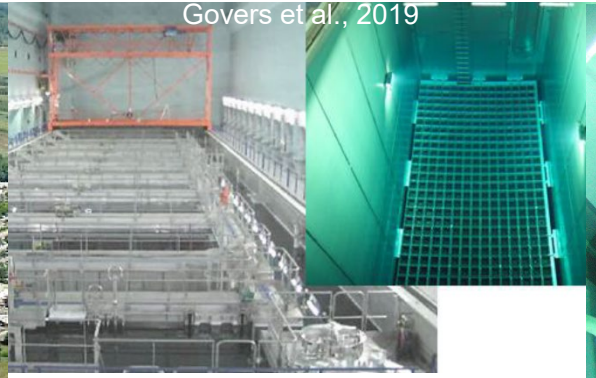

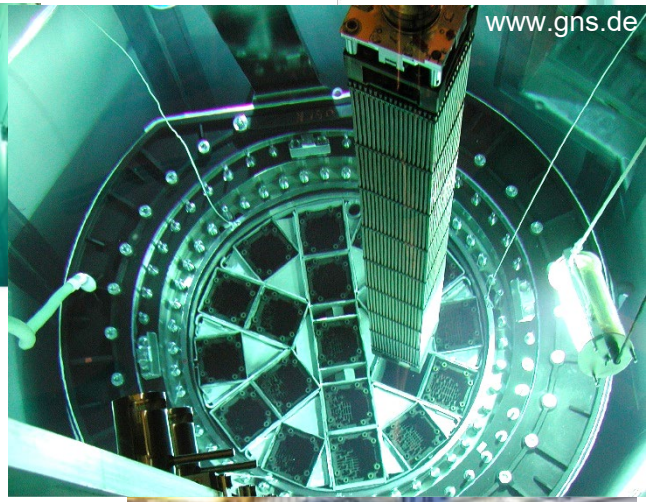

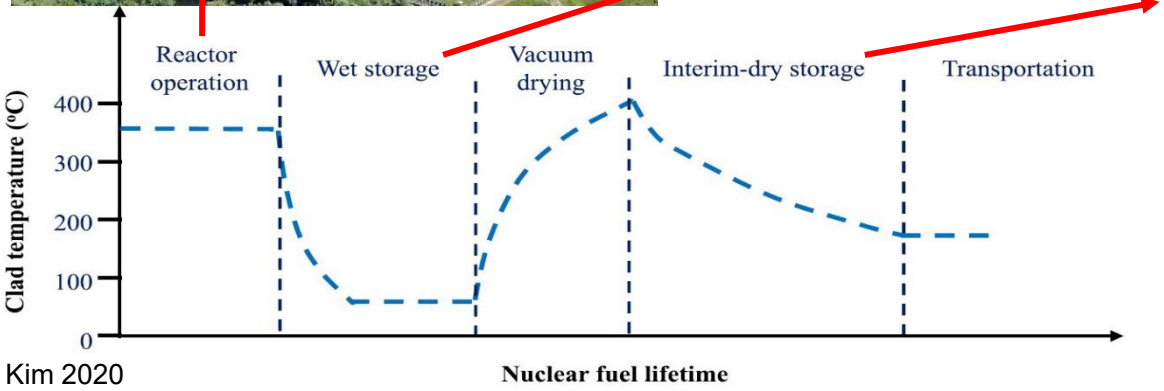

Kim 2020

Overview

Neutron Imaging of hydrogen in cladding tubes

- Neutron Imaging
- HT oxidation — NuMat 2022
- Interim dry storage phase: T_{max} conditions — SPIZWURZ

Theory - Neutron Imaging

NR = Neutron Radiography

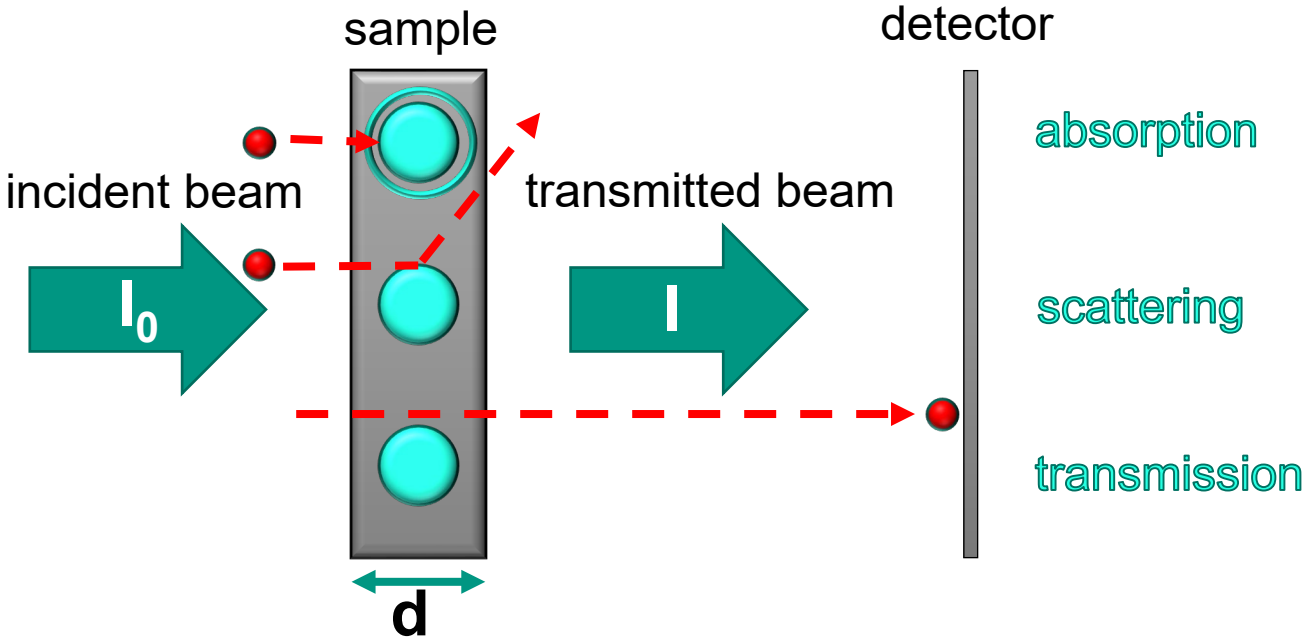

$$I = I_0 e^{-\sigma N d}$$

$$\Sigma = \sigma N$$

I: intensity
T: transmission
σ: microscopic neutron cross section
N: number density
d: sample thickness
Σ: macroscopic neutron cross section/ neutron attenuation coefficient

Theory - Neutron Imaging

PAUL SCHERRER INSTITUT

Karlsruher Institut für Technologie

X-rays

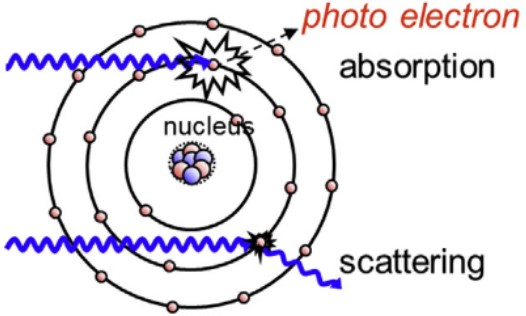

Attenuation coefficients with X-ray [cm²/g]

1a	2a	3b	4b	5b	6b	7b	8			1b	2b	3a	4a	5a	6a	7a	0
H 0.02																	He 0.02
Li 0.06	Be 0.22											B 0.28	C 0.27	N 0.11	O 0.16	F 0.14	Ne 0.17
Na 0.13	Mg 0.24											Al 0.38	Si 0.33	P 0.25	S 0.30	Cl 0.23	Ar 0.20
K 0.14	Ca 0.26	Sc 0.48	Ti 0.73	V 1.04	Cr 1.29	Mn 1.32	Fe 1.57	Co 1.78	Ni 1.96	Cu 1.97	Zn 1.64	Ga 1.42	Ge 1.33	As 1.50	Se 1.23	Br 0.90	Kr 0.73
Rb 0.47	Sr 0.86	Y 1.61	Zr 2.47	Nb 3.43	Mo 4.29	Tc 5.06	Ru 5.71	Rh 6.08	Pd 6.13	Ag 5.67	Cd 4.84	In 4.31	Sn 3.98	Sb 4.28	Te 4.06	I 3.45	Xe 2.53
Cs 1.42	Ba 2.73	La 5.04	Hf 19.70	Ta 25.47	W 30.49	Re 34.47	Os 37.92	Ir 39.01	Pt 38.61	Au 35.94	Hg 25.88	Tl 23.23	Pb 22.81	Bi 20.28	Po 20.22	At	Rn 9.77
Fr	Ra 11.80	Ac 24.47	Rf	Ha													

*Lanthanides	Ce 5.79	Pr 6.23	Nd 6.46	Pm 7.33	Sm 7.68	Eu 5.66	Gd 8.69	Tb 9.46	Dy 10.17	Ho 10.91	Er 11.70	Tm 12.49	Yb 9.32	Lu 14.07
*Actinides	Th 28.95	Pa 39.65	U 49.08	Np	Pu	Am	Cm	Bk	Vf	Es	Fm	Md	No	Lr x-ray

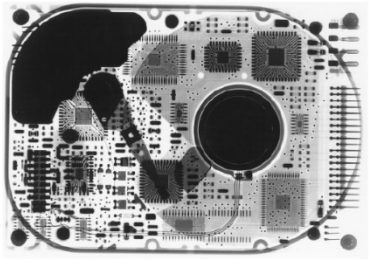

neutrons

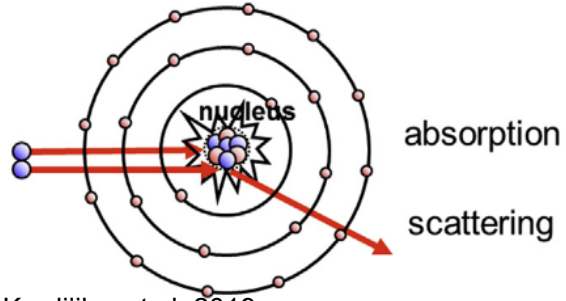

Attenuation coefficients with neutrons [cm²/g]

1a	2a	3b	4b	5b	6b	7b	8			1b	2b	3a	4a	5a	6a	7a	0
H 3.44																	He 0.02
Li 3.30	Be 0.79											B 101.60	C 0.56	N 0.43	O 0.17	F 0.20	Ne 0.10
Na 0.09	Mg 0.15											Al 0.10	Si 0.11	P 0.12	S 0.06	Cl 1.33	Ar 0.03
K 0.06	Ca 0.08	Sc 2.00	Ti 0.60	V 0.72	Cr 0.54	Mn 1.21	Fe 1.19	Co 3.92	Ni 2.05	Cu 1.07	Zn 0.35	Ga 0.49	Ge 0.47	As 0.67	Se 0.73	Br 0.24	Kr 0.61
Rb 0.08	Sr 0.14	Y 0.27	Zr 0.29	Nb 0.40	Mo 0.52	Tc 1.76	Ru 0.58	Rh 10.88	Pd 0.78	Ag 4.04	Cd 115.11	In 7.58	Sn 0.21	Sb 0.30	Te 0.25	I 0.23	Xe 0.43
Cs 0.29	Ba 0.07	La 0.52	Hf 4.99	Ta 1.49	W 1.47	Re 6.85	Os 2.24	Ir 30.46	Pt 1.46	Au 6.23	Hg 16.21	Tl 0.47	Pb 0.38	Bi 0.27	Po	At	Rn
Fr	Ra 0.34	Ac	Rf	Ha													

*Lanthanides	Ce 0.14	Pr 0.41	Nd 1.87	Pm 5.72	Sm 171.47	Eu 94.58	Gd 1479.04	Tb 0.93	Dy 32.42	Ho 2.25	Er 5.48	Tm 3.53	Yb 1.40	Lu 2.75
*Actinides	Th 0.59	Pa 8.46	U 0.82	Np 9.80	Pu 50.20	Am 2.86	Cm	Bk	Cf	Es	Fm	Md	No	Lr neut.

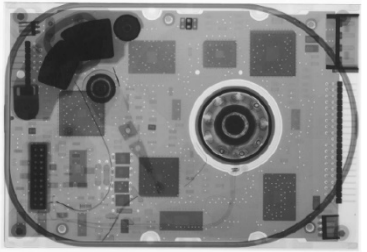

Kardijilov et al. 2019

Lehmann 2012

Theory - Neutron Imaging

attenuation coefficients

H	Fe	Cr	Zr	Sn	O
3.44	1.19	0.54	0.29	0.21	0.17

Grosse et al. 2021

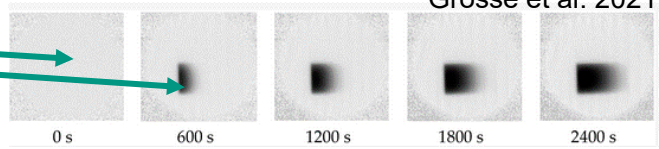

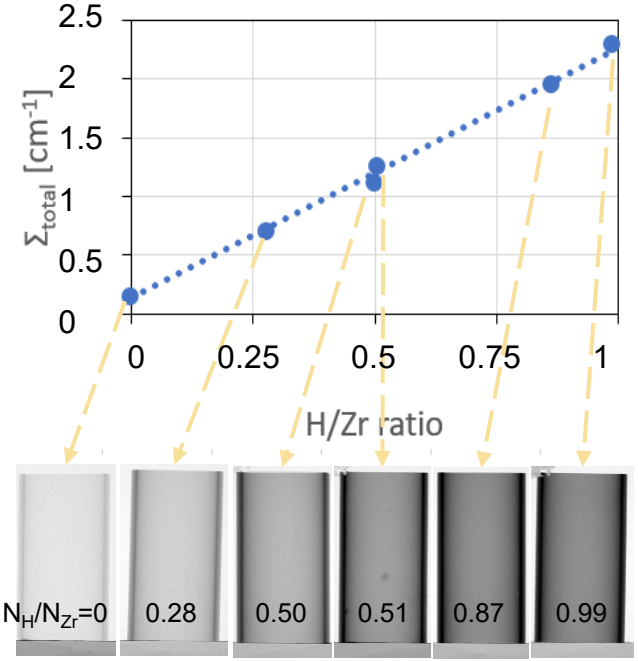

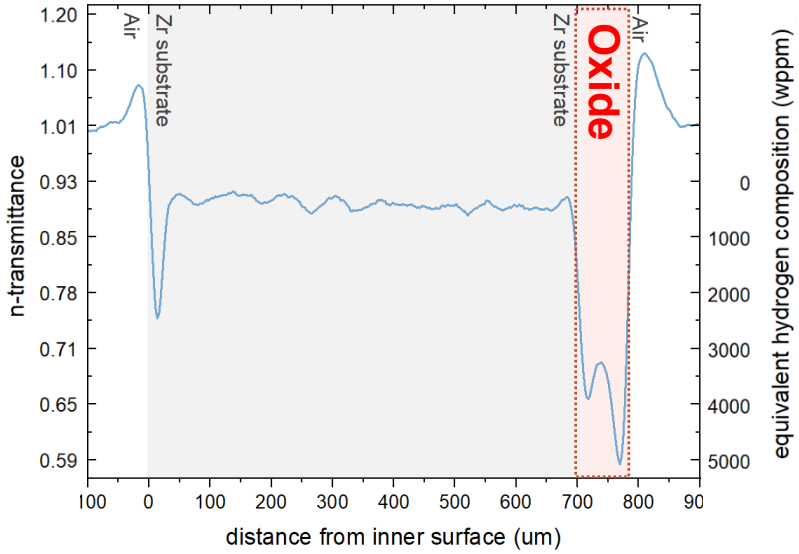

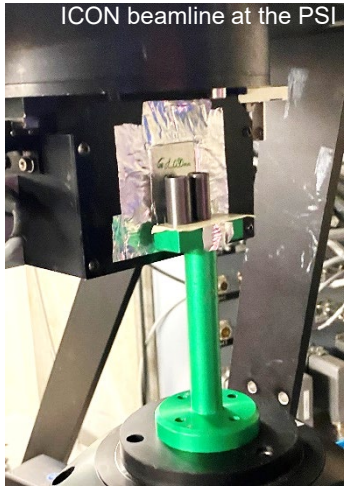

Hydrogen investigation after HT oxidation

- Breakaway in oxygen environment
- Deformations due to severe oxidation and crack formation may influence the quantification locally
- What is the reason for strong attenuation ?

→ Cracks, trapped hydrogen in cracks and/or hydrogen in the oxide layer ?

Oxygen 1000 °C 90min

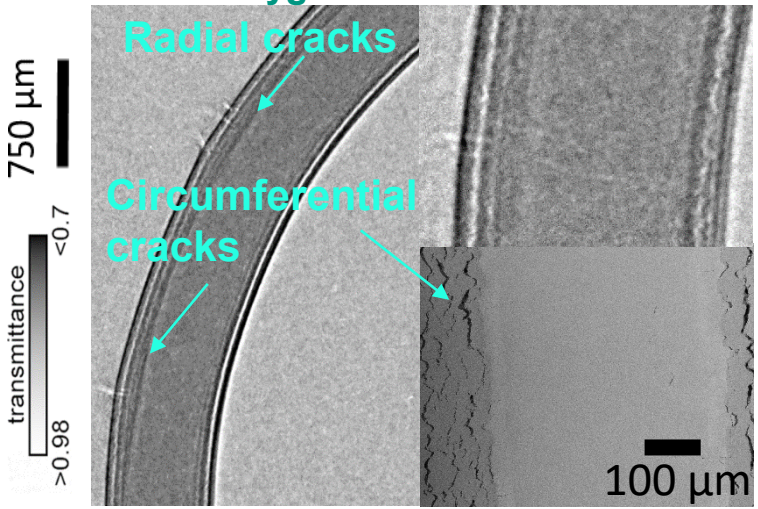

Oxygen 1100 °C 90min

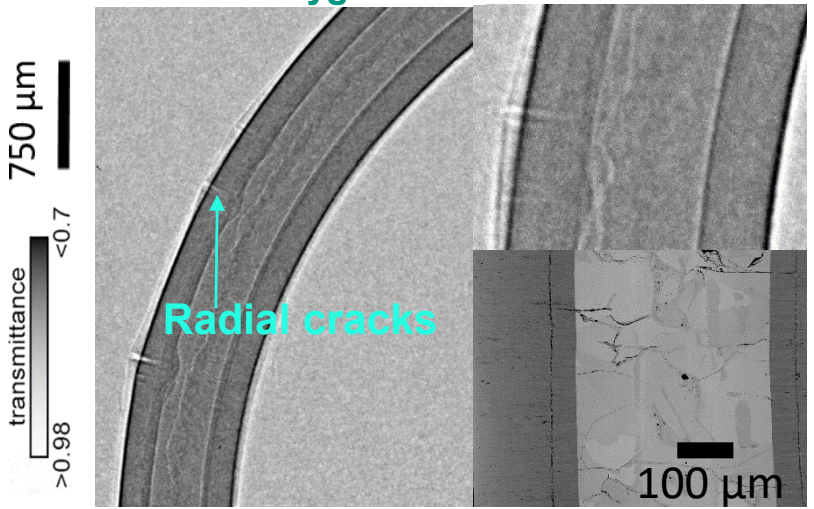

Hydrogen investigation after HT oxidation

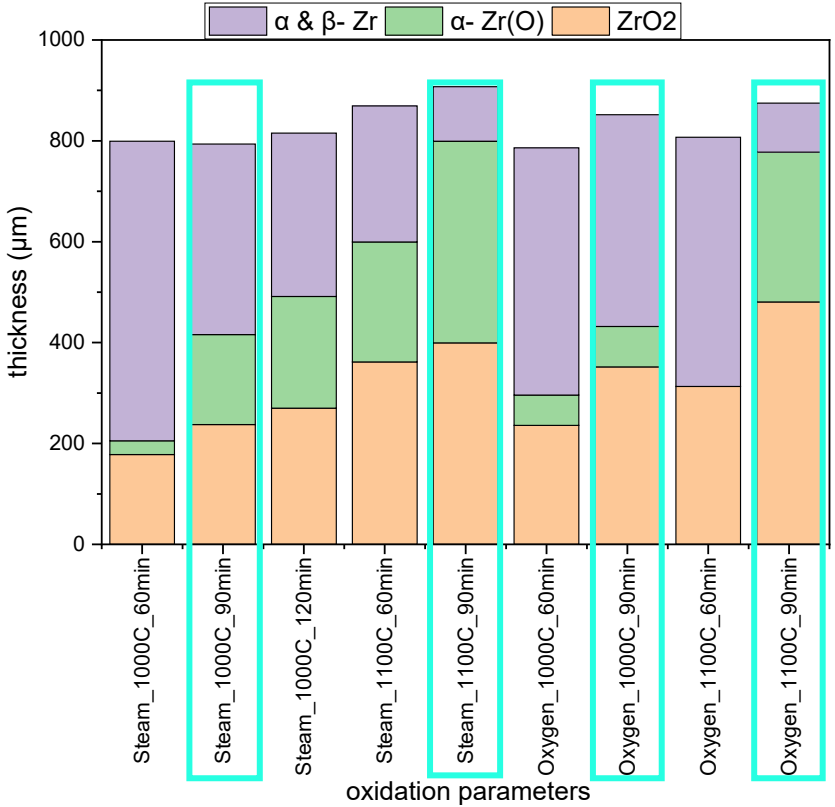

Hydrogen investigation after HT oxidation

- α- Zr(O): in steam higher attenuation than in oxygen

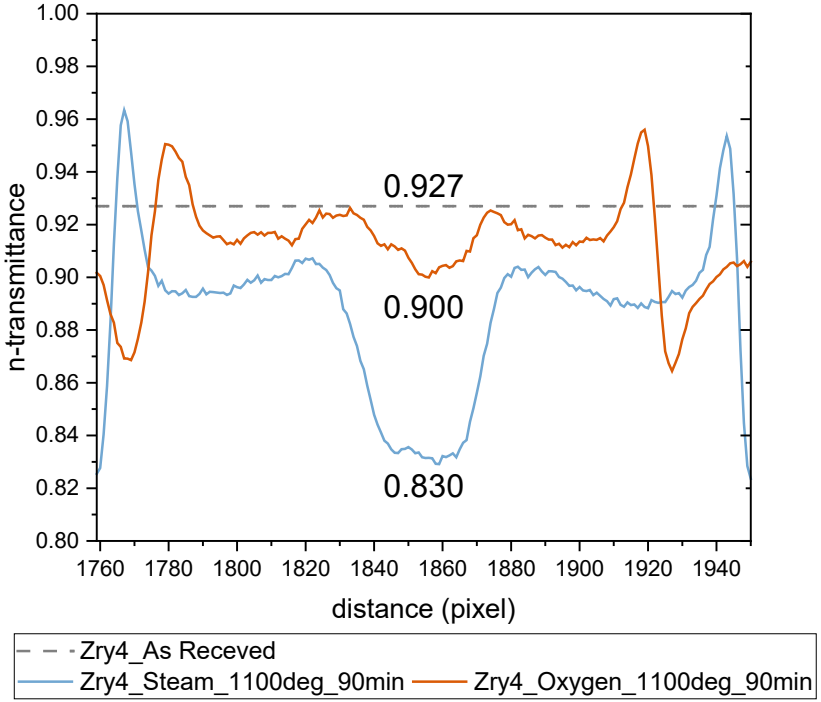

T_{Zr} = 0.927
$T_{Cr+Fe+Zr+O}$ = 0.900
$T_{Cr+Fe+Zr+O+H}$ = 0.830

$$c_H = \sim \mathbf{840\ wppm\ (0.070)}$$

Hydrogen investigation after HT oxidation

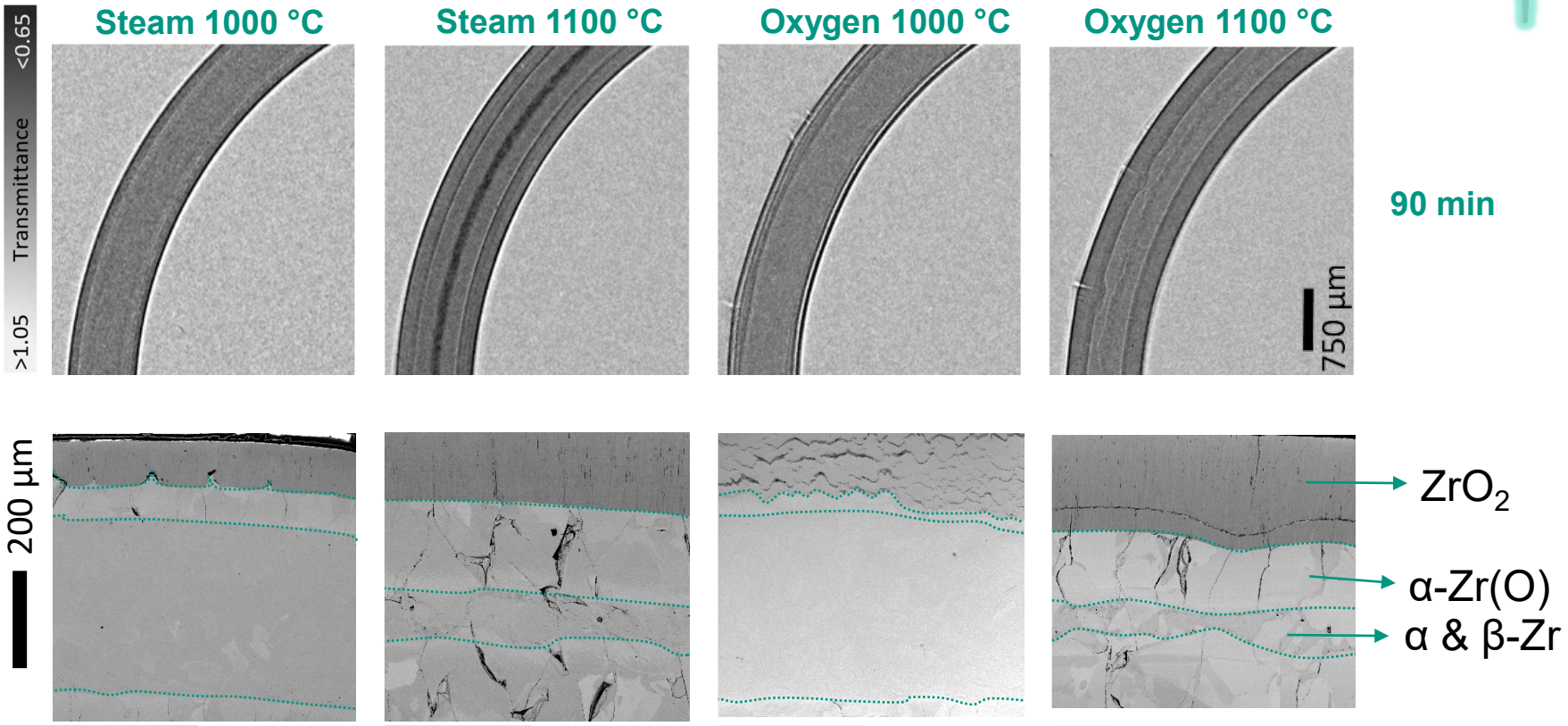

Hydrogenation – ex-situ/ in-situ

- From gas phase or with contact method
- Different diffusion velocities in *c*- and *a*-axis
- Hydrogenation in axial (*c*-axis) and/or circumferential (*a*-axis) direction
- Pre-oxidation essential

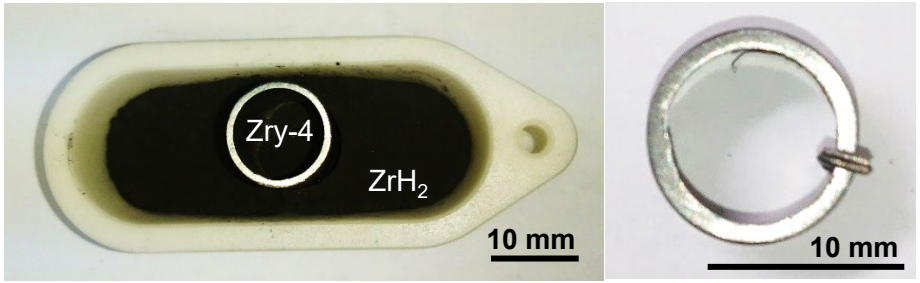

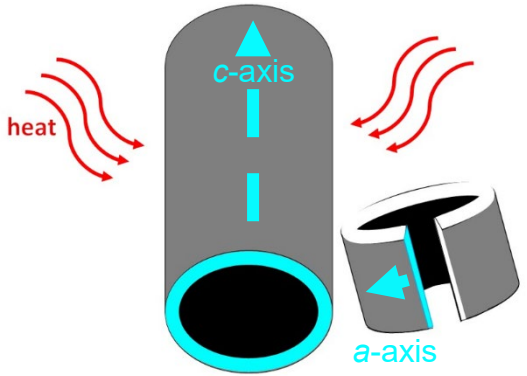

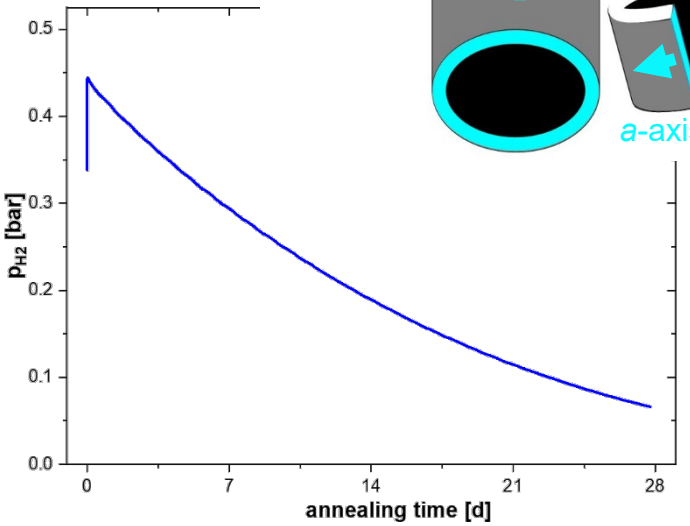

Dry Storage – NI of hydrogenated clads

- ZrH_2 powder, Ar, 400°C, 3h

$$c(x,t) = c_0\left(1 - erf\left(\frac{x}{2\sqrt{Dt}}\right)\right) + c_i$$

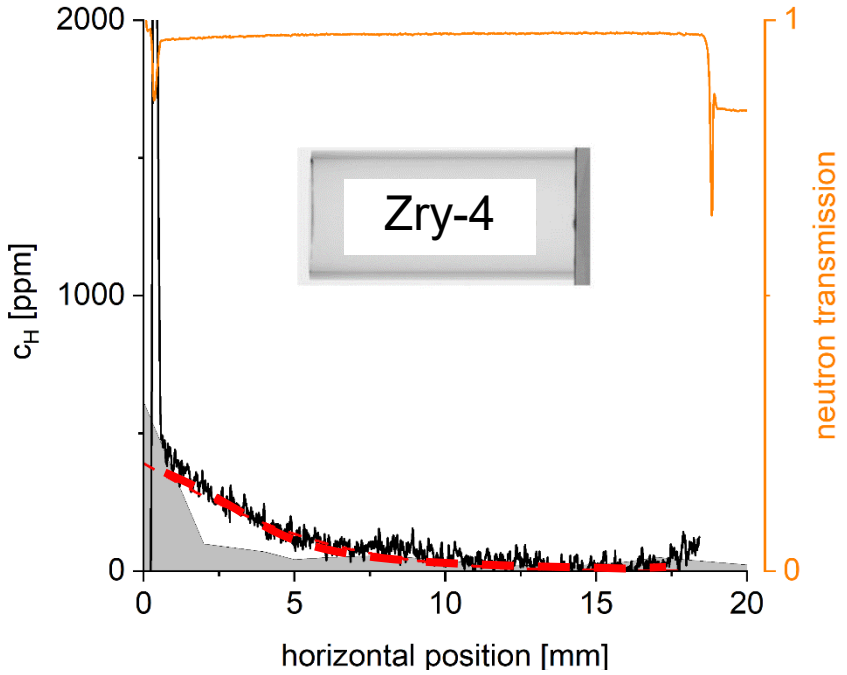

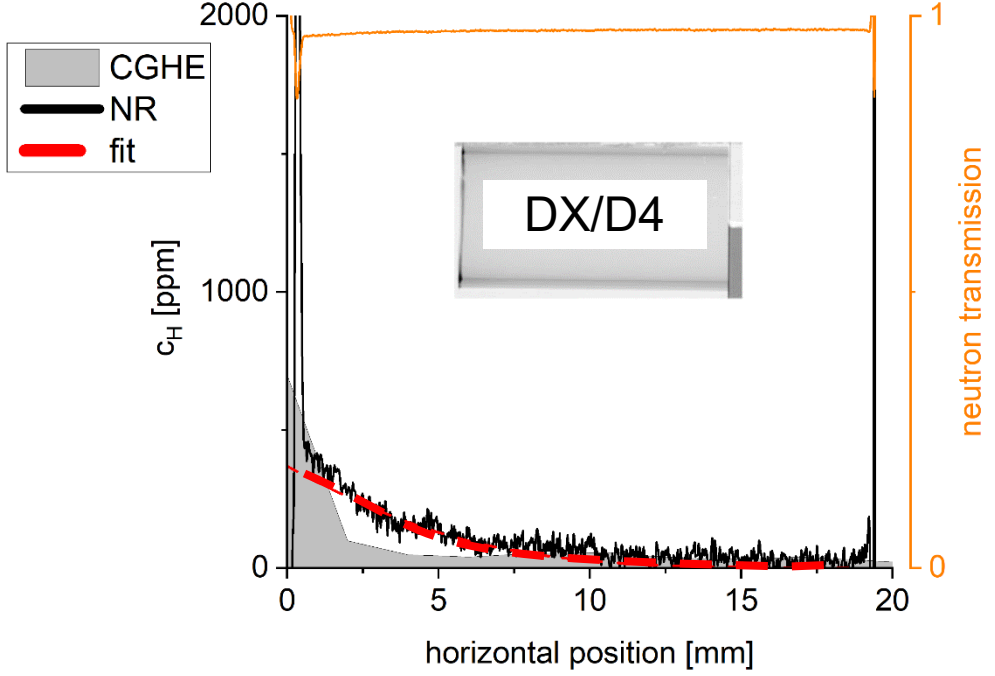

Dry Storage – NI of hydrogenated Zr

- Zr single crystals preparation and measurements:
  → XRD, grinding, NI

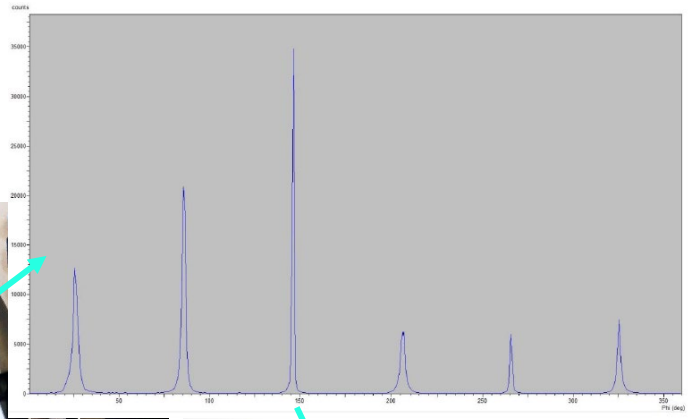

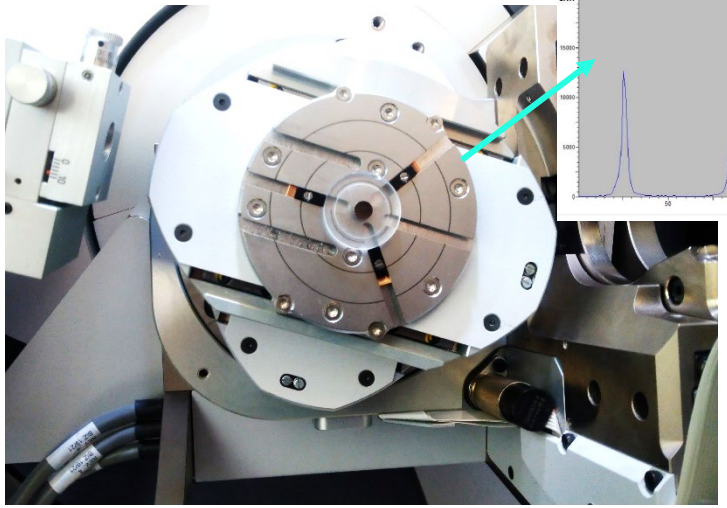

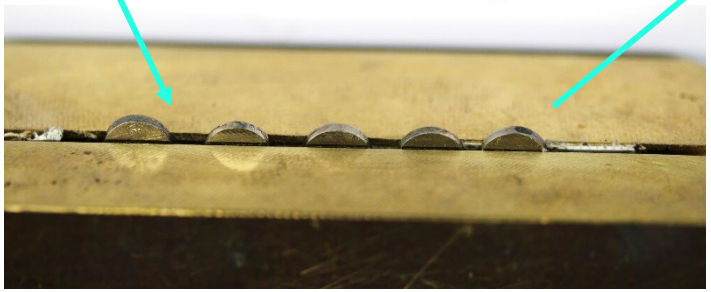

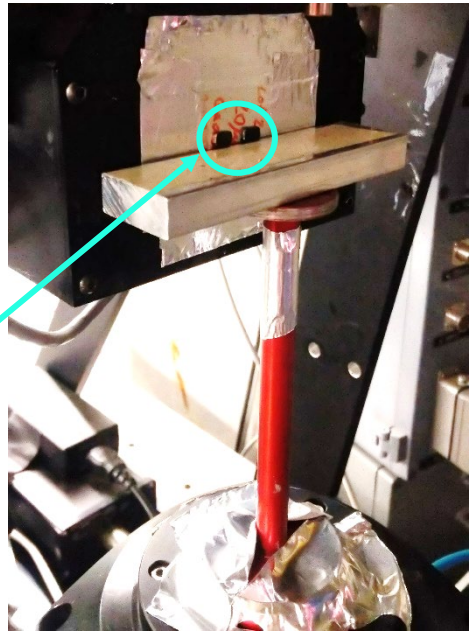

Dry Storage – NI of hydrogenated Zr

Zr single crystals, 450°C, 6h, pre-ox.

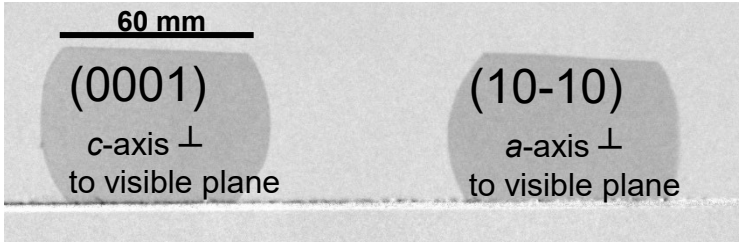

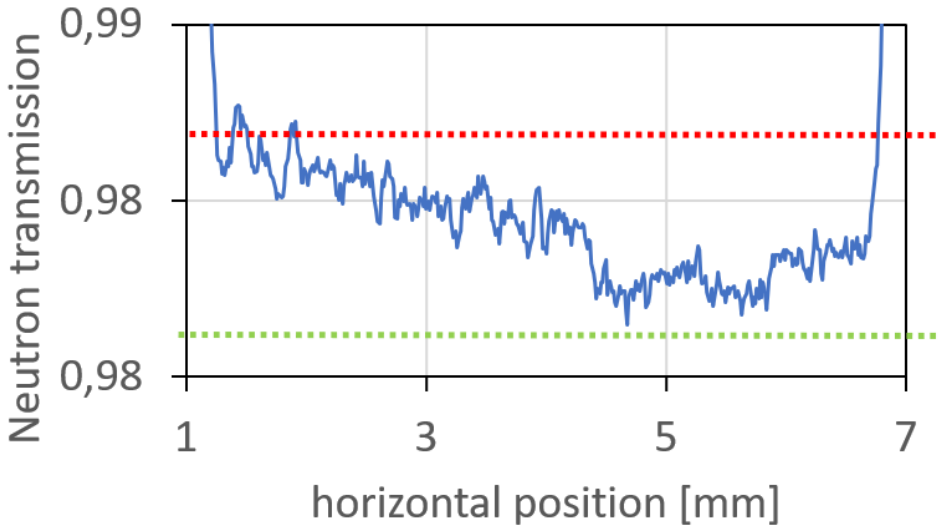

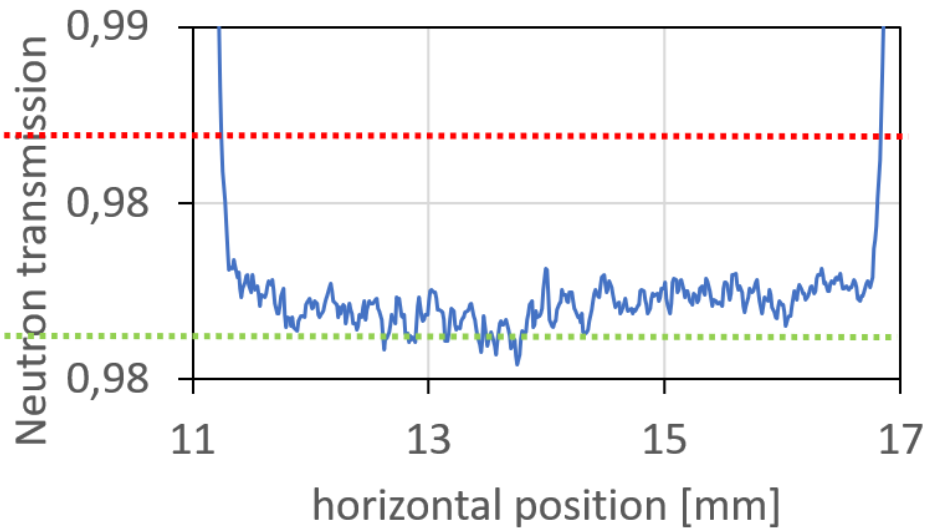

Dry Storage – NI in-situ of clads

- With hydrogenated plate (18.000 ppm H_2) or ZrH_2 powder
- Vacuum, 425°C

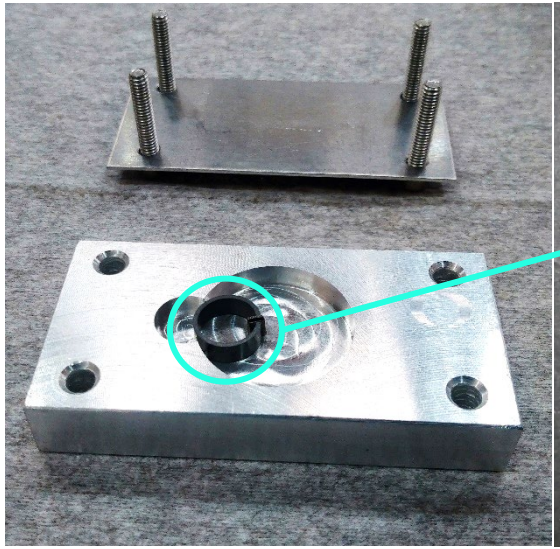

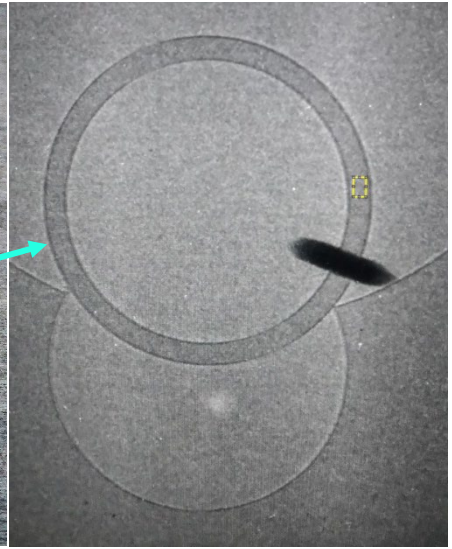

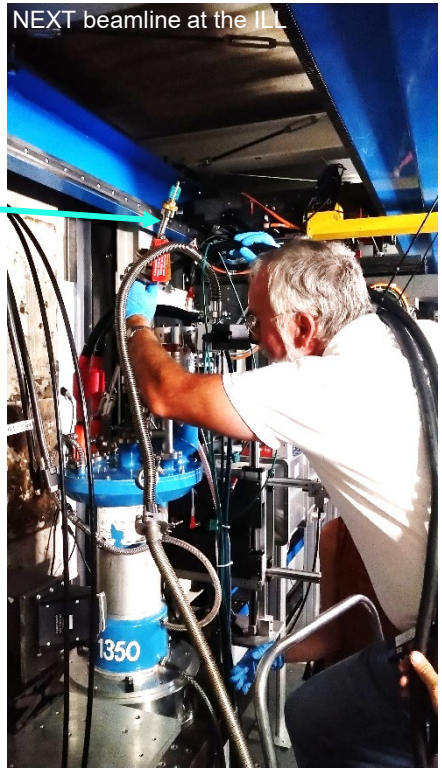

Dry Storage – NI in-situ of clads

- ZrH_2 powder, He, 450°C

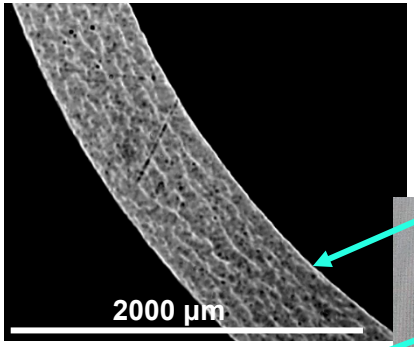

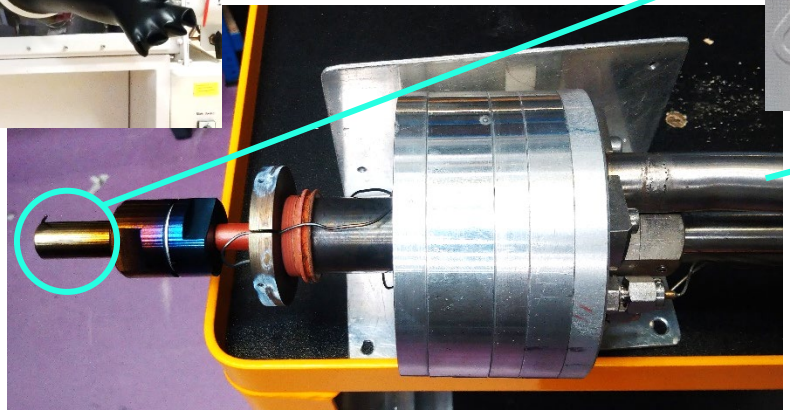

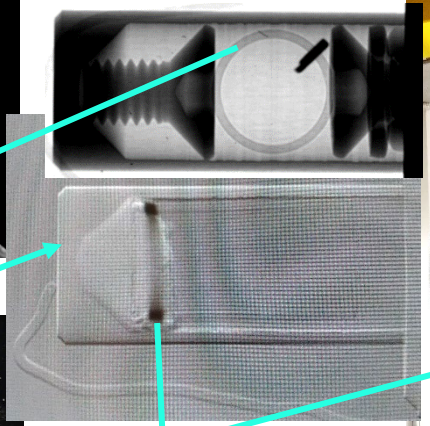

Conclusion

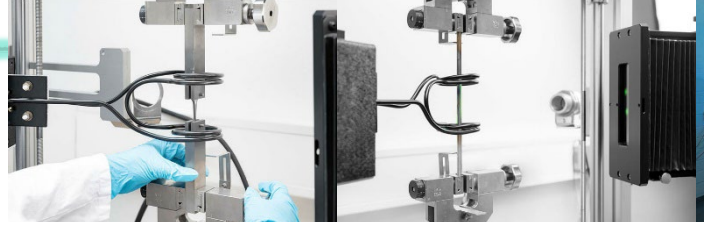

- Neutron Imaging very reliable for investigations of cladding tubes at HT oxidation and dry storage conditions

- HT oxidation

→ NI precise for Zr, ZrH_2, Fe & Cr SPPs; *NEW*: for oxides

→ ZrO_2 shows stronger attenuation than Zr metal with HR-NI; its attenuation behaviour varies with its chemistry and porosity

→ The hydrogen concentration in ZrO_2, α-Zr, and α+β-Zr varies in dependence of the oxidation parameters

→ Hydrogen concentration: ~ 280 wppm at 1100°C, ~ 160 wppm at 1000°C (high amount in α+β-Zr)

- Dry storage

→ hydrogen diffusion coefficients vary with axis direction

→ quantitative in-situ measurements possible

PAUL SCHERRER INSTITUT PSI

KIT Karlsruher Institut für Technologie

Outlook

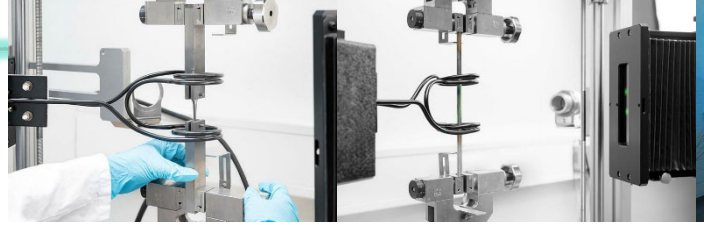

- First studies with NI → improvements and consequent measuring campaigns are already condsidered or were/will be conducted

- HT oxidation

→ same investigations with 500 & 800°C at BOA, PSI

- Dry storage

→ quantitative in-situ measurements with Zr single crystals, cladding tubes and tensile samples

PAUL SCHERRER INSTITUT PSI

KIT Karlsruher Institut für Technologie

Acknowledgements

- PSI & Matteo Busi for assistance
- ILL & Alessandro Tengattini & Ana Fredrigo for assistance
- Framatome for providing the cladding tubes
- The SPIZWURZ project (FKZ 1501609B) is funded by the Federal Ministry for the Environment, Nature Conservation, Nuclear Safety and Consumer Protection (BMUV)

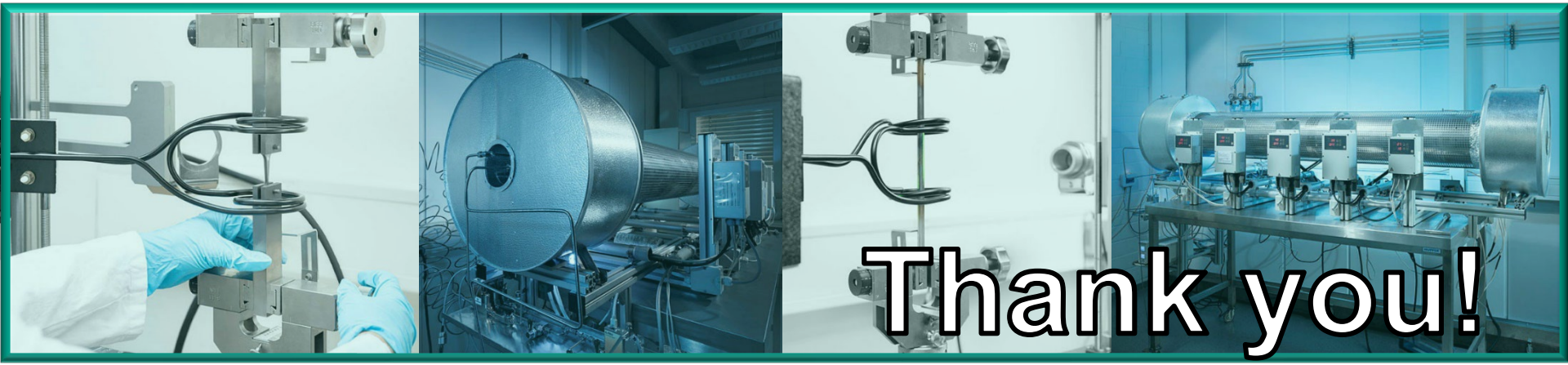

Y. Lee

SNU

Structural integrity of hydrided Zircaloy and its implications for safety extended dry storage

Difficulty to characterize reactor-grade Cold Work Stress Relieved (CWSR) Zircaloy with EBSD has hampered the direct observation of many of the mesoscale characteristics of Zirconium hydrides crucial to understanding the behavior of hydrided Zircaloy, including but not limited to, hydride precipitation, hydride-induced embrittlement, and hydride reorientation. This talk presents successful EBSD characterization of hydrided CWSR Zircaloy, and demonstrates how it advances the current understanding and gross assumptions of hydrided Zircaloy. The EBSD characterization reveals incoherent interface of hydride and reactor-grade Zircaloy matrix for both circumferential and radial hydrides. This implies a similar level of misfit strains for circumferential and radial hydrides, if any, the difference primarily arises from different shapes of circumferential and radial hydrides. The observed parameters were used as inputs to hydride reorientation model development. The developed hydride reorientation model gives a good agreement with experimental data. Ring Compression Tests (RCTs) show that Radial Hydride Fraction (RHF) is found to be an effective correlating factor for Strain Energy Density (SED) of hydrided Zircaloy when it is greater than 5%. SED is strongly correlated to the inverse of the maximum radial hydride length for all tested cases, demonstrating that radial hydrides serve as the pre-existing crack for material fracture in terms of fracture mechanics.

Structural integrity of hydrided Zircaloy and its implications for safety extended dry storage

2023. 12. 5.

Youho Lee*, Dahyeon Woo, Changhyun Jo, Chansoo Lee, Wei Chen Low
Donghyun Son

Department of Nuclear Engineering, Seoul National University, Korea

*leeyouho@snu.ac.kr

Table of Contents

1. Microstructure characterization of hydrided Zircaloy

EBSD characterization of reactor-grade CWSR Zircaloy

- **Challenges of hydrided CWSR Zircaloy characterization using EBSD**
  - TEM – There are some past studies, but TEM cannot provide statistical information.
  - EBSD – Difficult to get results from reactor-grade (CWSR) cladding tube.

Journal of Microscopy

Journal of Microscopy, Vol. 272, Issue 1 2018, pp. 25–34 doi: 10.1111/jmi.12729
Received 17 December 2017; accepted 4 June 2018

The challenge of acquiring a satisfactory EBSD result of CWSR Zircaloy-4 cladding tube

K.-C. LAN*, W. ZHONG*, P.A. MOUCHE*, H.-M. TUNG†, H. LEE*, B.J. HEUSER* & J.F. STUBBINS*
*Department of Nuclear, Plasma, and Radiological Engineering, University of Illinois at Urbana-Champaign, Urbana, Illinois, U.S.A.
†Nuclear Fuels and Materials Division, Institute of Nuclear Energy Research, Longtan, Taoyuan, Taiwan, ROC

- **Exploring the micro-structure of hydrided reactor-grade CWSR Zircaloy via EBSD**

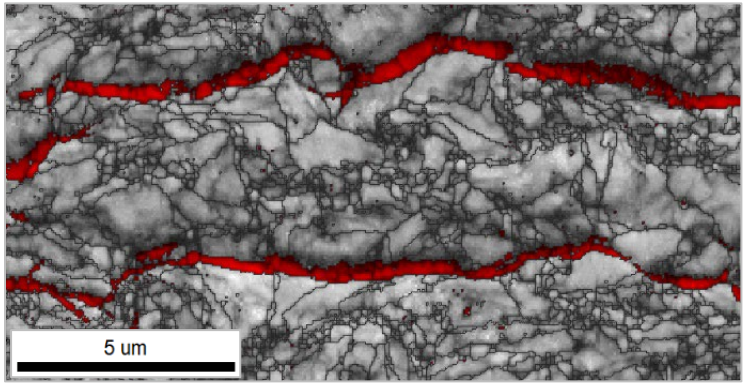

<Successful EBSD characterization of hydrides in SNU>

'It opens a new avenue to advance the current understanding and modeling of hydrided Zircaloy'

Simplified vs real hydride-Zircaloy interface

- **Simplified radial basal pole texture**

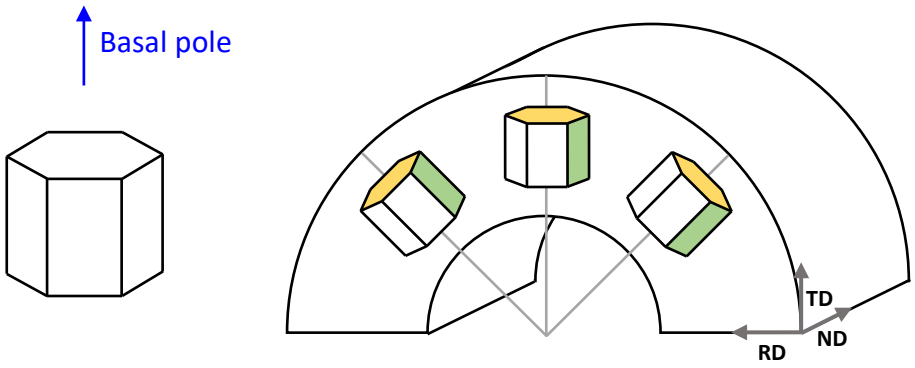

- **Ideal pole figure**

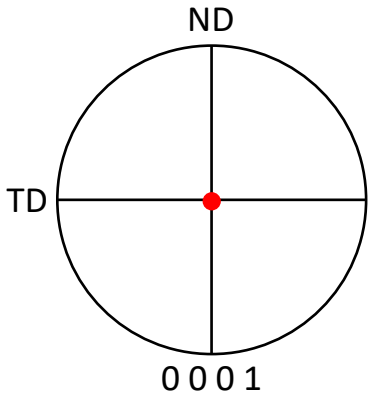

- **Real radial texture of basal pole**

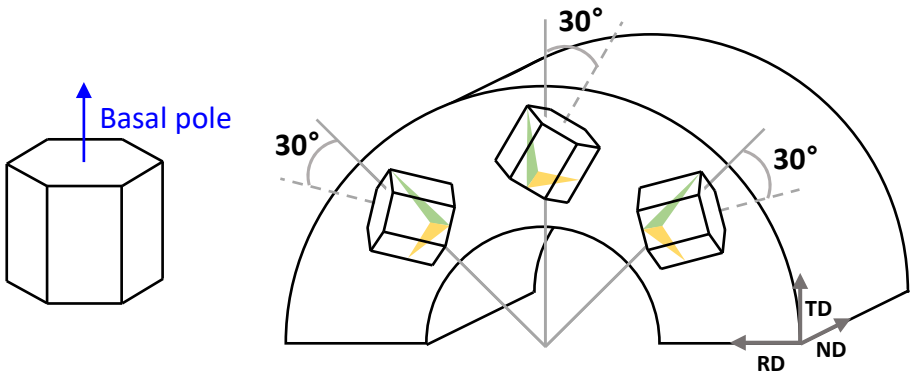

- **Real pole figure**

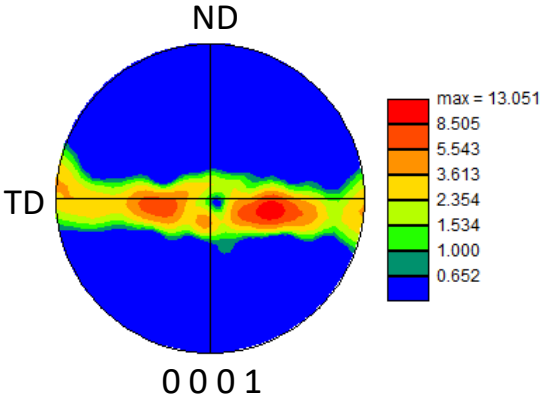

- Theoretically, it was considered that circumferential hydride precipitates at basal plane and radial hydride precipitates at the prismatic plane.[5]

[5] W. Qin, J.A. Szpunar, J. Kozinski, Hydride-induced degradation of hoop ductility in textured zirconium-alloy tubes: A theoretical analysis, Acta Mater. 60 (2012) 4845–4855.

Hydride-reorientation experiment in detail

- **Experimental conditions**

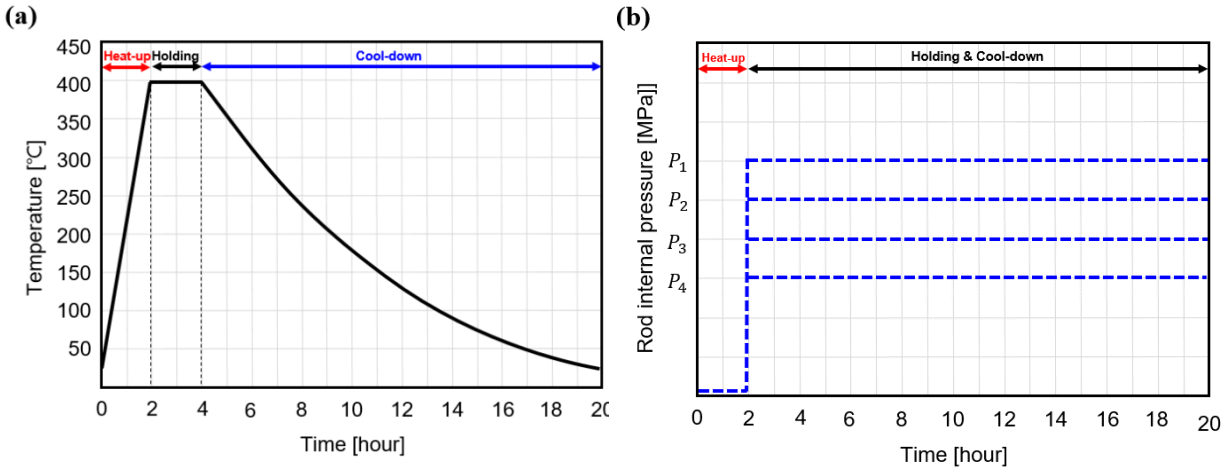

<Applied temperature and pressure profile>

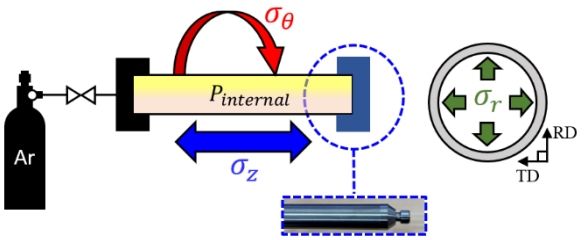

<Multi-axial Stress state of internally pressurized cladding>

- **Hydride reorientation experiment facility**

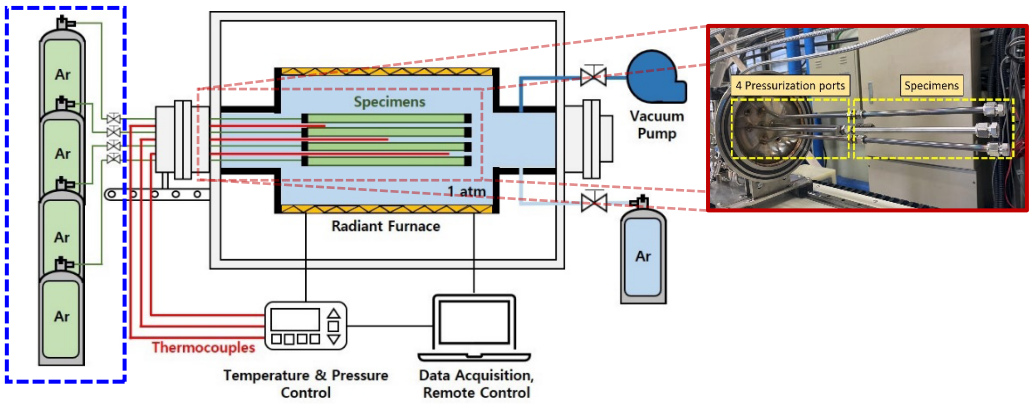

<Multi-axial stress test facility>

- Reactor-grade Zr-Nb1% cladding (CWSR and unirradiated) was used.
- The furnace was filled with Ar gas of 1 atm during pressurization.
- Radial hydrides were precipitated during the cool-down process.

EBSD Analysis of hydride in reactor-grade (CWSR) Zriconium

<EBSD Image quality map>

- **0 MPa / Circumferential hydrides (216 wppm)**

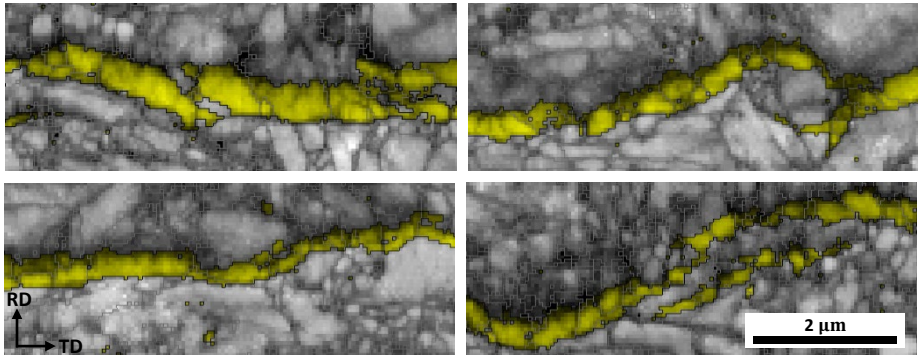

- **11 MPa / Radial hydrides (216 wppm)**

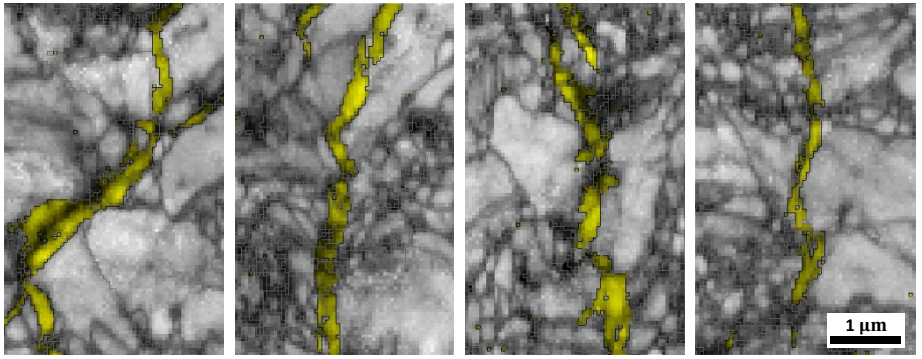

- **14 MPa / Radial hydrides (201 wppm)**

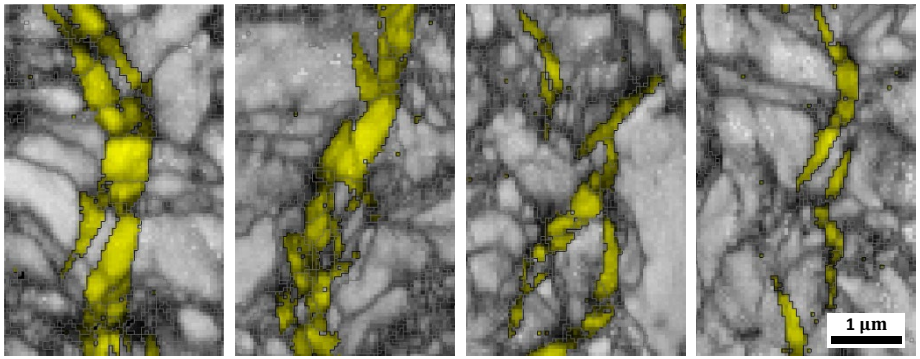

- **18 MPa / Radial hydrides (211 wppm)**

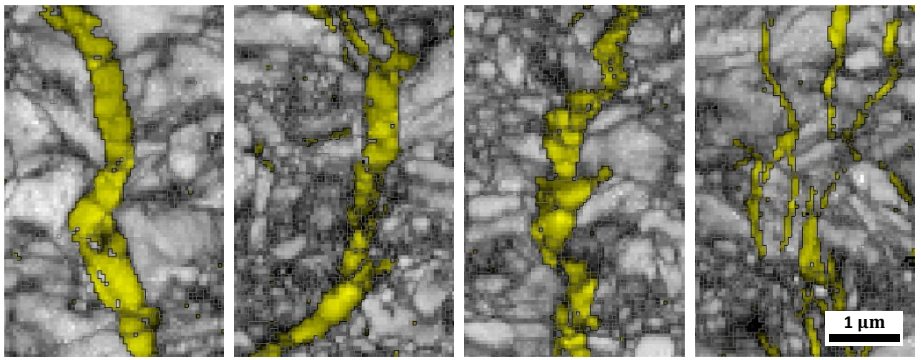

- To exclude the effect of the undissolved circumferential hydride on the precipitation of the radial hydride, specimens with low H concentration (~200 wppm) were prepared.

EBSD Analysis of hydride in reactor-grade (CWSR) Zircaloy

- **Quantification of interface: 5 Degrees of freedom**

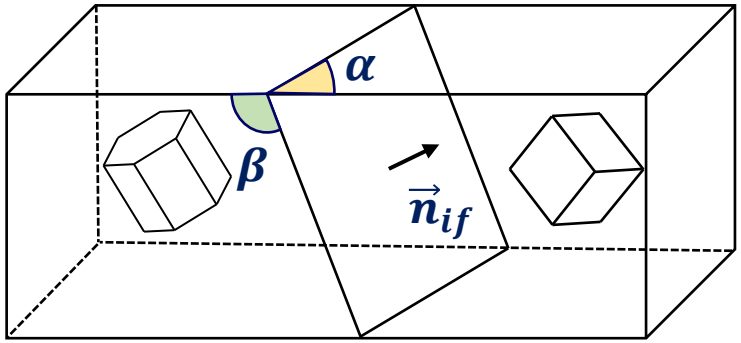

1. Orientation Relationship (3 degrees of freedom)

① OR1 (Euler angles of crystal)
② OR2 (Euler angles of crystal)
③ Misorientation axis/angle

[Burgers orientation relationship]
Attainable via typical EBSD

2. Interface information (5 degrees of freedom)

①, ②, ③ +
④ α …… attainable with typical EBSD
⑤ β …… The root of the matter
(Serial sectioning or stereological method)

or $\vec{n}_{if}$

- **Axially parallel grains + prevailing Intergranular hydrides due to pilgering allows 3D interface quantification using 2D EBSD result for reactor-grade Zircaloy ($\beta \approx 90^o$)**

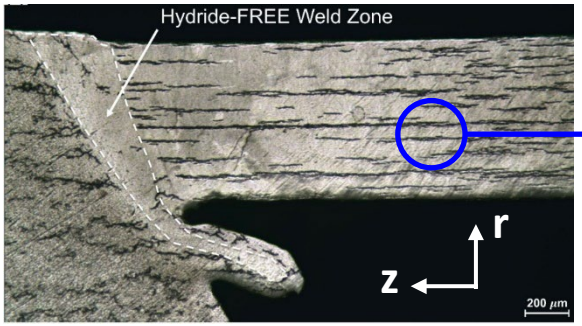

Axially parallel grain boundaries and intergranular hydride interface

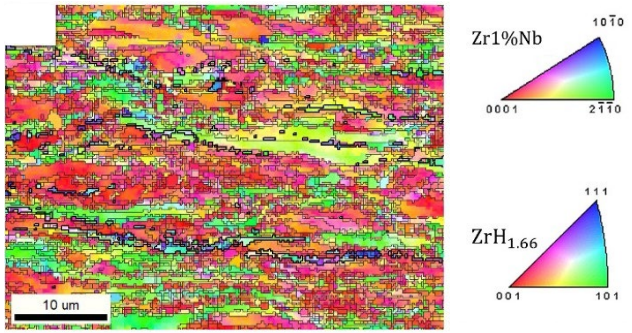

Construction of 3D Interface data using 2D EBSD

- **Phase boundary reconstruction**

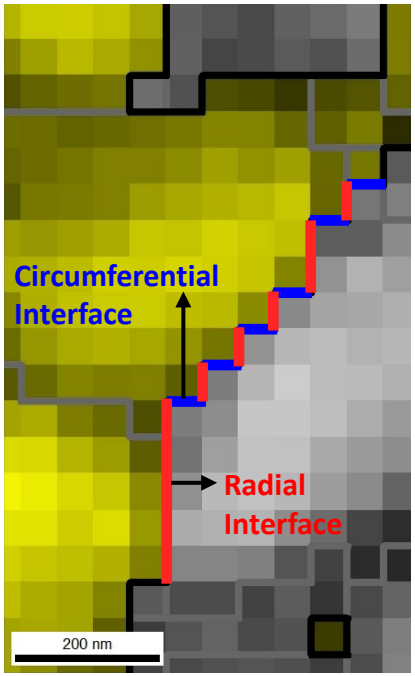

<Pixel based interface>

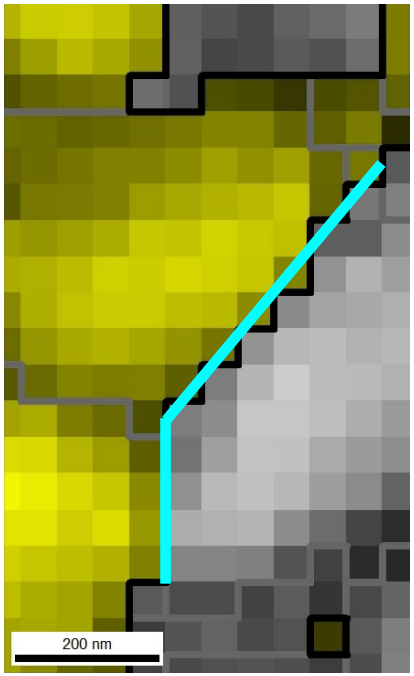

<Boundary reconstruction>

- **Axial interface detection via FIB/SEM**

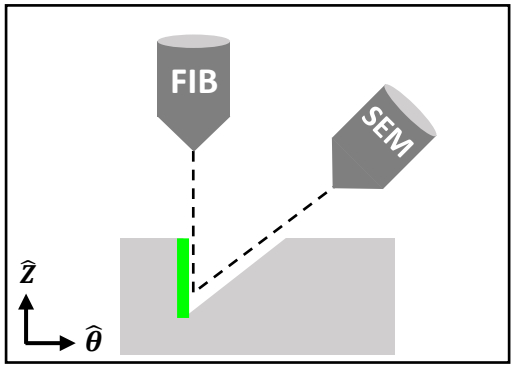

<FIB/SEM cross-beam angle configuration>

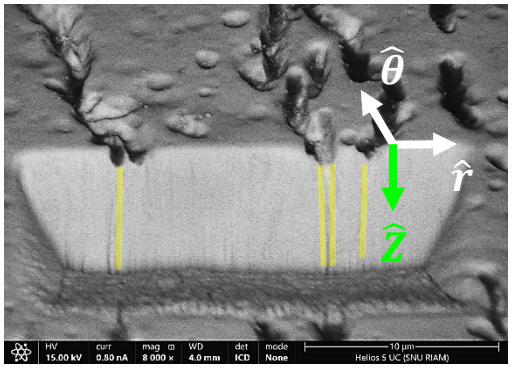

<SEM Image>

- **Total analyzed interface length**

	0 MPa	11 MPa	14 MPa	18 MPa
Interface length	137.62 μm	60.4 μm	96.66 μm	81.82 μm

Additional consideration of grain orientation

- **Defining the orientation of interface**

	0° Tilted basal pole	90° Tilted basal pole
Basal plane (0° from basal plane)	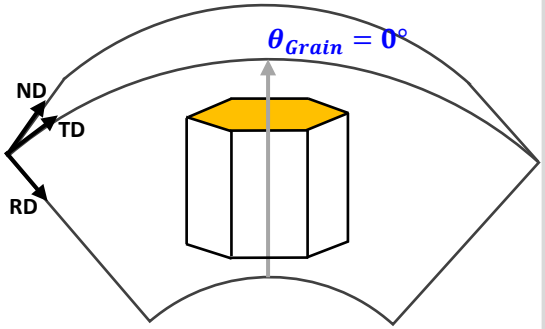 Circumferential interface	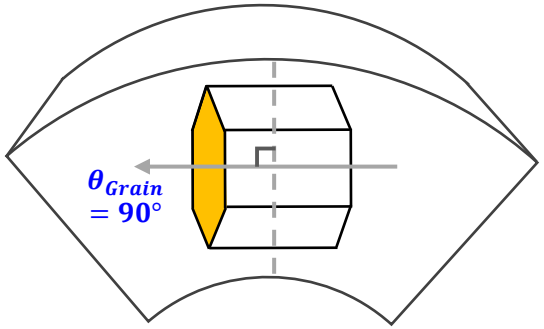 Radial interface
Prismatic plane (90° from basal plane)	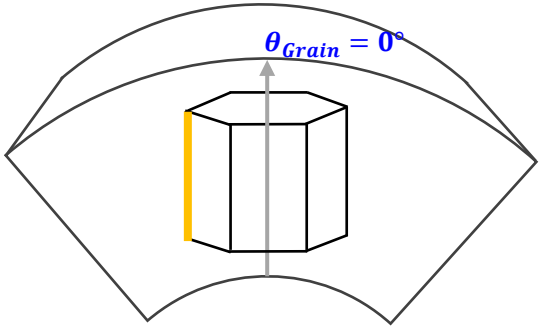 Radial interface	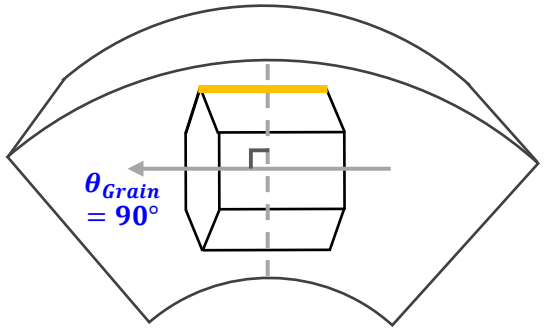 Circumferential interface

- While exhibiting the same interface plane, each interface is available to result in the different orientation (radial / circumferential) of the hydride according to the tilted angle of Zirconium.

Hydride orientation with two angles

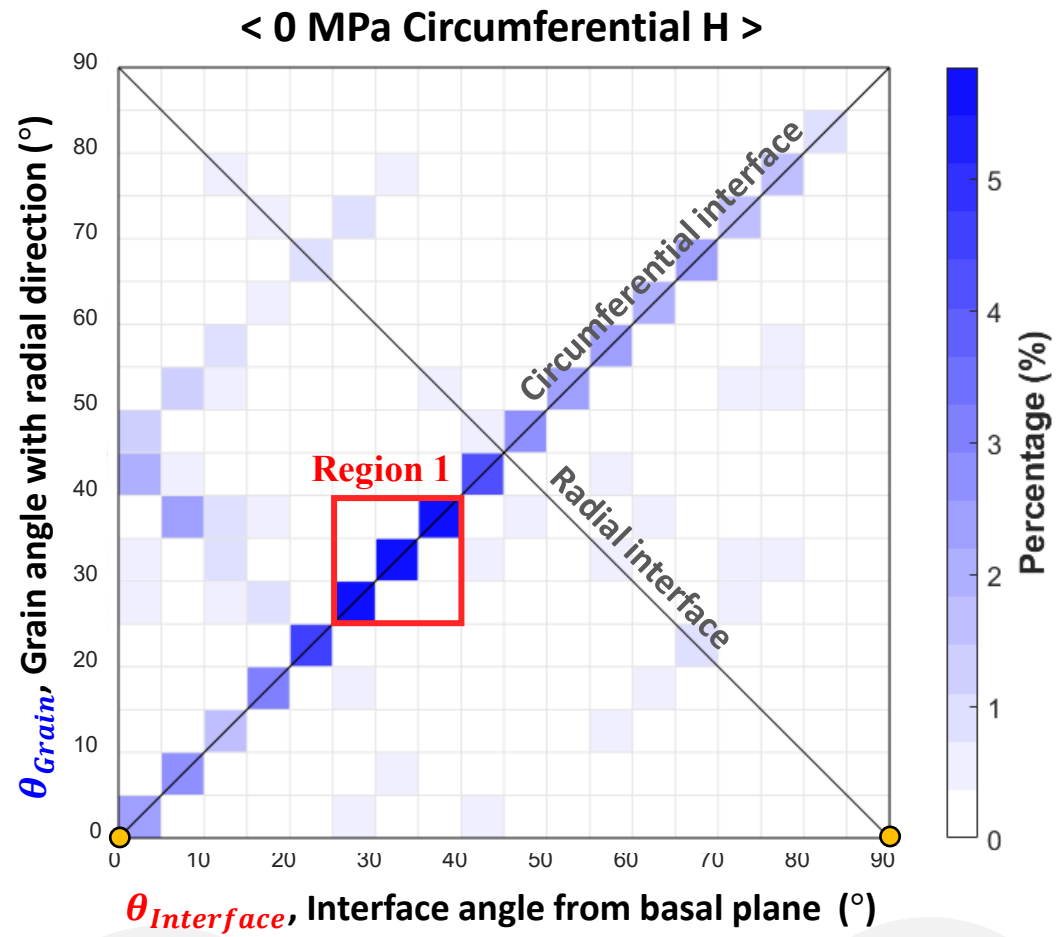

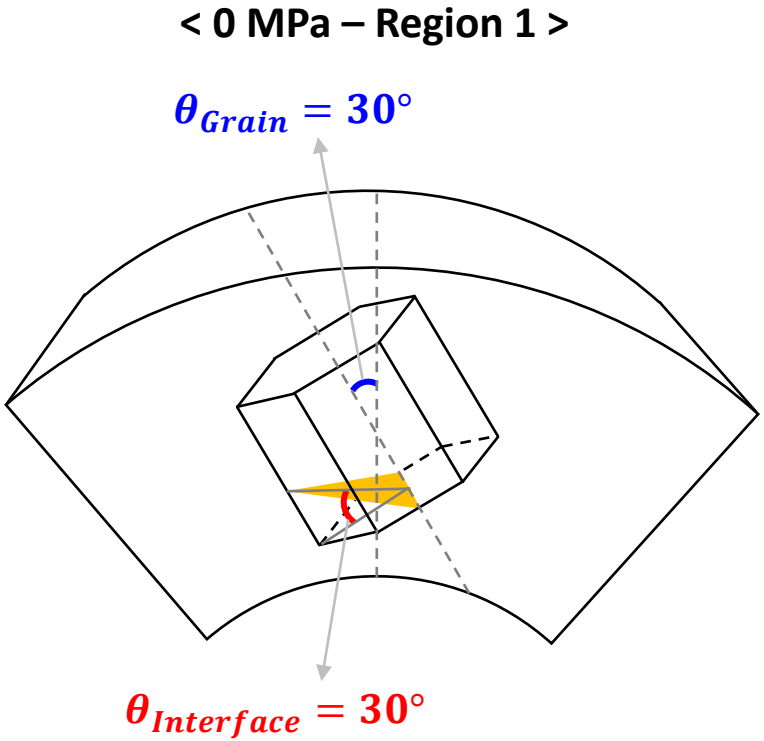

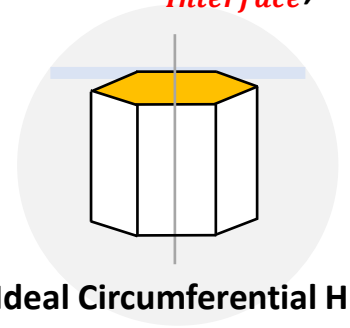
Ideal Circumferential H

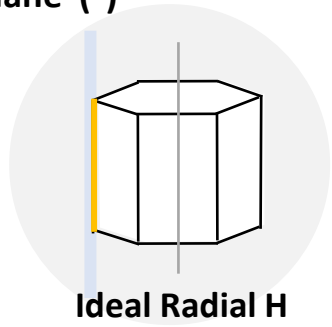
Ideal Radial H

Hydride orientation with two angles

< 0 MPa Circumferential H >

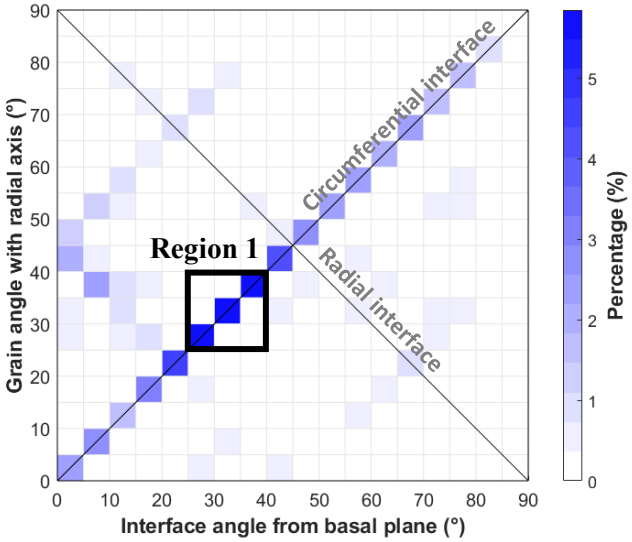

< 11 MPa Radial H >

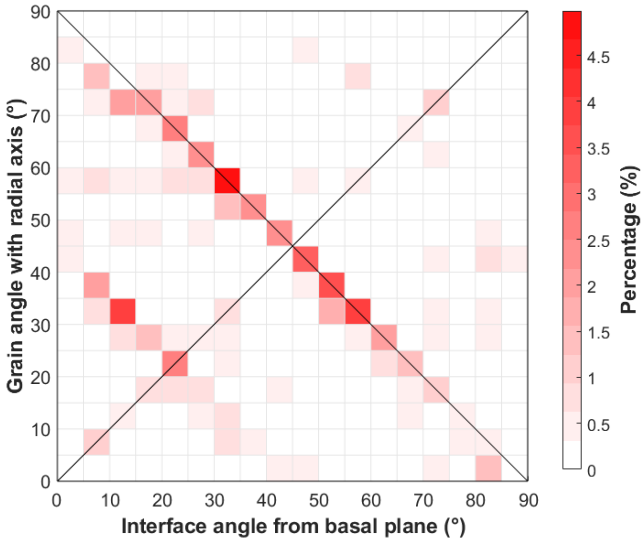

< 0 MPa – Region 1 >

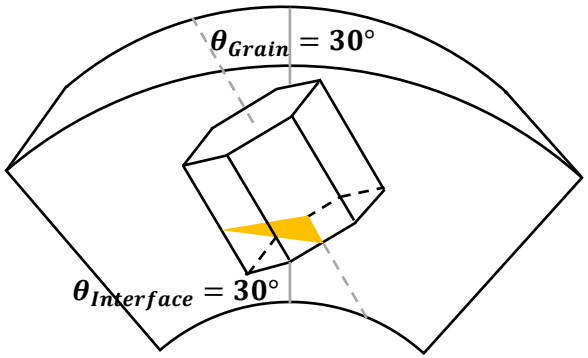

< 14 MPa Radial H >

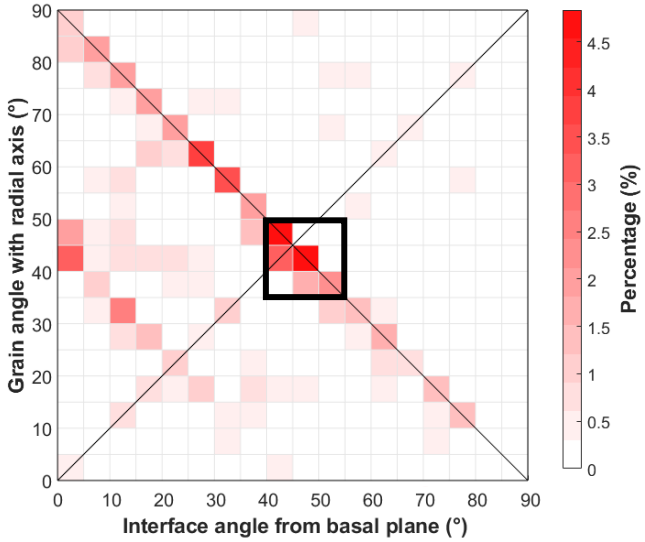

< 18 MPa Radial H >

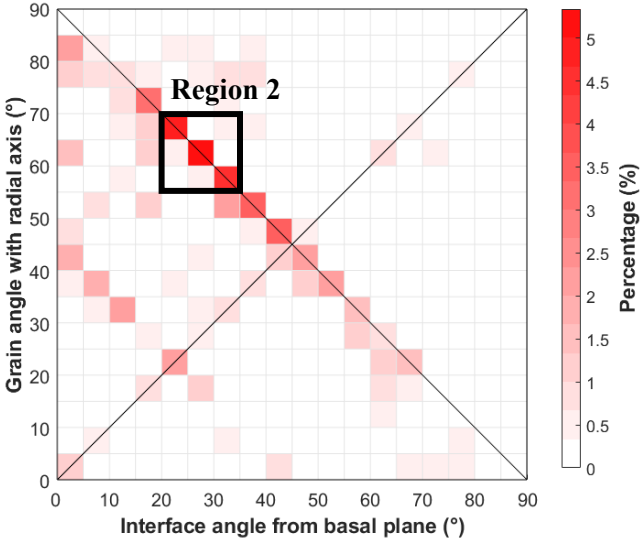

< 18 MPa – Region 2 >

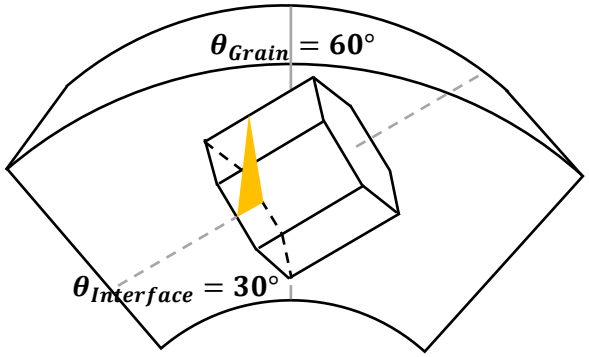

Hydride orientation with two angles

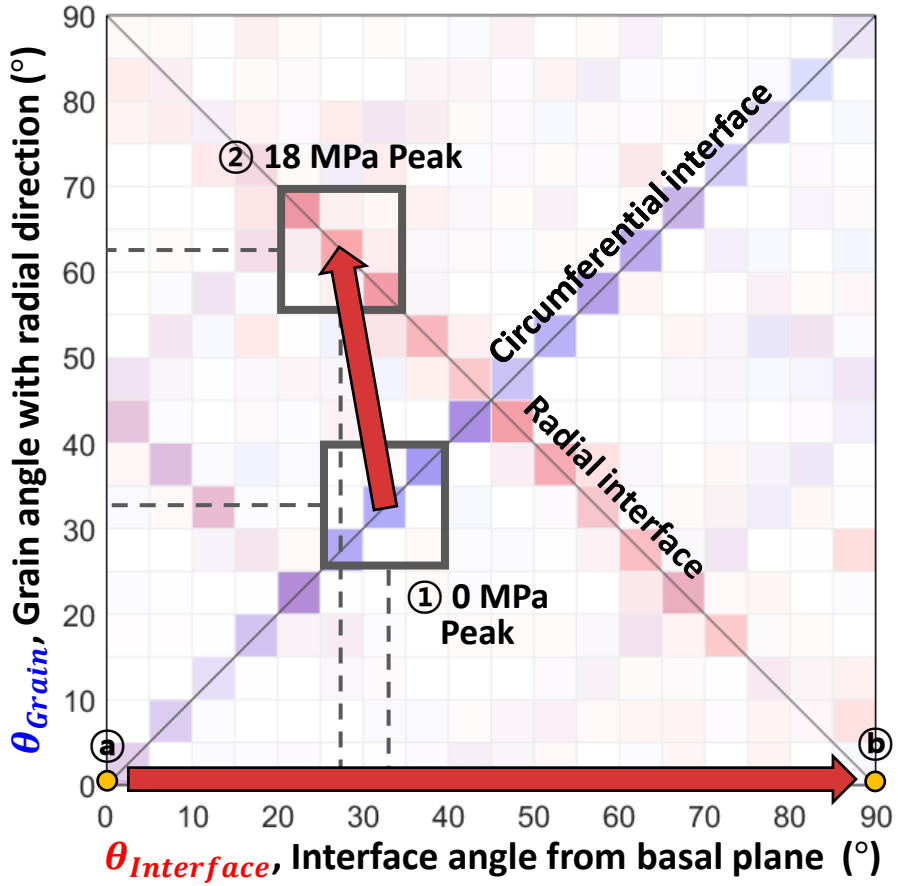

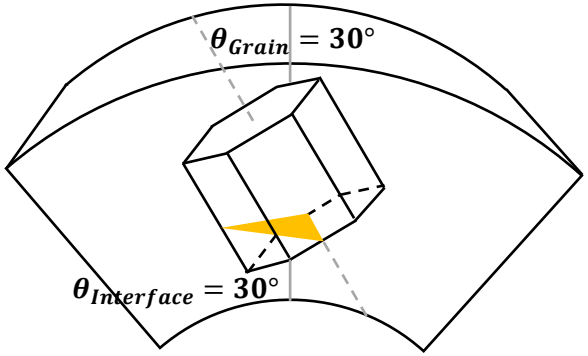

① Real Circumferential H

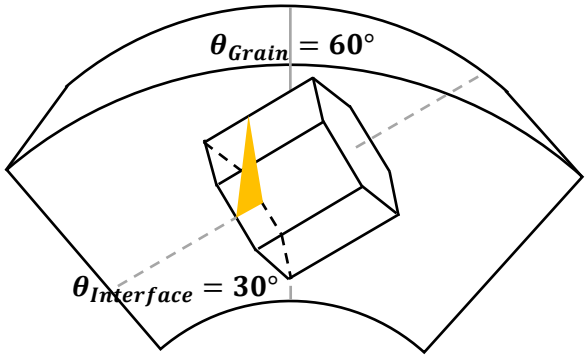

② Real Radial H

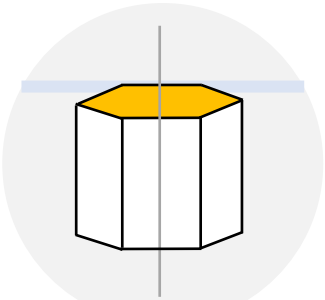

ⓐ Ideal Circumferential H

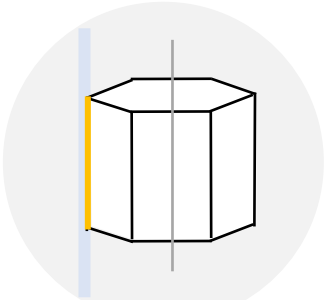

ⓑ Ideal Radial H

Texture of Zr matrix with hydride precipitation

- **Grains with hydride precipitation**

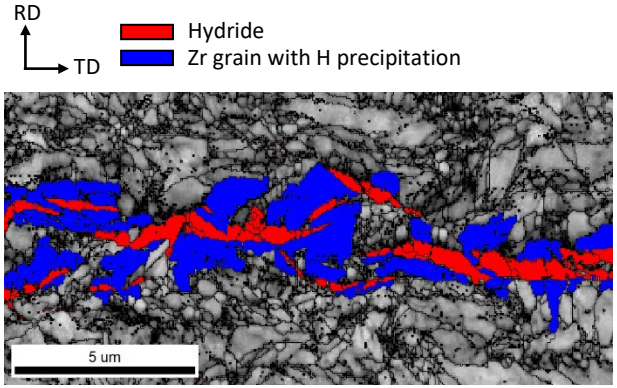

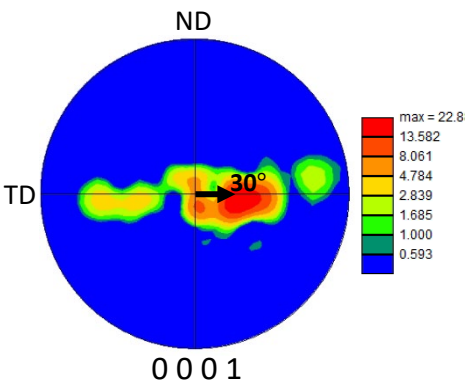

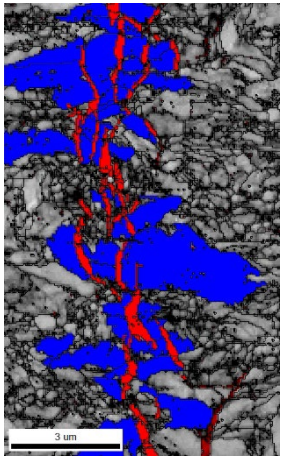

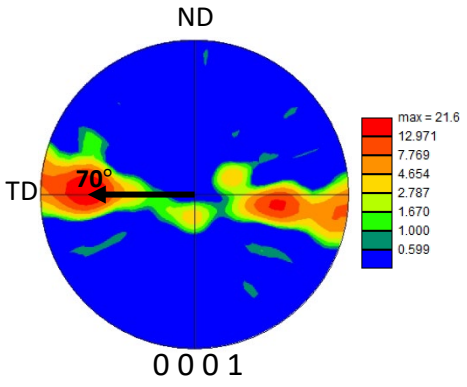

< 0 MPa Circumferential H > **< 18 MPa Radial H >**

- **Circumferential hydride:** precipitates at most common grains (statistically favorable) which have ±30° tilted radial basal pole.

- **Radial hydride (under hoop stress):** picks up the grains which contain appreciable radial grain boundaries. Grains which have ±60-70° tilted radial basal pole were found to contain appreciable extent of radial grain boundaries.

- **Modeling Implications:** Limited difference in misfit strain between circumferential and radial hydrides (if any, it's primarily due to the shape of hydrides) . Hydride segregation at the radial grain boundary under hoop stress is the key driving mechanism for hydride reorientation .

Hydride (FCC) Interface analysis result

- **Total analyzed hydride interfaces**

< 0 MPa Circumferential H>

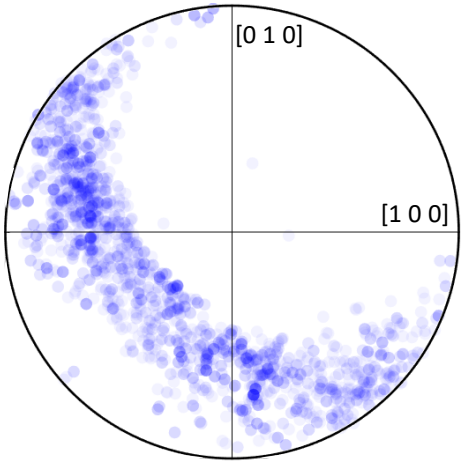

< 18 MPa Radial H >

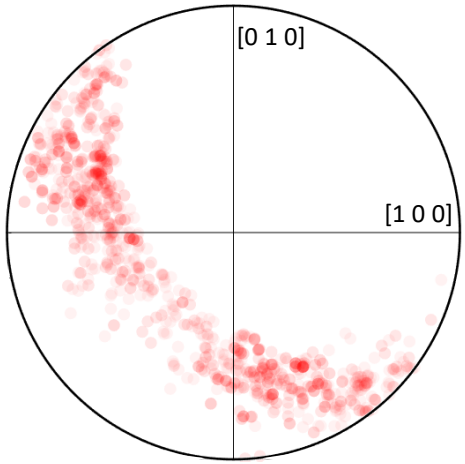

- **Hydride interface at most probable HCP interace region**

< 0 MPa Circumferential H (Region 1)>

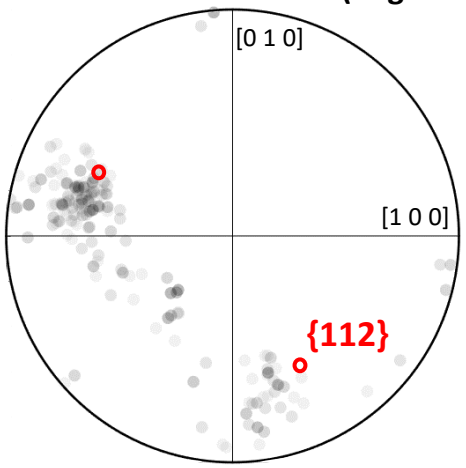

< 18 MPa Radial H (Region 2)>

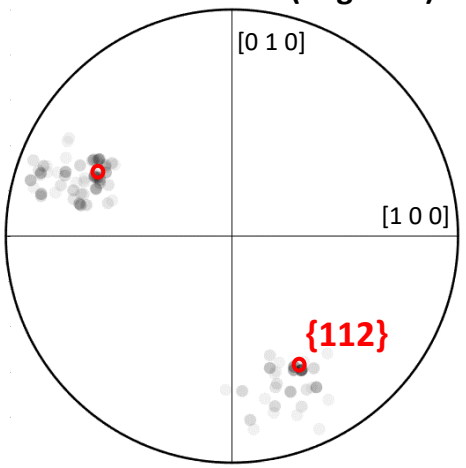

- Both circumferential and radial hydride exhibited specific preference in FCC crystal. It was stronger at radial hydride , and the preferential site was around {112} family.

Orientation relationship and interface determination via TEM

- **0 MPa Circumferential H**
  - ✓ OR: $[1\bar{2}10]//[110]$ & $(0001)//(111)$ & Interface: $(10\bar{1}3)//(110)$

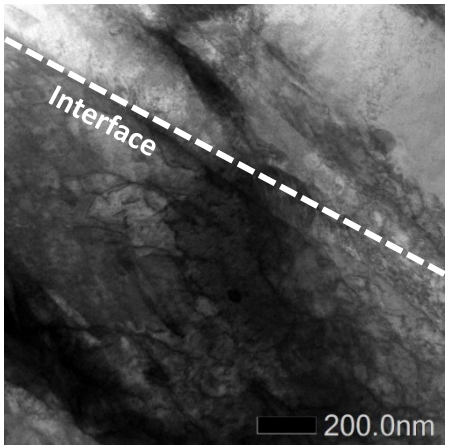

<BF-STEM Image>

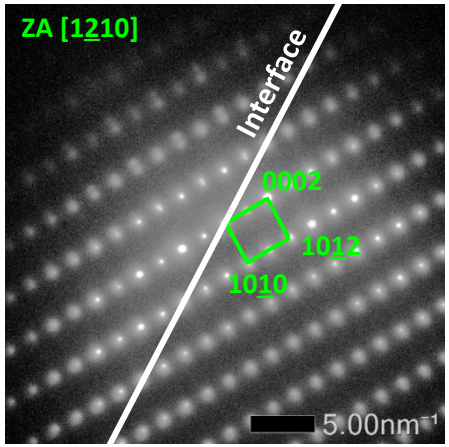

<Zr Matrix (HCP)>

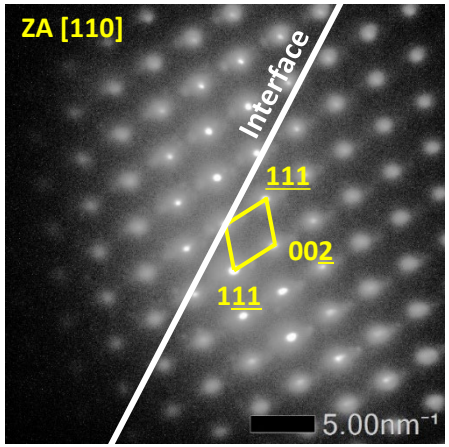

<ZrH (FCC)>

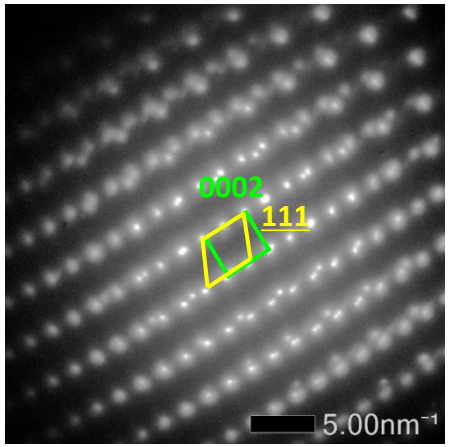

<Interface>

- **18 MPa Radial H**
  - ✓ OR: $[0001]//[001]$ & $(1\bar{2}10)//(110)$ & Interface: $(10\bar{1}0)//(110)$

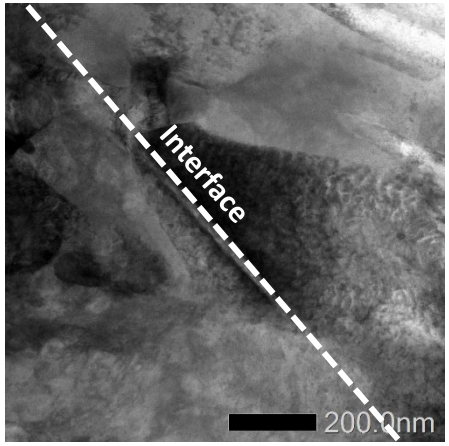

<BF-STEM Image>

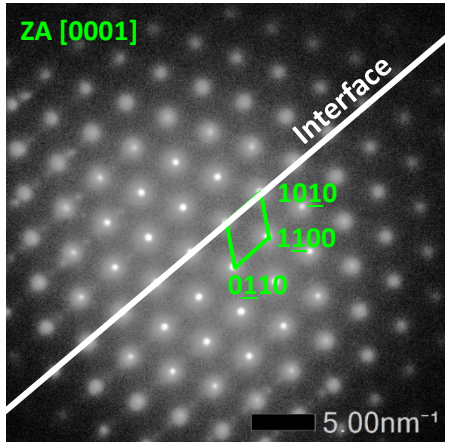

<Zr Matrix (HCP)>

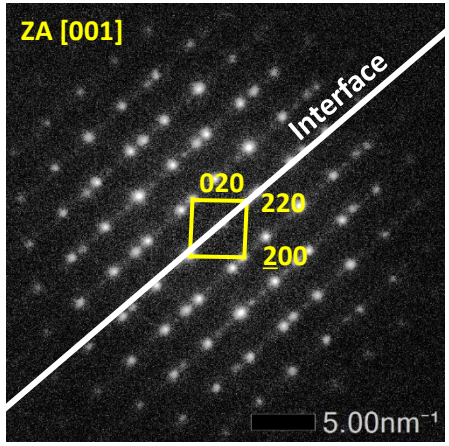

<ZrH (FCC)>

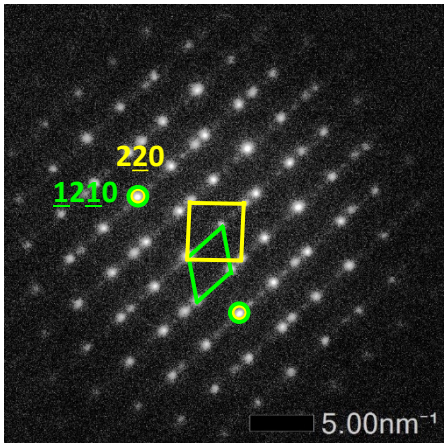

<Interface>

Orientation relationship in summary

- **OR analysis in TEM**

	OR	0 MPa	18 MPa
OR 1	$[1\bar{2}10]//[110]$ & $(0001)//(111)$	5	2
OR 2	$[1\bar{2}10]//[110]$ & $(0001)//(001)$	-	1

- **OR analysis in EBSD**

➢ Angle between HCP {0001} and FCC {111} in each interface.

<0 MPa>

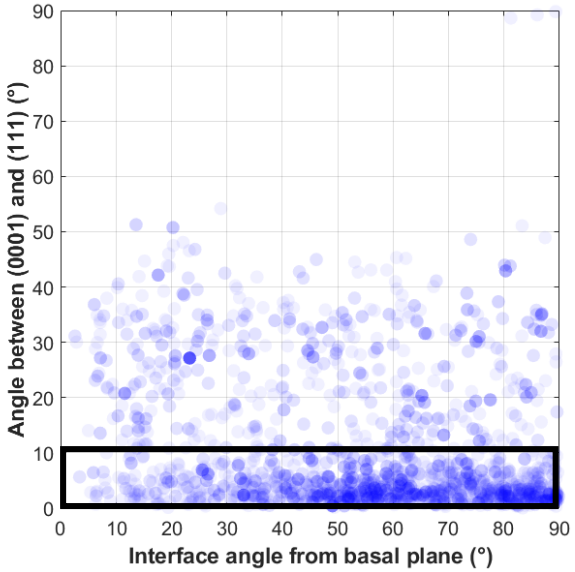

<18 MPa>

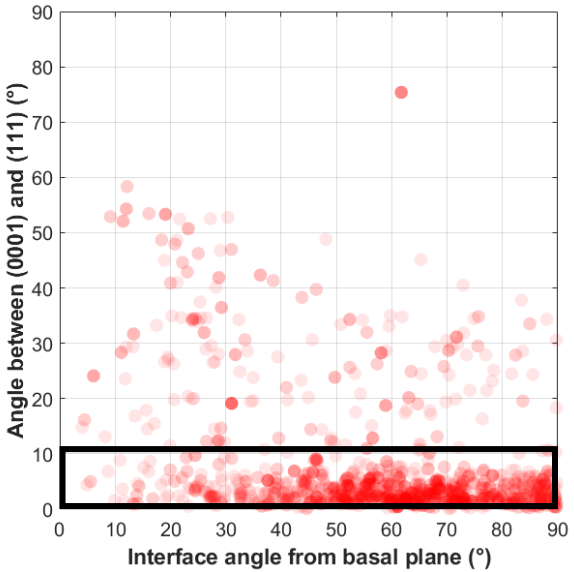

$(10\bar{1}0)//(111)$

$(0001)//(111)$

- (0001)//(111) orientation relationship was dominant in both TEM and EBSD analyses.

Solubility analysis

- **TSSd analysis result**

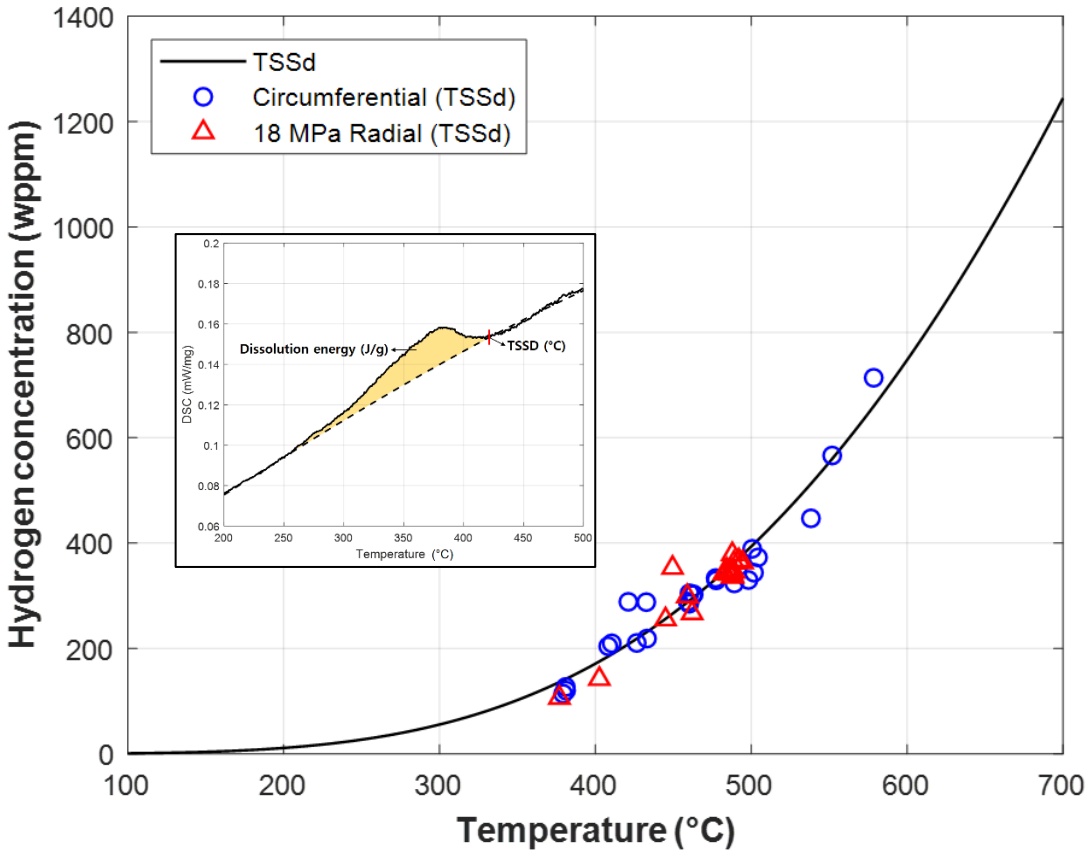

- Measured TSSd fits very well with the theoretical value[6], and there was no difference in TSSD between the radial hydride and the circumferential hydride.

[6] G. Sabol, G. Moan, Zirconium in the Nuclear industry: Twelfth International Symposium, 2000.

Dissolution energy analysis

- **Dissolution analysis result**

- Temperature profile: 25°C - 600°C -25°C (20°C/min)

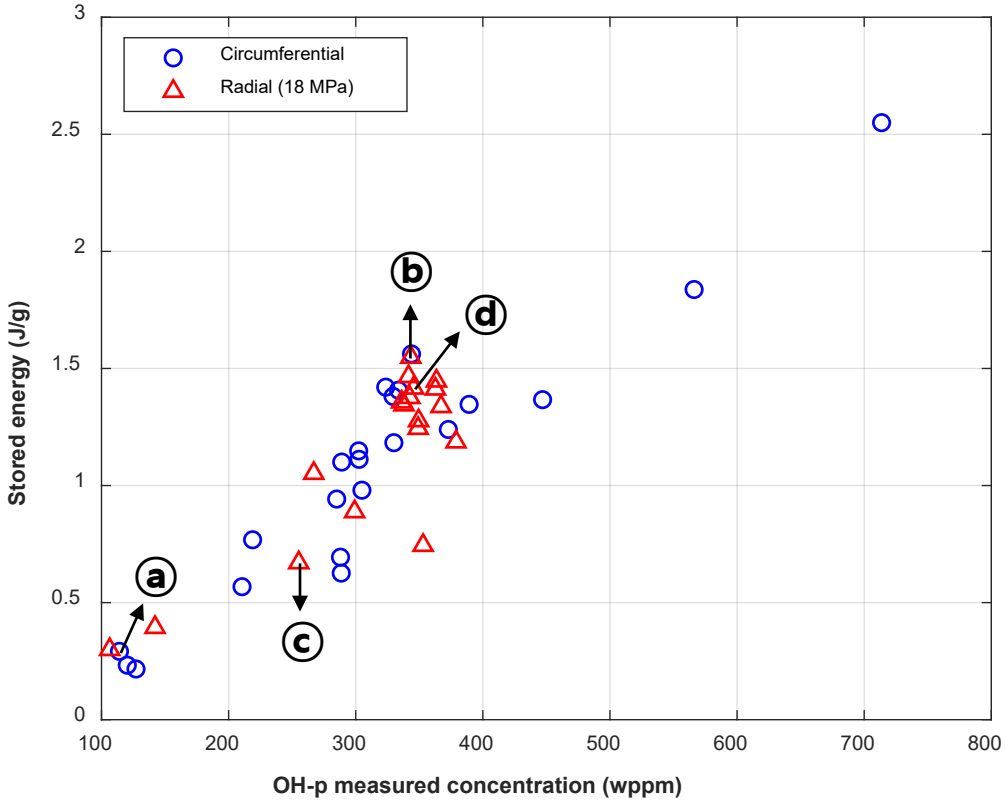

<Calculated stored energy of all specimens>

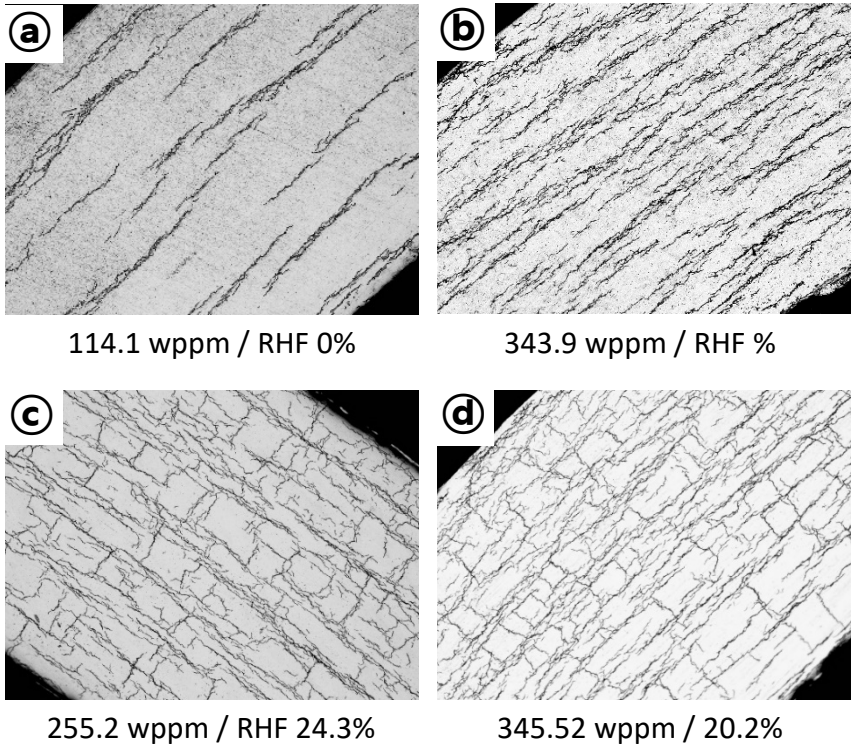

114.1 wppm / RHF 0%

343.9 wppm / RHF %

255.2 wppm / RHF 24.3%

345.52 wppm / 20.2%

<Optical microscope images>

- No significant difference was observed between circumferential and radial hydride specimens.

Conclusion: Implications and planned research

"Interface Microstructure Characterization"

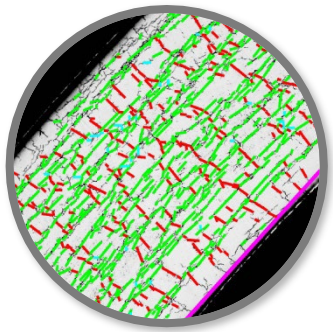

#1. Modeling hydride reorientation

Q. Is Misfit strain difference between radial hydride and circumferential hydride that significant ?

A. No significant preference in interface, thereby no significant misfit strain difference.

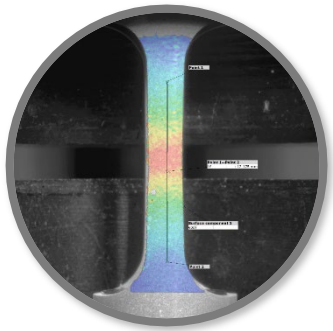

#2. Understanding axial mechanical strength

Q. What is the essential difference in terms of the dissolution energy?

A. Dissolution energy during heating process was similar in all tested specimen.

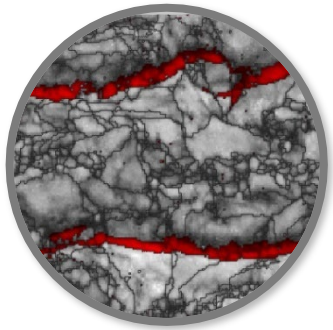

#3. Understanding solubility

Q. Is there any differences in solubility of radial hydride?

A. There is no appreciable difference.

2. Radial hydride precipitation model development and validation

Frame of radial hydride precipitation model I: Thermodynamic model

- **Gibbs free energy change for hydride precipitation**

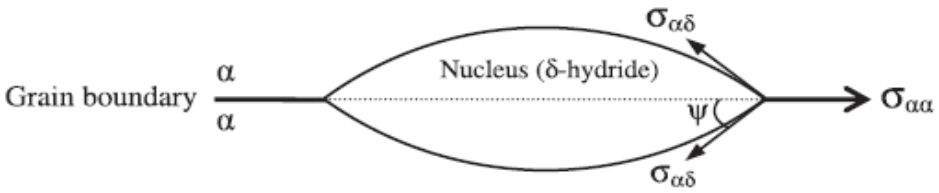

$$\psi = \cos^{-1}\left(\frac{\sigma_{\alpha\alpha}}{2\sigma_{\alpha\delta}}\right)$$

$$\Delta G = \frac{4}{3}\pi r^3 f(-\Delta G_{chem} + \Delta G_{strain}) + 4\pi r^2(1 - cos\psi)\,\sigma_{\alpha\delta} - (\pi r^2 \sin^2\psi)\,\sigma_{\alpha\alpha}$$

Hydride volume | [Driving force] Chemical free energy | [Retarding force] strain energy energy | Interface area | [Retarding force] Interface energy | GB area | [Driving force] Grain boundary energy

- **Critical GB energy and Radial hydride precipitation model**

$$\Delta G^* = \frac{16\pi\sigma_{\alpha\delta}^3}{3(-\Delta G_{chem}+\Delta G_{strain})^2} f \quad \text{with} \quad f = 1 - 1.5cos\psi + 0.5cos^3\psi$$

ΔG^* : Critical nucleation energy of hydrides at GB, f: Hydride shape factor

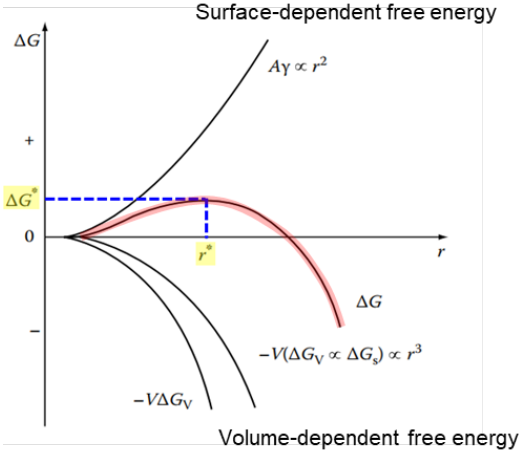

- **Radial hydride precipitation model**

$$\frac{J_{rad}^*}{J_{circ}^*} = \frac{(Z\beta^* N)_{rad}\exp\left(-\frac{\Delta G_{rad}^*}{kT}\right)}{(Z\beta^* N)_{circ}\exp\left(-\frac{\Delta G_{circ}^*}{kT}\right)} \Rightarrow RHF = \frac{\int_o^t J_{rad}^*\,dt}{\int_o^t J_{circ}^*\,dt + \int_o^t J_{rad}^*\,dt}$$

Frame of radial hydride precipitation model II: Kinetic model coupled to mHNGD

[Input] $C_t,\ T(t),\ \sigma_h(t)$

Solve kinetics ODEs

$C_{ss}(t_j),\ C_{pp}^{nucl}(t_j),\ C_{pp}^{grth}(t_j)$

Nucleation

Distribute C_{pp}^{nucl} proportional to J_{rad}^* and J_{circ}^*

Growth

Distribute C_{pp}^{grth} proportional to $C_{pp,rad}(t_{j-1})$, and $C_{pp,circ}(t_{j-1})$

Calculate $C_{pp,rad}(t_j)$, $C_{pp,circ}(t_j)$ and $RHF(t_j) = C_{pp,rad}(t_j)/(C_{pp,rad}(t_j) + C_{pp,circ}(t_j))$

$t_j < t_f$?

No

$t_{j+1} = t_j + dt$

Yes

[Output] $RHF(t), C_{pp,rad}(t), C_{pp,circ}(t)$

mHNGD model (kinetics)
: Calculate precipitation behavior (Nucleation, growth, dissolution)

Thermodynamic model
: Allocate orientation of precipitate

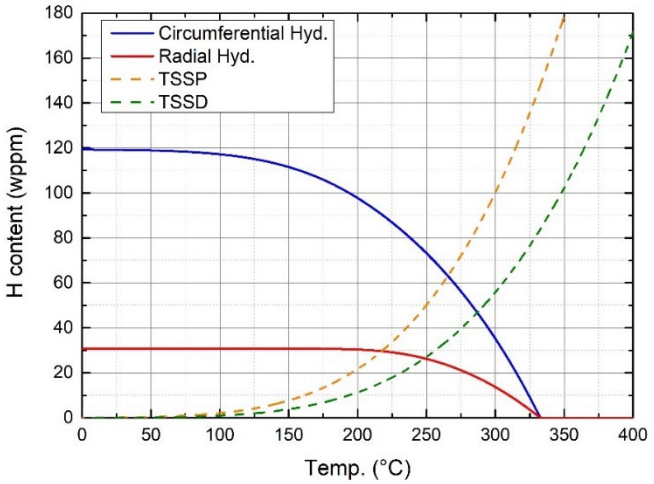

<150 wppm, 15MPa, 0.667 ℃/min>

Detailed constitutive models and experimentally attained parameters I

- **Critical GB energy and Radial hydride precipitation model**

$$\frac{J^*_{rad}}{J^*_{circ}} = \frac{(Z\beta^* N)_{rad}\exp\left(-\frac{\Delta G^*_{rad}}{kT}\right)}{(Z\beta^* N)_{circ}\exp\left(-\frac{\Delta G^*_{circ}}{kT}\right)} \quad \text{where} \quad \Delta G^* = \frac{16\pi\sigma^3_{\alpha\delta}}{3(-\Delta G_{chem}+\Delta G_{strain})^2} f \quad \text{with } f = 1 - 1.5cos\psi + 0.5cos^3\psi$$

$$\psi = \cos^{-1}\left(\frac{\sigma_{\alpha\alpha}}{2\sigma_{\alpha\delta}}\right)$$

- ΔG_{chem} : Chemical free energy change during precipitation ⇒ $\Delta G^{rad}_{chem} = \Delta G^{cir}_{chem}$

$$\Delta G_{chem} = \frac{RT}{\bar{V}_{hyd}}[(x+1)\ln(x+1) - x\ln(x)] \quad (x = 1.66 \text{ for } \delta\text{-hydride})$$

- ΔG_{strain} : Free energy stored in Zr matrix due to misfit strain ⇒$\Delta G^{rad}_{chem} \approx \Delta G^{cir}_{chem}$

$$\Delta G_{strain} = \Delta G^0_{strain}(\text{Strain energy with no stress}) + \Delta G^{int}_{strain}(\text{Interaction energy})$$

$$= 6\mu\chi^2 \cdot f\left(\frac{c}{a}\right) - \chi\omega$$

μ : Shear modulus
c/a : aspect ratio of hydride
χ : misfit strain
$\bar{\omega}$: tensile stress

The same hydride volume + interface misfit ($\chi_{rad} \approx \chi_{circ}$)

Shape of hydrides

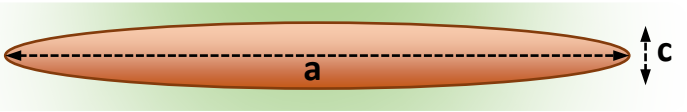

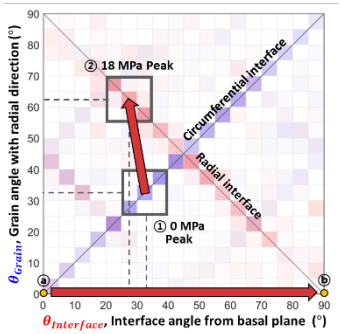

0 MPa / Circumferential hydrides (216 wppm)

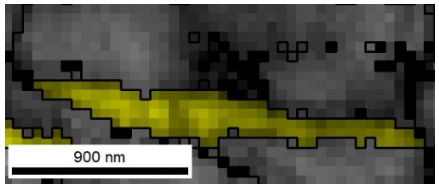

$$f(c/a)_{cir} \approx \frac{3}{4}\pi\left(\frac{c}{a}\right)_{cir} = \frac{3}{4}\pi 0.1521 = 0.3584$$

18 MPa / Radial hydride (211 wppm)

$$f(c/a)_{rad} \approx \frac{3}{4}\pi\left(\frac{c}{a}\right)_{cir} = \frac{3}{4}\pi 0.1774 = 0.4180$$

Detailed constitutive models and experimentally attained parameters II

- **Critical GB energy and Radial hydride precipitation model**

$$\frac{J^*_{rad}}{J^*_{circ}} = \frac{(Z\beta^* N)_{rad} \exp\left(-\frac{\Delta G^*_{rad}}{kT}\right)}{(Z\beta^* N)_{circ} \exp\left(-\frac{\Delta G^*_{circ}}{kT}\right)} \quad \text{where} \quad \Delta G^* = \frac{16\pi\sigma^3_{\alpha\delta}}{3(-\Delta G_{chem}+\Delta G_{strain})^2} f \quad \text{with} \quad f = 1 - 1.5cos\psi + 0.5cos^3\psi$$

$$\psi = \cos^{-1}\left(\frac{\sigma_{\alpha\alpha}}{2\sigma_{\alpha\delta}}\right)$$

- N_{rad}/N_{circ} : Nucleation site density ⇒Grain boundary length ratio

$$\frac{N_{rad}}{N_{circ}} \approx 0.2$$

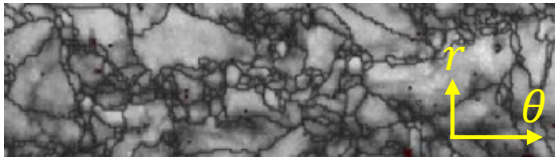

Circumferentially elongated grains in reactor grade CWSR Zircaloy

- $\sigma_{\alpha\alpha}$: Free energy stored in Zr matrix due to misfit strain ⇒ $\sigma_{\alpha\alpha,rad} > \sigma_{\alpha\alpha,circ}$ under tensile hoop stress

$\sigma_{\alpha\alpha,rad} = \sigma_{\alpha\alpha,circ} + k_{GB}\bar{\omega}$ …… For GB⊥$\bar{\omega}$ hydride segregation increases at the radial grain boundaries

It is the primary driving mechanism for radial hydride precipitation

: Applied tensile $\bar{\omega}$ $(+)\sim \sigma_{\alpha\alpha,rad} \uparrow \sim \psi_{rad} \downarrow \sim f_{rad} \downarrow \sim \Delta G^*_{rad} \downarrow \sim J^*_{rad} \uparrow \sim RHF \uparrow$

RHF analysis result

- **RHF assessment of various hydride morphologies using PROPHET**

  Green : circumferential / Cyan : mixed / Red : radial hydride

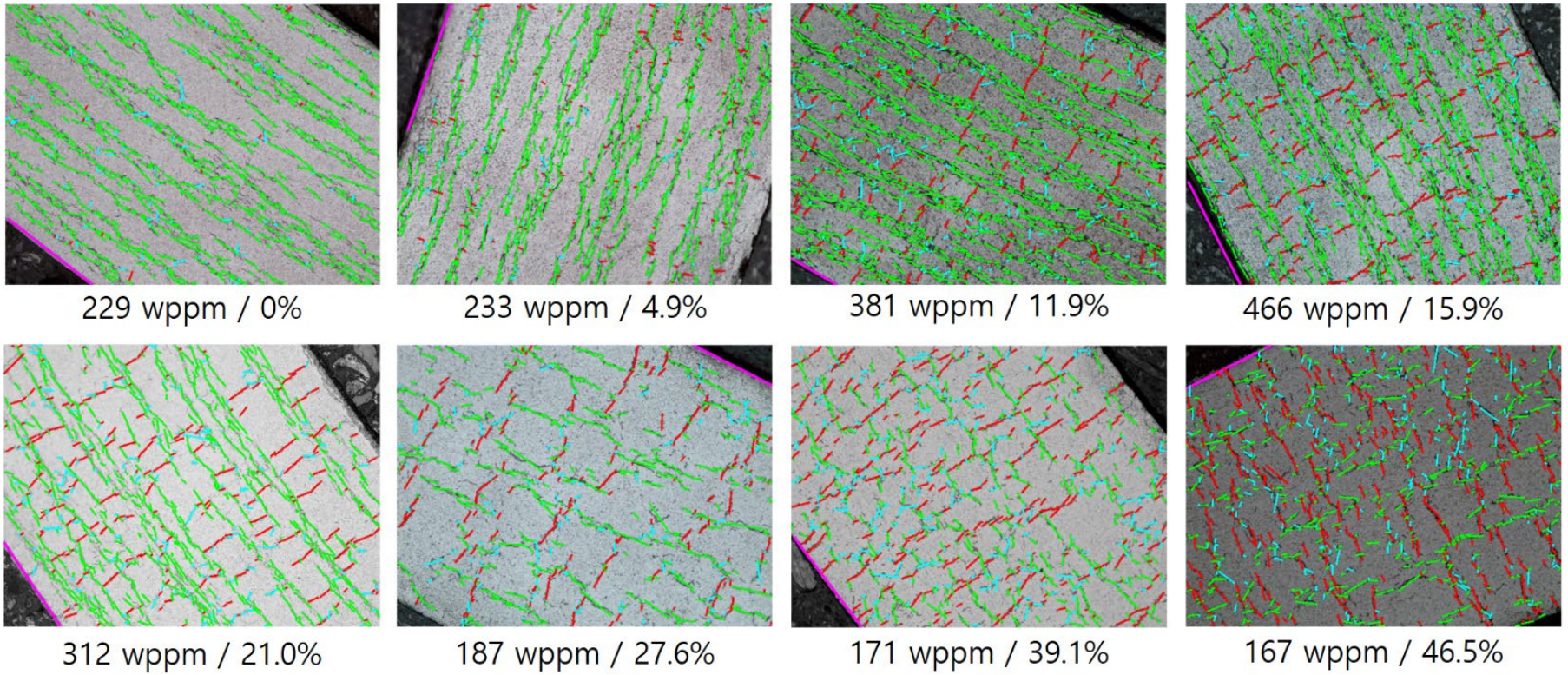

PROPHET : SNU-developed hydride image analysis code[4]

Available at http://fuel.snu.ac.kr

(a)

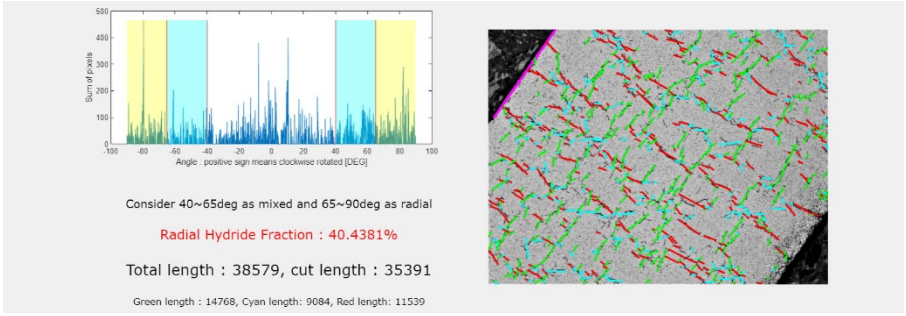

(b)

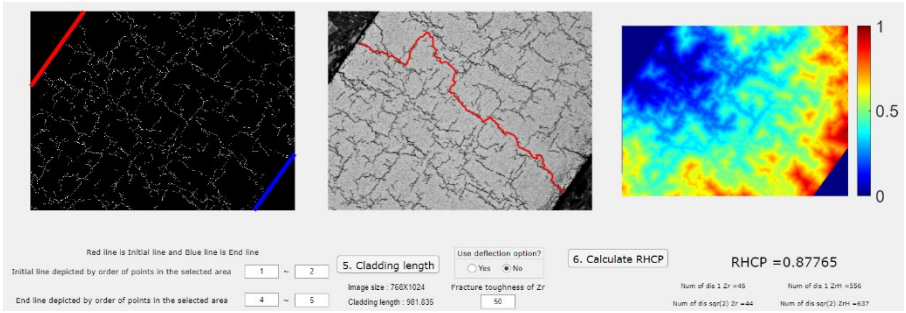

(c)

<Output screens of PROPHET analysis>

1. Radial Hydride Fraction (RHF)

$$RHF = \frac{\sum_i L_i f_i}{\sum_i L_i}$$ [5]

$$f_i = \begin{cases} 0\text{: } 0° \le \theta < 40°\text{: } circumferential \\ 0.5\text{: } 40° \le \theta < 65°\text{: } mixed \\ 1\text{: } 65° \le \theta < 90°\text{: } radial \end{cases}$$

2. Radial Hydride Continuous Path (RHCP)

$$RHCP = \frac{Lw_{Zr} - (x_{Zr}w_{Zr} + x_{ZrH}w_{ZrH})}{L(w_{Zr} - w_{ZrH})}$$ [6]

Relative cost of Zr matrix and hydride:

$w_{Zr} = 50\ MPa\sqrt{m}$, $w_{ZrH} = 1\ MPa\sqrt{m}$

0= Minimum cost path consists of 100% Zr matrix (Straight Zr path)

1= Minimum cost path consists of 100% ZrH (Straight hydride path)

3. Maximum length of radial hydride

[4] D. Kim et al., Development of an image analysis code for hydrided Zircaloy using Dijkstra's algorithm and sensitivity analysis of radial hydride continuous path. J Nucl Mater, 2022.
[5] P. Raynaud et al., Crack growth in the through-thickness direction of hydride thin-wall Zircaloy sheet, J Nucl Mater, 2012.
[6] P. Simon et al., Quantifying the effect of hydride microstructure on zirconium alloys embrittlement using image analysis, J Nucl Mater, 2021.

Experimental validation of the SNU RHF model

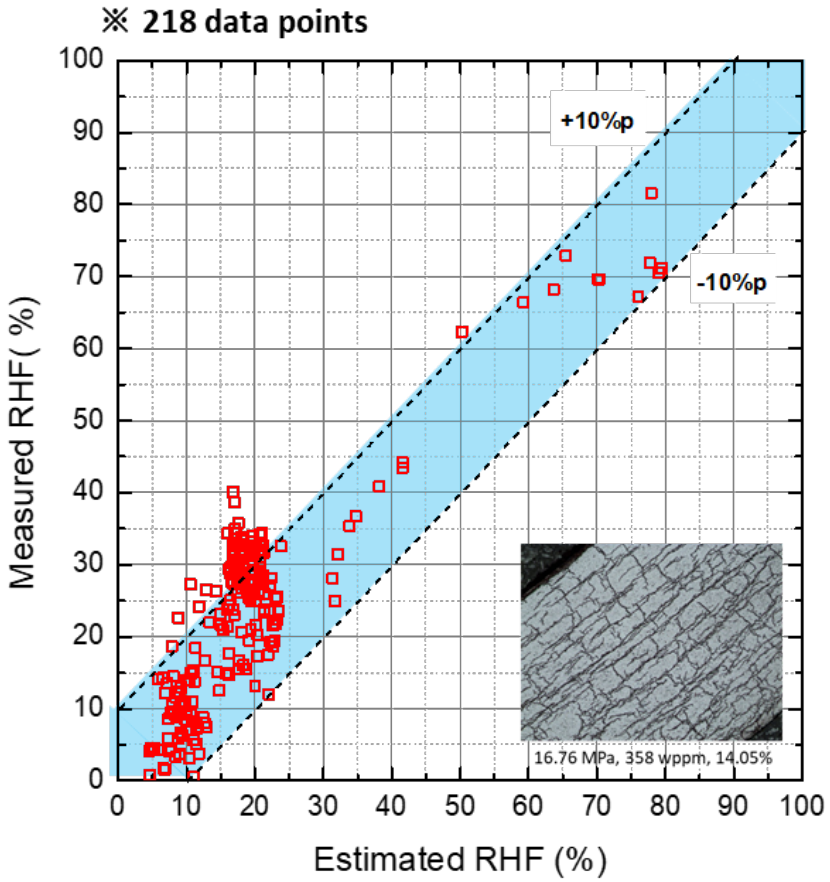

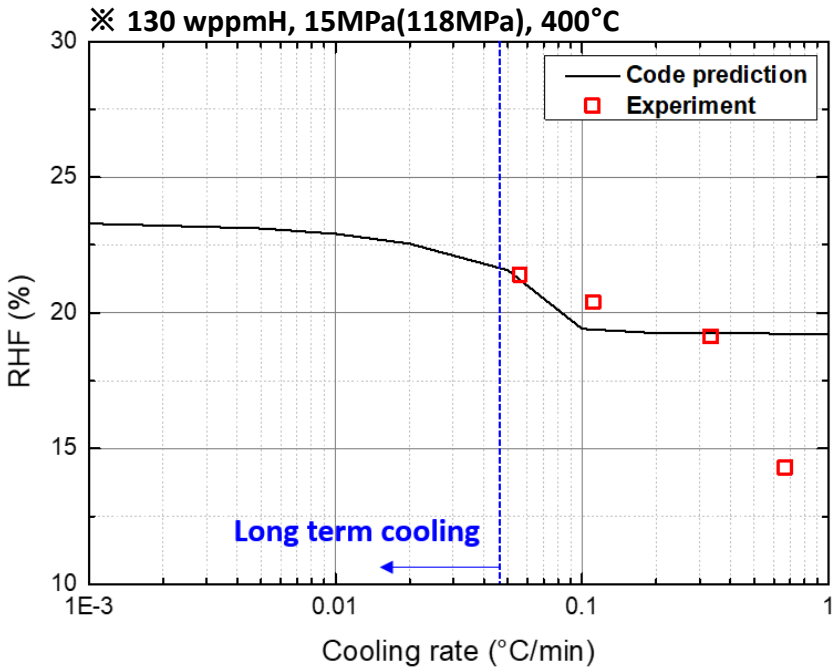

Collaboration for long-term cooling experiment is welcome

Employed parameters:

$\sigma_{\alpha\alpha,circ} = 0.12 J/m^2$, $\sigma_{\alpha\delta} = 0.16 J/m^2$, $k_{GB} = 7.5 \times 10^{-11}$m

Notable advancement in modeling by incorporating directly measured microstructural parameters (interface, grain size, hydride shape, nucleation site density, etc):

The ideal texture & interface treatment gives ~1.8 Gpa for threshold stress (Qin et al., Acta Materialia, 2011). The current model mechanistically captures key sensitivities.

3. Mechanical integrity analysis of hydrided Zircaloy

Image analysis for mechanical integrity of hydrided Zircaloy

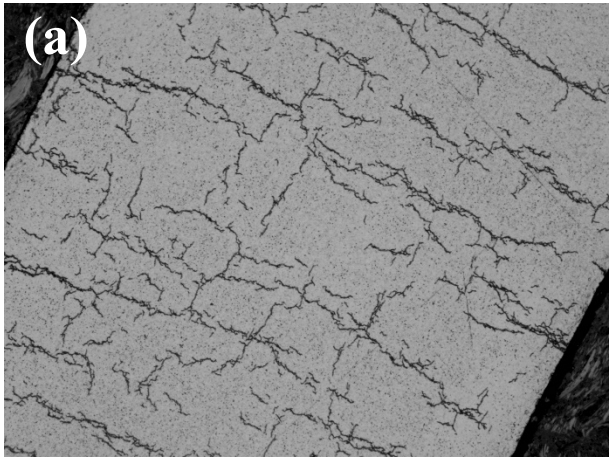

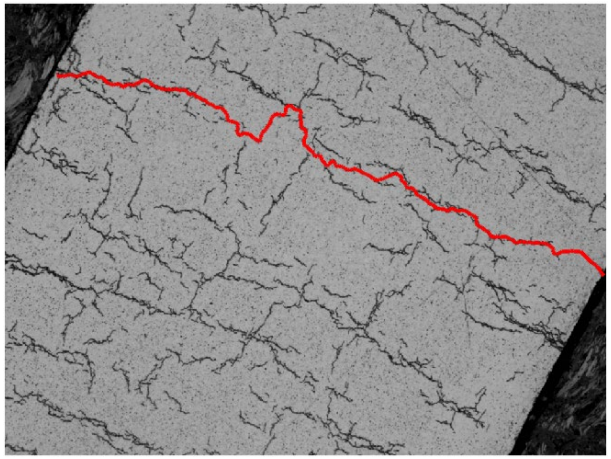

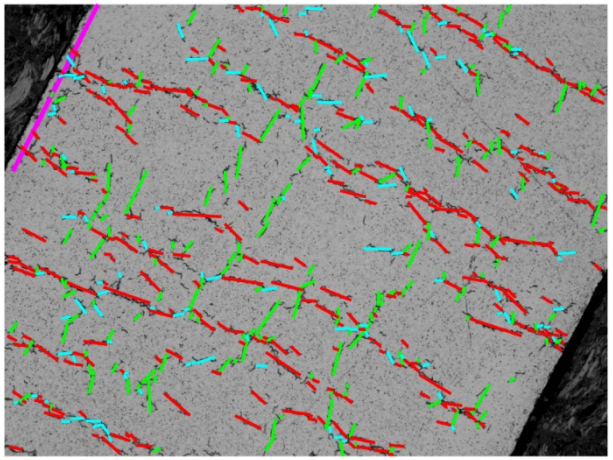

143.7 wppm / 18 MPa

RHCP = 0.902

SED=4 J/m

RHF = 47.3%

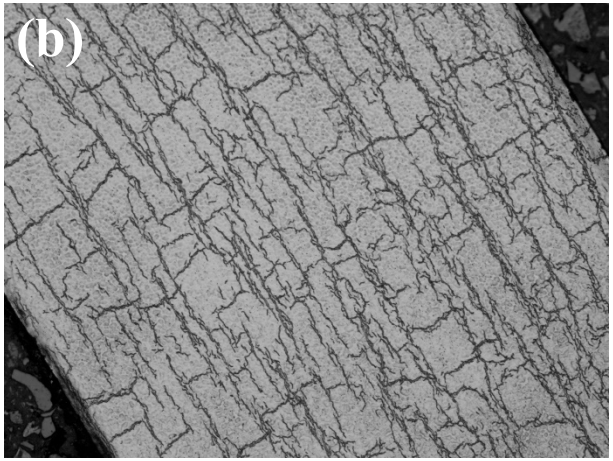

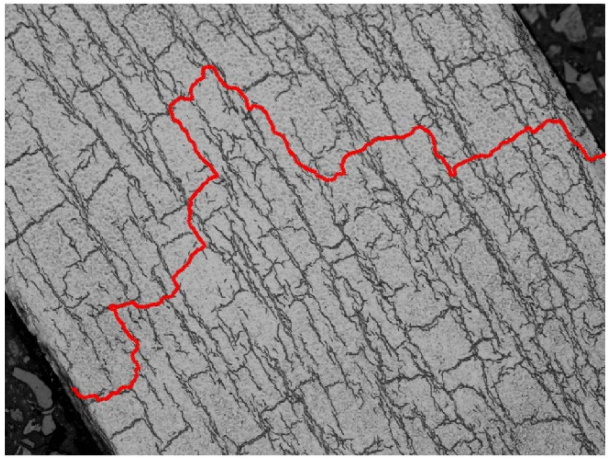

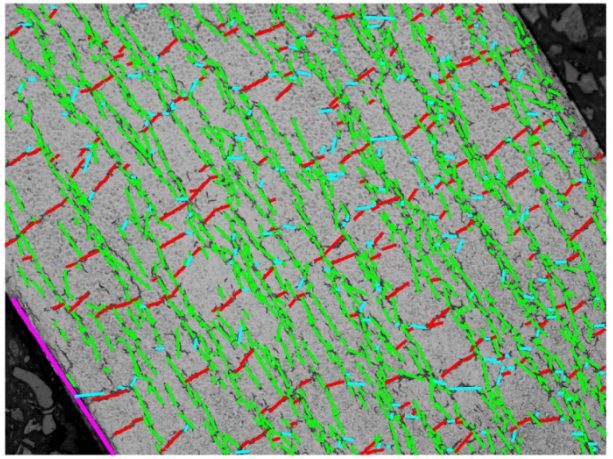

522.4 wppm / 18 MPa

RHCP = 0.883

SED=12J/m

RHF = 15.9%

<OM, RHF, RHCP images for applied pressure of 18 MPa: (a) low total hydrogen case of 143.7 wppm, (b) high total hydrogen case of 522.4 wppm>

RHF (>5%) is a powerful metric to predict SED

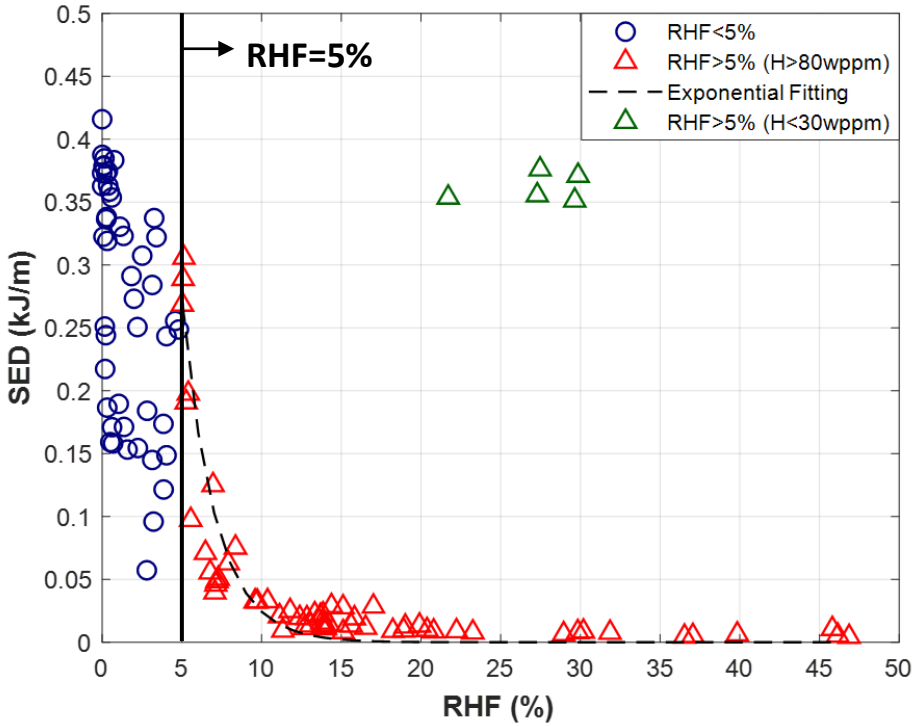

<SED change with RHF>

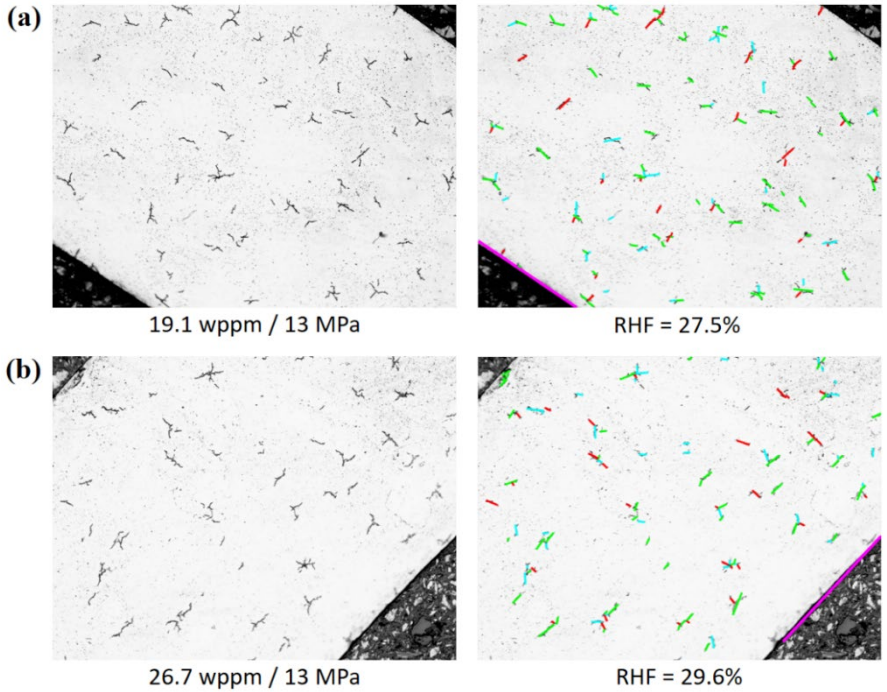

<Extremely low H concentration specimens>

- Radial Hydride Fraction (RHF) is a powerful metric for the strength for RHF > 5%.
- However, radial hydrides in an unconnected morphology (H < 30wppm) has limited effect on material strength.

Fracture mechanics relevant to radial hydride length

- **Fracture Mechanics Approach:** Treating the maximum radial hydride as the pre-existing flaw
  - For cladding tube with uniformly distributed maximum radial hydrides,

($l_{H,max}$: Maximum length of radial H & p_c: Critical load for the major load drop)

$$146.77 \exp\left(-2.06a \frac{\boldsymbol{l_{H,max}}}{\delta_{thick}}\right) = \frac{\boldsymbol{p_c}}{\sqrt{r_o}\,\delta_{thick}}\left[-1.61 \exp\left(-7.48 \frac{\boldsymbol{l_{H,max}}}{\delta_{thick}}\right) + 2.45\right]$$

Fracture toughness [7] of Zircaloy with 100% radial hydrides

Stress intensity factor [8] for the compressively loaded ring with a single radial crack

➢ SED associated with a major load drop of fairly elastic material:

$$\text{SED} \approx \frac{1}{2} p_c d_c \approx \frac{1}{2E} {p_c}^2$$

$$\textbf{SED} \approx \left[\frac{\mathbf{1}}{\boldsymbol{A' exp\left(B l_{H,max}\right) + C' exp\left(D l_{H,max}\right)}}\right]^{\mathbf{2}}$$

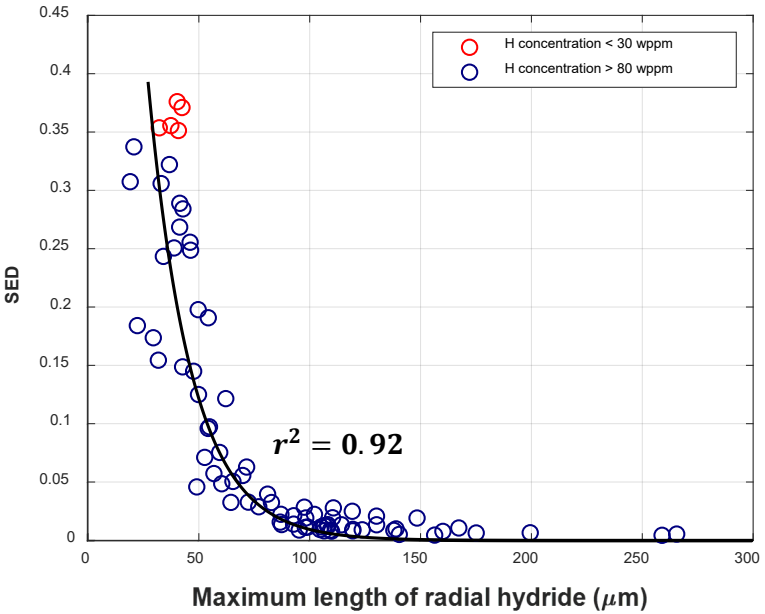

- Cladding tube with radial hydrides obeys the classical fracture mechanics and radial hydrides play as the critical flaw.

[7] Gopalan et al., Effect of radial hydride on room temperature fracture toughness of Zr-2.5 Nb pressure tube material, J Nucl Mater, 2021.
[8] Grandt et al., Two dimensional stress intensity factor solutions for radially cracked rings. AIR FORCE MATERIALS LAB WRIGHT-PATTERSON AFB OH, 1975.

Effect of radial hydride on mechanical property

- **Uniaxial tensile test**

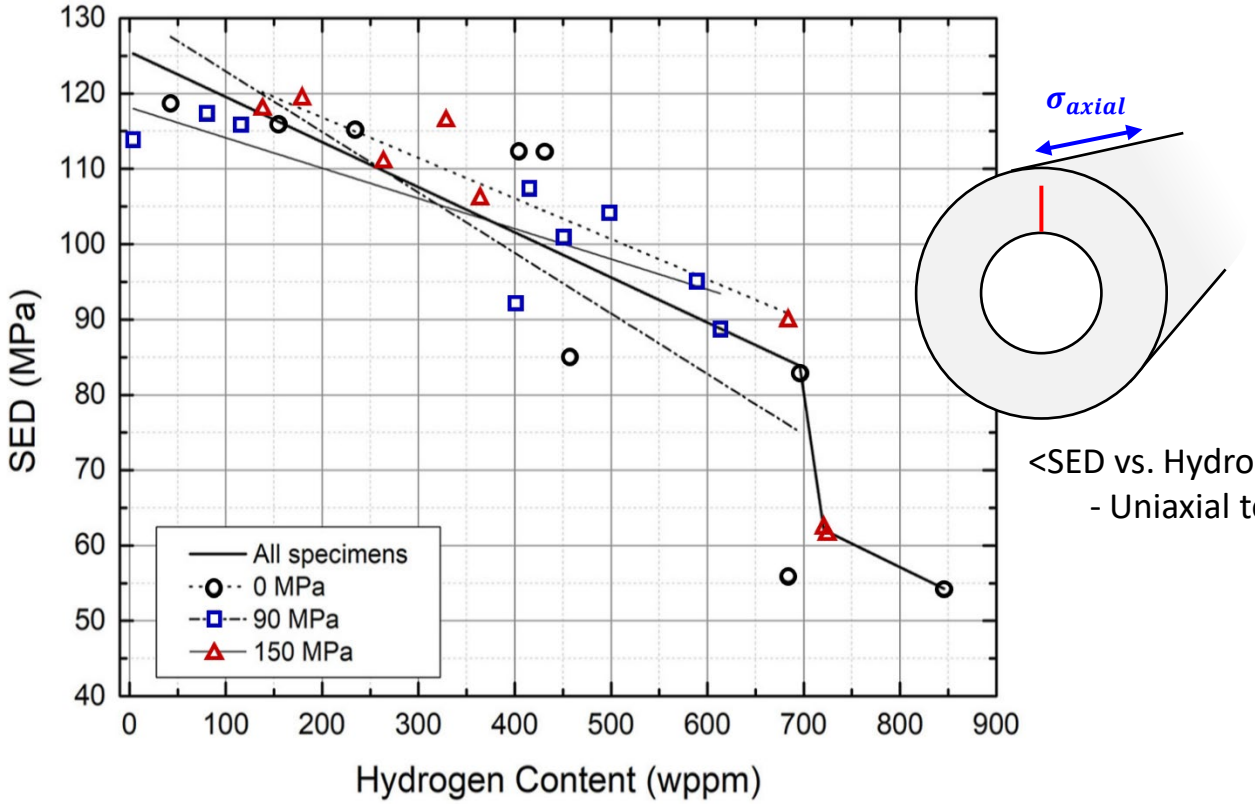

<SED vs. Hydrogen content>[2]
- Uniaxial tensile tests

- **The same effect with circumferential hydrides on uniaxial SED:** Having almost the identical interface hence misfit strain as we confirmed from the EBSD analysis, radial hydrides and circumferential hydrides exhibit the same influence on the SED of hydrided Zircaloy subjected to uniaxial tension along Z direction.

[1] Dahyeon Woo, Youho Lee, Understanding the mechanical integrity of Zircaloy cladding with various radial and circumferential hydride morphologies via image analysis, Journal of Nuclear Materials, 2023. (Submitted, under review)

[2] Shinhyo Bang, Ho-a Kim, Jae-soo Noh, Donguk Kim, Kyunghwan Keum, Youho Lee. Temperature-dependent axial mechanical properties of Zircaloy-4 with various hydrogen amounts and hydride orientations, Nuclear Engineering and Technology, 54 (5) 1579-1587, 2022.

Conclusion and pathforward: Multi-scale approach

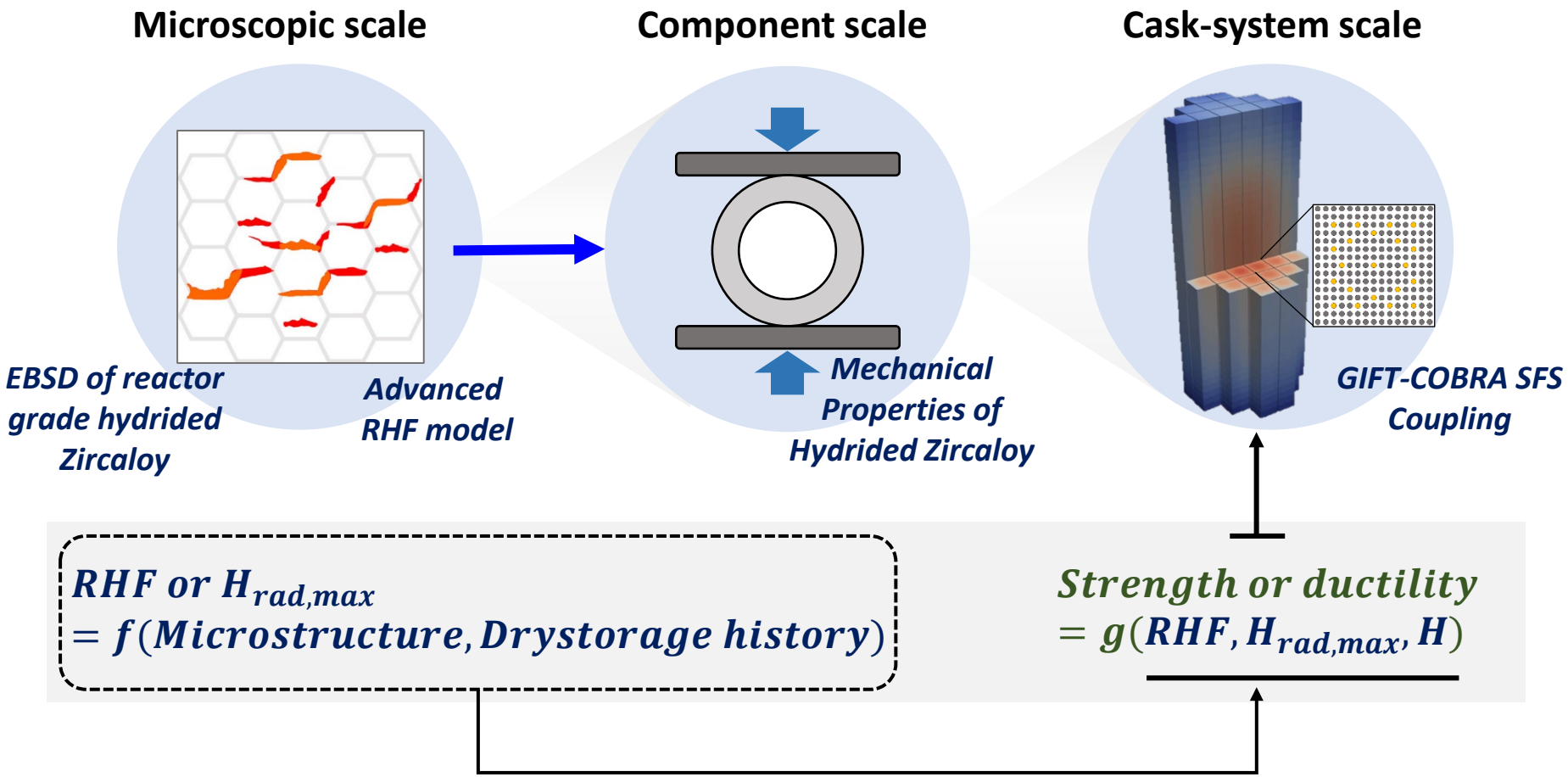

Conclusion and pathforward

<Extracting mechanical properties from RCT using ABAQUS-ISIGHT Optimization Solver>

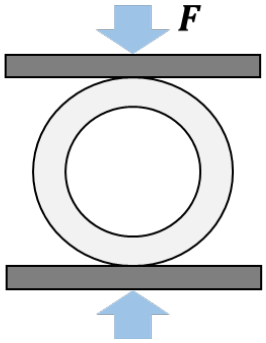

<Ring Compression Test>

<Experimental Curve>

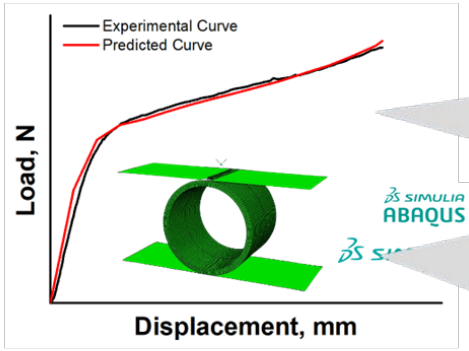

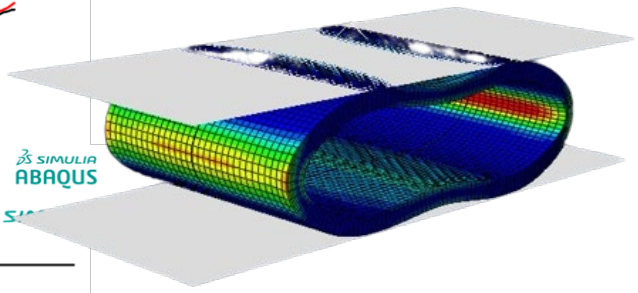

<Predicted Curve>

<GIFT-COBRA SFS Integrated Code Platform and Implementation of Hydrided Zircaloy model>

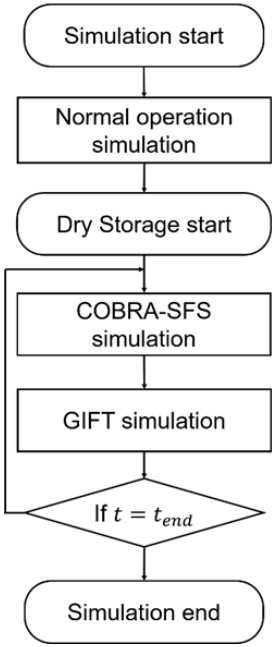

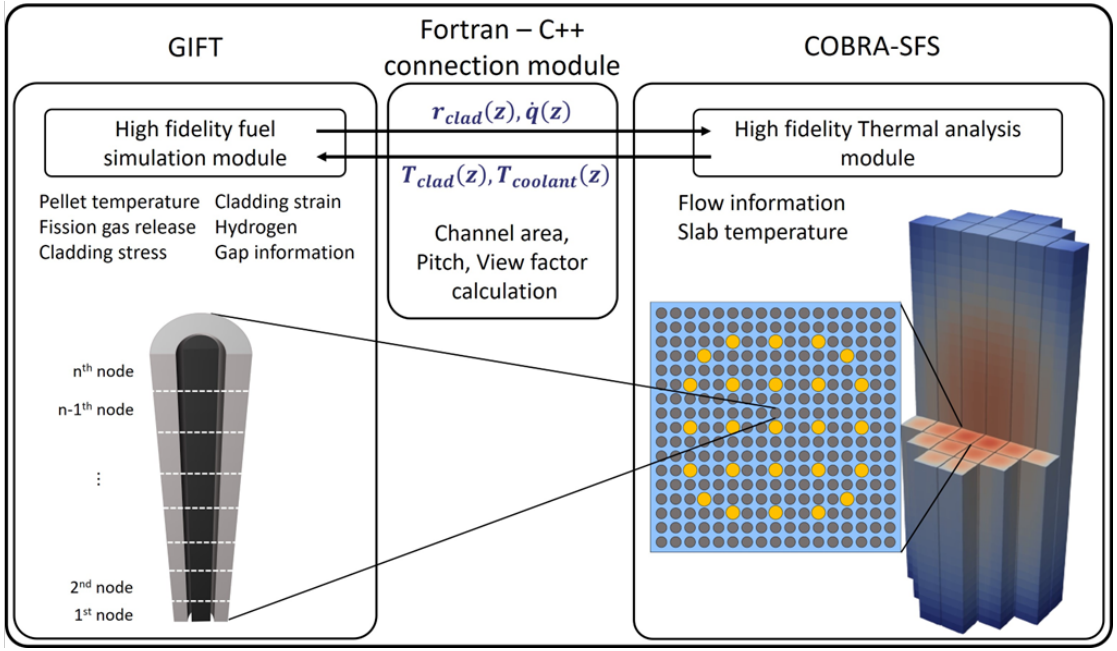

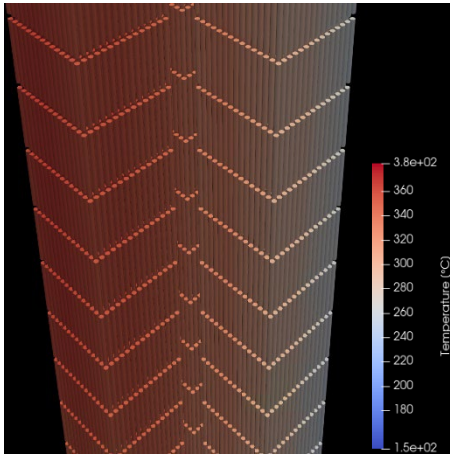

Thank you for your attention.

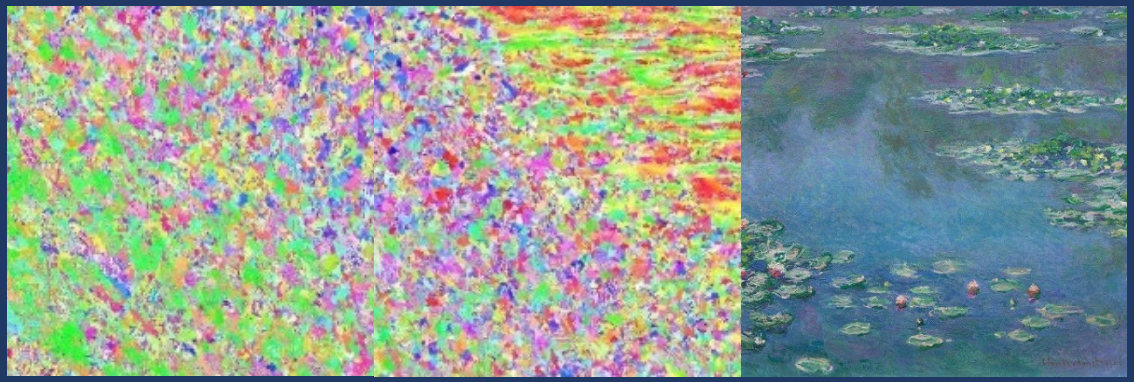

<Monet>

Supplementary slides

Ongoing research efforts: Integrating multi-scale understanding and analysis tools

Microscopic scale

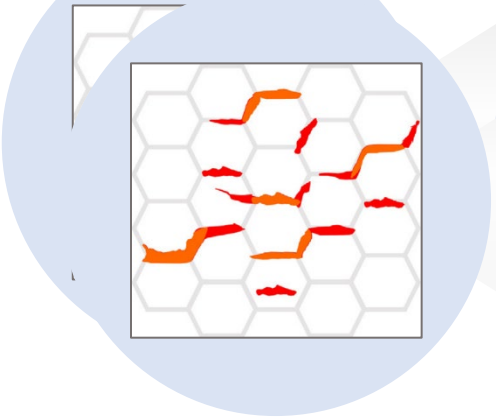

- EBSD
- TEM

- EBSD
- TEM

Component scale

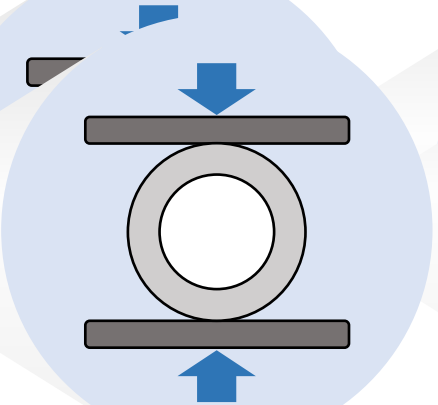

- Ring compression test
- Mechanical properties

- Ring compression test
- Mechanical properties

Cask-system scale

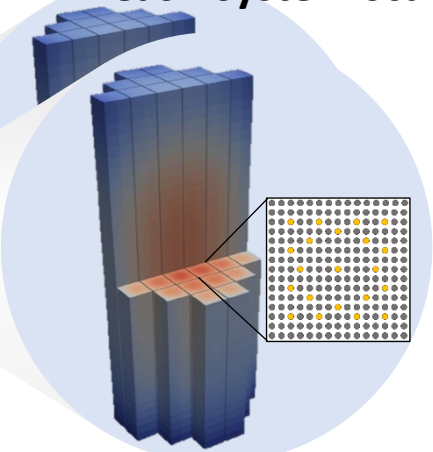

- COBRA-SFS
- GIFT

- COBRA-SFS
- GIFT

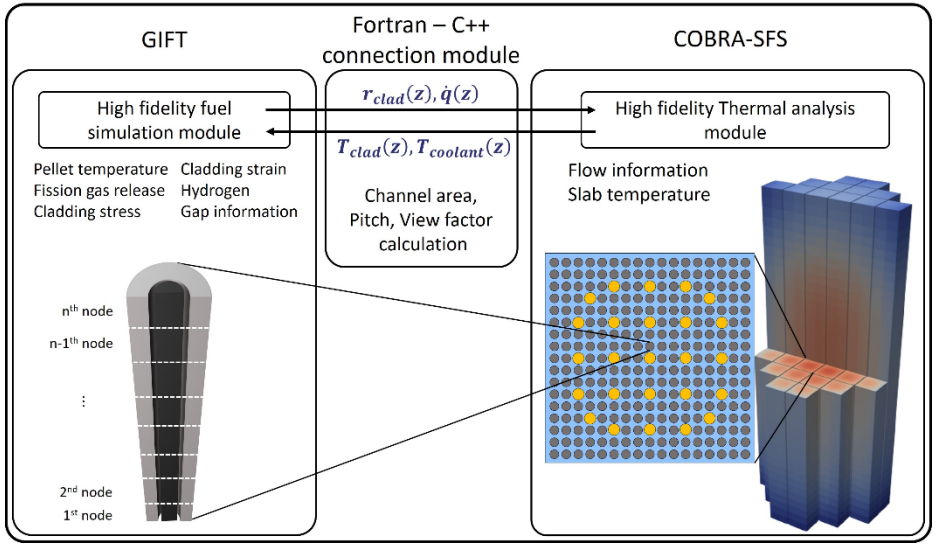

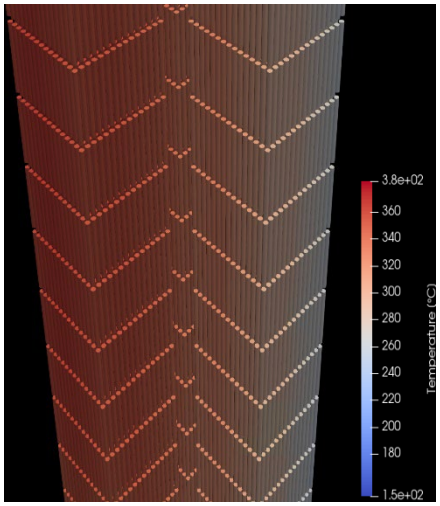

Motivation for fuel-TH coupled analysis for extended dry storage

- Improved discharge burnup and extended dry storage require more sophisticated predictions of nuclear fuel conditions during dry storage.

Fuel analysis

- Predict precise fuel behavior on full-cycle.
- Use simplified temperature as an input.

Thermal analysis

- Calculate accurate heat/temperature.
- Use simplified fuel information as an input.

Fuel – thermal integrated analysis

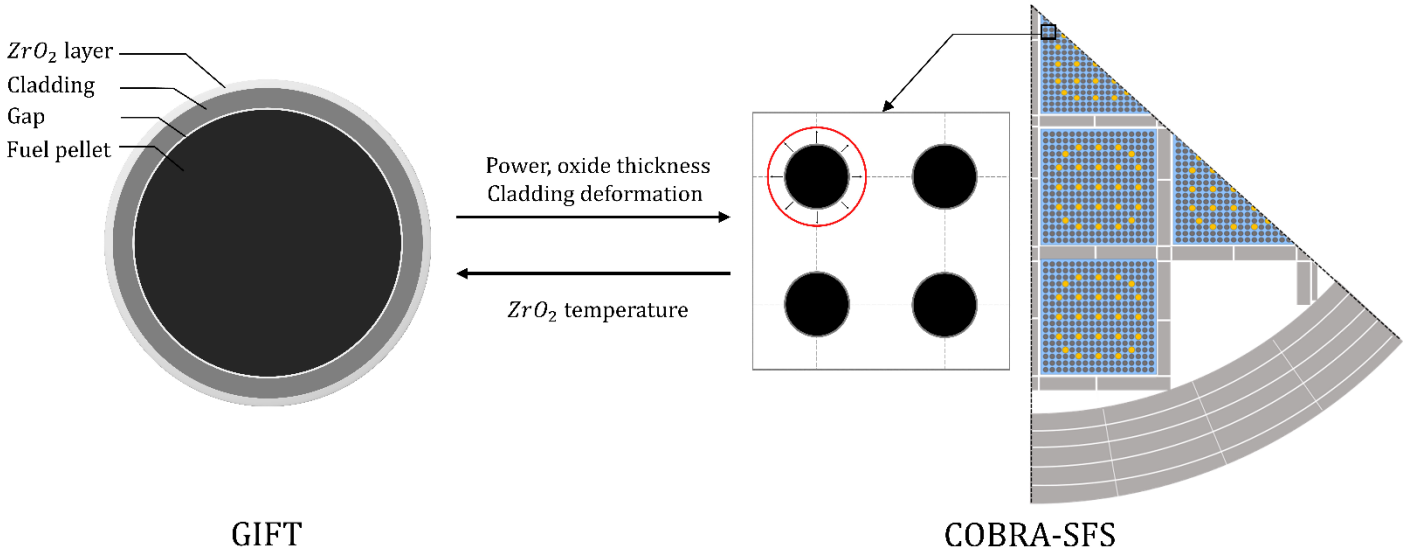

- Improve prediction accuracy of fuel behavior and temperature based on full-cycle simulation.
- Detailed status of spent fuel can be tracked based on burnup dependent realistic information.

GIFT/COBRA-SFS integration scheme

- GIFT - C++ based fuel analysis code with spent fuel module

Properties	Detailed features in spent fuel period
Pellet swelling[1]	α-decay induced pellet swelling after discharge
Fission and decay gas release[1]	Suppressed fission and decay gas release under 1000 K
Axial hydrogen migration[2]	Hydrogen prediction considering phase change and diffusion.
Cladding creep	EDF creep model, considering grain boundary sliding

- Flowchart of Integrated code

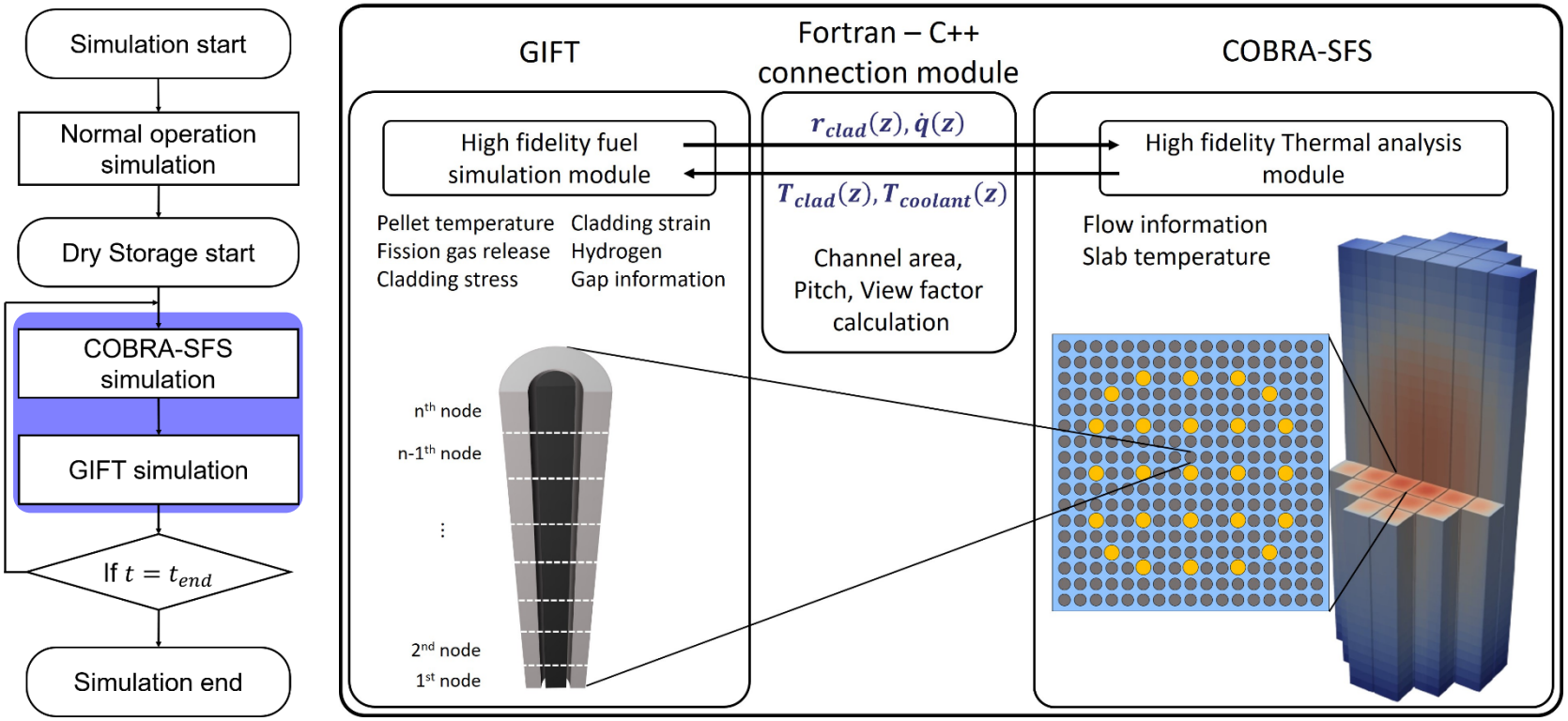

[1] Dahyeon Woo, Youho Lee, Spent fuel simulation during dry storage via enhancement of FRAPCON-4.0: Comparison between PWR and SMR and discharge burnup effect, Nucl. Eng. and Tech., Volume 54, Issue 12, 2022, 4499-4513
[2] Chansoo Lee, Youho Lee, Simulation of hydrogen diffusion along the axial direction in zirconium cladding tube during dry storage, J. of Nucl. Mater., Volume 579, 2023

GIFT/COBRA-SFS integrated code results

- Dry storage simulation condition

Fuel rod and dry cask information used in simulation					
Assembly, cladding type	WE 17x17 LOPAR, ZIRLO				
Bu_d [MWd/kgU]	50	55	60	65	70
U-235 enrichment [%]	4.2	4.5	4.95	5.5	6
Decay heat	ORIGEN data				
Cask type	TN-24P				
Assembly decay heat	Same decay heat applied for all assemblies				

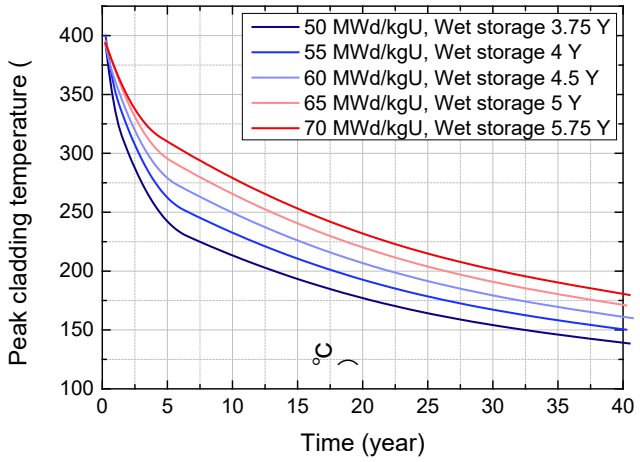

- Dry storage simulation thermal analysis result

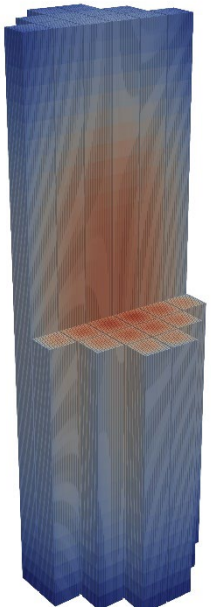

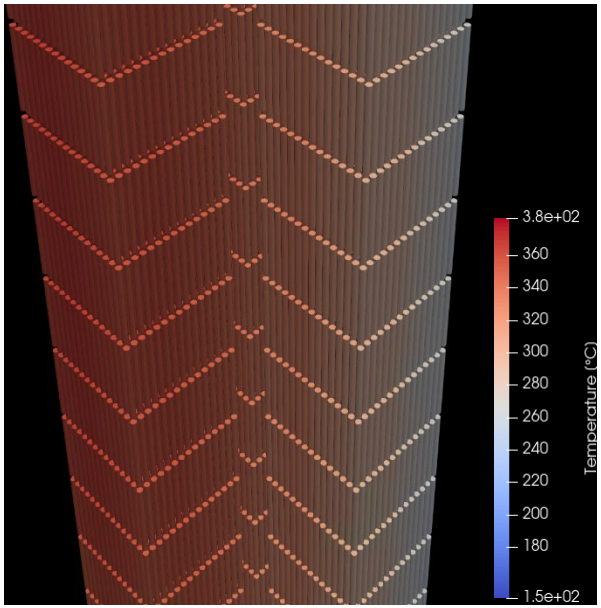

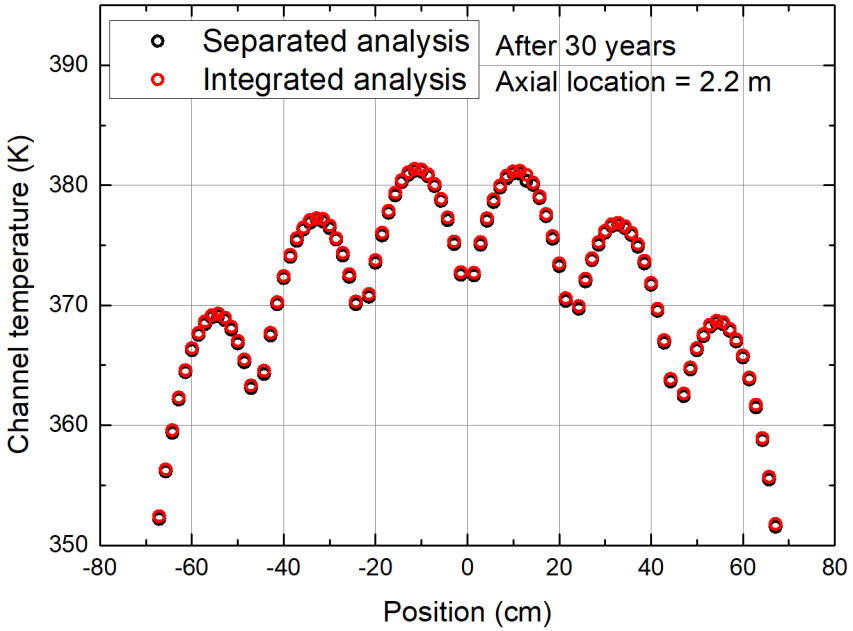

GIFT/COBRA-SFS integrated code results

- Dry storage simulation spent fuel analysis result

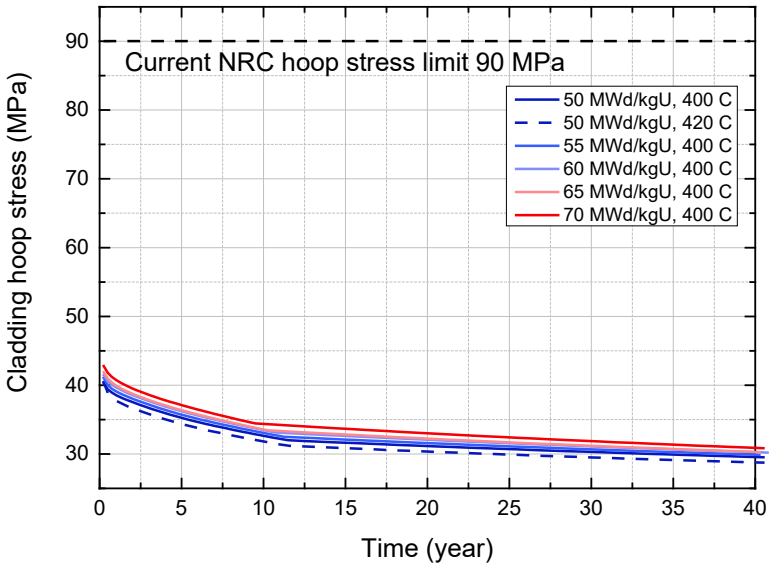

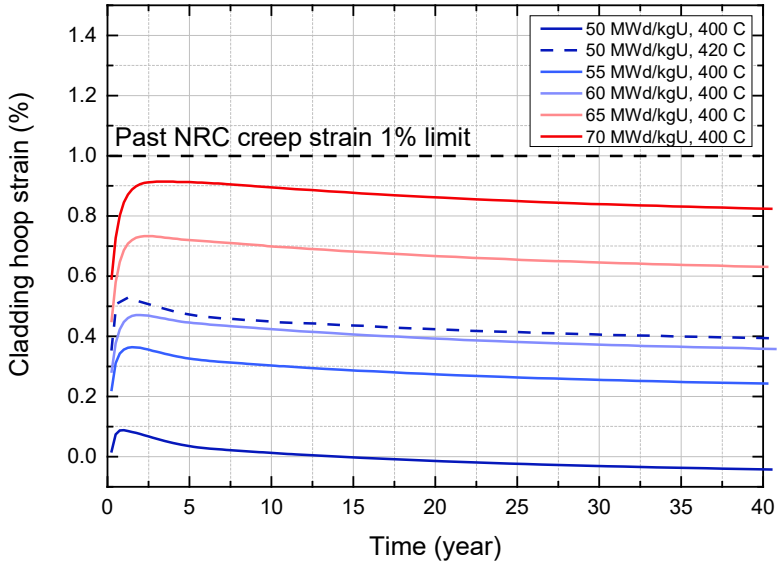

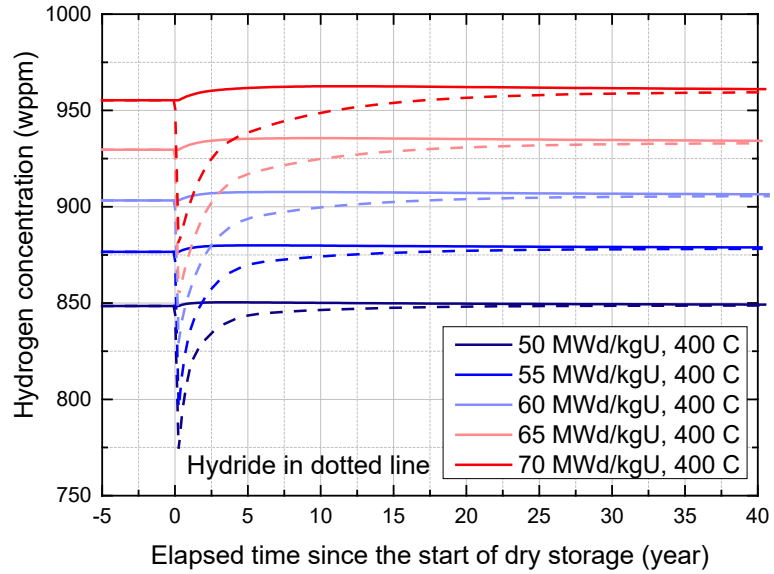

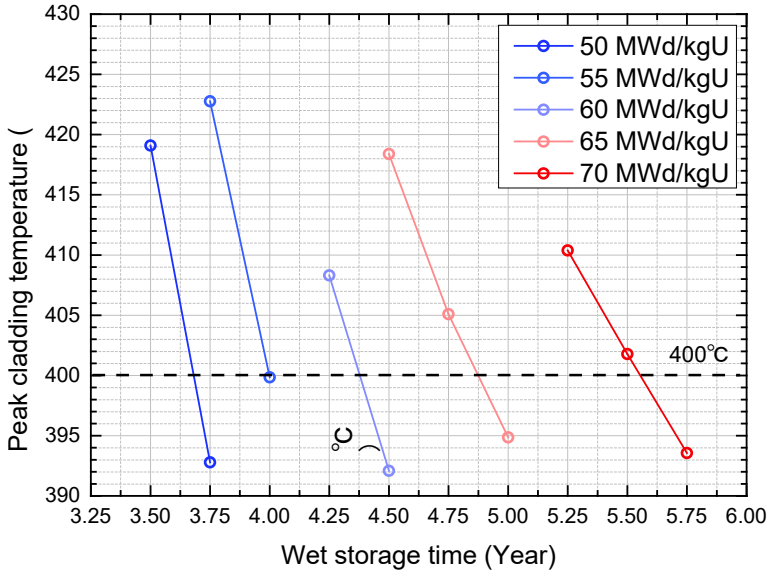

Safety envelope of extended dry storage

- Dry storage simulation spent fuel analysis result

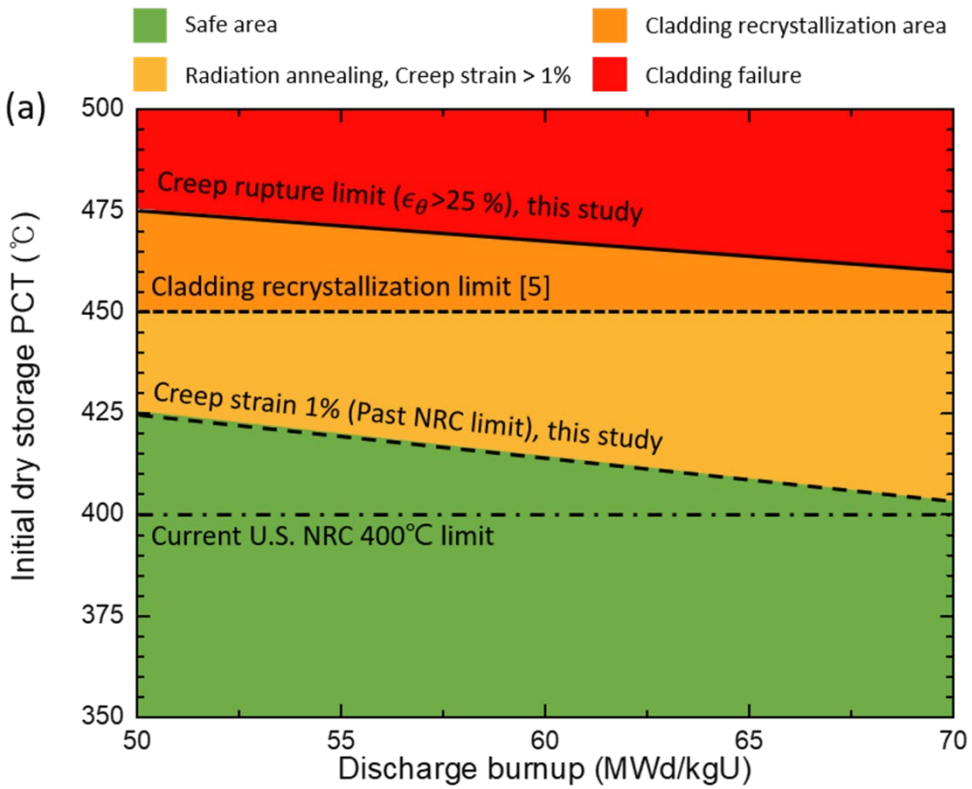

Supplementary slides

Conclusion

Microscopic Level

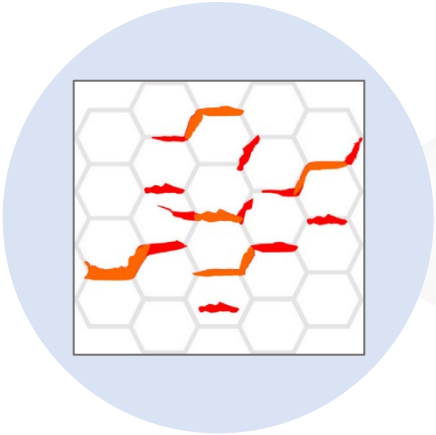

- EBSD
- TEM

Component Level

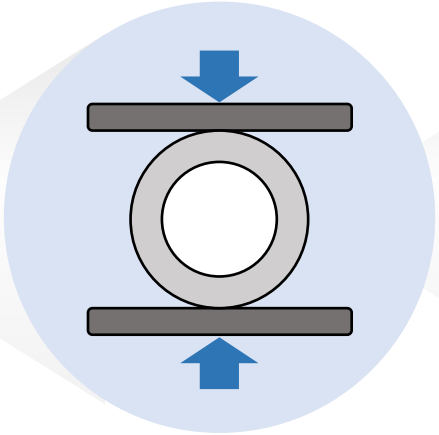

- Ring compression test
- Mechanical properties

Cask Level

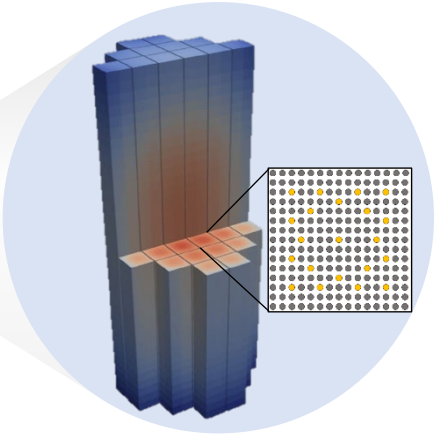

- COBRA-SFS
- GIFT

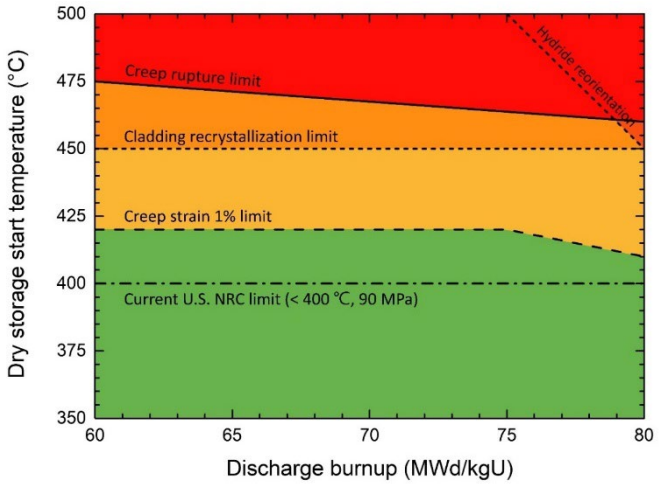

Spent nuclear fuel safety & Regulatory implication

Prediction of hoop mechanical properties

- **Background and Methodology**

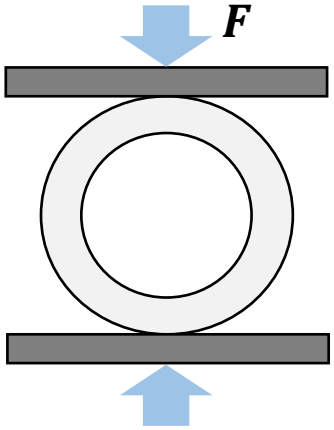

<Ring Compression Test>

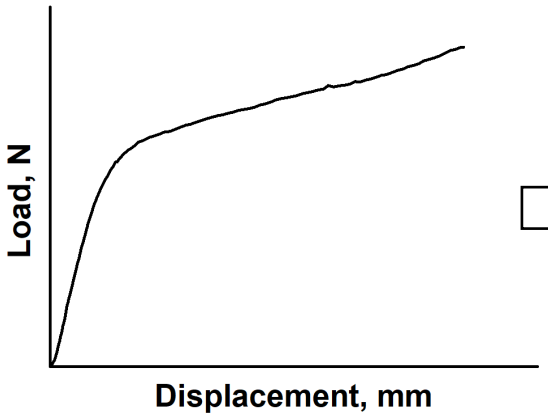

<Experimental Curve>

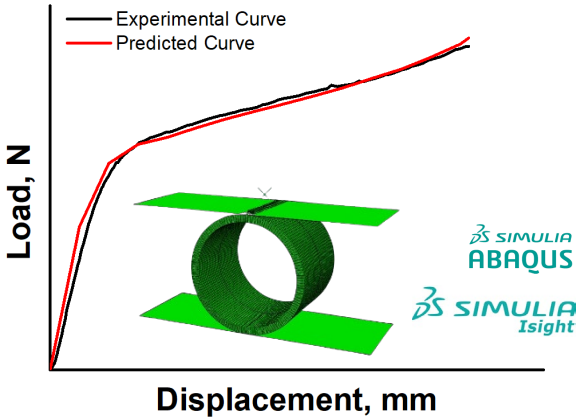

<Predicted Curve>

- Load displacement curve can be obtained from RCT.
- Hoop mechanical properties of the cladding cannot be obtained directly from the RCT.
- This research aims in obtaining the hoop mechanical properties via the RCT and Finite Element Analysis (FEA).
- Optimum predicted curve (k, ε_0, n) is based on the iteration method by using ABAQUS and ISIGHT.

Prediction of hoop mechanical properties

- **Extracting the hoop mechanical properties**

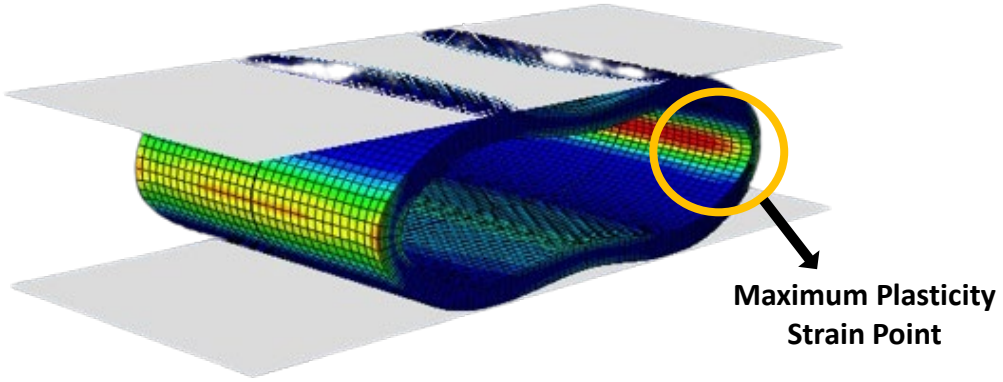

<Optimized modeled fractured specimen in Abaqus>

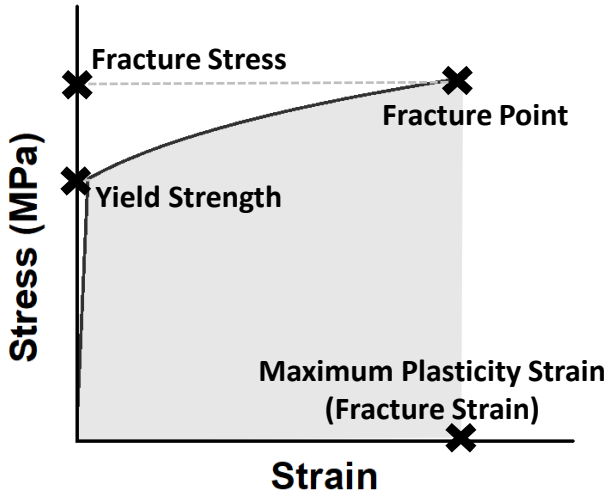

<Predicted Stress Strain Curve>

- Strain energy density (SED) can be obtained via the integration of internal energy over the whole specimen then be divided by the specimen length.
- Fracture is assumed to occur at the point of maximum plasticity strain.
- The plasticity stress strain curve was calculated by the strain hardening model $\boldsymbol{\sigma = k(\varepsilon_0 + \varepsilon)^n}$ [1-3].

[1] DeRuntz Jr, J.A. and P.G. HODGE JR, Crushing of a tube between rigid plates. 1962, ILLINOIS INST OF TECH CHICAGO.

[2] Nemat-Alla, M., Reproducing hoop stress–strain behavior for tubular material using lateral compression test. International Journal of Mechanical Sciences, 2003. 45(4): p. 605-621.

[3] Reddy, T.Y. and S. Reid, *On obtaining material properties from the ring compression test.* Nuclear Engineering and Design, 1979. **52**(2): p. 257-263.

Prediction of hoop mechanical properties

- **Result for specimens without radial H**

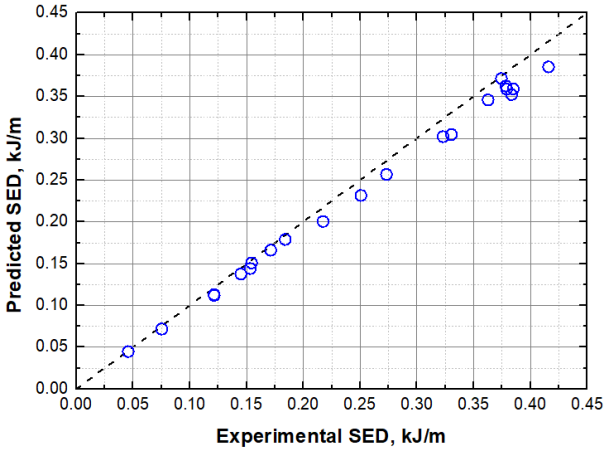

< Experimental SED vs Predicted SED>

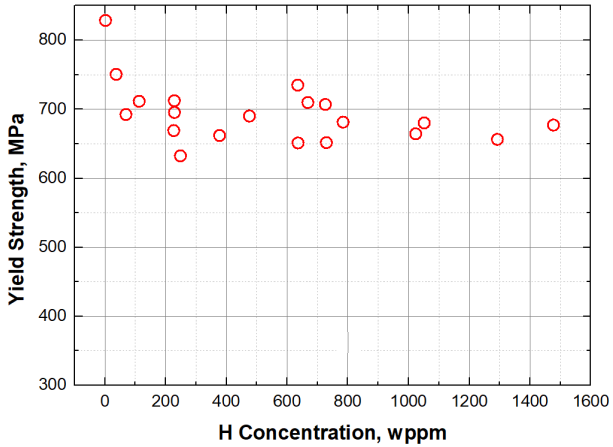

<Yield Strength>

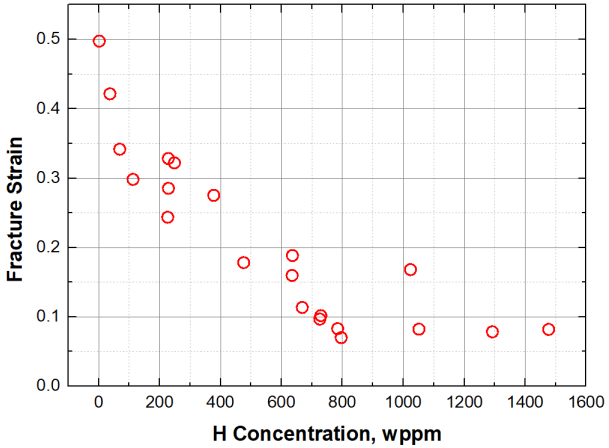

<Fracture Strain>

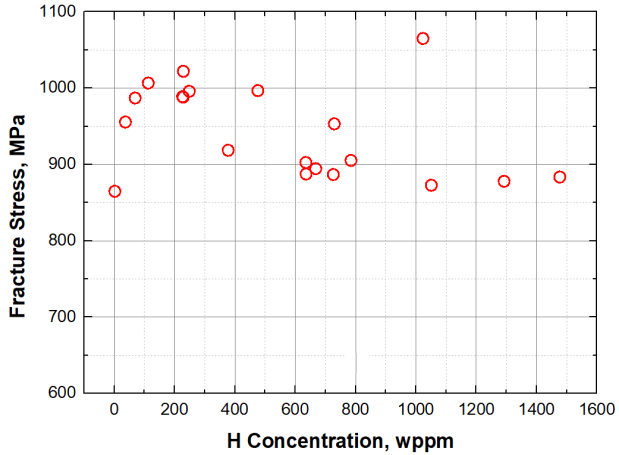

<Fracture Stress>

- SED and fracture strain decreases with the H concentration while yield strength and fracture stress do not have a strong correlation with the H concentration.

Hydride-induced embrittlement mechanisms

- **Embrittlement mechanisms in hydrided Zirconium**

  ① Intrinsic brittleness of hydrides

  - Fracture toughness: ZrH (~1 MPa·$m^{1/2}$) < Zr (~40 MPa·$m^{1/2}$) [3]

  ② Volume change due to hydride precipitation

  - The δ-hydride that was fabricated from α-zirconium exhibits numerous inner cracks due to the large volume change. [4]

  ③ Interface mismatch

  - Lattice mismatch between α-zirconium and δ-hydride occurs.

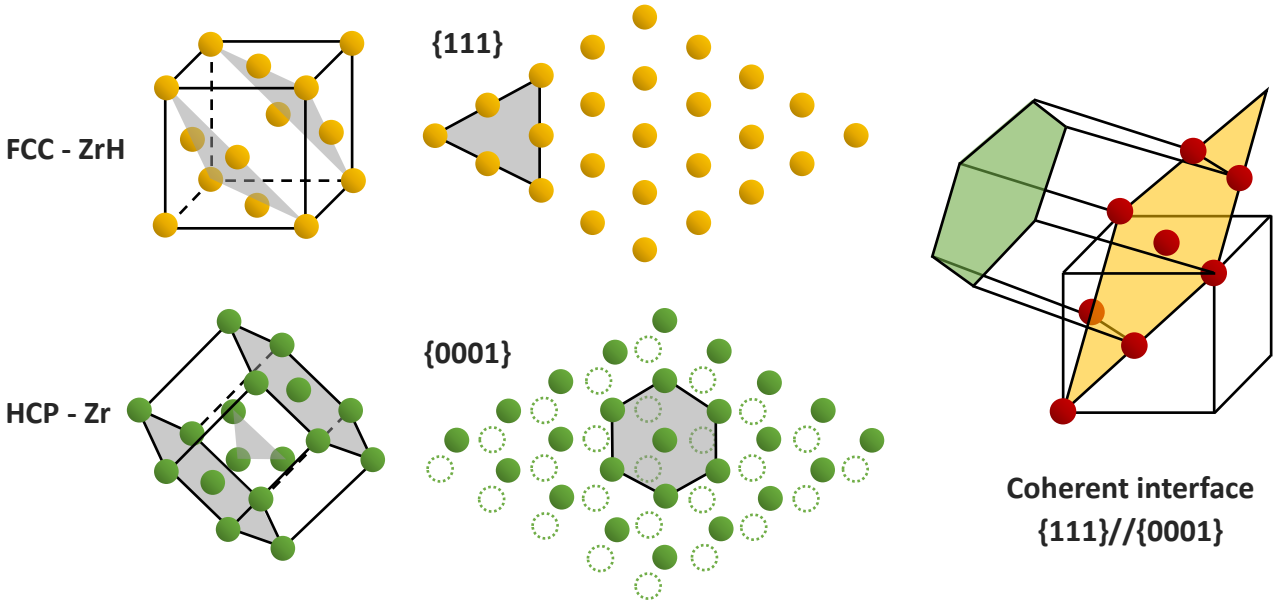

[3] Yu-Jie Jia et al., Mechanisms of Hydride Nucleation, Growth, Reorientation, and Embrittlement in Zirconium: A Review, Materials, 2023.
[4] Hiroaki Muta et al., Effect of hydrogenation conditions on the microstructure and mechanical properties of zirconium hydrides, Journal of Nuclear Materials, 2018.

Ongoing research using HR-TEM

- **HR-TEM Interface analysis**

<18 MPa Radial H>

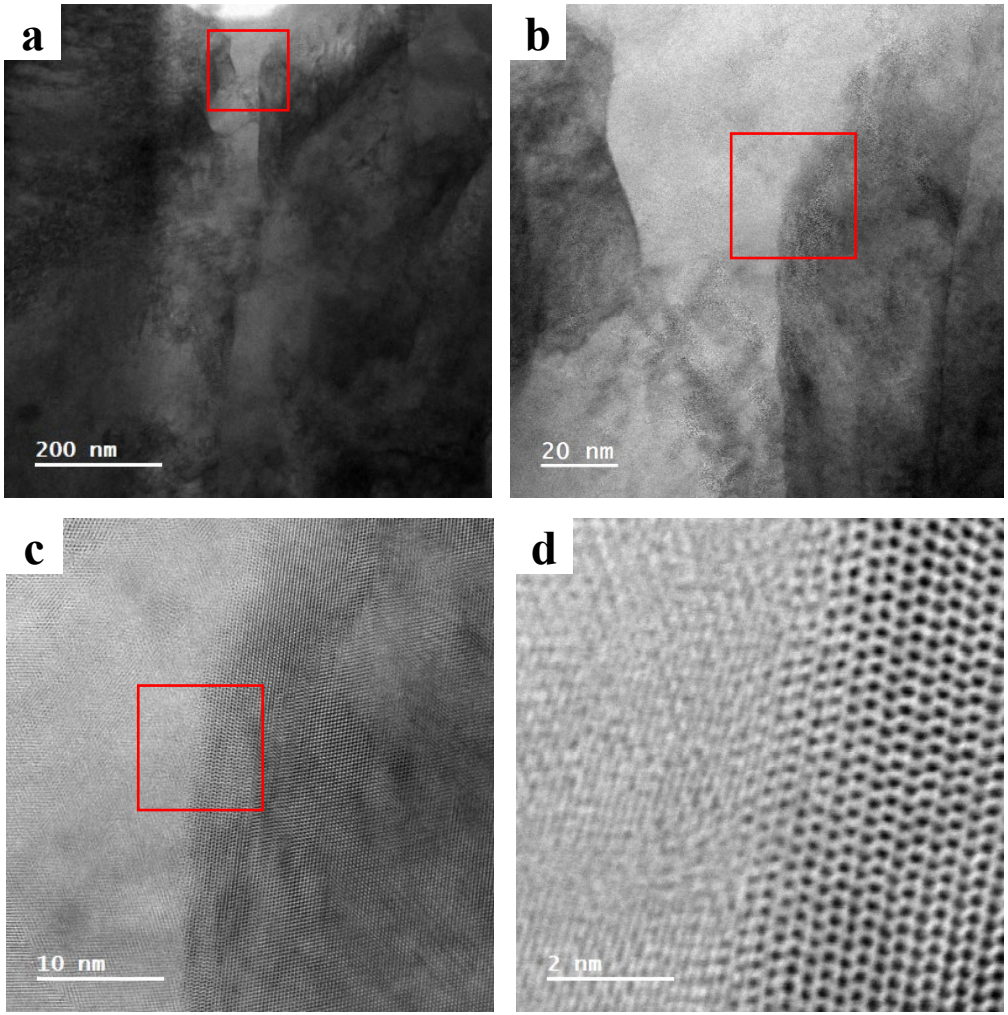

- Interface can be observed in atomic order using HR-TEM analysis method.

Interface analysis in summary

▣ Key findings of EBSD analysis

1. No significant interface difference between circumferential and radial hydrides.
2. There are no strongly preferred interface plane in both cases.
3. The analyzed planes exhibited large scatter.

▣ Key findings of TEM analysis

1. Interface plane was different in circumferential and radial hydrides.
2. Lack of data, yet it is predicted that there will be no unified interface plane in analyzed hydrides.

No significant difference in hydride-Zr matirx interface energy between circumferential and radial hydrides.

Q. No significant difference in solubility between circumferential/radial hydrides ?

Supplementary: Interface in HCP

- **Two angle information from HCP interface plane**

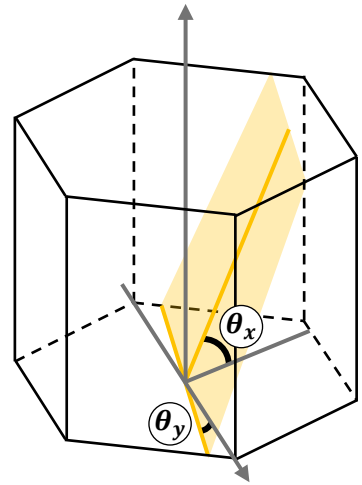

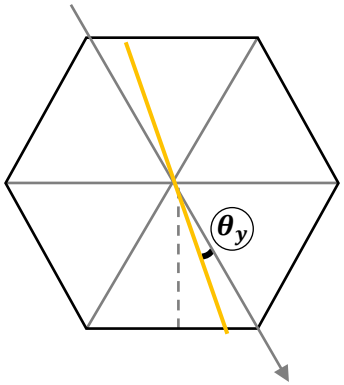

- Cutting angle in basal plane
- Min: 0° / Max: 30 °

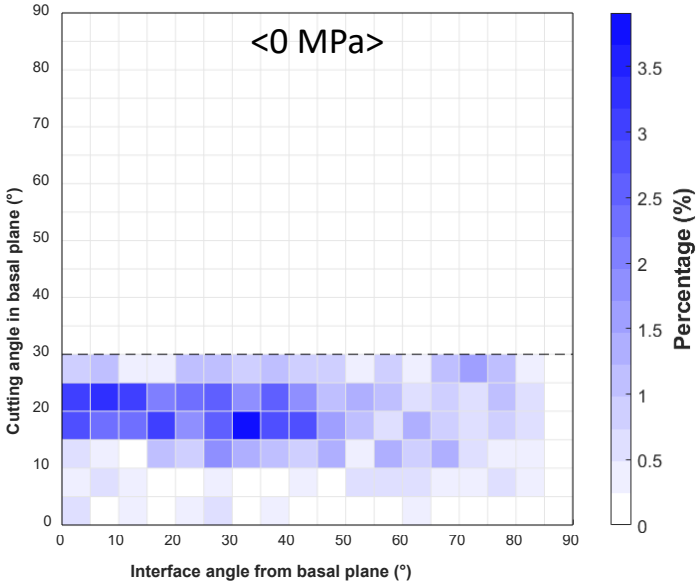

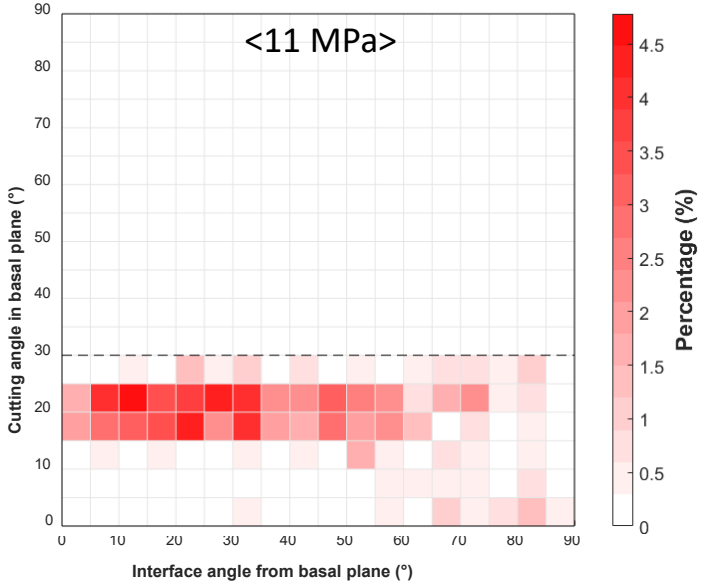

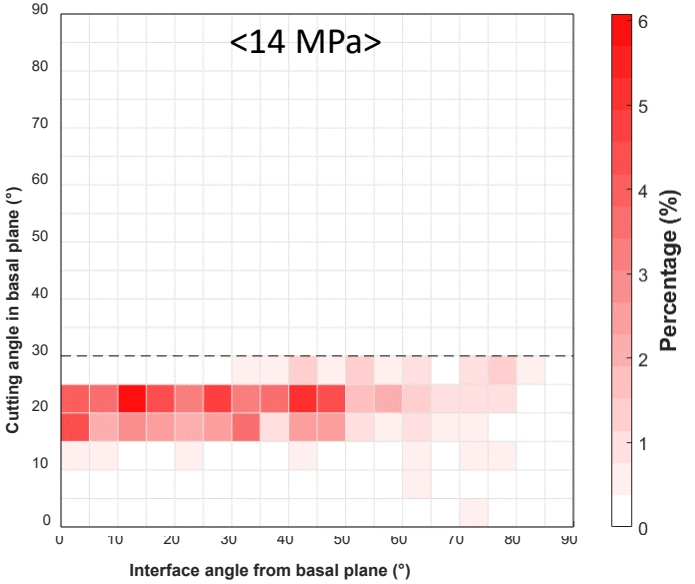

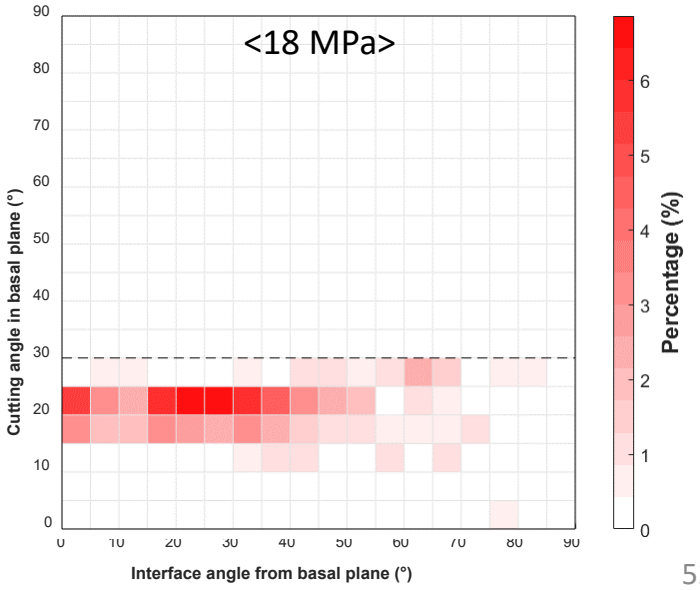

Supplementary: OR Analysis in EBSD

- **OR analysis in EBSD**

➢ Angle between HCP {0001} and FCC {111} in each interface.

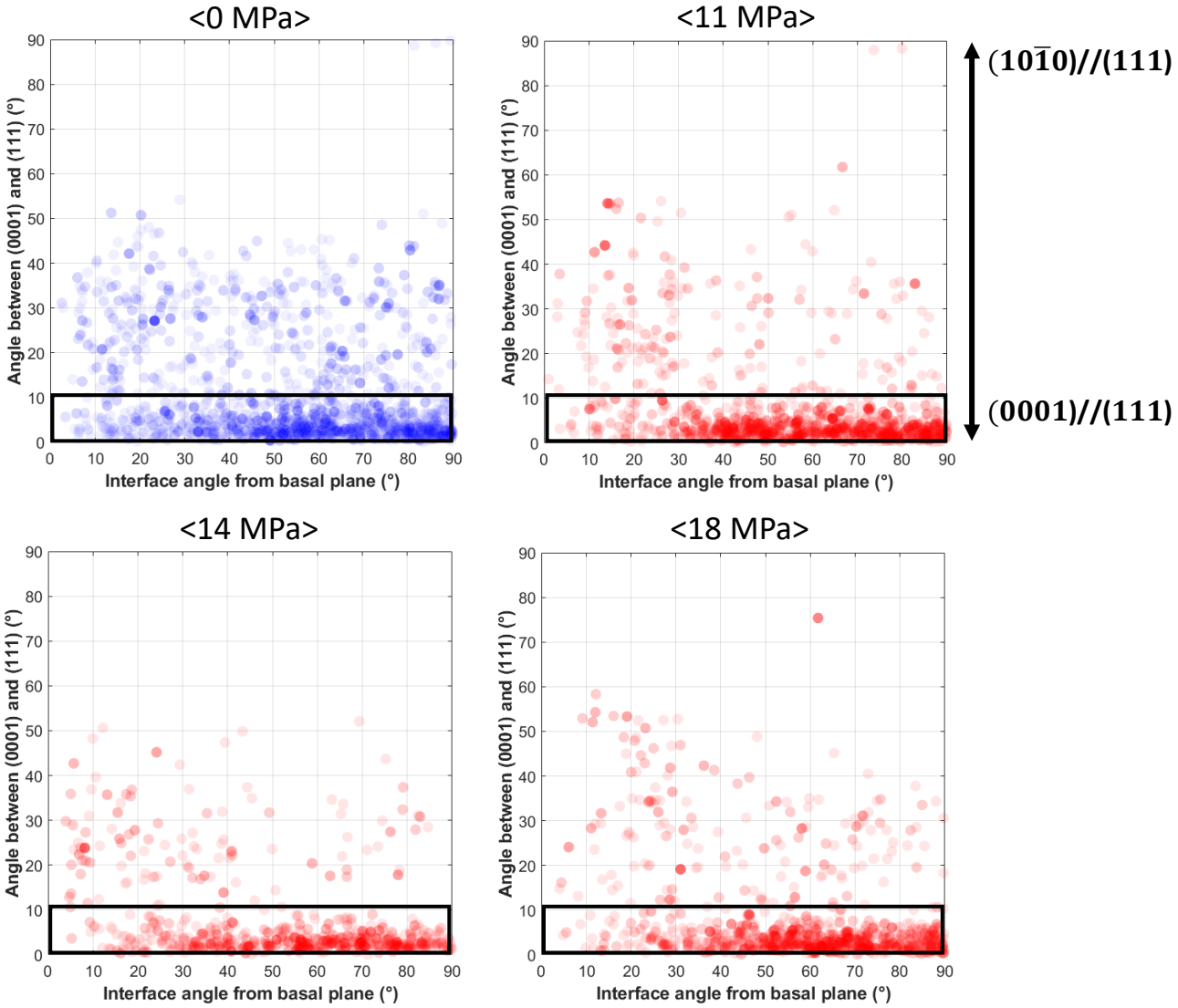

Microstructural Characterization: Foundation of understanding hydride using EBSD & TEM

“Interface Microstructure Characterization”

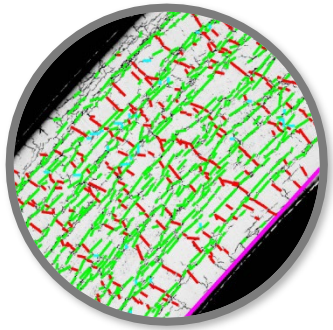

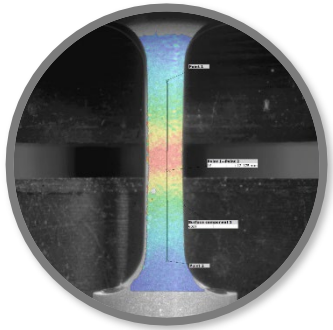

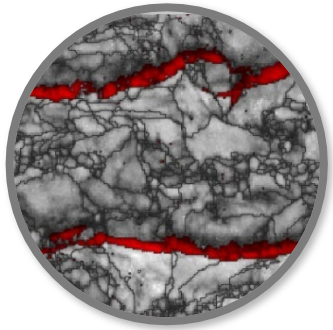

#1. Modeling hydride reorientation

- Traditional misfit strain assumption
  : Circumferential hydride — Basal plane
  Radial hydride — Prismatic plane

- **Is it applicable to the reactor-grade Zirconium cladding ?**

#2. Understanding axial mechanical strength

- Effect on axial mechanical strength
  : Circumferential hydrides ≈ Radial hydrides

- **What is the essential difference in terms of the dissolution energy ?**

#3. Understanding solubility

- Some countries experience extremes in temperature due to environmental factors
  : Effect of thermal cycling (repeated freeze-thaw cycles)
  Repeated dissolution and precipitation of hydrides

- **Is there any difference in solubility of radial hydride ?**

Orientation relationship and interface

- **Orientation Relationship**

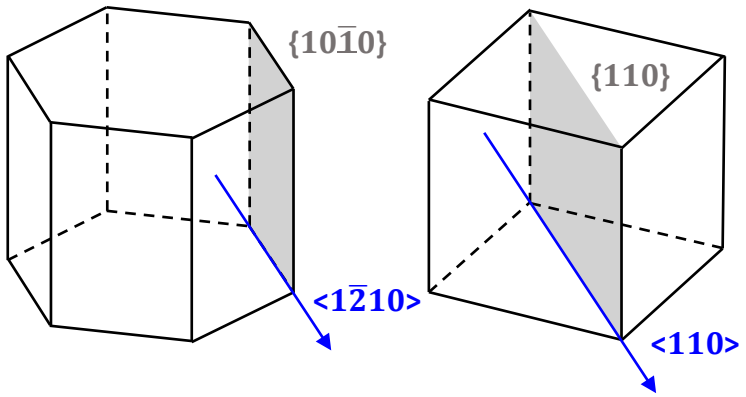

OR	HCP	FCC
Plane Parallel	{10$\bar{1}$0}	{110}
Direction Parallel	<1$\bar{2}$10>	<110>

- **Interface**

- The interface separates two different phases that can have different crystal structures.

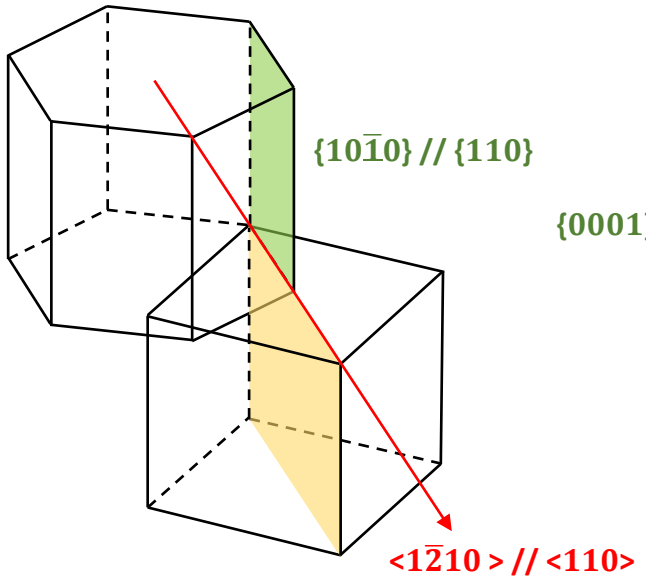

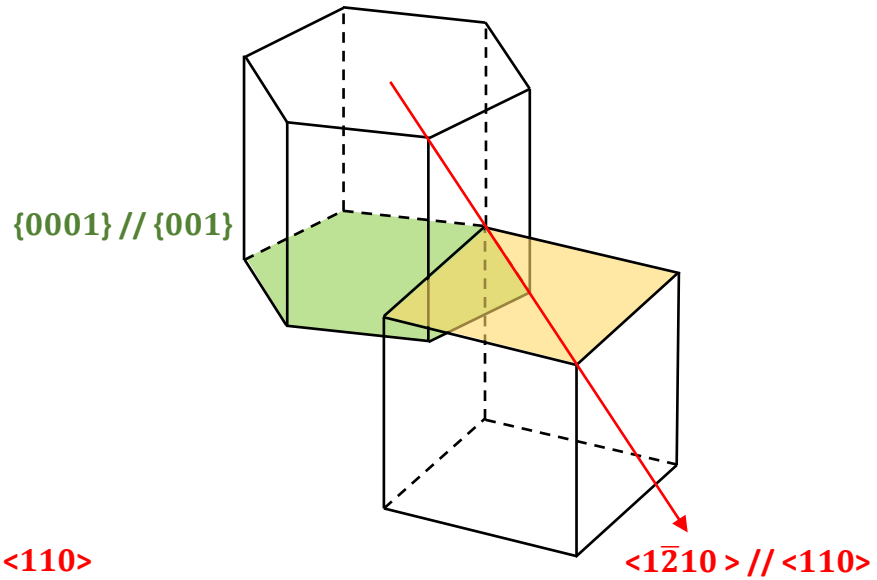

Introduction

- Since spent nuclear fuel is a kind of High Level Radioactive Waste, it is important to successfully remove decay heat and radiation.

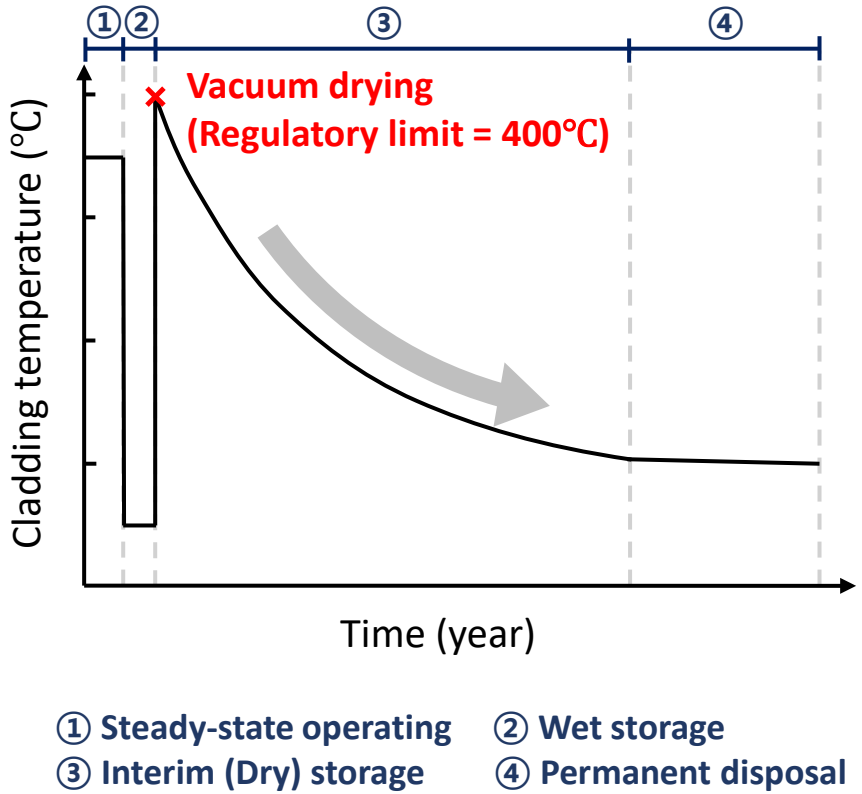

<Circumferential hydride>

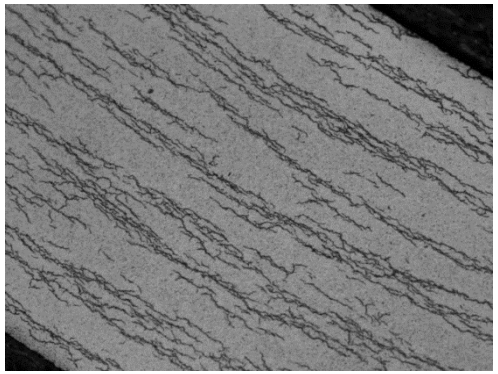

<Radial hydride>

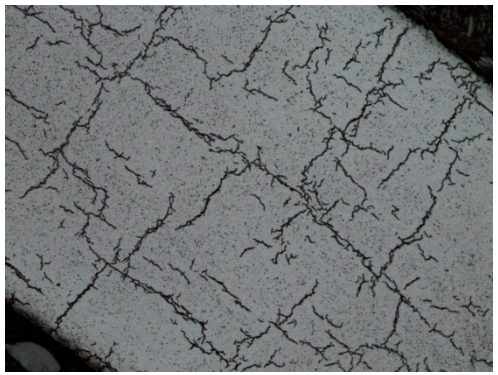

- As cladding cools down from 400℃, hydrogen precipitation occurs during dry storage.
- Hydrides precipitate in radial direction rather than circumferential direction due to applied stress higher than a threshold hoop stress.

Dissolution energy and solubility analysis

- **Sample preparation**

1. ~4mm ring specimen

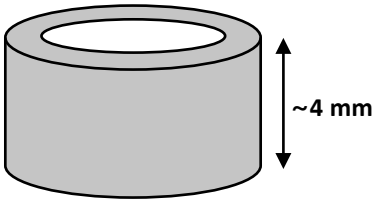

2. Cut into 4 sub-specimens

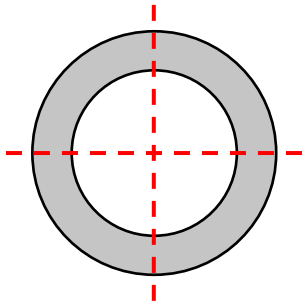

3. Polish the bottom plane

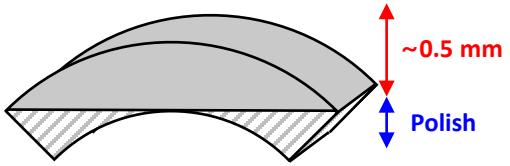

- **Determining H contencentration**

<Exemplary result of DSC – Heating>

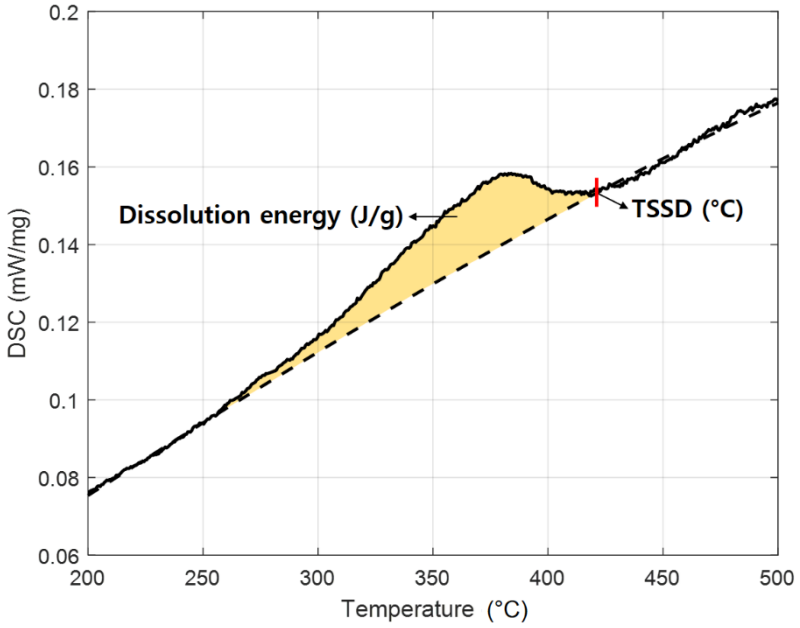

<Cross-validation of H concentration>

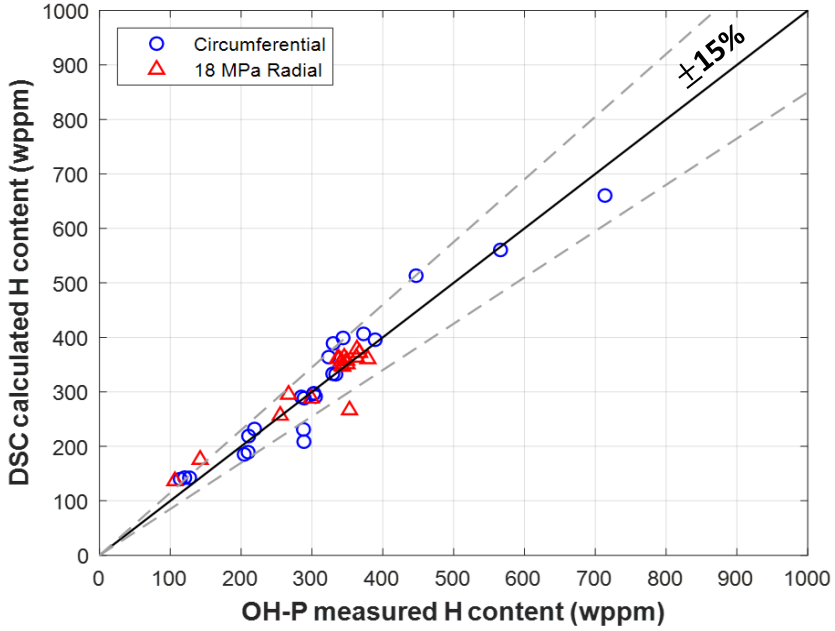

J. Bertsch

PSI

Hydrogen diffusion and precipitation in fuel cladding under stress, at various temperatures and under the influence of a liner, using neutron imaging

At the hot surface of nuclear fuel rods being operated in a light water reactor, water is dissociated, whereas the oxygen leads to oxidation, and a certain fraction of hydrogen is picked up. The hydrogen diffuses freely in the Zr-alloy cladding. When the solubility limit is reached, the hydrogen forms a hydrogen-metal compound, hydrides, which are brittle. Of interest are the location and morphology of hydrides, possible hydrides accumulations, and the driving forces which lead to respective hydrides arrangements. A high hydrides concentration and/or a disadvantageous orientation of hydrides lead to a deterioration of the mechanical properties of the cladding.

There are four driving forces for hydrogen diffusion, (i) the concentration gradient (diffusion from high to low hydrogen concentration), (ii) a temperature gradient (diffusion from areas with higher temperature to those with lower temperature), (iii) a stress gradient (diffusion from areas with lower tensile stress to those with higher stress), and (iv) the gradient of electrochemical potential (e.g. different adjacent materials, different hydrogen solubilities).

In the present work examples are shown for the hydrogen relocation under a stress gradient, for cladding material with a gradient of the electrochemical potential having a so-called liner, and under different cooling conditions. Claddings can have an inner or outer liner. Those with an outer liner are used in pressurized water reactors, and the liner shall improve the corrosion resistance. Claddings with an inner liner are applied in boiling water reactors, and the liner mitigates effects of pellet-cladding interaction (PCI). The liner, in contrast to the cladding substrate, is a bit softer, has a somewhat purer Zr-alloy and typically larger grains. Its thickness is a couple of tens of micrometers. In post-irradiation examinations, the liner often shows a high concentration of hydrides, i.e., the liner acts as hydrogen / hydrides sink.

An excellent method to visualize the hydrogen or hydrides distribution in a cladding is neutron imaging (NI) because hydrogen attenuates neutrons much stronger than zirconium. We have performed NI using PSI's neutron microscope, applied to cladding sections in axial direction with a length of 4-5 mm. The spatial resolution of the NI is below 10 microns, the concentration resolution for hydrogen is about few tens of wppm. The claddings tested for this work exhibit integral hydrogen concentrations of several hundred wppm.

Examples shown are the diffusion of hydrogen towards the liner as function of cooling rate. An additionally applied stress leads to reduced or increased hydrogen precipitation in the liner close to its interface with the substrate, depending on whether the stress gradient works in line with the hydrogen-attracting liner or inversely. The orientation and reorientation of the hydrides platelets is also determined. Further, examples of so-called Delayed Hydride Cracking (DHC) are shown, whereas an inner liner slows down the crack propagation rate of an outside-inside crack because of holding back of hydrogen in the liner. Finally, the stress induced hydrogen relocation can be seen in ring compression creep tests, giving hints for creep modelling. For the examples, the hydrogen concentration distribution could be mapped and quantified.

PAUL SCHERRER INSTITUT

PSI

Johannes Bertsch :: Nuclear Fuels :: Paul Scherrer Institut

L. Duarte, A. Colldeweih, F. Fagnoni, M. Meyer, D. Mota, D. Sanchez, P. Trtik, O. Yetik, R. Zubler

Hydrogen diffusion and precipitation in fuel cladding under stress, at various temperatures and under the influence of a liner, using neutron imaging

28th Quench Workshop, 5 Dec 2023

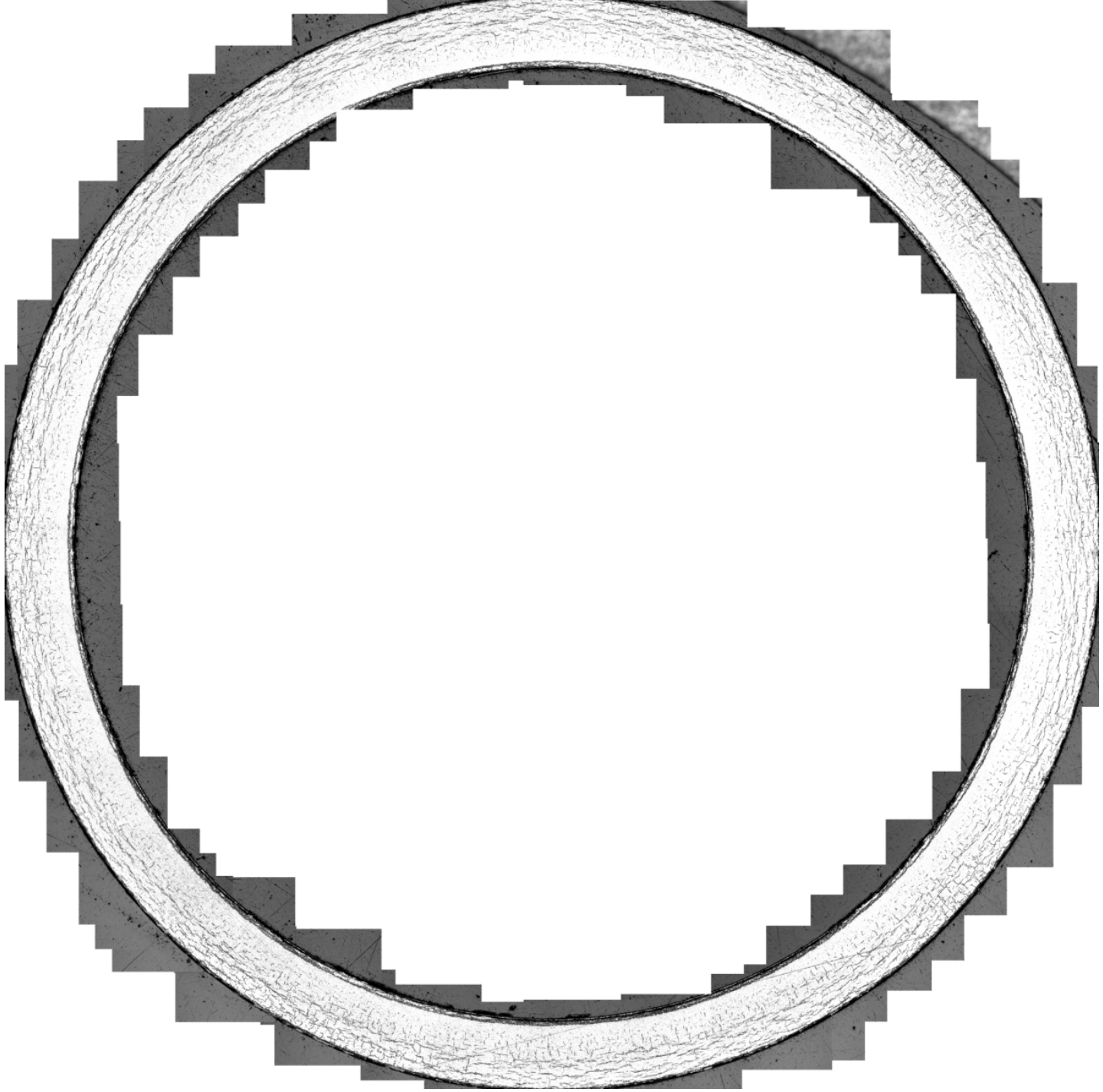

Hydrogen in Cladding

Hydrogen

Where does it go and what does it do? – solid solution

- Diffusion
  - Concentration gradient
  - Temperature gradient
  - Stress gradient
  - Electrochem. potential gradient (material, microstructure, TSSP)

The 4 gradients

$$Zr + 2\ H_2O \rightarrow ZrO_2 + 2\ H_2$$

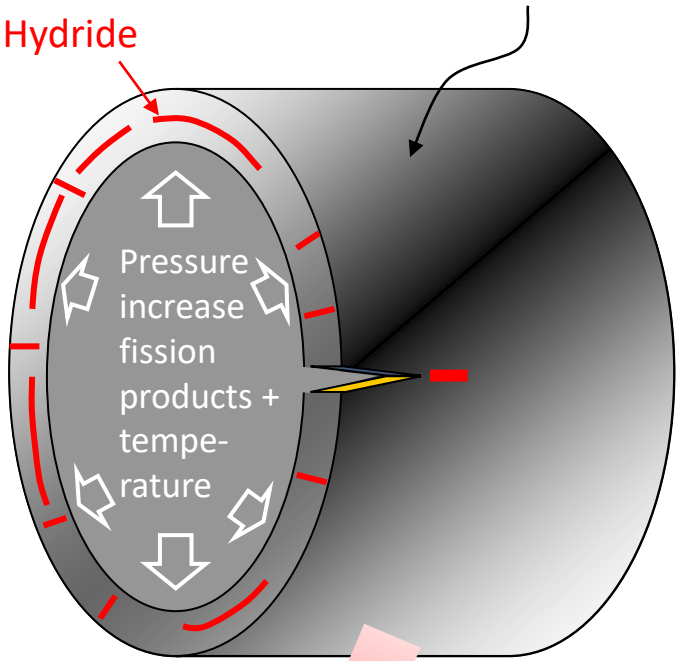

Where does it settle and how does it look like? – precipitation

- Temperature development
- Solubility limit
- Microstructure, texture
- Stress
  - Orientation
  - Location and DHC

Not yet very well understood is trapped hydrogen, neither at higher temperatures (solid solution) nor in the form of hydrides.

We are interested in …

Hydrogen

Solid solution / Diffusion

- Stress
- Temperature (time)
- Liner

Precipitation / Hydrides

- Stress
- Temperature (time)
- Liner

⇨ Hydrides characteristiques
(where, how much, how do they look like, …?)

⇨ **Neutron imaging**

⇨ Synchrotron investigations

⇨ Metallography

Hydrogen redistribution	Hydrides reorientation	Delayed Hydride Cracking (DHC)	Creep

Neutron imaging

Neutron Imaging

Various beam lines at PSI

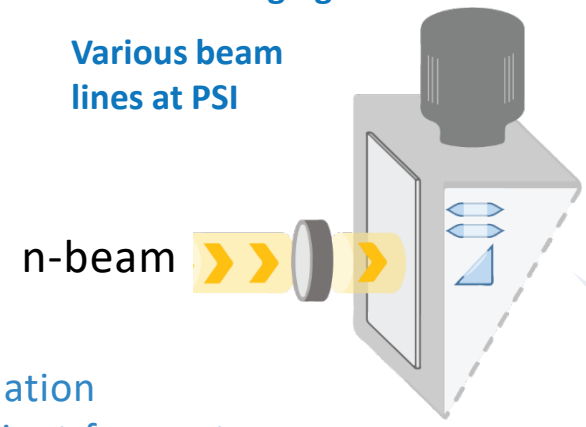

Attenuation coefficient for neutrons

H	Zr
3.44	0.29

Image (n-microscopy resolution < 10 µm)

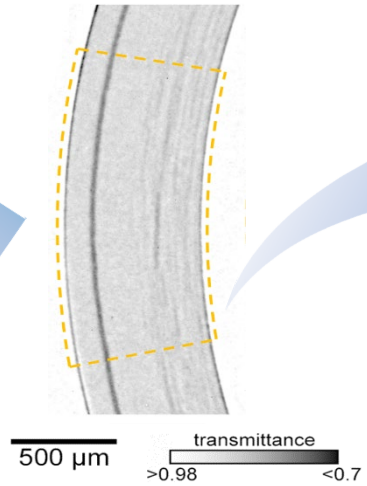

Quantification

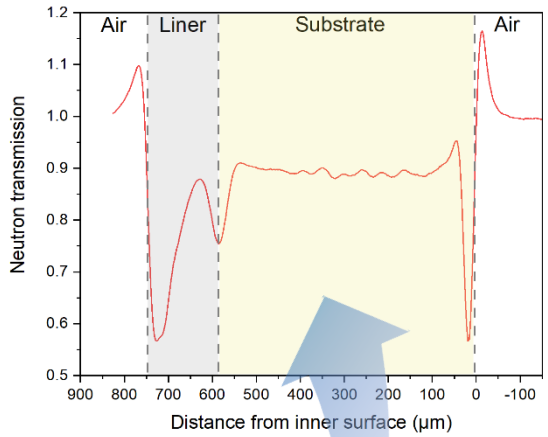

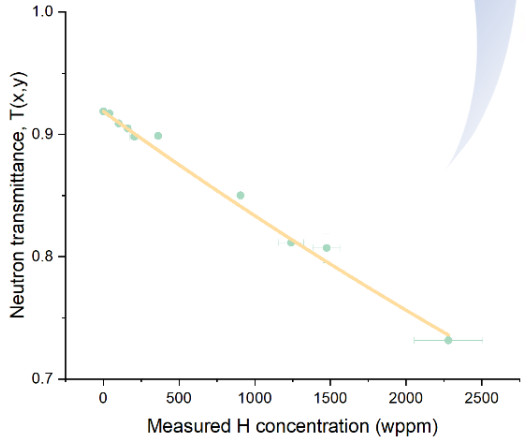

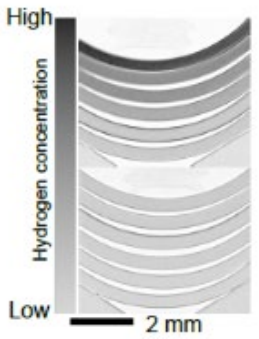

Hydrogen redistribution

Hydrides reorientation

Delayed Hydride Cracking (DHC)

Creep

all 200 wppm hydrogen

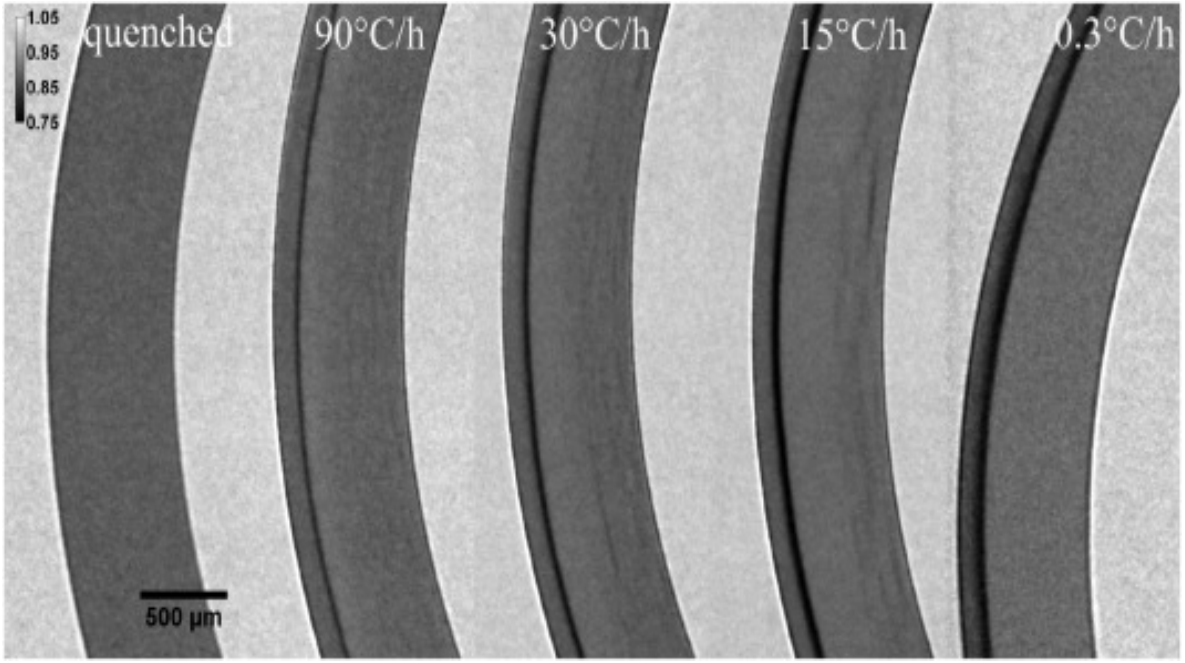

W. Gong, P. Trtik, A.W. Colldeweih, L.I. Duarte, M. Grosse, E. Lehmann, J. Bertsch; JNM, 526 (2019) 151757

PAUL SCHERRER INSTITUT

PSI

- Hydrogen redistribution
- Hydrides reorientation
- Delayed Hydride Cracking (DHC)
- Creep

all 200 wppm hydrogen

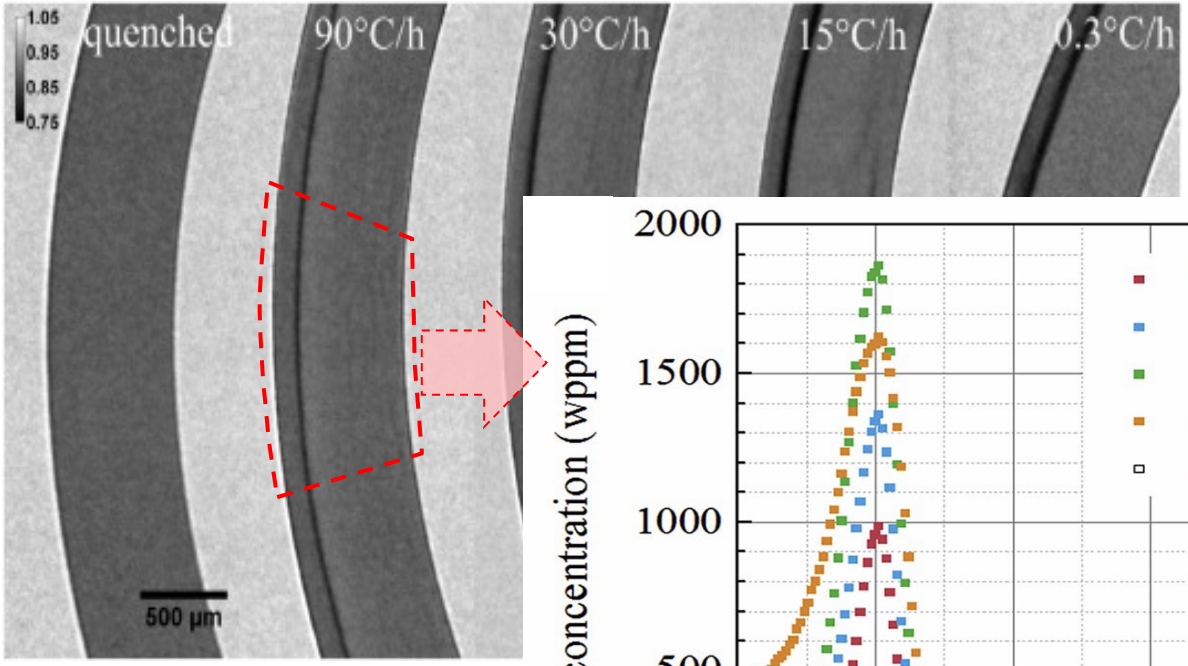

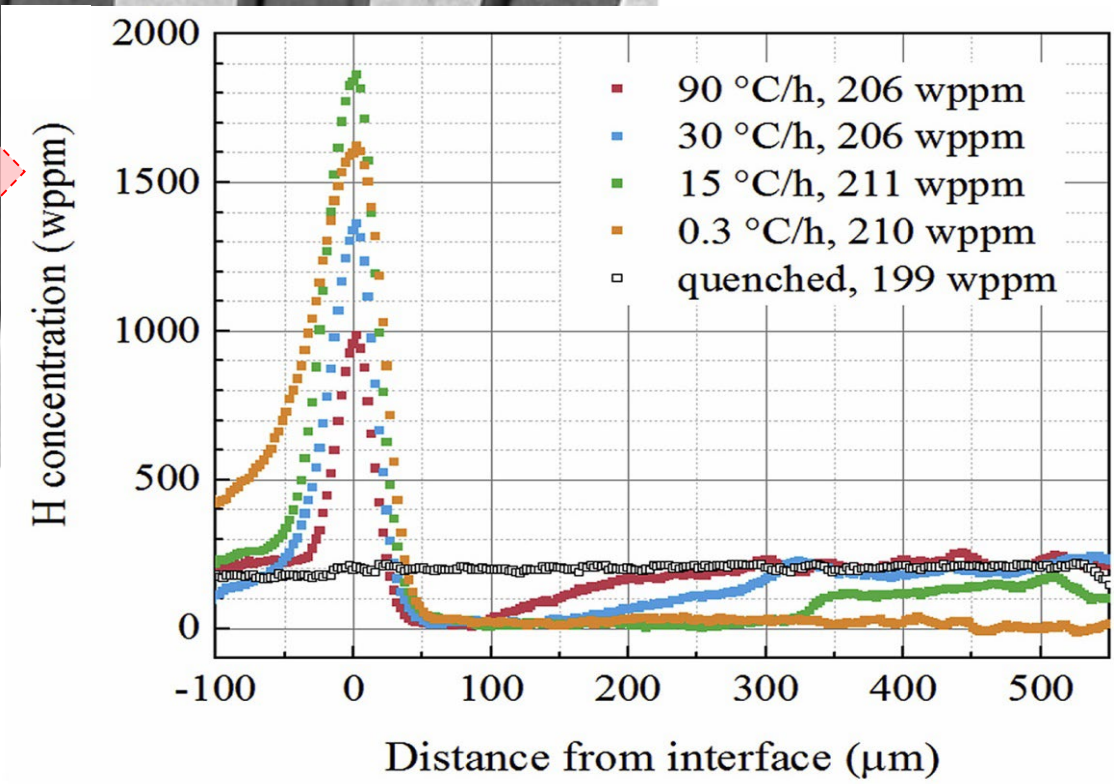

W. Gong, P. Trtik, A.W. Colldeweih, L.I. Duarte, M. Grosse, E. Lehmann, J. Bertsch; JNM, 526 (2019) 151757

Hydrogen redistribution

Hydrides reorientation

Delayed Hydride Cracking (DHC)

Creep

Double half cylinder test

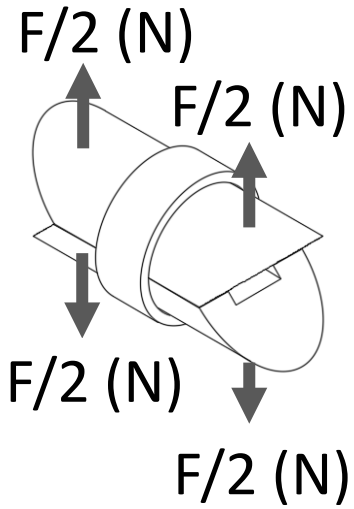

Stress distribution

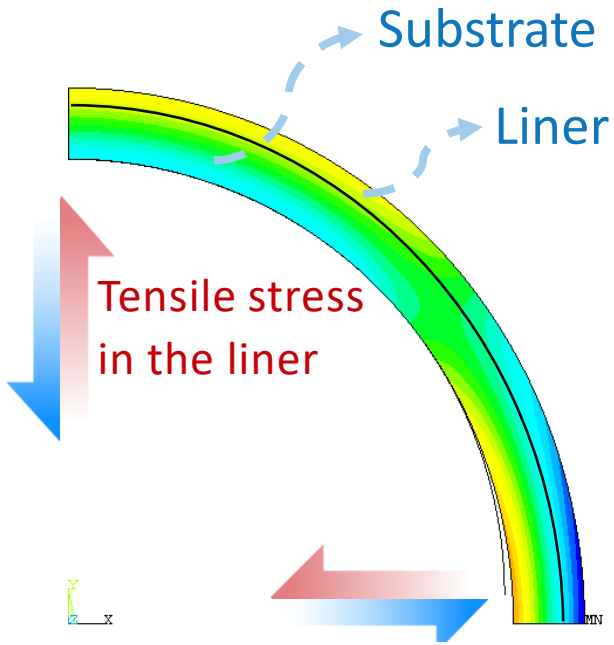

O. Yetik et al, Influence of Irradiation Damage and Thermomechanical Treatments on the Hydride Distribution in Zirconium-Based Nuclear Fuel Claddings, E-MRS 2023 fall meeting, 18-21 Sept 2023, Warsaw, Poland

PAUL SCHERRER INSTITUT

PSI

Hydrogen redistribution

Hydrides reorientation

Delayed Hydride Cracking (DHC)

Creep

Load and temperature curves

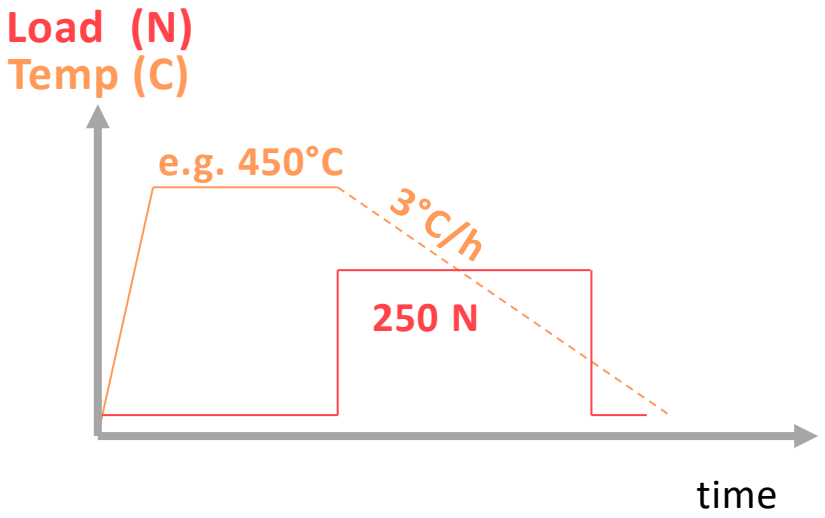

Hydrogen driving forces

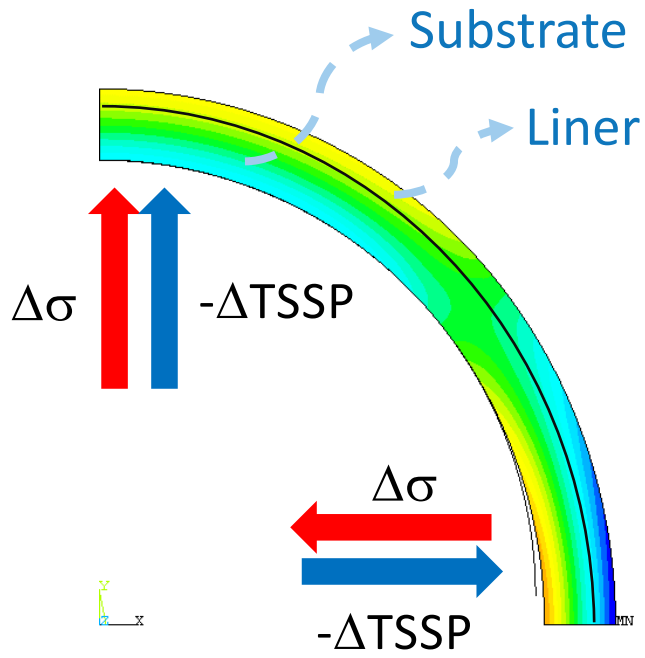

O. Yetik et al, Influence of Irradiation Damage and Thermomechanical Treatments on the Hydride Distribution in Zirconium-Based Nuclear Fuel Claddings, E-MRS 2023 fall meeting, 18-21 Sept 2023, Warsaw, Poland

PAUL SCHERRER INSTITUT

PSI

Hydrogen redistribution

Hydrides reorientation

Delayed Hydride Cracking (DHC)

Creep

non-irradiated, DX-D4, homogenized at 450˚C (incomplete hydrides dissolution)

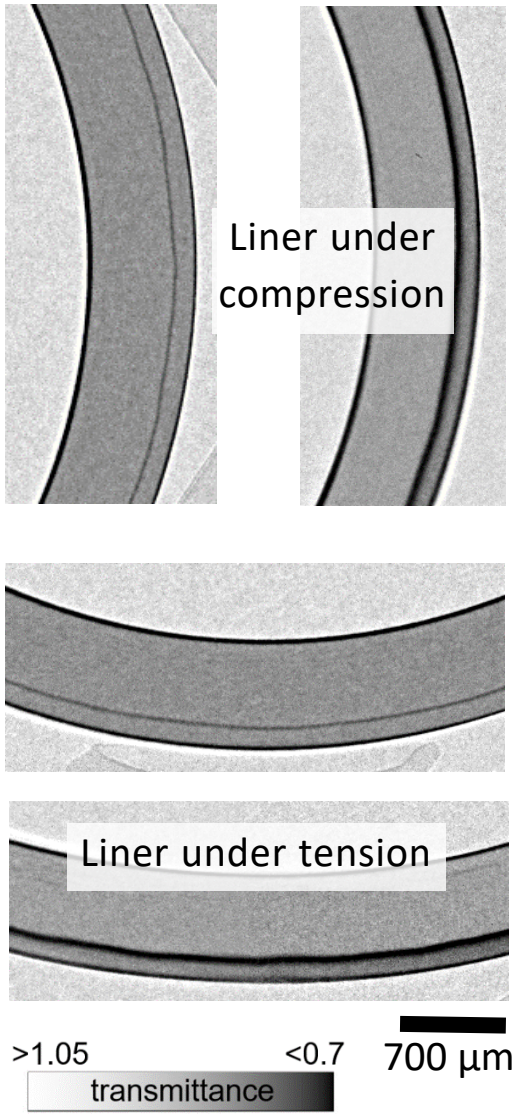

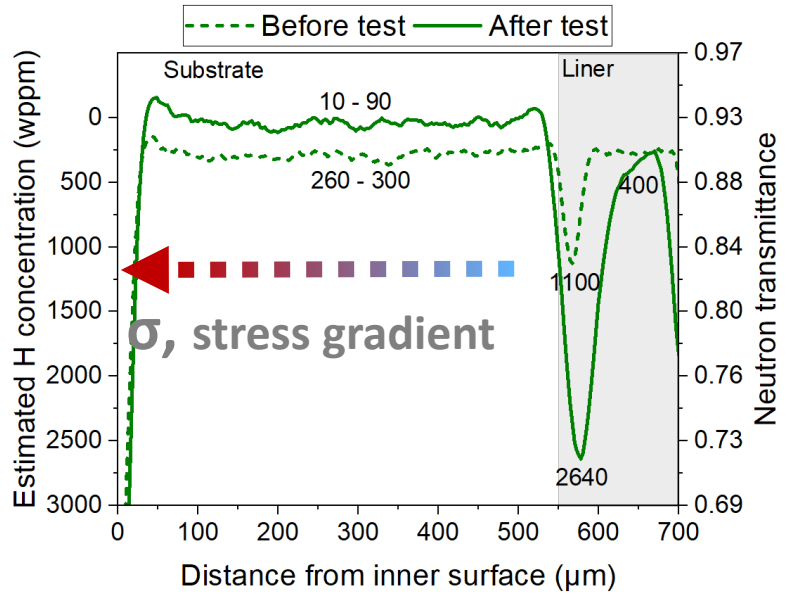

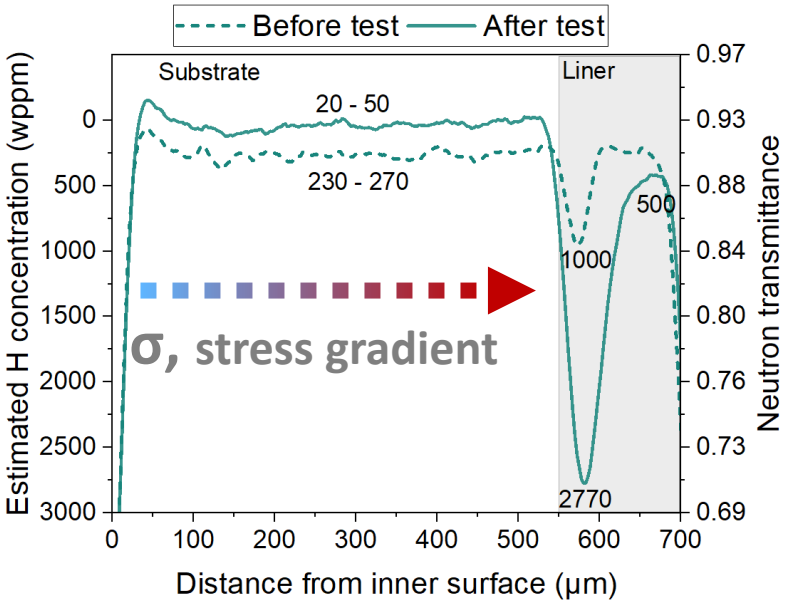

PAUL SCHERRER INSTITUT

PSI

Hydrogen redistribution

Hydrides reorientation

Delayed Hydride Cracking (DHC)

Creep

Irradiated, DX-D4, not homogenized

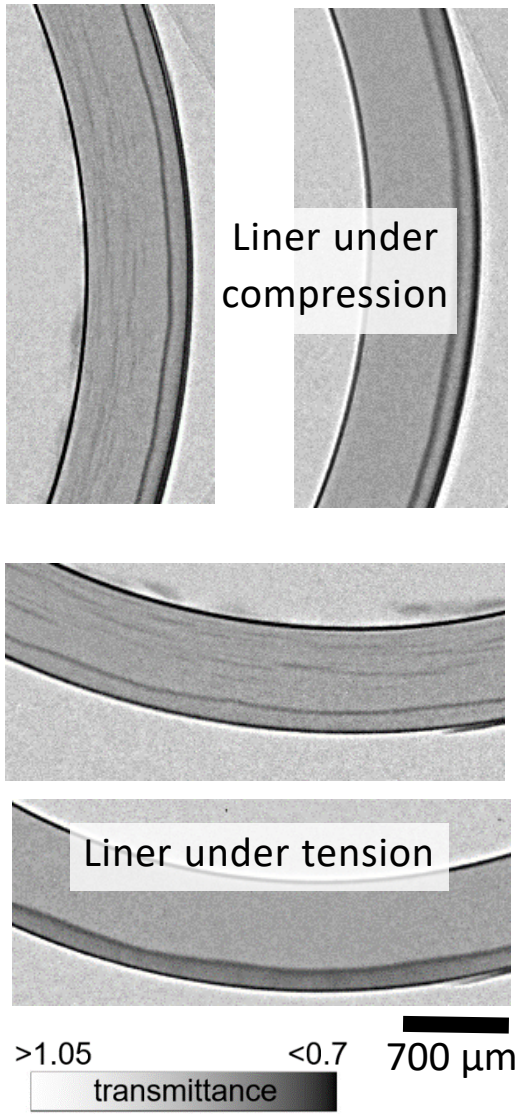

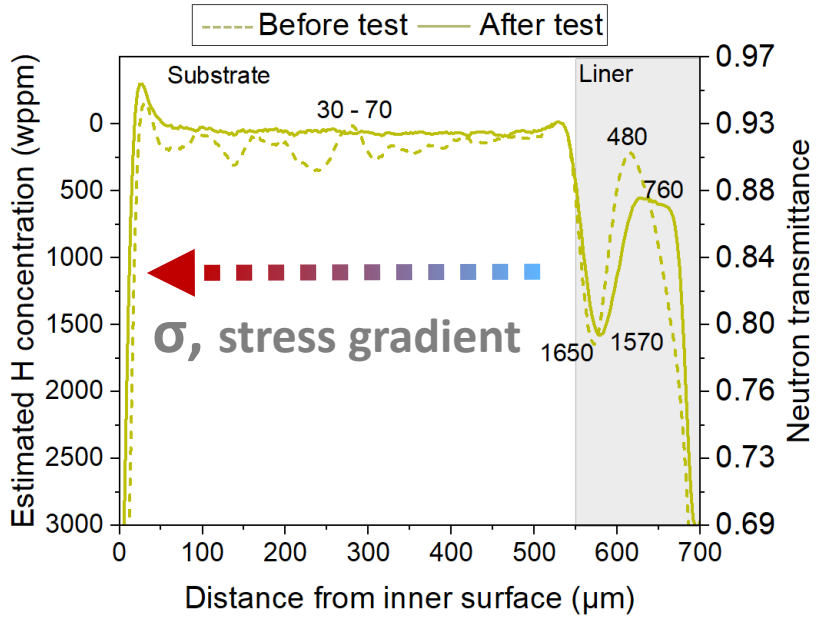

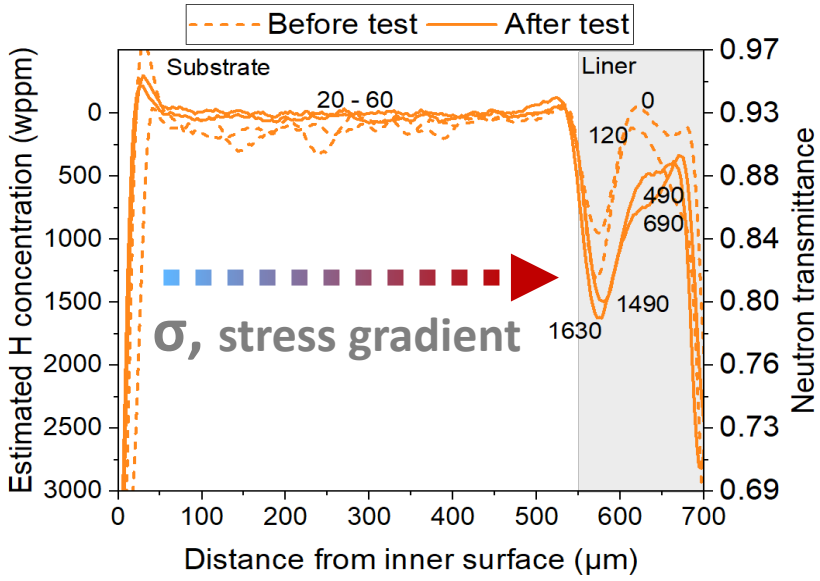

PAUL SCHERRER INSTITUT

PSI

Hydrogen redistribution

Hydrides reorientation

Delayed Hydride Cracking (DHC)

Creep

We had earlier performed hydrides reorientation tests, also with cycling, not very much considering the effect of the liner (the result was as expected with a reorientation threshold of about 75 Mpa).

Heat treatment 400°C, cooling 30°C/h
(faster than the slow cooling tests)

We took the images for 200 wppm hydrogen (full dissolution at the first cycle) again and looked separately at the different regions of the cladding, i.e. **liner under tension** and **liner under compression**

PAUL SCHERRER INSTITUT

Hydrogen redistribution

Hydrides reorientation

Delayed Hydride Cracking (DHC)

Creep

H concentration
200 wppm

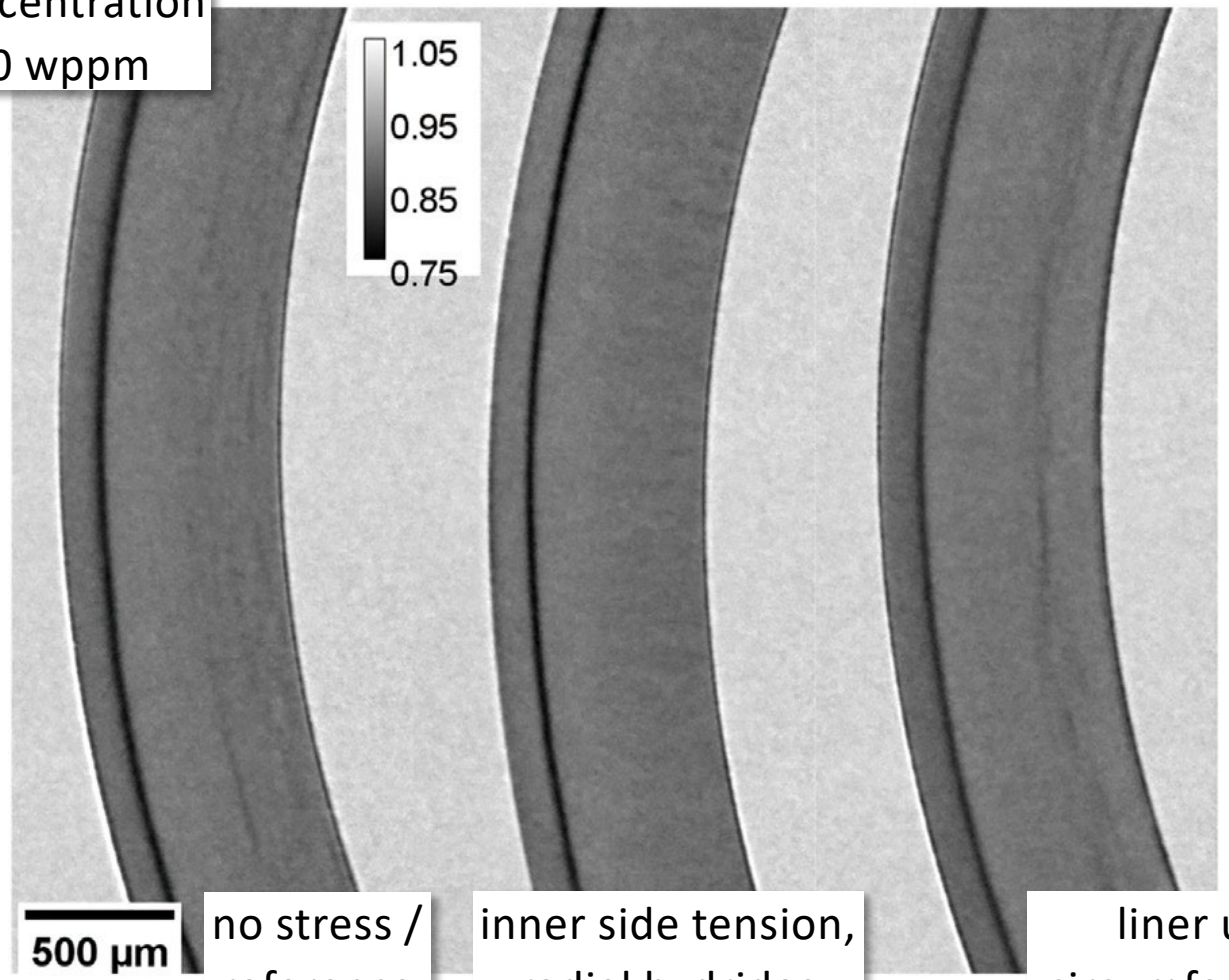

1 cycle
T_{max} = 400°C
$\Delta T_{cooling}$ = 30°C/h

no stress / reference

inner side tension, radial hydrides

liner under tension, circumferential hydrides in substrate

W. Gong, P. Trtik, F. Ma, Y. Jia, J. Li, J. Bertsch, Hydrogen diffusion and precipitation under non-uniform stress in duplex zirconium nuclear fuel cladding investigated by high-resolution neutron imaging, JNM 570 (2022) 153971

PAUL SCHERRER INSTITUT

PSI

- Hydrogen redistribution
- **Hydrides reorientation**
- Delayed Hydride Cracking (DHC)
- Creep

H concentration
200 wppm

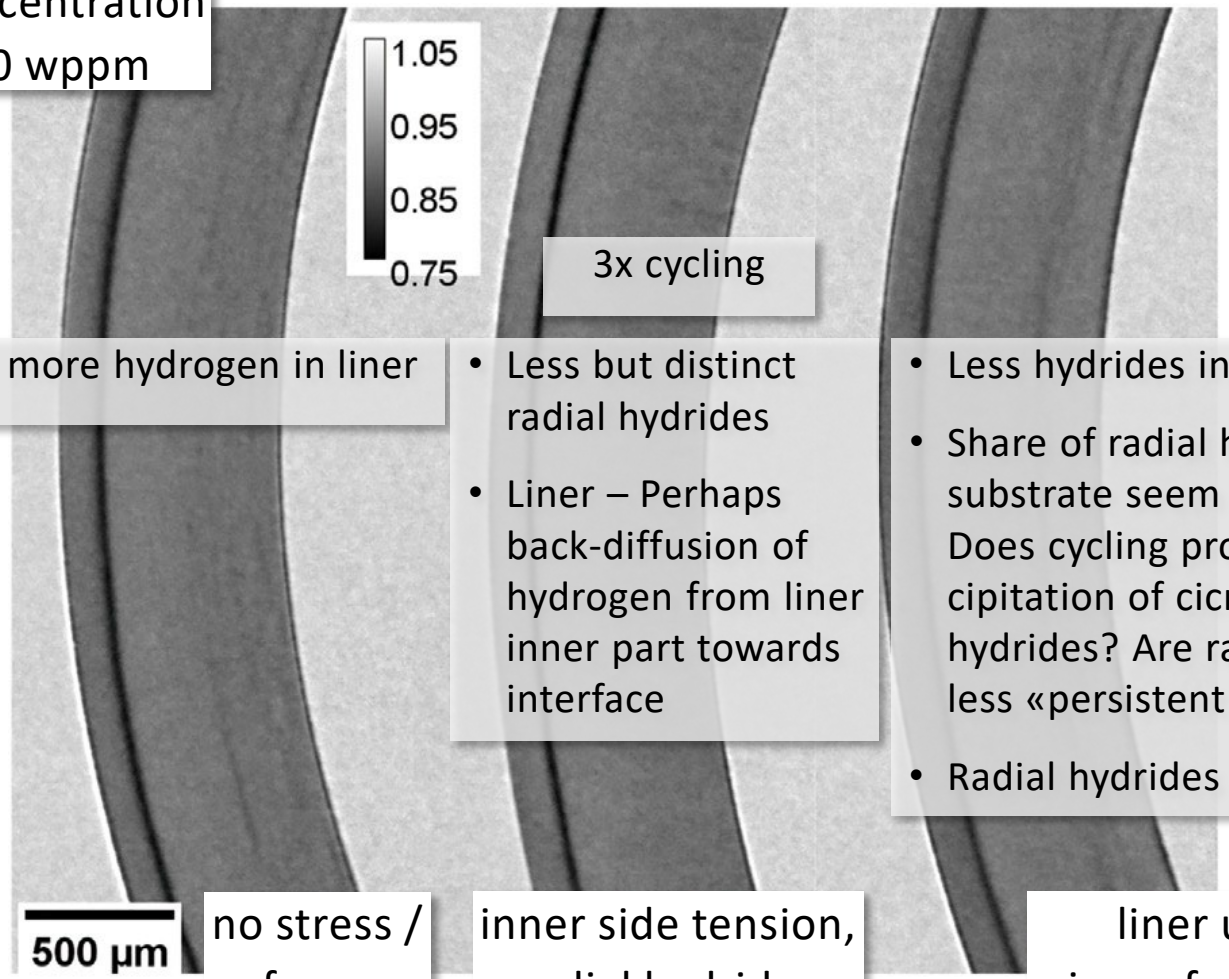

1 cycle
T_{max} = 400°C
$\Delta T_{cooling}$ = 30°C/h

3x cycling

no stress / reference	inner side tension, radial hydrides	liner under tension, circumferential hydrides in substrate
• more hydrogen in liner	• Less but distinct radial hydrides • Liner – Perhaps back-diffusion of hydrogen from liner inner part towards interface	• Less hydrides in substrate • Share of radial hydrides in substrate seem to decrease: Does cycling promote repre-cipitation of cicrcumferential hydrides? Are radial hydrides less «persistent»? • Radial hydrides occur in liner.

W. Gong, P. Trtik, F. Ma, Y. Jia, J. Li, J. Bertsch, Hydrogen diffusion and precipitation under non-uniform stress in duplex zirconium nuclear fuel cladding investigated by high-resolution neutron imaging, JNM 570 (2022) 153971

Hydrogen redistribution

Hydrides reorientation

Delayed Hydride Cracking (DHC)

Creep

Universal mechanical testing machine :

- γ-Shielding
- α-box (low pressure inside)
- highly radioactive samples up to 750° C
- long-distance microscope

Hydrogen redistribution

Hydrides reorientation

Delayed Hydride Cracking (DHC)

Creep

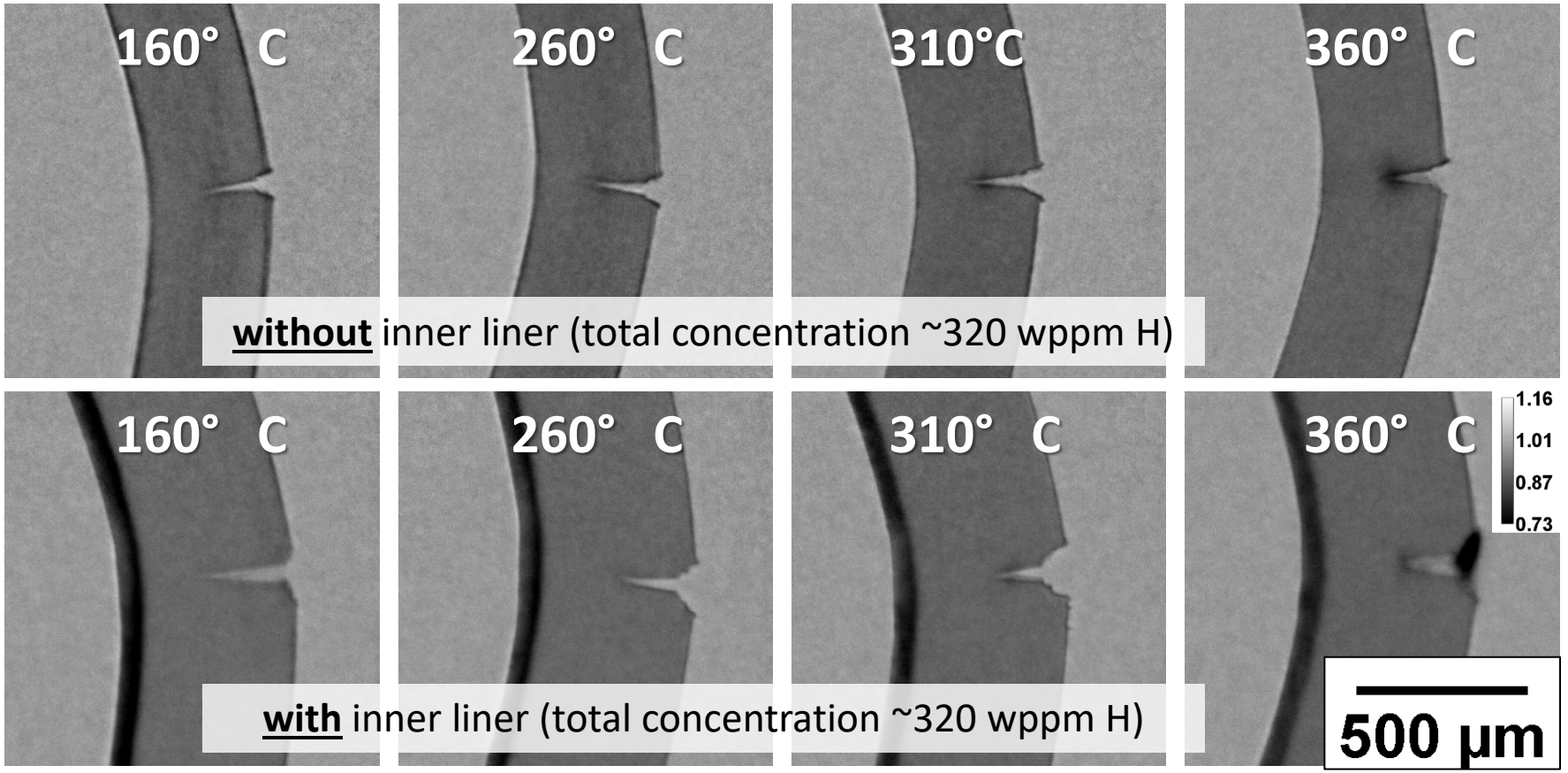

A. Colldeweih et al.; presented at ASTM 2022, 20th International Symposium on Zirconium in the Nuclear Industry, Ottawa

A. Colldeweih et al.; Journal of Nuclear Materials 561 (2022) 153549

PAUL SCHERRER INSTITUT

PSI

Hydrogen redistribution

Hydrides reorientation

Delayed Hydride Cracking (DHC)

Creep

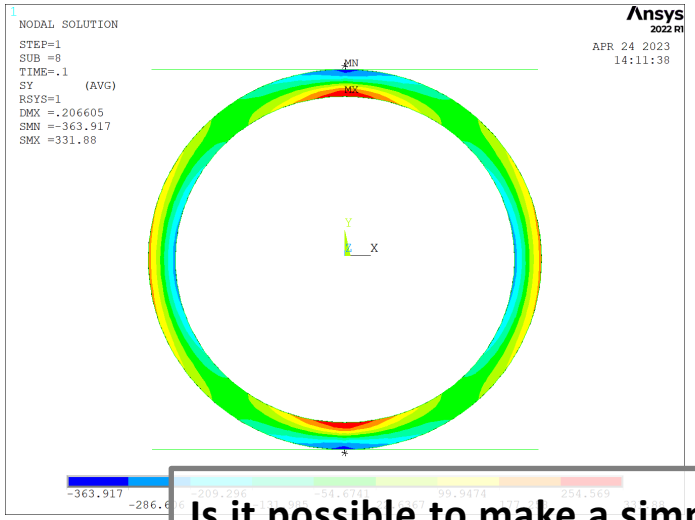

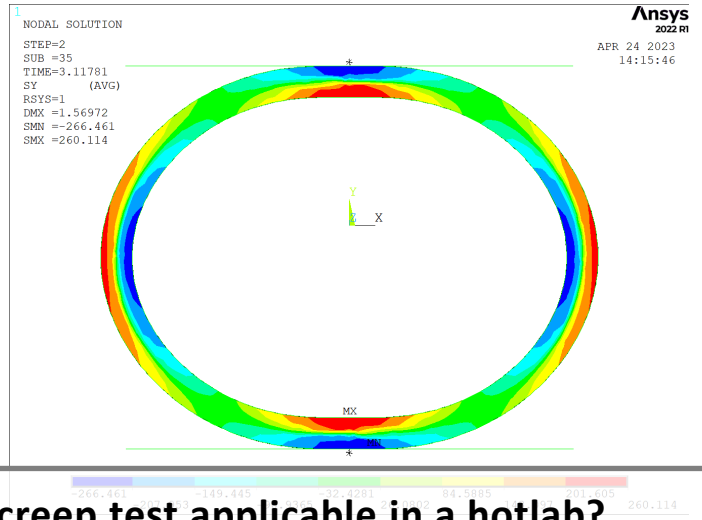

Is it possible to make a simple creep test applicable in a hotlab?

- Creep laws can be established according to the different stages.
- Assesment of the creep is difficult because of combined tension and compression at given circumferential positions, like equator or pole.

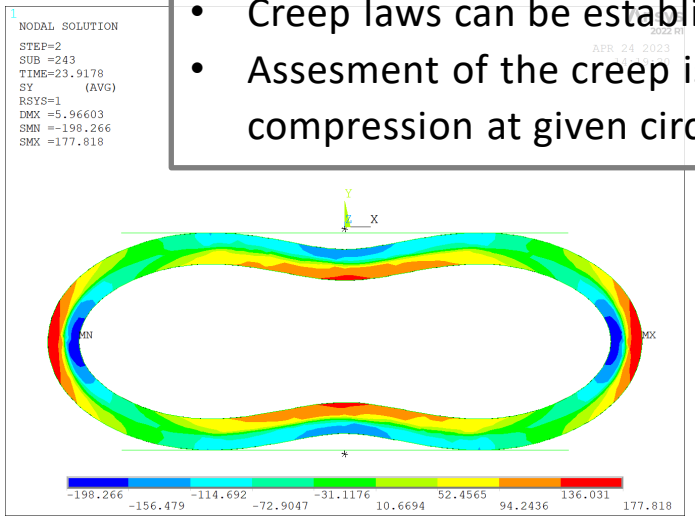

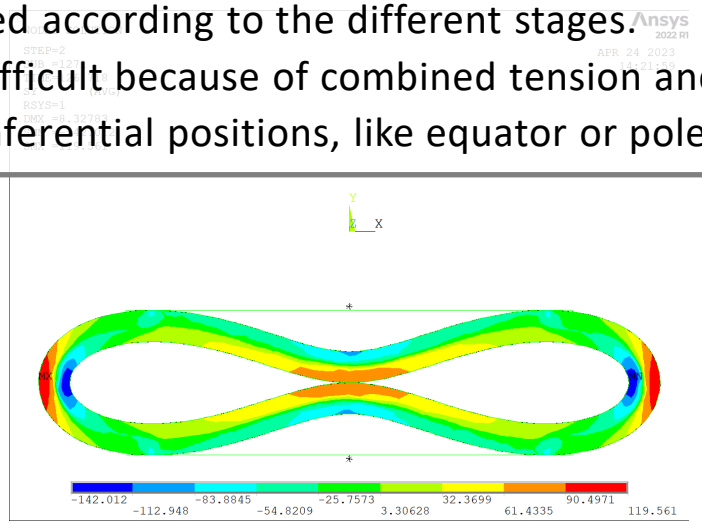

Diego Sanchez, Ring Compression Creep Testing for Zircaloy Claddings, Master Thesis, EPFL, Aug 2023

PAUL SCHERRER INSTITUT

PSI

- Hydrogen redistribution
- Hydrides reorientation
- Delayed Hydride Cracking (DHC)
- **Creep**

- Low intensity = high amout of hydrogen
- Redistribution from compression to tensile
- Softening due to hydroge is not (yet) in the model.

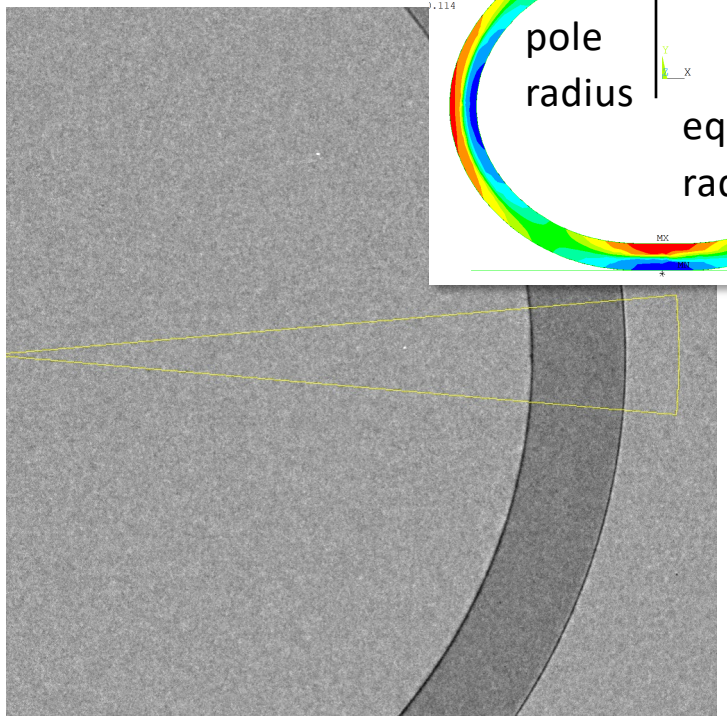

neutron image of 200 wppm hydrogen sample with region of interest (equator), angular integration

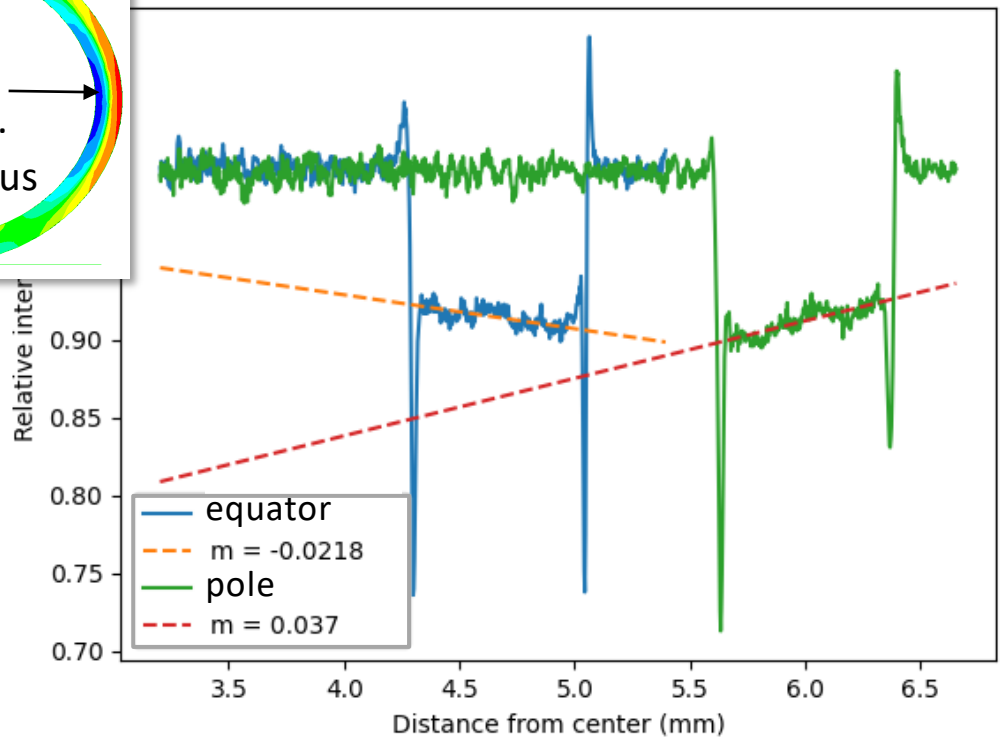

Relative intensity (transmission) of integrated neutron image, at equator and pole, 200 wppm hydrogen

Diego Sanchez, Ring Compression Creep Testing for Zircaloy Claddings, Master Thesis, EPFL, Aug 2023

Some further ideas?

Hydrogen redistribution	Learn more about the diffusion and precipitation kinetics and locations
Hydrides reorientation	Dissolution / reprecipitation of radial hydrides (differences in «memory effect» or in hysteresis)
Delayed Hydride Cracking (DHC)	DHC with outer liner
Creep	Active samples

Take away messages:

- Several relevant driving forces for hydrogen diffusion and precipitation
- Neutron radiography is excellent tool for hydrogen detection and quatification
- Examples ***Hydrogen Redistribution***, ***Hydrides Reorientation***, ***DHC*** and ***Creep***

My thanks go to

- ***swiss***nuclear
- PSI Hot Laboratory
- SINQ and Applied Materials Group (LNS, NUM)

K. Frederick
Westinghouse

Accident tolerant fuel: Cr coated cladding development at Westinghouse

In response to the nuclear industry's desire for longer coping times following the Fukushima accident in Japan in 2011, Westinghouse's **EnCore®*** accident tolerant fuel (ATF) program, is developing and commercializing an advanced fuel cladding and fuel pellet with the main goals of improving safety and economic performance. The program is a two-pathway approach, cladding and fuel, with each pathway having an intermediate product and long-term product; both of which are in testing and development phases. The cladding pathway will be the emphasis of this presentation as it is directly tied to the QUENCH testing being performed by KIT. The chrome coated cladding is undergoing testing in various settings and at various facilities. LTR and LTAs campaigns are currently underway with utility partners. These campaigns provide real-world data on the performance of the coating. Supporting testing at both the Westinghouse Churchill and Columbia facilities are occurring in parallel to provide valuable results in the development of the design and specification of the chrome coating.

This material is based upon work supported by the Department of Energy under Award Number DE-NE0009033.

Accident Tolerant Fuel: Cr Coated Cladding Development at Westinghouse

Katerina Frederick

28th International QUENCH Workshop

December 5-7, 2023

Westinghouse **VISION & VALUES**

together

we advance technology
& services to power a
clean, carbon-free future.

- Customer Focus & Innovation
- Speed & Passion to Win
- Teamwork & Accountability

Safety • Quality • Integrity • Trust

Westinghouse

The following material is based upon work supported by the United Stated Department of Energy under Award Number DE-NE0009033

Outline

- Westinghouse **EnCore®** Fuel Program
- LTA and LTR Status
- Coated Cladding Testing
- 2nd Test ATF-Quench Program

Westinghouse's EnCore® Fuel Program

The EnCore® Fuel program is developing and commercializing advanced fuel products to improve safety and economic performance

Advanced Cladding

- Cr-Coated Zr – increases safety & operational margin, may enable high burnup
- Silicon Carbide Cladding – safety and operational benefits

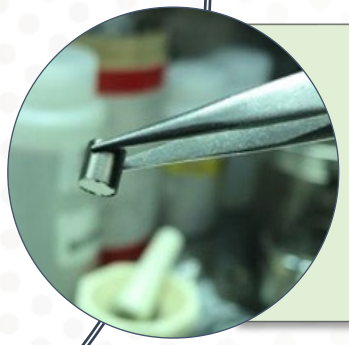

Advanced Fuel

- **ADOPT** fuel pellets – higher density
- Advanced Pellet (UN) - benefits to fuel cycle costs, may support high burnup, thermal properties, and lower operating temperatures

Chromium-Coated Zr Cladding

SiGA® Silicon Carbide (SiC) Composite Cladding

Photo courtesy of General Atomics

ATF Product Evolution

Enables HEF

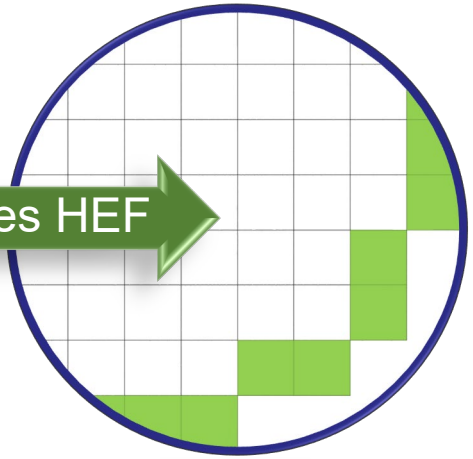

ADOPT Pellets

Uranium Nitride (UN) Pellets

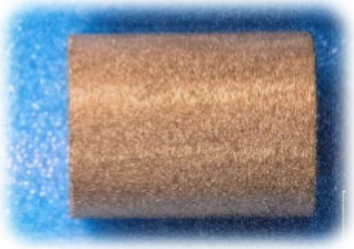

$U^{15}N$ Fuel

Photo courtesy of Los Alamos National Lab

Step 1: ~68 GWd/MTU for rods that do not rupture in a LOCA or experience DNB beyond 62 GWd/MTU

Step 2: Entire core to ~75 GWd/MTU with enrichment increase

LTA and LTR Status

Lead Test Rod/Assembly (LTR/A) campaigns with utility partners provide critical data to support fuel qualification

	Cr Coated Cladding	ADOPT Pellets	High Density Pellets	High Enriched Pellets
Byron Unit 2 (2019)	✓	✓	✓	
Doel Unit 4 (2020)	✓		✓	
Vogtle Unit 2 (Manufacturing Underway)	✓	✓		✓
EDF LTRs (Manufacturing Underway)	✓	✓		

Byron 2 LTAs: As-Fabricated

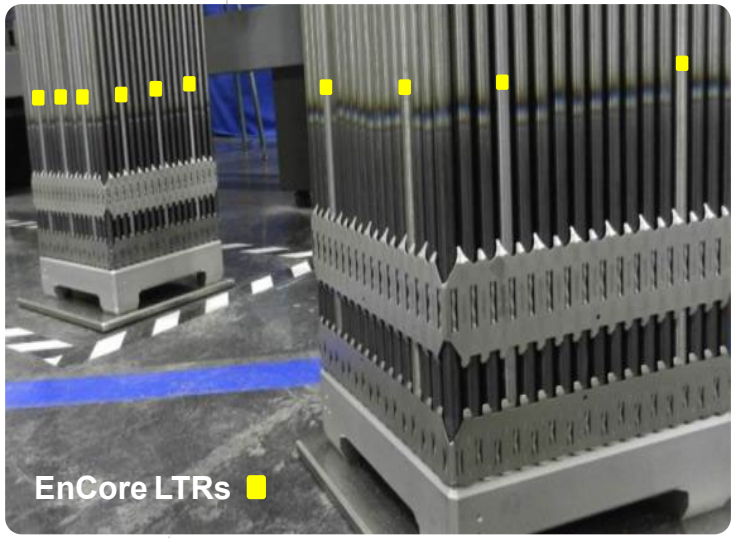

Pellet Inspections

Westinghouse

Commercial reactor testing confirms excellent performance of Westinghouse ATF products

Byron Unit 2 LTRs

EOC 1

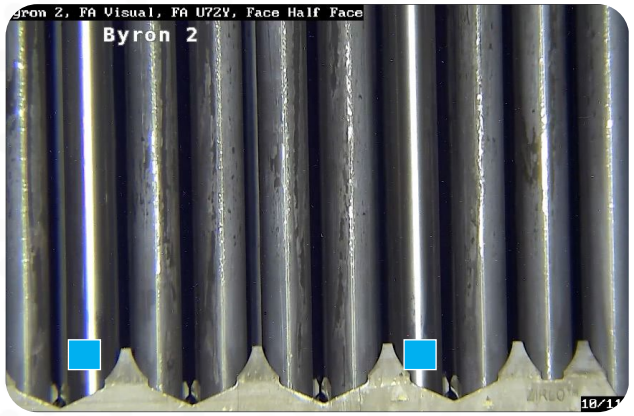

EOC 2

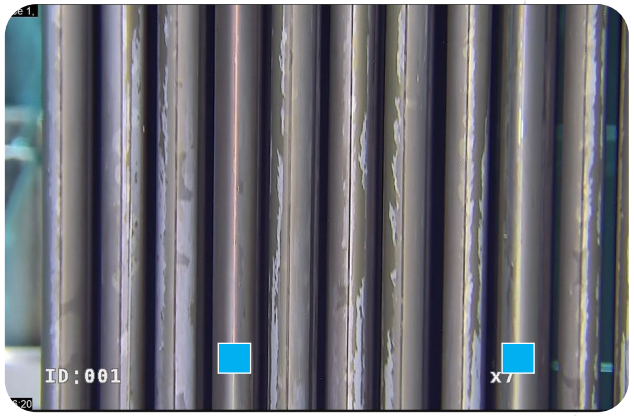

Doel Unit 4 LTRs

EOC 1

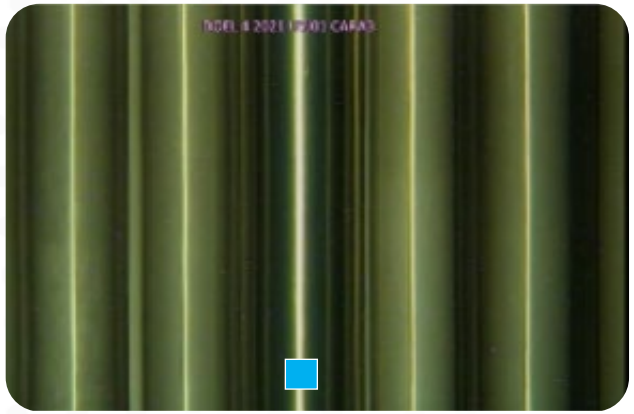

EOC 2

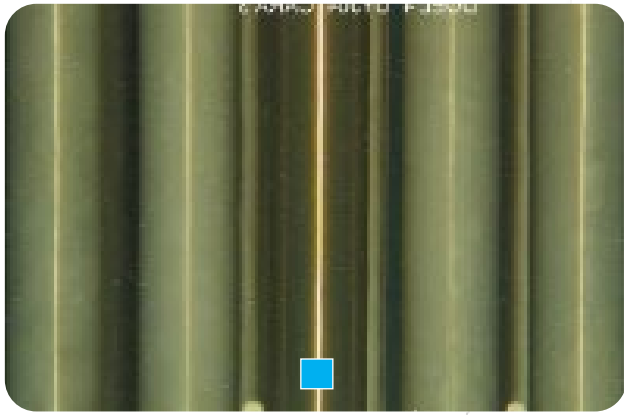

■ Cr Coated Rods

- Byron 1st and 2nd cycle visuals, rod extraction with rod length, fiberscope profilometry, and eddy current
- Hot cell examination of 1st burned rods underway. 2nd burned rods shipping to hot cell 2023.
- Doel 2nd Cycle poolside exam was in Spring 23
- Operating for 3rd cycle

ATF rods appear "pristine" with excellent coating adherence and little indication of crud.

Hot cell examinations of one cycle irradiated **EnCore®** Cr coated rods confirm excellent fuel performance

3 ATF and 4 high burnup rods received mid-2021

Credit: ORNL Photographer Carlos Jones

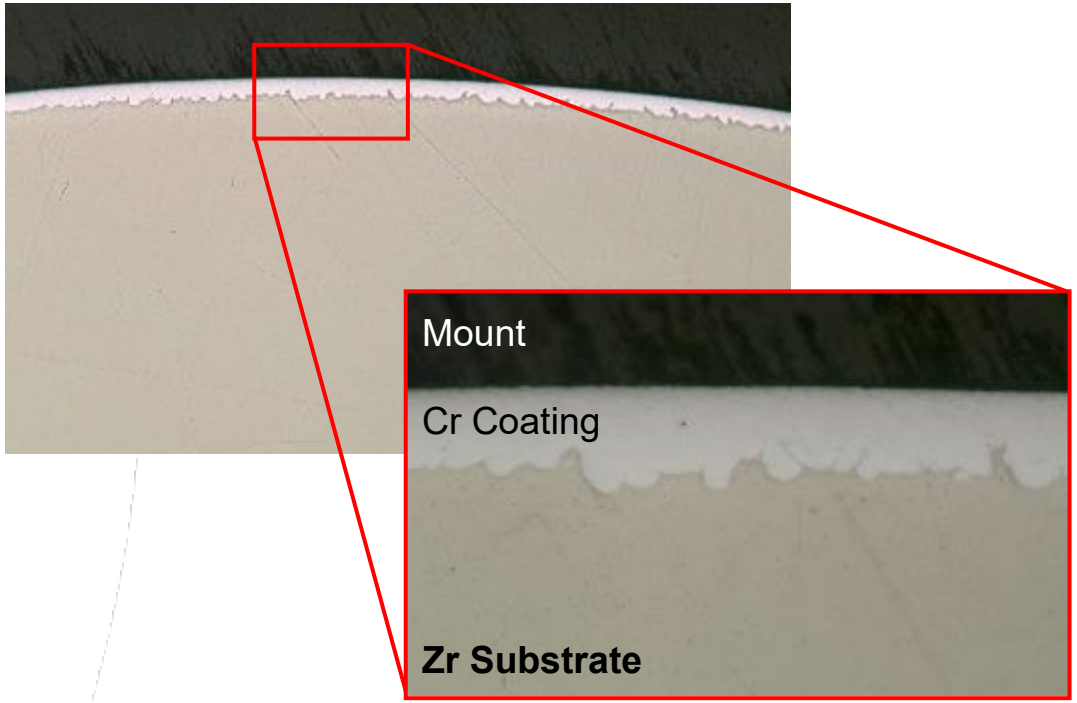

Excellent cold sprayed Cr coating integrity with complete protection of substrate

Hydride Etched metallography shows no unfavorable hydride orientations or rim

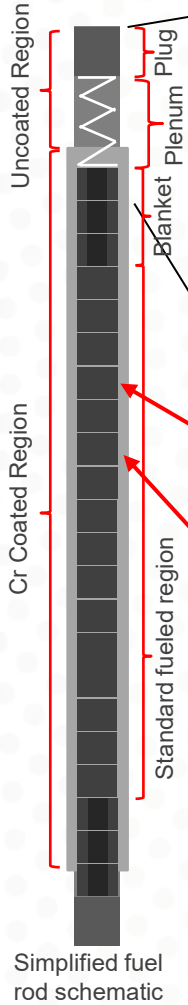

Simplified fuel rod schematic

~4in above coating
HPU: 26 ± 1 ppm

~1in above coating
HPU: 30 ± 5 ppm

at transition ~0.08in into coating
HPU: 20 ± 3 ppm

~2in into coating, ~0.4in above blanket
HPU: 11 ± 1 ppm

well into coating, ~4in above peak corrosion location for an uncoated rod
HPU: 24 ± 26 ppm & 16 ± 7 ppm

well into coating, near peak corrosion location for an uncoated rod
HPU: 19 ± 3 ppm

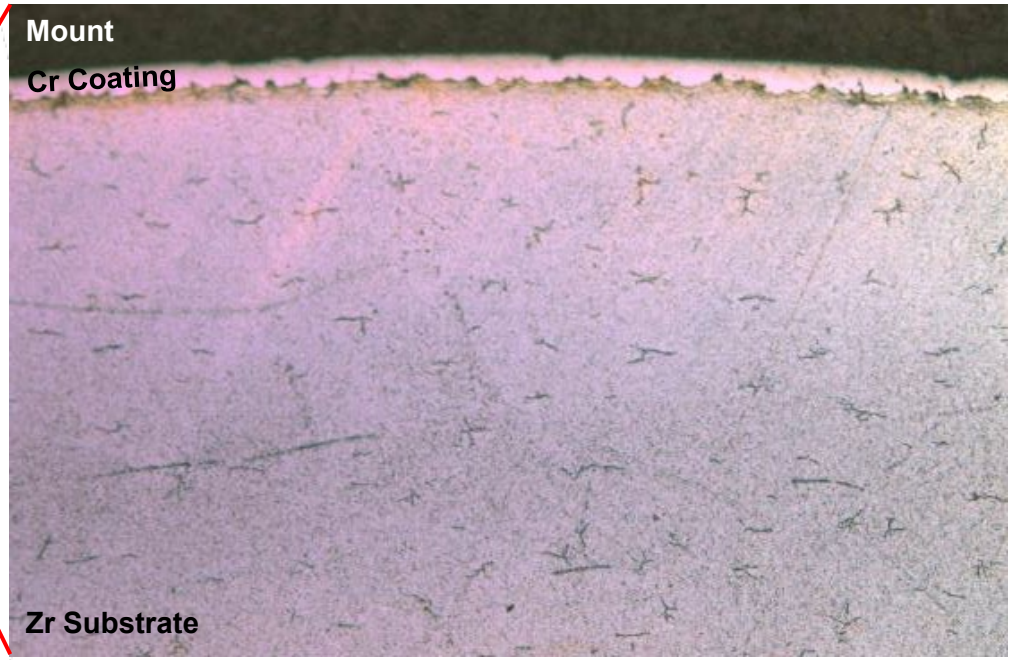

Shipment of 2nd cycle rods to INL hotcells planned for Q4 2023
Reactivity Insertion Accident and ramp testing planned at INL in 2024-2025

Westinghouse

Coated Cladding Testing

Helium and nitrogen cold spray both result in highly dense coatings

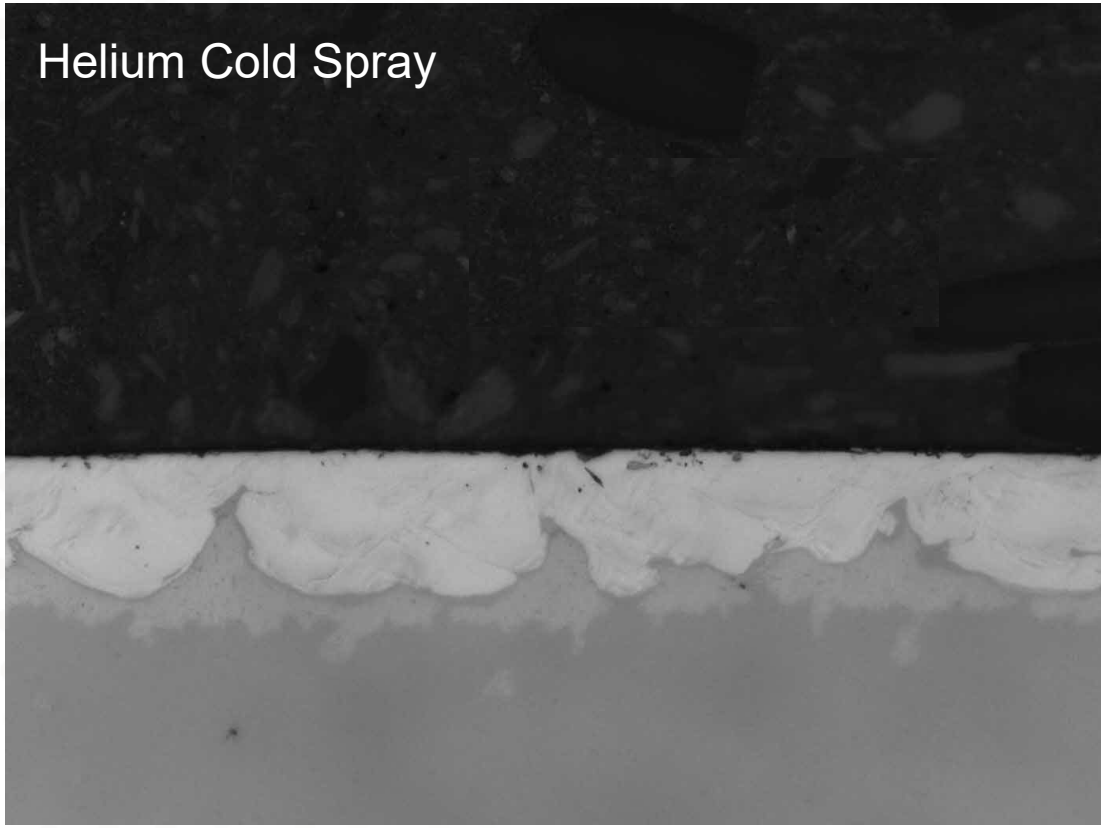

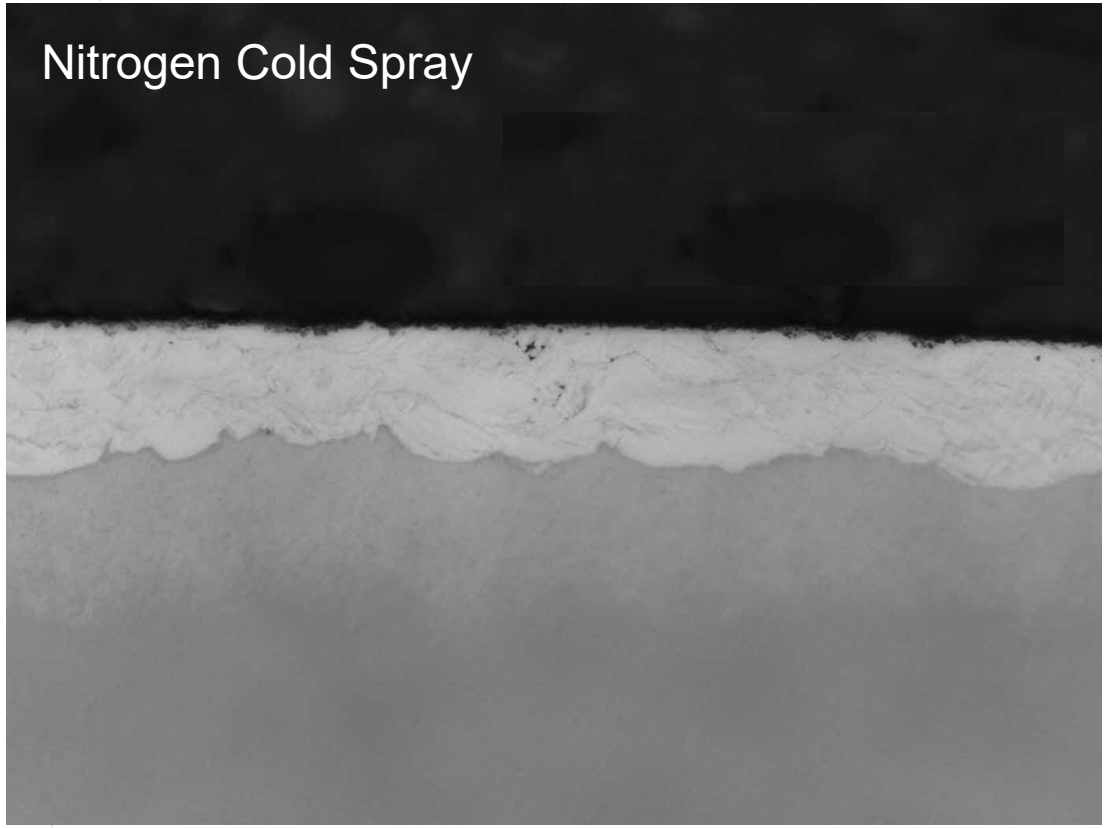

NCS demonstrated similar adhesion with no delamination, the same as HeCS

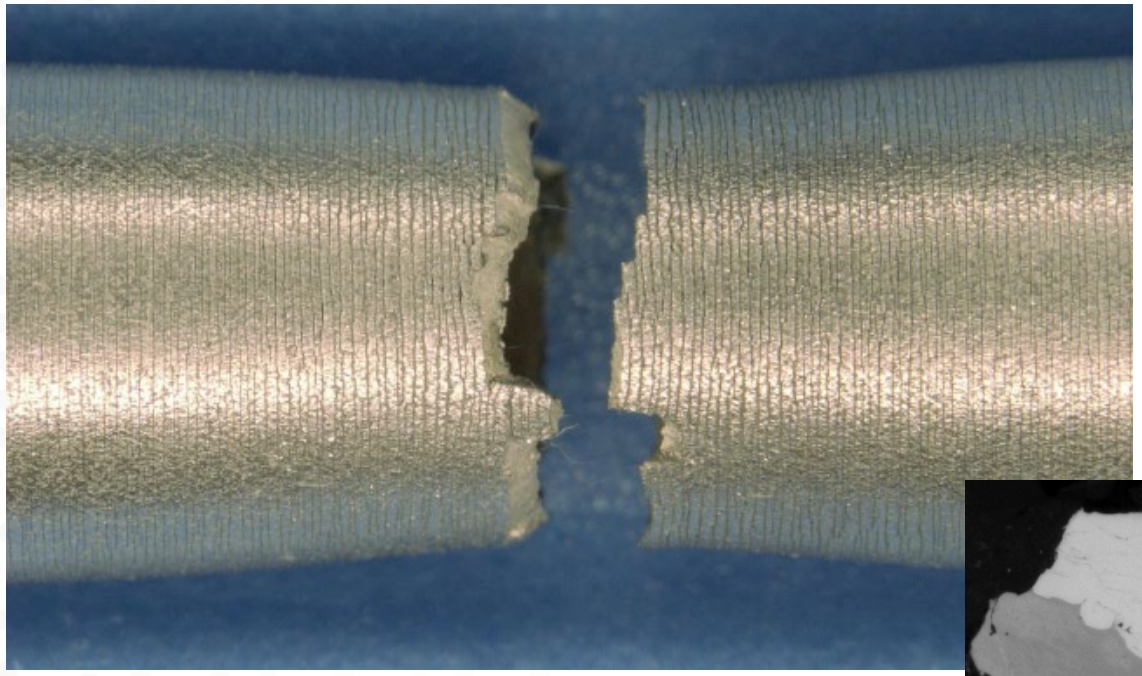

- Cracking of the coating begins to occur around ~3% strain
- Increase in elastic modulus and tensile strength
  - ~25% and ~12% respectively

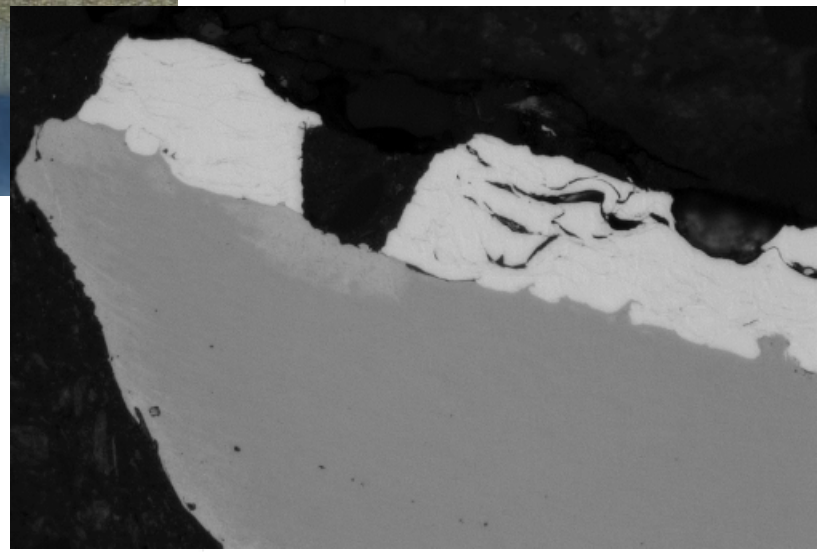

Cr coated samples significantly improve balloon and burst performance

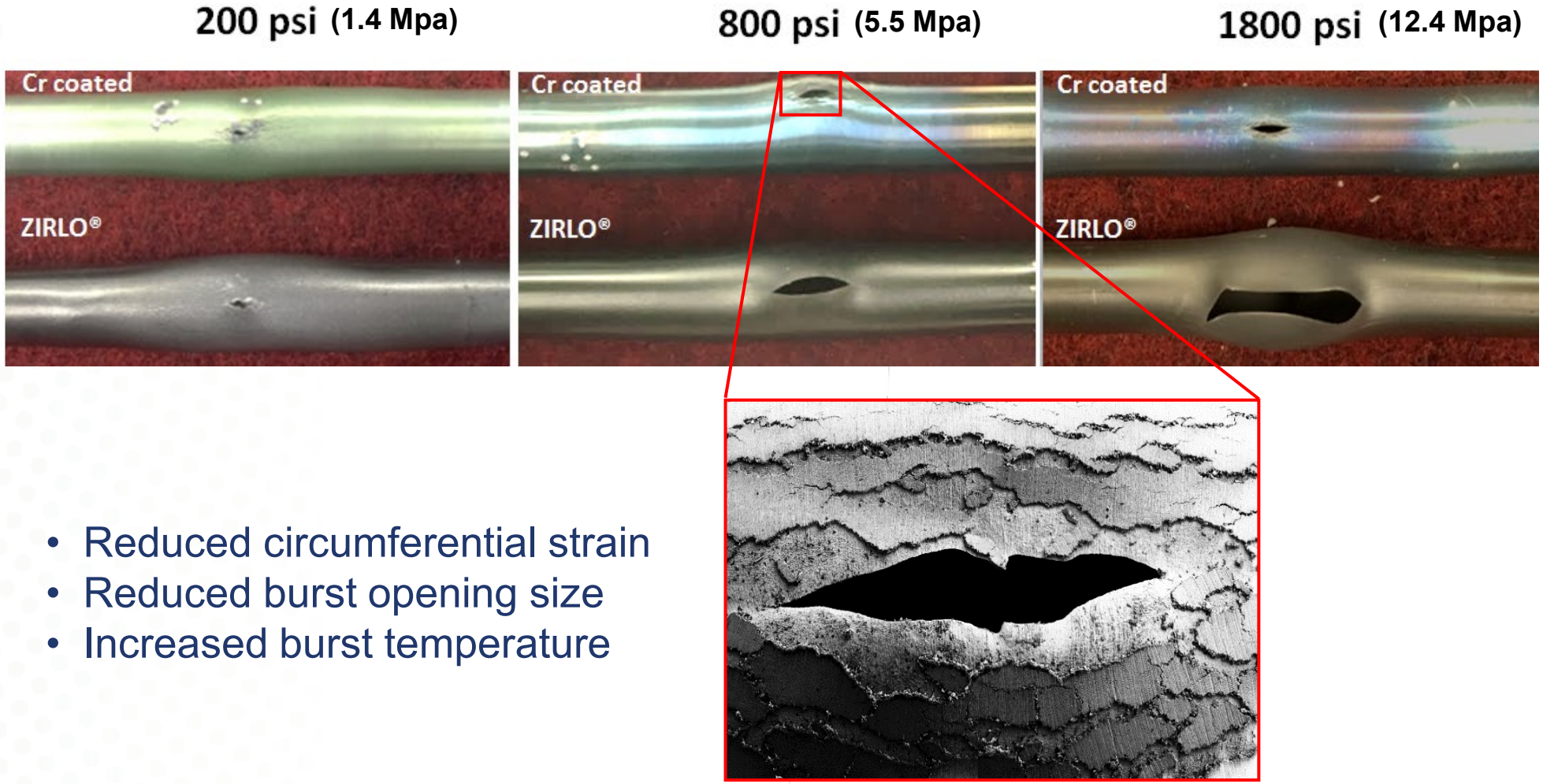

- Reduced circumferential strain
- Reduced burst opening size
- Increased burst temperature

Cr coating protects cladding at high temperatures in steam and retains ductility

Test Conditions: 1200°C for 525 seconds
Samples intentionally hydrided

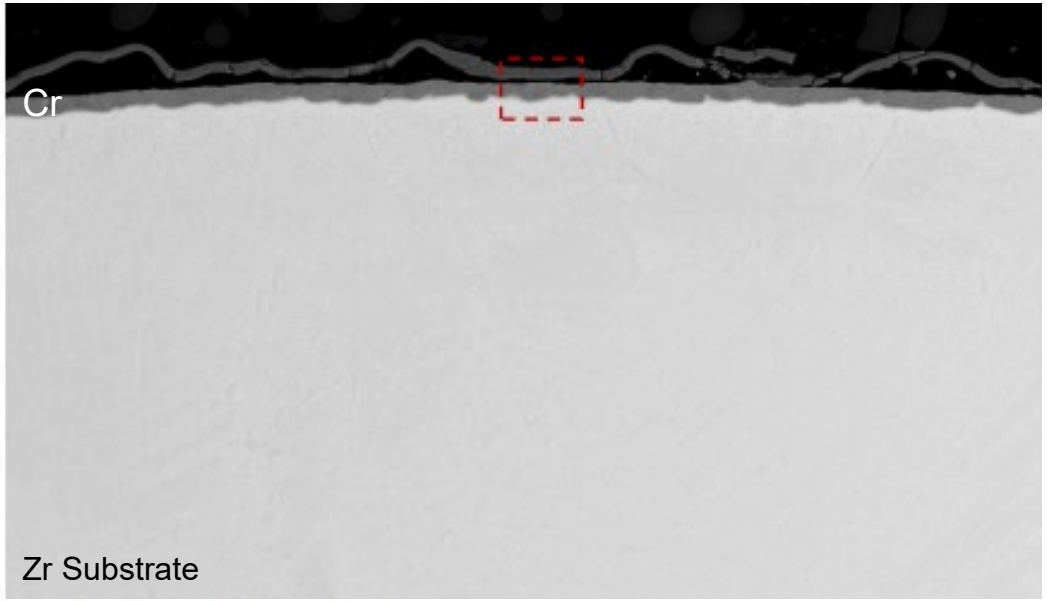

Sample	Offset Strain (%)	Break Load (lbf)	Peak Displacement (mil)
Uncoated	1.96	72.25	19.85
Cr Coated	34.27	89.90	145.80

Confirmatory testing to support licensing and understanding of benefits is ongoing

- Fatigue Testing
- Corrosion Studies
- High Temperature Oxidation
- Ring Compression Testing
- Ultra-High Temperature Testing
- DNB Testing
- Burst Testing
- PIE Analysis

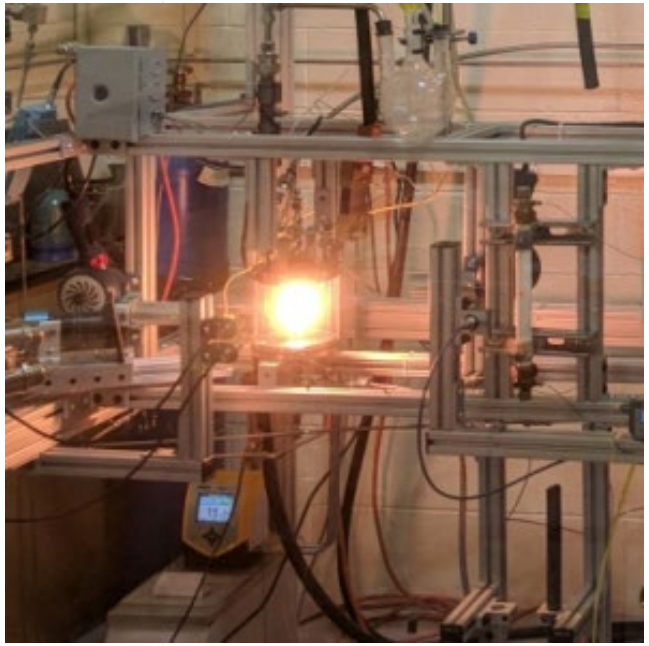

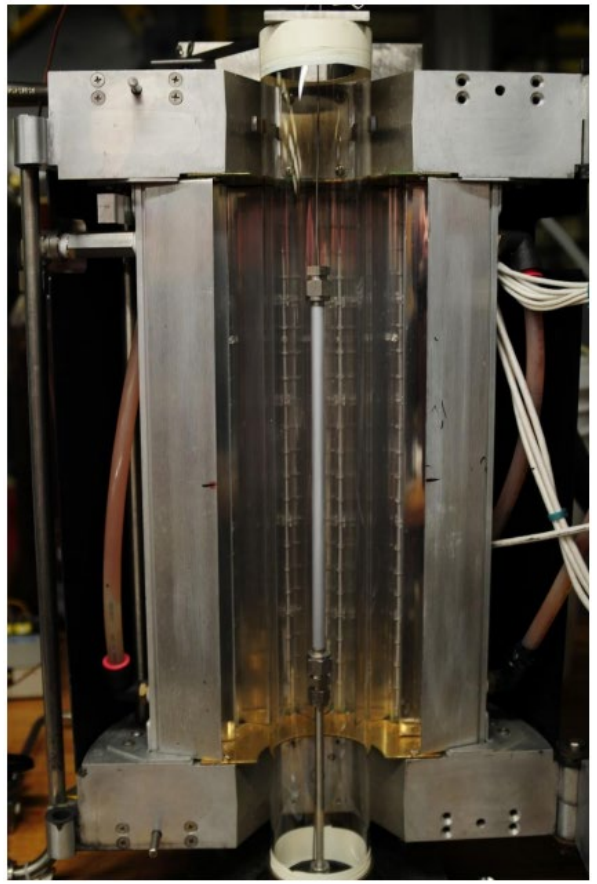

2nd Test ATF-Quench Program

Projected test parameters for a severe accident are planned

- Max Temperature
  - 1550 °C
- Heat Rate
  - 10 °C/min
- Quench at 1550 °C

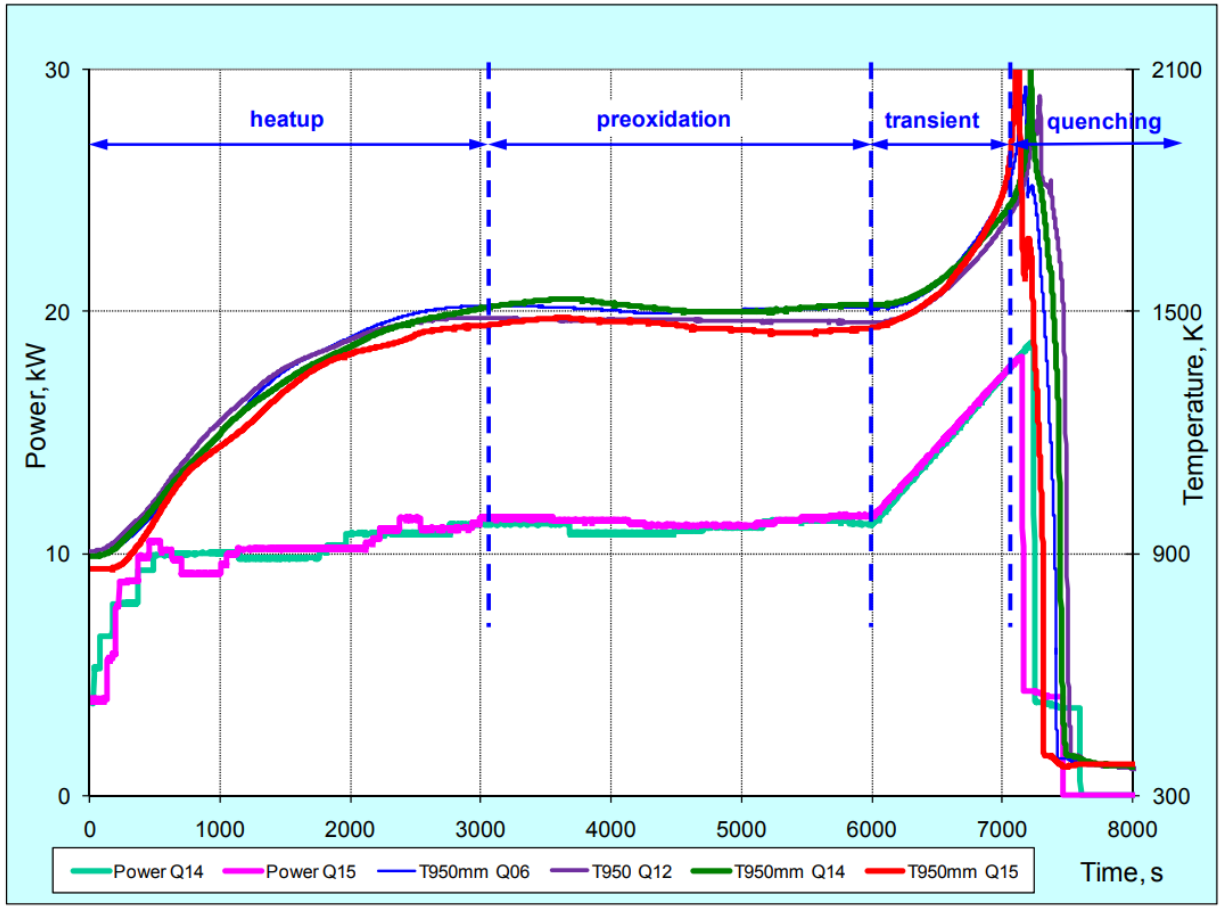

Samples were shipped to KIT and testing is planned for March/April 2024

- Tubes
  - 30 full length tubes (~2.5m in length)
  - Chromium cold spray coating
    - NCS and HeCS tubes
- Grids
  - 17x17 grid construction
  - Standard mid-grid

Thank You

 Westinghouse Electric Company

 @WECNuclear

 Westinghouse Electric Company

 wecchinanuclear

westinghousenuclear.com

Westinghouse

Y. Lee

SNU

Exploring safety limits of Cr-coated ATF cladding using separate effect and integral LOCA experiments

This talk presents experimental investigation on the safety limits of Cr-coated Zircaloy. Post quench ductility assessments were conducted on steam oxidized Cr-coated Zircaloy in compliance with the U.S NRC's test protocols. The test results demonstrate that the single-side (inner wall) ECR limit of ~19% can conservatively serve as the lower envelope of various Cr-coated modern-Zircaloy claddings. The microstructural analysis was conducted to explore the mechanism behind the loss of Cr coating protectiveness. The evidence of oxygen ingression through grain boundaries of Cr coating which led to the formation of ZrO_2 was observed. The loss of Cr protectiveness has limited significance to the Design Basis Accident (DBA) limit; loss of cladding ductility via the inner wall oxidation occurs before appreciable loss of Cr coating protectiveness. The safety analysis with the obtained DBA limit result reveals that potential burnup uprate with the modern Zircaloy (i.e., HANA-6 or M5) is comparable to that of Cr-coated ATF. This is because accident tolerance mainly comes from steady-state corrosion resistance, and modern Zircaloy alloys exhibit desirable steady-state corrosion resistance to ensure post-quench ductility in postulated DBAs. The allowable discharge burnup limit will be likely to be determined by the concerns surrounding Fuel Fragmentation Relocation and Dispersal (FFRD) issue. The fuel dispersal experiments with the Seoul National University's *i*-LOCA facility are presented, highlighting the sensitivity of post-burst cladding strains with respect to the azimuthal temperature distribution which is affected by the type of the inner fuel surrogates (i.e., pellet or powder types). The result indicates that the dispersal fraction would undergo a dramatic variation in the range of fuel burnup of 60 – 90 MWd/kgU.

28th International Quench Workshop
Karlsruhe Institute of Technology, Campus North, 5-7 December 2023

Exploring safety limits of Cr-coated ATF cladding using separate effect and integral LOCA experiments

2023. 12. 5.

Youho Lee*, Hyunwoo Yook, Dongju Kim, Sunghoon Joung

Department of Nuclear Engineering, Seoul National University, Korea

*leeyouho@snu.ac.kr

Table of Contents

1. Separate effect safety limit studies: PQD limit and loss of coating protection

Post-Quench ductility near the burst hole: a key DBA limit

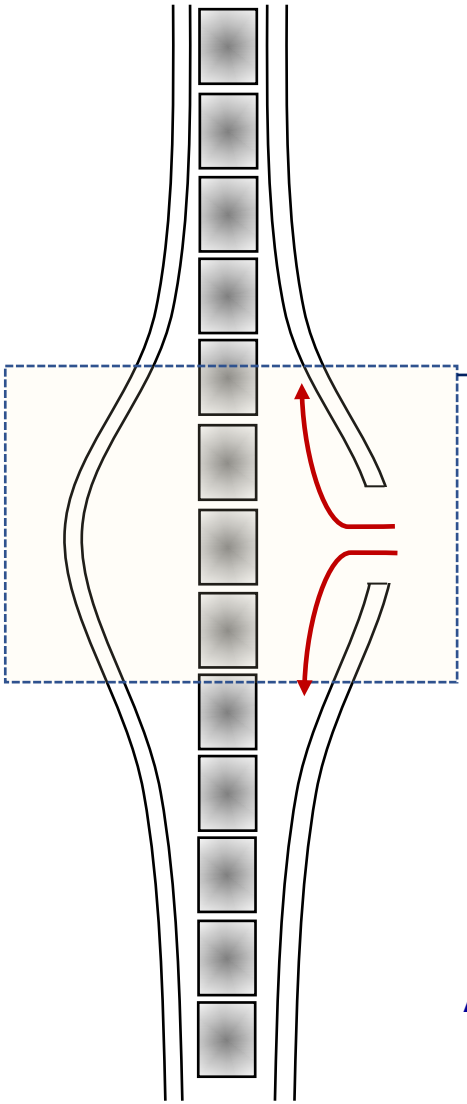

Exacerbated embrittlement near the burst region

① **Inner side oxidation**

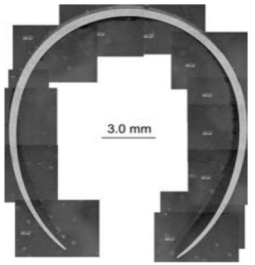

② **Thinning of the wall**

$$ECR_{double-sided} = c * \frac{\Delta W_{CP,double}}{\delta_{avg,deformed}}$$

① + ② also take place for Cr-coated cladding

NUREG 2119, U.S NRC: "No exception in the burst hole"

『..ring compression data to limit oxidation is **applied uniformly to the entire rod**, with the provisions for the balloon outlined in the existing rule to use the **average wall thickness** in the rupture region to calculate the CP-ECR…』

ATF-ISG-2020-01, U.S NRC:

『..Hence, the applicability of the **17% ECR analytical limit**, more generally, the use of **maximum local oxidation** as a surrogate SAFDL for cladding **is questionable** …』

Experimental procedure: simulated LOCA experiment

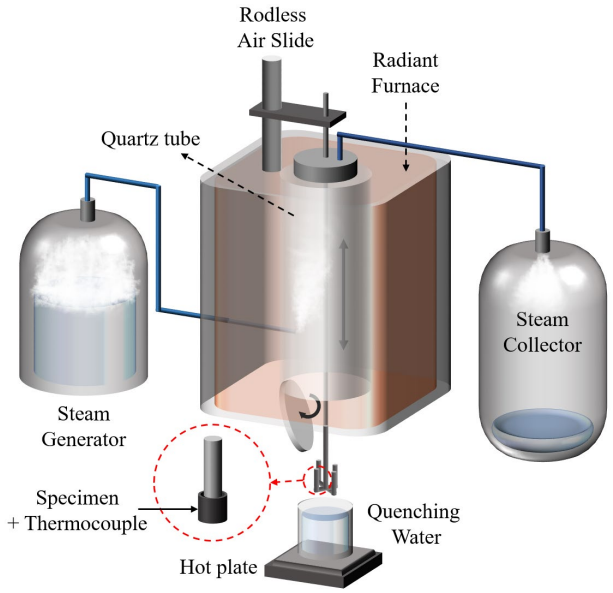

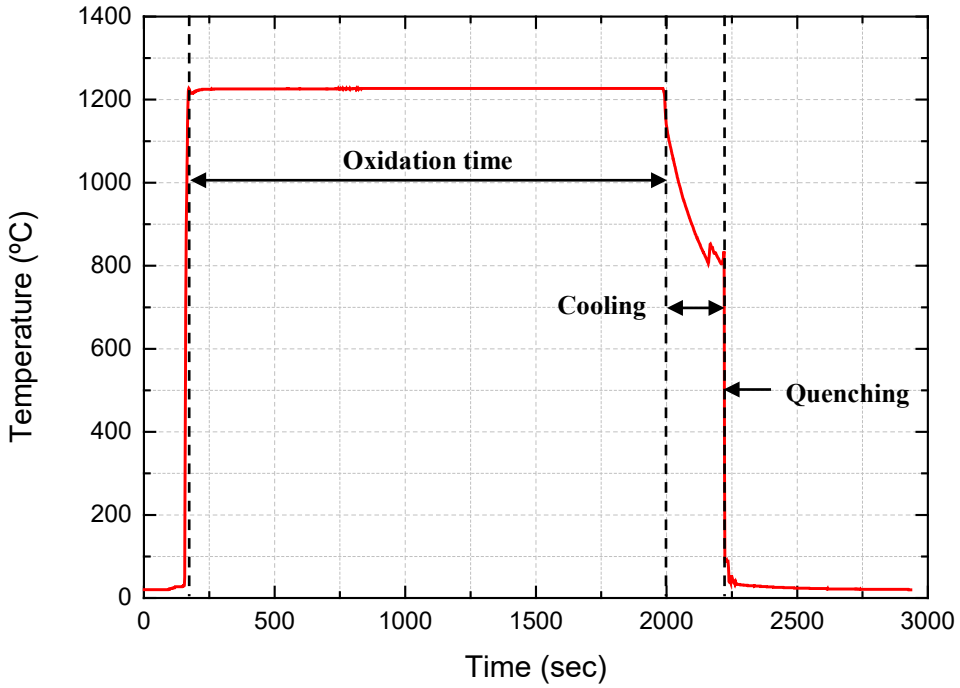

Sample holder

-Cladding OD: 9.5mm
-Thickness: 0.57mm
-:Length:8mm
-Various claddings

Specimen temperature measured with attached K-type thermocouple

Four specimens were oxidized at a same time and thermocouple was attached to one of the four specimens.

	NRC's protocol	SNU
Steam flowrate	0.8~30 [mg/cm^{2}s]	3.94 [mg/cm^{2}s]
Cooling rate (1200°C-800 °C)	> 2 [°C/s]	2 ~ 4 [°C/s]
Weight measurement resolution	0.0001 [g]	0.00001 [g]

- **The experimental procedure conducted by SNU conforms to the NRC's protocol.**

Experimental procedure: Ring Compression Test (RCT)

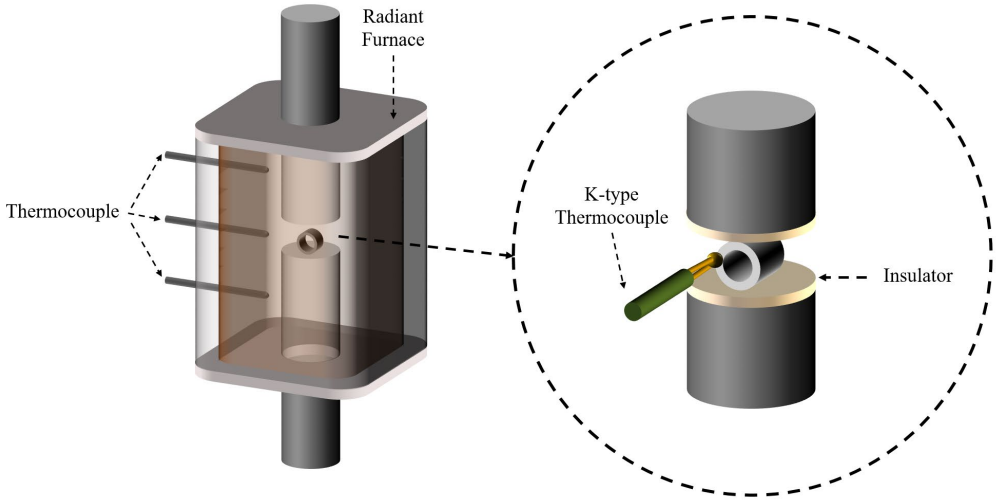

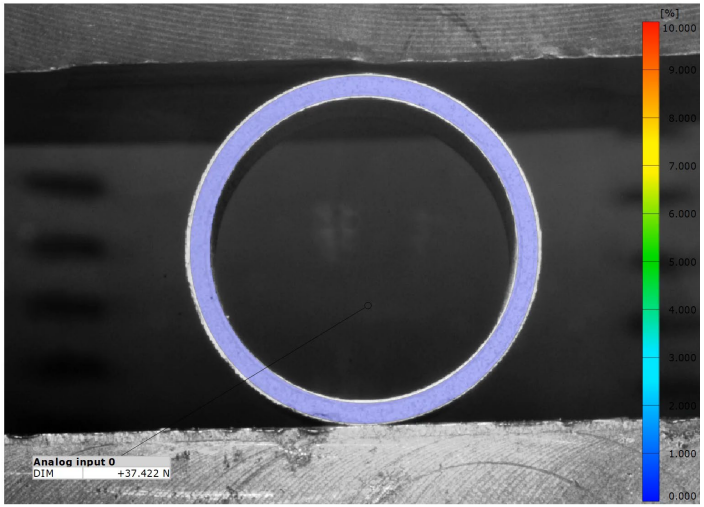

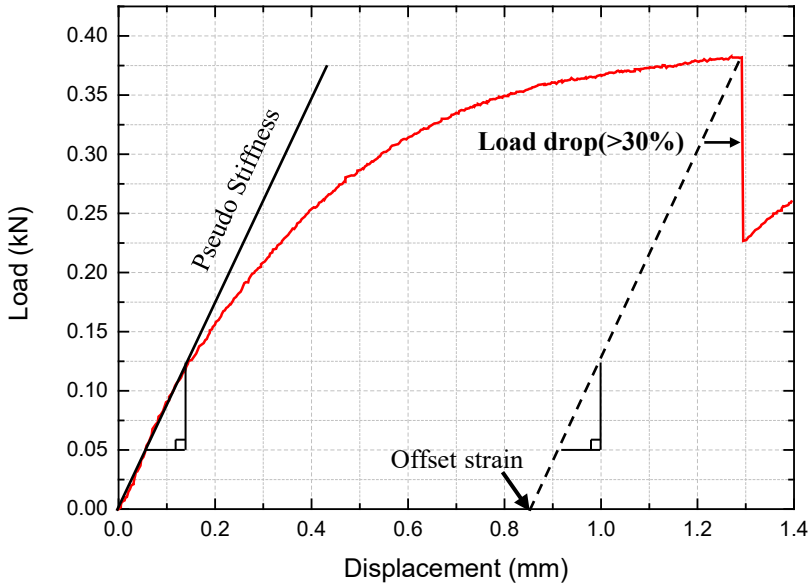

- Displacement rate : 0.033 mm/s
- Temperature of specimens : 135±3℃
- INSTRON 8516 (load cell 10 kN)
- Through wall crack : steep load drop (>30%)
- **The experimental procedure conducted by SNU conforms to the NRC's protocol.**

Regulatory limit (ECCS criteria) exploration for Cr-coated ATFs

<Zircaloy-4 offset strain validation with U.S NRC data>

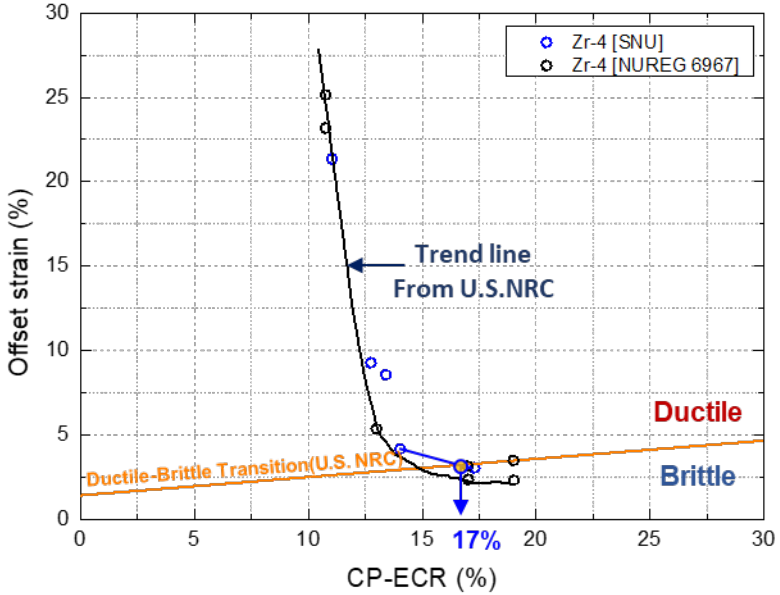

<Cr coating on Zircaloy-4 base material>

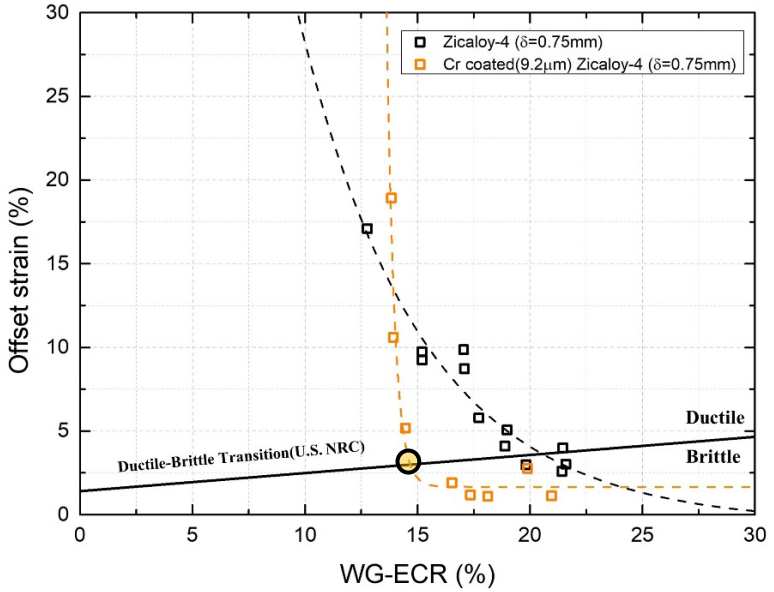

<Cr and Cr/CrN coating on Opt.ZIRLO™ base material>

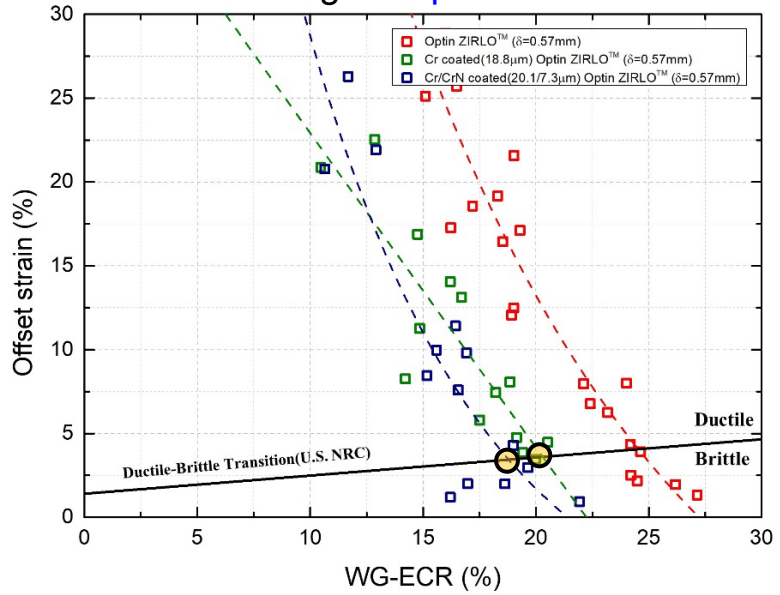

<Cr coating on HANA-6 base material>

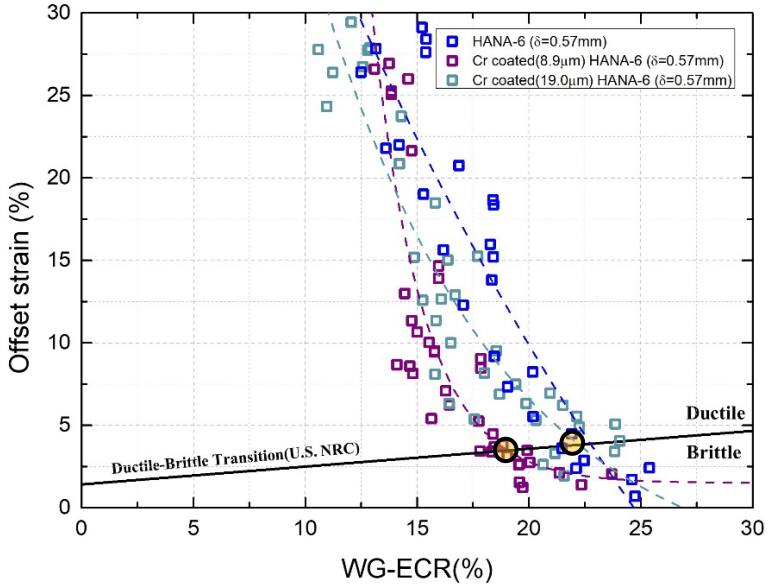

PQD limits of various Cr coated ATF in summary

Substrate	Coating	Method	ECR limit	Provider
HANA-6 cladding (17x17)	Bare cladding		23%	KNF(KOREA)
	Cr (8.9 [um])	AIP(400℃↑)	**19%**	KNF(KOREA)
	Cr (19.0 [um])	AIP(400℃↑)	**22%**	KNF(KOREA)
Zircaloy-4 (14x14)	Bare cladding		20%	KIT(Germany)
	Cr (9.2 [um])	Magnetron(400℃↓)	**15%**	KIT(Germany)
Optimized ZIRLO™ (17x17)	Bare cladding		24%	CTU(Czech)
	Cr (18.8 [um])	Magnetron(400℃↓)	**20%**	CTU(Czech)
	Cr/CrN (20.1/7.3 [um])	Magnetron(400℃↓)	**19%**	CTU(Czech)
Zircaloy-4 (17X17)	Bare cladding		17%	MIT(USA)
	Cr (39.6 [um])	Cold spray(400℃↓)	**14%**	MIT(USA)

IAEA

Tests were conducted at SNU under the ongoing IAEA CRP for ATF

*ECR limit for Cr-coated ATF is based on single-side oxidation

- Compared to conventional cladding, **the Cr coating results in a reduction of ductility, leading to a decrease of the DTB limit by 1-5%, on average 3%.**
- Ductility decrease after Cr coating is independent of the coating method.

Mechanisms for premature ductile to brittle transition of post-LOCA Cr-coated cladding under RCT

Uncoated HANA-6

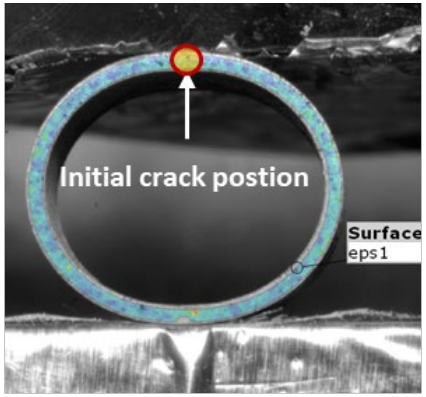

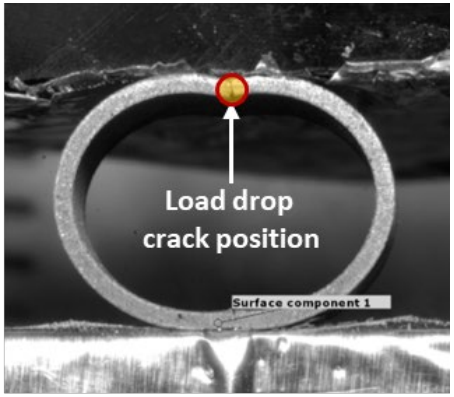

Cr-coated HANA-6

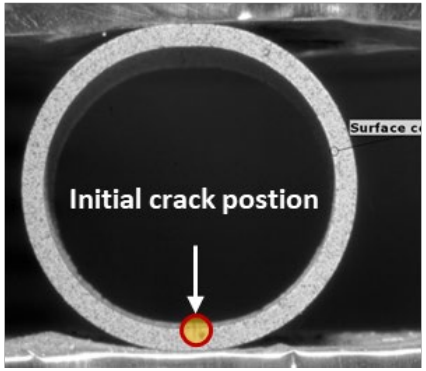

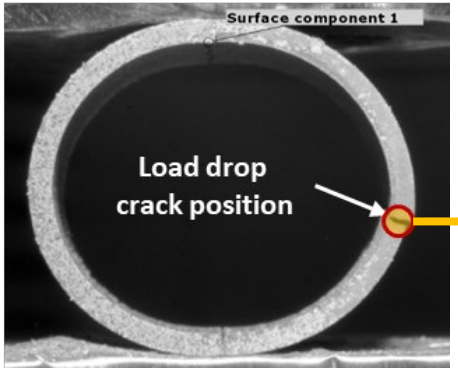

<Change of major load drop through-wall crack position>

displacement = 0.4mm

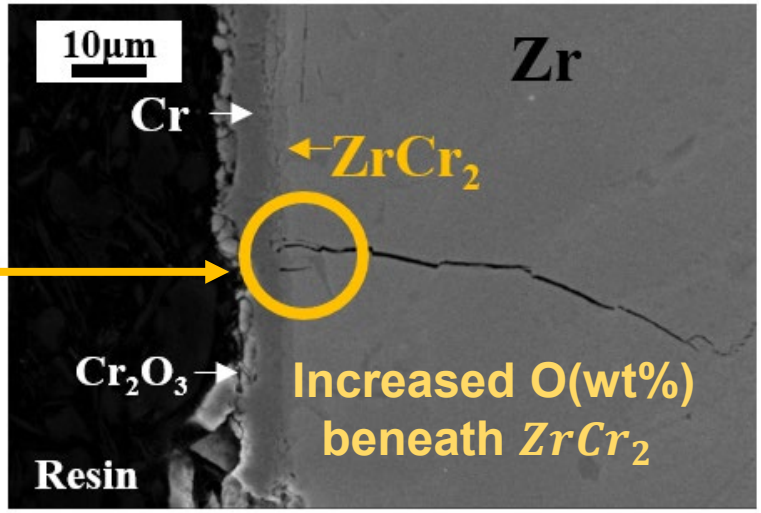

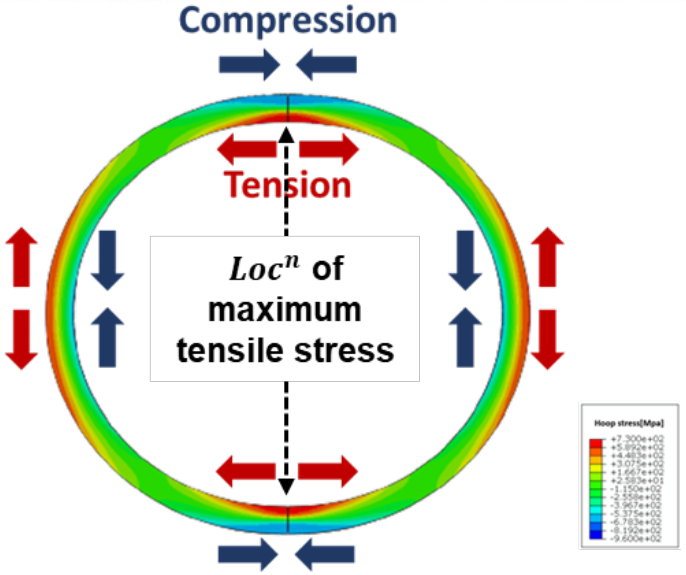

<Stress fields during RCT>

PQD Limits of Cr coated ATF (Modern Zircaloy base materials)

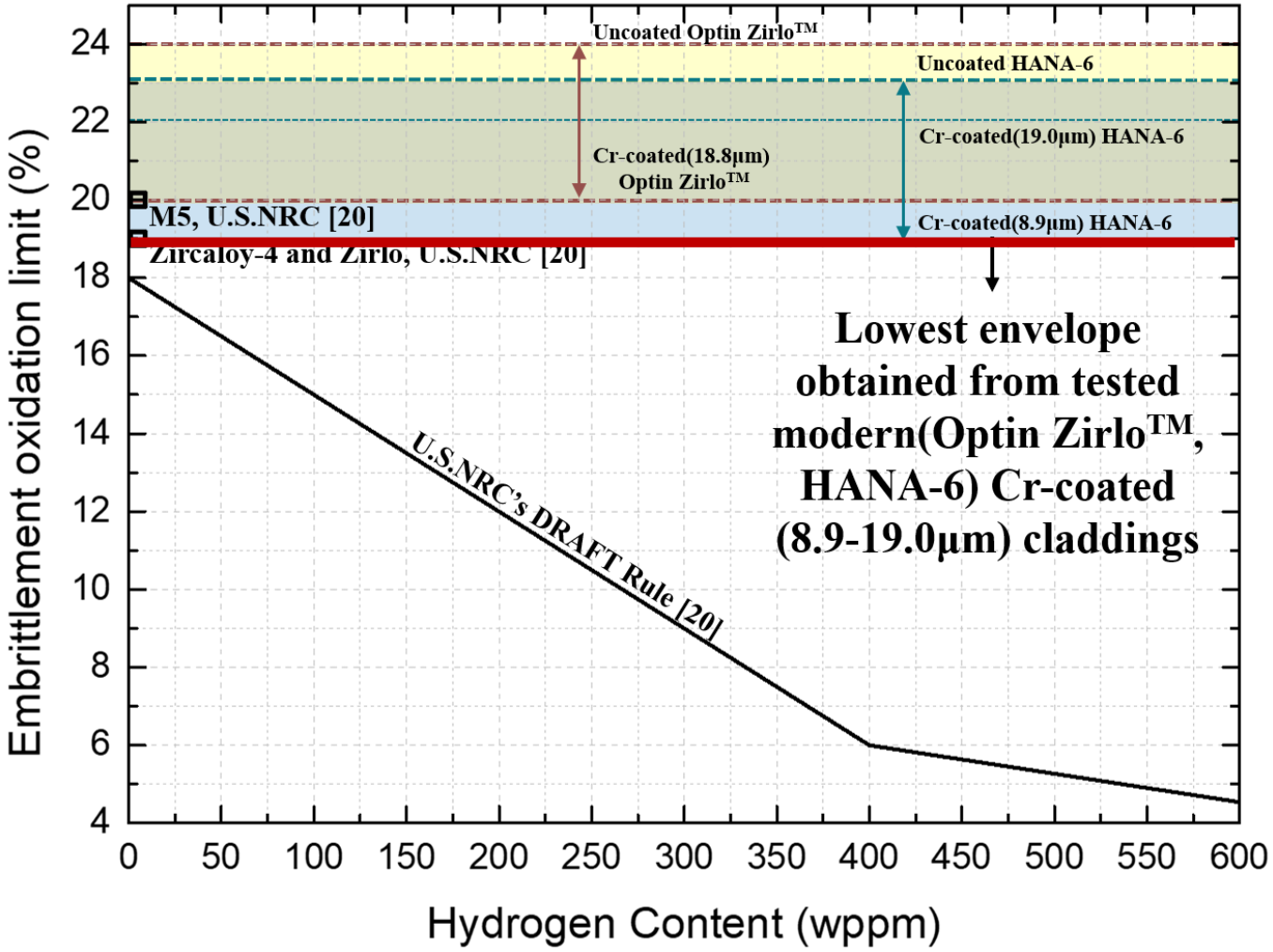

- This may imply that we can just use the current ECR limit (18%) of one-sided oxidation for the bounding limit Cr-coated Zircaloy.

Loss of coating protection during extended steam oxidation

- Setaram TGA coupled with steam generator

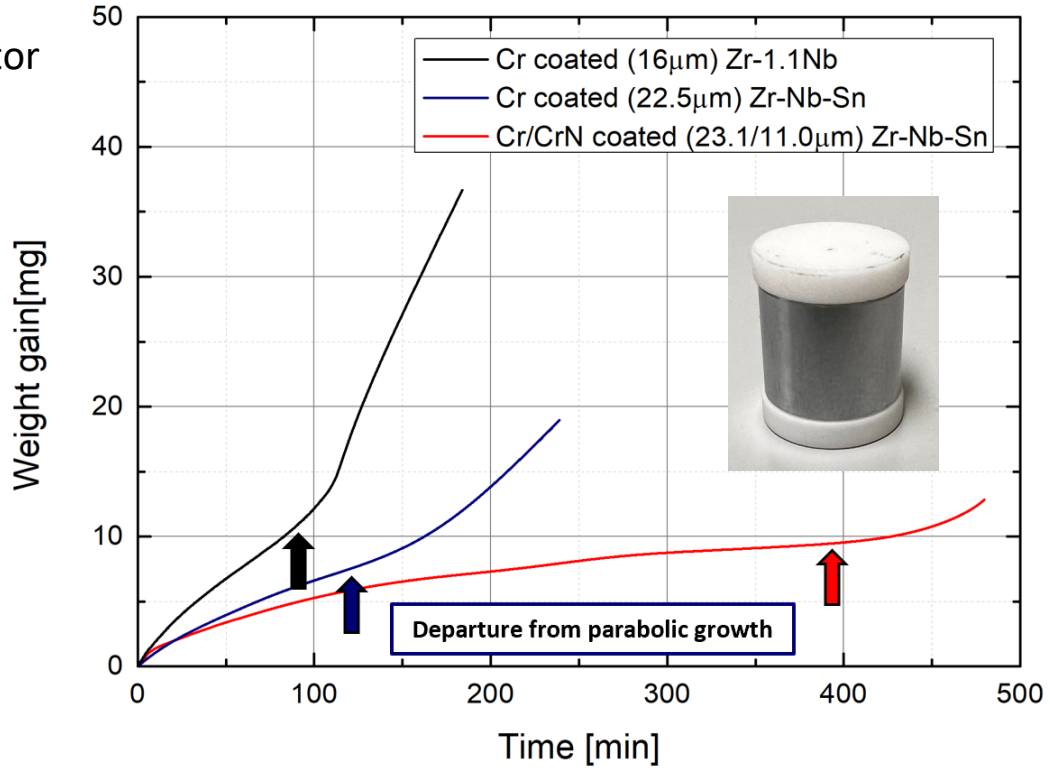

<In-situ weight gain at 1200 ℃, oxidized only at outer surface>

Specimen	Transition time [min]	Transition CP-ECR [%]	Peak weight gain rate [mg/min]
Cr/CrN coated Zr-Nb-Sn	395	72.9	~0.13
Cr coated(22.5 μm) Zr-Nb-Sn	128	41.5	0.14
Cr coated(16 μm) Zr-1.1Nb	94	35.7	0.39

Quick look at the transition time and post loss of protection weight gain rate

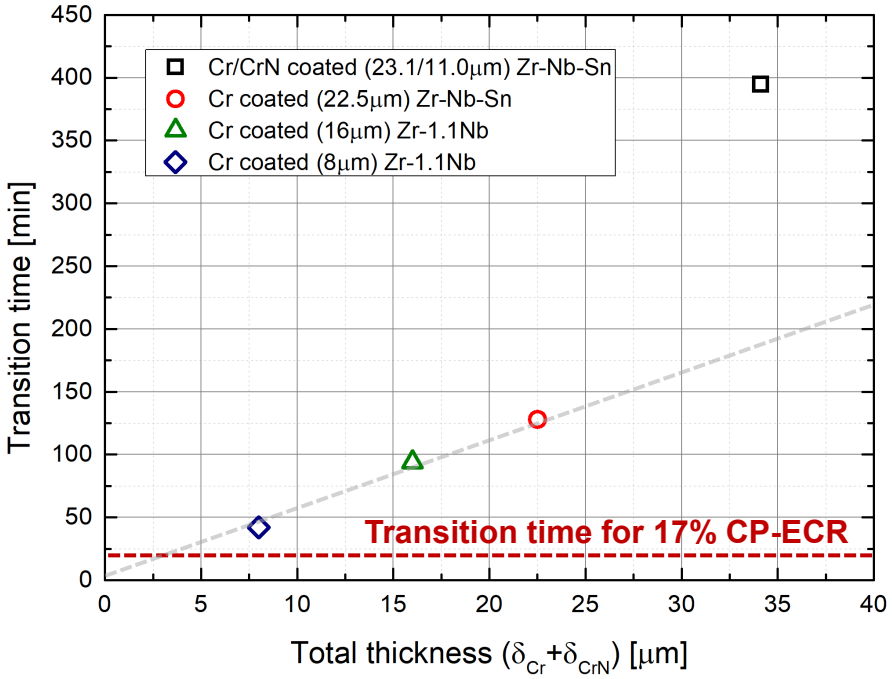

<Transition time w.r.t coating thickness>

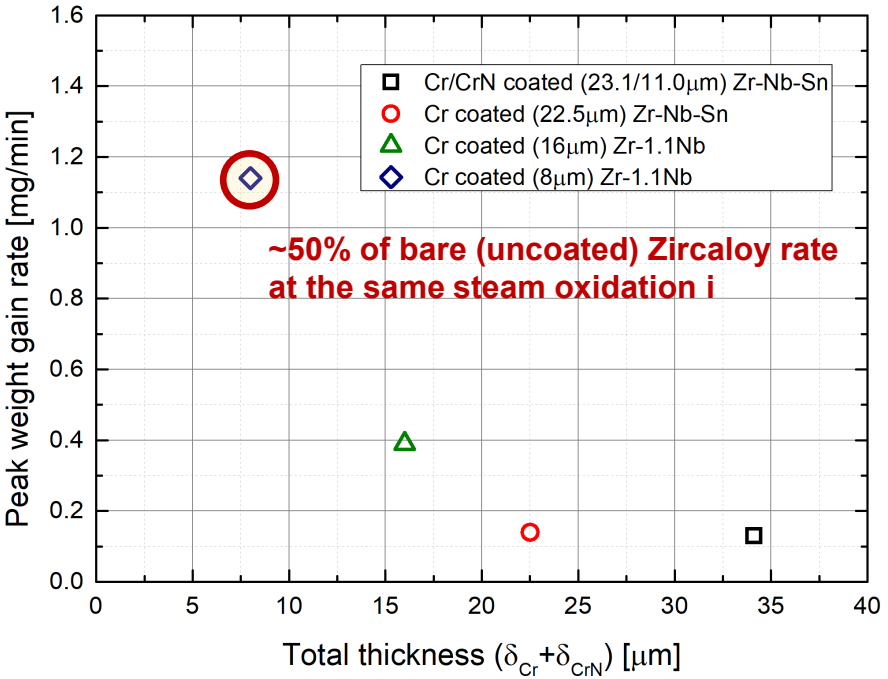

<The maximum post loss of protection weight gain rate>

- Transition time linearly increases with coating thickness for Cr/Zircaloy case.
- The maximum post-weight gain rate decreases with the initial coating thickness.
- It is remarkable to note the maximum post-weight gain rate reaches up to a significant fraction of the bare Zircaloy rate.

Phenomenological complexities and modeling frame work for updating TRANOX for Cr-Zr-O system

Mechanistic model for the loss of Cr coating protectiveness

Oxygen ingression model in Cr coating

Instantaneous Cr thickness

Site density for intergranular Zr diffusion in Cr

Transient coating thickness model

Fabrication effect

Cr coating recrystallization model

Loss of Cr mass to Cr_2O_3

Loss of Cr mass to Zr matrix

Cr grain density change with time

Cr coating oxidation exp & model

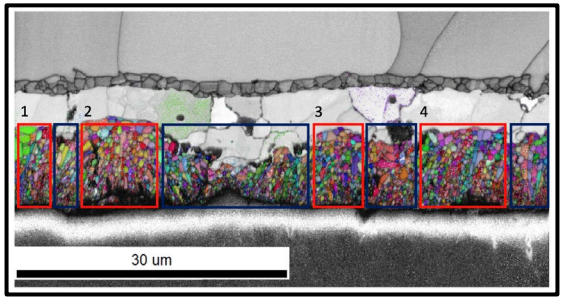

Completed. Pending submission

Cr diffusion to base material

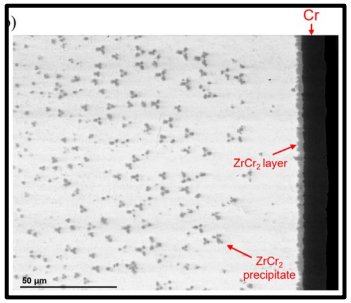

D.Kim, Y.Lee. Surface & Coatings Technology (2023)

Cr coating recrystallization investigation

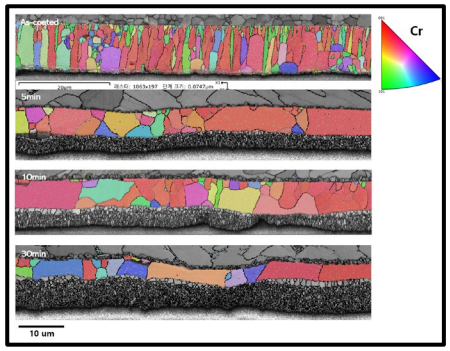

Completed. Pending submission

TEM&TKD analysis for Cr-coated specimen oxidized at 1200 ℃ for 105min (after protection loss)

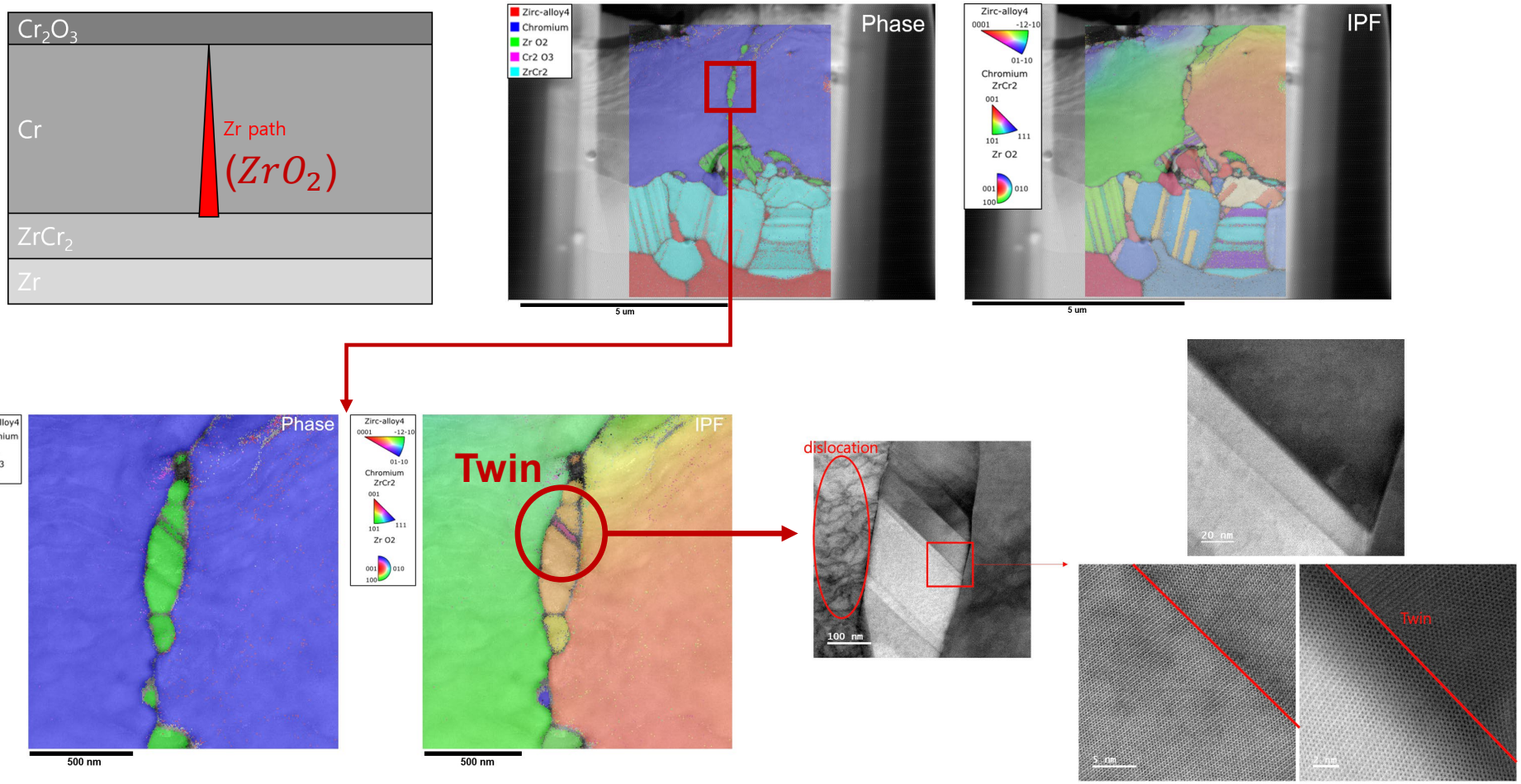

- **Sign of strong tensile stresses near ZrO_2:** The elastic stress fields near the ZrO_2 may lower the local chemical potential, thereby accelerating the oxygen diffusion along the grain boundaries via steeper diffusion potential gradient. This may hold a clue to understanding the eccentrically fast oxygen diffusion across the Cr thickness upon the loss of its protection.

TEM&TKD analysis for Cr-coated specimen oxidized at 1200 ℃ for 30min (protective)

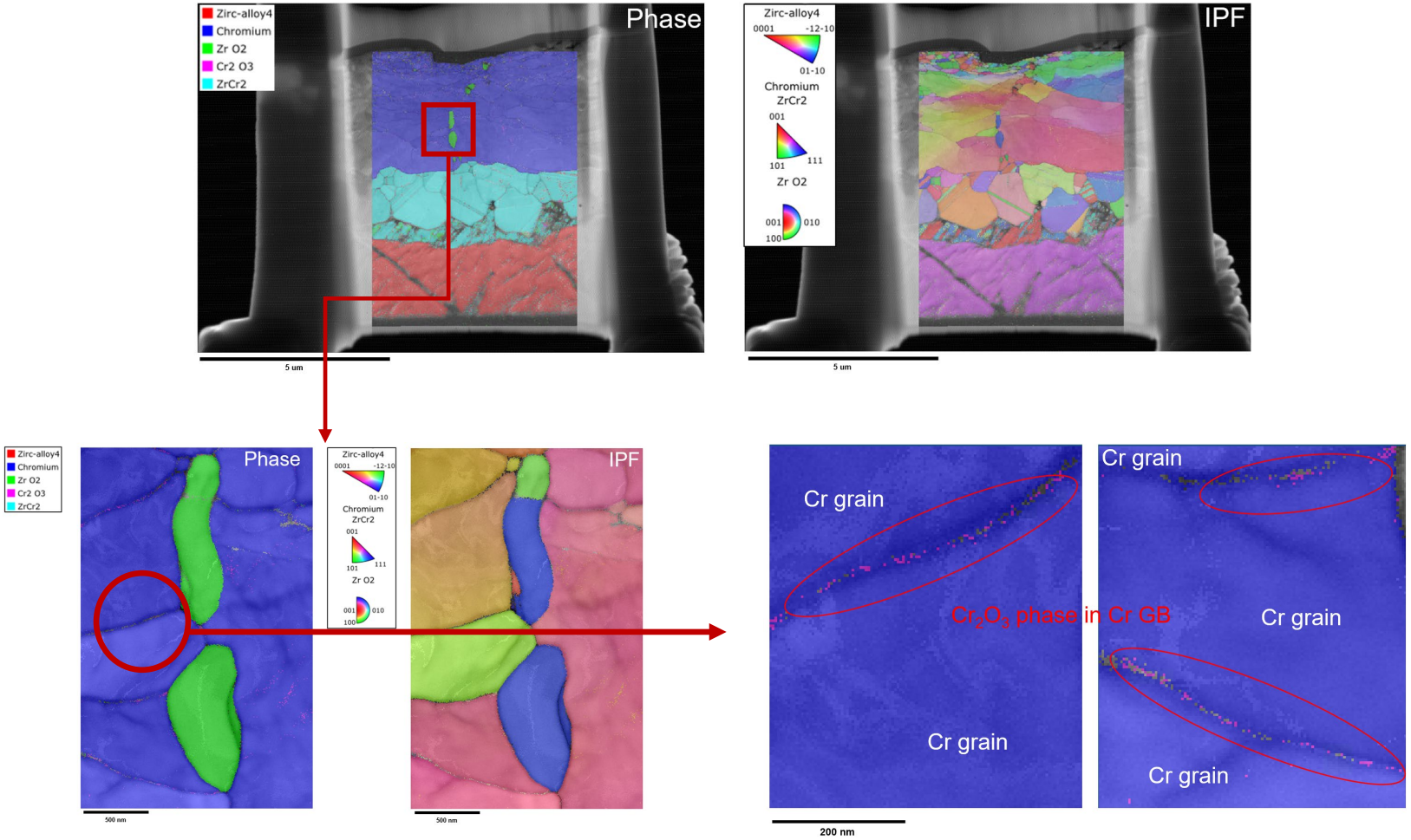

- **Sign of oxygen ingression through Cr grain boundary and early formation of ZrO_2:** ZrO_2 formation may occur before Zr reaches the top surface (Cr_2O_3). Zr may pick up oxygen from the Cr_2O_3 present in the grain boundaries and becomes ZrO_2 along its way to the top.

Tentative understanding of Cr coating safety limits

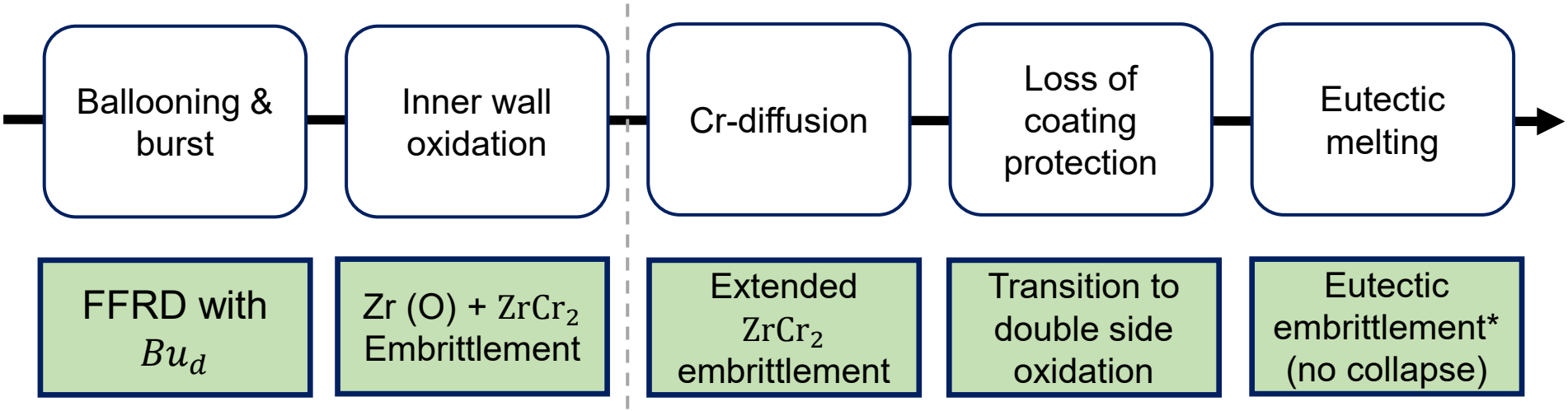

Tentative understanding:

Can be a burnup extension limiting factor

ECR=19% (single side oxidation)

PCT = 1204℃ (2200F)

Needs minimum ~10^1mins to be appreciable.

Modeling capability ready.

If coating is ~>15μm, it requires ~10^2mins at 1200 ℃.

Once it happens at >1310℃, no structural integrity should be expected. The ceiling of possible PCT limits. No fuel structural collapse with oxygen

DBA-relevant
(i.e., ECCS Criteria
10 CFR 50.46)

BDBA progression-relevant
(DEC condition)

2. Implications of safety limits of ATFs on burnup extension and integral LOCA experiments

Applying the Cr-coated limits for DBA safety analyses

- **Oxidation (ECR) Limits**

Uncoated Zr-based alloys:

$$ECR_{double-sided} = 87.8 * \frac{\Delta W_{CP,double}}{F_{thinning,avg}\left(\delta_{cladding} - \frac{ZrO_2}{1.56}\right)} \geq ECR_{limit}(\mathrm{H})$$

Metal substrate consumed by pre-transient oxidation [Pilling Bedworth ratio =1.56]

f(Bu) (i.e. 3.8% for 60MWd/kgU)

Cladding thinning factor due ballooning (average wall thickness reduction factor)

Metal substrate thickness after pre-transient oxidation

Cr-coated Zr-based alloys:

$$ECR_{single-sided} = 87.8 * \frac{\Delta W_{CP,single}}{F_{thinning,avg}\delta_{cladding}} \geq 18\%$$

Assumption: pre-transient consumption of metal substrate via steady-state corrosion is nil.

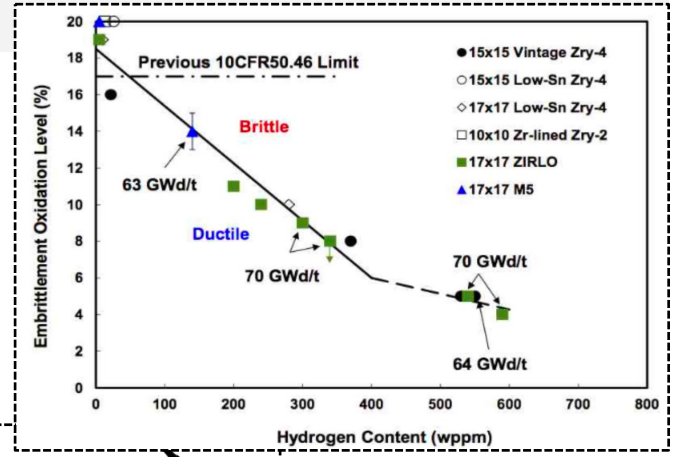

- **PCT Limits**

Uncoated Zr-based alloys: 1204℃

Cr-coated Zr-based alloys: 1204℃

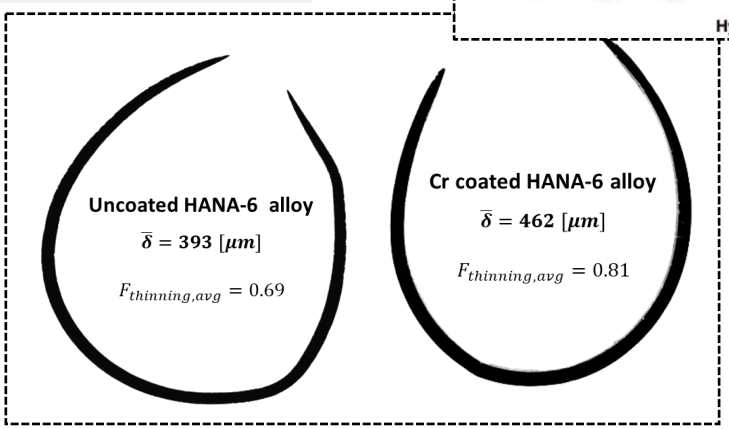

$F_{thinning,avg}$

Crucial importance of steady-state corrosion resistance

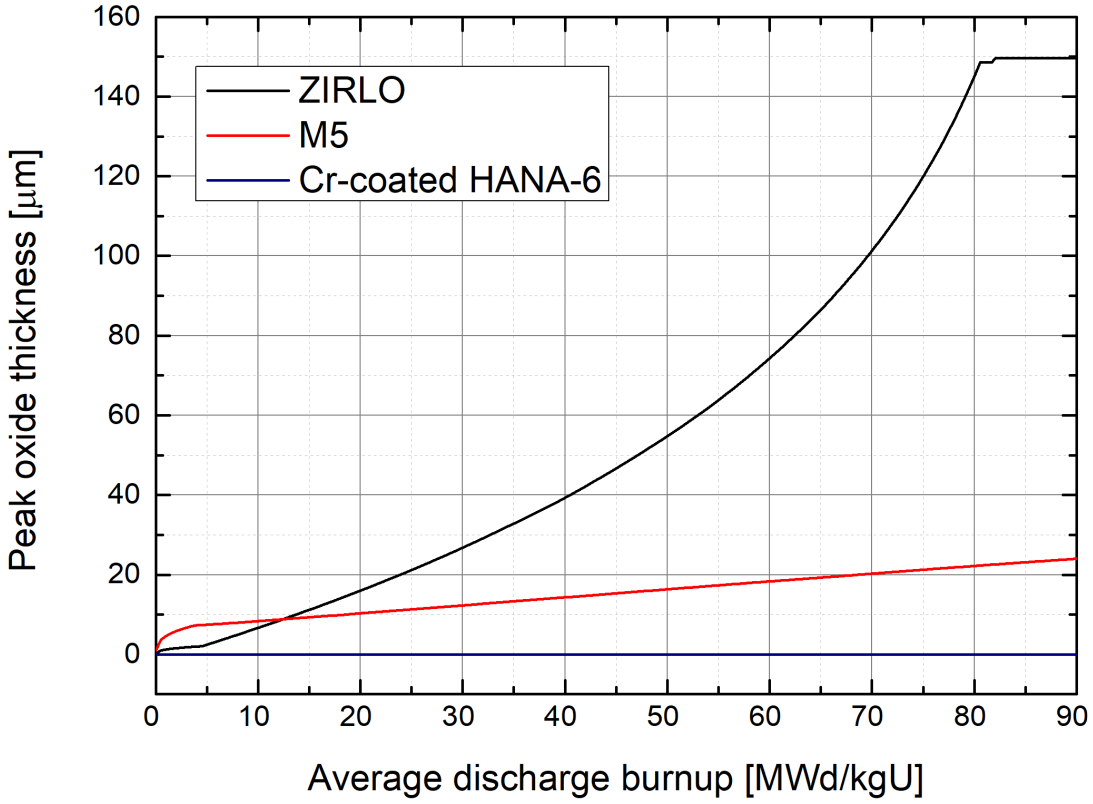

- **Accident tolerance comes from steady state corrosion resistance:** Steady-state corrosion resistance is a key performance metric that has direct ramifications on accident safety margin. Suppression of steady-state corrosion and resulting hydrogen pickup directly increases safety margin (i.e., ECR margin) of limiting DBA cases (i.e., LBLOCA).

Investigating the allowable discharge burnup with modern Zircaloy and Cr-coated ATF (APR-1400)

<Zirlo>

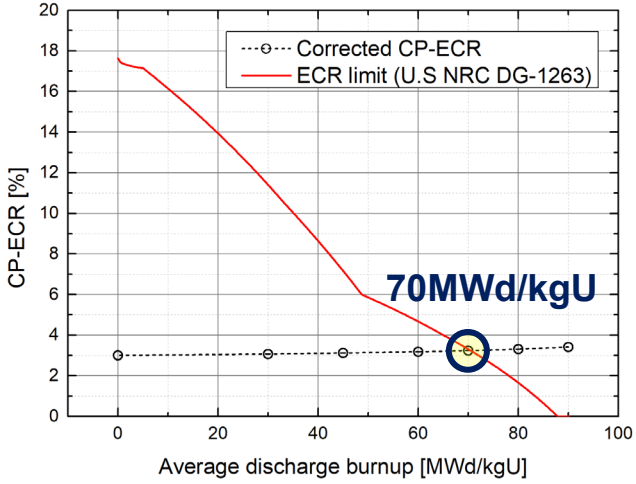

<Modern Zircaloy (HANA-6, M5)>

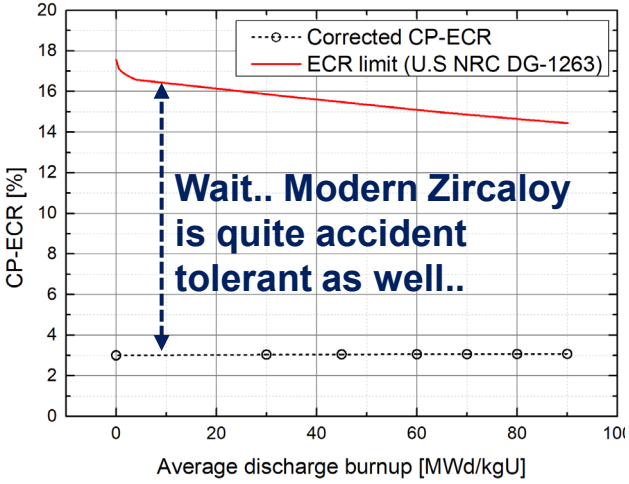

<Cr-coated ATF>

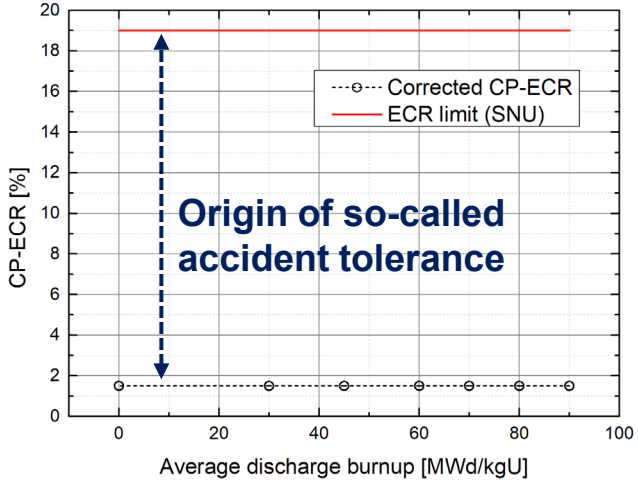

LBLOCA safety analysis (MARS)

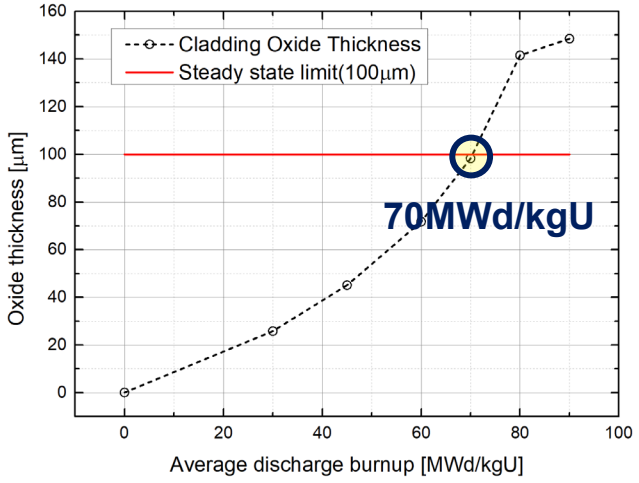

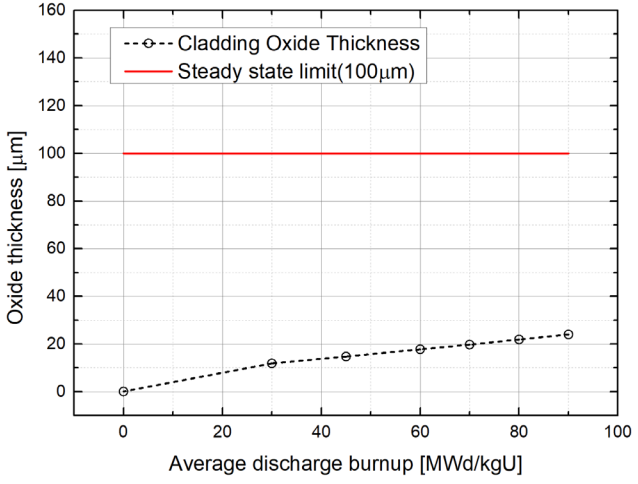

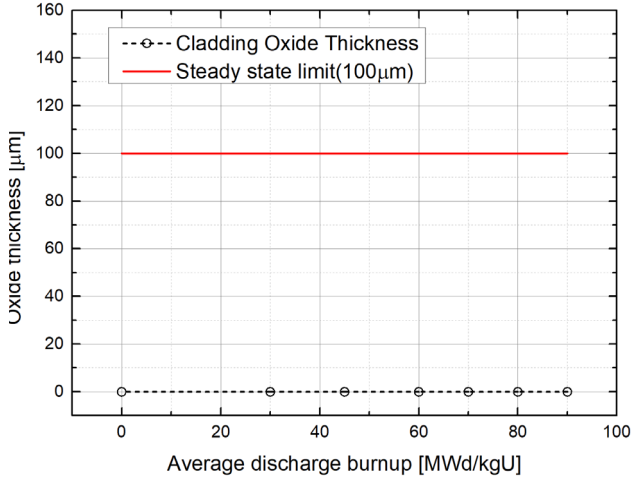

Steady-state fuel simulation (GIFT, developed by SNU)

Insight into the attainable performance of ATFs

Then, what will be the key limiting factor for fuel burnup increase ?

- **Key implications:**
  1. Modern Zircaloys may be as accident tolerant as Cr-coated ATFs.

  2. Accident tolerance comes from steady-state corrosion resistance. Modern Zircaloy is quite corrosion–resistant under the typical LWR operating conditions.

  3. Value of ATF needs to be addressed from the viewpoint of effective suppression on hydrogen production at certain temperature range.

  4. Cladding has done its job; burnup extension is contingent upon **FFRD**.

Schematic of SNU's integral LOCA experiment (*i*-LOCA facility)

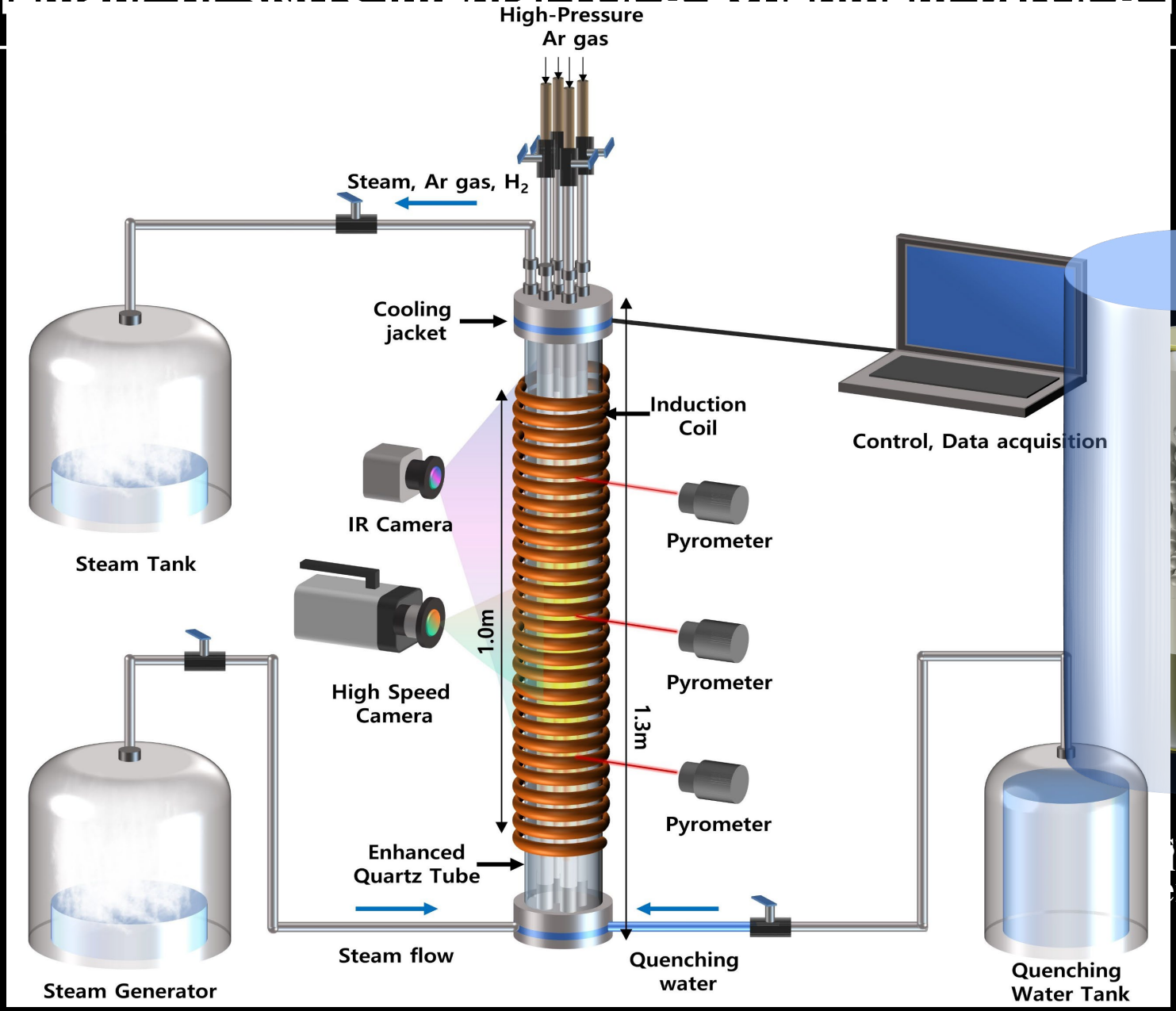

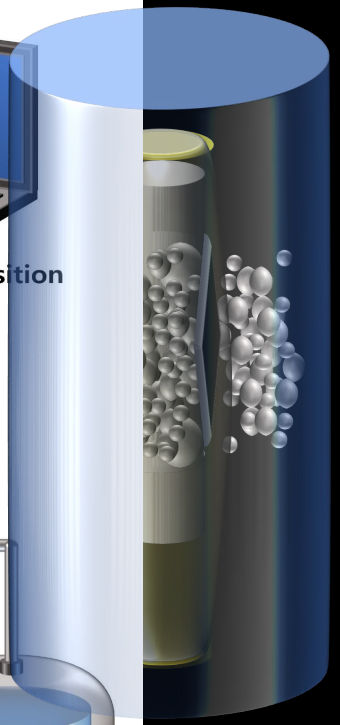

t & Fuel
looning
ent Dispersal

Integral LOCA experiment at Seoul National University (i-LOCA facility)

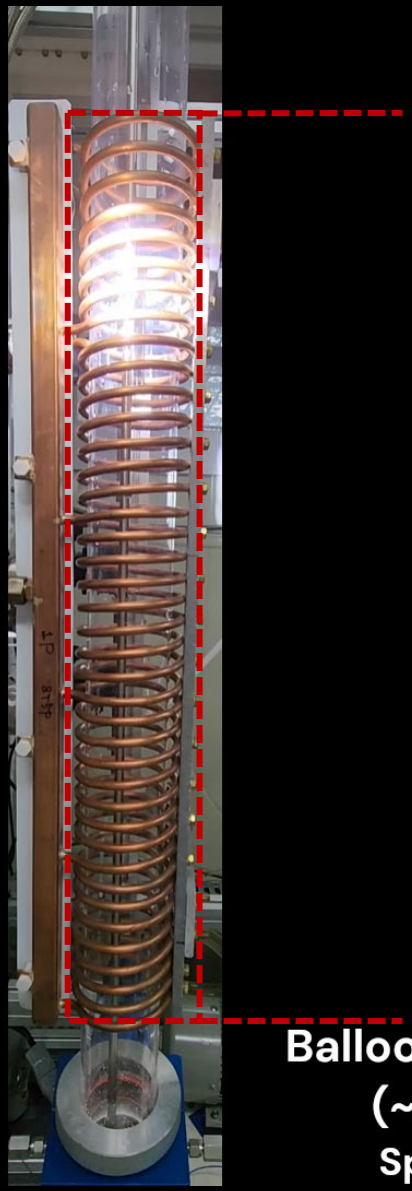

Ballooning&Burst
(~800°C)
Speed x10

<Digital camera> <IR camera>

<Schematic of LOCA procedure>

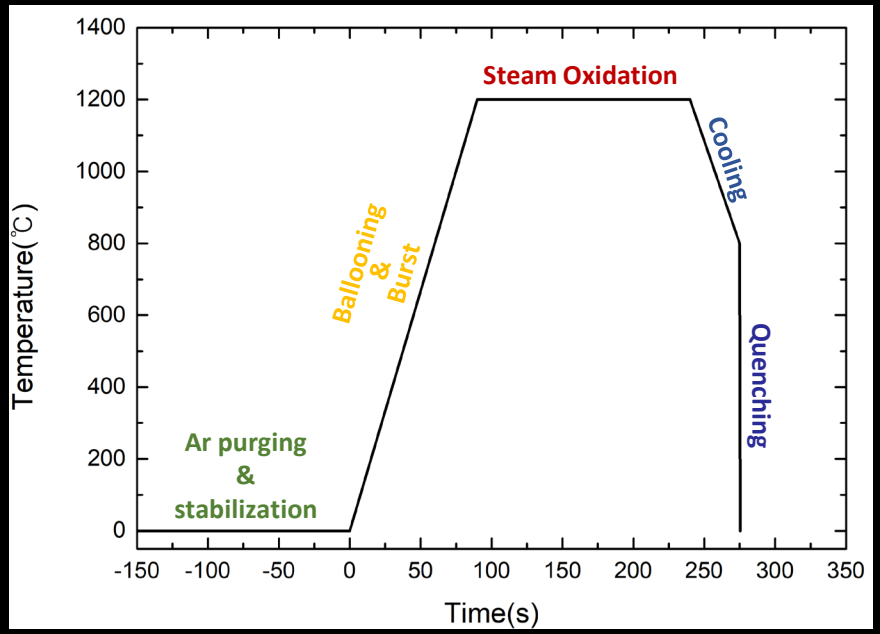

Integral LOCA experiment at Seoul National University (i-LOCA facility)

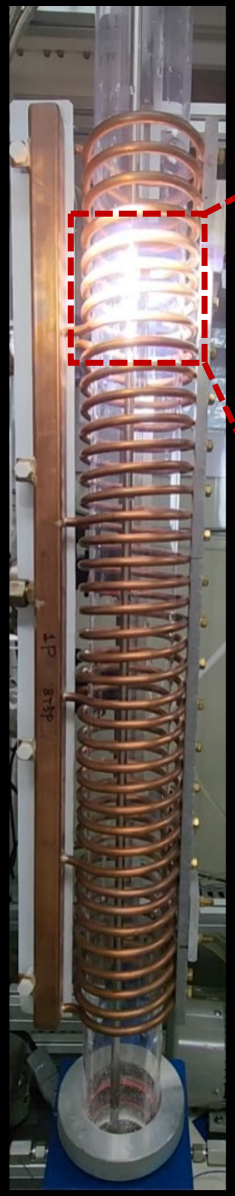

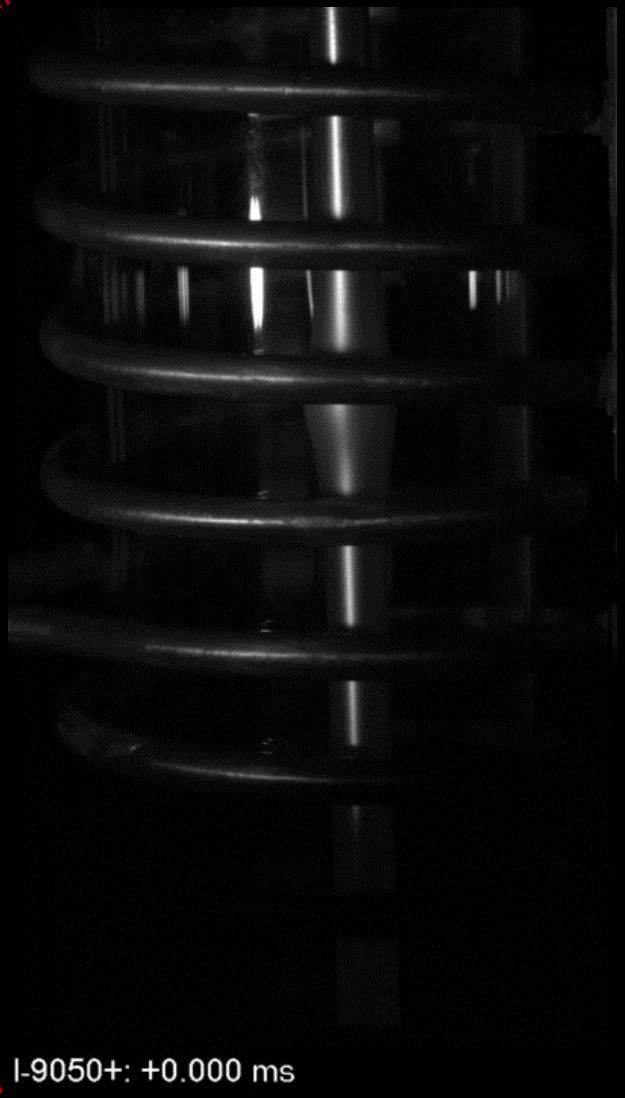

<Digital camera>

<High speed video camera>

Temperature validation of facility

IR camera

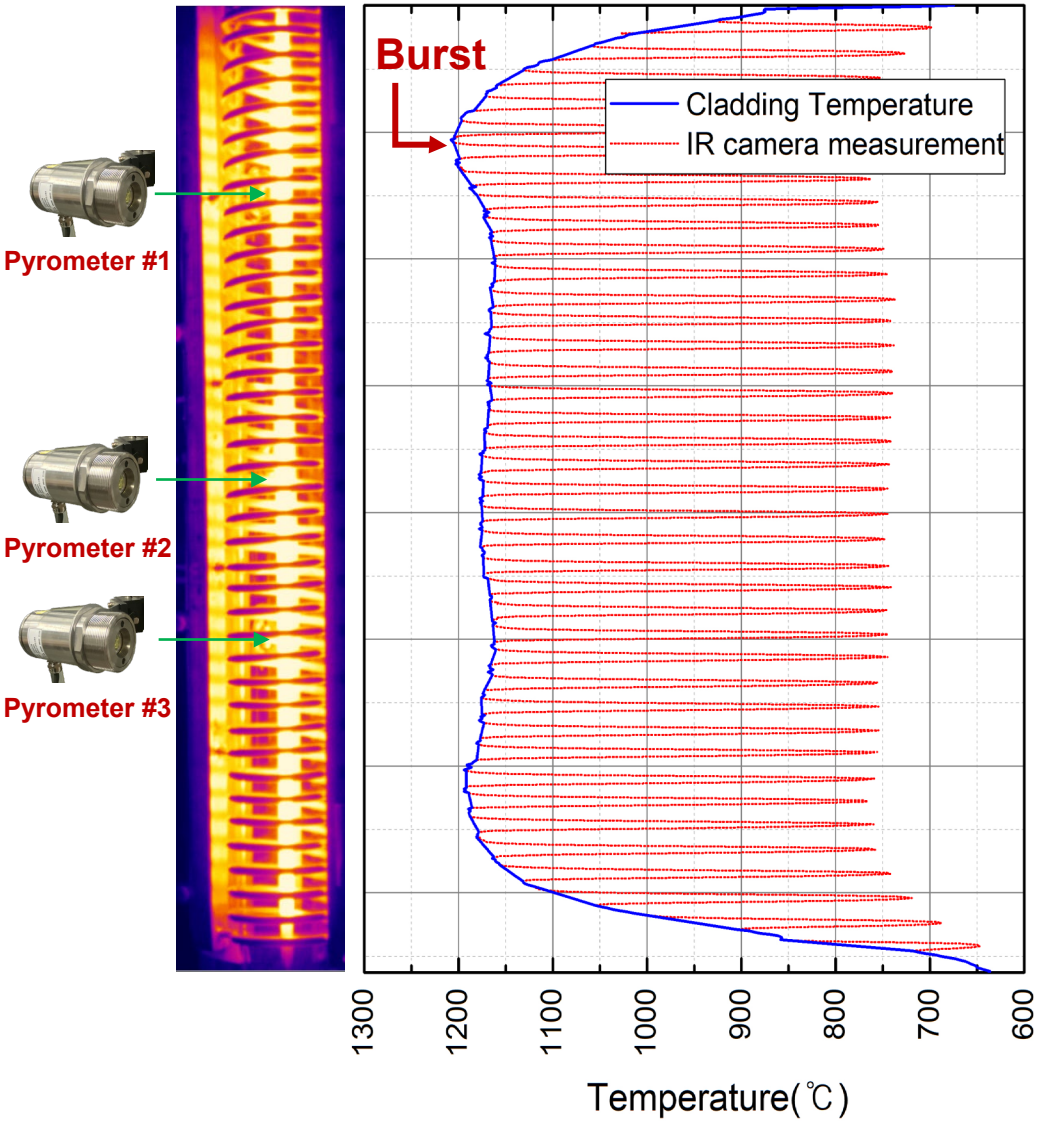

Oxide thickness measurement & calculation

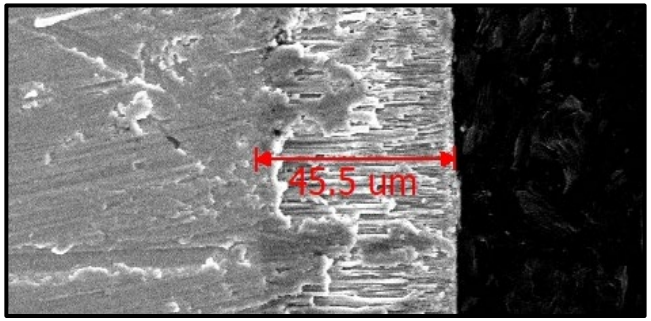

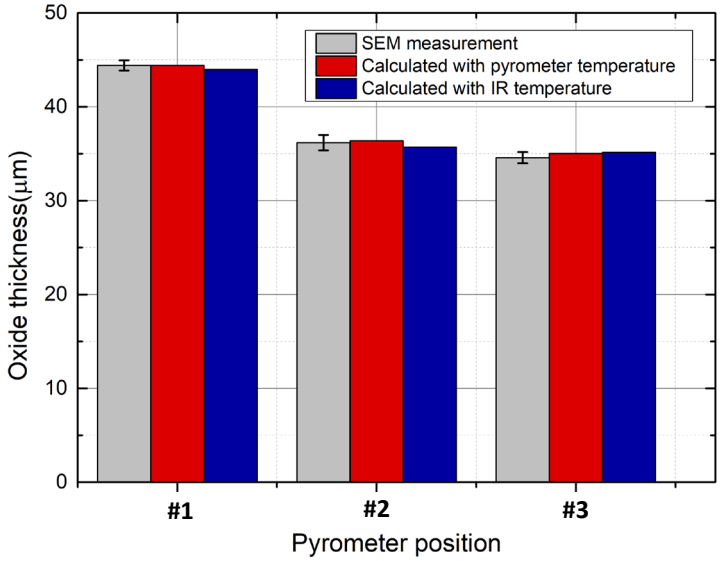

- Oxide thickness calculated with temperature profile of pyrometer and IR camera were consistent with SEM measurement

Surrogate pellets to study dispersal behavior

- **Surrogate ZrO_2 powder/powder mixture simulating fragmented pellets**

① Cylinder Pellet
Bu < 60 GWd/MTU
(d=8.192mm)
Packing fraction : 96%

② Mixed Powder Pellet
Bu ≈ 68 GWd/MTU
(d=0.3,1,2,3,5 mm
with the same mass fraction)
Packing fraction : 62.5%

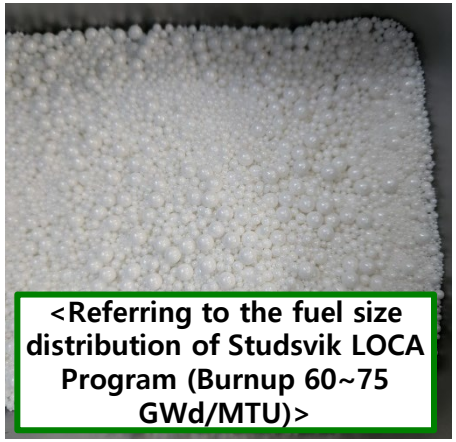

<Referring to the fuel size distribution of Studsvik LOCA Program (Burnup 60~75 GWd/MTU)>

③ Single Powder Pellet
Bu > 80 GWd/MTU
(d=0.5mm)
Packing fraction : 62.1%>

<Powder loading into the cladding>

Experimental test matrix

- Cladding : ZIRLO, HANA-6 (Zr-1.1Nb), Cr-coated HANA-6 (16μm, AIP)
- Rod cold void volume : 30 cm^3
- Powder pellet zoning length : 30 cm
- Heating rate : 70-80 ℃/s

ZIRLO	Rod internal pressure			
	1 MPa	3 MPa	5 MPa	7 MPa
Cylinder pellet 	2 ea	2 ea	2 ea	2 ea
Mixed powder 	2 ea	2 ea	2 ea	2 ea
Single powder 	2 ea	3 ea	3 ea	1 ea

HANA-6 & Cr-coated HANA-6	Rod internal pressure			
	1 MPa	3 MPa	5 MPa	7 MPa
Cylinder pellet 	1 ea	1 ea	1 ea	1 ea
Single powder 	1 ea	1 ea	1 ea	1 ea

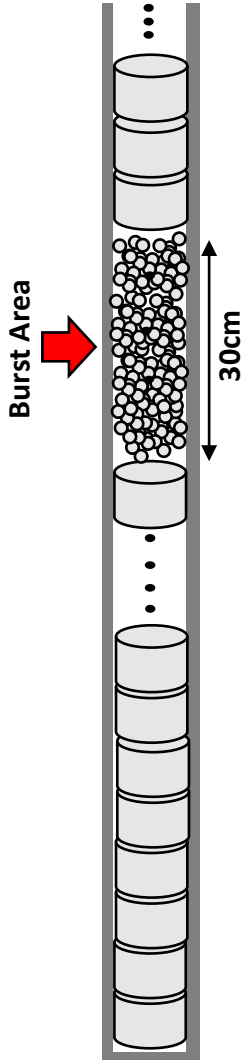

Post-burst characterization using 3D scanner: Burst Genome projects

ZIRLO Burst Results

	Cylinder pellet	Mixed powder	Single powder
10 bar	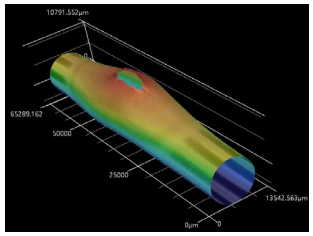	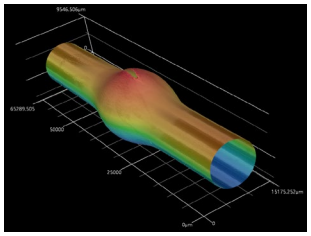	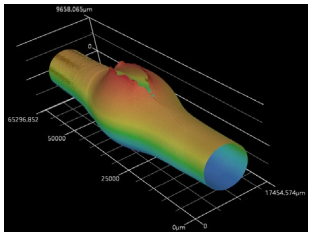
30 bar	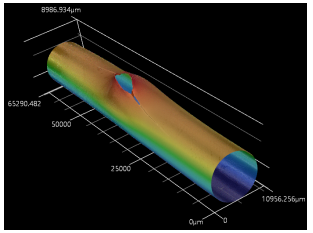	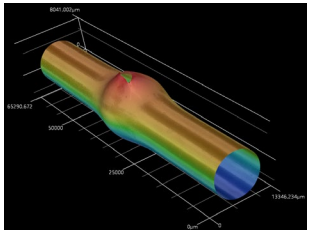	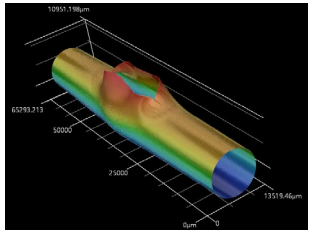
50 bar	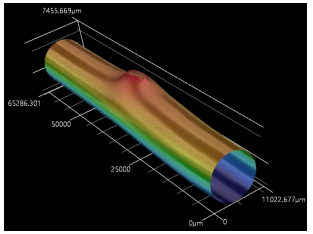	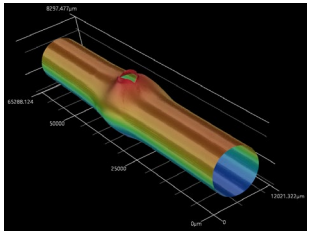	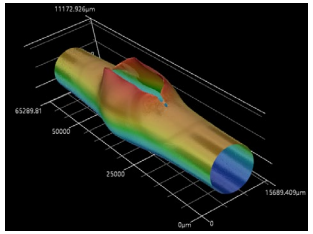
70 bar	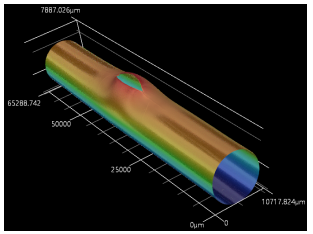	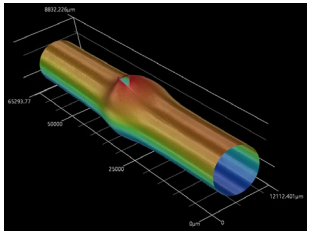	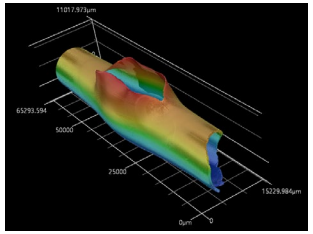

SNU burst result comparison with references

Burst temperature comparison with surrogate pellet inserted data

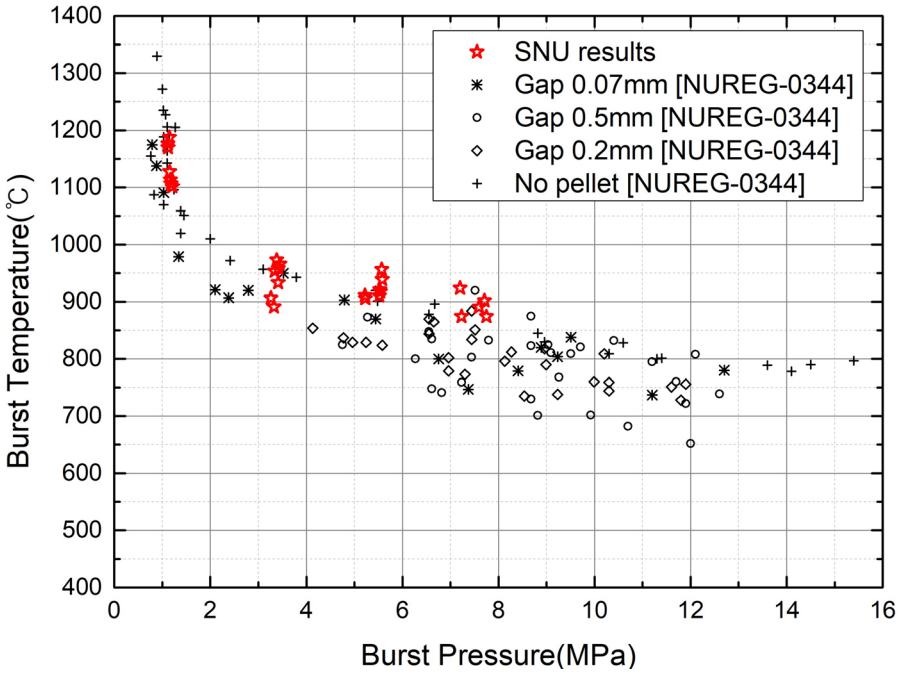

Engineering burst stress comparison with reported data

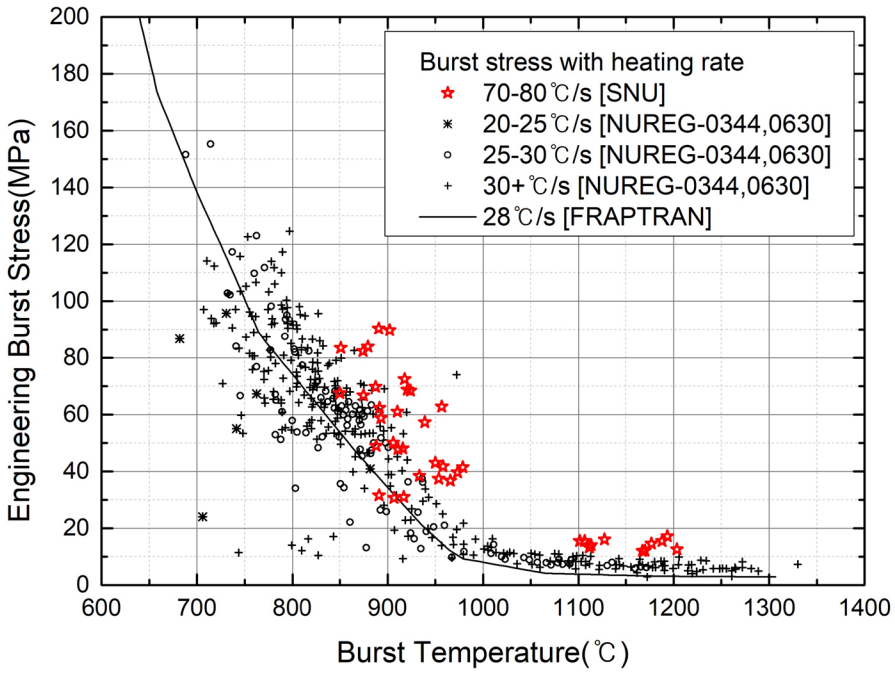

- Burst temperature and engineering stress showed slightly higher results in SNU
- Considering the **higher heating rate in SNU**, the difference is acceptable

Burst behavior for the different pellet types

Rod pressure 1 MPa, cold void volume 30cm^3

<Cylinder pellet>

I-10732+: +0.000 ms

<Single powder>

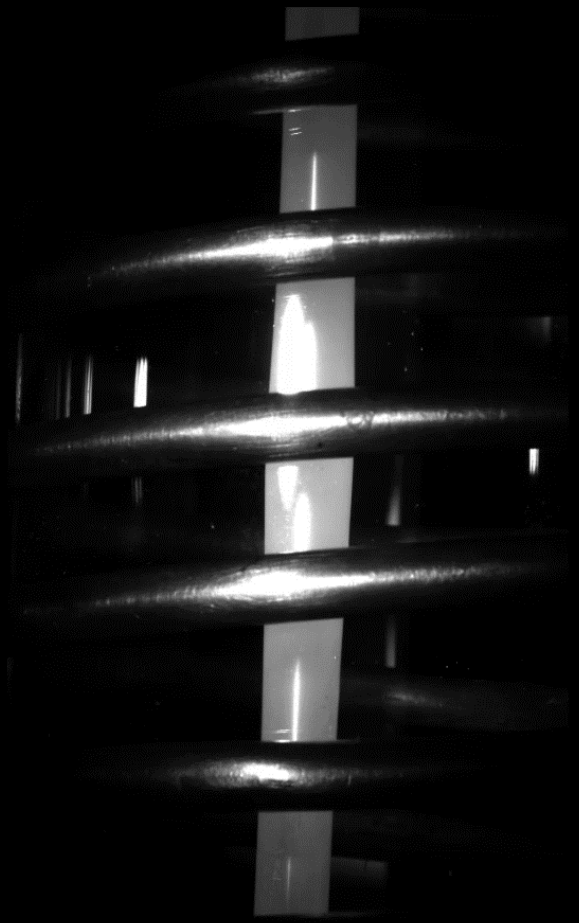

I-10312+: +0.000 ms

- **Cladding is heated more uniformly and deform larger with single powder**

ZIRLO post-burst characterization results

<ZIRLO 3 MPa burst results>

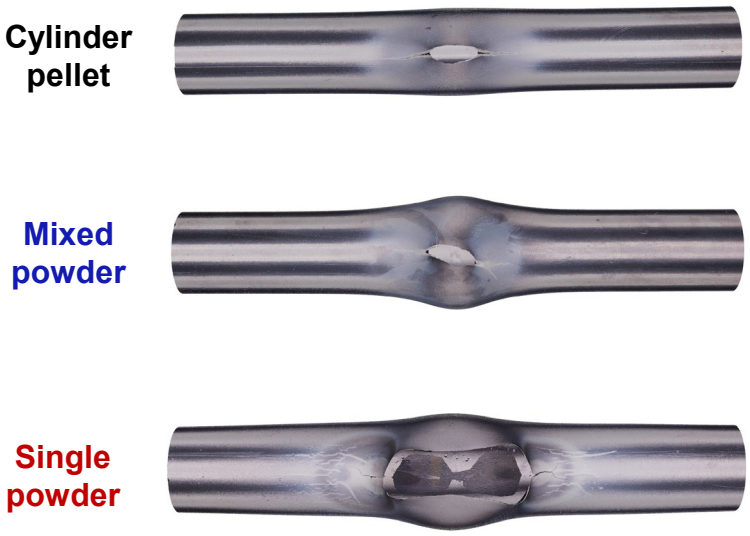

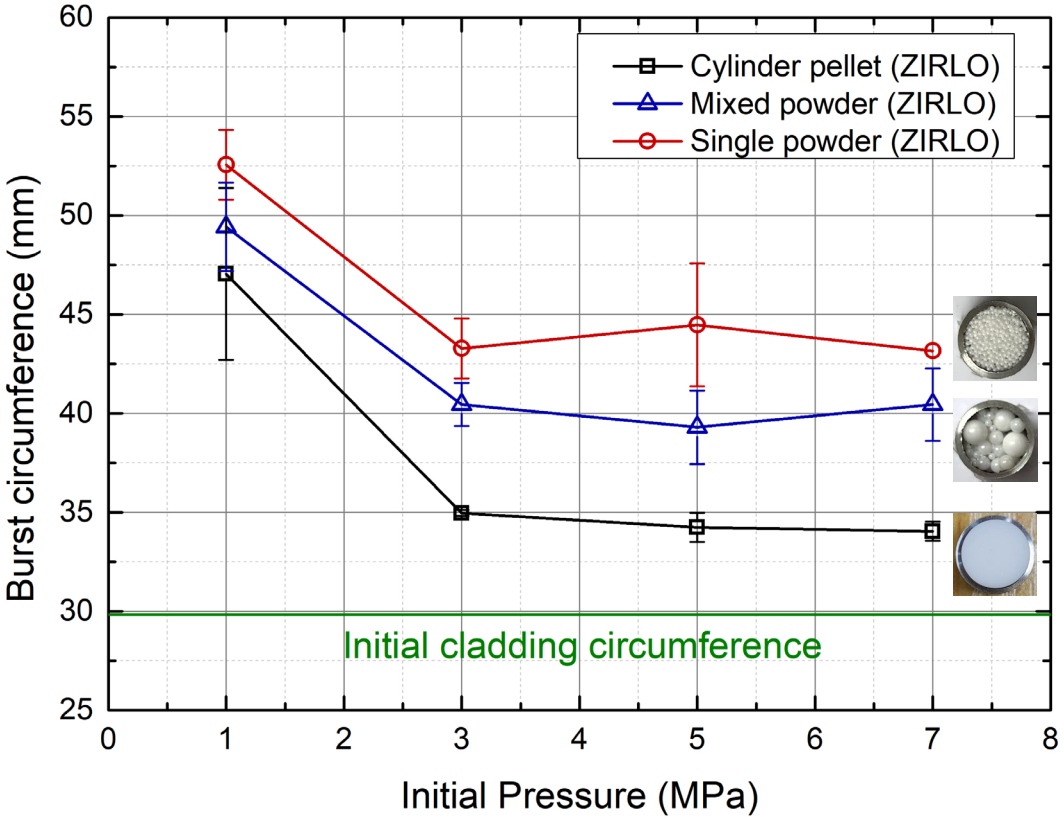

- Burst geometry was clearly different depending on the types of pellet
- **Type of pellet seemed to have greater effect on burst geometry** than rod pressure.

Burst behavior is sensitive to Azimuthal T affected by the pellet type

ZIRLO 3 MPa burst results

Cylinder pellet

Mixed powder

Single powder

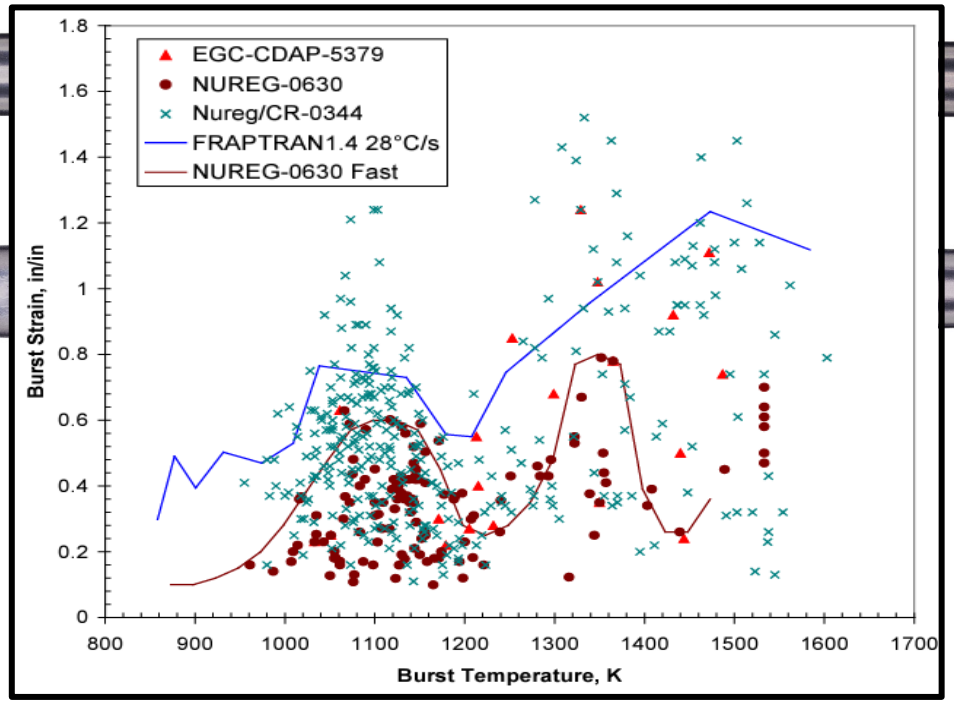

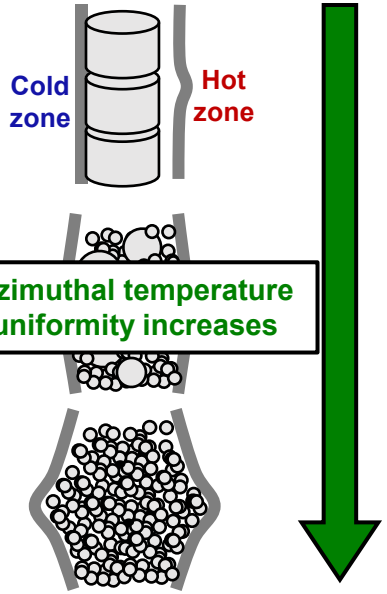

The size and distribution of fragmented fuel have a significant effect on burst behavior

Dispersal behavior for the different pellet types

Rod pressure 1 MPa, cold void volume 30cm^3

<Mixed powder>

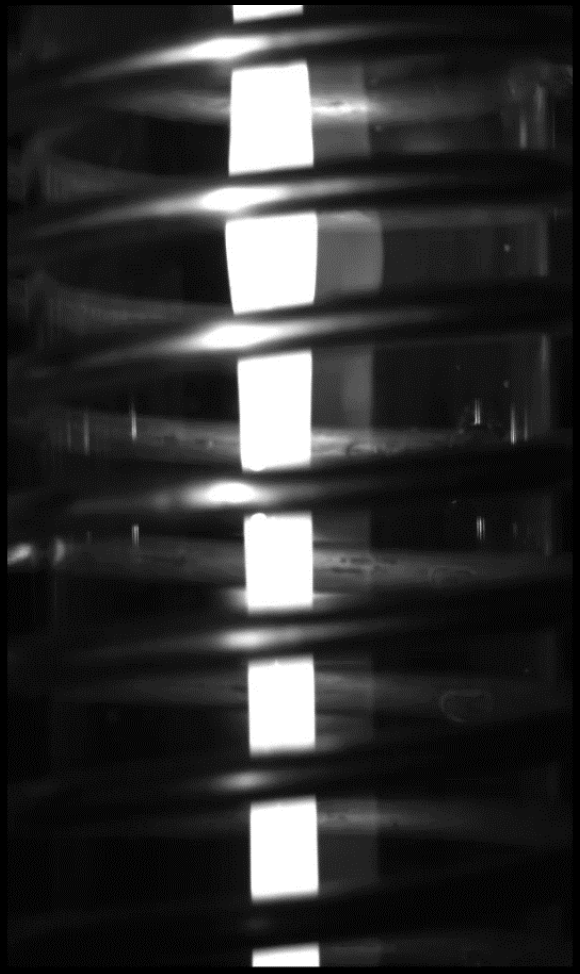

I-7661+: +0.000 ms

<Single powder>

I-6207+: +0.000 ms

- **Single powder is more dispersed compared to mixed powder**

Dispersal behavior for various rod pressures

Single powder case, cold void volume $30cm^3$

<1 MPa> **<3 MPa>** **<5 MPa>** **<7 MPa>**

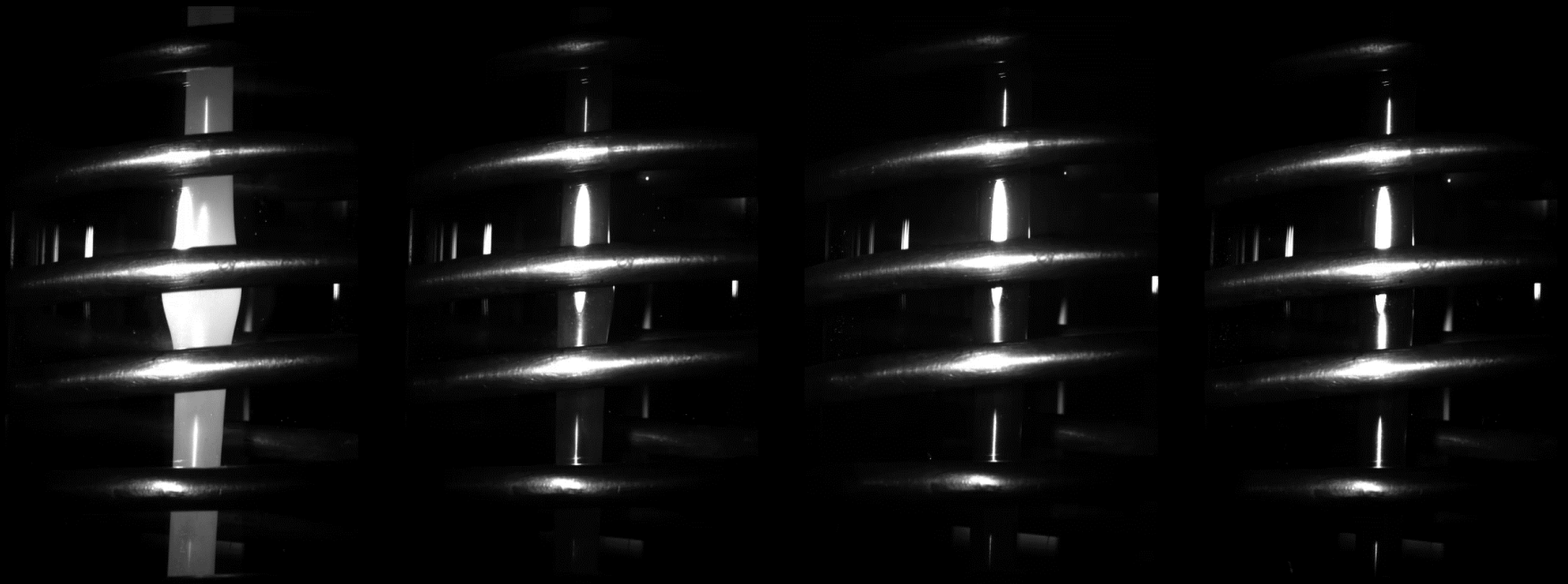

I-4511+: +0.000 ms I-5002+: +0.000 ms I-4901+: +0.000 ms I-4493+: +0.000 ms

- **The higher the rod pressure, the more particles were dispersed**

Fuel dispersal results

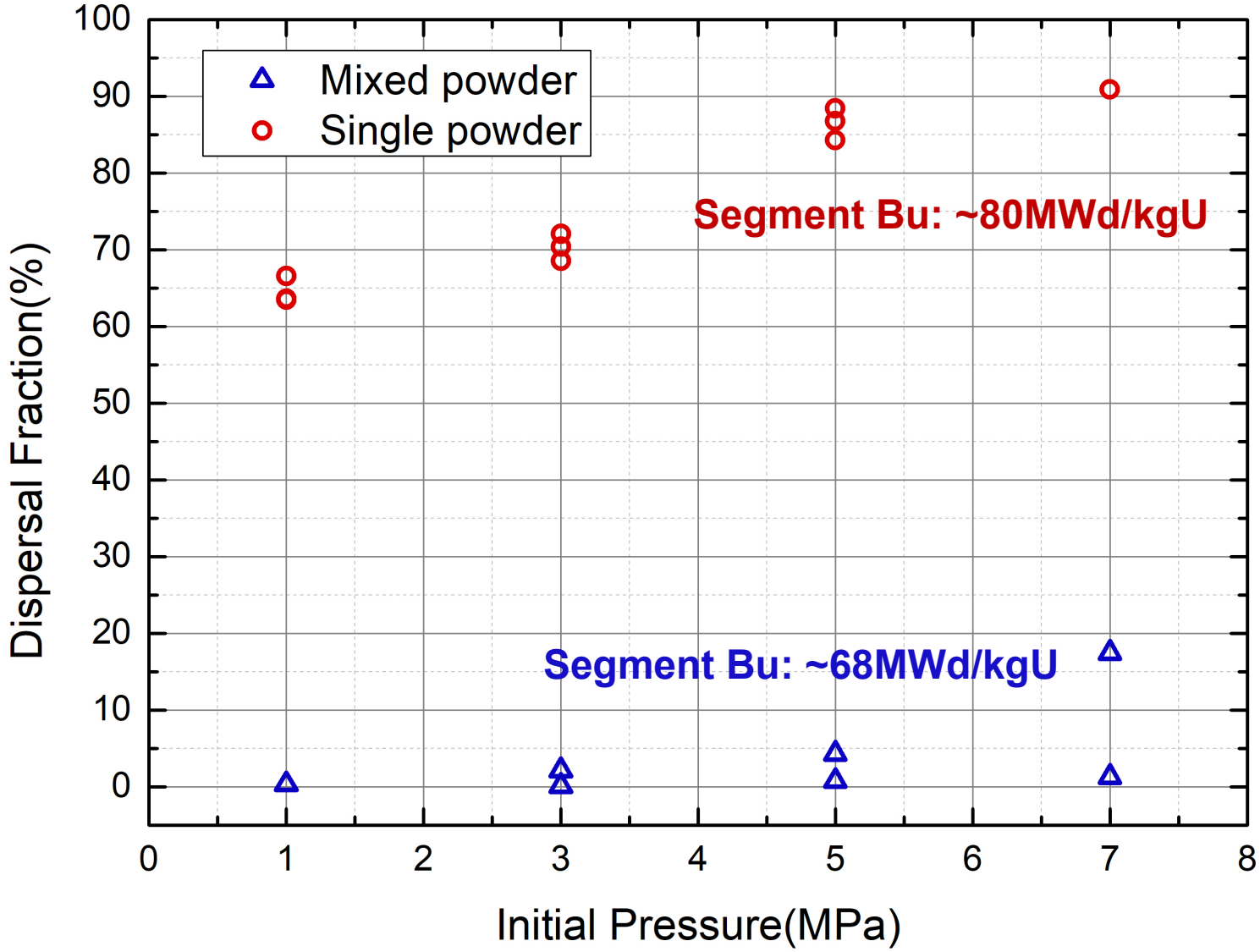

Cr coating influence on burst geometry and resulting fuel dispersal

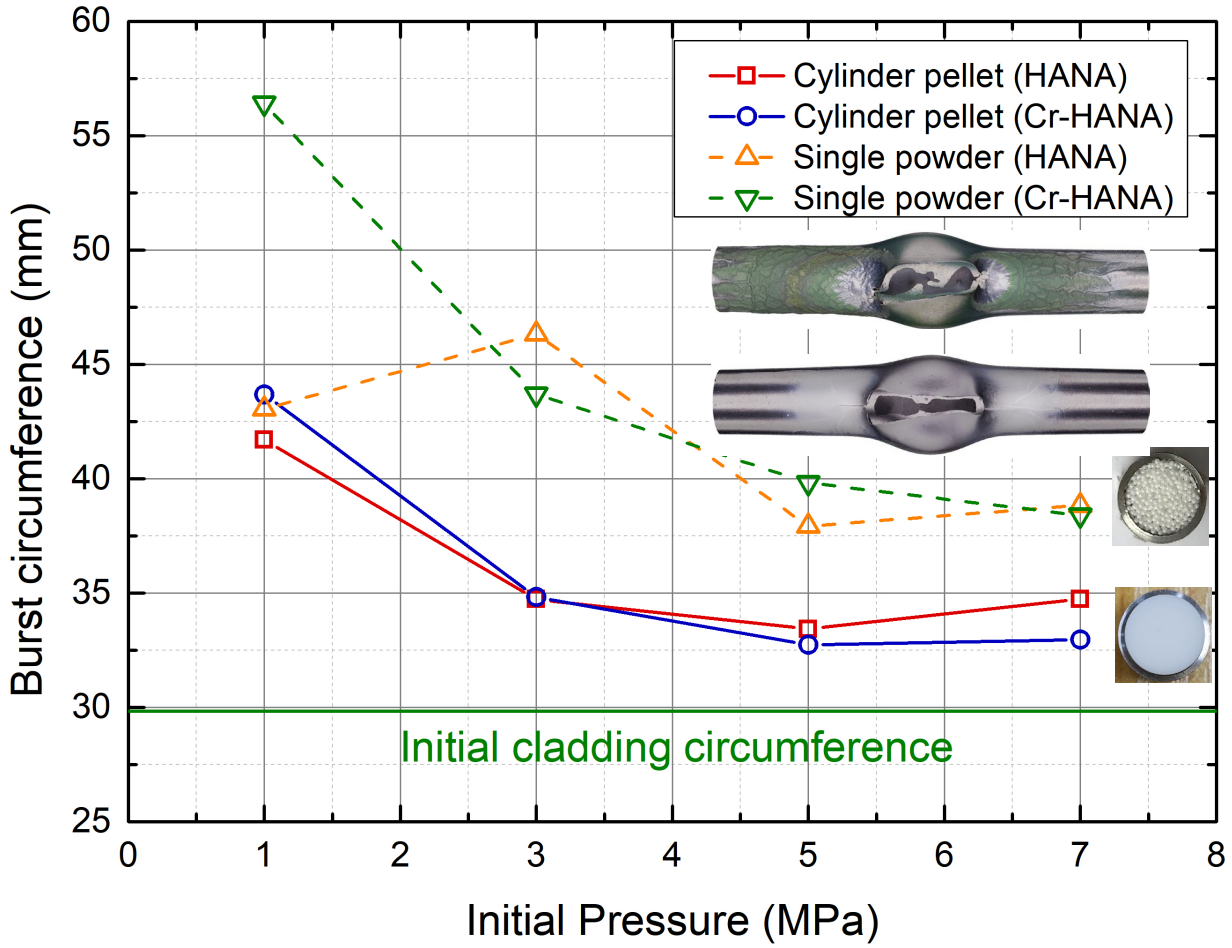

- Little burst circumference difference was observed with Cr-coated cladding
- **Type of pellet have greater effect on burst geometry** than coating effect.

Post-LOCA cladding embrittlement characterization

Rod pressure 5 MPa, cold void volume $30cm^3$

<Cr-coated HANA (16μm) >

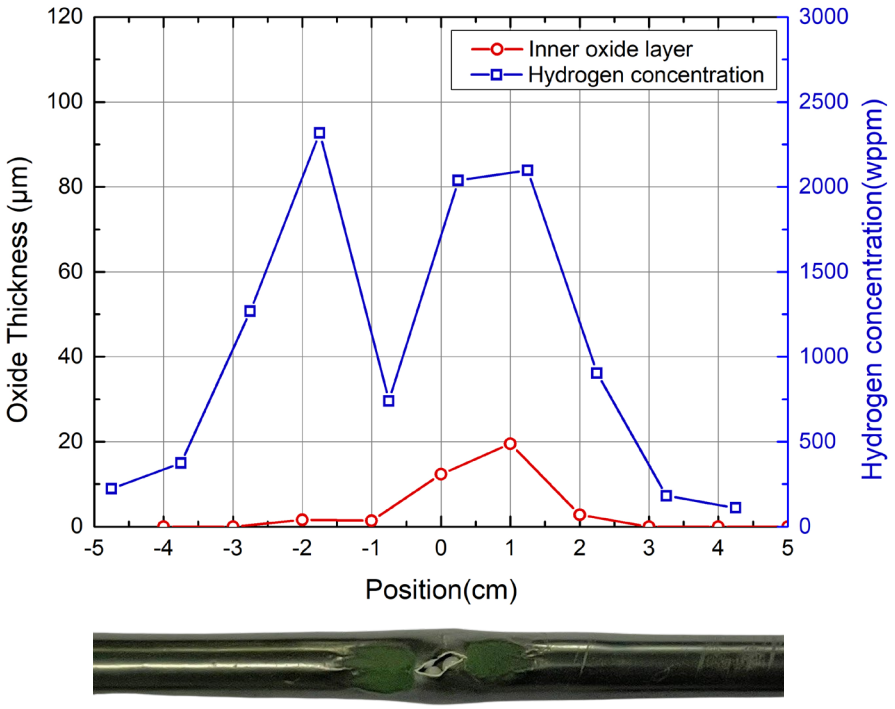

<HANA>

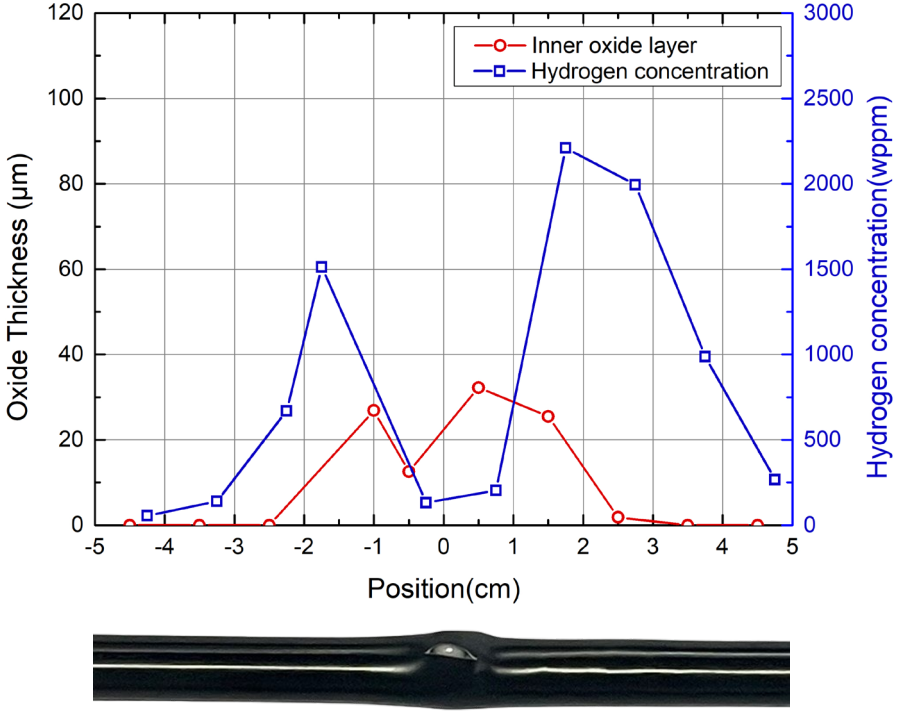

- Inner side oxidation and secondary hydriding behavior showed **little difference between coated and uncoated cladding**
- Inner side oxidation was limited to **±4cm from the burst hole, consistent with U.S.NRC ECCS evaluation models** (appendix K to part 50)

Extent of inner oxidation and secondary hydride formation w.r.t to burst hole size

Rod pressure 3 MPa, cold void volume 30cm^3

<Mixed Powder>

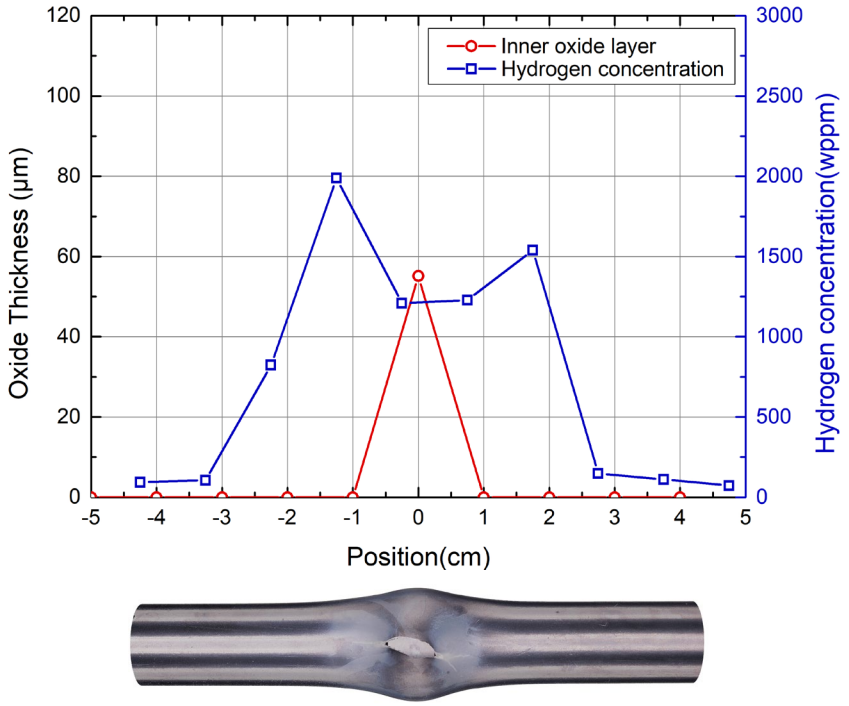

<Single powder>

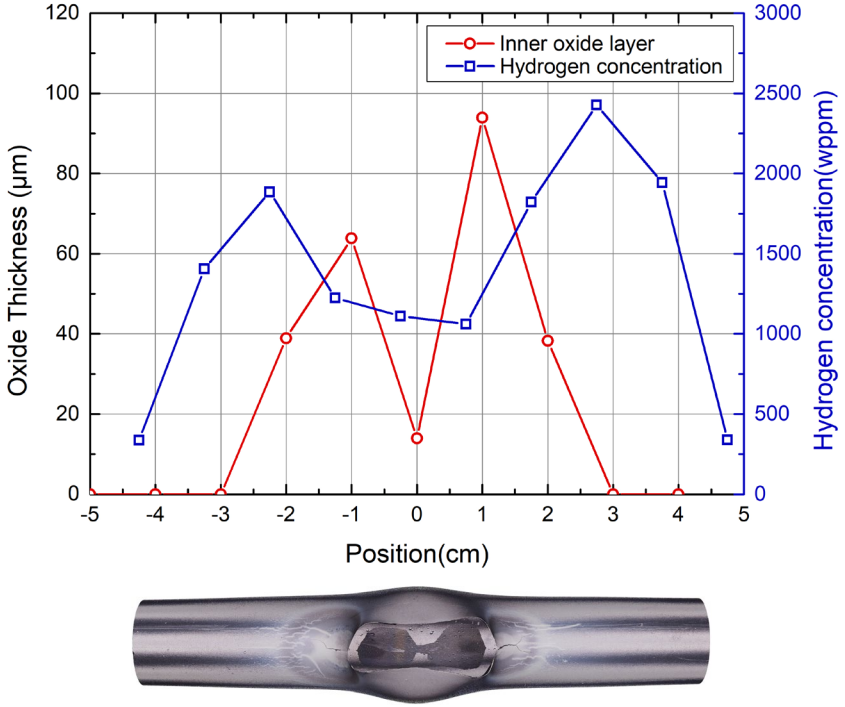

- The larger the hole, the larger the inner oxidation and secondary hydride formation

Post-oxidation characterization : weight gain results

- **Surface coating crack after ballooning & burst**

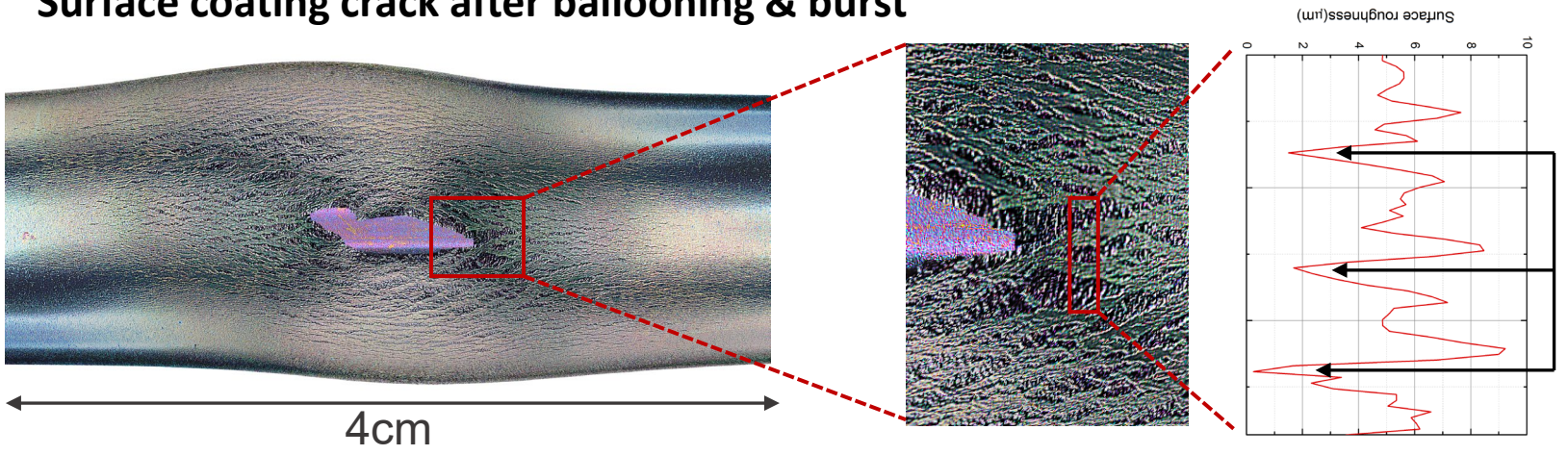

- **Post-burst steam oxidation tests: separate double side oxidation tests with cut burst parts**

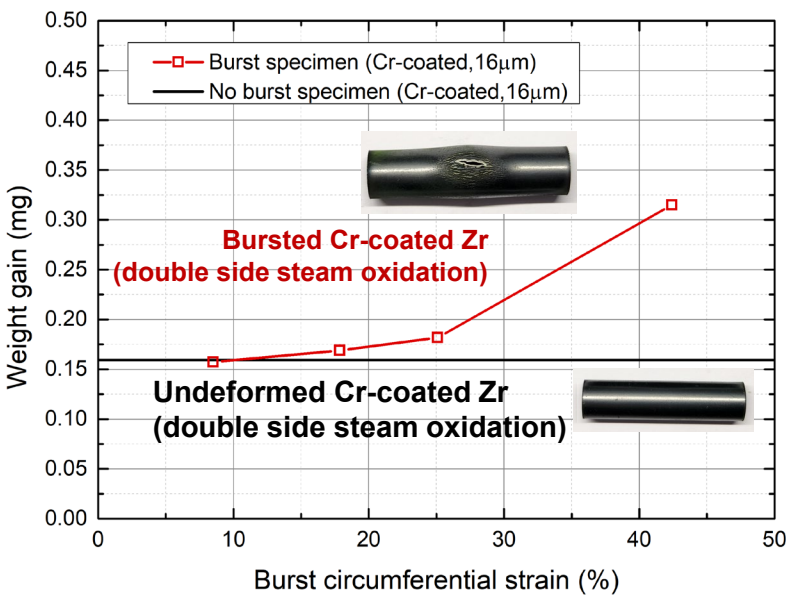

Normalized by surface area

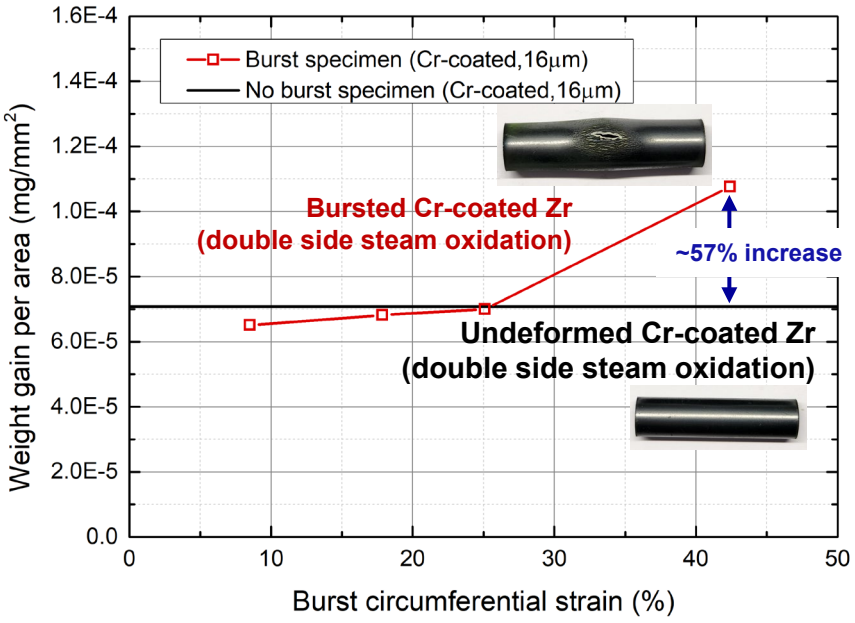

Conclusion : key deliverables

1. **Origin of accident tolerance**
   - Accident Tolerance comes from steady-state corrosion resistance and resulting decrease in hydrogen pickup.
   - Modern Zircaloy (i.e., HANA-6, M5) seems to be the earlier version of Accident Tolerant Fuels.

2. **Fuel ballooning and burst**
   - Post-burst geometry is sensitive to cold-void volume, and azimuthal temperature gradient which is affected by type of pellet inserts: some level of unification to reality is needed for cross-comparison of international benchmark programs.
   - The prevailing treatment of dispersal fraction (50% or 100%) is excessively conservative

3. **What's next ?**
   - Untapped potential of burnup extension for LEU+ (5-10% enrichment)/Modern Zircaloy or ATF fueled FFRD-free SMRs.

Thank you for your attention!

Global FFRD research

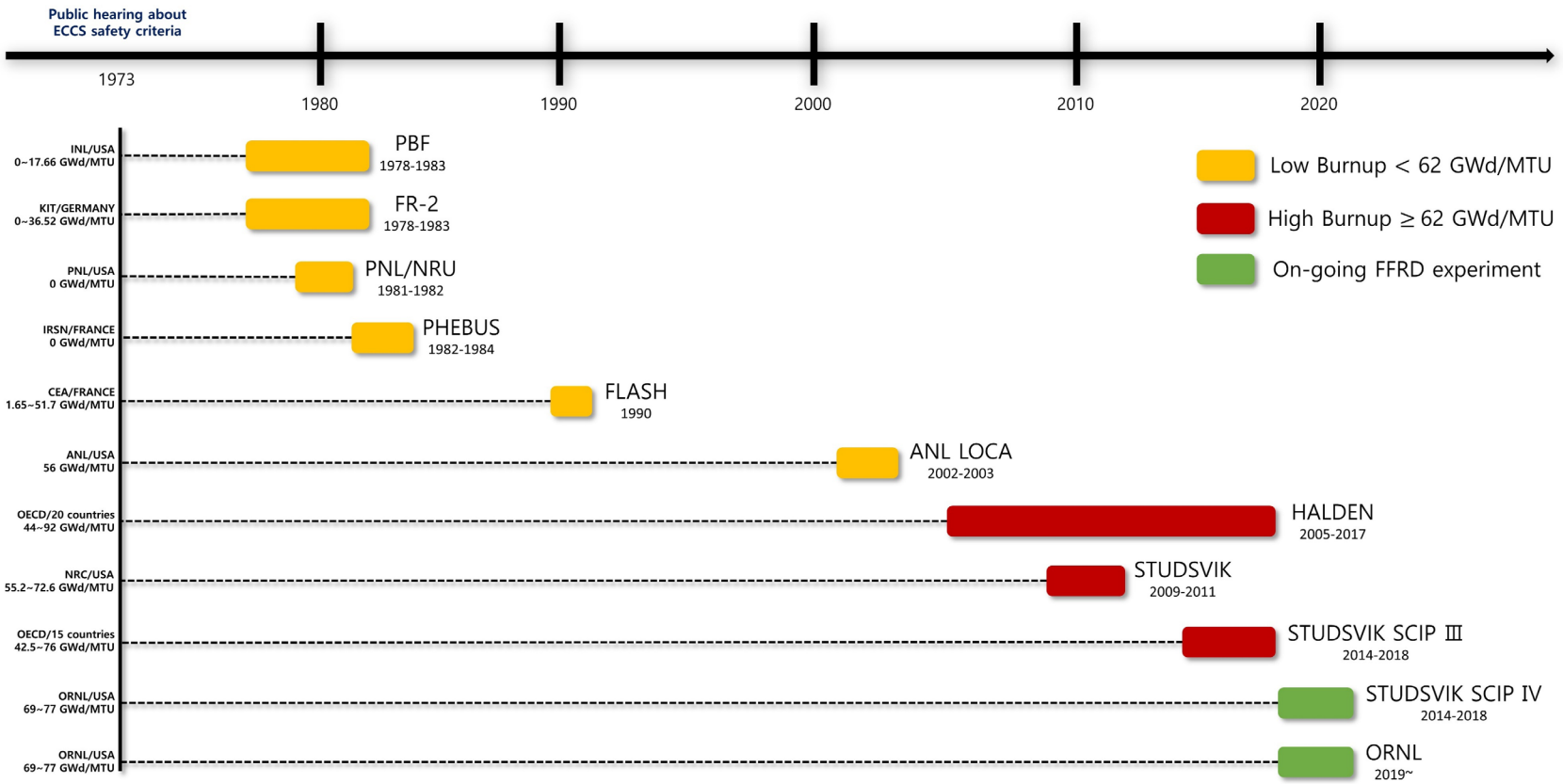

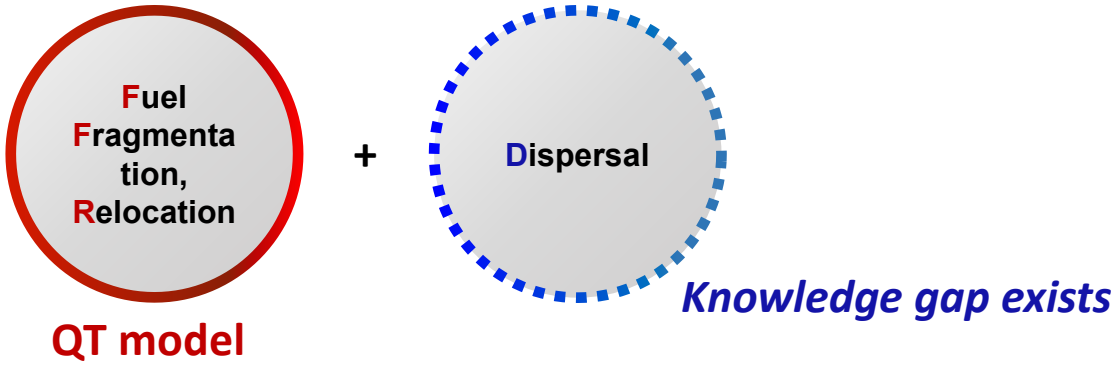

A. Charbal

CEA

Study of chromium coating (on zirconium based-cladding substrate) cracking under thermomechanical loadings

The ongoing research and development of enhanced accident tolerant fuel (EATF) claddings has provided various solutions and potential candidates [1]. Chromium coatings deposited on zirconium-based cladding by PVD [2]–[6] have been shown to give clear improvements in Loss-of-Coolant Accident (LOCA) conditions, providing additional coping time before reaching quenching and post-quenching embrittlement and potential loss of cladding integrity.

The cladding during normal or hypothetical accidental situations could undergo small to large deformations. The mechanical response of the chromium coating varies depending on its thickness, its microstructural state and the testing temperature (among other parameters). Coating damage (e.g., cracking and spallation) during thermomechanical loading needs to be further studied and quantified. Thus, this presentation will illustrate some CEA's experimental approaches to investigate such phenomenon, under nominal or hypothetical accidental scenarios.

Crack monitoring by acoustic emission (AE) during tensile test as-coated material at temperatures between 20°C and 350°C has proven to be an efficient and simple method to implement [2]. Results have shown good agreements with strain fields obtained from digital image correlation [7] or optical observations. AE techniques provides satisfactory results and could, in the future, be integrated to mechanical testing performed in "hot cells". Meanwhile preliminary results on neutron irradiated Cr-coated claddings (2dpa) at 330°C has shown promising results toward the remaining ductility of the protective layer. Indeed, post-mortem analyses highlighted no crack formation below ~2% of circumferential strains [8].

In LOCA scenarios, chromium-coated cladding exhibits higher ductility. Even in cases of significant ballooning and cladding rupture, negligible cracking and no coating spallation has been observed in many cases [6]. Post-mortem analyses such as metallographic observations or X-Ray tomography help to determine the correlation between the crack density and circumferential deformation.

Acknowledgment: The presented works have been supported by the CEA-EDF-FRAMATOME "Innovation COMBustible" project. Special thanks to Stéphane Valance (CEA), Edouard Pouillier & Antoine Ambard (EDF), Thomas Garnier, Thorsten Marlaud and Karl Buchanan (FRAMATOME) for their fruitful feedbacks and corrections.

Study of chromium coating (*on zirconium based-cladding substrate*) cracking under thermomechanical loadings*,**

A. Charbal, J-C. Brachet, Y. Taïbi, V.D. Nguyen, G. Touze, J.P. Bonthonneau, M. Dumerval, L., M. Bono, T-H. Pham, Gelebart, E. Rouesne, C. Lorrette, F. Bernachy-Barbe, M. Le Saux, E. Pons, J.-L. Flament and A. Sarrazin

* *The presented works are supported by the CEA-EDF-FRAMATOME triparty "Innovation COMBustible" project.*

PVD-HiPIMS Cr coating *on zirconium based-cladding substrate*

High density and thickness uniformity + strong adherence

HIPIMS PVD process

Brachet et al., 2017, WRFPM

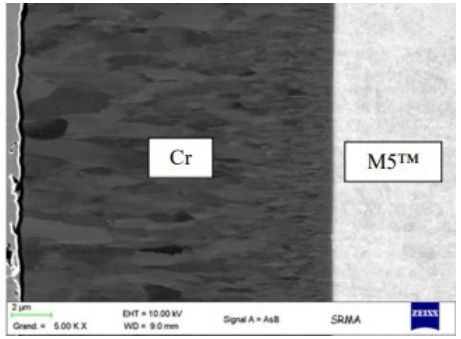

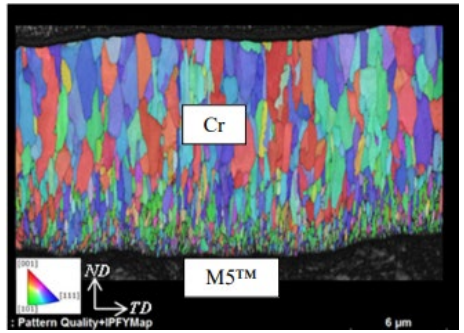

- Investigated chromium coating thickness range: 5-30 µm
- Zirconium alloy substrate:
  - Diameter 9.5 mm
  - Wall thickness 0.580 mm

PVD-HiPIMS Cr coating *on zirconium based-cladding substrate*

High density and thickness uniformity + strong adherence

HIPIMS PVD process

Brachet et al., 2017, WRFPM

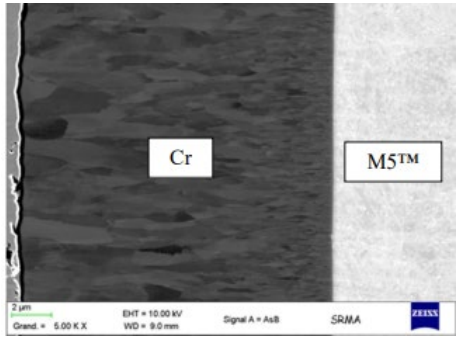

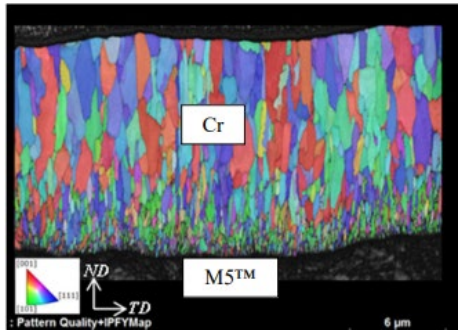

- Investigated chromium coating thickness range: 5-30 µm
- Zirconium alloy substrate:
  - Diameter 9.5 mm
  - Wall thickness 0.580 mm

High Temperature performances (LOCA)

Dumerval et al., 2018, Top Fuel

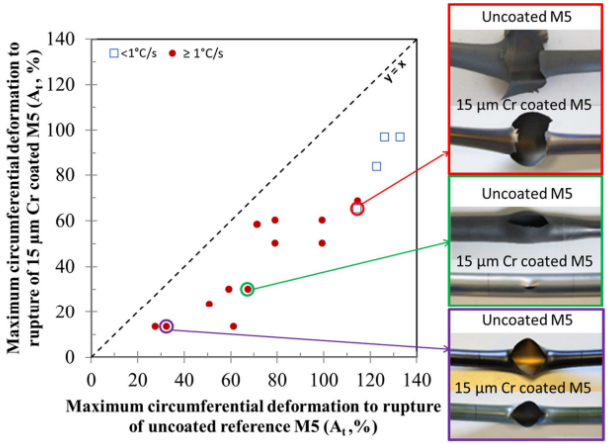

Brachet et al., 2020, Corr. Sc.

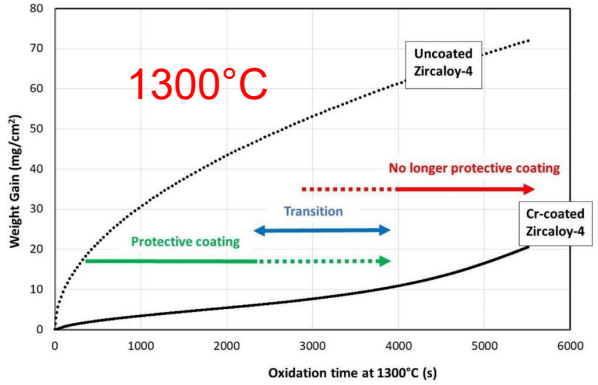

- Strengthening effect upon HT incursion + internal pressure → Decrease in balloon size
- Oxidation kinetics and associated gaseous H_2 production, strongly reduced
- Enhanced quenching and post-quenching resistance

PVD-HiPIMS Cr coating *on zirconium based-cladding substrate*

High density and thickness uniformity + strong adherence

HIPIMS PVD process

Brachet et al., 2017, WRFPM

High Temperature performances (LOCA)

Dumerval et al., 2018, Top Fuel

Brachet et al., 2020, Corr. Sc.

- ❖ **Properties are process dependent**
- ❖ **Good mastering of deposition process is key for obtaining chosen microstructure/properties**
- ❖ **Results cannot be generalized to any Cr coating deposition processes**

- Diameter 9,5 mm
- Thickness 0,580

- Oxidation kinetics and associated gaseous H_2 production, strongly reduced
- Enhanced quenching and post-quenching resistance

Cr coating *on zirconium based-cladding substrate*

Impact of coating damage on performance?

- **Cr-coating damage in nominal conditions and possible consequences?**
  - Damage could be generated during in-service / post-service conditions.
  - Possibility to create localized area favorable for accelerated corrosion/hydriding and/or coating spallation?

Cr coating *on zirconium based-cladding substrate*

How the enhanced performances could be affected by coating damage?

- **Cr-coating damaged in nominal conditions and possible consequences?**
  - Damage could be generated during in-service / post-service conditions.
  - Possibility to create localized area favorable for accelerated corrosion/hydriding and/or coating spallation?
- **Cr-coating damage during LOCA (*and other hypothetical accident scenarios*) and possible consequences?**
  - Ballooning of cladding can damage the Cr-coating
  - What are the consequences of cladding ballooning and burst on the coating's protectiveness of the coating upon further high temperature oxidation?

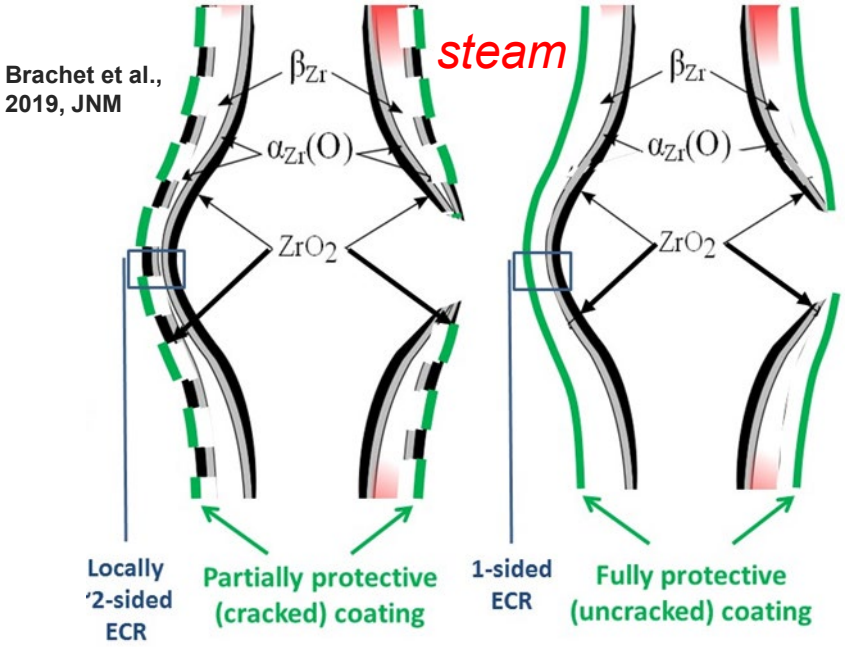

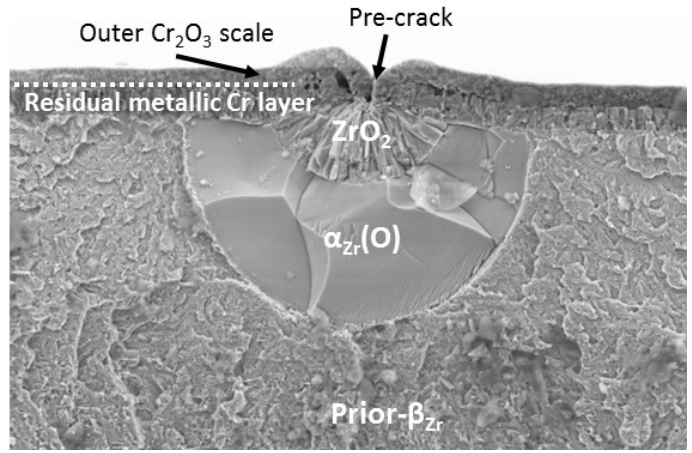

Cr coating *on zirconium based-cladding substrate*

How the enhanced performances could be affected by coating damage?

- Cr-coating damaged in nominal conditions and possible consequences?

Need for a better understanding & quantification of the Cr-coating damage in both nominal and hypothetical accident *scenarii* (LOCA & beyond, RIA…)

- Ballooning of cladding can damage the Cr-coating
- What consequences on the cladding ballooning and burst and on the protectiveness of the coating upon further high temperature oxidation?

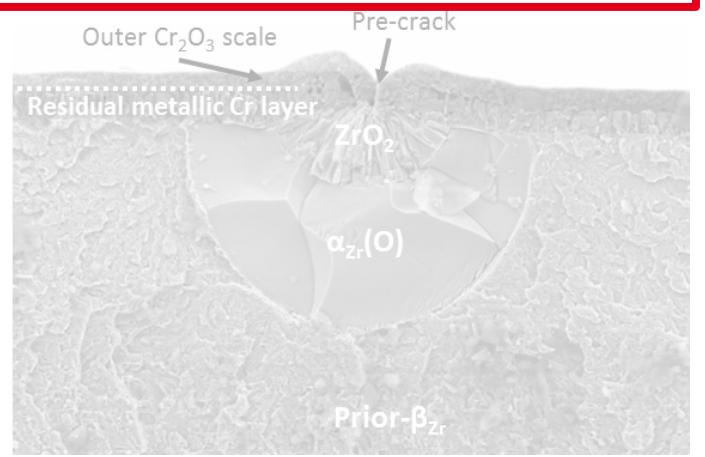

Scope of the presentation

- Focus on **CEA's current work on Cr-coating cracking under thermomechanical sollicitations**:
  - Reminder of previous work performed at ambient temperature *(penalizing and conservative conditions)*
  - "Nominal" conditions ~ 350 °C
  - "LOCA" conditions ("EDGAR" tests under internal pressure and at 600-1000°C)

Scope of the presentation

- Focus on **CEA's current work on Cr-coating cracking under thermomechanical sollicitations**:
  - Reminder of previous work performed at ambient temperature *(penalizing and conservative conditions)*
  - "Nominal" conditions ~ 350 °C
  - "LOCA" conditions ("EDGAR" tests under internal pressure and at 600-1000°C)

- Provide first results and observations on Cr-coating cracking behavior

Scope of the presentation

- Focus on **CEA's current work on Cr-coating cracking under thermomechanical sollicitations**:
  - Reminder of previous work performed at ambient temperature *(penalizing and conservative conditions)*
  - "Nominal" conditions ~ 350 °C
  - "LOCA" conditions ("EDGAR" tests under inner pressure at 600-1000°C)

- Provides first results and observations on Cr-coating behavior toward cracking

- Insights from several experimental techniques such as:
  - Acoustic Emission (AE) for in-situ Cr cracking detection and quantification
  - *Post-mortem* analyses by optical microscopy
  - *Post-mortem* analyses by X-ray tomography

Recall of the study performed at room temperature

Investigation of the multiaxiality effect on coating cracking

Biaxial testing machine – *as-coated samples*

- Facility provides the capacity to perform **biaxial testing with various biaxality (from 0 to ∞) ratios on cladding tubes**
- **Extensometers:** axial and radial extensometers for monitoring deformations
- **Camera with high magnification lens:** capture images of the sample outer layer and determine strain fields and cracking
- **Acoustic Emission sensor:** monitoring cracking by detecting the emitted sound

$$\sigma_{\theta\theta} = P\frac{\phi_i}{2e}$$

$$\sigma_{zz} = \frac{F_i + F_e}{S}$$

$$\gamma = \frac{\sigma_{zz}}{\sigma_{\theta\theta}}$$

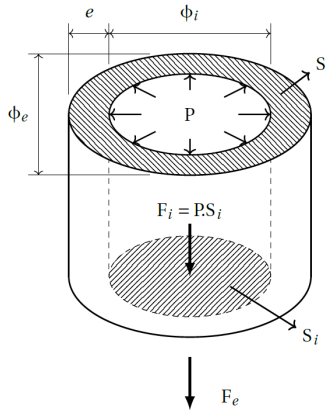

D.V. Nguyen, et al. , 2022 , JNM

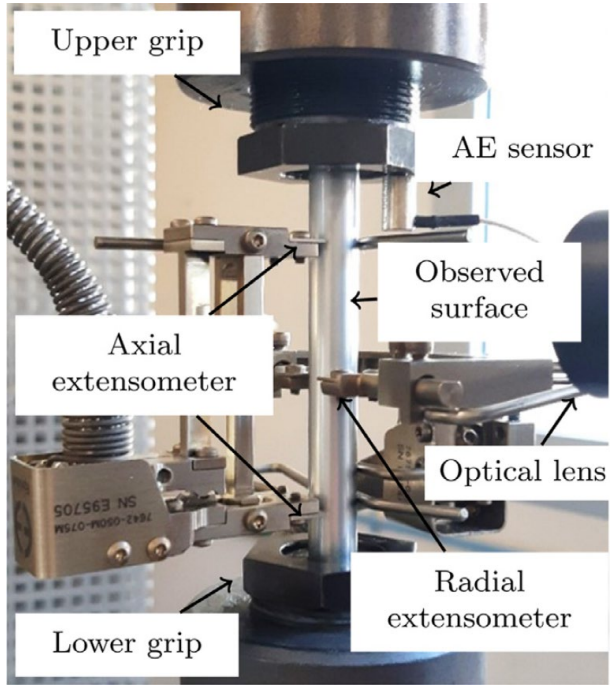

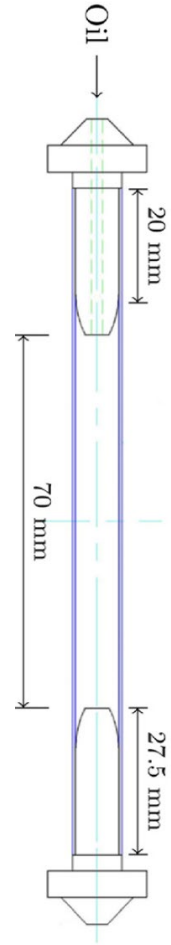

Recall of the obtained results at room temperature

AE and DIC for monitoring coating cracking

Biaxial testing machine – *as-coated samples*

- Facility provides the capacity to perform **biaxial testing with various biaxality (from 0 to ∞) ratios on cladding tubes**
- **Extensometers:** axial and radial extensometers for monitoring deformations
- **Camera with high magnification lens:** capture images of the sample outer layer and determine strain fields and cracking
- **Acoustic Emission sensor:** monitoring cracking by detecting the emitted sound

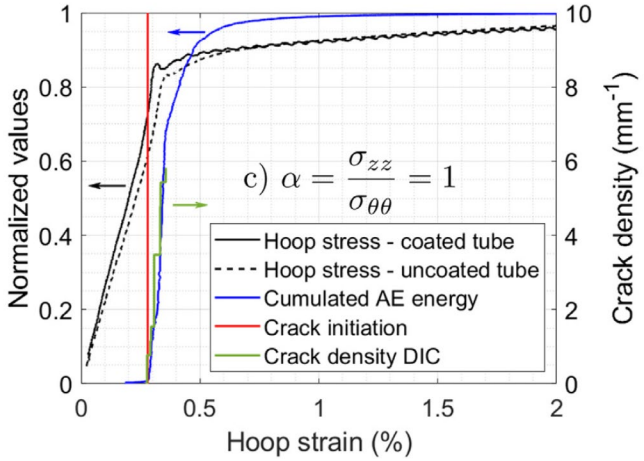

D.V. Nguyen, et al. , 2022 , JNM

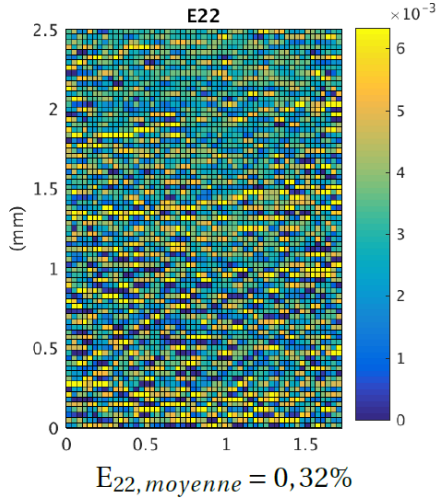

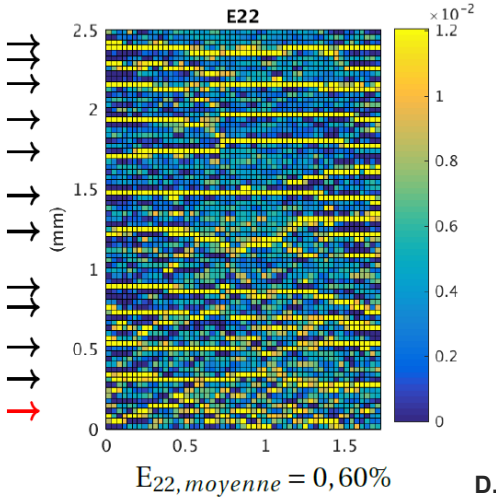

D.V. Nguyen, PhD thesis , 2021

Some conclusions from investigations at 20°C

Biaxiality doesn't affect the strain level for crack initiation

Crack propagation

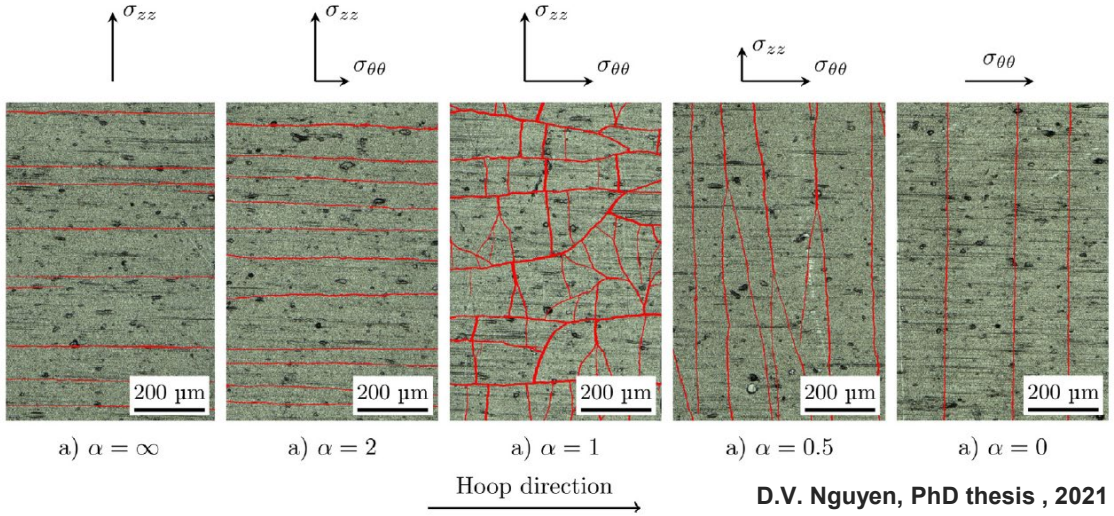

D.V. Nguyen, PhD thesis , 2021

- **Cracks initiation independent of** biaxiality state *(however, it affects cracks' orientation and distribution)*

Some conclusions from investigations at 20°C

Biaxiality doesn't affect the strain level for crack initiation

Crack propagation

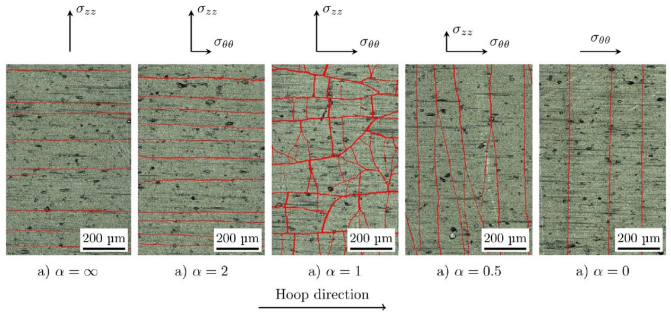

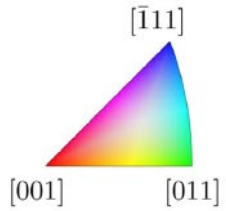

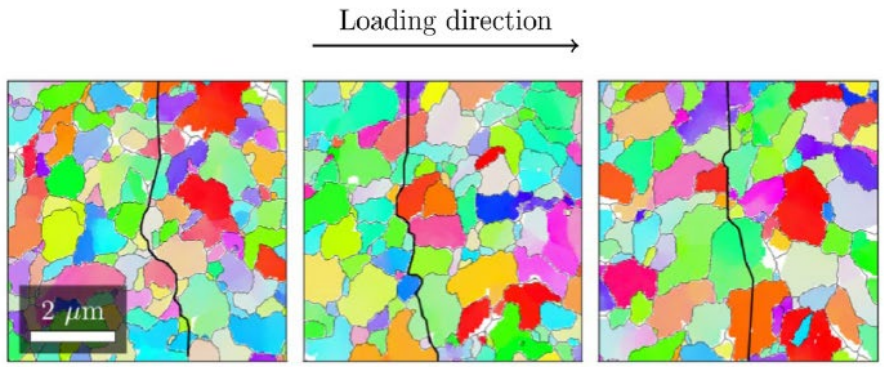

D.V. Nguyen, PhD thesis , 2021

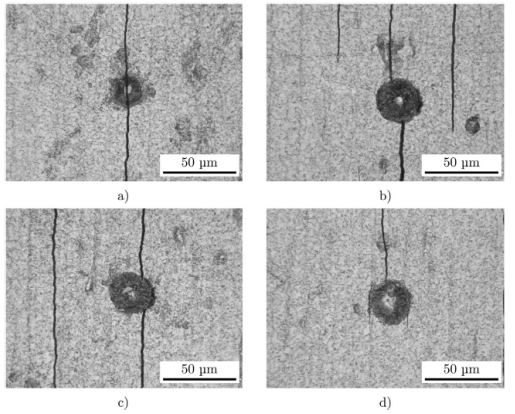

- **Cracks initiation independent of** biaxiality state *(however, it affects cracks' orientation and distribution)*
- **~50% intergranular cracks propagation** observed/emerging at the coating surface
- Cracks propagate through the Cr layer without significant **penetration to the substrate**
- **Cr coating remains fully adherent** up to high strain levels
- Limited effects of the (scarce) coating "imperfections" on the cracks propagation & density => should be different for other coating deposition processes / microstructures?

Uniaxial mechanical testing at 350°C

Nominal conditions temperature range

Uniaxial testing machine – *as-coated samples*

- Facility provides the capacity to perform **uniaxial testing** (biaxality ∞) **at temperatures from -20°C to 700 °C :**
- **Extensometer:** axial extensometers for monitoring axial deformation
- **Camera with intermediate magnification lens:** capture images of the sample outer layer and determine strain fields and cracking
- **Acoustic Emission sensor:** monitoring cracking by detecting the emitted sound

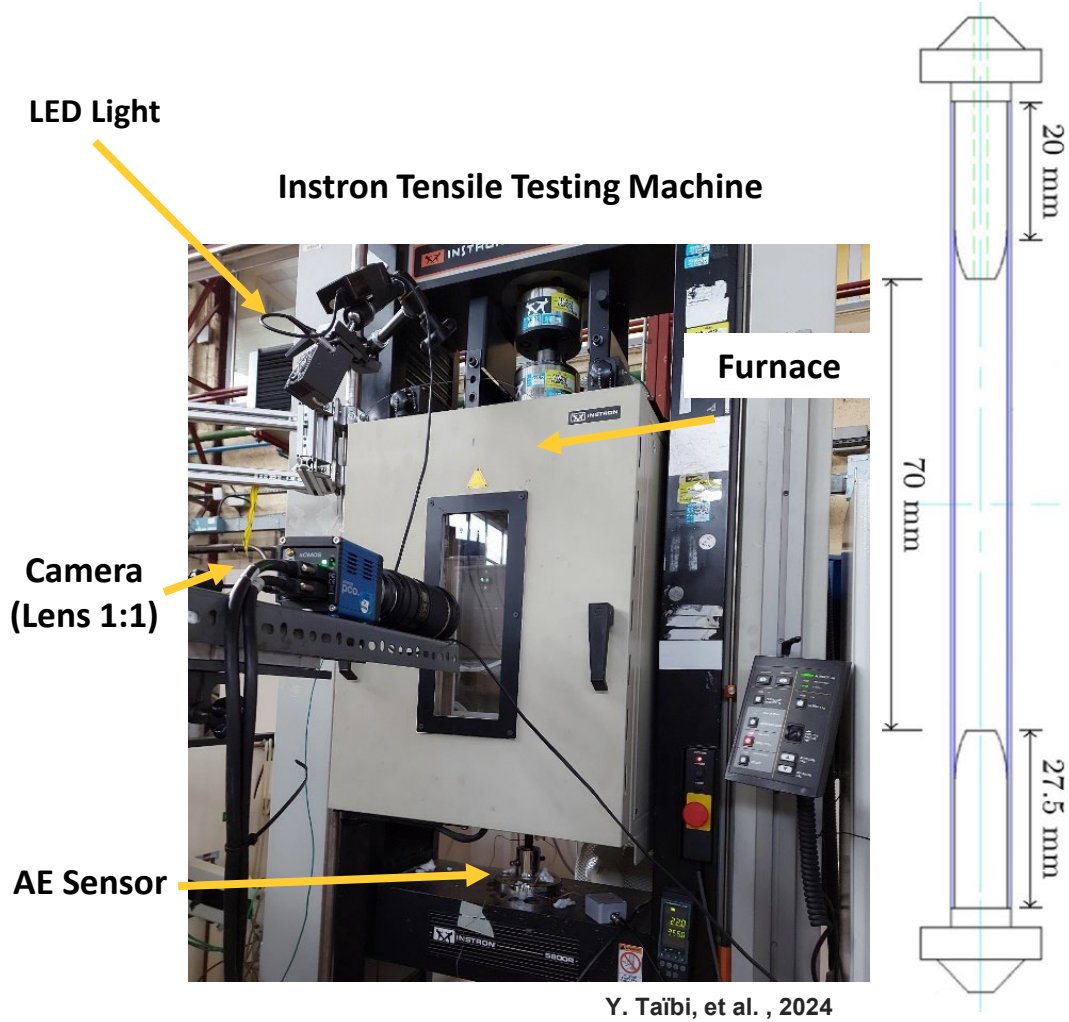

Y. Taïbi, et al. , 2024

Tensile testing at 350°C (non irradiated samples)

First cracks detected at ~2-3 %

Biaxiality ∞

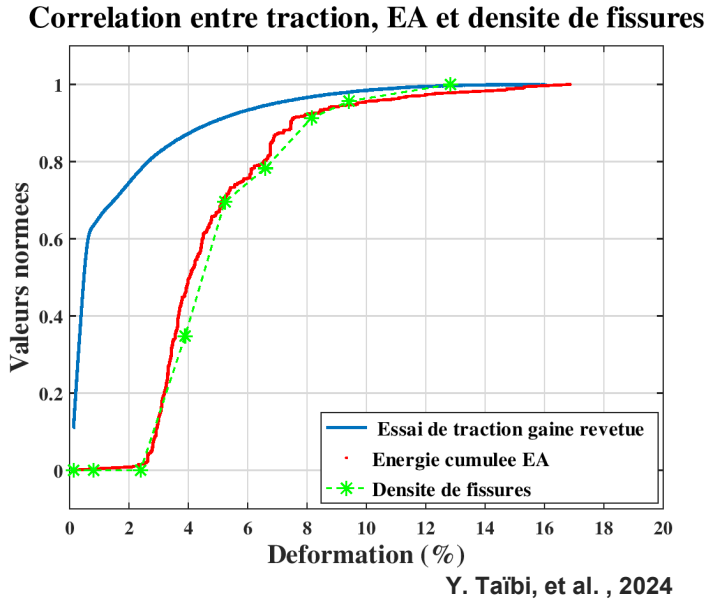

Y. Taïbi, et al. , 2024

- Good agreement between optical observations and AE
- First cracks are detected at ~2-3 %

Tensile testing at 350°C (non irradiated samples)

First cracks detected at ~2-3 %

Biaxiality ∞

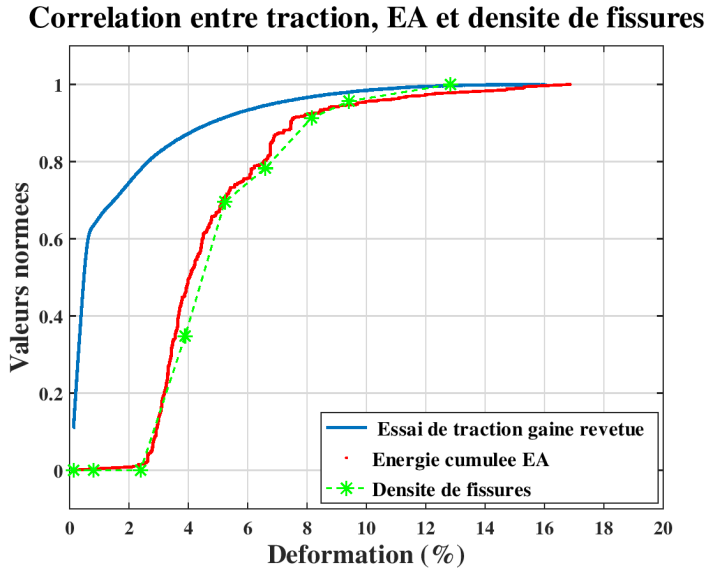

Y. Taïbi, et al. , 2024

Optical observations at different strain levels

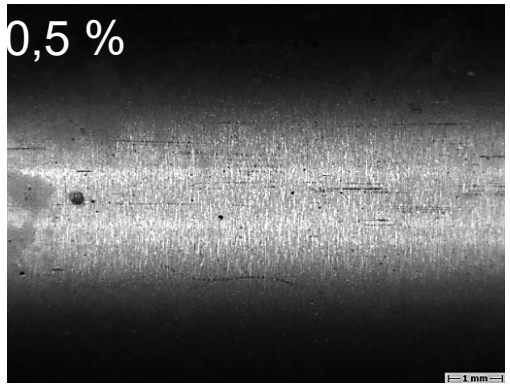

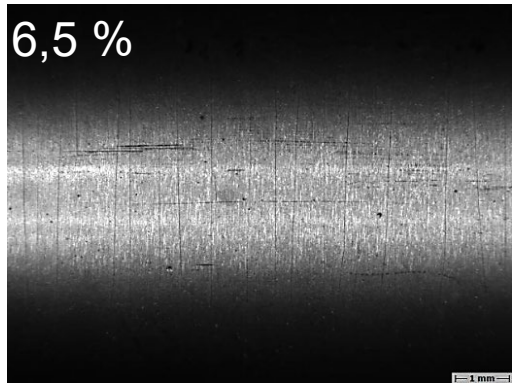

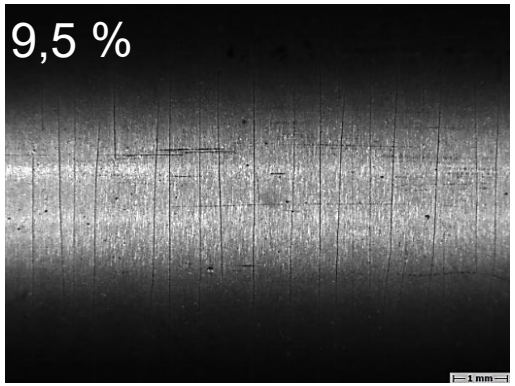

Y. Taïbi, et al. , 2024

- Good agreement between optical observations and AE
- First cracks are detected at ~2-3 %
- Crack detection by AE confirmed by optical observations
- Tensile test performed with several interruptions

Expension Due to Compression tests

Testing temperature 350°C on neutron irradiated samples

(CEA-Saclay LECI hot cells laboratory)

EDC (biaxiality 0) – circumferential testing machine in hot cell

- Facility provide the capacity to perform **thermomechanical testing on irradiated samples** (with a biaxiality ~ 0 **to be close to in-service PCMI loading conditions…)**
- **Joule effect heating** : slow and fast thermal loading can be applied (0.1°C/s to 200°C/s) up to 1200°C
- **Free / Fixed Extremities :** tests presented are with restrained ends
- **Identical experimental setup for non-irradiated samples** providing a support for a better interpretation/exploitation of results
- **Irradiated samples** in OSIRIS **up to 2 dpa,** and on-going/further tests planned on Cr-coated materials irradiated in commercial LWRs

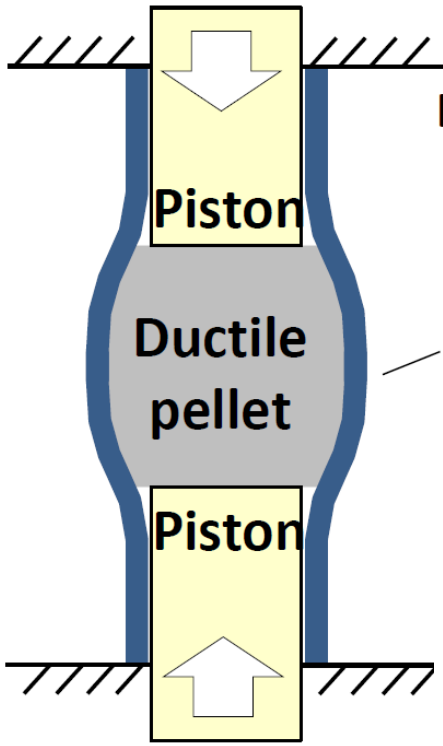

End restraining fixture

Irradiated cladding sample

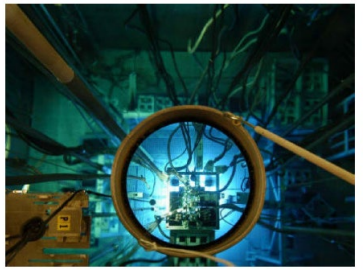

Bono et al. , 2020 , NUMAT

Circumferential loading at 350°C on Irradiated tubes

Crack initiation detected at >2 % circumferential clad deformation

Results obtained on 1st generation Cr-coated cladding tubes irradiated in OSIRIS

Fixed-end EDC tests at 350°C
Loading similar to pellet-cladding interaction conditions

Unirradiated coated cladding
Hoop strain at fracture
~ 30%

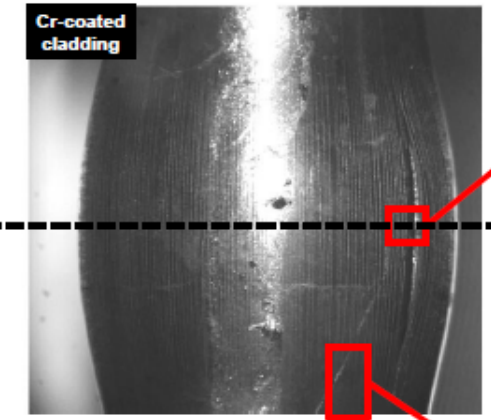

Irradiated coated cladding
Hoop strain at fracture
≥ 15%

2 dpa_{Zr}
Identical substrate and coating

Overall, significant post-irradiation coated cladding ductility

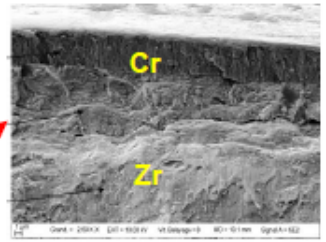

Metallographic observations

- No flaws
- No coating delamination
- No crack propagation into the substrate

SEM observations on Cr/Zr interface

Very good adhesion of coating at local strains in excess of 15%

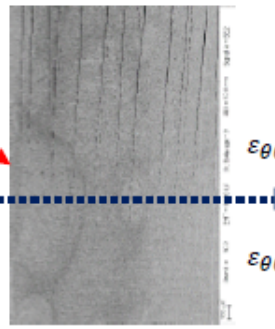

$\varepsilon_{\theta\theta} \geq 2\%$

$\varepsilon_{\theta\theta} < 2\%$

SEM observations of EDC tested coating surface

Neutron irradiated (1st. generation) 2-8µm thick Cr-coatings studied here can withstand a hoop strain up to 2% without cracking (similar to unirradiated cladding)

Bono et al. , 2020 , NUMAT

EDGAR, ballooning and burst
LOCA conditions temperature ranges

EDGAR 1&2 facilities:

- Designed in the late 70s, since **more than 4000 cladding tubes** have been tested
- EDGAR facilities provide the capacity to perform **thermomechanical testing under controlled inner pressure & temperature**
- **Joule effect heating**: slow and fast thermal loading can be applied (0.1°C/s to 200°C/s) up to 1200°C
- **Contactless temperature control and measurements**:
  IR pyrometers and internal thermocouple
- **Internal pressure** can be controlled up to 200 bars
- **In-situ contactless hoop-strain monitoring** (laser) during ballooning / burst
- Sample length representative of inter-grid distance in assemblies

EDGAR 1

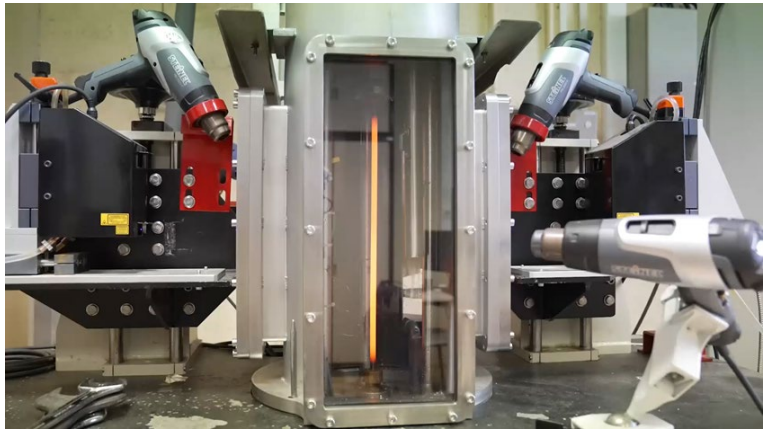

EDGAR, ballooning and burst

EDGAR 1&2 facilities:

- Designed in the late 70s, since **more than 4000 cladding tubes** have been tested
- EDGAR facilities provide the capacity to perform **thermomechanical testing under controlled inner pressure & temperature**
- **Joule effect heating**: slow and fast thermal loading can be applied (0.1°C/s to 200°C/s) up to 1200°C
- **Contactless temperature control and measurements**:
  IR pyrometers and internal thermocouple
- **Internal pressure** can be controlled up to 200 bars
- **In-situ contactless hoop-strain monitoring** (laser) during ballooning / burst
- Sample length representative of inter-grid distance in assemblies

EDGAR 1

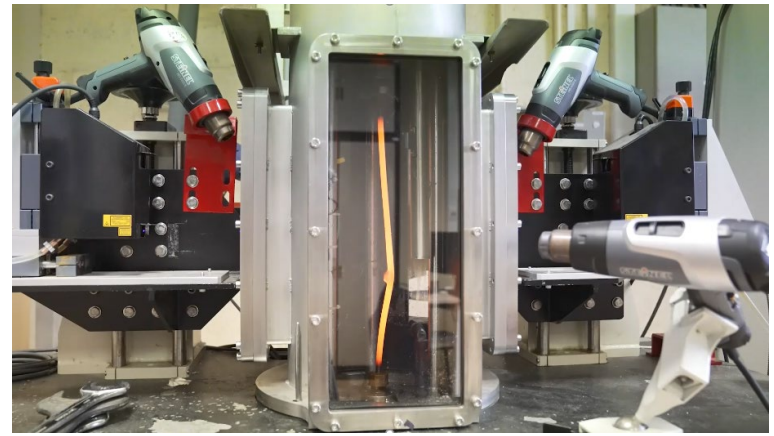

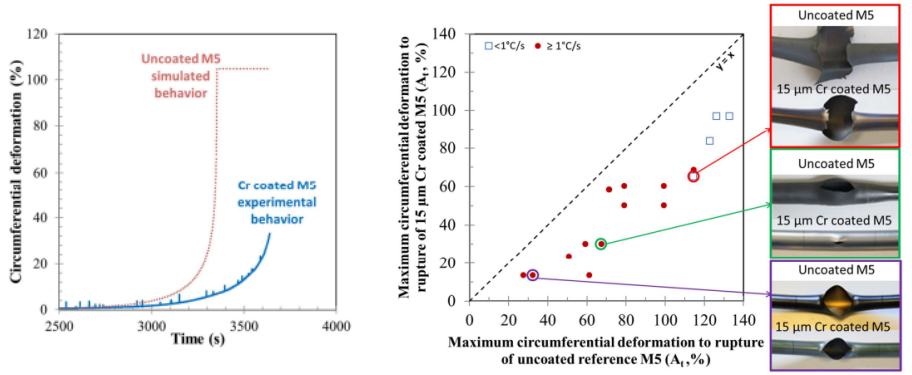

Dumerval et al., 2018, Top Fuel

Post-mortem inspections
Cr-coating gain in ductility *(to be compared with 20-350°C)*

Selection of Cr-coated cladding after burst : optical inspections at different height

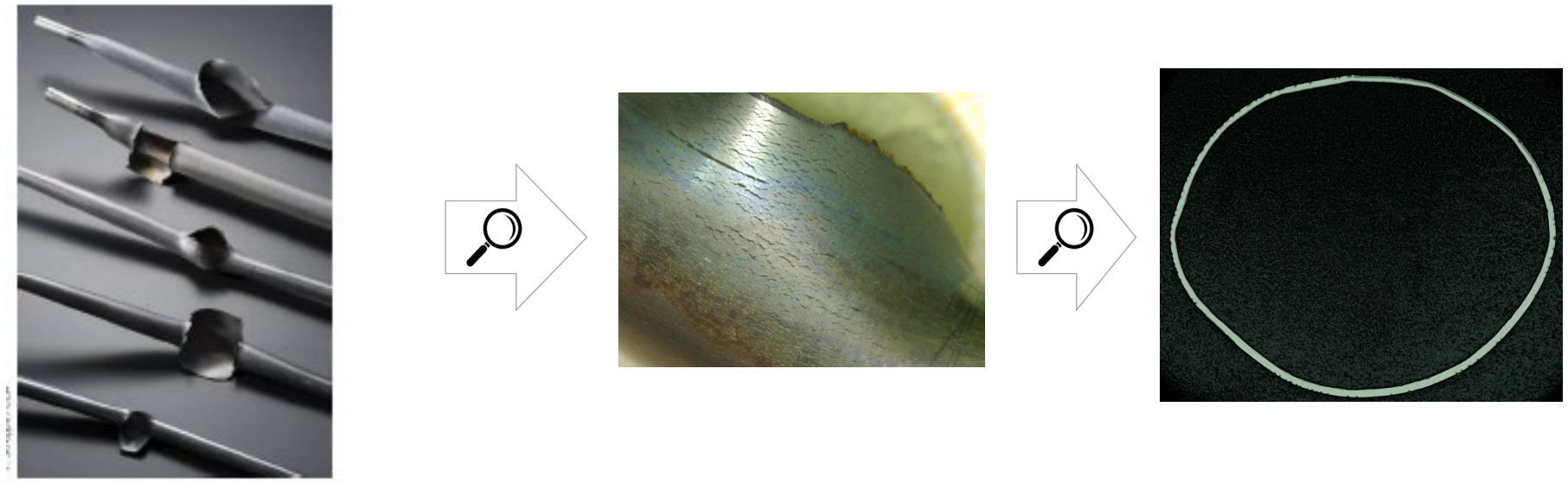

- Selection of a set of Cr-coated cladding after burst with high circumferential deformation
- Optical inspections to damage quantification
- Provides an estimate of damage level as function of hoop strain

Post-mortem inspections
Cr-coating gain in ductility *(to be compared with 20-350°C)*

Selection of Cr-coated cladding after burst : optical inspections at different height

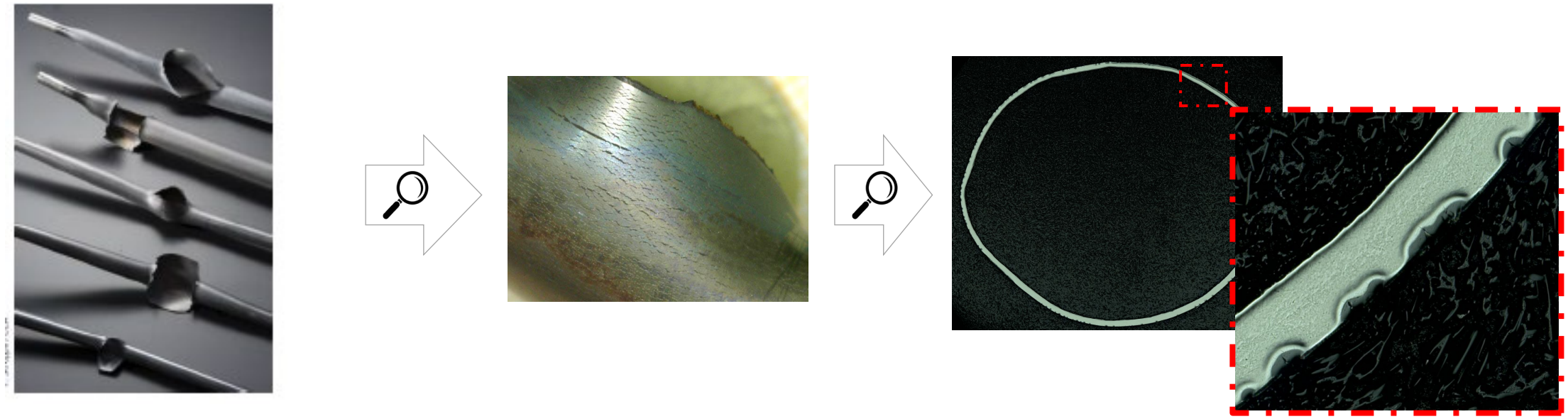

- Selection of a set of Cr-coated cladding after burst with high circumferential deformation
- Optical inspections to damage quantification
- Provides an estimate of damage level as function of hoop strain

Toward a better quantification by Optical Miscroscopy

High quality images, *measurements realized at a specific height*

High resolution optical observations

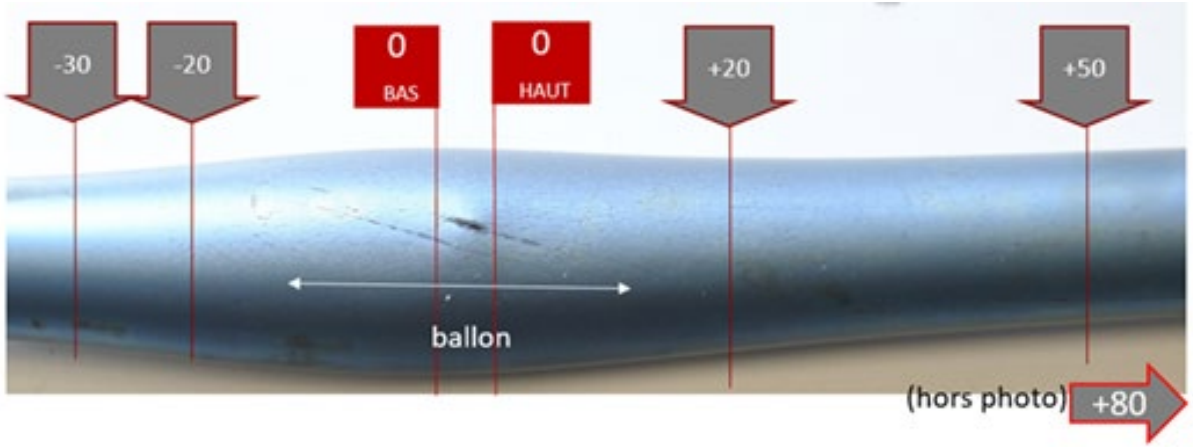

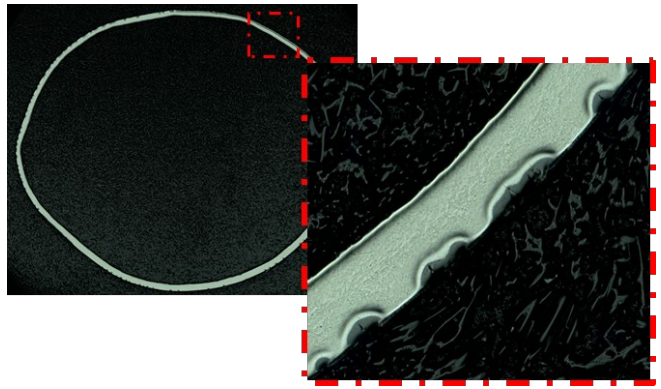

- Needs a metallographic preparation
- Resolution up to 1µm detect small cracks
- High quality image provides a good contrast for analyses
- Requires preparation effort and can be time consuming if a large data base is needed

Toward a better quantification by Optical Miscroscopy

High quality images, *measurements realized at a specific height*

Automated counting

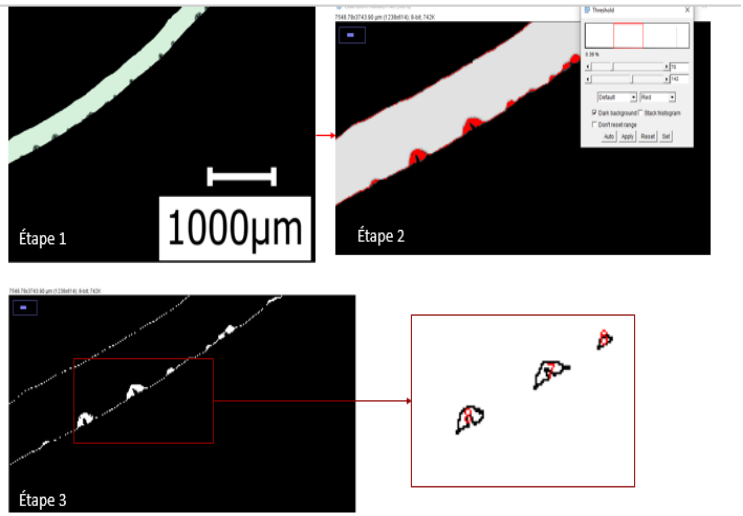

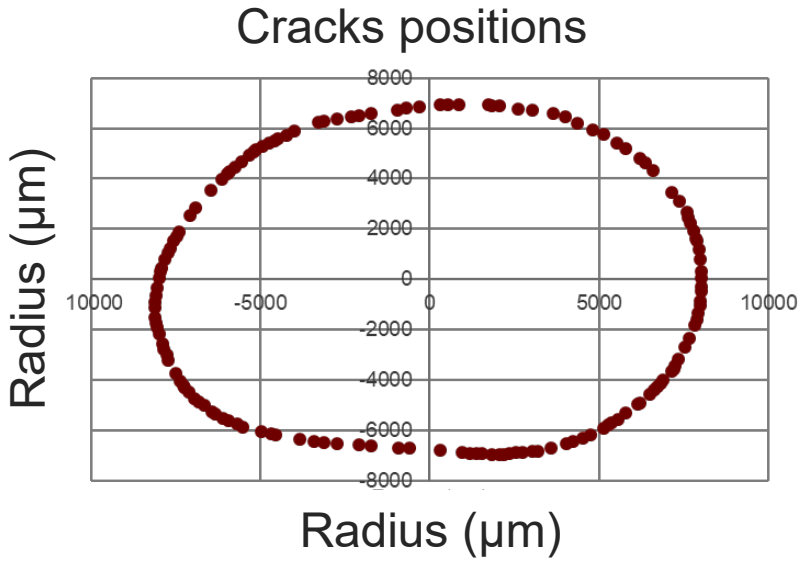

- Use of image processing and machine learning toolboxes (here Fiji & Weka plugin)
- Good detection rate of cracks on the optical images

Toward a better quantification by Optical Miscroscopy

High quality images, *measurements realized at a specific height*

Automated counting

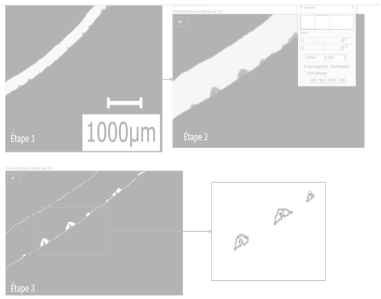

Measurement on the same cladding tube
(Tested with a heating rate of 1°C/s)

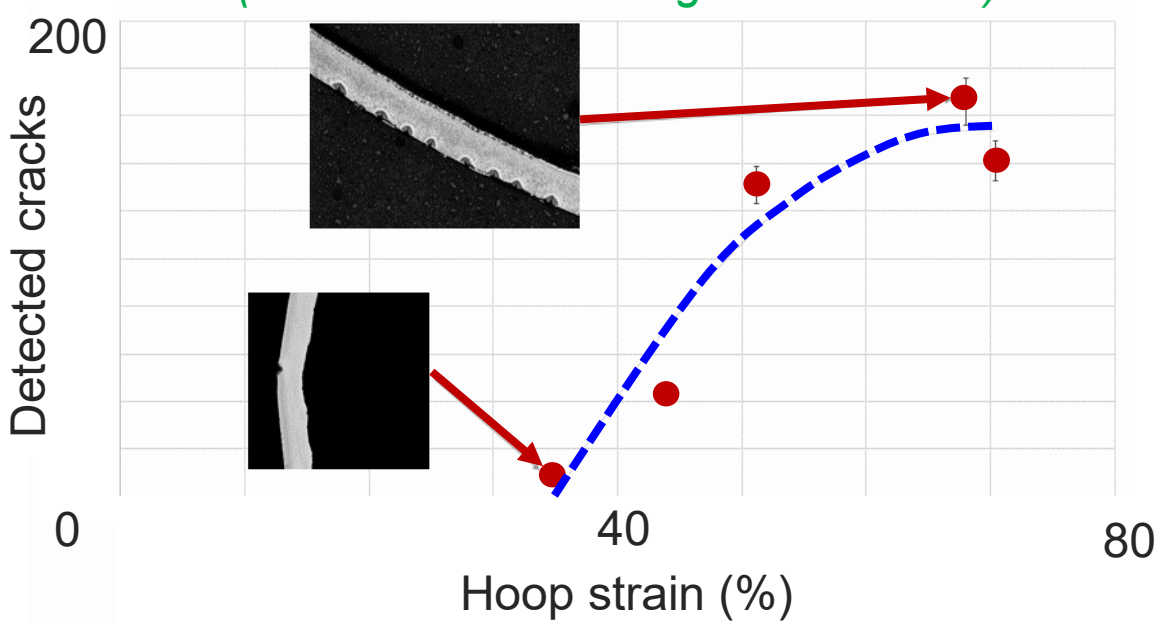

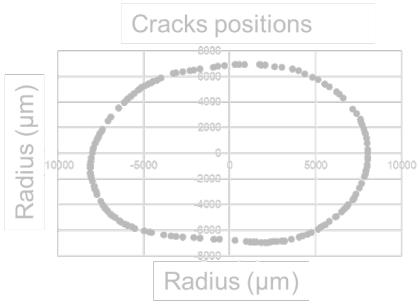

- Use of image processing and machine learning toolboxes (here Fiji & Weka plugging)
- Good detection rate of cracks on the optical images
- ***Higher Cr-coating ductility and resistance to cracking confirmed***

Toward a better quantification by X-Ray Tomography

Large amount of information with less preparation effort!

Volumic observations

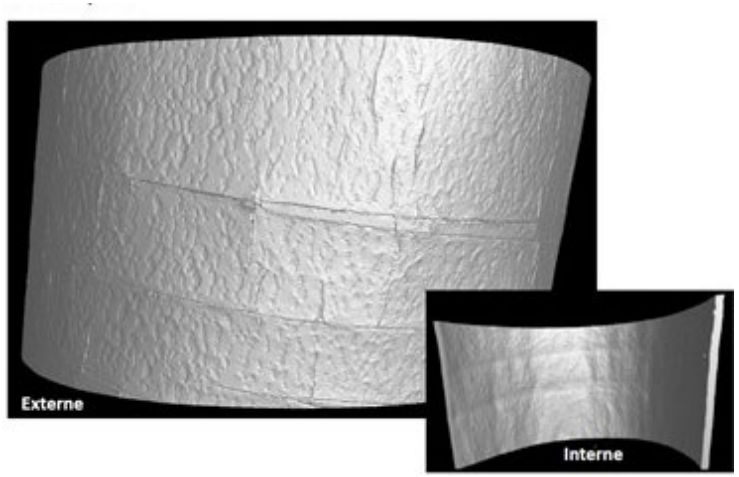

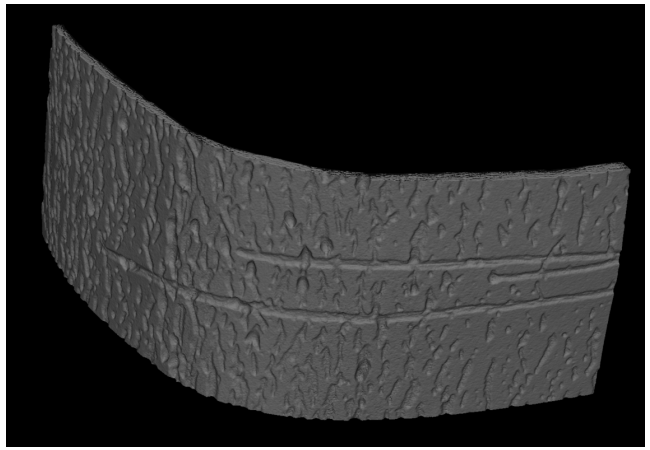

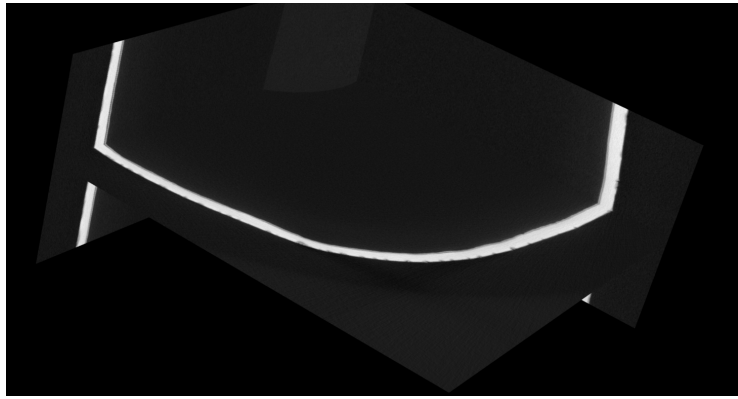

- No needs for preparation
- Large volumes can be scanned
- Resolution up to 10-15 µm per voxel
- Lower resolution and contrast than optical microscopy

Toward a better quantification by X-Ray Tomography

Large amount of information with less preparation effort!

Automated counting

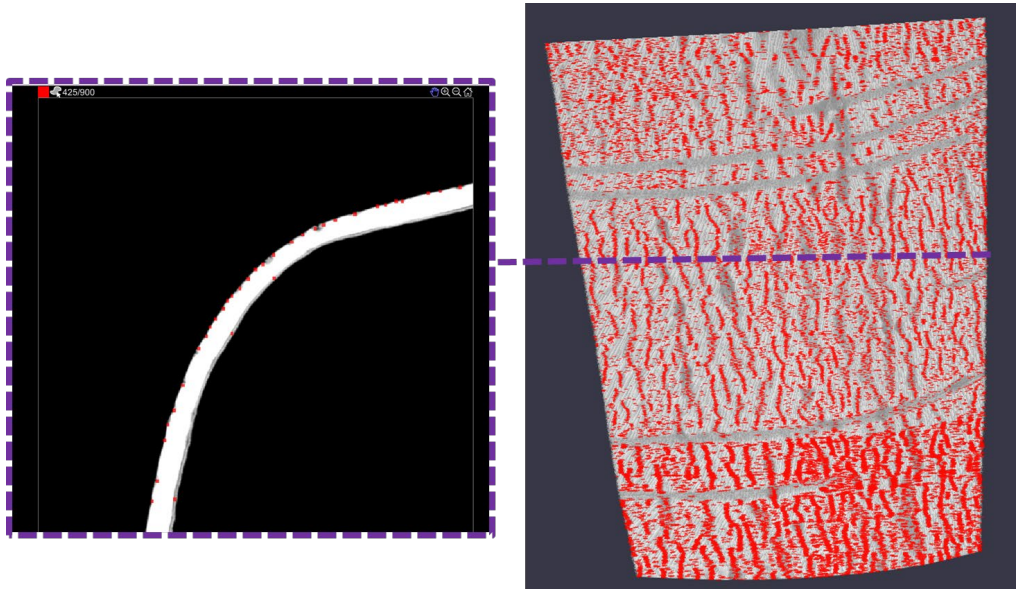

- Use of image processing (here “homemade codes” via Matlab)
- Satisfactory detection rate but still needs improvement
- Machine learning as a solution → needs extra work (vs. Optical Microscopy Images)

Conclusions

- **For all the tested samples in any conditions the coating remains perfectly adherent after high deformations**
- **Recall of the concluding remarks for the room temperature study :**
  - **Acoustic Emission confirmed by DIC measurements**
  - **The biaxiality state affects the cracks' orientation/pattern and density at saturation**
  - **The microscopic observations shows ~50% of intergranular crack propagations emerging at the coating surface**

Conclusions

- **For all the tested samples in any conditions the coating remains perfectly adherent after high deformations**
- **Recall of the concluding remarks for the room temperature study :**
  - **Acoustic Emission confirmed by DIC measurements**
  - **The biaxiality state affects the cracks' orientation/pattern and density at saturation**
  - **The microscopic observations shows ~50% of intergranular crack propagations emerging at the coating surface**
- **350°C temperature testing concluding remarks :**
  - **Acoustic Emission detected cracking confirmed by optical observations (on as-coated sample)**
  - **The first crack is detected/observed above 2 % of strain for both non-irradiated and neutron irradiated samples**
  - **Cr-coating ductility:**
    - **→ improved at 350°C (vs. 20°C)**
    - **→ not affected by neutron irradiation up to at least 2dpa (further investigations needed at higher burn up)**

Conclusions

- **For all the tested samples in any conditions the coating remains perfectly adherent after high deformations**
- Recall of the concluding remarks for the room temperature study :
  - Acoustic Emission confirmed by DIC measurements
  - The biaxiality state affects the cracks' orientation/pattern and density at saturation
  - The microscopic observations shows ~50% of intergranular crack propagations emerging at the coating surface
- 350°C temperature testing concluding remarks :
  - Acoustic Emission detected cracking confirmed by optical observations (on as-coated sample)
  - The first crack is detected/observed above 2 % of strain for both non-irradiated and neutron irradiated samples
  - Cr-coating ductility: improved at 350°C (vs. 20°C) / not affected by neutron irradiation up to at least 2dpa (further investigations needed at higher burn up)
- **EDGAR (LOCA) testing concluding remarks :**
  - ***Post-mortem* inspections indicate higher Cr-coating ductility (vs. 20-350°C range)**
  - **Optical Microscopy provides high image quality and exploitable data for machine learning, but requires significant sample preparation effort**
  - **Xray Tomography provides three-dimensional data with less sample preparation effort than OM: requires more data processing due to lower spatial resolution and image quality (contrast)**

References

- J.-C. Brachet *et al.*, « On-going studies at CEA on chromium coated zirconium based nuclear fuel claddings for enhanced accident tolerant LWRs fuel », in *TopFuel 2015-Reactor Fuel Performance Meeting*, 2015.
- J. C. Brachet « Behavior of Cr-coated M5^{TM} claddings under LOCA conditions », in *Proceedings of 2017 Water Reactor Fuel Performance Meeting,(Sept. 10-14, 2017), Jeju Island, Korea*
- M. Dumerval, Q. Houmaire, J.-C. Brachet, H. Palancher, J. Bischoff, et E. Pouillier, « Behavior of chromium coated M5 claddings upon thermal ramp tests under internal pressure (loss-of-coolant accident conditions) », in *Topfuel 2018-Light Water Reactor (LWR) Fuel Performance Meeting 2018*, 2018.
- J.-C. Brachet *et al.*, « Early studies on Cr-Coated Zircaloy-4 as enhanced accident tolerant nuclear fuel claddings for light water reactors », *J. Nucl. Mater.*, vol. 517, p. 268-285, 2019.
- M. Bono *et al.*, *Mechanical Testing of Irradiated ATF Chromium-coated Zr-based Claddings*. 2020. doi: 10.13140/RG.2.2.34085.52964.
- J.C. BRACHET, E. ROUESNE, J. RIBIS, T. GUILBERT, S. URVOY, G. NONY, C. TOFFOLON-MASCLET, M. LE SAUX, N. CHAABANE, H. PALANCHER, A. DAVID, J. BISCHOFF, J. AUGEREAU, E. POUILLIER, « High temperature steam oxidation of chromium-coated zirconium-based alloys: Kinetics and process », Corrosion Science 167 (2020) 108537, https://doi.org/10.1016/j.corsci.2020.108537
- D. V. Nguyen *et al.*, « Mechanical behavior of a chromium coating on a zirconium alloy substrate at room temperature », *J. Nucl. Mater.*, vol. 558, p. 153332, 2022.
- D. V. Nguyen PhD thesis., « Comportement mécanique à température ambiante d'un revêtement de chrome déposé sur un substrat en alliage de zirconium », Thèse en mécanique des matériaux université Paris-Saclay, 2021. http://www.theses.fr/2021UPAST009/document

Acknowledgment: The presented works have been supported by the CEA-EDF-FRAMATOME “Innovation COMBustible” project. Special thanks to Stéphane Valance (CEA), Edouard Pouillier & Antoine Ambard (EDF), Thomas Garnier, Thorsten Marlaud and Karl Buchanan (FRAMATOME) for their fruitful feedbacks and corrections.

K. Nakamura
CRIEPI

Preliminary BDBA tests of Cr-coated Zr alloy cladding at DEGREE facility

If the Cr coating on the outer surface of the Zr-based cladding tubes is damaged at extremely high temperatures and Zr metal substrate remains on the surface, chemical reaction heat accompanying the Zr-water reaction may be generated rapidly. In this case, the temperature rise could be accelerated compared to the conventional uncoated cladding material, and the possibility of early core damage cannot be denied [1]. Resolving this issue requires confirmation by bundle tests at different accident scenarios, CRIEPI is conducting some simulated beyond design-basis accident (BDBA)-LOCA tests with Cr-coated Zr-based cladding tubes using an induction heating furnace at the CRIEPI's DEGREE facility in a research project of the IAEA/ATF-TS.

A Zircaloy-4 fuel cladding tube (outer diameter: 10.75 mm, wall thickness: 0.725 mm, length: 235 mm) coated with Cr or Cr/CrN by the PVD method was used in the test. Alumina annular pellets and tungsten rods were loaded into the fuel rods to simulate the fuel pellets and susceptor as internal heating material, respectively. The rod internal pressure was set to be 6 MPa of He gas at room temperature.

Single rod and bundle tests were performed under simulated BDBA conditions in high temperature steam environment. Single rod was placed in the center of eight surrounding heater rods, which were tungsten rod inserted into alumina tubes (*single rod test*). A 3×3 type coated Zircaloy-4 test bundle with a fuel pitch of 14.5 mm was applied (*bundle test*). After heating to the peak cladding surface temperature (1350℃ or 1600℃) at a heating rate of 2-3 K/s in a steam flow rate of 0.4 g/s, the heating power supply was switched off and at the same time the atmosphere was switched from steam to Ar gas leading to cool down without quenching with water.

Online measurements were made of cladding surface temperature, fuel rod internal pressure, and hydrogen generation amount. The following post-test examinations are reported: the interdiffusion layer formation between the Cr or Cr/CrN coating layer and the Zr-based alloy substrate, redistribution of Cr, Zr, oxygen, and hydrogen, radial profile of microhardness; and ballooning and bursting behavior.

References

[1] M. Steinbrück, et al., JNM 559(2022)153470.

Preliminary BDBA tests of Cr-coated Zr alloy cladding at DEGREE facility

CRIEPI Kinya Nakamura, Kenta Inagaki
KIT Juri Stuckert
CTU Martin Ševeček

28th International QUENCH Workshop

December 5-7, 2023

Fortbildungszentrum für Technik und Umwelt (FTU), Auditorium (Aula)

Karlsruhe Institute of Technology, Germany

CRIEPI Central Research Institute of Electric Power Industry

Motivation

ATF bundle behavior under accident conditions

- Lack of knowledge regarding the degradation behavior of ATF bundles and delays in developing fuel performance models
- Potential more intense temperature runaway (M. Steinbrück, 2022)

Strong needs to accumulate experimental data under various accident scenarios

International research project on material science-based ATF behavior during accidents

QUECH-19 (2018)	OECD/NEA/QUENCH-ATF (2021-2025)	IAEA/CRP/ATF-TS (2021-2024)	OECD/NEA/TCOFF-2 (2022-2025)
First ATF bundle test  *FeCrAl(Y) @1460 ℃* J. Stuckert, et al., QWS-24, 2018.	Three bundle tests under DBA and BDBA conditions 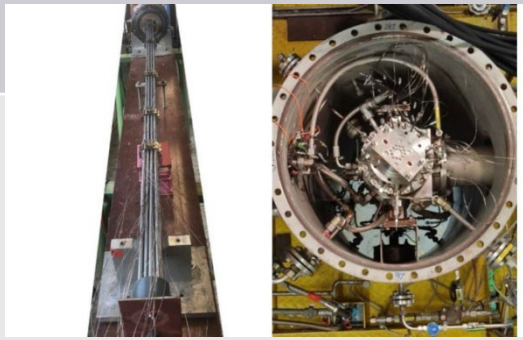 *Cr-coated opt ZIRLO* https://www.oecd-nea.org/jcms/pl_72063/first-results-from-the-quench-atf-joint-project	● Bundle tests (WT 1.2) ● Fuel Bundle Simulation (WT 2.2) 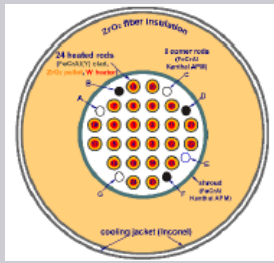 QUENCH-19 (KIT) 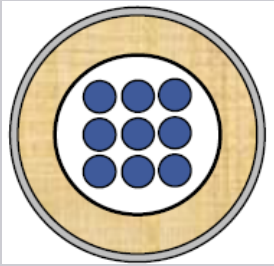 DEGREE (CRIEPI) 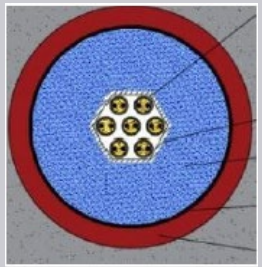 CODEX-ATF (MTA EK)	● From the perspective of materials science and thermodynamics, prioritization of issues specific to UO_2-Zry system and advanced fuels such as ATF ● Advances in fuel performance models and their implementation in the SA code

IAEA / ATF-TS project

"Testing and Simulation for Advanced Technology and Accident Tolerant Fuels (ATF-TS)"

CRP Structure

Work Task (WT)	Sub-tasks	WT Coordinators
WT 1: Experimental Programme	1.1 Separate Effect Tests (SETs)	M. Sevecek (Czech Republic)
	1.2 Bundle Tests	J. Stuckert (Germany)
WT 2: Fuel Modelling and Benchmark Exercise	2.1 Fuel Rod Modelling and Simulation	A. Boulore (France) M. Cherubini (Italy)
	2.2 Fuel Bundle Simulation	J. Stuckert (Germany) Z. Hozer (Hungary)
WT 3: LOCA Evaluation Methodology	3.1 Validation of Fuel Codes for LOCA Analysis	J. Zhang (Belgium)
	3.2 LOCA Fuel Safety Evaluation Methodology	
WT 4: Material Properties database for ATF	4.1 Literature Assessment	Ch. Allison (USA)
	4.2 Model/Correlation Development	
Co-Chairs		J. Zhang (Belgium), M. Sevecek (Czech Rep)
Sci. Secretary		K. Sim (IAEA)

CRIEPI's contribution

WT1.2 Bundle tests

- **Small-scale bundle tests with ATF cladding materials under DBA/BDBA conditions using DEGREE facility (Single rod & Bundle)**

WT 2.2 Fuel Bundle Simulation

- Benchmark exercise of DEGREE bundle test using FRAPTRAN

DEGREE facility

- The out-of-pile integral test facility “DEGREE” was built at CRIEPI in 2015*.
  - To deepen understanding of the core degradation processes BDBA
  - To strengthen accident management measures for LWRs

- Several performance tests have been conducted so far.
  - Unpressurized Zry-4 **bundle tests in steam environment up to 2000℃** to simulate early stages of SA such as SBO and LBLOCA scenarios
  - Ballooning and burst tests of pre-hydrided Zry-2 and Zry-4 single rods in steam-air mixture under LOCA at SFP
  - Performance tests of accident tolerant control rods (ATCR) under BDBA conditions
  - Pressurized/unpressurized **coated Zr-alloy bundle tests under BDBA conditions** (This presentation)

Degraded Zry-4 bundle under steam-starved condition heated up to 2013℃ (D-H27-02)

** within a framework “Advanced Multi-scale Modeling and Experimental Test of Fuel Degradation in Severe Accident Conditions” supported by METI, Japan.*

DEGREE facility

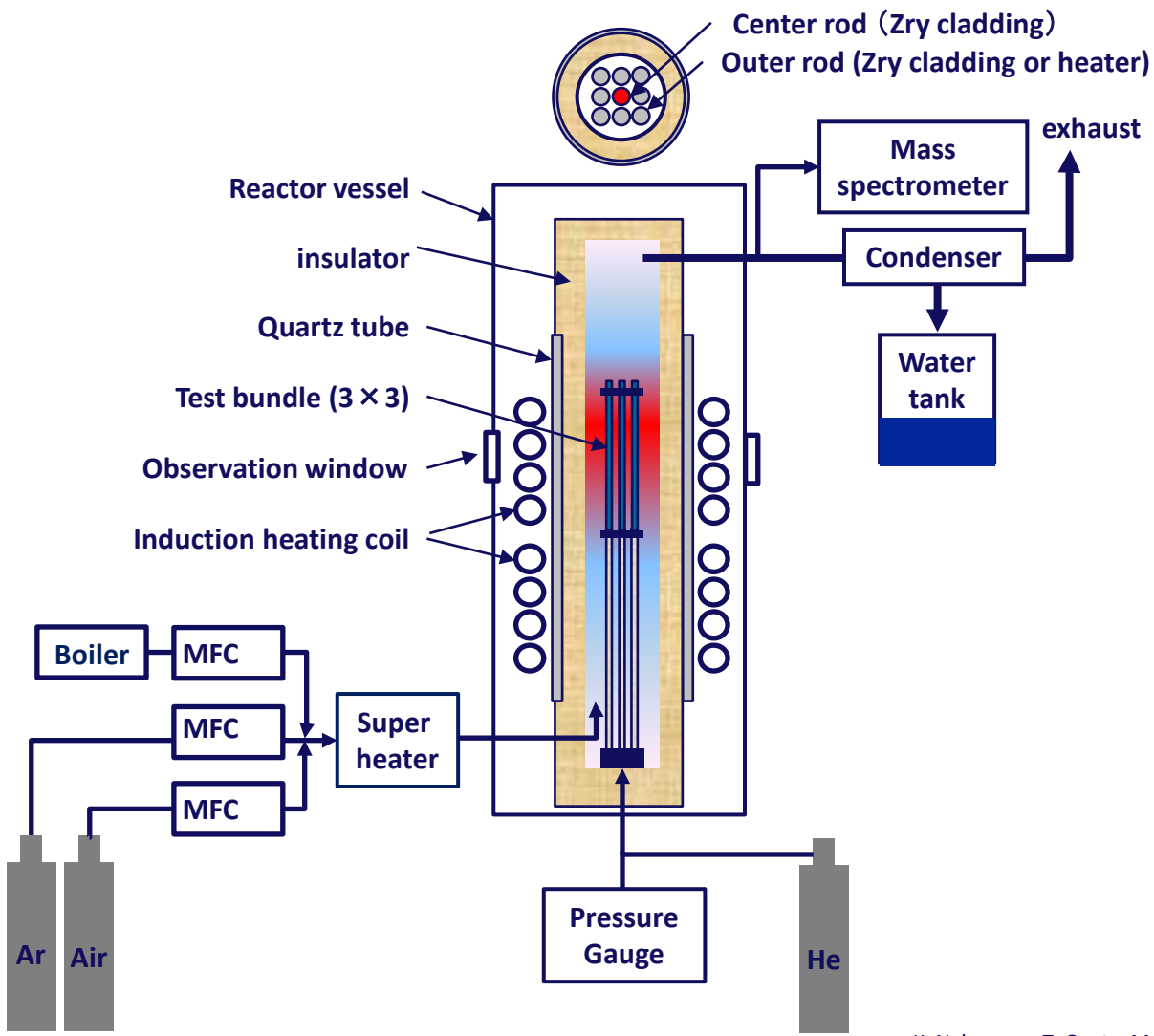

Major specification

Test Bundle	3 × 3 rods
Carrier gas	Steam, Ar, Air or their mixture
Heating rate	< 7 K/s
Cooling rate	> 3 K/s
Heating method	**Induction heating**
Max. temperature	ca. 2000℃
Heating region	200mm (upper), 300mm (lower)
System pressure	Atmospheric
Rod internal pressure	<12 MPa
Load cell	Not furnished
Quench medium	Argon gas
Nuclear material	Not available
Instrumentation	Thermocouples, Pyrometers, Pressure gauges, GC, QMS, Video recording system

K. Nakamura, T. Ogata, M. Kurata, OECD/NEA WORKSHOP-TCOFF PROJECT, July 10-12, 2019, J-village, Fukushima, Japan.

Induction heating method

- Primarily heat the central tungsten rod as a susceptor
- Secondarily heats the cladding itself
- Eddy currents also generated in the thin-walled balloon region of the cladding

Test rod

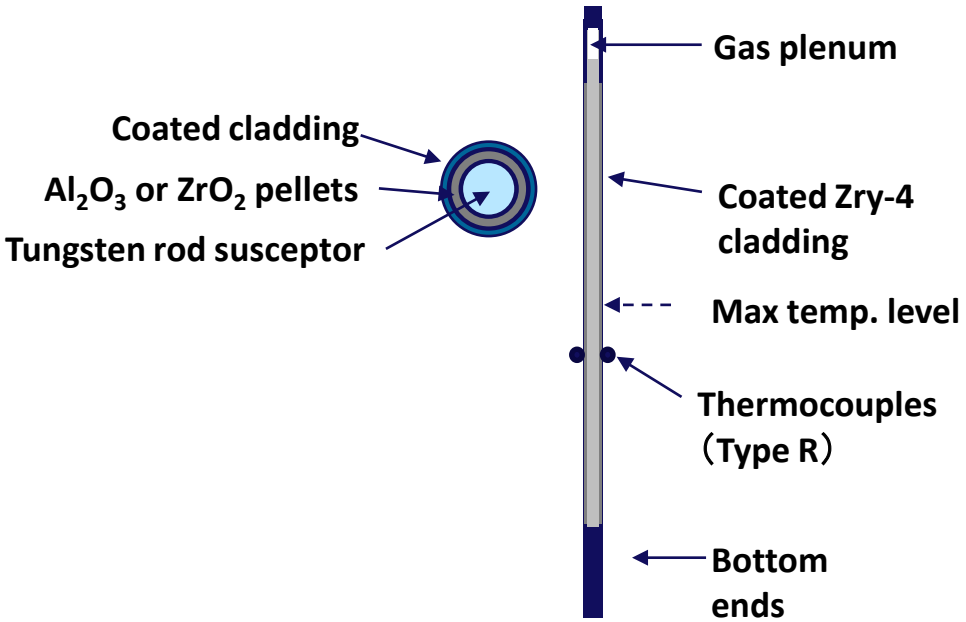

Pressurized test rods

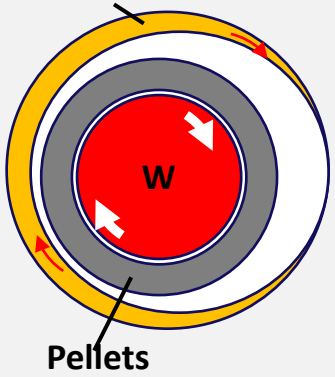

- Hoop strain
- Ballooning & Burst
- Secondary hydriding

- **After burst, heating is not anymore homogeneous (C. Duriez, QWS27)**
- **It is thought that the thin-walled balloon region has a higher temperature gradient than the actual phenomenon.**

Apart from burst region or Un-pressurized test rods

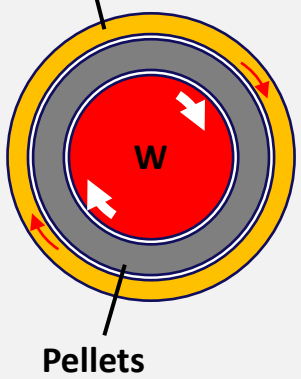

- Negligible hoop strain
- No Burst
- No secondary hydriding

- **The absence of ballooning in the cladding is expected to reduce the occurrence of excessively high temperature gradients and improve the simulation of accident behavior.**

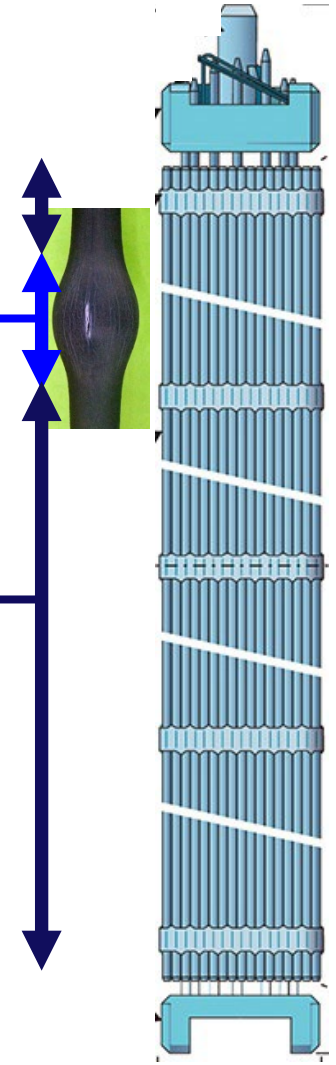

Preliminary BDBA tests at DEGREE facility

ATF Cladding Tube Material

Coating Materials	Cladding	Provided by
10 µm Cr	Zircaloy-4	KIT
20 µm Cr	Zircaloy-4	CTU
16/10 µm Cr/CrN	Zircaloy-4	CTU
20 µm Cr	opt. ZIRLO	CTU
15 µm multilayer Cr/CrN	E110	AEOI

✓ All Zircaloy-4 tube provided by KIT

- Sim. Fuel pellet Al_2O_3 or ZrO_2
- Susceptor Tungsten
- RIP 6.0 MPa at RT (He)
- Gas Plenum ca. 10 cc
- Fuel pitch 14.5 mm

Test rod

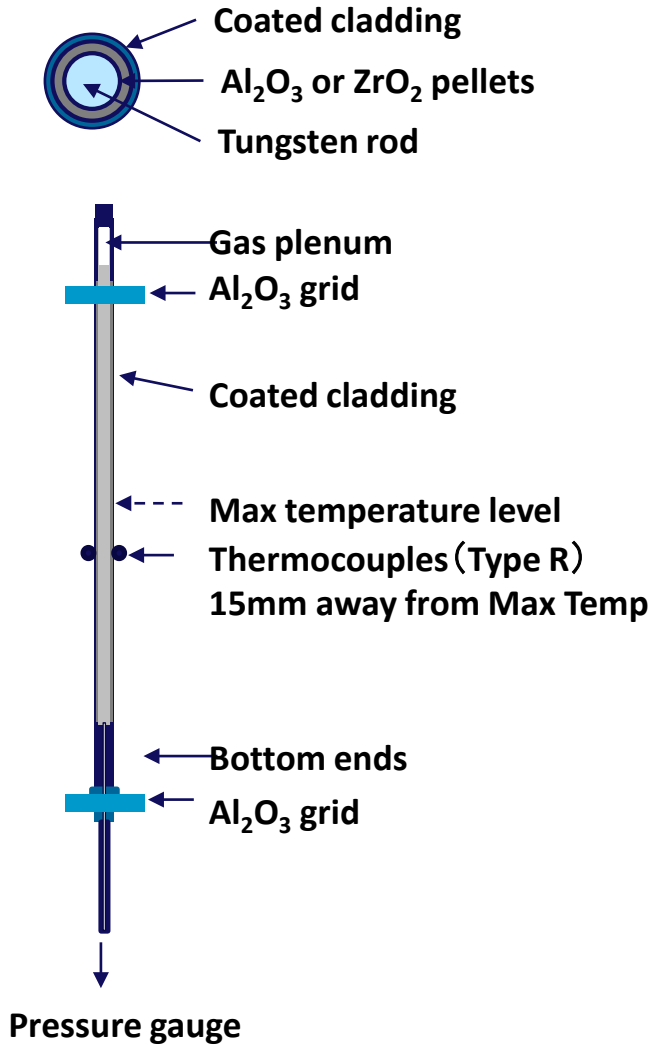

Cross section of as-deposited

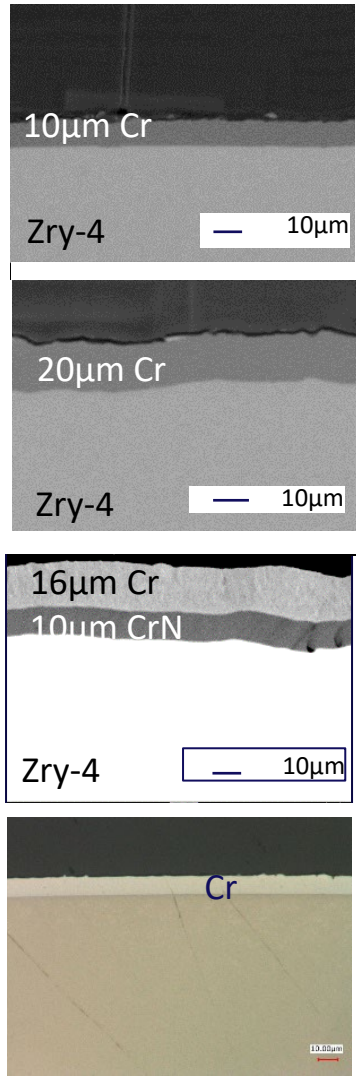

Preliminary BDBA tests at DEGREE facility

Single-rod test

Bundle test

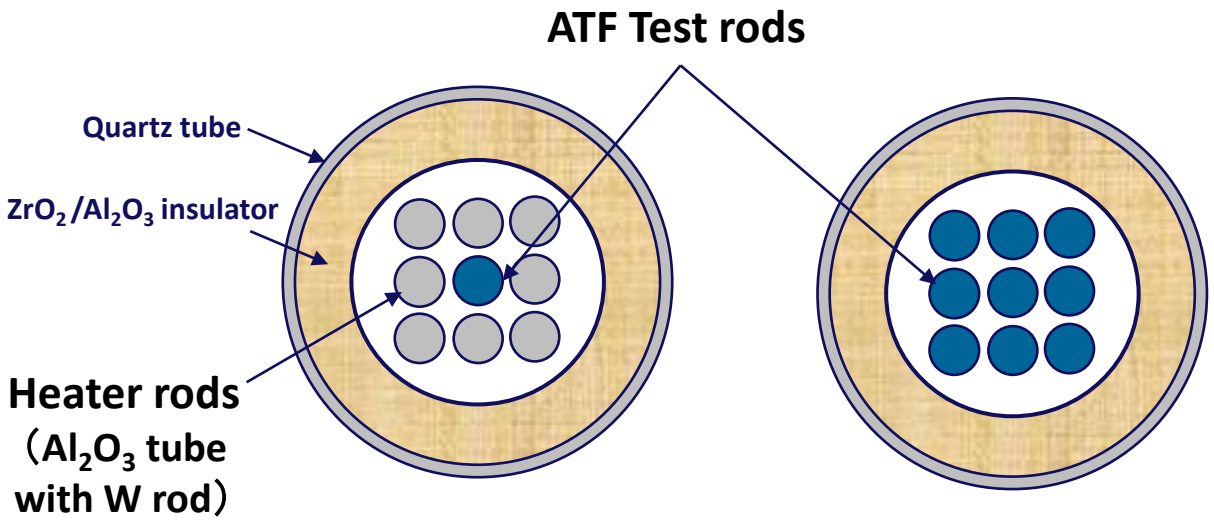

- 1350℃
- 1600℃

- 1350℃

Time history

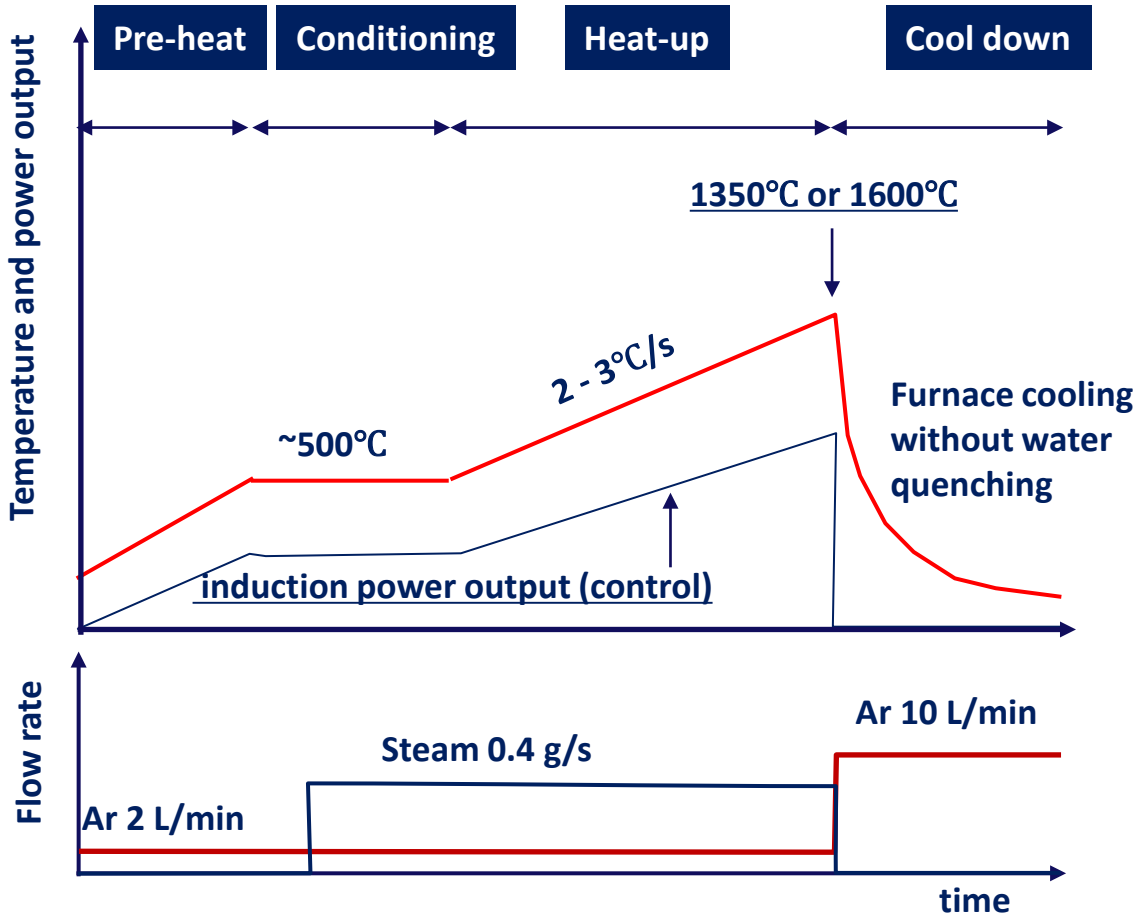

Single rod tests (RIP=6.0 MPa)

Effect of coating thickness and materials on burst behavior

Item	S1’	S2	S3	S4	S5	S6
Coating layer	-	10 μm Cr	20 μm Cr	16/10 μm Cr/CrN	10 μm Cr	20 μm Cr
Max temperature (℃)	1350				1600	
Heating rate (K/s)*	3.5-1.5	1.5	2.4-1.8	2.5-2.2	3.0-1.6	3.0-1.8
Photos of Burst Opening	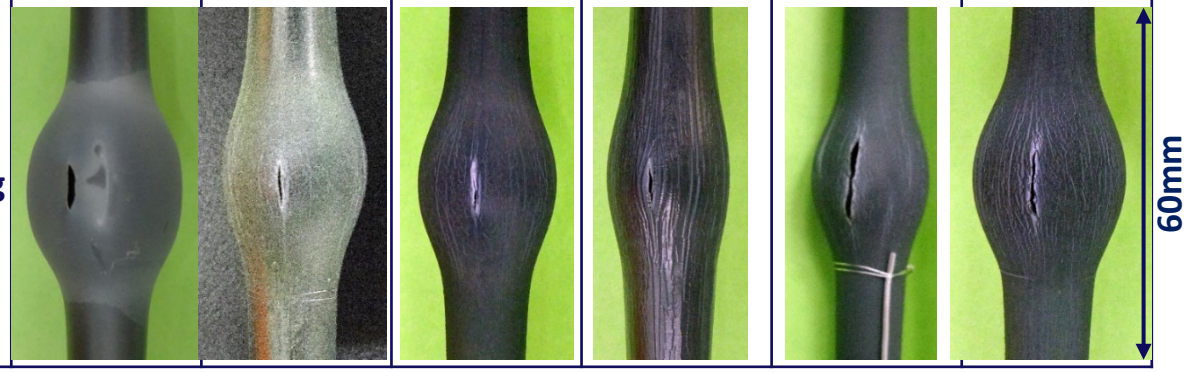					

* Temperature range above 1000℃

Little change in burst temperature and pressure regardless of coating thickness or material

Hoop strain >80%

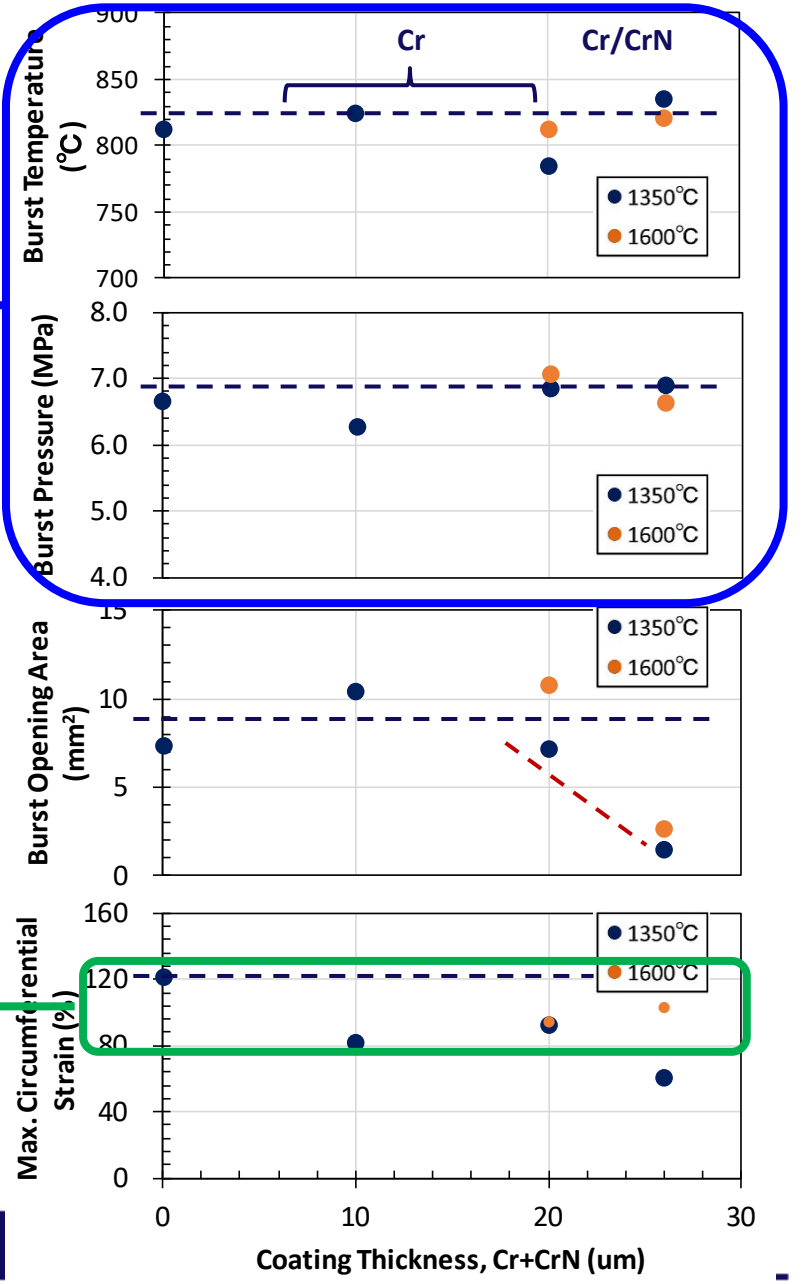

Single rod tests (RIP=6.0 MPa, 1350℃, Cr or Cr/CrN coated Zry-4)

Hydrogen concentration distribution

Vertical direction

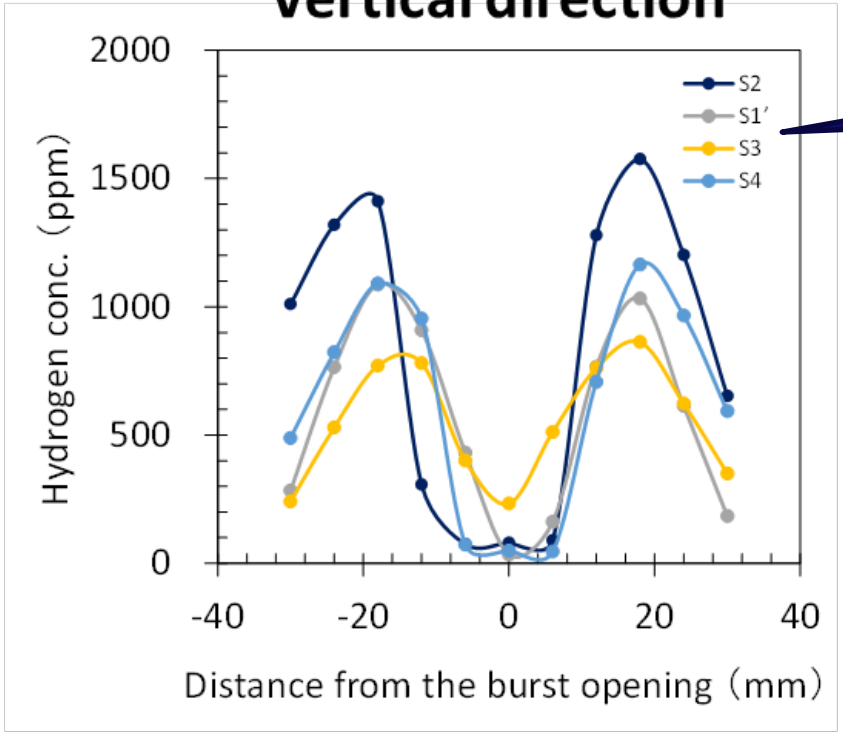

uncoated

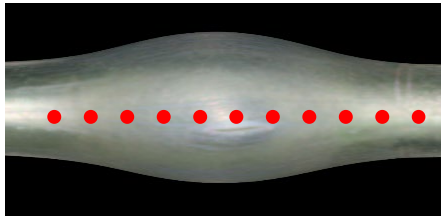

top

Circumferential direction

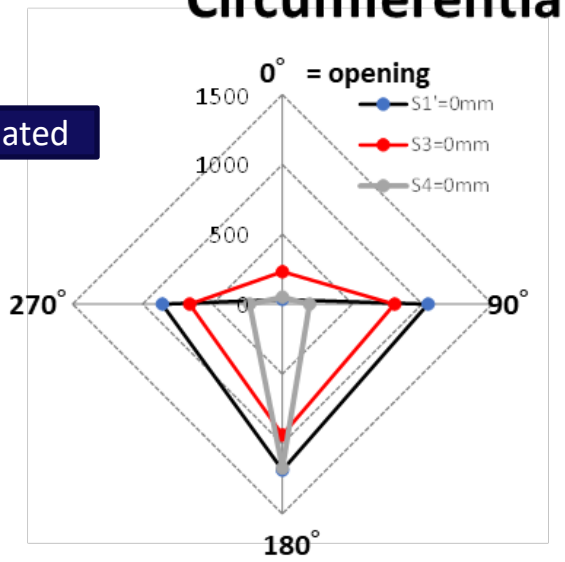

At Burst opening height

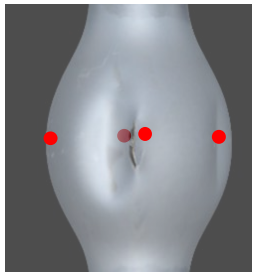

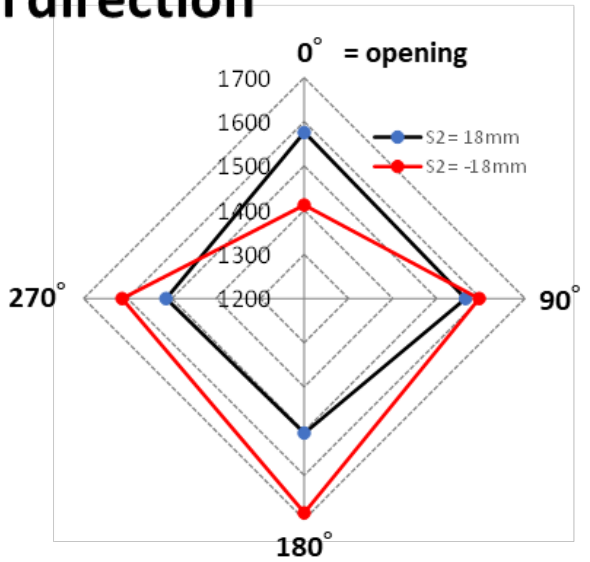

At 18mm away from Burst opening

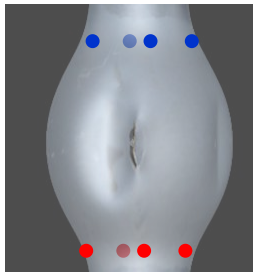

Single rod tests (RIP=6.0 MPa, 1350℃, Cr or Cr/CrN coated Zry-4)

20 µm Cr coated Zry-4

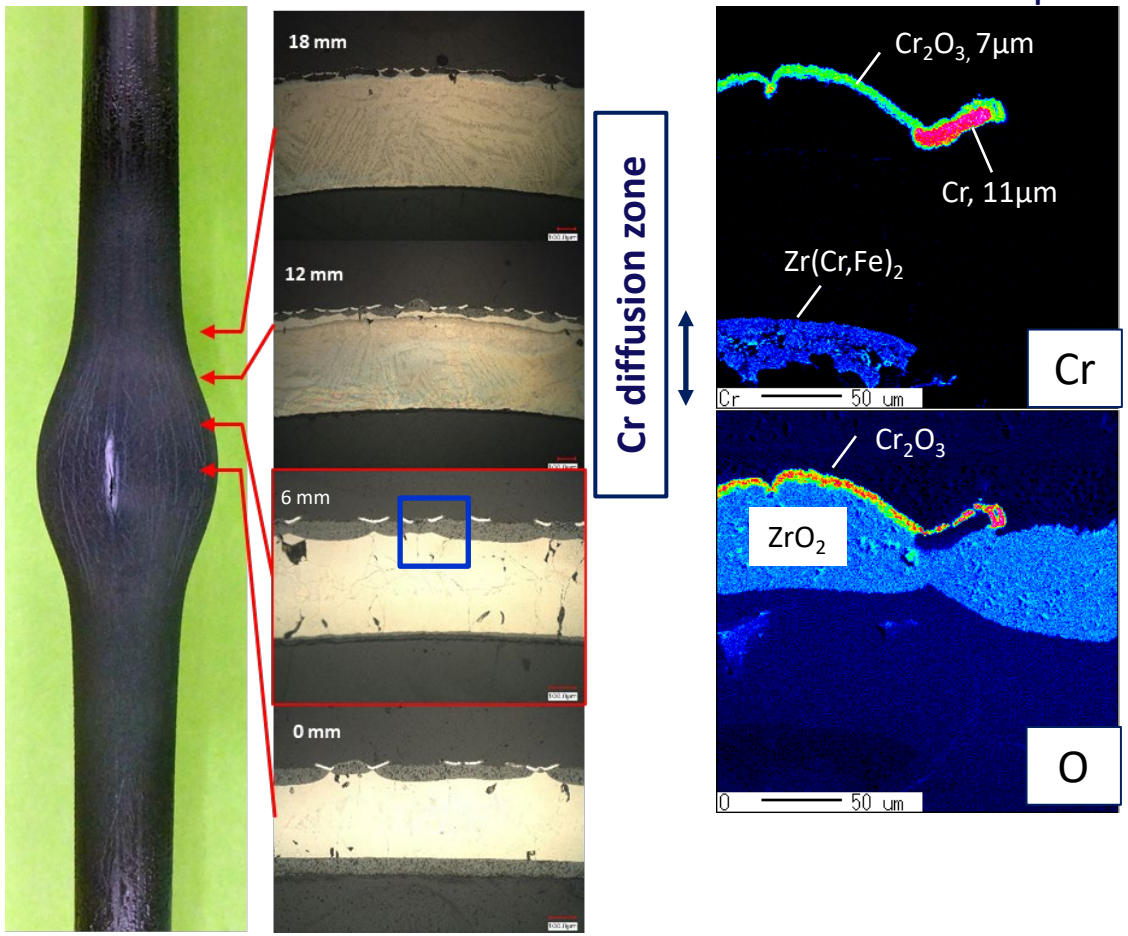

6 mm above from burst opening

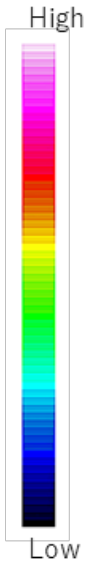

16/10 µm Cr/CrN coated Zry-4

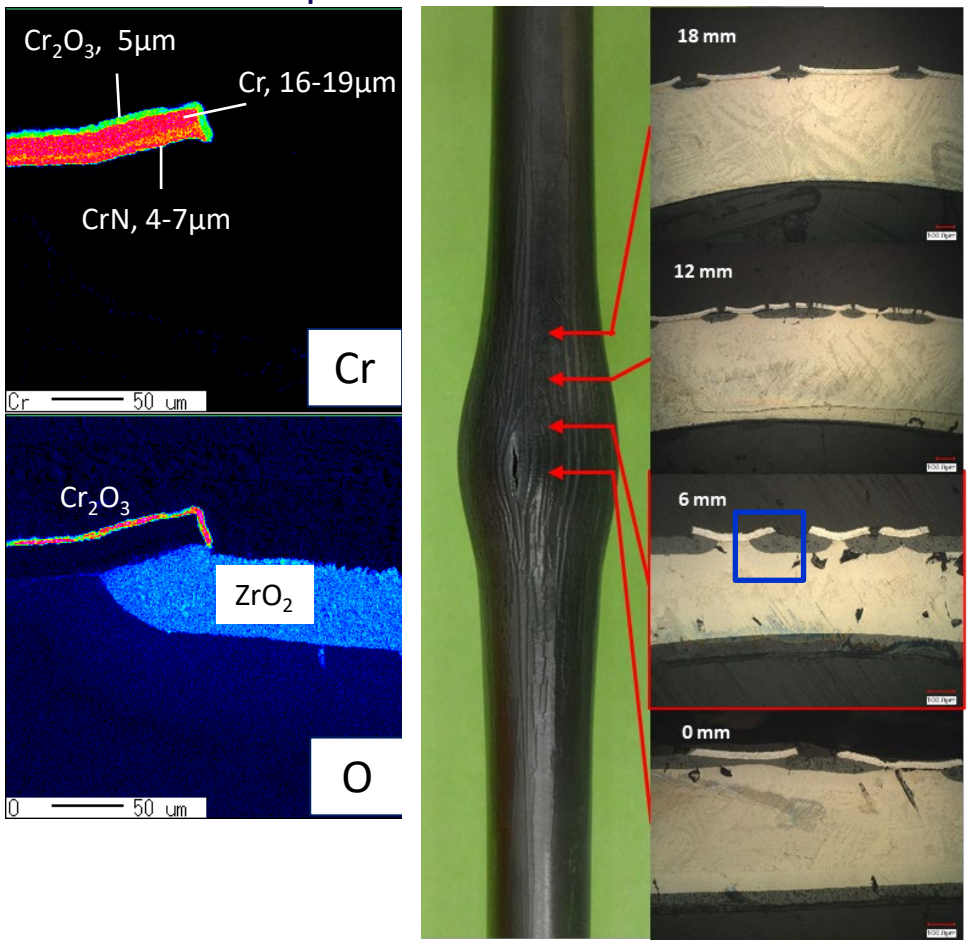

Single rod tests (RIP=6.0 MPa, 1600℃, Cr coated Zry-4)

Vertical Cross Section

10 µm Cr coated Zry-4

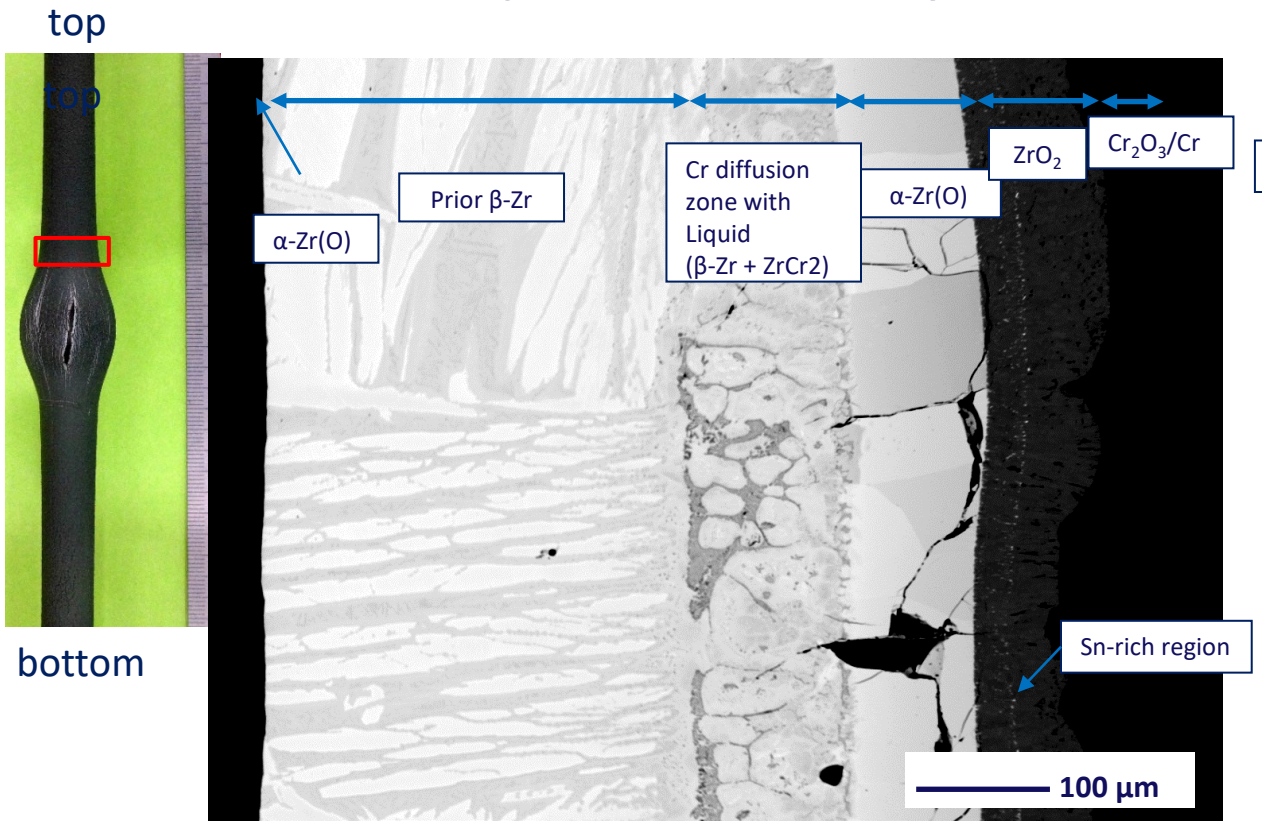

20 µm Cr coated Zry-4

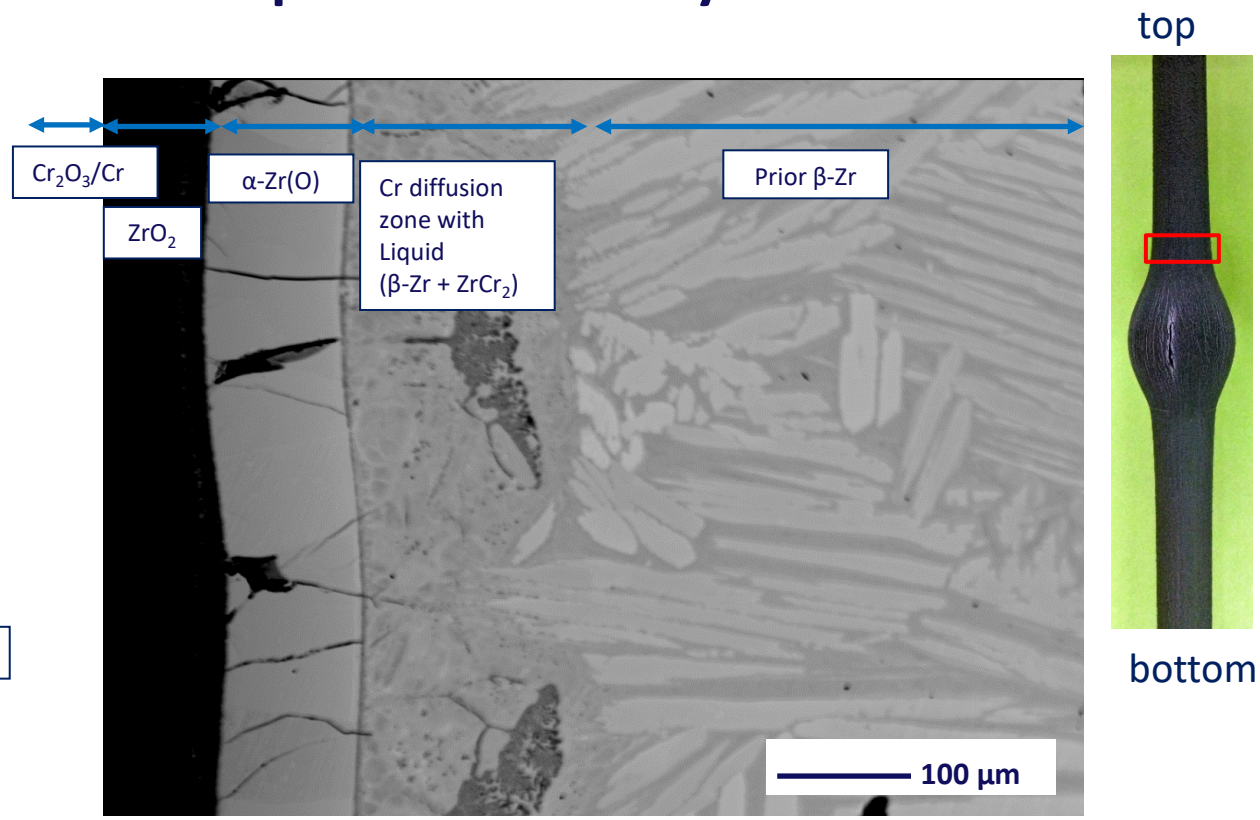

Single rod tests (RIP=6.0 MPa, 1600℃, 20 μm Cr coated Zry-4)

Microhardness

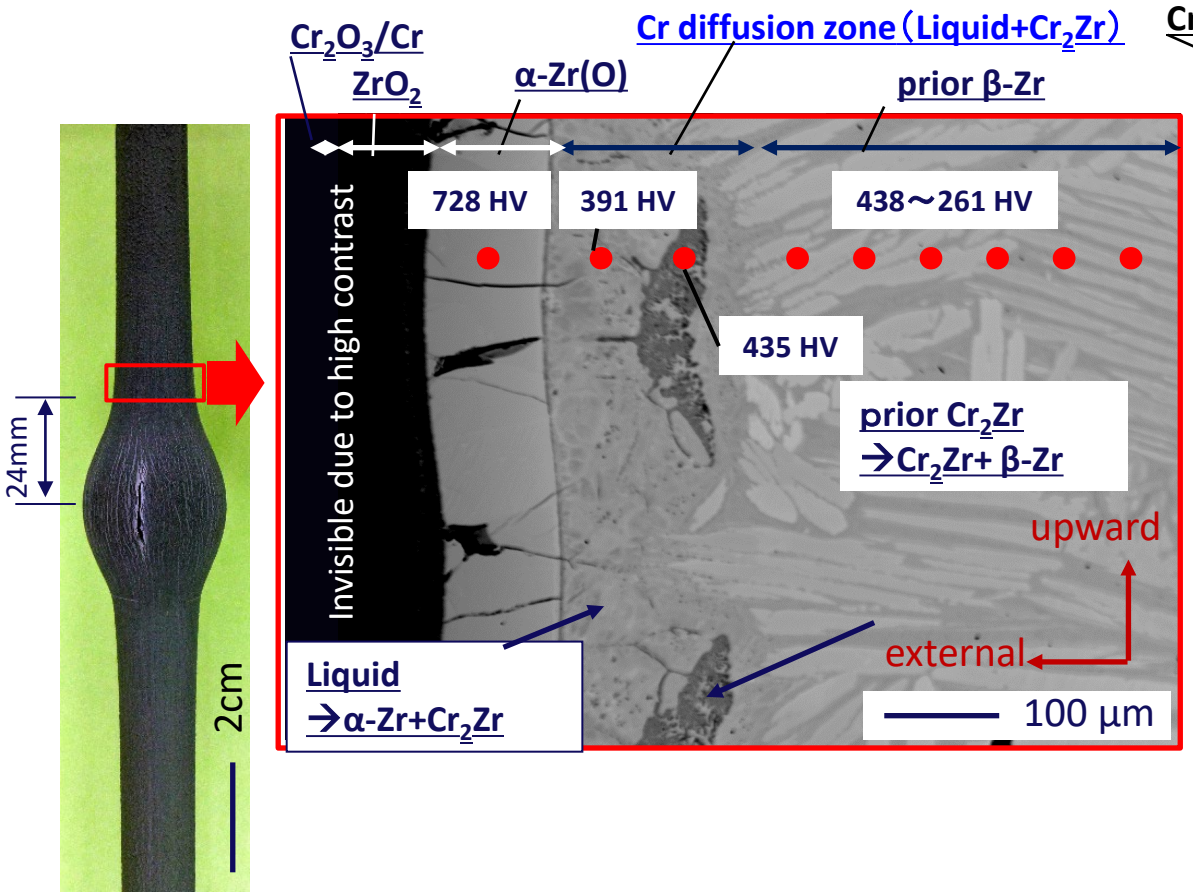

Element mapping

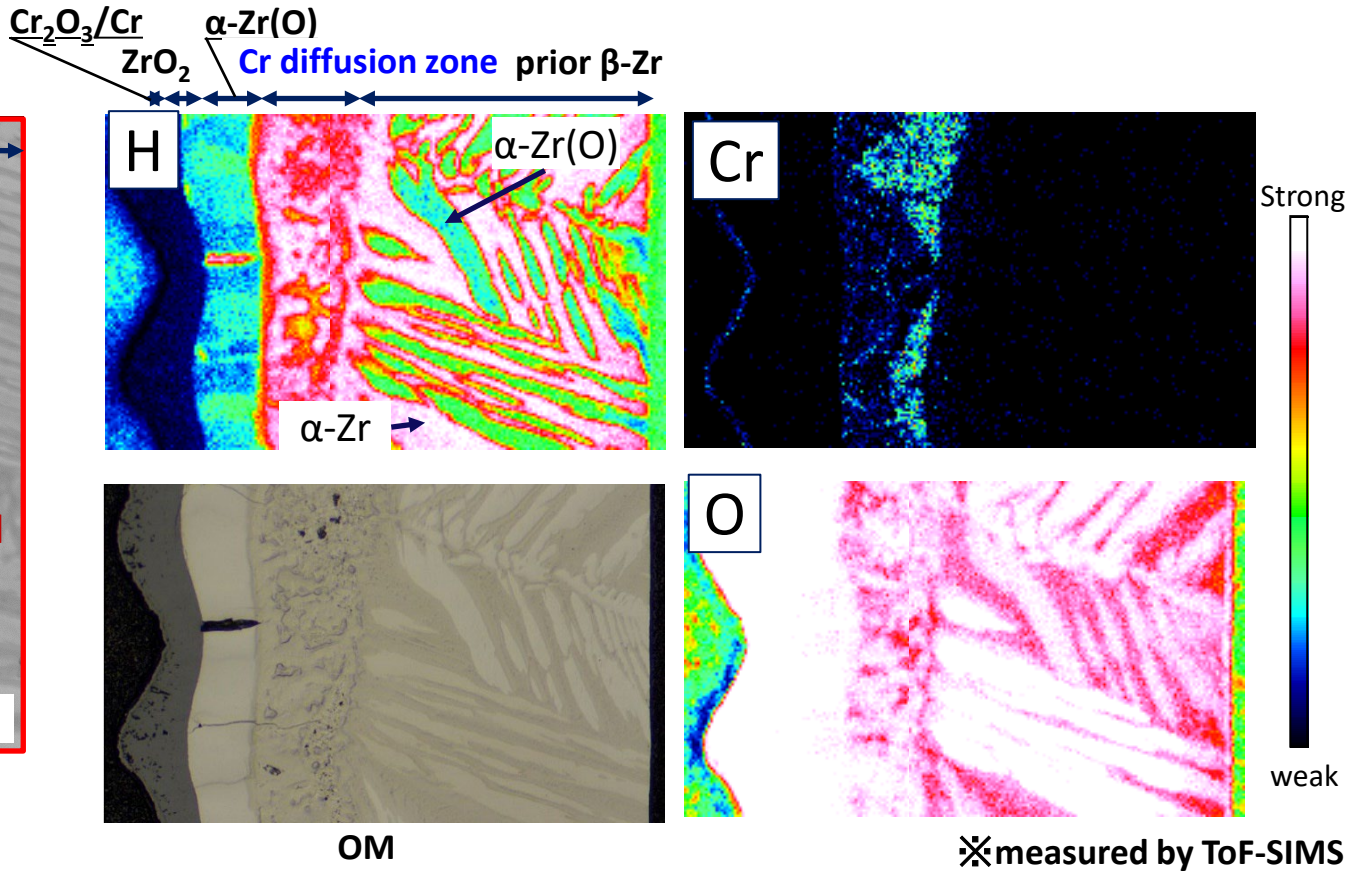

Bundle test (RIP=6.0 MPa, 1350℃, 20 μm Cr coated Zry-4)

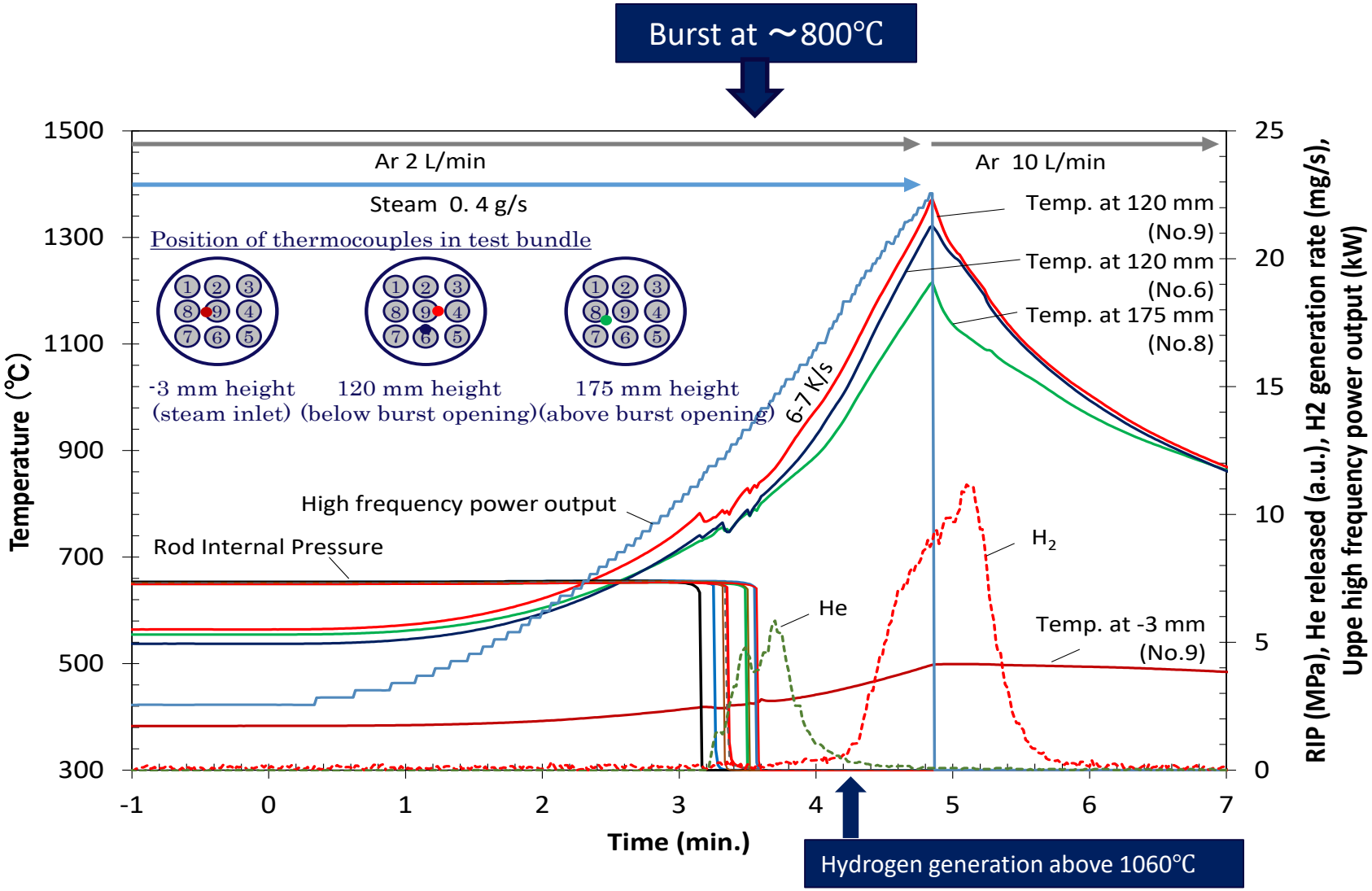

- Formation of Cr_2O_3 at hot region
- Burst inward
- Same burst temperature range as single rod test（～800℃）
- Contact/Bonding with neighboring rods
- Rapid Hydrogen generation above 1060℃

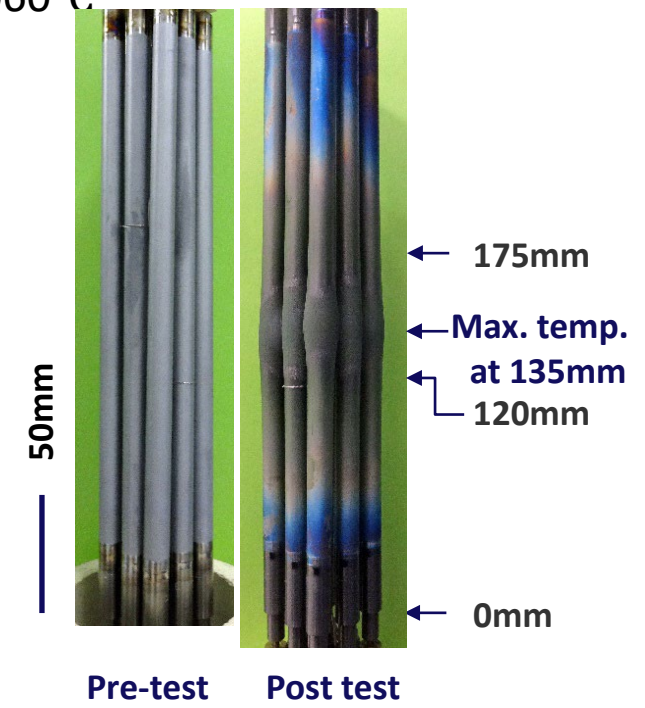

Bundle test (RIP=6.0 MPa, 1350℃, 20 μm Cr coated Zry-4)

Contact/Bonding with neighboring rods

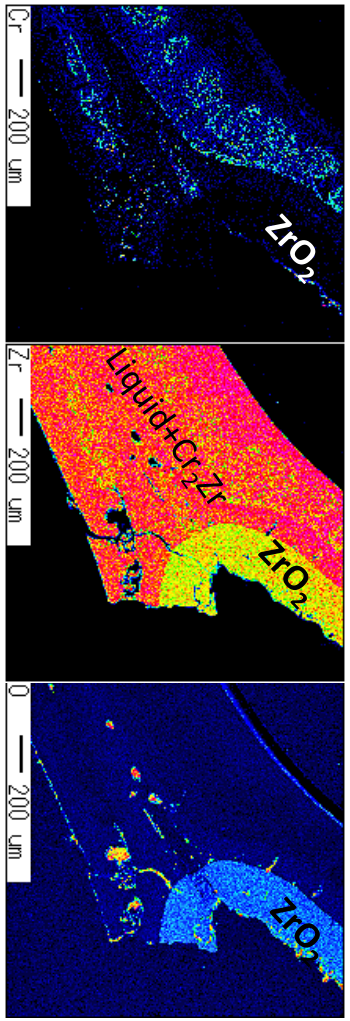

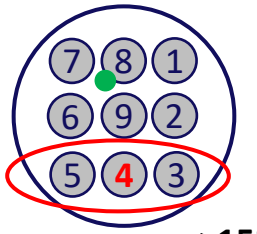

>1526℃

Formation of eutectoid microstructure :

$\gamma ZrO_2 \rightarrow \beta ZrO_2 + \alpha$-Zr(O)

1350℃

Measured by TC

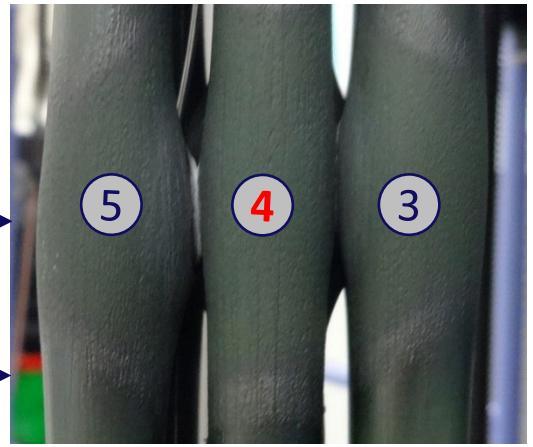

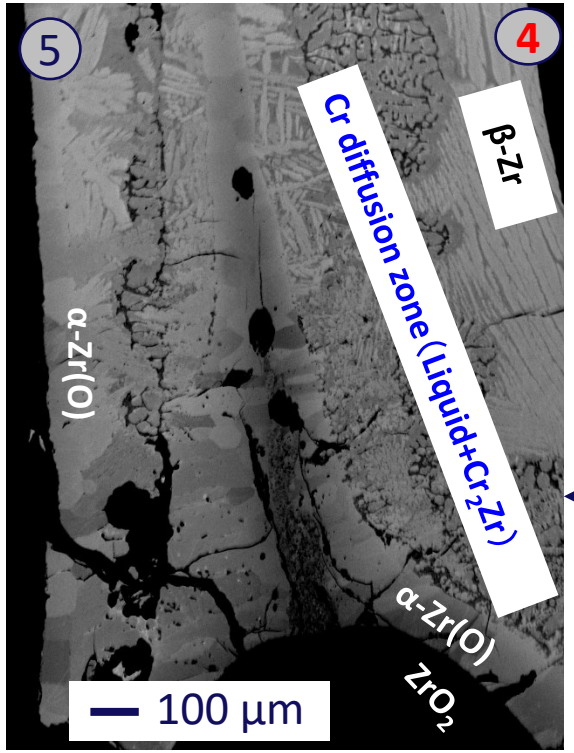

Center rod

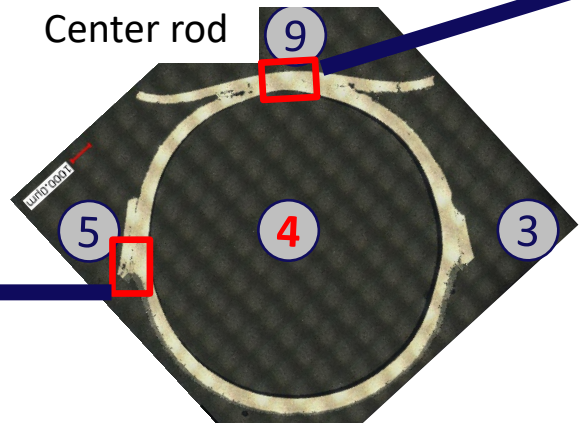

Outside surface

Cross section at burst level

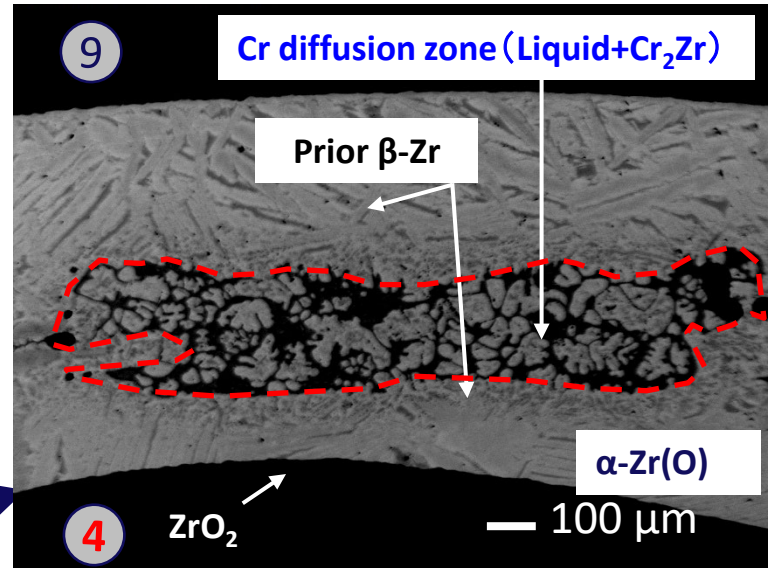

- Ballooning prior to Cr_2O_3 formation and contact with neighboring test rods to form liquid phase

Eutectoid microstructure near the interface of fuel rods ③-④

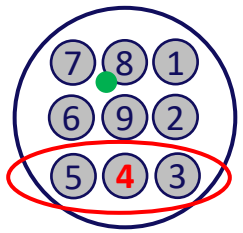

Inside

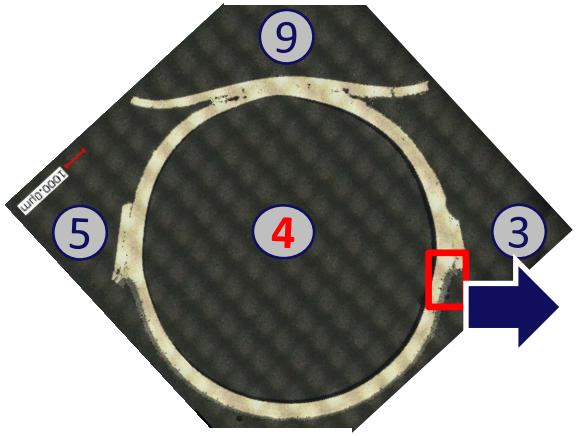

Outside

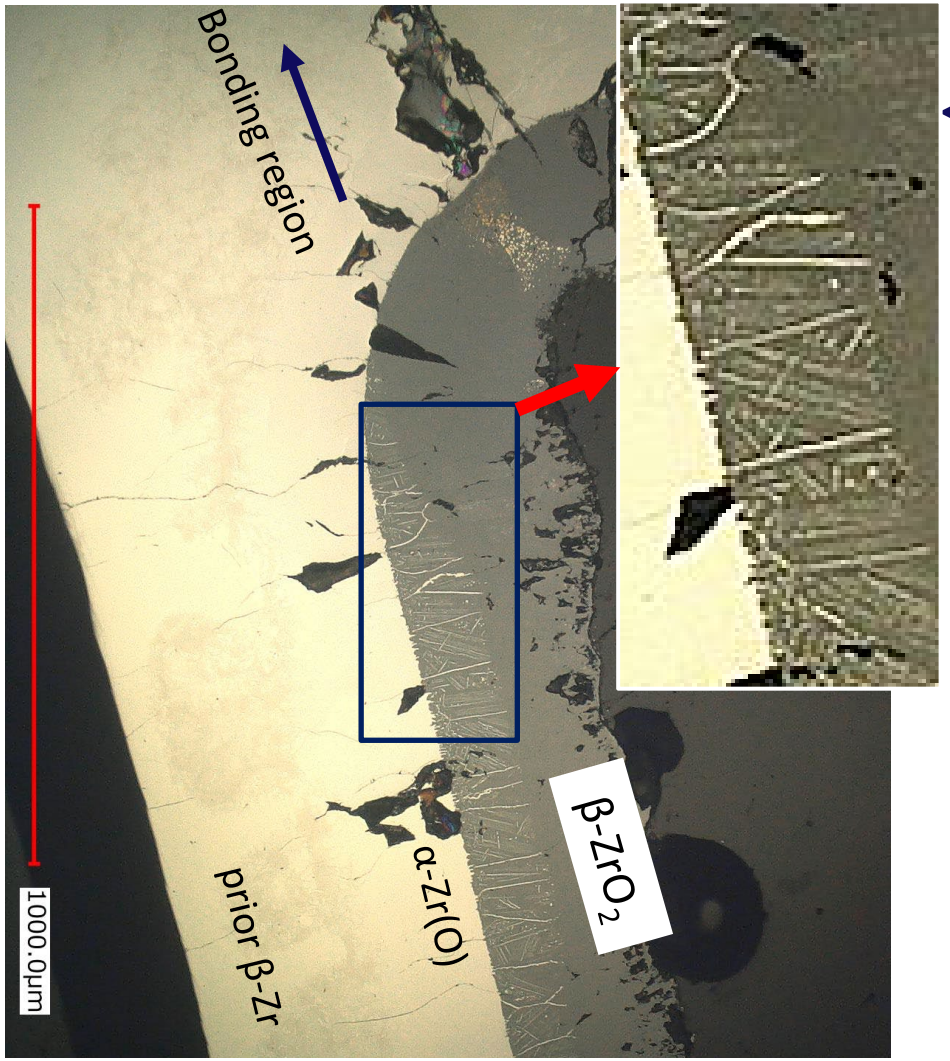

Potential phase transformation reactions at > 1526℃

- α-Zr(O) + γ ZrO_2 → α-Zr(O) + β ZrO_2

or

- γ ZrO_2 → α-Zr(O) + β ZrO_2

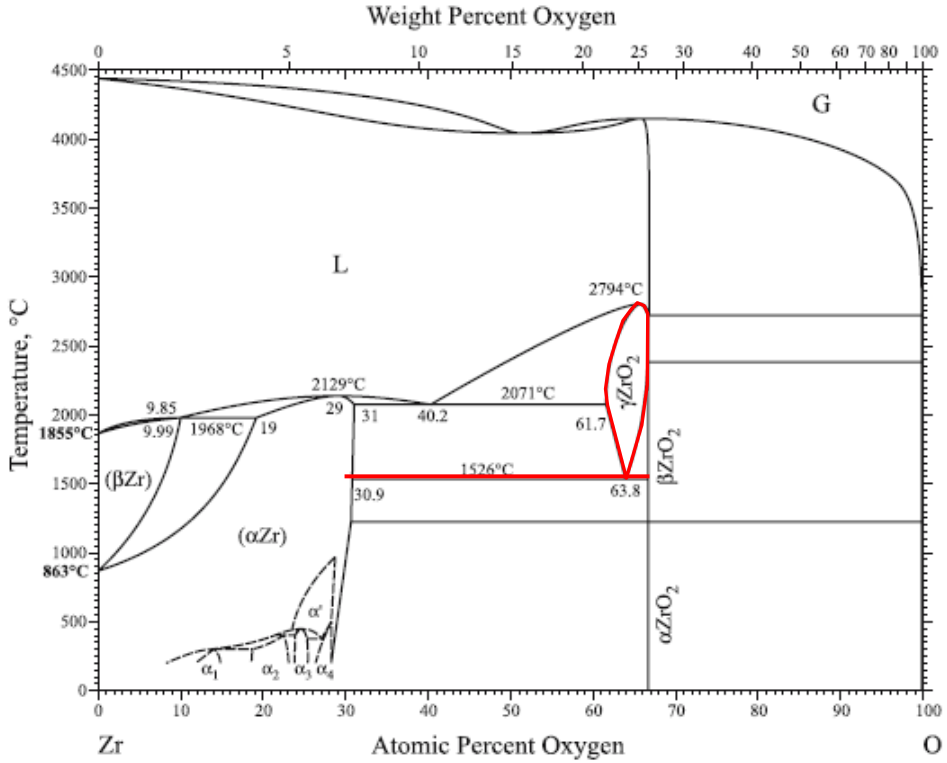

H. Okamoto, Phase diagrams for binary alloys, ASM international, 2010.

Suggests that a large temperature gradient of more than 180 ℃ occurred in the 15 mm length between the neck region and burst level.

Hoop strain over 80%

No reports exceeding 80% hoop strain

- In-pile tests such as FR2 and Halden
- Ex-reactors such as QUENCH

Over 80% hoop strain observed in this study

- In addition to the central W rod as a susceptor, Joule heating is generated by the eddy currents on the outer surface of the thinned cladding.

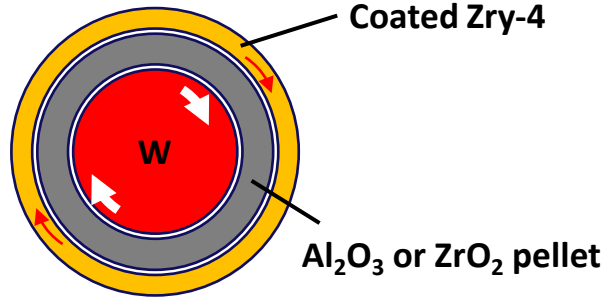

FR2 in-pile tests

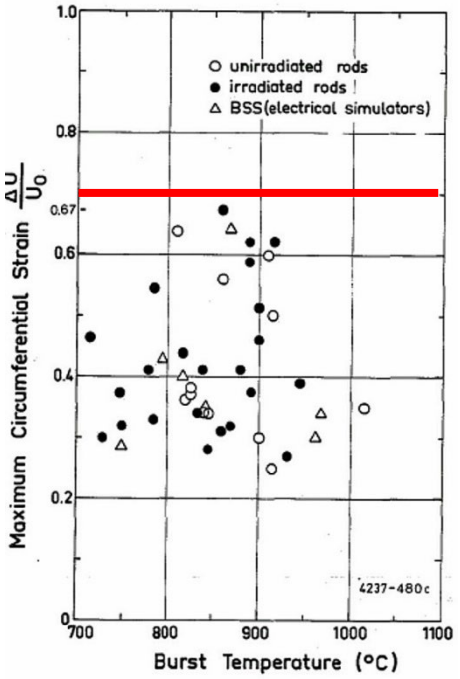

KfK 3346, 1983.

Halden reactor tests

test #	2	7	6	11	10	12	13	3	5	9	4
burnup, MWd/kg	0	44.3	55.5	56	60	72.3	74.1	81.9	83	90	92
balloon strain, %	54	23	49	25	15	40	45	8	15	61	62
ballon area, mm^2	270	8	?	1,5	38	1	10		7	224	434
fragment size	coarse	coarse	coarse	coarse	coarse & some fine	coarse & fine	coarse (& fine?)	medium & fine	medium & fine	medium & fine	medium & fine
gamma scan flask bottom →		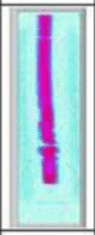	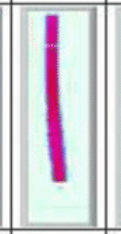		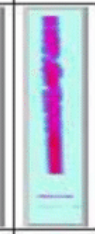	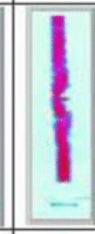				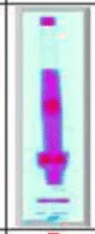	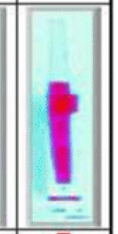
HBS width											
dispersal (qualitative)	none	none	none	none	some	some more	nearly none		much	much more	much more

NEA/CSNI/R(2016)16

- Possibility that the observed results of this study deviate from the previous reports
  - ➢ Accelerated strain and thinning
  - ➢ Larger local temperature gradients

Conclusion

- Preliminary single rod and bundle tests of coated test rods under BDBA conditions are being conducted at DEGREE facility in the framework of IAEA CRP ATF-TS project.
- Due to induction heating, a local high temperature gradient is created in the thin-walled cladding after burst, which may cause a phenomenon different from the actual behavior.

Future works

- Bundle tests without pressurization in order to reproduce the actual phenomenon

CRIEPI
Central Research Institute of Electric Power Industry

Acknowledgment

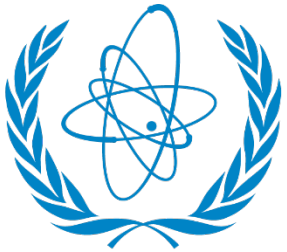

IAEA
International Atomic Energy Agency

Thank you for your attention!

R. Farkas
EK Budapest

The CODEX-ATF experiment

An integral bundle test was carried out in the framework of the IAEA Testing and Simulation for Advanced Technology and Accident Tolerant Fuels (ATF-TS) project in the CODEX (COre Degradation Experiment) facility. The test section included an electrically heated seven-rod bundle composed of 3 pieces uncoated and 4 pieces Cr coated optZIRLO cladding tubes. The main parameters of the scenario were selected on the basis of pre-test calculations.

Electrical heating with two tungsten heaters in each rod was applied. The heated length was 650 mm. The rods were pressurized during the test in order to reach ballooning and burst in the early phase of the experiment. The rods in the bundle were fixed by two spacer grids made of Zr1%Nb alloy. The bundle was placed into a hexagonal shroud. The shroud material was Zr2.5%Nb alloy, the total length of the shroud was 1000 mm. The bundle was heated by direct current power supply units. The steam generator provided hot steam to the test section. The water injection into the steam generator was performed with precision pump at constant flow rate. For heating up, argon gas was also injected into the steam generator.

In the preparatory phase the facility was heated up to 600 °C in 0.2 g/s steam and 0.2 g/s argon flow rates using both external heaters and fuel rod heaters. The heat-up phase continued with the same flow rates and with 1000 W heating power on the rods and 800 W power of external heaters. The rods were pressurised and cladding burst took place at ≈900 °C on most of the rods. The temperature increase was very smooth. At the initiation of water quench, the cladding temperature in the top of the bundle was above 1600 °C. In the upper part of the fuel rods 1400 °C was reached. It is expected that intense Zr-Cr eutectic formation took place at these temperatures. During the quench phase, room temperature water was injected to the bottom of the test section. The total hydrogen production during the experiment was about 3 g, which indicated significant oxidation of the Zr components.

HUN REN | Centre for Energy Research

HUN-REN Hungarian Research Network

HUN-REN Centre for Energy Research

The CODEX-ATF experiment

Róbert Farkas, Nóra Vér, Berta Bürger, Péter Szabó, Zoltán Hózer

28th International QUENCH Workshop
Egg.-Leopoldshafen, Germany, 5-7 December 2023

Research. Innovation. Impact.

Introduction

- During the discussions with ATF-TS project partners, EK proposed to carry out an integral bundle test in the CODEX facility.
- Czech Technical University (CTU) offered to provide Cr-coated (18 µm) and uncoated optimised ZIRLO^{TM} tubes for the experiment with 650 mm length and 9.1 mm diameter.

The main characteristics of the tests were agreed as follows:

- The bundle should include both coated (4 pieces) and uncoated cladding (3 pieces) tubes in order to allow direct comparison of their behaviour under serious accident conditions.
- The maximum local cladding temperature should be above 1300 °C for the observation of high temperature Zr-Cr interactions (eutectic formation).

CODEX-ATF test section

- Hexagonal 7-rod bundle in VVER geometry
- Length of heated rods 650 mm
- Tungsten heaters in the rods + external heating
- Zirconia and alumina pellets insulate the tungsten
- Rod pressurisation by argon
- Zr2.5%Nb shroud
- Thermal insulation layers

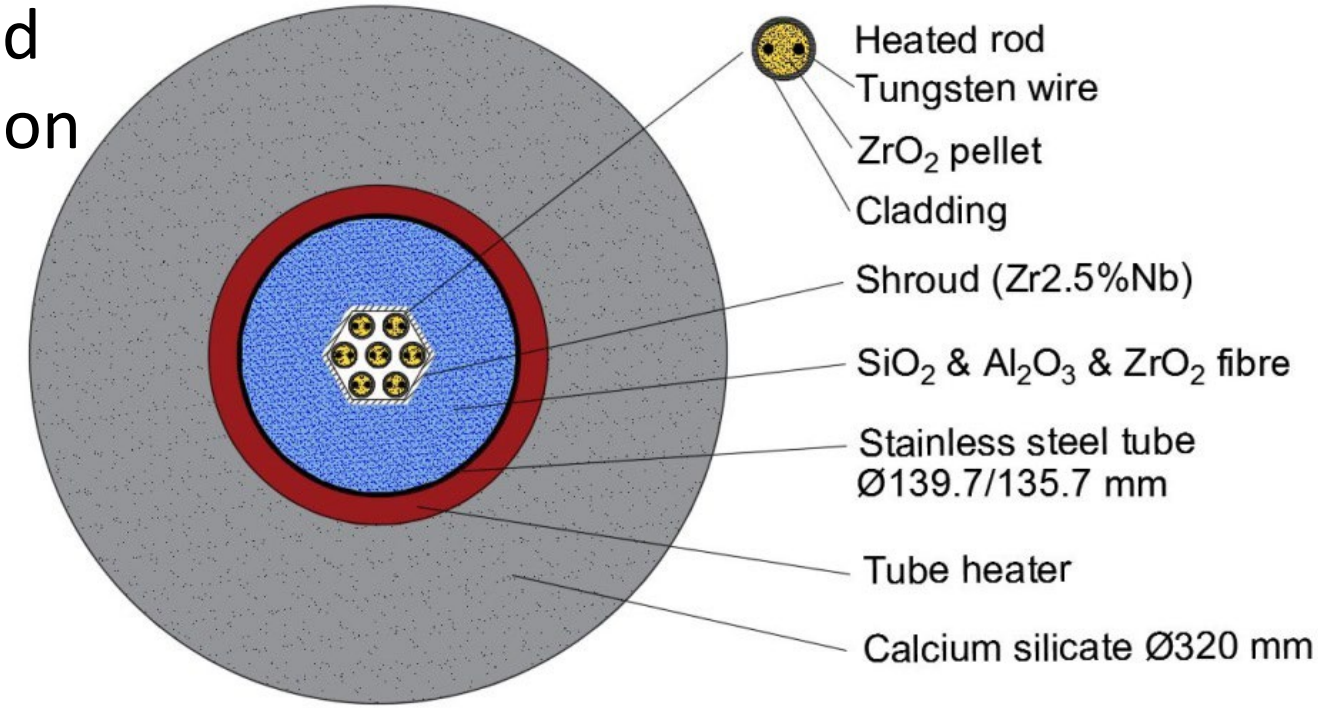

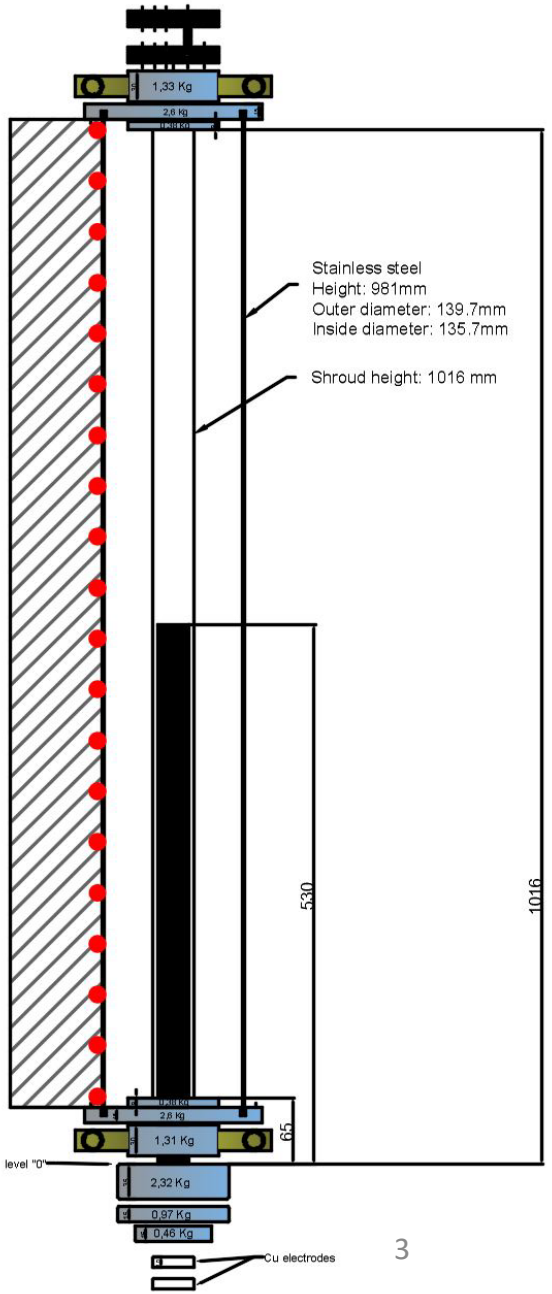

CODEX-ATF facility

Number of fuel rods	7
Cladding of fuel rods No. 2., 4. and 6.	optZIRLO™
Cladding of fuel rods No. 1. (central), 3., 5. and 7.	Cr-coated optZIRLO™
Length of fuel rods	650 mm
External diameter of fuel rods	9.1 mm
Cladding wall thickness	0.58 mm
Pellet material	ZrO_2
Pellet material in the bottom of the rods	Al_2O_3
Height of pellet	10 mm
Diameter of pellet	7.65 mm
Hole diameter in the pellet	2 mm
Spacer grid material	Zr1%Nb
Height of spacer grid	10 mm
Thickness of spacer grid	0.4 mm
Number of spacer grids	2
Shroud material	Zr2.5%Nb
Shroud thickness	2 mm
Length of shroud	1000 mm
Shroud key size	39 mm

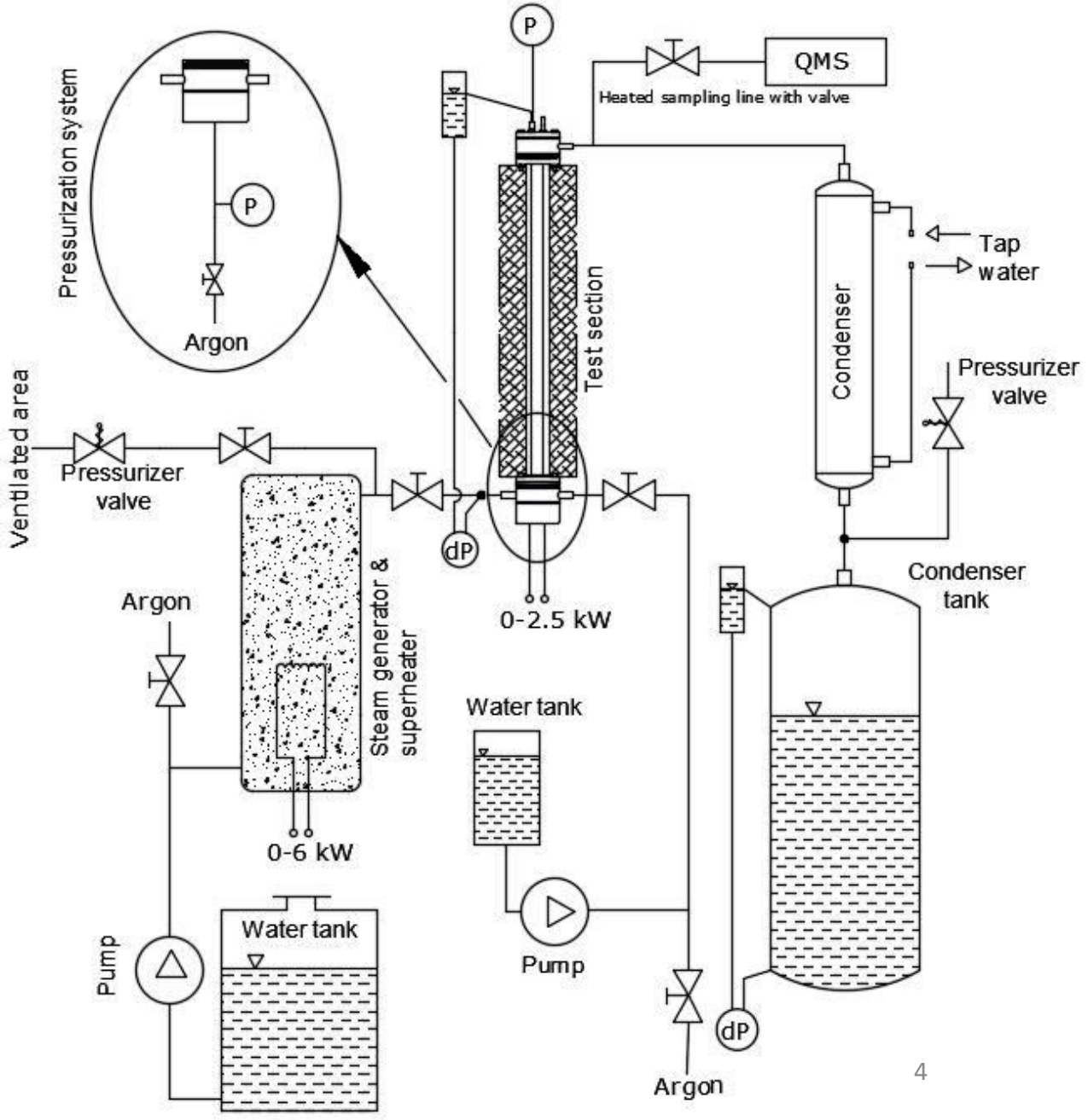

Thermocouple positions of the CODEX-ATF facility

High temperature thermocouples (6 pieces)

- ① W5Re/W26Re at elevation 550 mm with orientation of 180°
- ② W5Re/W26Re at elevation 500 mm with orientation of 300°
- ③ W5Re/W26Re at elevation 400 mm with orientation of 60°
- ④ W5Re/W26Re at elevation 200 mm with orientation of 60°
- ⑤ W5Re/W26Re at elevation 400 mm with orientation of 180°
- ⑥ W5Re/W26Re at elevation 300 mm with orientation of 180°

K-type thermocouples (33 pieces)

- ⑨ "K" type at elevation 50 mm with orientation of 0°
- ⑩ "K" type at elevation 50 mm with orientation of 180°
- ⑪ "K" type at elevation 150 mm with orientation of 300°
- ⑫ "K" type at elevation 150 mm with orientation of 120°
- ⑬ "K" type at elevation 500 mm with orientation of 240°
- ⑭ "K" type at elevation 200 mm with orientation of 240°
- ⑮ "K" type at elevation 300 mm
- ⑯ "K" type at elevation 400 mm
- ⑰ "K" type at elevation 500 mm

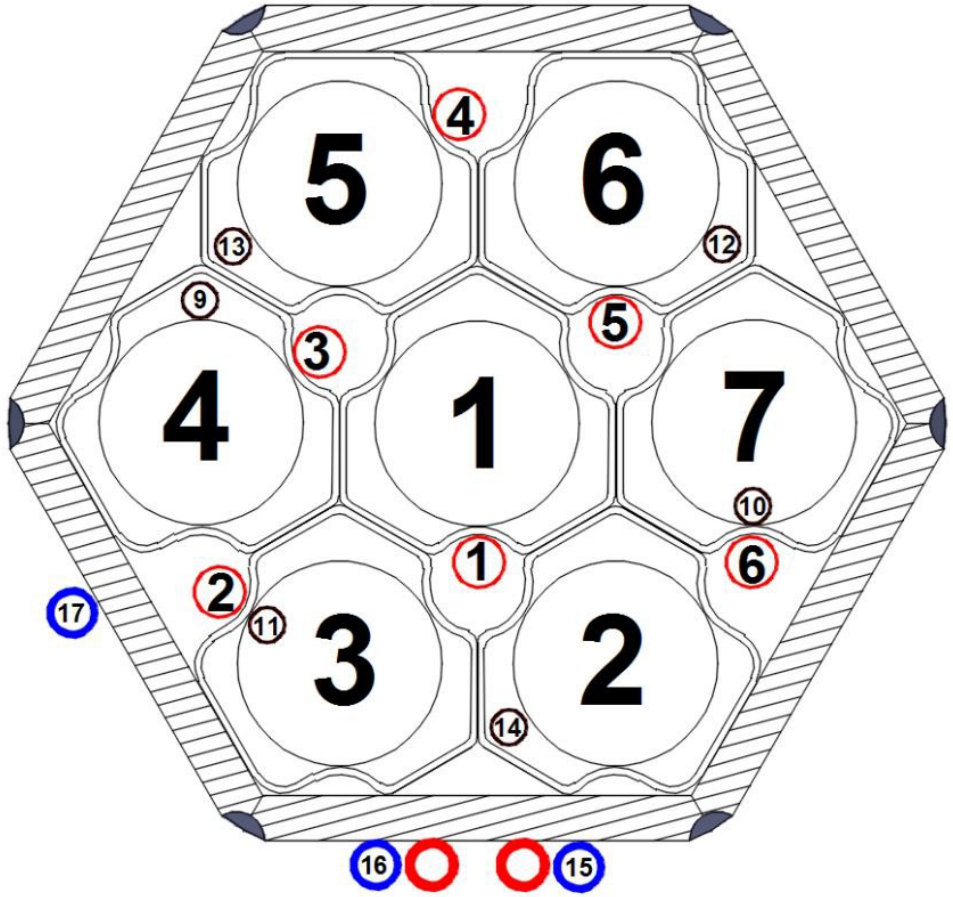

Proposed scenario

The proposed scenario will focus on covering several phenomena of fuel behaviour during accidents.

- **Ballooning and burst** will take place due to pressurisation of fuel rods (rod pressures between 1-3 MPa, all of them will burst between 800-1000 °C).

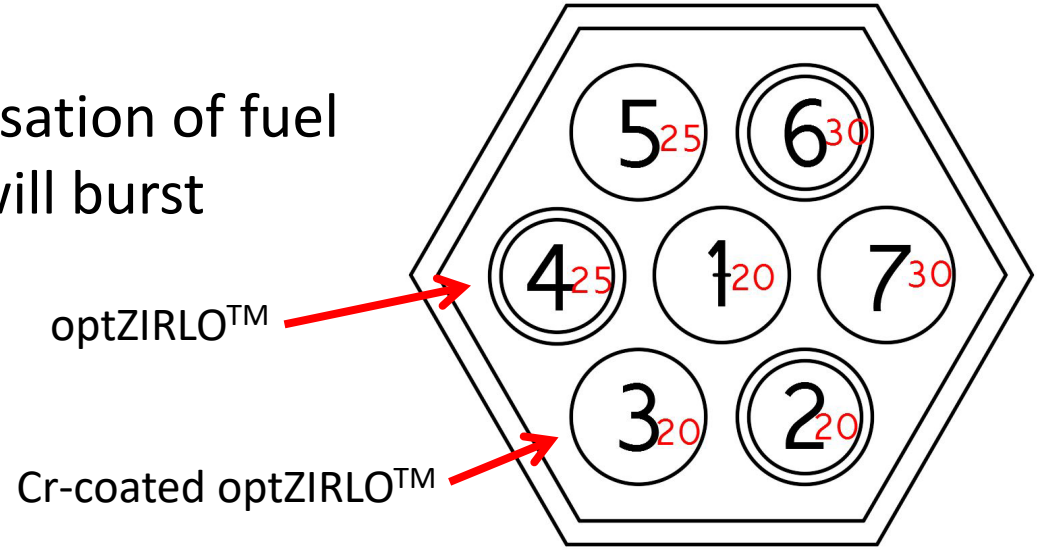

- **Oxidation of cladding external surface** will be observed in high temperature steam, the degree of oxidation will depend on the local temperatures.
- **Oxidation of inner cladding surface** and secondary hydriding may take place after cladding burst and penetration of steam into the fuel rods.
- **Eutectic formation** between Zr-Cr is expected above 1300 °C.

It is not intended to cover a representative NPP scenario in details, but the proposed sequence of events may be interpreted as a station blackout (SBO) event with combination of small break LOCA with recovery of emergency water supply when the cladding temperature reaches 1400 °C.

Proposed scenario

technological heat-up of the facility, initiation of steam supply, moderate power and target temperature of 600 °C

further heat-up with increased power, pressurization of fuel rods to reach burst, target temperature of 1000 °C

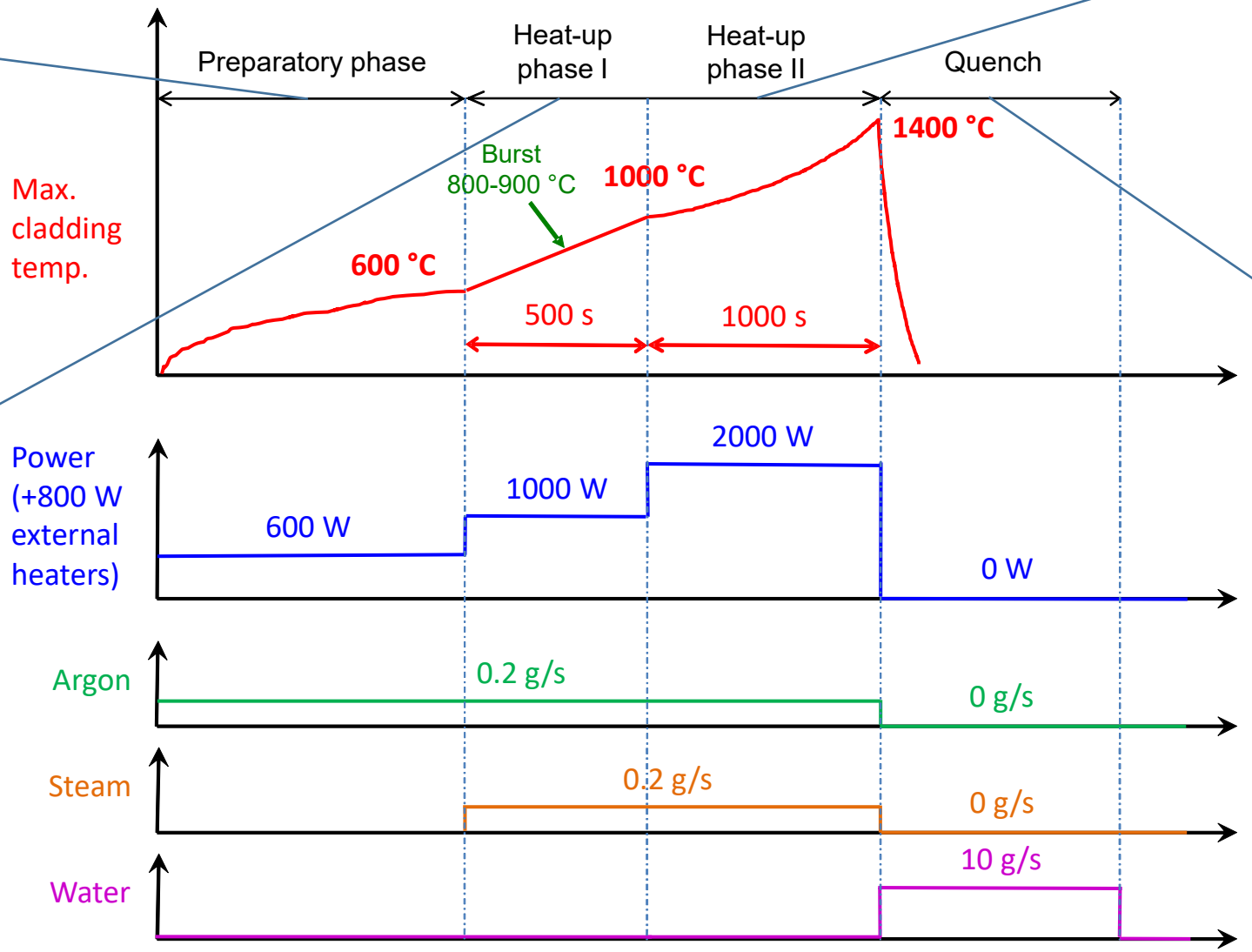

further heat-up with increased power, target temperature of 1400 °C

injection of water, switching off power and steam supply

Measurements

During the tests there will be on-line measurements and data acquisition:

- temperatures,
- pressures,
- flowrates,
- power,
- outlet gas composition.

Pre-test calculations by IBRAE, NUBIKI, GRS

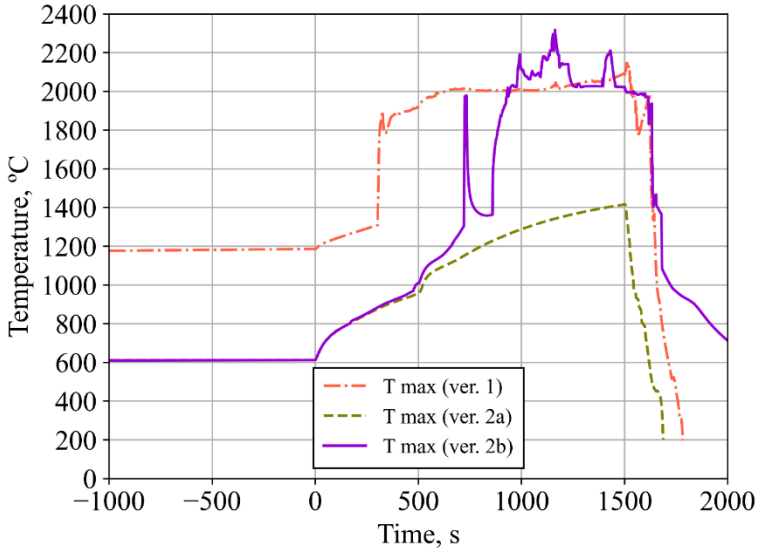

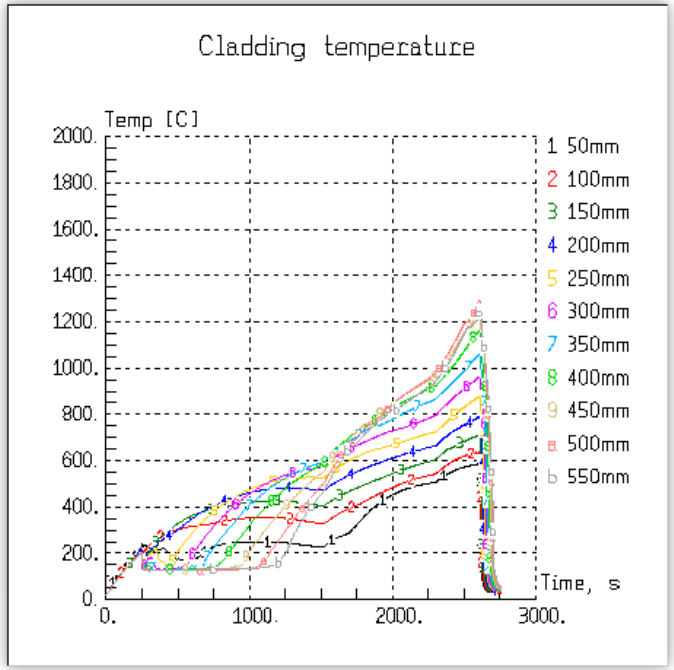

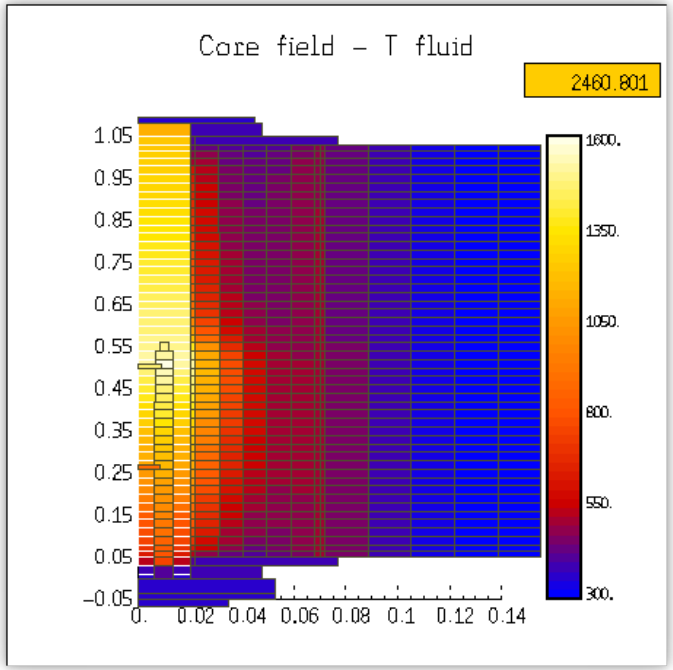

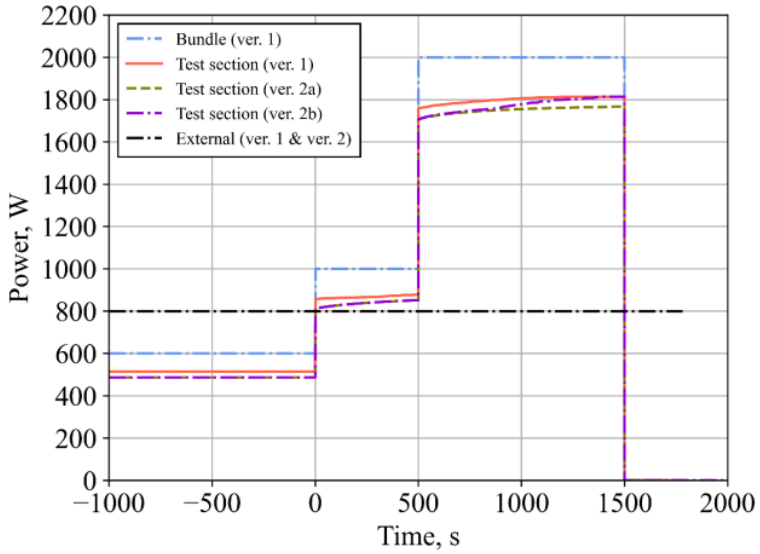

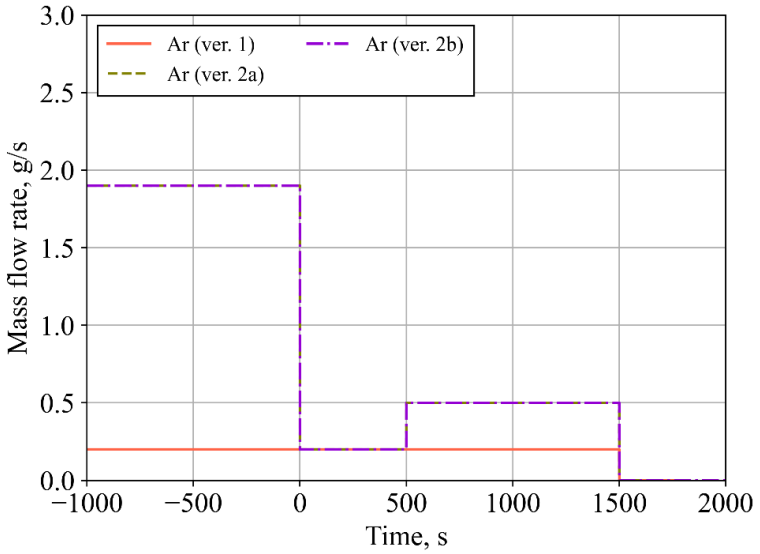

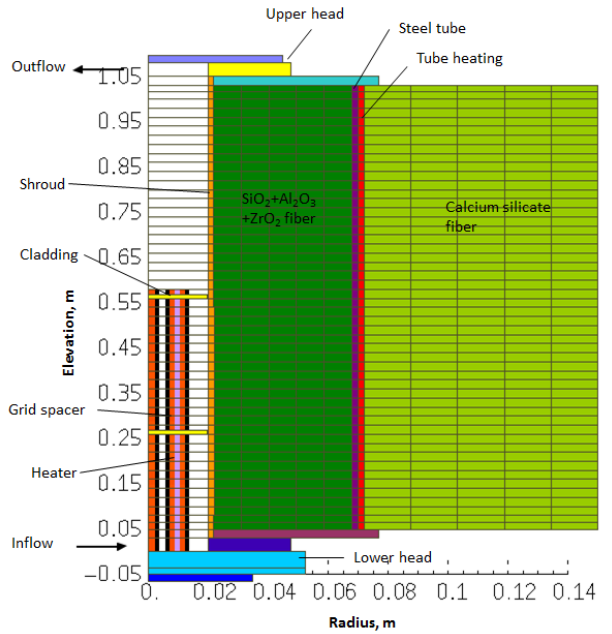

Assembly of the bundle

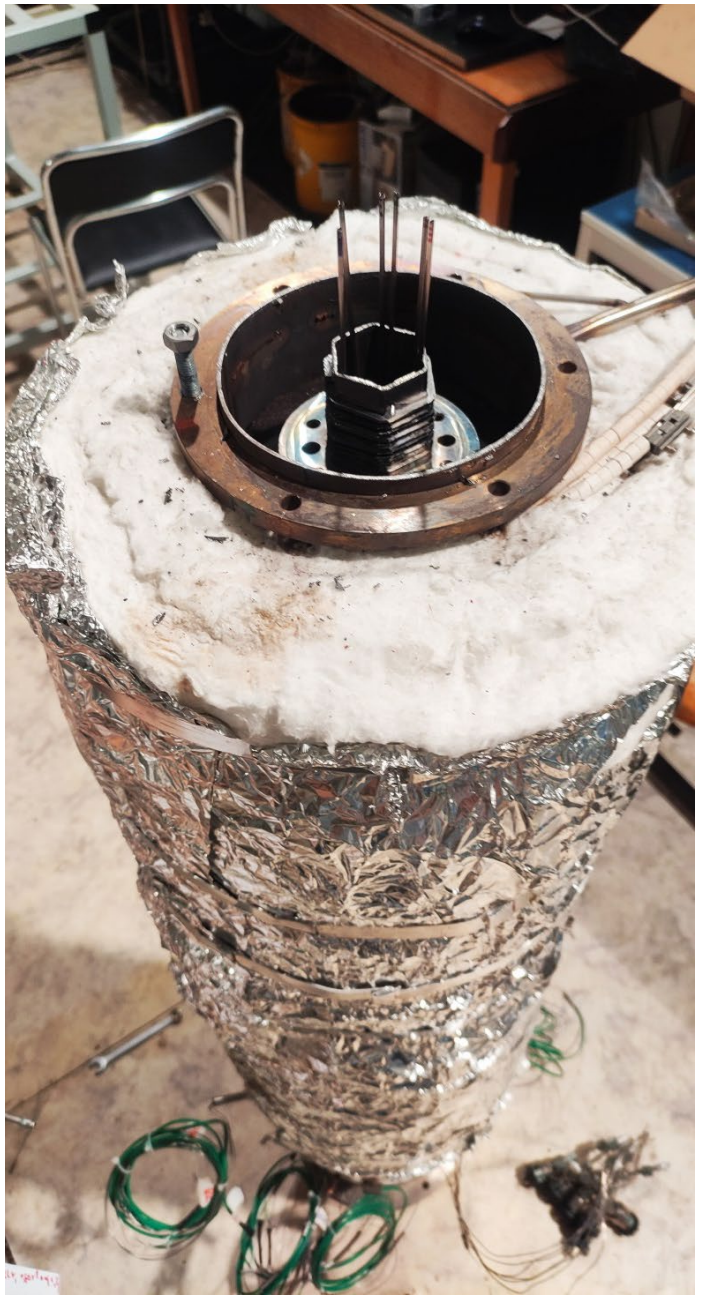

Comissioning test No. 1.

- The heating included the operation of both bundle heater and external heater systems. Stepwise power changes were performed with the fuel rod heaters in argon atmosphere (0.2 g/s). The maximum power was set to 500 W for the rods and 800 W for the external heaters.

- The total duration of the heated period was about 1 hour. The maximum rod temperature was close to 650 °C at 500 mm elevation, while one of the measured shroud temperatures reached 550 °C at the same elevation.

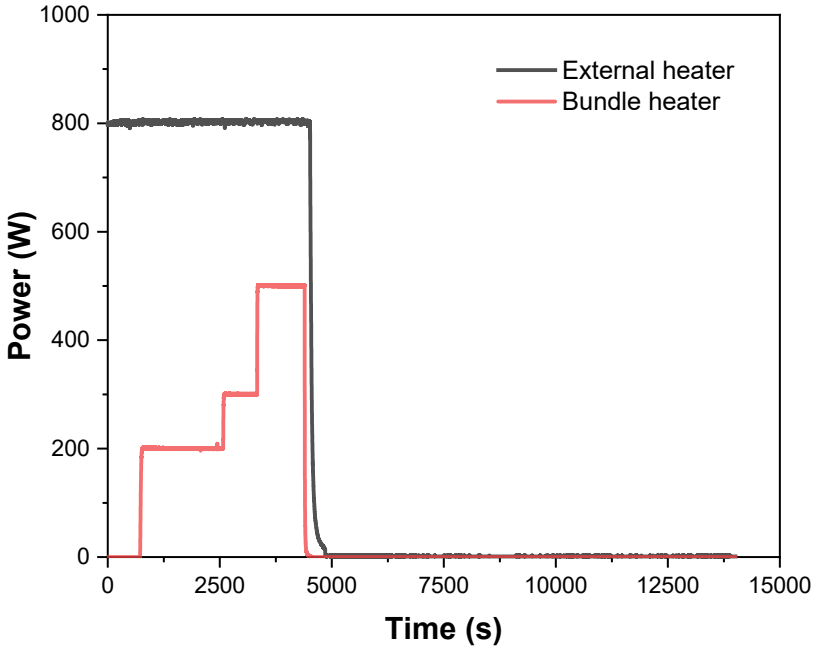

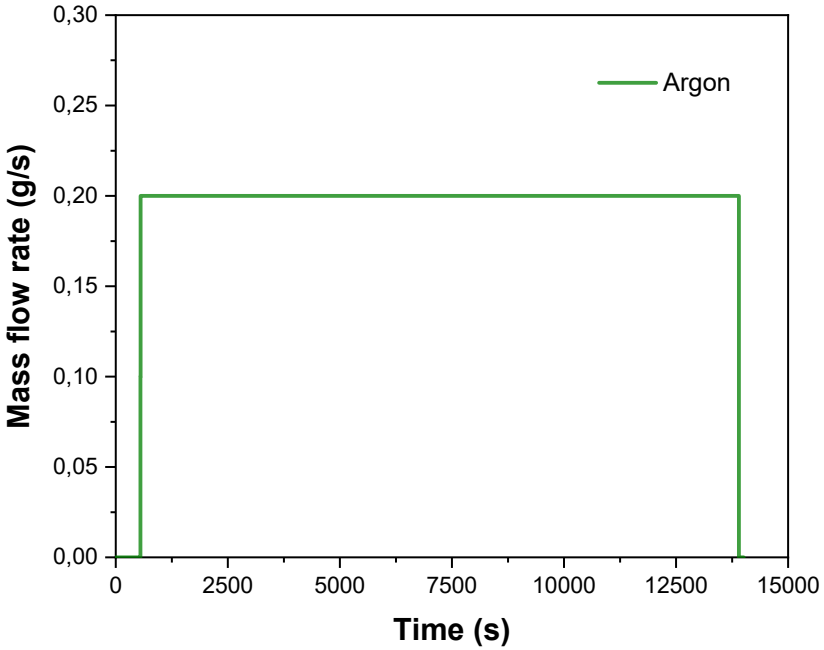

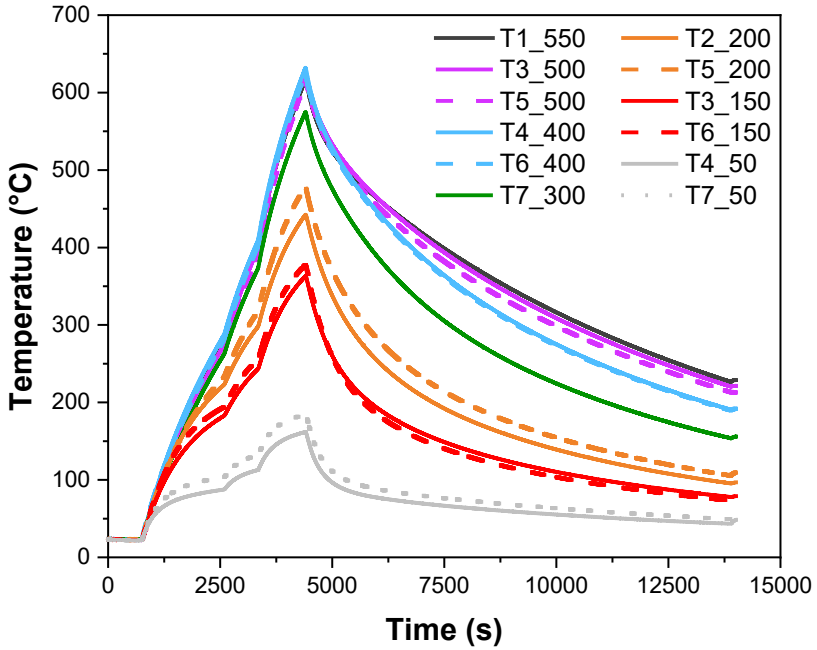

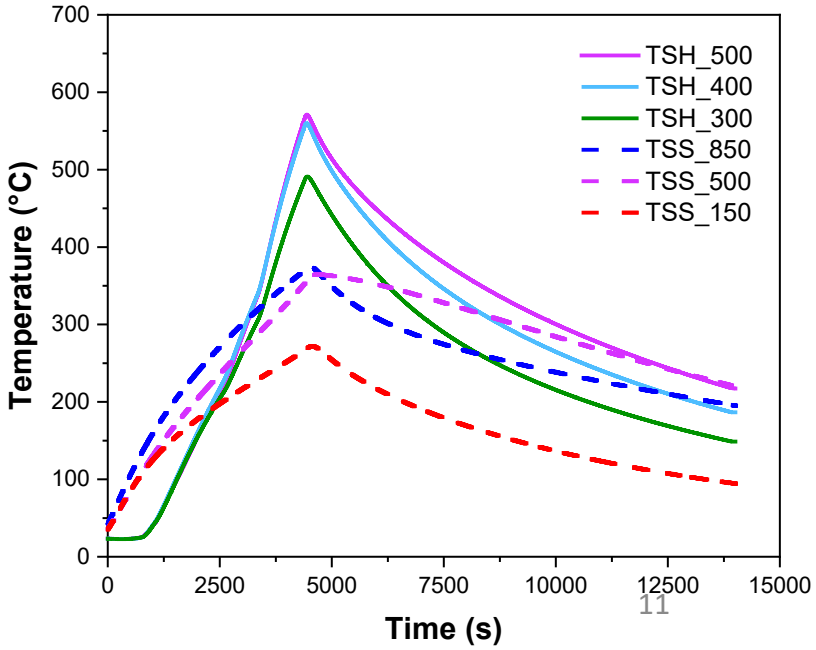

Comissioning test No. 2.

- The maximum power reached 1600 W for the rods (no external heater). The total duration of the heated period was 30 min. The maximum rod and shroud temperatures reached 650 °C and 450 °C at 500 mm elevation.
- The argon flow rates were varied.
- The pressurization of individual rods was tested several times during this commissioning test.
- The operation of steam generator was also tested.

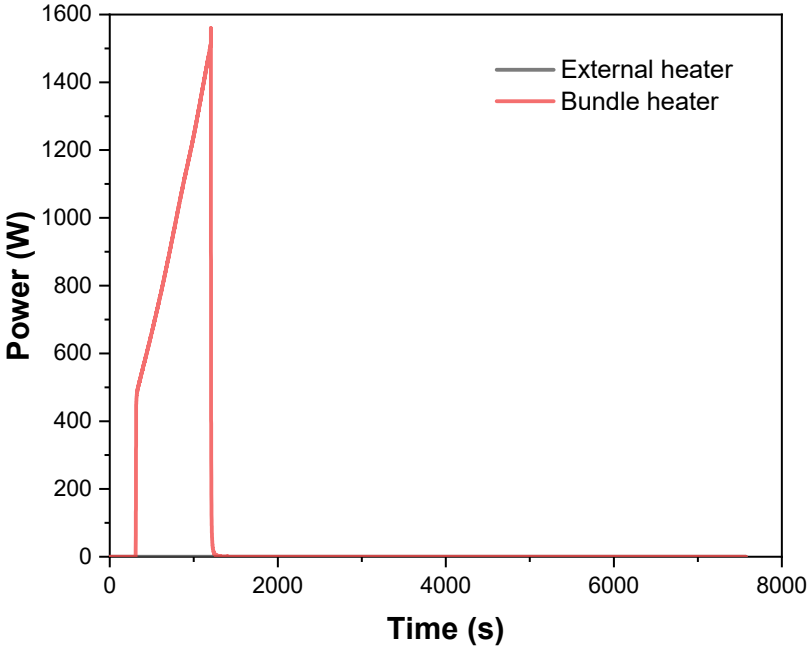

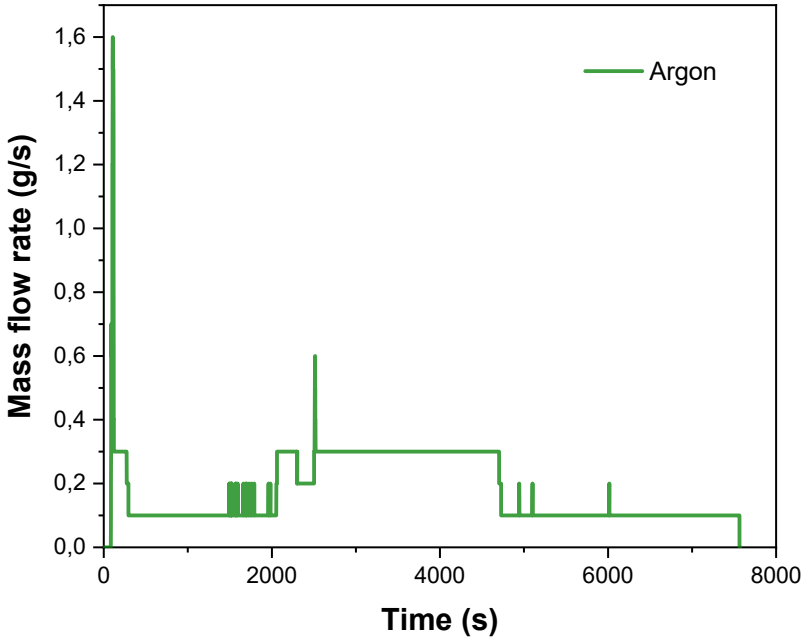

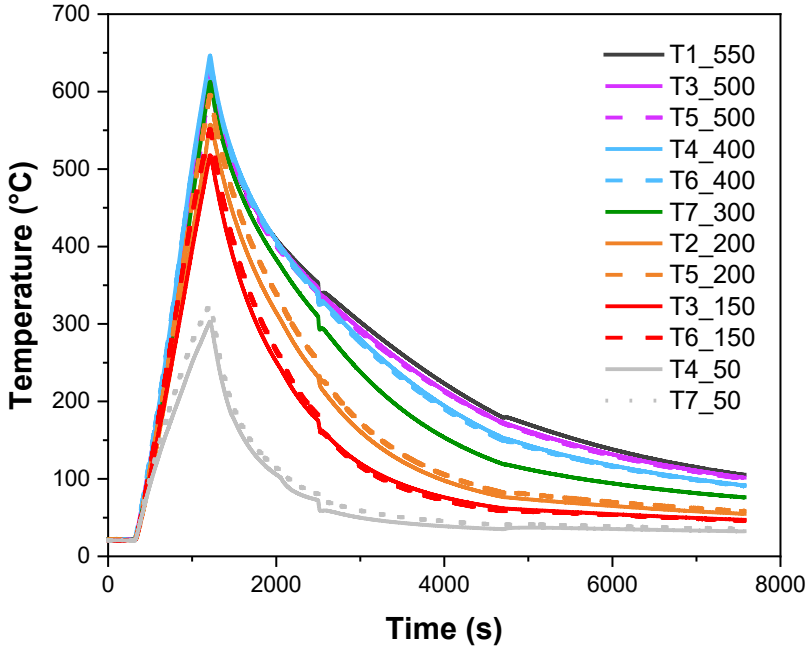

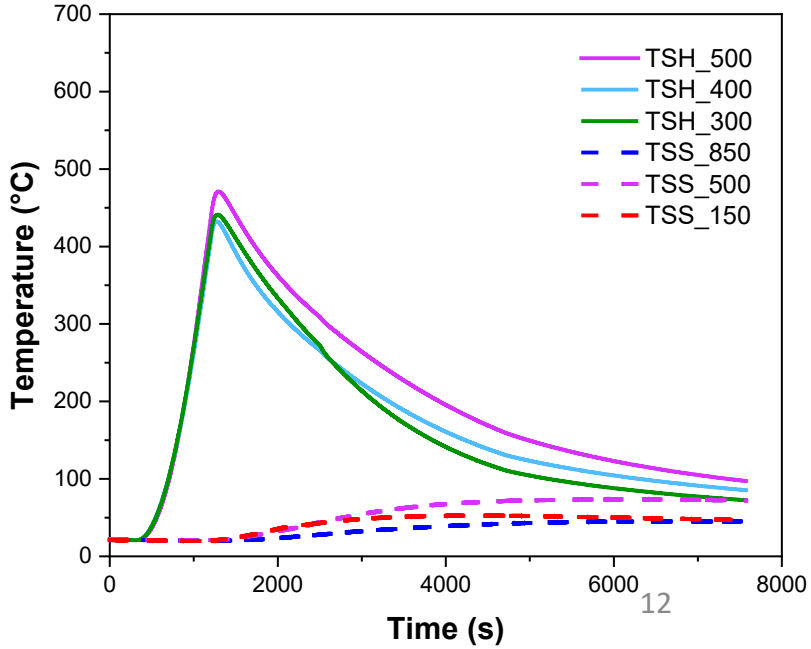

CODEX-ATF results

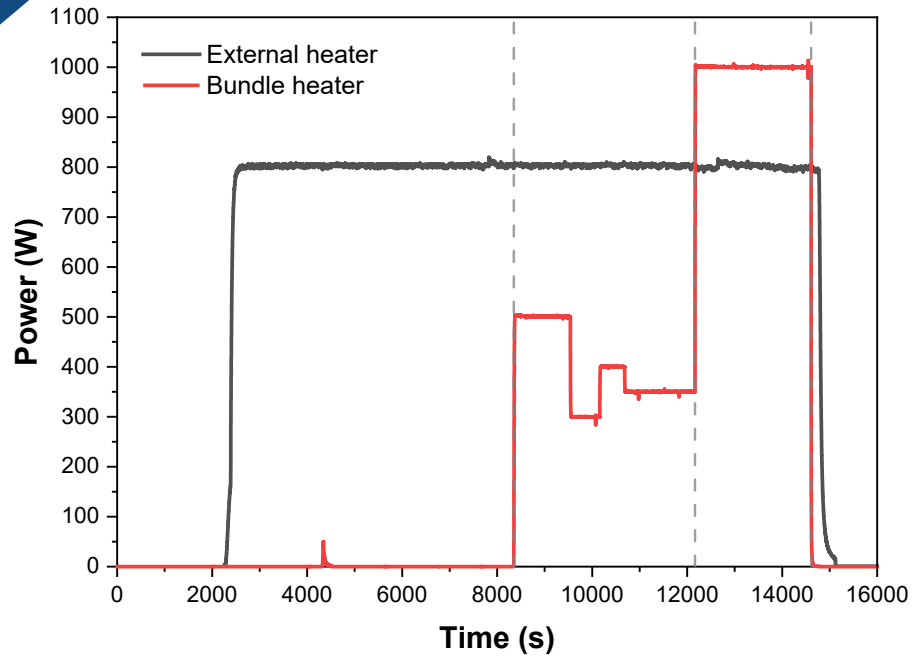

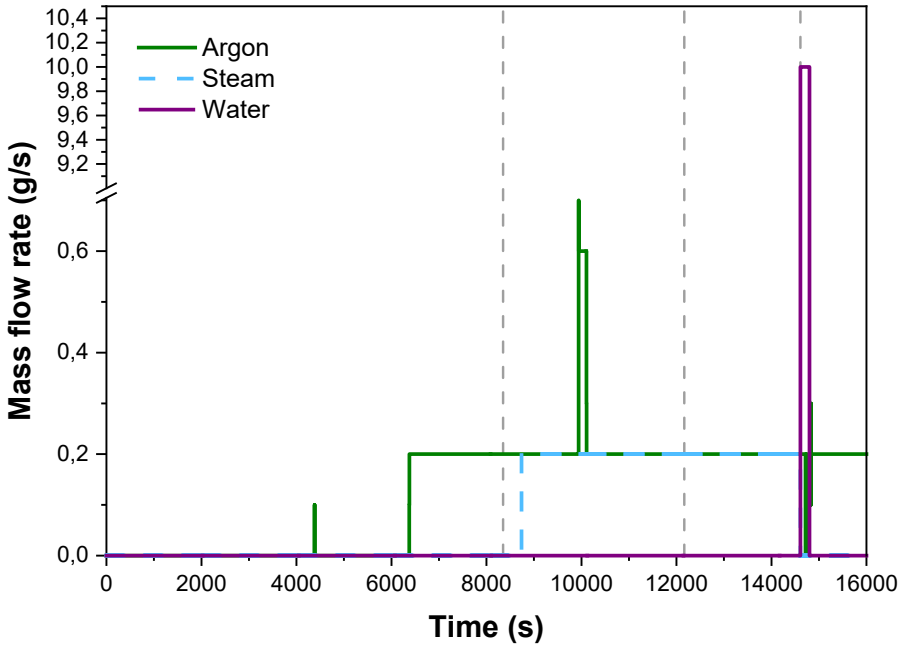

Maximum rod temperature T1_550mm, 1655 °C

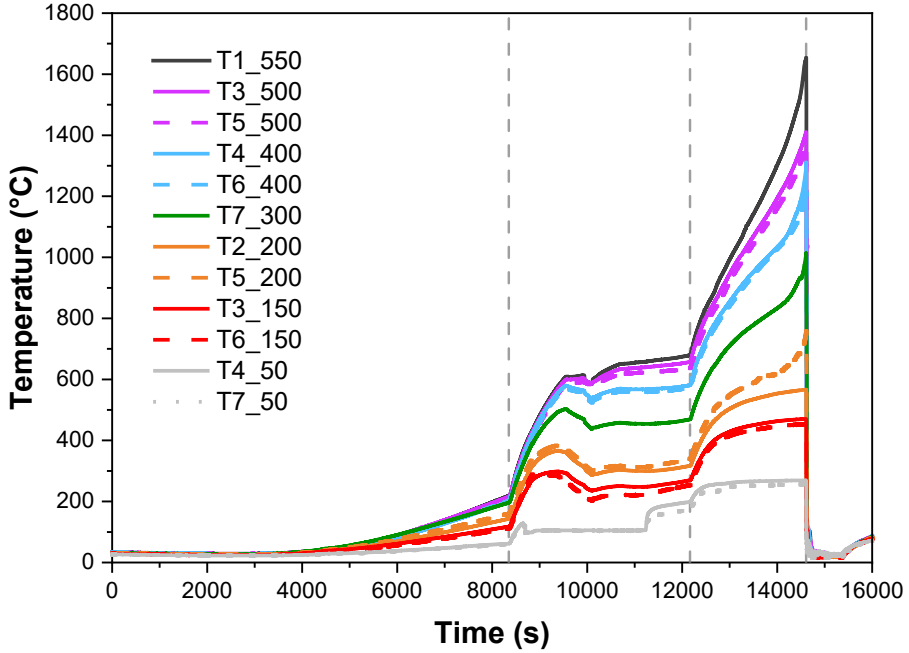

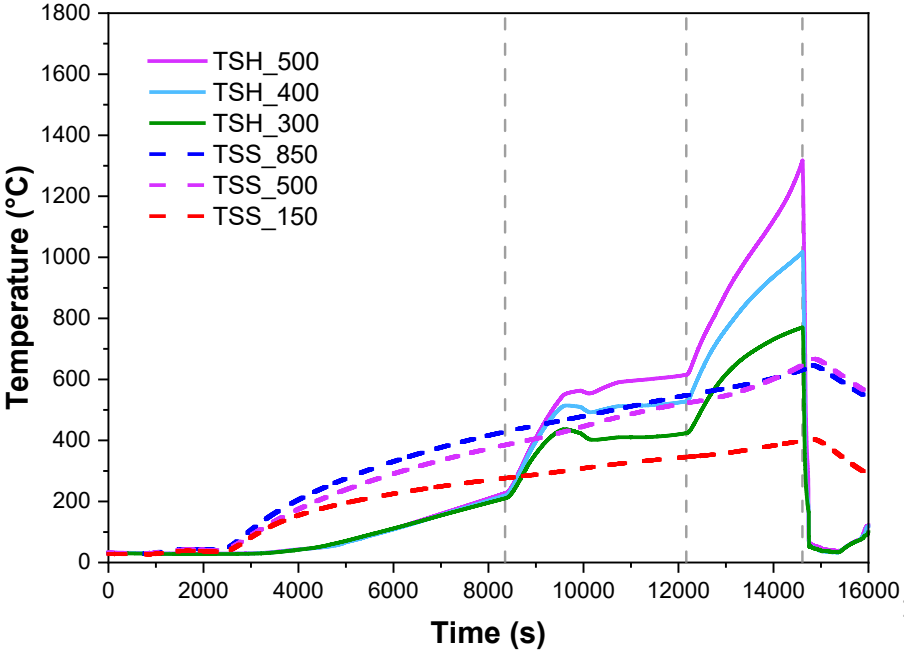

CODEX-ATF results

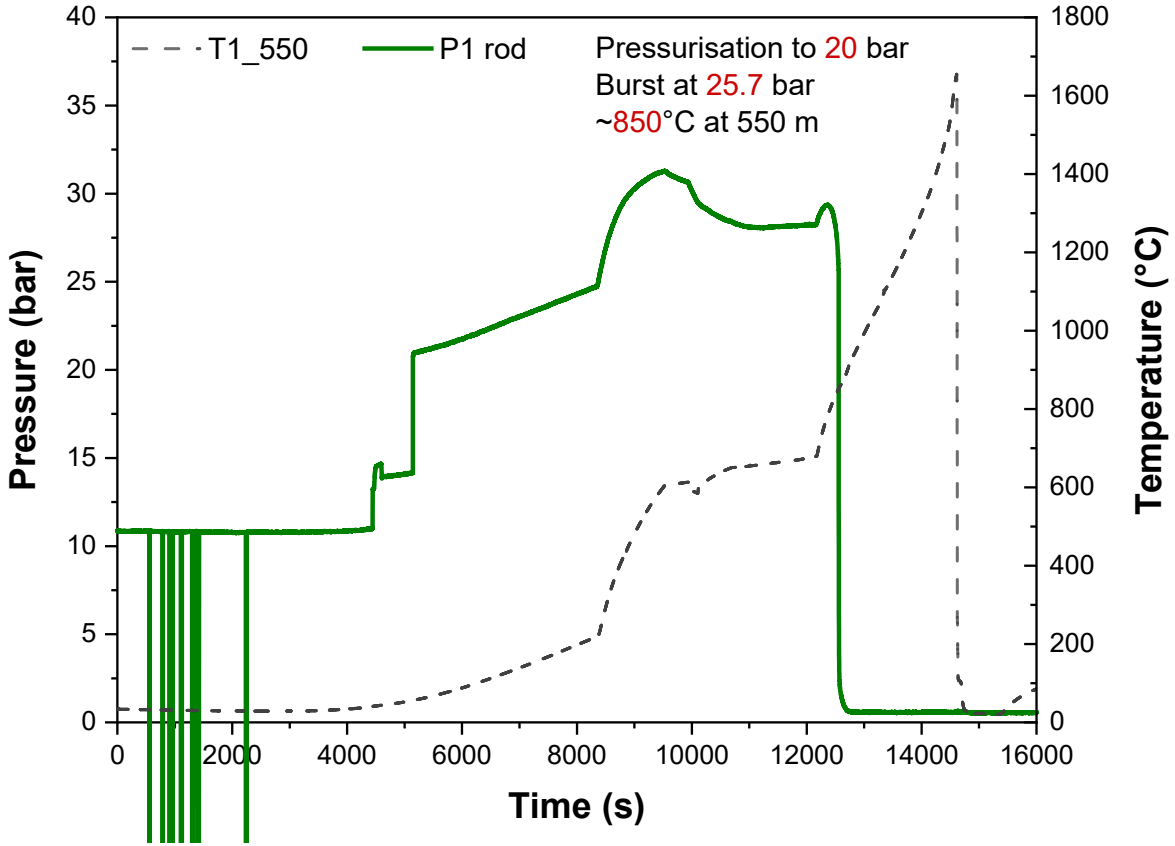

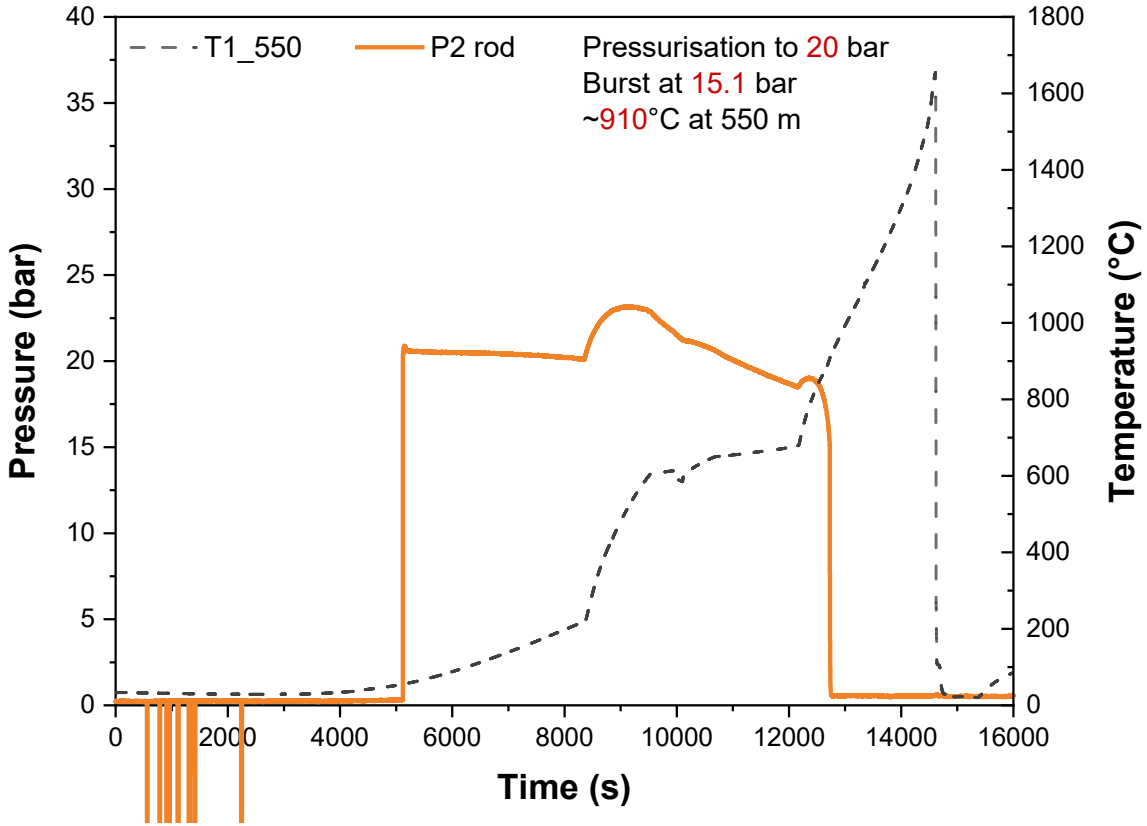

CODEX-ATF results

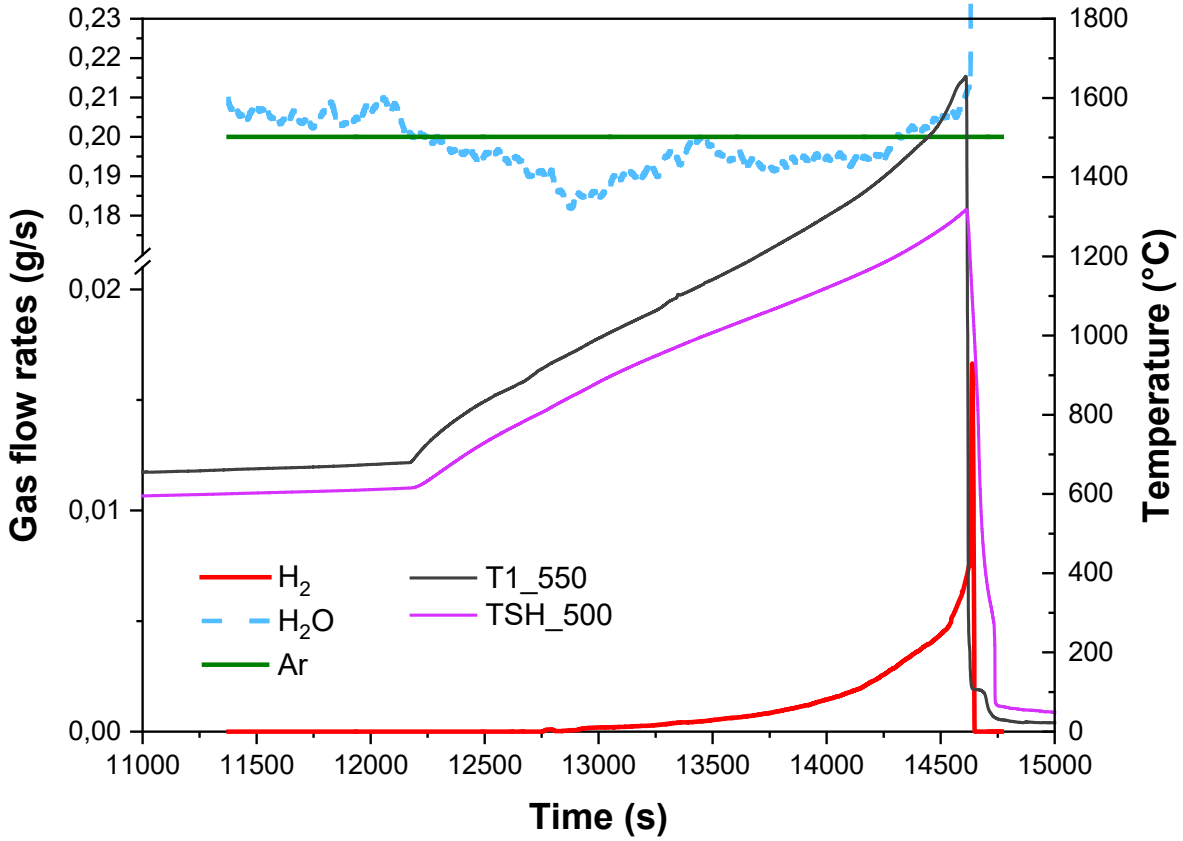

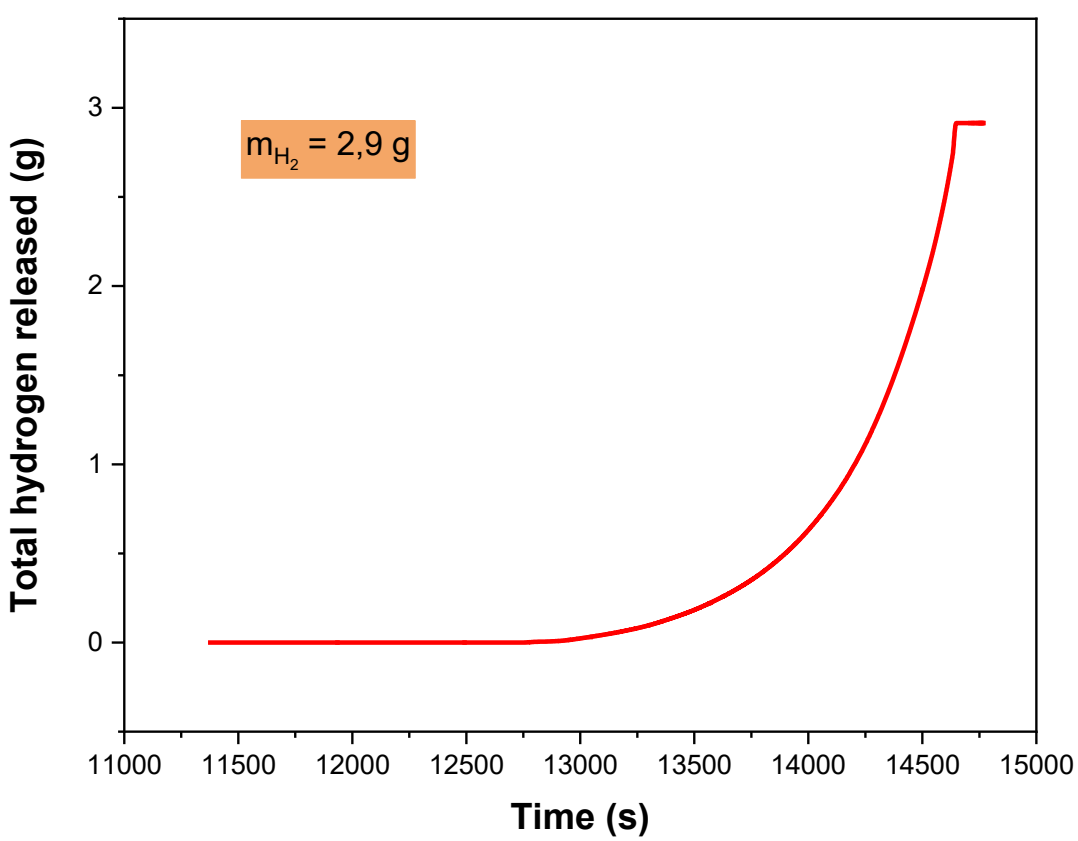

Images of the bundle (endoscopic)

Top of the bundle

Oxide layers were formed on the upper part of the bundle and the shroud

Removed fuel rod segments ~590-630 mm, T_{max}>1350 °C

Rod No. 3 - Cr-coated optZIRLO™

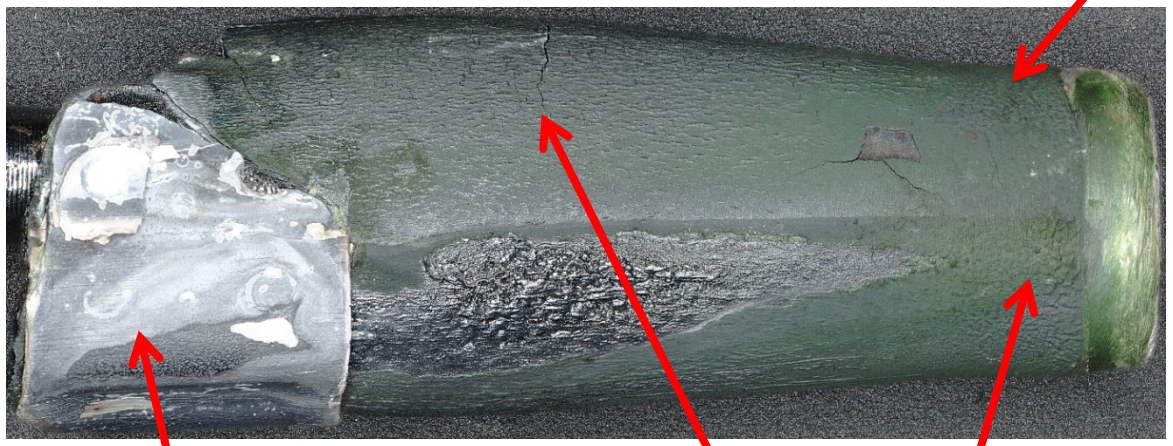

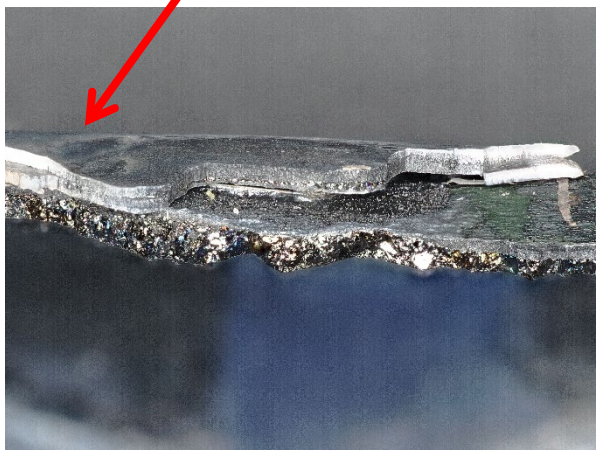

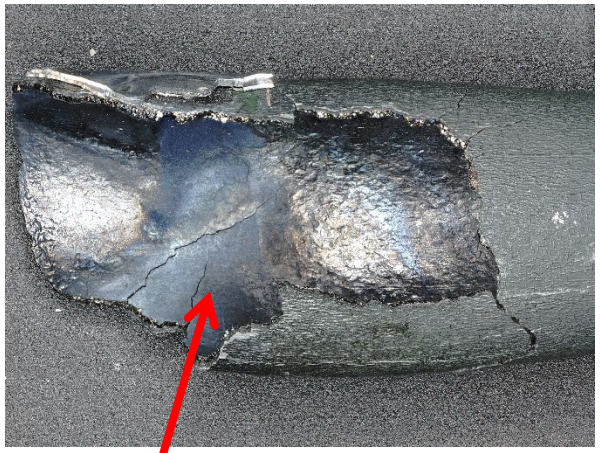

Rod No. 4 - optZIRLO™

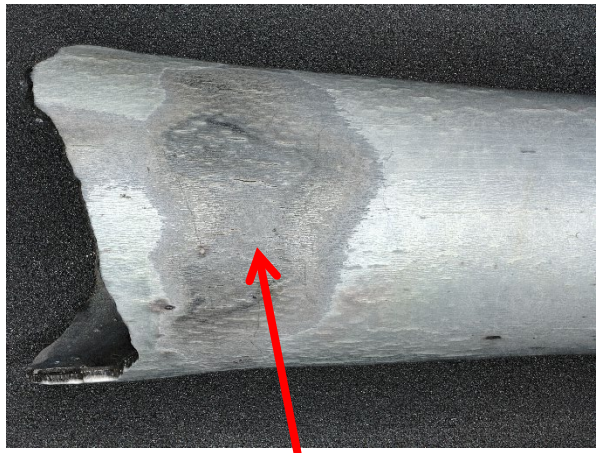

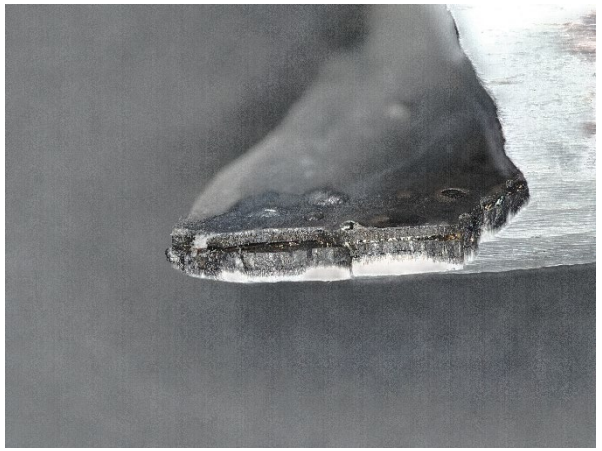

Scanning electron microscope images

Sample from the upper part (~590-610 mm) of Rod No. 3 - Cr-coated optZIRLO™

cracks 200-300 µm

Cr-oxide rich region

Zr rich particles

melted area

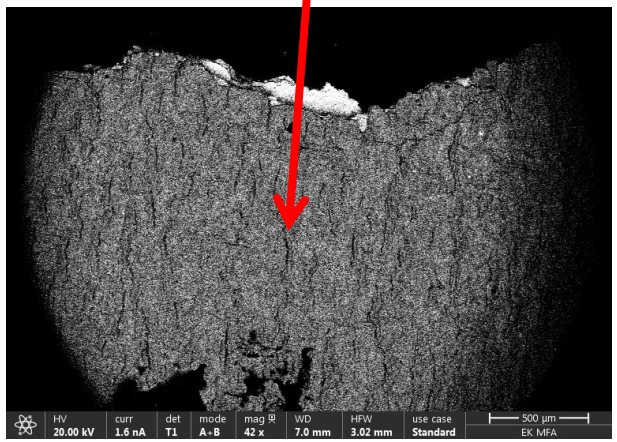

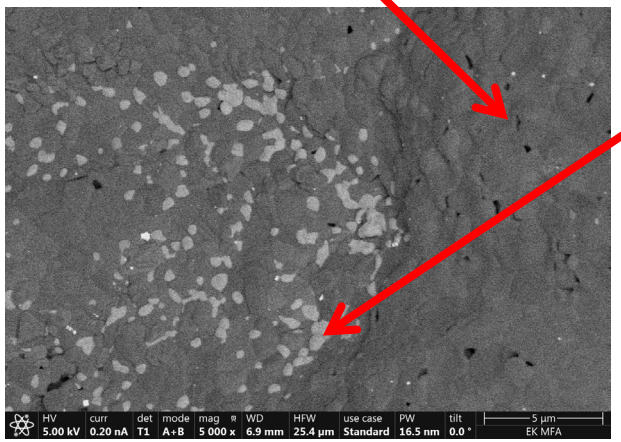

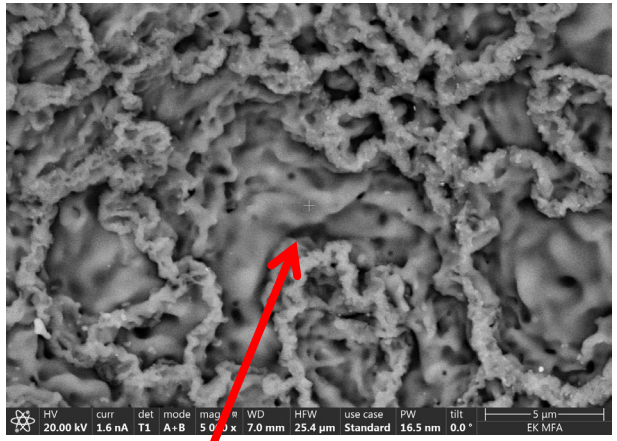

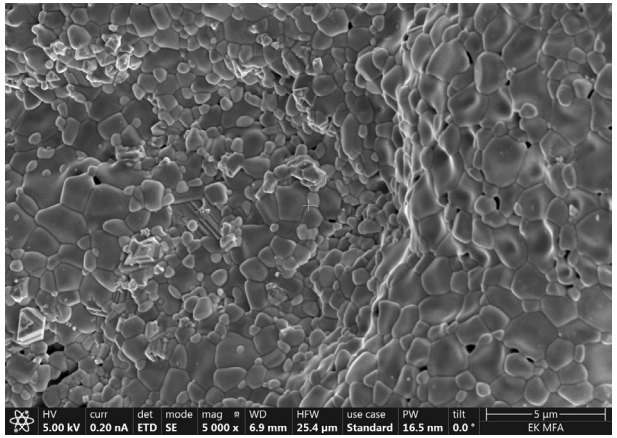

melted area

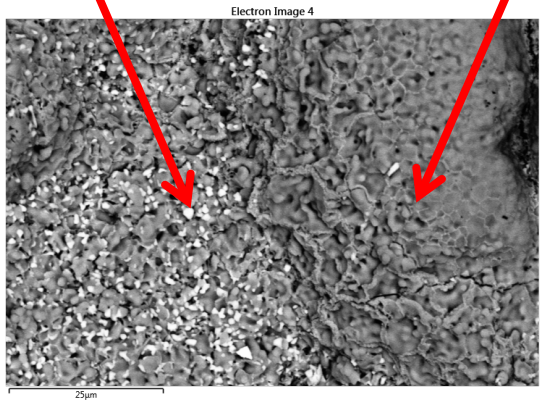

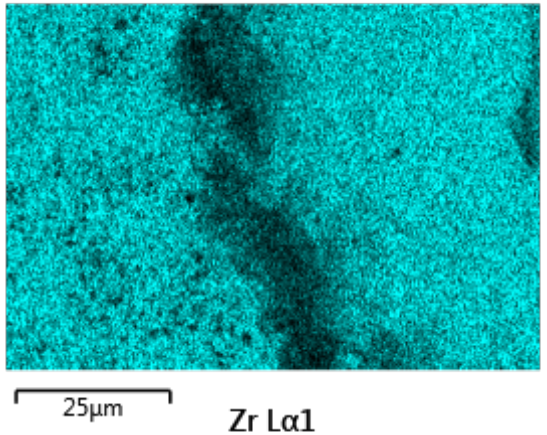

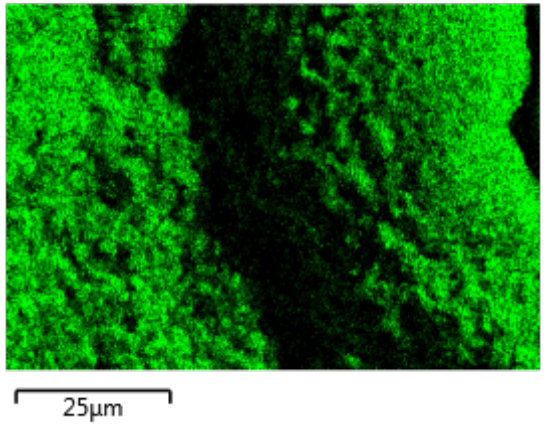

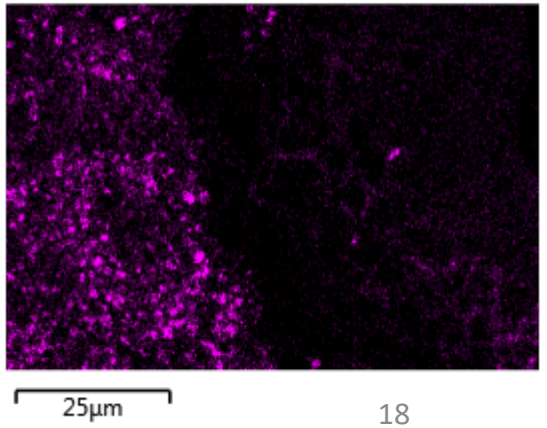

Summary (reached and further steps)

- The CODEX-ATF experiment was successfully carried out.
- The temperature values during the experiment were consistent with the results of the pre-test calculations (NUBIKI, GRS, IBRAE).
- During the experiment the temperature reached 1400 °C, above which eutectic formation occurs.
- Cladding burst took place due to high inner pressure. Consequence of the opening the coolant entered to the rod and started chemical reactions on both sides of the cladding.
- Oxidation of zirconium produced 2.9 g of hydrogen. Cool-down of the bundle was performed with water quench.
- After the experiment, the bundle showed a significant degree of degradation: two cladding broke, debris was created and fell from the upper segment.
- The bundle was pouring with epoxy resin.
- Further steps: post-test examination of CODEX-ATF bundle
  - Computed Tomography (CT) scan of the bundle (measure the geometry of each rod – in progress)
  - Metallography will show the level of oxidation of the bundle (cutting into cross sections, grinding, polishing - optical and scanning electron microscopy).

HUN-REN Centre for Energy Research

A. Endrychova

UJP

Oxidation of various ATF fuel cladding concepts

The presentation deals with the corrosion experiments and high-temperature oxidation of various ATF concepts. The most promising near-term concept is based on Zr-alloys with protective coatings. Thin layers of Cr, CrN, or multilayers such as CrNCr were deposited on the Zr-alloy substrate using the PVD method under various conditions. These protective coatings are used to improve the mechanical and corrosion properties of commonly used Zr-alloys during accident conditions. Another promising concept is the use of new materials for fuel cladding such as chromium– nickel alloys or FeCrAl, which have very high corrosion resistance and good mechanical properties even at high temperatures.

All the mentioned alloys were tested in autoclaves with VVER environment for long-term corrosion tests and in an electric resistance furnace were exposed to high temperatures from 900 to 1300°C for LOCA accident simulation. After the tests, the mechanical and microstructural properties of the different alloys were exanimated by optical or electron microscopy and mechanical testing. The measured data were then used to determine the thickness of the oxide layer, hydrogen absorption and residual ductility, which are the fundamental limits of fuel cladding. The determination of these properties will be essential for the implementation of ATF in commercial reactors.

Oxidation of various ATF cladding concepts

J. Krejčí[1], A. Endrychová[1,2], J. Kabátová[1], V. Rozkošný[1]

[1] UJP PRAHA a.s., [2] ČVUT FS

5.11. 2023, Karlsruhe

ATF CLADDING CONCEPTS

UJP PRAHA

- Development and testing of different concepts of **A**ccident **T**olerant **F**uels (**ATFs**) - 2 concepts:

1. **Protective coatings on zirconium-based alloys**
   - Cr, CrN, CrNCr (IAEA ATF-TS)
2. **New materials**
   - CrNi
   - FeCrAl

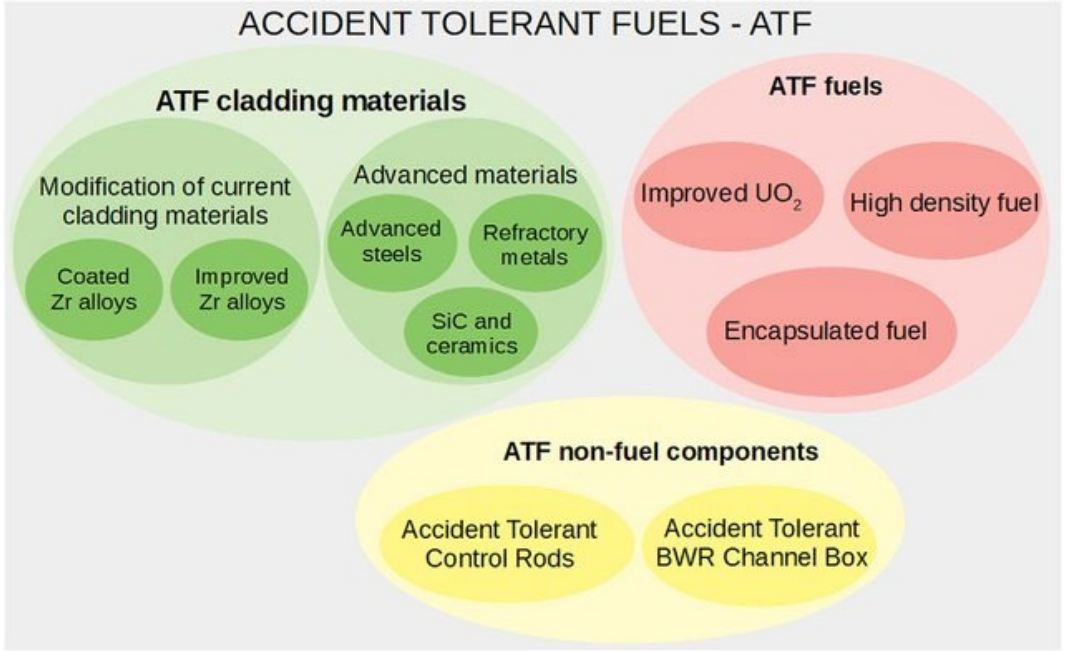

Krejci, Jakub & Sevecek, Martin & Kabátová, Jitka & Manoch, František & Kočí, Jan & Cvrček, Ladislav & Malek, Jaroslav & Krum, Stanislav & Sutta, Pavol & Bublíková, Petra & Halodova, Patricie & Namburi, Hygreeva. (2019). Development and testing of multicomponent fuel cladding with enhanced accidental performance. Nuclear Engineering and Technology. 52. 10.1016/j.net.2019.08.015.

Long-term corrosion tests in autoclaves

UJP PRAHA

Corrosion tests in autoclaves

- Static autoclaves (volume 4 dm^3)
- Environment:

  VVER (B: 1050 ppm, K: 16 ppm, Li: 1 ppm):
  360 °C, 18.6 MPa

Sample	Alloy	Coating	Thickness of coating (μm)	Methods of deposition
ICr	Zr1Nb	Cr	6,4	arc-PVD
ICrN	Zr1Nb	CrN	5,4	arc-PVD
ICrNCr	Zr1Nb	Cr/CrN	7,3	arc-PVD

Alloy	Cr	Al	Y	Mn	Ni	Balance
CrNi	41-43	< 0,4	-	< 0,2	balance	Ni
FeCrAl (B136Y3)	13	6,2	0,03	-	-	Fe
ADSS #B51	16,3	6,14	-	1,04	18,7	Fe

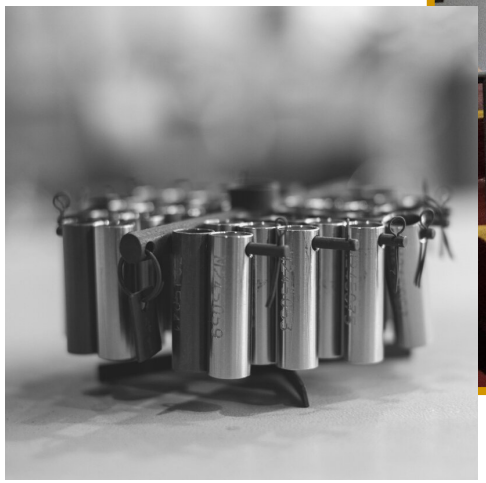

Long-term corrosion tests in autoclaves

UJP PRAHA

VVER (B: 1050 ppm, K: 16 ppm, Li: 1 ppm): 360 °C, 18.6 MPa

Coated samples – oxidation 10x lower

CrNi, **ADSS** – almost no oxidation

FeCrAl (B136Y3) - dissolves

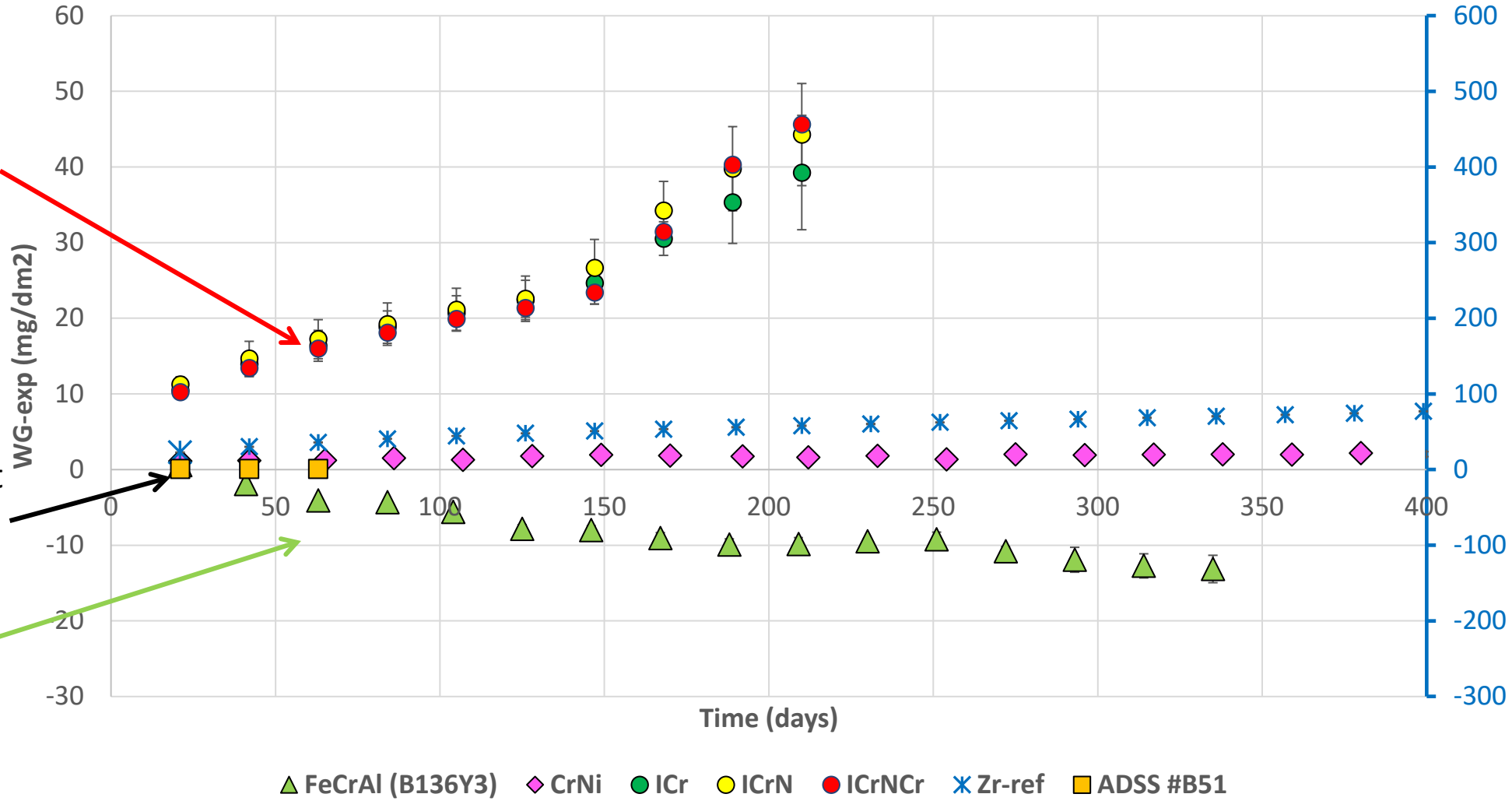

LOCA: high-temperature oxidation

UJP PRAHA

High-temperature oxidation in steam

- Electric resistence furnance
- Steam + Ar at atmospheric pressure
- Double-sided oxidation + direct quenching
- Post-experimental examination
  - WG
  - Destructive analyses

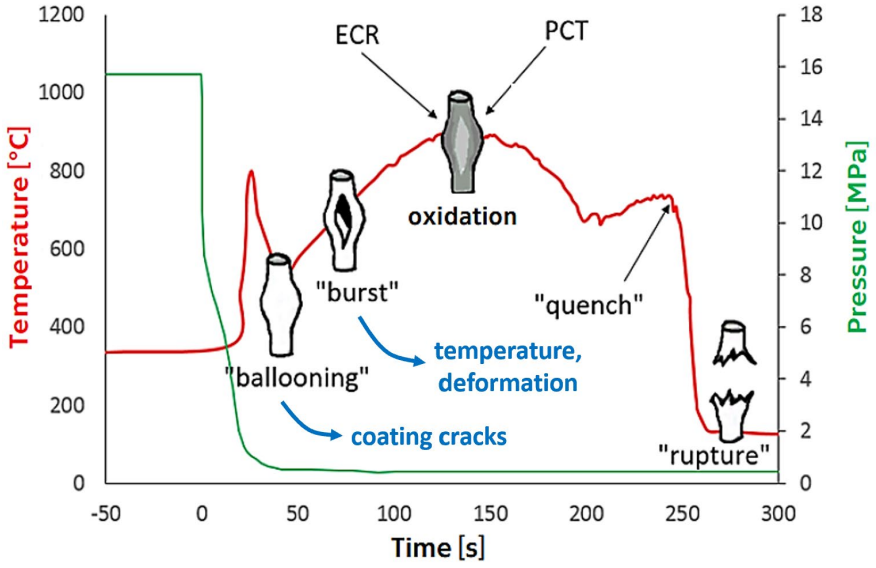

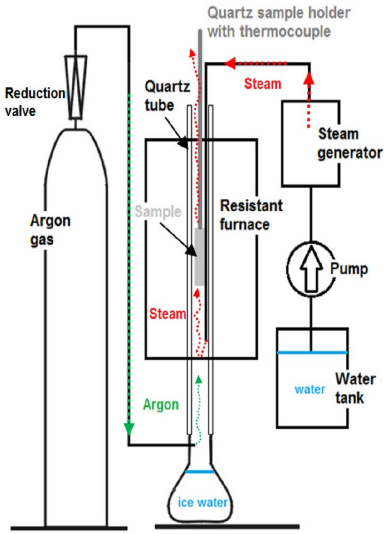

1. Protective coatings on zirconium-based alloys

UJP PRAHA

1. **Uncoated Zr (Zr1Nb)**
   - ∅ 9.1 × 7.9 mm
   - Fuel cladding
2. **Zr1Nb + Cr-coating**
   - PVD method (Hauzer Flexicoat 850)
   - Thickness of coating 6,4 µm
3. **Zr1Nb + CrN-coating**
   - Thickness of coating 5,4 µm
4. **Zr1Nb + CrNCr-coating**
   - Thickness of coating 7,3 µm

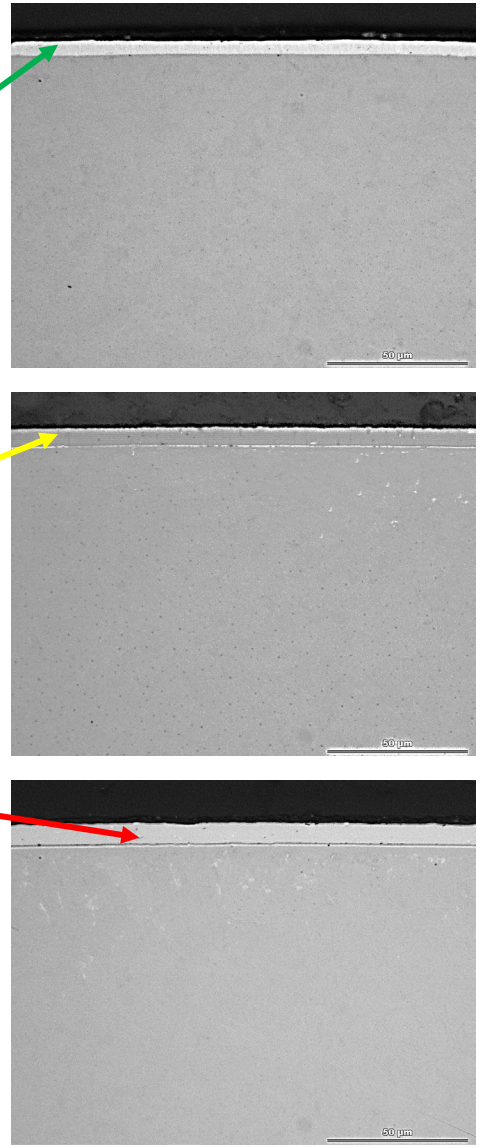

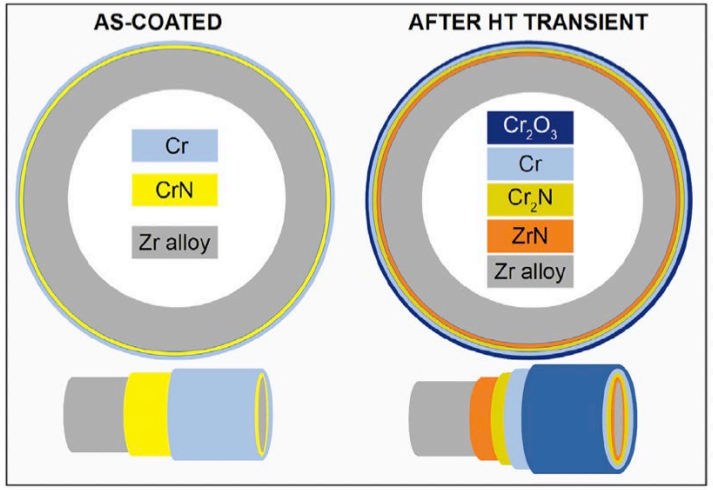

Fig. 19. The design of the multicomponent cladding that avoids Zr–Cr eutectic reaction and material inter-diffusion during high-temperature transients. Nitrogen is released from CrN to form ZrN above 975°C.

KREJČÍ, J.; KABÁTOVÁ, J.; MANOCH, F.; KOČÍ, J.; CVRČEK, L.; MÁLEK, J.; KRUM, S.; ŠUTTA, P.; BUBLÍKOVÁ, P.; HALODOVÁ, P.; NAMBURI, H. K.; ŠEVEČEK, M. Development and testing of multi- component fuel cladding with enhanced accidental performance. Nuclear Engineering and Technology

HT oxidation of zirconium-based alloys with protective coating - results

UJP PRAHA

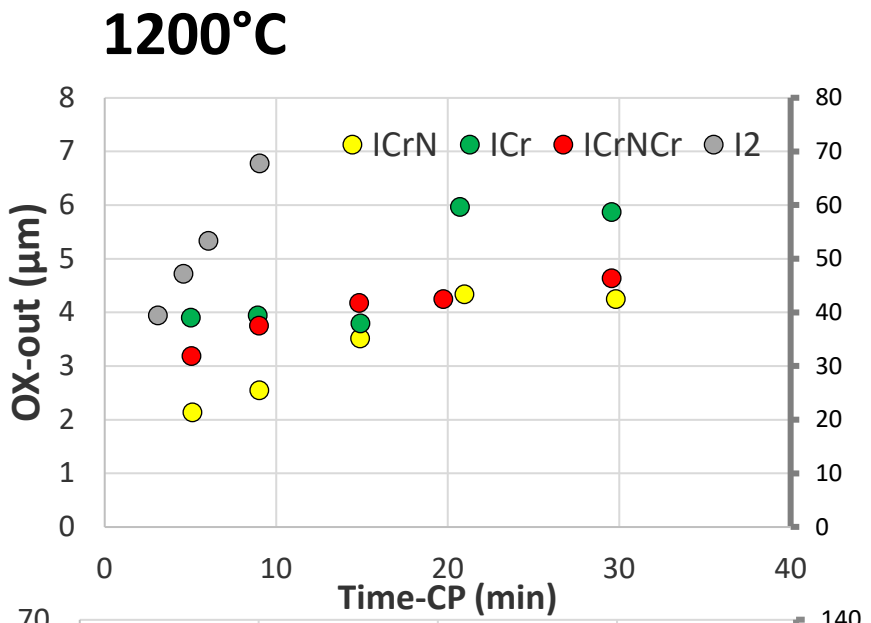

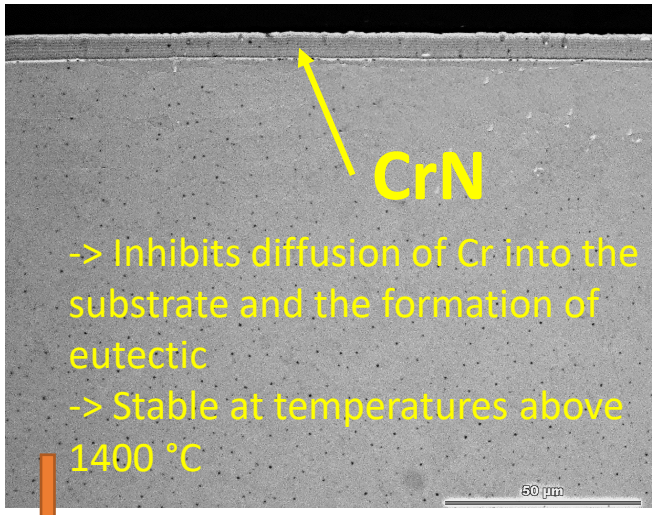

Zr1Nb+CrN (before oxidation)

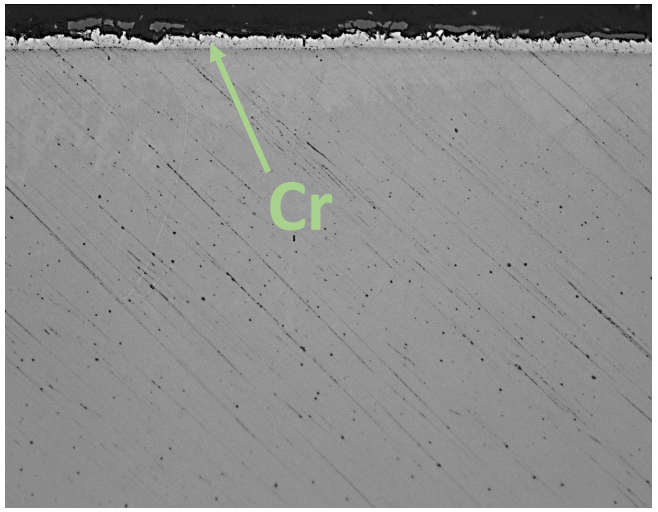

Zr1Nb+Cr (1200°C / 9 min)

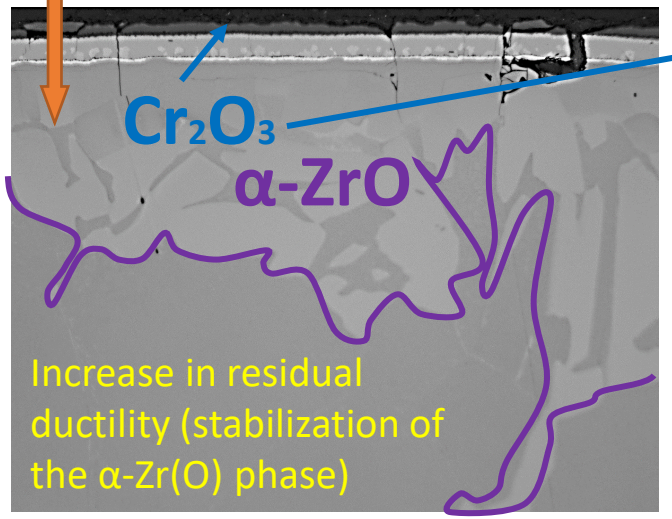

Zr1Nb+CrN (1200°C / 30 min)

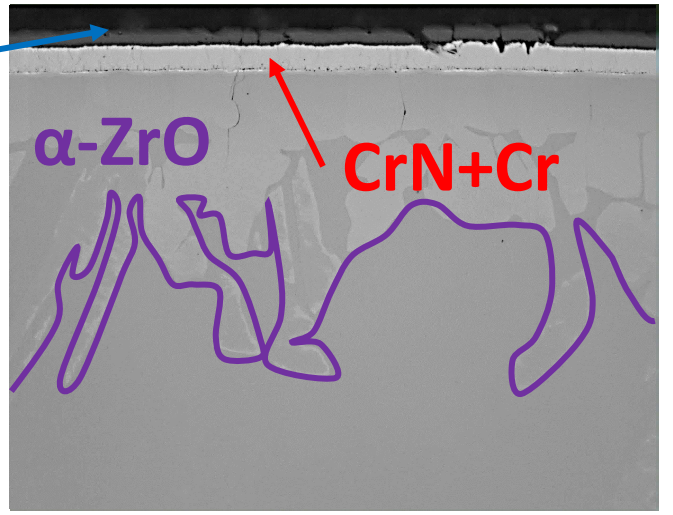

Zr1Nb+CrNCr (1200°C / 30 min)

HT oxidation of zirconium-based alloys with protective coating - results

UJP PRAHA

- **Weight gain**
  - Coating effectively prevents oxidation through the outer wall of the coating (~10x lower than uncoated samples)

- **Residual ductility**
  - The coating extends the ductile-brittle transition time
  - Degradation of Cr-coating because of diffusion (X CrN)

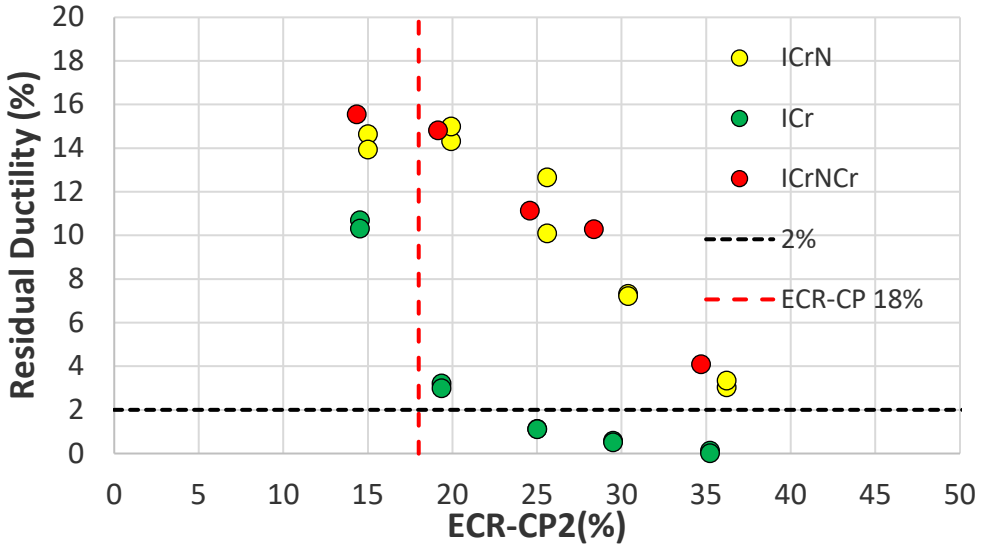

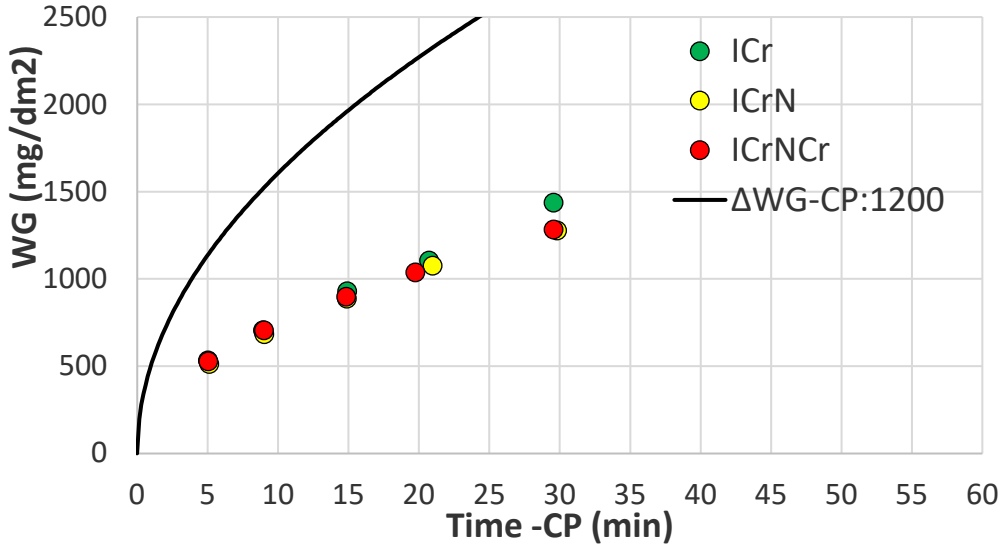

HT oxidation of zirconium-based alloys with protective coating

UJP PRAHA

- **Degradation of Cr-coating**
  - Difussion of Cr into Zr-substrate (L-phase formation at the interface + enrichement of β-Zr Cr) – brittle phase at Cr above ~ 1.5wt.%
  - Diffusion of Cr into Zr -> stabilization of ß-Zr -> increased solubility of O -> embrittlement even in areas of undamaged coating
  - Degradation of the coating by transport of Zr to the outer interface
  - Fast acceleration of kinetics after loss of protective properties of Cr

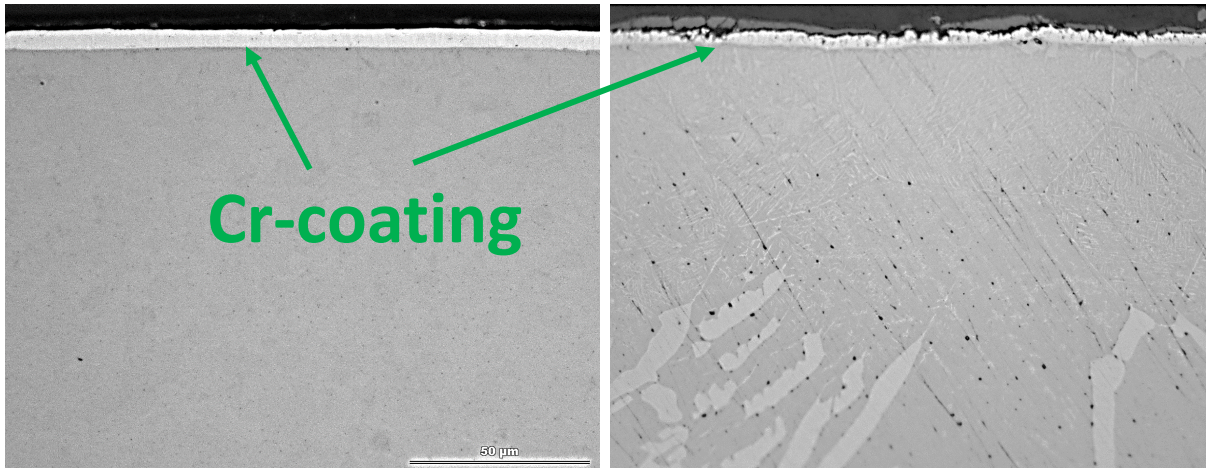

Zr1Nb+Cr (before oxidation, 1200°C / 15 min)

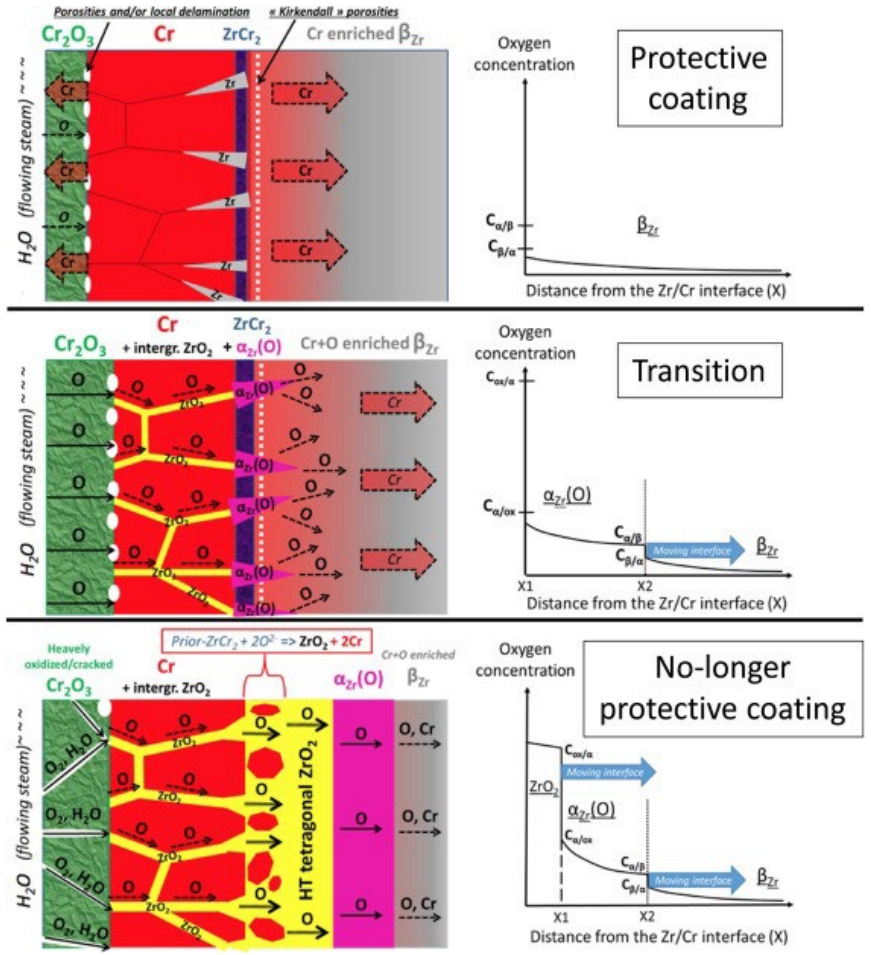

Brachet et al. High temperature steam oxidation of chromium-coated zirconium-based alloys: Kinetics and proces, Corrosion Science, 2020

HT oxidation of zirconium-based alloys with protective coating – coating methods

UJP PRAHA

- Different coating methods
  - Arc depositioning
  - Magnetron sputtering
  - Coldspray
- The quality of the coating does not depend on the method used, but on the parameters (energy, temperature)
- Coating damage-> oxidation under the layer

Zr1Nb+Cr (1200°C / 9 min)

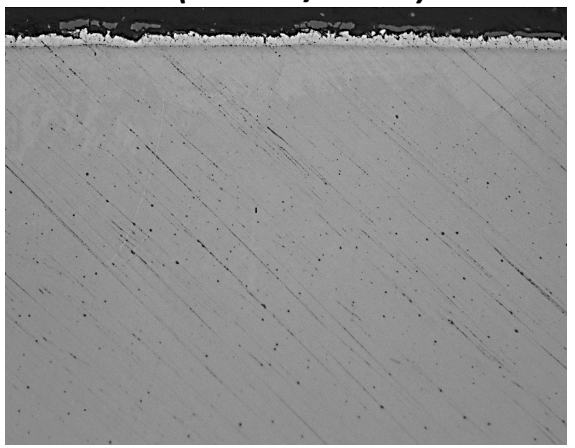

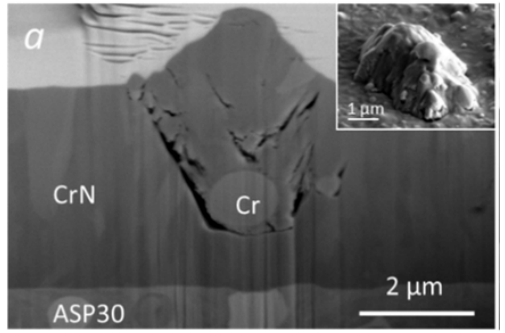

Defect - droplet

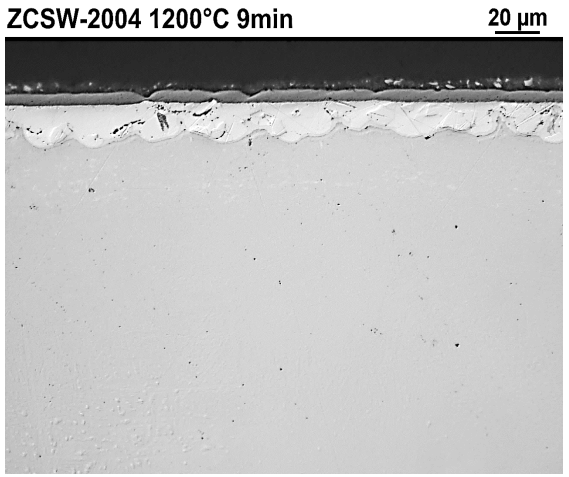

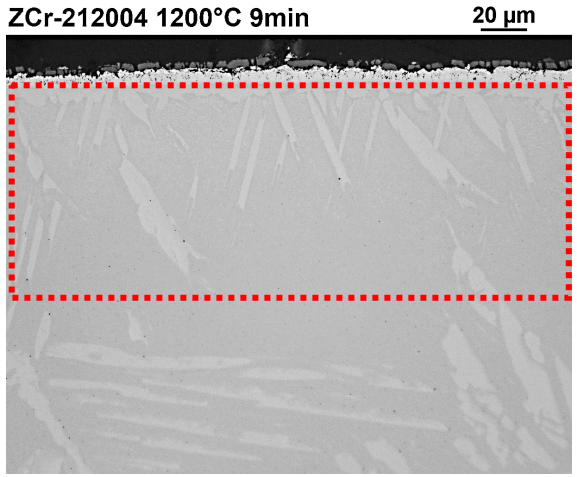

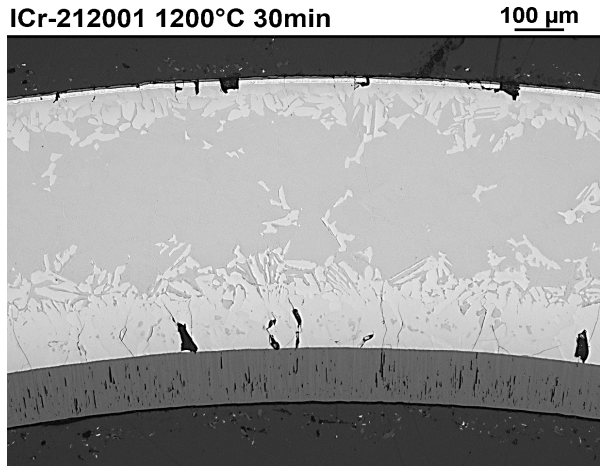

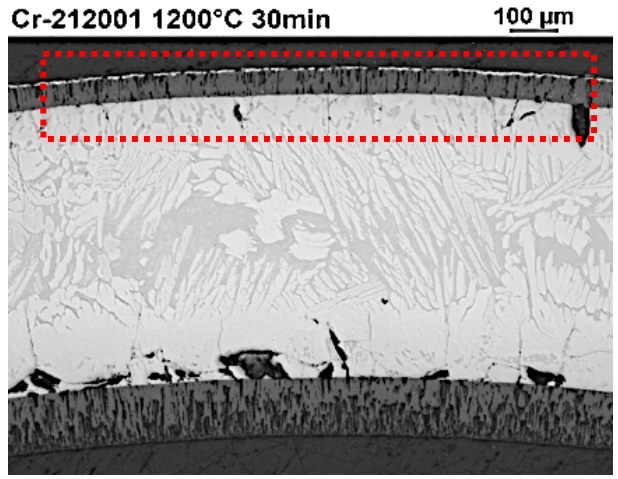

ZCSW - coldspray

Panjan, Peter & Drnovšek, Aljaž & Gselman, Peter & Cekada, Miha & Panjan, Matjaž. (2020). Review of Growth Defects in Thin Films Prepared by PVD Techniques. Coatings. 10. 447. 10.3390/coatings10050447.

2. FeCrAl

- Ferritic alloy (Kanthal®), various content of Fe-Cr-Al
- **Highly corrosion resistant**–Al_2O_3 oxide formation
- High effective cross section for neutron absorption (-> cladding 400 μm)
- Material tested
  - B136Y3 from QUENCH-19 experiment, fabricated by Oak Ridge National Laboratory, Fe-6.2Al-13Cr-0.03Y (supplied from KIT 2022)

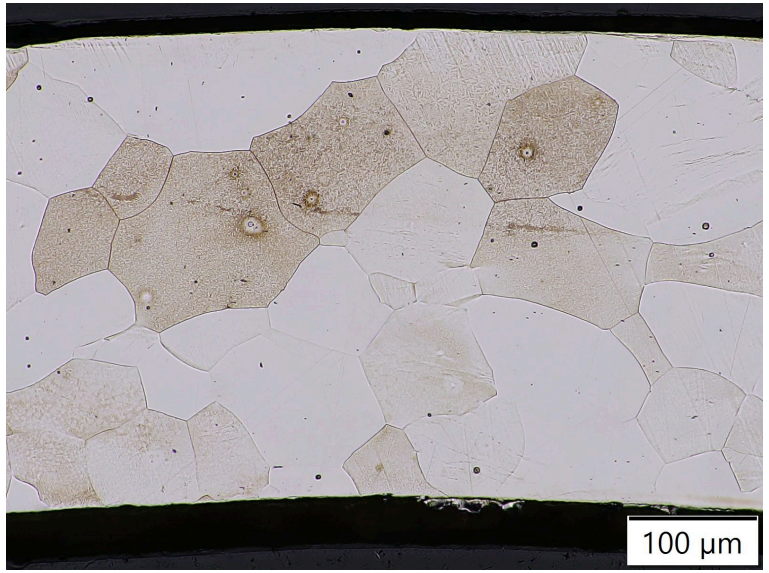

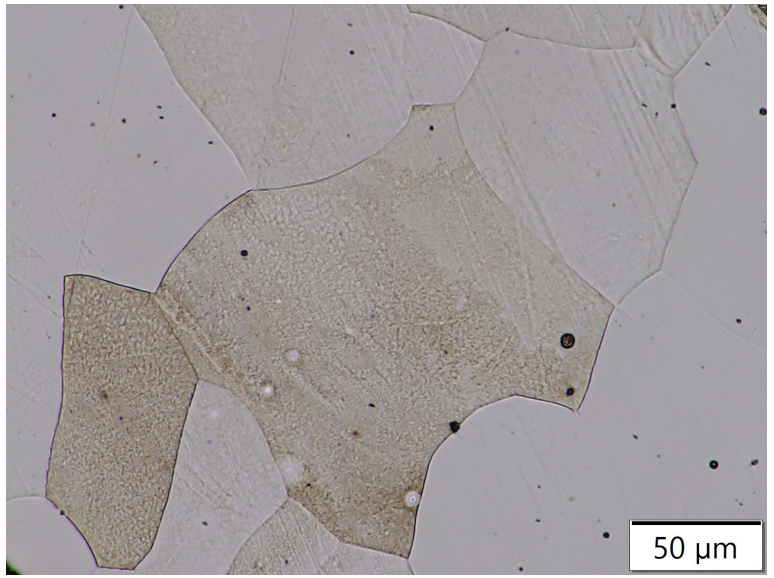

HT oxidation of FeCrAl

- Formation of **α-Al_2O_3** -> hight oxidation resistence
- At temperatures ~ 1360°C Fe oxides significaly faster kinetics
- **Al_2O_3 formation depends on heating rate** -> ramp gradually, otherwise it breaks down and Fe oxides are formed
- Above 1350°C kinetics cannot be done without continuous sample weighing

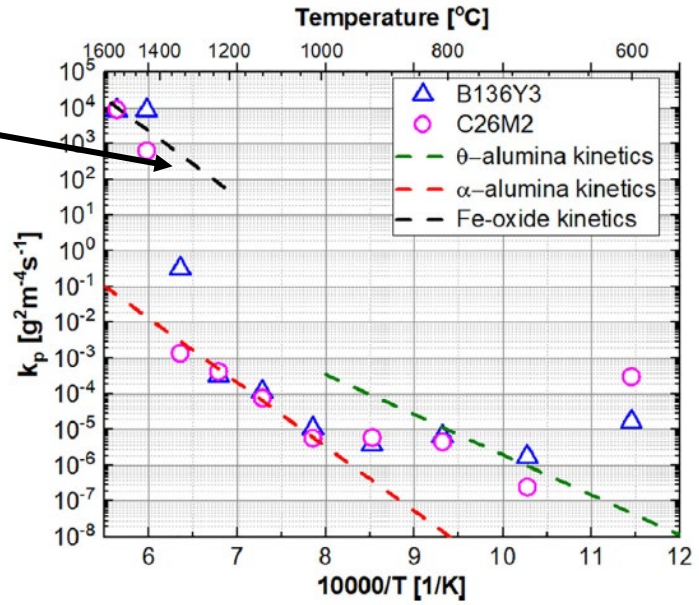

Fig. 10. Parabolic rate constants of B136Y3 and C26M2 as a function of temperature with the parabolic constants of Fe-oxide [18], α-alumina [18] and θ-alumina [19].

Chaewon Kim, Chongchong Tang, Mirco Grosse, Yunhwan Maeng, Changheui Jang, Martin Steinbrueck, Oxidation mechanism and kinetics of nuclear-grade FeCrAl alloys in the temperature range of 500–1500 °C in steam,Journal of Nuclear Materials, Volume 564, 2022, 153696, ISSN 0022-3115, https://doi.org/10.1016/j.jnucmat.2022.153696.

HT oxidation of FeCrAl B136Y3

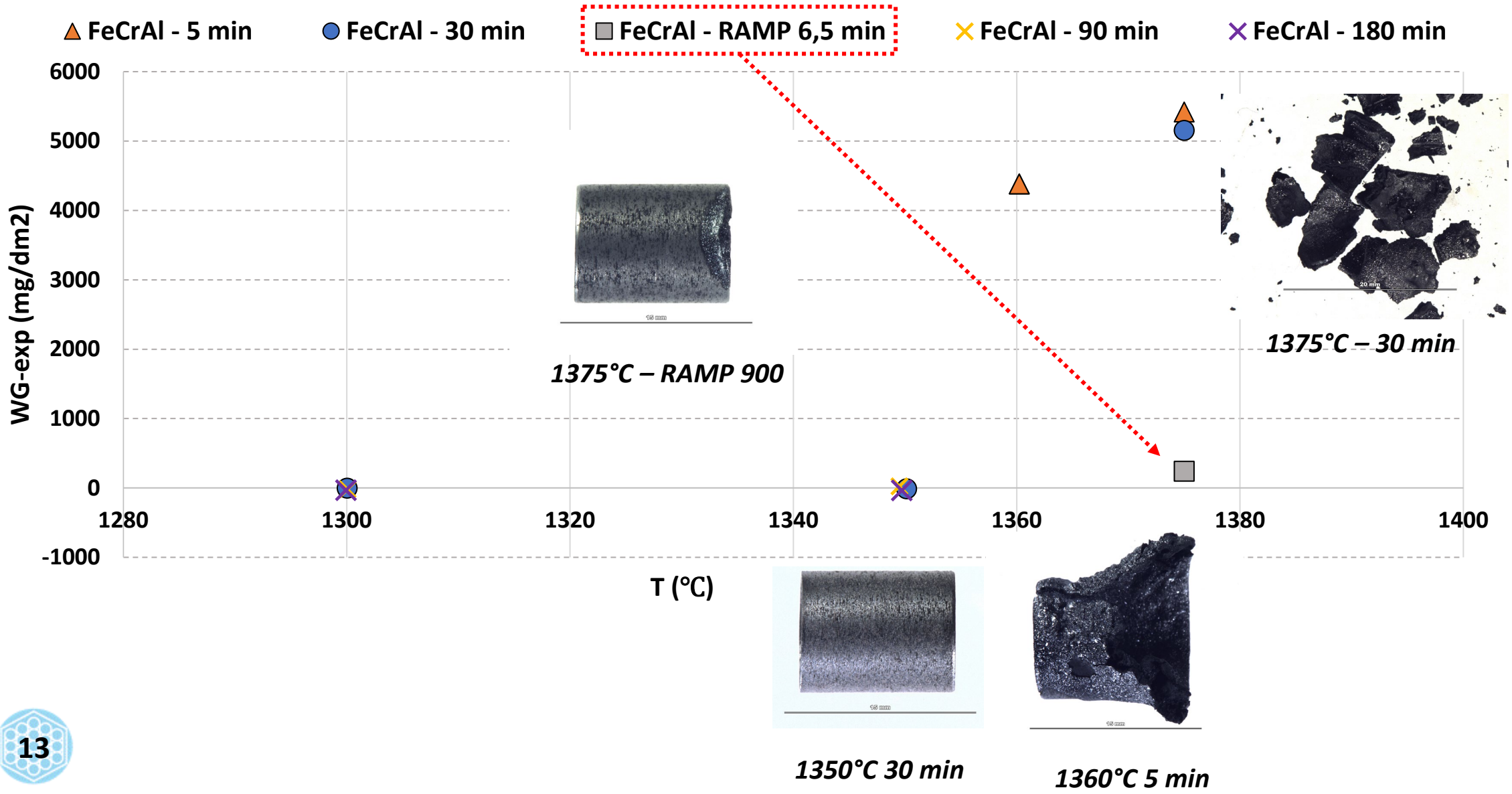

HT oxidation of FeCrAl – SEM

Fe-6.2Al-13Cr-0.03Y

Elt.	Line	Intensity (c/s)	Error 2-sig	Conc	Units
Al	Ka	10.88	0.518	4.11	wt.%
Cr	Ka	37.14	0.904	10.53	wt.%
Fe	Ka	169.72	1.802	85.36	wt.%

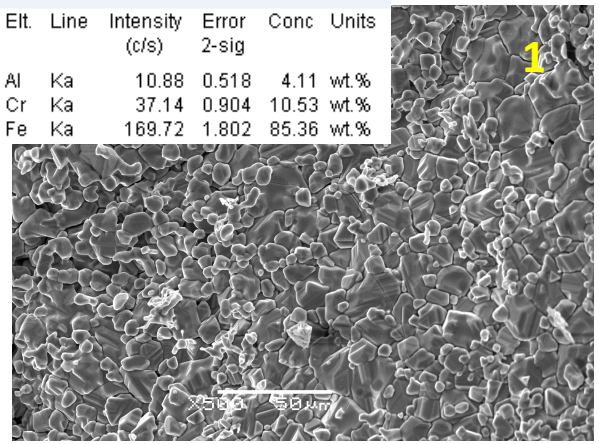

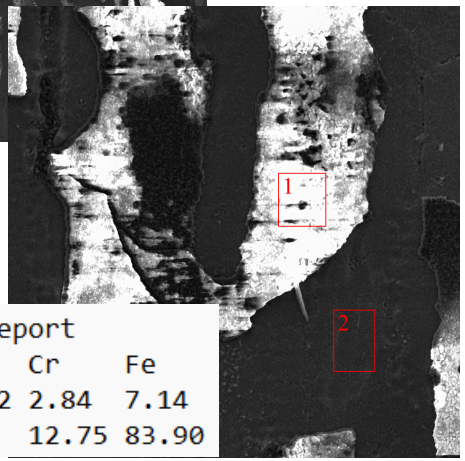

Conc Spectrum Report			
Spectrum	Al	Cr	Fe
Image1-1	90.02	2.84	7.14
Image1-2	3.34	12.75	83.90

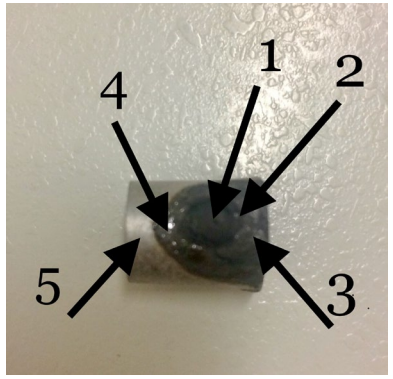

Elt.	Line	Intensity (c/s)	Error 2-sig	Conc	Units
Al	Ka	1.01	0.454	0.33	wt.%
Cr	Ka	1.75	0.488	0.26	wt.%
Fe	Ka	243.16	2.457	99.41	wt.%

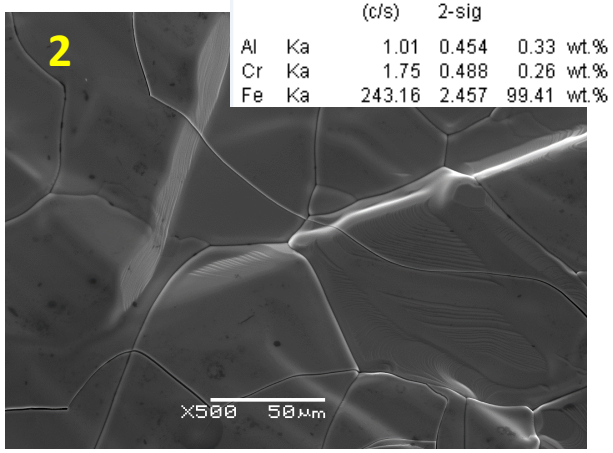

Elt.	Line	Intensity (c/s)	Error 2-sig	Conc	Units
Al	Ka	9.97	0.457	4.33	wt.%
Cr	Ka	5.14	0.406	1.32	wt.%
Fe	Ka	168.96	1.653	94.35	wt.%

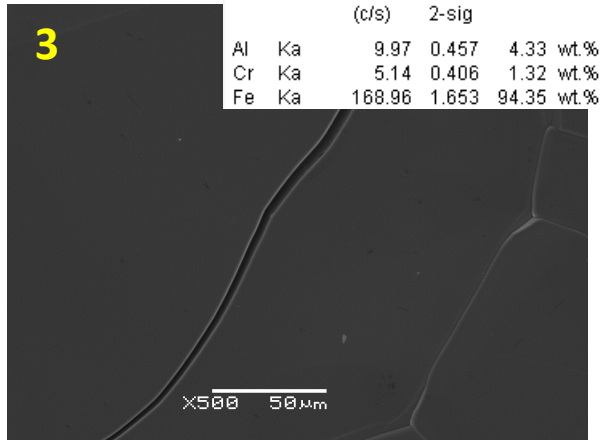

3. Chromium-Nickel alloy

- ∅ 8.2 × 7.2 mm
- Ni-(42%)Cr-(1.5%)Mo
- FCC austenitic structure
- Grain size ~ 10.5 µm
- Oxidation rate several orders of magnitude lower than Zr-alloys

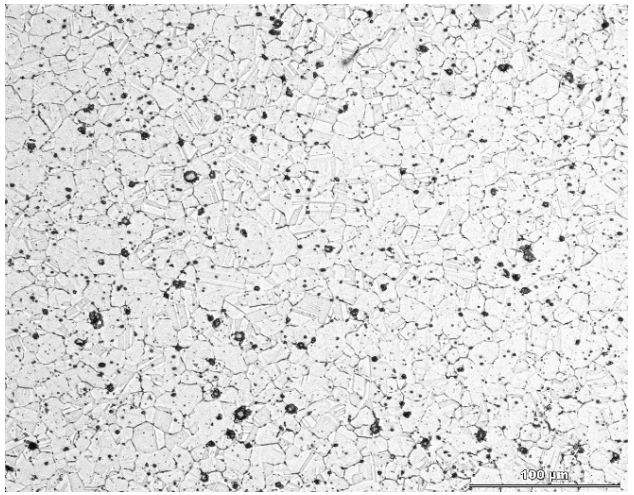

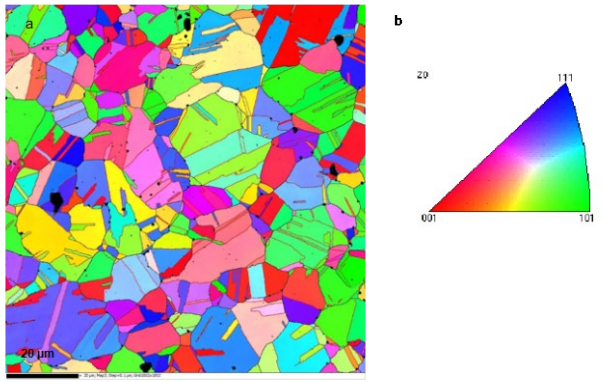

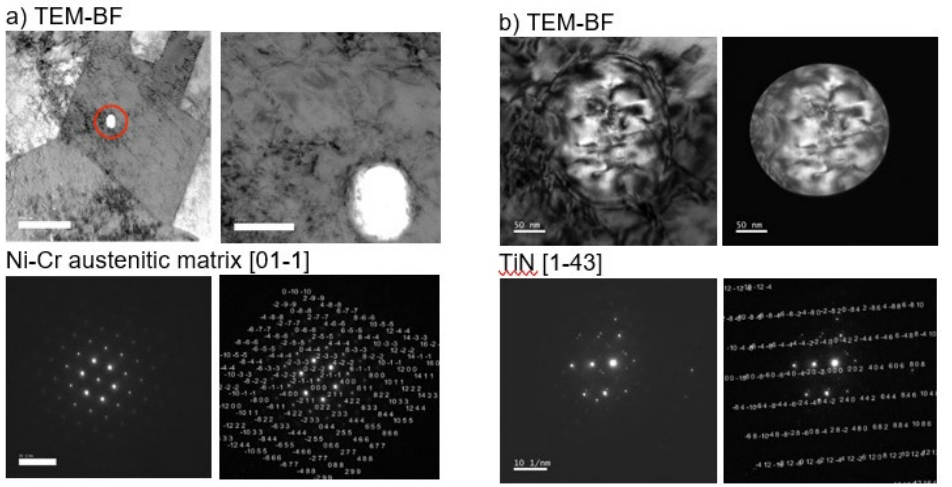

HT oxidation - metallography

- Determination of kinetics in the temperature range 800 to 1300°C based on weight gain and metallography results
- Determination of oxide (Cr2O3) and metal thickness => **no significant wall loss**
- Difficult to determine for **lower temperatures** (for long exposures maximum units of µm)
- **Oxide depletion at temperatures above 1200 °C** => Effect on determination of oxidation kinetics (must use metallography data)

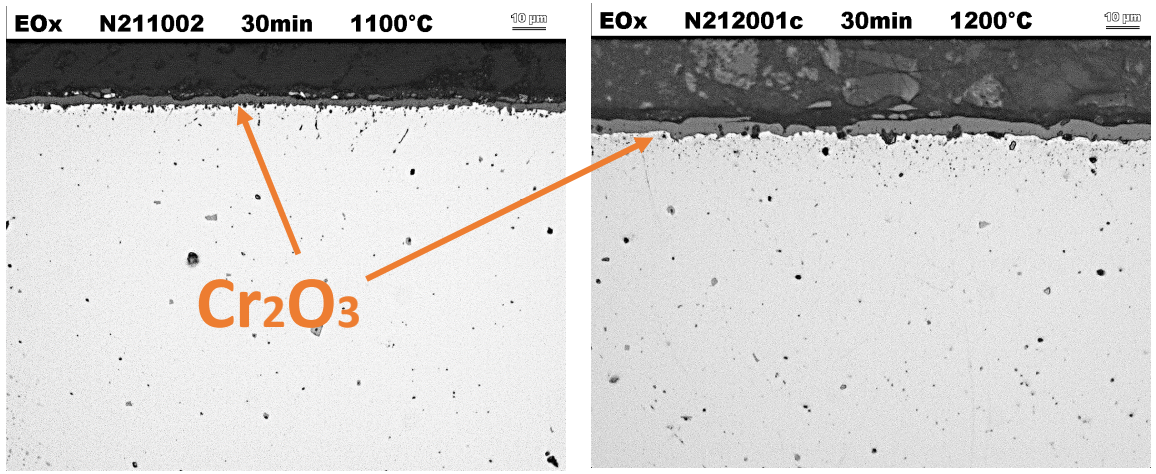

Growth of the oxide layer- steam + Ar

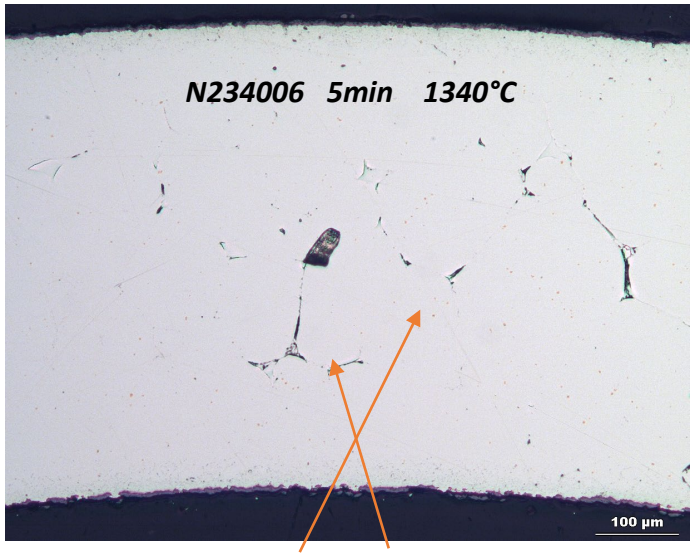

near the eutectic (1346°C), melting occurs in the region at the grain boundaries

Conclusion

UJP PRAHA

	Advantages	Disadvantages
Zr-alloy	• Low Σ_a • High resistance to corrosion cracking	• Oxidation and hydrogen production/absorption
Zr-alloy with protective coating	• Lower weight gain and do not absorb hydrogen • Effectively prevents oxidation at elevated temperatures • Reduction of hydrogen production (X reaction of zirconium with water) and also heat production	• The coatings are hard, brittle and less able to resist plastic deformation • Diffusion of Cr into Zr and stabilization of beta-Zr
FeCrAl	• Significantly reduced oxidation (normal and emergency conditions) • Significantly reduced hydrogen absorption • High residual ductility after steam oxidation	• Corrosion -> dissolution of Al-oxides • Radiative embrittlement • Reduction of strength at higher temperatures • High effective cross section for neutron absorption (cladding 400 μm)
CrNi	• No embrittlement at low temperatures • High corrosion resistance • Good mechanical properties at high temperatures • Resistance to corrosion cracking	• Degradation of mechanical properties in the temperature range 450-550 °C • Melting at ~ 1355 °C • High Σa for thermal neutrons

Thank you for your attention

This work was perfomed within project IAEA ATF-TS, TAČR
K04030168, TN02000018, TM04000018

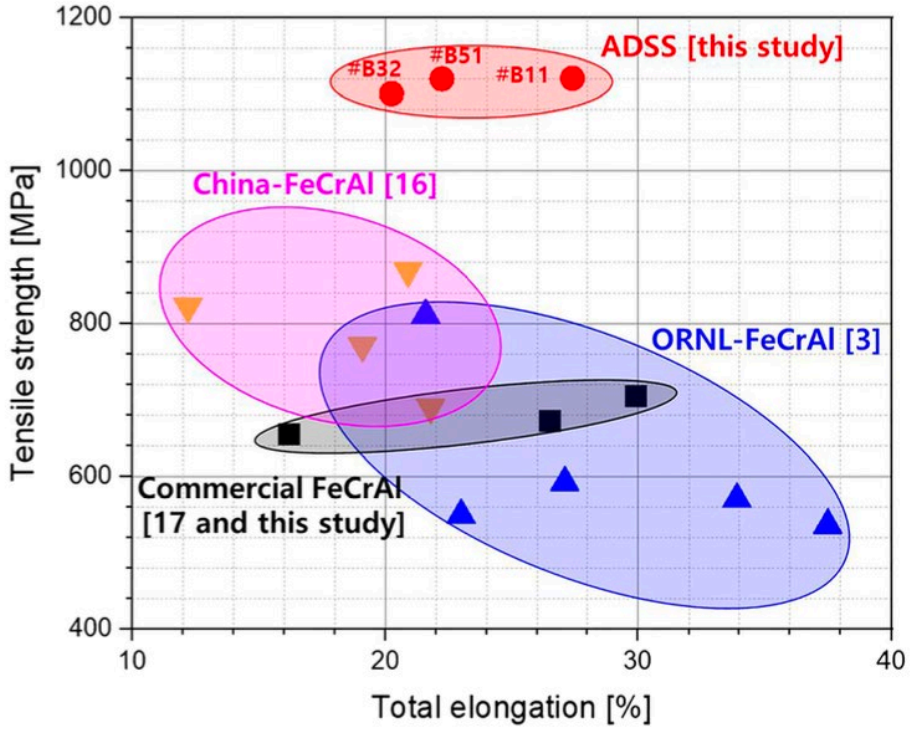

FIGURE 8 Tensile strength as function of total elongation of alumina-forming duplex stainless steel (ADSS) alloys, wrought FeCrAl model alloys, and commercial FeCrAl alloys [Colour figure can be viewed at wileyonlinelibrary.com]

TABLE 2 Tensile properties tested at room temperature for reference materials and alumina-forming duplex stainless steel (ADSS) alloys

Materials (Grade)	Remark	Yield Strength, MPa	Tensile Strength, MPa	Elongation, %
ADSS #B11	CR + FA condition	929 ± 30	1198 ± 10	20.5 ± 0.4
ADSS #B32		1026 ± 9	1264 ± 12	13.9 ± 1.0
ADSS #B51		930 ± 32	1129 ± 38	18.5 ± 0.8
APM	Commercial alloys	528 ± 19	698 ± 13	11.9 ± 0.6
310S		299 ± 8	580 ± 15	51.9 ± 1.1
DSS 2205		629 ± 24	830 ± 24	34.2 ± 1.2
Zircaloy-4	Reference materials	298 ± 9	481 ± 1	18.2 ± 0.6

A. Mohamad

JAEA

Transition of the $Zr(Cr, Fe)_2$ intermetallic phase up to the eutectic temperature

The development of Accident Tolerant Fuel (ATF) had been started by conducting the investigation on new concepts to improve the safety of Light Water Reactors (LWRs). It is well known that the Cr coating on Zry cladding has shown an improvement in behavior under accident conditions and normal operation [1-4]. Many research groups around the world have conducted the high-temperature oxidation and LOCA tests on Cr-coated Zry under accident conditions and proposed a mechanism for the degradation of Cr-coated up to 1500 °C under steam atmosphere [1-3]. In the Cr-Zr system, the eutectic phase of ZrCr2 is present at 1332 °C and forms as intermetallic compounds. Fe as alloying element in Zry-4 leads to the dissolution of Fe and segregtion of the Zr(Cr, Fe)2 intermetallic phase. There is still lack of data on the evolution of the intermetallic phase when the oxidation temperature reaches the eutectic temperature of Cr-Zr. Therefore, the purpose of this study will be to understand the solid-to-liquid phase transition of $Zr(Cr, Fe)_2$.

In this study, a high-temperature oxidation test was performed by using a tubular type of Cr-coated Zry cladding with an initial composition of Sn = 0.8, Nb = 0.5, Fe = 0.2, and Cr = 0.1 (wt%). High temperature oxidation tests were performed in a steam atmosphere to the target temperature (i.e., 1100 °C, 1200 °C, 1300 °C, 1350 °C, and 1400 °C) for different exposure times of 5, 30, and 60 min. Steam was introduced at target temperature and cooled down under Ar flow. After the test, the microstructures and chemical compositions of the specimens were characterized by using electron probe mciroanalysis (EPMA, JEOL JXA-iHP200F, Japan).

From the tests, the transition of $Zr(Cr, Fe)_2$ that formed at the Cr-Zr interface and also that precipitated in the Zry cladding were studied with varied oxidation time and temperatures. The microstructural evolution of the intermetallic phase was observed in the Zr substrate within the progress of the oxidation of Cr-coated Zry. A dendritic structure was observed at 1400 °C, indicating the formation of the $Zr(Cr, Fe)_2$ liquid phase when the oxidation temperature is above the eutectic temperature. The details of the oxidation behaviour and microstructural evolution obtained in this study and reported in [5] will be discussed in the presentation.

References:

[1] Brachet et al. Corrosion Science, 167 (2020) 108537.
[2] Liu et al. Corrosion Science, 192 (2021) 109805.
[3] Yeom et al. J. Nuclear Materials, 526 (2019)151737.
[4] Okada et al. TOPFUEL 2021 Proceeding, 2021.
[5] Mohamad et al. Corrosion Science, 224 (2023) 111540.

28th Quench Workshop
5~7 December 2023 @KIT

Transition of the $Zr(Cr, Fe)_2$ intermetallic phase up to the eutectic temperature

Afiqa Mohamad [a], Yoshiyuki Nemoto [a], Kenichiro Furumoto [b], Yuji Okada [b], Daiki Sato [b]

[a] Japan Atomic Energy Agency
[b] Mitsubishi Heavy Industries, LTD.

Background

Cr-coated Zry cladding as a near-term accident tolerant fuel (ATF) development.

Okada et al. (2021):
Corrosion testing using an autoclave showed that the weight gain of the Cr-coated Zry cladding was significantly lower compared to the uncoated Zry cladding.

Purpose:

- The oxidation behaviors/mechanisms are well reported by others e.g. Brachet et al.(2020) & Liu et al. (2021).
- To understand the transition of the intermetallic phase when reaches $T_{eutectic}$.

Contents have been published in Mohamad et al. Corrosion Science, 224 (2023)111540.

Intermetallic phase

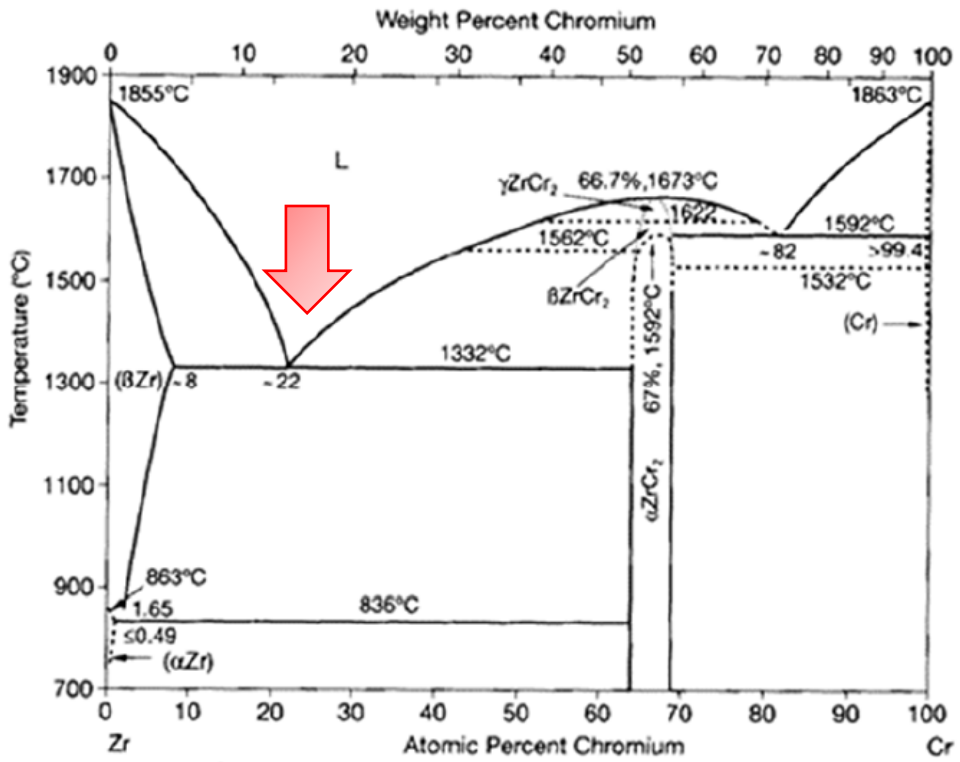

Zr-Cr phase diagram. (Arias, 1986)

- Lowest $T_{eutectic}$ = 1332 °C
- Cr has max. solubility ~8 at% in β-Zr (1332°C)
- Cr has max. solubility ~0.49 at% in α-Zr (836°C)

Alloying element in Zry cladding e.g. Fe
→ Dissolution of Fe in the Zry substrate
→Formation of $Zr(Cr,Fe)_2$ phase

wt%

Alloy	Sn	Nb	Fe	Cr	Zr
M5	N/A	1	0.05	0.015	Bal.
ZIRLO	0.6-0.79	0.8-1.2	0.09-0.13	N/A	Bal.
Zry-4	1.20-1.45	N/A	0.28-0.37	0.1	Bal.
MDA	0.8	0.5	0.20	0.1	Bal.

Example of formation of $Zr(Cr, Fe)_2$ phase from the Cr-coated Zry cladding.

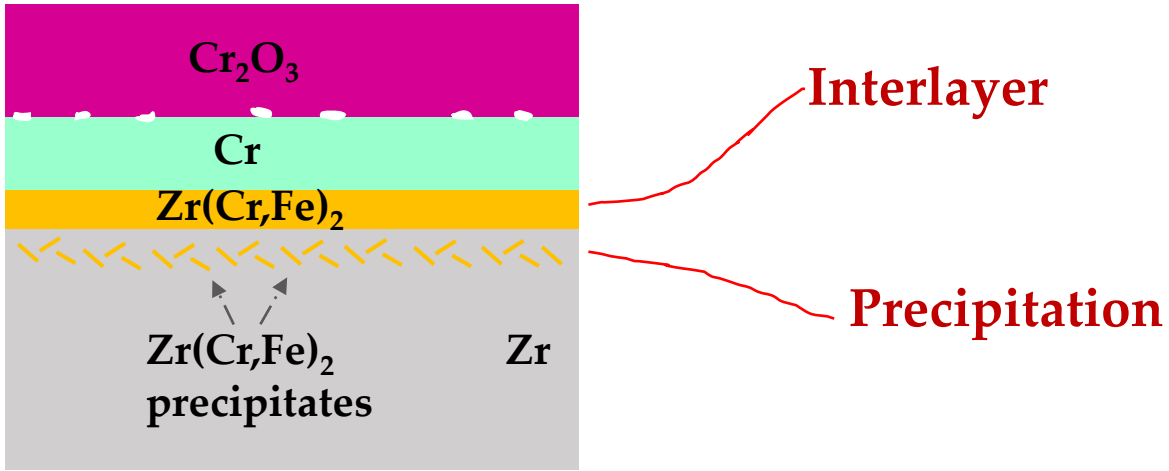

Experimental

Sample

Cr-coated Zry
(MDA-Mitsubishi Developed Alloy)
Thickness: 10 µm
Coating technique: Sputtering deposition

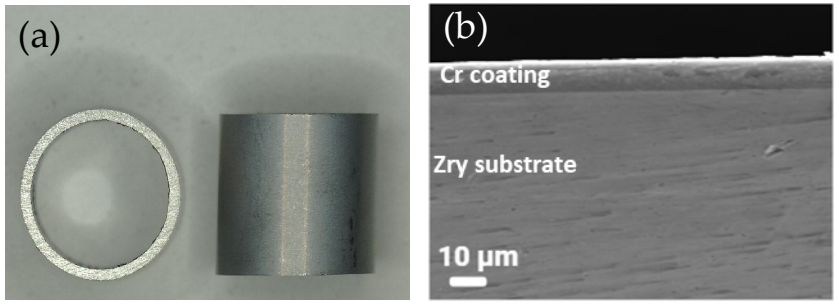

Fig. (a) Cladding tube and (b) cross-sectional of Cr-coated Zry cladding manufactured by MNF. (As-received)

One-sided coating on the outer surface of MDA Zry cladding. (Double-sided oxidation test)

Oxidation test

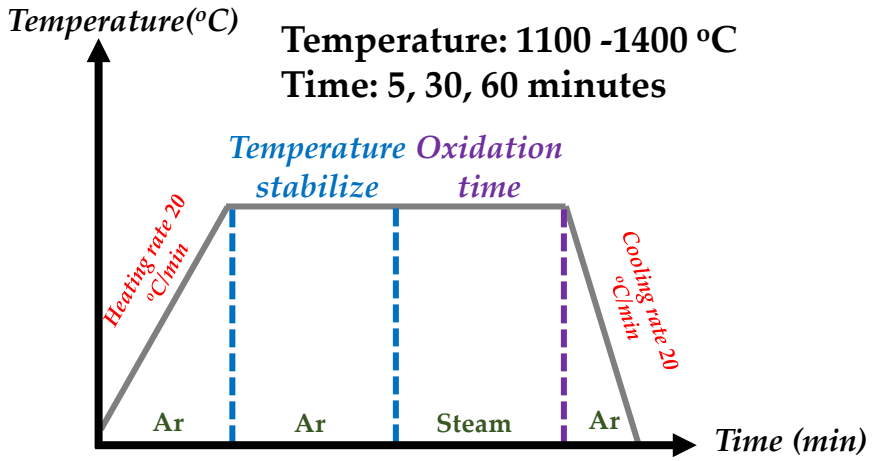

Steam was introduced at target condition.

Characterization

EPMA
Electron probe micro analyzer

RAMAN spectroscopy

Characterization on the cross-sectional samples.

Results: Intermetallic phase <$T_{eutectic}$

1200 °C-5min

e.g. Protective coating

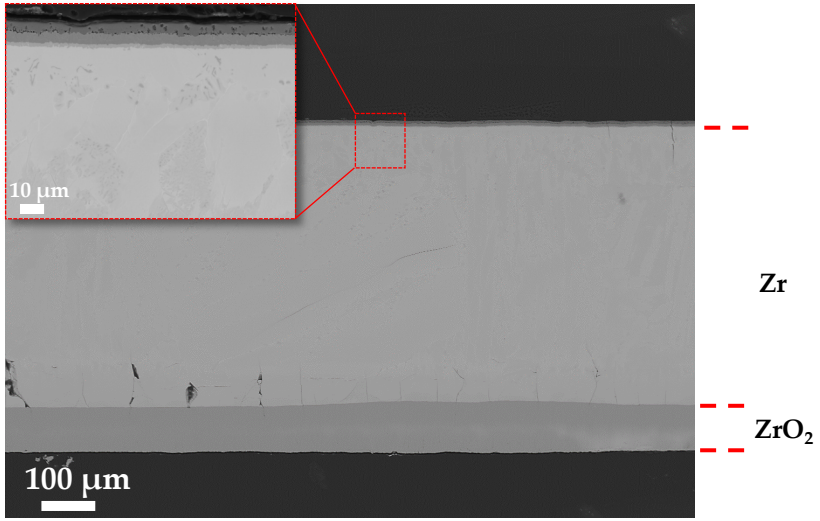

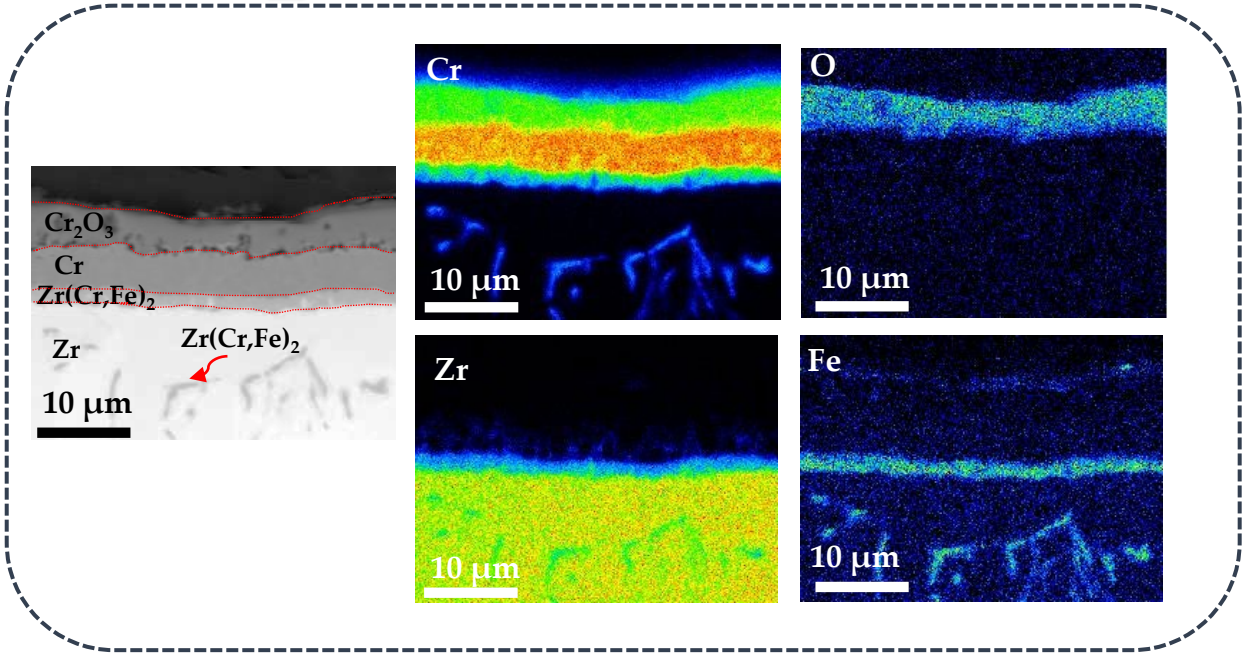

Interlayer:

$Zr(Cr, Fe)_2$ phase formation at the coating/substrate interface and beneath the Cr-metal layer.

→ Solid-state reaction between the coating and substrate

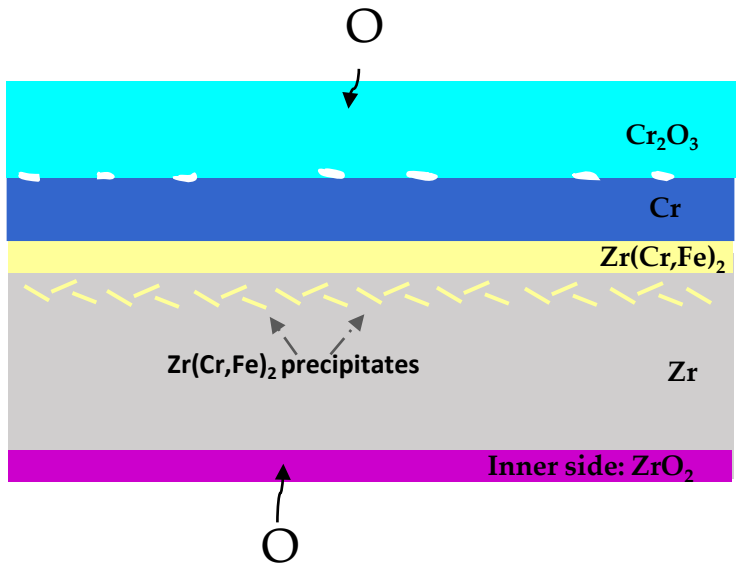

Substrate:

$Zr(Cr, Fe)_2$ phase precipitation within the substrate

→Inward diffusion of Cr into Zr (Cr own higher diffusion coefficient than Zr)

$Zr(Cr,Fe)_2$ exist at the interlayer and precipitate within Zry substrate.

Results: Intermetallic phase ≈$T_{eutectic}$

1300 °C-5min

e.g. No longer protective coating

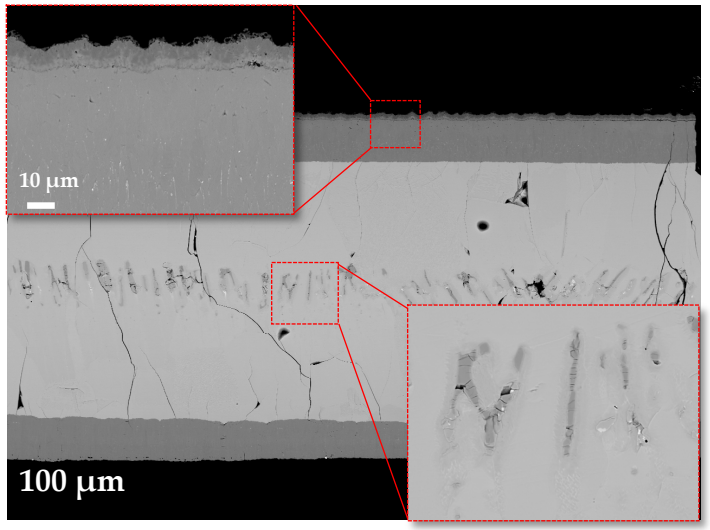

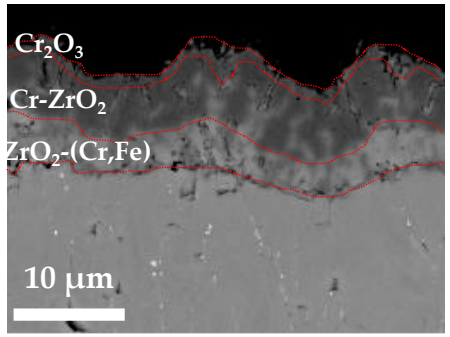

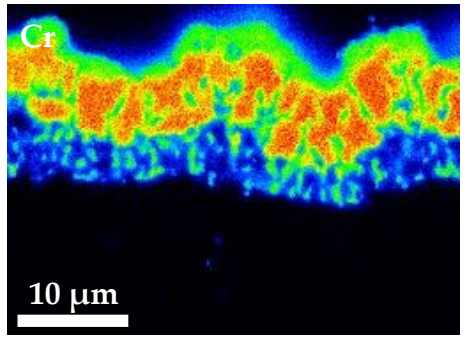

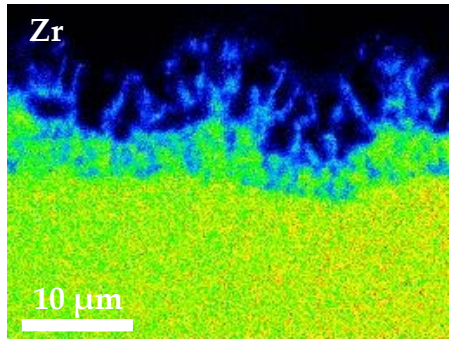

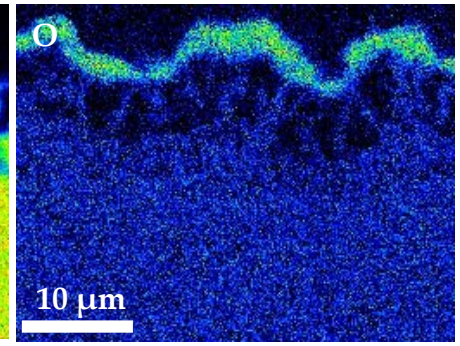

Interlayer:

$Zr(Cr,Fe)_2$ oxidize at initial stage

→ZrO_2, Cr+Fe (no Raman spectra)

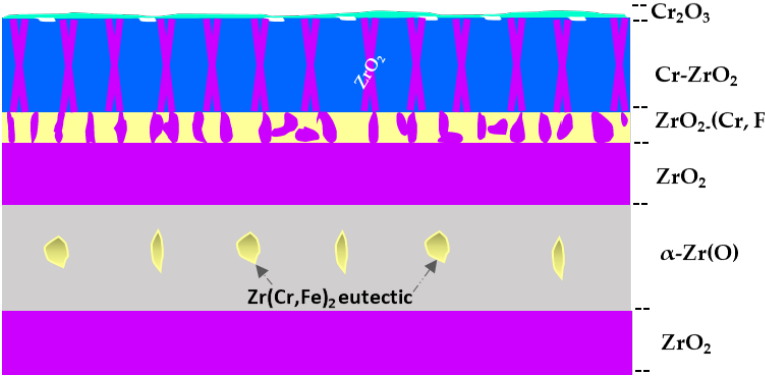

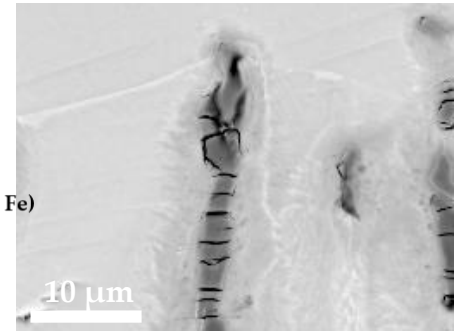

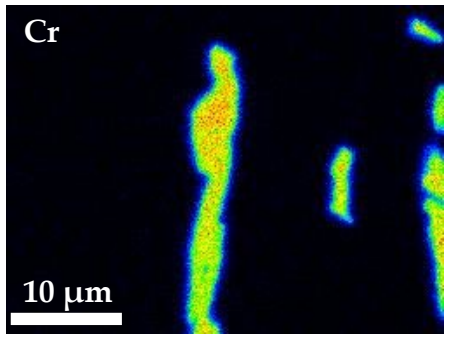

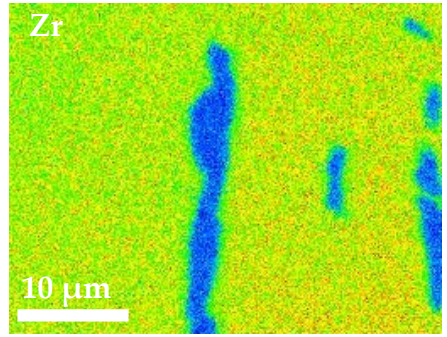

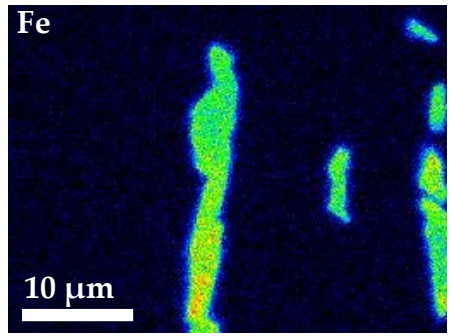

Substrate:

$Zr(Cr,Fe)_2$ phase are present as globule microstructure (center Zr substrate)

→Inward diffused Cr precipitate between β-Zr and α-Zr(O)

<u>$Zr(Cr,Fe)_2$ at the interlayer is oxidized and forms a globule microstructure within the Zry substrate.</u>

Results: Intermetallic phase >$T_{eutectic}$

1400 °C-5min *(Oxygen become saturated)*

e.g. No longer protective coating

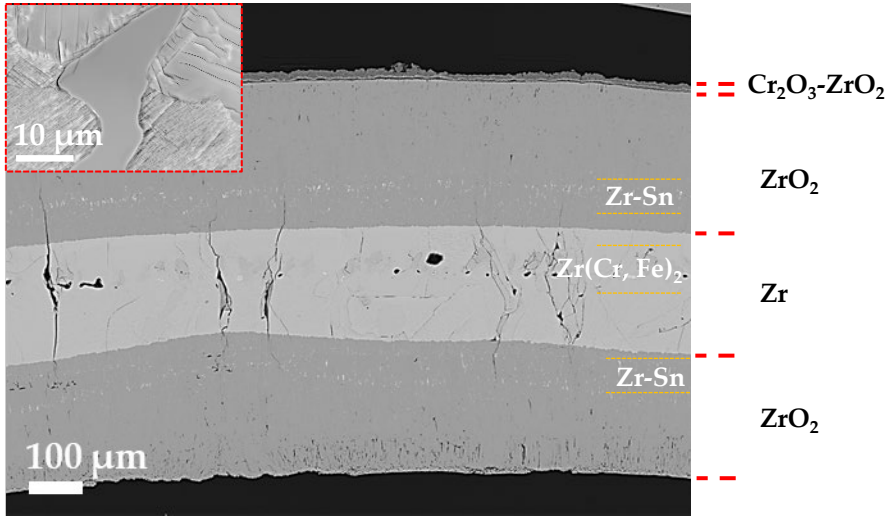

Interlayer:

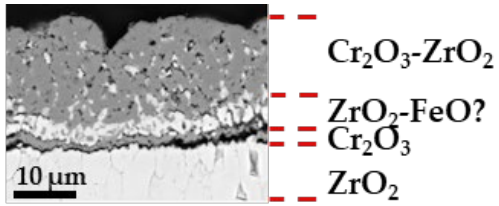

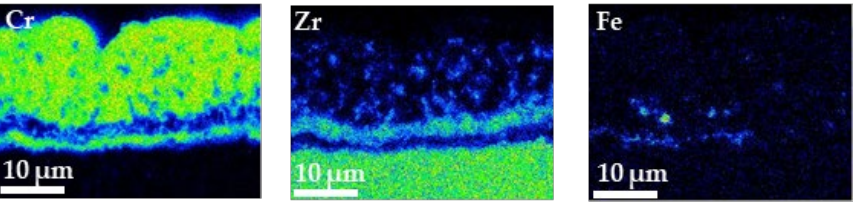

Raman spectroscopy

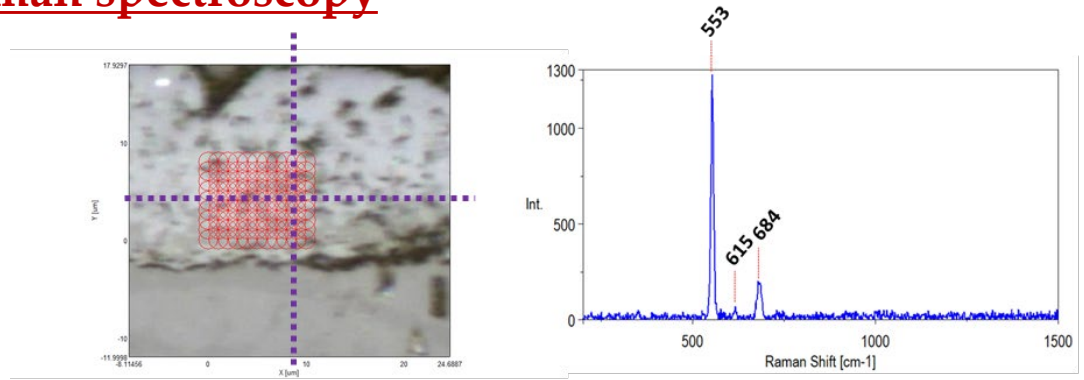

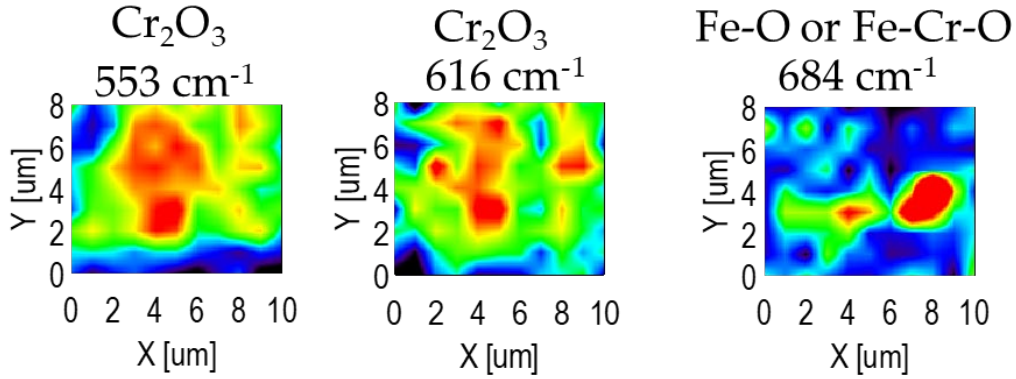

Interlayer:

Intermetallic phases are completely oxidized and produced Cr_2O_3, FeO agglomerate in the ZrO_2 layer.

→Migration rates of Fe in ZrO_2 is much higher than Cr_2O_3. [Pecheur et al. 1994]

Substrate:

$Zr(Cr, Fe)_2$ phase is positioned within the α-Zr(O) and ZrO_2.

Results: Intermetallic phase >$T_{eutectic}$

1400 °C-30min *(Oxygen become saturated)*

e.g. No longer protective coating

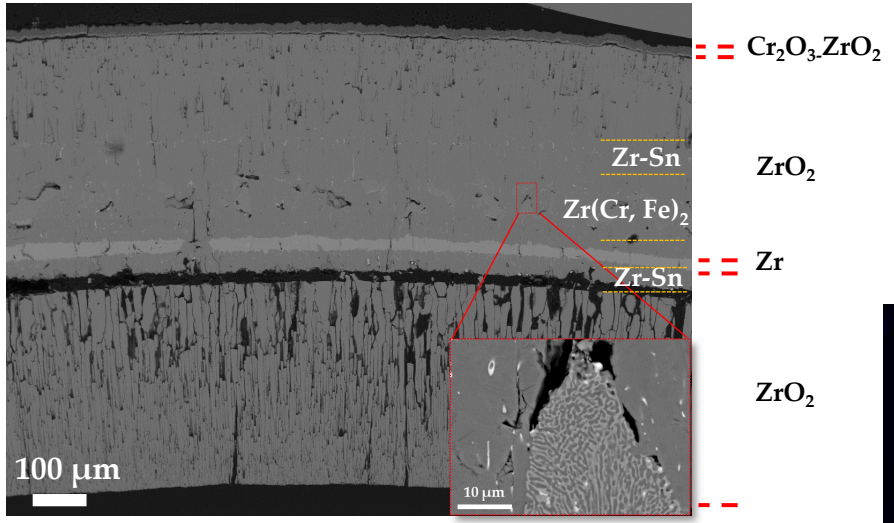

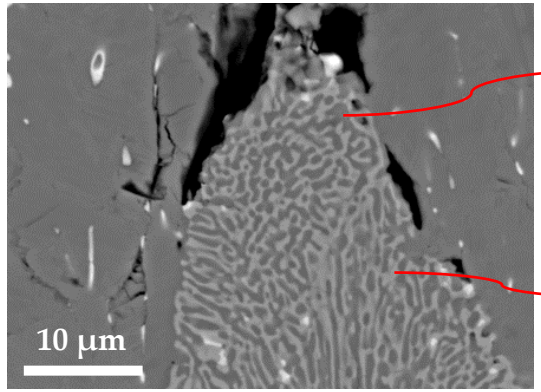

Dark grey region:
Cr-Fe rich region

Light grey region:
Zr rich region

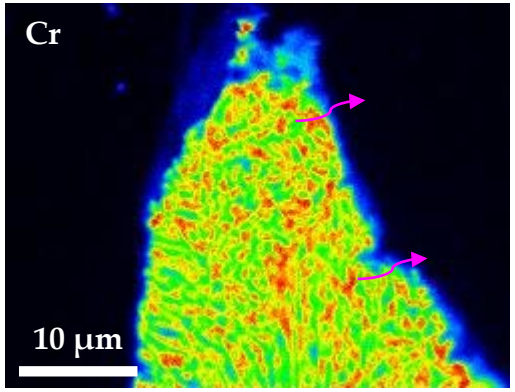

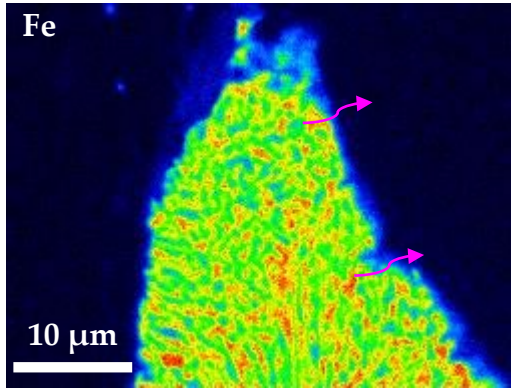

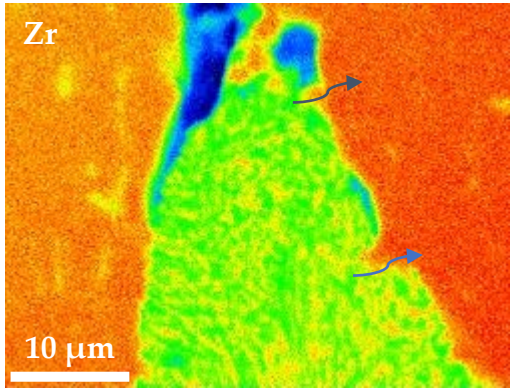

Beginning of oxidation:
Migration of Cr into β-Zr

Significant oxygen (both sides):
Remaining Zr substrate approximately 18μm (almost become saturated with O)

Significant oxygen (both sides):
Cr migration driving force may disappeared
→liquid formation at ZrO_2 (outer side)

<u>$Zr(Cr,Fe)_2$ within the substrate becomes the liquid phase.</u>

Results: Intermetallic phase >$T_{eutectic}$

Reported by Brachet et al. Corrosion Science 167 (2020)108537

Cr-coated M5$_{Framatome}$ Zry cladding

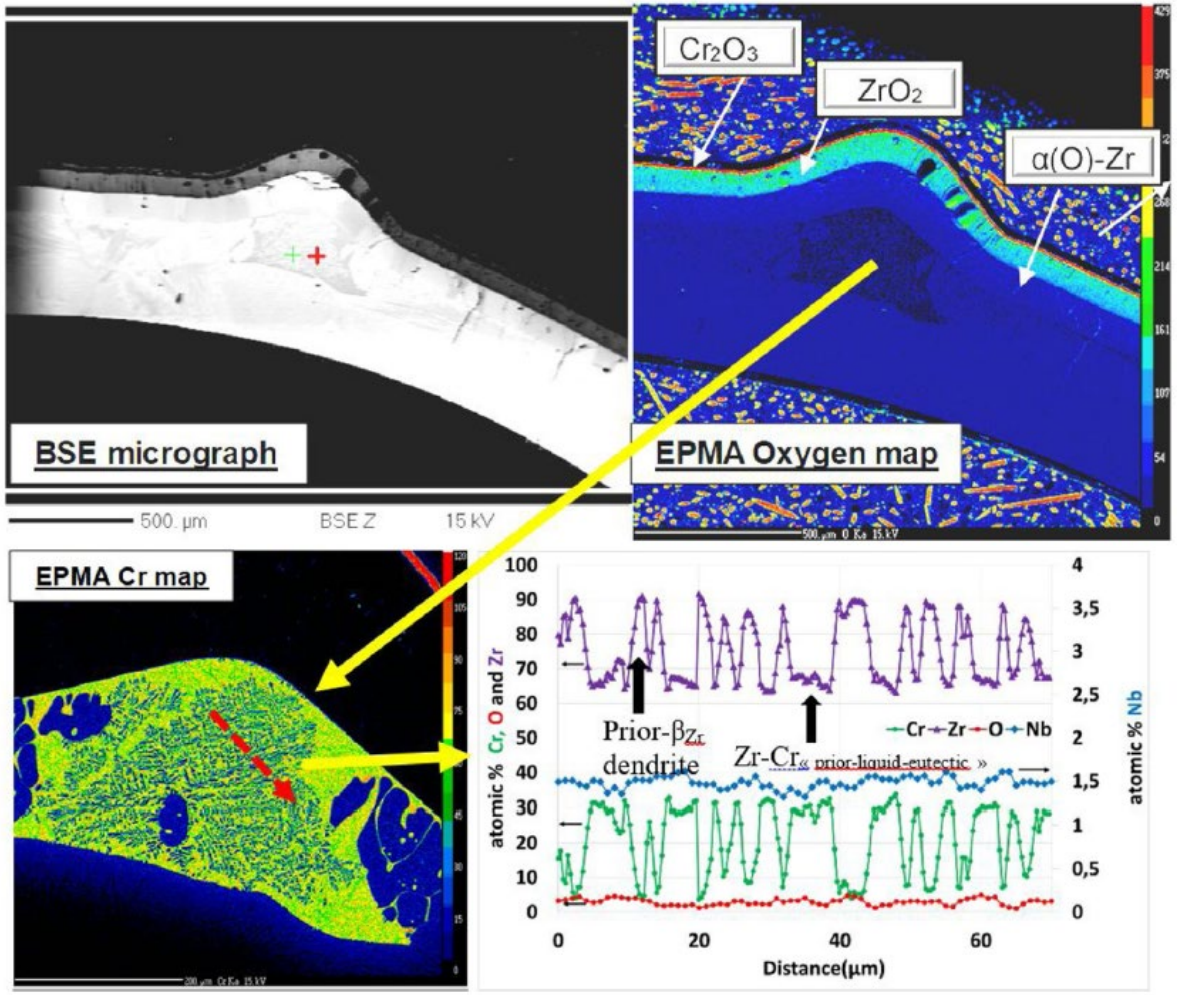

One-sided steam oxidation test at 1400-1405 °C for 100s with water quenching to RT.

Present study

Cr-coated MDA-Zry cladding

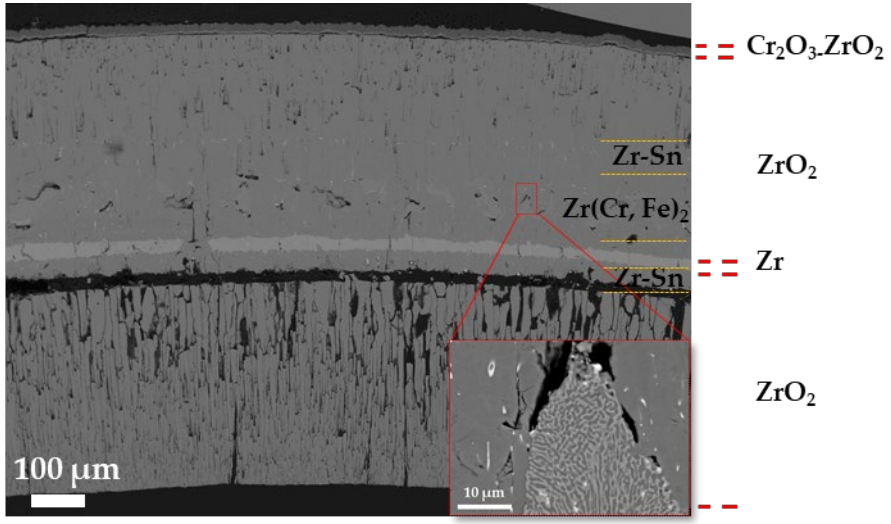

Double-sided steam oxidation test at 1400 °C for 360s.

Brachet et al	Present study
Liquid phase is observed in the α-Zr(O) ➢ Not saturated with O	Liquid phase is observed along the ZrO_2 ➢ Saturated with O

The difference in the liquid phase structure between Brachet et al and this study may due to the Fe concentration between M5 and MDA.

Discussion-1: Phase transformation

Cr-Zr-Fe system from TAF-ID database

✦ Position of the chemical compositions obtained from EPMA.

1200 °C

Cr: 62, Fe:3, Zr: 35 (at%)

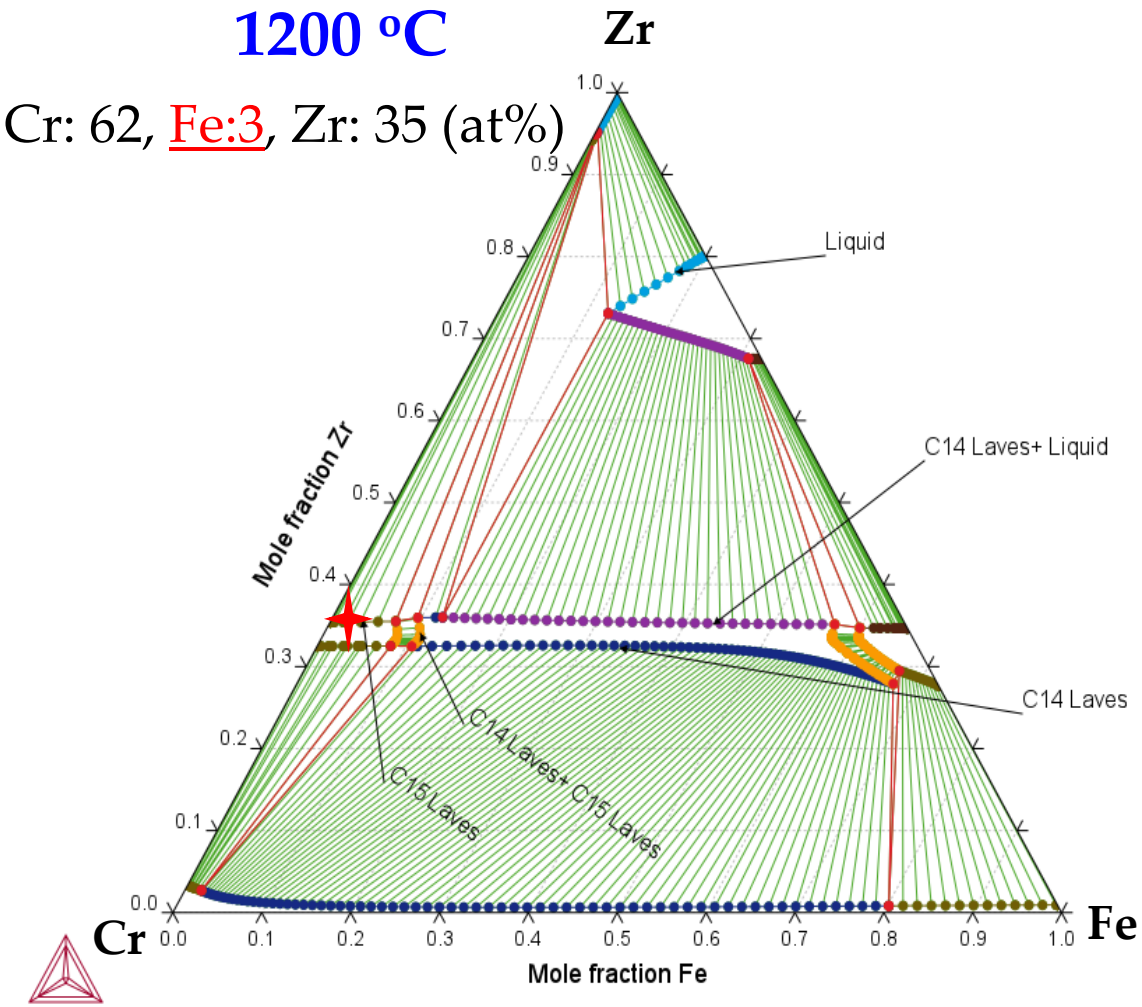

1300 °C

Cr: 52, Fe:13, Zr: 35 (at%)

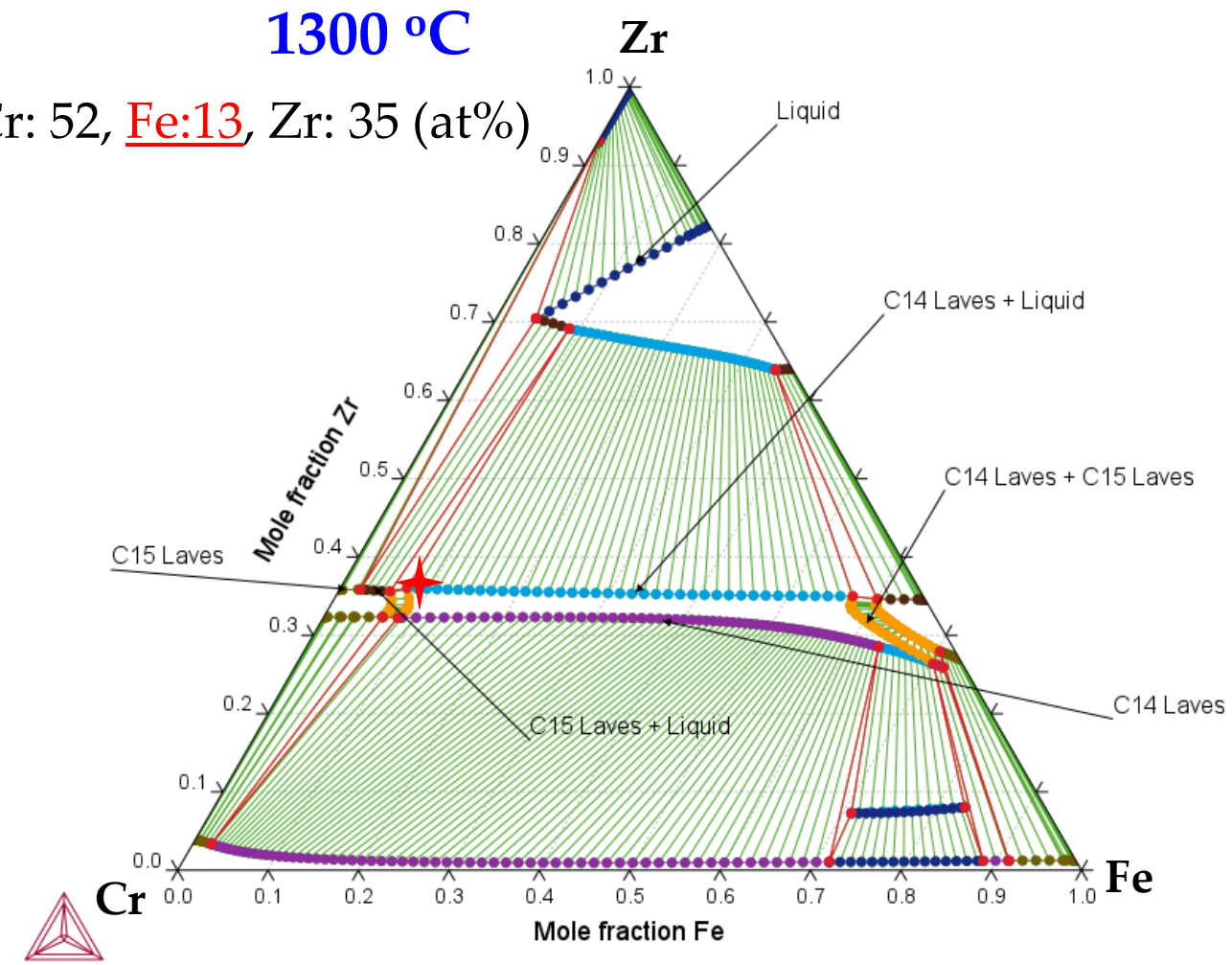

1200 °C: C15 Laves phase of $Zr(Cr, Fe)_2$

1300 °C: C14 Laves phase of $Zr(Cr, Fe)_2$.. Fe enrichment

Identified the Fe difference below and up to the $T_{eutectic}$:

Discussion-2: Transition of $Zr(Cr, Fe)_2$

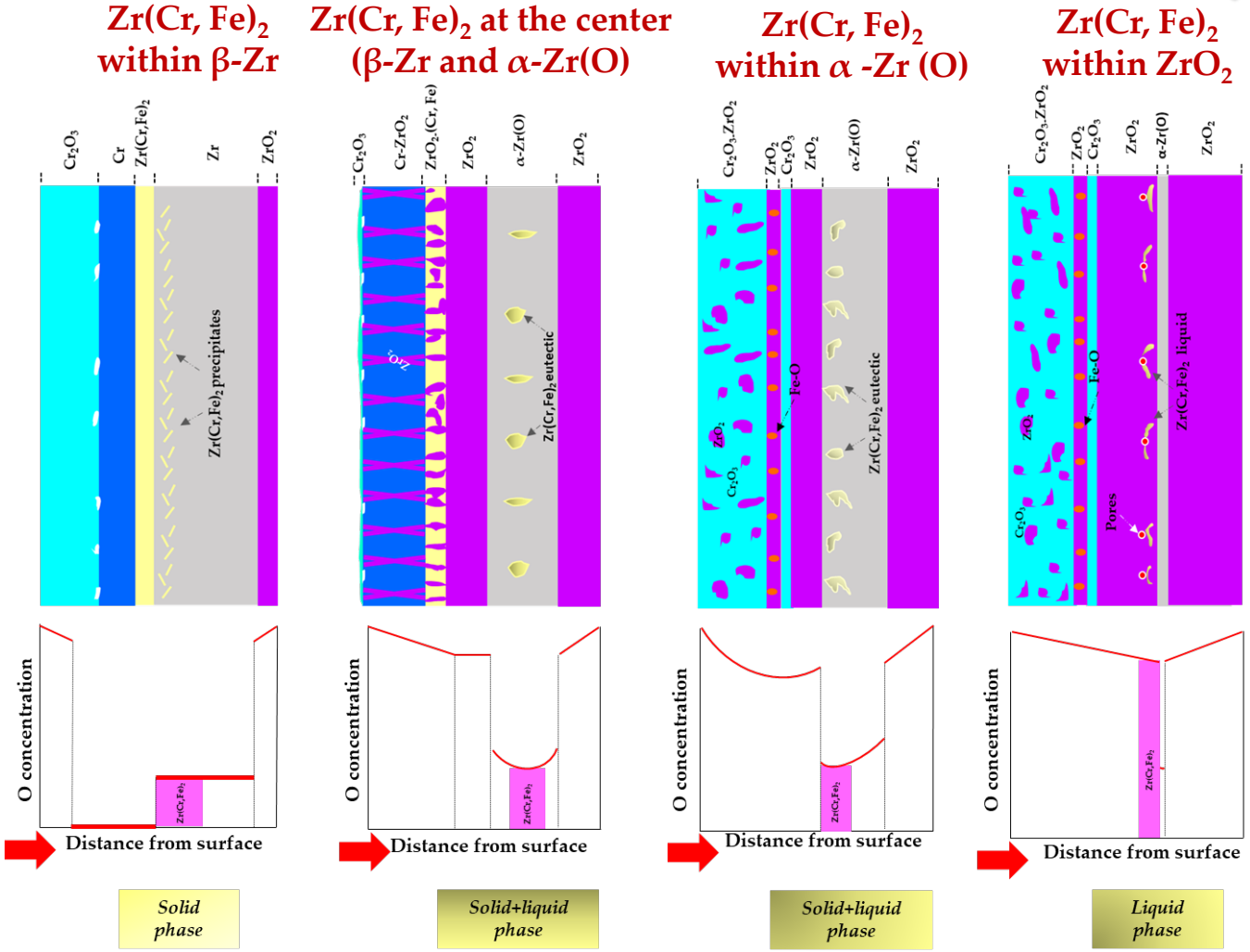

①Intermetallic at interlayer

→Oxidize to ZrO_2, Cr_2O_3, and Fe-O

②Intermetallic within substrate

→ Transformation from solid to liquid

Thickness of the ZrO_2 layer or oxidation from the inner/outer play a significant role in the formation of the $Zr(Cr,Fe)_2$ phase within Zry substrate.

Conclusions

Major phenomena observed under an isothermal oxidation condition

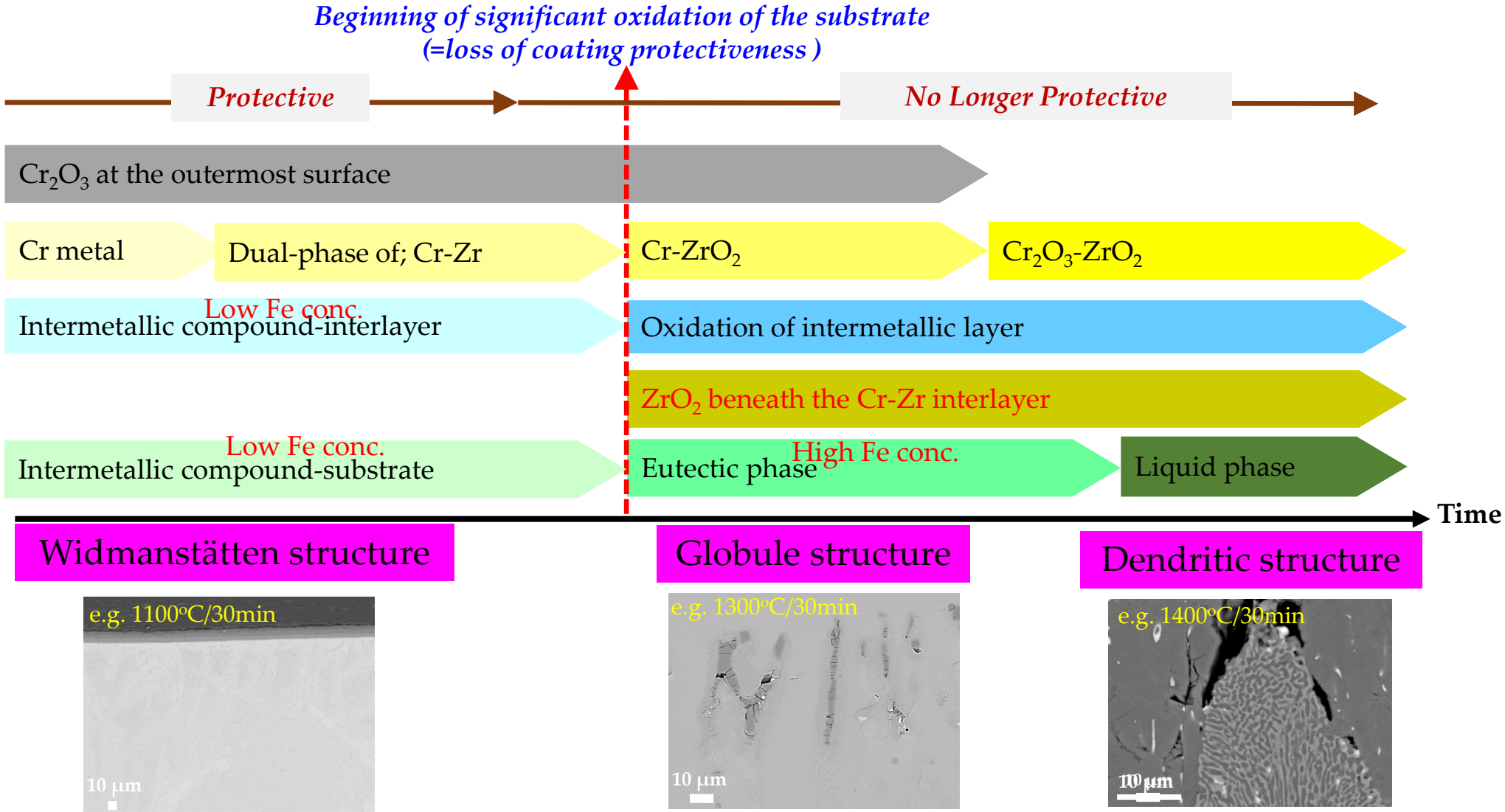

Future work: Need to confirm the ductility/brittleness of the cladding (LOCA/HT).

Additional slides

Results: Protective & no longer~

Declaration: The current data correspond to double-sided oxidation test using tube sample. Other sample and test types may produced different data.

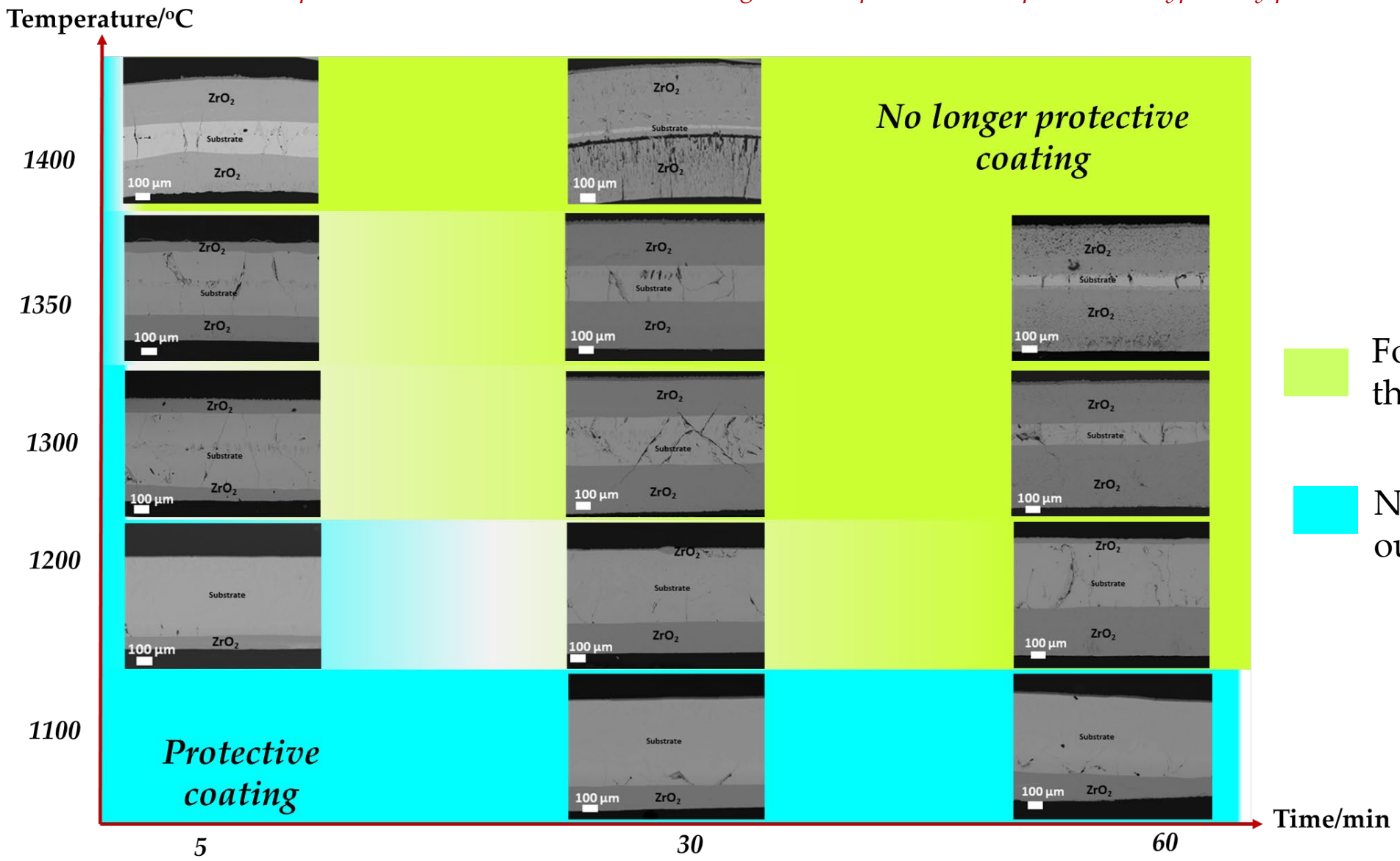

Results: Protective & No longer

1100 °C/ 30 min

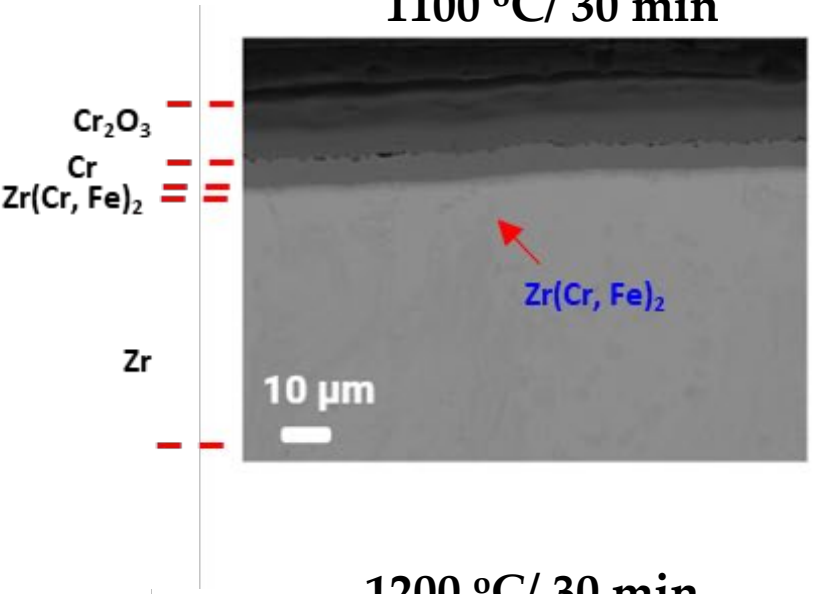

1100 °C/ 60 min

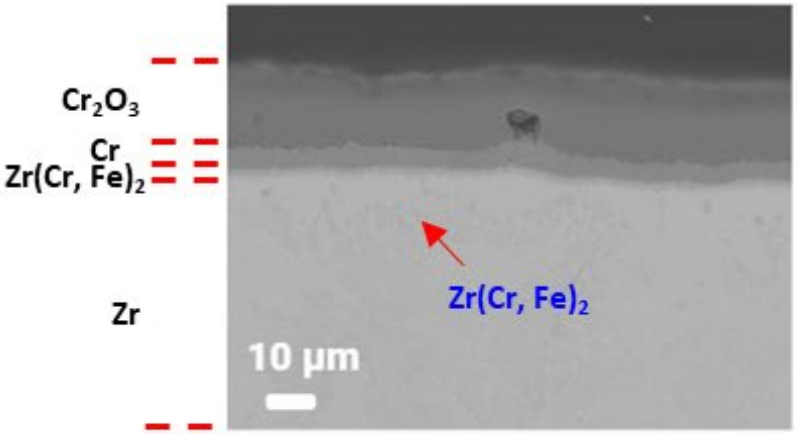

1200 °C/ 5 min

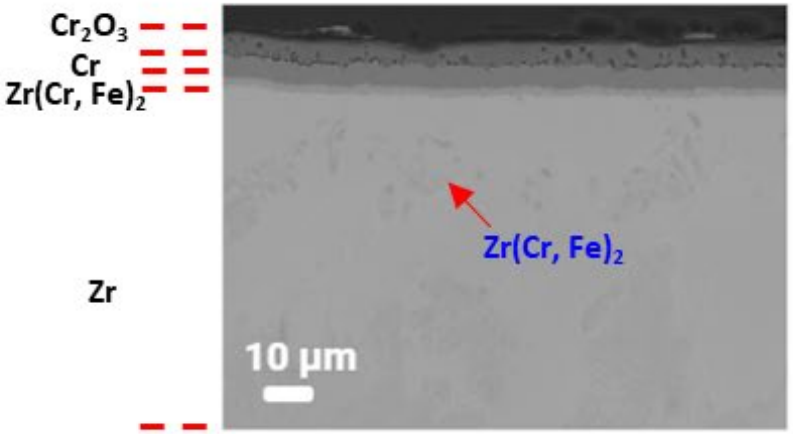

1200 °C/ 30 min

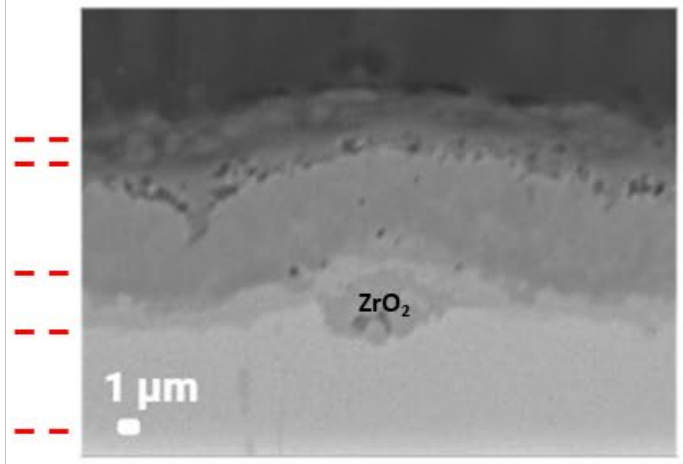

1200 °C/ 60 min

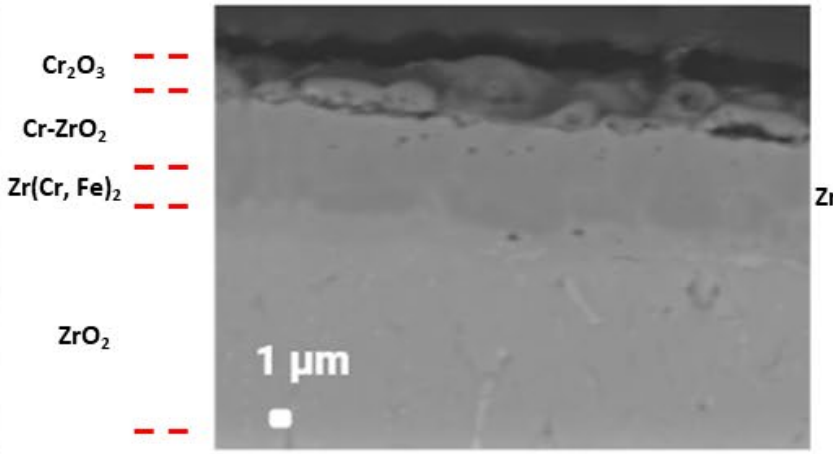

1300 °C/ 5 min

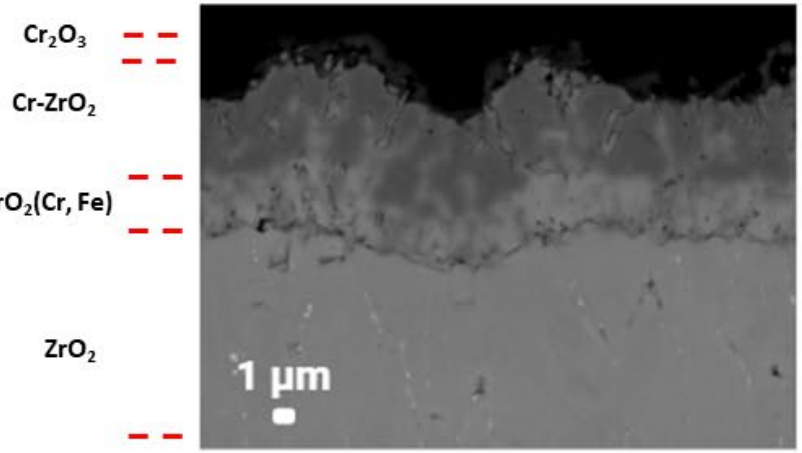

Results: Surface analysis

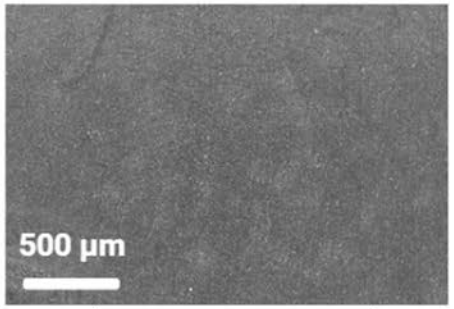

1200 °C/5 min (#C)

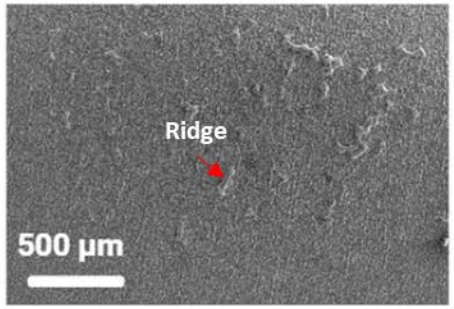

1300 °C/5 min (#F)

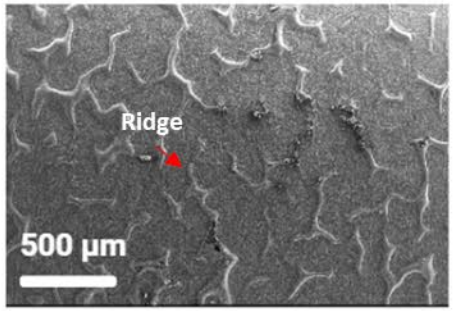

1350 °C/5 min (#I)

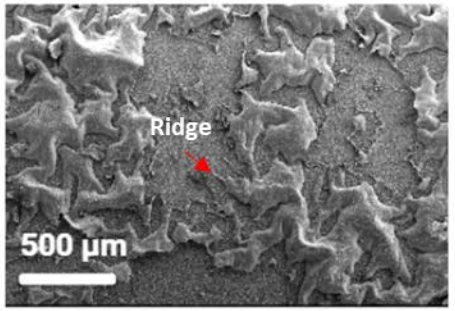

1400 °C/5 min (#L)

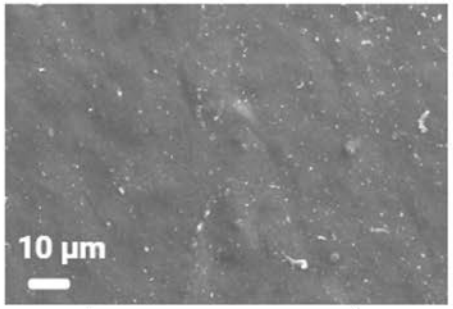

1100 °C/30 min (#A)

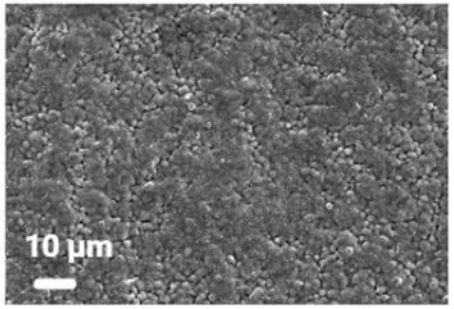

1200 °C/30 min (#D)

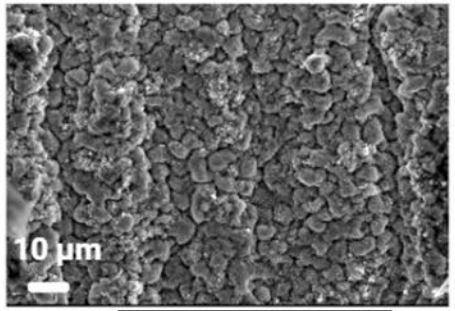

1300 °C/30 min (#G)

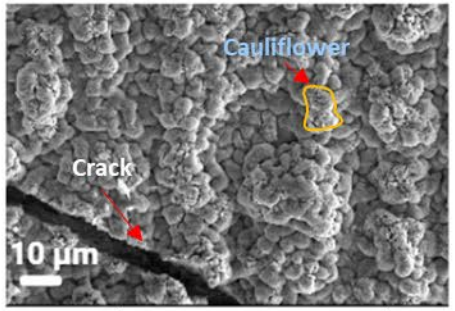

1350 °C/30 min (#J)

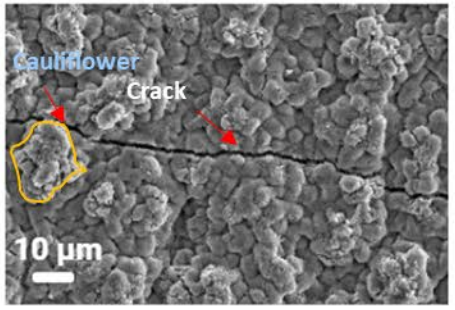

1400 °C/30 min (#M)

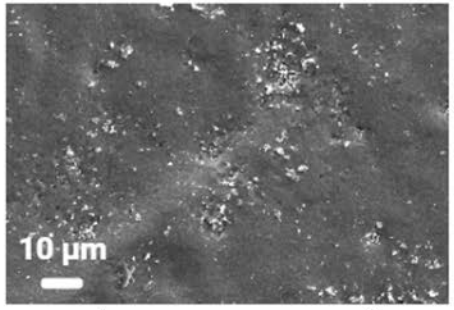

1100 °C/60 min (#B)

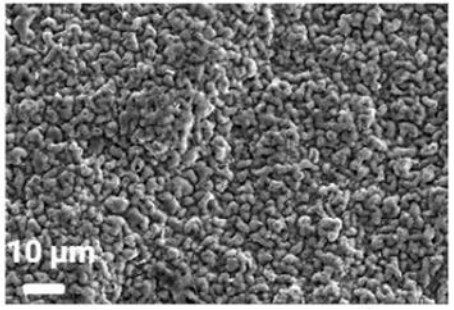

1200 °C/60 min (#E)

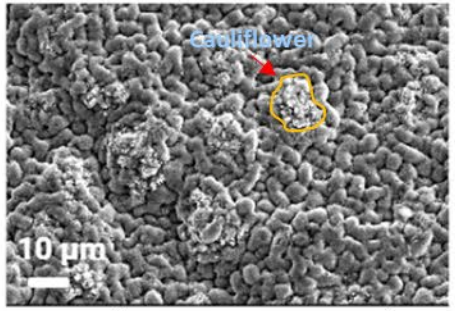

1300 °C/60 min (#H)

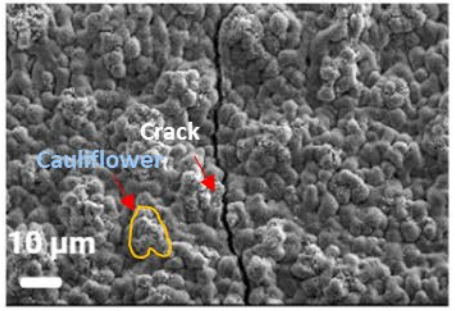

1350 °C/60 min (#K)

Results: Surface analysis

1200 °C/ 5 min

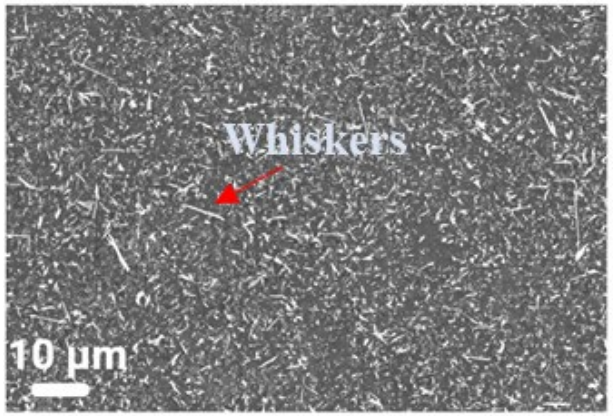

1300 °C/ 5 min

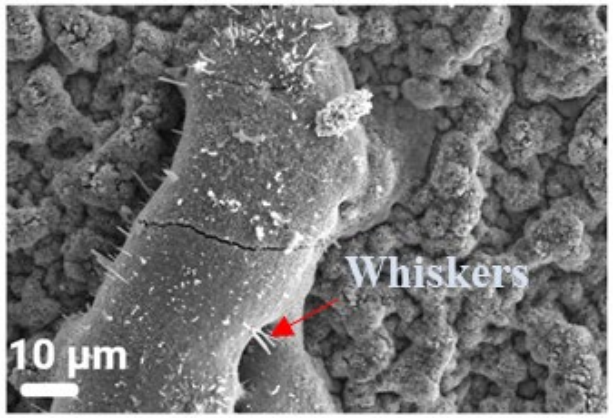

1350 °C/ 5 min

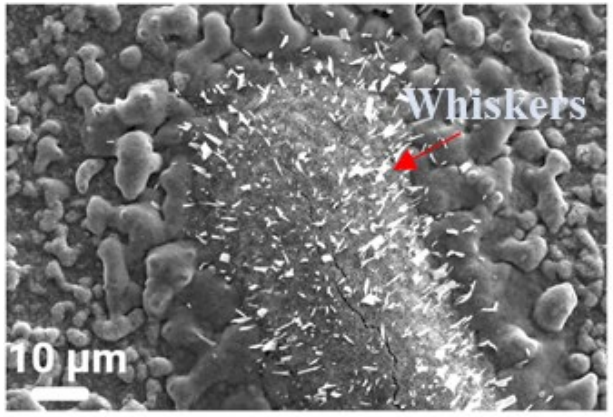

1400 °C/ 5 min

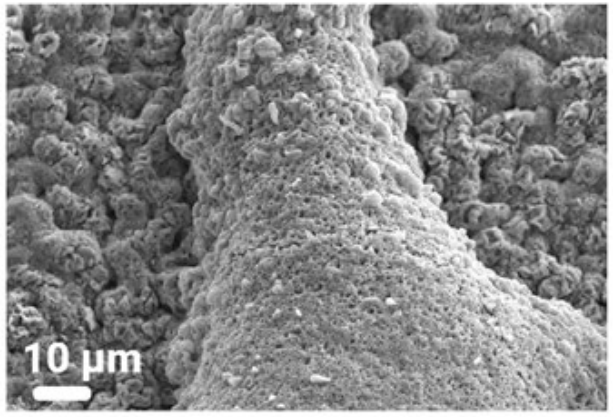

Results: Thickness

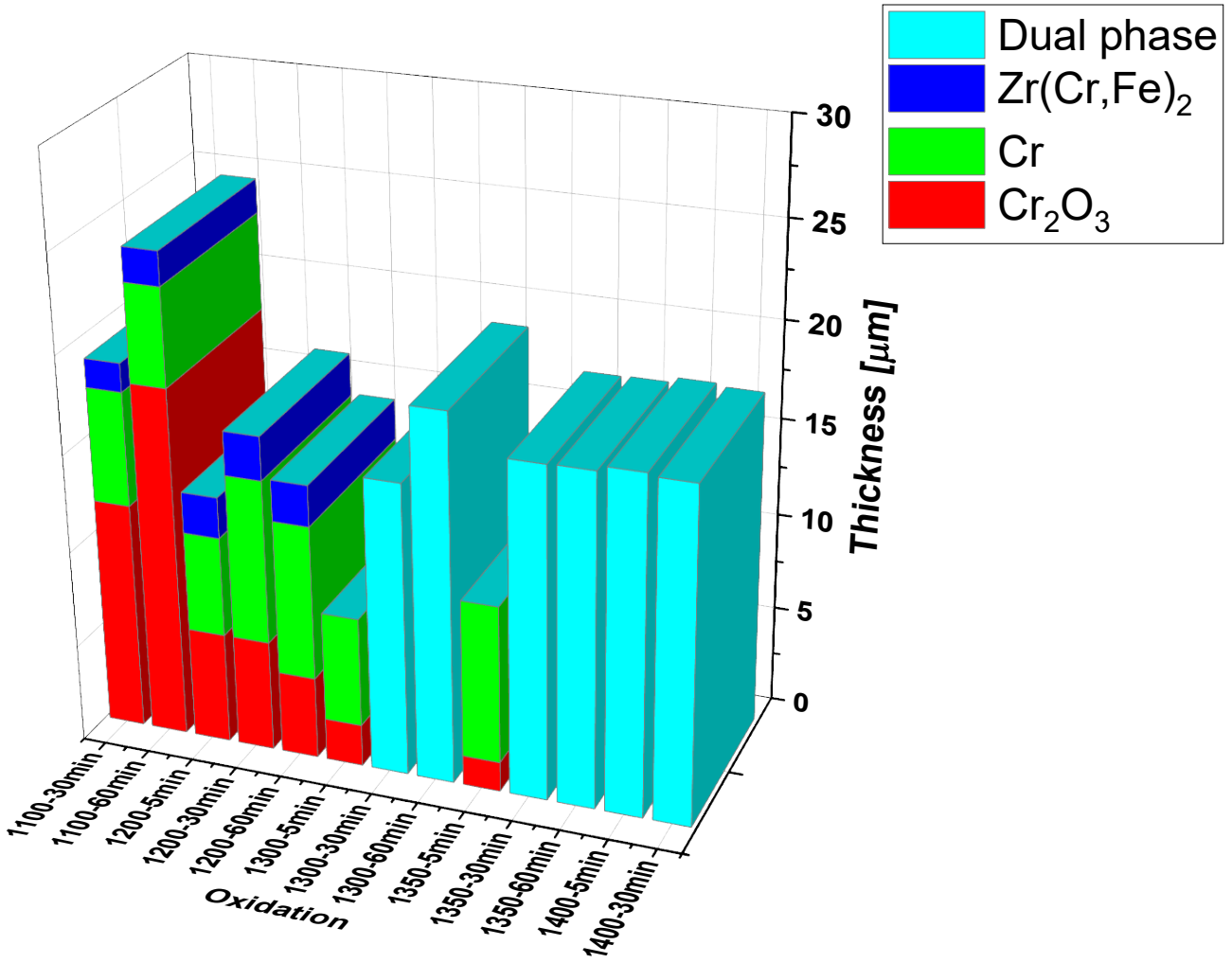

M. Steinbrück

KIT

Recent and ongoing experiments on the high-temperature oxidation and degradation of Cr-coated Zr alloy

The oxidation and degradation of Cr-coated zirconium alloy cladding alloys has been extensively investigated during the recent years and the mechanisms are widely understood. For modelling and validation of models, data are needed reflecting the effects of coating thickness (and quality), ambient atmosphere and accident scenario. Recent and current experimental activities at KIT took this into account.

Thermal balance systems were used to investigate the effects of transient heating rate, Cr coating thickness and atmosphere composition on the oxidation kinetics and degradation. The results presented here are partially preliminary.

The effect of transient heating rate was investigated from 2 K/min to 50 K/min up to 1380°C (i.e., 50 K above eutectic temperature) in oxygen atmosphere. The results have been published in https://doi.org/10.1016/j.jnucmat.2023.154538. Coating failure at eutectic temperature connected with accelerated oxidation rates was observed for the 5-50 K/min tests. Higher mass gain rate (= oxidation rate, = H2 release rate) of coated samples compared to non-coated samples after failure of Cr coating were seen. The higher the heating rate, the higher was the oxidation rate after failure. The mechanisms are discussed based on metallographical post-test examination, and potential effects on accident progression are considered.

Various test serious on the effect of Cr coating thickness (5-25 µm) on the degradation of the protective effects are ongoing. Transition time from protective to non-protective coating increases with Cr thickness in isothermal test series at 1000 and 1200°C as well as in transient tests with 30 K/min heating rate. Local coating failure was observed for the thickest coating (25 µm).

Very preliminary tests with Cr-coated Zry-4 plates in O_2, H_2O, and H_2O+O_2 showed an effect of the atmosphere on mass gain curves and post-test appearance. Strongest oxidation was observed for the mixed atmosphere. However, these results have to be confirmed, also because of relatively strong (non-coated) edge effects observed for all samples.

Karlsruhe Institute of Technology

Institute for Applied Materials

Recent and ongoing experiments on the high-temperature oxidation and degradation of Cr-coated Zr alloy

M. Steinbrück, D. Kim, I. Lee, M. Große, C. Tang, U. Stegmaier

28th International QUENCH Workshop, Karlsruhe Institute of Technology, 5-7 Dec 2023

Institute for Applied Materials, Programme NUSAFE

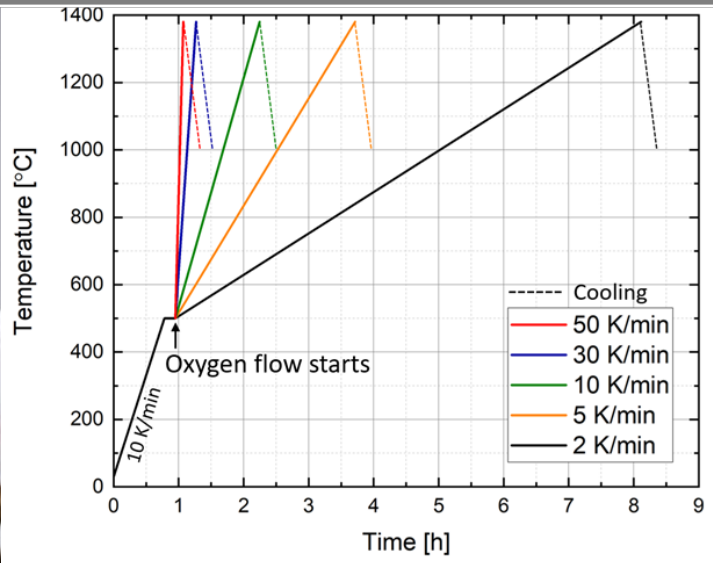

Outlook

- Experimental facility
- Effect of heating rate (published)
- Effect of Cr thickness (ongoing)
- Effect of atmosphere (preliminary)
- Conclusion

Experimental setup

- Netzsch STA449 in TG mode coupled with steam generator and mass spectrometer

Steam supply

STA with two furnaces

Mass spectrometer

Hanging sheet sample on TG holder

Transient tests
Effect of heating rate

Journal of Nuclear Materials 583 (2023) 154538

Contents lists available at ScienceDirect

Journal of Nuclear Materials

journal homepage: www.elsevier.com/locate/jnucmat

Eutectic reaction and oxidation behavior of Cr-coated Zircaloy-4 accident-tolerant fuel cladding under various heating rates

Dongju Kim [a,b,*], Martin Steinbrück [a], Mirco Grosse [a], Chongchong Tang [a], Youho Lee [b]

[a] Institute for Applied Materials IAM-AWP, Karlsruhe Institute of Technology, 76021 Karlsruhe, Germany
[b] Department of Nuclear Engineering, Seoul National University, 08826 Seoul, Republic of Korea

https://doi.org/10.1016/j.jnucmat.2023.154538

Effect of heating rate on eutectic reaction and oxidation of Cr coated Zr alloy

- Cr coated Zry-4 plates (17 µm PVD)
- Thermal balance
- Ar/oxygen atmosphere
- Heating up to 1380°C (50 K above eutectic temperature) with varying heating rates from 2-50 K/min

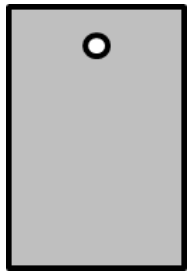

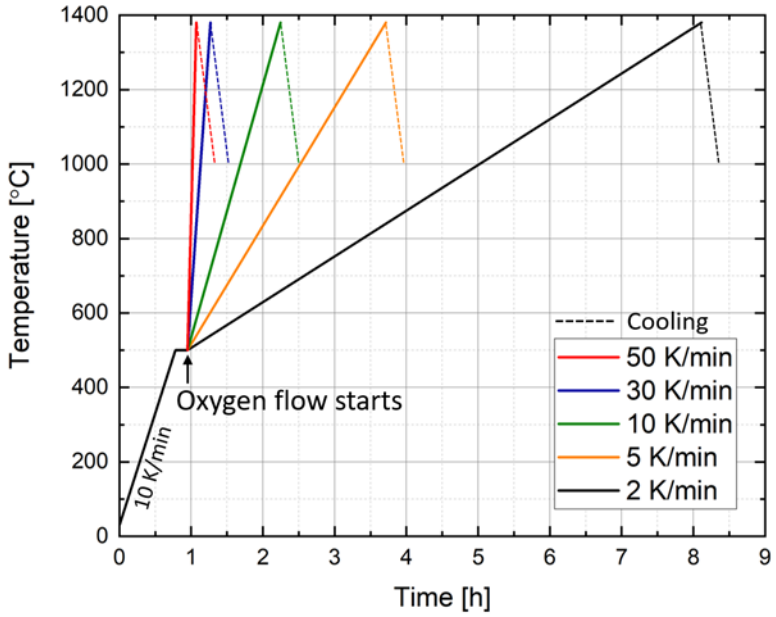

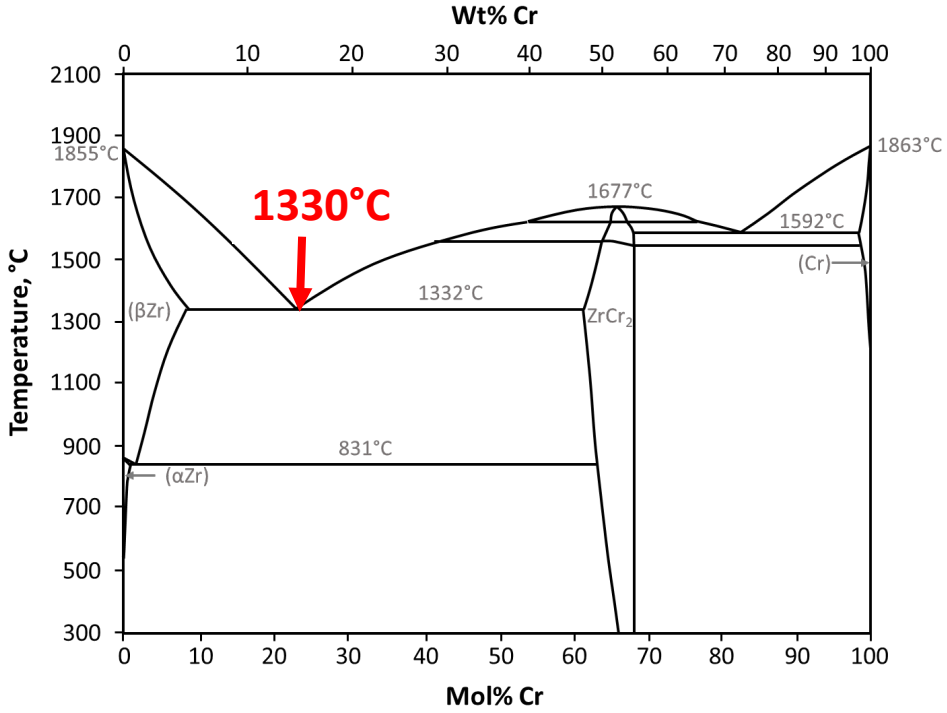

TG results

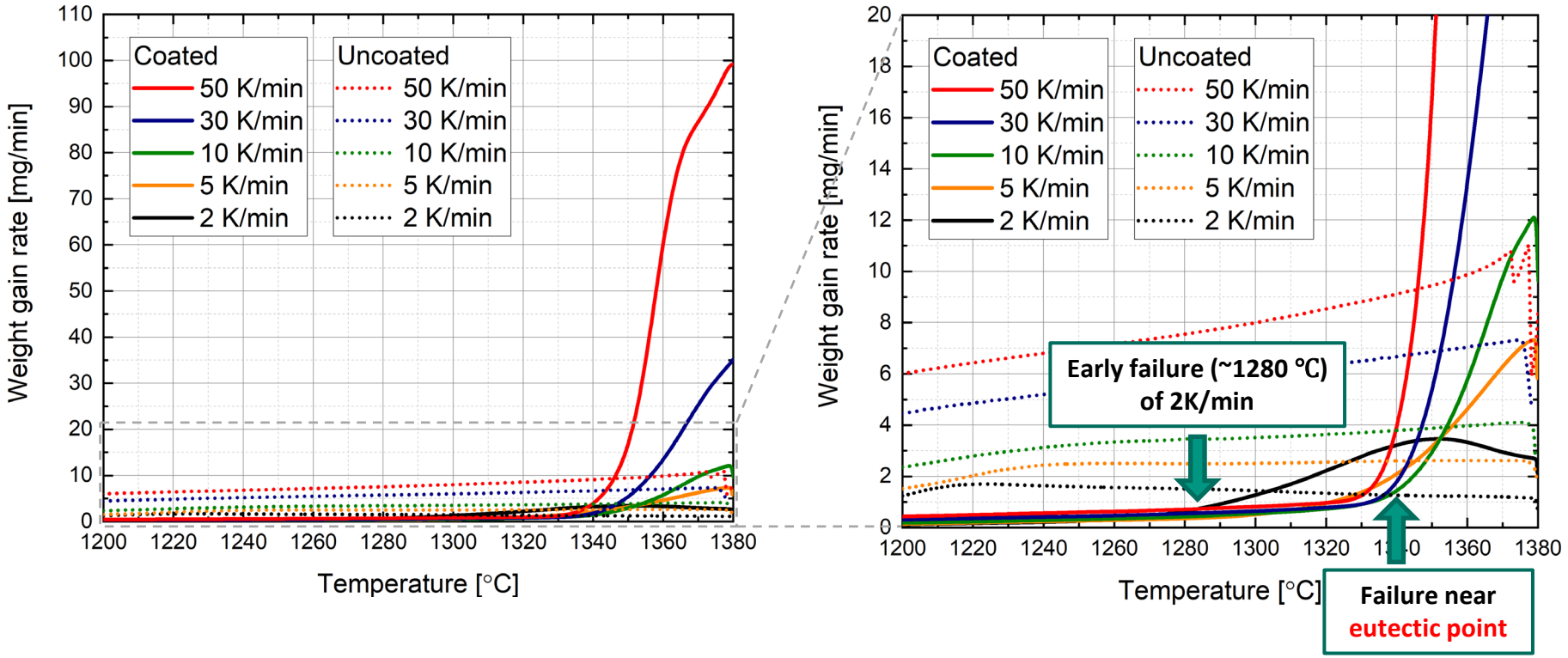

- Coating failure (5-50 K/min) at eutectic temperature
- Higher mass gain rate (= oxidation rate, = H_2 release rate) of coated samples compared to non-coated samples after failure of Cr coating
- The higher the heating rate, the higher the oxidation rate after failure

Post-test appearance

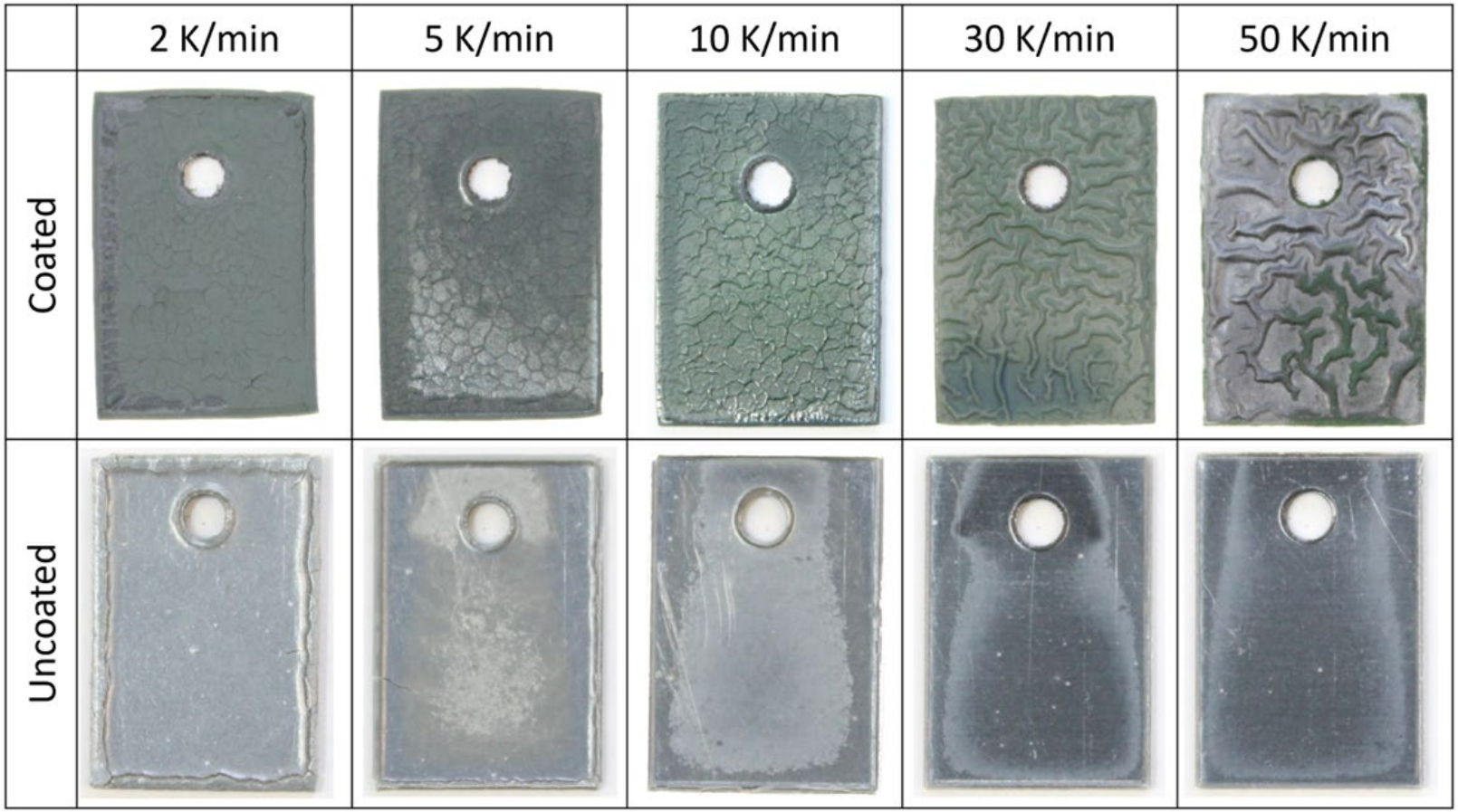

- More pronounced “crocodile skin” surface at higher heating rate is an indication for more melt formation

Micrographs of cross sections

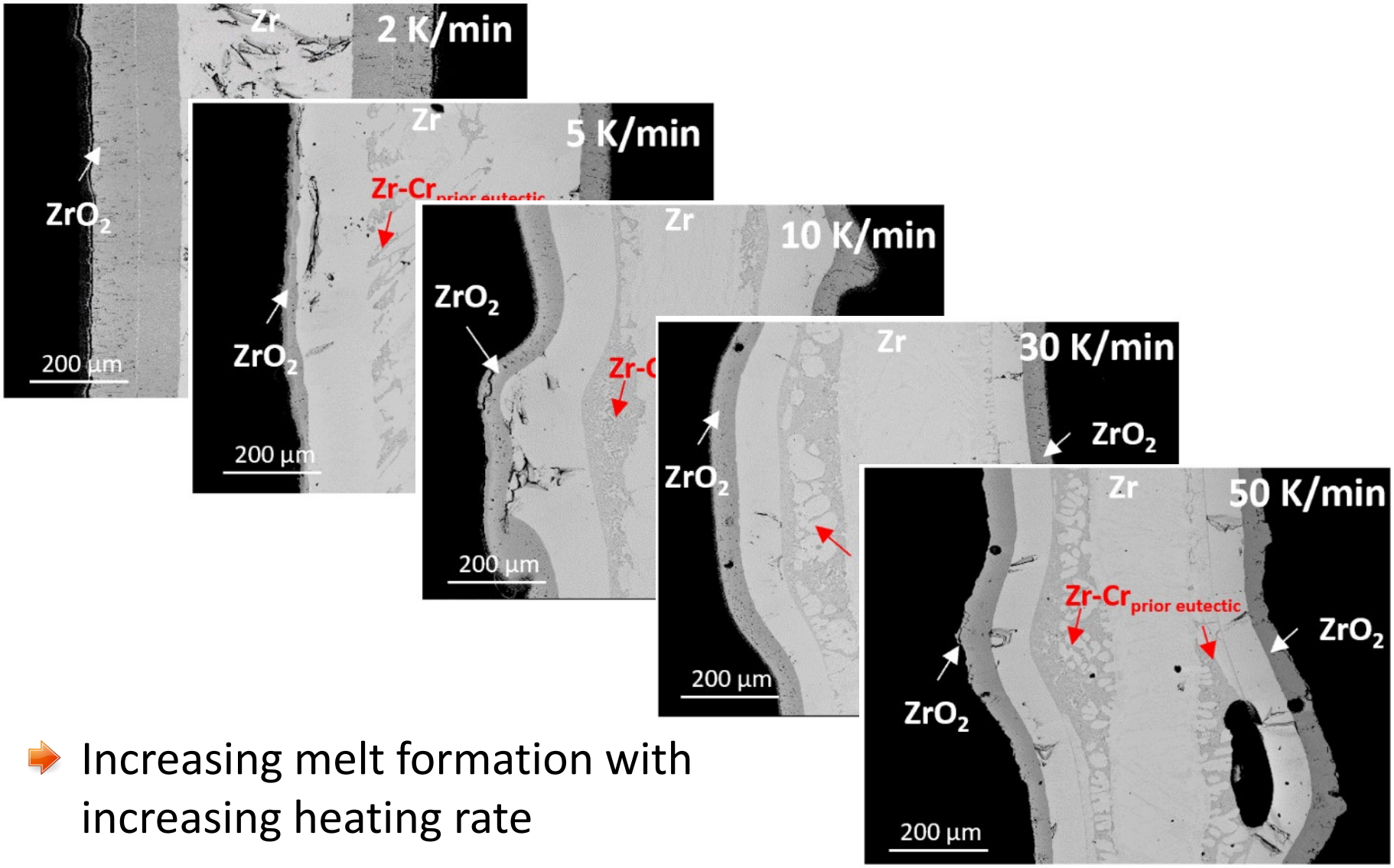

- Increasing melt formation with increasing heating rate

Mechanism

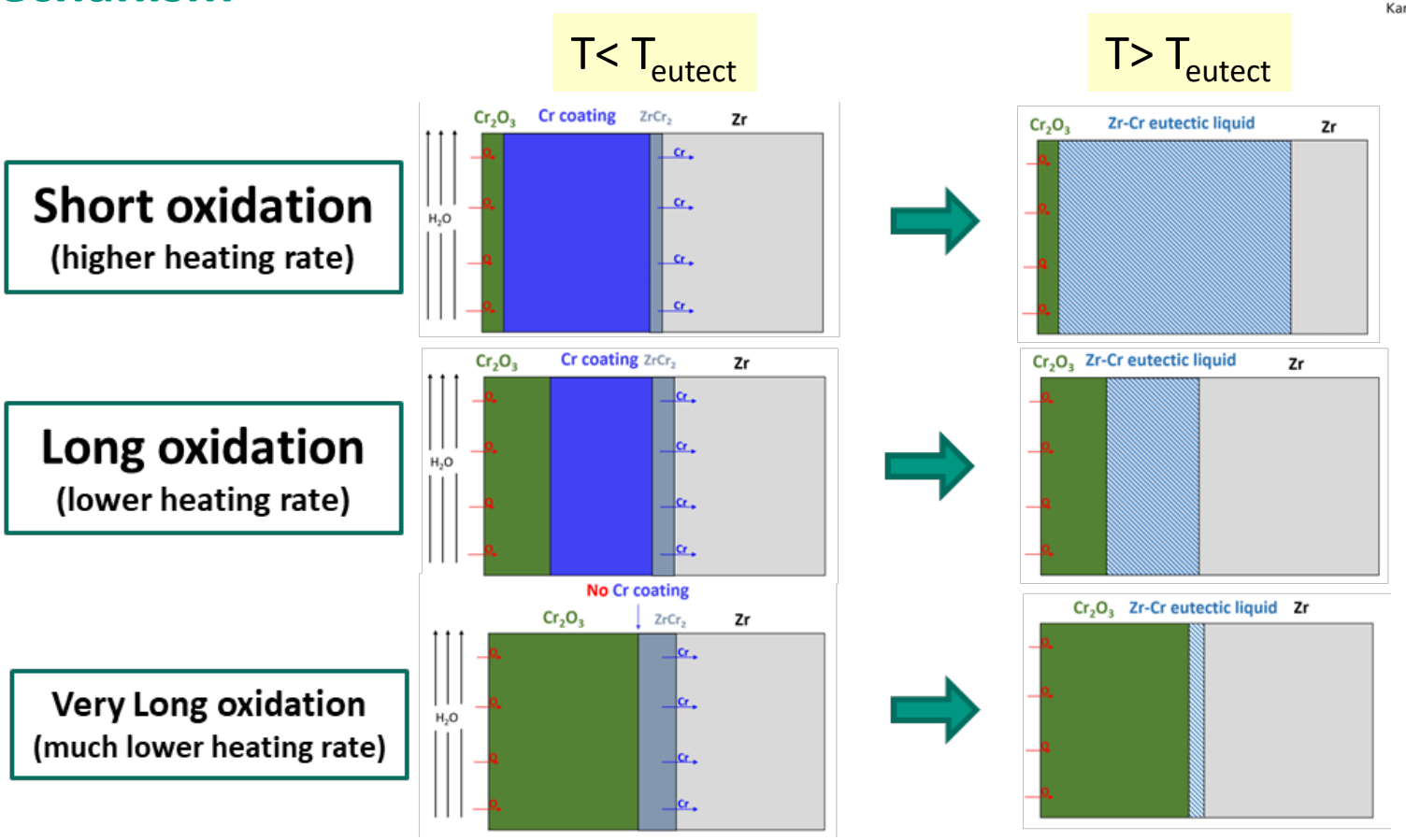

- Thicker remaining metallic Cr layer at eutectic temperature during shorter oxidation at higher heating rates
- More eutectic melt formation at higher heating rate

Estimated heat generation due to oxidation in steam after coating failure

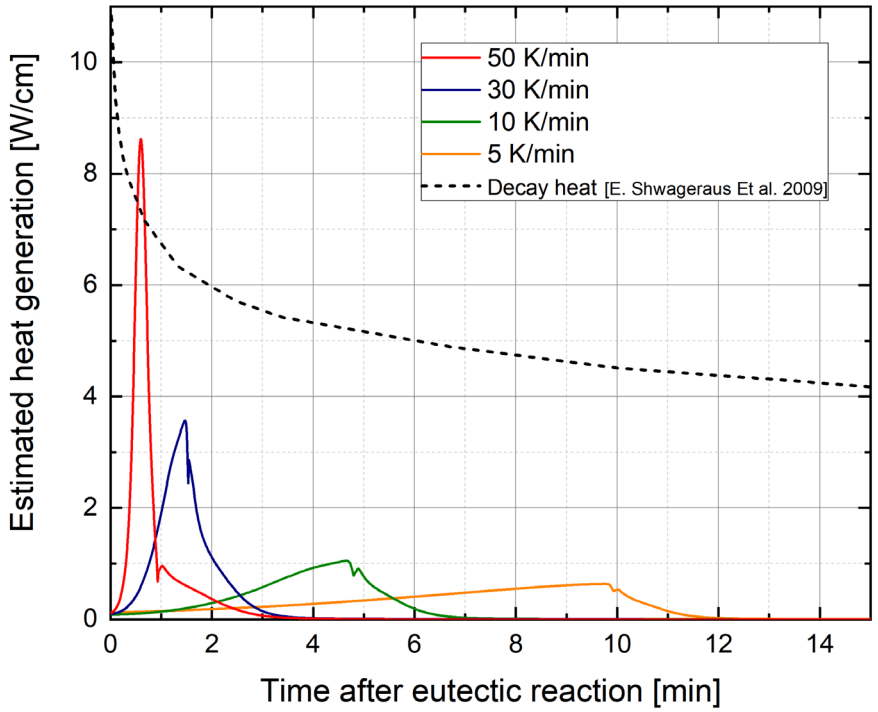

- Significant heat generation after eutectic temperature is reached and coating had failed
- For highest heating rate chemical heat can be higher than decay heat after shutdown
- Prototypical heating rates will be even higher and T_{eutect} will be reached later after shutdown

Effect of Cr thickness

(ongoing study)

Test matrix

- Zry-4 samples were coated by magnetron sputtering with Cr in five different thicknesses: 5, 10, 15, 20, and 25 µm
- Test series in STA *(conducted)*
  - 2 hours at 1000°C in steam
  - 1 hour at 1200°C in steam
  - Transient tests up to 1380°C in O_2
- Test series in BOX furnace *(planned)*
  - In steam at temperature >1200°C to be defined

TG results isothermal tests

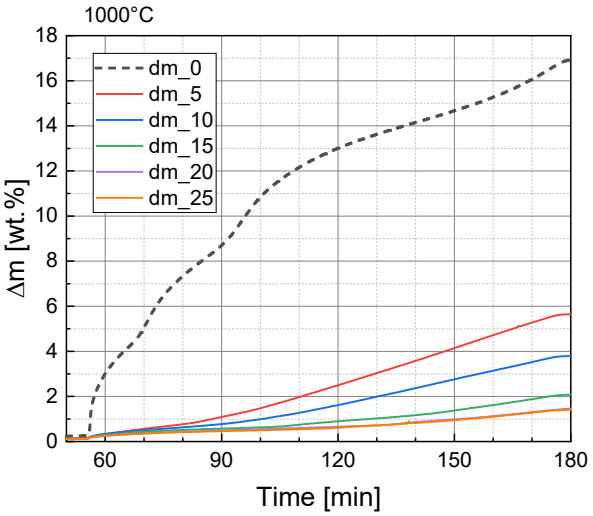

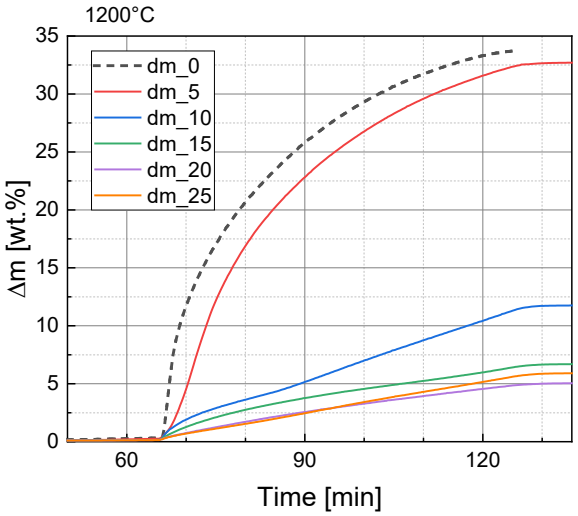

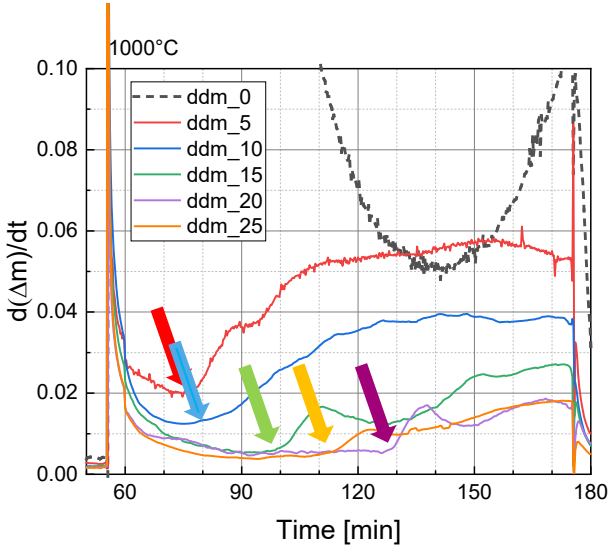

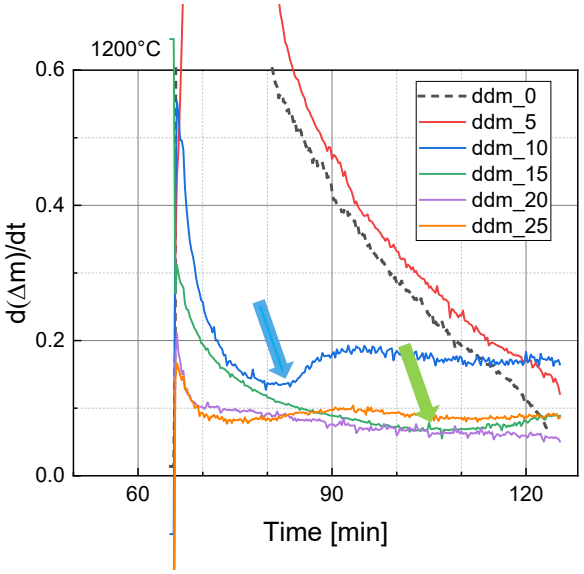

TG results transient tests

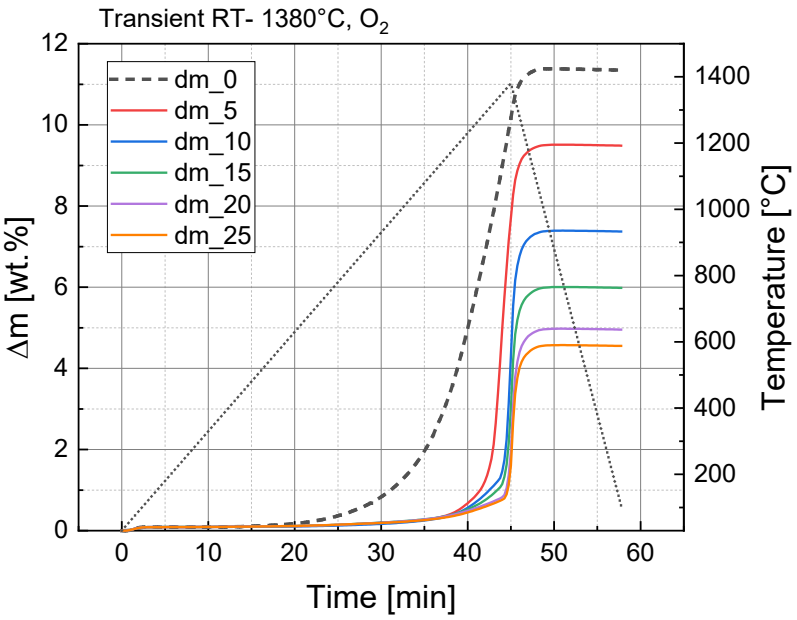

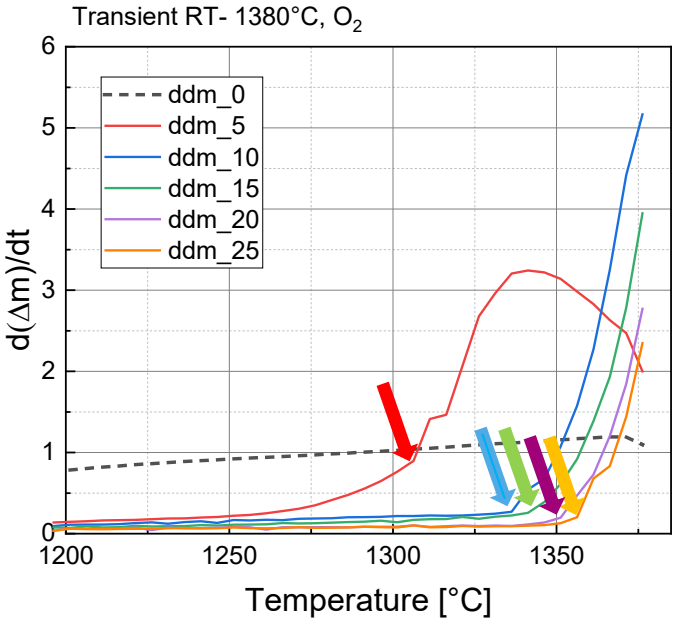

- Transition time from protective to non-protective coating increases with Cr thickness for all three test series

Post-test appearance of 1200°C samples

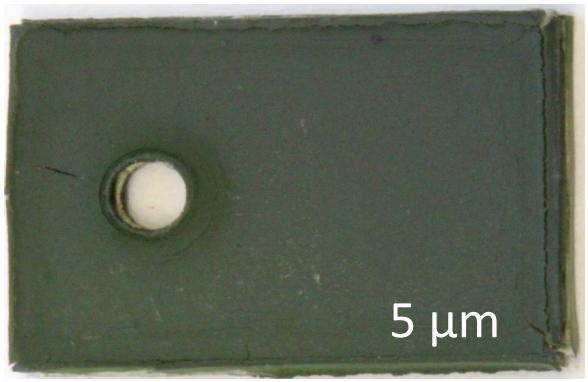

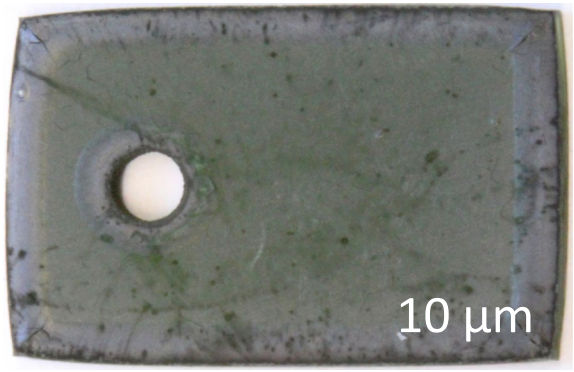

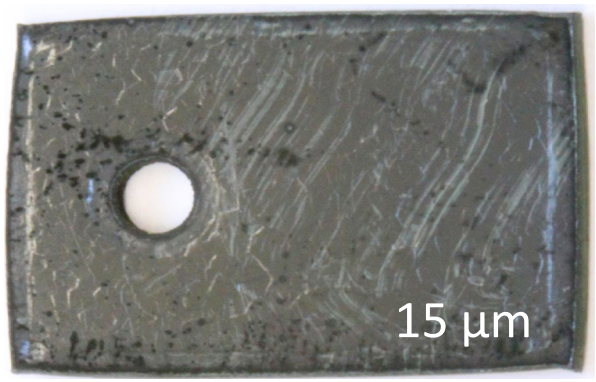

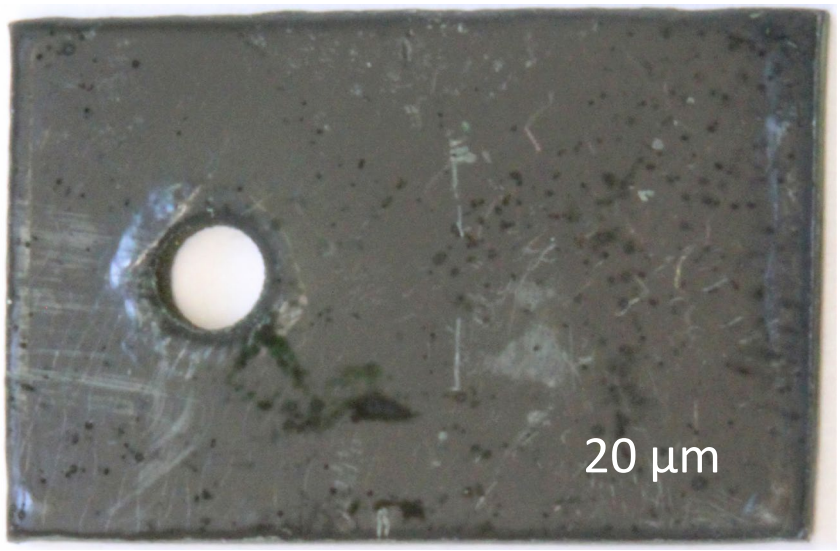

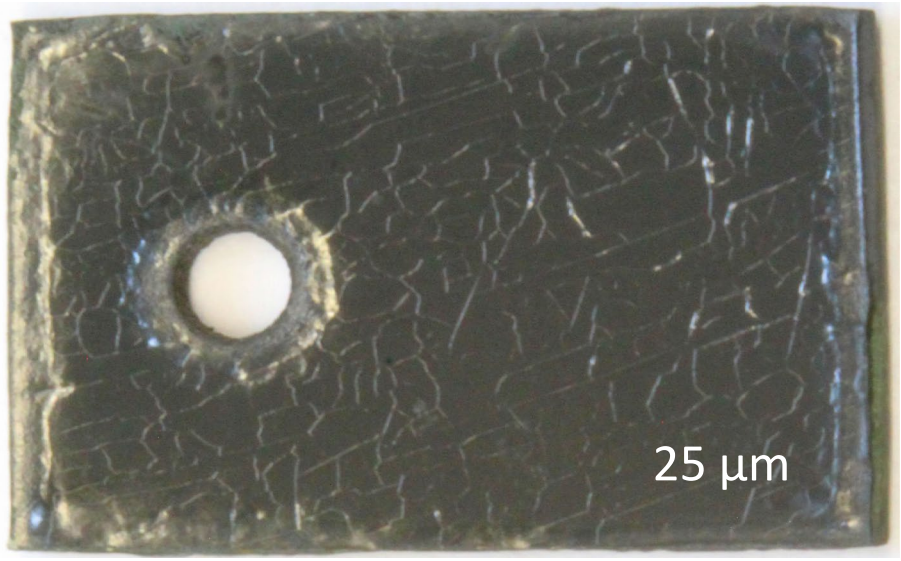

Ridge formation on 25 µm Cr samples

Isothermal tests at 1200°C in steam: macrographs

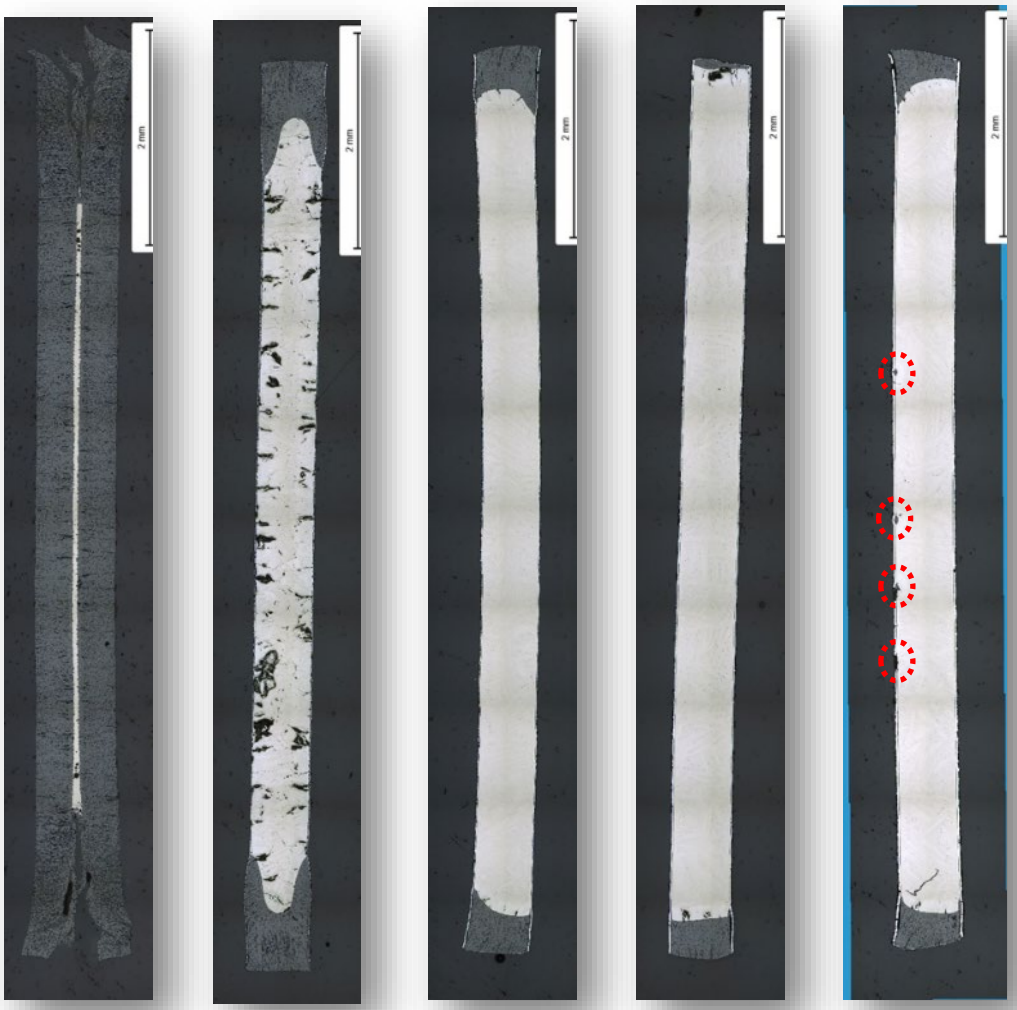

- Significant ridge effects
- Uncoated reference sample fragmented
- Almost complete oxidation of the 5-µm sample
- α-Zr(O) formation in 10-µm sample
- Local effects at 25-µm sample

SEM BSE images of 1200°C samples

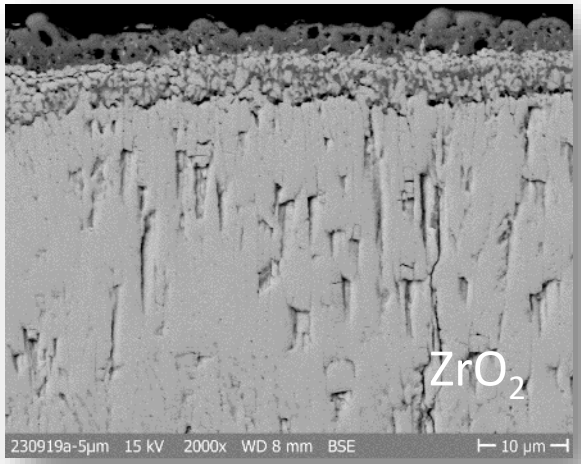

5 µm

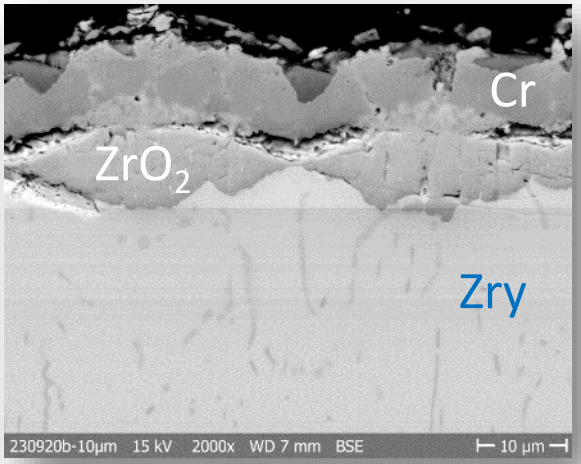

10 µm

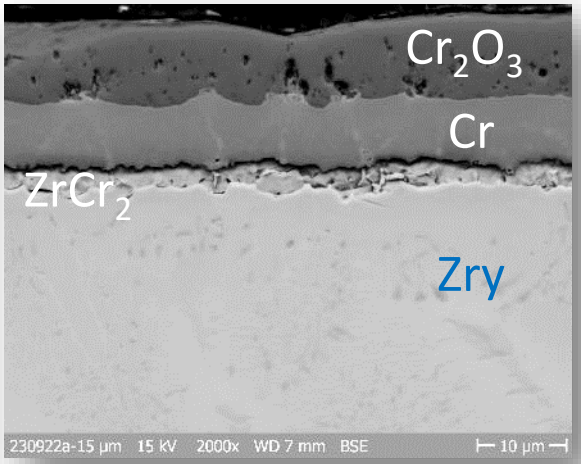

15 µm

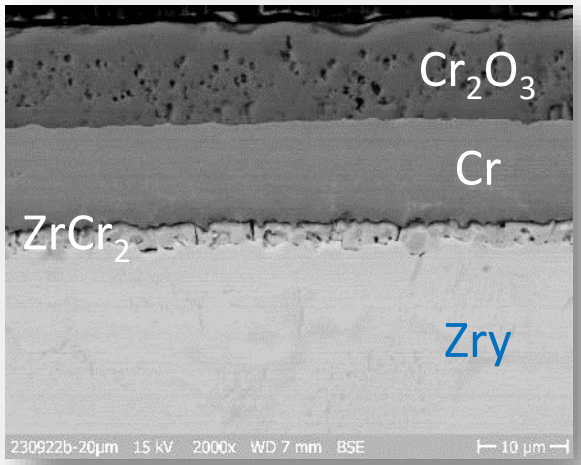

20 µm

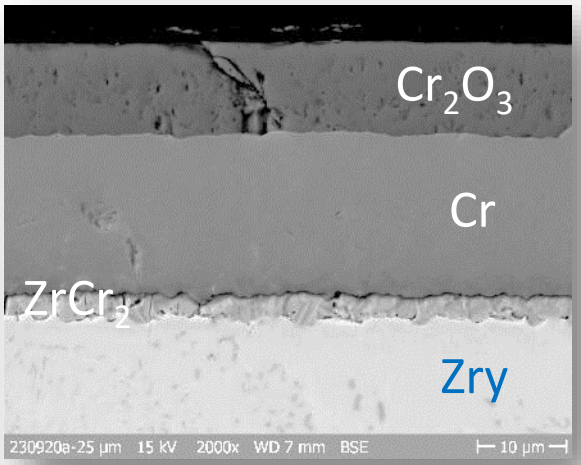

25 µm

EDS mappings of 1200°C samples

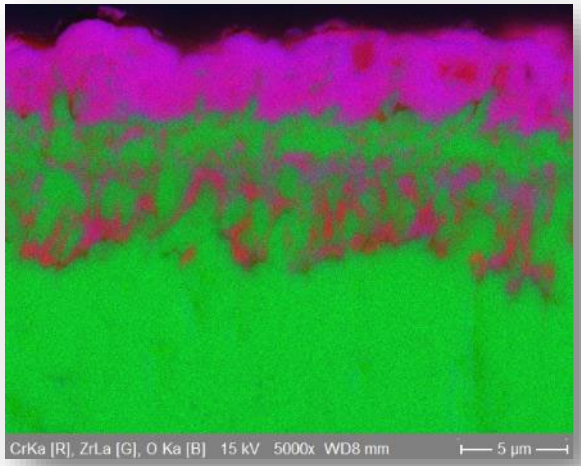

5 µm

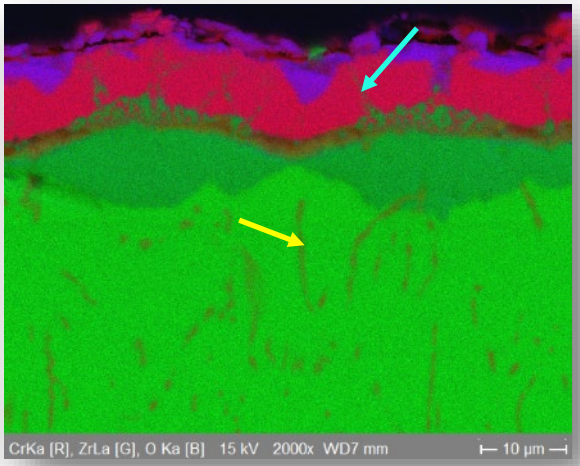

10 µm

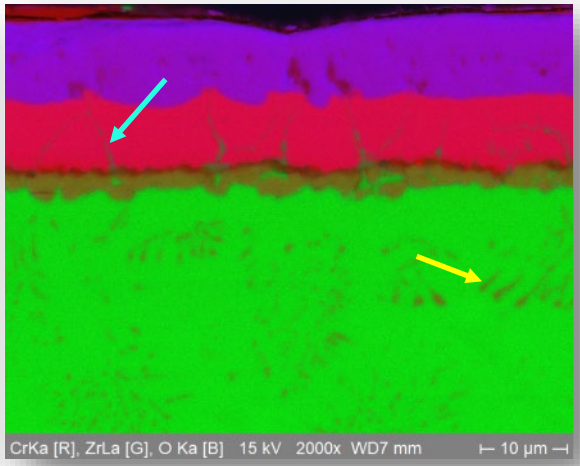

15 µm

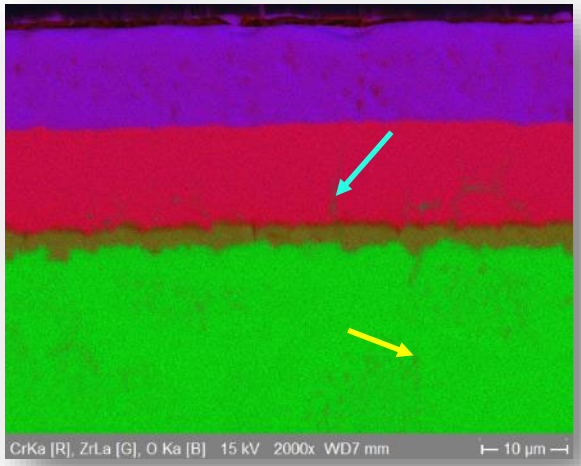

20 µm

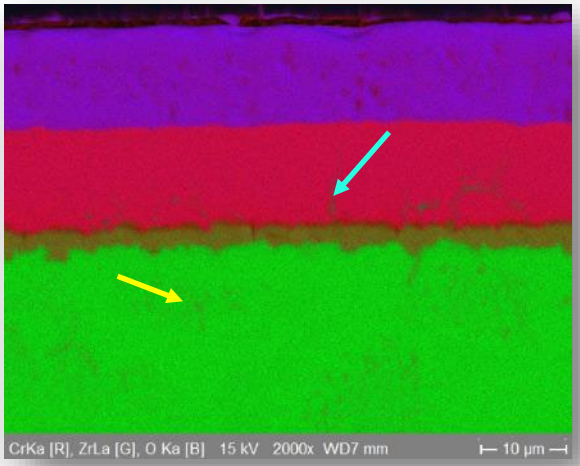

25 µm

- ZrC_2 precipitates in Zry
- ZrO_2 pathes along Cr grain boundaries (not through-going for 20/25 µm)

Special feature only for the 25 µm sample

Failure of Cr coating
during oxidation

Indication for too thick Cr coating resulting in thermo-mechanical mismatch?

Effect of atmosphere

(very preliminary results)

Background

- According to Brachet (Cor. Sci 2020), volatility of Cr_2O_3 is negligible up to 1300°C
- However, volatility is strongly dependent on composition of atmosphere

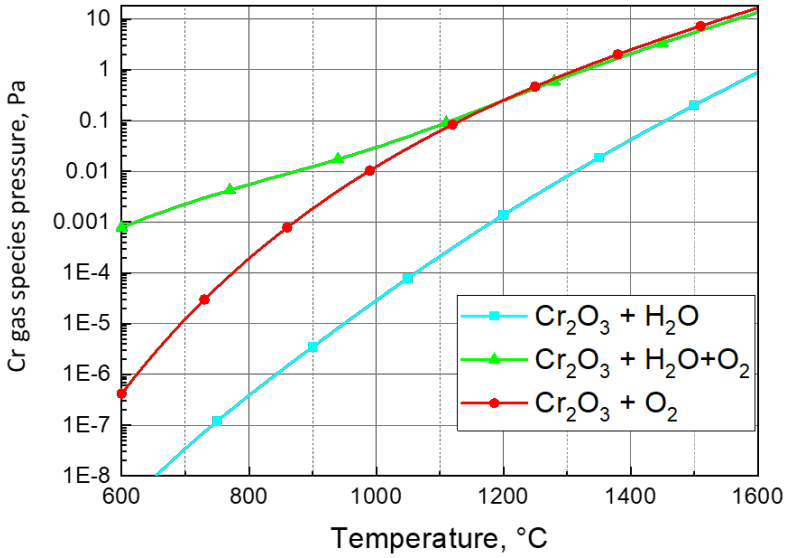

- Effect of gas composition on oxidation?
- Oxidation of Cr-coated Zry-4 plates at 1200°C in
  - H_2O
  - O_2
  - $H_2O + O_2$

$$Cr_2O_3(s) + 2H_2O(g) + 1.5O_2(g) \rightarrow 2CrO_2(OH)_2(g)$$
$$Cr_2O_3(s) + 1.5O_2(g) \rightarrow 2CrO_3\ (g)$$

TG results

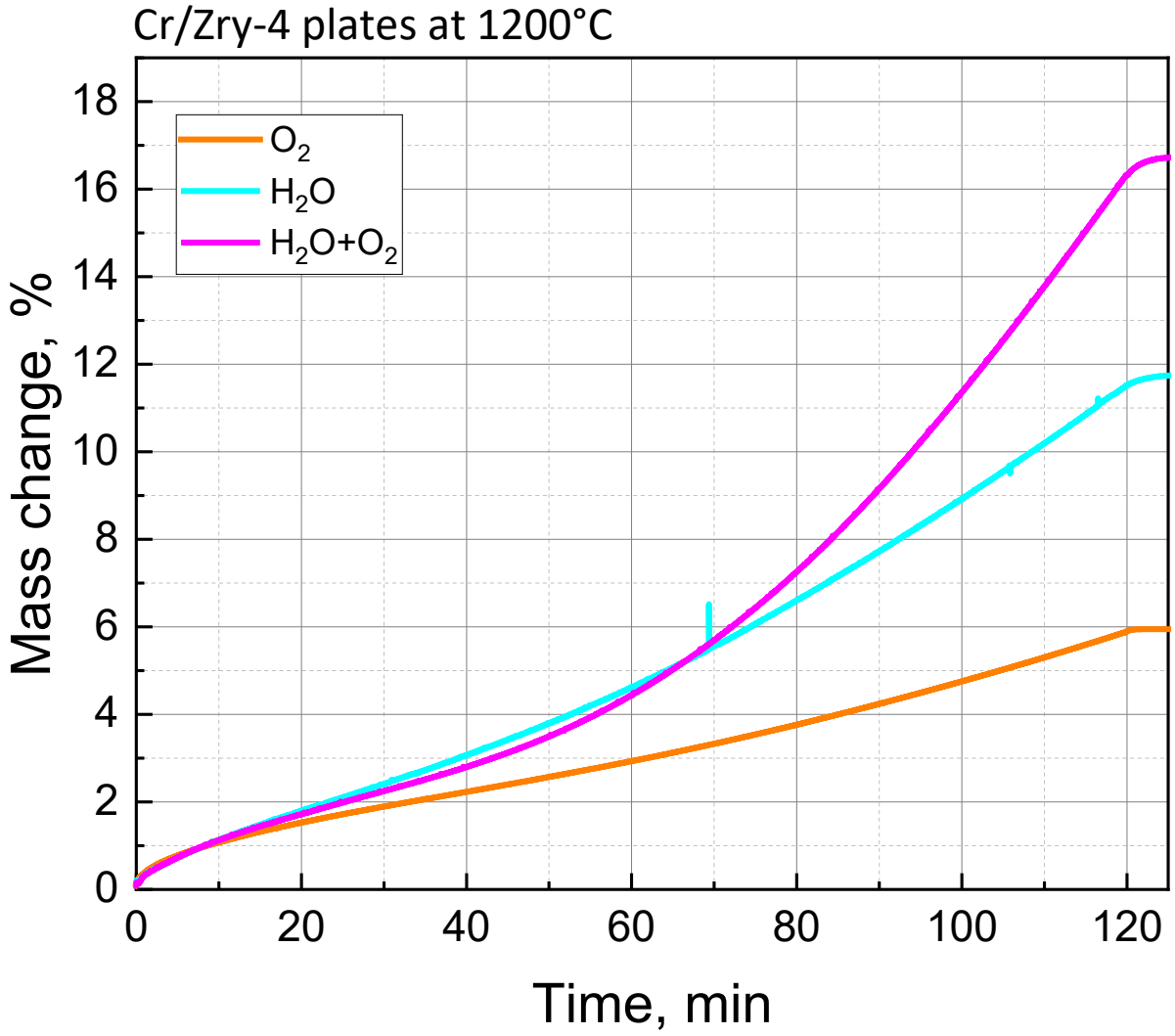
Cr/Zry-4 plates at 1200°C
O2
H2O
H2O+O2
Mass change, %
Time, min
0
2
4
6
8
10
12
14
16
18
0
20
40
60
80
100
120

Post-test appearance

O_2 H_2O H_2O+O_2

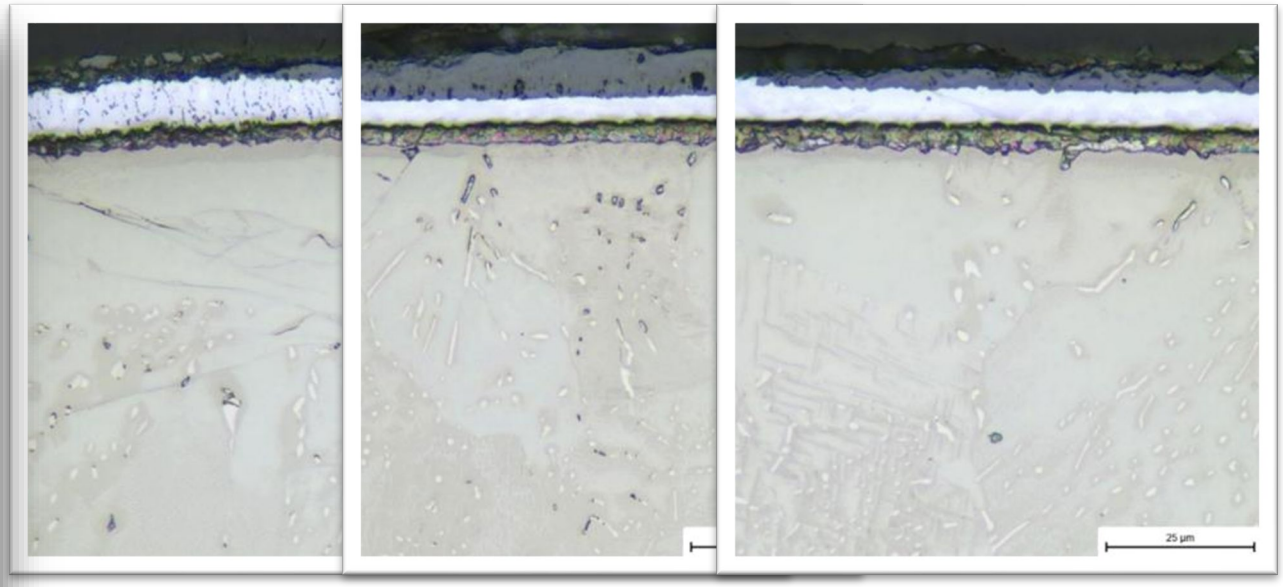

O_2 H_2O H_2O+O_2

- Significant edge effects
- Strongest overall oxidation in steam-O_2 mixture
- Thickest Cr oxide scale in steam
- More systematic experiments needed

Conclusion

- The oxidation and degradation mechanisms of Cr-coated Zr alloys are understood
- Coating thickness (and quality), temperature history (heating rates) and boundary conditions (composition of ambient atmosphere) affect oxidation kinetics, mechanisms and duration of protective behavior of Cr coatings
- 15-20 µm Cr thickness (PVD) seems to be the best compromise between protectiveness and mechanical compatibility with Zry bulk of the coating

M. Kolesnik (presented by J. Stuckert)
KIT

Modeling of hydrides morphology in zirconium tubes loaded by internal pressure after slow cooling

Hydrogen embrittlement of zirconium alloys occurs due to the presence of a hydride phase in the metal matrix. The ductile-to-brittle transition in the fracture mode of hydrogenated zirconium alloys can arise when hydrides form an interconnected network and provide a path for the brittle crack through the thickness of the loaded specimen. Therefore, the morphology of the hydrides largely determines the fracture mode of hydrogenated zirconium alloys. This presentation is dedicated to numerical approaches for simulating the morphology of hydrides in zirconium alloys. It focuses on the modelling of fuel rod cladding under conditions typical for spent nuclear fuel handling and storage. The basic approach simulates average values of the following main morphology parameters during heating and cooling: orientation, average size and spacing between hydrides. The effect of cooling rate in a wide range on morphology has been analyzed based on the numerical study. Further development of the approach simulates hydride continuity metrics widely used in practice. Coupled with the Monte Carlo method, it is possible to predict not only average values of the morphology parameters, but also their statistical distribution, and thus the probability of local critical hydrogen embrittlement.

28th International QUENCH Workshop
Karlsruhe Institute of Technology, North Campus
December 5 – 7, 2023

Modelling of hydride morphology in zirconium tubes loaded by internal pressure after slow cooling

Mikhail Kolesnik
/presented by J. Stuckert/
Karlsruhe Institute of Technology

Hydrogen embrittlement of Zr alloys:
the role of hydrides

Hydrides serve as fracture nucleation sites

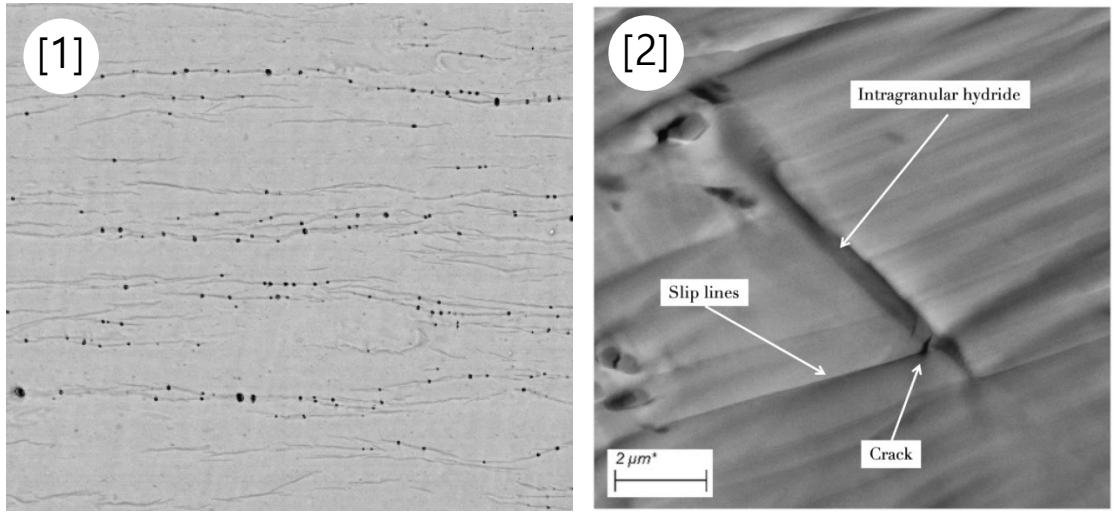

Hydrides proved an easy pathway for the brittle crack propagation

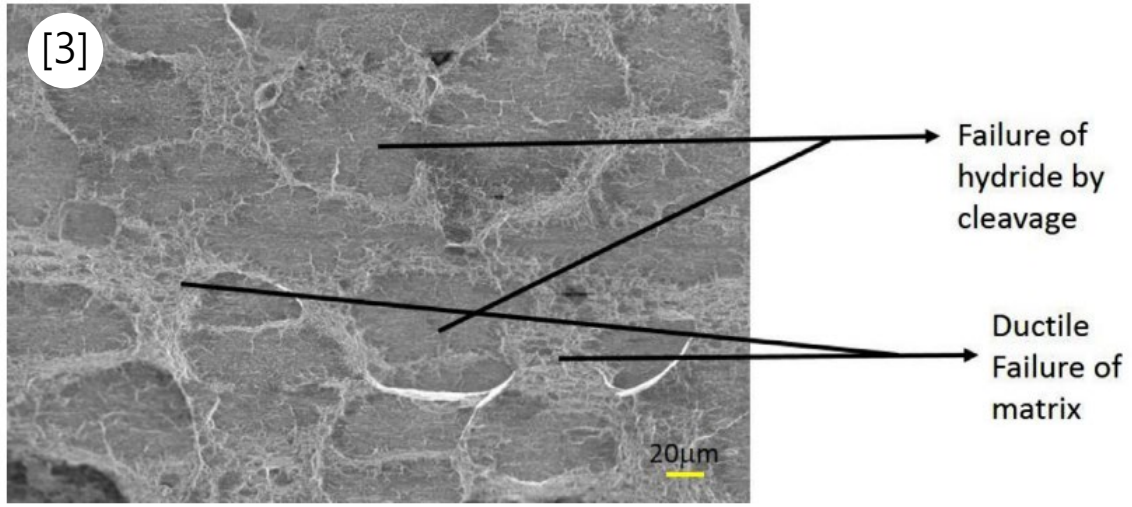

Brittle fracture of Zr alloy is localized in hydrides

[1] Le Saux *et al. Eng. Fail. Anal.*, 17 (2010) 683–700; DOI: 10.1016/j.engfailanal.2009.07.001
[2] Reali *et al. J. Mech. Phys. Solids*, 147 (2021) 104219; DOI: 10.1016/j.jmps.2020.104219
[3] Gopalan *et al. J. Nucl. Mater.*, 544 (2021) 152681; DOI: 10.1016/j.jnucmat.2020.152681

Hydride morphology and ductile-to-brittle transition (DBT): *a brittle crack percolation*

Hydrides can be considered as platelets and characterized by three following parameters:

(1) orientation
(2) length
(3) spacing

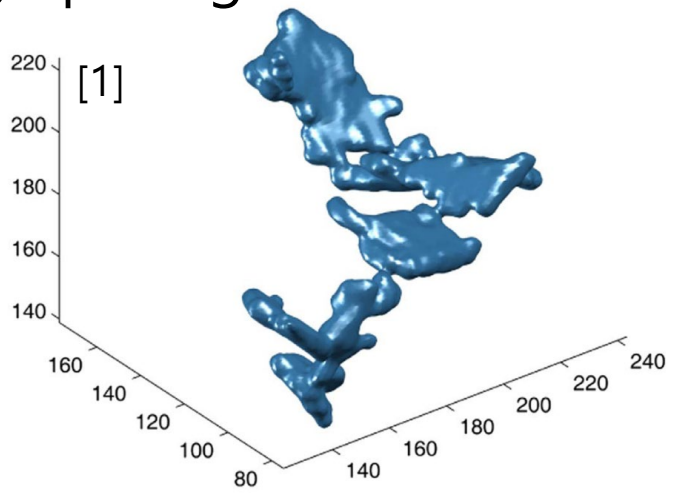

Integral morphology metrics: continuity of hydrides

Accumulated Hydride Length (AHL)
Hydride Continuity Coefficient (HCC)

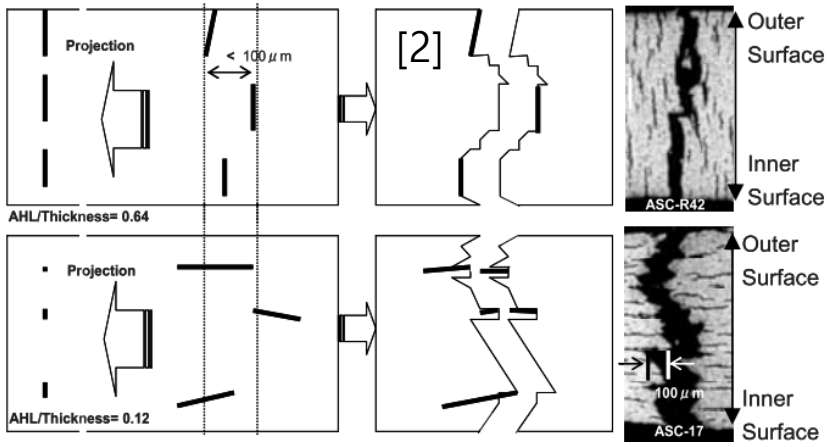

Radial Hydride Continuity Factor (RHCF)

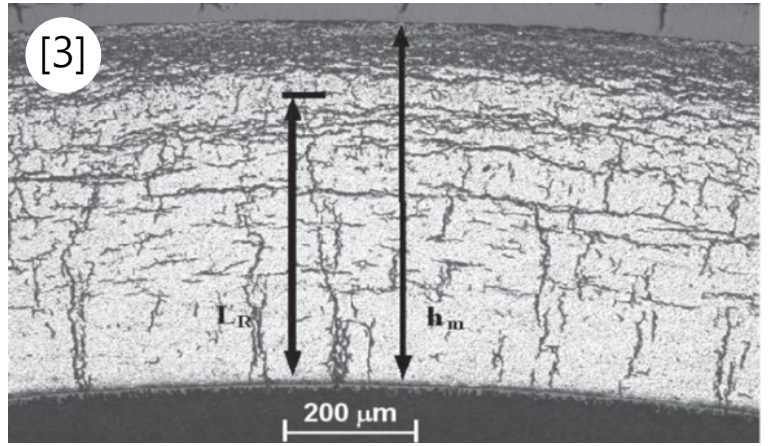

DBT condition is the threshold continuity of hydrides

[1] Fang *et al. Mat. Charact.*., 134 (2017) 362–369; DOI: 10.1016/j.matchar.2017.11.013
[2] M. Nakatsuka and S. Yagnik *J. ASTM int.* 8 (2010); DOI: 10.1520/JAI102954
[3] M. C. Billone *et. al. J. Nucl. Mat.* 433 (2013) 431-448; DOI: 10.1016/j.jnucmat.2012.10.002

What processes determine the morphology of hydrides?
nucleation of hydrides

Approach: heterogeneous nucleation in the classical approximation

Governing equations:

$$R = NZj^* \cdot \exp(-\Delta G^*/kT)$$ nucleation frequency

$$\Delta G^* = \Omega^*(g_m - \Delta\mu/v) + S^*\gamma - G_d$$ Gibbs free energy change

$$\Delta\mu = \chi \cdot kT \cdot \ln(C_s/C_e)$$ chemical energy change

$$g_m \approx \sigma_y \epsilon$$ mechanical energy

$$\frac{dn}{dt} = \int_{vacant\ sites} R(G_d) \cdot dG_d$$ increment of hydrides

R	nucleation frequency	$\Delta\mu$	chemical energy change
N	density of nucleation sites	v	atomic volume of Hydrogen
Z	Zeldovich factor	γ	metal/hydride surface energy
j^*	diffusion flow of H to the critical nucleus	γ_{gr}	grain boundary surface energy
ΔG^*	Gibbs free energy of the critical nucleus	χ	molar fraction of H in hydride
Ω^*	volume of the critical nucleus	C_s	H concentration in solid solution
S^*	surface area of the critical nucleus	C_e	equilibrium H concentration
g_m	mechanical energy of the critical nucleus	σ_y	yield stress of Zr matrix
G_d	defect energy	ϵ	volume dilatation

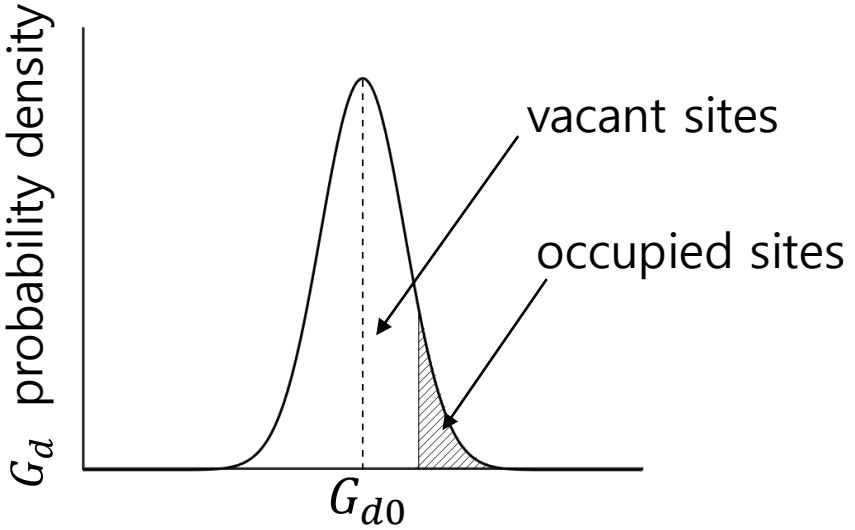

distribution of nucleation sites over the defect energy

What processes determine the morphology of hydrides?
diffusion growth and orientation function

Diffusion growth of hydrides:

H concentration in solution C_s tends to its equilibrium value C_e with characteristic time τ_0

$$\frac{\mathrm{d}C_s}{\mathrm{d}t} - \frac{1}{\tau_0}(C_s - C_e) = 0, \qquad \tau_0 = \frac{\Delta^2}{\alpha D}$$

Δ	spacing of hydrides
D	diffusion coefficient
α	geometric factor

Orientation function:

The Gibbs energy change difference of hydrides with two orientations is assumed to be a linear function of external stresses. Assuming $C_r = \theta \cdot C_h$:

$$\begin{cases} \dfrac{\mathrm{d}C_r}{\mathrm{d}t} = C_h \dfrac{\mathrm{d}\theta}{\mathrm{d}t} + \theta \dfrac{\mathrm{d}C_h}{\mathrm{d}t} \\ \dfrac{\mathrm{d}C_r}{\mathrm{d}t} = F_r \dfrac{\mathrm{d}C_h}{\mathrm{d}t} \end{cases} \Rightarrow \frac{\mathrm{d}\theta}{\mathrm{d}t} = \frac{F_r - \theta}{C_h} \cdot \frac{\mathrm{d}C_h}{\mathrm{d}t}$$

$$F_r = \frac{1 - f_t}{1 + \exp(-(\Delta G_t^* - \Delta G_r^*)/kT)} + f_t$$

$$\Delta G_t^* - \Delta G_r^* = \sigma \cdot \Delta\Omega^* - kT \cdot \ln f_0$$

C_h	H concentration in hydrides
C_r	H concentration in radial hydrides
θ	fraction of H in radial hydrides
F_r	orientation function
f_t, f_0	texture and microstructure factors

Average morphology parameters simulation
ODE system numerical solution

ODEs for precipitation:

$$\begin{cases} \dfrac{\mathrm{d}C_s}{\mathrm{d}t} = \dfrac{C_s - C_{e,p}}{\tau_0} \\ \dfrac{\mathrm{d}\theta}{\mathrm{d}t} = \dfrac{F_r - \theta}{C_r} \cdot \dfrac{\mathrm{d}C_r}{\mathrm{d}t} \\ \dfrac{\mathrm{d}n_r}{\mathrm{d}t} = F_r \cdot \int\limits_{vac.site} R(G_d) \cdot \mathrm{d}G_d \\ \dfrac{\mathrm{d}n_t}{\mathrm{d}t} = (1 - F_r) \cdot \int\limits_{vac.site} R(G_d) \cdot \mathrm{d}G_d \end{cases}$$

ODEs for dissolution:

$$\begin{cases} \dfrac{\mathrm{d}C_s}{\mathrm{d}t} = -\dfrac{C_s - C_{e,d}}{\tau_0} \\ \dfrac{\mathrm{d}\theta}{\mathrm{d}t} = const \\ \dfrac{\mathrm{d}n_r}{\mathrm{d}t} = const \\ \dfrac{\mathrm{d}n_t}{\mathrm{d}t} = const \end{cases}$$

Independent variables:

C_s	H in solid solution
θ	fraction of H in radial hydrides
n_r	volume density of rad. hydrides
n_t	volume density of tan. hydrides

The model can simulate:

1. average orientation
2. average size
3. average spacing

The model can not simulate:

1. continuity metrics
2. spatial and statistical distributions of parameters

Simulation results: slow stepwise cooling
approach based on ODE system solution

Simulation parameters:

Samples: gas-filled tubes, Zircaloy-4
H concentration: 100 and 300 ppm
Internal gas pressure: 106 and 146 bar ($\sigma_{\theta\theta}$ = 88 and 121 MPa)
Maximal temperature: 400 ºC
Minimal temperature: 200 ºC
Cooling rate at step: ~ 10^{-3} ºC/sec (5 ºC/hour)
Average cooling rate: ~ 10^{-5} ºC/sec (1 ºC/day)

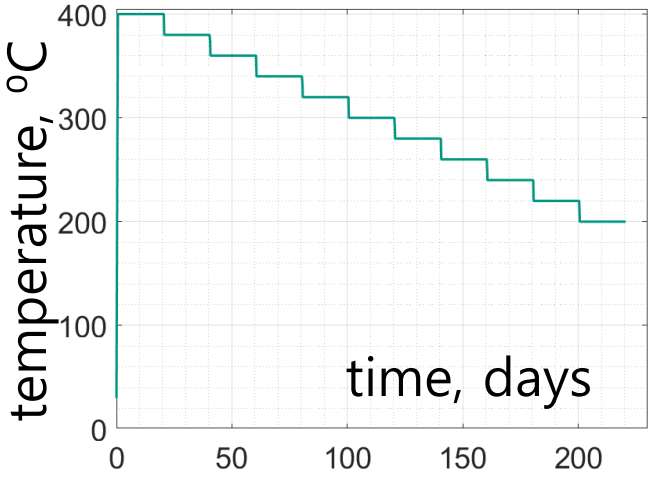

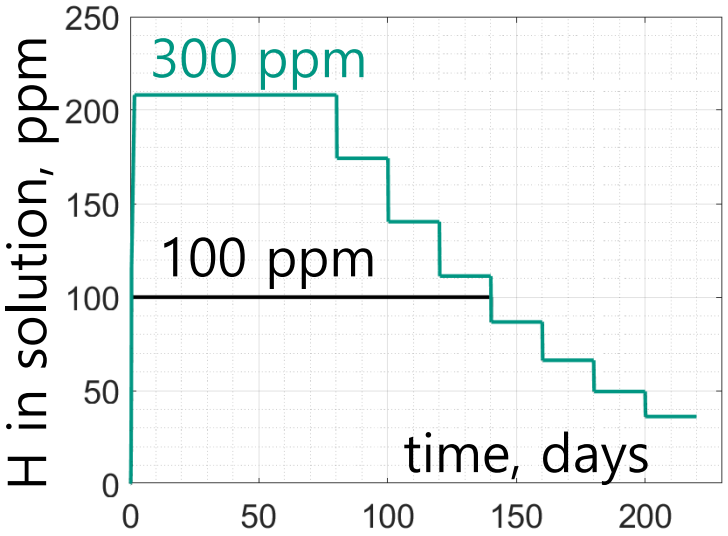

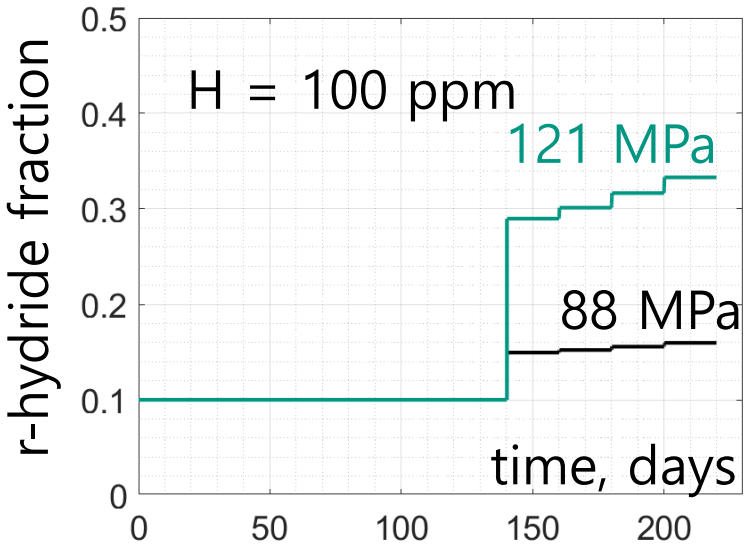

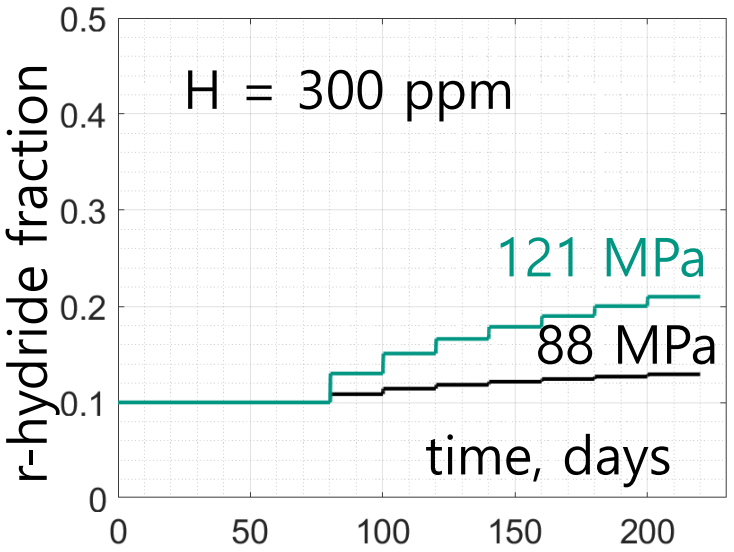

Simulation results: slow stepwise cooling
approach based on ODE system solution

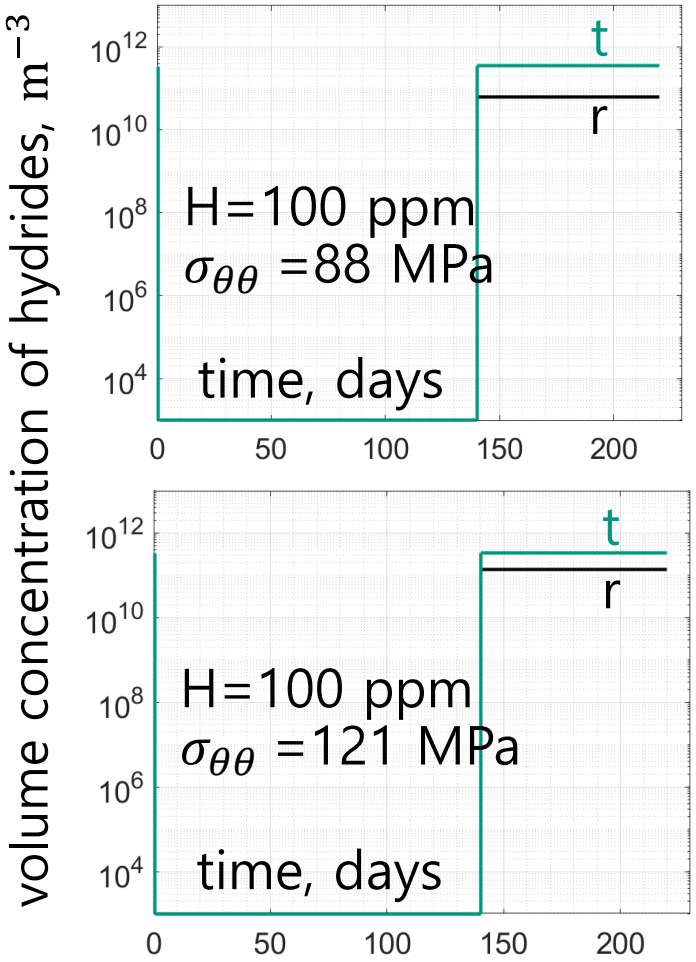

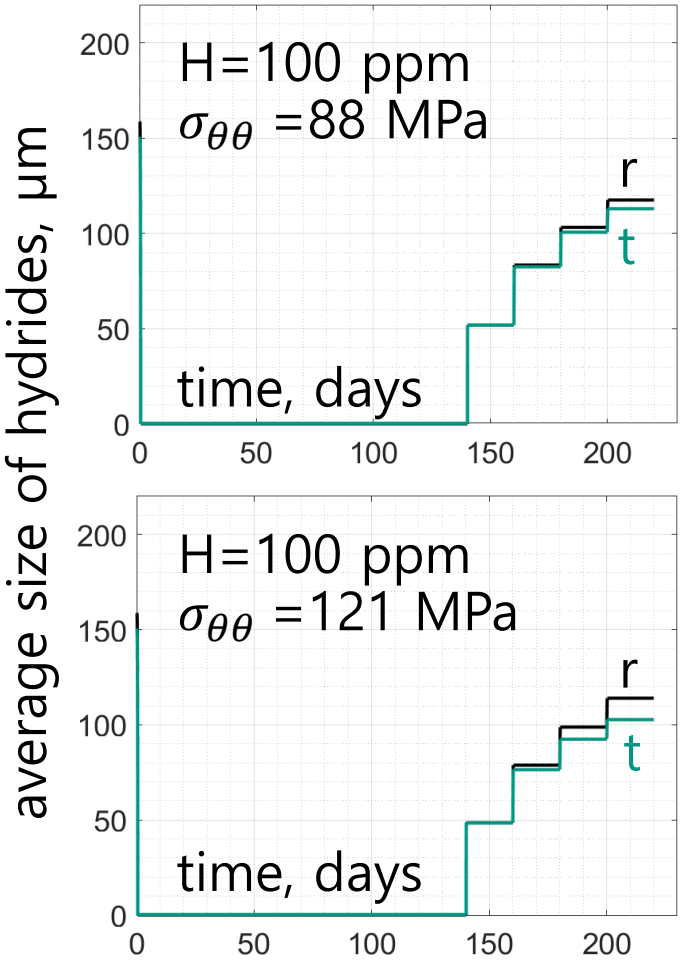

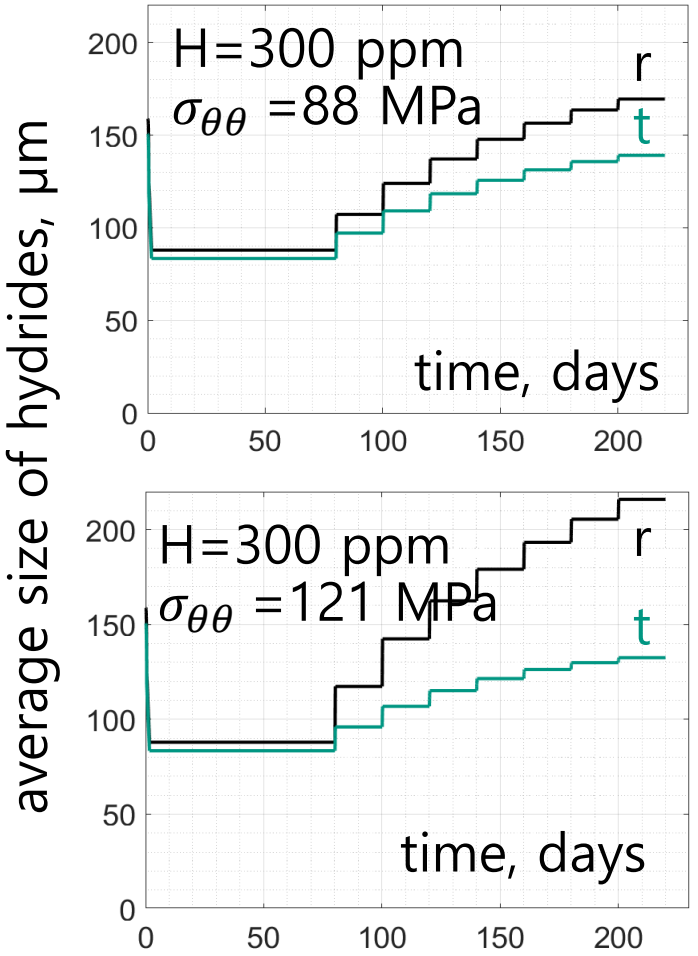

The morphology of the hydrides is a function of their initial state in the 300 ppm samples, but not in the 100 ppm samples.

Simulation results: the effect of cooling rate
approach based on ODE system solution

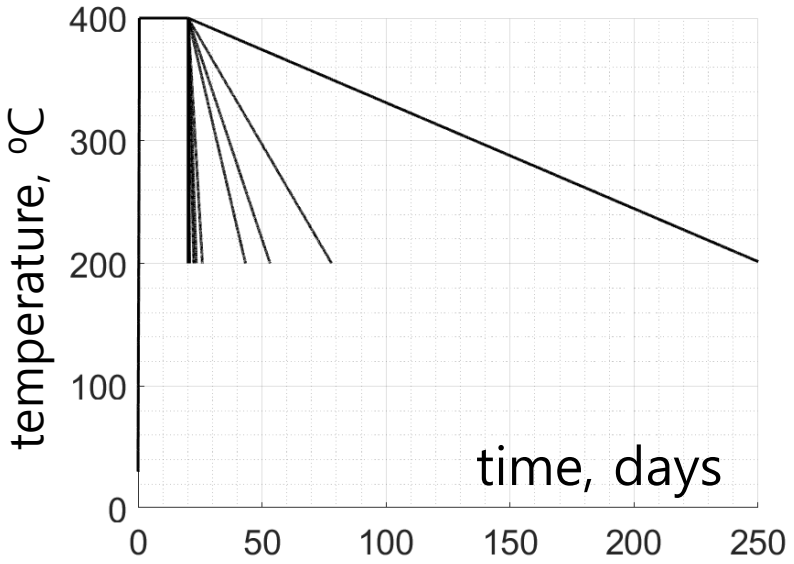

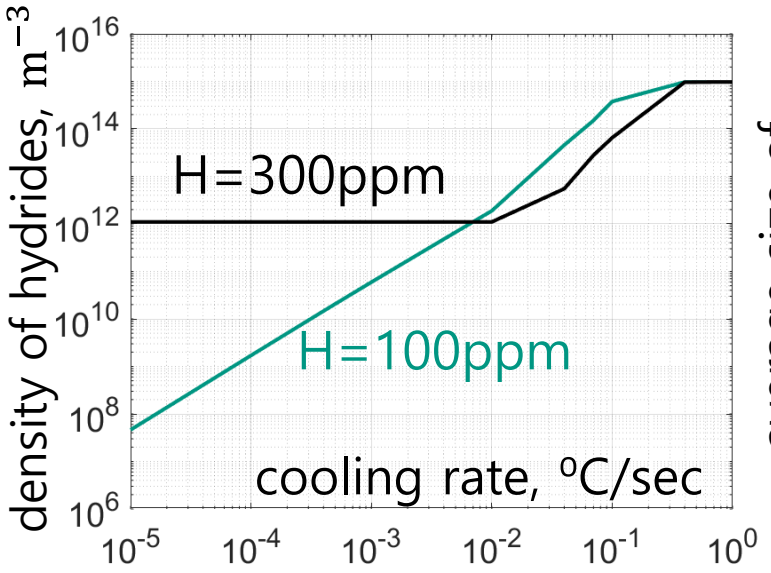

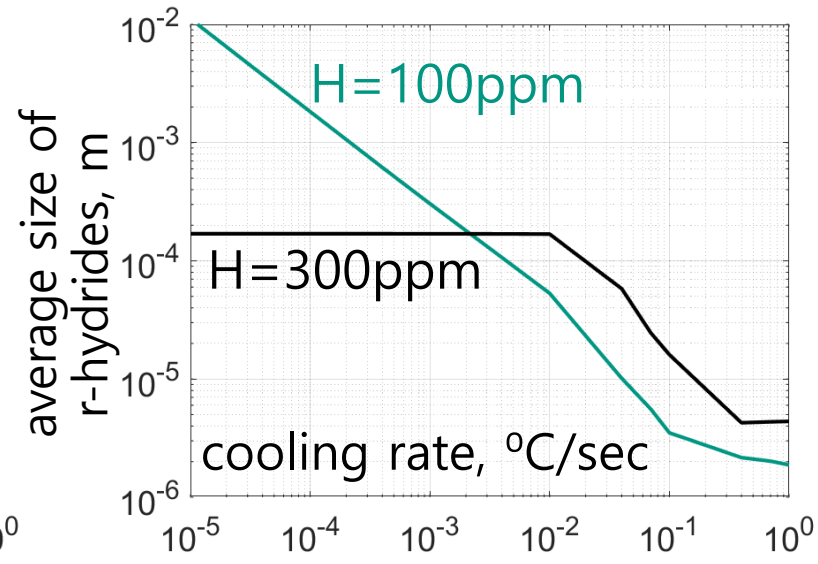

Partial dissolution of hydrides (300 ppm, 400 °C):
Hydride morphology is weakly dependent on cooling rate. Laboratory tests simulate dry storage conditions well.

Complete dissolution of hydrides (100 ppm, 400 °C):
Morphology is strongly dependent on cooling rate. Laboratory tests conducted at higher cooling rates may not produce conservative estimation of ductility for the purpose of justifying dry storage conditions.

How to simulate statistical distribution of morphology parameters?
coupling with Monte Carlo method

The simplest approach: randomise hydrides in 3D domain (with given density, size and orientation)

Additional assumptions:
1. simulate nucleation and growth of hydrides (randomize the hydride density)
2. consider competition among neighboring hydrides for Hydrogen (clustering effect)

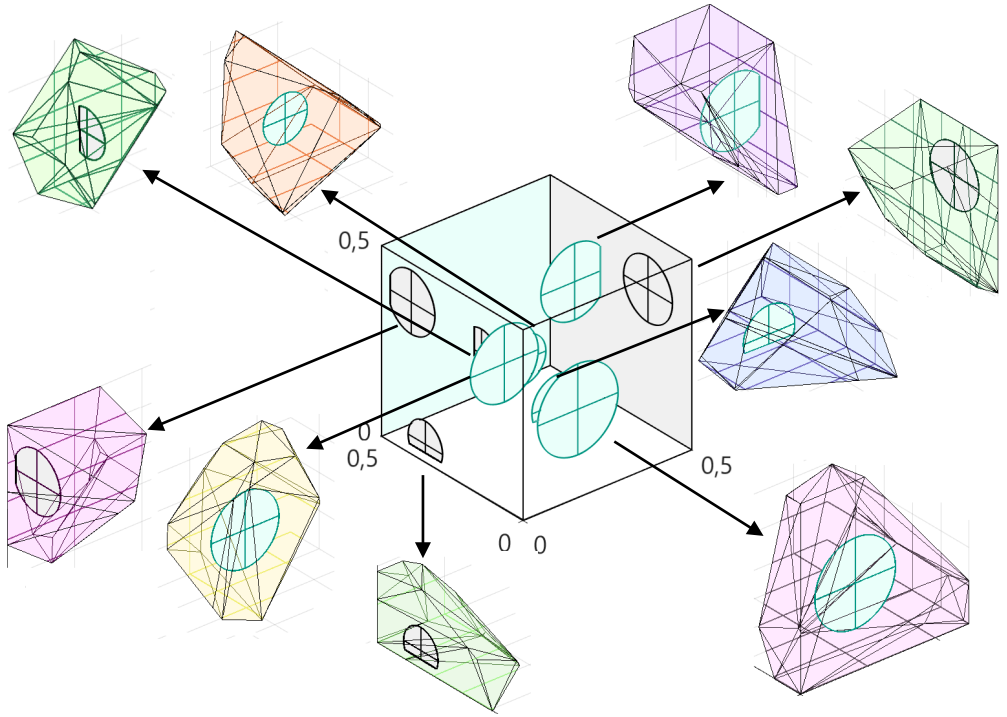

A 3D domain with nine random hydrides and Voronoi tessellation.
Voronoi cells limit the amount of hydrogen available to each hydride.

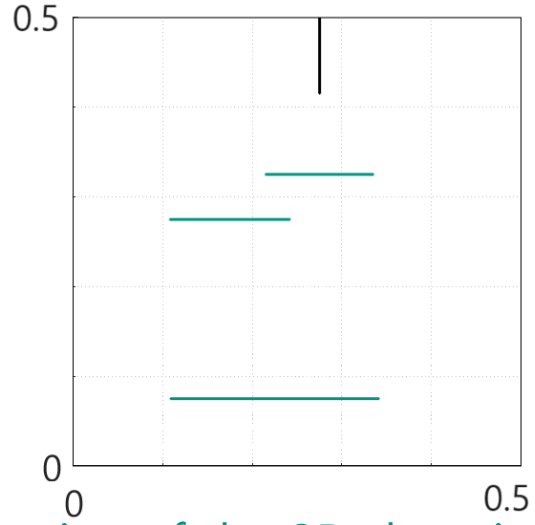

Cross-section of the 3D domain and four hydrides as a result of simulation.
Any morphology metric can be estimated as in experiments on micrographs.

Simulations result: continuity metrics and their distribution
coupling with Monte Carlo method

Simulation parameters:

3D domain: 0.1x0.6x0.3 mm
H concentration: 100 ppm
External stress: 88 and 121 MPa
Temp. scenario: stepwise cooling
Maximal temp.: 400 ºC
Minimal temp.: 200 ºC
Number of simulations: ~1000

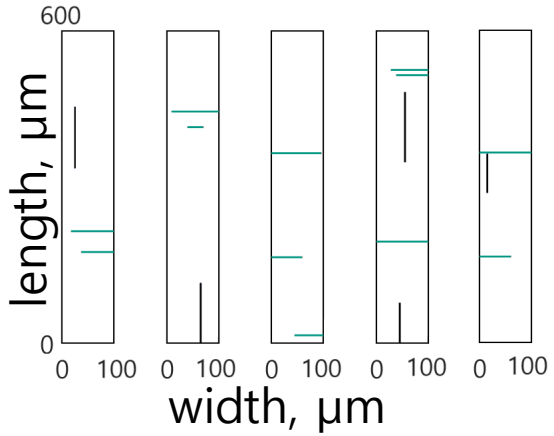

5 independent simulations

cross-sections with hydrides

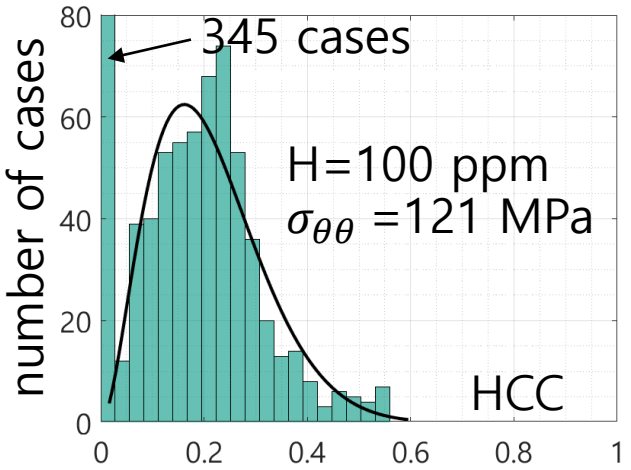

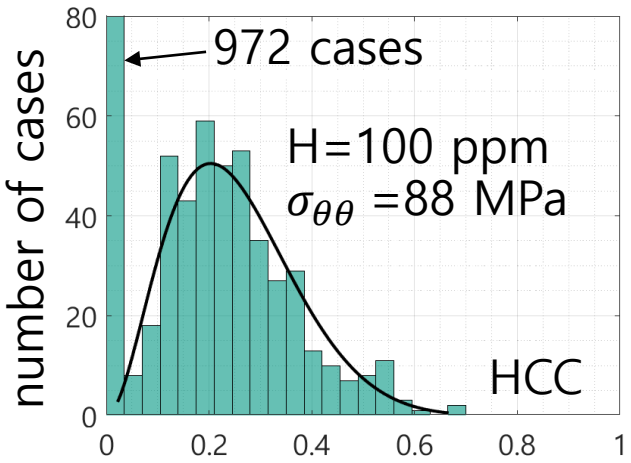

Calculated statistical distribution of HCC (AHL) metric:

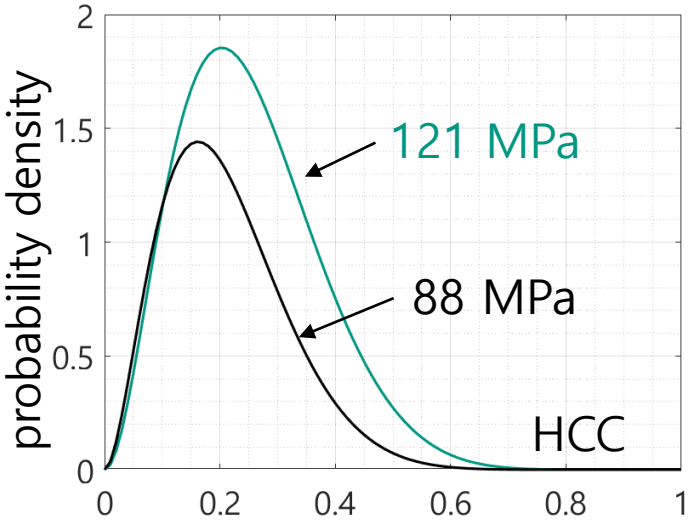

HCC is fitted by beta distribution, which has been applied for modeling of random values limed by an interval (like percentages)

Hydrogen Continuity Coefficient (HCC) or Accumulated Hydride Length (AHL):
the summary projection of hydride lengths within a 100 μm band onto radial direction.

The problem of small samples

Ring Tensile Test

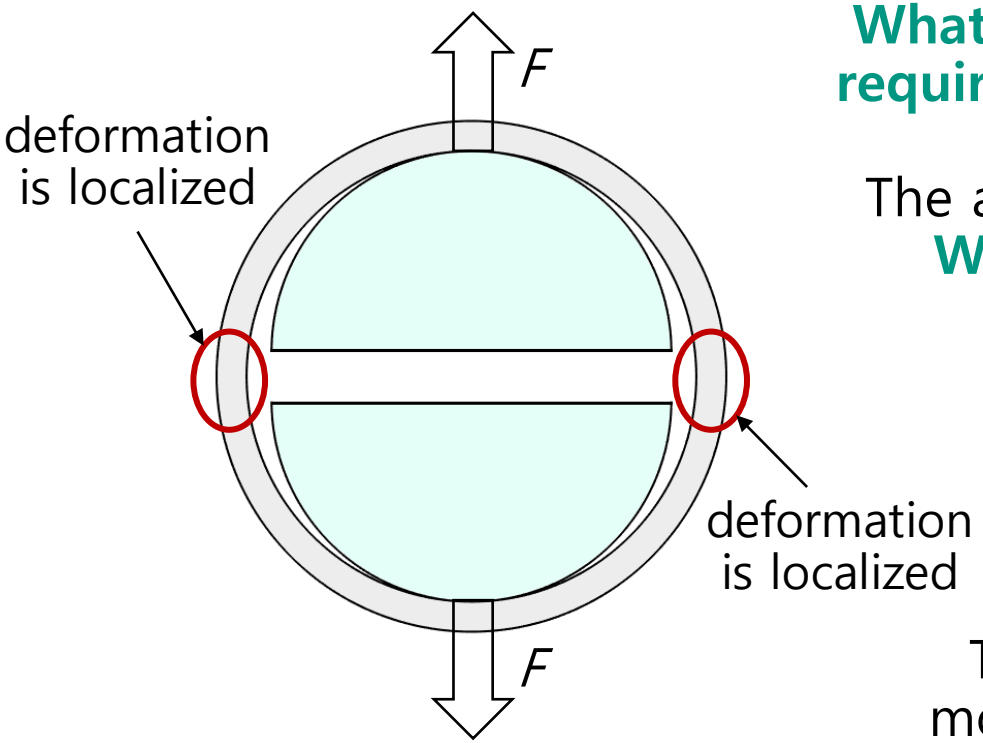

If the local hydrogen embrittlement degree is a random value,
What is the minimum volume (the number of ring specimens) required for a reliable estimation of the mechanical properties?

The answer can be found by first solving the following problem:
What is the probability of observing the critical hydride morphology in a random small volume Ω?

$$p_{crit} = 1 - \left[\int_0^{HCC_{crit}} \mathrm{pdf}(HCC) \cdot \mathrm{d}HCC \right]^{\Omega/V_0}$$

The probability density function (pdf) of HCC (or any other morphology metric) can be estimated either experimentally or computationally, as shown on the previous slide.

$^{*}V_0$ – minimal volume defining HCC (~0.1x0.6x0.3mm)

Summary

- The average values of orientation, size, and spacing of hydrides, has been simulated by the solution of the ordinary differential equation system. The hydride continuity coefficient and its statistical distribution have been estimated by coupling with the Monte Carlo method.
- If hydrides dissolve partially (300 ppm), then the final morphology is largely determined by their initial state. If hydrides dissolve completely (100 ppm), then the final morphology is largely determined by the cooling rate.
- It has been demonstrated that there are two potential sources of nonconservative assessments of hydrogen embrittlement degree in the end of dry storage:
  - If the hydrides dissolve completely, their length at the end of dry storage may exceed that under comparable conditions, but faster cooling. Therefore, the laboratory tests can underestimate the embrittlement degree;
  - Fracture testing of small specimens examines their local properties, which is a random value. Therefore, there is a possibility, that the most detrimental morphology of the specimen may be outside the fracture zone and test will show overestimated ductility.
- The described approach allows to justify both extrapolation to lower cooling rates, typical for dry storage, and the number of small samples for accurate measurements of hydrogen embrittlement degree.

G. Stahlberg
RUB

Development of a model for Cr-coated Claddings for System Codes

Unmitigated accidents in nuclear power plants can pose risks to the facility's integrity. This is due to factors like increasing temperatures, rising pressures, and the potential release of combustible gases. The fuel cladding, an important element of the defense-in-depth concept, plays a significant role in the progression of accidents. Zirconium (Zr) alloys commonly used as fuel cladding perform well under normal conditions. Their effectiveness is limited at higher temperatures during accidents, potentially leading to rapid accident progression and hydrogen production. Studies suggest that alternative materials, such as Iron-Chromium-Aluminum alloys (FeCrAl) or Chromium-coated claddings could establish another safety aspect in a reactor core. Ongoing developments on Accident Tolerant Fuels (ATF) aim to improve safety by exploring these concepts.

The presented works focus on the modelling of a Cr-oxidation model which is intended to be prospectively implemented into the severe accident code AC²-ATHLET-CD. The oxidation of structural materials or fuel rods can have significant implications for the overall behavior of the system. The accurate prediction of the accident progression is therefore crucial for developing effective mitigation strategies. The Cr-oxidation model is based on empirical correlations derived from experimental data. It considers various factors that influence the oxidation process, including temperature and the presence of steam. In a steam atmosphere the Cr-coating inhibits the inward oxygen diffusion and forms a protective chrome(III)-oxide layer (Cr_2O_3). It is intended to reduce hydrogen release and oxidation heat compared to uncoated Zry. This effect is represented by the overall lower oxidation kinetic and heat release during oxidation.

Sensitivity studies and the comparison with experimental data resulted in various suggestions for improvements of the in-house Cr-coating model. For example, by applying the model on beyond design basis accidents especially the coating failure is key for a reliable prediction of oxidation behavior and the integral hydrogen generation. The coating failure relies on different influential parameters like microstructure, thickness and degradation phenomena, which is currently not modelled in detail due to code simplifications regarding the oxidation calculation. The diffusion of oxygen into the binary system of Cr/Zr as well as diffusion processes between the coating and substrate result in a loss of protectiveness of the coating. This results eventually in enhanced oxidation kinetics. Current studies suggest a similar oxidation kinetic to Zr-alloy after coating failure, which is modelled by setting up a threshold value for the switching of the kinetics from Chromium to the Zirconium correlation of AC². The implementation of the Cr-oxidation model into the in-house version of AC²-ATHLET-CD involves modifying and extending the existing code structure. The model was validated against experimental data showing reasonable agreement between the predicted and measured weight gain. First applications to experiments of the QUENCH facility at KIT resulted in plausible predictions of the calculated sequence progression.

RUB

RUHR-UNIVERSITÄT BOCHUM

Development of a model for Cr-coated Claddings for System Codes

Gregor Stahlberg, Marco K. Koch

28th International QUENCH-Workshop | Karlsruhe, Germany | December 5th to 7th, 2023

PSS Plant Simulation and Safety
Prof. Dr.-Ing. Marco K. Koch

Motivation and Objective

Postulated plant accidents with fuel damage

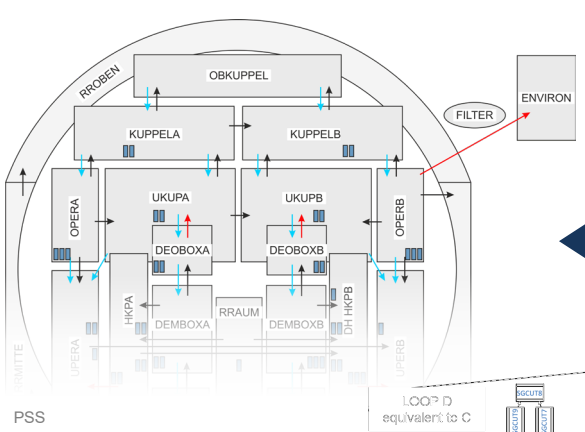

AC²

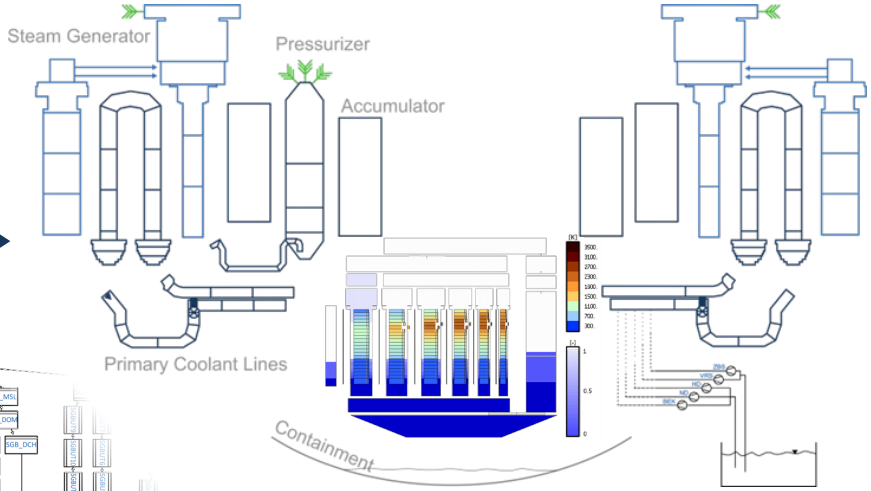

Stahlberg et al. 2021, PSS

ASTEC

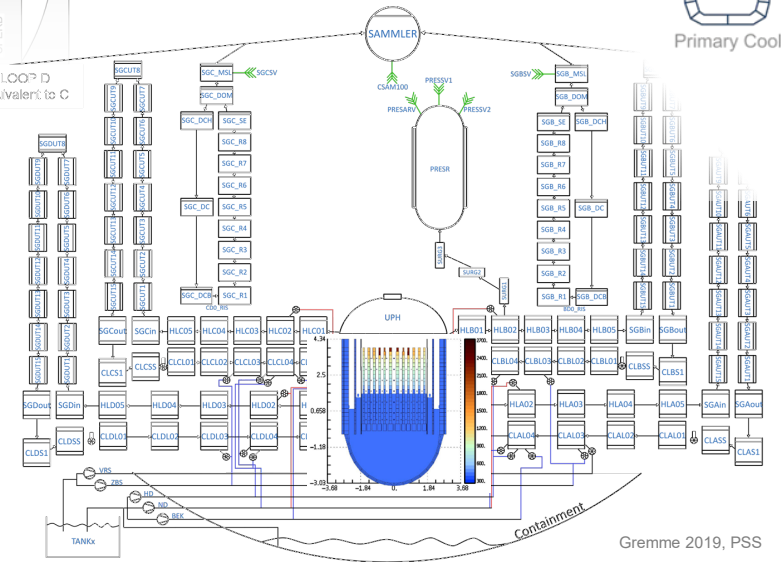

Gremme 2019, PSS

Motivation and Objective

Postulated plant accidents with fuel damage

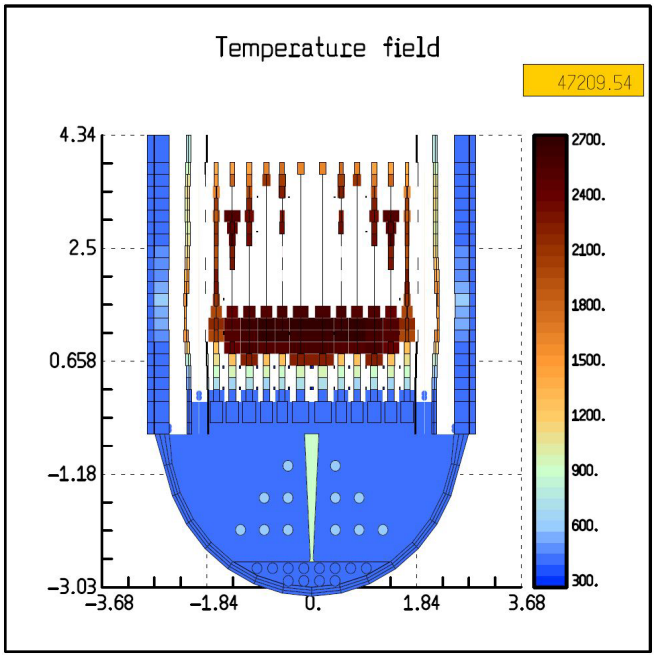

How to increase the coping time?

One key factor is influencing
the accident tolerance!

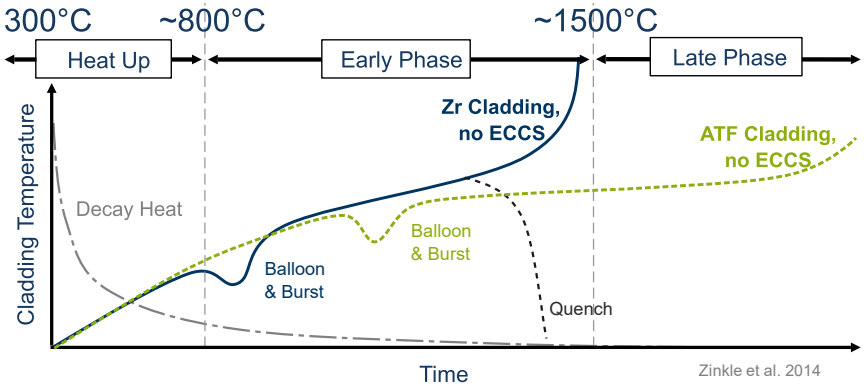

PSS Plant Simulation and Safety
Prof. Dr.-Ing. Marco K. Koch
RUHR UNIVERSITÄT BOCHUM
RUB

ACCIDENT TOLERANT FUEL
Cr-Coating Concept

- Material with higher (oxidation) resistance acting as diffusion barrier to protect underlying Zry
- Reduced oxidation heat (~3.5 MJ/kg_{Cr}), slower oxidation kinetics → Goal: increased coping time and reduced H_2 as well as heat release
- Development of new model for oxidation of Cr-coated claddings available as new option for AC² at RUB PSS (ongoing development)
- Applied on transient bundle experiments on ATF in Joint Project QUENCH-ATF as third party of GRS (validated against Q-ATF-1)

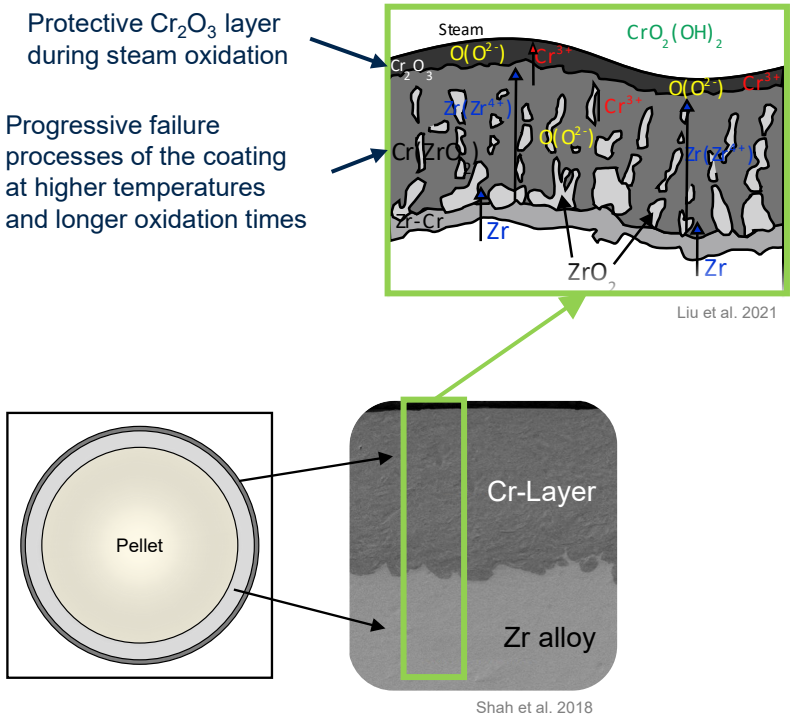

PSS Plant Simulation and Safety
Prof. Dr.-Ing. Marco K. Koch
RUHR UNIVERSITÄT BOCHUM
RUB

Accident Tolerant Fuel
Cr-Coating Concept

National funded Project

QUENCH-ATF
OECD-NEA

Development of Model for Cr-Coated Claddings

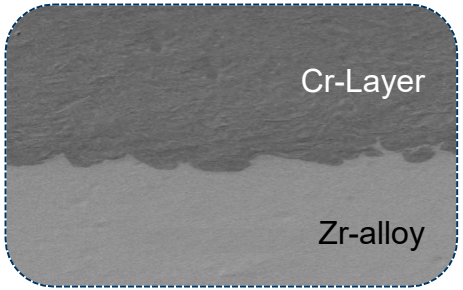

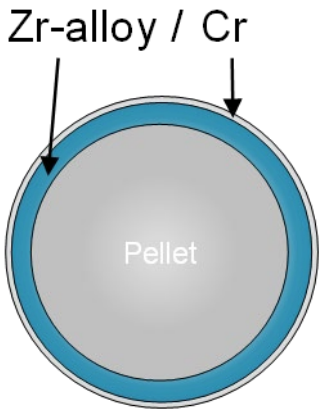

Modelling

MODELLING
Properties

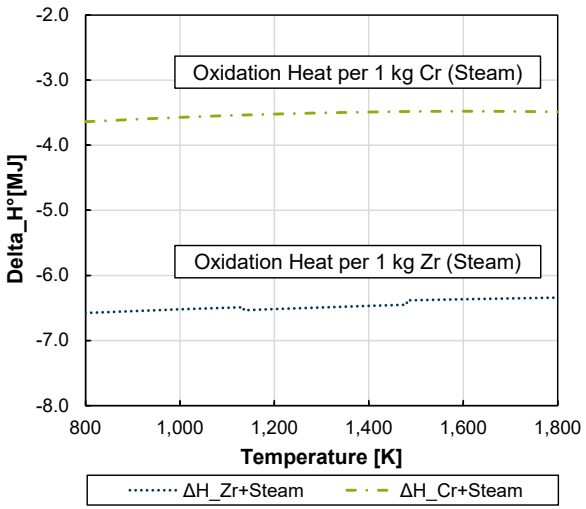

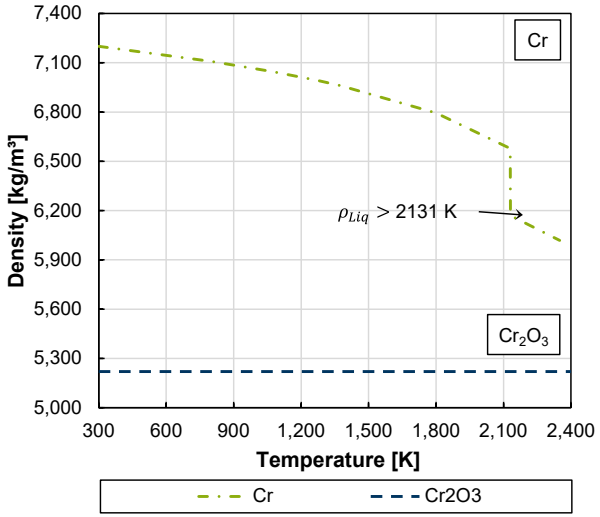

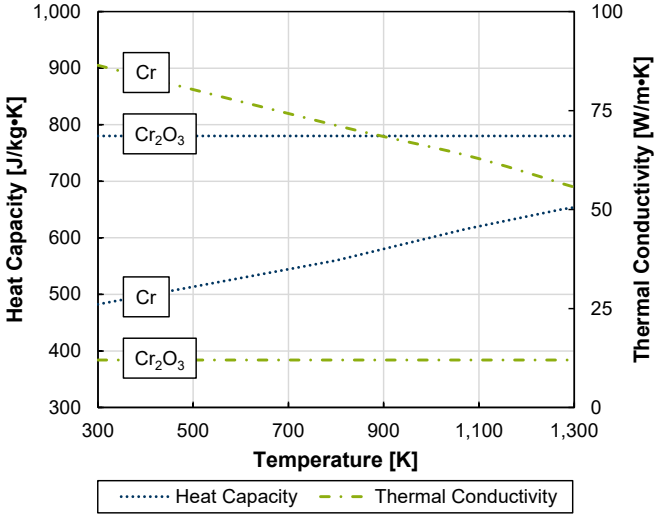

- Reaction heat per kg metal (Cr/Zr) calculated via database for chemical thermodynamics
- Data for c_p and λ based on literature, Zr data assumed after eutectic point (~1,332°C)

MODELLING
Correlation for Cr

- The oxidation rate is determined by the resistance to oxygen diffusion, it is based on a parabolic law derived from the analytical solution of diffusion eq.

$$\begin{cases} dX^2 = k_p dt \\ k_p(T) = AKOEFF * \exp\left(-{}^{Ea}/_{R\boldsymbol{T}}\right) \end{cases}$$

- The oxidation rate can be determined and oxidized mass per time step can be calculated

$$\begin{cases} \frac{dX}{dt} = \frac{k_p}{X} \end{cases} \Rightarrow \boxed{X = \left(k_p * t\right)^{0.5}}$$

⌛ The resulting heat flow due to oxidation depends on the oxidized mass and is eventually added to the outermost layer → ongoing analyses of code if molar masses are used correctly (and calculated consumed metal) for Cr-coated claddings (Cr/Zr)

MODELLING
Correlation for Cr

- Data from Brachet 2020 et al. used for correlation modelling

! Mass gain (m) of metal is used by AC²

Layer (X) Growth $= (k_p(T) * t)^{1/2}$ **[cm]** Stahlberg et al. 2022 and 2023

with $k_p(T) = \boldsymbol{AKOEFF^X} * \exp(-{}^{Ea}/_{RT})$

and $AKOEFF^{\boldsymbol{X}} = AKOEFF^{\boldsymbol{m}} * \left(\frac{M_{Clad}}{M_{O_2} * \rho_{Clad}}\right)^2$ Wu, Shirvan 2020

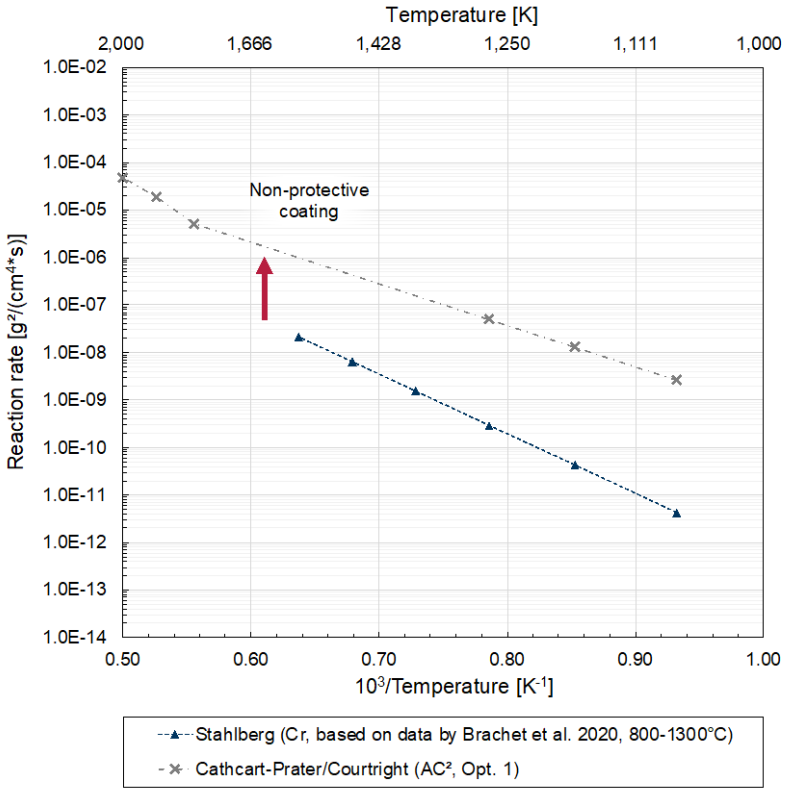

PSS Plant Simulation and Safety
Prof. Dr.-Ing. Marco K. Koch
RUHR UNIVERSITÄT BOCHUM
RUB

MODELLING
Correlation for Cr

- Data from Brachet 2020 et al. used for correlation modelling

! Mass gain (m) of metal is used by AC²

Layer (X) Growth $= (k_p(T) * t)^{1/2}$ [**cm**] Stahlberg et al. 2022 and 2023

with $k_p(T) = \boldsymbol{AKOEFF^X} * \exp(-{}^{Ea}/_{RT})$

and $AKOEFF^{\boldsymbol{X}} = AKOEFF^{\boldsymbol{m}} * \left(\frac{M_{Clad}}{M_{O_2} * \rho_{Clad}}\right)^2$ Wu, Shirvan 2020

- Additionally, for comparative assessment, most deviating weight gain data at 1,200°C are used by author to derive further Cr-correlations

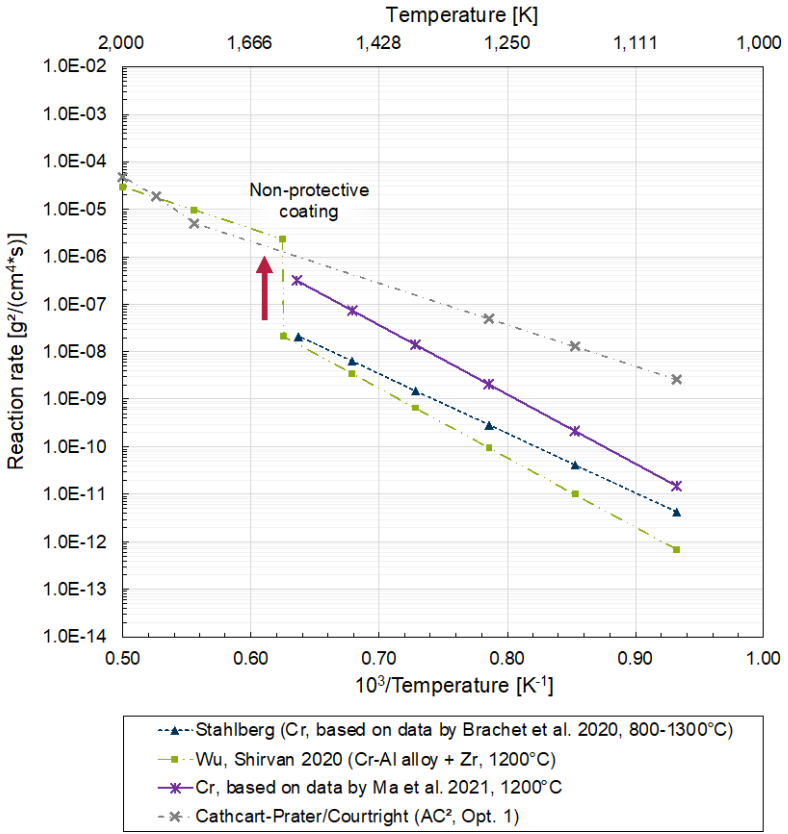

PSS Plant Simulation and Safety
Prof. Dr.-Ing. Marco K. Koch
RUHR UNIVERSITÄT BOCHUM
RUB

MODELLING
Current approach under development

- The newly modeled correlation is part of a model framework
  - Correlation is based on exp. data from Brachet et al. 2020
  - Transition from Cr → Zr after asssumed coating failure at variable (user) temperature
  - Heat of oxidation depends on active correlation
  - Inner oxidation (Zr) after cladding failure

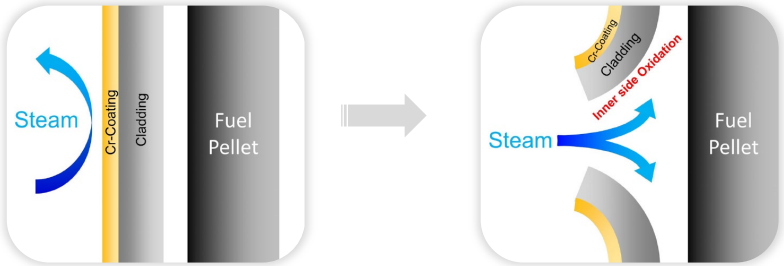

Yook et al. 2022

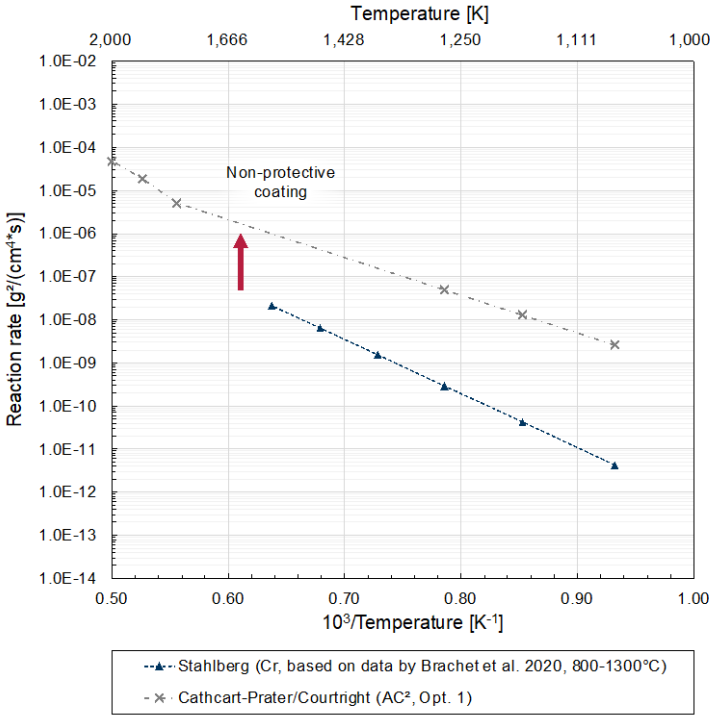

PSS Plant Simulation and Safety
Prof. Dr.-Ing. Marco K. Koch
RUHR UNIVERSITÄT BOCHUM
RUB

Verification and Application

VERIFICATION
Correlation for Cr, 1,000-1,100°C

- Derived correlation for Cr
  - Based on layer growth data from **Brachet et al. 2020** for **800-1,300°C**
- Curves show calculated mass gain for 1,000 and 1,100°C
  - Excellent agreement for *Bra19* at 1,000°C and *Kas22* at 1,050°C, but data by *Bra18* at 1,000/1,100°C are app. 30-60% overestimated
- For further modelling, separate coefficients for different temperature regions are under consideration
- Few experimental data available for verification

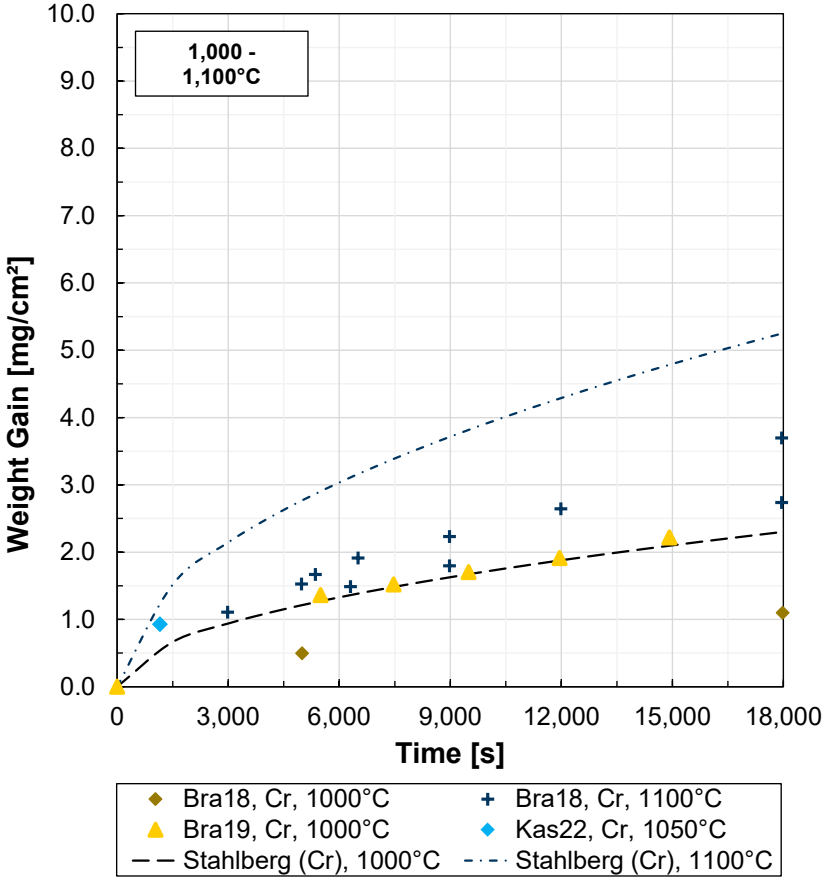

PSS Plant Simulation and Safety
Prof. Dr.-Ing. Marco K. Koch
RUHR UNIVERSITÄT BOCHUM
RUB

VERIFICATION
Correlation for Cr, 1200°C

- Calculated mass gain curve shows good agreement at 1,200°C
  - Most data are captured well or are slightly overestimated (few *not* captured like *Kim15*)
  - Coating failure seems to occur after 5,000-6,000 s, see *Bra18*, *Bra19 and Bou19*
  - Increased kinetics similar to Zr

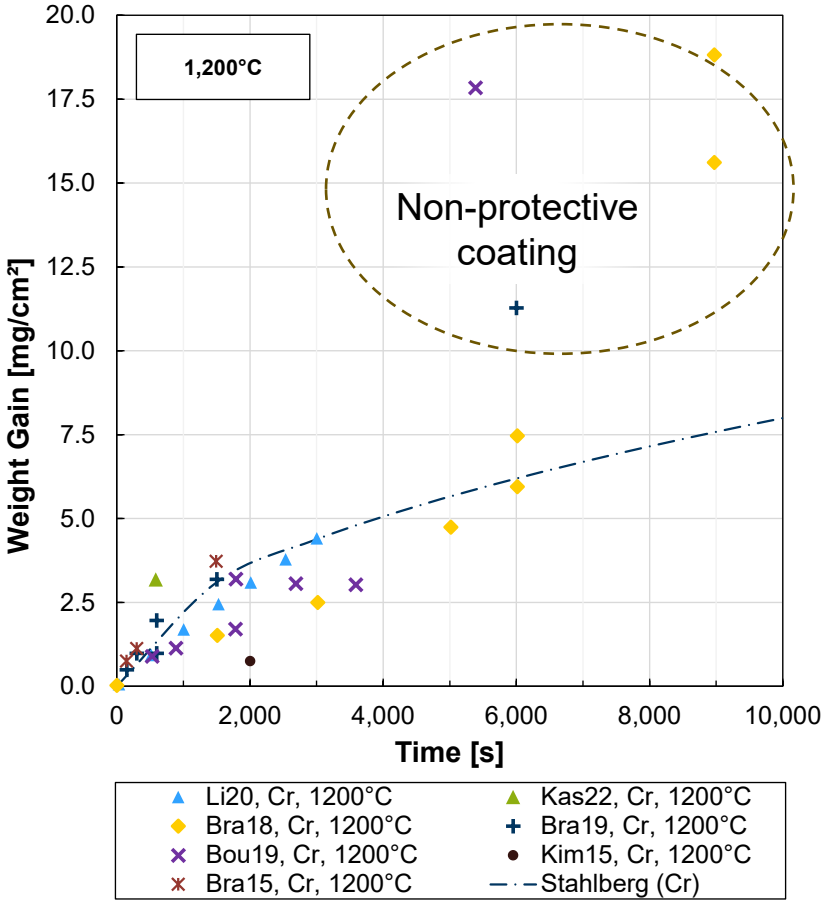

VERIFICATION
Correlation for Cr, 1,300°C

- Calculated mass gain at 1,300°C
  - Calculated curve shows mostly good agreement to data of *Bra20*, depending on state of coating (transition/non-protective)
  - However, measured data points only seem to fit a parabolic progression during first ~2,500 s
  - Increased kinetics after ~3,000-4,000 s
  - Data of *Ma21* follow a parabolic law but show **significantly higher values** compared to other measured data (see also correlation on slide 10)
  - Limited data available for verification, close to the eutectic point → QUENCH-SR simulations?

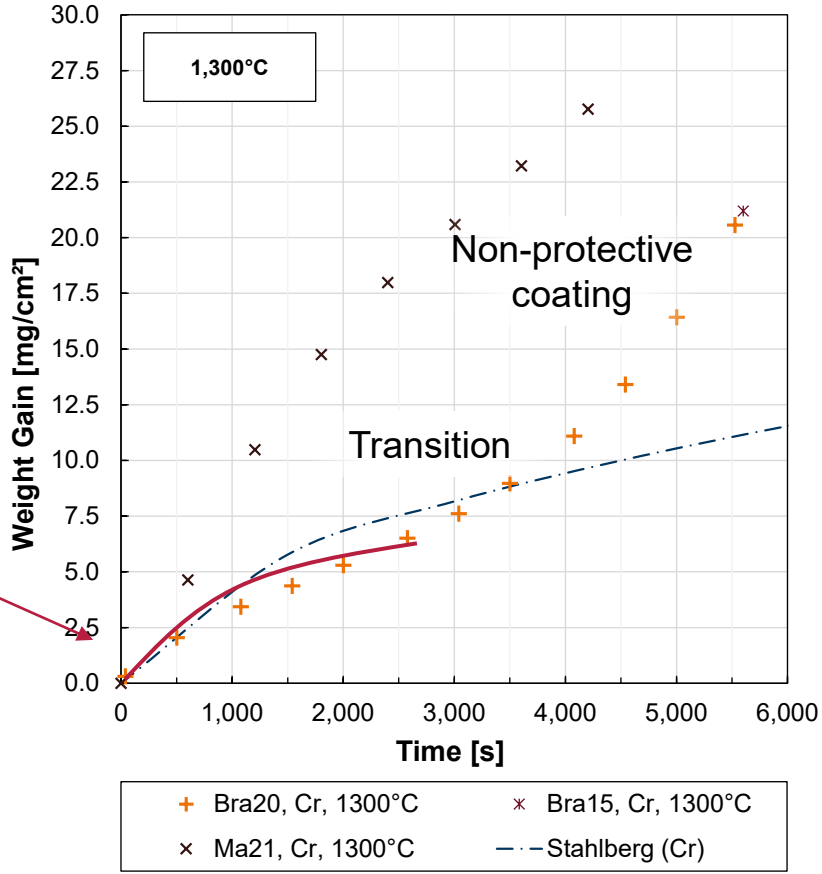

PSS Plant Simulation and Safety
Prof. Dr.-Ing. Marco K. Koch
RUHR UNIVERSITÄT BOCHUM
RUB

VERIFICATION
Correlation for Cr, 1,300°C

- Calculated mass gain at 1,300°C
- Current approach after failure of coating is using Zr-kinetics built into AC², see possible progression of weight gain with “Zr (Opt. 1)”

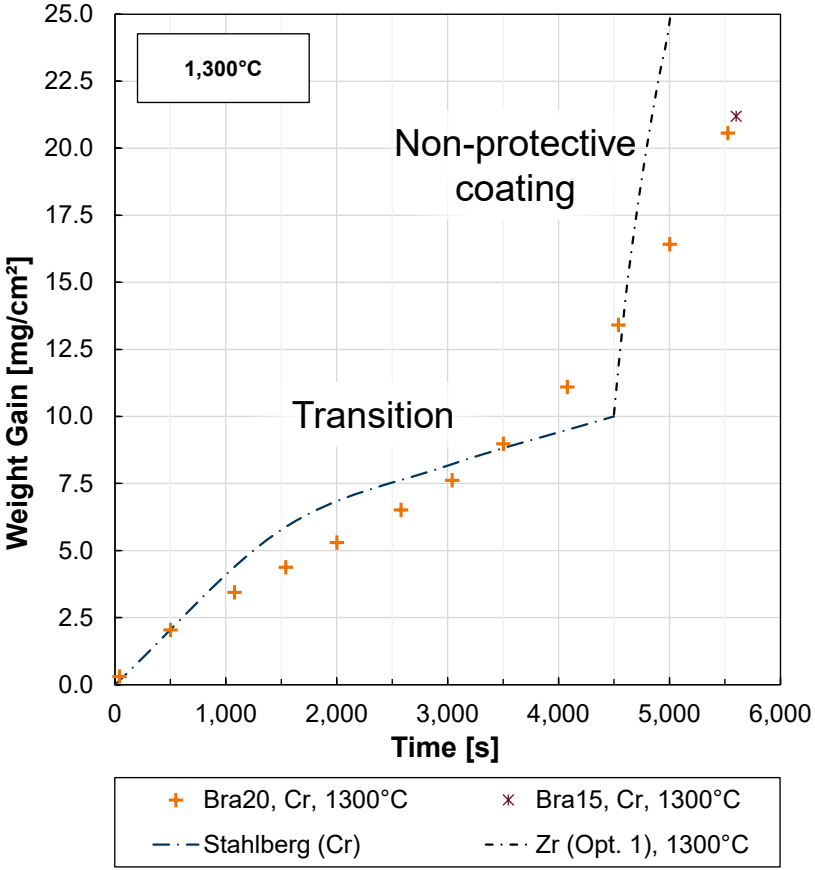

PSS Plant Simulation and Safety
Prof. Dr.-Ing. Marco K. Koch
RUHR UNIVERSITÄT BOCHUM
RUB

APPLICATION
QUENCH-LOCA-3 - PWR Bundle (opt. ZIRLO) - DBA

- LOCA-3 (opt. ZIRLO) with peak cladding temperature of just **~1,050°C**
  - Calculation with AC² shows thermal behavior is slightly underestimated (see H_2 as well) with *opt. ZIRLO,* but overall well reproduced
- Application of Cr-coated cladding to design basis accident (*AC²_mod*)
  - As expected, low hydrogen release, given the active correlation at this **low temperatures and short oxidation times**
  - Lower peak temperature
  - In consideration of the underestimation using AC², a maximum release of approx. 0.1 g is expected using new model

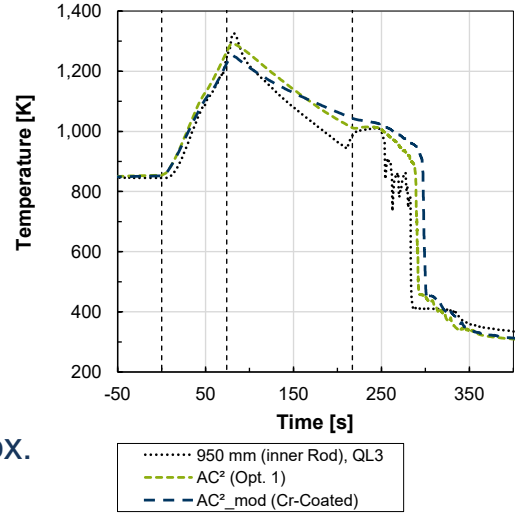

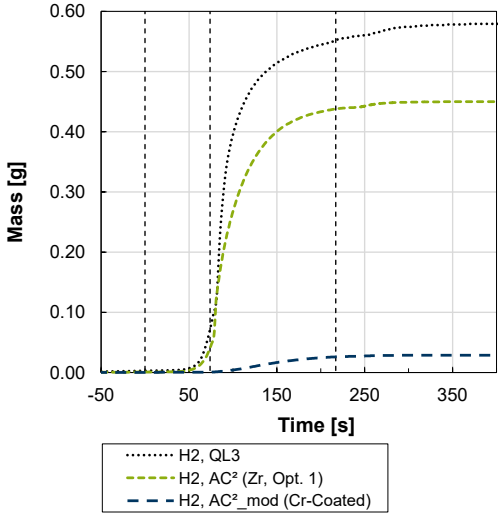

PSS Plant Simulation and Safety
Prof. Dr.-Ing. Marco K. Koch
RUHR UNIVERSITÄT BOCHUM
RUB

See Application of this model to BDBA QUENCH Experiments.
- common contribution presented by Thorsten Hollands.

ACKNOWLEDGEMENT

This work is funded by the German Federal Ministry for the Environment, Nature Conservation, Nuclear Safety and Consumer Protection (BMUV) under grant number 1501629 based on a decision by the German Bundestag.

Responsibility for the content lies with the authors.

The results were obtained using an in-house version at PSS of the GRS software package AC² 2021.0.

Supported by:

Federal Ministry
for the Environment, Nature Conservation,
Nuclear Safety and Consumer Protection

based on a decision of
the German Bundestag

Thank you for your attention!

Gregor Stahlberg

Gregor.Stahlberg@pss.rub.de

Marco K. Koch

Marco.Koch@pss.rub.de

RUHR-UNIVERSITÄT BOCHUM

PSS Plant Simulation and Safety

Prof. Dr.-Ing. Marco K. Koch

Building: IC | Floor 2

Universitätsstr. 150

D-44801 Bochum

pss.rub.de

References

[Bou19] Bourdon, Gauthier; Ševecek, Martin; Krejčí, Jakub; Cvrček, Ladislav: HIGH-TEMPERATURE STEAM AND AIR OXIDATION OF CHROMIUM-COATED OPTIMIZED ZIRLO™. Acta Polytechnica CTU Proceedings, 24, 2019. DOI: 10.14311/APP.2019.24.0001.

[Bra15] Brachet, Jean-Christophe; Le Saux, Matthieu; Le Flem, Marion; Urvoy, Stephane; Rouesne, Elodie; Guilbert, Thomas; Cobac, C.; Lahogue, F.; Rousselot, J. L.; Tupin, Marc; Billaud, Pierre; Hossepied, Charles; Monsifrot, Eric: On-going studies at CEA on chromium coated zirconium based nuclear fuel claddings for enhanced accident tolerant LWRS fuel, cea-02492582, Top Fuel 2015 - Reactor Fuel Performance Meeting, Zurich, Switzerland, 2015.

[Bra18] Brachet, Jean-Christophe; Guilbert, T.; Le Saux, Matthieu; Rousselot, J.; Nony, G.; Toffolon-Masclet, C.; Michau, Alexandre; Schuster, Frederic; Palancher, Herve; Bischoff, Jeremy; Augereau, J.; Pouillier, Edouard: BEHAVIOR OF Cr-COATED M5 CLADDINGS DURING AND AFTER HIGH TEMPERATURE STEAM OXIDATION FROM 800°C UP TO 1500°C - LOSS-OF-COOLANT ACCIDENT & DESIGN EXTENSION CONDITIONS, Top Fuel 2018 - Reactor Fuel Performance, Prague, Czech Republic, 2018.

[Bra19] Brachet, Jean-Christophe; Idarraga-Trujillo, Isabel; Le Flem, Marion; Le Saux, Matthieu; Vandenberghe, Valérie; Urvoy, Stephane; Rouesne, Elodie; Guilbert, Thomas; Toffolon-Masclet, Caroline; Tupin, Marc; Phalippou, Christian; Lomello, Fernando; Schuster, Frédéric; Billard, Alain; Velisa, Gihan; Ducros, Cédric; Sanchette, Frédéric: Early studies on Cr-Coated Zircaloy-4 as enhanced accident tolerant nuclear fuel claddings for light water reactors. Journal of Nuclear Materials, 517, S. 268–285, 2019. DOI: 10.1016/j.jnucmat.2019.02.018.

[Bra20] Brachet, Jean-Christophe; Rouesne, Elodie; Ribis, Joël; Guilbert, Thomas; Urvoy, Stéphane; Nony, Guillaume; Toffolon-Masclet, Caroline; Le Saux, Matthieu; Chaabane, Nihed; Palancher, Hervé; David, Amandine; Bischoff, Jérémy; Augereau, Julien; Pouillier, Edouard: High temperature steam oxidation of chromium-coated zirconium-based alloys: Kinetics and process. Corrosion Science, 167, 2020. DOI: 10.1016/j.corsci.2020.108537.

[Gre19] Gremme, Florian: Analyse des Einflusses anlageninterner Notfallmaßnahmen auf die Kernkühlbarkeit bei auslegungsüberschreitenden Störfällen in Druckwasserreaktoren. PhD thesis. Ruhr-University Bochum. Plant Simulation and Safety (PSS). Shaker-Verlag. Bochum. Germany. 2019. ISBN 978-3-8440-6516-9.

[Kas22] Kashkarov, E. B.; Sidelev, D. V.; Pushilina, N. S.; Yang, J.; Tang, C.; Steinbrueck, M.: Influence of coating parameters on oxidation behavior of Cr-coated zirconium alloy for accident tolerant fuel claddings. Corrosion Science, 203, S. 110359, 2022. DOI: 10.1016/j.corsci.2022.110359.

[Kim15] Kim, Hyun-Gil; Kim, Il-Hyun; Jung, Yang-Il; Park, Dong-Jun; Park, Jeong-Yong; Koo, Yang-Hyun: Adhesion property and high-temperature oxidation behavior of Cr-coated Zircaloy-4 cladding tube prepared by 3D laser coating. Journal of Nuclear Materials, 465, S. 531–539, 2015. DOI: 10.1016/j.jnucmat.2015.06.030.

REFERENCES

[Li20] Li, Guangbin; Liu, Yanhong; Zhang, Yingchun; Li, Huailin; Wang, Xiaojing; Zheng, Mingmin; Li, Yusha: High Temperature Anti-Oxidation Behavior and Mechanical Property of Radio Frequency Magnetron Sputtered Cr Coating. Metals, 10, S. 1509, 2020. DOI: 10.3390/met10111509.

[Liu21] Liu, Junkai; Tang, Chongchong; Steinbrück, Martin; Yang, Jianqiao; Stegmaier, Ulrike; Große, Mirco; Di Yun; Seifert, Hans Jürgen: Transient experiments on oxidation and degradation of Cr-coated Zircaloy in steam up to 1600 ℃. Corrosion Science, 192, 2021. DOI: 10.1016/j.corsci.2021.109805.

[Ma21] Ma, Hai-Bin; Yan, Jun; Zhao, Ya-Huan; Liu, Tong; Ren, Qi-Sen; Liao, Ye-Hong; Zuo, Jia-Dong; Liu, Gang; Yao, Mei-Yi: Oxidation behavior of Cr-coated zirconium alloy cladding in high-temperature steam above 1200 °C. npj Materials Degradation, 5, 2021. DOI: 10.1038/s41529-021-00155-8.

[Sha18] Shah, Hemant; Romero, Javier; Xu, Peng; Oelrich, Robert; Walters, Jorie; Wright, Jonathan, Gassmann, William: Westinghouse-Exelon EnCore® Fuel Lead Test Rod (LTR) Program including Coated cladding Development and Advanced Pellets, WAAP-10756, Top Fuel 2018 - Reactor Fuel Performance, Prague, Czech Republic, 2018.

[Sta21] Stahlberg, Gregor T., et al.: Externe Validierung und Modellanalyse der Codesysteme AC² und ASTEC mit unterstützenden CFD-Detailanalysen (VAMOCAAD) - Abschlussbericht zum Forschungsvorhaben BMWi 1501568, PSS-TR-19, Bochum, 2021.

[Sta22] Stahlberg, Gregor, T., et al.: Preliminary Simulation Results of the Experiments QUENCH-L3HT and QUENCH-ATF-1 Regarding High-Temperature Oxidation Mechanisms Using the System Code AC^2, 27th International QUENCH Workshop, KIT, Karlsruhe, 2022. https://doi.org/10.5445/ir/1000152245

[Sta23] Stahlberg, Gregor T., et al.: Comparative analyses of the QUENCH experiments L3HT and ATF-1 on high temperature oxidation mechanisms using AC^2, in Proceedings of NURETH-20 - International Topical Meeting on Nuclear Reactor Thermal Hydraulics, pp. 5450–5461, 2023. https://doi.org/10.13182/nureth20-39989

[Wu20] Wu, Xu; Shirvan, Koroush: System code evaluation of near-term accident tolerant claddings during boiling water reactor short-term and long-term station blackout accidents. Nuclear engineering and design, 2020. DOI: 10.1016/j.nucengdes.2019.110362.

[Yoo22] Yook, Hyunwoo; Shirvan, Koroush; Phillips, Bren; Lee, Youho: Post-LOCA ductility of Cr-coated cladding and its embrittlement limit. Journal of Nuclear Materials, 558, 2022. DOI: 10.1016/j.jnucmat.2021.153354.

T. Hollands
GRS

Simulation of QUENCH-03 and -15 Scenarios with the Code AC² modified for Cr-coated Claddings compared with ASTEC

One of the key factors influencing the progression of unmitigated accidents is the fuel cladding. It is an important part of the defense-in-depth concept. Zirconium (Zr) alloys perform well under normal operational conditions. At higher temperatures the accident progression can escalate due to a strong exothermic reaction. Various studies have indicated that alternative materials could partially enhance the behavior under accident conditions. Currently, there are ongoing developments in Accident Tolerant Fuels (ATF). Of particular interest are iron-chromium-aluminum (FeCrAl) alloys or the coating of existing Zr alloys, which are already widely used in nuclear power plants.

The main objective of the presented works is the application of a newly developed first in-house model for ATF at the PSS Group at RUB. This model specifically addresses the oxidation of Chromium (Cr)-coated claddings. It is implemented into a modified AC² version, a system code package developed by GRS gGmbH for the simulation of selected phenomena or complete accident sequences in nuclear power plants.

The investigated large scale bundle experiments were conducted at the QUENCH test facility of KIT. In these tests, beyond design basis conditions in light water reactors with subsequent re-flooding were considered. The sequences consist of a stabilisation, heat-up, transient and quench phase. Comparing both sequences, QUENCH-15 was conducted additionally with a pre-oxidation phase before the transient phase. QUENCH-03 / QUENCH-15 aim at investigating the hydrogen source term when water or steam is injected into an uncovered and overheated core of a light water reactor. These experiments were conducted with Zry-4 / ZIRLO™ for the test fuel rod simulators and temperatures of 2000°C / 1880°C were measured. Thus, severe accident conditions were reached with temperatures beyond the eutectic melting temperature of the binary Zr-Cr system. This marks the very latest failure time for the protective chromium layer at around 1332°C.

The conducted sequences were calculated as they were. However, the new option for Cr-coating oxidation in AC² is used for fuel rod simulators and shroud, assuming a dense chromium layer on the Zr-alloy. The QUENCH-03 input deck was furthermore altered from the original 21- to a 24-rod layout, as in QUENCH-15. Additionally, the newest ASTEC version was applied to QUENCH-15 using correlations for Cr-coating of KIT via user input. This allows a code crosswalk of both codes.

The analyses of the simulation results focus primarily on the code capabilities to represent the thermal behaviour of the rods as well as the oxidation behaviour in comparison with original Zr-oxidation. Both input decks were optimized for the particular sequence. This ensures reliable results when reviewing original hydrogen generation using Zr-alloy oxidation kinetics and the hypothetical potential benefit of the Cr-coating. The tentative simulations using Cr-oxidation show overall slightly lower temperatures than the experimental data of the QUENCH tests with Z-alloy as well as significantly lower hydrogen generation, as expected.

Simulation of QUENCH-03 and -15 Scenarios with the Code AC² modified for Cr-coated Claddings compared with ASTEC

Thorsten Hollands, GRS
Gregor T. Stahlberg, RUB PSS
Fabrizio Gabrielli, KIT

28th QUENCH Workshop, Karlsruhe
05.-07.12.2023

Outline

- Motivation and Objective
- Modelling Approach
  - Correlation
  - Modelling in AC² and ASTEC
- Experiment and Simulation Results
  - QUENCH-15 (AC² and ASTEC)
  - QUENCH-03 (AC²)
- Conclusions

Motivation and Objective

- Qualifying and further developing AC² regarding ATF application
  - Available so far is FeCrAl-Oxidation (derived from QUENCH-19), flexible user oxidation (same Δh as FeCrAl), ongoing development e.g. B136Y hard coded…
  - Experiment for validation: QUENCH-19
- New model for coating oxidation (Cr/Zr)
  - Under development in national funded project by RUB PSS
  - Experiment for validation: QUENCH-ATF series of joint project OECD NEA QUENCH-ATF led by KIT
  - Further experiments are under preparation like CODEX or DEGREE ATF series

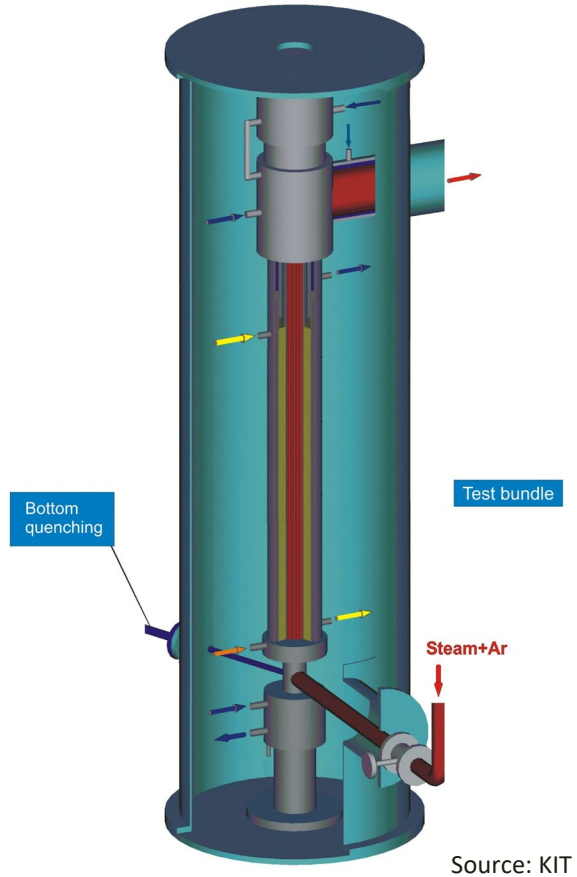

Source: KIT

Modelling Approach – Correlation

- Model framework
  - Correlation based on experimental data
  - Transition from Cr → Zr (incl. Δh)
  - Inner oxidation (Zr) after burst

$$K^{m}_{p,AC^2} = \begin{cases} 14.393 \exp\left(-\frac{120{,}000}{RT}\right) & \left[\frac{kg}{m^2 s^{0.5}}\right], Cr \\ A_{Zr} \exp\left(-\frac{E_{Zr}}{RT}\right), \; T \geq T^{*}_{Fail} & \left[\frac{kg}{m^2 s^{0.5}}\right], Zr \end{cases}$$

* T_{Fail} as user defined failure Temperature for coating

$$K^{m,d\ **}_{p,ASTEC} = \begin{cases} K^{m}_{p} = 6.19 \cdot \exp\left(\frac{-123783}{RT}\right) & \left[\frac{kg}{m^2 s^{0.5}}\right], Cr \\ K^{d}_{p} = 3.77E\text{-}3 \cdot \exp\left(\frac{-123783}{RT}\right) & \left[\frac{m}{s^{0.5}}\right], Cr_2O_3 \end{cases}$$

** Restart with Zr-Correlations of ASTEC (mass gain, thickness) when reaching 1300°C

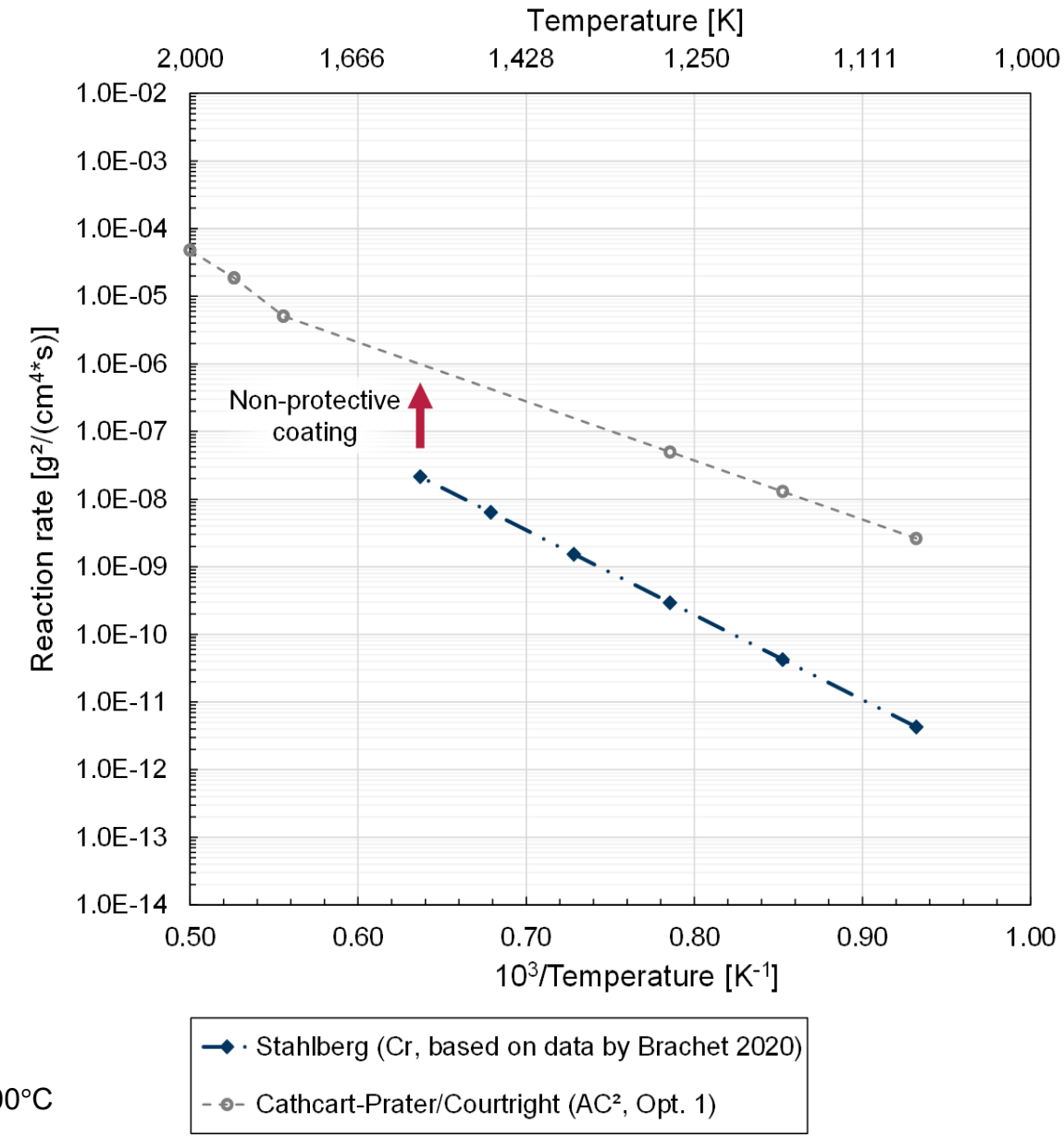

Modelling Approach – Modelling in AC² and ASTEC

- AC²
  - 3 RODs : 4, 12, 8 rods
  - Coating applied to relevant components
  - Zr for spacer as well as coated components at higher temperatures (2 cases: 1300°C and 1200°C)

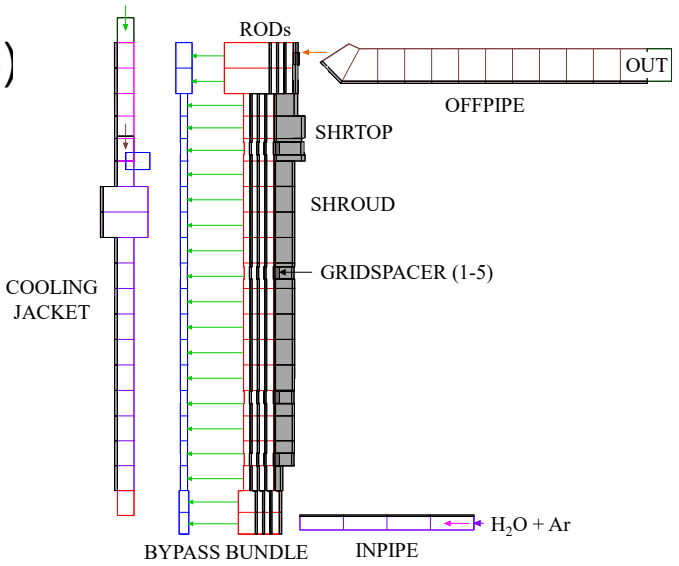

- ASTEC
  - 3 RODs: 4, 12, 8 rods
  - Coating applied to relevant components
  - Transition from Cr → Zr oxidation at 1300°C

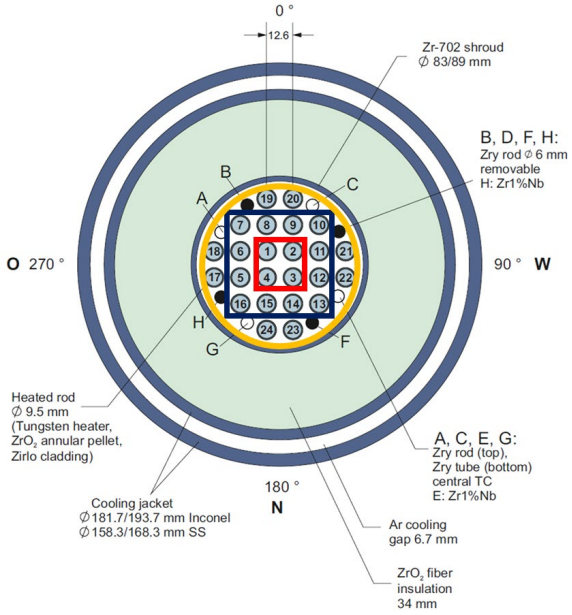

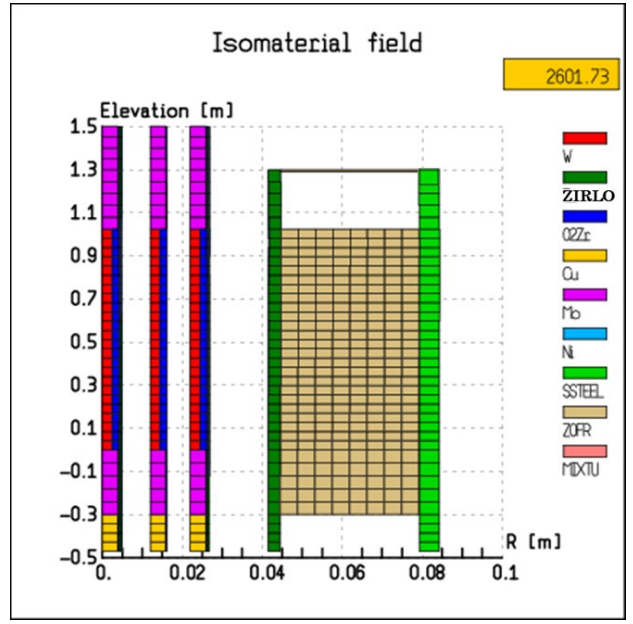

QUENCH-15

Test Bundle and Conduct

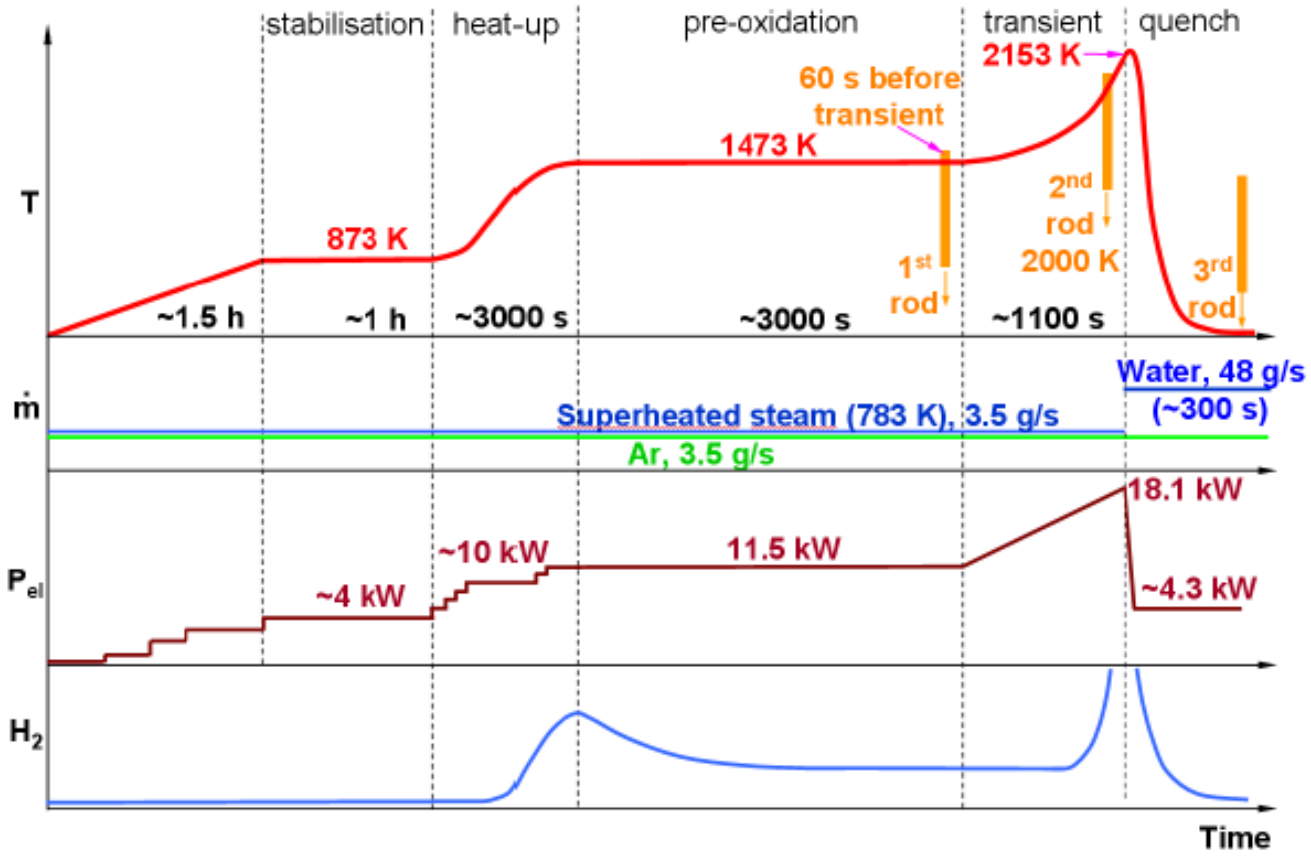

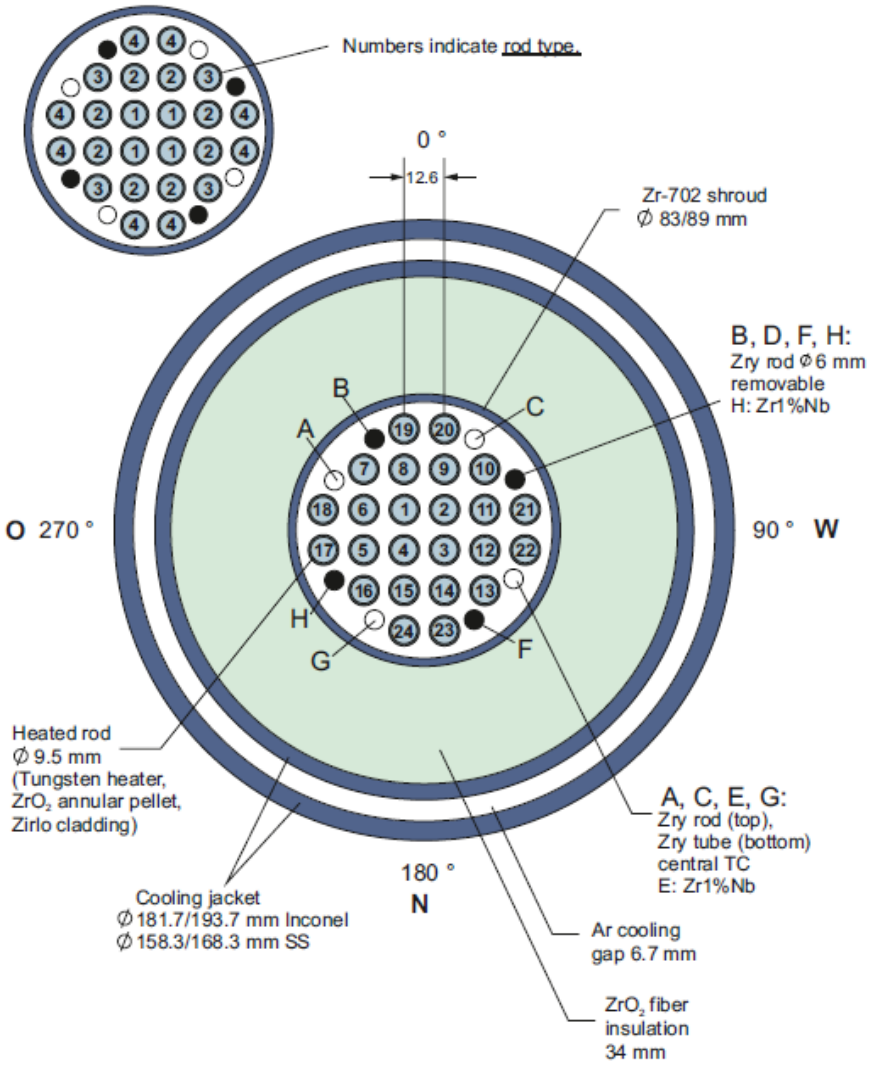

Source: KIT

Simulation Results – Cladding Temperatures at 550 mm

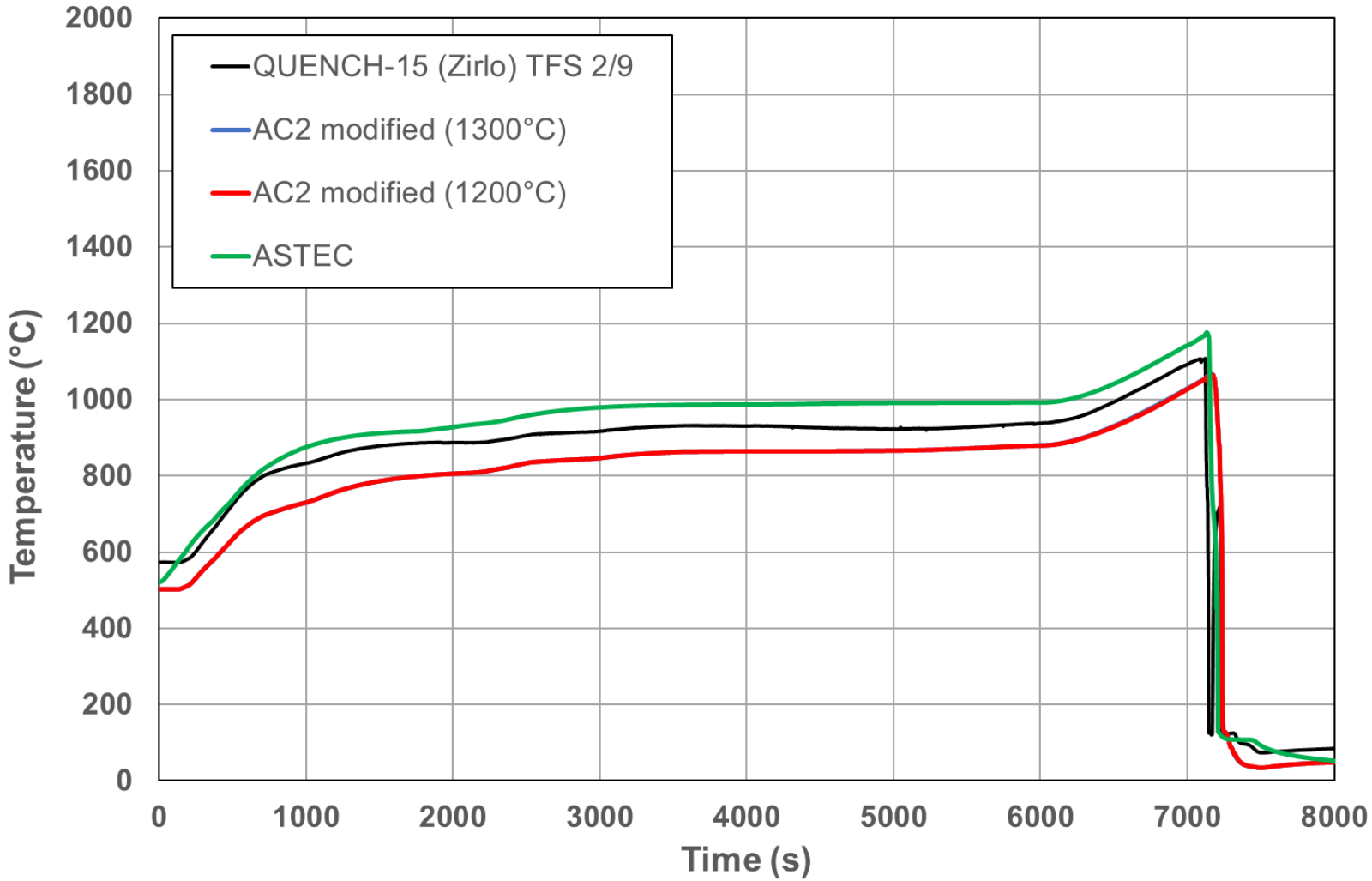

- AC² and ASTEC models were qualified for QUENCH-15 with ZIRLO rods
- Both codes show a comparable qualitative behaviour for Cr-coating, but ASTEC predicts higher temperatures
- No simulation reach the transition temperature to Zr oxidation in the middle bundle elevation

Simulation Results – Cladding Temperatures at 750 mm

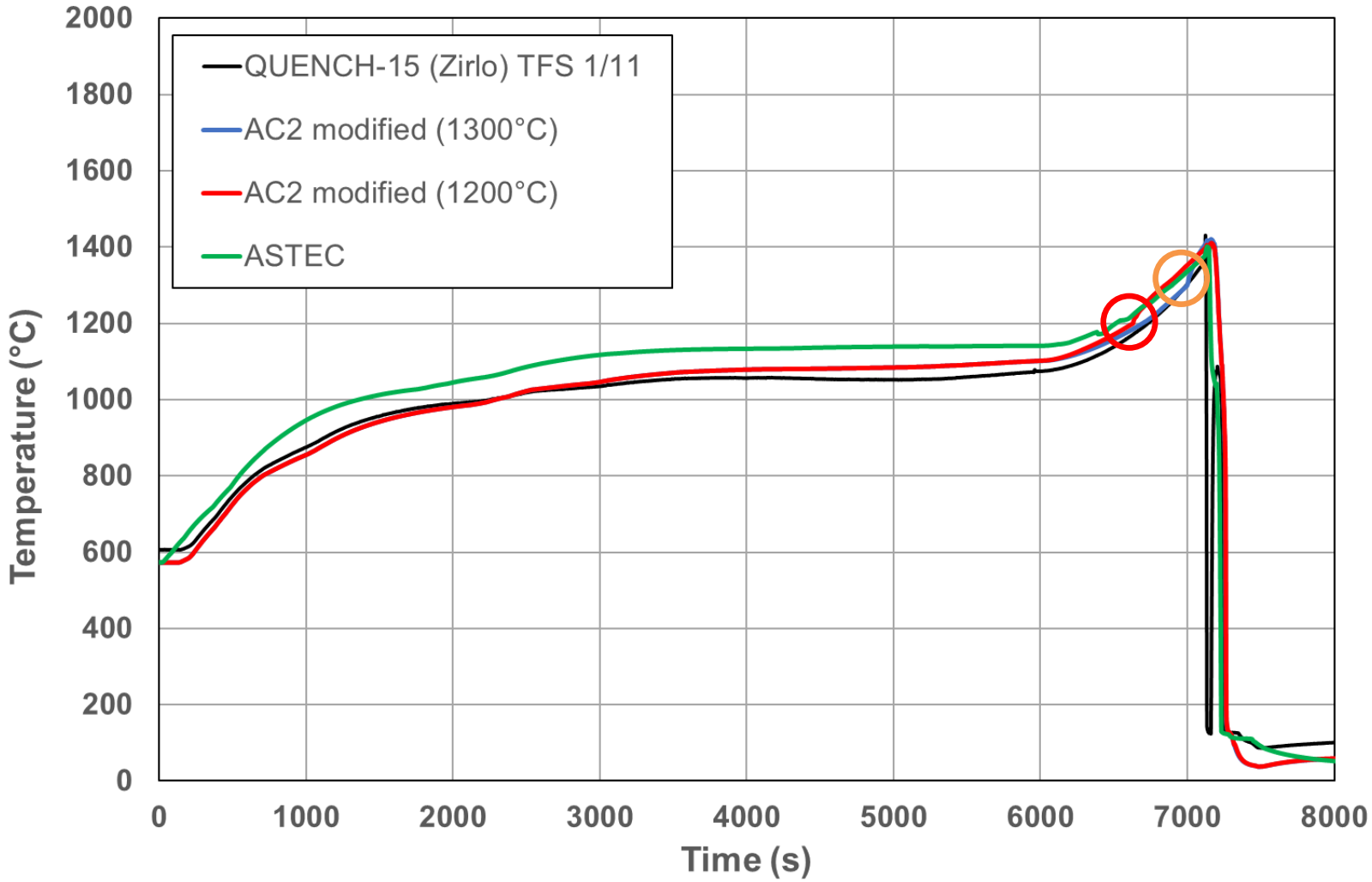

- All simulations reach the transition temperature to accelerated Zr oxidation
- The predicted temperatures for Cr-coating are comparable to original QUENCH-15 ZIRLO behaviour

Simulation Results – Cladding Temperatures at 850 mm

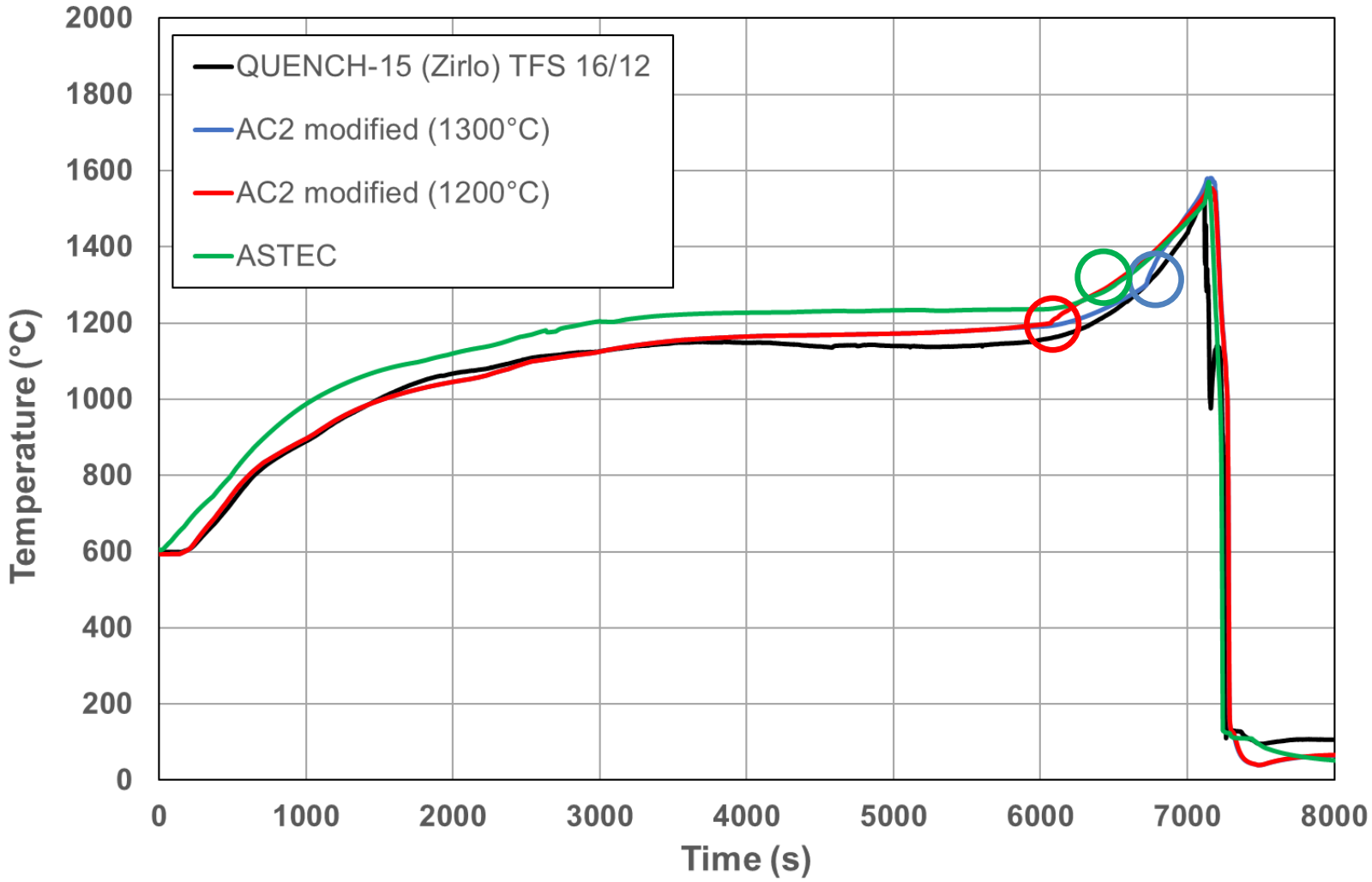

- All simulations reach the transition temperature to accelerated Zr oxidation
- The predicted temperatures for Cr-coating are comparable to original QUENCH-15 ZIRLO behaviour

Simulation Results – Cladding Temperatures at 950 mm

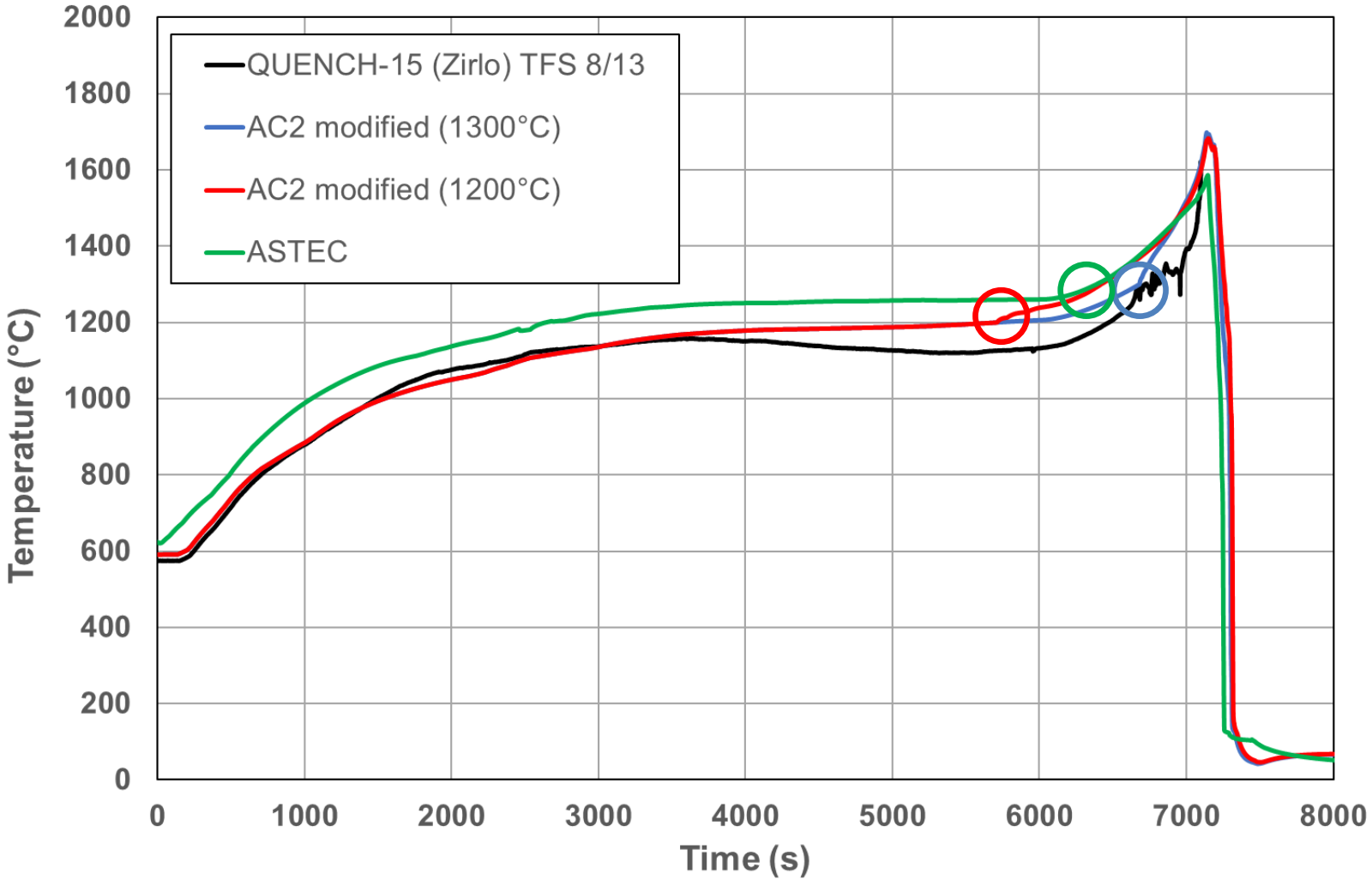

- All simulations reach the transition temperature to accelerated Zr oxidation
- The predicted temperatures for Cr-coating are comparable to original QUENCH-15 ZIRLO behaviour

Simulation Results – Hydrogen Generation

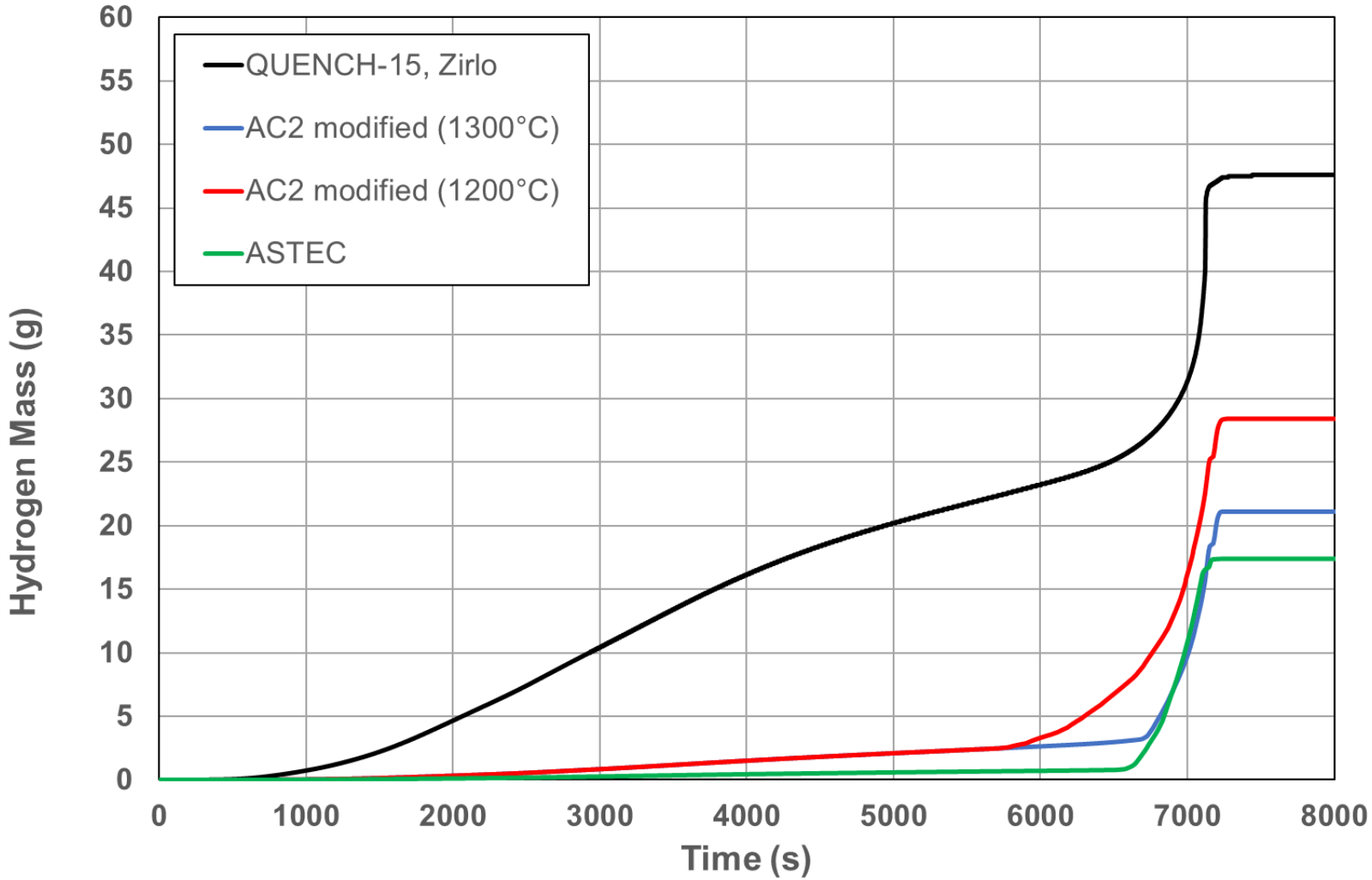

- Although the temperature evolution is comparable to QUENCH-15 with ZIRLO claddings the mass of hydrogen is less than in QUENCH-15
- During pre-oxidation the hydrogen generation is significantly lower with Cr-coated components
- The increase of hydrogen is strongly connected to the transition temperature in each simulation
- When Zr oxidation occurs after failure of Cr-coating the hydrogen generation is higher than for ZIRLO claddings with pre-oxidation

QUENCH-03

Test Bundle and Conduct

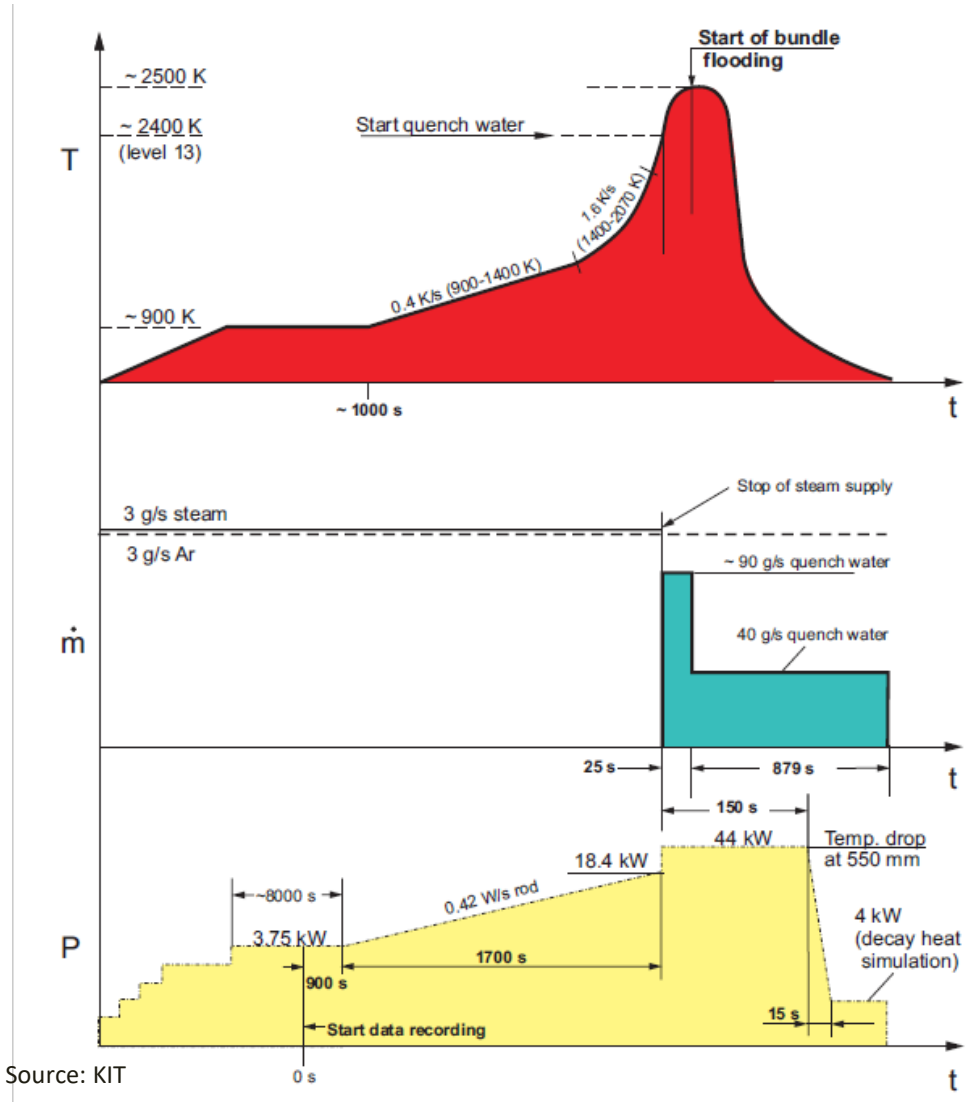

Source: KIT

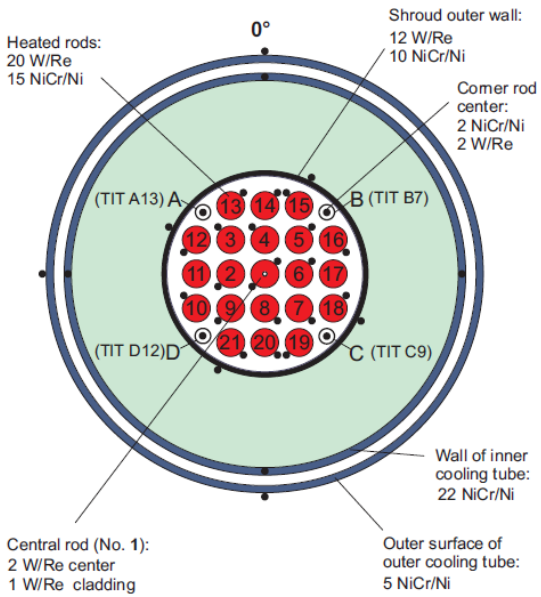

- Validation of the input deck against QUENCH-03 with 21 Zry claddings
- Application of QUENCH-03 scenario on QUENCH-15 configuration with 24 rods with
  - ZIRLO cladding
  - Cr-coated ZIRLO cladding

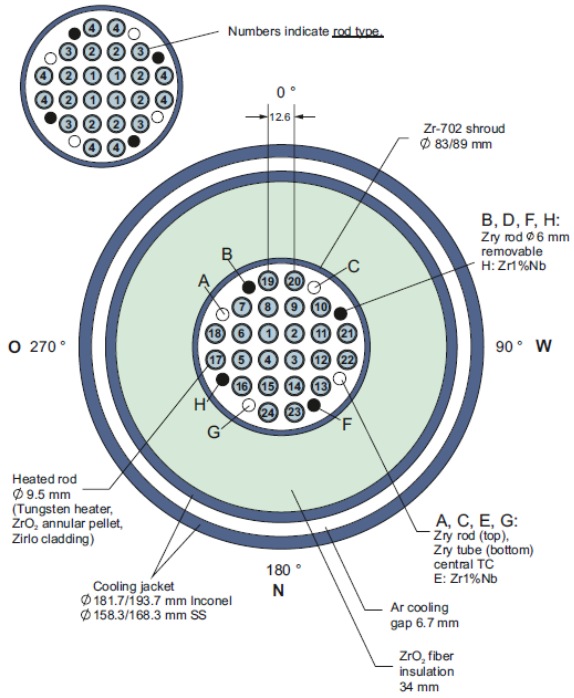

Source: KIT

Simulation Results – Cladding Temperatures at 550 mm

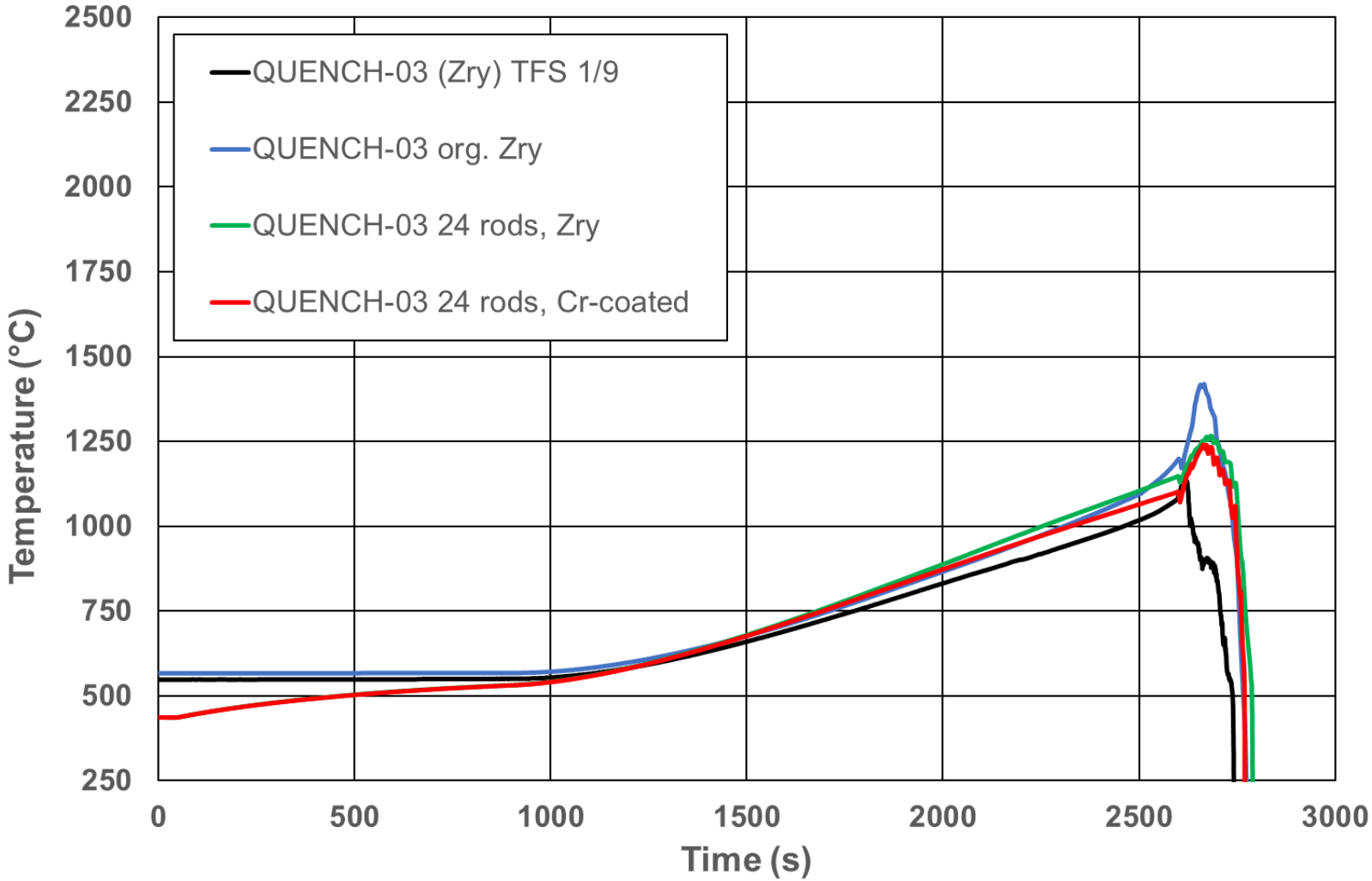

- Temperature is overestimated during transient phase of QUENCH-03 original configuration (21 rods)
- Using the QUENCH-15 configuration (24 rods) with ZIRLO the calculated temperature escalation is lower
- The application of Cr-coated cladding is comparable to ZIRLO claddings, because the transition temperature is not reached at 550 mm

Simulation Results – Cladding Temperatures at 750 mm

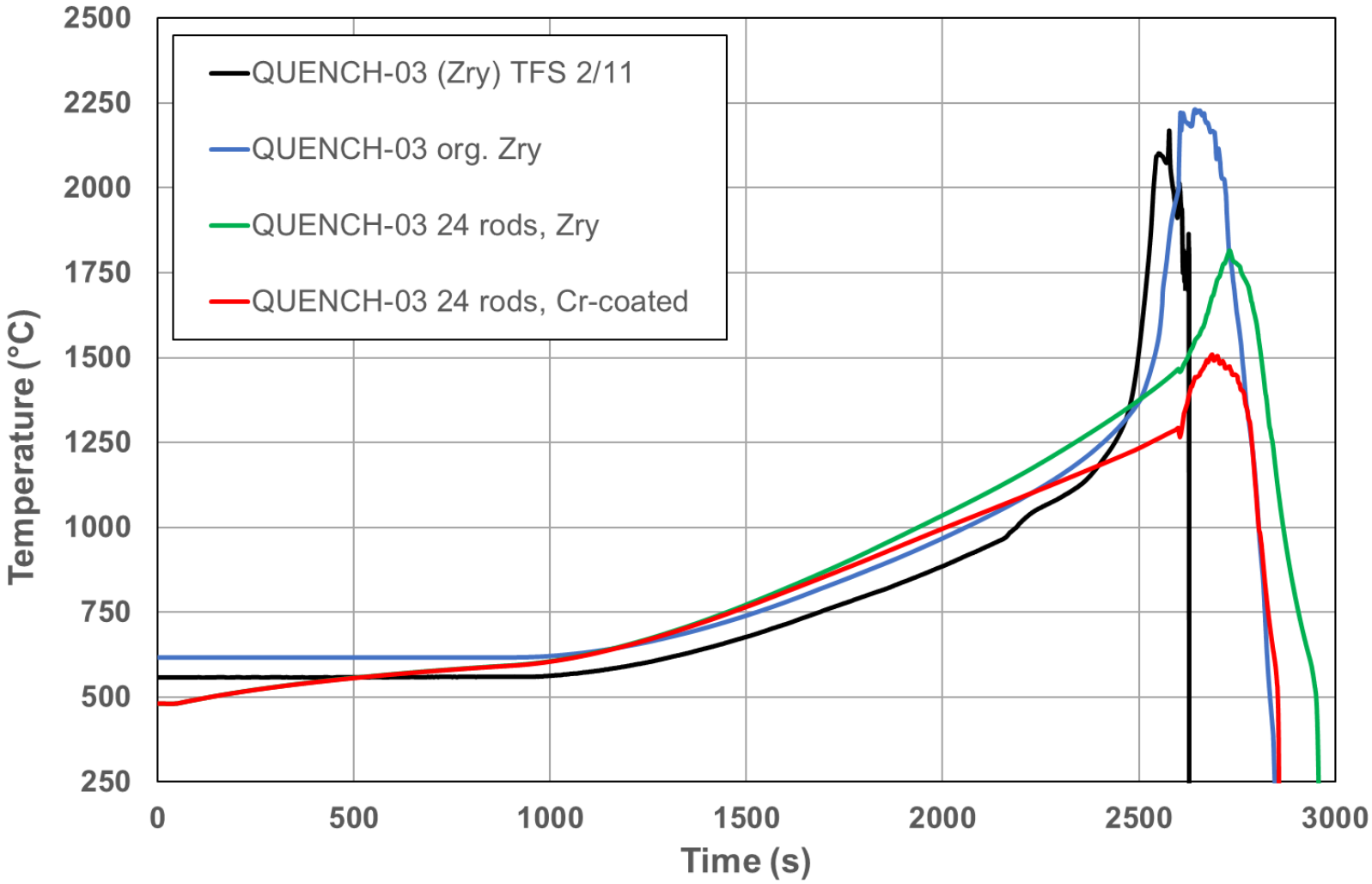

- For the original QUENCH-03 configuration the temperature is predicted plausible to the measured data
- For the 24 rod bundle with ZIRLO the temperatures are much lower, but show a significant increase
- The temperatures for Cr-coated claddings are again lower, but reaching the transition temperature (1300°C) leads to a sharp increase

Simulation Results – Cladding Temperatures at 950 mm

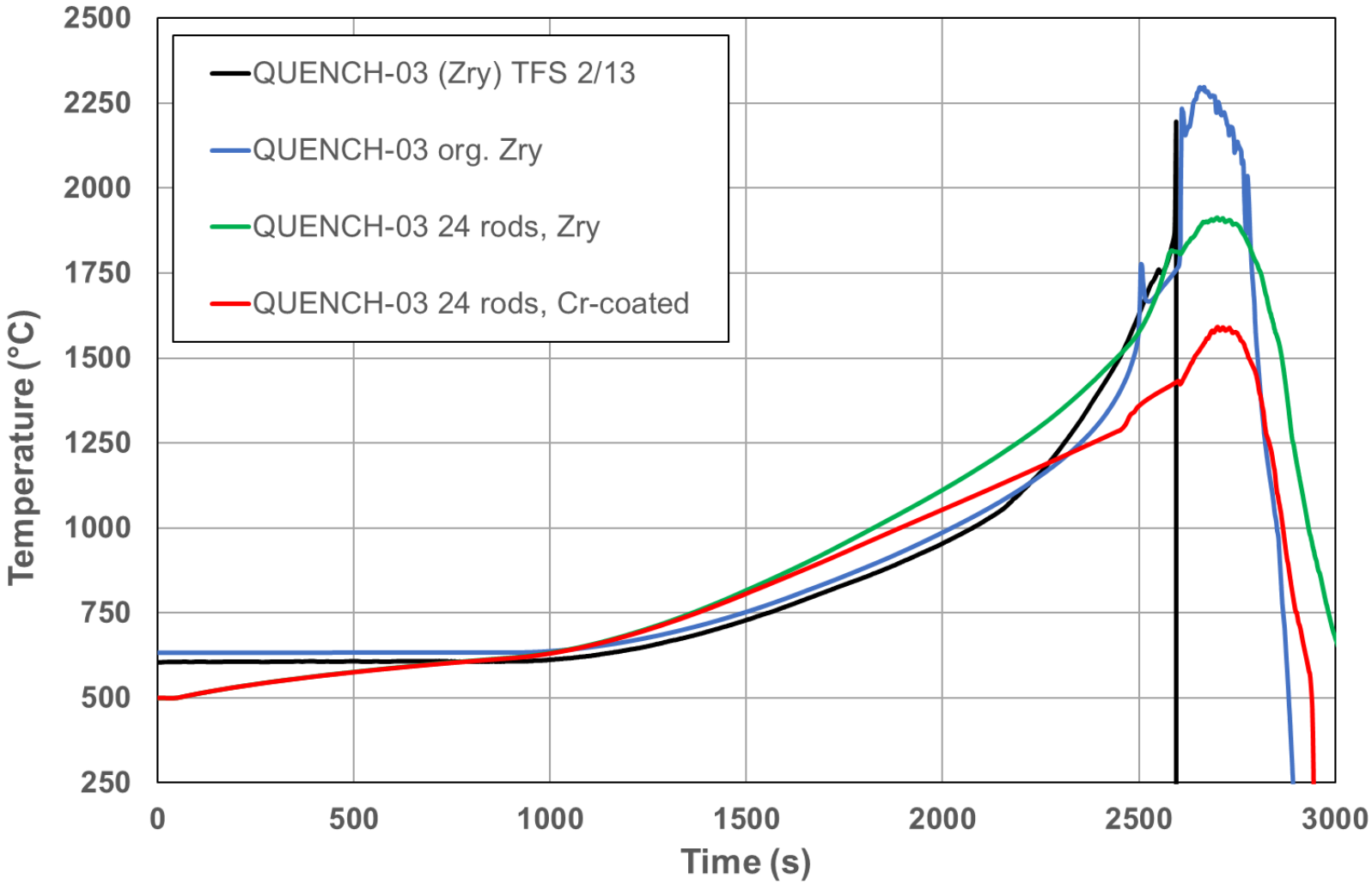

- For the original QUENCH-03 configuration the temperature is predicted plausible to the measured data
- For the 24 rod bundle with ZIRLO the temperatures are much lower, but show a significant increase, melting temperature is matched
- The temperatures for Cr-coated claddings are again lower, but reaching the transition temperature (1300°C) leads to a sharp increase

Simulation Results – Hydrogen Generation

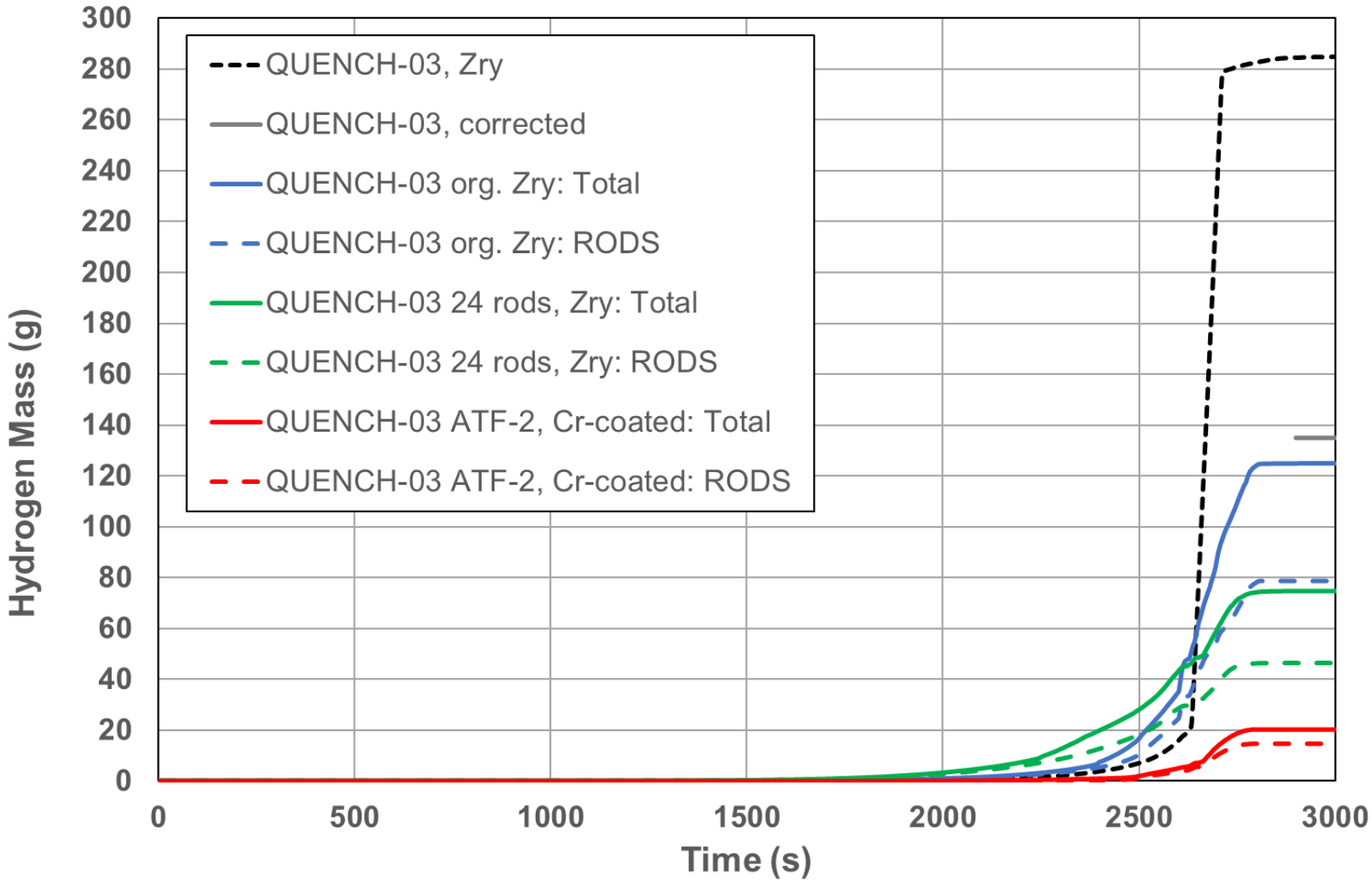

- The total amount of hydrogen is predicted quite well for the original QUENCH-03 scenario with Zry claddings
- For the 24 rod configuration with ZIRLO less hydrogen generation is predicted
- The application of Cr-coated claddings leads to only 20 g H_2 in the AC² simulation

Conclusions

- AC² and ASTEC are able to predict scenarios with Cr-coated claddings applied on the conducted QUENCH tests QUENCH-15 and QUENCH-03
- For the QUENCH-15 scenario nearly no influence on the temperature behaviour is predicted by the application of Cr-coated claddings, but
  - The hydrogen generation is less for Cr-coated claddings due to the low hydrogen generation as long as Cr acts as a protective layer
  - Afterwards, the hydrogen generation is higher compared to the ZIRLO cladding oxidation
- For the application of the QUENCH-03 scenario on the 24 rod bundle leads to lower temperatures most likely due to the different power to volume/mass ratio
  - Additionally, the consideration of Cr-coated claddings leads to further decrease of the cladding temperatures
  - The hydrogen generation is directly affected by the temperatures and vice versa which leads to less hydrogen for the Cr-coated claddings compared to ZIRLO (24 rods) and especially to Zry (21 rods, QUENCH-03)
  - The QUENCH-03 scenario is not prototypical because of the short pre-oxidation phase

Acknowledgement

The work of RUB PSS is funded by the German Federal Ministry for the Environment, Nature Conservation, Nuclear Safety and Consumer Protection (BMUV) under grant number 1501629 based on a decision by the German Bundestag.

The work of GRS is funded by the German Federal Ministry for the Environment, Nature Conservation, Nuclear Safety and Consumer Protection (BMUV).

Responsibility for the content lies with the authors.

The results were obtained using

- an in-house modified version of the GRS software package AC² 2021.0 at PSS and GRS,
- ASTEC V3, developed by IRSN, at KIT.

Supported by:

Federal Ministry
for the Environment, Nature Conservation,
Nuclear Safety and Consumer Protection

based on a decision of
the German Bundestag

M. Valincius
LEI

NPP accident analyses under LOCA and SBO conditions using system computer codes

Development of computer tools for accident analyses in NPPs is the area where scientific investigations are necessary to improve the models and reduce uncertainties of the results obtained by these tools. LEI has participated in several Euratom program projects, where the focus is specifically on numerical simulation of accident scenarios and accident progression. The IVMR (H2020-Euratom 2015-2019) project was initiated, to evaluate In-Vessel Retention strategy in high power NPPs, identify the needs for model updates, and harmonize the methodology of In-Vessel Retention. The MUSA (H2020-Euratom 2019-2023) project was focused on severe accident progression and uncertainties, related to core damage, accident progression and the resulting consequences. The ELSMOR (H2020-Euratom 2019-2023) project was focused on SMR safety, including modelling of SMRs, with some analyses of severe accident cases. SASPAM-SA (Euratom, 2022-2026) project was initiated to further analyze SMRs safety, with a full scope of safety analysis – from accident initiation up to emergency zone planning.

The presentation consists of brief presentation of LEI performed analyses and key findings obtained during the implementation of IVMR, MUSA, ELSMOR, SASPAM-SA projects, as well as plans for the near future of on-going SASPAM-SA project.

LITHUANIAN ENERGY INSTITUTE

NPP accident analyses under LOCA and SBO conditions using system computer codes

Dr. Mindaugas Valinčius
Laboratory of Nuclear Installation Safety
Lithuanian Energy Institute

28th International QUENCH Workshop

KIT, Karlsruhe, Germany, 5-7th December 2023

Outline

Modelling of accident scenarios in NPPs at LEI:

- IVMR project (2016-2019)
- MUSA project (2019-2023)
- ELSMOR project (2019-2023)
- SASPAM-SA project (2022-2026) (ongoing)

IVMR: In-Vessel Melt Retention Severe Accident Management Strategy for Existing and Future NPPs

- In-Vessel Melt Retention (IVMR) appears as an attractive solution that would stabilize molten corium and minimize the risks of containment failure (less Hydrogen produced, no corium-concrete interaction), if it can be proved to be feasible.
- The project aimed at relevant assumptions and scenarios to estimate the maximum heat load on the vessel wall, improved numerical tools for the analysis of IVMR issues and a harmonized methodology on the IVMR.

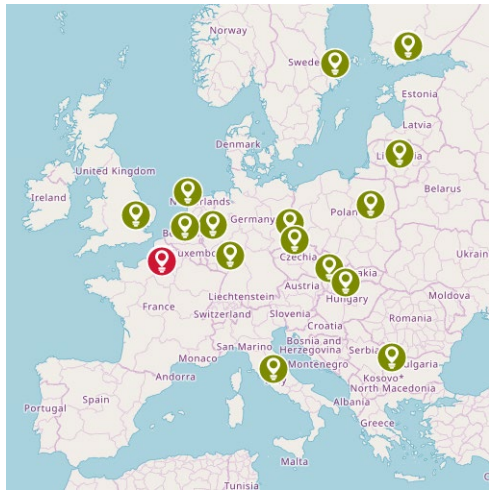

Brief Description Of The Modelled BWR

- Similar to BWR-5;
- Vessel total height 20.8 m, diameter 5.30 m and thickness 13 -19 cm;
- 2029 MWt;
- Total mass of UO2 fuel = 91.2 tons;
- Total mass of Zr = 26.4 tons;
- RELAP/SCDAPSIM mod 3.4;
- Event of LB LOCA + total failure of all emergency core cooling systems (reactor scram is activated) was assumed.

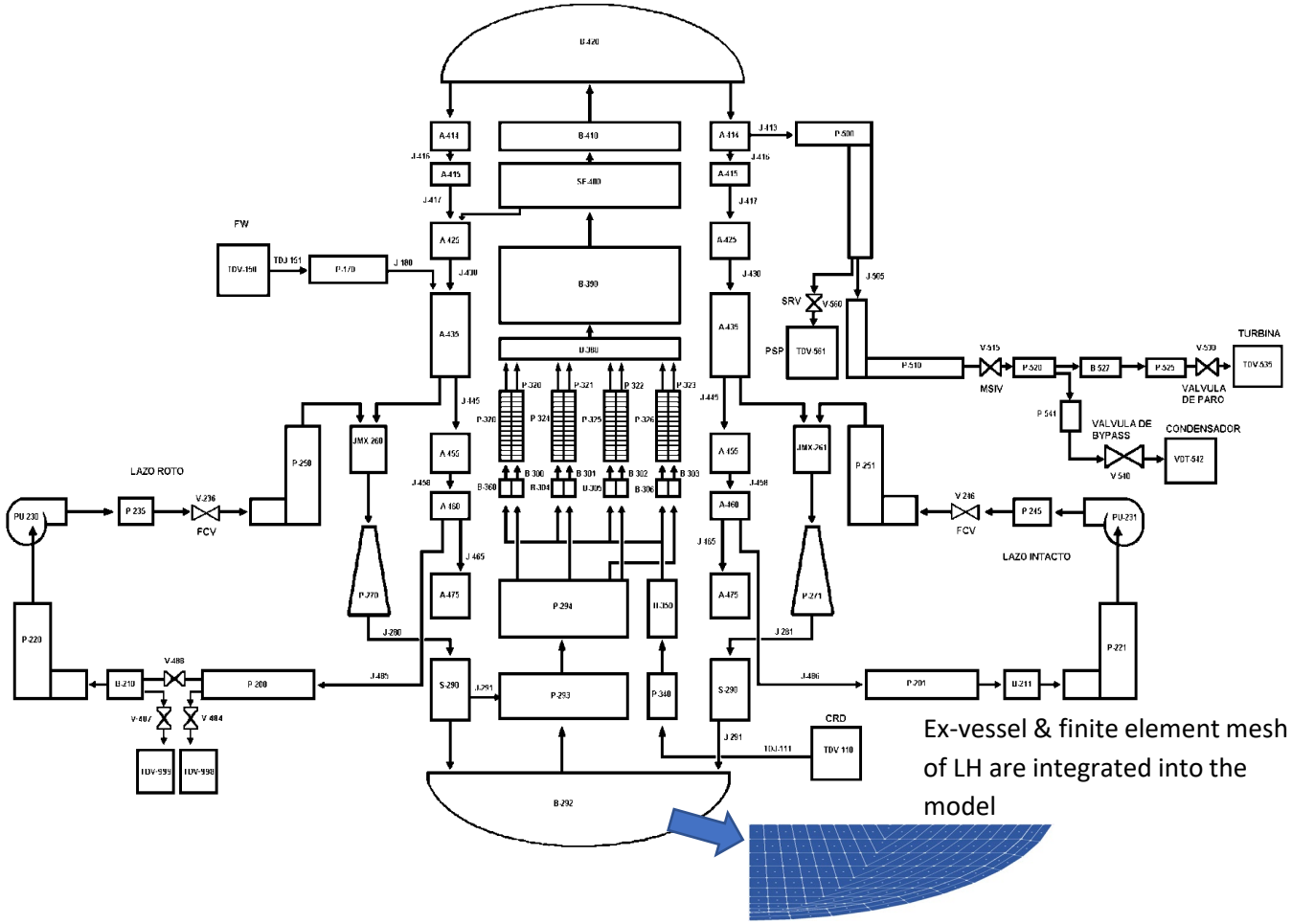

Key events and accident sequence

KEY EVENT	TIME (s)
LOCA+SBO	0
Reactor emergency shutdown (SCRAM) initiating	0.0
Turbine trip initiating	0.0
Trip of recirculation pumps initiating	0.0
Reactor cavity flooded for external cooling (with constant 15 kg/s water supply to prevent boil-off)	0.0
Core Uncovers/ First heat up of the core	32
Core fully uncovered	50
Start of core relocation to lower head	847
Dry out of the lower head	3000

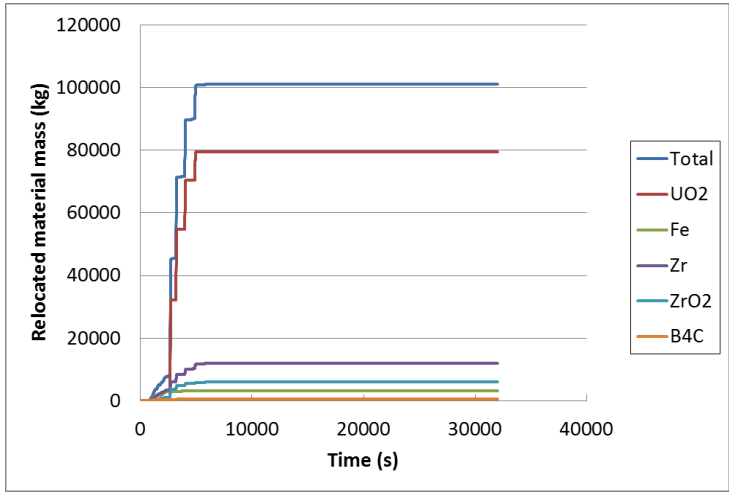

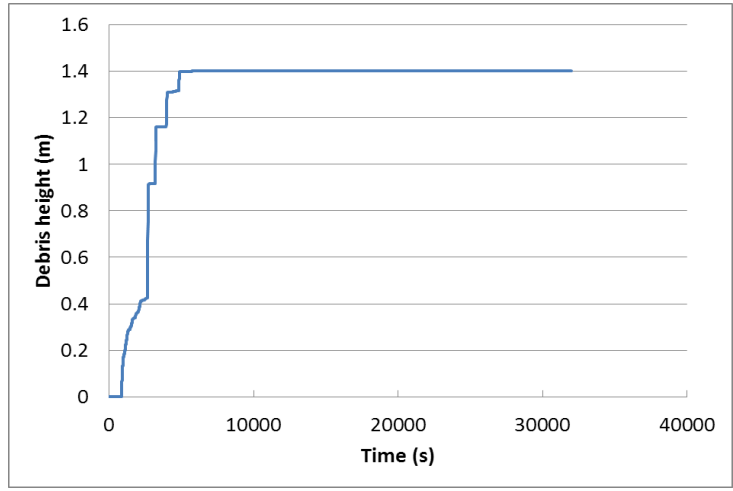

Mass of different materials and debris height in the lower head.

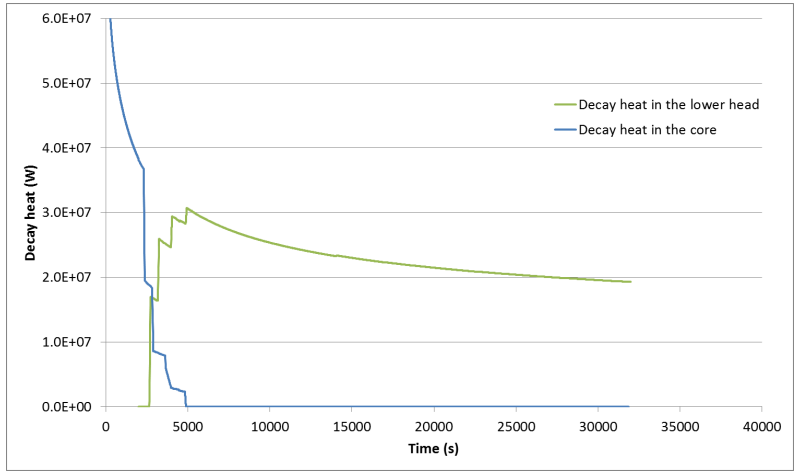

Decay heat in the reactor core and the corium in the lower head.

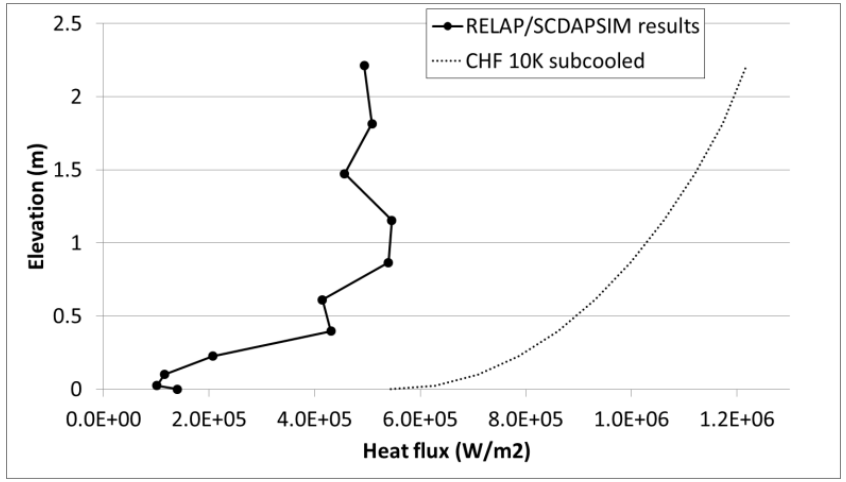

Maximum heat flux at the external surface of the RPV wall calculated by RELAP/SCDAPSIM.

Corium layers. Standard configuration vs RELAP/SCDAPSIM

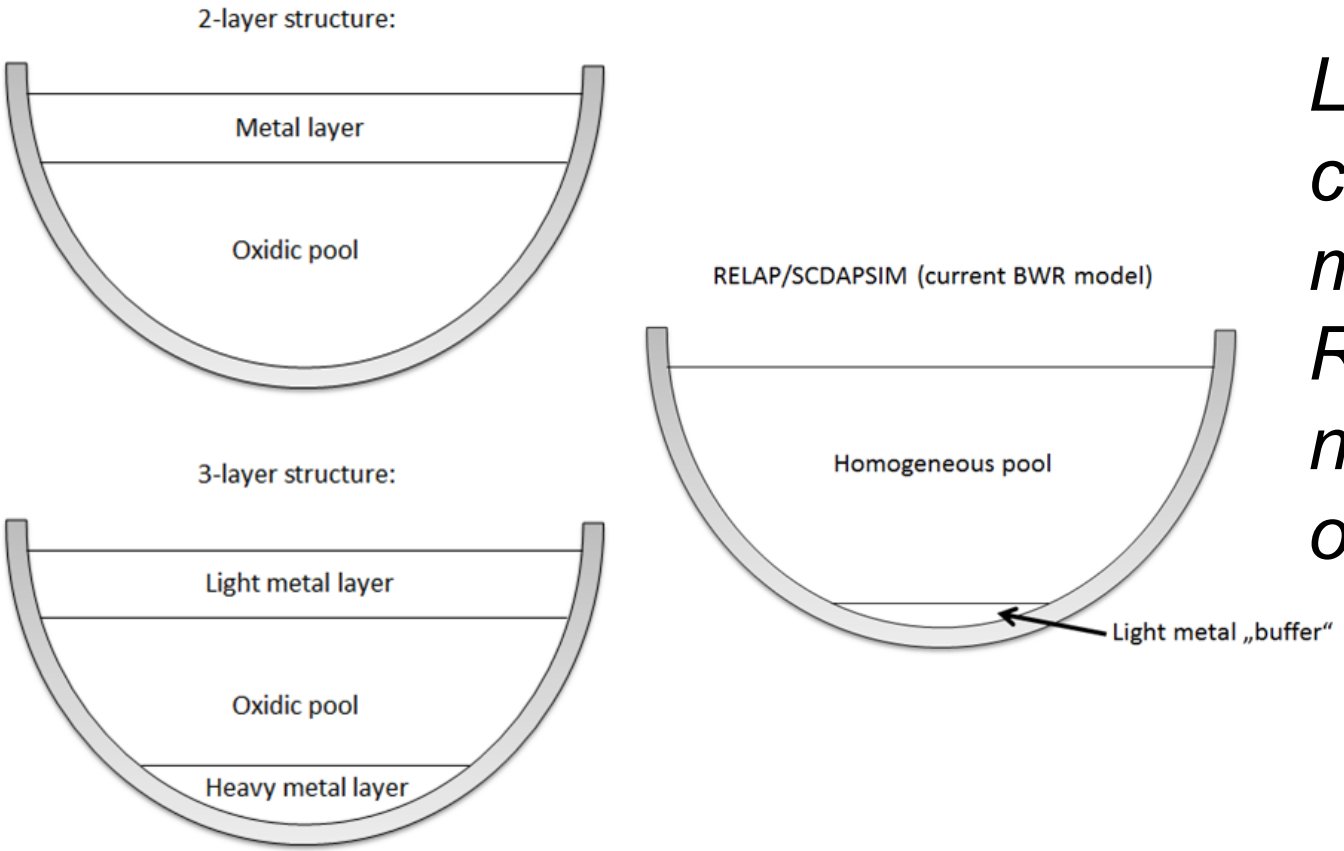

Layer formation in debris bed compared to RELAP/SCDAPSIM model.
RELAP/SCDAPSIM model does not take into account separation of oxidic and metallic layers.

ATHLET-CD calculations

ATHLET-CD code (AIDA module) was used to simulate stand-alone problem of IVR.
As we can see, with the corium composition from RELAP/SCDAPSIM calculations and without any additional steel, 10 MW of decay heat could be removed and the minimum residual wall thickness is ~4.5 cm.

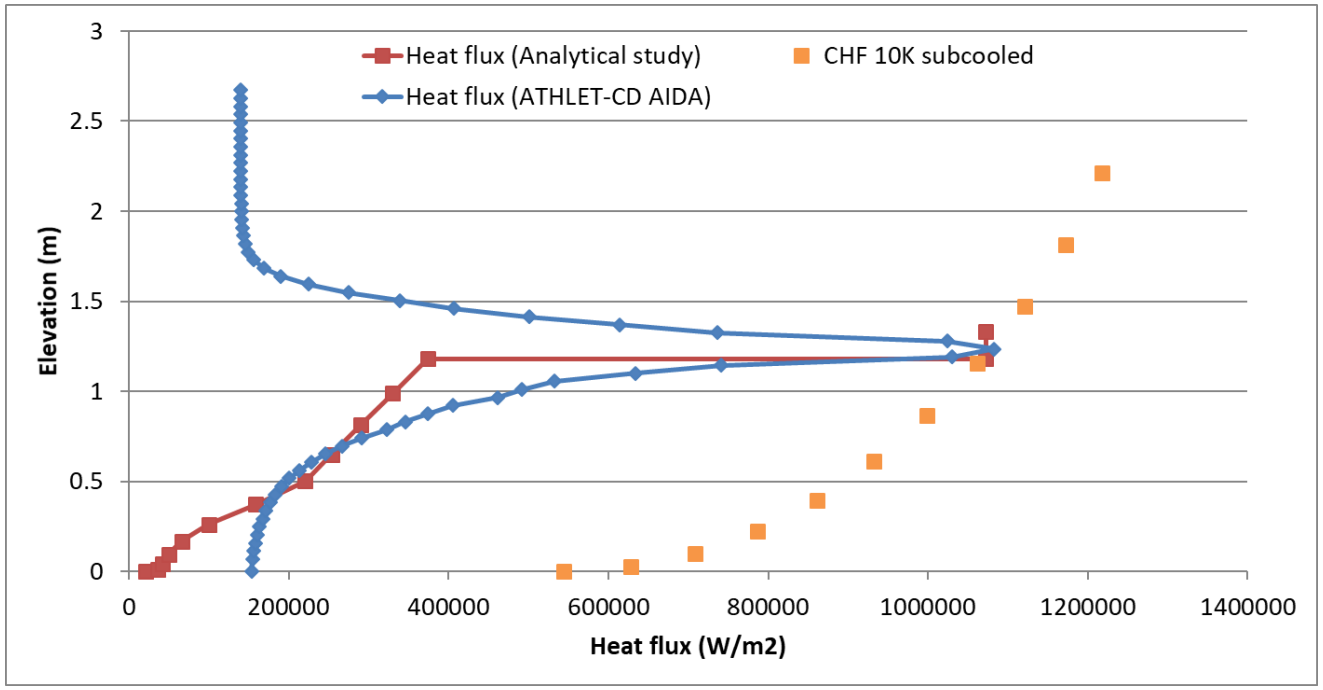

Heat flux comparison between analytical study and ATHLET-CD AIDA calculations.

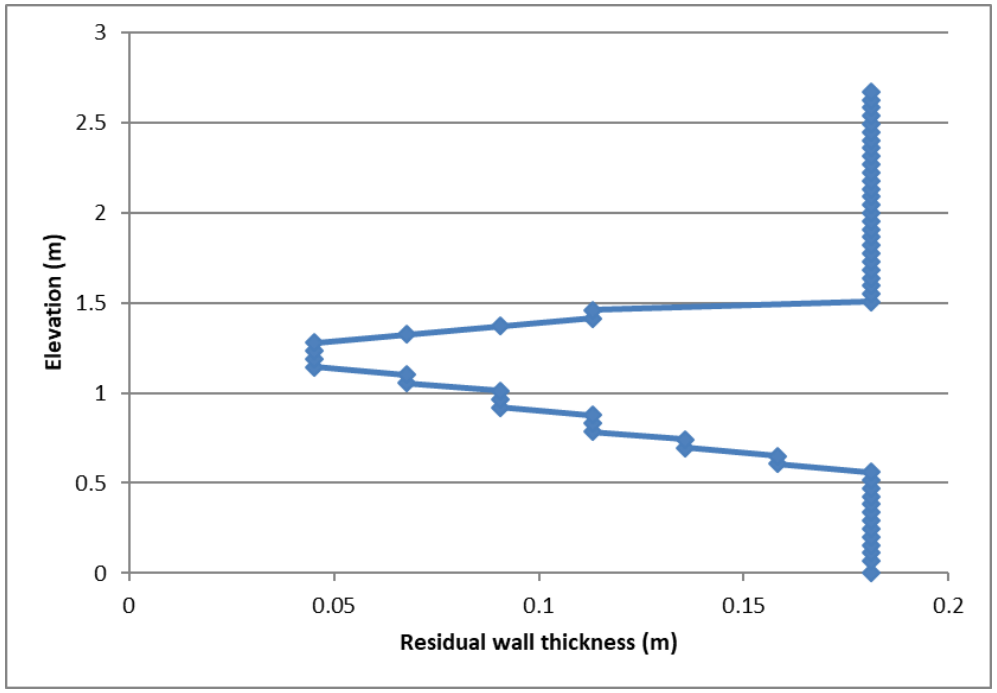

Residual wall thickness from ATHLET-CD AIDA calculations.

Conclusions

- **Message: Use the correct tools for the analysis!**

- RELAP/SCDAPSIM can be used to calculate normal plant operation thermal hydraulics, accident sequence, core heat-up and relocation of the core materials.
- RELAP/SCDAPSIM MOD3.4 is not suitable for detailed analysis of heat transfer between debris bed and RPV wall.
- ATHLET-CD AIDA model with IVMR updates is able to predict the focusing effect and take into account wall ablation. RELAP/SCDAPSIM integral calculation results can be used as input data for ATHLET-CD stand-alone model for detailed analysis, where RELAP/SCDAPSIM is not applicable.

MUSA: Management and Uncertainties of Severe Accidents

Key activities:

- Identification and quantification of uncertainty sources in severe accident analyses
- Review and adaptation of uncertainty quantification methods
- Testing such methods against reactor and spent fuel pool accident analyses, including accident management

NPP modelling and SA Scenario

- **Short description:**
  - **the NPP model:**
    - A plant similar to BWR-5 operating at 2029 MWth was assumed.
    - The containment was not modelled, since RELAP/SCDAPSIM is not applicable for modelling processes in the containment.
  - **the SA scenario analyzed: <u>LBLOCA+SBO & LBLOCA +SBO +HPCS injection</u>**
    - The initiating event is considered to be a guillotine break in one of two recirculation loops, followed by immediate SBO.
    - The only safety systems in operation are control rods and turbine isolation valves. The control rods are activated at the beginning of the accident. The exit to the turbines (MSIV) and feedwater line are closed at the beginning of the accident.
    - In case of HPCS the water injection starts at different times after the break, applied for the base case. For the current tests it was assumed at 700 s after the break, when the PCT reaches 1700K (to allow limited initial oxidation and core damage)

Plant Nodalization

HPCS

155 → 175

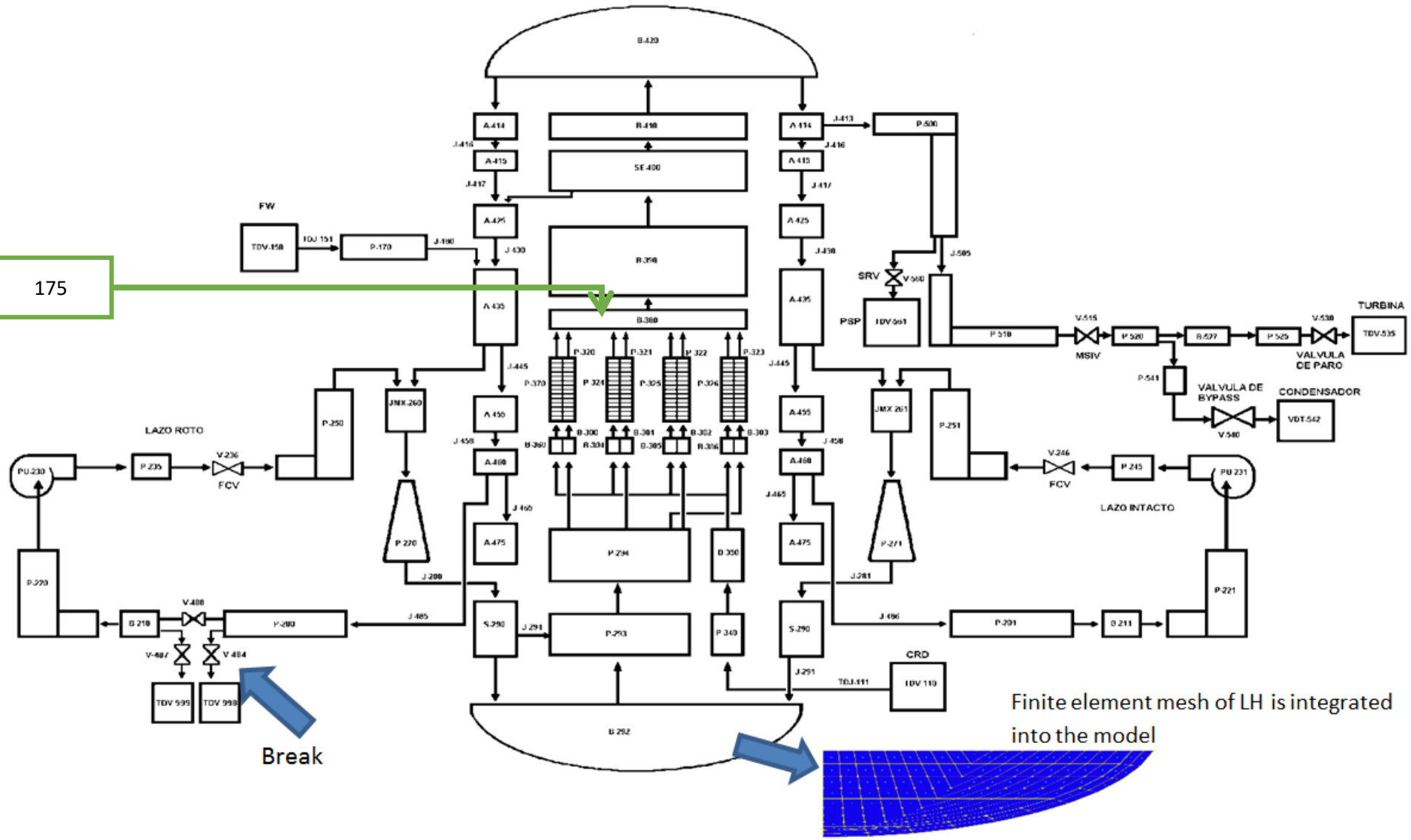

SA Code and UQ Tool Coupling

- **Severe accident code and version: RELAP/SCDAPSIM mod 3.4**
- **Uncertainty Tool and version: SUSA 4.0 (GRS)**
- **Number of calculations launched to perform the UQ: 100**
- **Number of calculations failed: 35 (=~1/3)**

- **Issues found in the SA/UQ tool coupling:**
  - Fission product element modeling:
    - CORSOR-M model to calculate Cs/I FP release from bundles (by using temperature calculation results), because there are problems with FP inventories in RELAP/SCDAPSIM model which still needs to be investigated.
    - The code is not applicable for FP modelling in the containment.

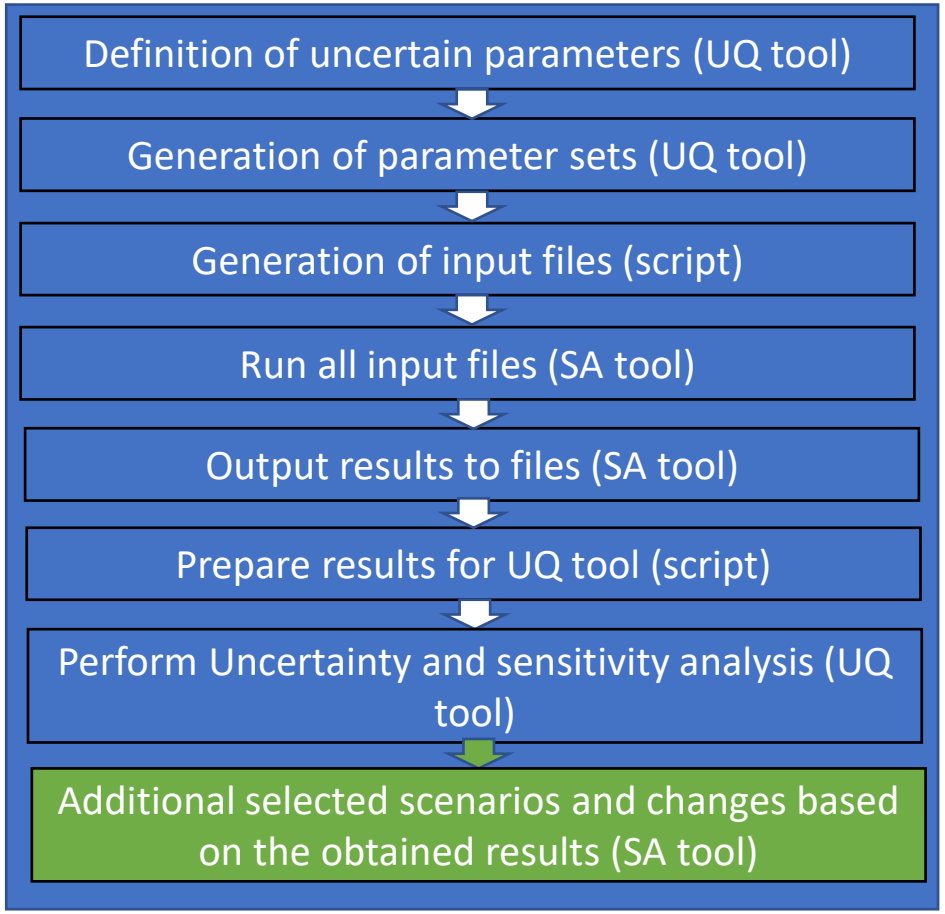

Assessment of the UQ Analysis: Uncertainty Parameters (1)

par#	Short description	Reference Value	Variation Range	PDF	Notes
1	Gamma heat fraction	0.026	0.013 - 0.039	Normal	
2	Zry-4 specific heat	1	0.8 - 1.2	Normal	Multiplier for $f(T)$
3	Zry-4 density	1	0.8 - 1.2	Normal	Multiplier for $f(T)$
4	Zry-4 thermal conductivity	1	0.8 - 1.2	Normal	Multiplier for $f(T)$
5	Gap specific heat	1	0.8 - 1.2	Normal	Multiplier for $f(T)$
6	Gap density	1	0.8 - 1.2	Normal	Multiplier for $f(T)$
7	Gap thermal conductivity	1	0.8 - 1.2	Normal	Multiplier for $f(T)$
8	Mass of grid spacer	0.0022	0.00176 - 0.00264	Normal	
9	Height of grid spacer	0.0413	0.033 - 0.0496	Normal	
10	Plate thickness of grid spacer	0.00762	0.0061 - 0.00914	Normal	

Assessment of the UQ Analysis: Uncertainty Parameters (2)

par#	Short description	Reference Value	Variation Range	PDF	Notes
11	Temperature for failure of oxide shell on outer surface of fuel and cladding	2500	2250 - 2750	Uniform	
12	Fraction of oxidation of fuel rod cladding for stable oxide shell	0.6	0.3 - 0.9	Uniform	
13	Cladding rupture strain and Transition strain multiplier	1	0.8 - 1.2	Normal	Multiplier for two parameters
14	Pressure drop caused by ballooning	0	0 - 1	Discrete	
15	Fraction of surface area covered with drops that results in blockage that stops local oxidation	0.2	0.1 - 0.3	Uniform	
16	Velocity of drops of cladding material slumping down outside surface of fuel rod	0.5	0.25 - 0.75	Uniform	

Assessment of the UQ Analysis: Failed cases – no observable pattern

- Failed = -1; Successful = 1

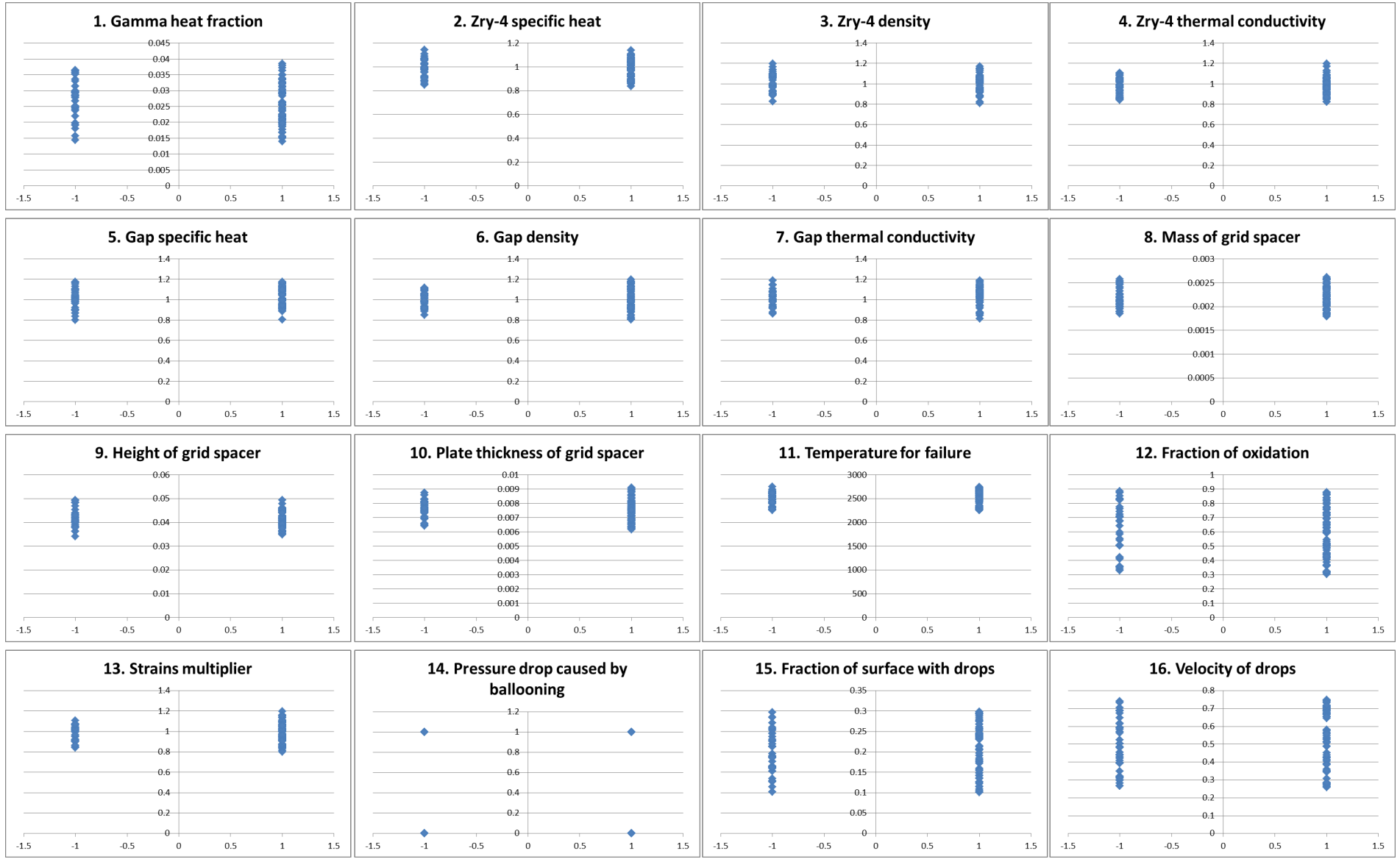

Assessment of the UQ Analysis: Figure-of-Merits

- **FoMs selected for the current analysis**

#	Figure-of-Merit
1	Total FP (Cs, I) released (mass fraction [% ii]) from fuel/core (in-vessel)
2	Mass of H2 produced in-vessel

- **Note: processes in the containment are not modelled by RELAP/SCDAPSIM.**

Results of the SAM Analysis (1)

- **(LBLOCA at 8000 s + HPCS at 8700 s)**

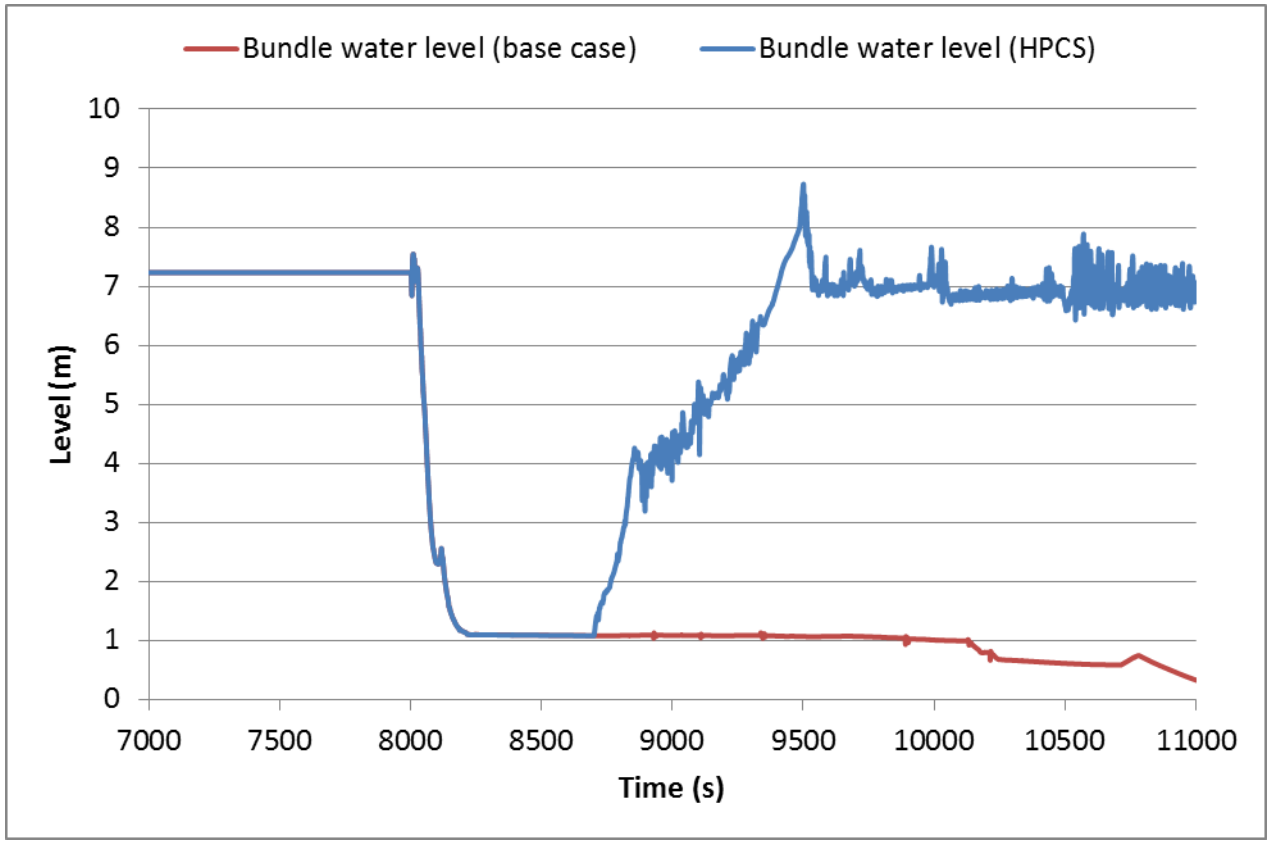

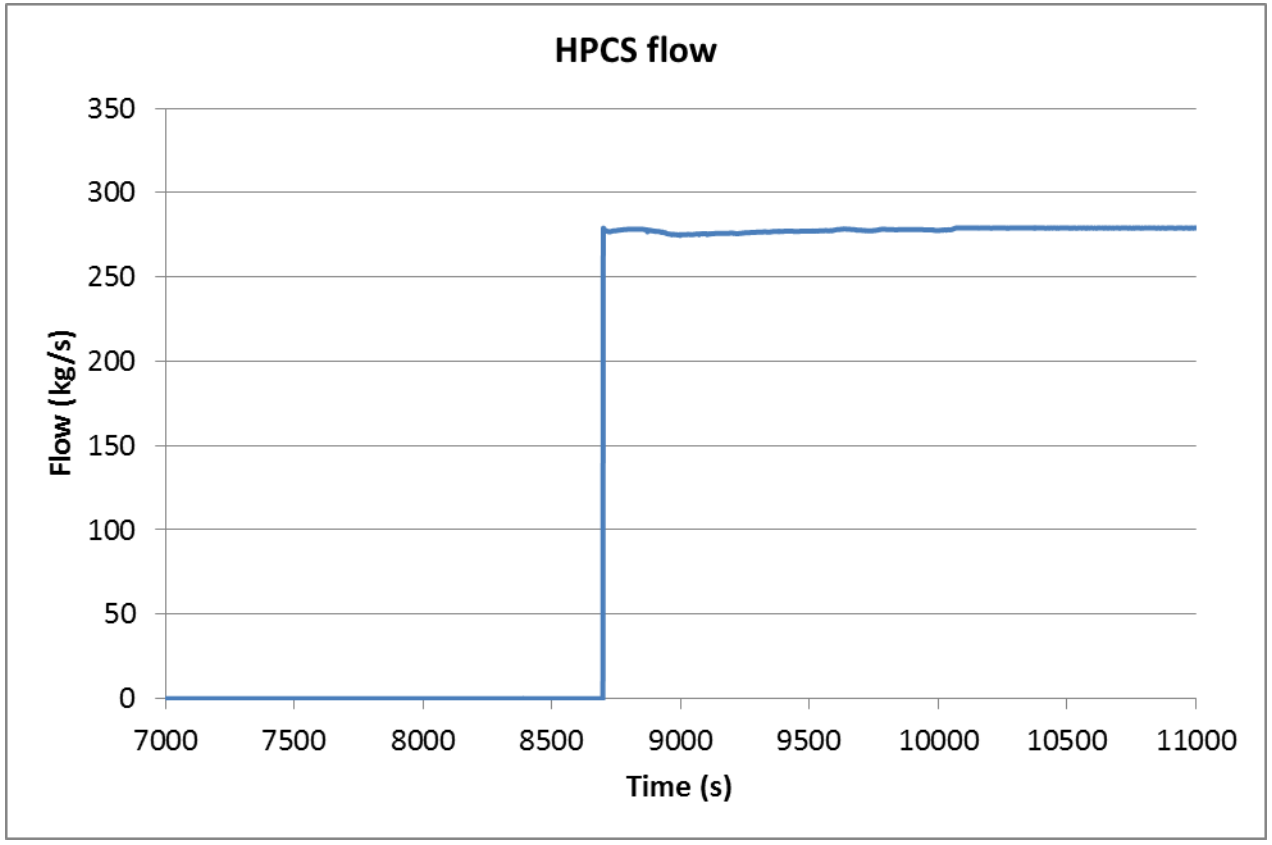

Results of the UQ Analysis (1)

- Cs/I release fraction from bundles
- (LBLOCA + SBO at 8000 s) & (LBLOCA at 8000 s + HPCS at 8700 s)

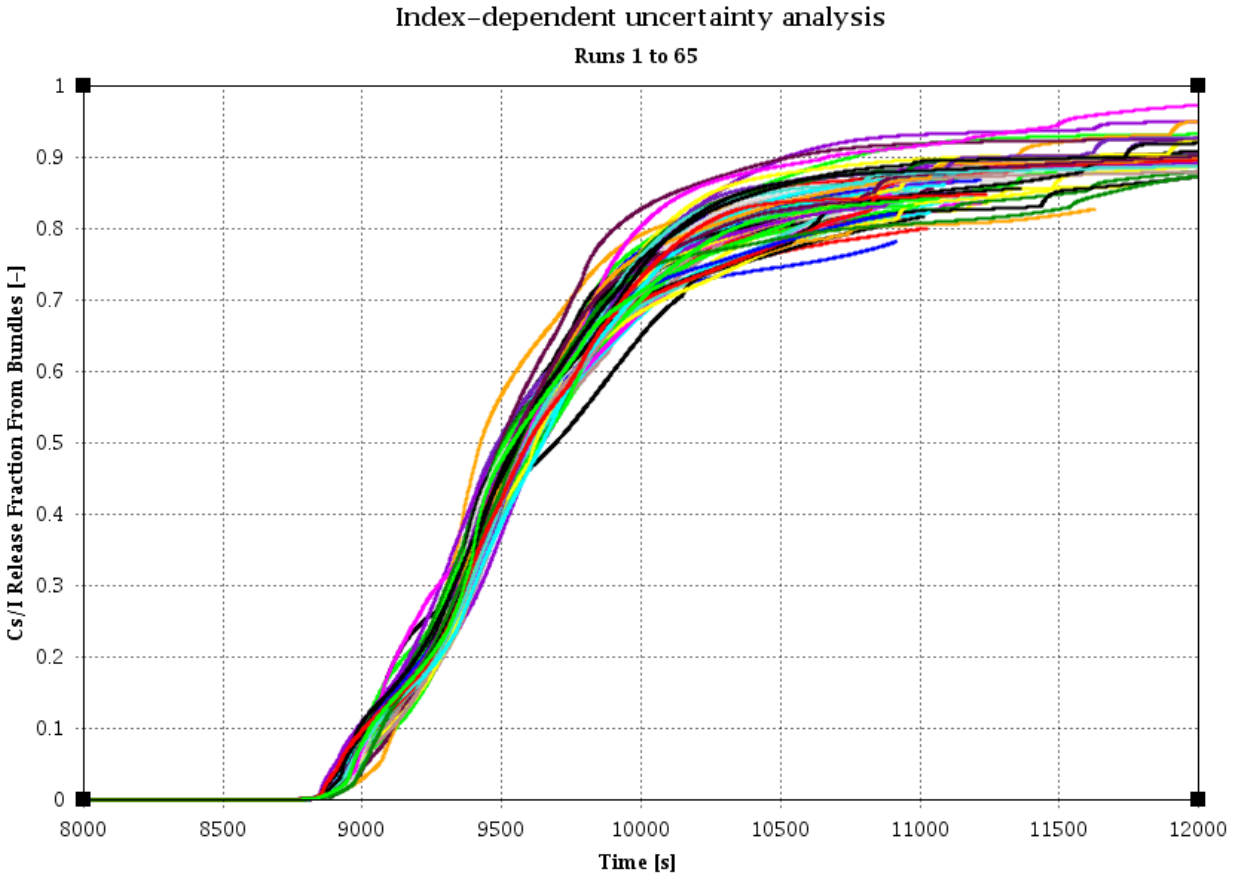

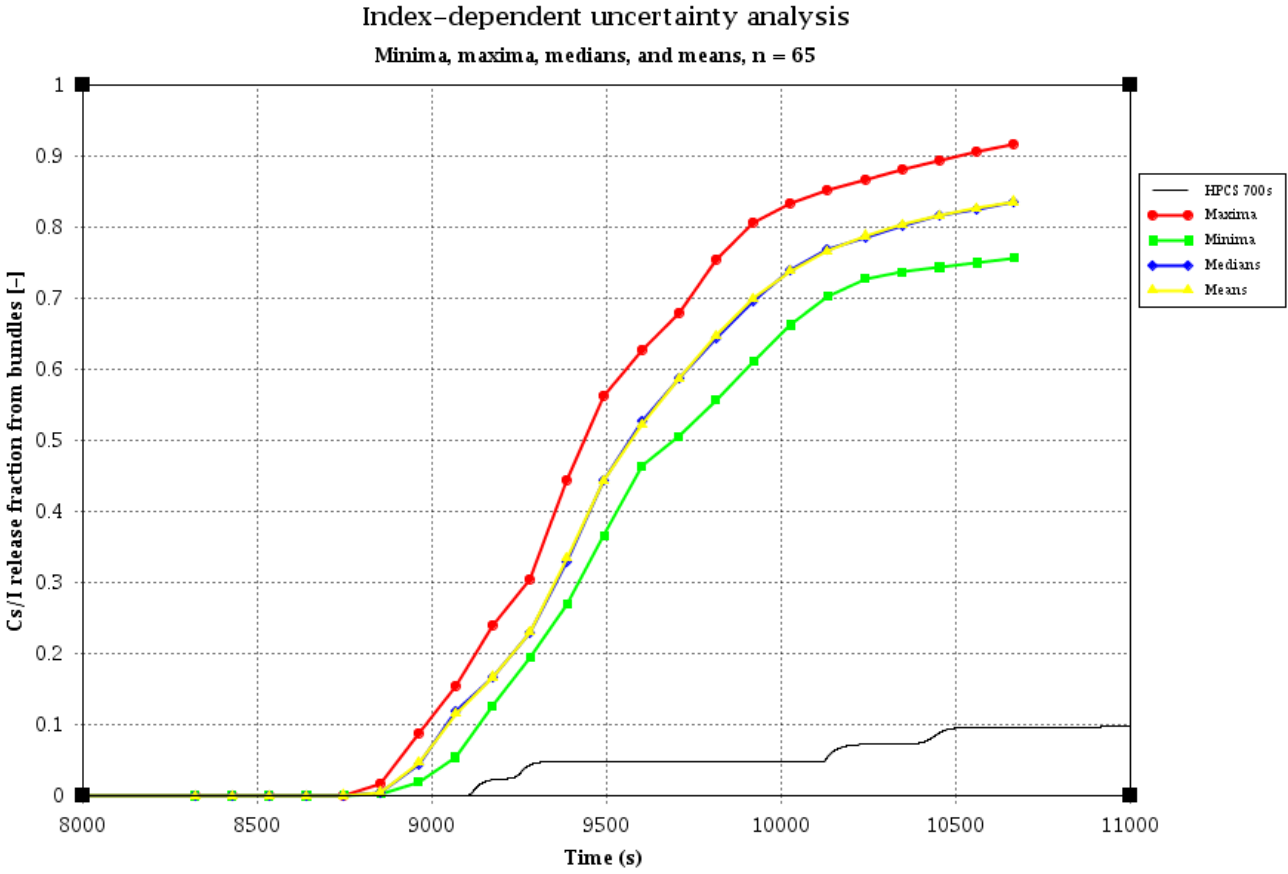

Results of the UQ Analysis (2)

- **Mass of H2 produced in-vessel**
- **(LBLOCA + SBO at 8000 s) & (LBLOCA at 8000 s + HPCS at 8700 s)**

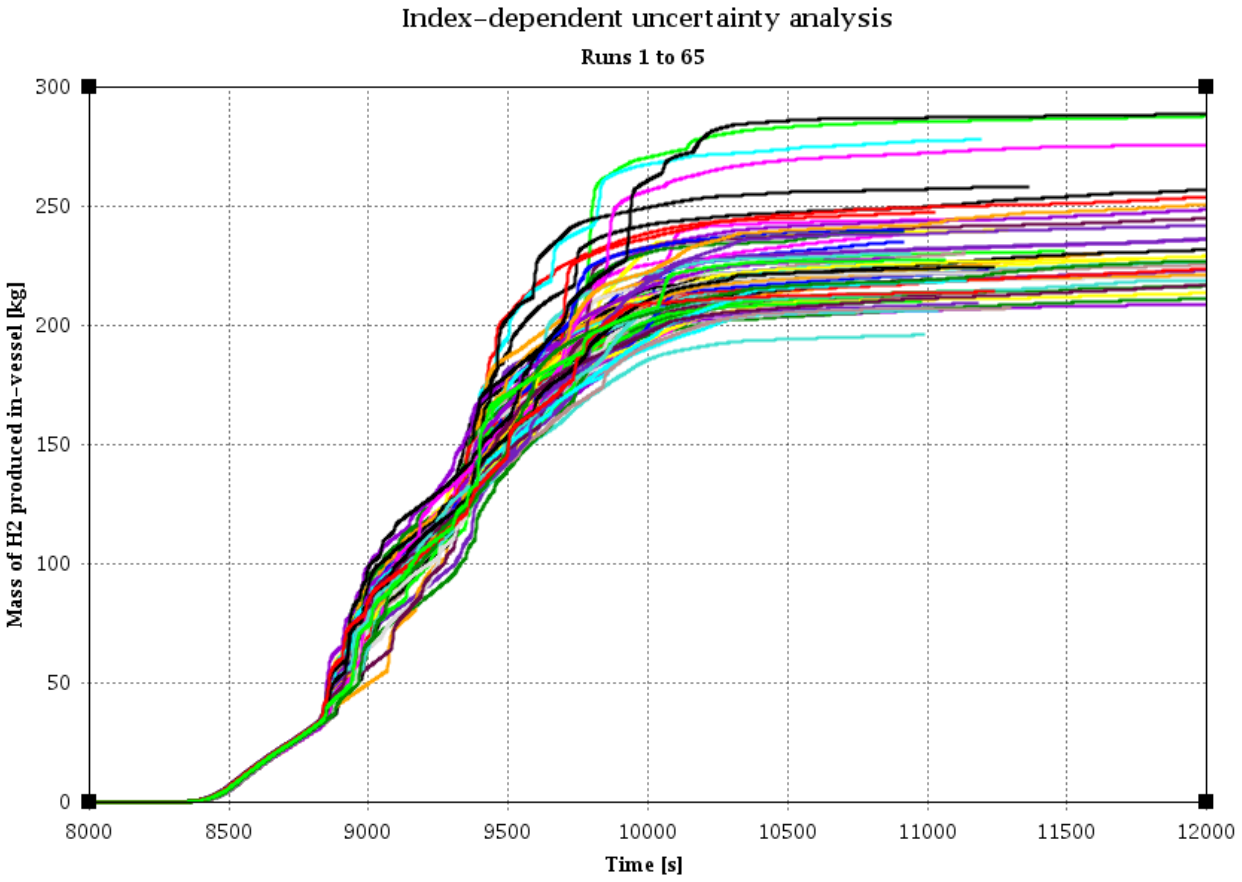

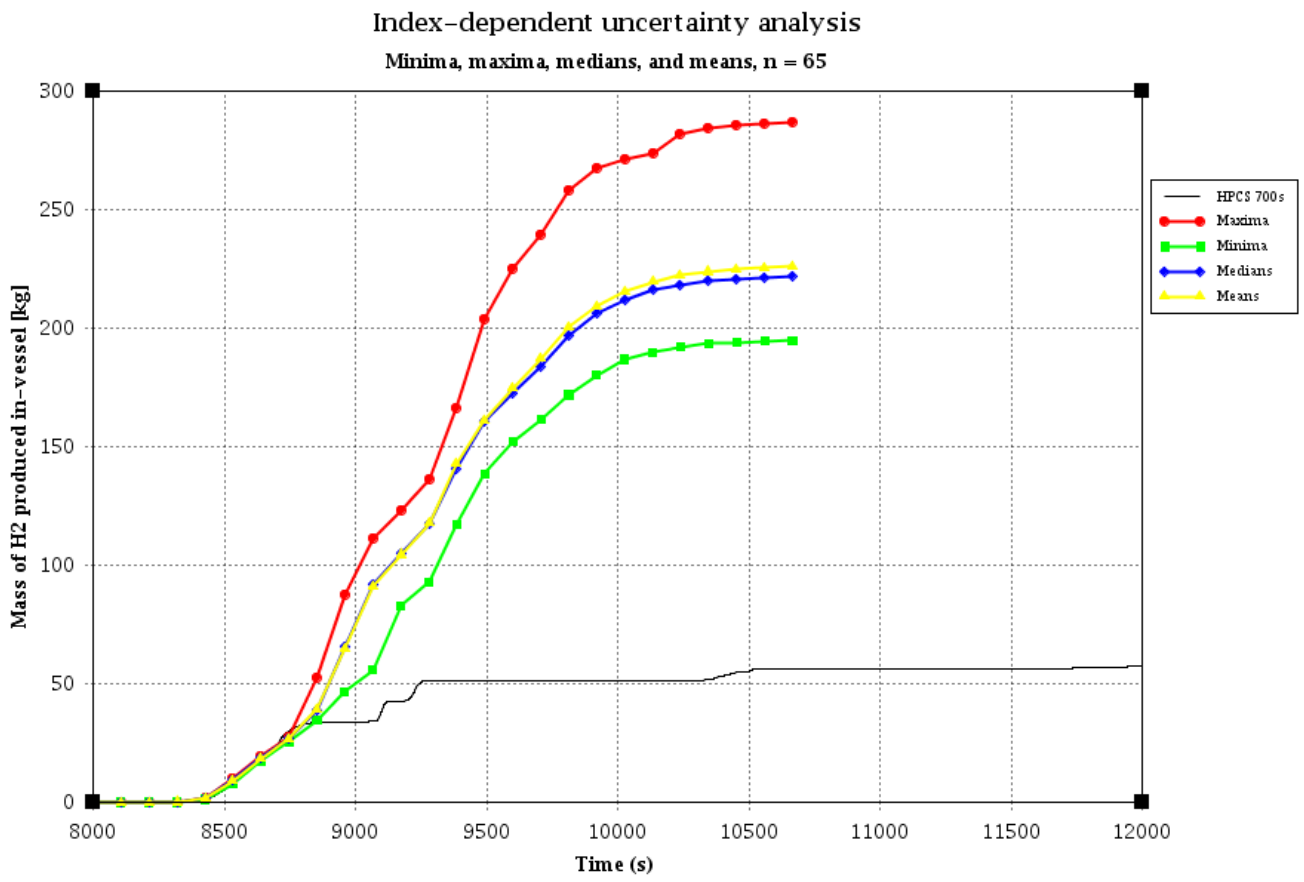

Summary

- **<u>Message: Use the correct tools!</u>**

- Limitation of the RELAP/SCDAPSIM code apply – not possible to model processes beyond RPV
- Code crashes is a huge issue – significant amount of time is required for manual time step adjustments and restarts. This might limit the investigated cases

ELSMOR “Towards European Licencing of Small MOdular Reactors” (2019-2023)

NUWARD SMR (France)

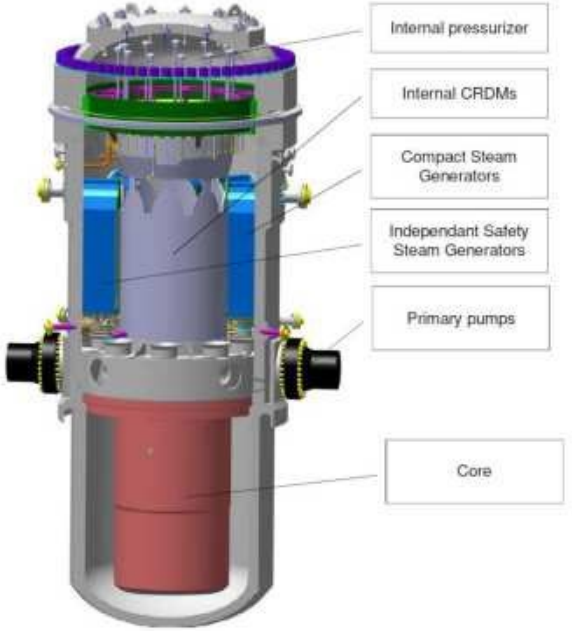

- **ELSMOR** aims to create methods and tools for the European stakeholders to assess and verify the safety of light water small modular reactors (LW-SMR) that would be deployed in Europe.
- **ELSMOR** advances the understanding and technological solutions pertaining to **light water SMRs** on several fronts:
  - Collection, analysis, and dissemination of the information on the **potential and challenges of Small Modular Reactors** to various stakeholders, including the public, decision makers and regulators.
  - Development of the high level methods to assess the **safety of LW-SMRs**
  - Improvement of the **European experimental research infrastructure** to assist in the evaluation of the novel safety features of the future LW-SMRs.
  - Improvement of the **European nuclear safety analysis codes** to demonstrate the capability to assess the safety of the future LW-SMRs

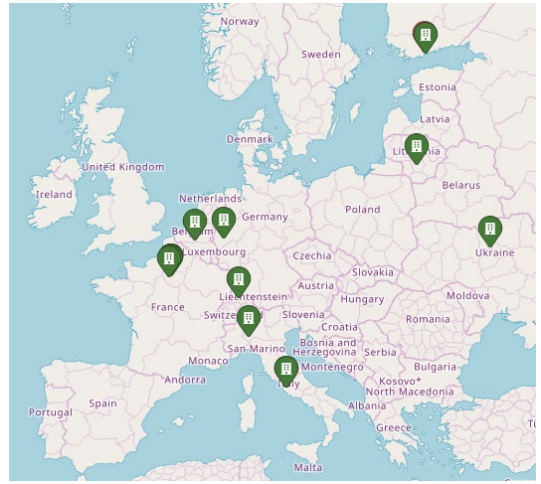

NUWARD SMR

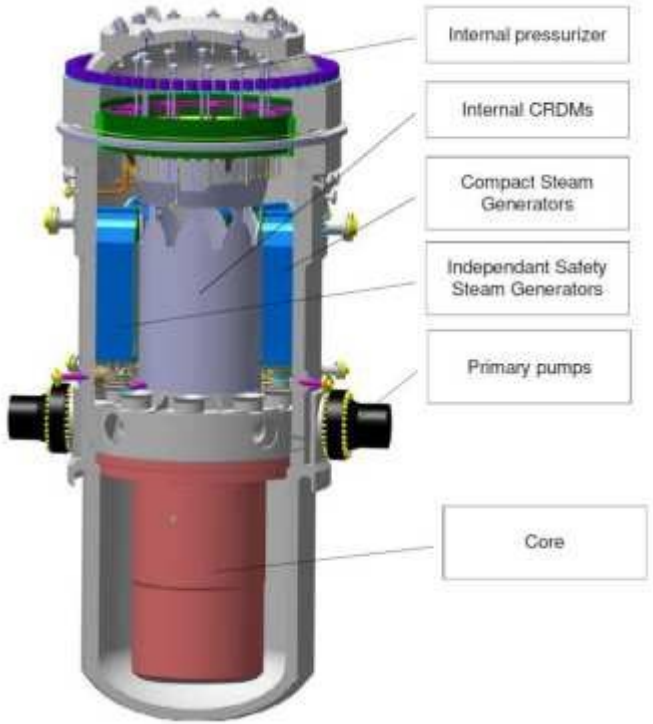
Internal pressurizer
Internal CRDMs
Compact Steam Generators
Independant Safety Steam Generators
Primary pumps
Core

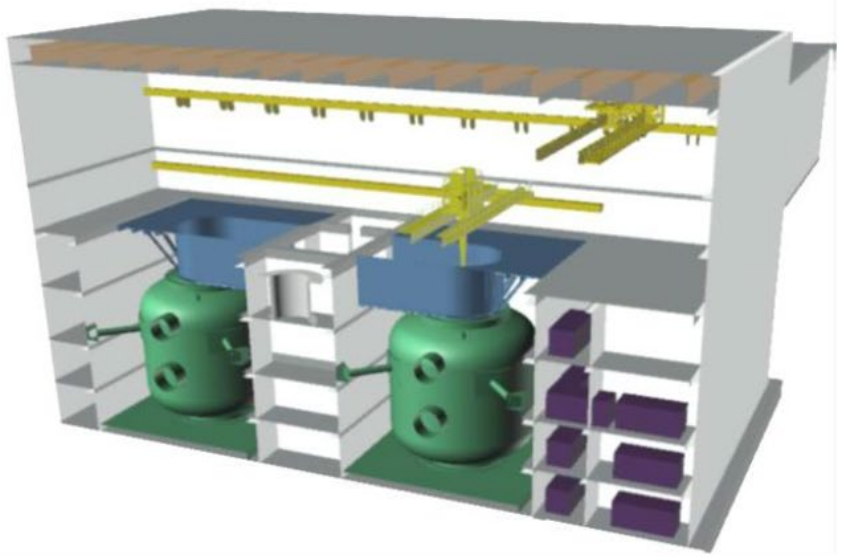

ELSMOR
towards European Licensing of Small MOdular Reactors

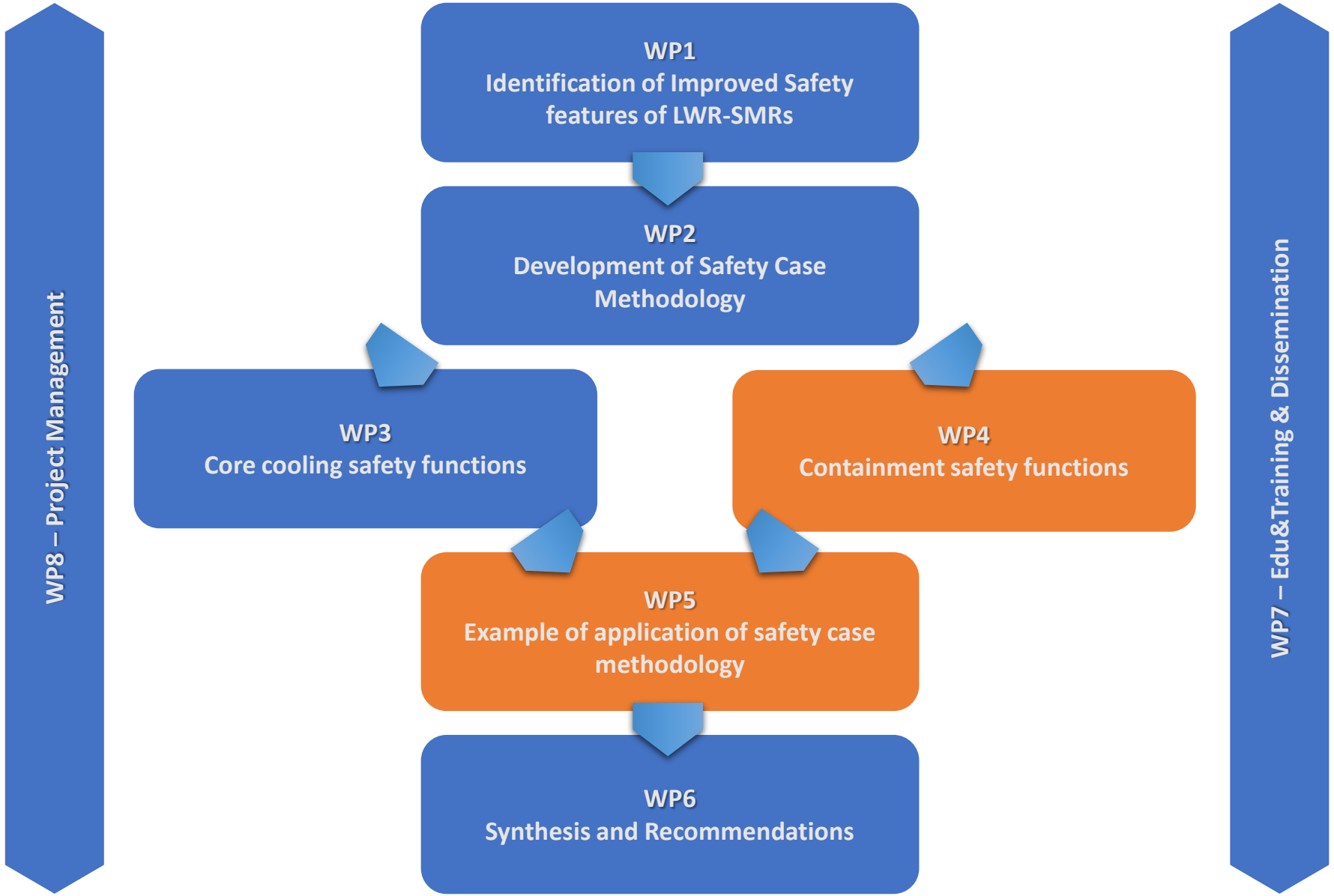

Model and Nodalization

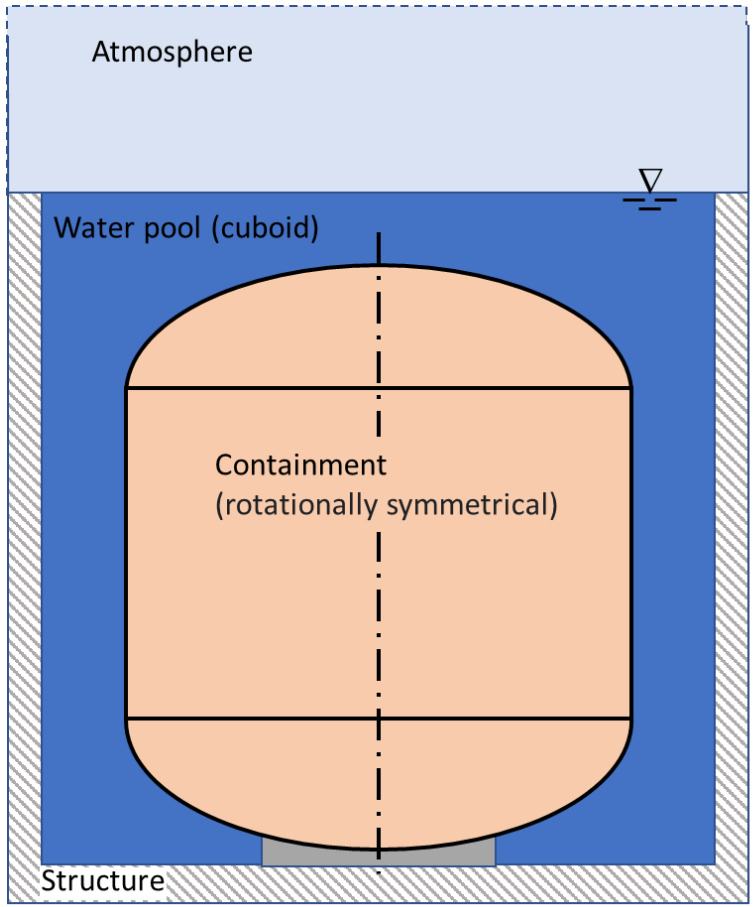

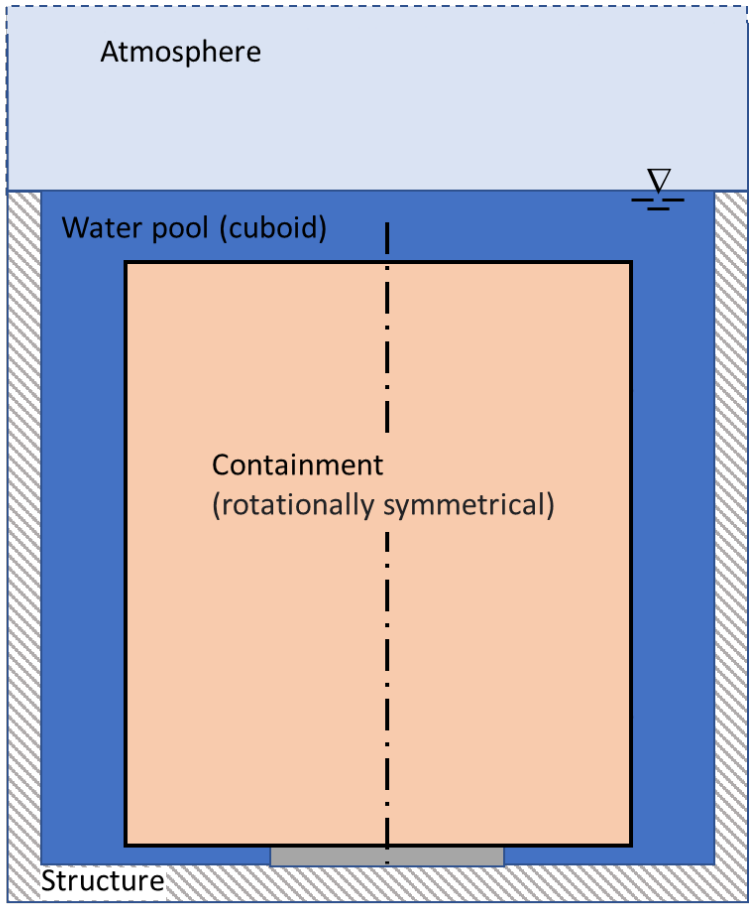

Pool size: 20x20x20 m
Water level: 20 m

Parameter	Value [m]
Diameter of Containment (outer)	15.00
Total height of containment	16.00
Height of upper head	3.05
Height of lower head	3.50
Height of cylindrical part	9.00
Height of containment support structure	1.05
Width of support structure	7.00
Containment wall thickness (uniform on all structures)	0.05

AC2, ATHLET-3D

- System thermal-hydraulic code, developed by GRS for NPP applications. 3D model implemented, which is based on 1D approach.
- Grids:
  - Coarse Cartesian/cylindrical grids
  - Grids are not meant to capture micro-scale phenomena, but rather macro-scale flow path
- Model & nodalization. 8x8x11 cuboid with cut-out 4x4x8 heated containment inside.

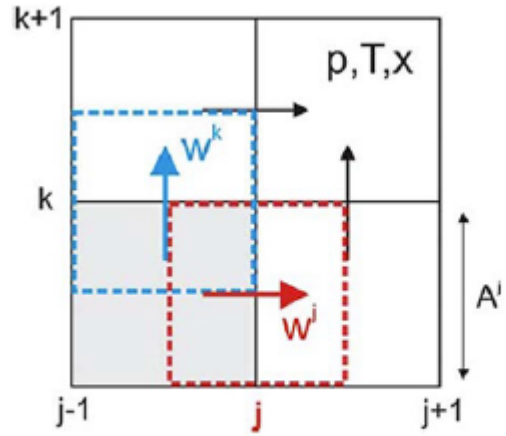

Staggered numerical grid with control volumes and junctions

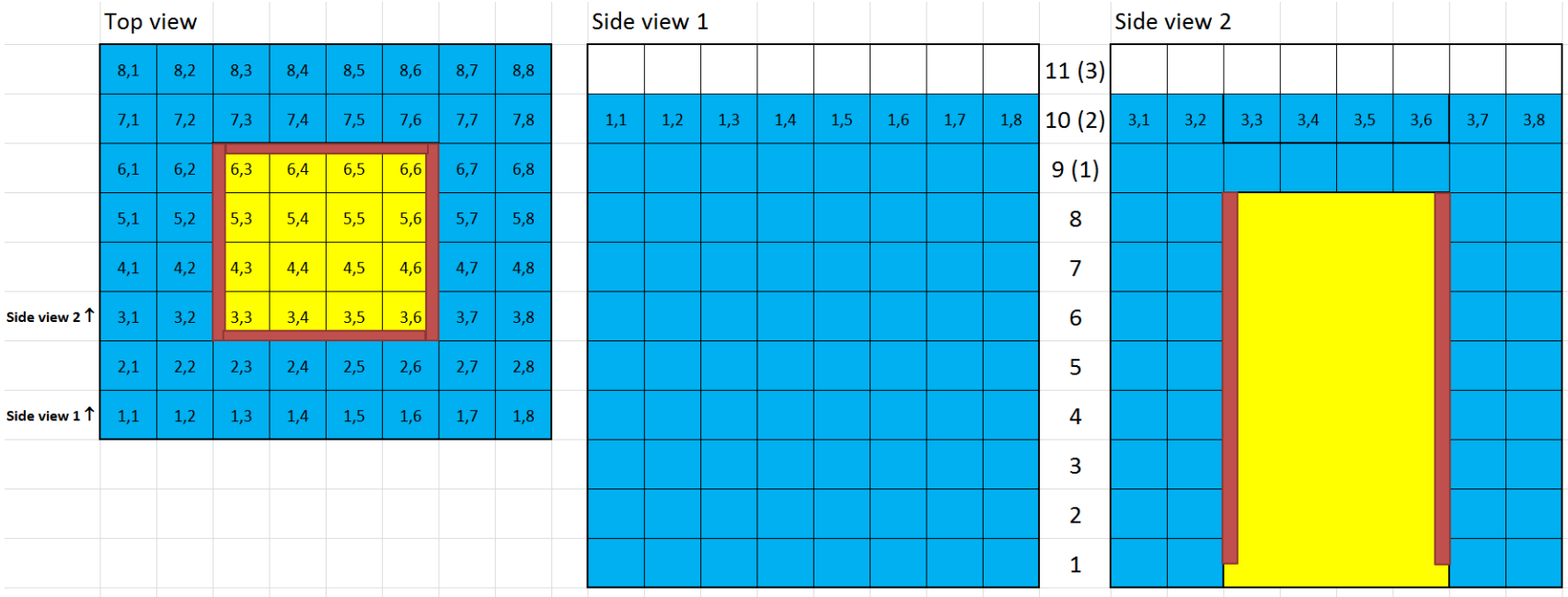

Model and Nodalization (too complex)

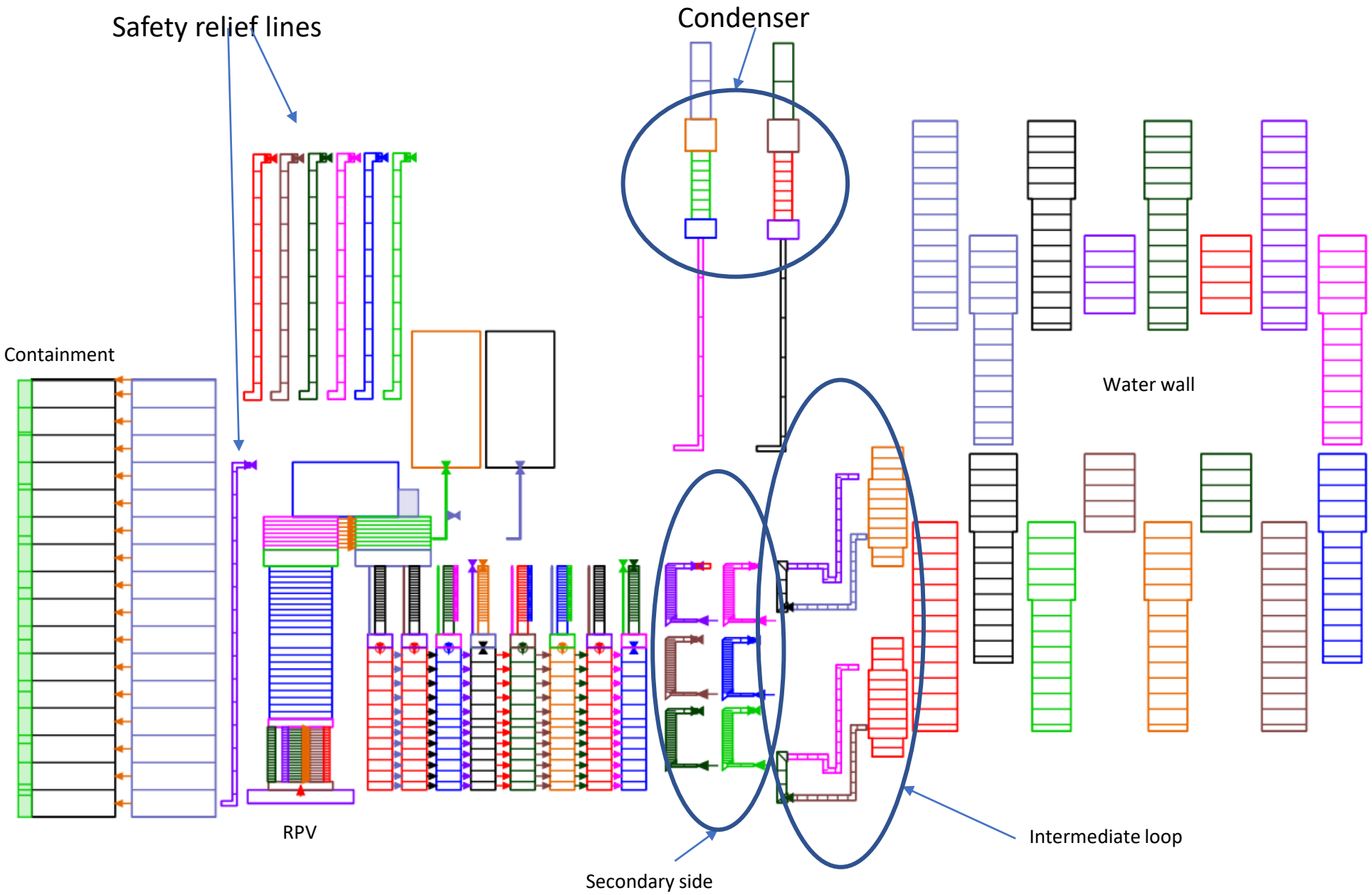

Model and Nodalization Simplified

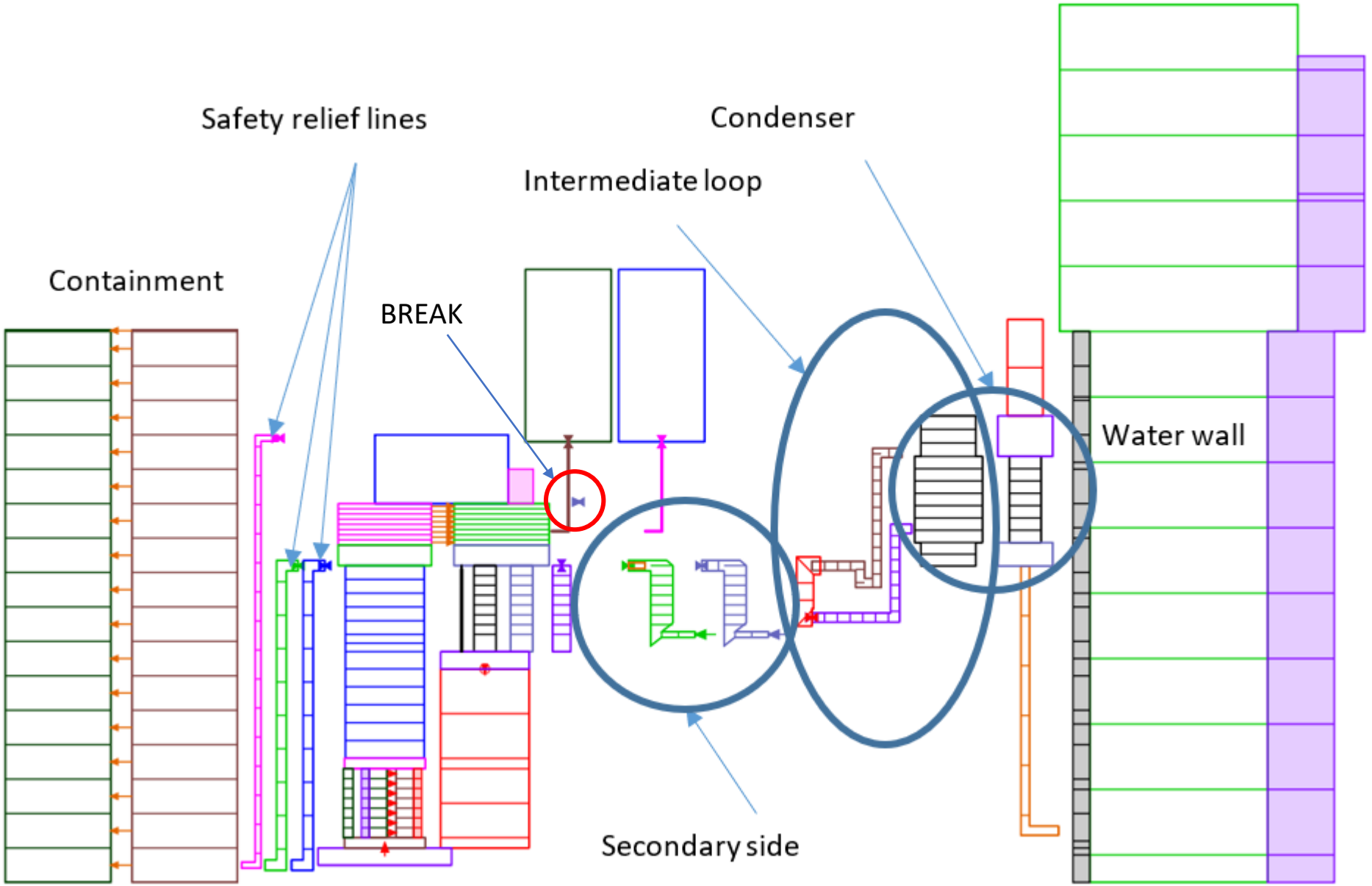

Model and Nodalization Simplified (2)

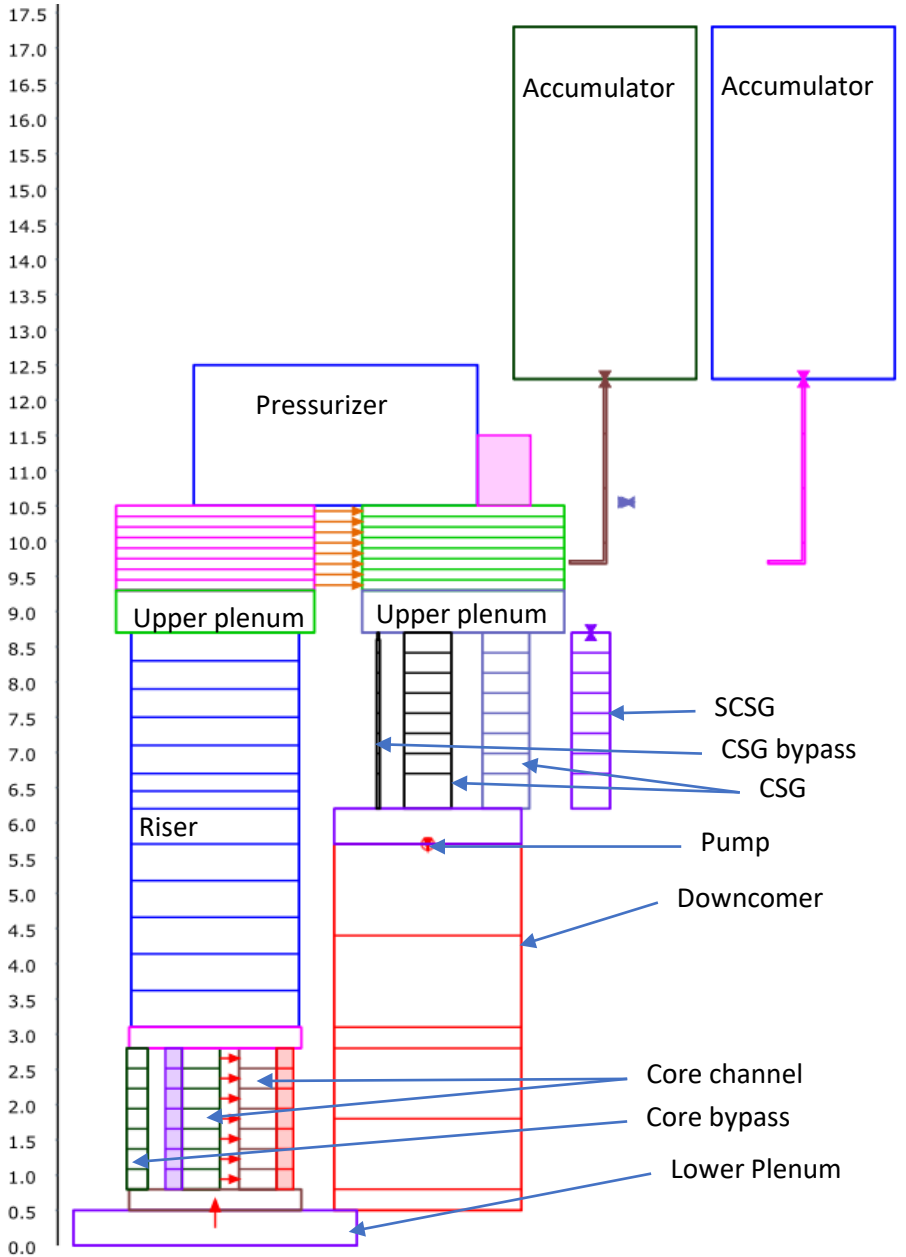

Steady state

Parameter	E-SMR	AC^2
Power (MW)	540.0	540.0
Primary pressure (bar)	150.0	149.9 (Lower Plenum)
Primary coolant flow rate (kg/s)	3700.0	3698.9
Secondary coolant flow rate (kg/s)	240.0	300.0
Core inlet temperature (°C)	280.0	279.9
Core outlet temperature (°C)	307.0	307.1
Core dp (bar)		0.33
Secondary pressure (bar)	45.0	45.1 (Main Steam Line)

Results - LOCA

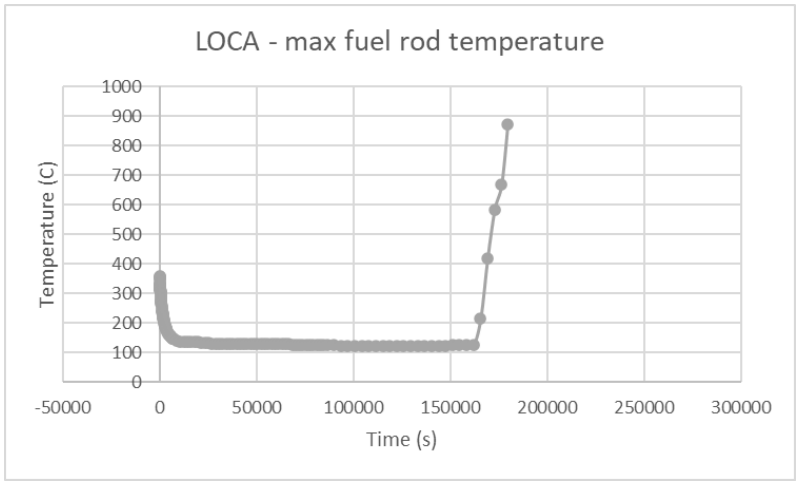

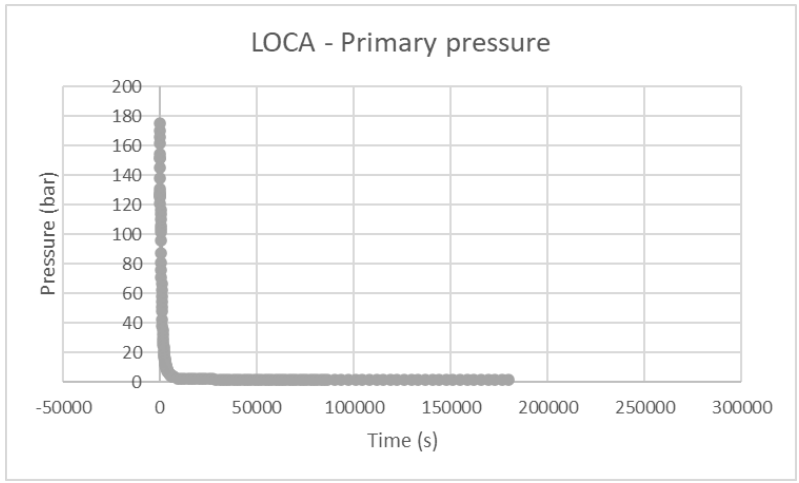

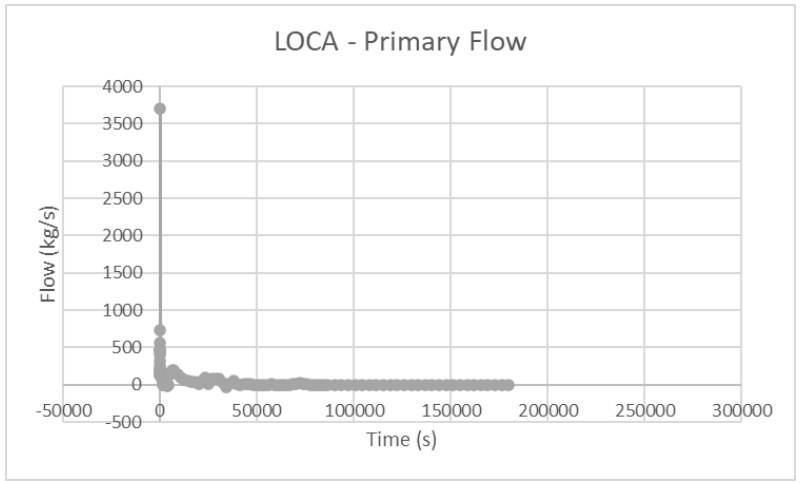

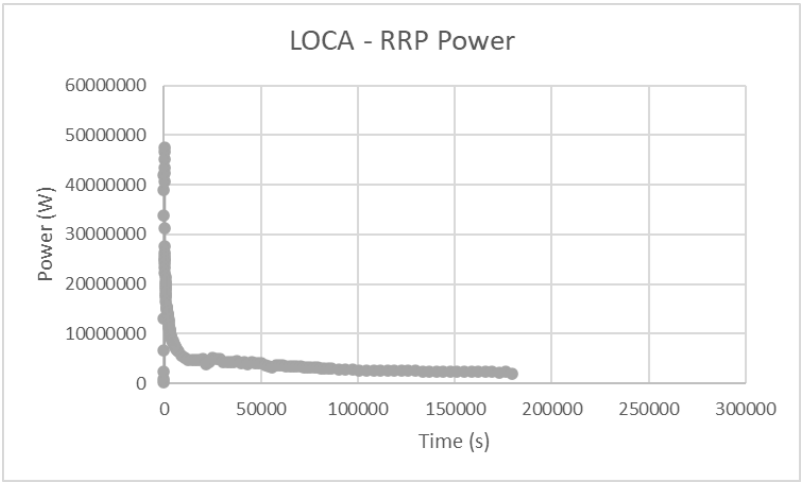

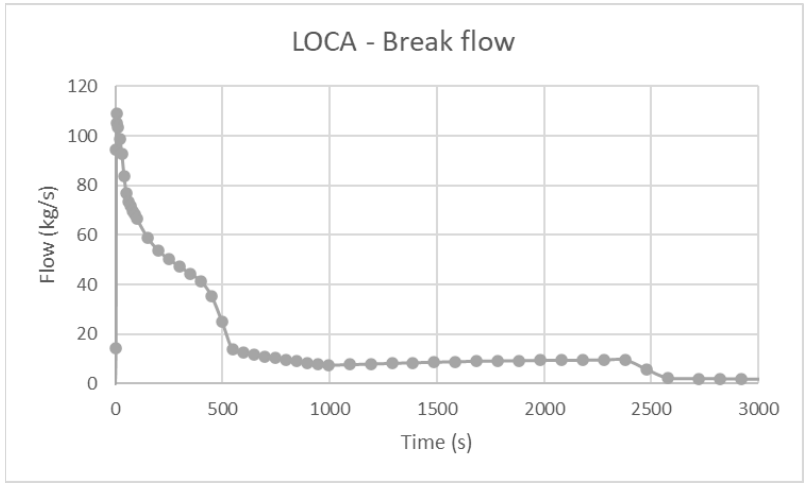

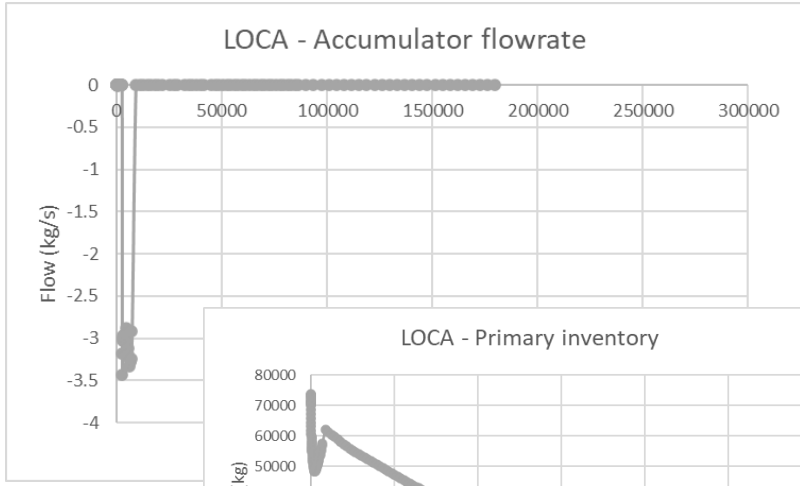

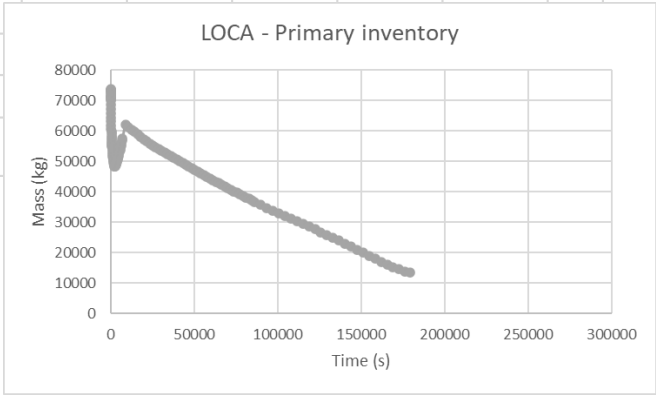

Conclusions of AC2 usage in ELSMOR project

- **<u>Message: Use the correct tools!</u>**

- Major issues in the simulation results were scenario/user input related, not code-related;
- The AC^2 code was applied for modelling of NUWARD-like SMR, and showed expected behavior trends in modelling of a 3D pool using ATHLET-3D, as well as processes inside the RPV and response of safety systems;
- The experience gained from ELSMOR project will be used in future activities.

SAFETY ANALYSIS OF SMR WITH PASSIVE MITIGATION STRATEGIES - SEVERE ACCIDENT

SASPAM-SA (**S**afety **A**nalyses of **S**MR with **P**assive **M**itigation strategies - **S**evere **A**ccident)
Horizon Euratom Project

KEY OBJECTIVE

- Key Objective of SASPAM-SA:
  - Investigate the applicability and transfer of the operating large-LWR reactor knowledge and know-how to the near-term deployment of integral PWR (iPWR), in the view of Severe Accident (SA) and Emergency Planning Zone (EPZ) European licensing analyses needs.

- Dedicated actions on:
  - Accident Tolerant Fuels (ATF)
  - In-Vessel Melt Retention (IVMR).

DESIGN 1

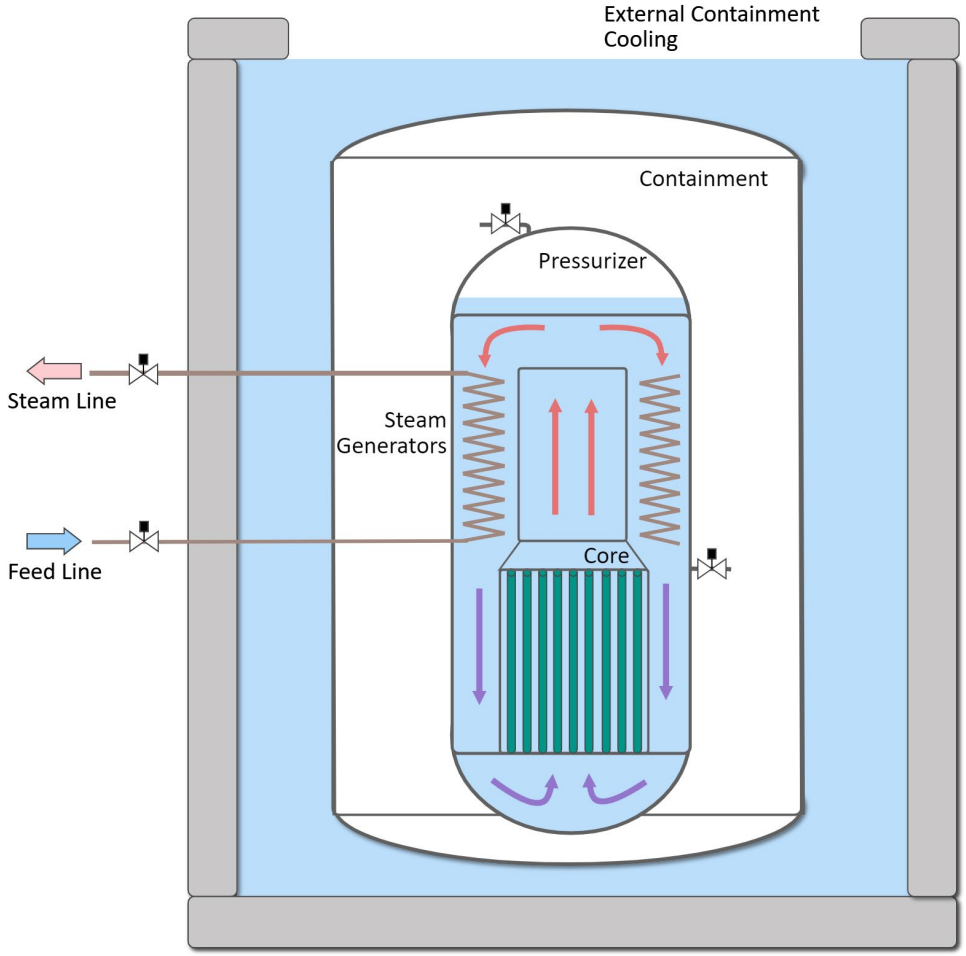

iPWR characterized by a submerged containment and electric power of about 60 Mwe

DESIGN 2

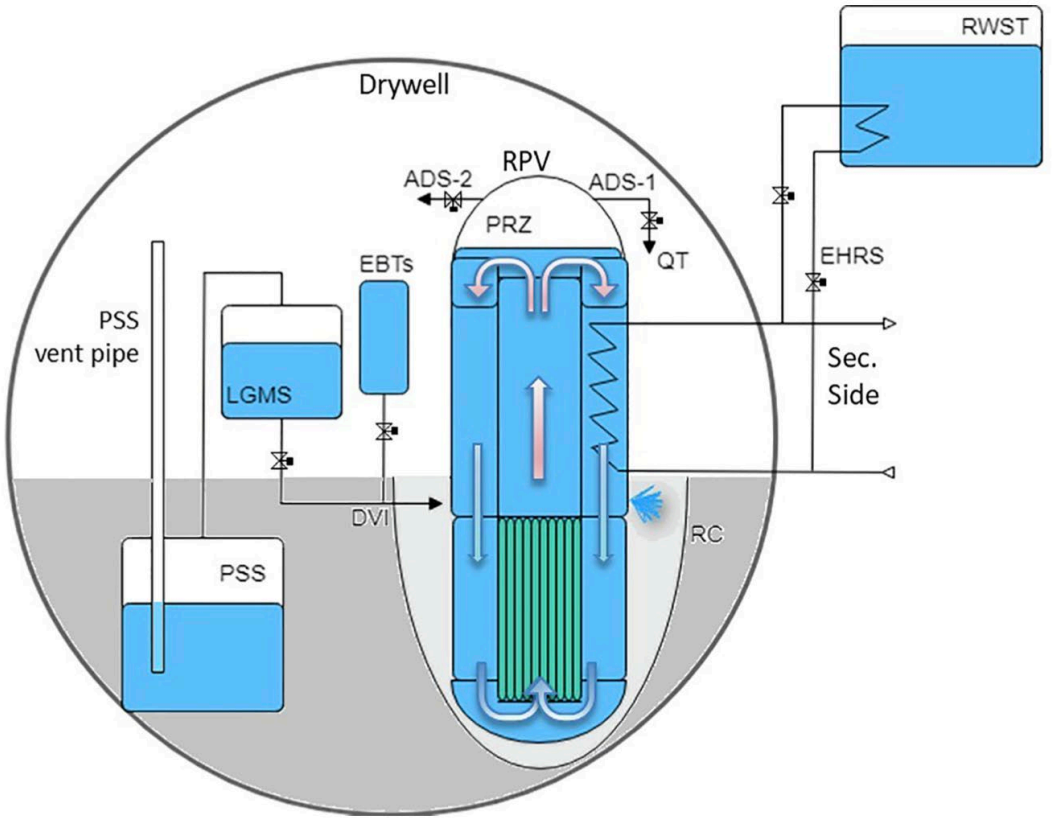

iPWR characterized by the use of several passive systems, a dry containment and an electric power of about 300 MWe,

Design-2 model in AC²

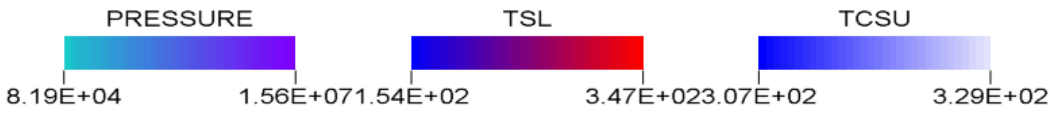

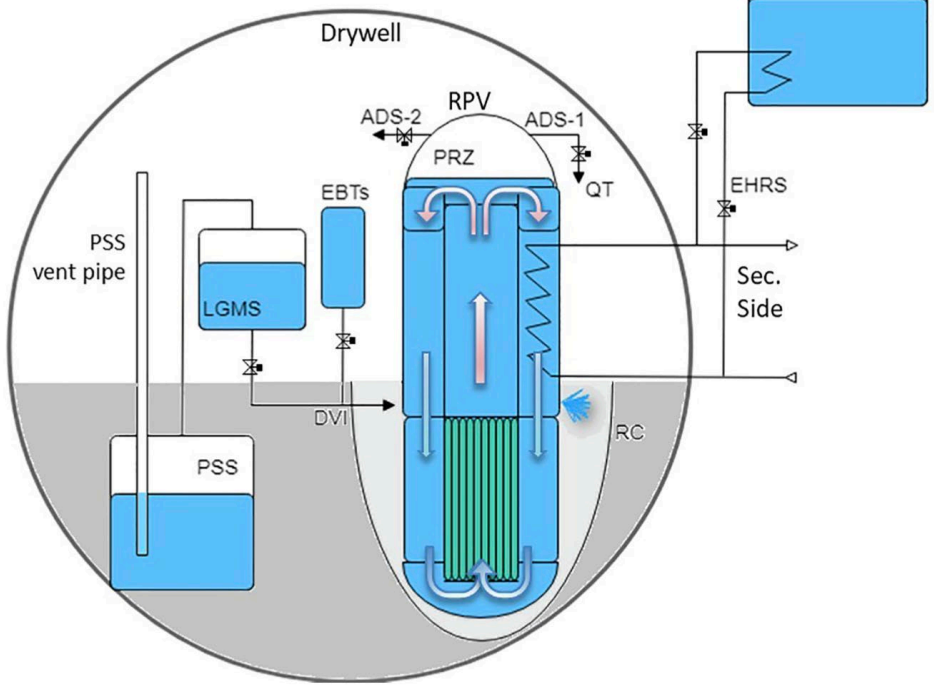

- ✓ **ATHLET**
- ✓ **ATHLET-CD**
  - ✓ ECOREMOD
  - FIPREM, SAFT, AIDA (…?)
- ✓ **COCOSYS**

COMPUTATIONAL TOOLS USED IN THE PROJECT

- For integral SA codes:
  - ASTEC (European code developed by IRSN),
  - AC2 (European code developed by GRS),
  - MAAP-EDF (non-European code developed by EPRI embedding EDF code changes),
  - MAAP (non-European code developedby EPRI)
  - MELCOR (non-European code developed by Sandia National Laboratories for the USNRC).

- For CFD codes:
  - ContainmentFOAM (European code developed by FZJ)
  - ANSYS CFX (non-European code developed by Ansys Inc.).

- For atmospheric dispersion codes:
  - ARANO (European code developed by VTT),
  - JRODOS (European code developed by KIT),
  - MACCS (non-European code developed by Sandia National Laboratories for the USNRC).

- For iodine chemistry:
  - IMPAIR (European code, developed by PSI in a framework of european collaboration).

First conclusions of using AC^2 in SASPAM-SA

- **<u>Message: Use the correct tools!</u>**

- The AC^2 code shows overall the expected NPP behavior;
- Major issues in the simulation results were scenario/user input related, not code-related;

LITHUANIAN ENERGY INSTITUTE

28th International QUENCH Workshop

KIT, Karlsruhe, Germany, 5-7th December 2023

M. Cazado
KIT

KIT Validation Activities of the ASTEC code against QUENCH Bundle Experments: Results and Outlook

Severe accident scenarios present a critical challenge in the assessment of nuclear power plant safety, constituting a primary focus at the Karlsruhe Institute of Technology (KIT). The continuous enhancement and validation of codes are essential for evaluating the progression and radiological consequences of severe accidents (SAs) in both existing and innovative nuclear power plants (NPPs). KIT extensively employs the ASTEC integral code, developed by IRSN, in this critical task. ASTEC validation against QUENCH experiments at KIT has been ongoing for an extended period, comprehensively analyzing nearly all QUENCH bundle tests.

Current research priorities are the expansion of ASTEC's application range and the evaluation of innovative reactor concepts, particularly Small Modular Reactors (SMRs) anticipated to utilize Advanced Tolerant Fuels (ATF) cladding materials. Validation efforts, exemplified by QUENCH experiments such as QUENCH-12 and -20, demonstrate good agreement between simulations and measurements in key figure of merits. KIT also prioritizes Uncertainty and Sensitivity Analyses, for which the KATUSA code was developed. Favorable results have been obtained from the ASTEC/KATUSA analyses of QUENCH-06 and -08.

A significant aspect of KIT's assessment involves the analysis of QUENCH experiments related to ATF in the framework of the OECD/NEA QUENCH-ATF and IAEA CRP ATF-TS projects. Initial ASTEC modeling of new cladding materials, such as FeCrAl and Cr-coated Zr alloys, required modifications in the material database of the code. While achieving reasonable results, identified deviations highlight the necessity of incorporating new physical models into the ASTEC code for more realistic simulations. In this context, ongoing development and implementation efforts include an oxidation model for new materials, particularly FeCrAl, with collaborative support from IRSN and the QUENCH team.

Karlsruhe Institute of Technology

KIT Validation Activities of the ASTEC code against the QUENCH Bundle Experiments: Results and Outlook

F. Gabrielli, O. Murat, A. Mercan, A. Stakhanova, M. E. Cazado, Z. Jimenez Balbuena, V.H. Sanchez-Espinoza

Institute for Neutron Physics and Reactor Technology

Motivation

- Assessment of Severe Accident (SA) scenarios at KIT is a key aspect → continuous improvement of the codes and their validations are fundamental to evaluate the progression and the radiological consequences of SAs in current and innovative NPPs.
- The ASTEC integral code, developed by IRSN, is extensively used at KIT
- **ASTEC validation against QUENCH experiments at KIT is ongoing → almost all the QUENCH bundle tests analyzed**
- Current research priorities:
  - Widening ASTEC applications, i.e., VVER (Q-12) and BWR (Q-20)
  - Safety assessment of the innovative reactor concepts, i.e., SMRs, expected to employ ATF cladding materials

ASTEC Validation against QUENCH-12

- **Framework: assessment of an ASTEC dataset of a generic VVER-1000 NPP**
- **QUENCH-12: VVER-type fuel assembly arrangement**
  - **Reflooding of pre-oxidized heated rods bundle**
  - Zr material data employed instead of Zr-1%Nb → work in progress at KIT

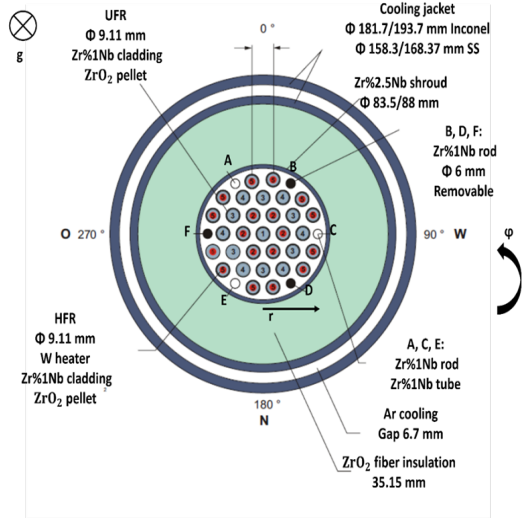

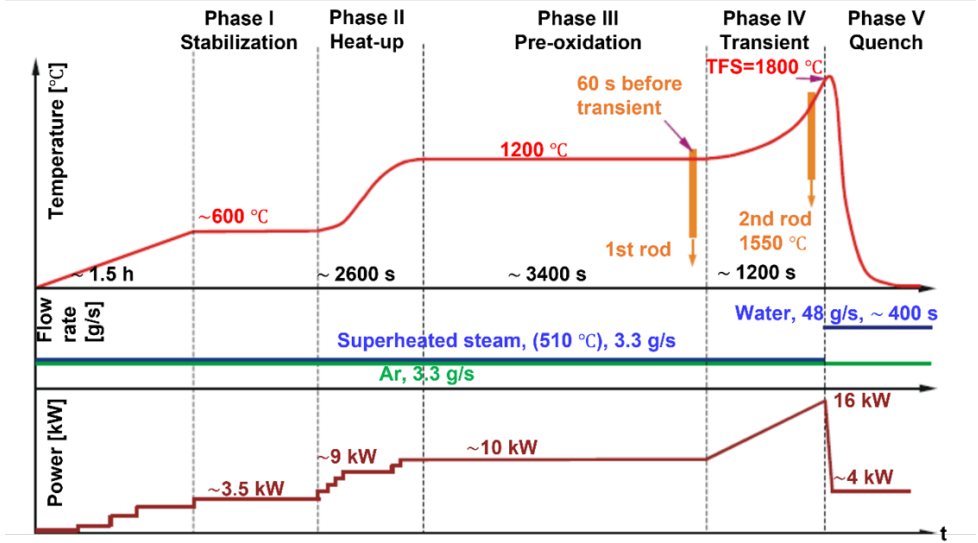

ASTEC Validation against QUENCH-12

- **Framework: assessment of an ASTEC dataset of a generic VVER-1000 NPP**
- **QUENCH-12: VVER-type fuel assembly arrangement**
  - **Reflooding of pre-oxidized heated rods bundle**
  - Zr material data employed instead of Zr-1%Nb → work in progress at KIT

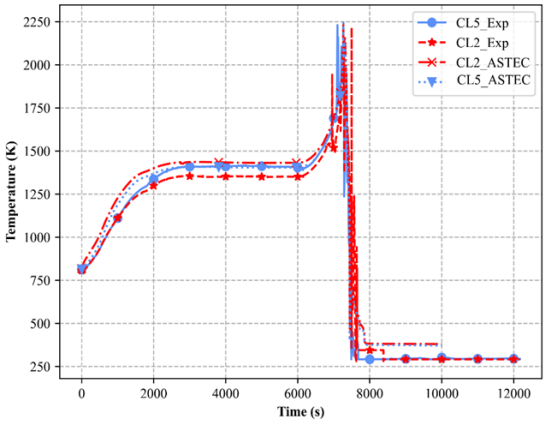

Heated rods at 950 mm height

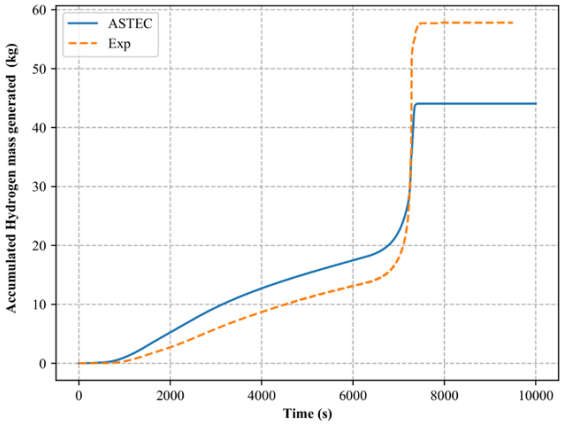

Hydrogen production

- **Good agreement on the temperatures of heated and un-heated rods**
- **Hydrogen production**
  - **Good agreement up to the beginning of the quenching phase**: 34.2 g (ASTEC) vs. 34.7g (Exp.)
  - **Underestimation during the quenching phase**: 9.9 g (ASTEC) vs. 23.1 g (Exp.) → due to the use of Zr-4 instead of Zr-1%Nb
- **The code is able to catch the physical phenomena of the experiment**

ASTEC Validation against QUENCH-20

- **Framework: assessment of an ASTEC dataset of a generic model of the Peach Bottom BWR NPP (first-of-its-kind)**
- **QUENCH-20: Test Bundle Cross Section (1/4 SVEA 96 OPTIMA-2)**

1. Pre-oxidation phase: power at 7.5 KW, steam and Ar flows
2. Transient phase: Electric power increases up to 18.2 kW
3. Quench phase: 50 g/s quench water Injected at the end of the transient phase, steam flow off

- **Efforts to properly model the power distribution in the bundle**
- **The electrical power is not the same for each rod**

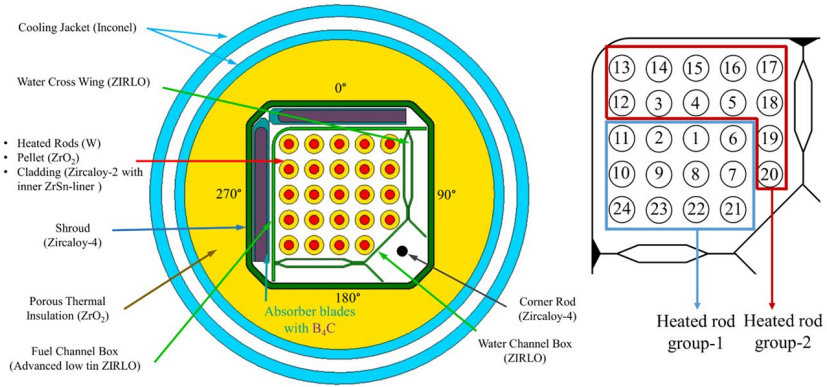

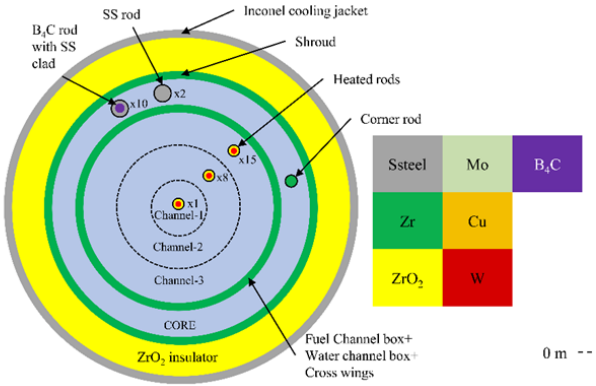

ASTEC Results vs. QUENCH-20 Experiment

Comparison at the end of transient phase and start of quench phase.

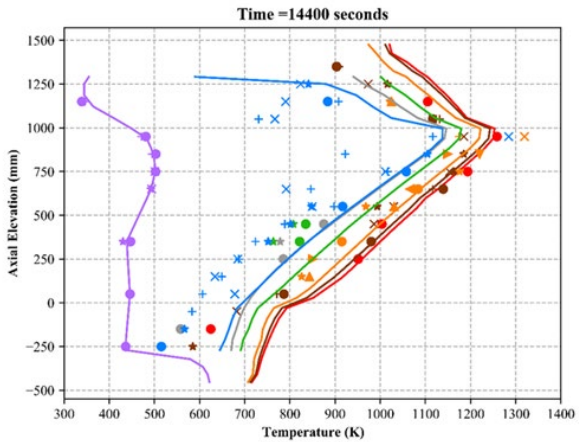

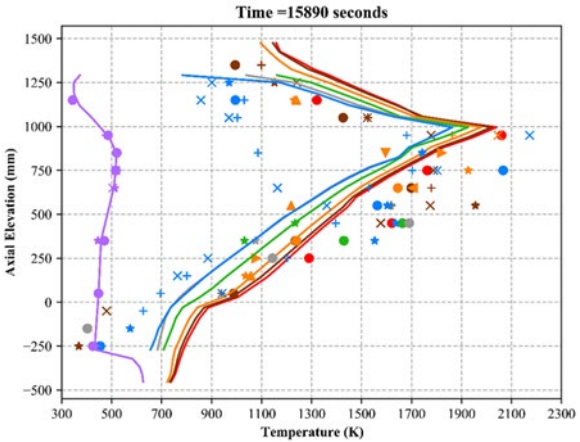

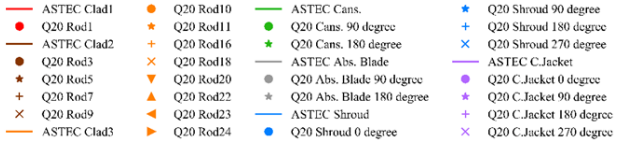

- **Considering the challenges in modelling the geometrical peculiarities of bundle, ASTEC reasonably well reproduces the temperature of the structures during the transient**

O. Murat, V.H. Sanchez-Espinoza, S. Wang, J. Stuckert, Preliminary validation of ASTEC V2.2.b with the QUENCH-20 BWR bundle experiment, NED 370, 2020

ASTEC Results vs. QUENCH-20 Experiment

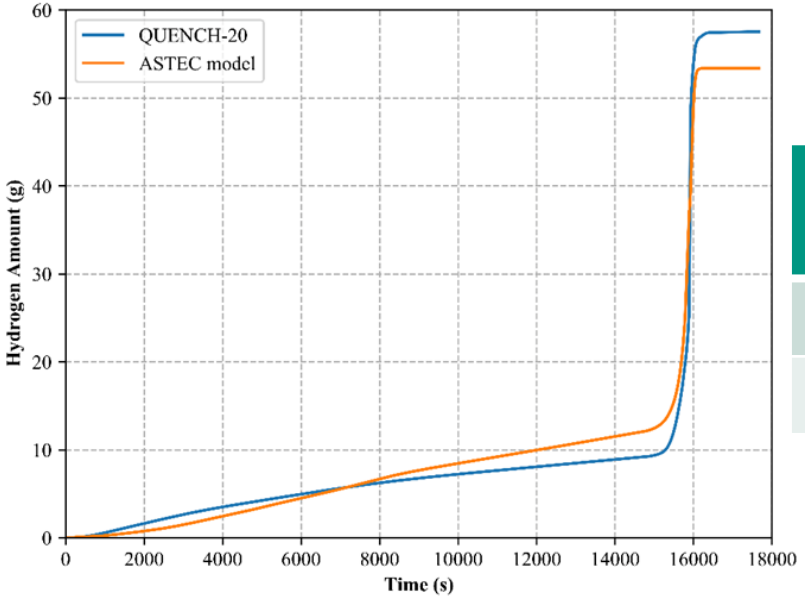

Contribution to H_2 production	Exp. [g]	ASTEC [g]
Total	**57.4**	**53.4**
B4C oxidation	**10.0**	**9.48**

➢ **ASTEC results on both the total and B4C contribution to the hydrogen production during the test are in good agreement with the experiment**

O. Murat, V.H. Sanchez-Espinoza, S. Wang, J. Stuckert, Preliminary validation of ASTEC V2.2.b with the QUENCH-20 BWR bundle experiment, NED 370, 2020

Uncertainty and Sensitivity Analyses (U&Sa)

- U&Sa of the ASTEC results became part of the calculation route in the KIT strategy for SA analyses
- The application of U&Sa methods to the ASTEC results for the QUENCH tests play a key role in order to:
  - Testing the U&S methodologies
  - Identifying bottlenecks in the code, when developing/employing new models devoted to new materials, i.e. ATF
- The KArlsruhe Tool for Uncertainty and Sensitivity Analyses (KATUSA) has been developed at KIT
- The ASTEC/KATUSA has been used for the QUENCH-08 and QUENCH-06 analyses

ASTEC Modelling of QUENCH ATF-Related tests

- **Large efforts on the analysis of the QUENCH ATF-related bundle tests on-going**
- **Framework: OECD/NEA QUENCH-ATF and IAEA CRP ATF-TS**
- Current approach in the ASTEC modelling: modifying the material database by including the correlations for such materials, i.e. FeCrAl

```
…..
STRUCTURE MODEL NAME 'BEST-FIT' LAW 'COEFF' VARIABLE 'T' VUNIT 'K' RUNLOW 0. RUNUPP 5000.
  SRG VALUE AGAIN 9.62D-10 BGAIN 0.0 ATHIC 2.252D-13 BTHIC 0.0 MODEL 0.5 TERM
  X  1473.K
  SRG VALUE AGAIN 3.0D+11 BGAIN 5.94354D5 ATHIC 3.371D3 BTHIC 5.94354D5 MODEL 0.5 TERM
  X  1648.K
  SRG VALUE AGAIN 2.4D+08 BGAIN 3.52513D5 ATHIC 0.008682D0 BTHIC 3.52513D5 MODEL 0.5 TERM
 END
```

- **Mid-term approach: development and implementation in ASTEC of an oxidation model for new materials (currently efforts devoted to FeCrAl)**

ASTEC Model of the QUENCH-ATF1 Test

➢ OECD/NEA QUENCH-ATF Project

Cr-coated ZIRLO Cladding

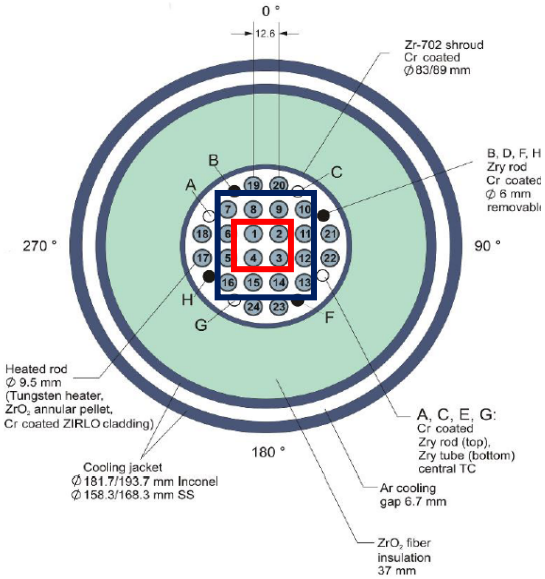

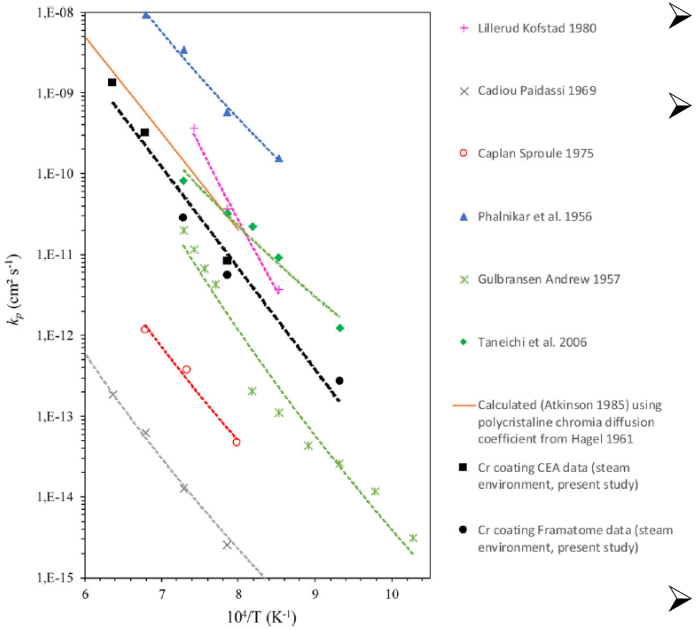

- **Brachet data**
- **Fitting functions for weight gain and thickness grown of the oxide layer provided by J. Stuckert**

$$\Delta m = 6.19 \cdot e^{-\frac{123783}{R \cdot T}} \cdot \sqrt{t}$$

$$\delta = 0.00377 \cdot e^{-\frac{123783}{R \cdot T}} \cdot \sqrt{t}$$

- **Correlations incorporated into the material database.**

Brachet, J.-C., et al., 2020. High temperature steam oxidation of chromium-coated zirconium-based alloys: Kinetics and process, Corrosion Science 167 (2020) 108537..

ASTEC Model of the QUENCH-19 Test

➢ IAEA ATF-TS Project

FeCrAl cladding

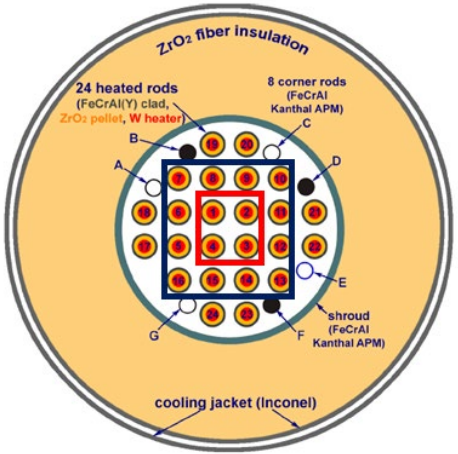

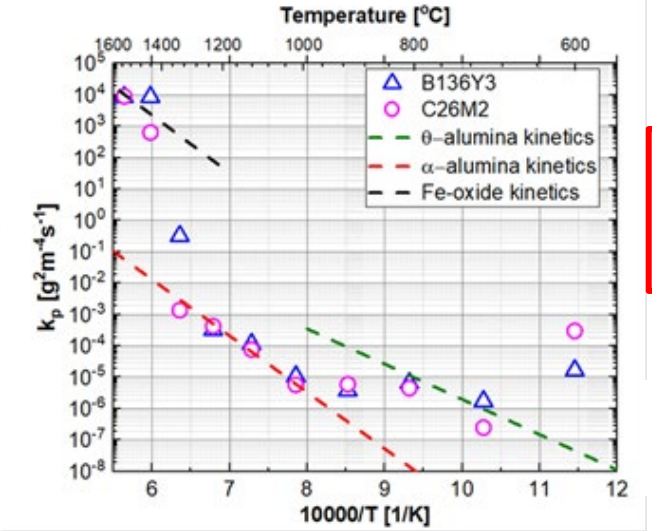

➢ **Fitting functions for weight gain provided by J. Stuckert**

$$K = \begin{cases} 9.62 \times 10^{-12}\,[\mathrm{g^2/cm^4 s}], & T \le 1473\ \mathrm{K} \\ A_B \exp\left(\frac{-E_B}{RT}\right), & 1473 < T < 1648\ \mathrm{K} \\ A_{Fe} \exp\left(\frac{-E_{Fe}}{RT}\right), & T \ge 1648\ \mathrm{K}\ (\textit{melting point of FeO}) \end{cases}$$

$A_B = 3 \cdot 10^9$ g²/cm⁴ s $E_B = 594354$ J/mol

$A_{Fe} = 2.4 \cdot 10^6$ g²/cm⁴ s $E_{Fe} = 352513$ J/mol

C. KIM, C. TANG, M. GROSSE, M. STEINBRUECK, C. JANG, Y. MAENG, „OXIDATION KINETICS OF NUCLEAR GRADE FeCrAl ALLOYS IN STEAM IN THE TEMPERATURE RANGE 600-1500°C", TopFuel 2021.

ASTEC Results for Quench-19: Cladding Temperatures

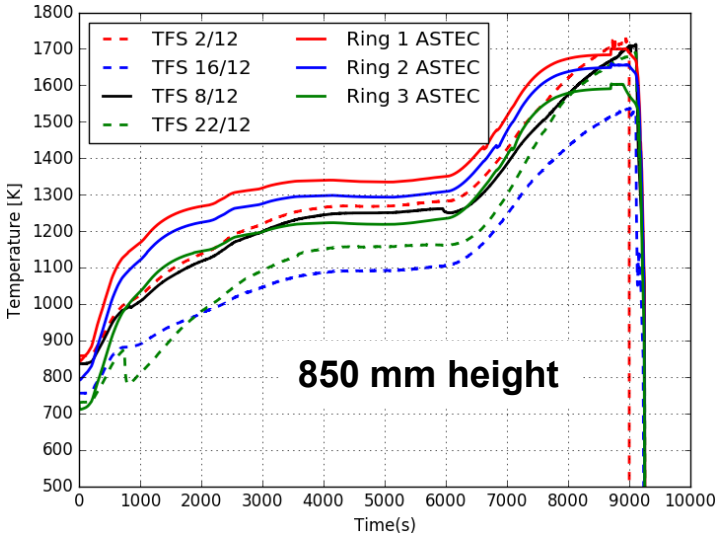

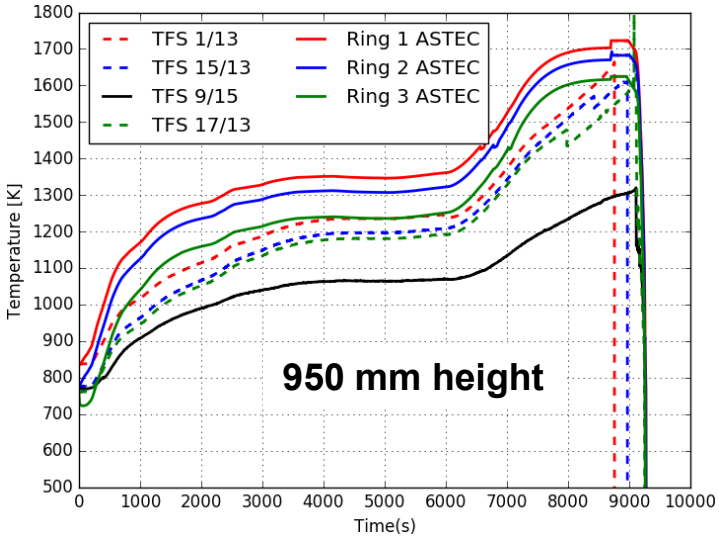

- Results exceed the exp. of about 100 degree in the pre-oxidation phase in Ring 1 (@850 mm) and in the Ring 1 and 2 (@950 mm height)
- Better agreement in Ring 2 and 3 (@850 mm) and Ring 3 (@950 mm)
- **Maximum temperatures reasonably well reproduced**

ASTEC Results for Quench-19 : Hydrogen Production

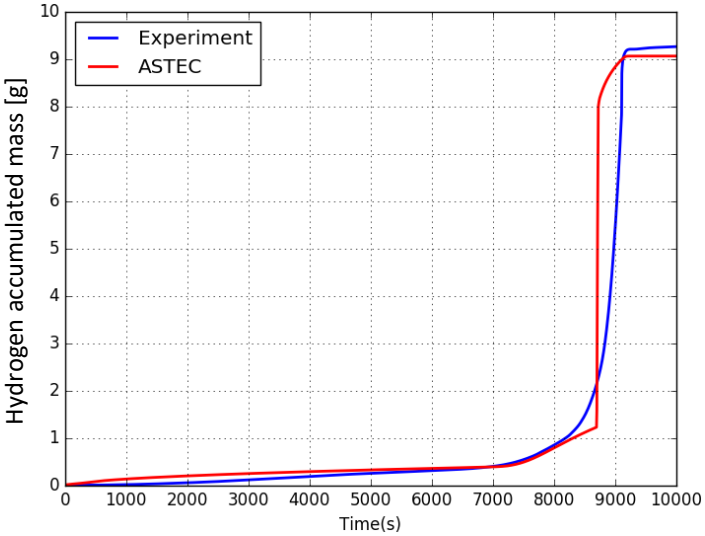

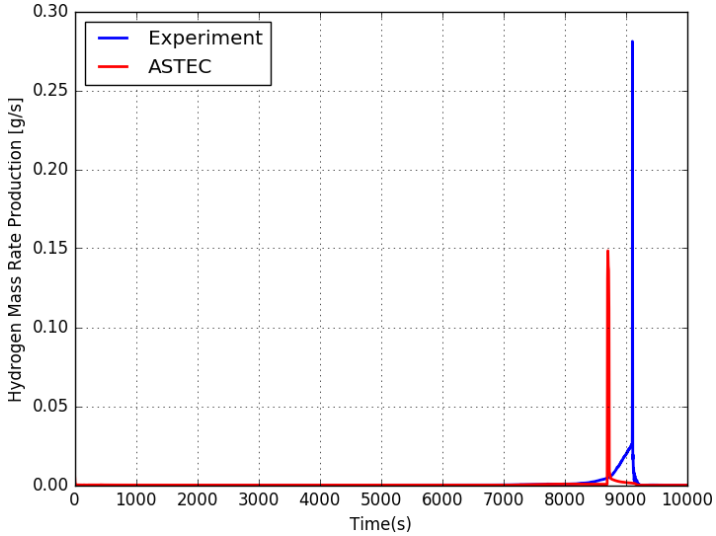

- **The final amount of H2 is reasonably well reproduced**
- ASTEC results show a good agreement with exp. up about 8000 s
- Escalation is anticipated in time with about 50% of the mass rate compared with the experiment
- **'Smooth' kinetics behavior is not reproduced**

Conclusion

- The validation of the ASTEC code against QUENCH bundle tests has been ongoing for an extended period.
- This activity is essential to analyze hypothetical SA scenarios in current and innovative NPPs.
- ASTEC is able to properly reproduce the main phenomena and/or the experimental results of the QUENCH bundle tests
- Efforts are currently devoted to analyze the QUENCH tests employing ATF materials in the frame of:
  - The OECD/NEA QUENCH-ATF project
  - The IAEA T12032 CRP ‘ATF-TS’
  - The development and the implementation in ASTEC of a physical model for the oxidation of FeCrAl cladding materials (tight connection with IRSN and the QUENCH team)

Acknowledgement

The authors wish to acknowledge the QUENCH team for the great support to the KIT/INR computation team

Special thank to J. Stuckert, M. Steinbrück, and M. Große for their continuous support, suggestions, and availability

J. Stuckert
KIT

Estimation of melt oxidation kinetics

The analysis of the viscous melt behavior in the CORA and QUENCH bundles and the image analysis of the frozen melt show the formation of ceramic precipitates in the melt even in the molten state. The driving mechanism for the formation of precipitates in the melt is the temperature gradient at the oxide-melt interface. The high temperature Prater-Courtright correlation, used usually in computer codes to simulate the oxidation of Zr melt, was obtained based on the oxidation of very thin samples, which does not allow taking into account processes in the bulk melt. Simulation of the melt oxidation by the mechanistic SVECHA code, verified on the basis of many crucible tests, gives more correct result. This takes into account not only the formation of an external oxide layer around the molten pool, but also the formation of ceramic precipitation inside the melt. A numerical calculation carried out for the case with an operating temperature of 2473 K and a temperature gradient at the melt boundary of 50 K showed that the oxidation process occurs parabolically and three times faster than predicted by the Prater-Courtright correlation. The estimated activation energy for the melt oxidation correlation of Arrhenius-type proposed on the basis of SVECHA calculations is 85.9 kJ/mol, which is noticeably lower than the Prater-Courtright activation energy of about 110 kJ/mol.

Karlsruhe Institute of Technology

IAM
Institute for Applied Materials

Estimation of melt oxidation kinetics

J. Stuckert

QWS-28, Karlsruhe

Institute for Applied Materials; Program NUSAFE

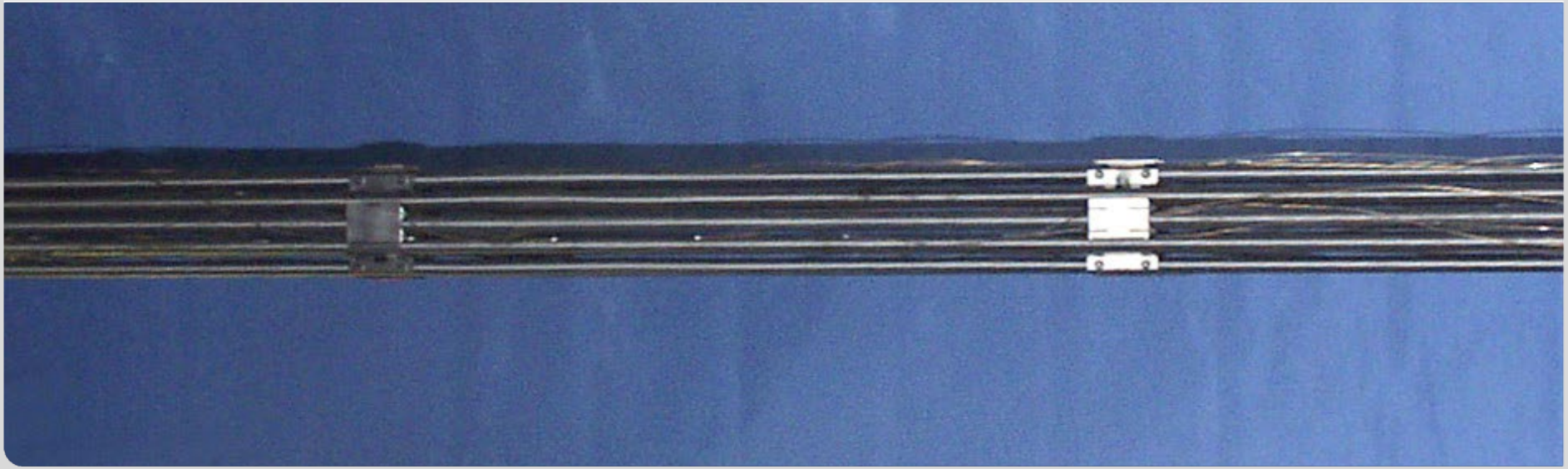

Melt relocation : rivulets and droplets in CORA-PWR tests (CORA-12, window at elevation 400 mm)

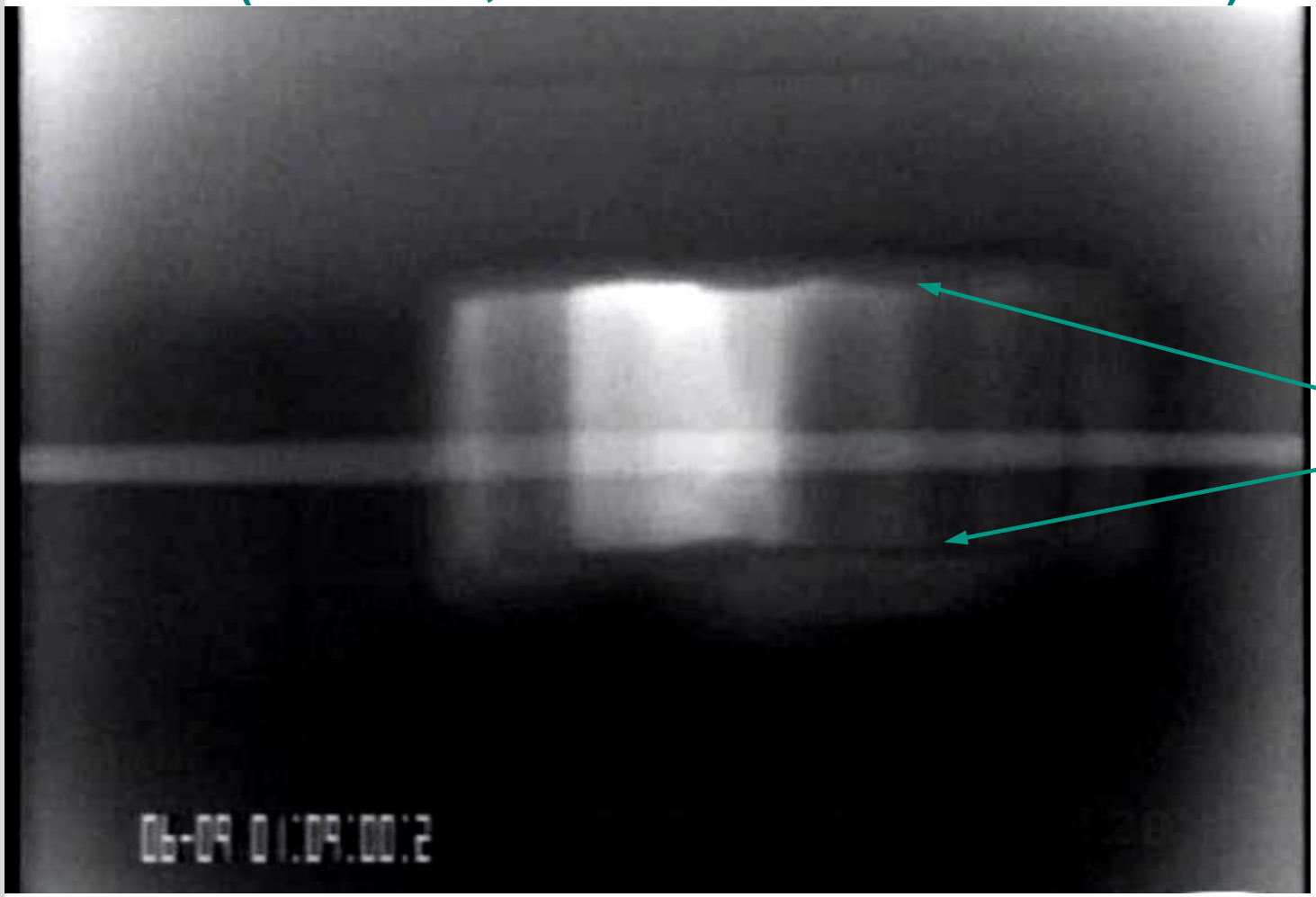

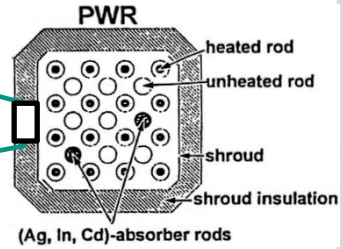

- rapid relocation of early metallic rivulets and later slowed relocation of partially oxidised rivulets
- relocation velocity of metallic rivulets $v_{metal} \approx 20$ cm/s;
- melt with ceramic precipitates (with volumetric part f) $v \sim 1/\eta(f)$, η – viscosity of the melt

Melt relocation : rivulets and droplets in CORA-PWR tests (CORA-12, window at elevation 400 mm)

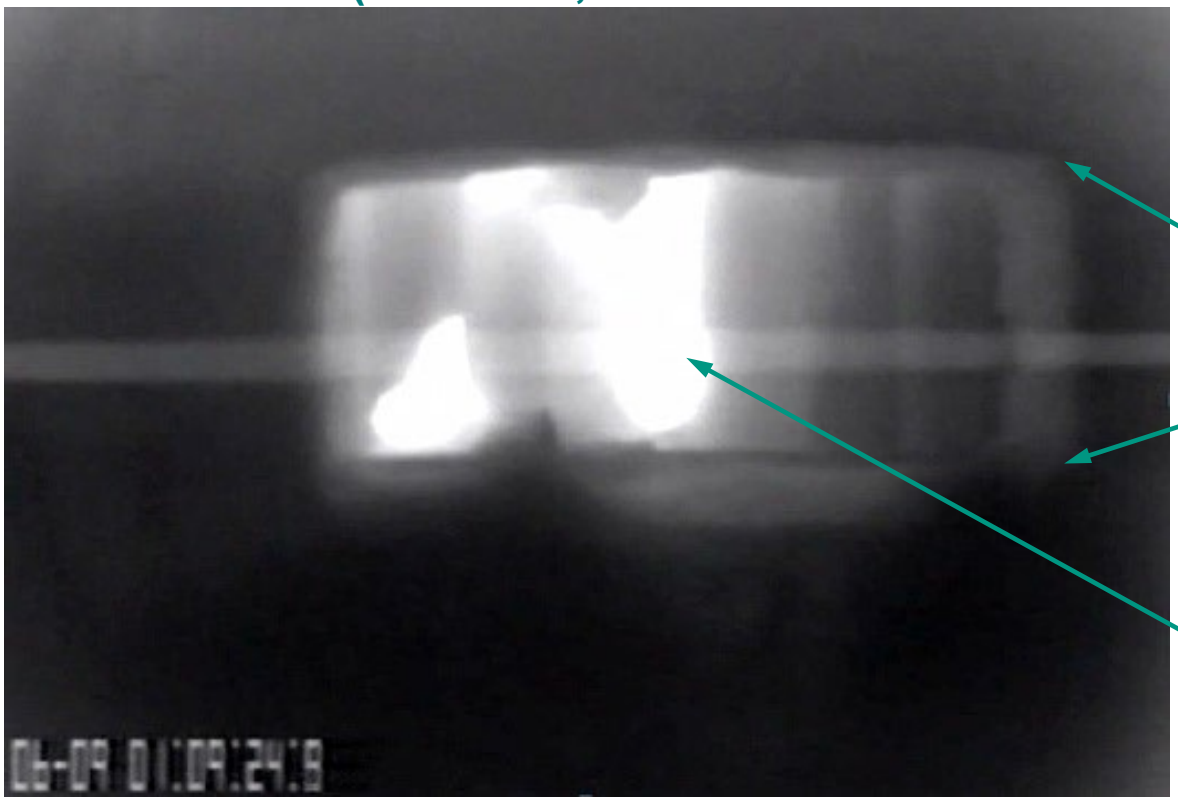

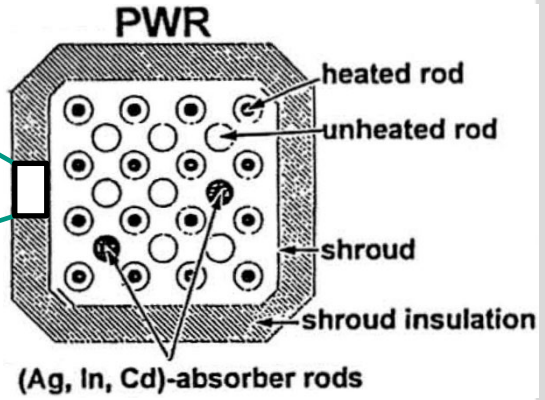

melt (Fe, Zr, U, (O), Ag, In, Cd,)

melt viscosity depends on temperature T and volume fraction of ceramic precipitates f

[M. Ramacciotti et al., NED 2001, https://doi.org/10.1016/S0029-5493(00)00328-9]: $\eta = \eta_{liq}(T) \cdot exp(2.5 \cdot C \cdot f)$

with [Kaptay, 2004, https://www.hanser-elibrary.com/doi/pdf/10.3139/146.018080] $\eta_{liq}(T) = A(T) \cdot exp(E/RT)$,

$A(T) \sim T_m^{1/2}$, E = 54(Zr)...87(ZrO_2) kJ/mol [Veshchunov et al., NED, 2008, https://doi.org/10.1016/j.nucengdes.2007.10.015], C=3...4.5

for Zr(O) at 2200 °C:

$\eta_{Zr}(f=0) \approx 6$ mPa·s,

$\eta_{Zr + ZrO2}(f=0.2) \approx 30$ mPa·s → $v_{melt} = v_{metal}/5 = 4$ cm/s

significant slower relocation than for the pure metal melt

Melt release outside of claddings and formation of molten pools frozen in steam atmosphere at middle bundle elevations

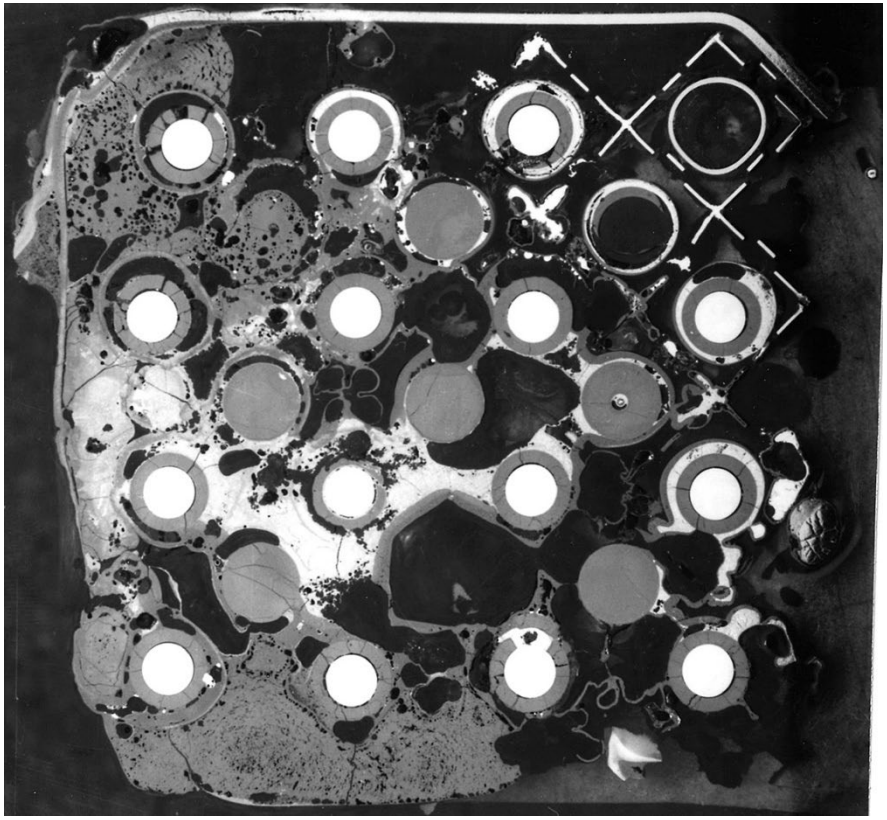

PWR CORA-15 ($T_{pct} \approx 2370\ K$), elevation 480 mm: melt collection **at spacer grid**

PWR QUENCH-11 ($T_{pct} \approx 2100\ K$), elevation 837 mm: formation of large molten pools below the bundle hot region

Cladding melt formation, oxidation and localization at the upper hottest bundle elevations for QUENCH bundles: formation of ceramic precipitates in the melt

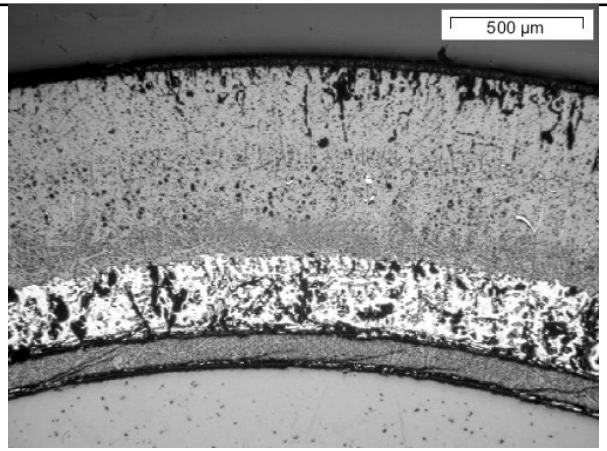

PWR QUENCH-06 (Zry-4), rod #12, 950 mm:
melt **captured** between clad oxide and pellet

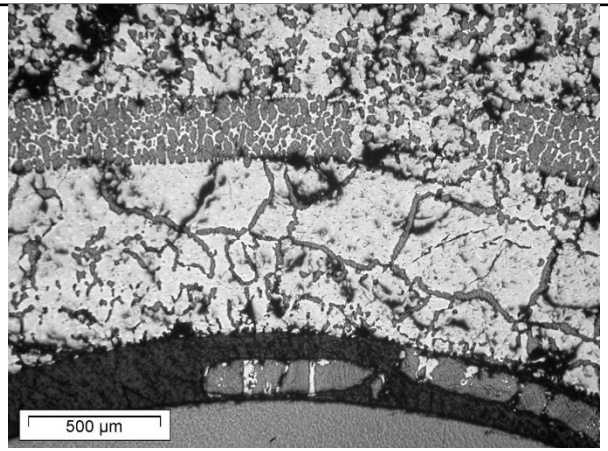

VVER QUENCH-12 (E110), rod #8, 950 mm:
melt **partial release through failed clad oxide**

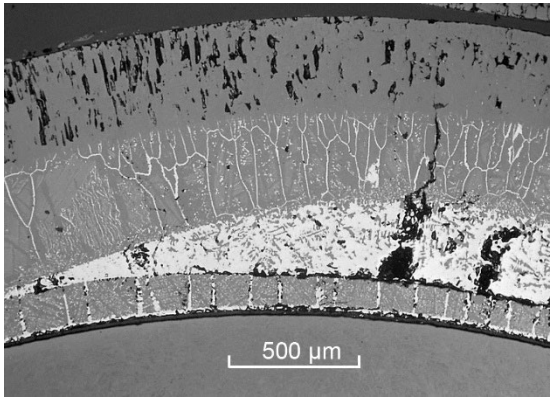

PWR QUENCH-14 (M5), rod #2, 1000 mm:
melt **captured** between clad oxide and pellet

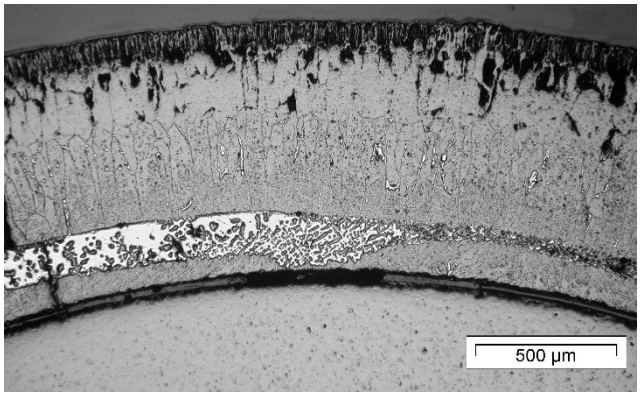

PWR QUENCH-15 (ZIRLO), rod #17, 1000 mm:
melt **captured** between clad oxide and pellet

Simplified equilibrium Zr-O phase diagram

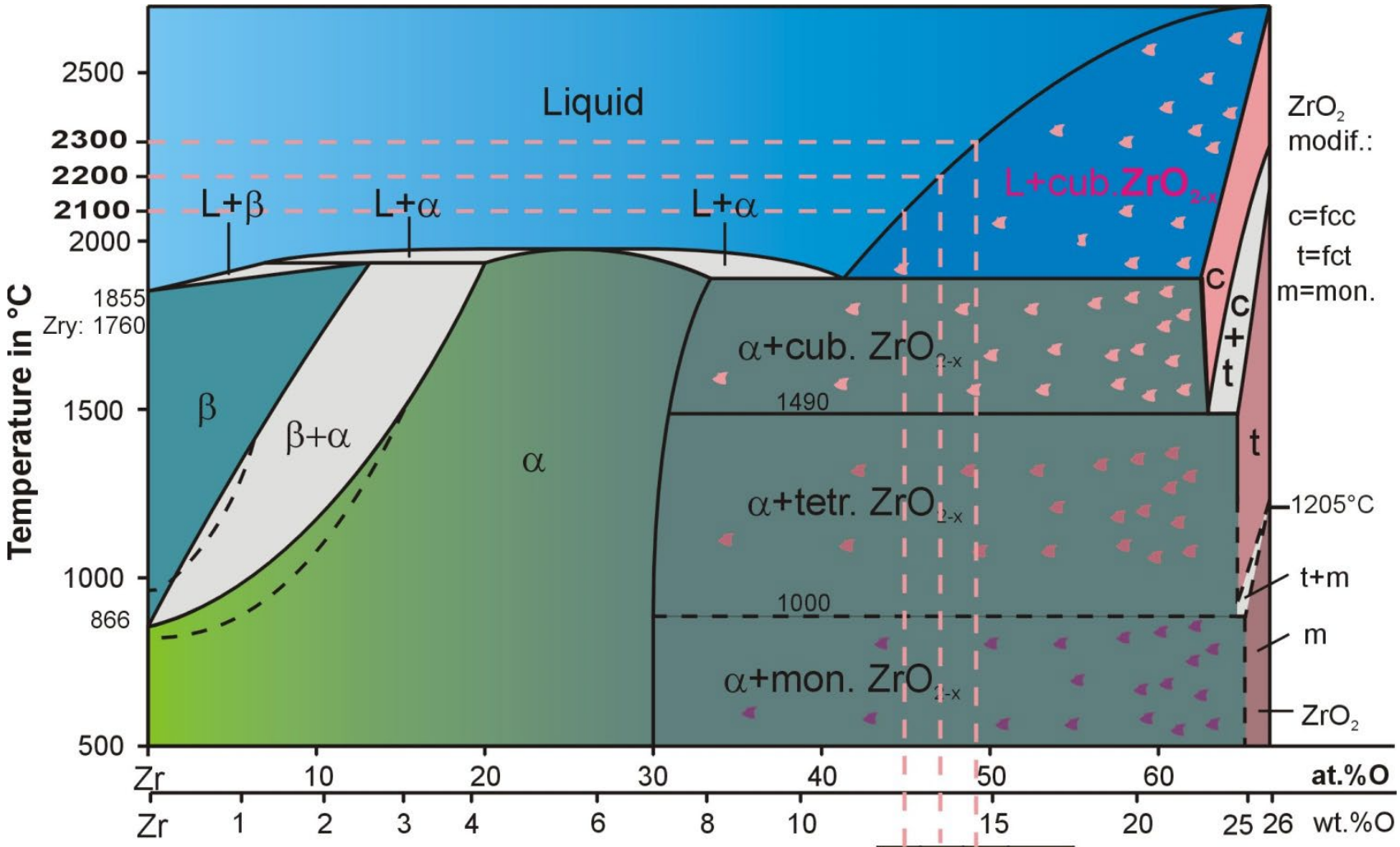

Solubility of oxygen in Zr liquid at 2100, 2200, 2300 °C:

45.3	47	49.5	at.%O
12.7	13.5	14.7	wt.%O

Crucible test, result of image analysis of the oxidized melt: partial formation of precipitates before cool-down (oversaturation)

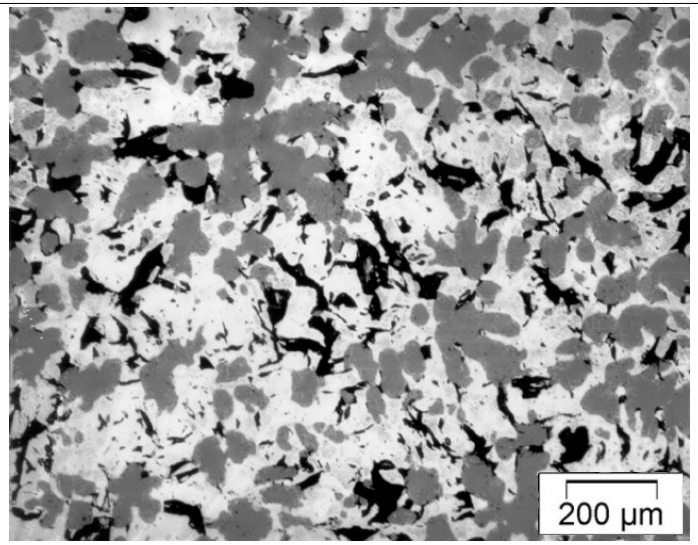

2100 °C, oxygen content **49 at%** (>solubility limit of 45%)

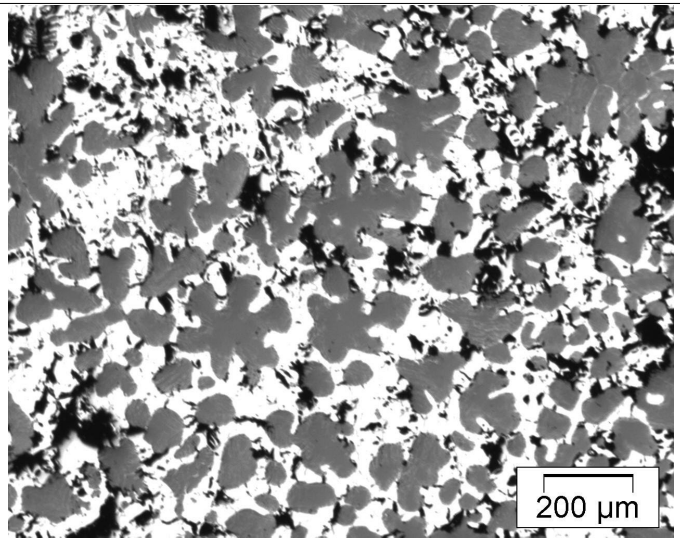

2100 °C, oxygen content **55 at%** (>solubility limit of 45%)

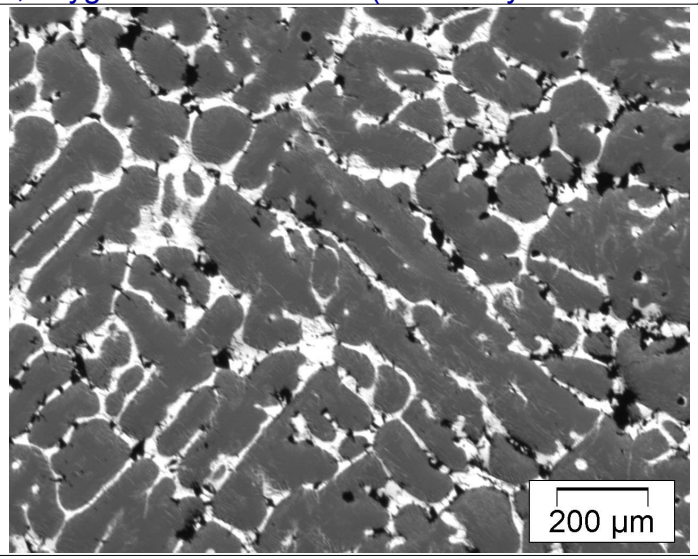

2200 °C, oxygen content **61.5 at%** (>solubility limit of 47%)

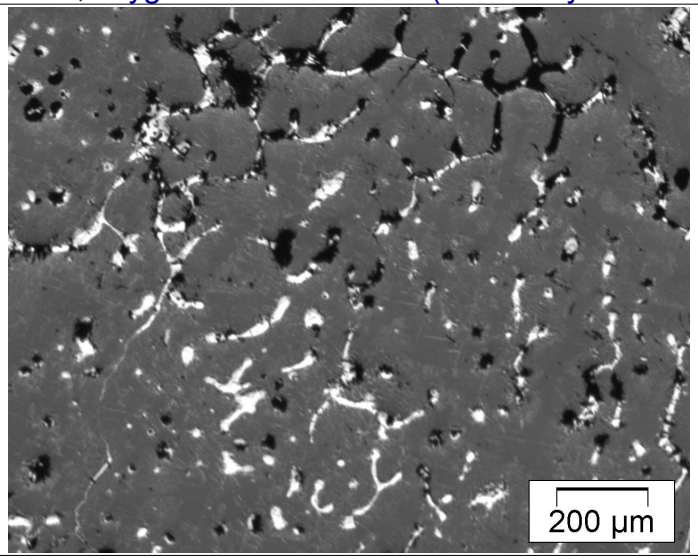

2200 °C, oxygen content **63.5 at%** (>solubility limit of 47%)

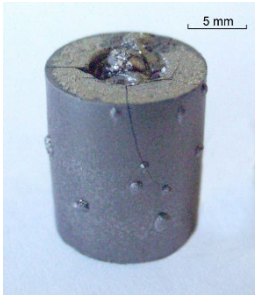

Mechanism of precipitates formation due to the temperature gradient at the liquid-solid interface: SVECHA model verified on the basis of crucible tests

[Veshchunov, Stuckert, Berdyshev, 2002, Karlsruhe, FZKA 6792, https://www.doi.org/10.5445/IR/270053667]

possible reasons of the temperature gradient: exothermic reaction of steam with metal and the axial temperature difference

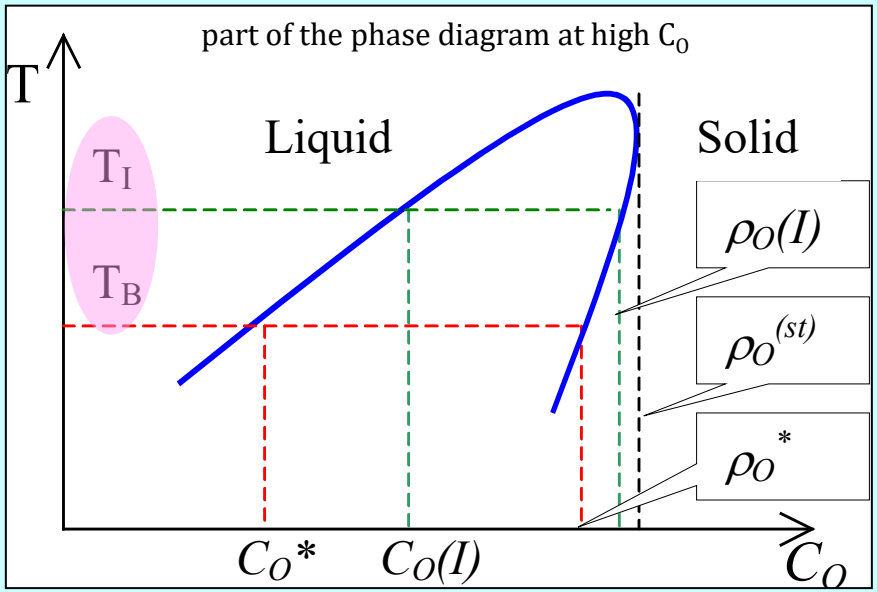

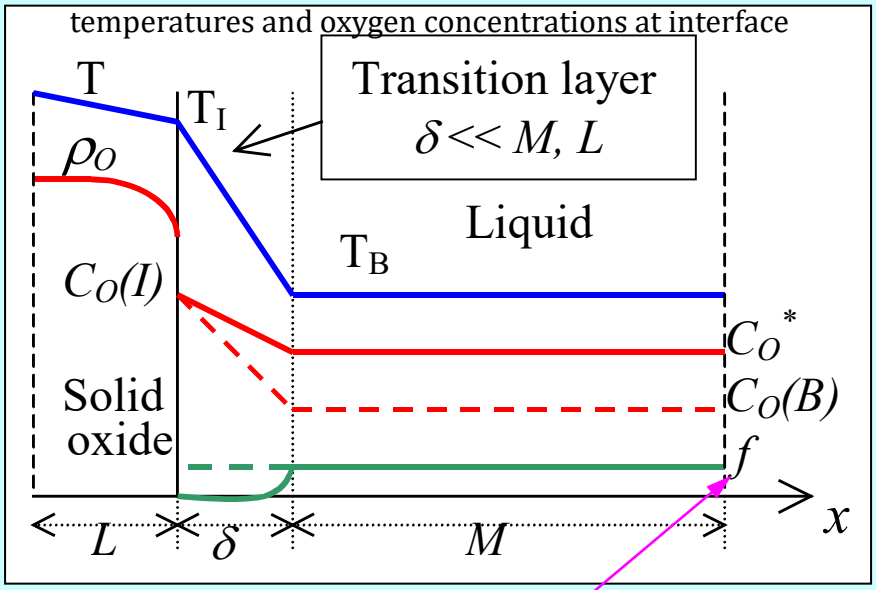

One-dimensional mass transfer equations in SVECHA during the precipitation stage

Mass balances

$$-D_O^{ZrO_2}\frac{\partial \rho_O}{\partial x}|_I - \rho_O(I)\frac{dL}{dt} = \frac{d}{dt}[c_O^* M(1-f) + \rho_O^* M f]$$

$$-\rho_{Zr}\frac{dL}{dt} = \frac{d}{dt}[c_{Zr}^* M(1-f) + \rho_{Zr} M f]$$

Flux matches

$$-D_O^{ZrO_2}\frac{\partial \rho_O}{\partial x}|_I - \rho_O(I)\frac{dL}{dt} = c_O(I)\left(\mathrm{u} - \frac{dL}{dt}\right) + k_O e^{-2.5f}(c_O(I) - c_O^*)$$

$$-\rho_{Zr}\frac{dL}{dt} = c_{Zr}\left(\mathrm{u} - \frac{dL}{dt}\right),$$

u – net velocity of the melt, k – mass transfer coefficient in the melt

SVECHA modelling results of Zr melt oxidation at melt temperature 2473K and temperature drop in the transition boundary layer ΔT = 50 K for cylindrical molten pool with R_0=6 mm

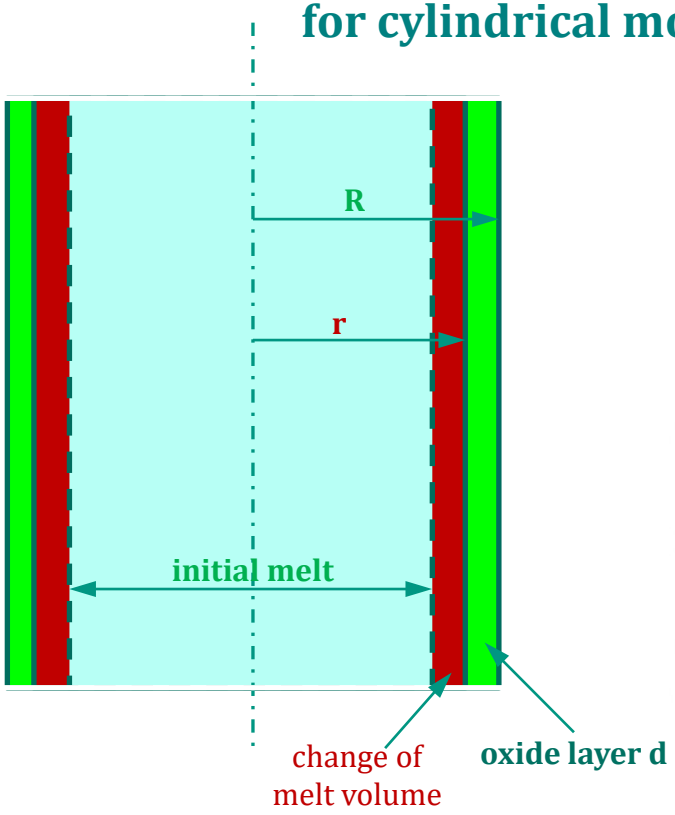

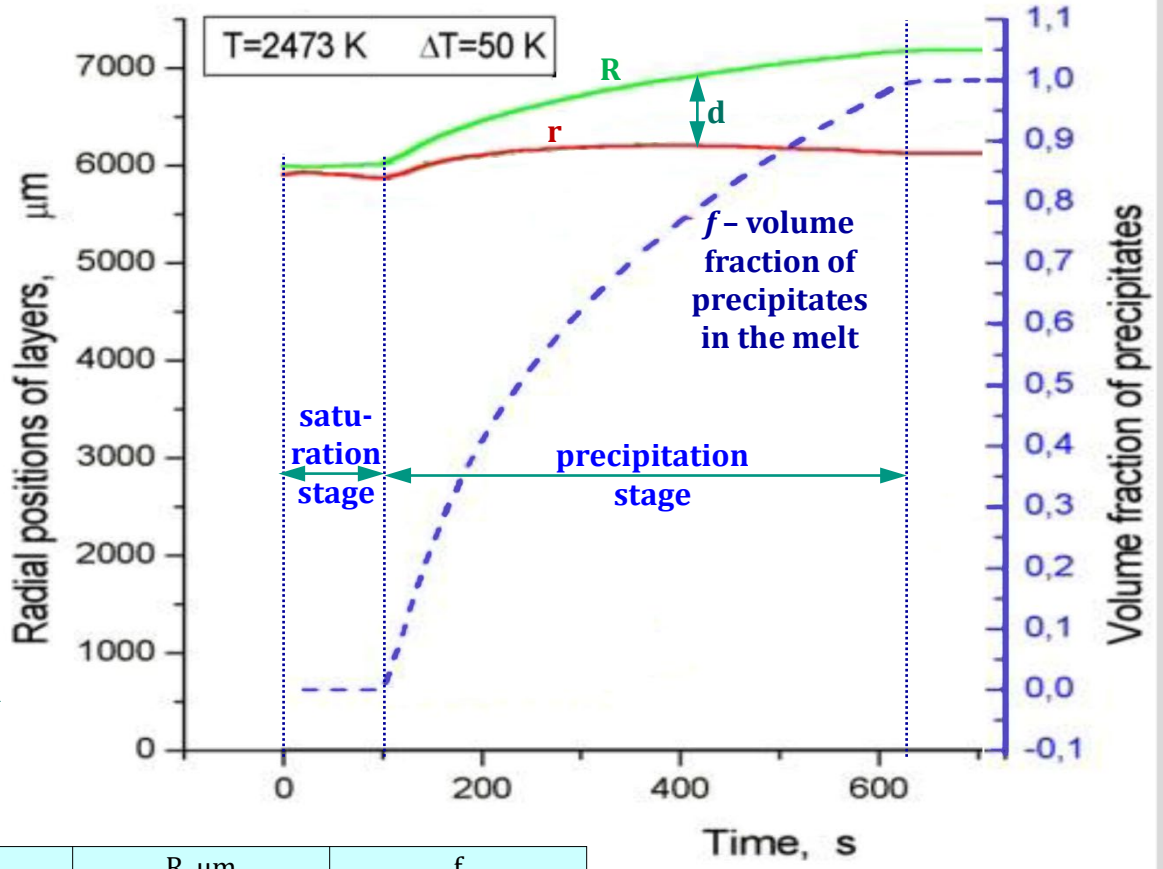

t, s	r, μm	R, μm	f
0	5876	6027	0
100	6114	6459	0.41
200	6189	6708	0.62
300	6211	6902	0.77
400	6178	7043	0.88
500	6135	7151	0.97

Derivation of weight gain next slide

Oxygen uptake by molten pools at 2200 °C: comparison of two models (SVECHA vs. Prater-Courtright)

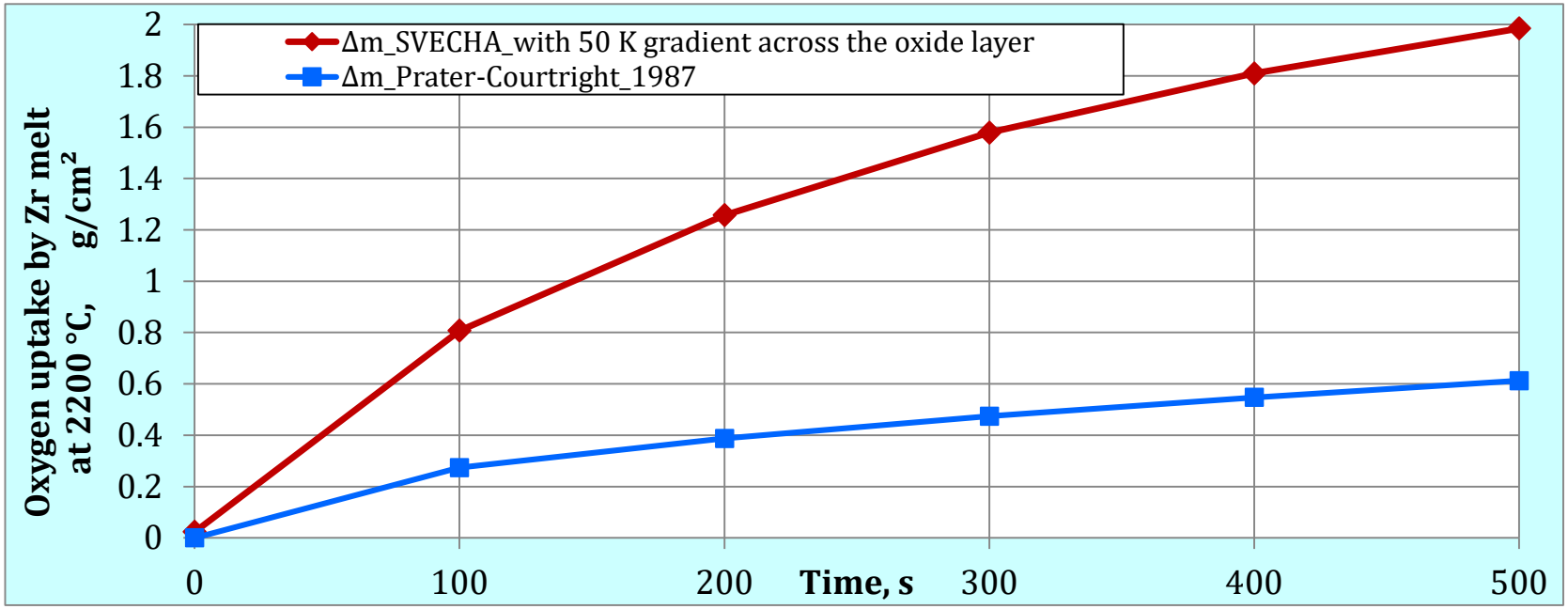

t, s	mass gain by ZrO_2 layer $\Delta m_{R\text{-}r}$, g/cm²	mass gain by ZrO_2 precipitates in melt m_f, g/cm²	total mass gain Δm_{SVECHA}, g/cm²	*Prater-Courtright mass gain Δm_{PC}, g/cm²*	$\Delta m_{SVECHA}/\Delta m_{PC}$
0	0.023	0	**0.023**	0	
100	0.057	0.751	**0.807**	0.274	3.0
200	0.088	1.169	**1.257**	0.387	3.2
300	0.120	1.458	**1.578**	0.474	3.3
400	0.153	1.657	**1.809**	0.547	3.3
500	0.182	1.803	**1.984**	0.612	3.2

- **accelerated melt oxidation due to formation of ceramic precipitates: factor 3 in comparison to the Prater-Courtright**
- **suggested kinetics:** $K_{mod}=5.74*\exp(-85900/RT)$, $g/cm^2/s^{0.5}$ *(instead $K_{PC}=5.74*\exp(-109911/RT)$, $g/cm^2/s^{0.5}$)*

Conclusions

- The analysis of the viscous melting behavior in bundles and the image analysis of the frozen melt show the formation of ceramic precipitates in the melt even in the molten state.
- The driving mechanism for the formation of precipitates is the temperature gradient at the oxide-melt interface.
- The high temperature Prater-Courtright correlation used usually in computer codes was obtained based on the oxidation of very thin samples, which does not allow taking into account processes in the bulk melt.
- Simulation of the melt oxidation by the mechanistic SVECHA code, verified on the basis of many crucible tests, gives more correct result. This takes into account not only the formation of an external oxide layer, but also the formation of ceramic precipitation inside the melt.
- A numerical calculation carried out for the case with an operating temperature of 2473 K and a temperature gradient at the melt boundary of 50 K showed that the oxidation process occurs parabolically and *three times faster* than predicted by the Prater-Courtright correlation.
- Activation energy of the new suggested correlation is 85.9 kJ/mol, which is noticeably lower than the Prater-Courtright activation energy of about 110 kJ/mol.
- It is advisable to carry out additional calculations to specify more precisely the activation energy and the pre-exponential factor in the correlation for different temperature gradients at the solid-melt interface.

Thank you for your attention

http://www.iam.kit.edu/awp/163.php

http://quench.forschung.kit.edu/

A. Khaperskaia
IAEA

IAEA ongoing activities to support advanced nuclear fuel technologies development

The IAEA has supported power-reactor fuel technologies for many decades by means of providing platforms to exchange information, through organizing IAEA meetings and developing IAEA publications, coordinating research activities (CRPs), maintaining databases (NFCFs, PIE) and fuel cycle modelling tools.

In the presentation, on-going programmes and near-term plan of the IAEA to support for advanced fuels for operating and innovative power reactors are introduced. This includes IAEA support for accident tolerant and advanced technology fuel (ATF), for fuels for recycling/multi-recycling, for advanced fuels in GENIV and small modular reactor (SMR).

Special attention is paid to Coordinated Research Projects (CRPs) on “Testing and Simulation of Advanced Technology and Accident Tolerant Fuels (ATF-TS)”, on Fuel Materials for Fast Reactors, “Standardization of subsized specimens for PIE and advanced characterization for SMR and advanced applications”, on “Fuel Modelling Exercises for Coated Particle Fuel for Advanced Reactors Including Small Modular Reactors”.

IAEA Member States can benefit from IAEA’s topical meetings and new coordinated research programmes (CRPs) that deal with cutting-edge technologies. To make it possible, the IAEA encourages Member States to actively participate in these activities.

.

IAEA
International Atomic Energy Agency

IAEA ongoing activities to support advanced nuclear fuel technologies development

Anzhelika Khaperskaia

Technical Lead (Fuel Engineering and Nuclear Fuel Cycle Facilities)
Nuclear Fuel Cycle and Materials Section
Division of Nuclear Fuel Cycle and Waste Technology
Department of Nuclear Energy
IAEA, Vienna, Austria

The 28th International QUENCH Workshop

Karlsruhe Institute of Technology
Germany, 5-7 December 2023

Organizational Chart

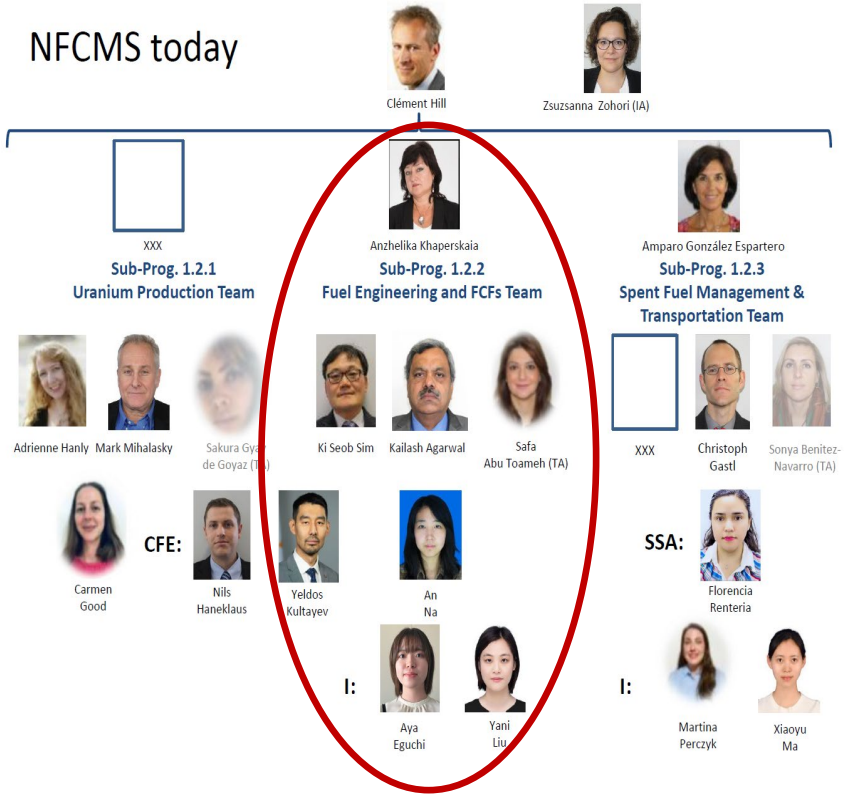

IAEA Sub-Programme 1.2.2: Nuclear Power Reactor Fuel and Fuel Cycle Facilities

Objectives:

- Support Member States (MSs) to understand and address factors affecting the design, fabrication and in-pile behaviour of currently operating and innovative nuclear fuels and materials for power reactors.
- Support MSs to technically implement IAEA Safety Standards when operating or upgrading existing nuclear fuel cycle facilities, and to understand and address factors affecting the ageing of these facilities.

Through:

- Organizing IAEA meetings and developing IAEA publications
- Coordinating research activities (CRPs)
- Maintaining databases (NFCFs, PIE) Integrated Nuclear Fuel Cycle Information System - IAEA INFCIS and modelling tools (NFCSS) Nuclear Fuel Cycle Simulation System (NFCSS) (iaea.org)
- Developing e-Learning Materials on nuclear fuel OPEN-LMS: All courses (iaea.org)
- Building up Networks among practitioners (NFE-Net) Pages - NFE Net (iaea.org)
- Supporting the IAEA Technical Cooperation Programme

Advised by the TWG FPT:

The Technical Working Group on Fuel Performance and Technology (TWG FPT) is a group of recognized experts from MSs to provide advice and support programme implementation, reflecting a global network of excellence and expertise in the area of nuclear power reactor fuel engineering (20 Members + Observers)

IAEA Publications on Fuel Engineering (2020-2023)

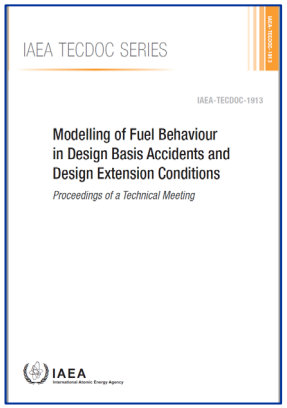

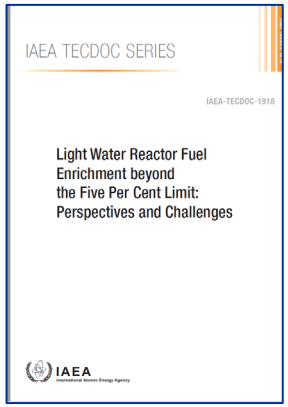

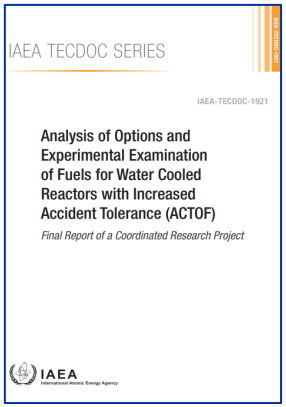

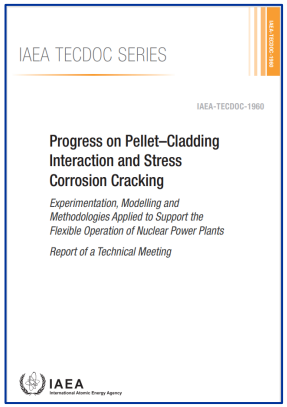

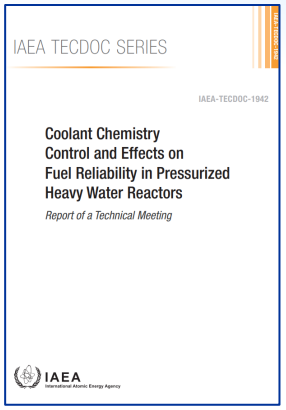

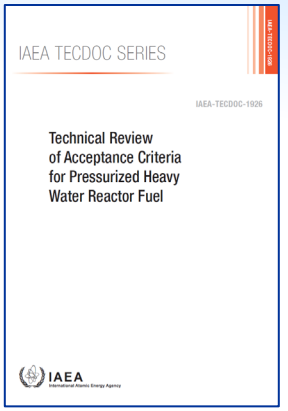

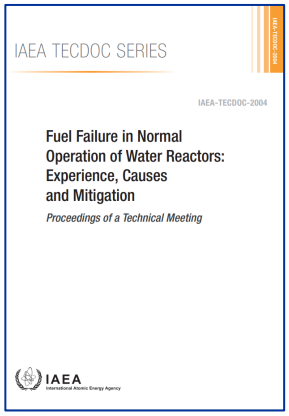

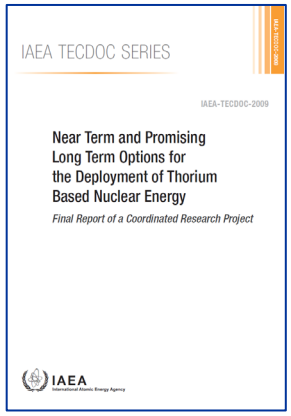

The three volumes of the IAEA *Book on the Metallurgy of Zirconium*

E-Learning courses on Nuclear Fuel Engineering (17 lectures)

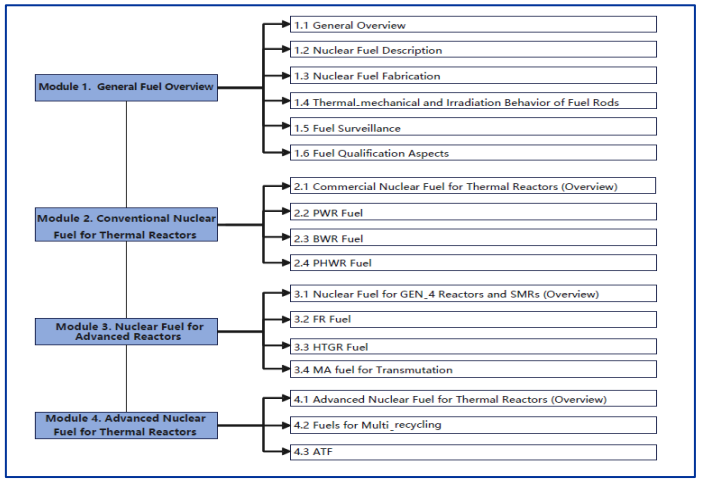

Drivers for the development of nuclear fuel technologies

- Generation IV
- SMR fuels (ranging from scaled down versions of LWR fuel designs to entirely new Gen-IV designs)

INNOVATIVE REACTOR

ENHANCED SAFETY

ATF designs (ranging from short-term evolutionary concepts e.g., coated Zr based claddings, to long-term breakthrough concepts e.g., SiC cladding)

- Zero defect campaigns
- Diverse fuel cycle options
- Higher burnup
- Multiple recycling
- Innovative methods for fuel manufacturing (AM)

IMPROVED ECONOMICS

IAEA ongoing activities to support the development of Water-Cooled Reactor fuels

Accident Tolerant Fuels

- CRP T12032 on "*Testing and Simulation of Advanced Technology and Accident Tolerant Fuels* (ATF-TS)" (2020-2024)
- TM on the "*Technical Review of ATF Technologies*: Progress on Design, Manufacturing, Experimentation, Irradiation, Case Studies for Industrialization, Safety Evaluation, and Future Prospects" (2025)
- Workshop on "*Quantification of the experimental assessment of the safety benefits of ATF*" (2025)

Fuels for recycling/multi-recycling

- TECDOC "*Mixed Oxide Fuels Design, Operation and Management*" (in progress)
- Technical meeting and IAEA publication on "*Challenges and Opportunities in Reprocessed Uranium Fuels*"

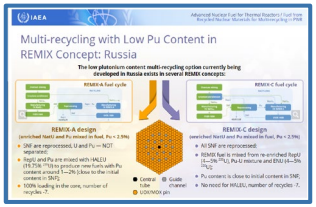

Conventional Water-Cooled Reactor fuels

- NF-G-2.1 on "*Quality and Reliability Aspects in Nuclear Power Reactor Fuel Engineering":* Guidance and Best Practices to Improve Nuclear Fuel Reliability and Performance in Water-Cooled Reactors (under publication)
- TECDOC on "*Review of Fuel Failures in Water Cooled Reactors (2016–2020)"* (in progress)
- TECDOC "*Advances in Nuclear Fuel Fabrication Technologies for Power Reactors"* – TM 2021, 2023 (in progress)
- TM on "*Advances in Fuel Design, Manufacturing and Examinations for Pressurized Heavy Water Reactors" (*November 2024, Argentina)

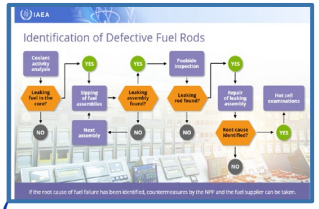

IAEA CRP Series on Fuel Behavior Modelling since 1982

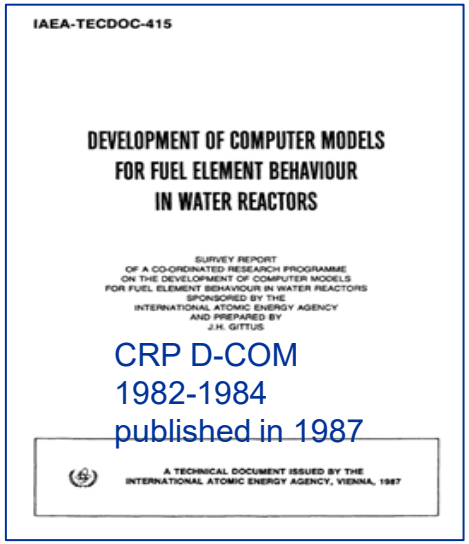

CRP D-COM
1982-1984
published in 1987

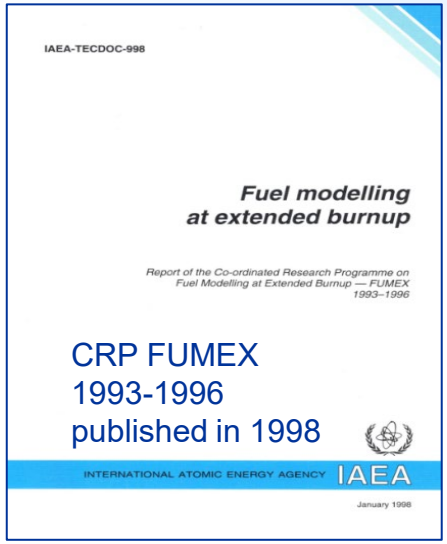

CRP FUMEX
1993-1996
published in 1998

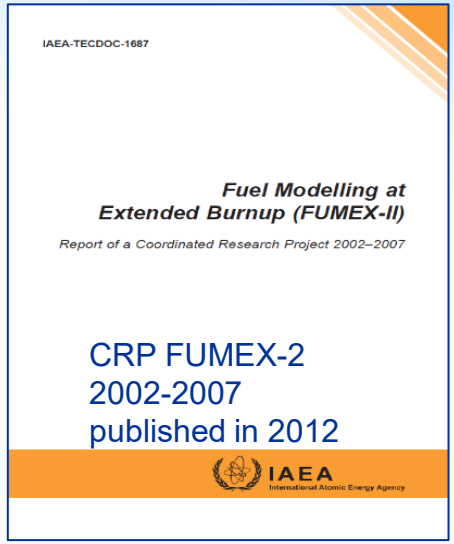

CRP FUMEX-2
2002-2007
published in 2012

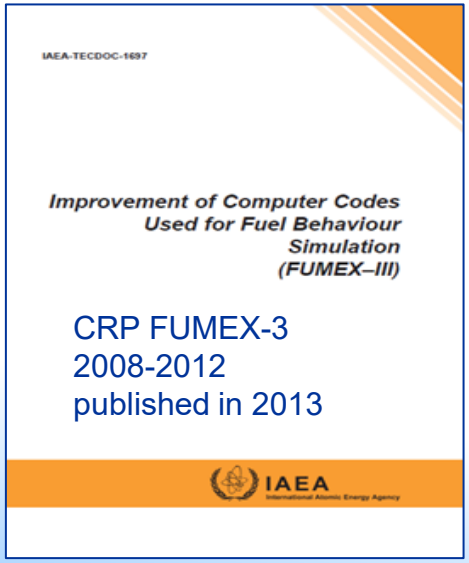

CRP FUMEX-3
2008-2012
published in 2013

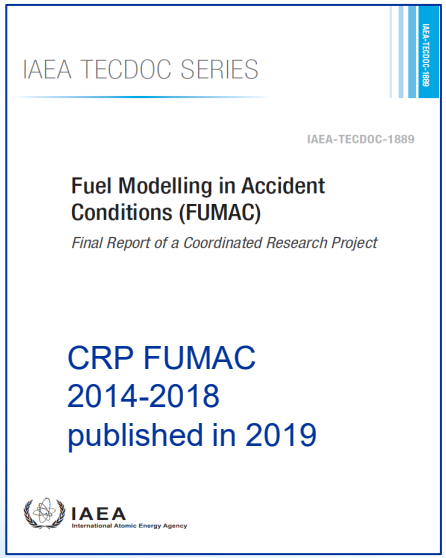

CRP FUMAC
2014-2018
published in 2019

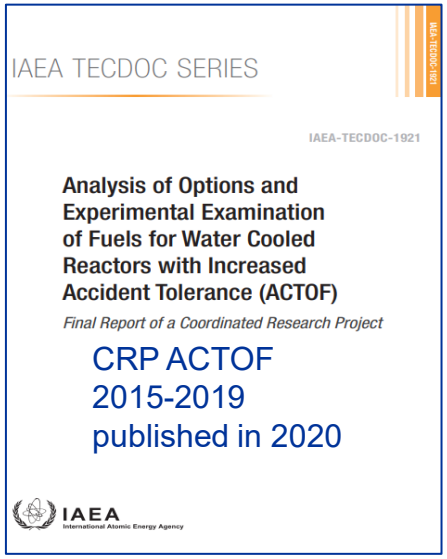

CRP ACTOF
2015-2019
published in 2020

Needs for ATF cladding

- Conventional Zr-based cladding has showed excellent performance as the 2nd physical barrier in defence-in-depth design for NPP (mainly related to the operational states of the plant)
- Safety system (Emergency Core Cooling System) is installed to maintain a coolable core and to avoid significant fuel degradation (i.e., core melting) during postulated accidents (LOCA, RIA)
  - BDBAs and severe accidents were not considered in the ECCS design due to a low probability of occurrence (< 10^{-5})
  - However, accidents at TMI (1979), Chernobyl (1986) and Fukushima-Daiichi (2011) indicated that the probability of occurrence was much greater than 10^{-5}
- IAEA Safety Standard SSR-2/1, revised in 2012 (Rev 1), requires considering of BDBA and severe accidents (design extension conditions) in the plant design

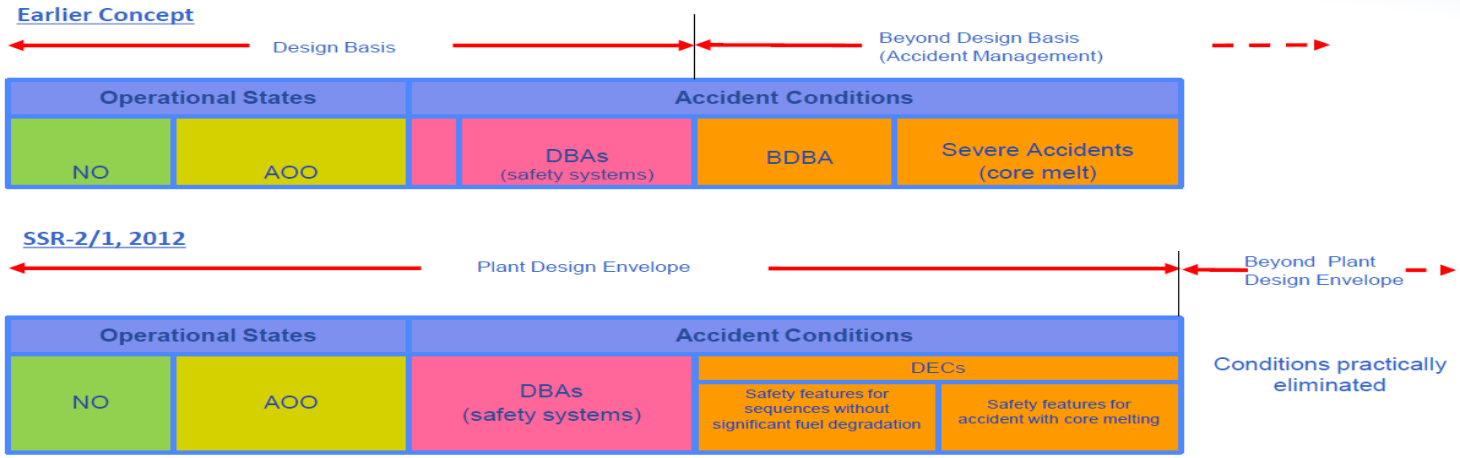

ATF cladding design - Motivation

- As the core becomes uncovered, the core temperatures rise further, and the fuel rods start to experience physical and chemical degradation
- Physical degradation occurs first at about 700-1000°C, involving ballooning and burst of the thin-walled cladding tube
- Chemical degradation by steam oxidation & high temperature:

$$Zr + 2H_2O = ZrO_2 + 2H_2 + 6.45x10^6 \text{ J/kg-Zr}$$

  - Exothermic reaction
  - Temperature escalation may take place in bundle geometry above 1200°C
  - Self-sustaining reaction above 1200°C
  - Chemical reaction power comparable to or even higher than the decay power →

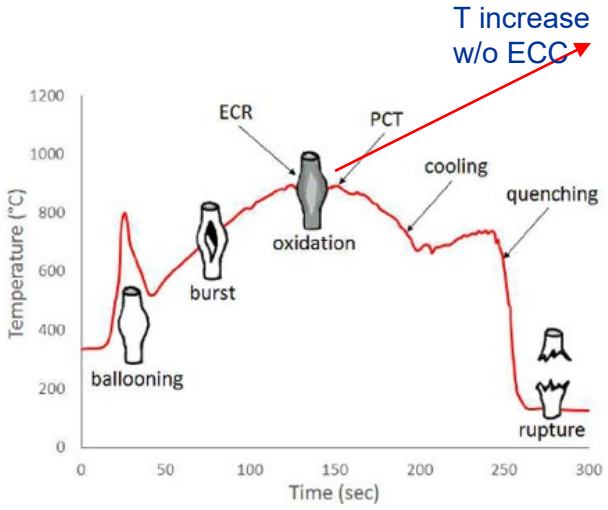

Need to decrease the rate and the total amount of heat generated and the build-up of hydrogen generated from cladding oxidation in hight temperature steam

ATF design – Basic concepts

- The oxidation rates for chromia, alumina and silica are about two orders lower than those of the oxides associated with traditional Zr alloy cladding
- Therefore, three cladding design options proposed are:
  - Chromia-coated Zr based cladding
  - Advanced steel (FeCrAl) cladding
  - SiC/SiC composites cladding
- Synergies with various improved pellet designs are pursued to enhance safety and economics (e.g., high burnup):
  - Doped UO_2
  - High thermal conductivity UO_2 (w/ metallic or ceramic addition)
  - High density fuel (U_3Si_2, (U,Pu)N, (U,Pu)C, U(-Pu)-Zr)

ATF projects

Two categories

- Not brand-new concepts: available on the shelves and move forward with priority worldwide upon request
- Two categories in terms of TRL:
  - Short term '**evolutionary**' concepts (coated or FeCrAl cladding + Cr-doped fuel, high density (U_3Si_2) fuel)
  - Longer term '**revolutionary**' concepts (refractory cladding, e.g., lined Mo, SiC cladding + microcell fuel, UN fuel, microencapsulated fuel)

ATF projects worldwide

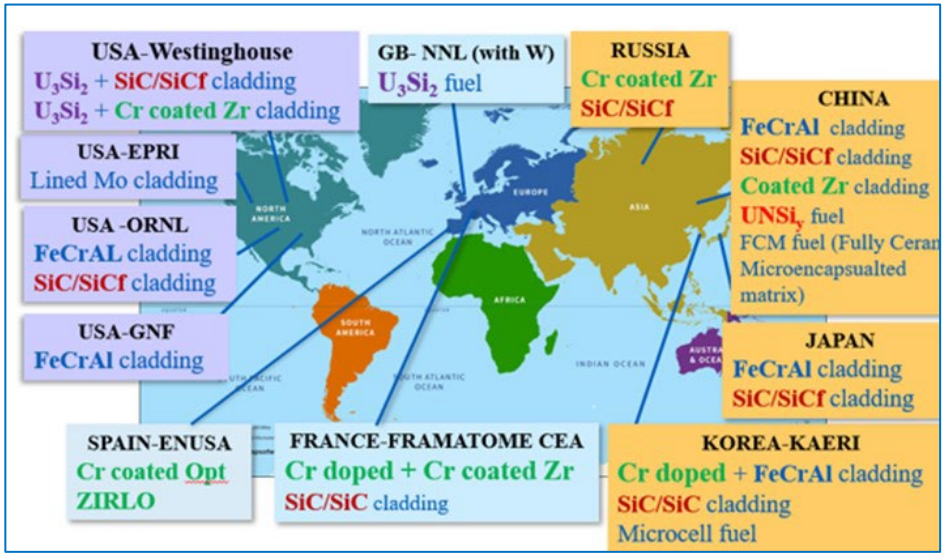

ATF/HBU

- Some countries anticipate significant benefits from high burnup operation beyond the current operating limit, especially when coupled with ATFs
- ATF lead test rods (LTRs) or assemblies (LTAs) are already being irradiated in several NPPs worldwide, and pool side inspections/PIEs are being performed, to support the qualification and licensing of ATF/HBU fuels
- Industry's two step approaches:
  - To a max burnup that does not require design changes
  - To 75 GWd/tU (rod average) or higher
- Some Member States have already developed roadmaps for licensing of ATF/HBU together with use of higher enrichment

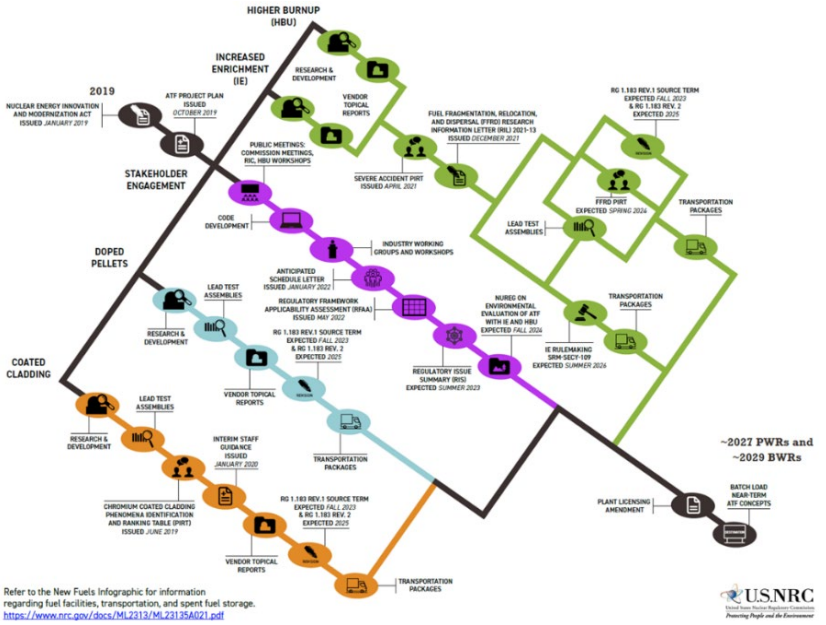

IAEA support to ATF development

CRP FUMAC (2014-18)

- Better understanding of fuel behaviour during LOCA
- 24 organizations (18 countries), 10 computer codes
- IAEA-TECDOC-1889

CRP ACTOF (2015-19)

- Better understanding of ATF cladding (FeCrAl) behaviour during normal operation and under accident conditions
- 5 organizations, 5 computer codes
- IAEA-TECDOC-1921

CRP ATF-TS (2021-24)

- Comprehensively understanding of ATF (cladding, rod, assembly) behaviour for all applicable plant conditions
- 29 organizations (18 countries)
- Mainly deals with short-term concepts

Objectives of the CRP T12032 “ATF-TS”

Overall

- To support Member States to understand and address factors affecting the design, fabrication and in-pile behaviour of currently operating and innovative nuclear fuels and materials for power reactors, to increase technology readiness for candidate ATF materials

Specific

- To perform experimental tests including single rod and bundle tests on ATFs' performance under normal, DB and DE conditions
- To benchmark fuel codes against new test data either obtained during the CRP or from existing data relevant to advanced fuel and cladding concepts from Member States' experimental Programmes
- To develop LOCA evaluation methodology for ATF performance with a view for NPP applications

CRP Testing and Simulation of Advanced Technology and Accident Tolerant Fuels (ATF-TS)(2020-2024)

The CRP brings together specialists from IAEA MSs with active ATF R&D programmes to share their national efforts and to contribute in any of the following objectives of the CRP:

- Round Robin tests on different ATF cladding concepts (e.g., coated Zr cladding, FeCrAl, SiC);
- Bundle tests under DB/DEC with ATF materials (e.g., with coated Zry-4 rods under SA and/or LOCA conditions);
- Collection of irradiation tests data;
- Code benchmarking against existing data, relevant for advanced fuel and cladding concepts from other experimental Programmes, as well as new tests data obtained during the CRP;
- LOCA evaluation methodology development for NPP applications including uncertainty and sensitivities studies.

Participants : 29 organizations from **18** MSs **Co-Chairs: J. Zhang (BEL), M. Sevecek (CZE)**

WT 1:
Experimental Programme
M. Sevecek (CZE)
J. Stuckert (GER)

WT 2:
Modelling
A. Boulore (FRA),
M. Cherubin (ITA),
J. Stuckert (GER),
Z. Hozer (HUN)

WT 3:
LOCA Evaluation Methodology for NPP Application
J. Zhang (BEL)

WT 4:
Material Properties database for ATF
Ch. Allison (USA)

Activity flow (interfaces) of CRP T12032 “ATF-TS”

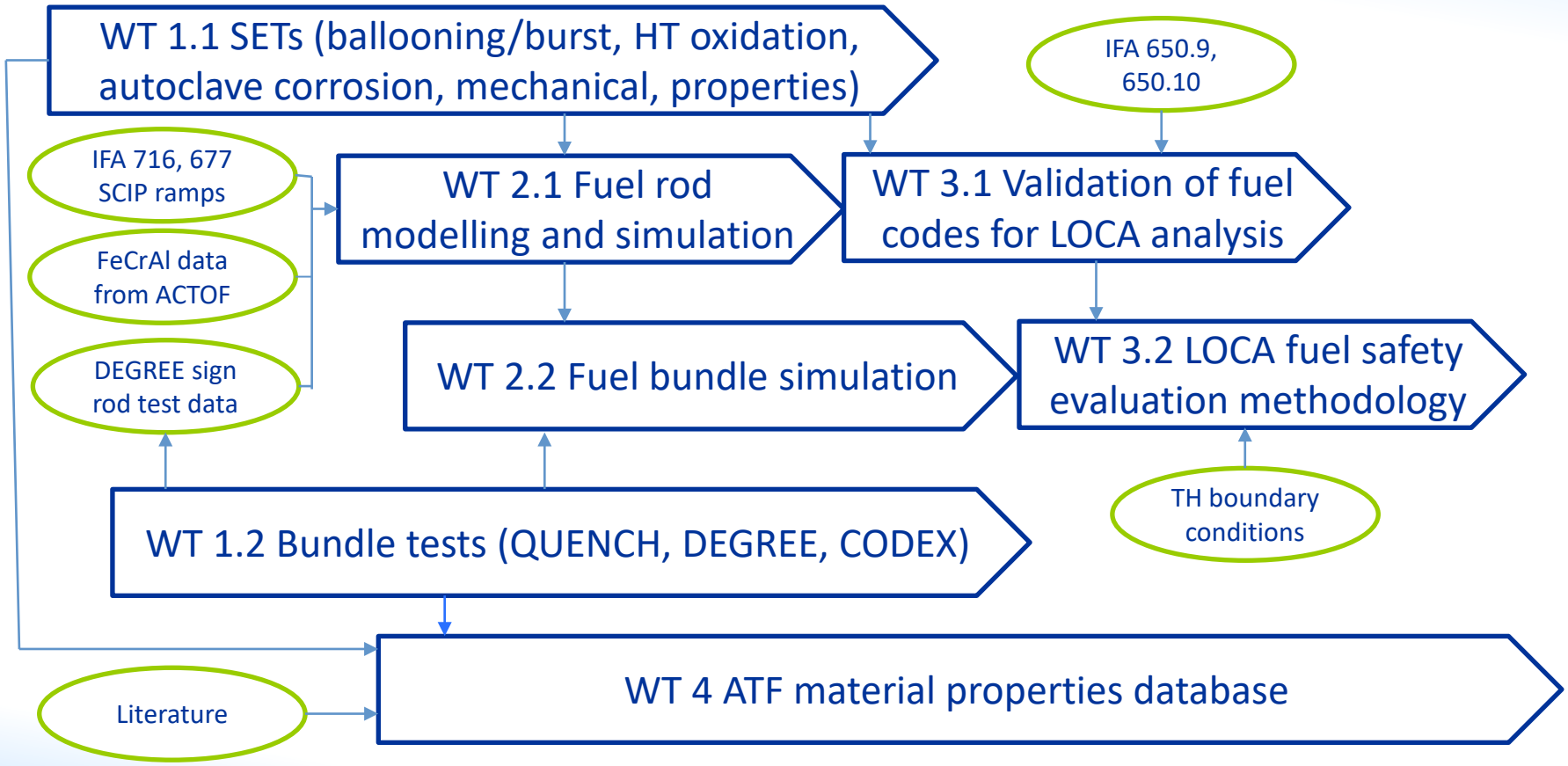

Meetings of CRP T12032 “ATF-TS”

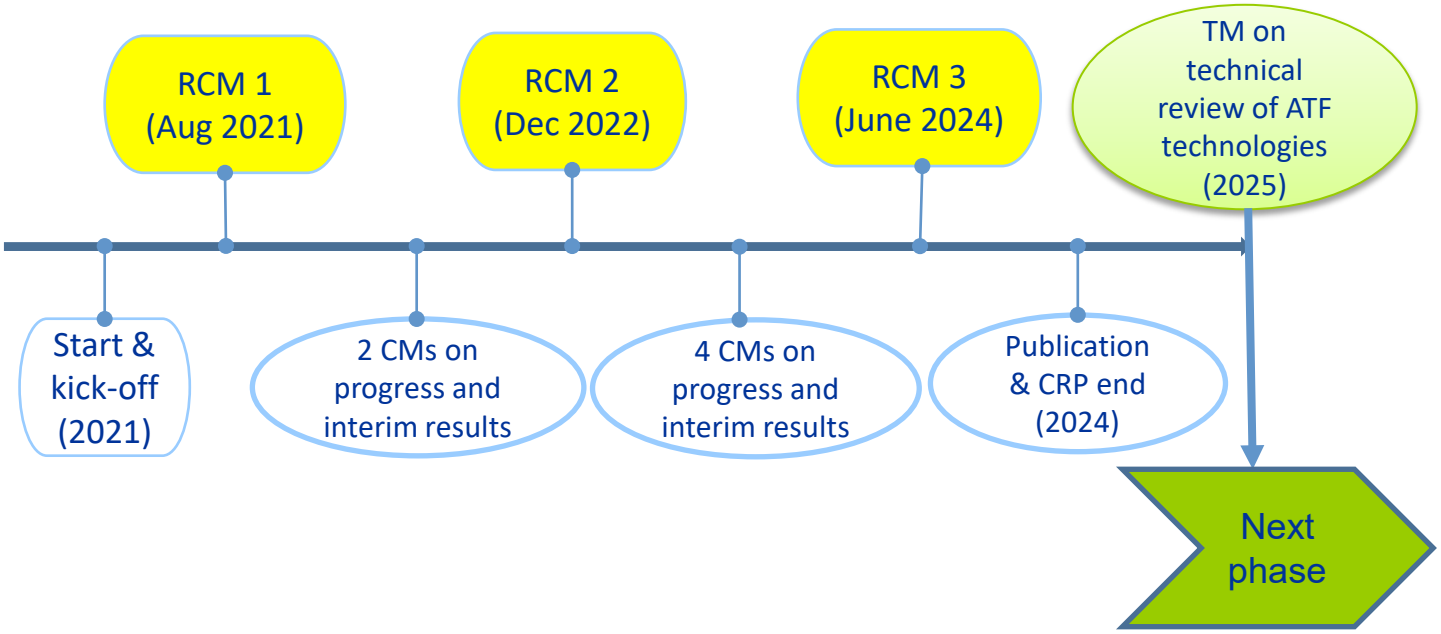

We plan a Technical Meeting in 2025 to assess the state-of-the art of the ATF including CRP results and to discuss path forward to complete the ATF technologies.

Fuels for recycling/multi-recycling

TECDOC "*U-Pu Oxide Fuel – Design, Operations & Management*"

State-of-the art report with information on the design, fabrication and operation of U-Pu oxide fuels, the feedback experience of MOX fuel utilization in thermal reactors, fuel concepts for multi-recycling in LWRs (such as REMIX, CORAIL or MIX type), and using MOX fuels in fast reactors

- Present status and trends of U-Pu oxide fuels
- U-Pu oxide fuels' properties
- U-Pu Oxide fuels' design and behaviour
- U-Pu oxide fuels' fabrication technologies and infrastructure
- Reactor operation experience with U-Pu oxide fuels
- Safety considerations for U-Pu oxide fuels

MOX for LWR.
Example of a MOX FA zoning
(average Pu content : 8,65%)

CORAIL

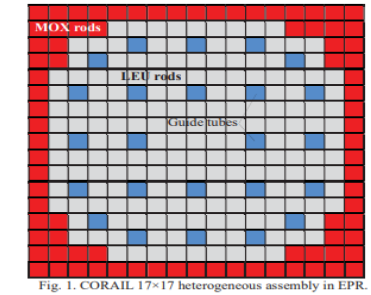

REMIX-C

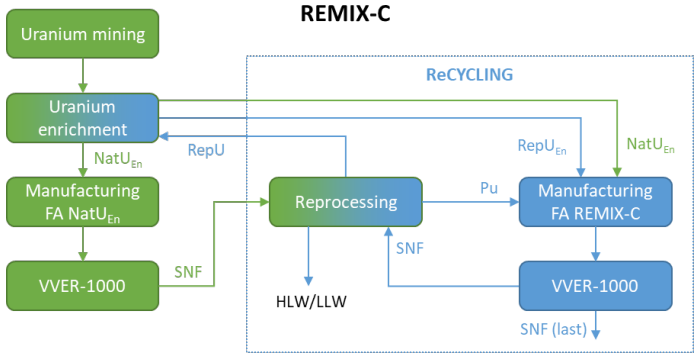

The TECDOC "U-Pu Oxide Fuel – Design, Operations & Management" is under finalization

Fuels for recycling/multi-recycling: Reprocessed Uranium Fuels

CMs in 2022 and 2023

Technical Meeting on the Challenges and Opportunities in Reprocessed Uranium Fuels (20 - 24 November 2023): 49 experts from 16 Member States

The participants recommended

- to revise and update the *IAEA Nuclear Energy Series NF-T-4.4* (2009)

- *TECDOC with Proceedings* of a Technical Meeting, 2023, with executive summary of the TECDOC, with high-level findings,
- *Infographics* (very high-level findings, with input from repU recycling into SDGs).
- New CO2 -reducing calculation *module for IAEA NFCSS*
- A *new database with PIE results* on the isotopic composition of irradiated fuel (for Nat U and rep U).

Technical Sessions

- National policies related to RepU, inventories and future arising of RepU
- Stages in implementation of different options of RepU fuel management.
- Loading into the reactor and behaviour of RepU fuel
- Management of spent ERU fuel. RepU recycling contribution into SDGs
- Market and economics of RepU
- Increasing of Proliferation Resistant of Uranium by using RepU

IAEA support to Advances in Nuclear Fuel Fabrication Technologies for Power Reactors

Two IAEA Technical Meetings held in Vienna

- ***8 – 10 November 2021:*** 48 participants from 18 MSs and 1 IO
- ***26–28 June 2023:*** 45 participants from 18 MSs and 1 IO

- **Powder and reconversion** (modelling of uranium oxide powder and dry conversion processes for fuel fabrication and improvements of reconversion processes, advanced sintering, doped (UO_2, MOX) pellets, new or higher content of burnable absorbers)
- **Sintering, pelletizing, advanced pellet fabrication** (modelling of fuel fabrication processes, thermal conductivity ATF pellet and burnable absorber fuel, fabrication and characterization of Gadolinium pellets for LWR-based SMR fuels)
- **Cladding, fuel rod/assembly components** (development of ATF and 3D printing technology, new type of Zirconium Alloy Cladding Tubes , advancement for PHWR fuel manufacturing)
- **Advancements in fuel fabrication facilities and inspection** (automatization, application of artificial intelligence technology to QC, passive scanner for Uranium and Gadolinium fuel rods inspection)
- **Adaptation of new technology** (3-D printing , Virtual reality, AI technology)
- **Fabrication technologies for new fuel development** (new type nuclear fuel for existing NPP, SMR Fuel Development and Fabrication)

The IAEA TECDOC on “Advances in Nuclear Fuel Fabrication Technologies for Power Reactors”- is under development

IAEA ongoing activities to support the development of innovative GEN-IV and SMR fuels

Water-cooled SMR fuels

- Workshop on "Core and Plant Simulation with an Emphasis on Fuel Behaviour in Light Water Reactor Based Small Modular Reactors (to compare results of SMR fuel behaviour simulation, common analysis), 27-29 February 2024

Fast reactor fuels

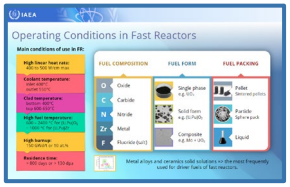

- **CRP T12031** on "Fuel Materials for Fast Reactors (FMFR)" (2020-2023) (TECDOC in progress)
- NES report "Nuclear Fuel Technologies for Liquid Metal Cooled Fast Reactors (LMFRs)" (in progress)

Gas-cooled SMR fuels

- TECDOC "Coated Particle Fuels for High Temperature Gas-Cooled, Small Modular Reactors – Progress in Design, Manufacturing, Experimentation, Modelling and Analysis Technologies" (currently under MSs' review)
- **CRP T12034** on "*Fuel Modelling Exercises for Coated Particle Fuel for advanced reactors including SMR*" (open for proposals)

Molten salt SMR fuels

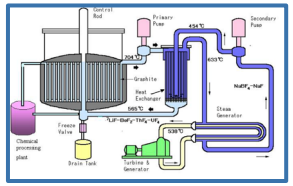

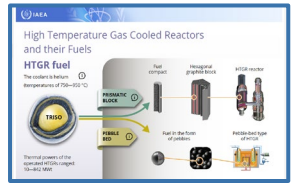

- Dedicated technical session during TWG FPT meeting, April 2024
- New Simulation tool module development for MSR with relevant fuel cycle

PIE for SMR

- **CRP T12033 on "***Standardization of Subsized Specimens for Post-Irradiation Examination and Advanced Characterization of Fuel and Structural Materials for Small Modular Reactor and Advanced Reactor Applications* **(PIE for SMR)" (**open for proposals**)**
- TECDOC on "*Assessment of Post-Irradiation Examination Techniques for Advanced Reactor Fuel and Materials" (under publication)*

Needs for collaborative activity in FR fuel

There is a growing interest from countries in the deployment of GEN-IV reactors (and small modular reactors, SMRs) based on liquid metal-cooled fast reactor technologies, but **very limited numbers of FR fuel experimental datasets, fuel behavior codes** and **published benchmark exercises exist**

Several demonstration projects, from small to large scales, are currently under study, design, and construction, and there are national and international efforts to develop suitable fuels and fuel cycles for different fast reactor technologies' demonstration

CRP T12031 “FMFR” on Fuel Materials for Fast Reactors (2019-2023)

MSs’ participation

- 8 organizations from 5 MSs + EC:
  India (IGCAR), France (CEA), Japan (CRIEPI, JAEA), Korea (KAERI), United States (ANL, INL), EC (JRC-Karlsruhe)
- NEA OECD is an observer

Chair: Dr T. Ogata (CRIEPI, Japan)

RCMs and CMs

- RCM-1: 2-4 October 2019 in Vienna
- *CM on the Status of the CRP FMFR: 22-23 October 2020 (virtually)*
- RCM-2: February 15-18, 2021 (virtually)
- *CM on the Status of the CRP FMFR: 25-27 January 2022 (virtually)*
- RCM-3: 17-21 November 2022 (hybrid)
- *CMs to prepare the draft TECDOC in May 2023 and November 2023.*

The main purpose of the CRP is to support the fuel and cladding materials performance assessments for the sodium-cooled fast reactor technology, in accordance with the Gen-IV requirements, through enhancing the fuel performance codes. Methodologies to achieve this goal are to collect irradiation test data and build a dataset that shall be shared among the IAEA Member States (MSs) to extend the validation basis of fuel performance phenomena

Two focused areas:

1) Collecting irradiation test data on fuel materials, including oxide (MOX) and metallic (U/U-Pu based alloys) fuels and steel-based claddings

2) Performing benchmarking exercises.

Current Status: Documentation of the CRP results is in progress

Results achieved in CRP T12031 “FMFR”

- **9 Fast Reactor fuel experimental datasets** were provided by the CRP participants
  - For FR Oxide fuel: FBTR, JOYO B5D2, SANTENAY, FFTF-FO2, SUPERFACT
  - For FR Metal fuel: X447 DP11, METAPHIX-1#1, METAPHIX-2#1
- **29 calculations** were performed on FR fuel experimental datasets, and various fuel performance codes were used
  - CEPTAR, GERMINAL, TRANSURANUS, CAMOX, ALFUS, MACSIS, LIFE-METAL, BISON

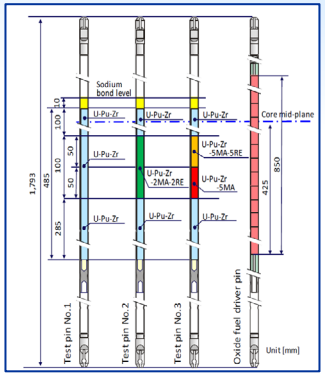

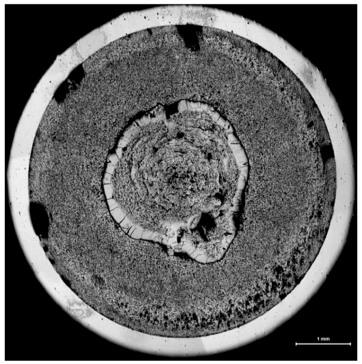

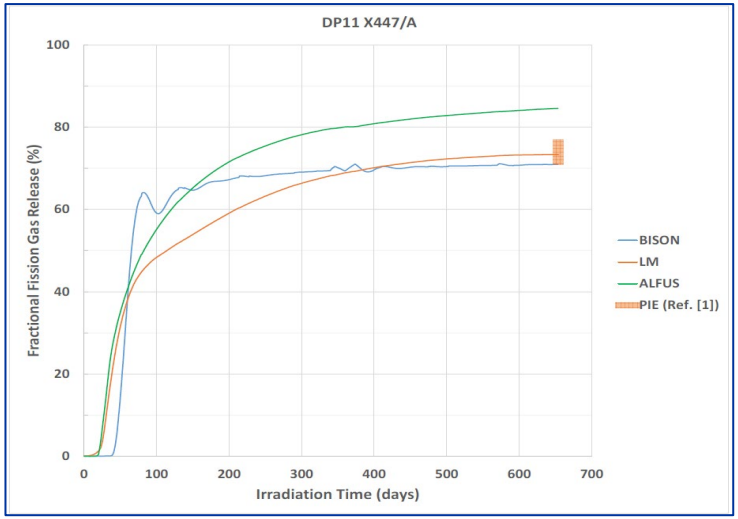

NES report “Nuclear Fuel Technologies for Liquid Metal Cooled Fast Reactors (LMFRs)”

The new document will update and complement the IAEA publication NF-T-4.1 (2011) for SFR fuels, with new technical information on the design, fabrication, and operation of fuels for Liquid Metal cooled FRs (LMFRs), including SMRs

16 experts from 11 MSs (*Czech Republic, China, Japan, Italy, France , Korea, India, Russia, Sweden, UK, USA)* developed the draft

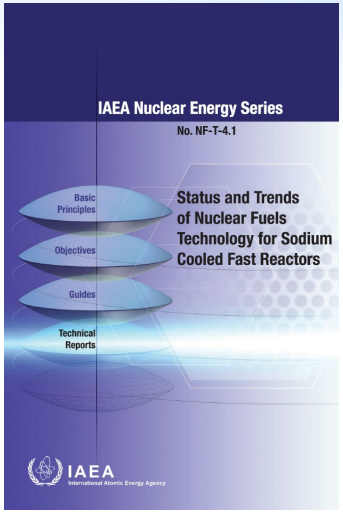

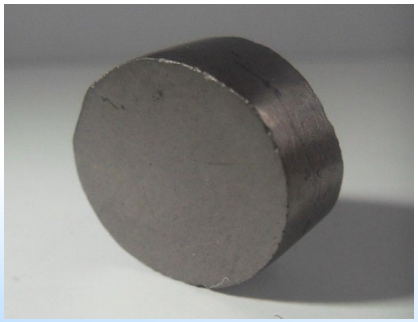

UN pellet produced by spark plasma sintering.
Courtesy of KTH, Sweden.

BN-600 Fuel assemblies with (U Pu) N
Courtesy of VNIINM, Russia

NES report “Nuclear Fuel Technologies for Liquid Metal Cooled Fast Reactors (LMFRs)” (cont.)

- Introduction (current situation on FRs, FR core and fuel assemblies, specifics of fuel technology for fast neutron SMR)
- Member States’ activities in LMFRs and their fuel cycles
- Oxide fuels for LMFRs (fabrication technologies and experience, fuel failure and irradiation behaviour and experience in LMFRs, advanced fuels with minor actinides)
- Nitride fuels for LMFRs
- Metallic fuels for LMFRs
- Cladding materials for LMFRs
- Fuel performance evaluation codes
- Recommendations for future activity

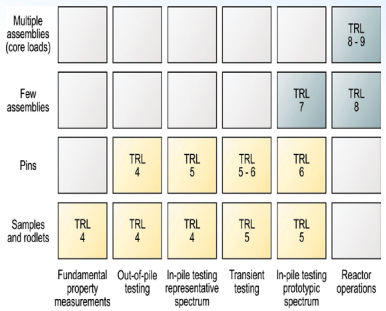

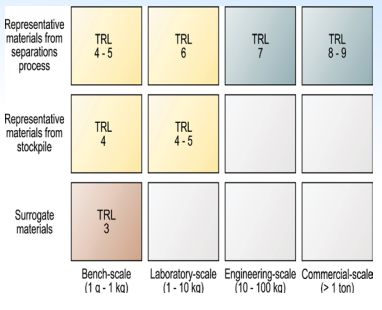

TRL (MAX international)	UOX	(UPu)O2	UN	UPuN	U Pu Zr	U-Zr
Fabrication/ irradiation experience	9/9	9/9	8/7	8/7	7/7	8/7

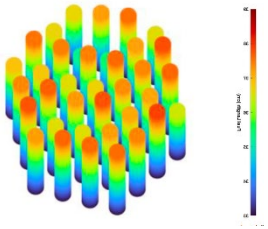

Example BISON Simulation of Axial Fuel Growth in an EBR-II Experiment

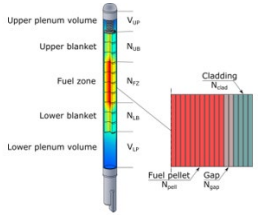

Fuel rod discretization scheme of the BERKUT-U code

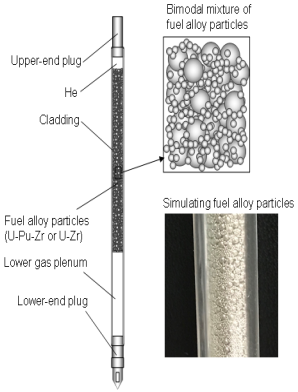

He bonded particulate metallic fuel pin concept

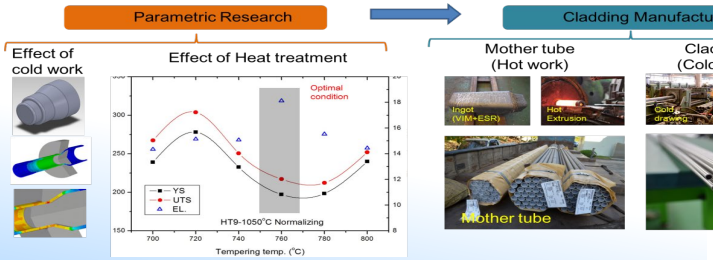

Manufacture of FC92 cladding tube

IAEA support to innovative fuels: new CRP for small sample PIEs

- The safety of nuclear reactors is strongly coupled with the reliability and performance of their fuel and materials in the reactor core
- Before use in the reactor, new fuels and materials should be qualified mainly by experimental data obtained through post-irradiation examinations (PIEs)
- The amount of experimental data is not comprehensive enough to cover all material properties and in-reactor performance aspects required for qualification, when compared to the amount of supporting irradiation data for currently operating reactor fuels and materials
- Mapping exercise on important performance parameters vs corresponding PIE capabilities has been conducted for several advanced reactor fuels:
  - Many gaps exist and it may take significant time to fill the gaps, as documented in an IAEA TECDOC on Assessment of Post-irradiation Examination Techniques for Advanced Reactor Fuel and Materials (in press)
- International experts proposed:
  - Accepting advances in examination techniques that enable the characterization and property measurements of very small samples into the qualification processes
  - Collaboration across borders

New CRP T12033 on "Standardization of subsized specimens for PIE and advanced characterization for SMR and advanced applications" (2024-2029)

IAEA

Overall objective

To support Member States by demonstrating that:

- Collaborative efforts for advanced characterization of innovative fuel types can be performed
- The required fuel performance parameters for a given fuel type or material can be properly assessed using small samples
- Sample preparation guidelines are well defined and similar across laboratories
- Irradiated sample transport is viable

Specific objectives

1. Develop a PIE roadmap (round-robin PIE plan)
2. Execute the round-robin PIE exercise
3. Demonstrate and look for efficiencies associated with transport of small/subsized samples

Expected outcome

- Expanded sets of PIE capabilities to support new or advanced fuel developments for innovative reactors
- Establishment of protocol for collaboration to expand PIE capabilities spanning 2 or more labs

Currently call for research proposals

Several organizations have already submitted their research proposals (Small sample preparation, homogenizations, Irradiation, Shipping irradiated/unirradiated sample materials, Tests, justification of test results, etc.)

TRISO –fuelled SMRs and MMRs

Increasing international interest, and significant efforts are underway in developing nuclear reactors using **TRISO-coated particle fuels (GENIV and SMR)** based on either pebble bed or prismatic designs

- This technology has a unique design with inherent safety features, which provide **excellent retention** of fission products at high temperatures

Reactors using TRISO fuels have the potential to **supply high temperature process heat**, and many other applications such as hydrogen production in addition to electricity generation

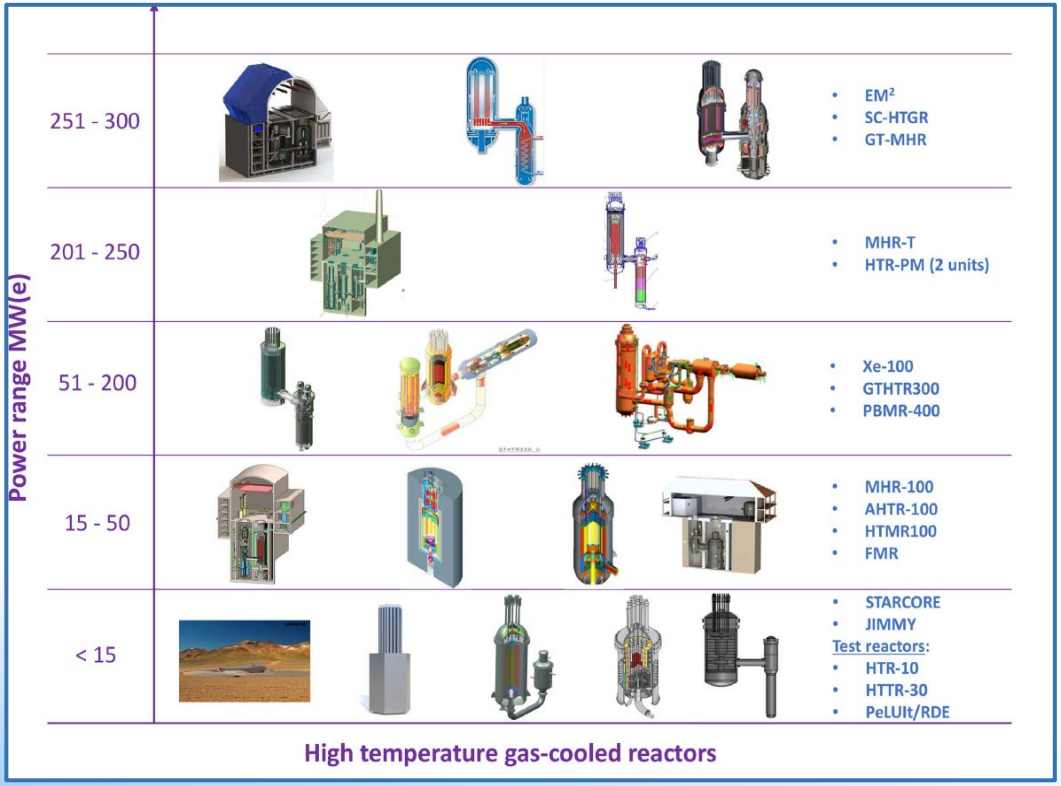

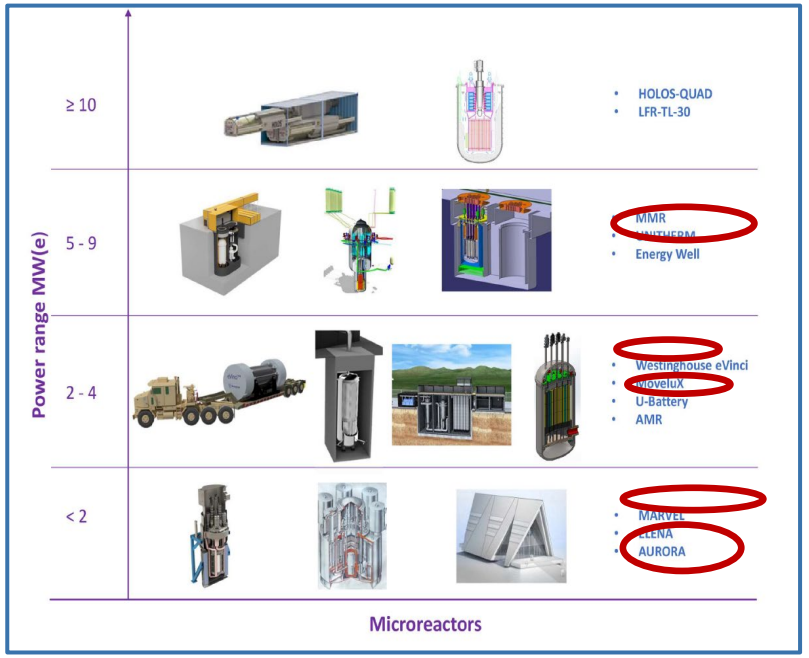

IAEA support to TRISO fuel development

- **IAEA-TECDOC-978** “Fuel performance and Fission product Behaviour in Gas Cooled Reactors” (1997)
  - A benchmark dedicated to the validation of predictive methods for fuel and fission products’ behaviour (fuel performance during normal and accident oxidizing and nonoxidizing conditions, transport of gaseous and metallic fission products during normal and accident conditions, performance of advanced fuels and GCR fuel design and fabrication programmes)
- **IAEA-TECDOC-1645** “High Temperature Gas Cooled Reactor Fuels and Materials” (2010)
  - A handbook and best practice document for use in training and education in coated particle fuel technology. The document covers: manufacture of coated particles, compacts and elements; design-basis; quality assurance / quality control and characterization techniques; fuel irradiations; fuel failure mechanisms; accident testing; fuel and fission product chemistry; fuel cycles; fission product transport; spent fuel management; and nuclear hydrogen production
- **IAEA-TECDOC-1674** “Advances in High Temperature Gas Cooled Reactor Fuel Technology” (2012)
  - Set of benchmarking activities to compare fuel performance codes under normal operation and operational transients
- **New TECDOC** “Coated Particle Fuels for High Temperature Gas-Cooled, Small Modular Reactors – Progress in Design, Manufacturing, Experimentation, Modelling and Analysis Technologies” (*currently under MSs’ review*)
  - A comprehensive review of HTGR particle fuel technologies (e.g., design, fabrication, characterization, irradiation performance, performance modelling) to provide up-to-date information on coated particle fuel technologies, covering the period after 2010, as the baseline reference to support fuel technologies of HTGR SMRs
- **New CRP** 12034 (2024-2029) on “Fuel Modelling Exercises for Coated Particle Fuel for Advanced Reactors Including Small Modular Reactors

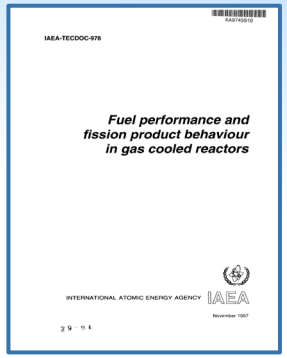

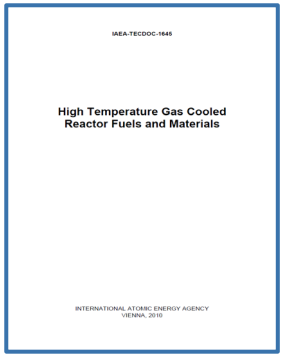

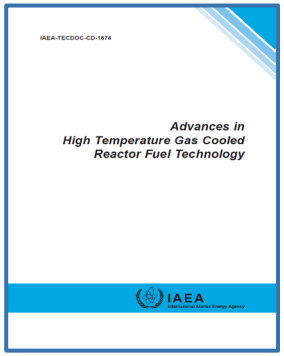

IAEA TECDOC on “Coated Particle Fuels for High Temperature Gas Cooled Small Modular Reactors”

IAEA-TECDOC-1674 is the latest publication that covers the R&D on coated particle fuel up to 2010: it does not address the applicability to SMRs

The new publication will focus on up-to-date information on fuel technologies to be used as the baseline reference to support fuel technologies of high temperature gas cooled SMRs

TECDOC content:

1. Introduction
2. Design description and design requirements
3. Updates in Member States
4. Coated particle fuel manufacturing
5. Quality control for fuel particle characterization
6. Irradiation tests, heating tests and post irradiation examinations
7. Fuel modelling and code developments
8. Fuel cycles and waste
9. Conclusions

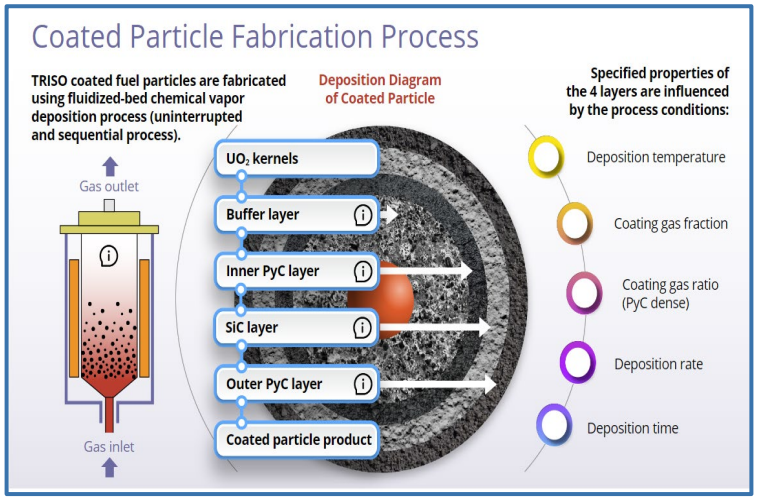

Needs for collaborative activities on TRISO fuel

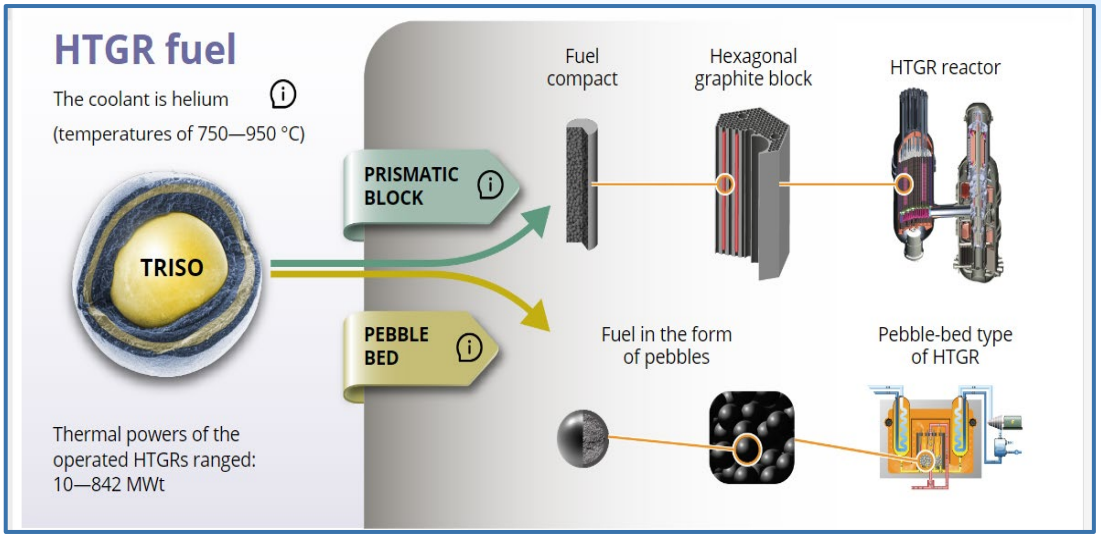

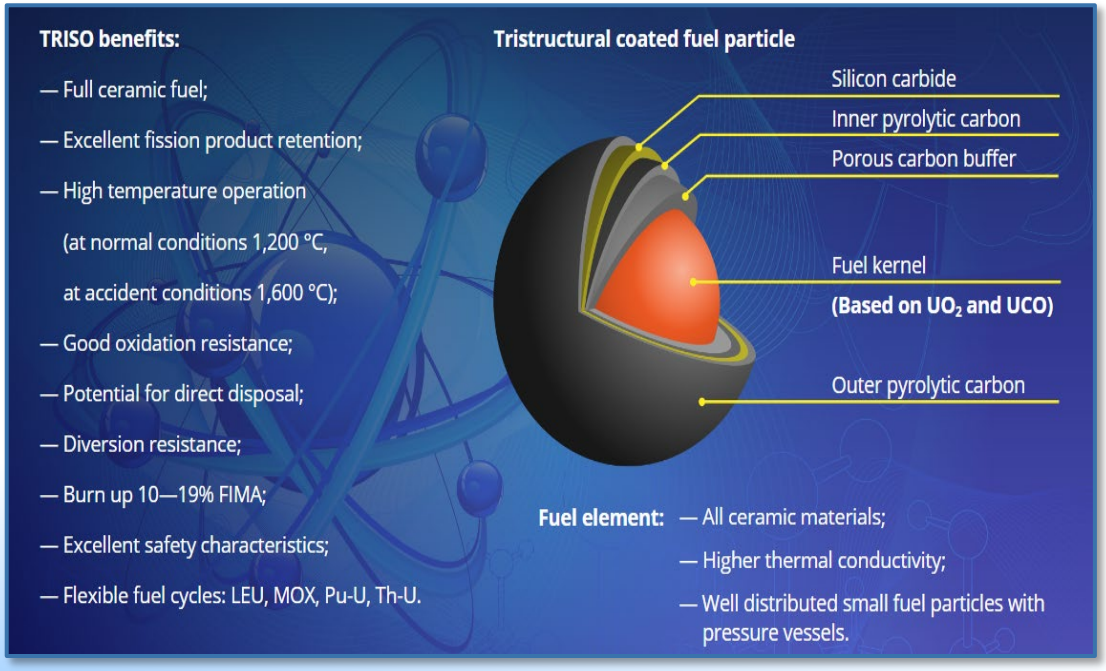

There is a gap in the knowledge of **material properties** and **fuel performance modelling**, which could hinder the deployment of HTGR technologies:

- Key TRISO fuel properties like diffusivities, creep, thermal conductivity, mechanical properties,
- Missing experimental data for reactivity-initiated accidents (RIA) on irradiated fuel
- Accurate list of dominant FPs for Source Term (current list for modelling: Ag, Cs, Sr, I/Kr/Xe, incomplete modelling parameters: Ba, Ce, Eu, Ru)

New CRP T12034 on "Fuel Modelling Exercises for Coated Particle Fuel for Advanced Reactors Including Small Modular Reactors" (2024 – 2029)

Overall Objective

– To support interested IAEA Member States (MSs) to enhance advanced modelling / simulation of TRISO fuel performance, improving the fundamental understanding of key TRISO fuel properties and radiation effects on TRISO fuels' properties in high-radiation environment, to deploy GEN-IV reactors, SMRs and MMRs, that use TRISO-coated particle fuels

Specific Research Objectives

– To strengthen international collaboration by bringing together experts to better utilize national R&D efforts:

- To promote the sharing of irradiation data from HTGR TRISO experiments, and associated post-irradiation examinations
- To optimize the use of available experimental data
- To identify methodologies for obtaining and measuring material properties relevant for modelling fuel performance

– To perform simulations of acquired datasets, using various fuel performance codes

- To compare, analyse and share simulation results among CRP participants, including recommendations on fuel performance codes enhancement

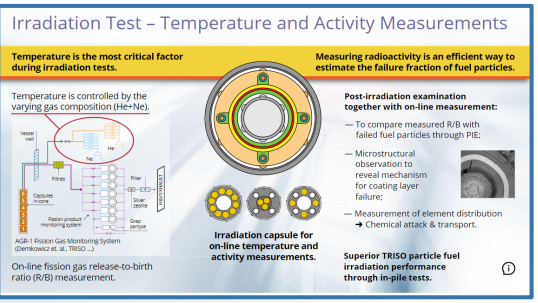

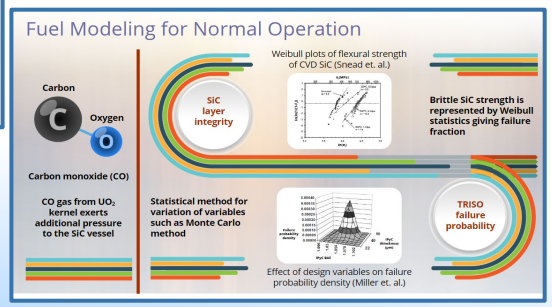

Open for research proposals

Specific Tasks of CRP T12034

- To improve knowledge and fill the gaps of key TRISO fuel properties for codes development (e.g., diffusivities, creep, thermal conductivity, mechanical properties, SiC strength) with new data (e.g., obtained from new experiments and/or generated by multiscale modelling) to provide input to these codes
- To implement all the important TRISO particle failure modes into fuel performance codes that will be used for the validation of TRISO fuel experiments
- To gather the operating and transient envelopes for TRISO-fueled reactors relevant to participating MSs for potential new measurements of fuel properties and new calculations
- To develop the list of fission products (FPs) that are of importance to the selective criteria to model their transport and release for licensing purposes, and to develop the methodology used to define the importance of each FP
- To develop a database based on existing experimental data and new dataset collection to validate codes
- To perform code benchmark exercises, including uncertainty propagation

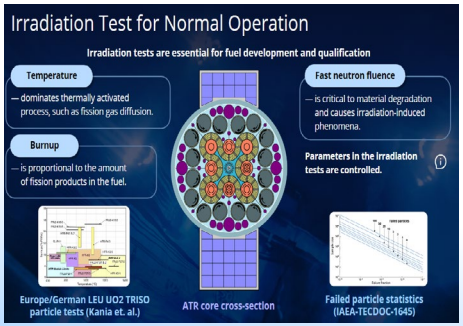

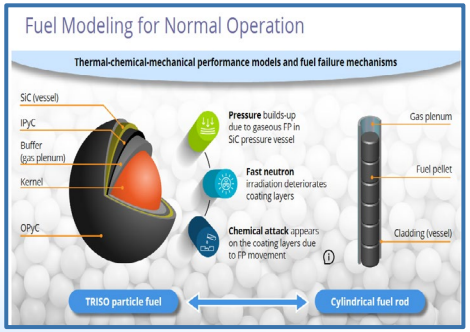

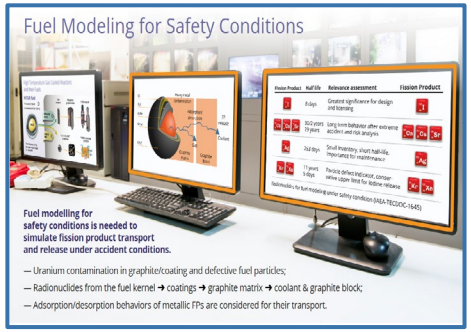

Expected outcome and results

Expected outcome

- A knowledge preservation for supporting fuel designs for coated particle fueled reactors, including SMRs
- Enhancing confidence in the use of fuel performance codes that support the deployment of coated particle fueled reactors

Expected results

- A database containing experimental data (existing and potentially newly collected data)
- Improved models/correlations for materials' properties (e.g., thermo-mechanical, such as SiC strength) and irradiation properties (e.g., diffusion coefficients of fission products in a given medium, such as SiC layer) to be implemented into fuel performance codes
- Results of computer modelling of a selected number of cases with the use of different fuel performance codes
- Scientific publications, presentations at international conferences and final CRP report (TECDOC)

Simulation tool (NFCSS)

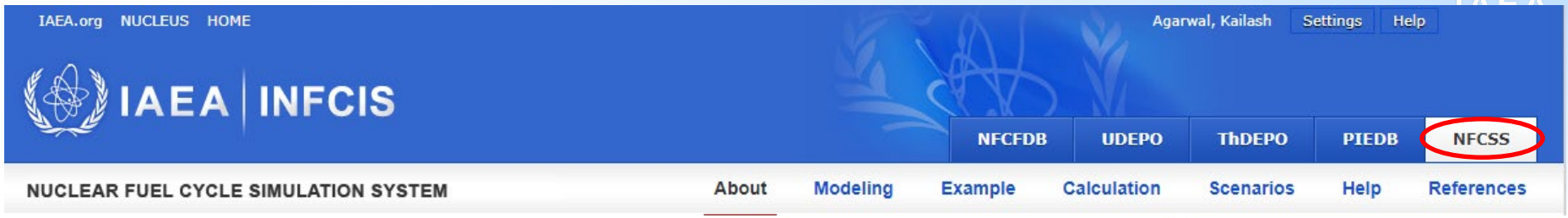

- NFCSS is a scenario-based publicly available computer model (web-based tool) for the estimation of nuclear fuel cycle material and service requirements
- 7 Types of reactors: PWRS, BWRs, PHWRs, RMBKs, AGRs, GCRs, WWERs
- UOX, MOX and ThOX fuel cycles
- Calculates the requirements for Nat U resources, enrichment and fuel fabrication services, etc. SF inventory, Minor Actinide Inventory, FP inventory, Decay Heat and Radio-toxicity with material Flow Diagrams up to 200 years
- FRs modelling
- A e-Tutorial Module is being developed

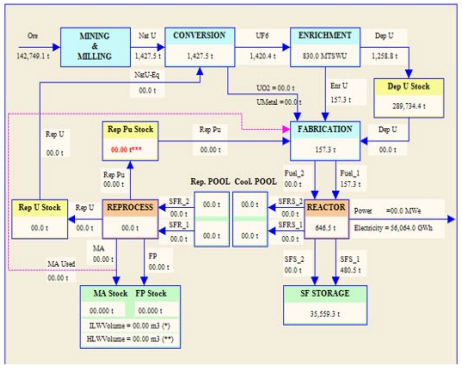

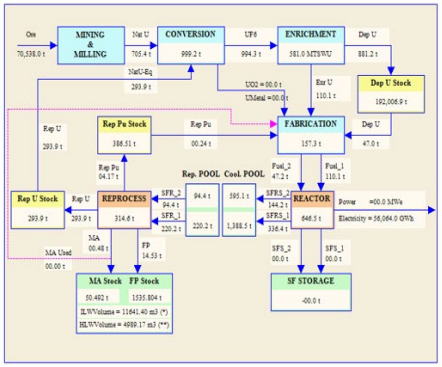

	Open cycle	Closed Cycle	
The total natural uranium (2025 to 2110)*	337831 tones	202973 tones	
The total spent fuel (or HLW) accumulated in the end of life cycle	37228 tones of SNF	High-level waste	5405 tones
		Plutonium	478 tones
		Minor actinides	54.7 tones

Nuclear Fuel Cycle Simulation System (NFCSS) (iaea.org)

* Example for calculation for NES with 10 PWRs (45GWd/t burn up) having a 60-years lifespan

Nuclear Fuel Cycle Simulation System (NFCSS): Further Developments

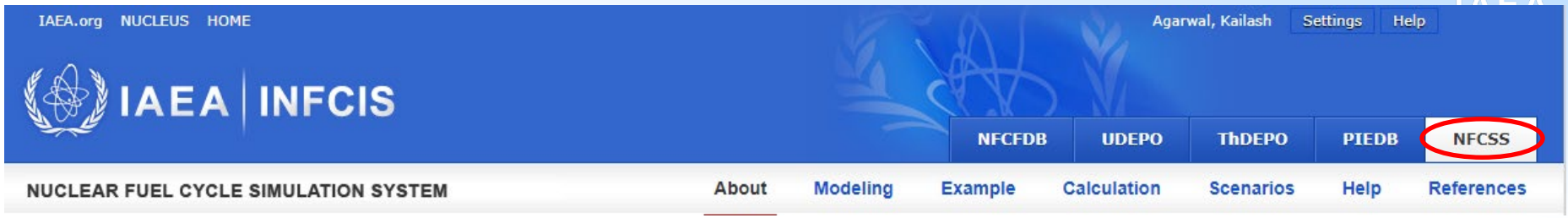

Activity completed:

- Migration to new IT platform (using modern software development standards and principles, eliminate security vulnerabilities)

In Progress

- Development of new simulation model for MSR fuel cycles
- Development of new simulation model for calculation DGR footprint
- Feasibility of adding fuel cycle cost calculation
- Integration of Radio-toxicity and Decay Heat calculations
- Simulation with MA containing fuel
- Scenario studies with HALEU fuel

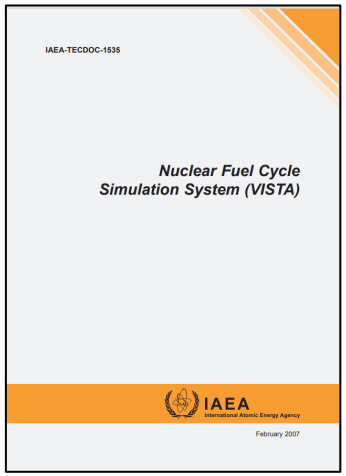

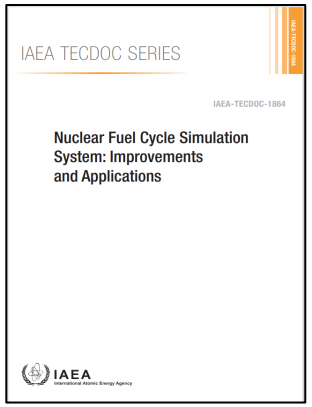

Nuclear Fuel Cycle Simulation System (NFCSS) (iaea.org)

NFCSS applicability to Advanced Reactors: MSR model (Th base Fuel cycle)

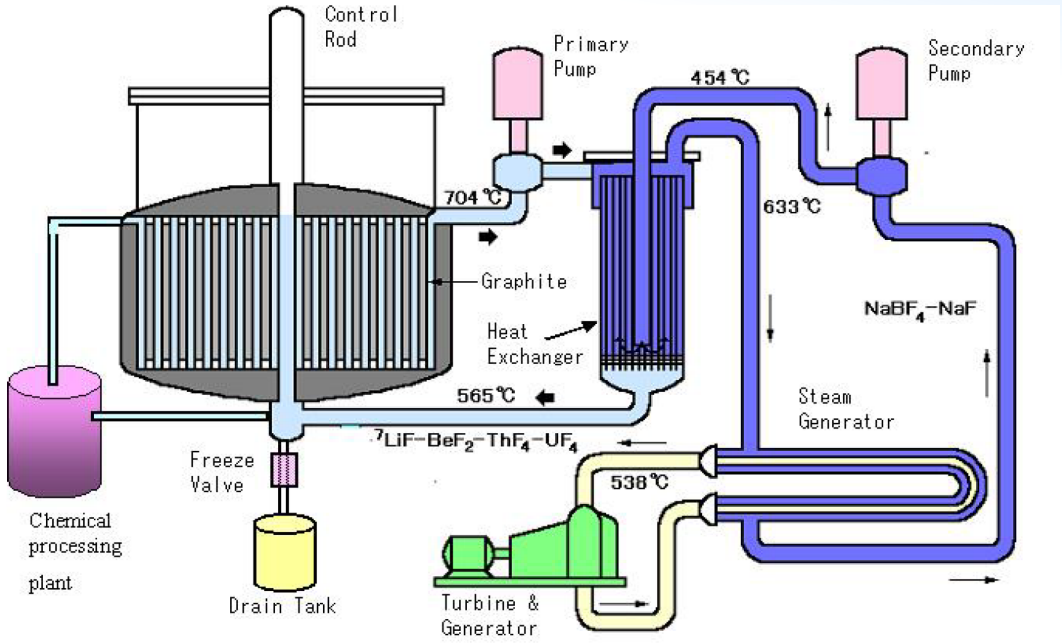

Case Studies for Simulation of MSRs

1. Case-1 Th/^{233}U fuel
2. Case-2 Th/Pu fuel
3. Case-3 Th/LEU fuel
4. Case-4: Fast spectrum MSR (Th/^{233}U fuel)

- *Batch reprocessing after 1 year*
- *Comparison with ORIGEN and SRAC codes*

Results

1. Case -1 Very close with ORIGEN (+/- 5%)
2. Case-2 Within 11.4%
3. Case-3 Within 12.9%
4. Case-4 Within 10%

E-Learning course on Nuclear Fuel Engineering, Fabrication and Operation Behaviour

The course comprises 4 Modules with 17 Lectures in total

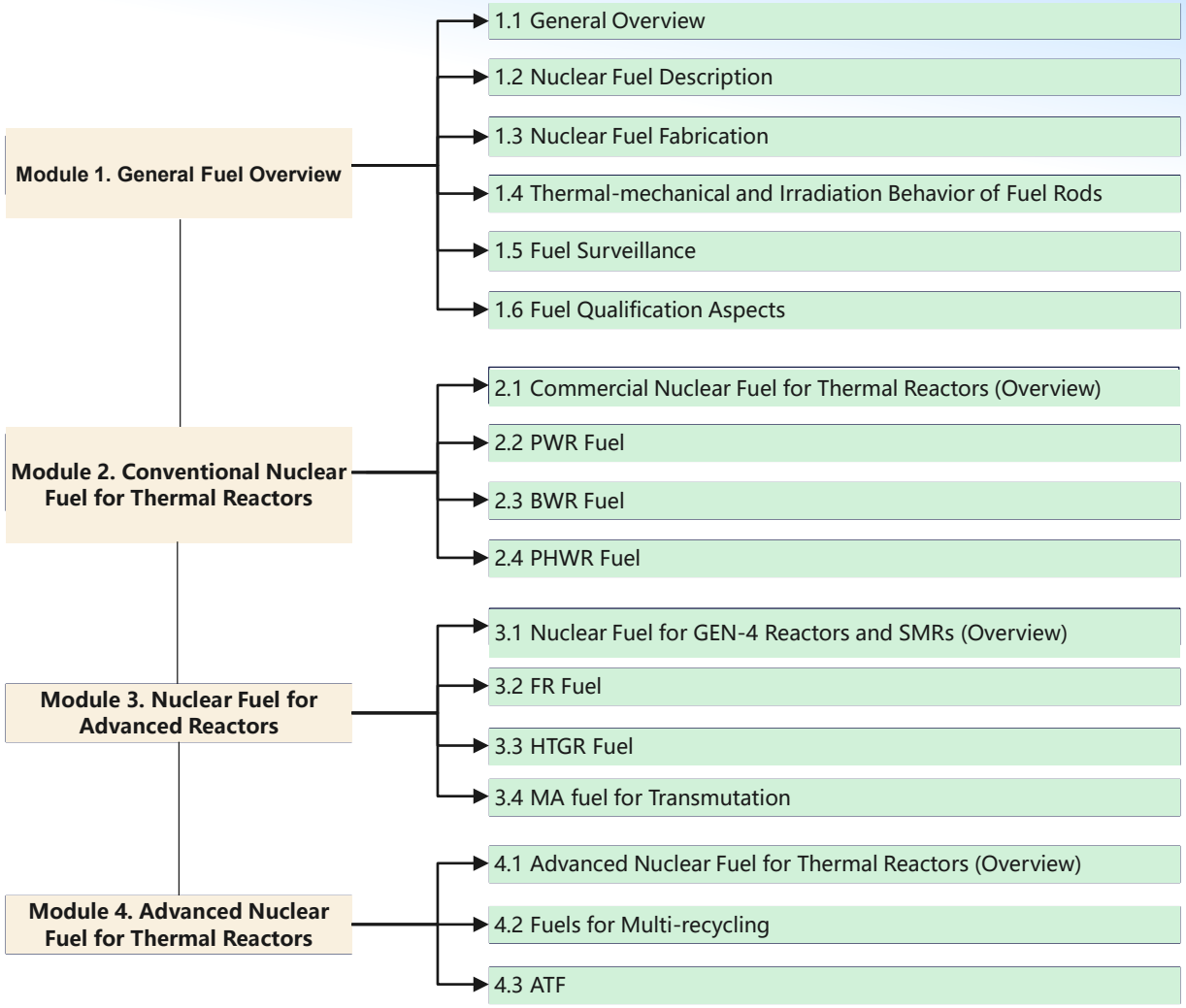

Each Lecture has a duration of about 45 minutes + Quiz (Q&A)

OPEN-LMS: All courses (iaea.org)

Module 3. Nuclear Fuel for Advanced Reactors

- **Lecture 3.1: Nuclear Fuel for Advanced Reactors (GEN-4) and SMRs (overview)**
- **Lecture 3.2: FR Fuel**
- **Lecture 3.3: HTGR Fuel**
- **Lecture 3.4: MA fuel for transmutation**

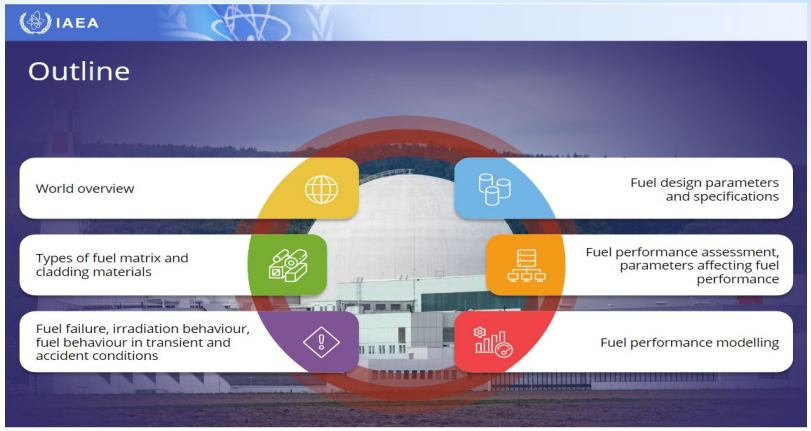

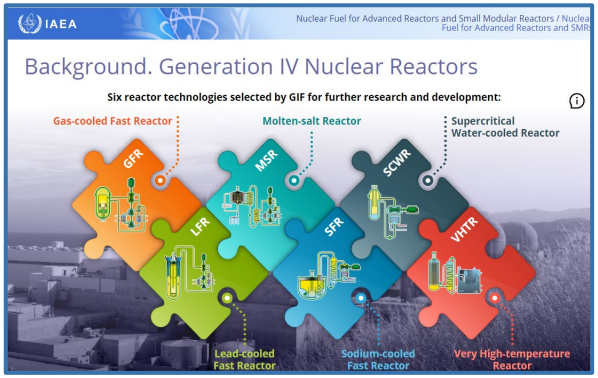

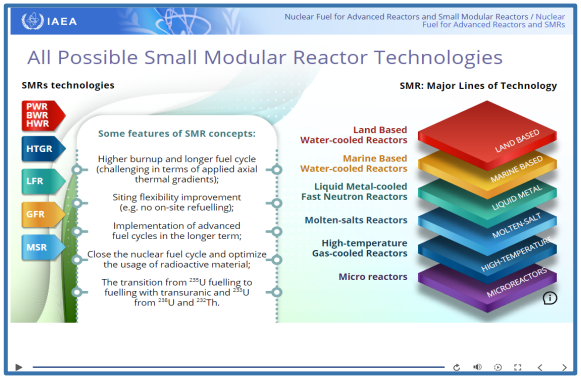

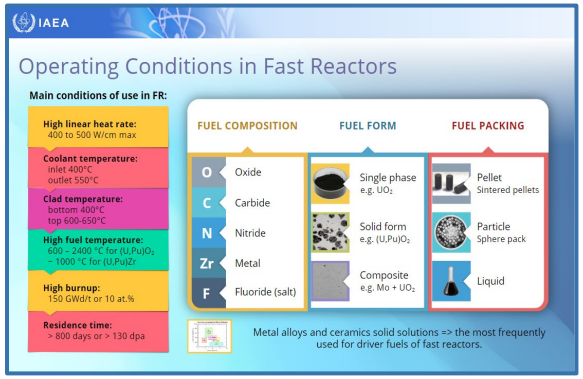

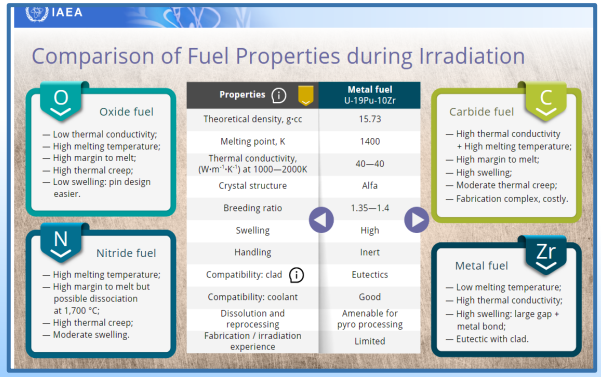

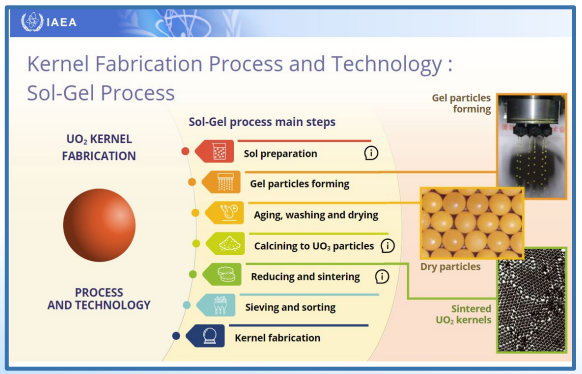

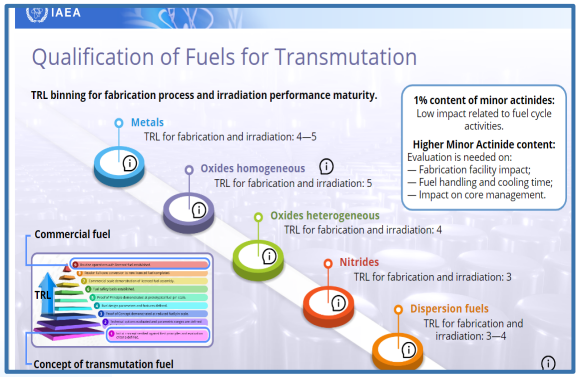

Module 4. Advanced Nuclear Fuel for Thermal Reactors

- **Lecture 4.1: Advanced Nuclear Fuels for Thermal Reactors (overview)**
- **Lecture 4.2 Fuels for multi-recycling**
- **Lecture 4.3: Accident tolerant fuel (ATF)**

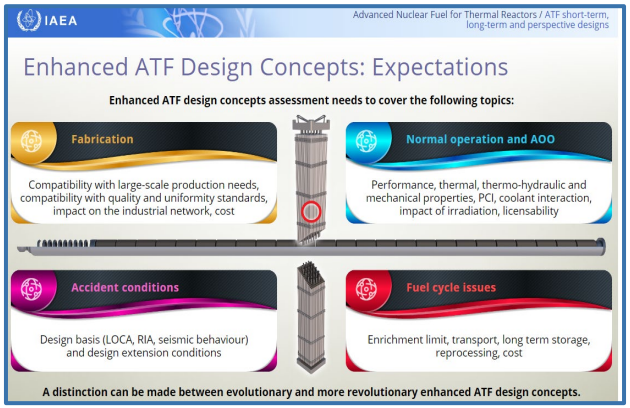

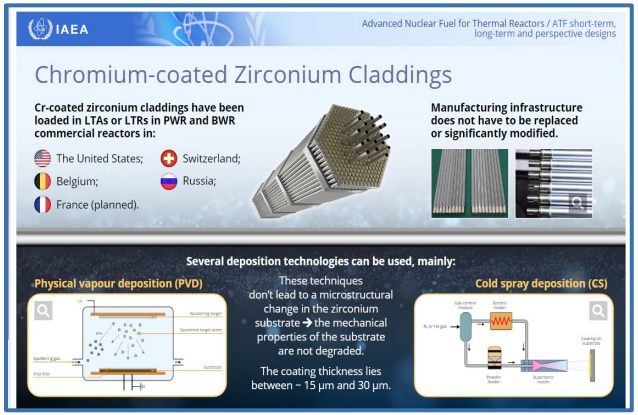

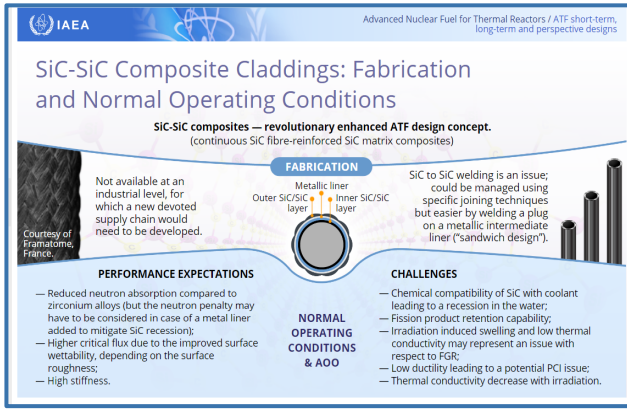

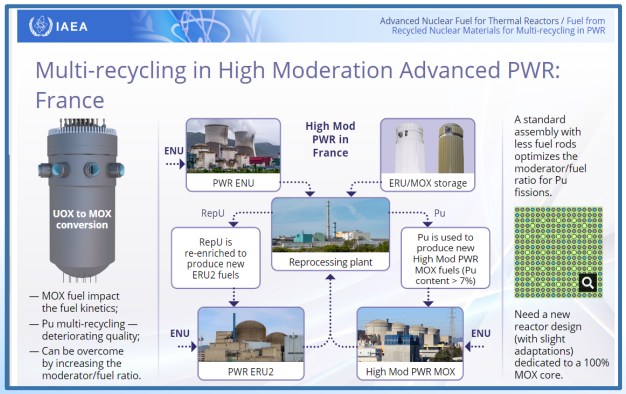

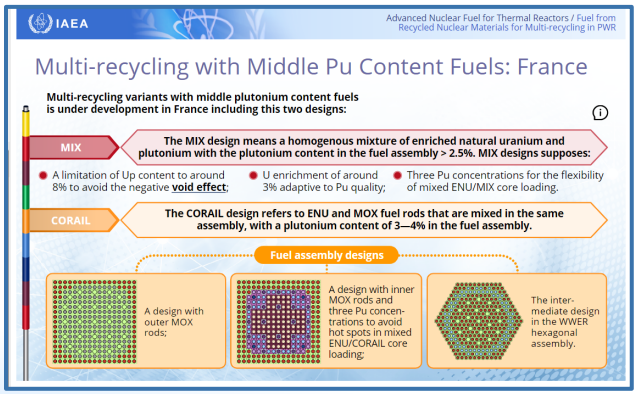

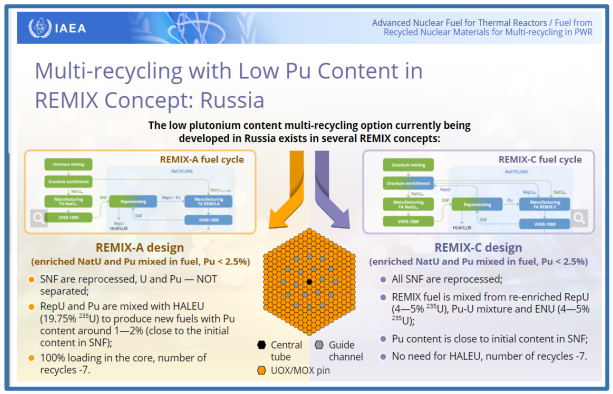

IAEA
International Atomic Energy Agency

Thank you

Contact information

Email: A.Khaperskaia@iaea.org

D. Bottomley
JRC Karlsruhe

Improving chemical thermodynamics knowledge of severe accidents within the OECD - TCOFF2 Project

The OECD project TCOFF-2 (Thermodynamic Chemistry of Fission Products - Part 2) is an extension of the original project that was part of the near-term projects intended to support the Fukushima Dai-ichi decommissioning efforts. This second part continues to be mainly financed by Japanese Ministry (MEXT) with JAEA-CLADS support. TCOFF2 started in August 2022 and includes certain new material requirements compared to the first TCOFF project. These are increased emphasis on accident tolerant fuels (ATFs), certain actinides and fission products related to volatility/leachability but also certain combinations of the ceramic oxide systems important for MCCI behaviour.

Following a PIRT review of phenomena in TCOFF 1, there was in TCOFF2 a Task 1 to prioritise current needs, particularly for relevance to severe accident phenomena and alternative materials (ATFs). This included a re-evaluation and ranking of the thermodynamic systems to make a Systems Identification and Ranking Table (SIRT) for the improvement of the thermodynamic database foreseen in TCOFF2. The further systems for evaluation were then proposed by the partners according to their particular requirements; this resulted in over 150 thermodynamic systems. In the mid-year meeting (June 2023) discussions were made to rationalise these into the most important 20 systems.

The rationale for the reduction of systems to this limit will be explained in the talk, both those systems that were omitted as well as those finally included.

These systems will then be used as a priority list of work for the experimental call to members that will be launched by the TCOFF-2 project towards the end of the year 2023 with the intention to initiate the first projects soon afterwards.

.

28th Quench Workshop, December 05-07, 2023, Karlsruhe
Institute of Technology, North Campus

Improving chemical thermodynamics knowledge of severe accidents within the OECD - TCOFF2 Project

C. Journeau (CEA, DES, IRESNE, DTN, Cadarache, F-13108 Saint-Paul-lez-Durance, France),

S. Bechta, A. Komlev (KTH, NPS, Stockholm, Sweden),

M. Kurata, H. Ohgi, T. Matsumoto, M. Afiqa (JAEA, Japan),

M. Barrachin (IRSN, France),

A. Quaini (Université Paris-Saclay, CEA, DES, ISAS, DMPC, Gif/Yvette, France),

D. Bottomley, D. Serrano-Purroy (JRC Karlsruhe, Germany),

A. Itoh (Tokyo Tech., Japan),

K. Nakamura (CRIEPI, Yokosuka, Japan),

M. Steinbrück (KIT, Karlsruhe, Germany).

A. Dufresne (NEA-OECD, Paris, France)

Presented by D. Bottomley

The joint project on Thermodynamic Characterization Of Fuel Debris and Fission Products (TCOFF) is based on a scenario analysis of severe accident progression at the Fukushima Daiichi nuclear power station (FDNPS). It was initiated within the Nuclear Science Committee (NSC) of Nuclear Energy Agency (NEA).
The project was launched by the Ministry of Education, Culture, Sports, Science and Technology - Japan (MEXT), which provided the entire financial funding (approx.720 kEuros) over three years (June 2017 – June 2020).
It was also well- integrated into other Fukushima Daiichi (FDNPS) -oriented projects, that were organized under the auspices of the OECD and used the wide variety of the project partners to produce an upto date review of the uses of thermodynamic data for understanding the fuel & cladding degradation as well fission product behaviour.
It was successfully concluded in December 2021 with the delivery of an end report that also pointed out the future thermodynamic data needs both for experimental and modelling.

Original TCOFF project 2017-2020

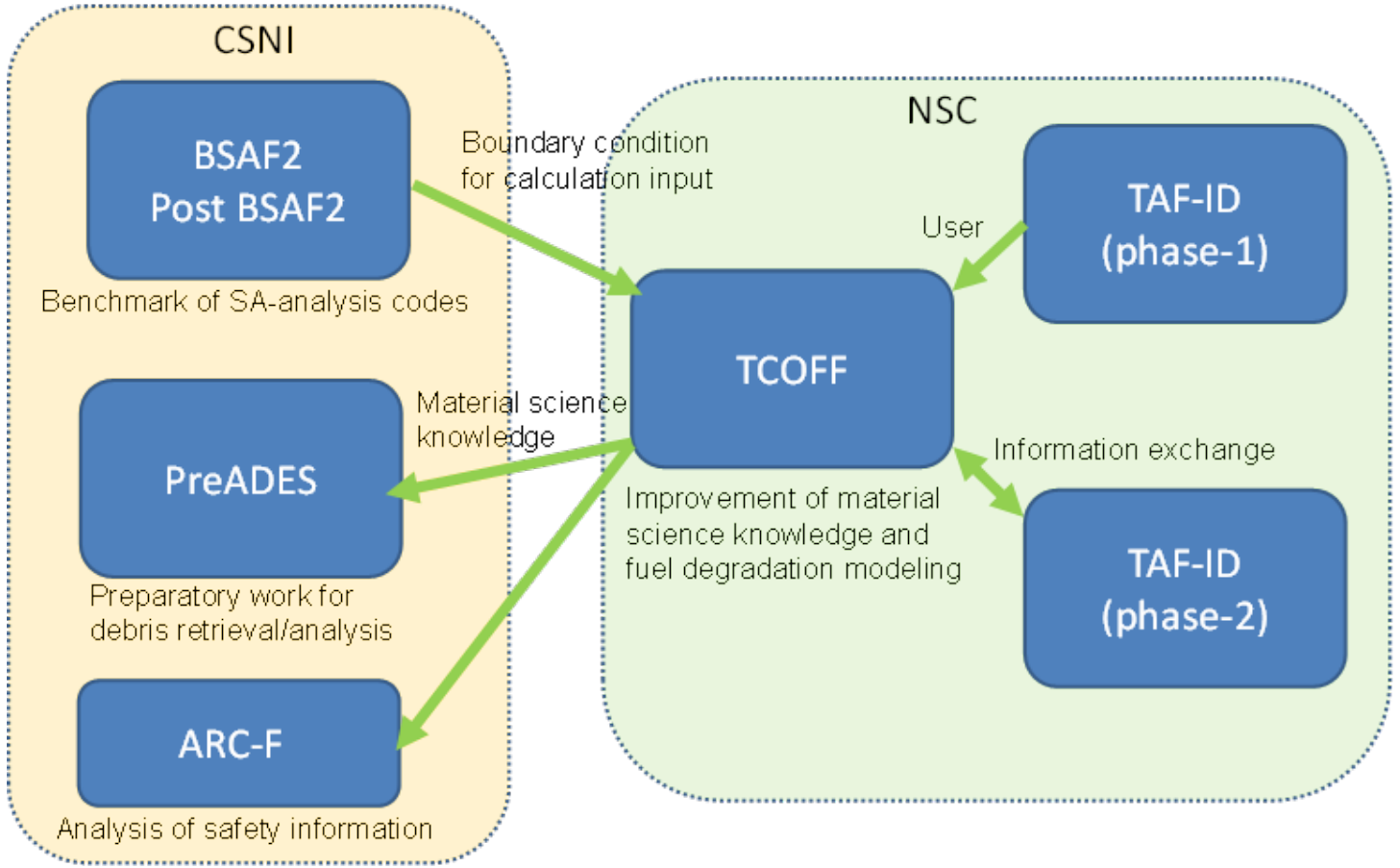

TCOFF = Thermodynamic Characterization of Fuel Debris and Fission Products

Task Force 1 was principally about Corium and Fuel elements and deepening of their thermodynamic knowledge and data, including TD databases extension, validation and testing.

Task Force 2 focused on Fission Product behaviour and chemistry in fuel and in primary circuit and containment buildings. The thermodynamic knowledge and data needed extension &/or improvement, validation and testing. Condition s relevant to the FDNPS were examined

Conclusions of the TCOFF project and formulation of TCOFF-2

As the TCOFF final report was finalised, a series of meetings of TCOFF participants + other interested institutes was held during summer 2020 to propose a second phase.

A draft programme of work based on the results of TCOFF was established and was successfully submitted to the

NEA Committee on the Safety of Nuclear Installation (CSNI) and the Nuclear Science Committee (NSC). Again MEXT ministry of Japan was contributing through JAEA a 50% total of the Funding.

The Program was divided into the five following tasks:

- Task-1: Prioritisation of the material science issues related to the severe accidents (SA) study
- Task-2: Improvement of the materials science knowledge regarding fuel core degradation and FP release (UO_2-Zry and ATFs)
- Task-3: Implementation of improved knowledge for the simulation of the accident behaviour (UO_2-Zry and ATFs)
- Task-4: Leaching phenomena
- Task-5: Training and Education

Notes (1) It was important to include an educational component – eg. young researchers exchanges to maintain competencies and promote young researchers skills in different SA research areas

(2) The Task 1 on prioritisation of material science issues and Thermodynamic systems was continued from the first project as needing updating in view of the new members and changes in members priorities. In particular, Task 3 (see above) was the inclusion of Accident–tolerant fuel (ATF) cladding systems that were under development by the Nuclear industry and authorities

The TCOFF-2 Project

Major tasks as in the TCOFF-2 Agreement with OECD- NEA are the following:

- **Task-1**: **<u>Prioritisation of the material science issues related to the severe accidents (SA) study</u>**

- **Task-2**: Improvement of the materials science knowledge regarding fuel core degradation and FP release (UO_2-Zry and ATFs)
- **Task-3**: Implementation of improved knowledge for the simulation of the accident behavior (UO_2-Zry and ATFs)

- **Task-4**: Extension of the leaching experimental database to better evaluate mid and long-term stability of degraded cores

Task 4 slightly modified

- **Task-5**: Training and Education

This will include workshops and an International Call for Research Proposals, this will sponsor students on exchanges & Courses.

Notes:
It will be linked to the parallel project: FACE: which follows the Pre-ADES & ARC-F projects that accompanied the TCOFF-1 project
There will also be links to the OECD-NEA QUENCH –ATF joint project and the IAEA CRP (Combined Research Proposal) ATF-TS

Database Systems & Models used in TCOFF 1 & 2: IRSN

Nuclear fuel databases developed at IRSN since 1988- **NUCLEA** for Corium applications & **MEPHISTA** for fuel & fission product chemistry

NUCLEA database (IRSN) is developed particularly for core degradation (In & Ex-Vessel).

- contains Gibbs Energies for 18 elements (O-U-Zr-Ag-In B-C-Fe-Cr-Ni-Ba-La-Ru-Sr-Al-Ca-Mg-Si + Ar-H (gas phase)) systems.
- More than 500 stoichiometric compounds are modelled as well as more 50 solution phases.
- Key systems for core degradation and corium progression in the vessel have only been fully assessed for ternary systems .
- MEPHISTA (IRSN) database is more specifically developed for the normal & accident conditions of fuel & FP.
- contains Gibbs energies for 14 elements (O-U-Pu-Zr-Fe-Si-C-Ba-Ce-Cs-La-Mo-Ru-Sr + Ar-H gas systems)
- more than 230 stoichiometric compounds and 40 solution phases.

Used for validation of large number of severe accident tests also for the ASTEC code for in-vessel retention & MCCI models.

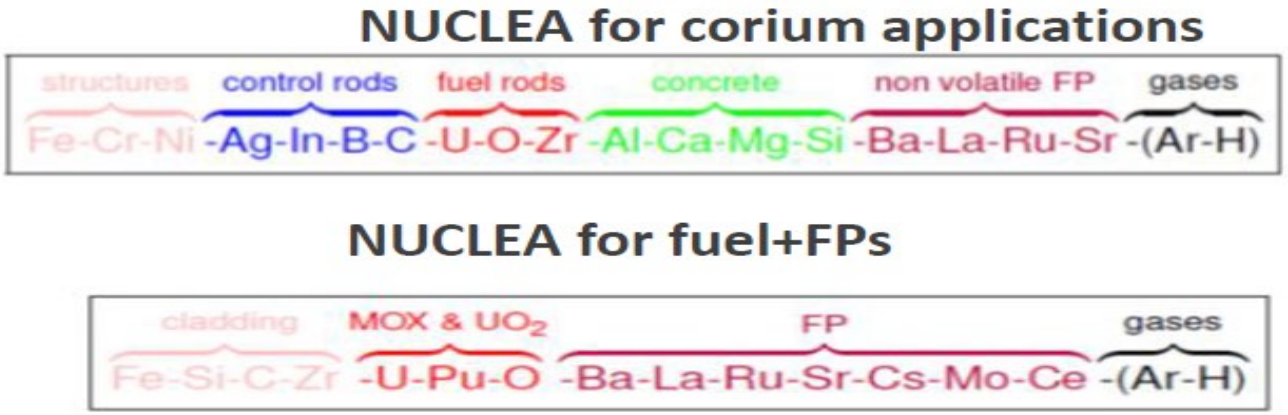

Comprehensive & reliable databases for Nuclear Fuels (oxides, carbides), Corium, Fission Products, & In- & Ex-Vessel Structural Materials

Current Version NUCLEA: 18 elements + Ar + H,
153 binary systems,
19 ternary systems,
95 pseudo binary oxide systems
15 pseudo ternary oxide systems

Current Version MEPHISTA: 14 elements + Ar + H,
91 binary systems,
18 ternary systems,
36 pseudo binary oxide systems,
2- pseudo ternary oxide systems

Database Systems & Models used in TCOFF 1 & 2: CEA & NEA

SUMMARY

The (CEA/NEA) TAF-ID database uses Calphad (Gibbs energy minimisation) for calculation and provides a total description as of Apr 2021, 206 binary and 72 ternary systems for modelling of different types of fuels & minor actinides, fission products and structural materials.

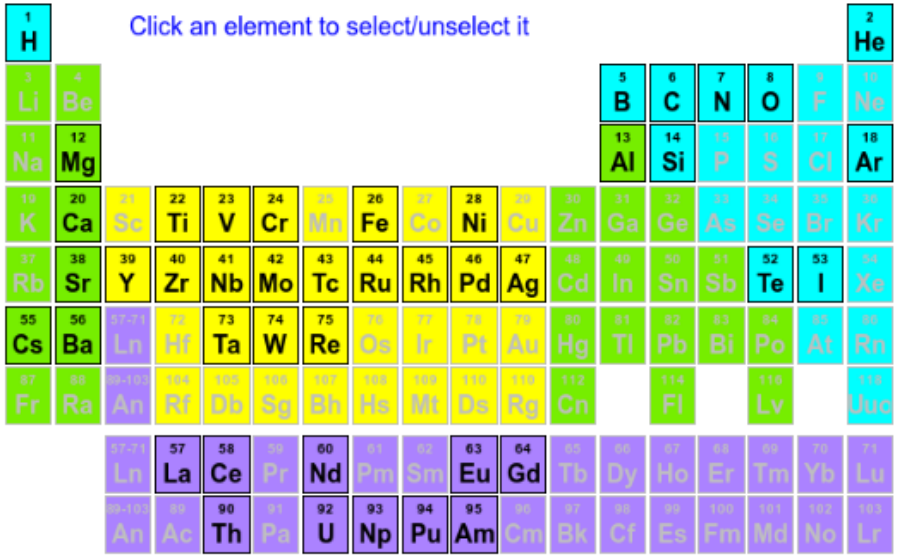

NEA joint project since 2013.

3rd phase - Thermodynamics of Advanced Fuels – International Database (TAF-ID) Project started in January 2023, with 11 member organisations from 7 countries and the European Commission

Comprehensive and reliable database for:

- Nuclear fuels (oxide, metallic, nitride, carbide) + MA
- Fission products
- Structural materials (in- and ex-vessel)

Current version (v16, summer 2023) includes 43 elements with:

- **247** binaries
- **114** ternaries
- **2** quaternaries

Areas of application:

- **Severe accident studies**, in- and ex- vessel
- **Fission product chemistry**, including 22 FP elements
- **Fuel chemistry**, including fuel cycle and fuel fabrication

See Guéneau et al. CALPHAD (72) 2021 and TAF-ID website

Database Systems & Models used in TCOFF 1 & 2: PSI & JAEA

PSI-GEMS Modelling Package & HERACLES Database

GEMS: flexible TD modelling package

- Aqueous elevctrolyte
- Non-ideal gaseous fluids, solis solns. & (ionic) melts
- Absorption, ion exchange
- Metastable species/ phases, kinetic
- ~ 30 different mixing models

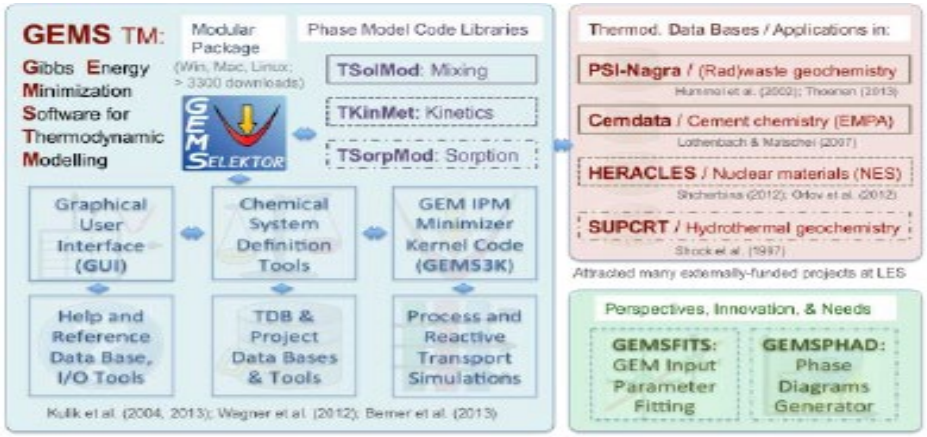

HERACLES: initially contained only oxides & carbides –for modelling of FP release

- It was futher extended for modelling of MSR–related issues (relevant fluoride & chlorides).
- Within TCOFF project has been extended to support Severe Accident modelling (Cr,Ni,B related spp., SS, Inconel).
- Currently covers metal, actinides, fission products gases salts
- >600 condensed compounds
- >400 gaseous & plasma species

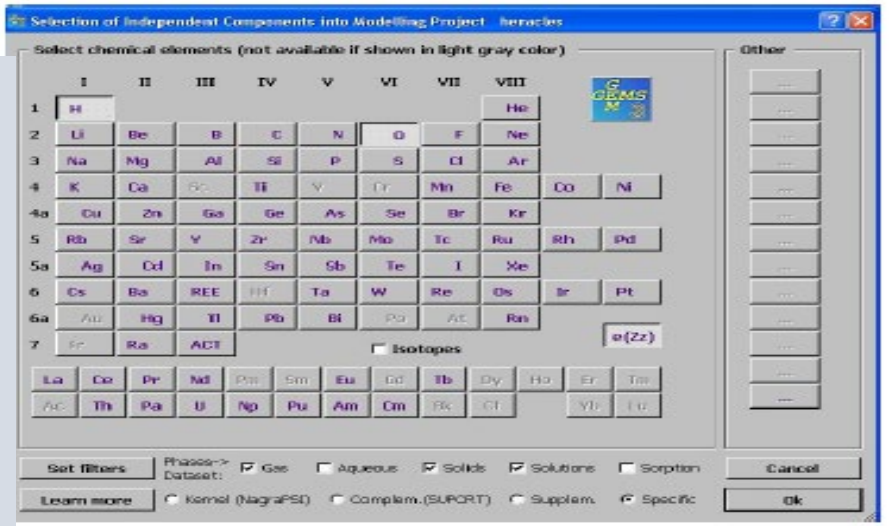

JAEA Database

JAEA database concentrates on MCCI interactions, and developed a thermodynamic database of Al_2O3-CaO-SiO_2-UO_2-ZrO_2-FeO/Fe_2O_3 quasi-hexagonal system using a cell model compatible with the SOLGASMIX code. It has assessed 28+15 = 43 ternary oxide systems;

14 binary oxide systems.

Systems examined in TCOFF

Task Force: 1 corium and fuel

(iii) U-Zr-O/U-Zr-Fe-O systems (+NITI) plus the effects of absorber elements/compounds Ag-In-Cd & B_4C

iv.) Multi element systems (Fe-Cr-Ni/B_4C/Zr/UO_2) and exptl. studies of fission products: Ba-Sr-Cs-Mo-O system;

v. In vessel corium and MCCI : Al_2O_3-CaO-SiO_2-UO_2-ZrO_2-FeO/Fe_2O_3

vi. FDNPS issues (examn.- testing of lava samples: U,Zr,Si,O systems

Task Force 2-Fission Products

ii. Cs-complex oxides ,Cs-SS interactions Cs-O-H; Cs-Mo-O; Cs-Si-O; Cs-Fe-Si-O + Sr,

iii. Semi-volatile FPs:

1); Ba-Mo-O; Cs–Ba-Mo-O; Cs-$(MoO_4^{2=})_n$, Cs_2O-SiO_2; Cs_2O-B_2O_3, $Cs_2$0-Fe_2O_3 Cs-Sr-Cl-O; Sr-Zr-O; Sr-Si-O

The major deficits identified are related to:

(i) the chemistry of the fuel corium (in-vessel) systems U-Zr-O and U-Zr-Fe-O,

(ii) the effects of absorbers Ag-In-Cd and B_4C,

(iii) the debris behaviour in the lower plenum and RPV failure,

(iv) the chemistry of the MCCI systems (e.g. CaO-Al_2O_3-SiO_2-MgO-$(Na,K)_2O$ + UO_2 + ZrO_2 + FeO), and

(v) testing of MCCI scenarios

Table 5: Status of the ternary sub-systems to describe the interaction between stainless steel: Fe-Cr-Ni and boron carbide: B_4C

Ternary sub-systems of Fe-Cr-Ni / B_4C	TAF-ID database	NUCLEA database
Fe-Cr-Ni	**Modelled**	**Modelled**
Fe-Cr-B	Not modelled	Not modelled
Fe-Cr-C	Not modelled	**Modelled**
Fe-Ni-B	Not modelled	Not modelled
Fe-Ni-C	Not modelled	**Modelled**
Fe-B-C	**Modelled**	**Modelled**
B-C-Ni	Not modelled	Not modelled
B-C-Cr	Not modelled	Not modelled
C-Cr-Ni	Not modelled	**Modelled**
B-Cr-Ni	Not modelled	Not modelled

Table 6: Status of the ternary sub-systems to describe the interaction between stainless steel: Fe-Cr-Ni, boron carbide: B_4C and zirconium

Ternary sub-systems of Fe-Cr-Ni / B_4C / Zr	TAF-ID database	NUCLEA database
Fe-Zr-Cr	Modelled	Not modelled
Fe-Zr-Ni	Not modelled	Not modelled
Fe-Zr-B	Modelled	Not modelled
Cr-Zr-Ni	Not modelled	Not modelled
Cr-Zr-B	Not modelled	Not modelled
Cr-Zr-C	Not modelled	Not modelled
Ni-Zr-B	Not modelled	Not modelled
Ni-Zr-C	Not modelled	Not modelled
B-Zr-Ci	Modelled	Modelled
C-Zr-Fe	Not modelled	Not modelled

TCOFF2 project: (ab Jan. 2023):
Task 1 SIRT - Identification of relevant systems

Report from Feb 1st, 2023 meeting of TCOFF2-Task1
System Identification and Ranking Table
by Christophe Journeau (CEA), Sevostian Bechta (KTH), Masaki Kurata (JAEA), Ayumi Itoh (TokyoTech)

Task 1: a) Prioritization of material science issues related to the SA study

- **Systems Identification and Ranking Tables**

- Adaptation of more classical Phenomena Identification and Ranking Tables to chemical thermodynamics and material science
  - Identification of systems of interest for various applications (fuel x accident phenomena)
    - Links with existing PIRTs and reviews (other projects…)
  - Figures of Merit (FoMs):

    These include : a) Importance for safety
    - severe accident phenomena
    - Fission Product behavior and source term

      b) Needs of further R&D
    - Lack of data –what is missing?
    - Need of improvement of database(s) –what is not well modelled

Task 1: a) Prioritization of material science issues related to the SA study

Both reactors with conventional fuel systems and Accident Tolerant Fuels (ATF) (incl. cladding and control rods) will be addressed.

The System Identification and Ranking tables will cover the following aspects:

- **Key systems** to be tackled for the **corium progression** and the **FPs behaviour** in the following phases of the accident :
  - Normal fuel performance ?
  - departure from normal operation,
  - fuel degradation,
  - fuel in-vessel relocation,
  - molten pool formation/debris formation,
  - RPV failure,
  - ex-vessel phenomena (typically, MCCI);

  Ideally, the prioritisation exercise will also identify the data where accident modelling/description is particularly sensitive to, thus indicate the level of accuracy required for the data.
- For each identified system: Assess the level of knowledge and identify most critical/pressing gaps in terms of TD modelling.
  - absence of thermodynamic modelling,
  - missing or poor data,
  - potentially critical lack of models' accuracy or range of accident conditions requiring modelling,
  - Education knowledge gap ;
- For each identified knowledge gap: evaluate possibility to address in the TCOFF 2 project, either through
- 1) in-kind contributions or
- 2)with focused R&D funded by the project, or both.

Task 1 –b) Identification of relevant systems –TCOFF2 task1 work plan

1st Semester of TCOFF2 project: Identification of relevant systems

- Focus just on the list of binary/ternary systems to be included (ranked on a 1-4 system (4 highest level) for a) importance to severe accidents, b) level of knowledge)
  - Possibility to introduce higher order systems (e.g. U-Zr-Pu-O)
- Organization of the System table and search for forgotten systems
  - TF1 core group (Deadline 15 March 2023)
- Need to use some “PIRT-like” tables to link phenomena of importance within a type of severe accident to the TD system considered.
  - Japanese team presented their tables for classical and advanced fuels that could serve as help for other participants.

  So a 2nd more detailed form was sent round by JAEA with an additional PIRT type evaluation where the important TD systems were noted for: a) the major reactor systems and b) by the major stages or types of the severe accident.

Extract of the first SIRT Table sent round of particular reactor systems or accidents. showing input from JRC-Ka (lines 129-140).

	Systems	Classical LWR	High BU, High enrichment fuel	Fukushima Daiichi, TMI2, Chernobyl	Short term ATF (Cr-coated Zry, FeCrAl)	Long Term ATFs SiC ; SiCf/SICm	Advanced Modular Reactors	Leaching	Other (specify)	Raw Data	Databases
System 1	Al,Cr,Fe										
	Al,Fe,O										
	Al,Fe,U										
	O,Sn,Zr										
	O,U,Zr										
System 94	Pu,U,Zr	Does this include U,Zr,Pu,O, or should this be included at the end of the pseudi-ternary diagrams									
	Si,Pu,U										
	SiO2,ZrO2										
	SiO2,ZrO2,UO2										
System 129	UO2,ZrO2,PuO2	Note 1	for MOX fuel -Zr-cladding system -maybe UO2-PuO2-ZrO2-Cr2O3 for Cr-coated Zr cladded systems								
	CaO,MgO,Al2O3,FeO	Note 2	additional pseudo-quinary system for cement+rebar 'baseline corium' composition ?								
	(Mi,M2,M3)Oy	Note 3	For all trimetallic systems - check selected mixtures for their oxides (M1,M2,M3)x(O)y -probably the most important would be the (Fe,Ni,Cr)x Oy spinels for conventional fast reactor cladding or (Fe,Cr, Zr)O mixed oxides-for Cr-coated-Zr/UO2 fuels.								
	Ru, O	Note 4	Ru oxides and mixed oxides								
	Ru, Cs, O										
	Ru,Mo,O										
	Ru,B,O										
	Sr,O										
	Sr,Cs,O	Note 5	add the System Cs,O, Sr etc. - for comparison with Cs, O,Zr (sys. No. 57) to check for CsSrO3 compounds as FP, and any potential volatility ?								
	Sr,Cs,U,O										
System 140	Sr,U,Zr,O										

Total systems now: >140

Input in lines 94, 129-140: JRC-KA proposals to include mixed-fuel Pu,Zr,U ,O systems and various FP systems such as Ru, Sr, Mo,Cs,O with B,U,Zr,O, + an MCCI system : CaO, MgO, Al_2O_3, FeO (for 1F).

SIRT working table (Example) provided by JAEA

As a helpful tool for discussion

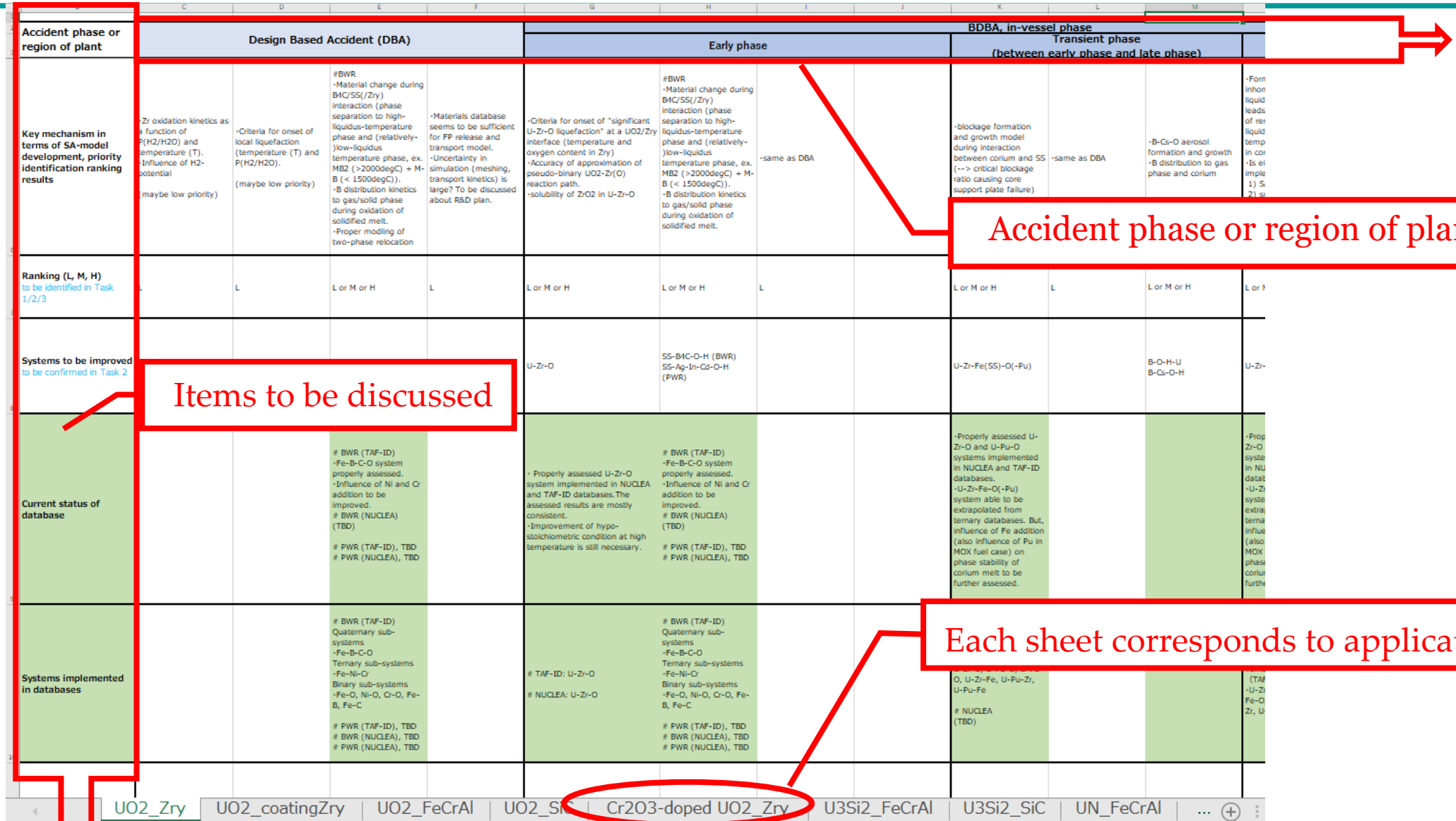

Accident phase or region of plant	Design Based Accident (DBA)				BDBA, in-vessel phase: Early phase				BDBA, in-vessel phase: Transient phase (between early phase and late phase)			
Key mechanism in terms of SA-model development, priority identification ranking results	·Zr oxidation kinetics as a function of P(H2/H2O) and temperature (T). ·Influence of H2-potential (maybe low priority)	·Criteria for onset of local liquefaction (temperature (T) and P(H2/H2O). (maybe low priority)	#BWR ·Material change during B4C/SS(/Zry) interaction (phase separation to high-liquidus-temperature phase and (relatively-)low-liquidus temperature phase, ex. MB2 (>2000degC) + M-B (< 1500degC)). ·B distribution kinetics to gas/solid phase during oxidation of solidified melt. ·Proper modling of two-phase relocation	·Materials database seems to be sufficient for FP release and transport model. ·Uncertainty in simulation (meshing, transport kinetics) is large? To be discussed about R&D plan.	·Criteria for onset of "significant U-Zr-O liquefaction" at a UO2/Zry interface (temperature and oxygen content in Zry) ·Accuracy of approximation of pseudo-binary UO2-Zr(O) reaction path. ·solubility of ZrO2 in U-Zr-O	#BWR ·Material change during B4C/SS(/Zry) interaction (phase separation to high-liquidus-temperature phase and (relatively-)low-liquidus temperature phase, ex. MB2 (>2000degC) + M-B (< 1500degC)). ·B distribution kinetics to gas/solid phase during oxidation of solidified melt.	·same as DBA		·blockage formation and growth model during interaction between corium and SS (--> critical blockage ratio causing core support plate failure)	·same as DBA	·B-Cs-O aerosol formation and growth ·B distribution to gas phase and corium	·Form inhom liquid leads of re liquid temp in co ·Is ei imple 1) S 2) su
Ranking (L, M, H) to be identified in Task 1/2/3	L	L	L or M or H	L	L or M or H	L or M or H	L		L or M or H	L	L or M or H	L or M
Systems to be improved to be confirmed in Task 2					U-Zr-O	SS-B4C-O-H (BWR) SS-Ag-In-Cd-O-H (PWR)			U-Zr-Fe(SS)-O(-Pu)		B-O-H-U B-Cs-O-H	U-Zr-
Current status of database			# BWR (TAF-ID) ·Fe-B-C-O system properly assessed. ·Influence of Ni and Cr addition to be improved. # BWR (NUCLEA) (TBD) # PWR (TAF-ID), TBD # PWR (NUCLEA), TBD		· Properly assessed U-Zr-O system implemented in NUCLEA and TAF-ID databases.The assessed results are mostly consistent. ·Improvement of hypo-stoichiometric condition at high temperature is still necessary.	# BWR (TAF-ID) ·Fe-B-C-O system properly assessed. ·Influence of Ni and Cr addition to be improved. # BWR (NUCLEA) (TBD) # PWR (TAF-ID), TBD # PWR (NUCLEA), TBD			·Properly assessed U-Zr-O and U-Pu-O systems implemented in NUCLEA and TAF-ID databases. ·U-Zr-Fe-O(-Pu) system able to be extrapolated from ternary databases. But, influence of Fe addition (also influence of Pu in MOX fuel case) on phase stability of corium melt to be further assessed.			·Prop Zr-O syste in NU datat ·U-Z syste extra terna influe (also MOX phase corium furth
Systems implemented in databases			# BWR (TAF-ID) Quaternary sub-systems ·Fe-B-C-O Ternary sub-systems ·Fe-Ni-Cr Binary sub-systems ·Fe-O, Ni-O, Cr-O, Fe-B, Fe-C # PWR (TAF-ID), TBD # BWR (NUCLEA), TBD # PWR (NUCLEA), TBD		# TAF-ID: U-Zr-O # NUCLEA: U-Zr-O	# BWR (TAF-ID) Quaternary sub-systems ·Fe-B-C-O Ternary sub-systems ·Fe-Ni-Cr Binary sub-systems ·Fe-O, Ni-O, Cr-O, Fe-B, Fe-C # PWR (TAF-ID), TBD # BWR (NUCLEA), TBD # PWR (NUCLEA), TBD			O, U-Zr-Fe, U-Pu-Zr, U-Pu-Fe # NUCLEA (TBD)			(TAF ·U-Z Fe-O Zr, U

Accident phase or region of plant

Items to be discussed

Each sheet corresponds to application

UO2_Zry | UO2_coatingZry | UO2_FeCrAl | UO2_SiC | Cr2O3-doped UO2_Zry | U3Si2_FeCrAl | U3Si2_SiC | UN_FeCrAl | ...

Reactor fuel systems for SIRT Application

- ✓ We prepared the following applications to be discussed. Name of sheet means a combination of fuel/cladding materials ("Fuel"_"Cladding").

Handouts: Bold-colored applications

1. **UO2_Zry sheet, *classical LWR***
2. **UO2_coatingZry, *conventional UO_2 pellet + Cr-coating cladding (ATF cladding)***
3. **UO2_FeCrAl, *conventional UO_2 pellet + Fe-Cr-Al cladding (ATF cladding)***
4. **UO2_SiC, *conventional UO_2 pellet + SiC/SiC cladding (ATF cladding)***
5. Cr2O3-doped UO2_Zry, *ATF fuel + conventional Zircaloy cladding*
6. U3Si2_FeCrAl, *ATF fuel + ATF cladding*
7. U3Si2_SiC, *ATF fuel + ATF cladding*
8. UN_FeCrAl, *ATF fuel + ATF cladding*
9. UN_SiC, *ATF fuel + ATF cladding*
10. **ATCR_Cr-coatingZrycladding, *Accident Tolerant Control Rod + ATF cladding***

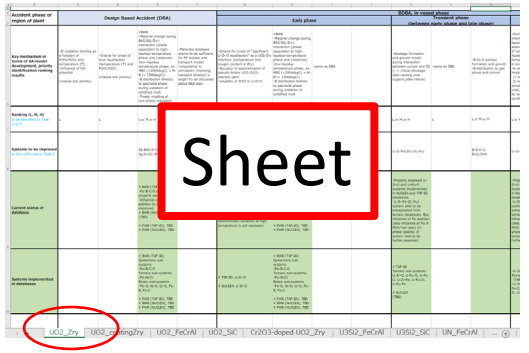

1 Sheet per reactor system.
green: previous systems (TCOFF);
black: added systems for TCOFF2

7 Stages of the Severe Accident (7 columns) in the JAEA SIRT table as filled out in Apr-Jun 23 for Task 1 Evaluation update

Time / Severity →

Accident phase or region of the plant	**Design Based Accident (DBA)**	**BDBA, in-vessel phase**			**Ex-vessel phase**		
		Early phase	"Transient phase(between early phase and late phase)"	Late phase	Relocation phase	MCCI	Uncategorized behaviors
Key mechanisms involved							
Ranking L,M, H importance							
Systems for improvement							
Current status of Database							
Systems implemented in database							

The lines for individual systems (eg. Pu-U-Zr-O or Al,Cs-O) were replaced by more detailed conditions for which particular TD system was important.

Systems
Al,Cr,Fe
Al,Fe,O
Al,Fe,U
Al,Fe,Ni
Al,Fe,Zr
Al,Ni,O
Al,Cs,O
Al,O,U
Al,O,Zr
Al,U,Zr

Task-1: Prioritisation of the material science issues related to the severe accidents (SA) study

The evaluation from the 1) Systems Identification and Ranking Table (SIRT),
that was derived from the 2) Phenomenon Identification Ranking Table (PIRT) now needed the next 2 stages:

3) incorporate the chemical thermodynamics and material science factors/problems and identify the thermodynamic systems for various accident scenarios/issues (ie *fuel* x *accident phenomena*) and
4) finally establish their Figures of Merit (FoMs) based on their importance for safety and the further R&D needs.

Discussions in SIRT between Jan & Jun 2023

Evaluation

The form was sent round and there a large number of imputs especially as this included needs for all reactor types and fuels as well as remaining systems that needed further investigation.
There had been requests to include:
1) (more) key fission products in the systems eg Ba, Sr, & Cs;
2) More Pu-containing systems for high burn-up and other fuels and also
3) Cs-Fe-Si (JAEA work in TCOFF) –Cs-steel contamination,
4) ATF fuels/ claddings required the inclusion of Ni/Cr/Fe (O) + U systems and Si/SiC+ U,O systems (SiC & SiC composite claddings).
5) Selected complex oxide systems for MCCI interactions for 1F concrete (JAEA), also key rare earths (eg. Eu) for checking their oxides as potential matrix tracers for UO_2 fuel

The total ended with over 200 systems for consideration, therefore rationalisation was necessary by regrouping elements into higher systems (eg. ternary oxides).

Example of Summary page of JAEA's SIRT Table showing the input from JRC-Ka for the first 2 systems: UO2-Zry & UO2_Cr-coated Zry (red writing in yellow squares)

System	Definition of system * corresponing to SIRT ~~ppt~~ report ? -p7	Accident phase or region of plant	Design Based Accident (DBA)				BDBA, in-vessel phase										
							Early phase				Transient phase (between early phase and late phase)			Late phase			
UO2_Zry	Classical LWR Fukushima Daiichi	Accident phenomena, for which improvement of understanding is necessary to be discussed with Task-1/2/3	Ballooning of Zry-cladding H2-absorption/desorption in Zry-cladding	Pellet/cladding interaction (DBA condition)	Control blade degradation (BWR) Control rod degradation (PWR) Interaction between metallic melt and channel box (BWR) and fuel rods (PWR)	FP release	Pellet/cladding interaction (BDBA condition)	Control blade degradation (BWR) Control rod degradation (PWR) Interaction between metallic melt and channel	FP release	Others	Slumping/candling (in-vessel relocation) Blockage (core permeability)	FP release FP transportation FP deposition	Others	Corium pool	Interaction between corium and RPV (including interaction with CRGT in BWR case)	FP release FP transportation FP deposition FP redistribution between oxidic/metallic phases	Others
		Systems to be improved to be confirmed with Task 2	U-Zr-O-H	U-Zr-O-H + Te,I	SS-B4C-O-H (BWR) Ag-In-Cd (PWR)	Ag, In, Cd, I, Ru, Te, B, Cs, U, Fe, Cr, O, Si,	U-Zr-O	SS-B4C-O-H (BWR) SS-Ag-In-Cd-O-H (PWR)	Ag, In, Cd, I, Ru, Te, B, Cs, U, Fe, Cr, O, Si,		U-Zr-Fe(SS)-O(-Pu	Ag, In, Cd, I, Ru, Te, B, Cs, U, Fe, Cr, O, Si,	B-O-H-U B-Cs-O-H	U-Zr-Fe(SS)-O(-Pu	U-Zr-Fe(SS)-O(-Pu	Ag, In, Cd, B, Cs, U, Fe, Cr, O, Si,	B-O-H-U
UO2_Cr-coating Zry	Short term ATF?	Accident phenomena, for which improvement of understanding is necessary to be discussed with Task-1/2/3	Ballooning of Cr-coated Zry-cladding H2-absorption/desorption in Cr-coated Zry-cladding	Pellet/Cr-coated cladding interaction (DBA condition) - corrosion cracking	Interaction between metallic melt and Cr-coated channel box (BWR) and Cr-coated fuel rods (PWR)	FP release (Influence of Cr-coating)	Pellet/Cr-coated cladding interaction (BDBA condition)	Interaction between metallic melt and Cr-coated channel box (BWR) and Cr-coated fuel rods (PWR)	FP release (Influence of Cr-coating)	Others	Slumping/candling (in-vessel relocation) Blockage (core permeability) Delayed relocation due to Cr-coating	FP release FP transportation FP deposition (influence of Cr-coexistence)	Others	Corium pool	Interaction between corium and RPV (including interaction with CRGT in BWR case)	FP release FP transportation FP deposition FP redistribution between oxidic/metallic phases	Others
		Systems to be improved to be confirmed with Task 2	Cr-Zr-O(-H) Zr-O-Sn(-H)	U-Zr-Cr-Cs-I-Te-O-H	Cr-O-SS-B4C-Zr Cr-O-SS-Ag-In-Cd	Cr-Cs-Mo-Sr-O	Cr-U-Zr-O	Cr-O-SS-B4C-Zr Cr-O-SS-Ag-In-Cd	Cr-Cs-Mo-Sr-O	Zr-Cr-O	Cr-U-Zr-O	B-Cr-Cs-Mo-Sr-O-H	B-O-H-U B-Cs-O-H			U-Zr-Fe-(Cr-Cs,Mo,Sr)-O	B-Cr-Cs-Mo-Sr-O-H

Showing the addition of Ba & Sr for MCCI systems & additional FP's eg Cs, Mo, Ru, Sr in B-O-H systems for Ex-Vessel aerosol transport

molten corium - concrete reaction FP redistribution between oxidic/metallic phases	FPs release and transport
U-Zr-Ba-O-(Al2O3, CaO, SiO2)-(Fe,Cr,Ni)-Sr	(Cs, I, Mo, Ru, Sr), (Fe, Si), (Ag, In-Cd), B, O, H

Ex-vessel phase

Relocation phase	MCCI			Uncategorized behaviors	
Interaction between molten corium and penetrations	Interaction with the sump coolant	molten corium - concrete reaction FP redistribution between oxidic/metallic phases	FPs release and transport	FPs transport via the primary coolant system	H2 explosion
U-Zr-(Fe,Cr,Ni)-O	U-Zr-(Fe,Cr,Ni)-O	U-Zr-Ba-O-(Al2O3, CaO, SiO2)-(Fe,Cr,Ni)-Sr	(Cs, I, Mo, Ru, Sr), (Fe, Si), (Ag, In-Cd), B, O, H	Cs, Fe, Cr, Mo, Ru, Si, H	reducing conditions, HP processes ??
Interaction between molten corium and penetrations	Interaction with the sump coolant	molten corium - concrete reaction FP redistribution between oxidic/metallic phases	FPs release and transport	FPs transport via the primary coolant system	H2 explosion
U-Zr-Fe-(Cr-Cs,Mo,Sr)-O		U-Zr-Ba-O-(Al2O3, CaO, SiO2)-Cr2O3	U-Cr-Cs-Mo-Sr-B-O-H		

Discussions in SIRT –contd.

Rationalisation (C.Journeau & S. Bechta)

- Focus was on the systems with the highest marks for the 11 selected accident applications of the SIRT table.
But there were 26 systems with high importance (>3.5/4 at least for one application) but combined with poor to medium knowledge.
- Systems were arranged in 2 classes corresponding to near term and long term applications;

Other systems, where thermodynamic factors are dominated by kinetics, eg. (H, O, U) have been discarded despite poor knowledge marks (1.5- 2.5/4);

- The U, Al system, initially overlooked was reinserted as it is important system for FeCrAl-fuel interactions, which is itself a very high priority for many members

• The Task-2 presented a comparison on UO_2-FeCrAl in steam that highlighted discrepancies between TAF-ID and NUCLEA, which led to the inclusion of the corresponding system Al_2O_3- Cr_2O_3, FeO, UO_2 in the list of high-priority systems.

Proposal (IRSN): R&D work could either focus on:

1) sub-systems to improve the database or on
2) multi-element compositions for direct inputs to SA codes (e.g. concrete mp. for MCCI codes

Following systems were suggested

• sub-systems for database improvement: Fe-Pu-O; PuO_2-UO_2-ZrO_2; Fe-Pu-U-Zr; Cr-Fe-Zr-O; U-Al; B-O-Zr; Cr-Cs-O; Cs-Si-O; B-Cs-O and Cs-O-Sr

• multi-element study: CaO-SiO_2-UO_2; FeO_x-Cr_2O_3-SiO_2-UO_2-ZrO_2; Al_2O_3-Cr_2O_3-FeO-UO_2

• This included ranking of importance

Discussions in SIRT –contd. (2)

Final Form of SIRT at TCOFF-2 Jun23 meeting where over 150 systems under consideration at March 23 were rationalised into 20 priority, multiple TD systems in reponse to specific needs (*ternary or higher)*

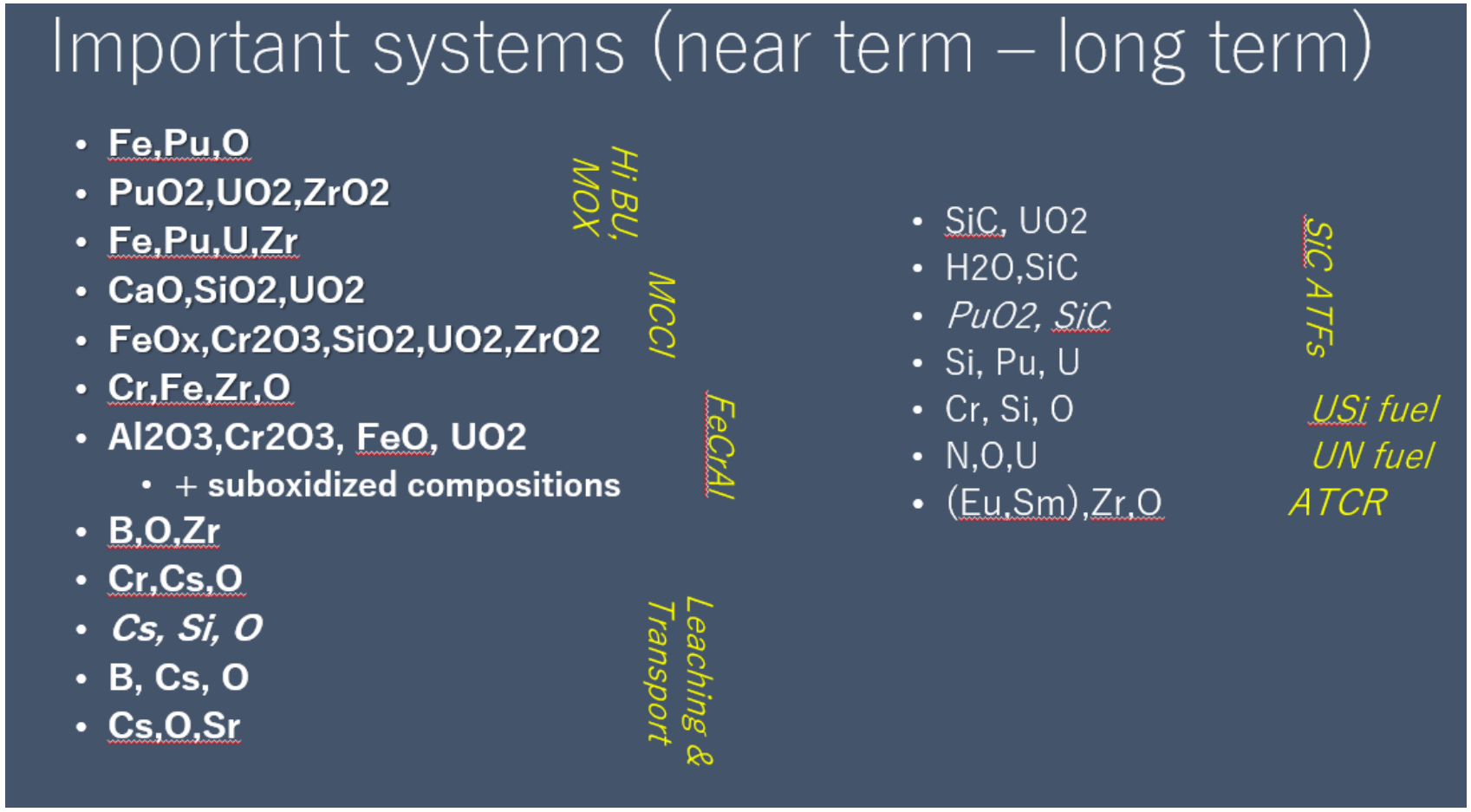

Figure 1 List of priority thermodynamic systems defined by Task-1 as proposed at the TCOFF-2 PRG Meeting in 26-27Jun23 along with the area of needs (marked in yellow)

PRG members provided confirmation of the 4 new systems included by Aug. 23.
New Syst: a) FeO_x,Cr_2O_3,SiO_2,UO_2,ZrO_2; b) Al_2O_3,Cr_2O_3, FeO, UO_2; c) SiC,H_2O; and d)(Eu,Sm),Zr,O.

Input into research proposals

1) The final updates in the second half of the year 2023 will have been incorporated into the final SIRT ranking for TCOFF2.

2) The committee for TCOFF2 technical proposal will also have had its first meeting and will have started the assessment of the first proposals received, based on the established SIRT table. There is 50k$ available pro year for upto 5 proposals (max. 1 year for any proposal).

Future Publications

- The finalised SIRT presented at the QUENCH workshop, 5-7 Dec. 2023;
- The SIRT to be presented at the ERMSAR conference, Stockholm in May 2024;

- A more specific paper will be written for submission to a journal (e.g. JNM), including more scientific background to justify selection of each system (~1 page/system);

Conclusions

- The second stage of the Thermodynamic Characterisation of Fuel and Fuel Debris (TCOFF-2) started end 2022/2023 and the initial task of re-evaluation of thermodynamic research priorities (Task 1: System Identification of Research Priorities - SIRT) is practically completed. After an initial review of the TD systems, it was extended to assess the various stages of a reactor accident for each reactor/fuel combination.
- It particularly includes new systems relating to Accident–Tolerant Fuels (ATF) and cladding systems and has been widened to consider other reactor fuel systems as well as revisiting ‘difficult’ combinations of complex fission product chemistry or higher BU and an additional MCCI system.
- This evaluation continues the series of assessment for severe accident research needs and then priorities (SARPs) and available facilities (Facilities evaluation) in nuclear countries in Europe and abroad eg. NUGENIA TA2/SARNET and SAFEST projects. This prioritization is necessary because of the expense and to optimize the benefits to nuclear safety and for nuclear facilities world-wide and the general public.
- This re-evaluation will already be used for the selection of first set of TCOFF-2 technical proposals that are being currently considered.
- In addition this SIRT table will assist other parallel projects at the OCED-NEA, particularly this should give direct support to on-going research and decontamination activities at Fukushima Daiichi.

J.-F. Martin
OECD-NEA

Update on the Nuclear Energy Agency's Activities related to Accident Tolerant Fuels

The OECD Nuclear Energy Agency serves its 33 member countries by addressing topics of shared interest in various fields related to nuclear energy generation. Both through its standing committees and working groups, as well as through ad-hoc joint undertakings, the Agency acts as a forum for its expert delegates to share progress on, and advance the developments of, advanced technology fuels among other topics.

The findings of recent NEA publications (oe.cd/neaatfsoar, oe.cd/neacsnitop19) focusing on ATF, HBU/HALEU and doped fuels are provided, notably focusing on the relevance and suggested adjustments of current safety frameworks in regards of such novel technologies. An overview of eight running joint undertakings, covering in-pile and out-of-pile transient testing as well as thermodynamic databases, allows to span the variety of activities developed by the OECD Nuclear Energy Agency in support of the deployment of advanced fuels.

The NEA assists its members with promoting international collaboration to support advanced fuel technologies by:

- Ensuring information exchanges between relevant international initiatives in the field
- Updating research priorities for ATF development, integrating, as far as feasible, state-of-the-art knowledge from R&D and implementation plans in NEA member countries
- Enhancing testing capabilities and developing FIDES-II as a framework for fuel testing in key research reactors, as well as other complementary joint projects
- Coupling experimentation with advanced modeling and simulation
- Preserving key experimental data and competencies

The author acknowledges contributions from fellow NEA colleagues Michelle Bales, Markus Beilmann, Alice Dufresne, Didier Jacquemain.

.

NEA
NUCLEAR ENERGY AGENCY

Update on NEA activities supporting ATF development

Julie-Fiona Martin

with input from M. Bales, M. Beilmann, A. Dufresne, D. Jacquemain

NEA committees (as of 1 January 2022)

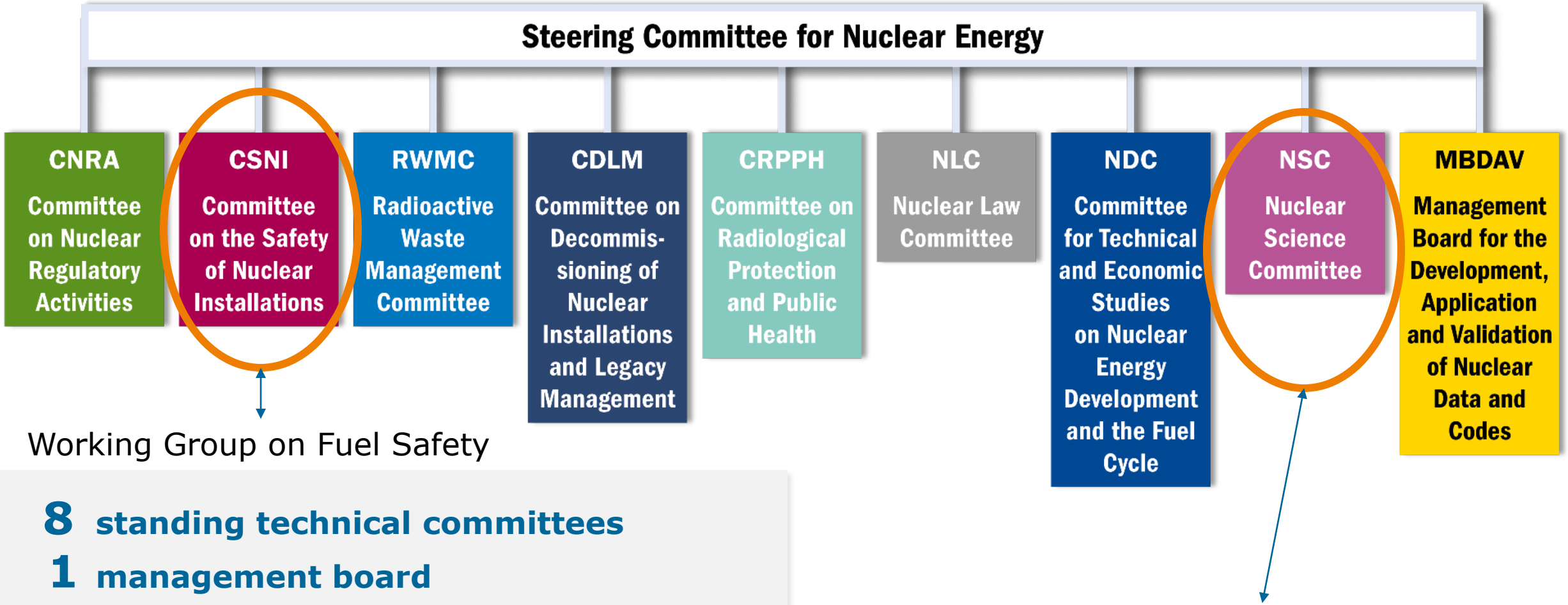

Working Group on Fuel Safety

Expert group on Reactor Fuel Performance

8 standing technical committees

1 management board

74 working parties and expert groups

Recently or soon-to-be published NEA reports on ATF

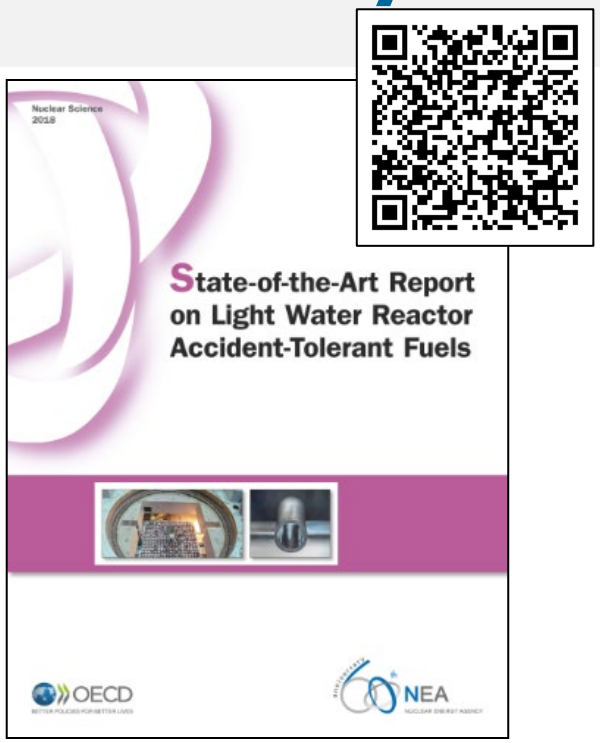

ATF design concept	EGATFL technology readiness level*	Relative impact on existing fuel safety criteria	Number of new phenomena	Relative magnitude of data gaps
Coated zirconium alloy cladding	4	Low	3	Low
FeCrAl cladding	3-4	Medium	2	Medium
Silicon carbide cladding	< 3	High	3	High
Doped UO_2 ceramic pellets	8	Low	0	Low
Uranium silicide ceramic pellets	< 3	High	1	High

* In 2018, the EGATFL report defined a TRL for each ATF design concept from 1 to 9, with 9 defined as *routine commercial-scale operation. Multiple reactors operating.*

CSNI and NSC both main contributors to ATF related studies with complementary approaches

- **State-of-the-Art Report on Light Water Reactor Accident-Tolerant Fuels**, 2018
- !RECENT! **Technical Opinion Paper No 19 on Applicability of Nuclear Fuel Safety Criteria to ATFs**, 2022
- !NEW! **Status report on fuel safety implication of extended enrichment**, in press

Safety research needs for ATFs, HBU/HALEU and doped fuels identified

NEA Joint Projects

Cooperation through projects

- Share world-wide expertise on safety topics and experimentation
- Share resources, leveraging investments and facilities
- Maintain key research facilities and competencies, support operating agents, contribute to education
- Facilitate cooperation between countries and various stakeholders

Applications and perspectives

- Understand phenomena that affect safety and sensitivities to safety (e.g. data for assessing accident management)
- Quantify and reduce uncertainties
- Obtain high quality data for safety code validation, benchmark safety codes
- Be ready for the future
  - License renewal of existing reactors
  - New reactor applications (light water, non-light water, SMRs)

On-going OECD/NEA joint undertakings addressing ATF

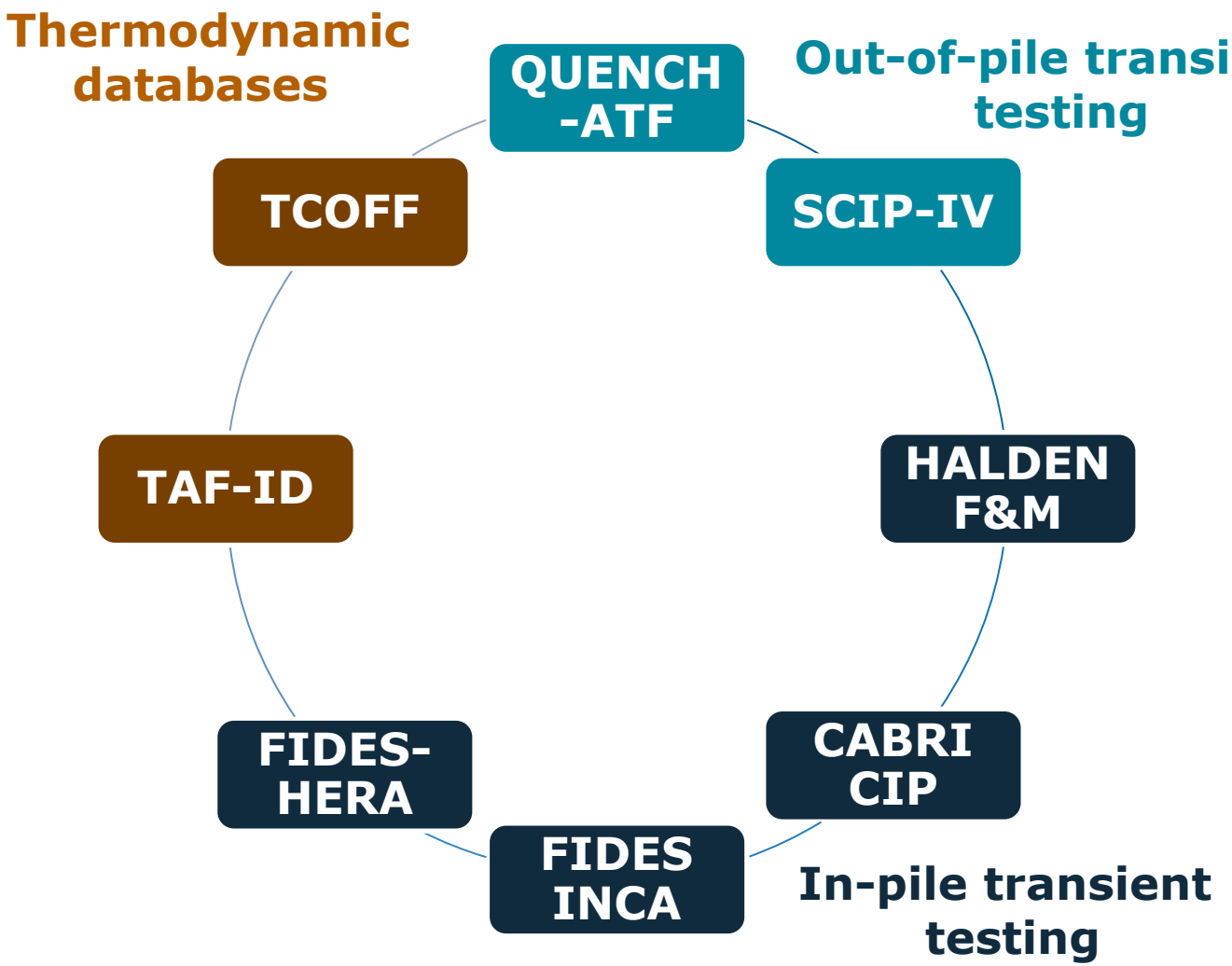

- **QUENCH-ATF** (2021-24)
- **SCIP-IV** (2019-24)
- **Halden Fuel & Materials** (2021-23)
- **CABRI CIP** (2000-26)
- **FIDES/HERA** (2021-24)
- **FIDES/INCA** (2021-24)
- **TCOFF** (2017-20, 2022-2025)
- **TAF-ID** (2013-2017, 2018-2021, 2022-2026)

QUENCH-ATF *(See presentation by M. Steinbrück)*

A joint project to investigate **ATF claddings** for enhanced performance and safety:

- Three large-scale bundle tests performed at the QUENCH facility (KIT, Germany)
- with ATF cladding materials:
- Simulating design-basis and severe accident scenarios
- Supporting separate-effects tests
- Complementary tests performed by IRSN, and CEA @ ILL
- Numerical simulation exercise: blind post-test benchmark coordinated by GRS

Participants: 19 organisations from 9 NEA countries

Project started in Autumn 2021, for 4 years

Programme Manager M. Steinbrück (GER), **MB Chair** H. Esmaili (US), **PRG Chair** Y. Nemoto (JPN), **NEA Secretariat** J.-F. Martin

QUENCH-ATF #1 (Jul. 2022)
- Cr coated Zr (Westinghouse US)
- Bundle with 24 heated rods
- Extended LOCA conditions
- Peak local temperature 1600 K
- Compares with QUENCH-L3HT

QUENCH-ATF #2 (S1 2024)
- Cr coated Zr
- Severe accident conditions
- Above Zr-Cr eutectic
- Compares with QUENCH-15

QUENCH-ATF #3 (2024-2025)
- Cr coated Zr, or SiC
- Scenario depending on material and results of previous tests

SCIP - Studsvik Cladding Integrity Project

Objectives:

- Understanding the fuel and cladding performance in interim storage conditions
- Investigate the fuel behavior during LOCA
- Analysis of the influence of the microstructure on PCI
- Support the experimental investigations with pre- and post-test modeling

Status of the project:

- Phase 4 ongoing (2019-2024), back-end topics were included for the first time
- Phase 5 under discussion, including ATF materials – irradiated Cr coated cladding mechanical properties, and ballooning and burst behavior
- Participants: 38 organisations from 15 countries
- Broad range of materials are used for the investigations (PWR, BWR, VVER, non-standard) including doped fuel (ADOPT, ALSi, GD, IFBA)

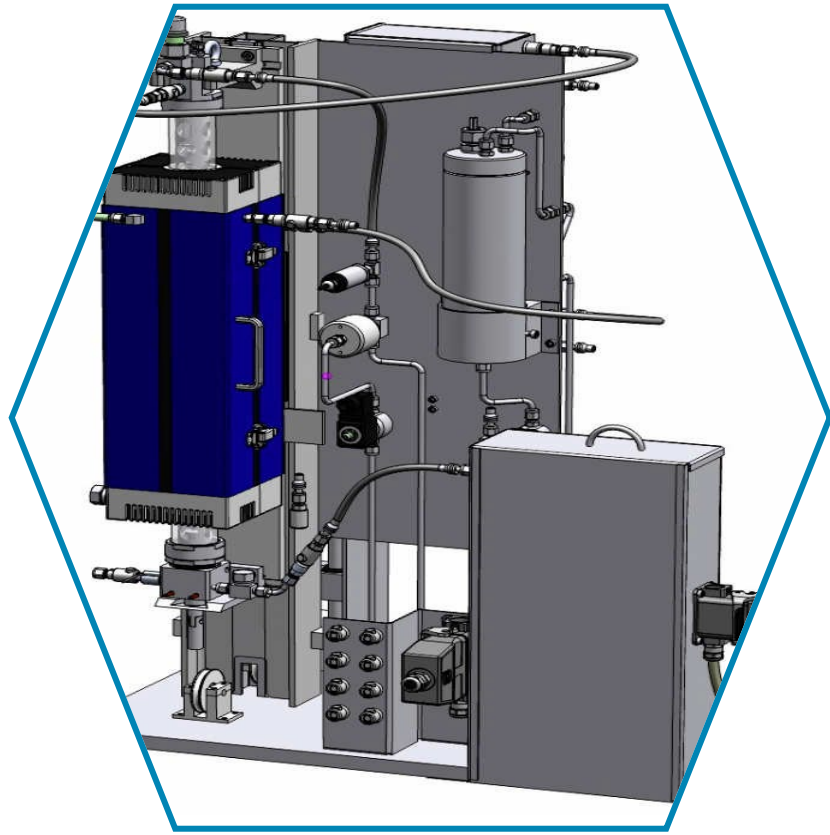

New LOCA apparatus.
Figure source: Studsvik

Programme Manager Per Magnusson (SWE) **MB Chair** Davis Shrire (SWE) **PRG Chair** Kurt Atkinson (UK) **NEA Secretariat** M. Beilmann

Halden Fuels & Materials (2021-2023)

Halden reactor

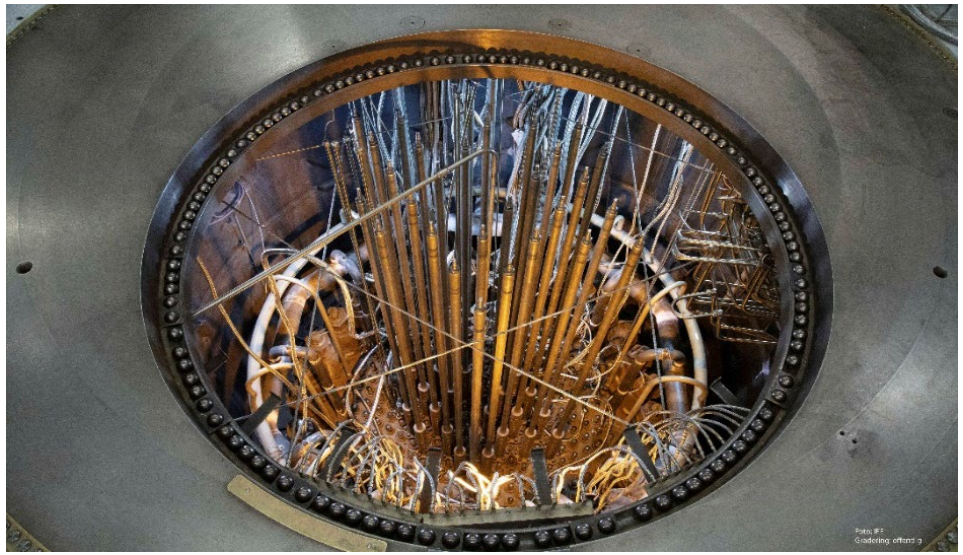

Figure source: IFE

Programme Manager Jon Kvalem (NOR)
NEA Secretariat D. Jacquemain

- Experiments on fuel safety and operational margins, incl. fuel and cladding performance and behaviour for **normal operation** and **transient conditions**
- Mandate 2021-2023, 17 countries and EC, operated by IFE
- ATFs investigation have been performed and were planned before reactor closure: **Cr, CrAl and FeCrAl coated claddings, UN, U3Si2, doped UO2**
- LOCA testing to be done via **Studsvik's SPARE** project
- Final meeting in May 2024 – wrapping up **65 years** of research
- The **legacy database** shall by available from the NEA for member countries **from 2024**

CIP Cabri International Programme

Objectives : HBU & ATF fuel and clad behavior in RIA

Project : mandate 2018-2026, 12 countries, operated by IRSN, complementary tests at NSRR in Japan

Experiments: 12 tests in CABRI reactor (IRSN, France)

ATFs: 4 tests dedicated to advanced fuels (Cr doped UO2) a/o advanced cladding (liners), scheduled in 2023, 2024

CABRI reactor

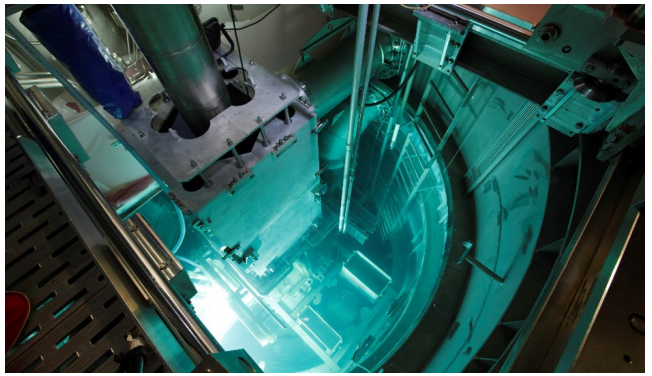

Figure source: IRSN

Operating agent contact F. Barré (FR) **NEA Secretariat** D. Jaquemain

Framework for Irradiation Experiments (FIDES-II)(13 countries and EC)

Second Framework for Irradiation Experiments – FIDES-II

- NEA joint undertaking, established pursuant to Article 5 of the NEA Statues in co-ordination with the Nuclear Science Committee (NSC) and the Committee on the Safety of Nuclear Installations (CSNI)
- A stable, sustainable, reliable platform for fuel and material testing using nuclear research reactors (RRs) in NEA member countries
- Generates experimental results and expertise for shared costs
- **FIDES-II Program of Work includes 4 Joint Experimental Programmes (JEEPs) & 3 cross cutting pillars**

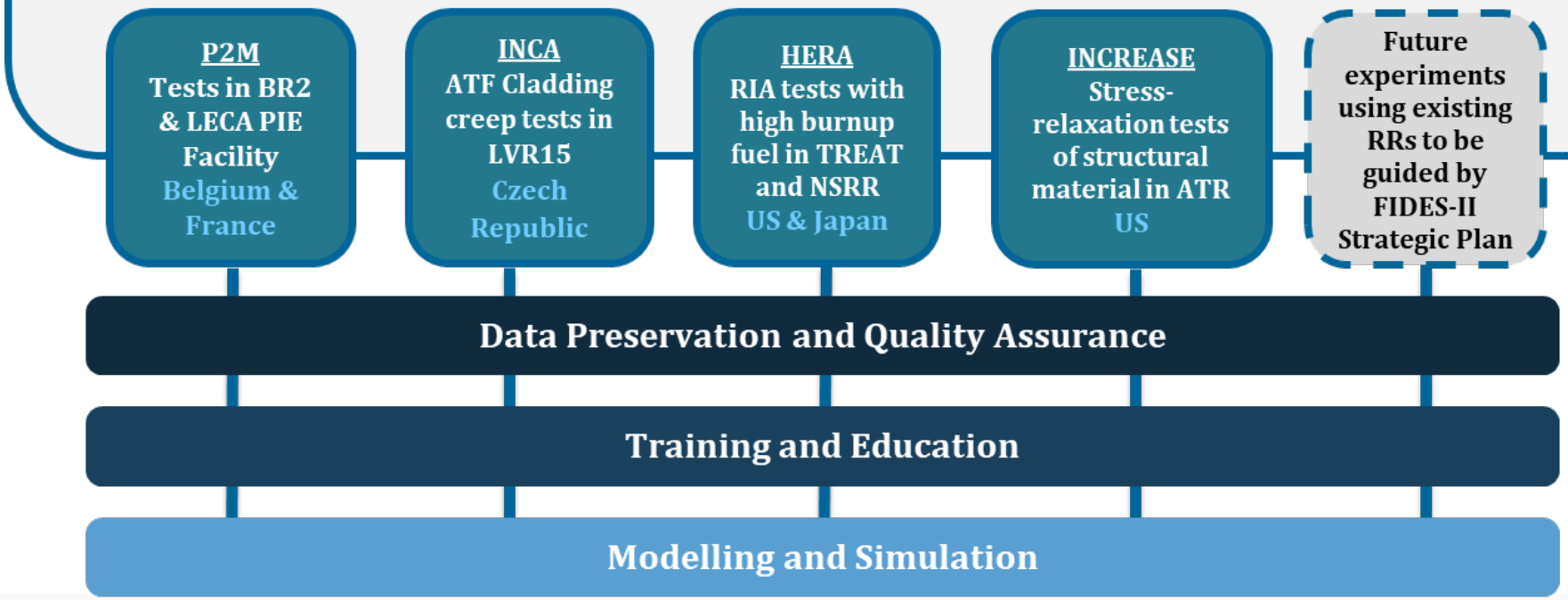

Chair R. Furstenau (US), G. Bignan (FR)
NEA Secretariat M. Beilmann, M. Bales

FIDES-II HERA
High Burnup Experiments in Reactivity Initiated Accidents

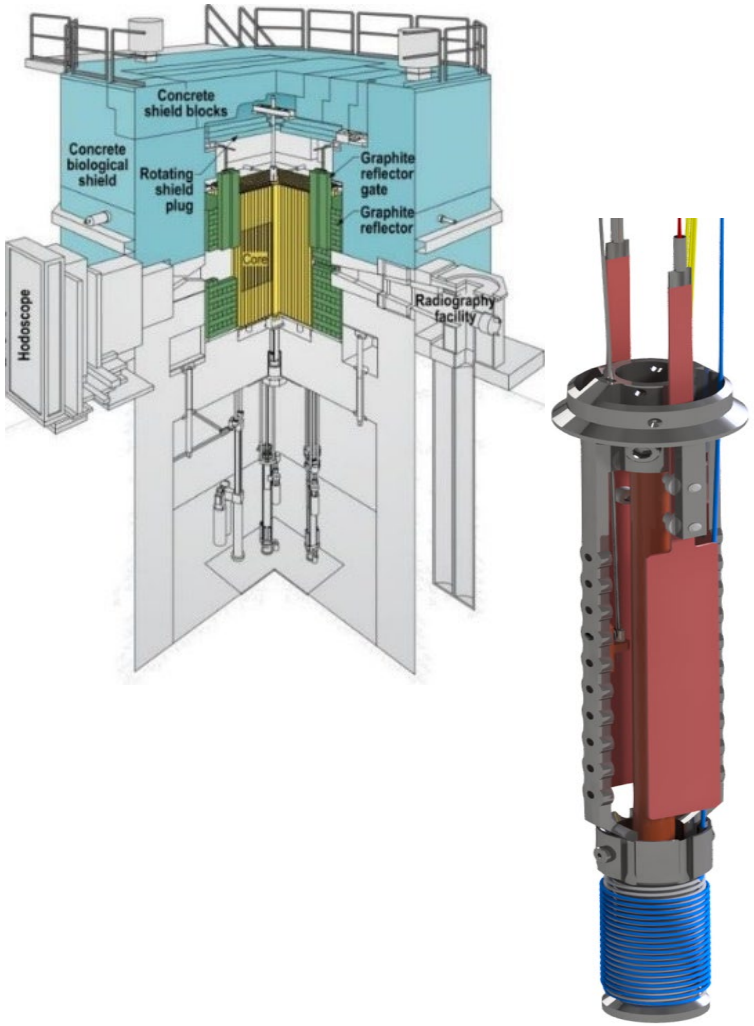

TREAT reactor & HERA rig. *Court. INL*

Objective: Investigate performance of modern high burnup fuel at representative pulse widths

Facility: TREAT reactor and hot cells, USA and NSRR reactor Japan

Scenario: 6 RIA tests with pre-hydride cladding and oversized UO2 pellets + 4 RIA test with actual HBU fuels

Materials: High burnup fuels & Cr-coated cladding

Experiment Status: Pre-hydride and pre-irradiated tests planned for 2022/23

Blind calculations on RIA experiments recently launched

Core Group: DOE, NRC, Westinghouse (US), JAEA (Japan), IRSN (France)

Programme Manager D. Kamerman (US) **NEA Secretariat** M. Bales & M. Beilmann

FIDES-II INCA
In-pile Creep Studies of ATF Claddings

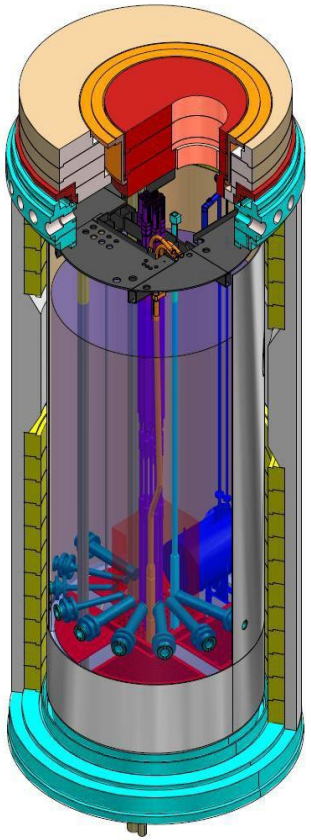

LVR-15 reactor & INCA rig. *Court. ÚJV Řež*

Objective: Provide comparative data on the irradiation induced creep of current Zr alloys and Cr coated samples under steady state conditions

Facility: LVR-15 reactor and hot cells, ÚJV Řež, Czech Republic

Materials: Coated ATF claddings

Experiment Status: Irradiation began May 2022

Core Group: CVR, UJV REZ, Alvel (CZ), VTT (Finland), CEA (France)

Programme Manager M. Miklos (CZ) **NEA Secretariat** M. Bales & M. Beilmann

Preparing FIDES-II's next triennial

Since the launch in 2021, the member's desire to expand has been significant

NEW Second Triennial Proposals (2024-2027) demonstrate FIDES-II is agile, able to respond to member interests rapidly.

- 4 **new facilities** proposed
- 2 JEEPs addressing **Advanced Reactor** technology
- 3 JEEPs focused on **accident tolerant fuels**
  - Metallic Cr coated Zr-based cladding tubes
  - Chemical-vapour deposition CrCx internal coating on Zr-based cladding tubes
  - SiC-SiC_f cladding tubes
  - Silicon carbides
  - Fe-Cr-Al cladding tubes
- Under steady state and transient conditions

TAF ID –Thermodynamic of Advanced Fuel International Database

Objectives

- Develop a thermodynamic database (phase diagrams + thermodynamic properties of the phases) for advanced fuel materials using the Calphad method

Systems of interest: materials for Generation II, III, IV

- Fuels: UO2, (U,Pu,Am,Np)O2 , (U,Th)O2, (U,Pu,Zr,Am,Np), **UN, (U,Pu)C**
- Fission products: Ba, Sr, Mo, Zr, Lanthanides (Ce, La, Nd, Gd), metallic FPs (Pd, Ru, Rh, Te, Tc), Volatile (Ag, Cs, I, Te)
- Structural materials: Fe-Cr-Ni, Zr alloys, Fe-Cr-Al-Y, Concrete (SiO2-CaO-FexOy-Al2O3-MgO), SiC, B4C

Status of the project (NEW!)

- Major update of the "public" version available to all NEA member countries released in August 2023, including 110 binaries, 22 ternaries and 2 quaternaries
- Phase 3 started early 2023: **increased focus on ATF materials** (UN, U3Si2, encapsulated fuels) and ATF cladding materials (Cr-coated Zry, FeCrAl, SiC) and their interactions with fission products, coolants, and structural materials

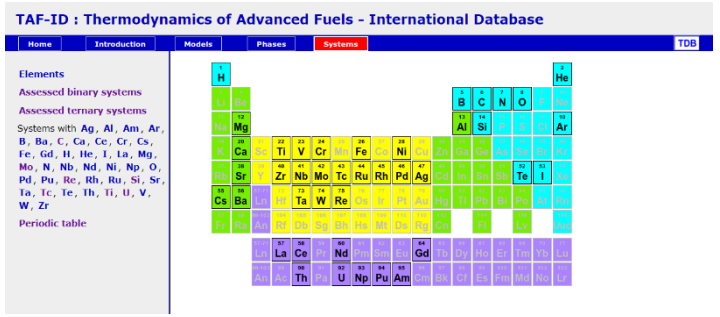

https://www.oecd-nea.org/science/taf-id/

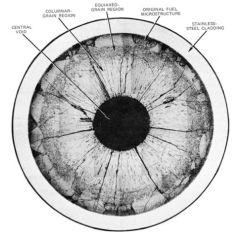

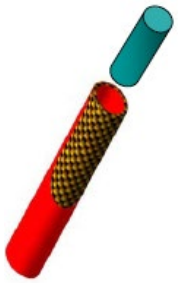

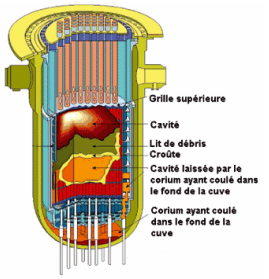

Chair C. Gueneau (FR), **vice-chair** T. Besmann (US), **NEA secretariat** A. Dufresne

TCOFF-2 – Thermodynamic Characterization Of Fuel Debris and Fission Products based on Scenario Analysis of Severe Accident Progression *(See presentation by D. Bottomley, JRC)*

Objectives

- Improve the models describing the core materials interactions and their role in the various phases of severe accidents;
- Improve the understanding of fission products behaviour during the severe accidents and their influence on the accident progression.

Status of the project

- Phase 1 completed (July 2020)
- Phase 2 launched Sept. 2022: broadened scope in terms of reactor design (not limited to BWR) and materials (the effect **of potential deployment of ATF materials** will be evaluated): U3Si2, UN, Cr2O3 doped UO2, Cr-coated Zry, FeCrAl, SiC/SiC
  - Task-1: Prioritisation of the material science issues related to the severe accidents study
    - Prioritisation summarised in a SIRT (System Identification Ranking Tables) detailed in the presentation of D. Bottomley
  - Task-2: Improvement of the materials science knowledge on fuel core degradation and FP release (UO2-Zry and ATFs)
  - Task-3: Implementation of improved knowledge for the simulation of the accident behaviour (UO2-Zry and ATFs)
  - Task-4: Leaching (with the development of a database)
  - Task-5: Training and Education consolidated with a NEST project, approved in Nov. 2023

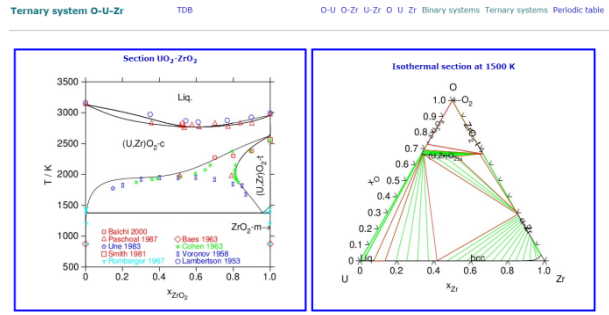

Phase relations in U-Zr-Fe-O system (metallic/oxidic melts in corium)

Phase relations in U-Zr-Fe-O system (oxidic/metallic melts in corium)

MB Chair H. Esmaili (US), C. Journeau (FR), **PRG Chair** M. Kurata (JPN), L. Lovasz (GER) **NEA Secretariat** A. Dufresne

Looking ahead

NEA assists its members with promoting international collaboration to support advanced fuel technologies by:

- Ensuring **information exchanges** between relevant international initiatives in the field
- Updating **research priorities** for ATF development, integrating, as far as feasible, state-of-the-art knowledge from R&D and implementation plans in NEA member countries
- **Enhancing testing capabilities** and developing FIDES-II as a **framework for fuel testing** in key research reactors, as well as other complementary **joint projects**
- Coupling **experimentation** with **advanced modeling and simulation**
- Preserving **key experimental data** and **competencies**

Thank you!

www.oecd-nea.org

M. Steinbrück
KIT

OECD-NEA Joint Undertaking QUENCH-ATF

The OECD-NEA Joint Undertaking QUENCH-ATF is the worldwide first large-scale bundle experimental series with Accident-Tolerant Fuel (ATF) cladding materials under DBA and severe accident conditions. It started in October 2021 and will last four years.

Within the project, three bundle experiments with ATF cladding are foreseen with the focus on Cr-coated cladding. The large-scale bundle tests are supported by dedicated separate-effects tests, post-test analyses at KIT and IRSN as well as by code support and code benchmark exercises coordinated by GRS.

The first bundle test with slightly extended LOCA conditions similar to QUENCH-L3HT was conducted in July 2022. All non-destructive post-test examinations have been completed, and the destructive ones are underway. Two benchmark exercises (blind and open post-test) have been completed.

The second experiment with a beyond DBA scenario (QUENCH-15 as reference test) will be conducted March/April 2024. The scenario of the third and last bundle tests will be discussed and decided after the first two tests have been analyzed.

Single-rod tests simulating potential scenarios (QUENCH-03, QUENCH-15) for the QUENCH-ATF2 experiment were conducted at KIT. No failure below eutectic temperature for both scenarios has been observed below the eutectic temperature, i.e., only very low hydrogen release was measured at these conditions. A strong acceleration of oxidation rate above 1330°C was observed for all tests being stronger/steeper, but shorter for the QU-03 scenario w/o pre-oxidation phase.

.

Karlsruhe Institute of Technology

NEA Nuclear Energy Agency

OECD-NEA Joint Undertaking QUENCH-ATF

M. Steinbrück, J. Stuckert, M. Grosse, J.-F. Martin

28th International QUENCH Workshop, 5-7 December 2023

Institute for Applied Materials IAM-AWP & Program NUSAFE

QUENCH-ATF Joint Undertaking

- Worldwide first large-scale bundle experimental series with Accident-Tolerant Fuel (ATF) cladding materials under DBA and severe accident conditions

Fact sheet

- Duration: Oct. 2021 – Oct. 2025
- Budget: 1.6 Mio €
- 20 participants from 9 countries

QUENCH-ATF Joint Undertaking

- Three bundle experiments with ATF cladding in the QUENCH facility
  - Focus on Cr-coated Zr alloys
  - Design basis and beyond design basis accident conditions
- Supporting separate-effects tests
  - at KIT
  - Complementary tests at IRSN and CEA (France)
- Code support for test preparation and code benchmark exercises, coordinated by GRS

QUENCH-ATF test matrix

QUENCH-ATF #1 (July 2022)

- **CS Cr-coated Zr** (provided by Westinghouse)
- Bundle with 24 heated rods, 12.6mm pitch
- **Extended LOCA** conditions: similar conditions as QUENCH-L3HT (LOCA 3 High Temperature) with optimized ZIRLO^{TM}, which will allow a comparison

QUENCH-ATF #2 (01/2024)

- **CS Cr-coated Zr** (WEC)
- **Severe accident conditions**

  (above Zr-Cr eutectic)
- ATCR

QUENCH-ATF #3 (04/2024)

- PVD Cr-coated Zr
- Scenario depending on results of previous tests

QUENCH-ATF1 experiment

Bundle assembly from component parts…

24 Opt. ZIRLO cladding tubes with Cr coating

5 grid spacers

2234 ZrO_2 pellets

24 W heaters

24 Mo/Cu electrodes

… to test bundle …

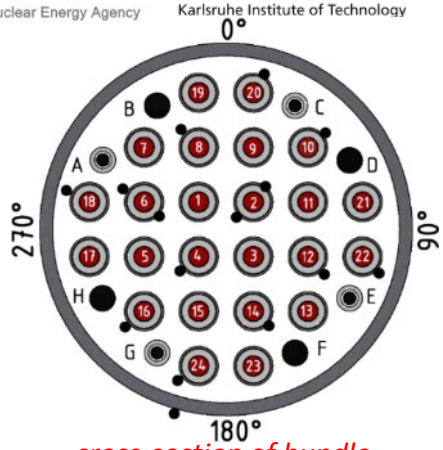

cross-section of bundle instrumented with thermocouples

- Improved handling of Cr coated cladding tubers during bundle assembly

… in the test section

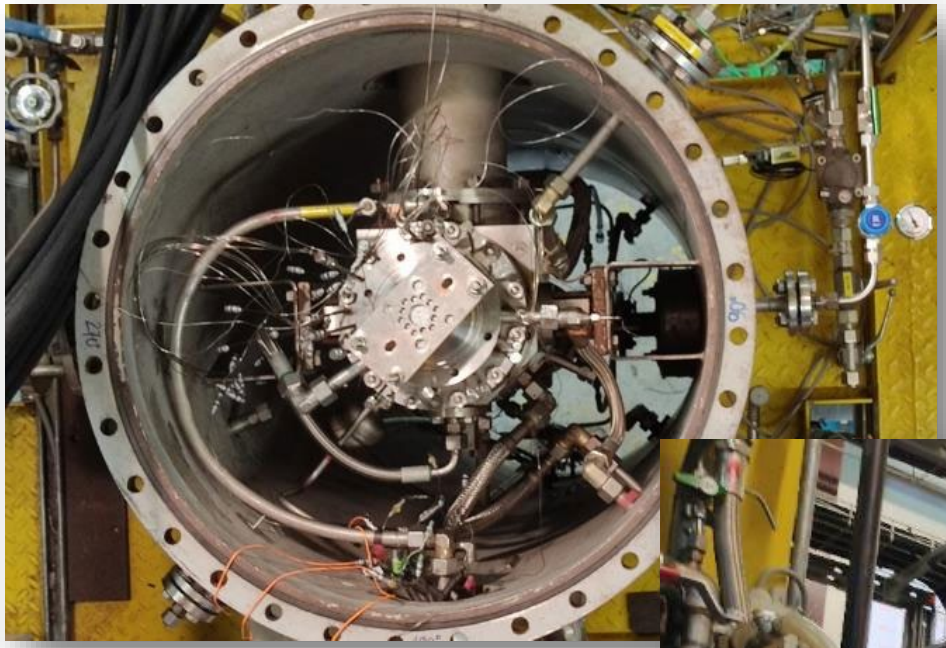

24 Mo/Cu electrodes

QUENCH-ATF 1 scenario

- Extended LOCA conditions
  - Heating-up rate during the heating in superheated steam 5 K/s
  - Peak cladding temperature at the end of the heat-up stage 1600 K
  - Duration of cool down stage 200s
  - Final quenching by water
  - QUENCH-L3HT with uncoated Opt. ZIRLO as reference test

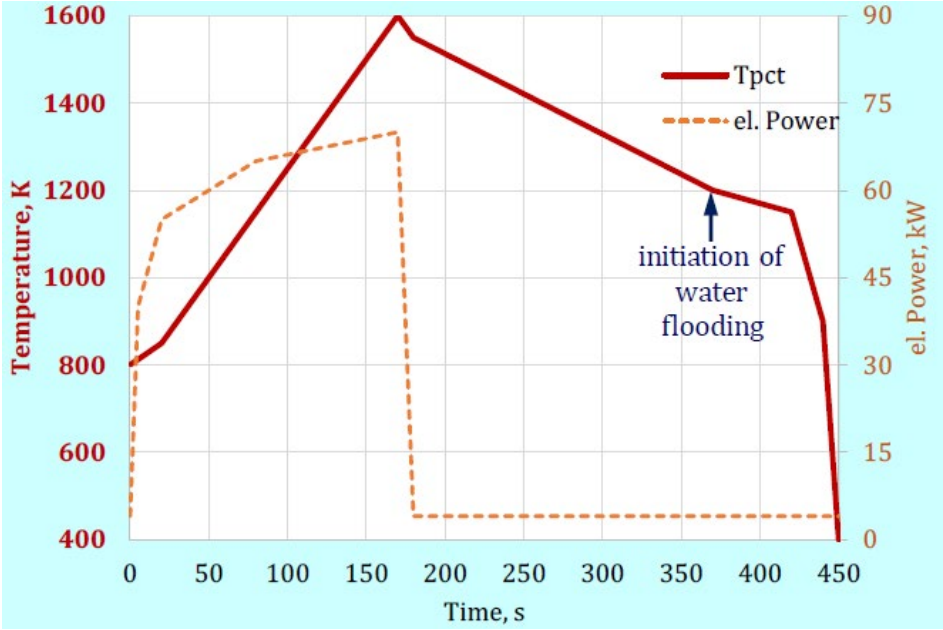

QUENCH-L3HT scenario

QUENCH-ATF1 post-test examinations (KIT/IRSN/CEA)

- ✓ Laser scanner profilometry (pre-/post-test)
- ✓ Burst opening parameters
- ✓ Internal cladding surface observation by videoscope
- ✓ Ultrasound measurement of wall thickness
- ✓ Neutron radiography and tomography (hydrogen concentration around burst location)
- Mechanical testing
- Fractography after tensile tests
- Metallography and EBSD analysis
- Chemical analyses (O,H content)

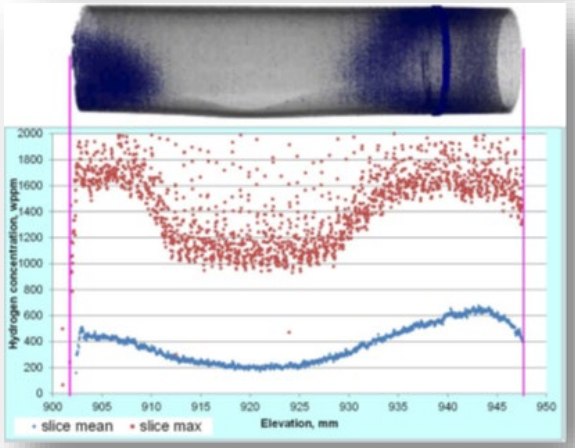

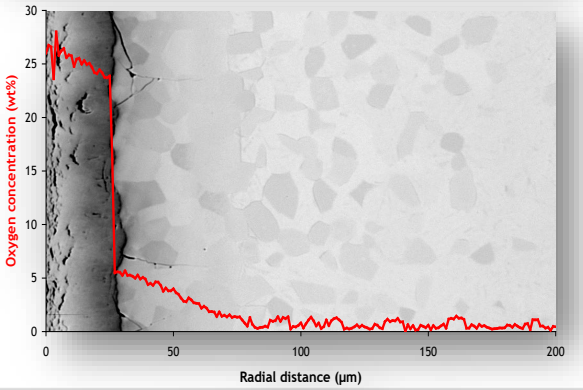

QUENCH-ATF1 benchmark exercise

Blind and open post-test benchmark

- Coordinated by Th. Hollands, GRS (DE)
- Simulation of bundle temperatures, hydrogen release and mechanical cladding behavior (ballooning and burst parameters)
- 7 organizations volunteered to participate:
  - UJV Rez with MELCOR
  - GRS with AC2/ATHLET-CD
  - RUB PSS with AC2/ATHLET-CD
  - KIT with ASTEC
  - IAE with SAMPSON
  - USNRC with MELCOR
  - EPRI with MAAP
- Blind phase completed 12/2022
- Open phase report under preparation

QUENCH-ATF2 experiment

QUENCH-ATF2 – scenario

- BDBA scenario with max. temperatures significantly above the Zr-Cr eutectic (1330°C)
- Cold spray Cr-coated Opt. ZIRLO (24 rods, OD 9.5 mm)
- QUENCH-15 (ZIRLO, 24 rods, OD 9.5 mm)
  - Pre-oxidation phase 3000 s at 1200°C in superheated steam
  - Transient phase up to 1600°C (tbd)
- Two accident tolerant control rods (Eu_2O_3/HfO_2 pellets produced by CRIEPI)
- Two rods pressurized similar to the QUENCH-18 bundle

Test scenario of QUENCH-15

- **Heatup** to ≈860 K and stabilization. Facility checks
- Heatup to ≈1470 K and **Preoxidation** of the bundle in superheated steam this temperature for ≈2800
- **Transient** heatup from ≈1470 to ≈2150 K (**≈1900 K for QUENCH-ATF2**) in superheated steam
- **Quenching** of the bundle by a flow of ≈50 g/s of water

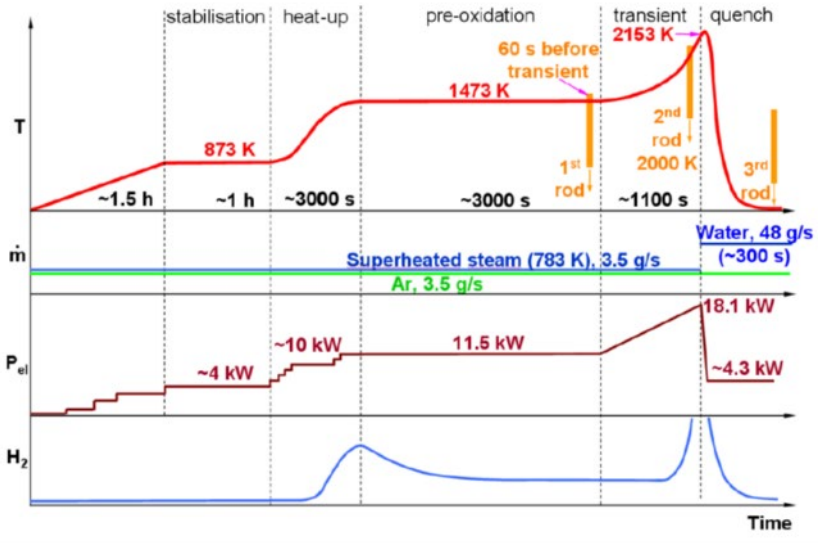

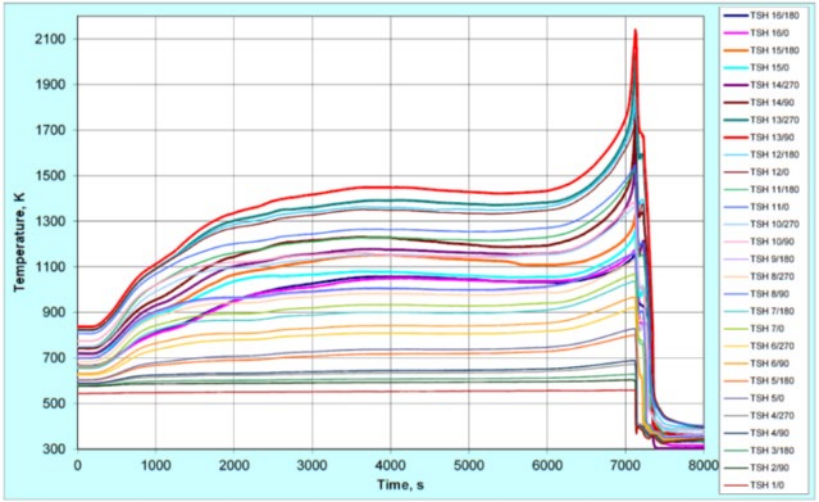

Pre-tests in the QUENCH-SR facility

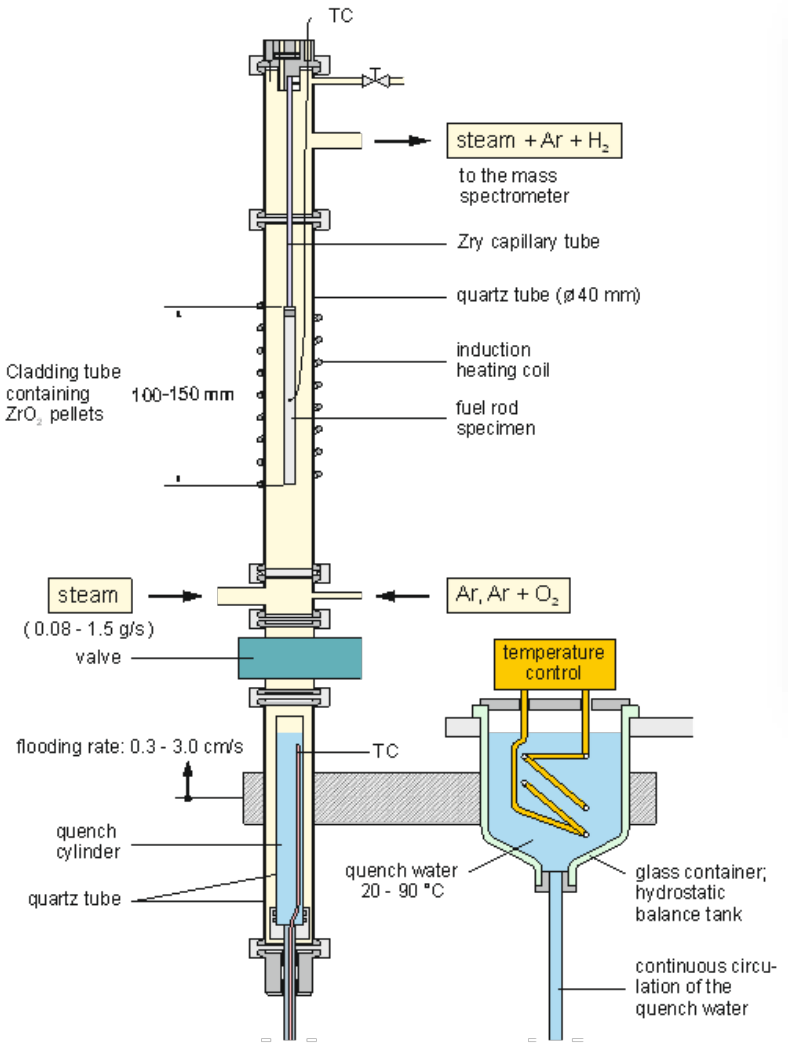

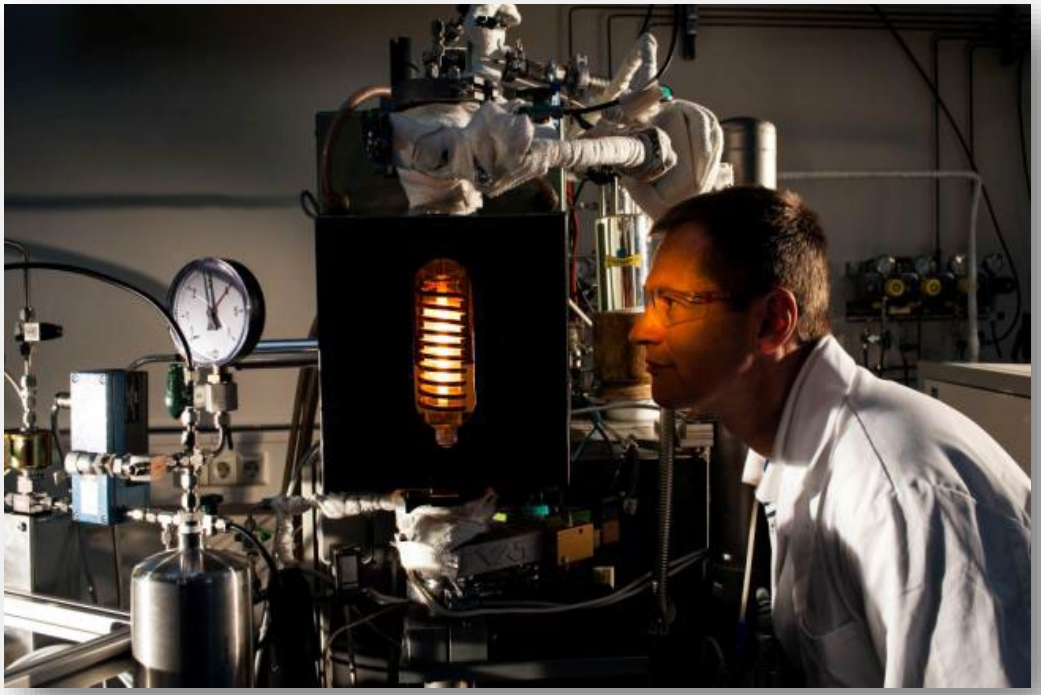

- Temp. up to 2000°C
- Oxidizing/reducing atmospheres incl. steam
- Quenching by water (not used)
- Coupled with MS

Samples and test matrix

- Eight experiments with 12-cm-long tube segment samples cut from Westinghouse cladding tubes
- Two slightly different coating methods
  - In helium (old)
  - In nitrogen (new)
- Two scenarios
  - QUENCH-15 (with PO)
  - QUENCH-03 (without PO)
- Two maximum temperatures
  - 1300°C (below eutectic temperature)
  - 1600°C (significantly above eutectic temperature)

QUENCH-ATF2 pre-test results: Temp. and H_2 rates

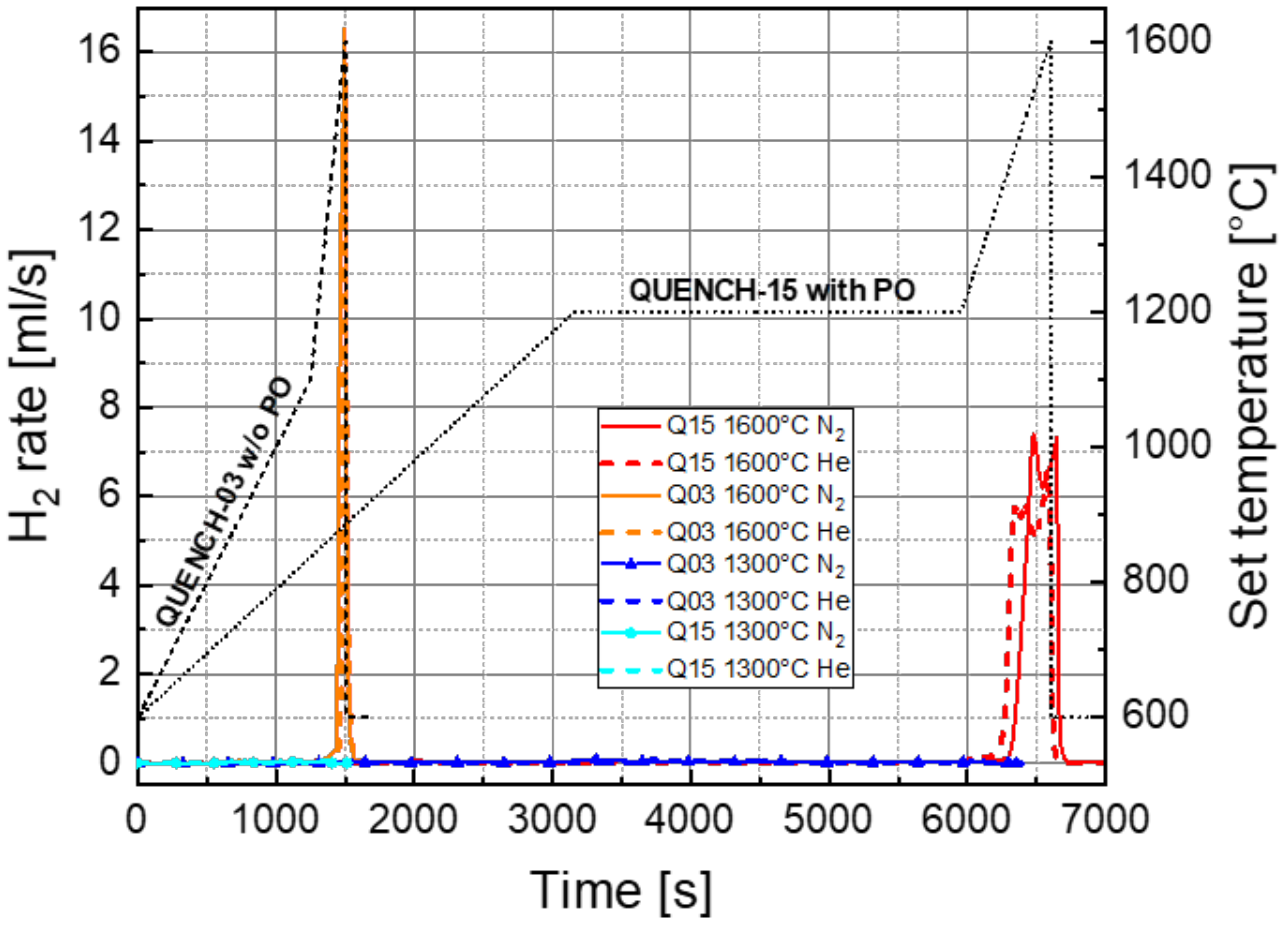

- No failure below eutectic temperature for both scenarios
- Strong acceleration of oxidation rate above 1330°C
- Stronger/steeper, but shorter acceleration for the QU-03 scenario w/o PO
- Inner TCs measured T>1600°C

QUENCH-ATF2 pre-test results: Post-test appearance

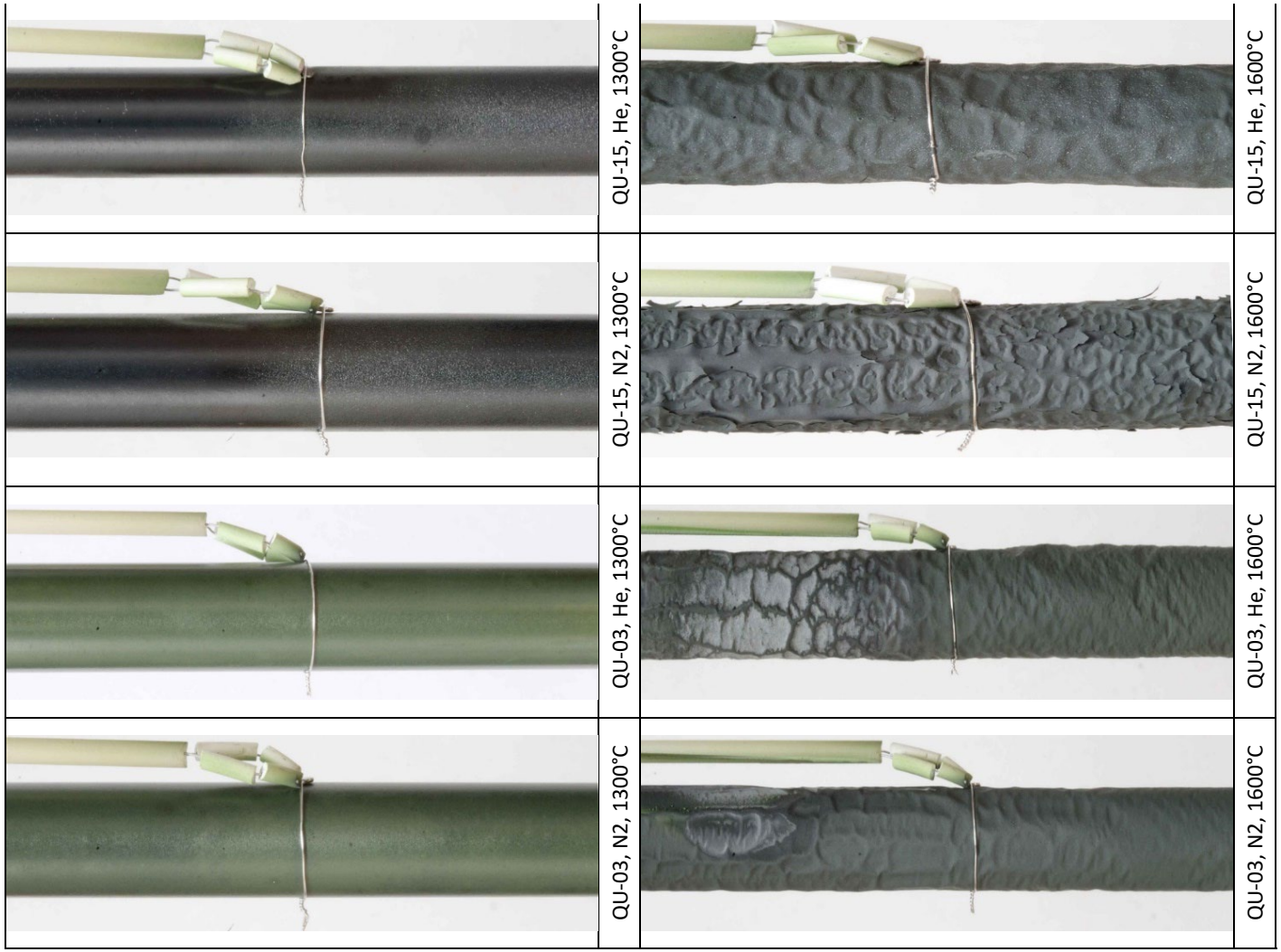

QUENCH-ATF2 pre-test results: Cross sections

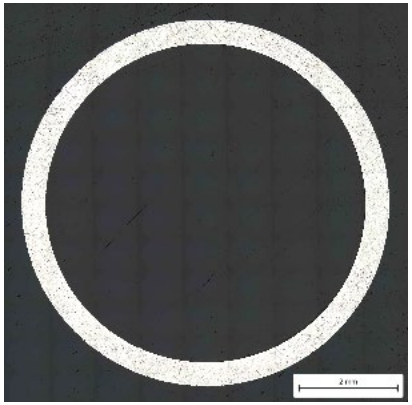

QU-03, N2, 1300°C

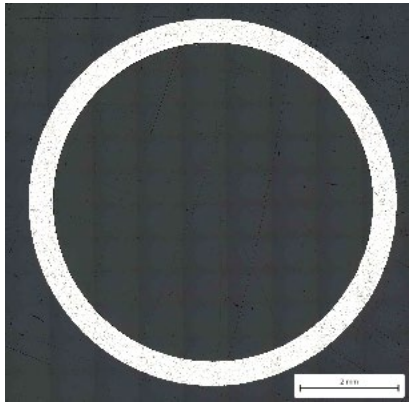

QU-03, He, 1300°C

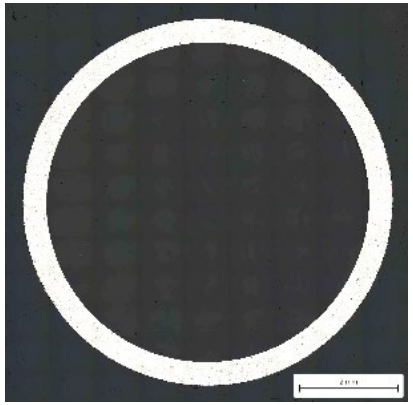

QU-15, N2, 1300°C

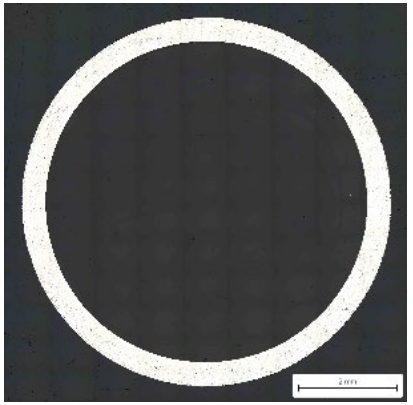

QU-15, He, 1300°C

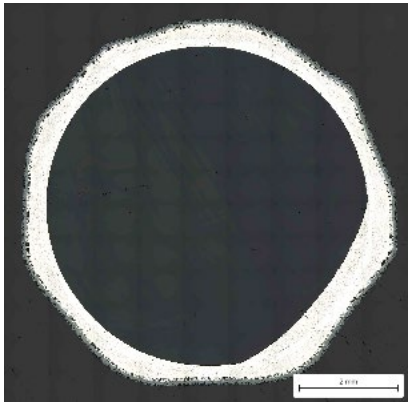

QU-03, N2, 1600°C

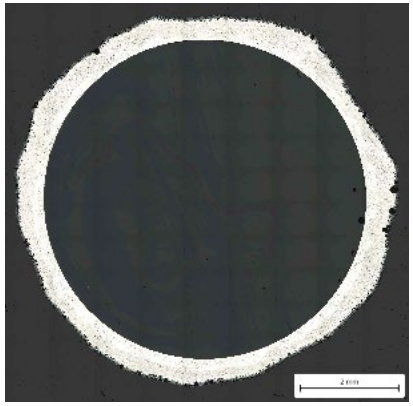

QU-03, He, 1600°C

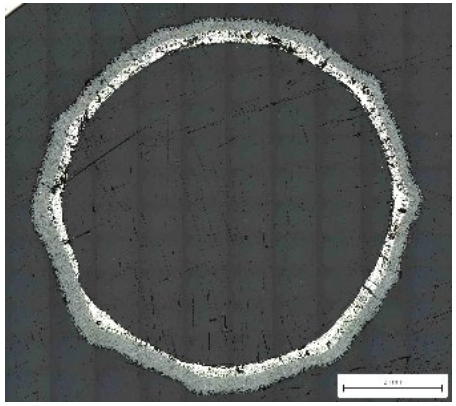

QU-15, N2, 1600°C

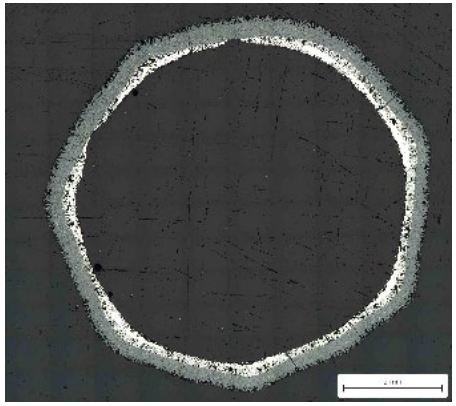

QU-15, He, 1600°C

QUENCH-ATF – status and next steps

- QUENCH-ATF1
  - Non-destructive post-test examinations completed
  - Destructive PTE at KIT and IRSN in progress
  - Completion of all benchmark activities soon
- QUENCH-ATF2
  - Cladding tubes and spacer grids provided by WEC
  - All other bundle components available/ordered/in production
  - BDBA scenario (QUENCH-15 with PO)
  - Application of 2 ATCR (CRIEPI) and two pressurized rods
- QUENCH-ATF3
  - Most probably PVD Cr coated with scenario tbd.

Why the QUENCH-ATF2 experiment could be exciting

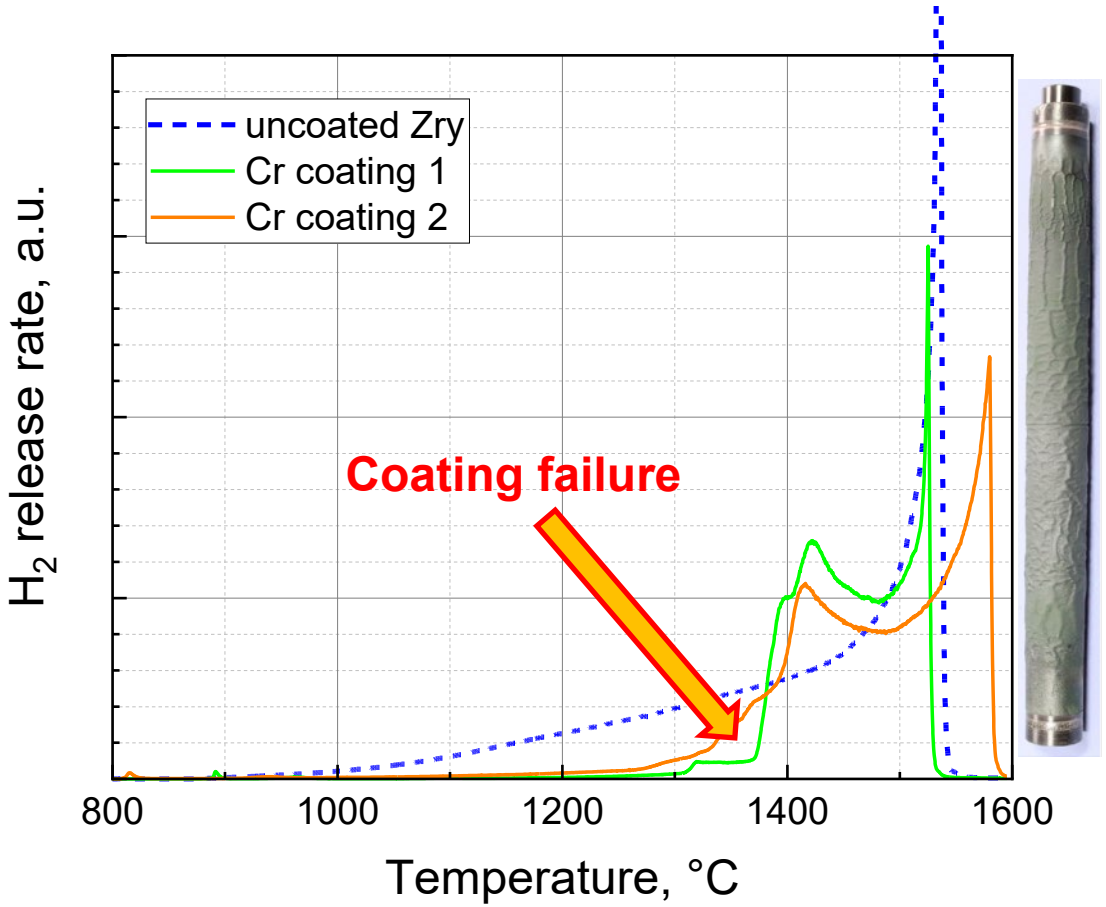

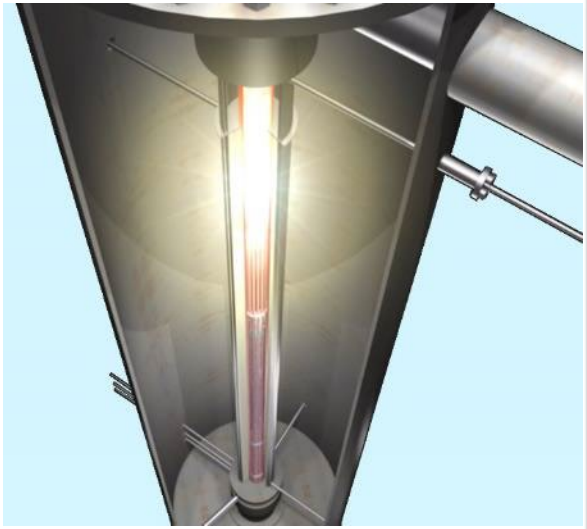

What will happen under almost adiabatic conditions in the well-insulated bundle?

Faster oxidation of coated samples after coating failure compared to Zry in single-rod experiments with high heat losses!


Thank You

G. Wang
PNNL

PNNL Research and Testing Capabilities

PNNL has a broad range of laboratory objectives, including nuclear material processing, scalable machine reasoning, reinventing chemical conversions, energy decarbonization, multiscale earth dynamics, and predictive phenomics. For example, as a challenge, nuclear stockpile modernization and next-generation energy technologies are hindered by a lack of science-based understanding of historical and emerging material systems. Thus, the National Security Directorate (NSD) stewards the accelerating development and characterization of nuclear material processing.

This presentation presents a few example cases with the following information. First, some background Information with reactor design evolution aligned with PNNL research and development activities are presented in certain level of details. Then, the PNNL's laboratory objectives are discussed in a high level. Thirdly, the PNNL capability high-level introduction is presented on five selected cases.

Solid Phase Processing (SPP) applications is the first selected case. Solid Phase Processing (SPP) involves the application of a high shear strain during metals synthesis or fabrication without bulk melting of the constitutive materials to produce high-performance microstructures in alloys, semi-finished products, coatings and engineered assemblies. PNNL has the expertise and machines on friction stir processes, cold spray and Shear Assisted Processing and Extrusion (ShAPE™) process. Secondly, PNNL has strong capability on material characterization, prediction and control. For example, the Solid Phase Processing Science Initiative (SPPSi) is coupling multi-scale models and measurements with demonstration of an integrated methodology. Thirdly, in the refractory electroplating area, PNNL has developed a novel method of electroplating thin metal films from deep eutectic solvents (DES). Refractory metals are used for their corrosion and erosion resistance, high melting temperature and excellent mechanical properties. The electroplating film quality is high and contamination is low. As the fourth example, stress corrosion cracking (SCC), creep, corrosion fatigue, and fracture toughness testing capabilities are introduced in this presentation. Especially, the PNNL's testing lab on Chloride-induced stress corrosion cracking (CISCC) has been performing a lot of tests to support the U.S. nuclear waste technical review board led by the Nuclear Regulatory Commission (NRC). Finally, PNNL's capability on post-irradiation examination (PIE) for Spent Nuclear Fuel is introduced. The PNNL's Radiochemical Processing Laboratory (RPL) is a Category 2 nuclear facility in operation since 1953. The RPL occupies 144,095 square feet, has 87 research laboratories, 21 gloveboxes, 143 fume hoods and 9 exhausted enclosures as well as 6 shielded research laboratories containing 16 hot cells. Typical PIE processes and measurements in a PNNL project may include rod puncture and fission gas analysis, rod sectioning and fuel dissolution, unetched for dimensions and microhardness, hydrogen analysis and etched to reveal hydrides. Also, the defueled mechanical property testing capability includes fatigue testing, tensile testing with digital image correlation, burst test, 4-point bend testing with digital image correlation, and radionuclide analysis/burnup analysis.

Pacific Northwest
NATIONAL LABORATORY

PNNL Research and Testing Capabilities

Guoqiang Wang
Pacific Northwest National Laboratory (PNNL)
December 5-7, 2023

U.S. DEPARTMENT OF ENERGY BATTELLE

PNNL is operated by Battelle for the U.S. Department of Energy

PNNL-SA-192541

Pacific Northwest
NATIONAL LABORATORY

Acknowledgement

The presenter/author would like to express his special thanks of gratitude to his colleagues at Pacific Northwest National Laboratory (PNNL) (Don Todd, Brady Hanson, Mychailo Toloczko, Lance Hubbard, Joshua Silverstein and Shenyang Hu for providing some of the slide information) as well as the management team (Bob Oelrich, Eric Smith, Mark Nutt, Stacy Torrey and others) and the review team at PNNL.

Pacific Northwest
NATIONAL LABORATORY

Abstract

PNNL has a broad range of laboratory objectives, including nuclear material processing, scalable machine reasoning, reinventing chemical conversions, energy decarbonization, multiscale earth dynamics, and predictive phenomics. For example, as a challenge, nuclear stockpile modernization and next-generation energy technologies are hindered by a lack of science-based understanding of historical and emerging material systems. Thus, the National Security Directorate (NSD) stewards the accelerating development and characterization of nuclear material processing.

This presentation presents a few example cases with the following information. First, some background Information with reactor design evolution aligned with PNNL research and development activities are presented in certain level of details. Then, the PNNL's laboratory objectives are discussed in a high level. Thirdly, the PNNL capability high-level introduction is presented on five selected cases.

Solid Phase Processing (SPP) applications is the first selected case. Solid Phase Processing (SPP) involves the application of a high shear strain during metals synthesis or fabrication without bulk melting of the constitutive materials to produce high-performance microstructures in alloys, semi-finished products, coatings and engineered assemblies. PNNL has the expertise and machines on friction stir processes, cold spray and Shear Assisted Processing and Extrusion (ShAPE™) process. Secondly, PNNL has strong capability on material characterization, prediction and control. For example, the Solid Phase Processing Science Initiative (SPPSi) is coupling multi-scale models and measurements with demonstration of an integrated methodology. Thirdly, in the refractory electroplating area, PNNL has developed a novel method of electroplating thin metal films from deep eutectic solvents (DES). Refractory metals are used for their corrosion and erosion resistance, high melting temperature and excellent mechanical properties. The electroplating film quality is high and contamination is low. As the fourth example, stress corrosion cracking (SCC), creep, corrosion fatigue, and fracture toughness testing capabilities are introduced in this presentation. Especially, the PNNL's testing lab on Chloride-induced stress corrosion cracking (CISCC) has been performing a lot of tests to support the U.S. nuclear waste technical review board led by the Nuclear Regulatory Commission (NRC). Finally, PNNL's capability on post-irradiation examination (PIE) for Spent Nuclear Fuel is introduced. The PNNL's Radiochemical Processing Laboratory (RPL) is a Category 2 nuclear facility in operation since 1953. The RPL occupies 144,095 square feet, has 87 research laboratories, 21 gloveboxes, 143 fume hoods and 9 exhausted enclosures as well as 6 shielded research laboratories containing 16 hot cells. Typical PIE processes and measurements in a PNNL project may include rod puncture and fission gas analysis, rod sectioning and fuel dissolution, unetched for dimensions and microhardness, hydrogen analysis and etched to reveal hydrides. Also, the defueled mechanical property testing capability includes fatigue testing, tensile testing with digital image correlation, burst test, 4-point bend testing with digital image correlation, and radionuclide analysis/burnup analysis.

Pacific Northwest
NATIONAL LABORATORY

Background Information: Reactor Design Evolution Aligned with PNNL Research and Development Activities

Evolution of Nuclear Reactor Technology

- Generation-0 Reactors
  - ❑Chicago Pile-1 (CP-1)
  - ❑B Reactor
- ≥ Generation III/III+
  - ❑Advanced Reactor Designs, e.g. AP1000
- Future Generation(s)
  - ❑Gen IV, and
  - ❑Fusion Reactors
  - ❑PNNL active in both
- Current Hot Topics
  - ❑Small and Micro Reactors

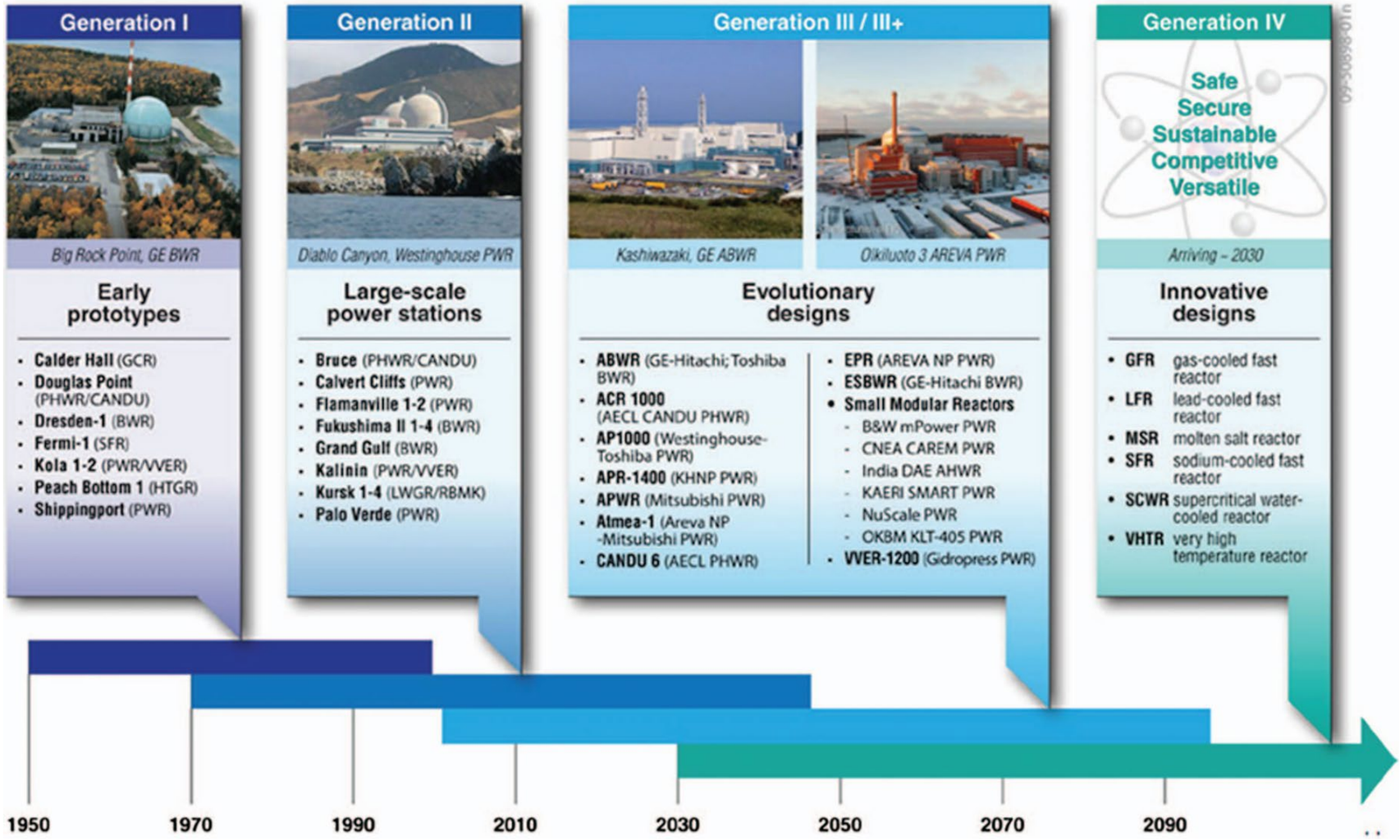

(From JANUARY 2017, Vol. 3 / 010801-1 of Journal of Nuclear Engineering and Radiation Science by J. Riznic, R. Duffey)

Generation-0 Reactors

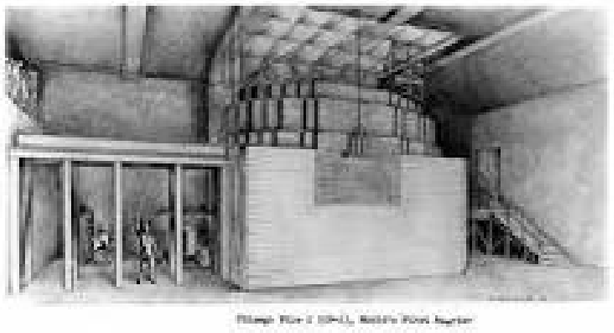

- Chicago Pile-1 (CP-1), the world's first artificial nuclear reactor
- Self-sustaining nuclear chain reaction initiated on December 2, 1942
- During an experiment led by Dr. Enrico Fermi
- Power ~ 200 Watts thermal (Wth)

- B Reactor, the world's 1st commercial nuclear reactor
- First nuclear chain reaction on September 26, 1944
- Based on experimental designs tested at CP-1 and X-10 Graphite Reactor
- Power ~ 250 MWth

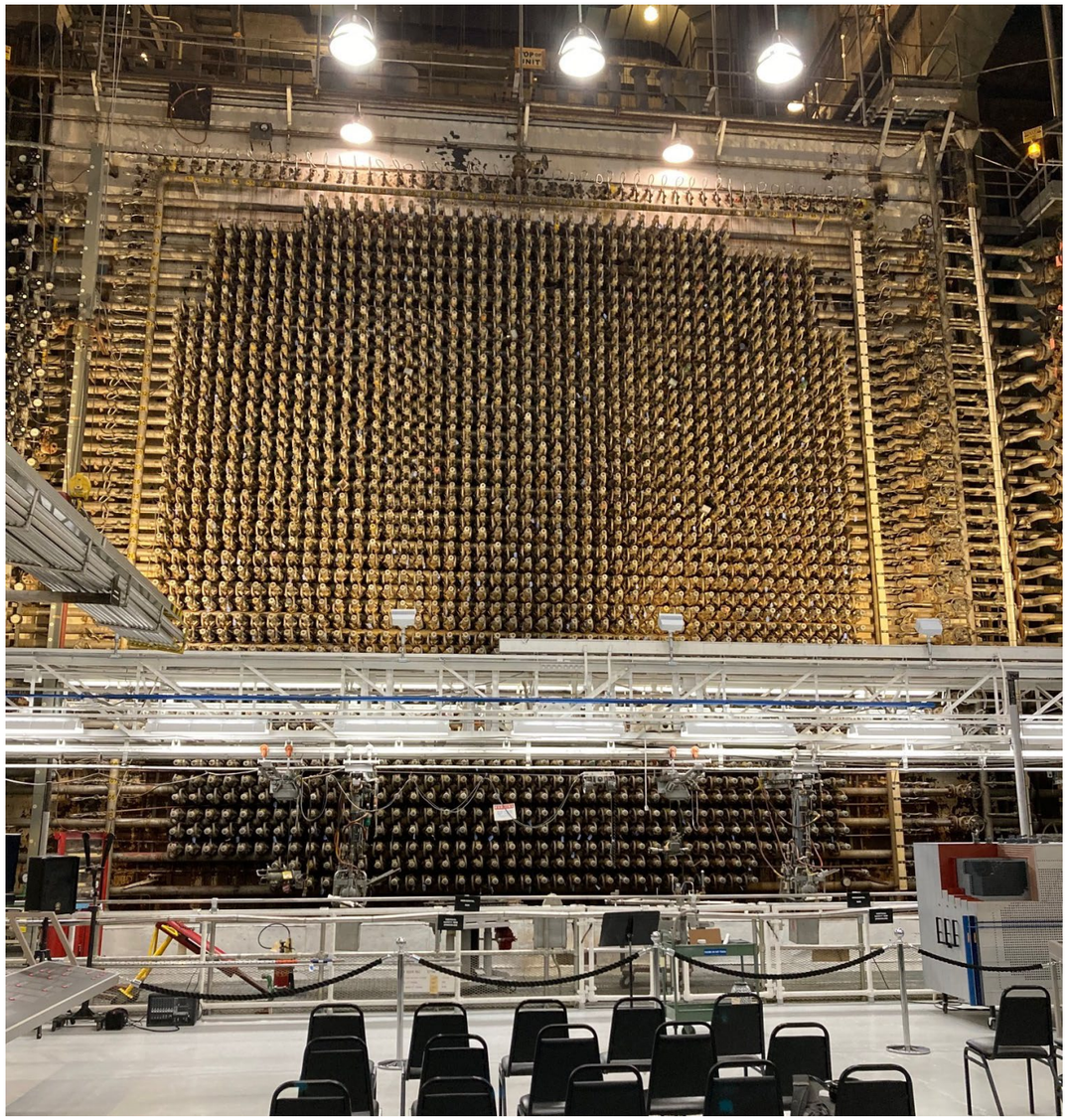

Picture taken on 5/12/2023 by Guoqiang Wang

Generation-0 Reactors (Cont.)

Prof. Enrico Fermi's house – renovated
- Located at Harris Ave., Richland, WA, USA
- Along the Columbia river

- B Reactor designed and built by E. I. du Pont de Nemours and Company, based on Prof. Enrico Fermi's CP-1 design
- 2004 fuel rods and cooling channel pressure monitoring
- Changed 1650 to 2004 fuel rods to avoid Iodine (^{135}I) pit or Xenon (^{135}Xe) poisoning. Applicable to today/future.
- Accumulator – partial **passive design**

Pictures Taken on 5/12 and 5/15/2023 by Mei Chen (Guoqiang Wang's wife)

Generation III+ Reactors (Sanmen Units 1 and 2)

(Taken on June 18, 2012)

- AP1000 China Bid negotiations
  - April to September 2005

A Picture from Previous ICONE Plenary Speeches by Westinghouse, Sanmen Units 1 and 2 Courtesy to Sanmen Nuclear Power Corp.

- AP1000 – A Sample GEN III+ reactor design with **passive features**

Pacific Northwest
NATIONAL LABORATORY

PNNL's Laboratory Objectives

PNNL's Laboratory Objectives

- PNNL has a broad range of Laboratory Objectives
- As an example, National Security Directorate (NSD) Stewards the Accelerating Development and Characterization of Nuclear Material Processing:
  - ❑ Challenge: Nuclear stockpile modernization and next-generation energy technologies are hindered by a lack of science-based understanding of historical and emerging material systems.
- This presentation only include some example cases.

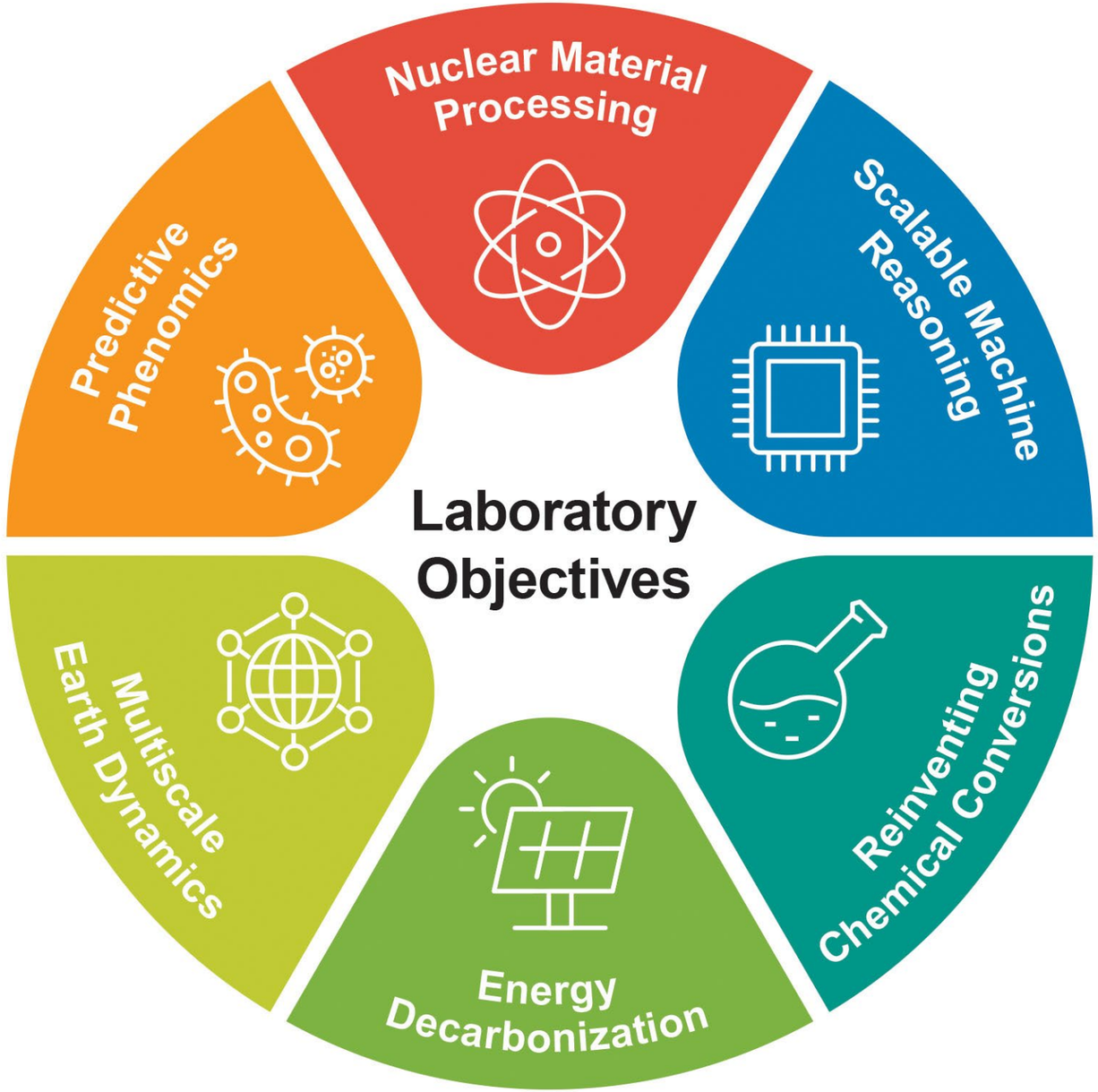

Pacific Northwest
NATIONAL LABORATORY

PNNL Capability: Solid Phase Processing Applications

Solid Phase Processing

- Solid Phase Processing (SPP) involves the application of a high shear strain during metals synthesis or fabrication without bulk melting of the constitutive materials, to produce
  - ❑ High-performance microstructures in alloys
  - ❑ Semi-finished products
  - ❑ Coatings and
  - ❑ Engineered assemblies

Friction Stir Processes

ShAPE™

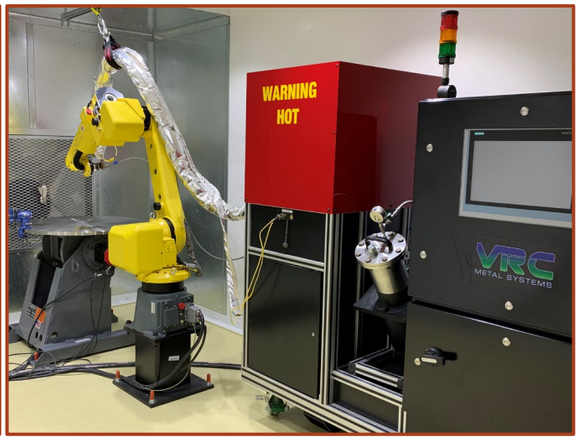

Cold Spray

Friction Extrusion and the ShAPE Process

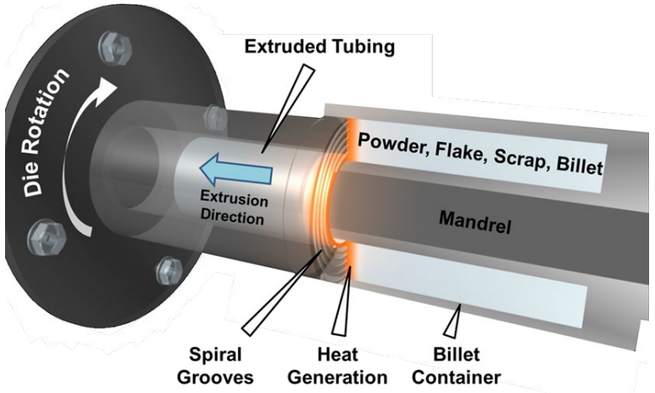

Extrusion process with a rotating die

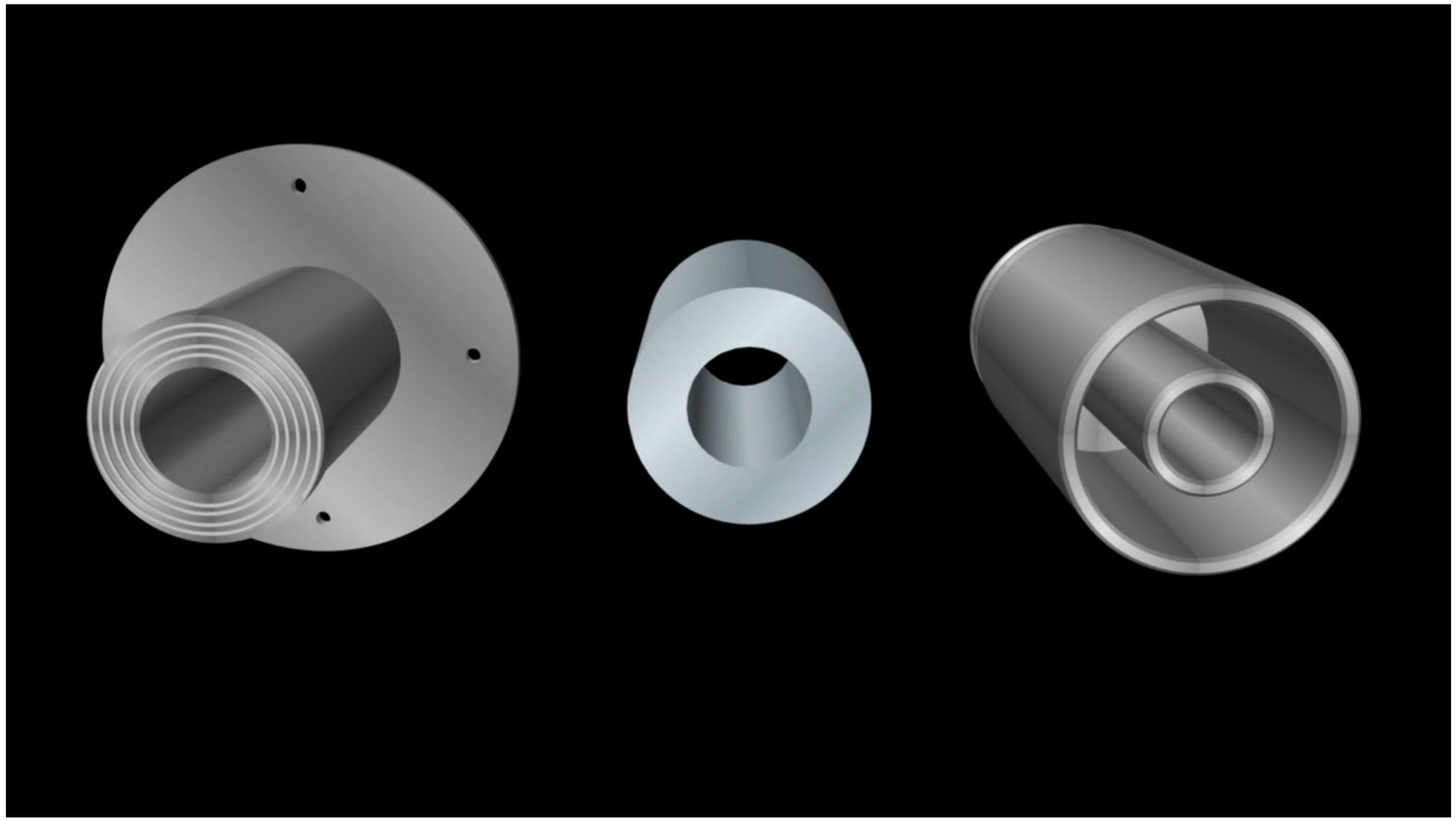

PNNL's Shear Assisted Processing & Extrusion (ShAPE™) process

ShAPE Applications

- New alloys and composites
- Improved properties through novel microstructures
- Enhanced fabricability for hard-to-process alloys
- Process intensification
- Recycled scrap into products

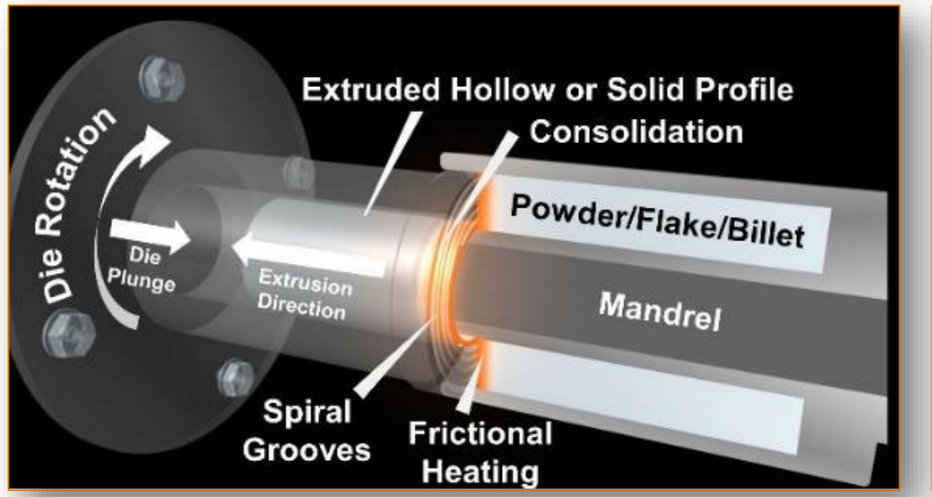

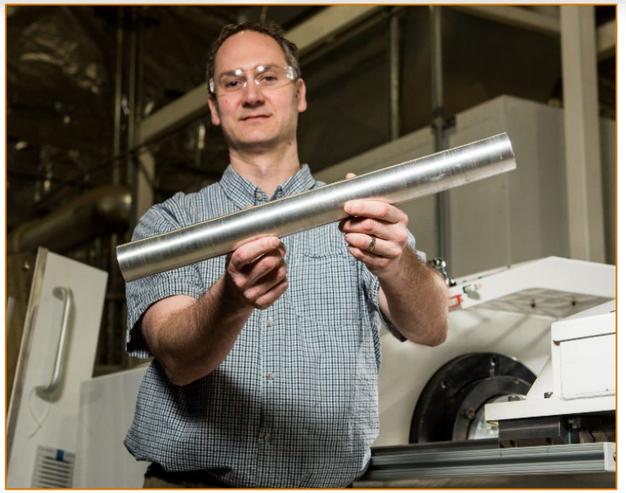

Friction Stir Welding and Processing

- Spinning, non-consumable tool is plunged into the surface of a material.
- Friction and plastic work energy heats the material sufficiently to lower the flow stress.
- When material softens, the tool is then translated along the joint line causing material in front of the pin to be deformed around to the back, and forged into the gap behind the traveling pin

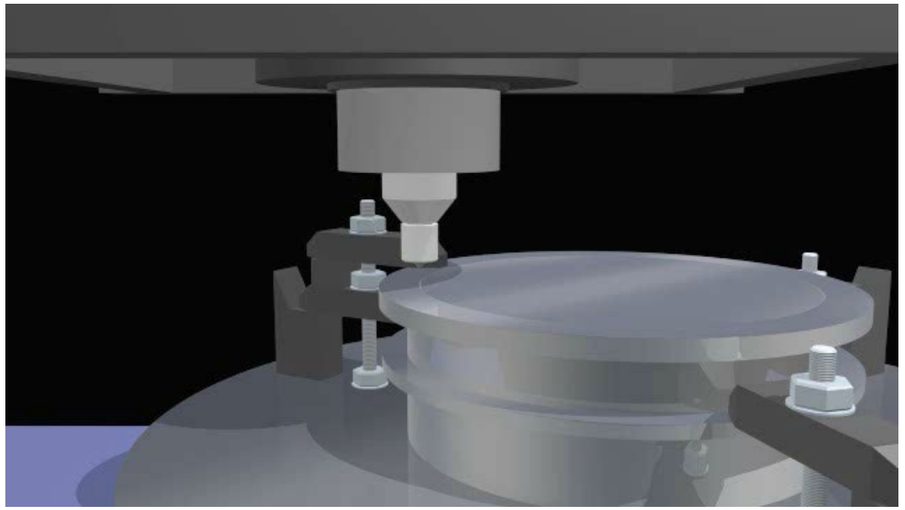

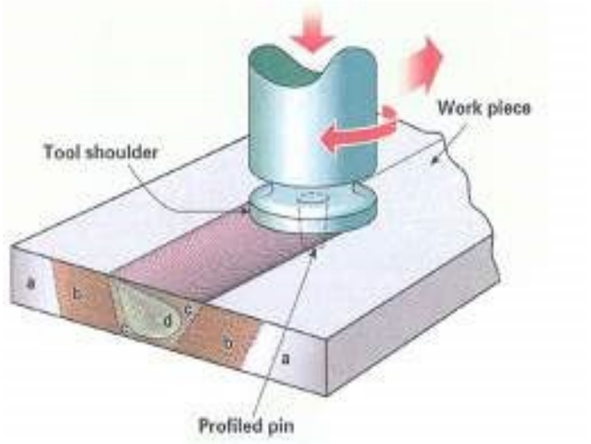

FSJ was invented and patented by TWI, Ltd. in 1991

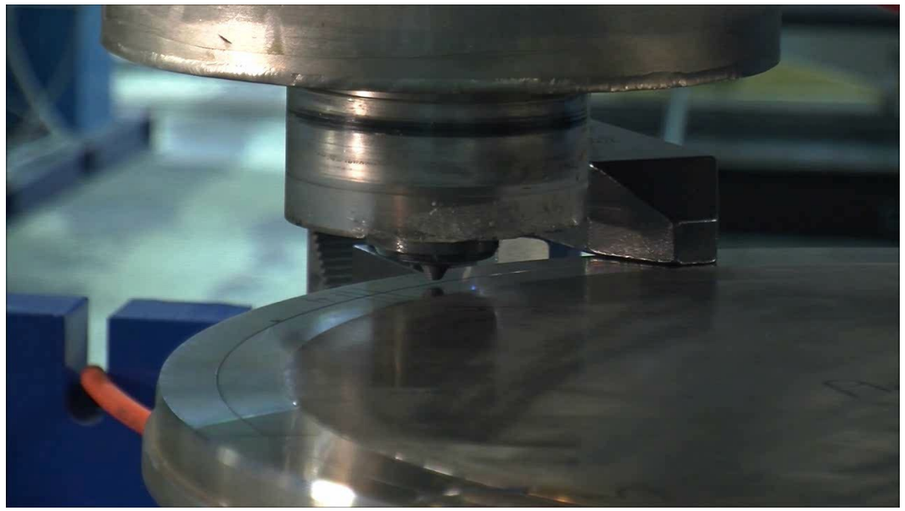

- Department of Energy's (DOE) Office of Environmental Management (EM)
- DOE Office of River Protection (ORP)

Pacific Northwest
NATIONAL LABORATORY

PNNL Capability: Material Characterization, Prediction and Control

Solid Phase Processing Science Initiative (SPPSi)

Coupling multi-scale models and measurements

Pacific Northwest NATIONAL LABORATORY

Multi-scale shear deformation

In situ friction stir welding apparatus (FlexiSTIR)

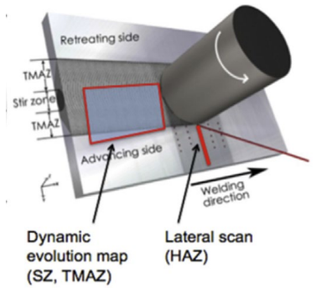

In situ high speed roto diamond anvil cell (DAC)

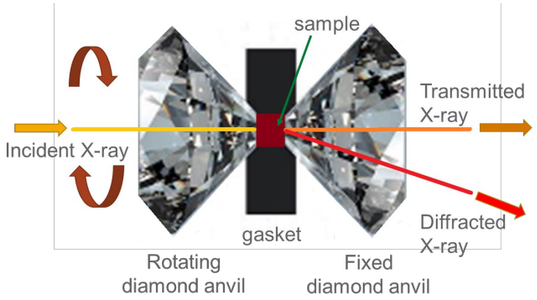

Atomic force microscope (AFM), PI88

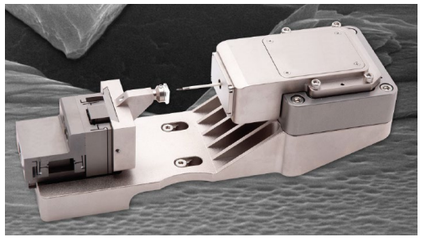

In situ transmission electron microscopy (TEM)

cm-mm → mm-μm → μm-nm → ~nm- Å

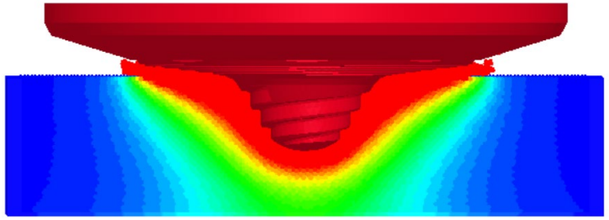

Smooth particle hydrodynamics(SPH): Process scale with high deformation

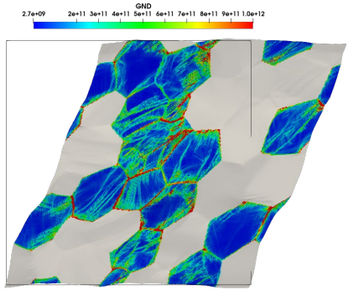

Crystal plasticity simulation: Dislocation density evolution

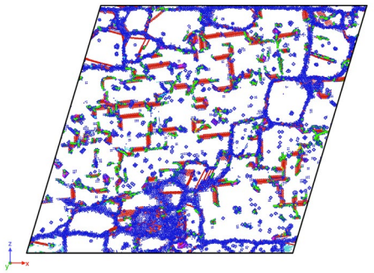

Molecular dynamics: dynamic defect evolution

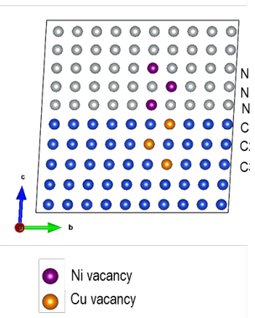

Density functional theory (DFT): Atomic scale mixing pathways & energetics

Pacific Northwest NATIONAL LABORATORY

Surrogate Modeling

Generation of Synthetic Micrographs

- Demonstrate data-driven, machine learning method for generation of:
  - Synthetic SEM images
  - Microstructural features
- Couple to Unified Micrograph Analysis

Utilize data-driven machine learning for prediction of

- Process → Microstructure relationships (grain-size, grain-orientation distributions)
- Process → Property relationships (microhardness)
- Microstructure → Property relationships (comparison to Hall-Petch relationship)

Demonstration of an Integrated Methodology

Use Case: Friction-Stir Processing of SS-316L

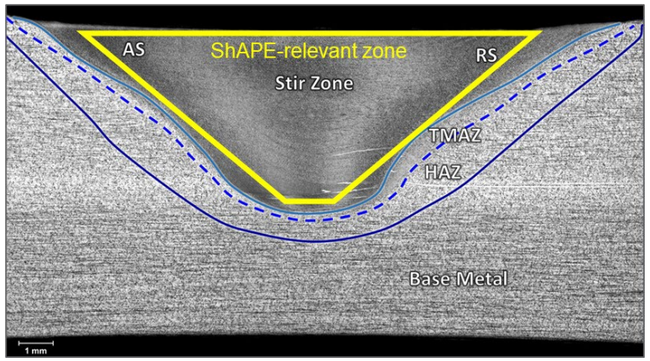

Representative Qualification Requirements

Microstructure (M)
Grain-size distribution
Grain-orientation distribution

Properties (P)
Hardness

Defects (D)
Predict and prevent

PREDICT and CONTROL System Response

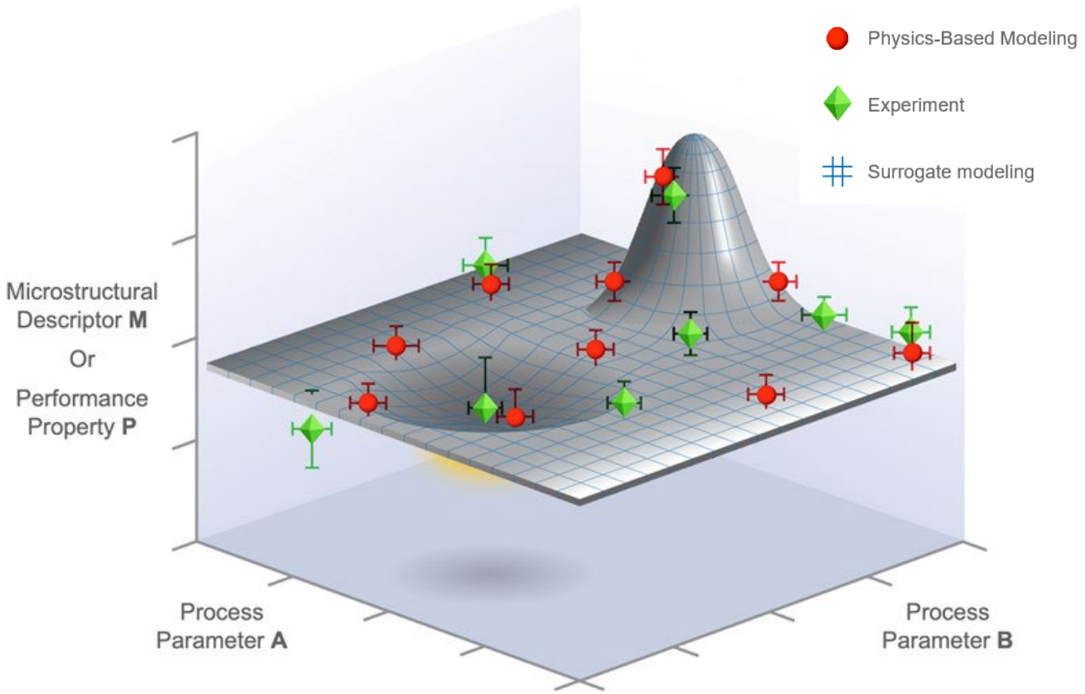

Automated UT Scanner

- Beam angle in specimen: 0˚
- Longitudinal wave
- **Flaw detection**

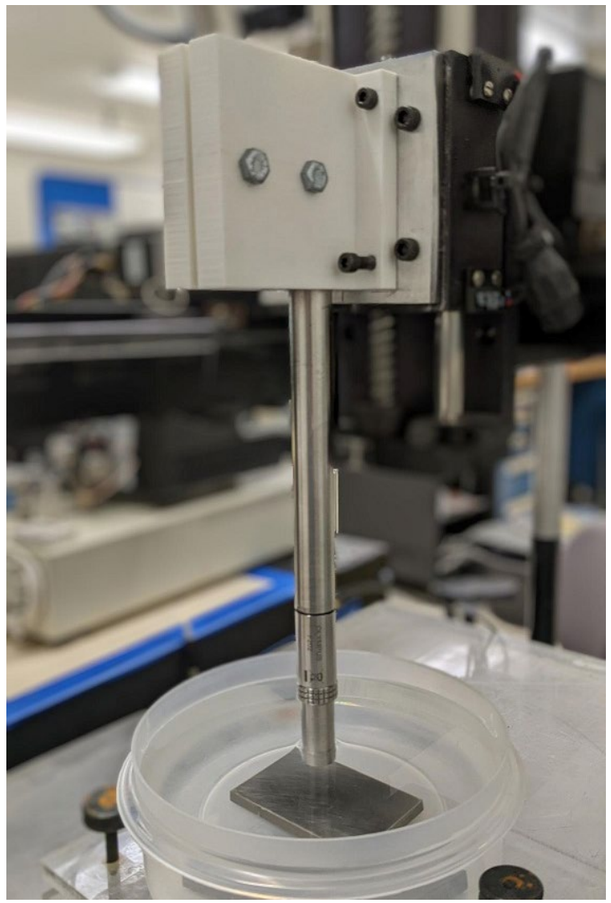

Raster scan

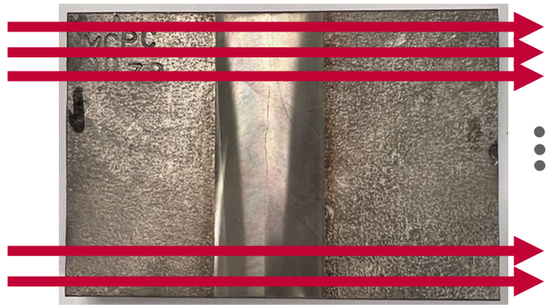

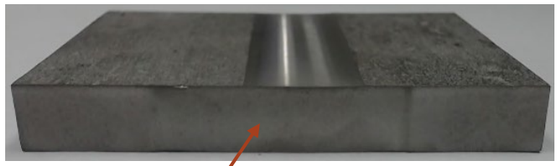

Transverse cross-section

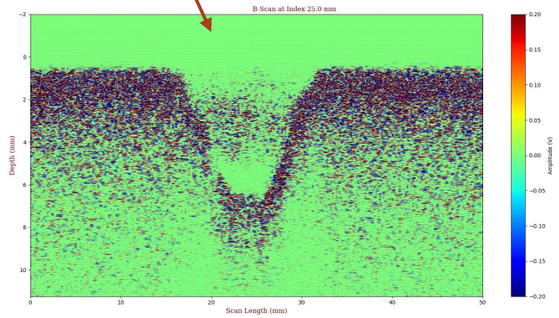

- Beam angle in specimen: 45˚
- Shear wave
- **Grain size measurement**

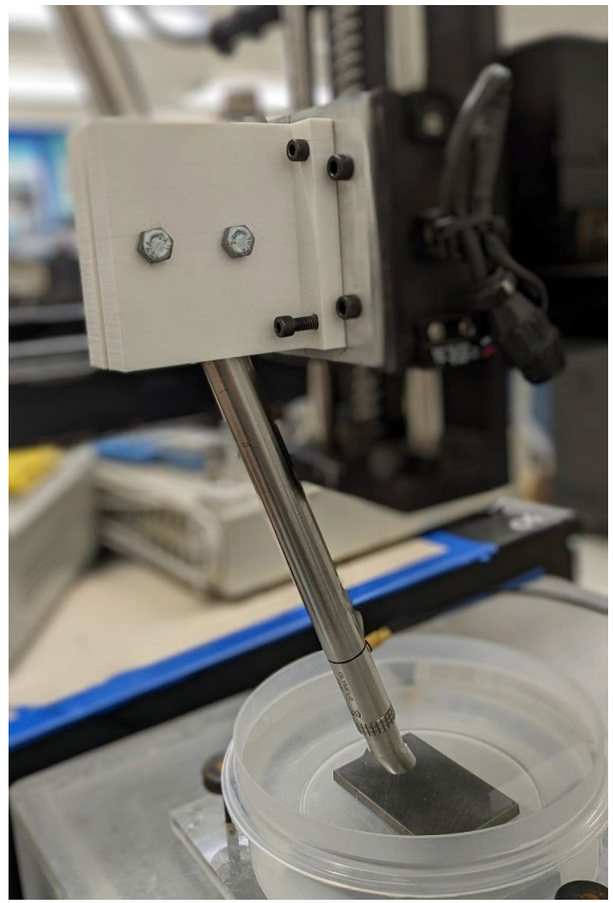

Partnering with Other Organizations

- Potential partners include
  - ❑ Intelligent Optical Systems – For Using Laser Ultrasonics
  - ❑ VRC – For Cold Spray
  - ❑ Westinghouse – For application cases, e.g. ATF development and production work

Solid Phase Processing

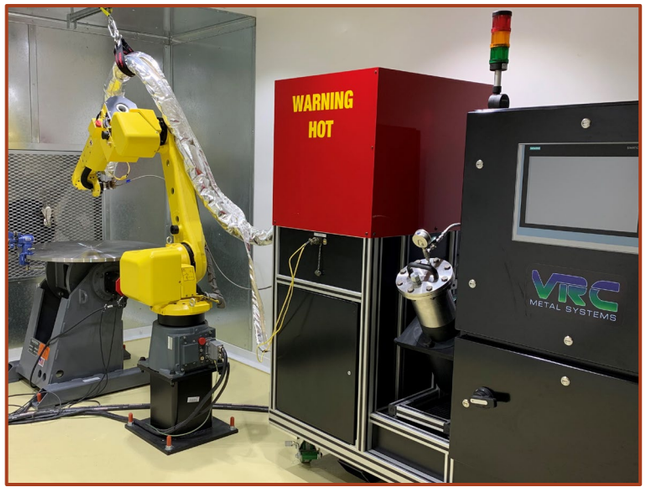

Cold Spray – VRC Gen-III at PNNL

Coated Cladding

Offline Laboratory Analysis

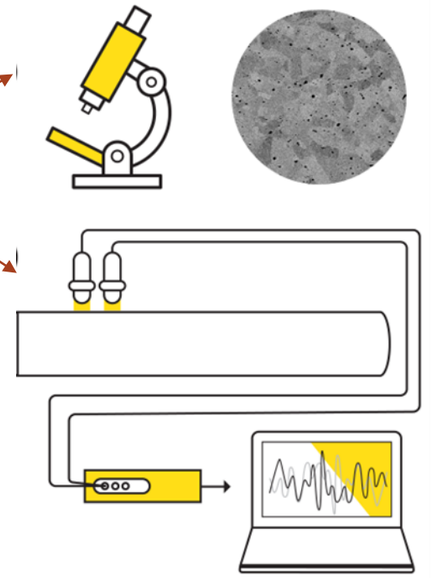

Online Nondestructive Monitoring

Solid Phase Process Monitoring and Quality Control

Pacific Northwest
NATIONAL LABORATORY

PNNL Capability: Refractory Electroplating

Introductory Overview: Refractory Electroplating

- We have developed a novel method of electroplating thin metal films from deep eutectic solvents (DES)
- Film quality is high and contamination is low
- Plating solvent constituents are not carcinogenic
- Refractory metals are used for their corrosion and erosion resistance, high melting temperature, and excellent mechanical properties
- Titanium and zirconium have been demonstrated in our system, but other metals are possible

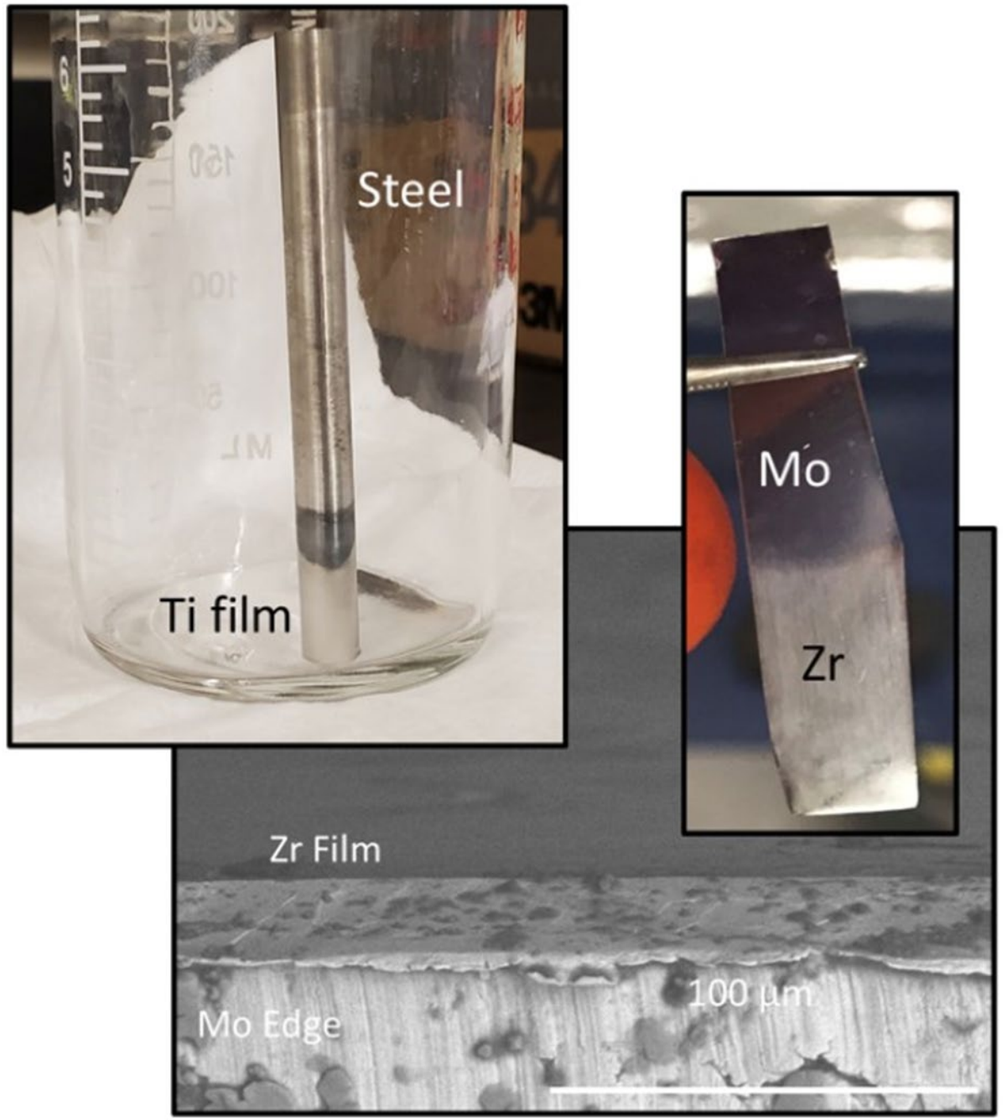

Pacific Northwest
NATIONAL LABORATORY

PNNL Capability: SCC, Creep, Corrosion Fatigue, and Fracture Toughness Testing Capabilities

Stress Corrosion Cracking Test Capabilities

- Test systems were designed and built in-house using a combination of custom and off-the-shelf parts.
  - 16 high temperature water test systems
  - 5 chloride salt test systems (for tests in salt solutions and humid air)
- Used for both crack initiation and crack growth rate measurements.
- In-situ measurement of cracking using a direct-current-potential-drop technique.
- Active control of load, stress intensity, temperature, many other environmental variables.

3-specimen test system

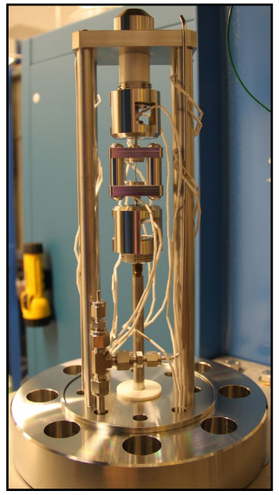

6-specimen test system

36-specimen test system

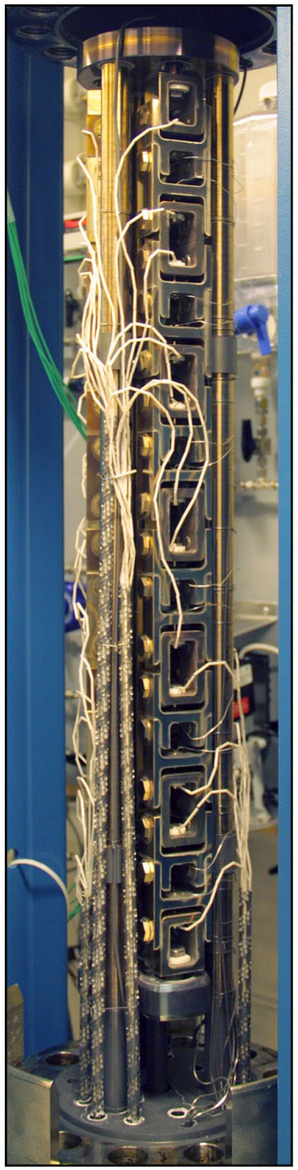

Pacific Northwest
NATIONAL LABORATORY

Other Test Capabilities

- Multi-specimen Creep Testing Capability
- Corrosion Fatigue Lifetime Testing
- Fracture Toughness Testing
- Microstructural Origins of Cracking Susceptibility

Pacific Northwest
NATIONAL LABORATORY

PNNL Capability: PIE for Spent Nuclear Fuel

Radiochemical Processing Laboratory (RPL) – A Category 2 Nuclear Facility in operation since 1953

- 144,095 square feet, ANS Historic Landmark
- 87 Research Laboratories
  - ❑ 21 Gloveboxes
  - ❑ 143 Fume Hoods and 9 Exhausted Enclosures
- 6 Shielded Research Laboratories containing 16 hot cells:
  - ❑ High Level Radiochemistry Facility - 3 interconnected hot cells
  - ❑ Shielded Analytical Laboratory - 6 interconnected hot cells
  - ❑ Shielded Isotope Separations Laboratory - 2 stand alone hot cells
  - ❑ High Activity Separations Laboratory - 1 stand alone hot cell
  - ❑ Shielded Process Development Laboratory - 2 stand alone hot cells
  - ❑ Shielded Materials Examination Laboratory - 2 stand alone hot cells
- $150M investment over the next decade to upgrade and extend service life

From Full-Length Rods to TEM Samples and Everything In-Between Under One Roof

Hot Cell Capacity and Adaptability

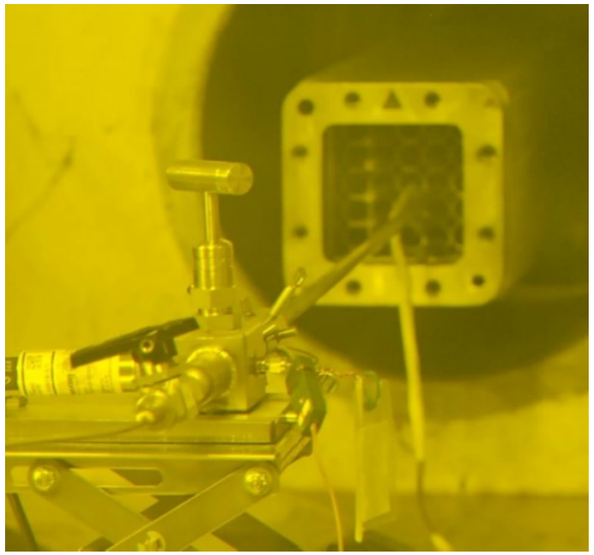

Rod Puncture/FGR

Fuel Dissolution/Chemical Burnup Analysis

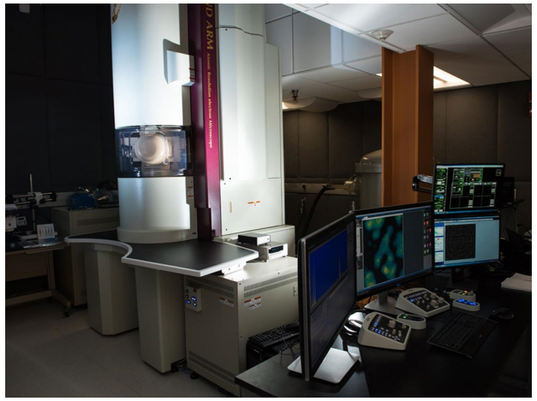

Aberration-Corrected Scanning Transmission Electron Microscope

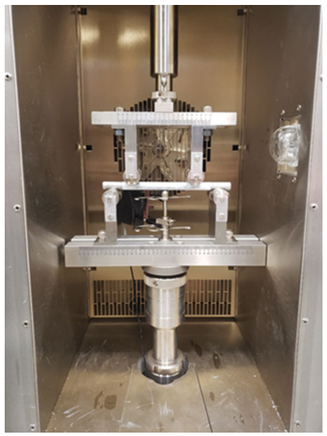

Mechanical Property Testing

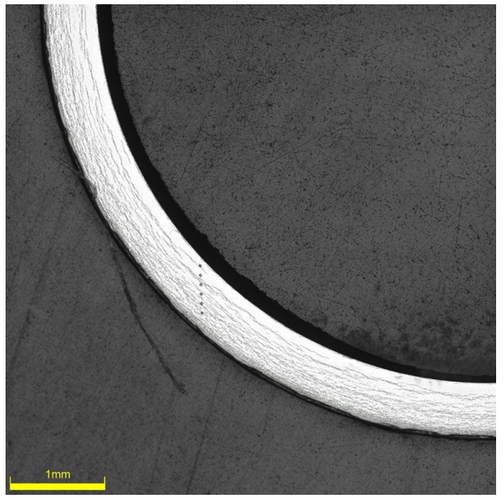

Metallography/OM/SEM/Microhardness/ Total Hydrogen Content

High Level Radiochemistry Facility (HLRF)

- Three interconnecting cells:
  - A-Cell 15’W x 8.5’D x 15’H
  - B- , C-Cells 6’W x 8.5’D x 15’H
- Viewing windows provide equivalent shielding as front face walls (oil-filled leaded-glass windows).
- A-Cell completely refurbished (window seals, crane, lights, operating deck) in 2022

- Front face and side shielding walls are 48” high-density concrete.
- Rear walls are 36” high density concrete.
- Main shield access doors are 18” steel.

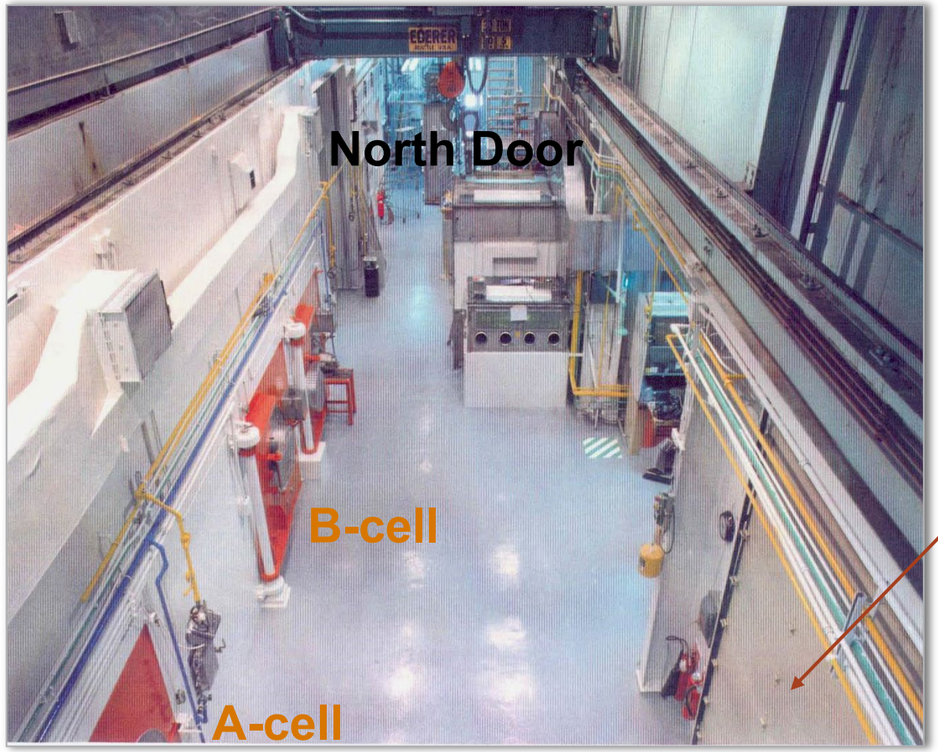

Shielded Analytical Laboratory (SAL)

Six Interconnected Cells

- 6’W x 5.5’D x 6’H
- Viewing Windows: 2 - 12” panes high-density leaded glass
- Shielding Walls are 26” high-density concrete for back wall and 12” iron for front wall

Process Development Cells (PDC)

PDC 1 and PDC 2

- Shielding Walls are 12” steel
- 5.5’W x 5’D x 12’H
- Viewing Window: 18” thick high-density leaded glass

- PDC1
  - Welding for end caps
  - Pressurization system
  - Laser welder
  - Optical micrometer

- PDC2
  - Oven
  - Saw
  - Videography

Materials Examination Cells (MEC)

MEC 1

12-inch steel shielding
10’W x 5’D x 12’H inside dimensions

MEC 2

12-inch steel shielding
7’W x 5’D x 12’H inside dimensions

EDM/mill will be installed later in CY 2023

PIE-Enabled Study of Aqueous Corrosion & Zr Hydriding in Cr-Coated Cladding

The I-NERI project PERSEUS core objective: Perform the advanced PIE (post-irradiation examination) of accident-tolerant fuel (ATF) cladding materials irradiated in the BR2 test reactor within the H2020 IL TROVATORE project (EURATOM fund; Grant Agreement No. 740415).

Material supply
Uncoated vs. Cr-coated Optimised ZIRLOTM (WH)

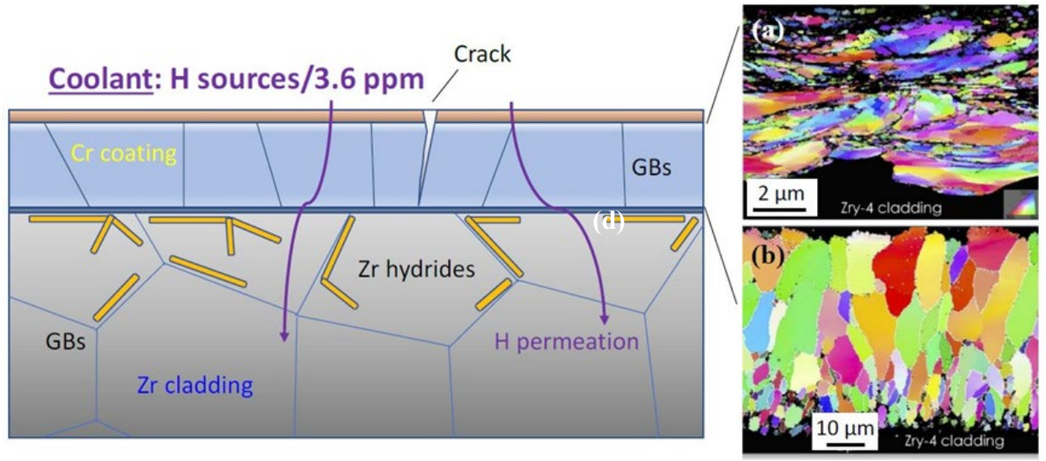

The multimodal comparative post irradiation examination (PIE), supported by a DOE GAIN Voucher, will aim at gaining unique insights into the hydrothermal corrosion effects and hydrogen transport mechanisms governing the formation of embrittling Zr hydrides in various Cr-coated ATF claddings concepts provided by Westinghouse Electric Company LLC (WH).

PNNL Experience and Expertise in Commercial Spent Nuclear Fuel

1980s

- Received, characterized, and tested commercial spent nuclear fuel as part of the Materials Characterization Center (MCC)
  - ❑ Approved Test Materials (ATM): -101, -103, -104, -105, -106, and -108
  - ❑ PWR and BWR fuel
    - Assembly or multiple rods
  - ❑ See e.g., “Characterization of Spent Fuel Approved Testing Material—ATM-104”, R.J. Guenther et al., Pacific Northwest Laboratory, December 1991, PNL-5109-104.

1980s-2008

- Lead laboratory for Waste Form Degradation testing in support of the Yucca Mountain Project and the National Spent Nuclear Fuel Project
  - ❑ Oxidation and dissolution studies

PNNL Experience and Expertise in PIE

Present

- Design authority and lead laboratory for PIE of the Tritium Producing Burnable Absorber Rods (TPBARs) receiving new rods approximately every 18 months
  - ❑ Latest receipt in January 2023
- Extended Storage and Transportation (NE-8)
- PNNL supporting Westinghouse GAIN voucher program on PIE of ATF samples (PERSEUS program)
- PIE on 10 high burnup spent fuel rods under the DOE-NE High Burnup Spent Fuel Data Project
- Sibling Pin Project
  - ❑ Phase 1 (2018 – 2023): Perform baseline characterization (as-irradiated) of rods to determine the condition and properties
  - ❑ Phase 2 (2023 – 2025 or longer): Focus on effects of drying and dry storage

Pacific Northwest
NATIONAL LABORATORY

Typical PIE Processes and Measurements

Typical PIE Processes and Measurements in a PNNL Project:

- Rod Puncture, and Fission Gas Analysis
- Rod Sectioning, and Fuel Dissolution
- Unetched for dimensions and microhardness
- Hydrogen Analysis, Etched to reveal hydrides
- Defueled Mechanical Property Testing Capability:
  - ❑Fatigue Testing,
  - ❑Tensile Testing with Digital Image Correlation,
  - ❑Burst Test,
  - ❑4-point Bend Testing with Digital Image Correlation,
  - ❑Radionuclide Analysis/Burnup Analysis

Pacific Northwest
NATIONAL LABORATORY

Thank you

Guoqiang Wang, Ph.D., ASME Fellow
Chief Engineer, National Security Directorate
Pacific Northwest National Laboratory (PNNL)
902 Battelle Boulevard
P.O. Box 999, MSIN K8-34
Richland, WA 99354, USA
Phone: +1 509.375.2101
Mobile: +1 412.378.1796
Email: Guoqiang.Wang@pnnl.gov

A.M. Kpemou
IRSN

A separate effects study of secondary hydriding during a LOCA transient

Secondary hydriding may occur during Loss of coolant Accident (LOCA) when nuclear fuel cladding is exposed to steam at high temperature. During a LOCA transient, the cladding may burst, and the steam ingress results in cladding inner surface oxidation in the vicinity of burst opening in the ballooned region. The inner gaseous environment is progressively enriched with hydrogen released during zirconium oxidation by steam. At a certain distance from burst opening the internal gaseous environment is highly enriched in hydrogen which can be partly absorbed by the cladding leading to a localized high hydrogen content that can reach up to several thousand wppm at the peak. Semi-integral devices were set up to experimentally reproduce LOCA transients consequences and usually lead to hydrogen enriched bands, at a few tens of a millimeter from burst opening. The complex nature of these tests combined to the uneven deformed cladding geometry obtained after burst impedes the direct study of the various parameters influencing secondary hydriding.

In the present study, burst opening size, pellet-cladding gap size, oxidation duration and other parameters influences are characterized using an axisymmetric testing procedure reproducing LOCA conditions including cladding oxidation and the final quench of the sample.

A non-deformed zirconium alloy cladding tube is inserted upwards in a vertical resistive furnace. The tube is opened on its upper end, tightly closed on the lower end, and is filled with stacked ceramic pellets (porcelain & alumina) and exposed to steam at high temperature (~1200 °C). As expected from semi-integral tests, the region of the cladding surface just below the top of the pellet stack is oxidized by steam penetrating in the cladding-pellet gap. Hydrogen gas release occurs, resulting from cladding oxidation process, and a high hydrogen uptake by the cladding is evidenced a few millimeters below the top of the pellet stack corresponding to a position where the thin internal oxide layer disappears. This procedure allows using close to axisymmetric LOCA tests to study the influence of several parameters on secondary hydriding. The generated data can be used to support secondary hydriding modeling using simple and well-defined conditions. A set of post-test analyses is systematically performed on the cladding samples subjected to this procedure. Post-quench material microstructure, including inner and outer oxide layer thickness axial profiles, were characterized using metallography. Hydrogen axial profiles were obtained mainly by Hot Vacuum Extraction (HVE). Neutron radiography was also used to perform hydrogen measurement. A sample was analyzed using Electron Probe Micro-Analysis (EPMA) and Micro Laser Induced Breakdown Spectroscopy (μ-LIBS) to map oxygen and hydrogen local concentrations in an extended region.

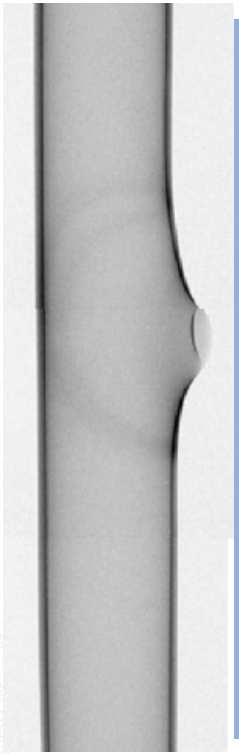

A SEPARATE EFFECTS STUDY OF SECONDARY HYDRIDING DURING A LOCA TRANSIENT

Apou Martial KPEMOU *(IRSN - INSA LYON)*

Marie-Christine BAIETTO *(INSA LYON / LAMCOS)*
Bernard NORMAND *(INSA LYON / MATEIS)*
Séverine GUILBERT *(IRSN)*
Tatiana TAURINES *(IRSN)*

Mirco GROSSE (KIT)
Julian SOULACROIX (EDF)
Antoine AMBARD (EDF)
Florent BOURLIER (Framatome)

28th International QUENCH-Workshop

LOCA – Secondary hydriding

LOCA transient

$$oxidation\ reaction: Zr + 2H_20 \rightarrow ZrO_2 + 2H_2$$

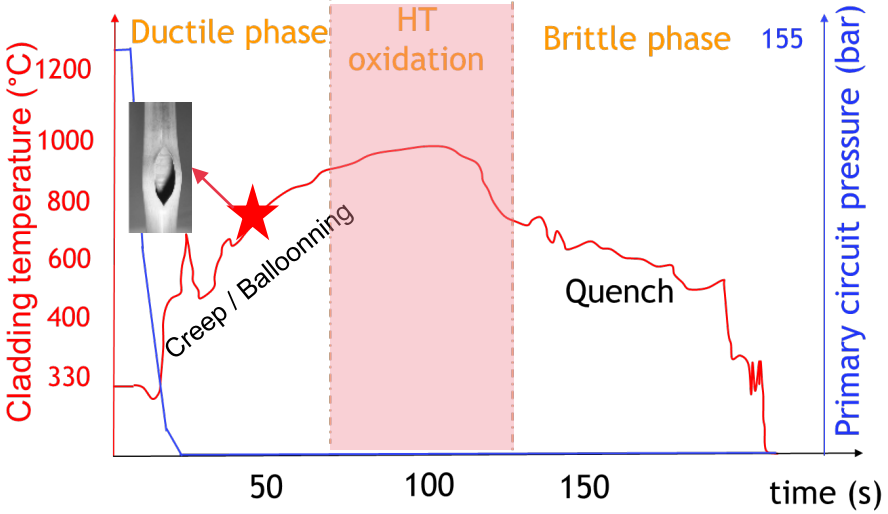

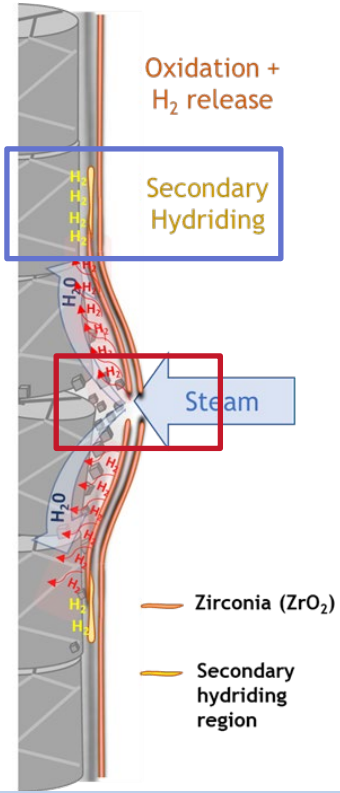

Illustration of secondary hydriding

Oxygen content (wt%)

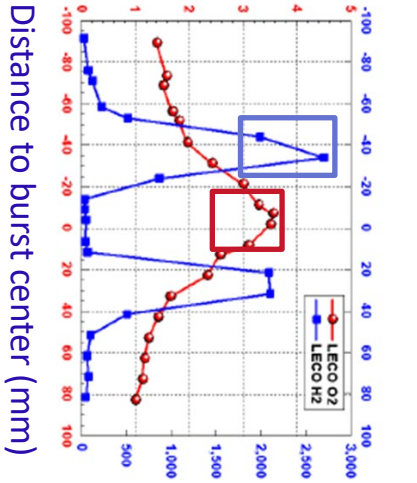

Hydrogen content (wppm)

[M. Billone, 2008] (OCL#22 unirradiated sample)

Ballooning → Burst → Steam ingress in the inner side of the cladding → oxidation → secondary hydriding

LOCA – Secondary hydriding

Semi – integral tests

- Understand the overall behavior of fuel rods during LOCA
- Highly coupled phenomena → Impede study of separate effects

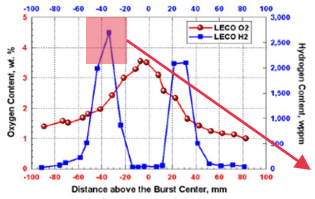

[M. Billone, 2008]

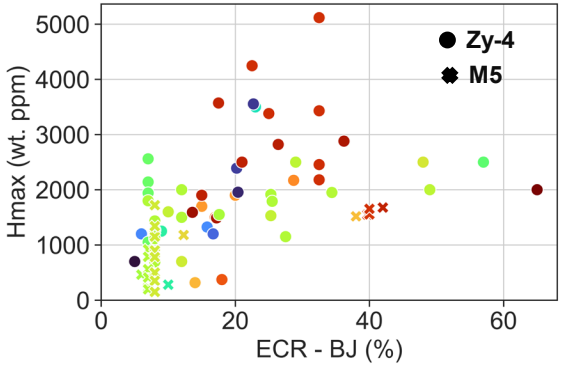

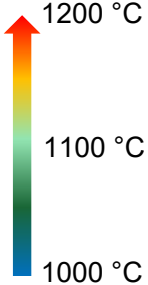

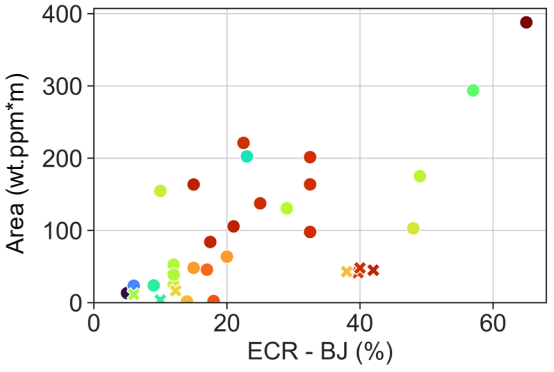

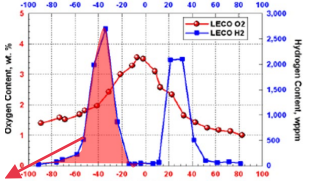

$$S = \int [H\ (wppm)]dz\ (m)$$

Data obtained from LOCA tests in literature regarding secondary hydriding on unirradiated cladding (JAEA, EDF, CEA, KIT, IRSN)

*M5 and $M5_{Framatome}$ are registered trademarks of FRAMATOME or its affiliates, in the USA or other countries

ECR : Equivalent Cladding Reacted (metric representing the degree of cladding oxidation)

LOCA – Secondary hydriding

Semi – integral tests

- Understand the overall behavior of fuel rods during LOCA
- Highly coupled phenomena → Impede study of separate effects

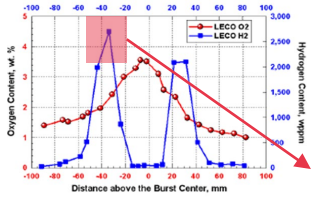

[M. Billone, 2008]

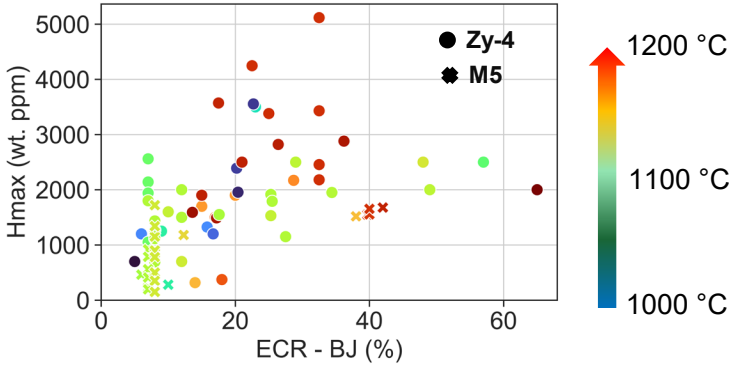

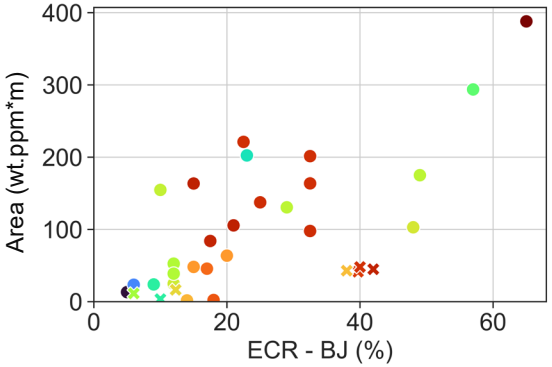

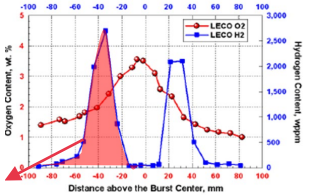

$$S = \int [H\ (wppm)]dz\ (m)$$

Data obtained from LOCA tests in literature regarding secondary hydriding on unirradiated cladding (JAEA, EDF, CEA, KIT, IRSN)

*M5 and $M5_{Framatome}$ are registered trademarks of FRAMATOME or its affiliates, in the USA or other countries

These results give an overall trend but depend on test parameters (oxidation temperature, cladding geometry after burst, opening size, gap size, etc…)

→ Separate Effects Tests (SETs)

ECR : Equivalent Cladding Reacted (metric representing the degree of cladding oxidation)

LOCA – Semi-integral tests vs SETs

Semi-integral tests

3D

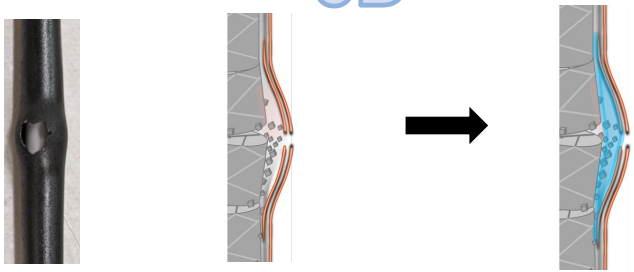

Deformed cladding

axially varying gap size

Influence of gap size

SETs

1.5D

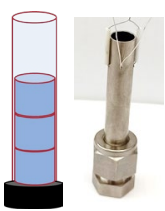

Undeformed cladding

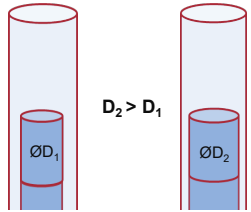

~uniform gap for each test

Modelling complexity → Separate effects analysis

LOCA – Semi-integral tests vs SETs

Semi-integral tests

3D

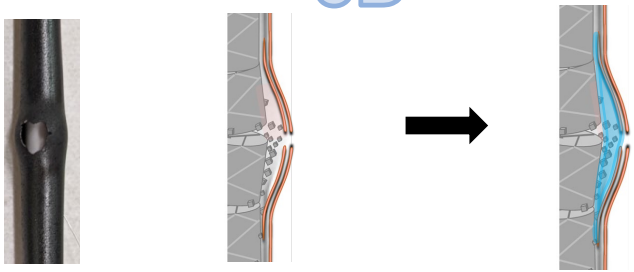

Deformed cladding

axially varying gap size

Influence of gap size

SETs

1.5D

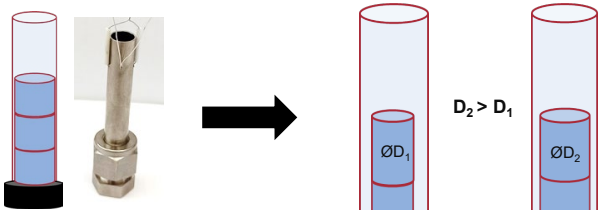

Undeformed cladding

~uniform gap for each test

Modelling complexity → Separate effects analysis

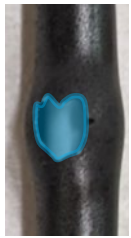

Variable opening size

Influence of opening size

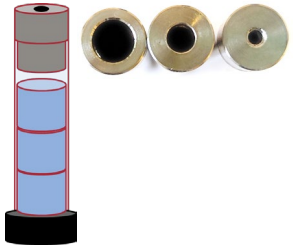

Cladding's cover with a defined opening size

SETs are suitable for modelling with well-defined boundary conditions

Sample geometry and material

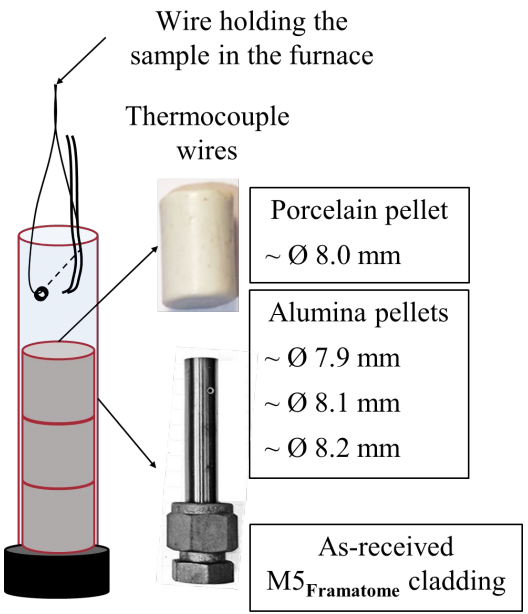

LOCA transient

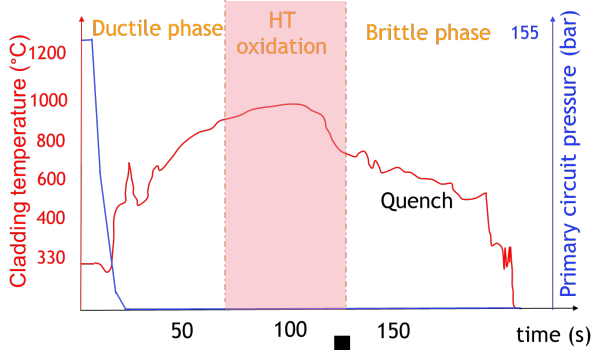

SETs thermal transient

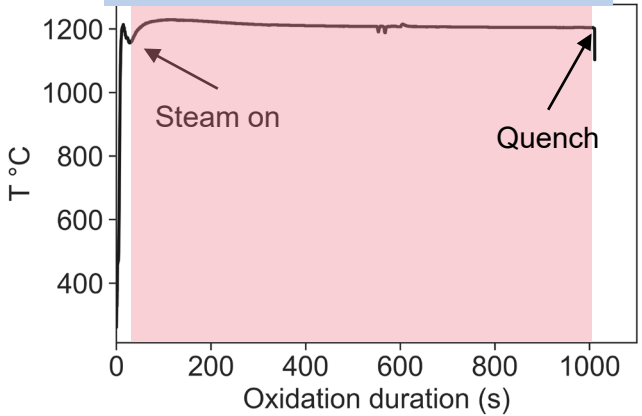

Tests in oxidizing environment (50% Ar + 50% H_2O) at ~1200 °C

Sample geometry and material

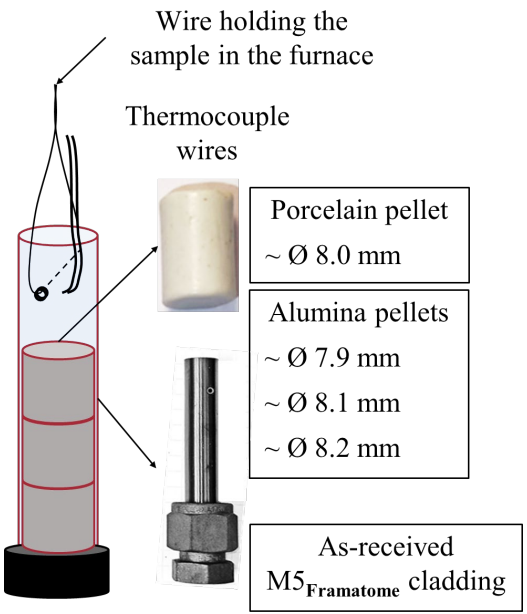

LOCA transient

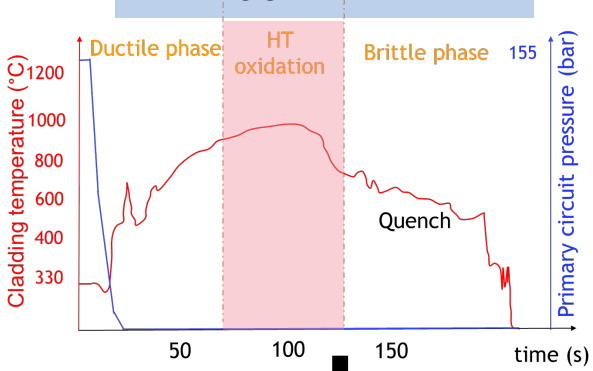

SETs thermal transient

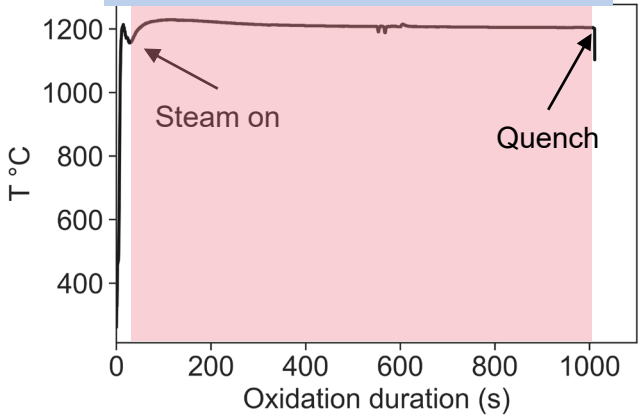

Vertical furnace for oxidation stage

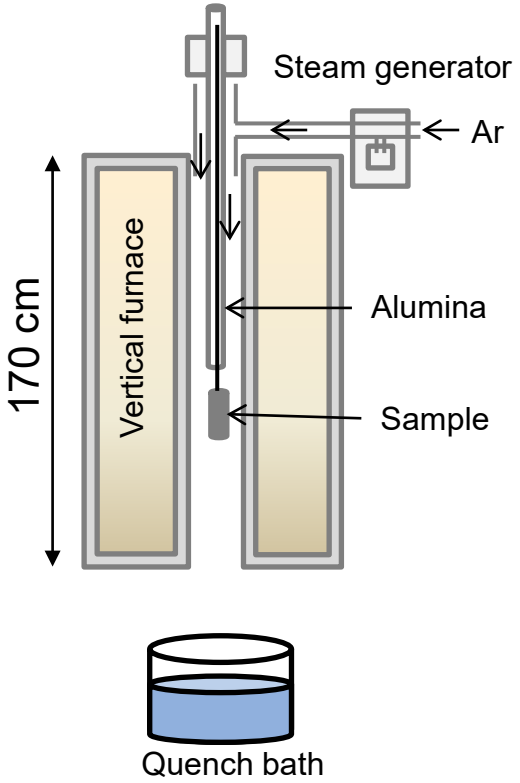

Tests in oxidizing environment (50% Ar + 50% H_2O) at ~1200 °C

Sample geometry and material

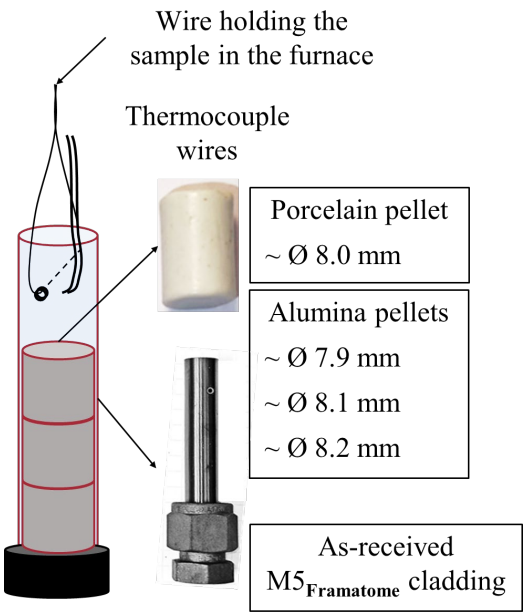

LOCA transient

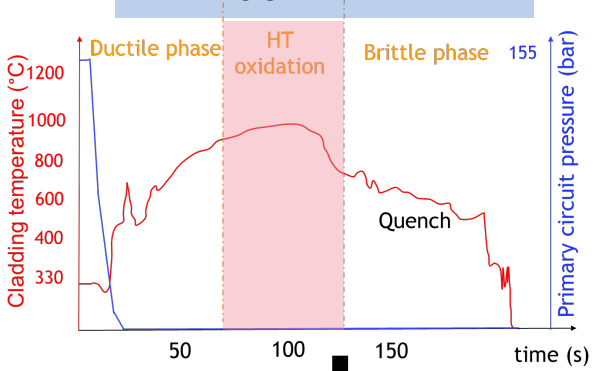

SETs thermal transient

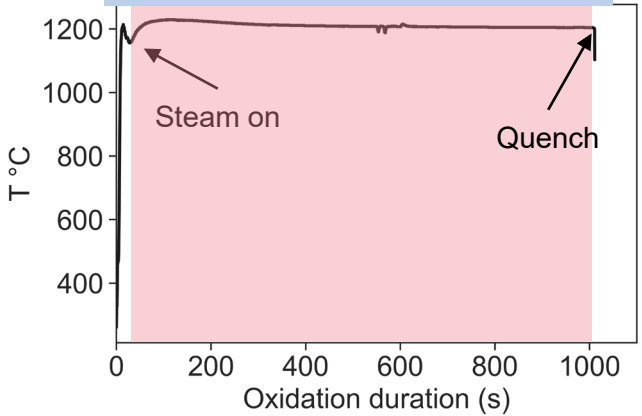

Vertical furnace for oxidation stage

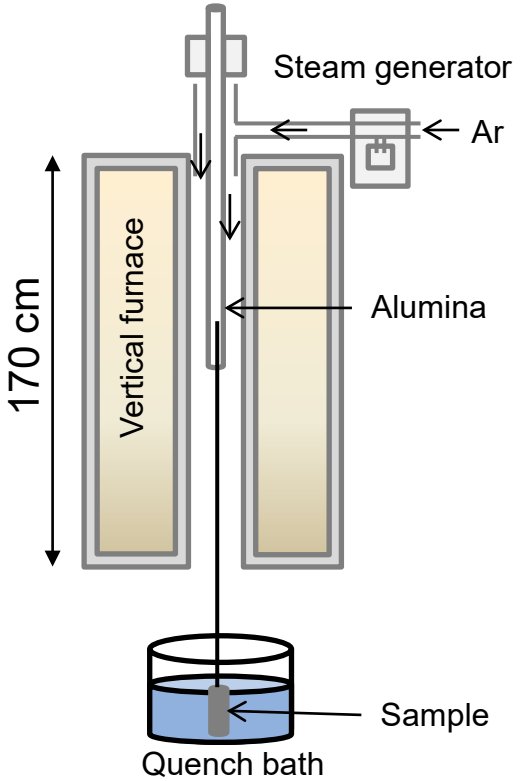

Tests in oxidizing environment (50% Ar + 50% H_2O) at ~1200 °C

SETs – Hydrogen measurements by HVE[1]

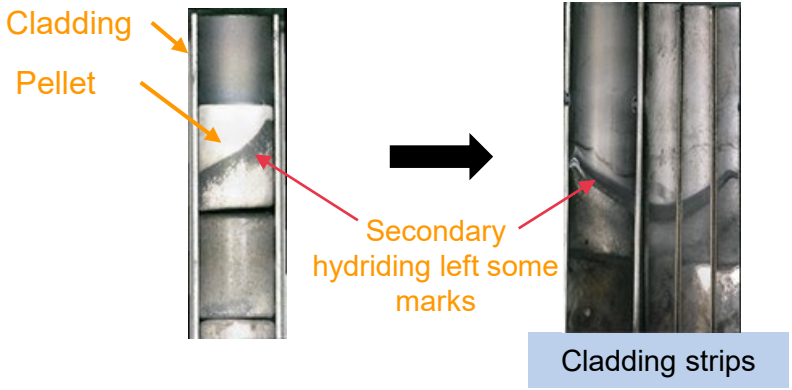

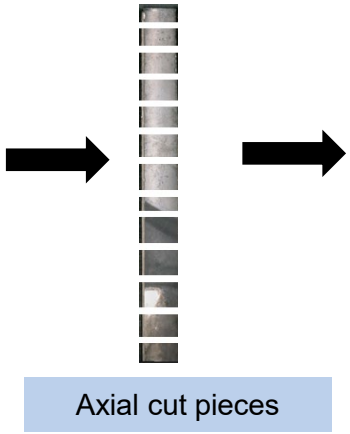

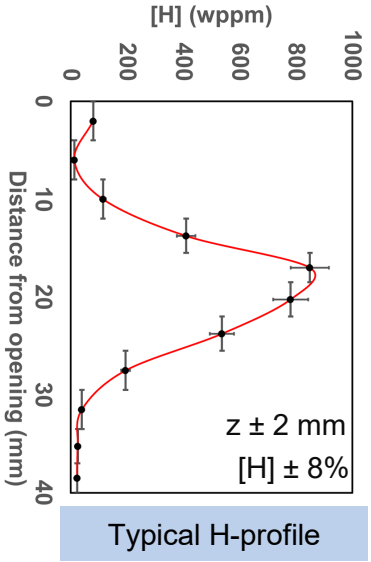

Hydrogen axial profile using Hot Vacuum Extraction (HVE)

[1]Hot Vacuum Extraction

SETs – Hydrogen measurements by HVE[1]

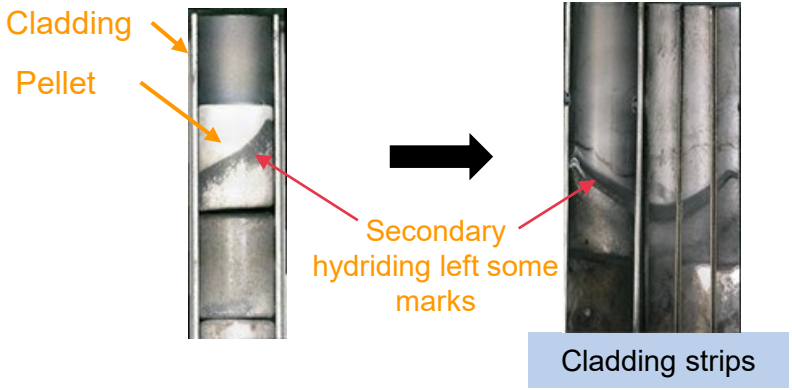

Cladding strips

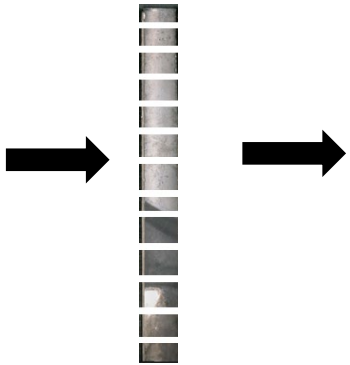

Axial cut pieces

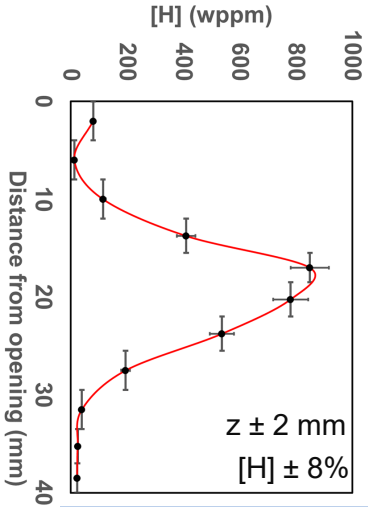

Typical H-profile

Hydrogen axial profile using Hot Vacuum Extraction (HVE)

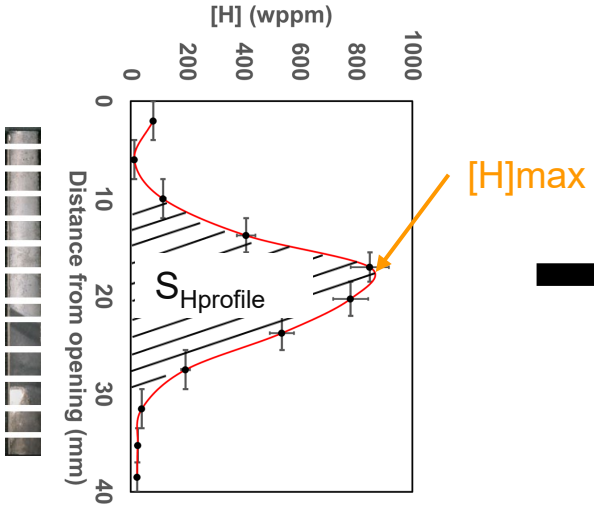

Characterization of each hydrogen axial profile

- Hydrogen content at the peak (Hmax)
- Integral hydrogen content uptake by the cladding ($S_{Hprofile}$)
- Full Width at Half Maximum (FWHM)

[1]Hot Vacuum Extraction

Post-test visual examinations of pellets and cladding inner surface

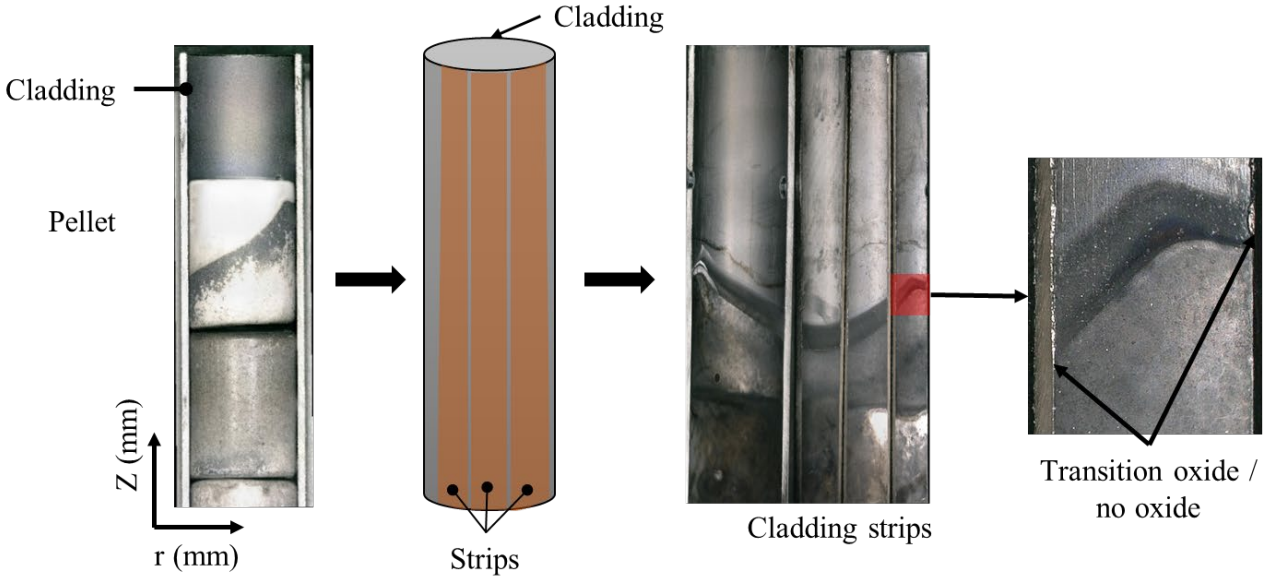

- Marks on pellets and cladding inner surface indicate secondary hydriding area
- Influence of pellets positioning on hydrogen azimuthal distribution was evidenced through neutron radiography measurements

Influence of pellets positioning on secondary hydriding

Heterogeneous distribution

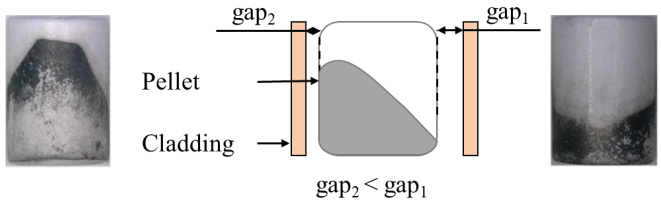

Non co-axial positioning of pellet

Influence of pellets positioning on secondary hydriding

Heterogeneous distribution

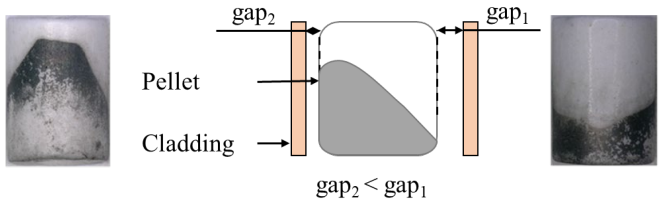

Non co-axial positioning of pellet

~ homogeneous distribution

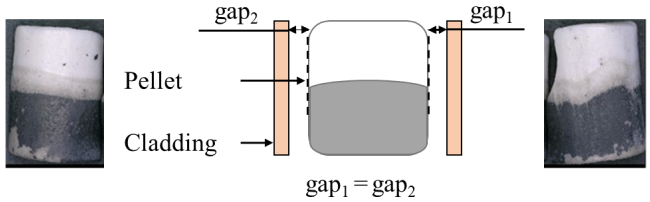

Co-axial positioning of pellet

Pellet positioning influences steam and hydrogen ingress inside the cladding

Influence of pellets positioning on secondary hydriding

Heterogeneous distribution

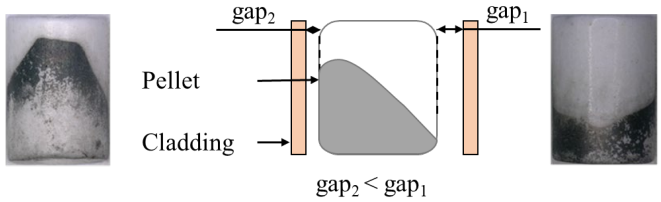

Non co-axial positioning of pellet

~ homogeneous distribution

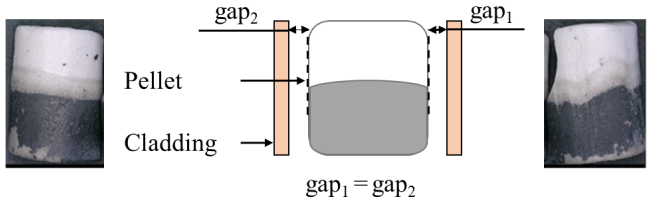

Co-axial positioning of pellet

Pellet positioning influences steam and hydrogen ingress inside the cladding

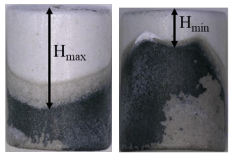

$$\delta_{Hsec} = \frac{H_{max} + H_{min}}{2}$$

Evolution of HSEC position over oxidation duration

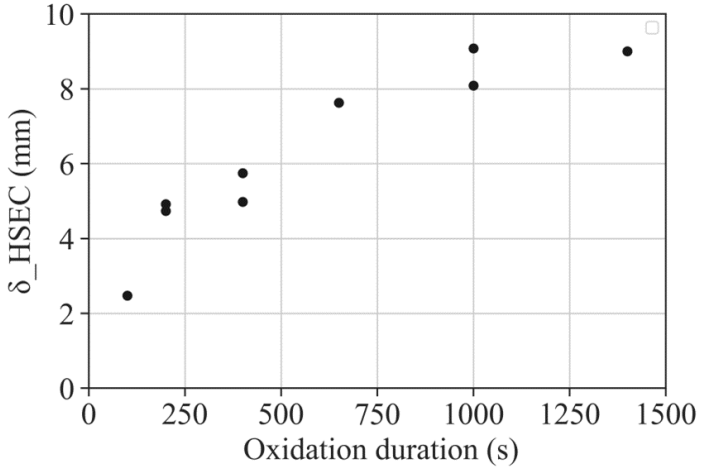

Hydrogen uptake shifts away ingress with oxidation duration

SETs – Influence of pellets positioning on hydrogen distribution

Hydrogen measurements using neutron radiography analysis

~1210 °C / 250 s

Cladding cuts in several strips

Hydrogen measurements using neutron radiography analysis

~1210 °C / 250 s

Cladding cuts in several strips

Neutron radiography analysis

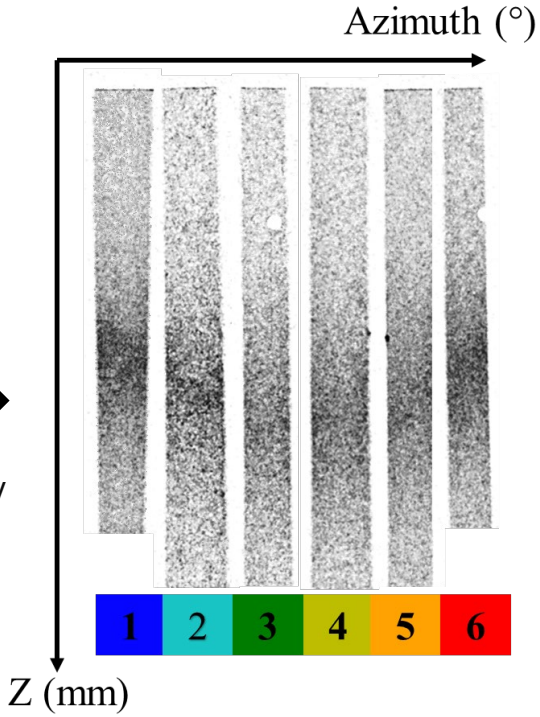

High hydrogen spots in dark area

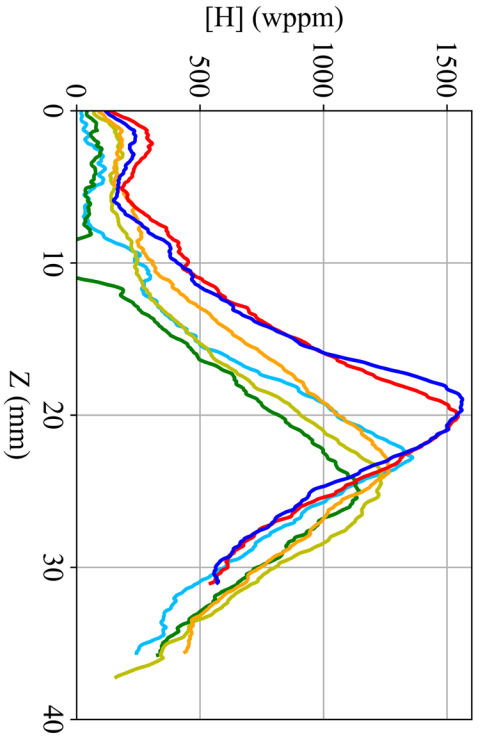

Hydrogen axial profiles

Influence of pellets positioning of hydrogen distribution

Azimuthal distribution of hydrogen regarding pellet positioning

Azimuthal distribution of marks on cladding

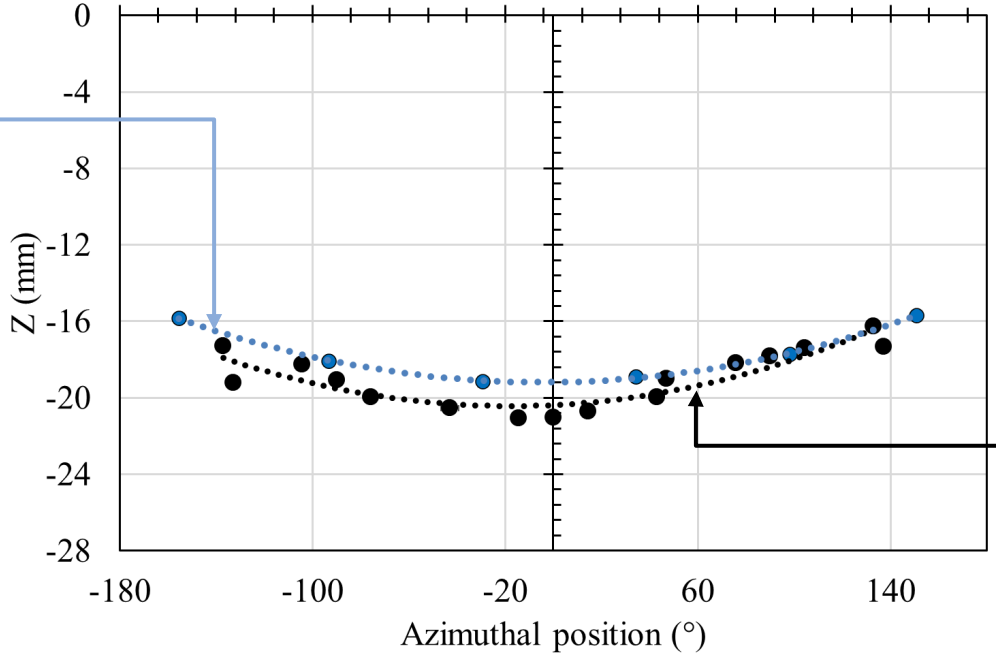

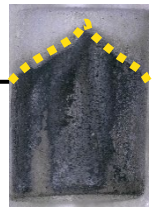

Azimuthal distribution of marks on pellet

The marks on both the inner cladding surface and pellet surface are coherent

Azimuthal distribution of hydrogen regarding pellet positioning

Azimuthal distribution of marks on cladding

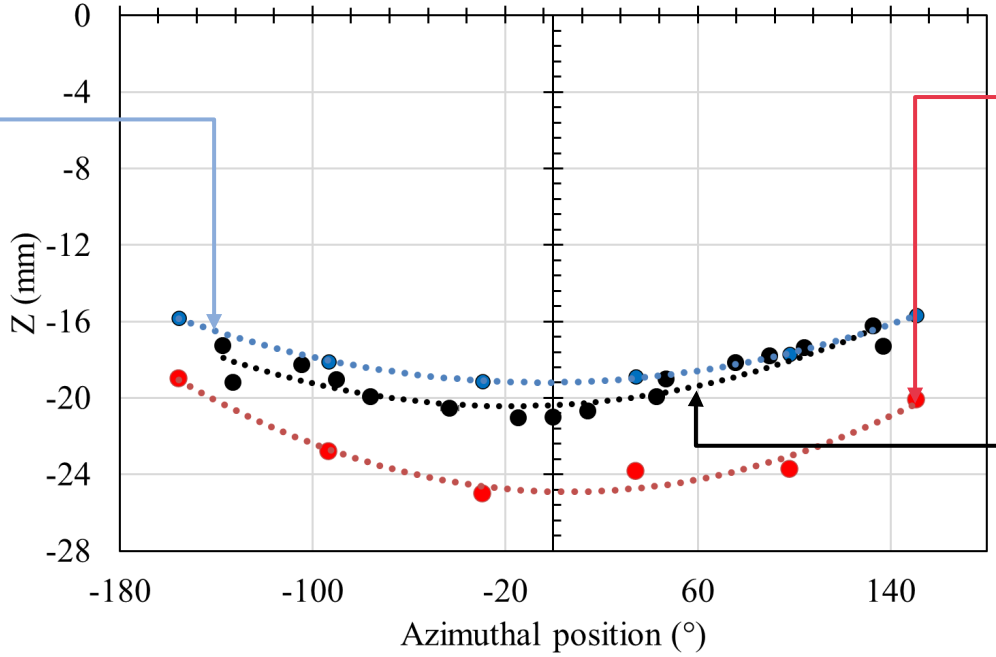

Azimuthal distribution of hydrogen peak position

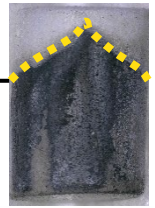

Azimuthal distribution of marks on pellet

The marks on both the inner cladding surface and pellet surface are coherent

Comparison between HVE[1] and neutron-radiography

Tox = ~ 1210 °C – tox = 250 s

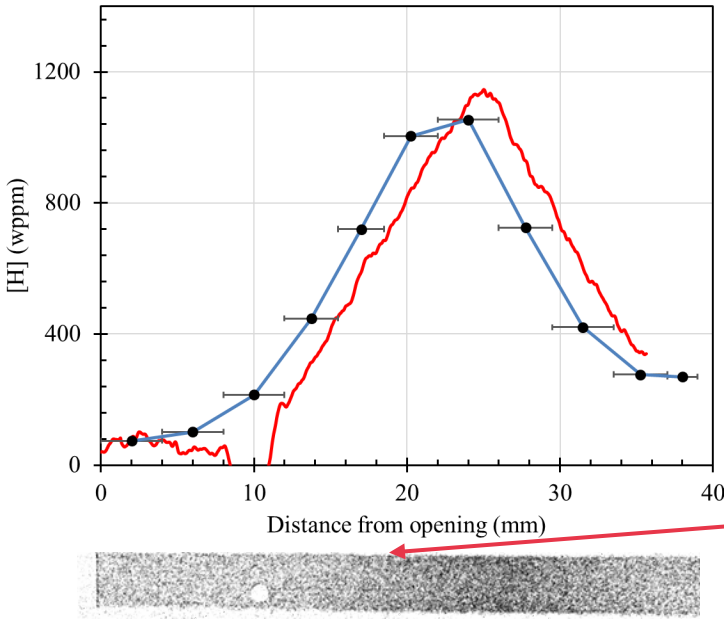

HVE ([H] ± 8%)

Neutron-radiography

Tox = ~ 1210 °C – tox = 600 s

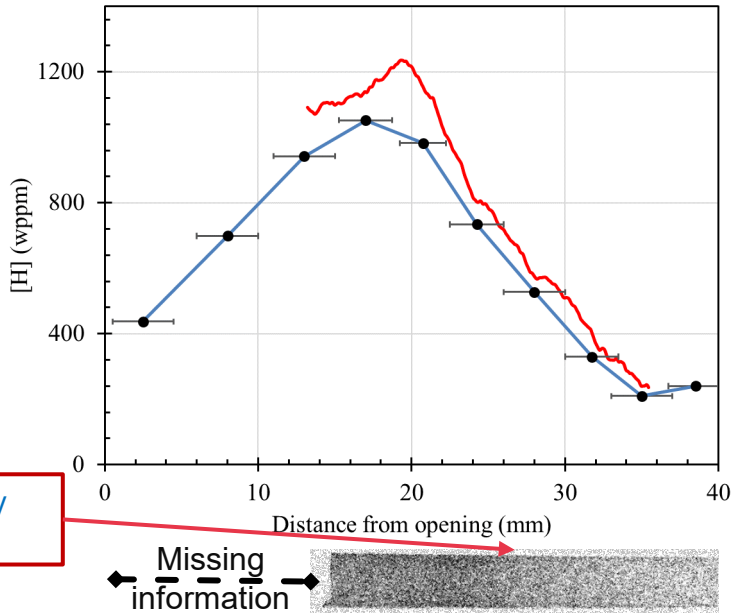

neutron-radiography image

Missing information

- Both measurements from HVE and neutron-radiography are coherent
- The hydrogen maximal content can be slightly be underestimate by HVE

[1]Hot Vacuum Extraction

Hydrogen axial profiles for different oxidation durations (Tox : ~1150°C – 1200°C)

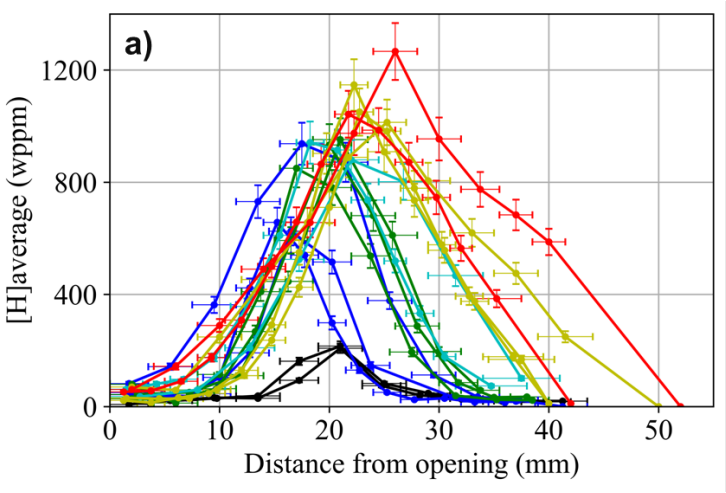

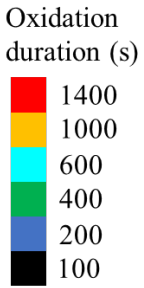

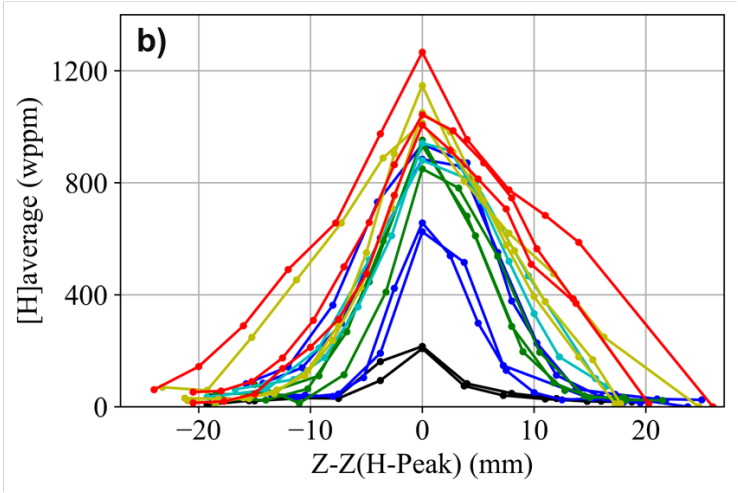

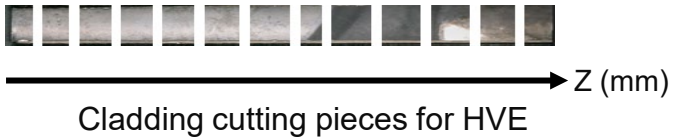

Cladding cutting pieces for HVE

- Hydrogen axial profile evolves with respect to oxidation duration
- The exact location of the peak is not well known due to the uncertainty on HVE & azimuthal variations

Influence of oxidation temperature and oxidation duration

Evolution of S with oxidation duration and temperature

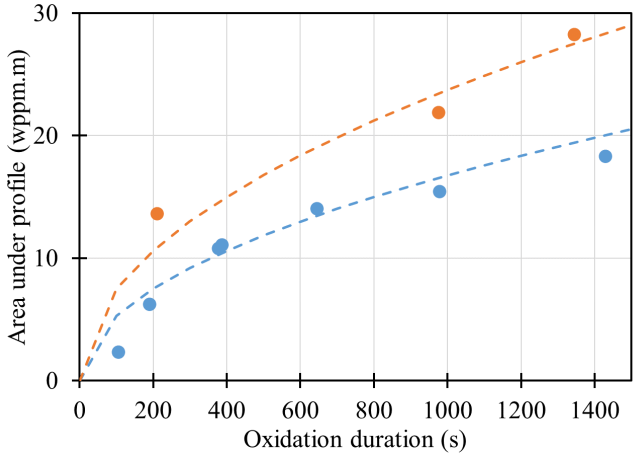

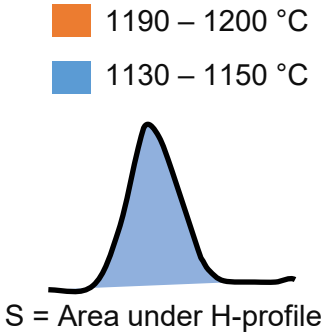

Evolution of S respect to ECR = f (Tox, tox) value

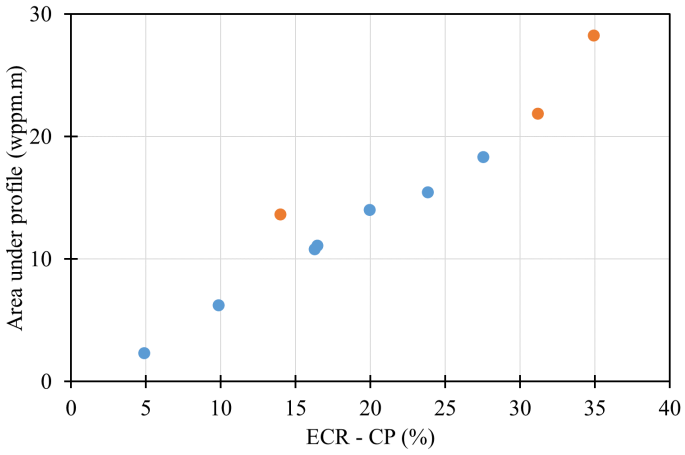

- The Hydrogen uptake increases with oxidation duration and temperature
- The overall hydrogen follows a linear trend with respect to ECR value (in double-sided configuration)

SETs – Micro-analysis

Oxidation duration (s)	Oxidation temperature (°C)
387	~1150

EPMA analysis : 6000 µm x 600 µm with a step of 3µm

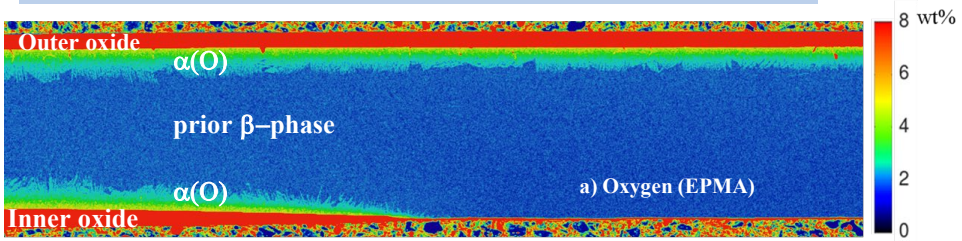

[1]ROI : Region of Interest

Oxidation duration (s)	Oxidation temperature (°C)
387	~1150

EPMA analysis : 6000 µm x 600 µm with a step of 3µm

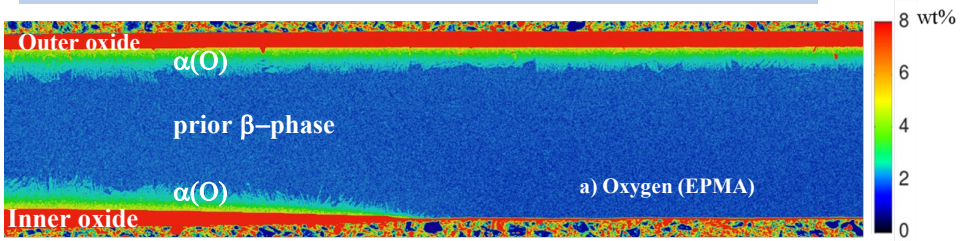

µ-LIBS analysis : 3000 µm x 600 µm with a step of 3µm

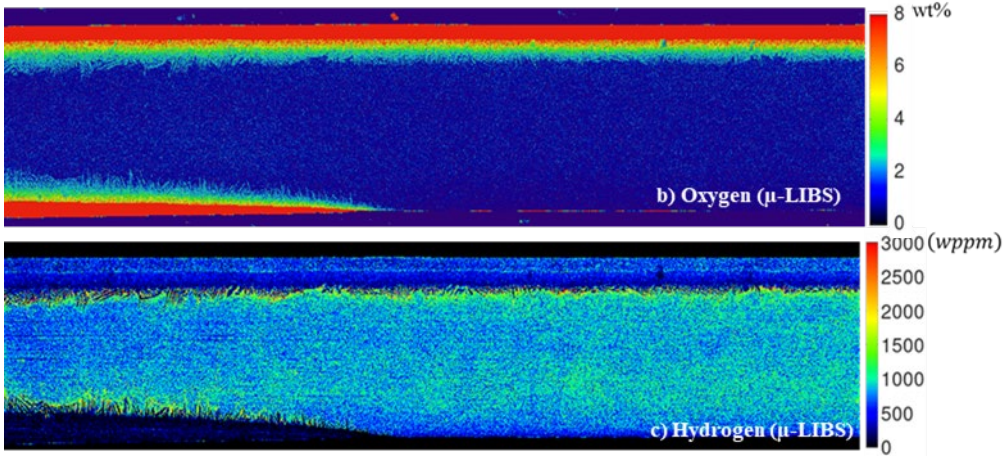

[1]ROI : Region of Interest

Oxidation duration (s)	Oxidation temperature (°C)
387	~1150

EPMA analysis : 6000 µm x 600 µm with a step of 3µm

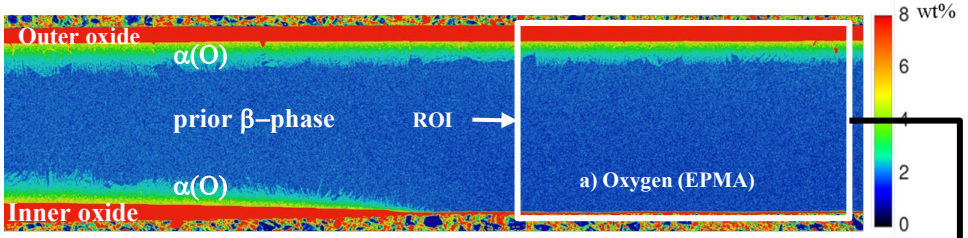

µ-LIBS analysis : 3000 µm x 600 µm with a step of 3µm

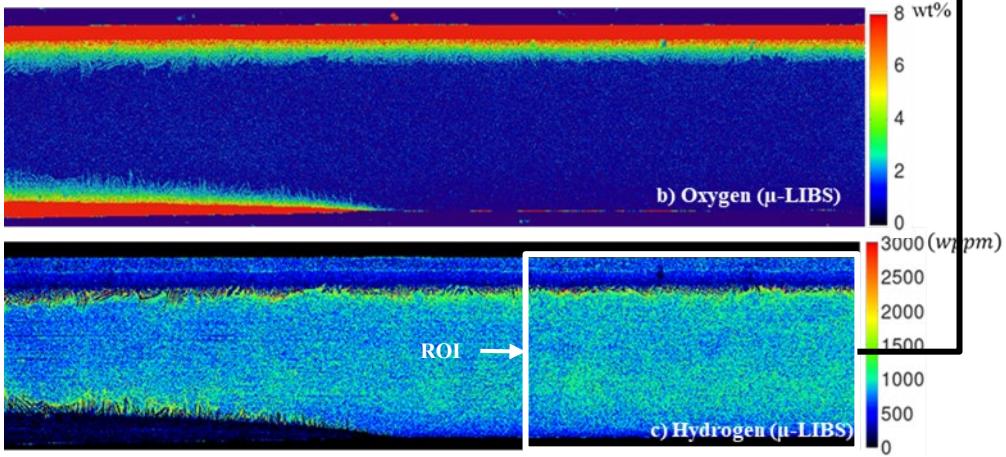

Oxygen and hydrogen radial distribution in the ROI

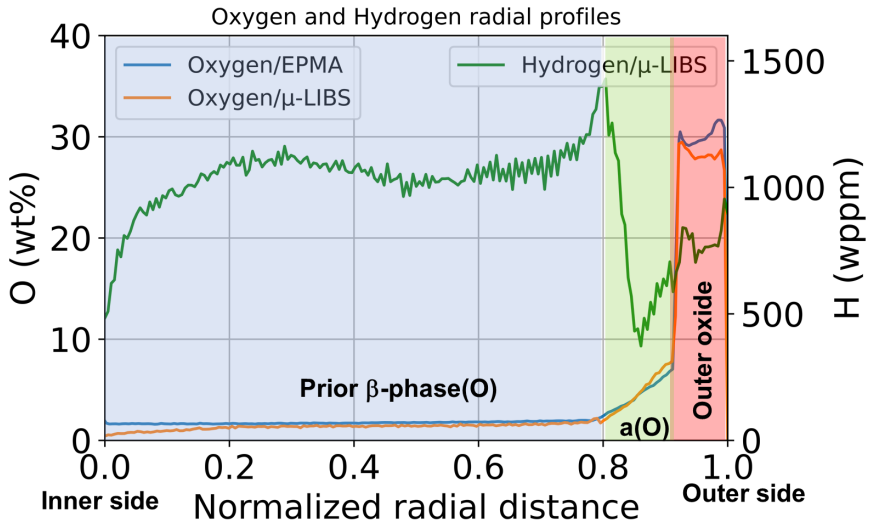

- Distribution of both elements in the different phases of the cladding after oxidation
- These analyses can help investigate any relationship between oxygen and hydrogen

Oxidation duration (s)	Oxidation temperature (°C)
387	~1150

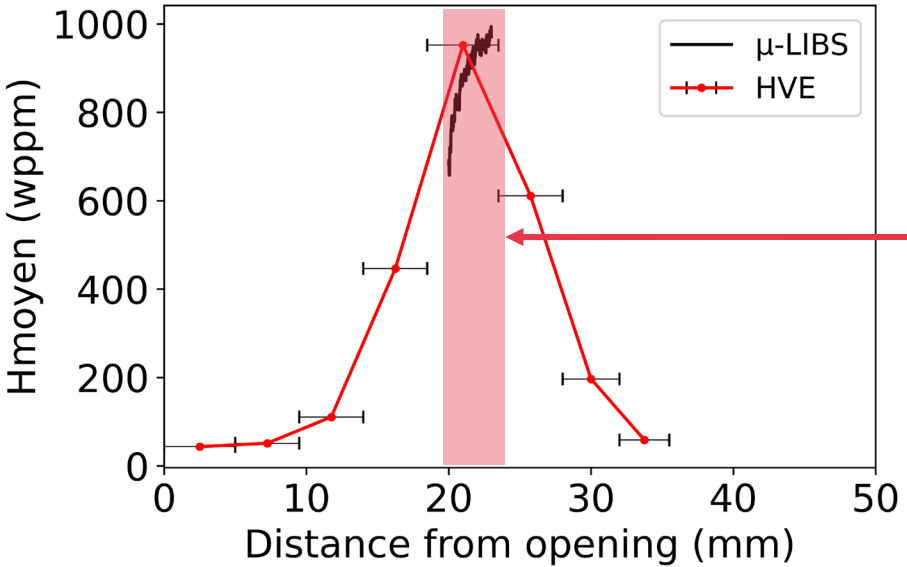

Hydrogen map from µ-LIBS

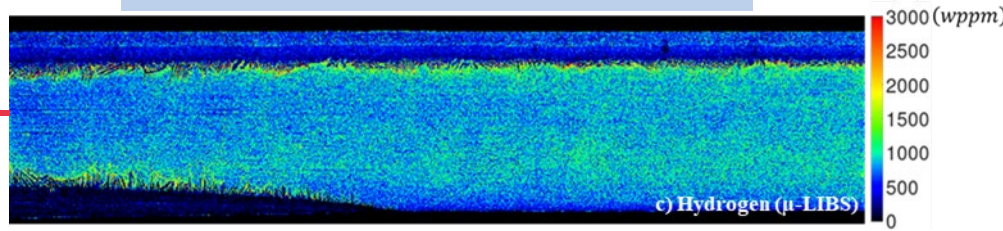

µ-LIBS analysis and HVE measurements are consistent

SETs– Summary

SETs are suitable for separate effects understanding and modeling :

- Tests help simulate secondary hydriding during a LOCA transient
- Pellets positioning inside the cladding influences the azimuthal distribution of hydrogen
- The hydrogen content related to secondary hydriding evolves with oxidation duration,
- Micro-analyses help quantifying oxygen and hydrogen local distribution within the cladding (Investigation of the binary O-H system)

Upcoming activities :

- Modelling of SETs with SHOWBIZ[2] is in progress
- µ-LIBS analysis for O & H mapping
- Comparison between different hydrogen measurement methods (HVE, µ-LIBS, and Neutron-radiography)
- Mechanical tests are performed to characterize both oxygen and hydrogen embrittlement on cladding

[2]SHOWBIZ is a new version of the code DIFFOX [DURIEZ C et al.., 2010] developed earlier at IRSN which aims to simulate secondary hydriding in LOCA conditions

Thanks for your attention

V. Boucek
UJP

High Temperature Creep of Zr Alloys with Internal Overpressure

This presentation shows findings from two distinct creep experiments conducted at UJP Praha, focusing on the performance of specimens featuring various protective coatings (Cr, CrN, CrN+Cr, CrN+Cr multilayer, CrNb) in comparison to uncoated specimens. Isothermal tests conducted at temperatures of 750 °C and 950 °C revealed prolonged time to burst for the coated specimens, as anticipated. Conversely, in the RAMP tests, reference specimens exhibited a higher burst temperature, likely attributed to protective layer cracking and localized stress concentration at the crack tip. To discern the occurrence of cracks throughout the experiments, acoustic emission was employed. While only 6 experiments with acoustic emission were completed at the time of presentation, initial results suggest that cracks in the protective coating emerged after the first third of the test duration.

UJP PRAHA

High Temperature Creep of Zr Alloys with Internal Overpressure

J. Krejčí[1], V. Bouček[1,2], et al.

[1] UJP PRAHA a.s., [2] FNSPE CTU

7. 12. 2023, Karlsruhe

28th International QUENCH Workshop

Outline

UJP PRAHA

- UJP equipment
- Constant temperature tests
- RAMP tests
- Acoustic emission

Equipment – burst tests

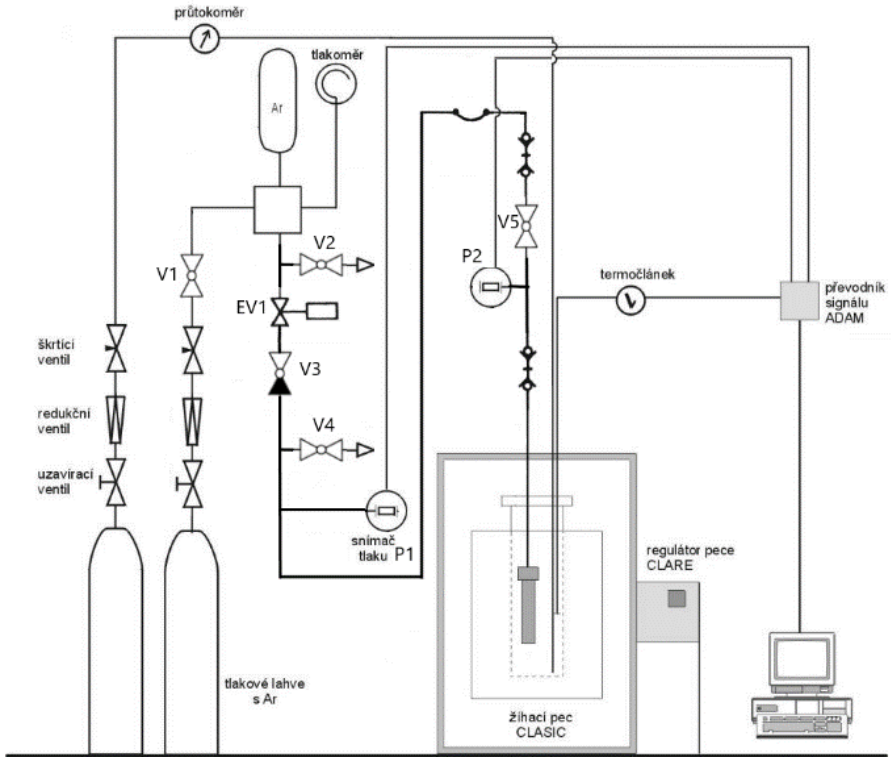

Specimen – burst tests

UJP PRAHA

- 1 or 2 thermocouples
  - Welded
  - As close as possible (not attached)
- „Swagelok“ endings

Isothermal tests

UJP PRAHA

- Heating
- α->β transformation
- Pressurizing
- Exposure

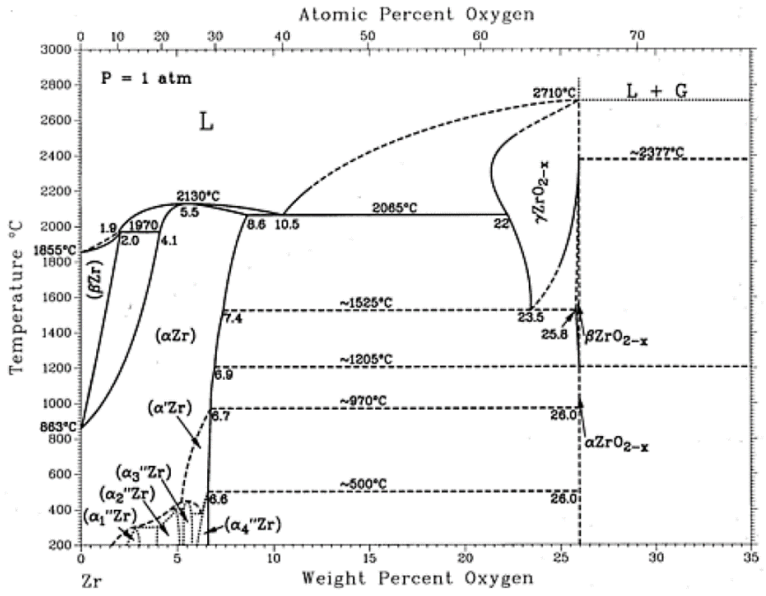

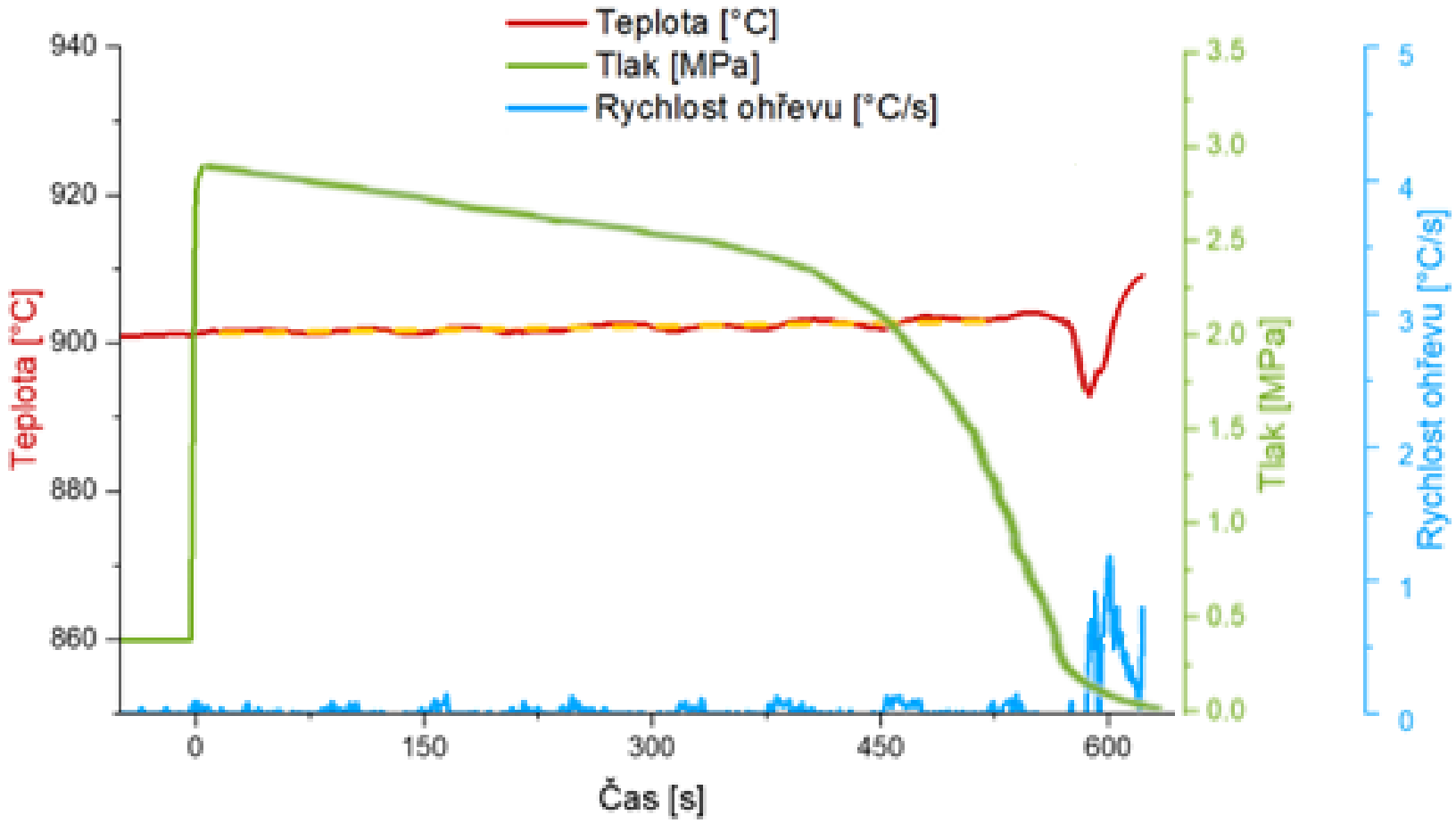

„RAMP“ tests

UJP PRAHA

- Pressurized specimen placed into the furnace
- Heating: 0-9 °C/s

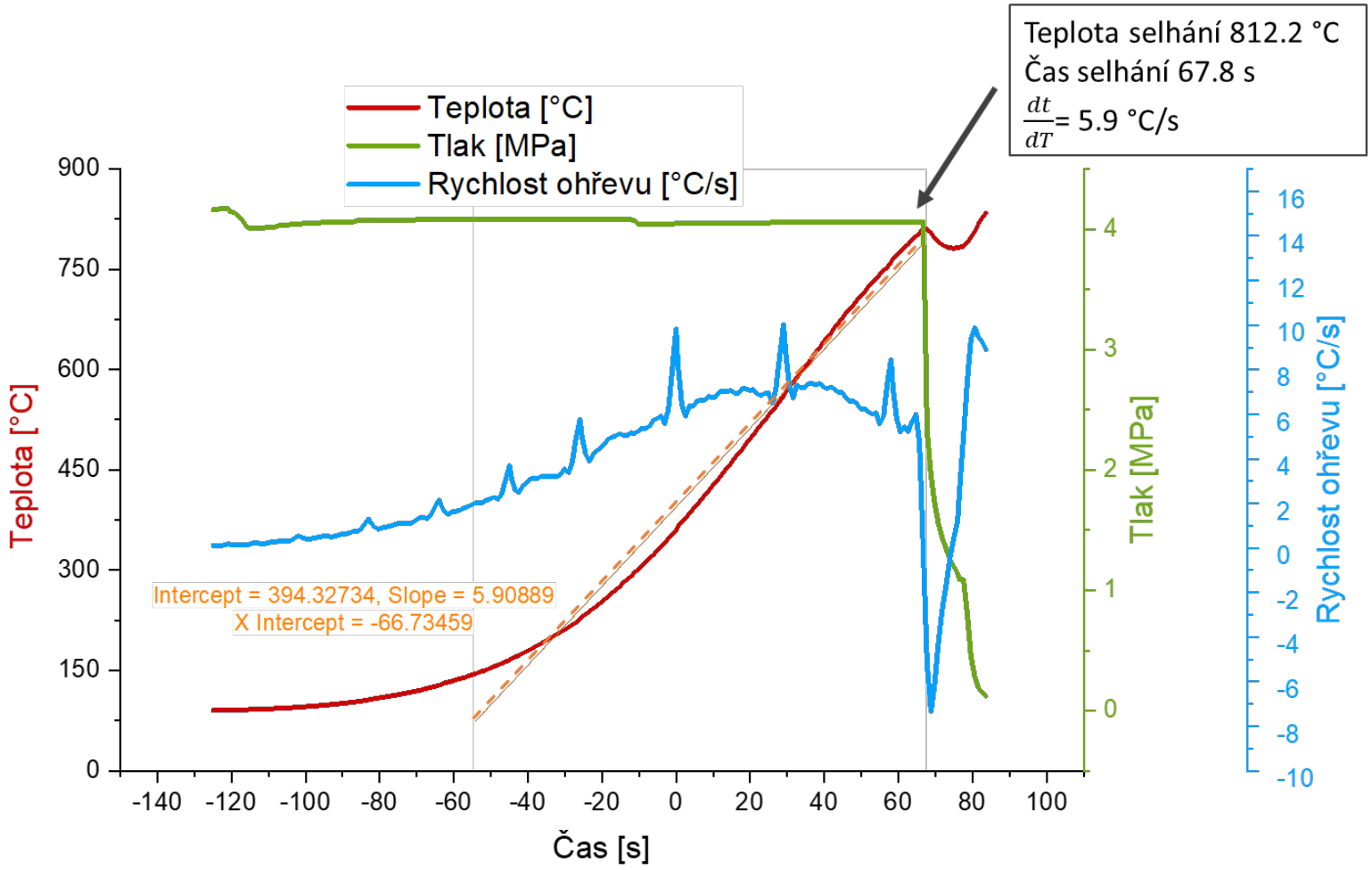

Protective coatings

UJP PRAHA

Layer	Thickness [µm]							
	Cr	CrN	Cr	CrN	Cr	CrN	Cr	Sum
CrN+Cr (22,6 µm)	19,4	3,2	-	-	-	-	-	22,6
CrN+Cr (16,7 µm)	11,4	5,3	-	-	-	-	-	16,7
Cr/CrN+Cr	10,8	1,6	1,2	1,2	1,0	1,3	0,6	17,6
$Cr_{90}N_{10}$	-	18,2	-	-	-	-	-	18,2
Cr	18,6	-	-	-	-	-	-	18,6
Cr70Nb30	-	-	-	-	-	-	-	7
Cr85Nb15	-	-	-	-	-	-	-	7

Results – isothermic tests

UJP PRAHA

- Time to burst

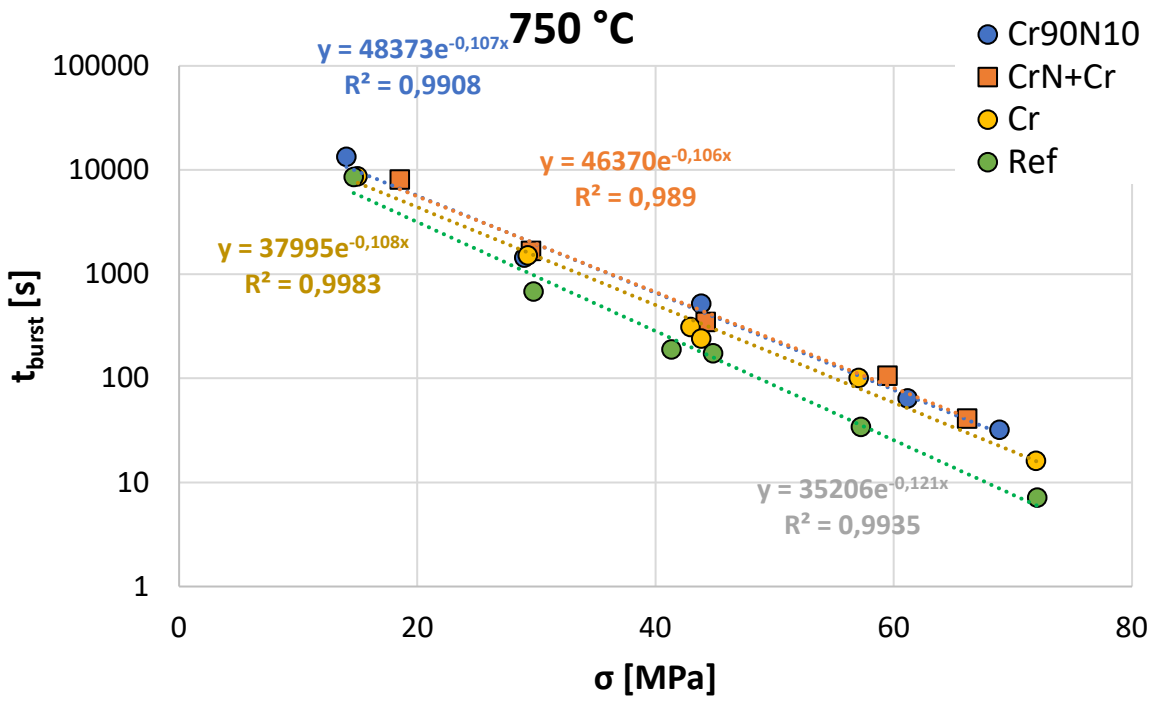

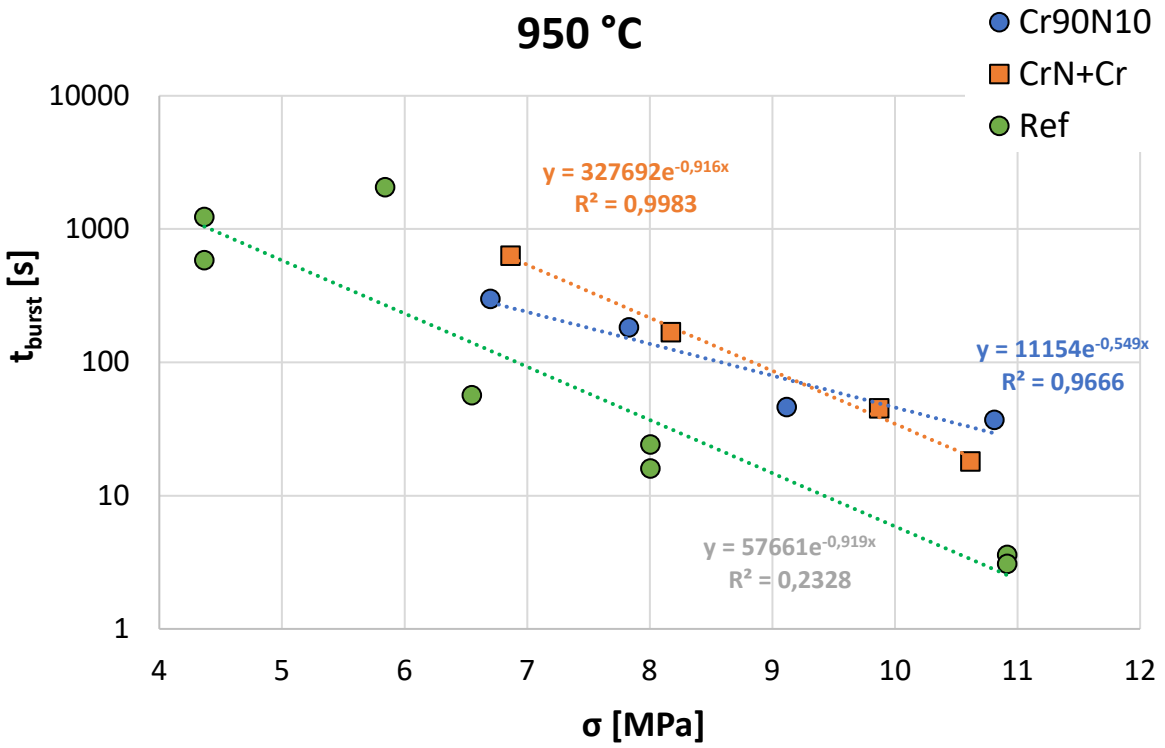

Results – isothermic tests

UJP PRAHA

- Time to burst
  - 750 °C and 950 °C

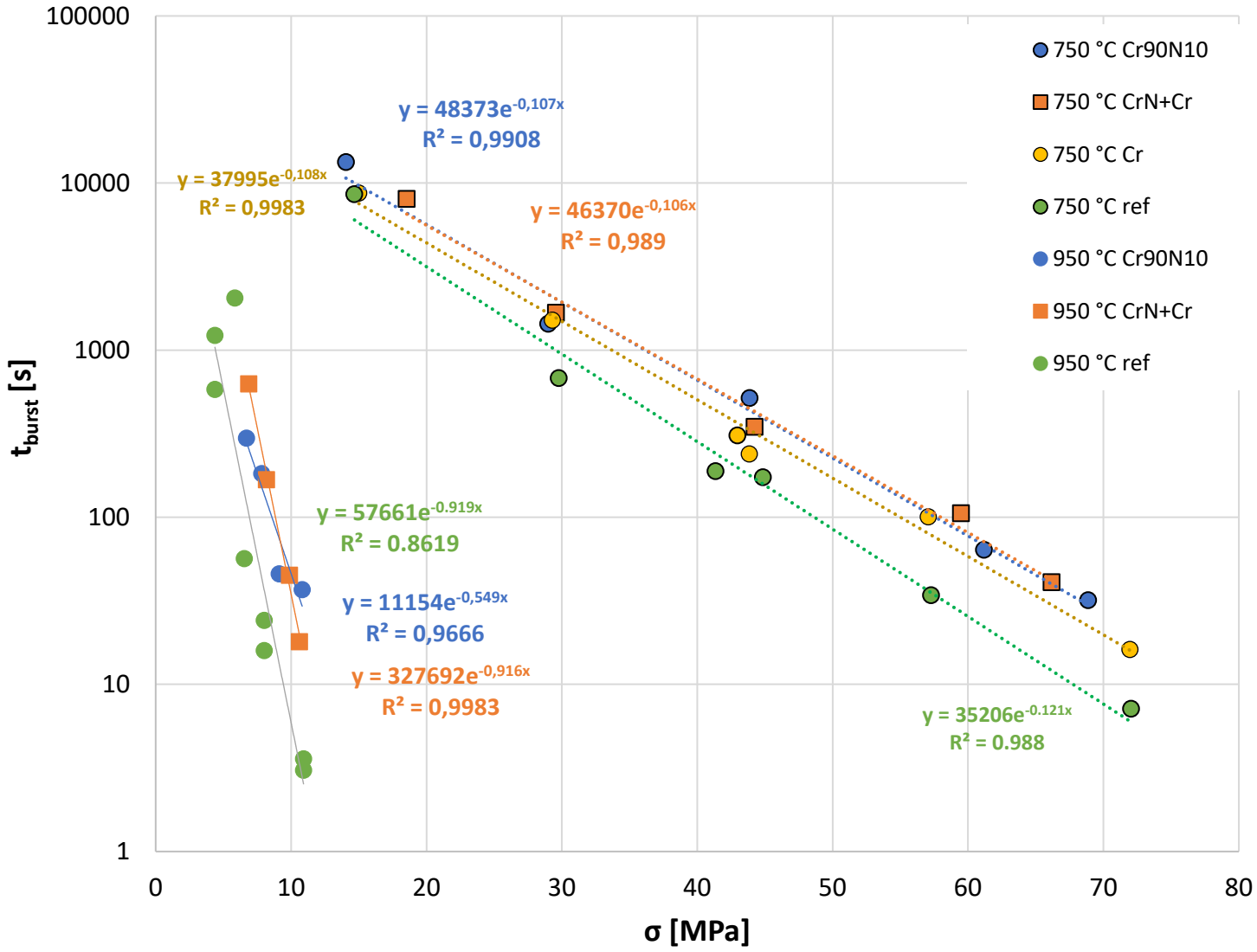

Results – isothermic tests

UJP PRAHA

- Maximum deformation

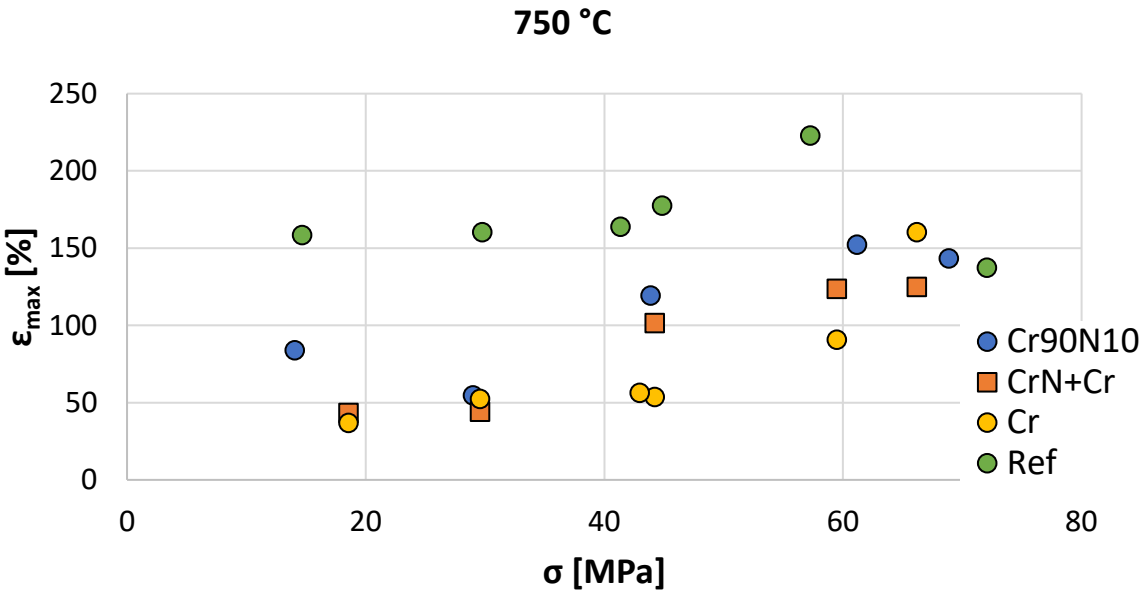

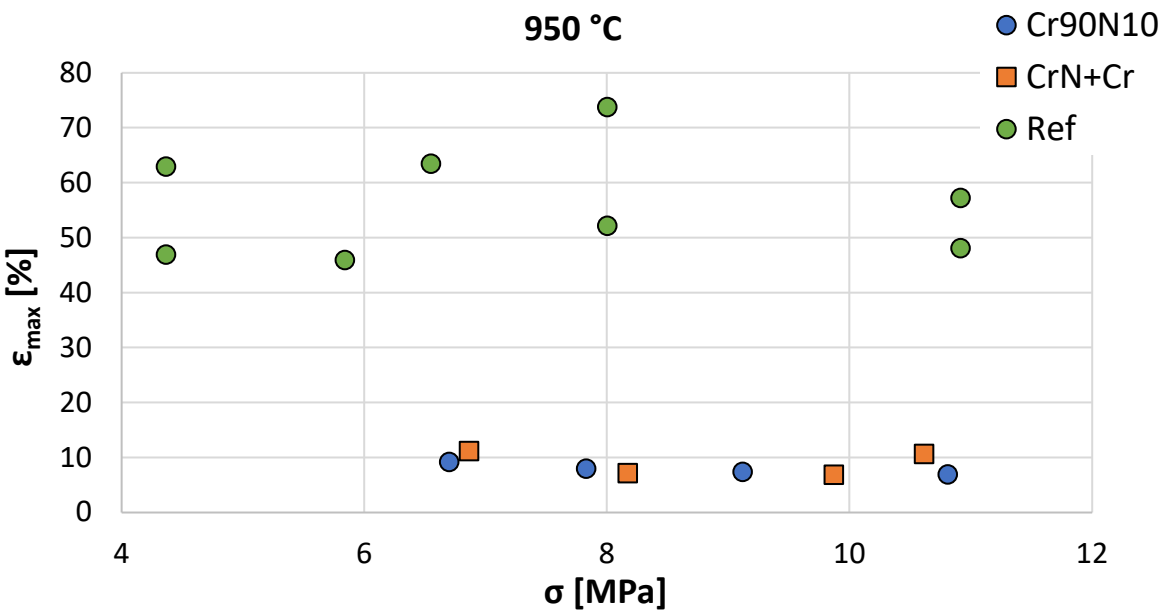

Results – RAMP tests

UJP PRAHA

- 6 °C/min (heating)

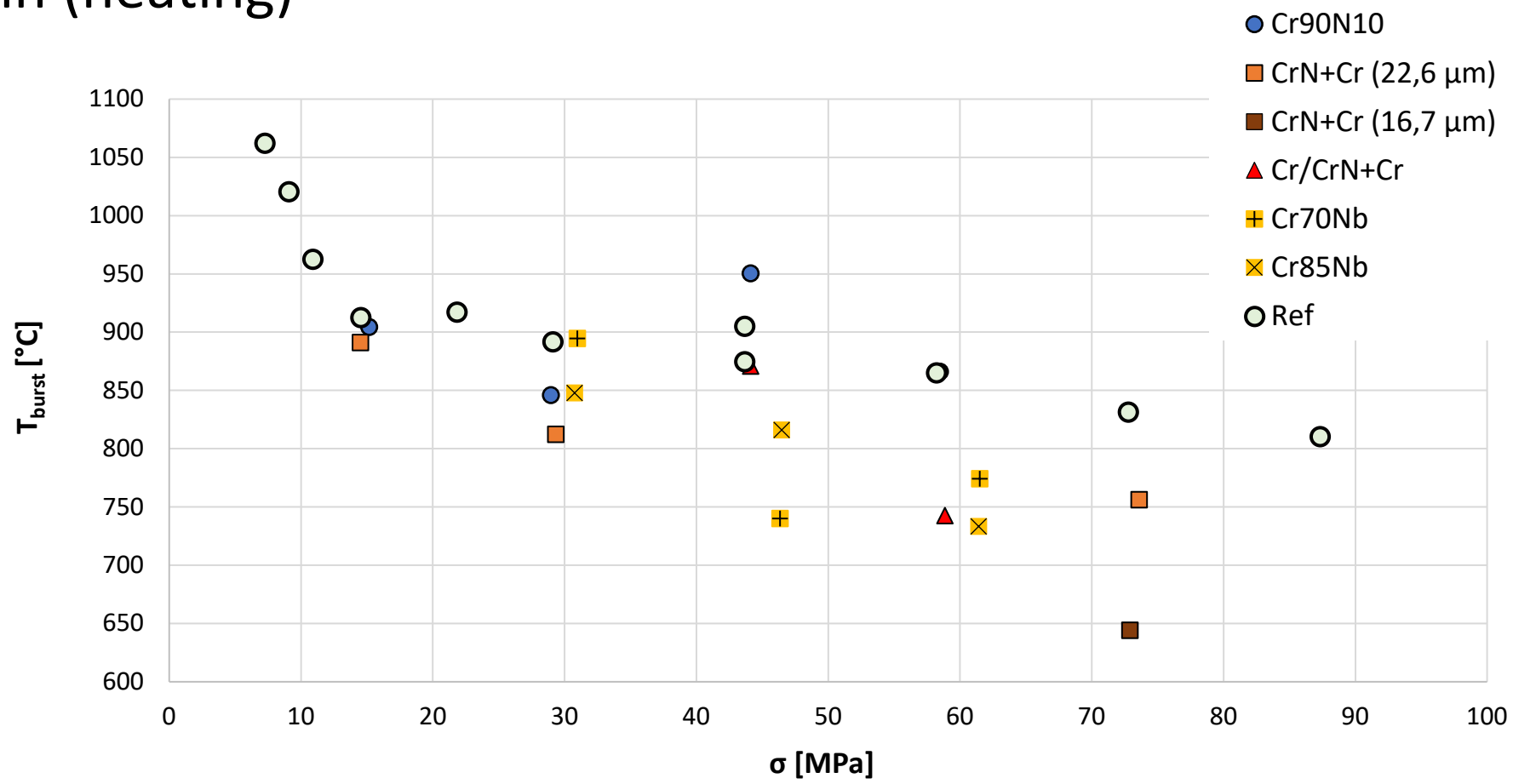

Conclusion

UJP PRAHA

- Coated/ uncoated specimens – different behaviour

- Isothermic tests:
  - Coated specimens: longer exposure time to burst
  - Coated specimens: lower creep rate

- RAMP tests:
  - Coated specimens: lower burst temperature compared to reference specimens
  - Probably caused by stress concentration in coating cracks tips

Acoustic emission

- Coating Cr, 15-20 µm
- Constant gas amount (isothermal test)

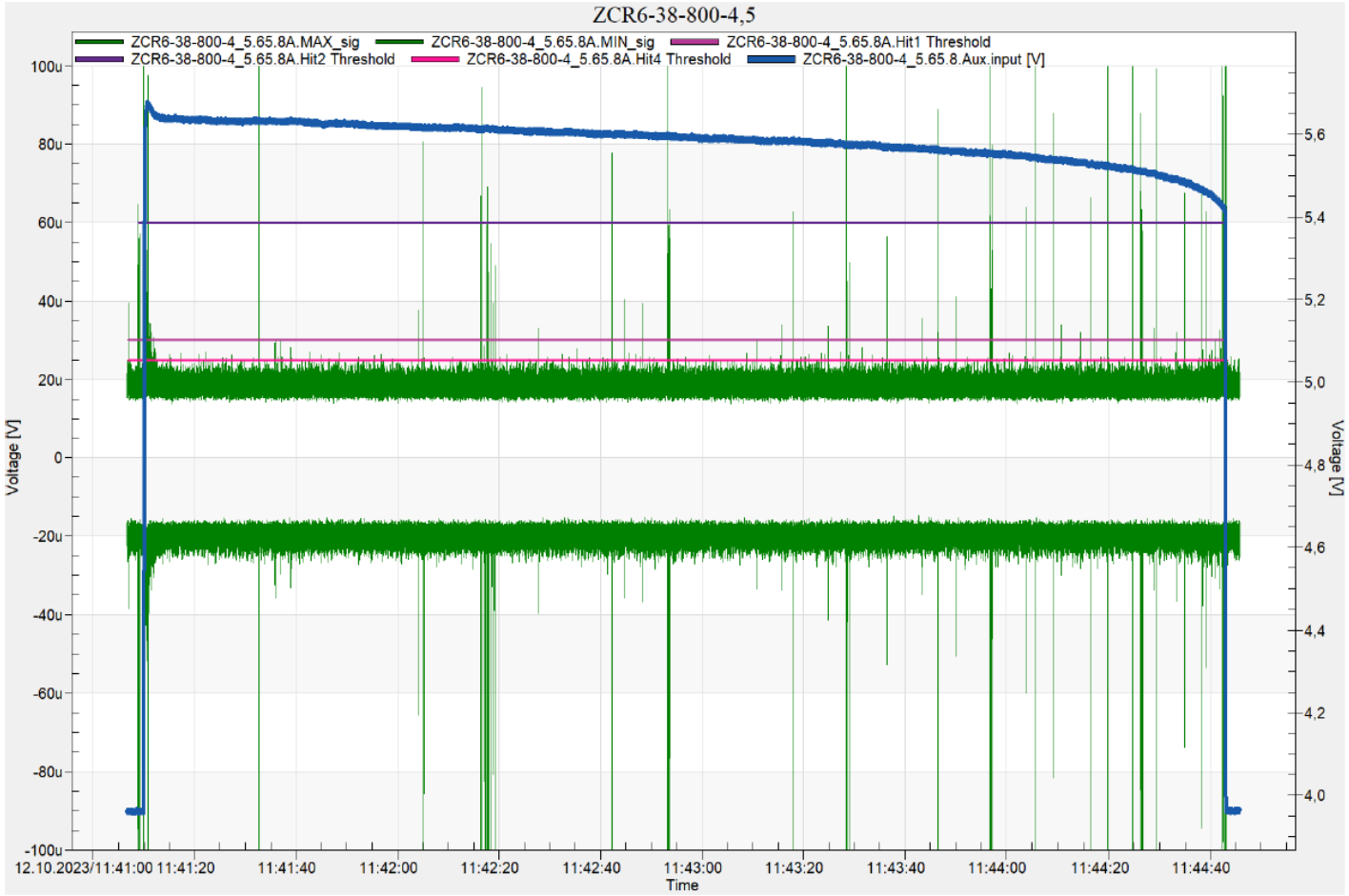

Acoustic emission

- Coating Cr, 15-20 µm
- Constant gas amount (isothermal test)

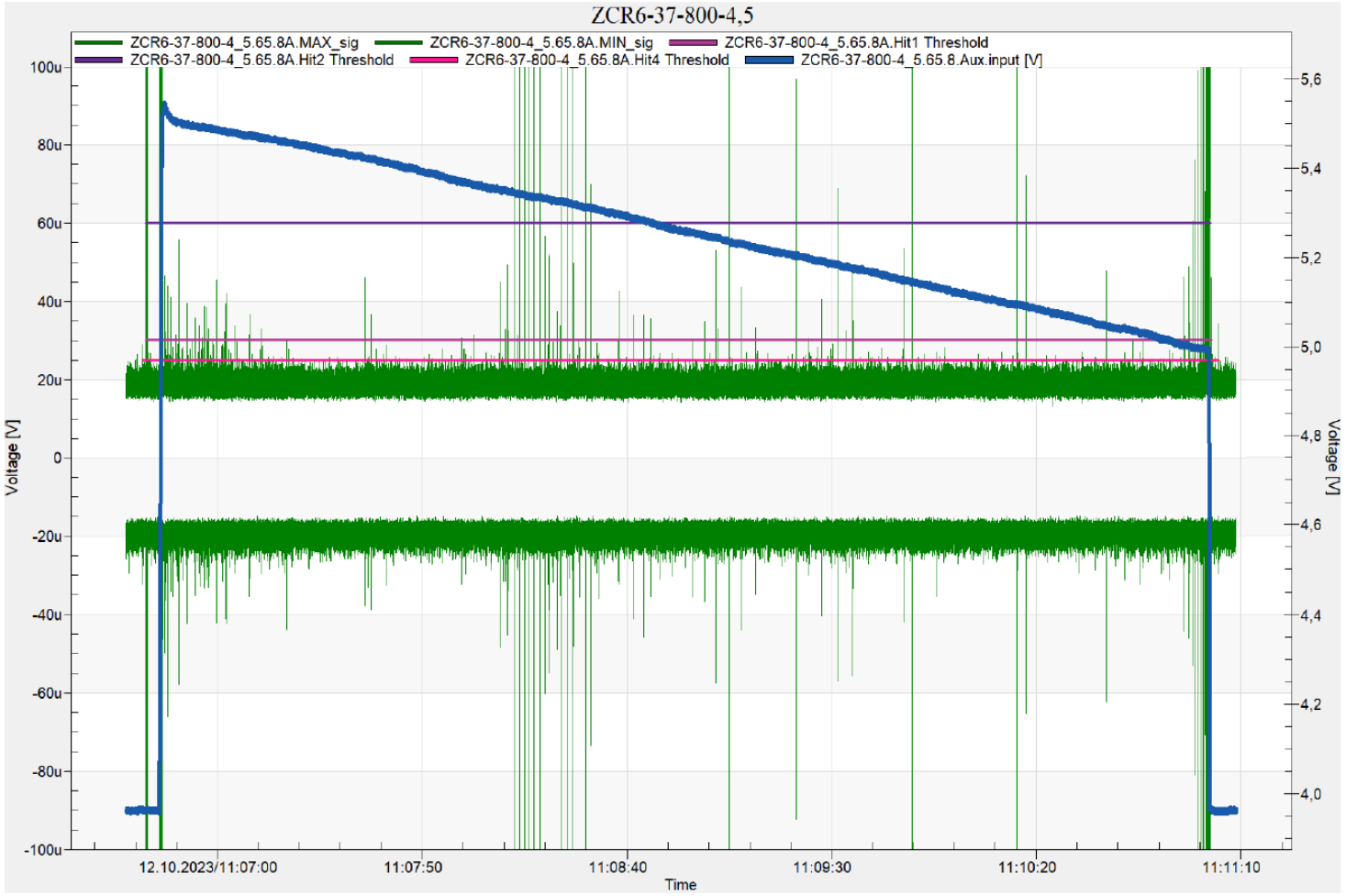

Accoustic emission - Conclusion

UJP PRAHA

- Primary creep, first phase of experiment
  - A lot of incidents
    - Filling with gas, primary creep
- Secondary creep
  - Cracking in ~ 1/3 of experiment
    - Probably cracking of protective layer
- Ballooning
  - Cracking of protective layer

- Uncoated specimens
  - Higher amplitude during first phase and secondary creep only

Thanks for attention!

M. Große
KIT

The EC SCORPION Project on SiC cladding: Overview and first results

SiC_f/SiC CMC is a rather revolutionary ATF cladding material concept. Before it really can be applied several problems has to be overcame:

- High corrosion rate in water
- Brittle behavior
- Irradiation-induced swelling

In order to develop an innovative approach for SiC_f/SiC CMC´s, the SCORPION project sponsored by the European commission was lounged. A consortia of 14 institutions from seven European countries, Japan and the USA produces and joins SiC_f/SiC CMC, These cladding tubes will be coated by ceramic films.

The paper gives an overview about the structure of the project and about the precursor projects IL TROVATORE and PERSEUS.

First results of high temperature oxidation tests at 1200°C for 1 h conducted at KIT are given. For the tests, bulk material of promising ceramic coatings on SiC was used. All materials tested show no or very low mass loss and very low hydrogen release under these conditions.

Finally, the paper gives an outlook about further high-temperature tests planned in atmospheres with varying hydrogen partial pressure.

The EC SCORPION Project on SiC cladding: Overview and first results

Konstantina Lambrinou, Mirco Grosse, et al.

KIT / Institute for Applied Materials – Applied Material Physics / Program NUSAFE

University of Huddersfield

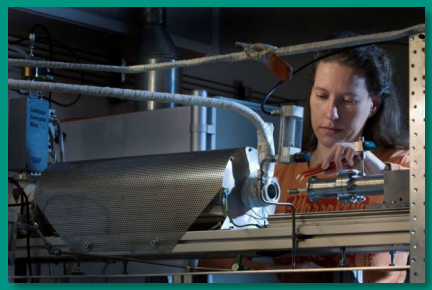
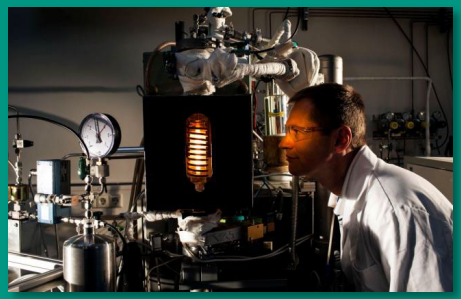
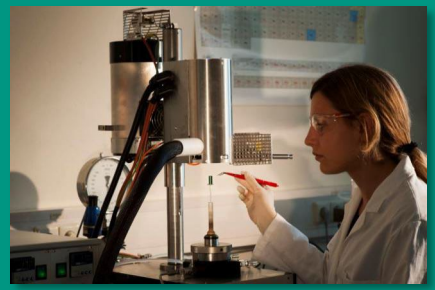
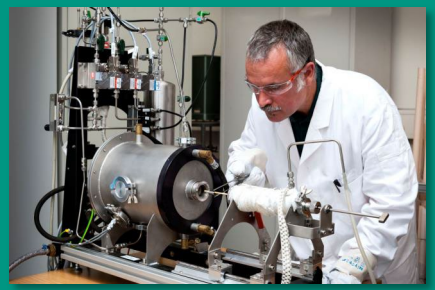

The project

HORIZON SCORPION

(SiC Composite Claddings: LWR Performance Optimisation for Nominal and Accident Conditions)

***Prof. Konstantina Lambrinou**, UoH (UK) & IIT (Italy)*

HORIZON European Research & Innovation Action (RIA)

The project

- Start: 9/2022
- Duration 4 y
- Participants: 14 institution from 7 European countries 1 from J and 1 of the US:
  - UK: Univ. Huddersfield, Oxford Univ.
  - B: Kath. Univ. Leuven,
  - D: RWTH Aachen, KIT, Friedrich-Alexander-Univ Erlangen-Nuremburg, Gesellsch. für Techn. Thermochemie &-physik,
  - S: Linkopings Univ.,
  - F: CEA,
  - I: Politecnico di Torino, IIT,
  - US: Univ.Michigan,
  - J: Kyoto Univ.,
  - CH: PSI

The project

- External Expert Advisory Committee (EEAC)
  - Industries:
    - Edward J. Lahoda & Luke Czerniak Westinghouse Electric Company LLC USA
    - Christian Deck General Atomics GA USA
    - Jeffrey Reed FRAMATOME FRAMATOME USA
    - Andrew J. Perry Rolls UK
    - Yoshitaka Ito NGS Advanced Fibres Co., Ltd. Japan
  - Research Instituts:
    - Robert L. Oelrich Pacific Northwest National Laboratory PNNL USA
    - Peng Xu Idaho National Laboratory INL USA
    - Takaaki Koyanagi Oak Ridge National Laboratory ORNL USA
  - Intern. Organisation:
    - Ki Seob Sim International Atomic Energy Agency IAEA

Project structure

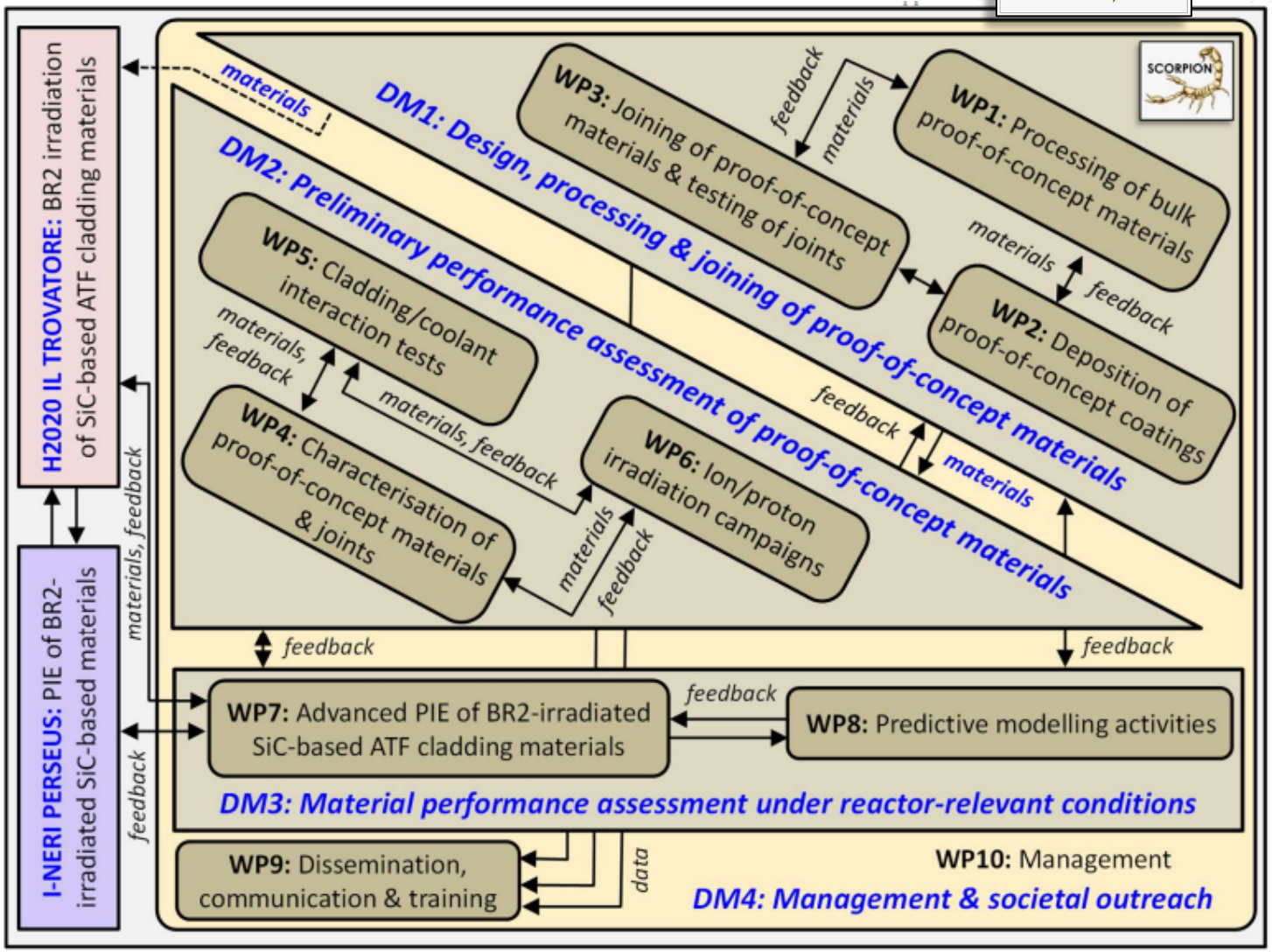

Background

- SiC/SiC CMC is a rather revolutionary ATF cladding material concept
- Must overcome
  - Incompatibility to the coolant (Strong corrosion in water)
    - $SiC(s) + 2H_2O(aq) = SiO_2(s) + CH_4(g)$
    - $SiC(s) + 2H_2O(aq) = SiO_2(s) + 2H_2(g) + C(s)$
    - $SiC(s) + 3H_2O(aq) = SiO_2(s) + 3H_2(g) + CO(g)$
    - $SiC(s) + 4H_2O(aq) = SiO_2(s) + 4H_2(g) + CO_2(g)$
    - $SiO_2(s) + 2H_2O(aq) = Si(OH)_4(aq)$
    - $2SiO_2(l) + SiC(s) = 3SiO(g) + CO\ (g)$
  - Radiation-induced swelling until a dos rate of ~ 2 dpa
  - Lack of ductility
- Porosity needed for quasi ductile behaviour and to compensate irradiation induced swelling but porosity can increase the corrosion/oxidation due to larger surface.
- Influence of water chemistry on the corrosion and high temperature steam oxidation (influence of the hydrogen partial pressure).

Precursor projects:

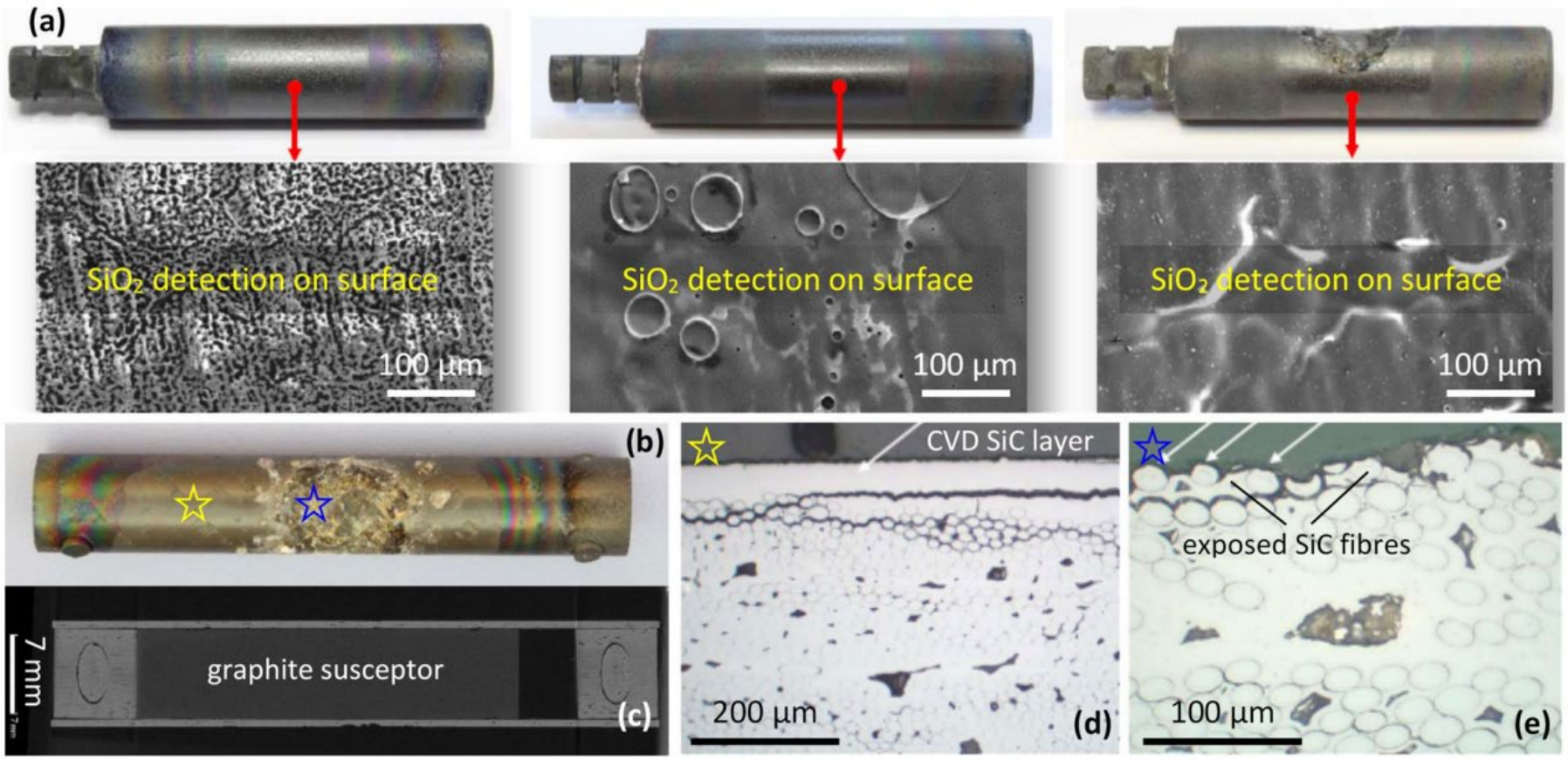

Precursor projects:






I-NERI Project PERSEUS

(Advanced PIE of Accident-Tolerant Fuel Claddings Neutron-Irradiated in the BR2 Test Reactor)

***Prof. Konstantina Lambrinou**, European Lead & **Robert Oelrich**, US Lead*

I-NERI (International Nuclear Energy Research Initiative) US/EURATOM Project

Irradiation Tests at Univ. Michigan

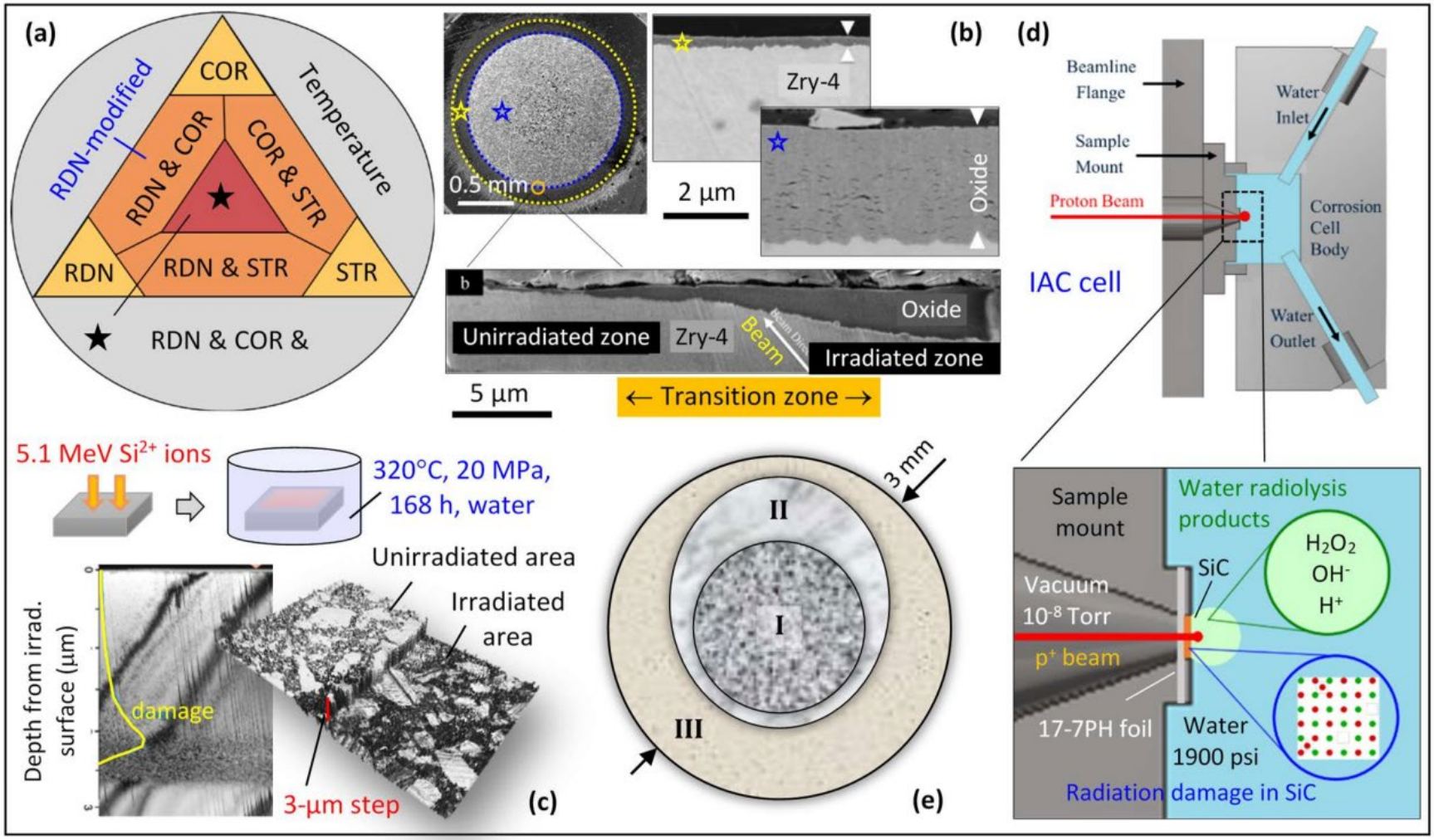

Compatibility with Coolant (Water, Steam)

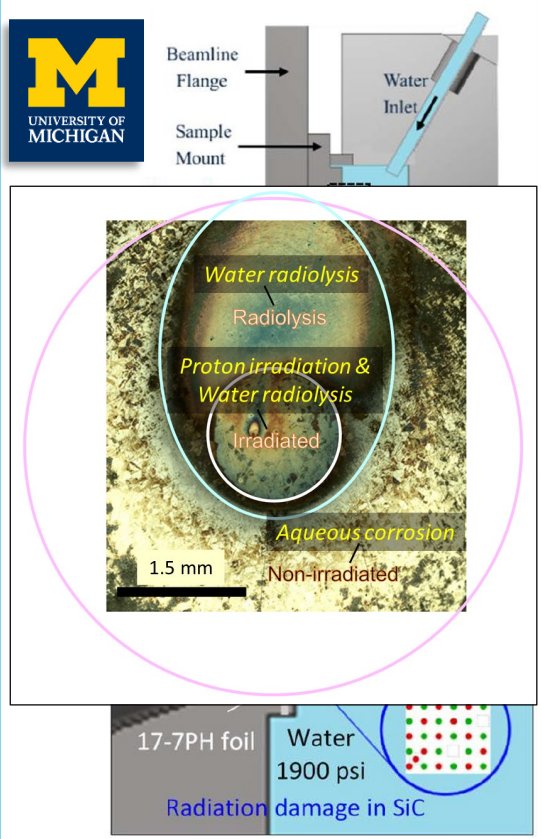

PIE by TEM/STEM/EELS (320°C, PWR water)

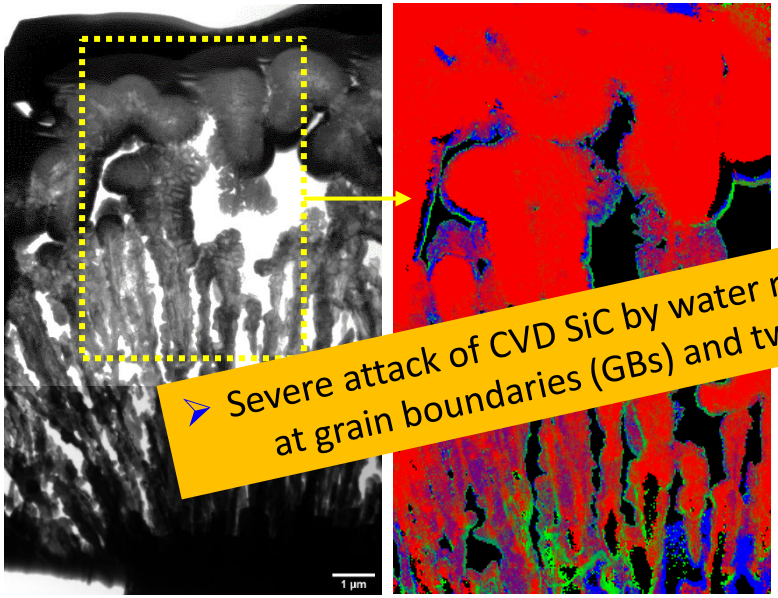

STEM

EELS

- Red = Carbon (C)
- Blue = Silicon (Si)
- Green = Oxygen (O)

PIE/TEM (288°C, BWR water)

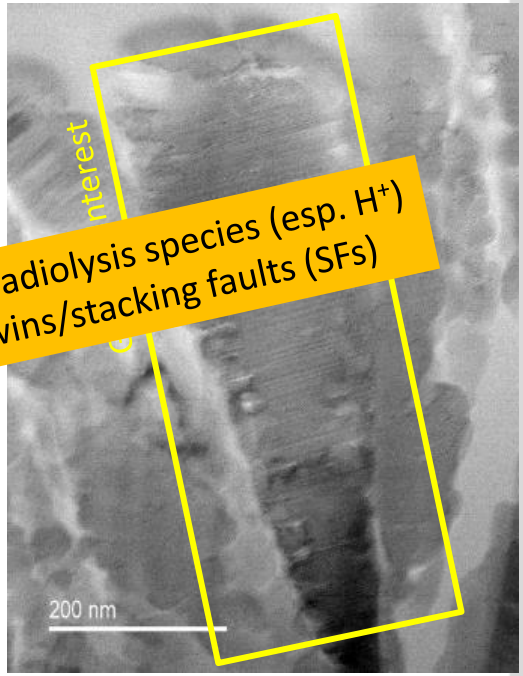

➢ Severe attack of CVD SiC by water radiolysis species (esp. H^+) at grain boundaries (GBs) and twins/stacking faults (SFs)

Pacific Northwest NATIONAL LABORATORY

Steam oxidation tests of promising cladding materials

- Y_2SiO_5
- $Y_2Si_2O_7$
- $Y_3Al_5O_{12}$
- Yb_2SiO_5
- $Yb_2Si_2O_7$
- $Yb_3Al_5O_{12}$
- $(Y,0.6Yb)_2SiO_5$

One or two steps process

Steam oxidation tests for 1 h at 1200°C

Steam oxidation tests of promising cladding materials

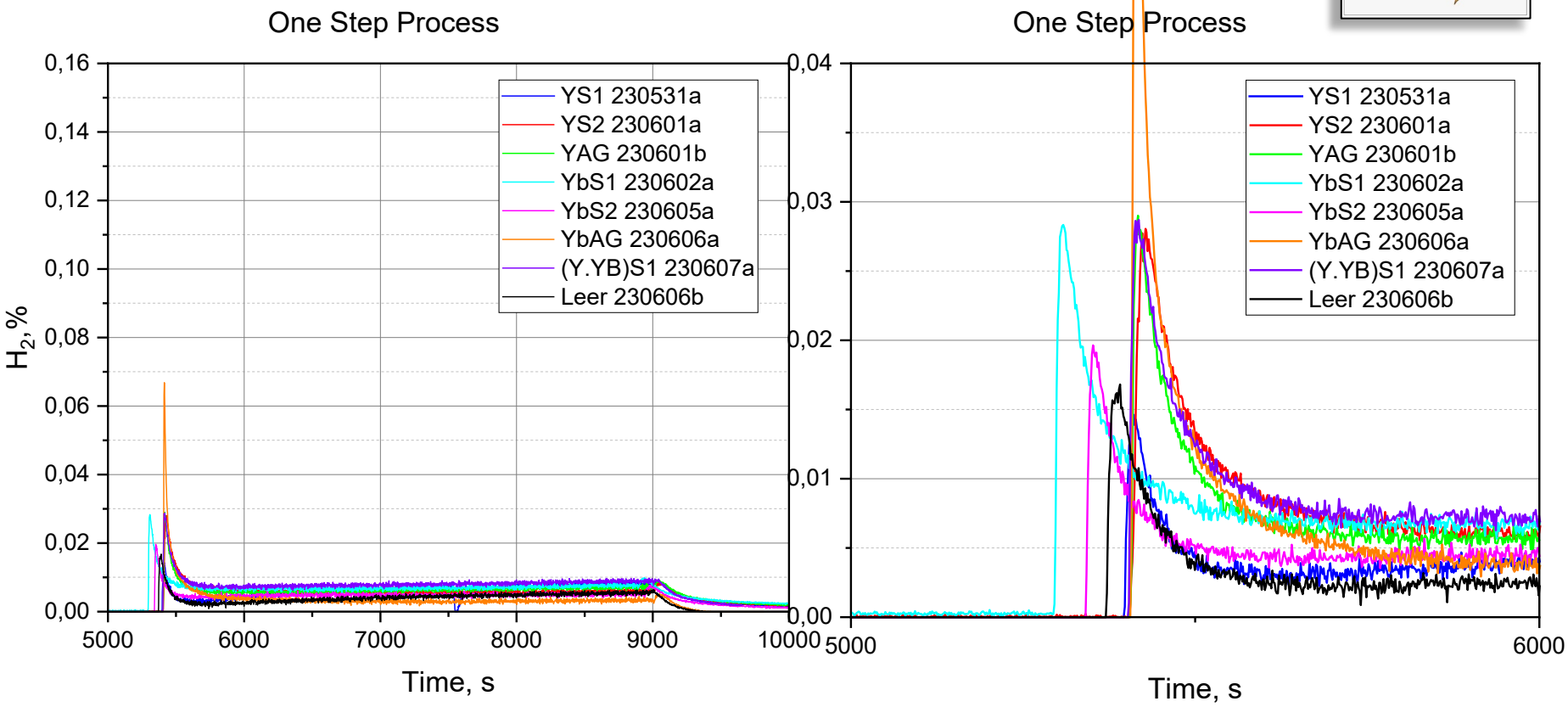

Steam oxidation tests of promising cladding materials

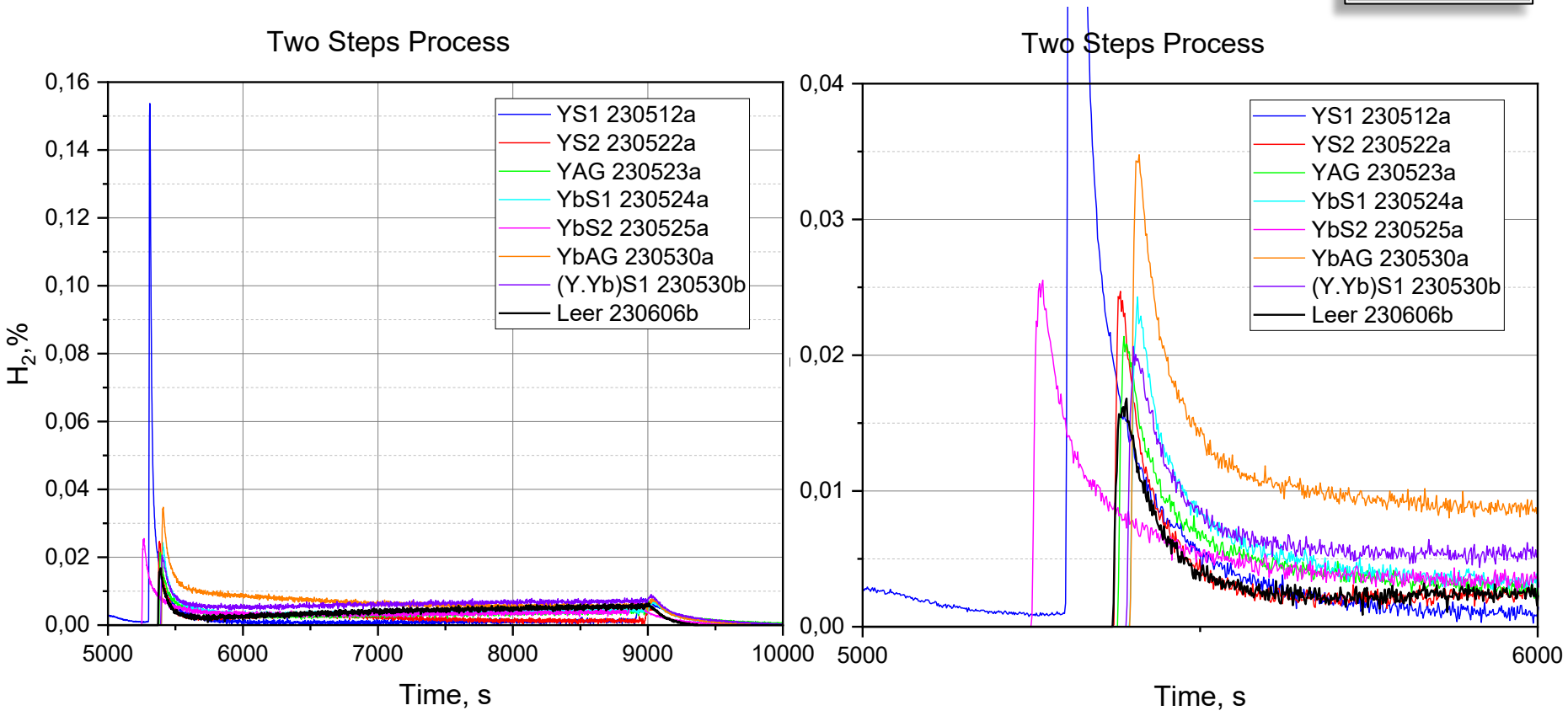

Summary

- Very challenging approach for SiC CMC claddings
- Steam oxidation tests at 1200°C for 1 h were already performed
  - Very low mass changes and hydrogen releases at all
  - No clear behaviour:
    - $Y_2Si_2O_7$ single step process had relative high mass gain but no significant hydrogen release,
    - $Yb_3Al_5O_{12}$ single step process and Y_2SiO_5 two step process showed higher hydrogen release but medium mass change.
- Next steps
  - Steam oxidation tests of the coating materials at 1600°C for 1 h
  - Steam oxidation tests of SiC with different porosities at 1200°C for 1 h
  - Steam oxidation tests with of monolithic SiC samples with different hydrogen partial pressure at 1600°C

Acknowledgement

The SCORPION project is supported by

EU Horicon 2020
Grant number **101059511**

The authors thank all colleagues all participants in the project,

Thank you for your attention

P. Doyle
ORNL

Analysis of Fuel Fragment Dispersal During Post-Burst Vibration Event

Loss-of-coolant accidents (LOCAs) in nuclear power plants lead to rapid heat transients in nuclear fuel rods that can reach up to 100 ℃/s, causing local balloon and burst of the fuel rod. Burst of the fuel rod can be accompanied by fuel relocation down the rod and some ejection through the burst region as the fuel itself fragments. This behavior is particularly acute at high burnup, where the high burnup microstructure creates particles ranging in size from 3 mm to <0.1 mm. Under design-basis accident conditions, the emergency coolant systems acuate rapidly and quench the core. This quenching process induces vibrations that may cause additional material loss through the burst region.

To evaluate the likely impact of these burst events, it is necessary to know 1) the dimensions of the burst region, and 2) the expected quench-induced fragment relocation out of the rod. Two analysis systems have been developed at ORNL to evaluate these effects. The first is a high-resolution profilometer, which consists of 3 axes of motion: length-wise along the rod, rotation of the rod, positioning of a camera. On each axis, scans can be conducted with step sizes of up to 0.1 mm and 0.1 degrees for axial and angular displacements, respectively. Post-examination data reconstruction can then be used to identify the precise burst geometry and to provide 3D burst data to modelers for replication. In this work, data on 4 tubes (3 having been burst) was collected at various axial and angular respective steps sizes. Large step sizes (5 mm and 45 degrees) were used to collect images on the camera for full rod image stitching. Rod edge and diameter data was then collected along the entire rod at steps of 1 mm and 5 degrees, respectively. This was followed by a higher resolution scan of the burst region at 0.2 mm and 1 degree step sizes to reveal burst geometry. For very small bursts (~ 3 mm maximum width) a higher resolution of 0.1 mm and 0.1 degrees was also used, for a total of around 900,000 data points. Data was then post-processed to extract burst edge information and compute circumference, tube circularity, and caliper-equivalent diameter at each point, as well as the maximum width and length of the burst region. These data, as relevant, were compared to caliper-measured burst parameters and found to be consistent with them.

Fuel dispersal has been measured using a system that induces sinusoidal oscillations in a post-burst rod and collects any dispersed material in a collection tray for real-time mass analysis and post-collection sieve analysis. In this work, out-of-cell testing on as-burst rods has been conducted by filling the rods with various sizes and shapes of fuel-surrogate particles in both dry and wet conditions, and with two different burst geometries. The rods were subjected to vibrations with peak-to-peak amplitudes of 2 – 25 mm at 2 – 5 Hz frequencies. Future work will demonstrate these results on actual fuel rods.

OAK RIDGE National Laboratory

Development of Tools for the Examination of Post-Burst Rods Exposed to LOCA-type Events in the SATS system

Peter Doyle

Yong Yang

Jason Harp

Mackenzie Ridley

Matthew White

ORNL is managed by UT-Battelle LLC for the US Department of Energy

U.S. DEPARTMENT OF ENERGY

Introduction – Severe Accident Test Station

- Objectives
  - Replicate LOCA conditions for surrogate fuel and as-burned fuel
- Description
  - Heats samples in variable atmosphere at up to 5℃/s, up to 1200℃
  - Pressurized tubes
  - In-cell and out-of-cell duplicate systems

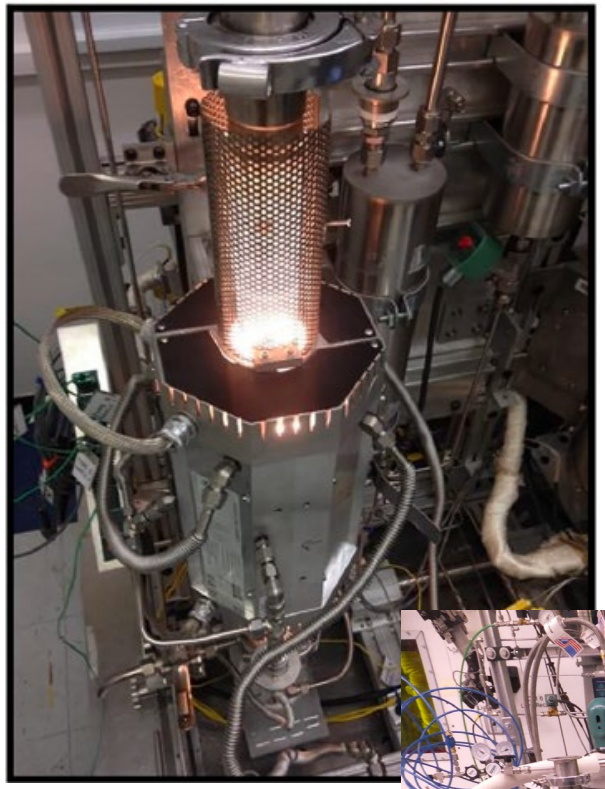

Capps et al., Nucl Eng Des 367 (2020) 110811

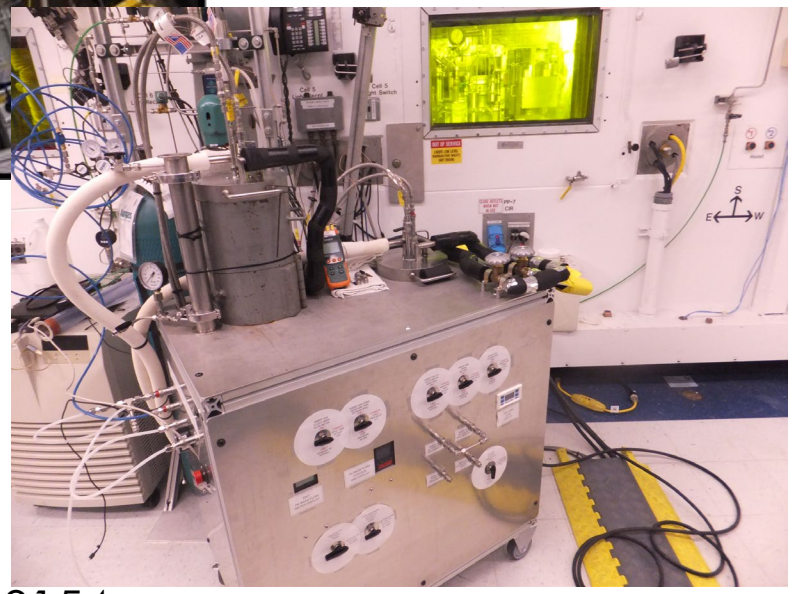

Yang et al, ORNL-SPR-2023-3154

Introduction – at burnup >62 GWd/MTU, fuel fragmentation relocation and dispersal is increasingly of concern

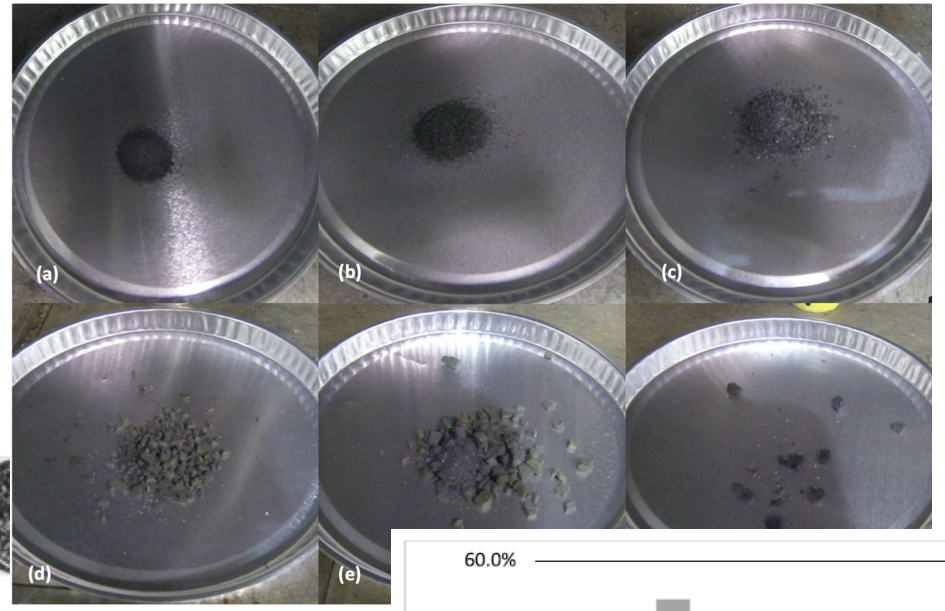

Capps et al., Nucl Eng Des 367 (2020) 110811

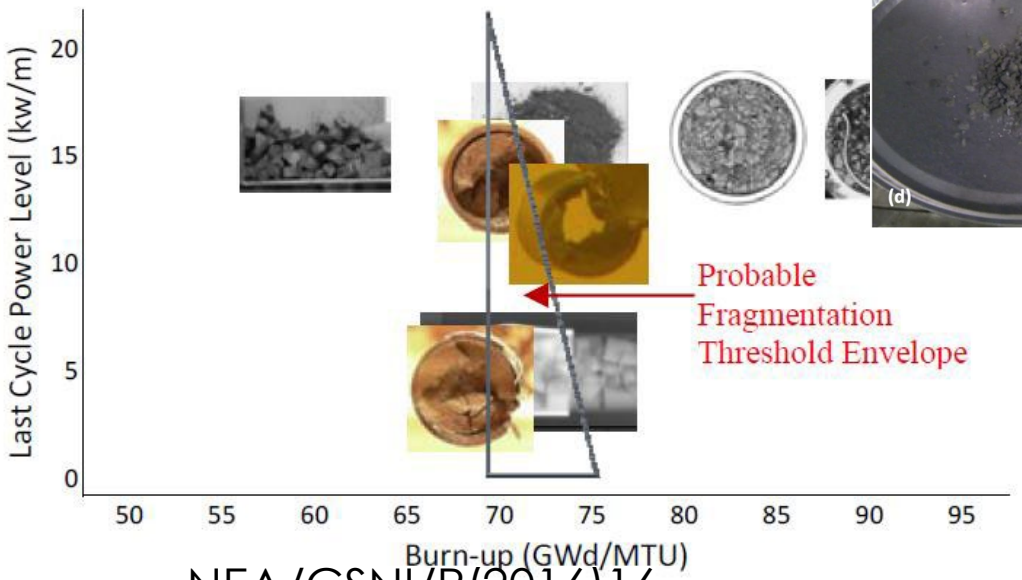

NEA/CSNI/R(2016)16

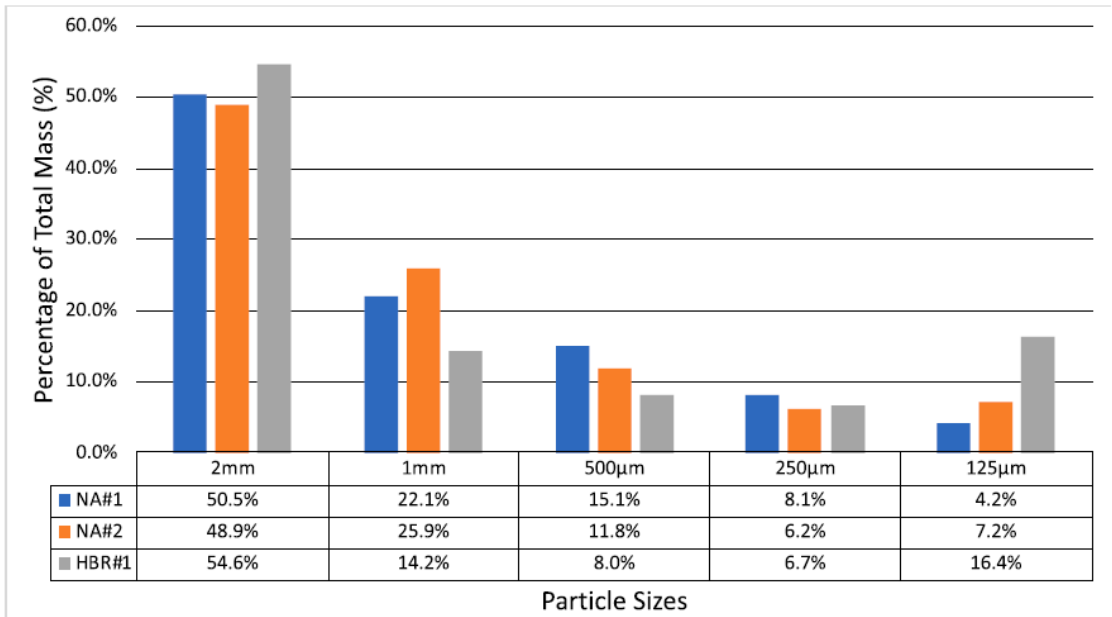

	2mm	1mm	500µm	250µm	125µm
NA#1	50.5%	22.1%	15.1%	8.1%	4.2%
NA#2	48.9%	25.9%	11.8%	6.2%	7.2%
HBR#1	54.6%	14.2%	8.0%	6.7%	16.4%

Objectives

- Develop system to improve characterization of fuel rod segments post-exposure to LOCA-type accidents
  - Improve uncertainty measurements
  - Increase inputs usable by the modeling community
- Develop a system to analyze fuel dispersal from vibrations following burst events

Advanced characterization of SATS-tested rods

- Standard method is caliper-based: burst length, width, circumference
- Fuel rod segment profilometry system (FRSPS) provides improved method of burst detection
  - Two instruments: camera and light curtain profilometer
  - Instruments are mounted on a moving stage that runs along the axial direction of the rod
  - The camera can move perpendicular to rod motion
  - A rotation motor allows the rod to be moved

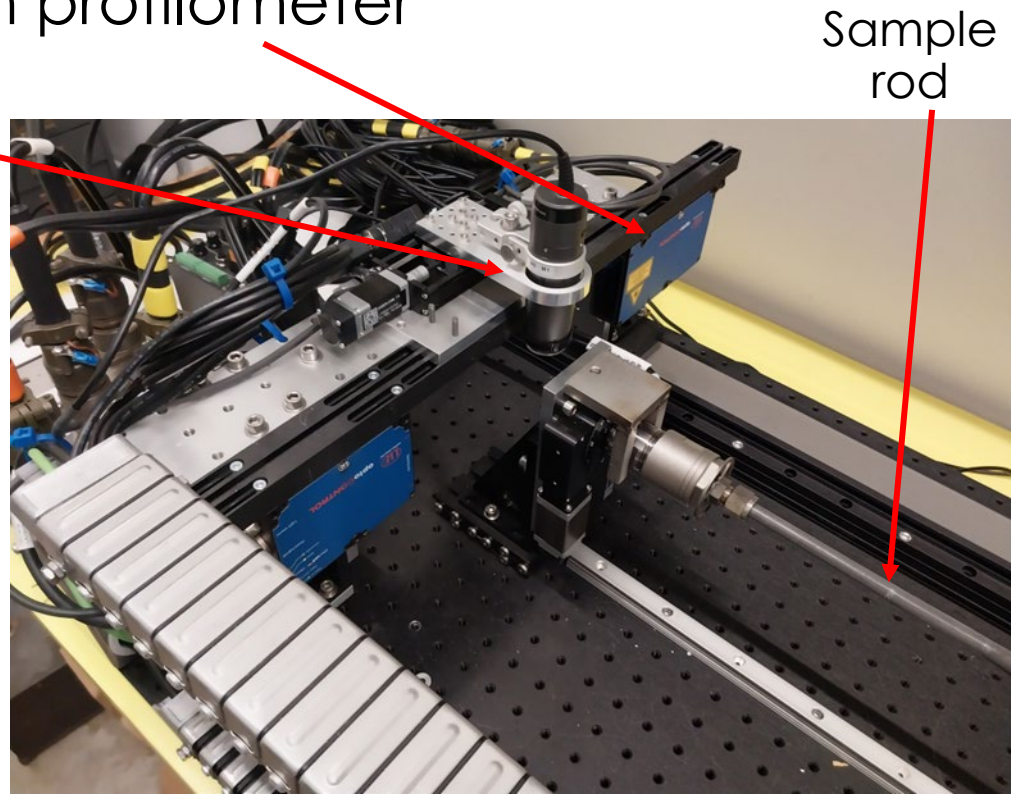

Optical analysis: stitched images

Burst test

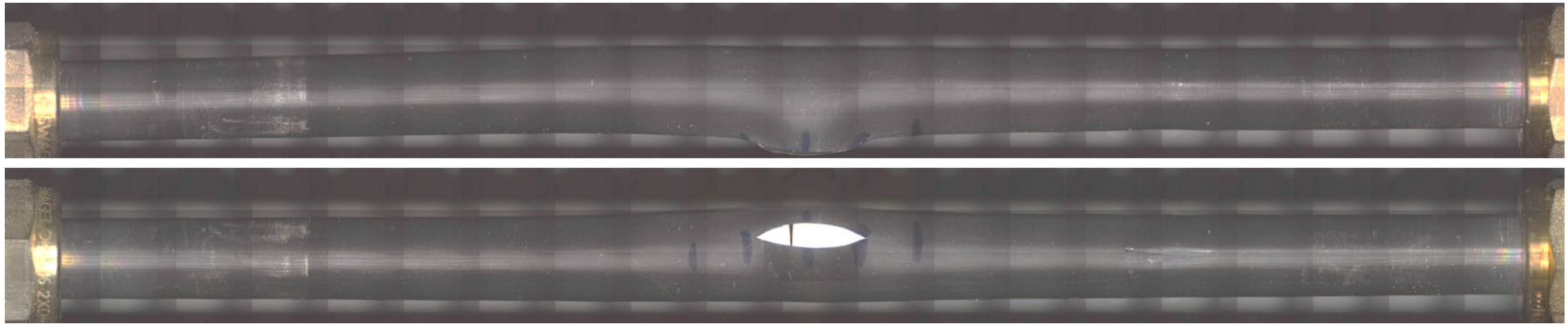

Creep test

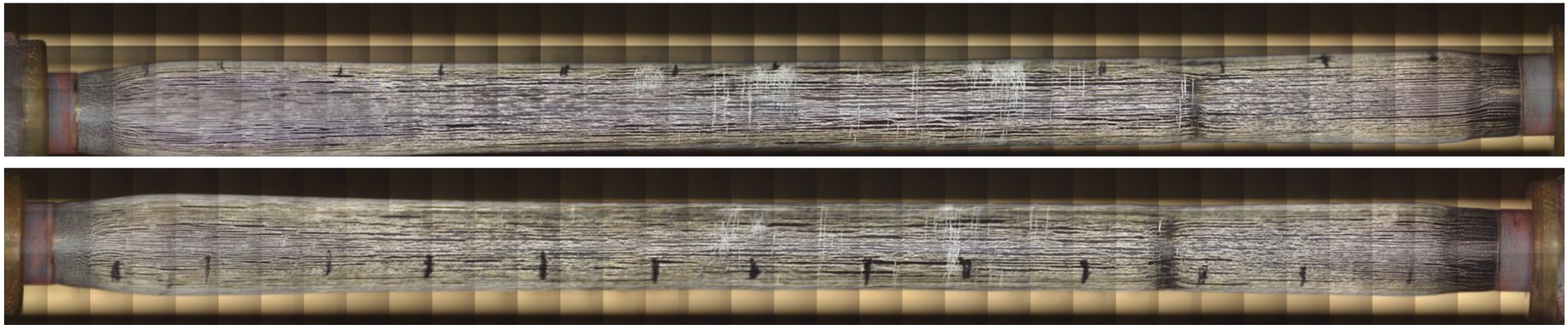

Light curtain profilometry - technique

- An LED source is parallelized and transmitted across an object
- The transmitted beam is recorded at a CMOS receiver
- Intensity thresholds are used to identify edges. Pixel interpolation allows precise determination of distance between edges

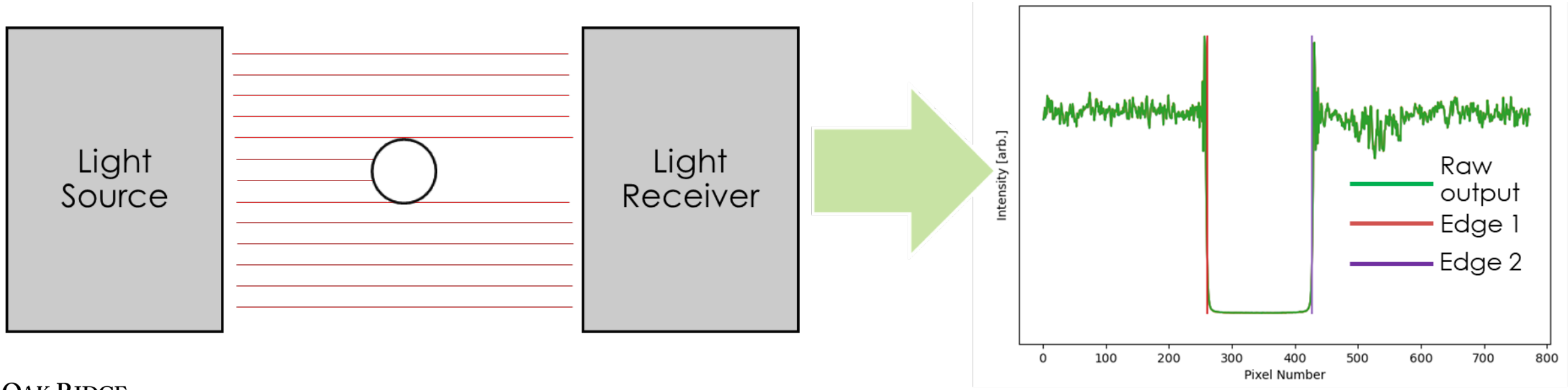

Light curtain profilometry – burst analysis

Scan sample:
- Minimum of 360 angular points
- Maximum of 1 mm increment axially

Two data points: edge 1 and edge 2, are saved at each location

Identify center of rod from center of stationary mount

Compute rod curvature from local center – ignoring burst

Recreate 3D object file with translation and rotation operations about the rod centerline

Identify burst center points – first-derivative analysis

Fit burst profile and compute burst geometry

Compute geometric properties of the rod, ignoring points related to the burst.

Reconstructed cross-sections of raw data at various slice locations along the tube

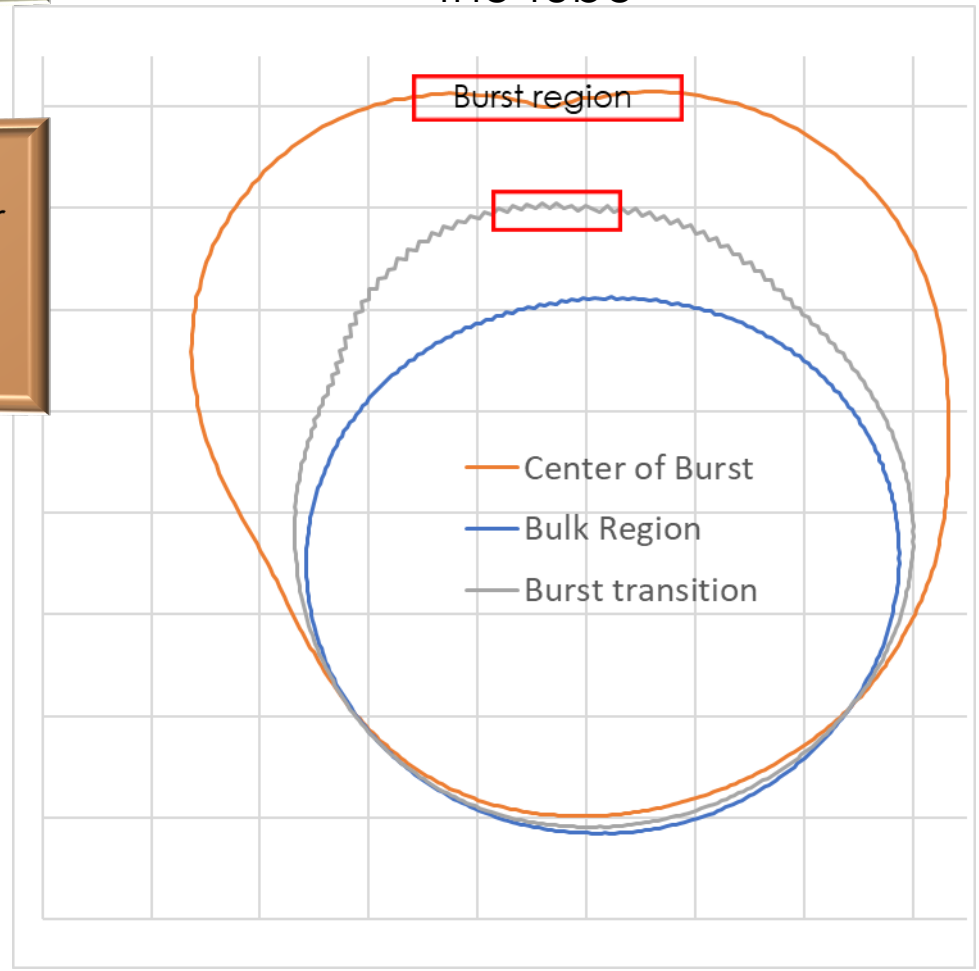

Light curtain analysis - burst example

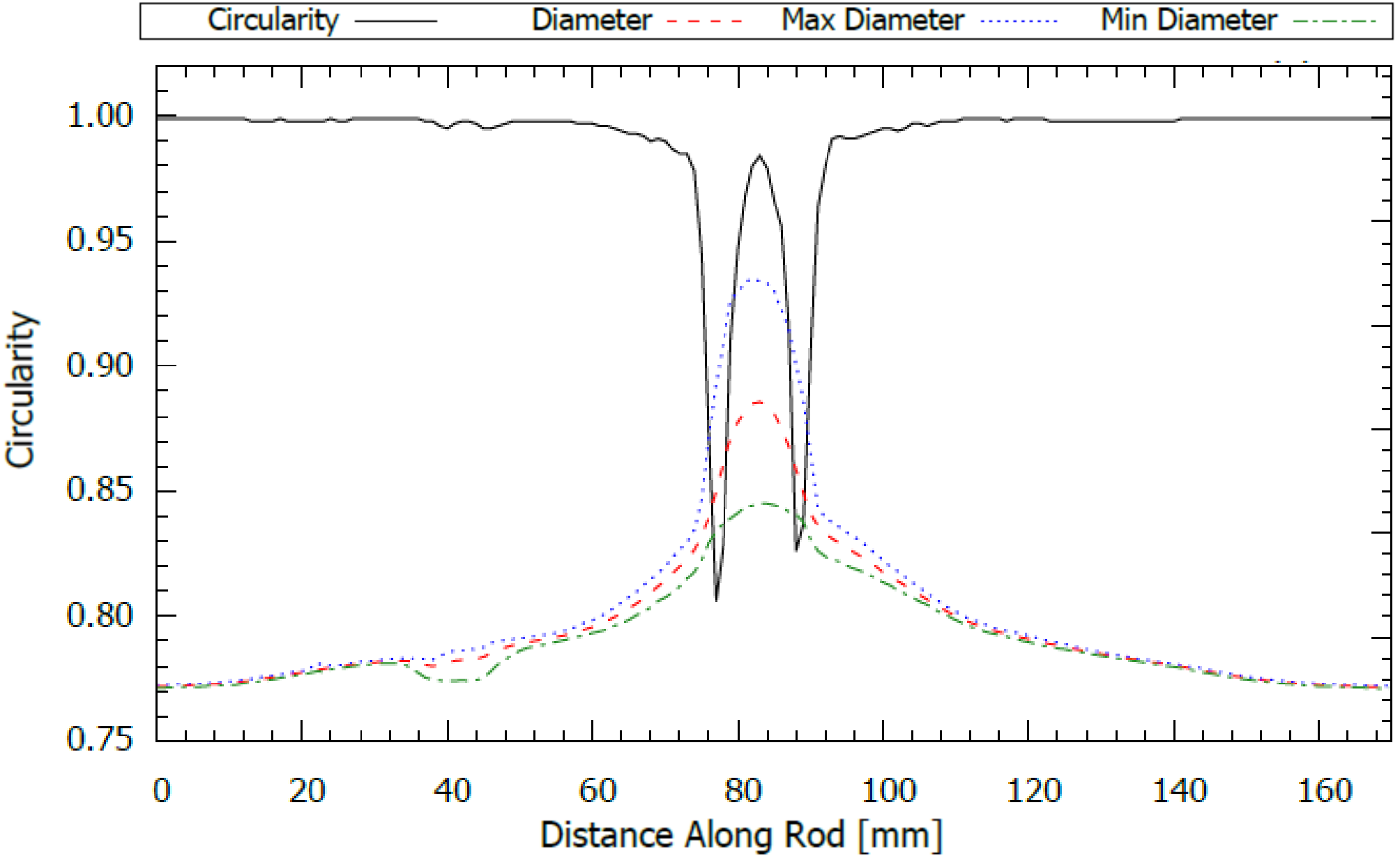

Fragment Relocation Induced by Accident Recovery (FRIAR)

- Objective:
  - Develop a tool for evaluation of fragmentation dispersal from post-burst fuel rods undergoing vibrations during post-LOCA quench
  - Identify conditions in which full fragment dispersal from the rod will occur, specifically the impacts of:
    - Frequency
    - Amplitude
    - Moisture
    - Particle geometry/mixture

FRIAR – Two types of particles examined in the present work

YSZ spheres, up to 0.3 – 3.0 mm

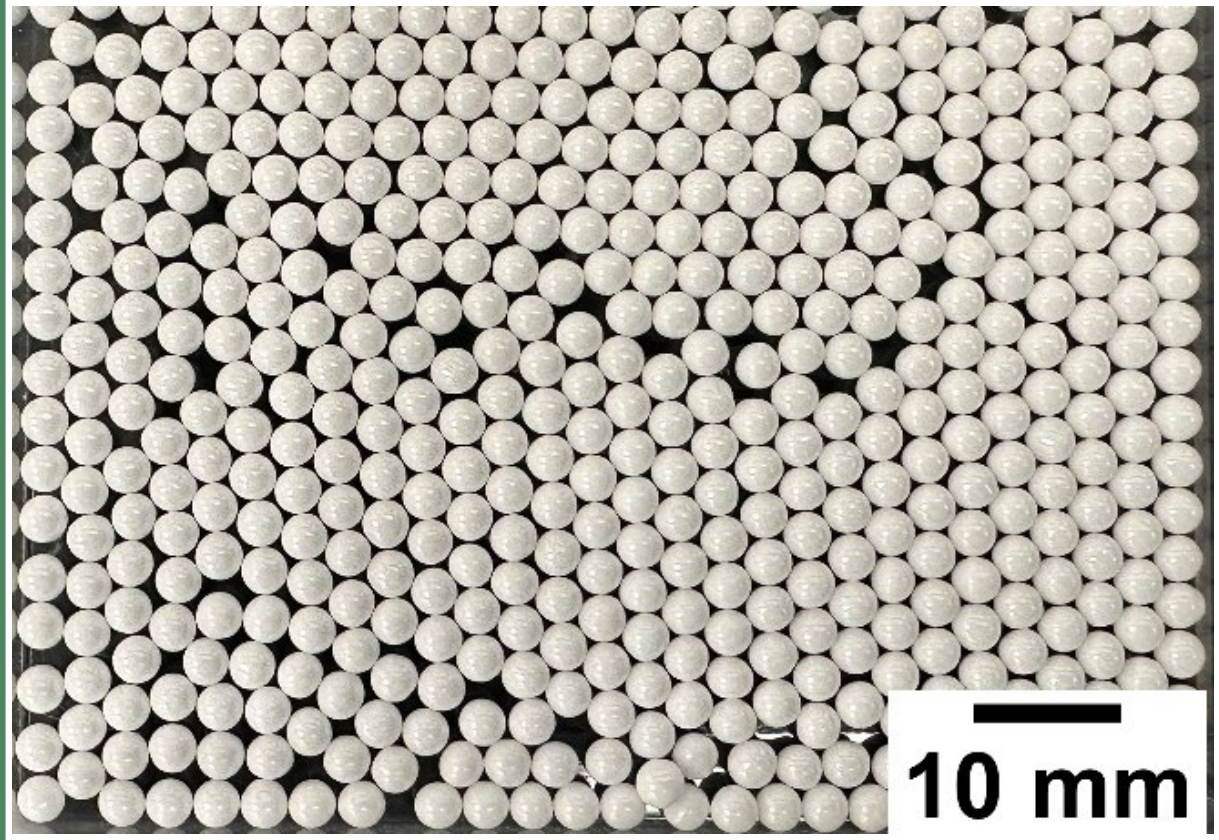

HfO_2 fragments, 3±1 mm

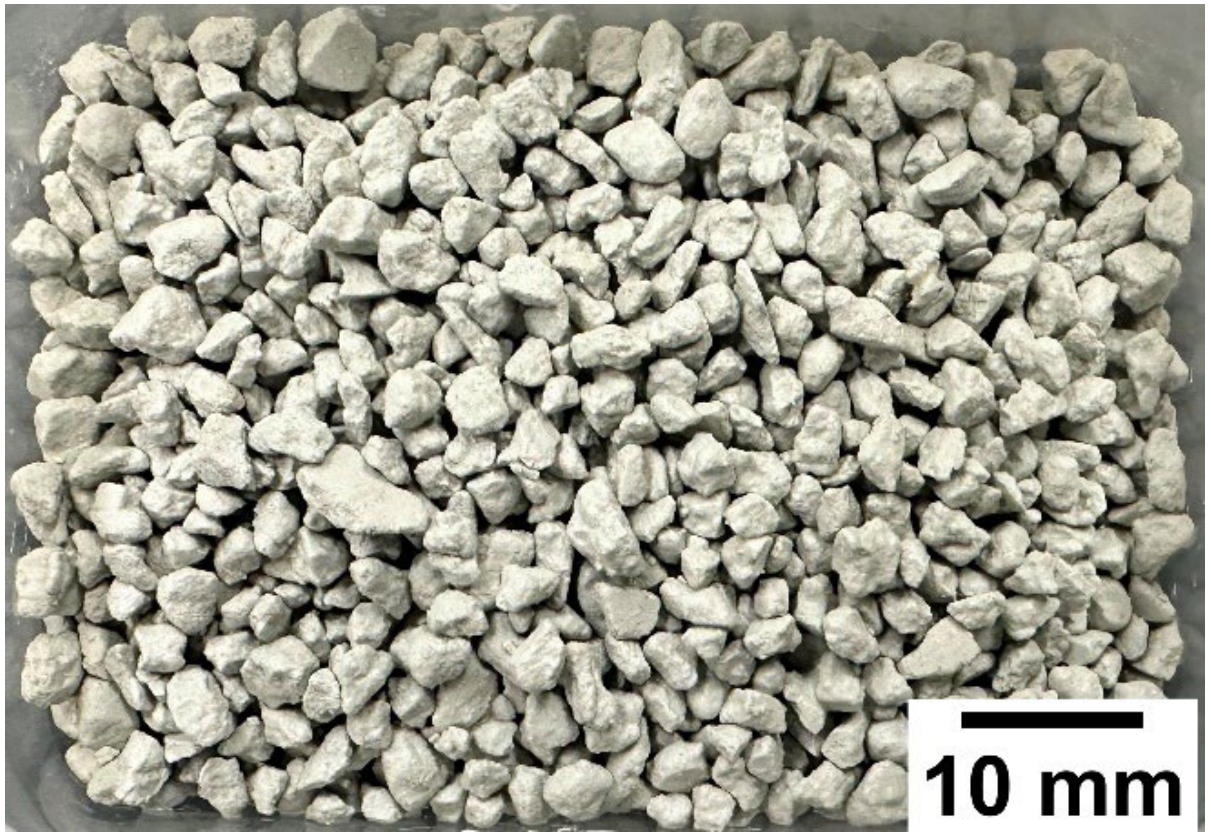

FRIAR – out-of-cell results accomplished through re-loading of pre-burst rods

- Out-of-cell SATS burst with pre-filled rods were universally non-prototypic
  - Significant burst-induced dispersal resulting in damage to equipment with large rod filler loss
  - Burst-induced dispersal far greater than real fuel tests
  - Refilled post-burst rod testing with FRIAR is expected to result in conservative dispersal estimates
- Reloading with spherical particles resulted in immediate gravity-induced loss through the burst: no packing retention
- Reloading with HfO_2 fragments or fragments mixed with smaller spheres resulted in packing

FRIAR apparatus and testing conditions

- SATS sample rod is mounted to a receiver plate, which is attached to a motor capable of producing sinusoidal vibrations
- A guide tube surrounds the rod, allowing dispersed material to be collected in a tray
- The collection tray is placed on a mass balance for time-resolved dispersal analysis
- Tests are universally run for 5 min in sets of at least 4

Fill Material	Burst width x length (mm)	Frequency (Hz)	Peak-to-peak amplitude (mm)
HfO_2 fragments	7 x 16	2	25
			10
			5
			2
		5	2
	5 x 15		10
			2
		2	25
Mixture*	5 x 15	5	10
			2
Wet Mixture**			10
	7 x 16	5	2

*Mixture is a combination of 60 wt% HfO_2 fragment, 25% 1 mm YSZ, 15% 0.3-0.4 mm YSZ, similar to particles recovered in NA2 (Capps et al., Nucl Eng Des 367 (2020) 110811)

**Wet mixture is the NA2 mixture with 5wt% addition of water

FRIAR – HfO_2 fragments partially pack and undergo full headspace loss less readily than spherical particles; full headspace loss occurs in 7x16 mm burst

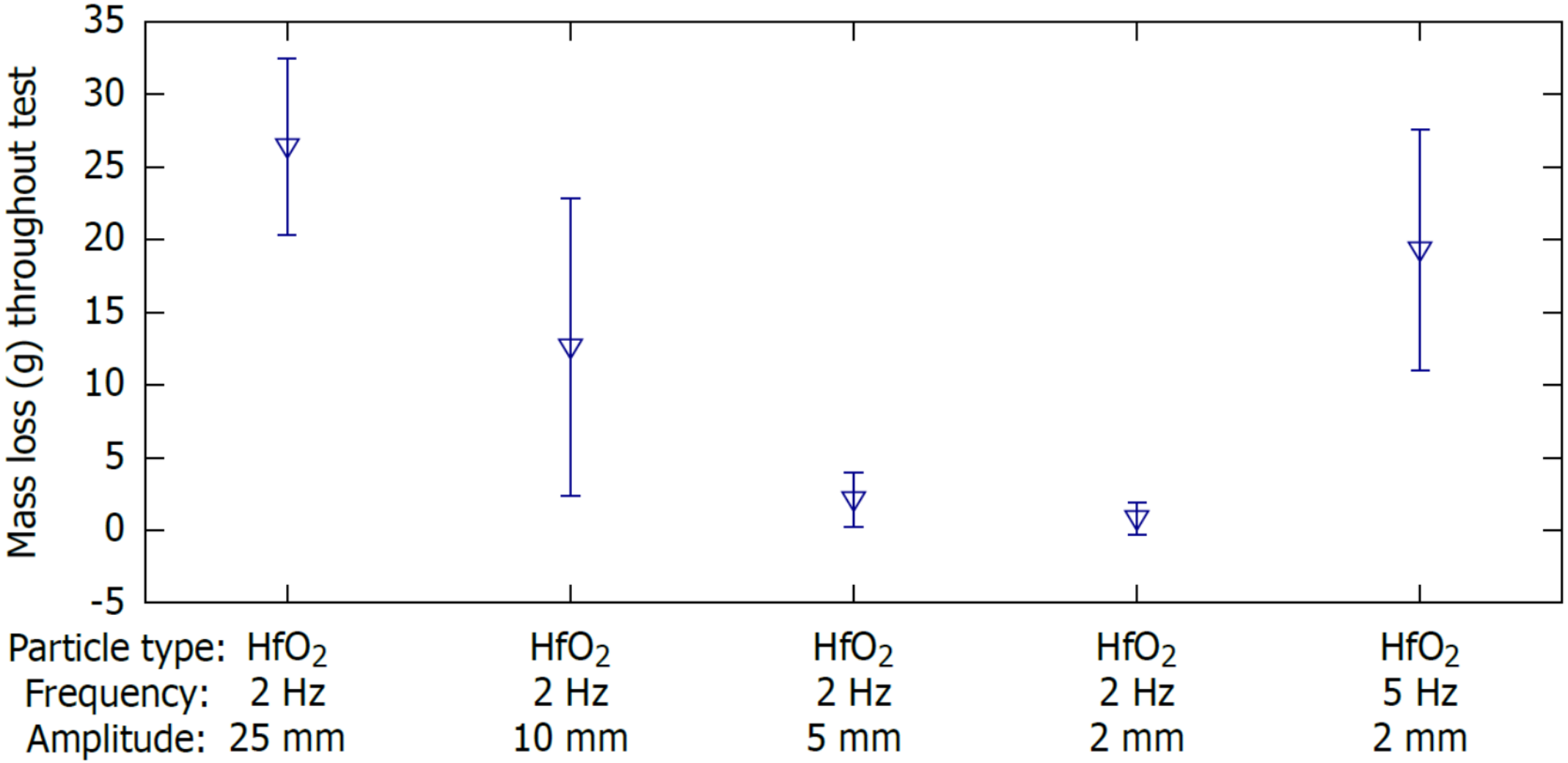

FRIAR – large fragment dispersal is localized to the burst when 5x15 mm burst; dispersal of small mixture fragments is nearly eliminated with moisture addition

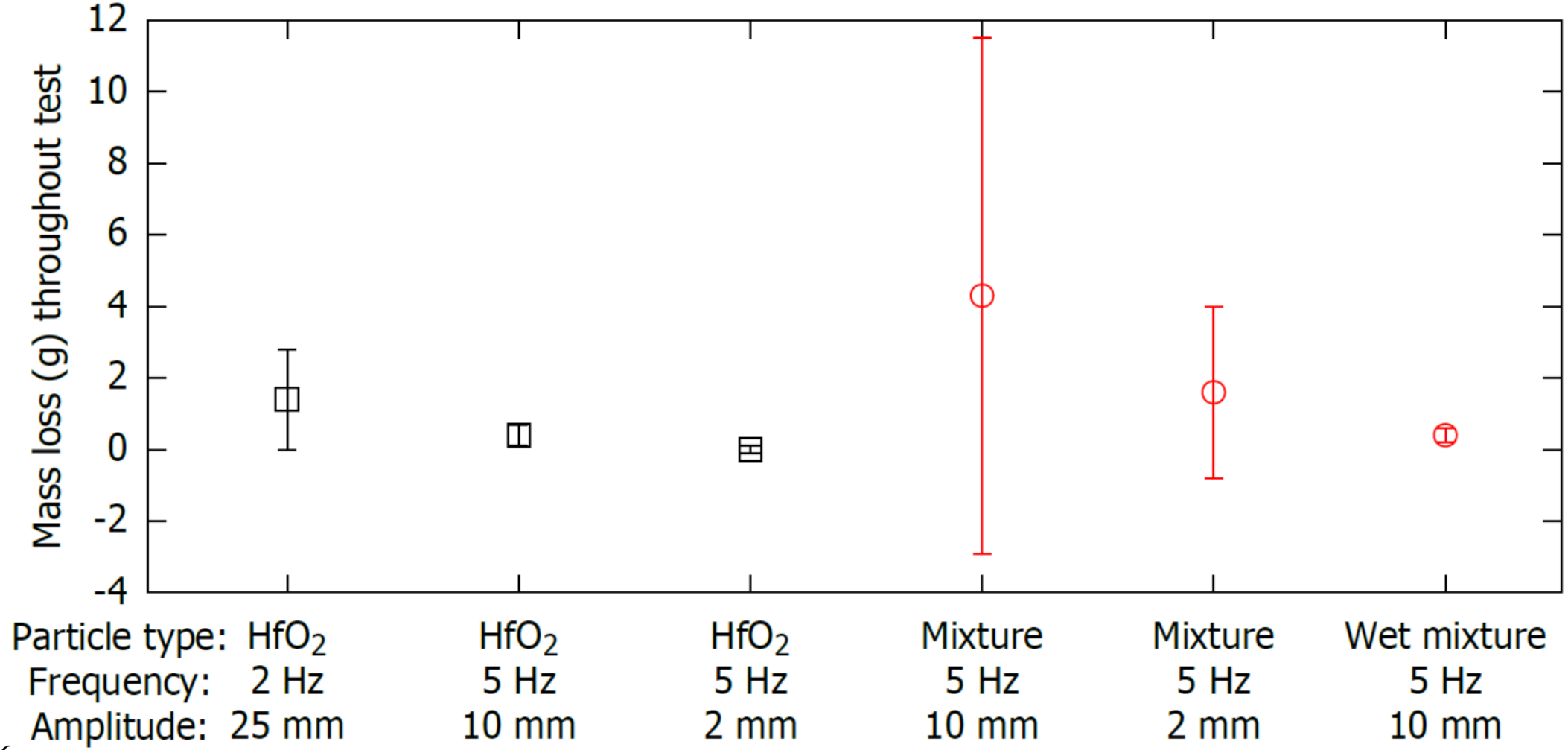

Conclusions

- The FRSPS at ORNL provides advanced characterization capability for post-burst nuclear fuel rods
  - Rod diameter is reported across the full length of the rod and at various radial increments
  - The burst region can be fully resolved with >100k data points
  - Data compares well with caliper-based results but is more expansive, aiding modelling efforts
- The FRIAR system at ORNL aids in analysis of the impacts of FFRD during core reflood following LOCA events
  - Fuel surrogate ceramic fragments have been tested
  - Fully fragmented fuel, including with small particulates, will be fully dispersed under severe and extended vibrations
  - Moisture addition and reduction of burst width significantly reduces the chance of headspace dispersion and increases dispersion time

28th International QUENCH Workshop
Participants

Nr.	Family Name	First Name	Institution	Country	e-mail
1	Bertsch	Johannes	Paul Scherrer Institut PSI	Switzerland	johannes.bertsch@psi.ch
2	Bottomley	David	JRC Karlsruhe	Germany	dboksb3@gmail.com
3	Boucek	Vaclav	UJP Praha	Czech Republic	boucek@ujp.cz
4	Brachet	Jean-Christophe	CEA	France	jean-christophe.brachet@cea.fr
5	Campell	Shawn	U.S. Nuclear Regulatory Commission	USA	shawn.campell@nrc.gov
6	Cazado	Mauricio Exequiel	KIT	Germany	mauricio.cazado@kit.edu
7	Charbal	Ali	CEA	France	ali.charbal@cea.fr
8	Doyle	Peter	Oak Ridge National Laboratory	USA	doylepj@ornl.gov
9	Endrychová	Alžběta	UJP PRAHA a.s.	Czech Republic	endrychova@ujp.cz
10	Esmaili	Hossein	U.S. Nuclear Regulatory Commission	USA	hossein.esmaili@nrc.gov
11	Fargette	Andre	FRAMATOME	France	andre.fargette@framatome.com
12	Farkas	Róbert	Centre for Energy Research (EK)	Hungary	robert.farkas@ek.hun-ren.hu
13	Frederick	Katerina	Westinghouse Electric Company	USA	katerina.frederick@westinghouse.com

28th International QUENCH Workshop
Participants

14	Grosse	Mirco	KIT	Germany	Mirco.Grosse@KIT.edu
15	Hollands	Thorsten	Gesellschaft fuer Anlagen- und Reaktorsicherheit (GRS) gGmbH	Germany	thorsten.hollands@grs.de
16	Howell	Jutta	KIT	Germany	jutta.howell@kit.edu
17	Jiménez Balbuena	Zaira Itzel	KIT	Germany	zaira.balbuena@kit.edu
18	Jo	Changhyun	Seoul National University	Republic of Korea	changhyun99@snu.ac.kr
19	Joung	SungHoon	Seoul National University	Rebulic of korea	brivin5386@snu.ac.kr
20	Khaperskaia	Anzhelika	IAEA	Austria	A.Khaperskaia@iaea.org
21	Kpemou	Apou Martial	IRSN	France	apou-martial.kpemou@irsn.fr
22	Krejci	Jakub	UJP PRAHA a.s.	Czech Republic	krejci@ujp.cz
23	Laier	Jutta	KIT	Germany	jutta.laier@kit.edu
24	Lee	Youho	Seoul National University	South Korea	leeyouho@snu.ac.kr
25	Lee	Injae	KIT	Germany	in.lee@partner.kit.edu
26	Lovasz	Liviusz	GRS	Germany	liviusz.lovasz@grs.de

28th International QUENCH Workshop
Participants

27	Martin	Julie-Fiona	OECD NEA: OECD Nuclear Energy Agency	France	julie-fiona.martin@oecd-nea.org
28	Mohamad	Afiqa	JAEA	Japan	mohamad.afiqa@jaea.go.jp
29	Nakamura	Kinya	Central Research Institute of Electric Power Industry	Japan	kinya@criepi.denken.or.jp
30	Peters	Ursula	KIT	Germany	Ursula.Peters@kit.edu
31	Piluso	Pascal	CEA	France	pascal.piluso@cea.fr
32	Rezchikova	Aleksandra	GRS	Germany	Aleksandra.Rezchikova@grs.de
33	Roessger	Conrado	KIT	Germany	conrado.roessger@kit.edu
34	Rougé	Emmanuel	IRSN	France	emmanuel.rouge@irsn.fr
35	Stahlberg	Gregor Tobias	Ruhr-Universität Bochum	Germany	stahlberg@pss.rub.de
36	Stegmaier	Boris	KIT	Germany	boris.stegmaier@kit.edu
37	Stegmaier	Ulrike	KIT	Germany	ulrike.stegmaier@kit.edu
38	Steinbrück	Martin	KIT	Germany	martin.steinbrueck@kit.edu
39	Stuckert	Juri	KIT	Germany	juri.stuckert@kit.edu

28th International QUENCH Workshop
Participants

40	Tang	Chongchong	KIT	Germany	chongchong.tang@kit.edu
41	Tiborcz	Livia	GRS	Germany	livia.tiborcz@grs.de
42	Valincius	Mindaugas	Lithuanian Energy Institute	Lithuania	mindaugas.valincius@lei.lt
43	Ver	Nora	HUN-REN Centre for Energy Research	Hungary	ver.nora@ek.hun-ren.hu
44	Wang	Guoqiang	Pacific Northwest National Laboratory (PNNL)	USA	Guoqiang.Wang@PNNL.GOV
45	Wang	Shisheng	KIT	Germany	Shisheng.Wang@kit.edu
46	Weick	Sarah	KIT	Germany	sarah.weick@kit.edu
47	Yook	Hyunwoo	Seoul National University	Republic of Korea	dbrgusdn96@snu.ac.kr